Talanta

The International Journal of Pure and Applied Analytical Chemistry

Publication information: *Talanta* (ISSN 0039-9140). For 2007, volumes 71–73 are scheduled for publication. Subscription prices are available upon request from the Publisher or from the Regional Sales Office nearest you or from this journal's website (http://www.elsevier.com/locate/talanta). Further information is available on this journal and other Elsevier products through Elsevier's website: (http://www.elsevier.com). Subscriptions are accepted on a prepaid basis only and are entered on a calendar year basis. Issues are sent by standard mail (surface within Europe, air delivery outside Europe). Priority rates are available upon request. Claims for missing issues should be made within six months of the date of dispatch.

Orders, claims, and journal enquiries: please contact the Customer Service Department at the Regional Sales Office nearest you:
Orlando: Elsevier, Customer Service Department, 6277 Sea Harbor Drive, Orlando, FL 32887-4800, USA; phone: (+1) (877) 8397126 [toll free number for US customers], or (+1) (407) 3454020 [customers outside US]; fax: (+1) (407) 3631354; e-mail: usjcs@elsevier.com
Amsterdam: Elsevier, Customer Service Department, PO Box 211, 1000 AE Amsterdam, The Netherlands; phone: (+31) (20) 4853757; fax: (+31) (20) 4853432; e-mail: nlinfo-f@elsevier.com
Tokyo: Elsevier, Customer Service Department, 4F Higashi-Azabu, 1-Chome Bldg, 1-9-15 Higashi-Azabu, Minato-ku, Tokyo 106-0044, Japan; phone: (+81) (3) 5561 5037; fax: (+81) (3) 5561 5047; e-mail: jp.info@elsevier.com
Singapore: Elsevier, Customer Service Department, 3 Killiney Road, #08-01 Winsland House I, Singapore 239519; phone: (+65) 63490222; fax: (+65) 67331510; e-mail: asiainfo@elsevier.com

USA mailing notice: *Talanta* (ISSN 0039-9140) is published monthly by Elsevier B.V. (P.O. Box 211, 1000 AE Amsterdam, The Netherlands). Annual subscription price in the USA US$ 3,818 (valid in North, Central and South America), including air speed delivery. Application to mail at periodical postage rate is paid at Rathway, NJ and additional mailing offices.
USA POSTMASTER: Send address changes to *Talanta*, Publications Expediting Inc., 200 Meacham Avenue, Elmont, NY 11003.
AIRFREIGHT AND MAILING in the USA by Publications Expediting Inc., 200 Meacham Avenue, Elmont, NY 11003.

Available online at www.sciencedirect.com
ScienceDirect
Talanta 71 (2007) 1470–1475
Talanta
www.elsevier.com/locate/talanta

Tunable separation of anions and cations by column switching in ion chromatography

Muhammad Amin, Lee Wah Lim, Toyohide Takeuchi *

Department of Chemistry, Faculty of Engineering, Gifu University, 1-1 Yanagido, Gifu 501-1193, Japan

Received 19 February 2006; received in revised form 7 July 2006; accepted 7 July 2006
Available online 24 August 2006

Abstract

A convenient ion chromatography method has been proposed for the routine and simple determination of anions (Cl^-, SO_4^{2-} and NO_3^-) and/or cations (Na^+, NH_4^+, K^+, Mg^{2+} and Ca^{2+}) using a single pump, a single eluent and a single detector. The present system used cation-exchange and anion-exchange columns connected in series via two 6-port switching valves or a single 10-port valve. The connection order of the ion-exchange columns could be varied by switching the valve(s). The present system therefore allowed the separation of either cations or anions in a single chromatographic run. While one ion-exchange column is being operated, the other ion-exchange column is being conditioned, i.e., the columns are always ready for analysis at any time. When 2.4 mM 5-sulfosalicylic acid was used as the eluent, the three anions and the five cations could be separated on the anion-exchange column and cation-exchange column, respectively. In order to obtain the separations of the target ions, the injection valve was placed between the two columns. Complete separations of the above anions or cations were demonstrated within 10 min each. The detection limits at S/N = 3 were 19–50 ppb (μg/l) for cations and 10–14 ppb for anions. The relative standard deviations of the analyte ions were less than 1.1, 2.9 and 2.8% for retention time, peak area and peak height, respectively. This proposed technique was applied to the determination of common anions and cations in river water samples.

Keywords: Ion chromatography; Tunable separation; Column switching; 5-Sulfosalicylic acid; Inorganic common ions

1. Introduction

Ion chromatography (IC) has become a mature analytical method since its introduction by Small et al. [1] owing to its wide applicability to the determination of ionic species in various water samples. Regularly, anions and cations are independently separated by using suppressed IC methods and nowadays, a great number of methods have been intimately developed for the simultaneous determination of anions and cations in a single chromatographic run, leading to achievement of more convenient, more simple and less solvent consuming systems [2–25].

There are two approaches currently known for the simultaneous determination of anions and cations in a single chromatographic run. The first approach uses a single column for this purpose based on chelation of cations to form anions [3–5], use of zwitterionic ion-exchangers [6–9] or mixed-bed ion-exchange columns [10], etc. However, these methods allow partially simultaneous separation of anions and cations. An alternative method involves mixed-mode separation such as ion-exclusion chromatography and cation-exchange chromatography [11–15]. This system provides a simple, rapid determination means for inorganic common ions. However, it is ineffective for a wide variety of anions contained in samples and an appropriate eluent should also be carefully selected.

The second approach uses two columns connected in series or parallel with or without column switching. For the approach without column switching [16–18], a suitable eluent should be chosen for the simultaneous separation of both anions and cations, but these peaks sometimes overlap and the method is not applicable widely. The determination of these common ions can be also achieved on short permanently coated silica monolithic anion-exchange and cation-exchange columns [19]. The both columns are connected in parallel arrangement. However, common monovalent cations such as Na^+, NH_4^+ and K^+ could not be separated when these ions contained in real samples.

* Corresponding author. Tel.: +81 58 2932806; fax: +81 58 2932806.
E-mail address: takeuchi@apchem.gifu-u.ac.jp (T. Takeuchi).

0039-9140/$ – see front matter © 2006 Elsevier B.V. All rights reserved.
doi:10.1016/j.talanta.2006.07.020

Two separation columns (cation-exchange and anion-exchange columns) can be connected in series via a single 6-port switching valve [20,21] or two switching valves [22]. We also developed separation systems using two 6-port switching valves for the determination of anions and cations and applied the developed system to the determination of ions in tap, river and pond water samples [23,24]. In our developed system named peak parking technique, cation-exchange and anion-exchange columns were connected in series via two 6-port switching valves. However, the above methods required accurate column-switching timing in order to avoid peak overlaps.

Yokoyama et al. [25] have also described a separation method using switching valves for the separation of anions and cations using cation-exchange and anion-exchange columns. They accumulated temporarily anions in loop while the cation IC was performed. Subsequently, the accumulated fraction was introduced into the anion-exchange column and then determined.

As a competitive practical method, this paper presents a convenient ion chromatography method to determine either of anions or cations in a single system. The method comprises one pump, one injection valve, an anion-exchange column, a cation-exchange column, two 6-port switching valves or a single 10-port switching valve and a conductivity detector. This method is easy and simple to operate compared with our previous method [23,24]. In previously method, good resolution of cations and anions was achieved when the peak parking technique was performed. However, the column switching timing had to be focused to control accurately in order to trap analyte anion on the anion-exchange column, i.e., to avoid peak overlaps.

In the present method, while one ion-exchange column is being operated, the other ion-exchange column is being conditioned. In other words, both the columns are being conditioned with the eluent and are possible to use at any time. Furthermore, column switching is needed only when the required separation will be changed. On that purpose, the two ion-exchange columns are then connected in series via two 6-port switching valves or a single 10-port switching valve while the injection valve is placed between the two columns to allow separating the target ion. The optimized operating system was then applied to the determination of anions and cations in river water samples.

2. Experimental

2.1. Apparatus

The diagrams of the apparatus employed in this study are illustrated in Fig. 1a and b. The ion chromatograph consisted of a PU-2080i plus HPLC pump (Jasco, Tokyo, Japan), a Rheodyne 5095 injector equipped with a 20 μl sample loop (Cotati, CA, USA), a CM-8020 conductivity detector (Tosoh, Tokyo, Japan), two Model 7000 6-port switching valves (Rheodyne) or a Model 7610-600 10-port switching valve (Rheodyne) and a Computer Aided Chromatography data processor (Nippon Filcon, Tokyo, Japan). The columns employed were a TSK_{gel} Super-IC-Cation column (150 mm × 4.6 mm i.d.) and a TSK_{gel} IC-Anion-PW_{XL} column (75 mm × 4.6 mm i.d.). Both columns were obtained from Tosoh (Tokyo, Japan).

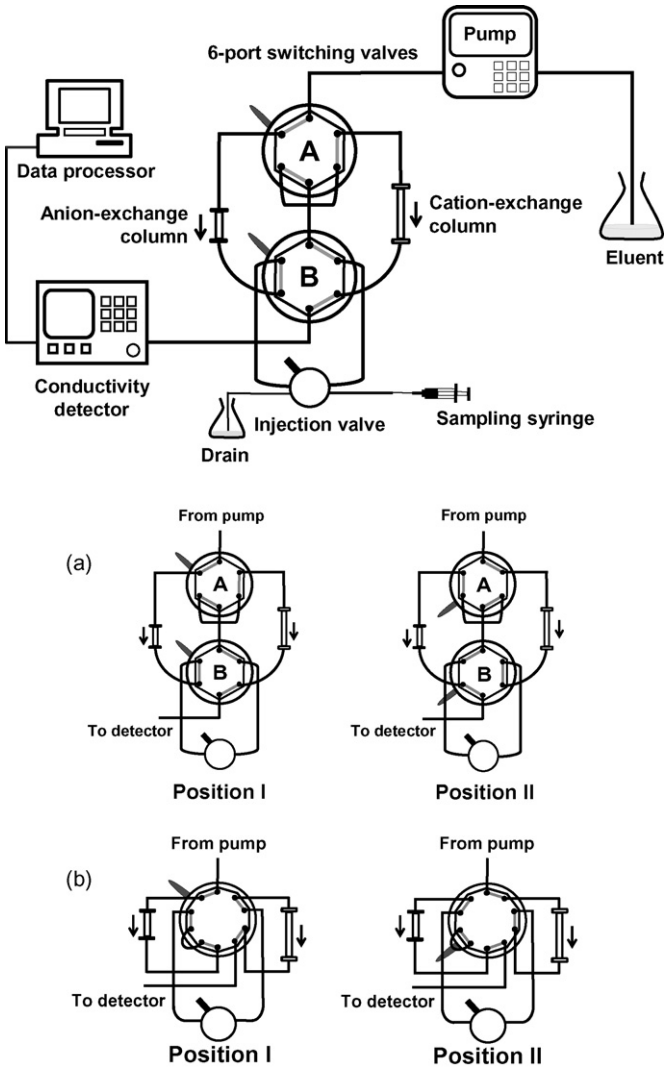

Fig. 1. Schematic diagrams of the instruments and the positions of the switching valve(s) for (a) two 6-port switching valves and (b) single 10-port switching valve. The injection valve was placed between anion-exchange and cation-exchange columns, which allowed the tuning of either cations separation or anions separation. Separation of cations (position I) and separation of anions (position II).

2.2. Reagents, standards and sampling

Analytical reagent grade chemicals were used and purchased from Nacalai Tesque (Kyoto, Japan), unless otherwise noted. Purified water was prepared in the laboratory by using a GS-590 water distillation system (Advantec, Tokyo, Japan). A single stock standard solution containing a mixture of all interest ions was prepared by dissolving 0.2 mM of each NaCl, $CaCl_2$, $MgSO_4$, NH_4NO_3 and KNO_3. All standard solutions were stored in polyethylene containers and kept under refrigeration at 4 °C. 5-Sulfosalicylic acid was obtained from Wako (Osaka, Japan) and used for the eluent.

The samples were taken from Ijira River located near the Gifu University, Gifu, Japan. The samples were filtered with a 0.45 μm membrane filter for IC and stored in polyethylene containers and kept under refrigeration at 4 °C. The samples were injected to the chromatographic system without dilution.

2.3. Eluent conditions

The eluent used for the determination of anions and cations was 2.4 mM 5-sulfosalicylic acid. The conditions were under isocratic mode. The pump was operated at a flow rate of 0.5 ml/min to keep the inlet pressure lower than 7.0 MPa.

2.4. Column switching procedures

Two columns were connected in series via two 6-port switching valves or a single 10-port switching valve. Fig. 1 illustrates of the equipment and the position of both 6-port switching valves and 10-port switching valve for the required separations. The injection valve is placed between the anion-exchange and cation-exchange columns, which allowed the tuning of either cations separation or anions separation. As in Fig. 1a, the separation system works at position as follows.

2.4.1. Position I

Both valves A and B are switched for the separation of cations position and the eluent passes through both cation-exchange and anion-exchange column until a straight baseline is obtained. A 20 μl volume of the sample solution is then injected to the chromatographic system. The analytes will pass on the cation-exchange column and then the cations will separate. The separation of cations can be repeated by re-injecting a new sample to the chromatographic system. While the separation of cations on the cation-exchange column is being operated, the anion-exchange column is being conditioned with the eluent; therefore, the anion-exchange column is ready for use at any time.

2.4.2. Position II

Both valves A and B are switched for the separation of anions position. A 20 μl volume of the sample solution is then injected to the chromatographic system. The analytes will pass on the anion-exchange column and then the anions will separate. The separation of anions can be repeated by re-injecting a new sample to the chromatographic system. While the separation of anions on the anion-exchange column is being operated, the cation-exchange column is being conditioned with the eluent; therefore, the cation-exchange column is ready for use at any time. This means that the separation of cations and/or anions in this work is tunable at any time.

Fig. 1b shows a simplified method for the separations of anions and cations. The two 6-port switching valves can be replaced by a single 10-port switching valve. The manual procedures are the same as for the two 6-port switching valves. However, the use of a single 10-port switching valve in the present work is recommended for avoiding complicated operation. It should be noted that the present system does not allow the simultaneous detection of both anions and cations. Either anions or cations can be detected in a single chromatographic run.

3. Results and discussion

3.1. Selection of eluent

In this work, 5-sulfosalicylic acid was used as the eluent for the separation of both cations and anions. It has been sometimes used in IC because cations and particularly anion selectivity may be adjusted by varying its concentration. 5-Sulfosalicylic acid was used by Lee et al. [11] for the simultaneous determination of anions and cations, where the analytes were separated in the ion-exclusion and cation-exchange chromatography modes. In our previous report [24], 5-sulfosalicylic acid was also used as the eluent to achieve separation of both anions and cations in the ion-exchange mode. It should be noted that SO_4^{2-} can be eluted from a commercially available anion-exchange column when 5-sulfosalicylic acid was used as the eluent [24].

3.2. Effect of 5-sulfosalicylic acid concentration

The influence of the 5-sulfosalicylic acid eluent on the retention time was investigated at different concentrations in the range 1.6–3 mM. As shown in Fig. 2, the retention factor (k) tended to decrease with increasing eluent concentration. When the eluent concentration was less than 2.4 mM, divalent cations (Mg^{2+} and Ca^{2+}) were retained longer and SO_4^{2-} overlapped with NO_3^- and at much lower concentration, SO_4^{2-} overlapped with the system peak. At the concentrations higher than 2.4 mM the resolution between Na^+ and NH_4^+ was poor. Considering of the above results, in this method, 2.4 mM was used in subsequent experiments. The elution order at the optimized concentration was $Na^+ < NH_4^+ < K^+ < Mg^{2+} < Ca^{2+}$ for the cations and $Cl^- < SO_4^{2-} < NO_3^-$ for the anions.

Almost linear relationships between the logarithm of the retention factor ($\log k$) and the logarithm of the eluent concentration are observed, as shown in Fig. 2. The slopes for the analyte cations were −0.86, −1.00, −1.11, −1.56 and −1.93 for Na^+, NH_4^+, K^+, Mg^{2+} and Ca^{2+}, respectively, whereas those for the analyte anions were −0.40, −0.79 and −0.45 for Cl^-, SO_4^{2-} and NO_3^-, respectively. If we assume that the eluent anion is divalent, the slope value should be −1 and −2 for the monovalent and divalent analyte cations, respectively. On the contrary, it should be −0.5 and −1 for the monovalent and divalent analyte anions. The above slight deviations from the expected values may be due to the fact that the dissociation of the carboxylic acid of 5-sulfosalicylic acid is not perfect. Actually, since the pK_a value of the carboxyl group of 5-sulfosalicylic acid is around 2.9, it is expected that a portion of 5-sulfosalicylic acid is present as a divalent anion. For example, the pH of 2.4 mM 5-sulfosalicylic acid is 2.1. The formation of complex between divalent cations and 5-sulfosalycilic acid may be another possible reason.

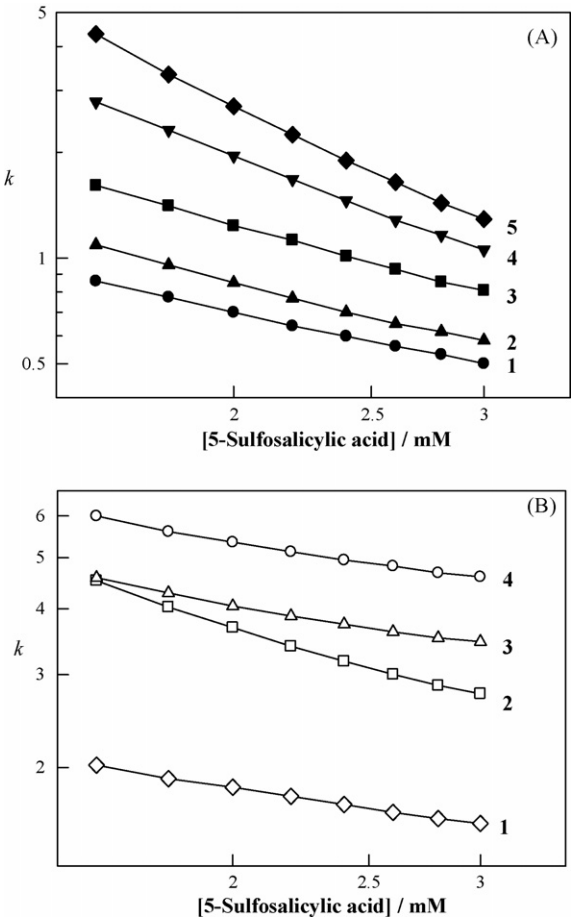

Fig. 2. The logarithm of the retention factor vs. the logarithm of the 5-sulfosalicylic acid concentration for cations (A) and anions (B). Eluent: 1.6–3.0 mM 5-sulfosalicylic acid. Columns: TSK_{gel} Super IC-Cation (150 mm × 4.6 mm i.d.) and TSK_{gel} IC-Anion-PW_{XL} (75 mm × 4.6 mm i.d.). Eluent flow-rate, 0.5 ml/min; column temperature, room temperature; injection volume, 20 μl; plot lines: (A) 1 = Na^+; 2 = NH_4^+; 3 = K^+; 4 = Mg^{2+}; 5 = Ca^{2+} and (B) 1 = Cl^-; 2 = SO_4^{2-}; 3 = NO_3^-; 4 = system peak.

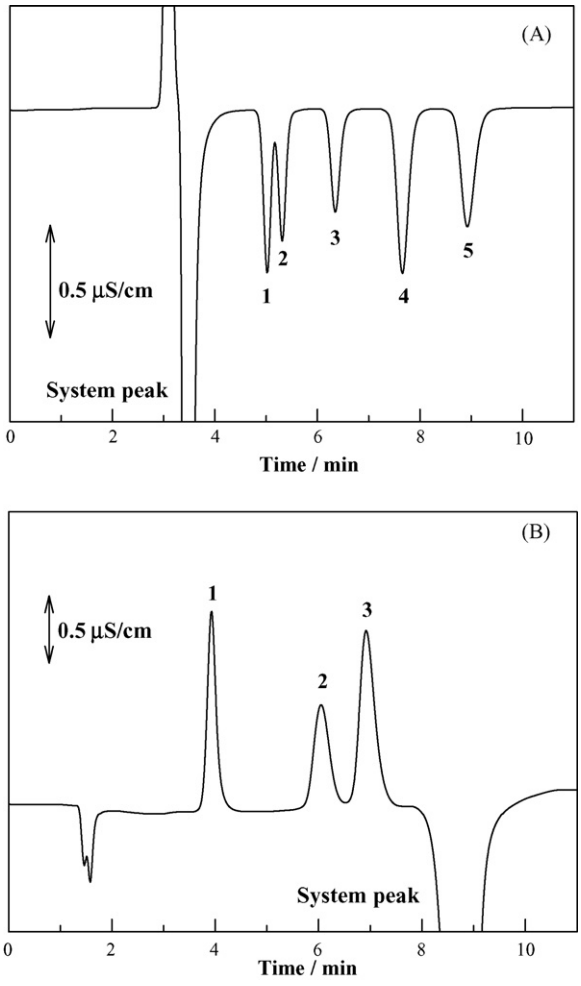

Fig. 3. Separation of cations and/or anions via column switching. Eluent: 2.4 mM 5-sulfosalicylic acid. Columns: TSK_{gel} Super IC-Cation (150 mm × 4.6 mm i.d.) and TSK_{gel} IC-Anion-PW_{XL} (75 mm × 4.6 mm i.d.), connected in series via two 6-port switching valves or a single 10-port switching valve. Analyte (concentration, in mM): (A) 1 = Na^+ (0.2); 2 = NH_4^+ (0.2); 3 = K^+ (0.2); 4 = Mg^{2+} (0.2); 5 = Ca^{2+} (0.2) and (B) 1 = Cl^- (0.6); 2 = SO_4^{2-} (0.2); 3 = NO_3^- (0.4); 4 = system peak. Other operating conditions as in Fig. 2.

3.3. System peaks

System peaks are usually generated by the difference in the composition between the sample solution and the eluent. In addition, the area and direction of the system peaks also depend on the eluent pH. The performances of system peak have been described in literature [26].

It was observed that at the optimized eluent concentration cationic species eluted just after system peaks on the cation-exchange column, whereas anionic species eluted before a system peak on the anion-exchange column. The system peaks did not overlap with analyte.

3.4. Cation-exchange separation

The five cations (Na^+, NH_4^+, K^+, Mg^{2+} and Ca^{2+}) were well eluted within 10 min. As described in Fig. 3A, a baseline separation between Na^+ and NH_4^+ was not achieved under the eluent concentration. However, both ions could be determined. The results were cross-checked under different eluent conditions. By reducing the molar composition of eluent (e.g., 1.4 mM), the baseline separation could be achieved and the obtained results with those obtained under the conditions in Fig. 3A.

3.5. Anion-exchange separation

The resolution and retention time of analyte ions were extremely dependent on the ionic strength of the eluent and its pH. For achieving good resolution, the eluent concentration must be adjusted carefully. Particularly for SO_4^{2-}, at lower 5-sulfosalicylic acid eluent concentration, it eluted just after NO_3^-. In contrast, at higher concentration (e.g., 2.4 mM), it is eluted before NO_3^-. As shown in Fig. 3B, complete separation of the three anions (Cl^-, SO_4^{2-} and NO_3^-) was also achieved within 10 min.

Table 1
Summarized data for the detection limits (LODs), correlation coefficient (r^2) and retention times (t_R) of major cations and anions obtained under the optimum chromatographic condition described in Fig. 3

Analyte	LOD (S/N = 3)		Correlation coefficient (r^2)	t_R/min
	(μM)	(ppb)		
Cations				
Na^+	0.91	22	0.9975	5.02
NH_4^+	1.19	21	0.9975	5.31
K^+	1.29	50	0.9967	6.35
Mg^{2+}	0.81	19	0.9982	7.65
Ca^{2+}	1.13	45	0.9913	8.93
Anions				
Cl^-	0.27	10	0.9936	3.93
SO_4^{2-}	0.15	14	0.9976	6.06
NO_3^-	0.19	11	0.9959	6.92

3.6. Validation of the proposed method

3.6.1. Calibration plots and detection limits

In order to evaluate the quantitative applicability of the proposed technique, five different concentration standard sample solutions were determined under the optimized conditions. The peak heights of ions were plotted against the concentration to get the calibration graphs. The correlation coefficients and detection limits are listed in Table 1. From the Table, the correlation coefficients $r^2 > 0.99$ proved good linearity of the present method. The detection limit at a signal-to-noise ratio (S/N) of 3:1 are also given.

3.6.2. Repeatability

Table 2 shows the repeatability of retention times, peak areas and peak heights under the optimum elution conditions. The results reveal that the relative standard deviations (R.S.Ds.%) of common cations and anions were less than 1.1% for retention time, less than 2.9% for peak area and less than 2.8% for peak height, respectively.

3.7. Application to river water sample

The proposed technique was applied to the determination of common anions and cations in river water samples. The samples were determined after filtration with a 0.45-μm membrane filter for IC. Good separations for all common inorganic anions and cations were achieved. The results showed that the contents of ionic species in samples were all higher than the detection limits. The chromatograms of this river water samples are shown in Fig. 4. Fig. 4A demonstrates the separation of cations, whereas Fig. 4B demonstrates the separation of anions. The concentrations of common anions and cations are determined by using the present column-switching technique and the results are shown in Table 3. In addition contamination of the samples by foreign ions are minimized because the samples were just filtrated using

Table 2
Relative standard deviations (R.S.Ds.) of major cations and anions obtained under the optimum chromatographic condition described in Fig. 3

Analyte	R.S.D. (%), $n = 5$[a]		
	Retention time	Peak area	Peak height
Cations	0.26–0.89	1.89–2.91	1.13–1.82
Anions	0.43–1.05	1.22–2.64	1.44–2.77

[a] n, Number of replicate measurements.

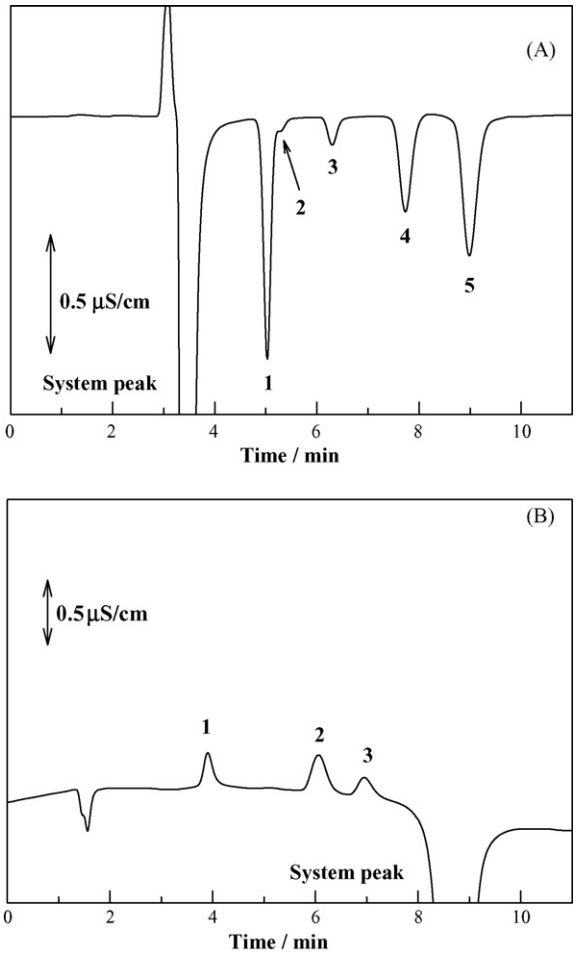

Fig. 4. Chromatograms of ions detected in river water sample for (A) cations and (B) anions. Chromatographic conditions as in Fig. 3 except for the samples.

Table 3
Determination of major cations and anions concentration in river water sample ($n = 5$) obtained using the proposed IC method

Analyte	River water sample	
	Mean (mM)	R.S.D. (%)
Cations		
Na^+	0.328	1.29
NH_4^+	0.005	2.01
K^+	0.038	1.34
Mg^{2+}	0.097	1.76
Ca^{2+}	0.203	1.97
Anions		
Cl^-	0.147	1.58
SO_4^{2-}	0.065	2.13
NO_3^-	0.039	2.01

a membrane filter for IC and stored in polyethylene containers and kept under refrigeration at 4 °C.

Bicarbonate is commonly found as a major anion in the river water samples. Since the pH of the river water sample determined in Table 3 is 7.02, bicarbonate is a dominant species. From the determination data in Table 3, ionic balance can be calculated. The bicarbonate concentration in the river sample in Table 3 is estimated to be 0.655 mM assuming that the contribution of trace ions can be neglected.

4. Conclusions

In conclusion, a novel column switching technique for ion chromatography is reported here. The described separation system offered simple and easy operation for determining anions and cations. Both anions and cations could be determined by using two ion-exchange columns, two 6-port switching valves or a single 10-port switching valve and a single detector. The eluent of 2.4 mM 5-sulfosalicylic acid was suitable for the determination of common anions and cations contained in water samples in a reasonable time. The present method will be applicable to the determination of anions and cations in various water samples.

References

[1] H. Small, T.S. Stevens, W.C. Bauman, Anal. Chem. 47 (1975) 1801.
[2] J. Weiss, Ion chromatography, second ed., VCH, Weinheim, 1995.
[3] M. Yamamoto, H. Yamamoto, Y. Yamamoto, S. Matsushita, N. Baba, T. Ikushige, Anal. Chem. 56 (1984) 832.
[4] K. Ohta, K. Tanaka, Anal. Chim. Acta 373 (1998) 189.
[5] K. Ohta, K. Tanaka, J.S. Fritz, J. Chromatogr. A 731 (1996) 179.
[6] W. Hu, H. Haraguchi, Anal. Chem. 66 (1994) 765.
[7] W. Jiang, K. Irgum, Anal. Chem. 71 (1999) 333.
[8] W. Jiang, K. Irgum, Anal. Chem. 73 (2001) 1993.
[9] M.G. Kiseleva, P.A. Kebets, P.N. Nesterenko, Analyst 126 (2001) 2119.
[10] D.J. Pietrzyk, D.M. Brown, Anal. Chem. 58 (1986) 2554.
[11] K.-P. Lee, S.-H. Choi, Y.-C. Park, Z.U. Bae, M.-S. Lee, S.H. Lee, H.-Y. Chang, S.-M. Kwon, K. Tanaka, Bull. Korean Chem. Soc. 24 (2003) 1324.
[12] Q. Xu, W. Zhang, C. Xu, L. Jin, Analyst 125 (2000) 1065.
[13] M.-Y. Ding, K. Tanaka, W. Hu, K. Hasebe, P.R. Haddad, Analyst 126 (2001) 567.
[14] K. Tanaka, K. Ohta, J.S. Fritz, S. Matsushita, A. Miyanaga, J. Chromatogr. A 671 (1994) 239.
[15] M. Mori, K. Tanaka, M.I.H. Helaleh, Q. Xu, M. Ikedo, Y. Ogura, S. Sato, J. Chromatogr. A 997 (2003) 219.
[16] H. Small, T.E. Miller Jr., Anal. Chem. 54 (1982) 462.
[17] Z. Iskandarani, T.E. Miller Jr., Anal. Chem. 57 (1985) 1591.
[18] D.-C. Gan, J.G. Tarter, J. Chromatogr. 404 (1987) 285.
[19] D. Connolly, D. Victory, B. Paull, J. Sep. Sci. 27 (2004) 912.
[20] R. Saari-Nordhaus, J.M. Anderson Jr., J. Chromatogr. 549 (1991) 257.
[21] R. Saari-Nordhaus, L. Nair, J.M. Anderson Jr., J. Chromatogr. 602 (1992) 127.
[22] K.J.B.A. Karim, J.-Y. Jin, T. Takeuchi, J. Chromatogr. A 995 (2003) 153.
[23] M. Amin, L.W. Lim, T. Takeuchi, Anal. Bioanal. Chem. 381 (2005) 1426.
[24] M. Amin, L.W. Lim, T. Takeuchi, Anal.Bioanal. Chem. 384 (2006) 839.
[25] Y. Yokoyama, N. Sawaguchi, H. Sato, Analyst 126 (2001) 989.
[26] M. Nishimura, M. Hayashi, A. Yamamoto, T. Horikawa, K. Hayakawa, M. Miyazaki, J. Chromatogr. A 708 (1995) 195.

Available online at www.sciencedirect.com
ScienceDirect
Talanta 71 (2007) 1817–1823
Talanta
www.elsevier.com/locate/talanta

Short communication

A novel cyclic hexapeptide as chiral selector: Application for HPLC separation of a series of dansyl amino and arylalkanoic acids

Claire André [a], Mireille Thomassin [a], Arunalyat Umrayami [b], Lhassane Ismaili [b], Bernard Refouvelet [b], Yves-Claude Guillaume [a,*]

[a] *Equipe des Sciences Séparatives et Biopharmaceutiques (2SB)-EA 3924, Laboratoire de Chimie Analytique, Faculté de Médecine Pharmacie, Place Saint Jacques, 25030 Besançon, Cedex, France*
[b] *Equipe des Sciences Séparatives et Biopharmaceutiques (2SB)-EA 3924, Laboratoire de chimie organique, Faculté de Médecine Pharmacie, Place Saint Jacques, 25030 Besançon, Cedex, France*

Received 3 March 2006; received in revised form 5 July 2006; accepted 24 July 2006
Available online 1 September 2006

Abstract

In this paper, the synthesis of a cyclic hexapeptide molecule was presented and evaluated for the enantiomer separation of a series of dansyl amino and arylalkanoic acids using high performance liquid chromatography (HPLC). It was clearly vizualized that this chiral selector allowed the separation of a great number of enantiomer pairs. The influences of the size and the hydrogen bonding donor (HBD) parameter of the organic modifier (OM) (THF (HBD = 0.00), propan-2-ol (HBD = 0.33), methanol (HBD = 0.43)) added in the mobile phase were also investigated on both the enantiomer-chiral selector association and enantioseparation.

Keywords: Cyclic hexapeptide; Chiral selector; Arylalkanoic acid; Dansyl amino acid; HPLC

1. Introduction

Because enzymes and other biological receptor molecules possess chiral structures, enantiomers of a racemic compound may be absorbed, activated and degraded by them in different manners. This phenomenon causes that, in many instances, two enantiomers of a racemic drug may have different or even opposite pharmacological activities. To ascertain these differing effects, the biological activity of each enantiomer often needs to be studied separately. This and other factors within the pharmaceutical industry have contributed significantly to the need for enantiomerically pure compounds and, thus, the need for chiral chromatography [1]. Various types of chiral selectors have been introduced as chiral stationary phases (CSPs). The chiral selectors commonly used for the production of CSPs are aminoacids [2–4], proteins [5–8], crown-ethers [9,10], oligo- and polyssacharides [11–13] or macrocyclic antibiotics [14–16]. Due to the wide structural variation of analytes, among the large number of chiral stationary phases, only a few demonstrated broad chiral selectivity. With the increasing number of racemic compounds that need to be resolved, a significant need exists to develop new chiral selector. Affinity chromatography is a technique that has been shown to be an efficient and accurate tool for the separation of the enantiomers of an analyte. In this high performance liquid chromatography (HPLC) method, a novel macrocyclic chiral selector synthetized in our laboratory was dissolved in the mobile phase. In this form of analysis, changes in the retention factor k of an analyte (*A*) on complexation with the chiral selector (*S*) present in the mobile phase can be correlated to the binding constant *K* using the following equation [17]:

$$k = \frac{k_0^A}{1 + K[S]_m} \quad (1)$$

This model correlates the selector concentration in the mobile phase [*S*] and the effective retention factor of the free solute, k_0^A. From the collected set of data (*K*, enantiomer association constant; α, apparent selectivity factor equal to the highest association constant between the two enantiomers divided by the lowest one ($\alpha \geq 1$)) and from the structure of the analytes,

* Corresponding author. Tel.: +33 3 81 66 55 44; fax: +33 3 81 66 56 55.
E-mail address: yves.guillaume@univ-fcomte.fr (Y.-C. Guillaume).

0039-9140/$ – see front matter © 2006 Elsevier B.V. All rights reserved.
doi:10.1016/j.talanta.2006.07.041

attempts are made to interpret the observed results. The addition of an organic modifier (OM) in the mobile phase affecting retention and separation of the D,L-enantiomers are also evaluated and discussed in the present work.

2. Materials and methods

2.1. Chemistry

Thin layer chromatography (TLC) was performed on silica gel plates Merck 60 F-254; spots of compounds were revealed by ninhydrin. Solvent systems for TLC development were: butanol/eau/acetic acid, 60:37:3 (v/v/v).

^{1}H NMR spectra were recorded on a brucker AC 300 spectrometer at 300 MHz using tetramethylsilane as internal standard. Chemical shifts are reported in parts per million and signals are quoted as s (singlet), d (doublet), t (triplet), q (quadruplet) and m (multiplet).

Elemental analyses were carried out at the Central Analysis, Centre National de la Recherche Scientifique (CNRS), 69390 Vernaison, France.

The synthesis of macrocycle **11** was prepared by the cyclisation of linear precursors [18] (Fig. 1). This intermediate **10** (hexapeptide) was obtained after removal Boc by TFA [19,20] and ester by hydrolysis [21,22] to compound **9** (Fig. 2).

The preparation of compound **9** (Fig. 2) consists of coupling two tripeptide: *N*-Boc-alanyl-alanyl-aminobutyric acid **7** and *N*-Boc-alanyl-alanyl-alanine **8**. The first tripeptide **7** was prepared by the coupling of aminobutyric acid dipeptide ester **4** using DCC, HOBT [23–25] based condition followed by removal of Boc. Similarly, the other tripeptide **8** was synthetized standing from dipeptide ester **4** and *N*-Boc-alanine then hydrolysis of ester.

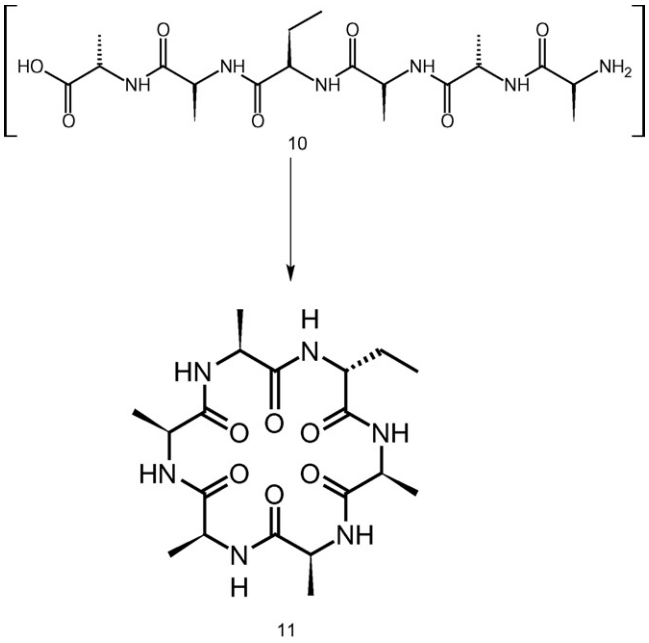

Fig. 1. Cyclisation of linear precursor (compound **10**) for the synthesis of cyclic hexapeptide (chiral selector **11**).

The active ester of *N*-Boc-ALAOH [26] was treated with methyl ester alanine to afford dipeptide **4** after removal quantitatively *N*-Boc protecting group [27] by HCL in dioxane.

2.1.1. Alanine ethyl ester 1

To a solution of alanine in dry ethanol (10 ml) was added $SOCl_2$ 2 equiv at 0 °C for 1 h and then refluxed for 17 h. After removal of the solvent, the residue was dissolved in dry ethanol (5 ml) and the ester hydrochloride was precipitated with dry ether. The solid was filtered and dried over P_2O_5 overnight.

NMR in $CDCl_3$ δ 0.9 (t, 3H); 1.2 (d, 3H); 3.9 (q, 2H); 4.0 (q, 1H); 8.7 (s, NH_2).

Anal. (%) Calcd for $C_5H_{11}NO_2$, C, 51.26; H, 9.46; N, 11.96. Found C, 51.41; H, 9.37; N, 11.82.

2.1.2. *N*-Boc alanine ***2a*** *and N*-Boc aminobutyric acid ***2b***

The α-amino acid 10 mmol was dissolved in 20 ml of water containing (0.4 g, 10 mmol) of sodium hydroxide. Sodium bicarbonate (1.63 g, 20 mmol, 2.00 equiv) and dioxane (20 ml) were added sequentially to the alkaline solution. The resulting solution was cooled in ice bath, and di-*tert*-butyl dicarbonate (Boc_2O) (2.54 g, 12 mmol, 1.2 equiv) was added to the reaction mixture at 0 °C. After stirring for 1 h, the reaction mixture was allowed to warm at room temperature, and was stirred at that temperature for 30 min. Water (50 ml) was added, and the aqueous product solution was extracted with ethyl acetate (120 ml). The organic layer was washed with 2% aqueous sodium bicarbonate solution (40 ml). The aqueous layers were combined, and the resulting solution was carefully acidified to pH 3.5 by the addition of saturated aqueous citric acid solution. The acidified solution was extracted with three portions of ethyl acetate (50 ml). The combined organic layers were washed with two portions of water (30 ml) and then were dried over sodium sulphate, filtered and concentrated in vacuo to give the *N*-Boc amino acid.

*2.1.2.1. N-Boc alanine **2a**.* NMR ($CDCl_3$) δ 1.1 (d, 3H); 1.3 (s, 9H); 3.9 (q, 1H); 5.1 (s, NH); 11.2 (s, OH).

Anal. (%) Calcd for $C_8H_{15}NO_4$, C, 50.78; H, 7.99; N, 7.40. Found C, 50.71; H, 7.97; N, 7.49.

*2.1.2.2. N-Boc aminobutyric acid **2b**.* NMR ($CDCl_3$) δ 0.9 (t, 3H); 1.2 (d, 3H); 1.3 (s, 9H); 3.7 (q, 1H); 3.9(q, 3H); 5.8(s, NH); 11.5 (s, OH).

Anal. (%) Calcd for $C_9H_{17}NO_4$, C, 53.19; H, 8.43; N, 6.89. Found C, 53.28; H, 8.37; N, 6.85.

2.1.3. General procedure for synthesis dipeptide ***3*** *and tripeptide **5** and **6***

Amino acid ester or dipeptide ester hydrochloride (10 mmol) was dissolved in methylene chloride and cooled in an ice bath with stirring. *N*-Methylmorpholine (NMM) (10 mmol) was added. After 5–10 min, the *N*-Boc amino acid or the *N*-Boc aminobutyric acid (10 mmol) and hydroxybenzotriazole (HOBT) (11 mmol) were added, followed by a solution of dicyclocarbodiimide (DCC) (10 mmol) in methylene chloride

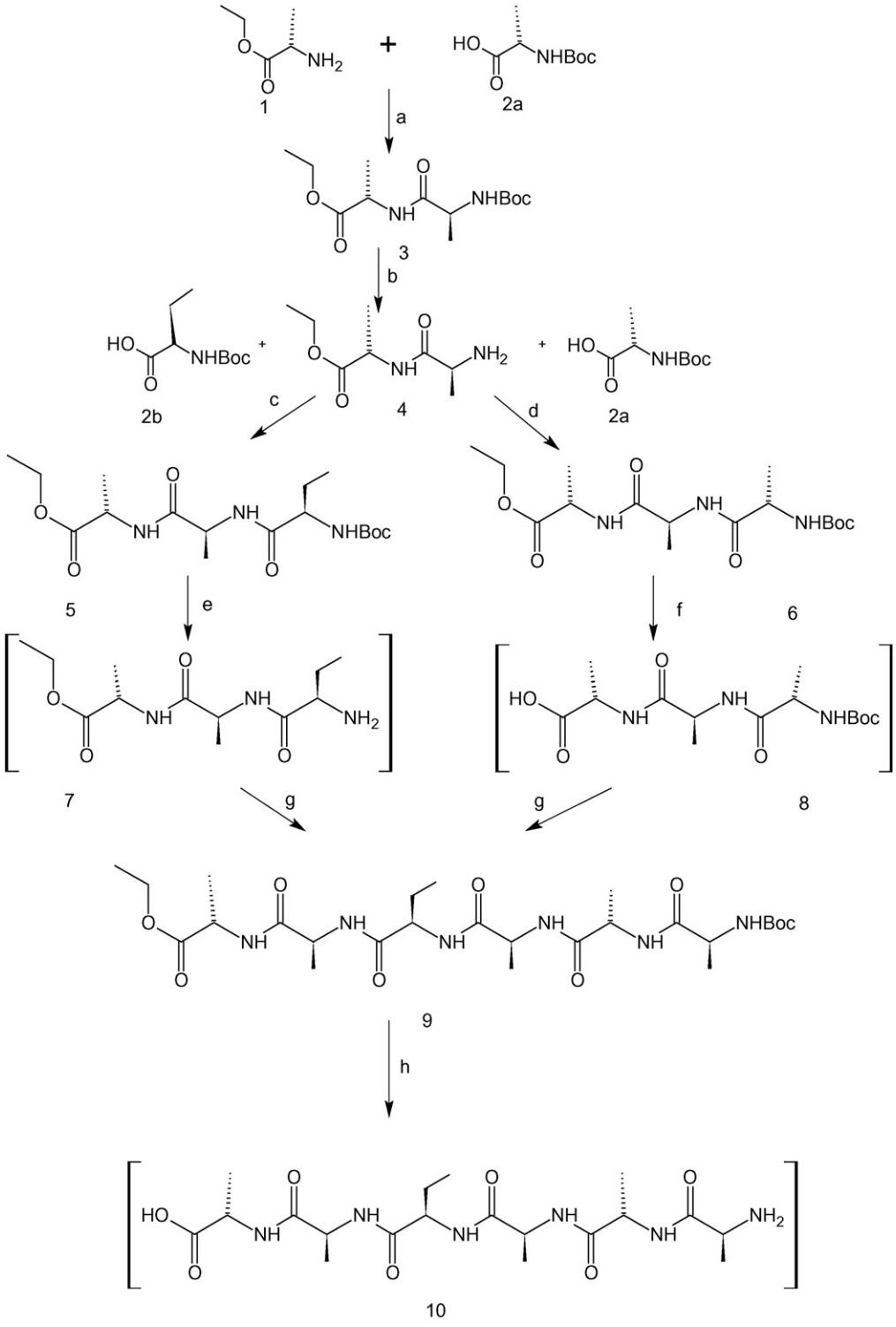

Fig. 2. General procedure to synthetize the linear precursor **10**: (a) NMM, DCC, HOBT, CH_2Cl_2; (b) HCl, dioxane; (c) *N*-Boc-aminobutyric acid, NMM, DCC, HOBT, CH_2Cl_2; (d) *N*-Boc-alanine, NMM, DCC, HOBT, CH_2Cl_2; (e) HCl, dioxane; (f) LiOH, THF–water; (g) NMM, DCC, HOBT, CH_2Cl_2; (h) CF_3COOH, LiOH, THF–water.

(Fig. 2). The reaction was carried out at 0 °C for 5 h, at 4 °C overnight (12–14 h, unless otherwise specified), and at room temperature for 3–5 h. The reaction mixture was filtered to remove dicyclohexylurea (DCU), and the filtrate was evaporated to dryness under reduced pressure. The residue was dissolved in ethyl acetate, washed successively with water, saturated $NaHCO_3$ (three times), water, 1 N citric acid (three times), and water, and then dried over anhydrous sodium sulphate. It was then purified by flash chromatography using silica gel as adsorbent [28].

*2.1.3.1. Dipeptide **3**.* NMR in $CDCl_3$ δ 1.5 (t, 3H); 1.6 (m, 6H); 1.7 (s, 9H); 4.3 (q, 2H); 4.4 (q, 1H); 4.5 (q, 1H); 5.3 (s, NH); 6.8 (s, NH).

Anal. (%) Calcd for $C_{13}H_{24}N_2O_5$, C, 54.15; H, 8.39; N, 9.72. Found C, 54.67; H, 8.31; N, 9.95.

*2.1.3.2. Tripeptide **5**.* NMR in $CDCl_3$ δ 0.9 (t, 3H); 1.3 (t, 3H); 1.4 (m, 6H); 1.45 (s, 9H); 4.2 (q, 2H); 4.3 (m, 2H); 4.3 (m, 2H); 4.4 (m, 1H); 4.6 (m, 2H); 5.5 (s, NH); 6.7 (s, NH).

Anal. (%) Calcd for $C_{17}H_{31}N_3O_6$, C, 54.68; H, 8.37; N, 11.25. Found C, 54.31; H, 8.25; N, 11.39.

*2.1.3.3. Tripetide **6**.* NMR in $CDCl_3$ δ 1.3 (t, 3H); 1.4 (m, 9H, $3CH_3$); 1.45 (s, 9H); 4.2 (q, 2H); 4.5 (m, 3H); 5.2 (s, NH); 6.5 (s, NH).

Anal. (%) Calcd for $C_{16}H_{29}N_3O_6$, C, 53.47; H, 8.13; N, 11.69. Found C, 53.77; H, 8.07; N, 11.44.

*2.1.4. General procedure to remove Boc fromdipeptide **3** and tripeptide **5** to afford compounds **4** and **7***

A solution of dipeptide **3** or tripeptide **5** (10 mmol) (Fig. 2) dissolved in dioxane (125 ml, previously saturated with HCl at 0–5 °C) was reacted at room temperature for 2 h. Next the solution volume was reduced under vacuum to about 10 ml. The resulting oil was triturated with ether (300 ml) and was allowed to precipitate. After 1 h the ether was decanted; the white solid was resuspended in ether (300 ml) and was allowed to precipitate again. After 1 h the ether solution was decanted and the white precipitate was concentrated under vacuum to yield the desired compound as a white solid.

*2.1.4.1. Dipeptide **4**.* NMR in $CDCl_3$ δ 0.9 (t, 3H); 1.4 (m, 6H); 3.9 (q, 2H); 4.2 (q, 1H); 4.3 (q, 1H); 5.5(s, NH_2).

Anal. (%) Calcd for $C_8H_{16}N_2O_3$, C, 51.05; H, 8.57; N, 14.88. Found C, 52.18; H, 8.34; N, 14.92.

*2.1.5. Hydrolysis of tripeptide **6** to afford compound **8***

To a solution of tripeptide **5** (1 g, 3.3 mmol) in THF–water (12 ml–12 ml) was added LiOH (0.21 g, 3.7 mmol) at room temperature (Fig. 2). After stirring for 30 min, water (30 ml) and saturated citric acid solution (1 ml) were added. The aqueous product solution was extracted with ethyl acetate (3 × 25 ml). The organic layer was washed with two 30 ml portions and then was dried over sodium sulphate, filtered and concentrated in vacuo to give the *N*-Boc tripeptide **8**.

*2.1.6. Synthesis of hexapeptide **9***

Tripeptide ester hydrochloride **7** (2 g, 5.8 mmol) was dissolved in methylene chloride and cooled in an ice bath with stirring. *N*-Methylmorpholine (0.59 g; 5.8 mmol) was added. After 5–10 min, the *N*-Boc amino tripeptide acid **8** (1.73; 5.8) and HOBT (0.87 g; 6.4 mmol) were added, followed by a solution of DCC (3.62 g; 17.6 mmol) in methylene chloride. The reaction was carried out at 0 °C for 5 h, at 4 °C overnight (12–14 h, unless otherwise specified), and at room temperature for 3–5 h. The reaction mixture was filtered. The white solid was extracted with absolute ethanol. The ethanol was evaporated to obtain hexapeptide **9** (Fig. 2).

NMR in $CDCl_3$ δ 0.8 (t, 3H); 1.2 (m, 18H); 1.3 (s, 9H); 3.8 (q, 2H); 4.1 (m, 6H); 4.2 (m, 2H); 5.8 (d, NH); 6.5 (d, NH); 7.8 (d, NH); 7.9 (d, NH); 8.2 (d, NH); 8.4 (d, NH).

Anal. (%) Calcd for $C_{26}H_{46}N_6O_9$, C, 53.23; H, 7.90; N, 14.32. Found C, 54.11; H, 7.67; N, 14.02.

*2.1.7. Synthesis of cyclic hexapeptide **11***

A solution of **9** (1 g; 1.7 mmol) in 20 ml of TFA was stirred for 1 h at room temperature. The solution was concentrated and the residue was triturated with ether and filtered. The product obtained above was dissolved in THF/H_2O and cooled with ice-water bath. To it was added LiOH, $1H_2O$ (43 mg, 3.4 mmol), and the resulting mixture was stirred for 10 h, neutralized with 1 N HCl to pH 7 and then extracted with ethyl acetate (Fig. 2). The combined organic phases were dried with anhydrous Na_2SO_4, filtered and concentrated. The residue was dissolved in THF (40 ml) and HOBT (0.87 g; 6.4 mmol) was added, followed by a solution of DCC (3.62 g; 17.6 mmol) in THF. The reaction was carried out at 0 °C for 5 h, at 4 °C overnight (12–14 h, unless otherwise specified), and at room temperature for 10 h. The reaction mixture was filtered. The white solid was extracted with absolute ethanol. The ethanol was evaporated to obtain the cyclic hexapeptide **11**, i.e., the chiral selector (Fig. 1).

NMR in DMSO δ 1.1–1.3 (m, 18H); 4.3 (m, 6H); 4.5 (m, 2H); 5.3 (d, NH); 6.4 (d, NH); 7.5 (d, NH); 7.6 (d, NH); 7.9 (d, NH); 8.1 (d, NH).

Anal. (%) Calcd for $C_{19}H_{32}N_6O_6$, C, 51.81; H, 7.32; N, 19.08. Found C, 52.05; H, 7.12; N, 18.84.

2.2. Chromatographic study

2.2.1. Apparatus

The HPLC system for these measurements consisted of a Merck Hitachi pump L7100 (Nogent sur Marne, France), an Interchim Rheodyne injection valve model 7125 (Montluçon, France) fitted with a 20 μl sample loop injection, and a Merck L4500 diode array detector. The column used was an Interchim C1 monolithic (100 mm × 4.6 mm i.d.) under controlled temperature conditions (25 °C) in an interchim TM 701 oven (Montluçon, France). The mobile phase flow-rate was fixed at 1 ml/min and the wavelength at 254 nm.

2.2.2. Solvents and samples

Water was obtained from an Elgastat option I water purification system (Odil, Talant, France) fitted with a reverse osmosis cartridge. Sodium hydrogen phosphate and potassium dihydrogen phosphate were supplied by Prolabo (Paris, France). The mobile phase derived from a phosphate buffer (at pH 5.60) with chiral selector concentration varying from 1 to 10 mM. This phosphate buffer was prepared by mixing 10 ml of sodium hydrogen phosphate (M/15) and 190 ml of potassium dihydrogen phosphate (M/15). The chiral selector was synthetized as described in materials and method. Sodium nitrate was used as a dead time marker (Merck, Saint Quentin Fallavier, France). Some chromatographic experiments were carried out using

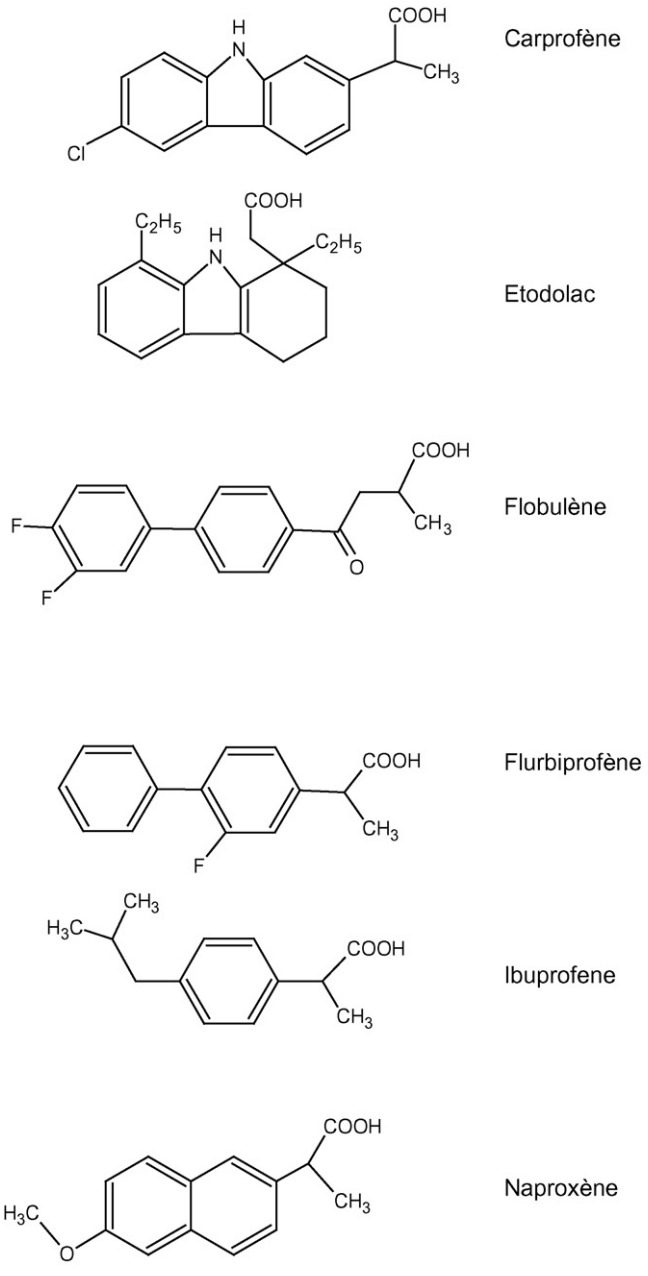

Fig. 3. Compound molecular structure.

successfully three different organic modifiers (THF, propan-2-ol, methanol (Sigma–Aldrich, Saint Quentin Fallavier, France)), with the same base solvent (phosphate buffer pH 5.60). Dansyl amino acids (i.e., dansyl-alanine (dan-ala), dansyl-valine (dan-val), dansyl-norvaline (dan-nor), dansyl-leucine (dan-leu), dansyl-phenylalanine (dan-phe), dansyl-tryptophane (dan-try)) and arylalakanoic acids, i.e., etodolac (eto), flobuphen (flo), ibuprophen (ibu), flurbiprophen (flu), naproxen (nap), sulindac (sul), racemic standard compounds and D-enantiomers were purchased from Sigma–Aldrich (Saint Louis, MO, USA). The molecular structure of these analytes are given in Fig. 3. Sample solutions were separately prepared at concentrations of 5 mM in the phosphate buffer. All samples and mobile phases were filtered with 0.45 μM syringe filter discs (Whatman, Clifton, NJ, USA) and degassed by sonification. Twenty microliters of each sample were injected and the retention times were measured.

Table 1
Association constant (K) and thermodynamic data (i.e., ΔH° and ΔS°) of the D-enantiomer, and enantioselectivity (α) for the compounds analysed in this study

Compound	K	ΔH° (kJ/mol)	ΔS° (J/mol/K)	α
Alanine	35	−9.82	−3.37	1.21
Valine	51	−12.02	−7.62	1.20
Norvaline	110	−28.44	−56.32	1.23
Leucine	76	−16.10	−17.99	1.22
Phenylalanine	92	−23.40	−40.90	1.13
Tryptophane	59	−14.15	−13.55	1.11
Edotolac	10	−6.12	−1.30	0
Flobuphen	280	−38.82	−83.38	1.31
Flurbiprophen	315	−44.20	−100.46	1.30
Ibuprofen	210	−33.10	−66.58	1.33
Naproxen	150	−31.20	−63.01	1.43
Sulindac	63	−14.16	−13.04	0

Mobile phase: phosphate buffer (pH 5.6, M/15)–methanol mixture (0.75/0.25) (v/v), $T = 25\,^\circ$C.

3. Result and discussion

From the enantiomer analyte retention time, the retention factor of all the enantiomers were determined for a phosphate buffer (pH 5.6) at $T = 25\,^\circ$C with the addition of a 0.25 (v/v) fraction of methanol. The use of a monolithic column allow us to obtain low retention times. All the experiments were repeated three times. The precisions of retention times of each enantiomer is characterized by relative standard deviation (R.S.D.) values comprised between of 0.21 and 0.40%. The variation coefficients of the K values were less than 1.5% in most cases, indicating a high reproducibility and good stability for the chromatographic system. Using a weighted non-linear regression, the K values were determined (Table 1). The correlation between the values predicted by the model (Eq. (1)) and experimental K values is excellent. The slope (0.997; ideal is 1.00) and r^2 (0.991) indicate that there is an excellent correlation between the predicted and the experimental retention factors. In the following of this work, the chiral selector concentration in all the used mobile phases was kept constant equal to 10 mM. From the data given in Table 1, the chiral selector was able to discriminate the enantiomers of dansyl norvaline. The L-enantiomer was more retained by the chiral selector than the D-enantiomer. As can be seen in Table 1 the molecule exhibited also discriminating properties for various other compounds. Representative chromatograms are shown in Fig. 4 illustrating the separation of enantiomers of dan-nor, dan-try, flur and nap. From the data reported in Table 1, some observations can be made about the structure enantioselectivity relationships with the chiral selector. For the dansyl amino acid series, the apolar groups (dimethylaminonaphtyl of the dansyl group and side chains R) acted as factors governing the analyte degree association with the selector. The overall association depended, at least in part, on the overall hydrophobic interaction between

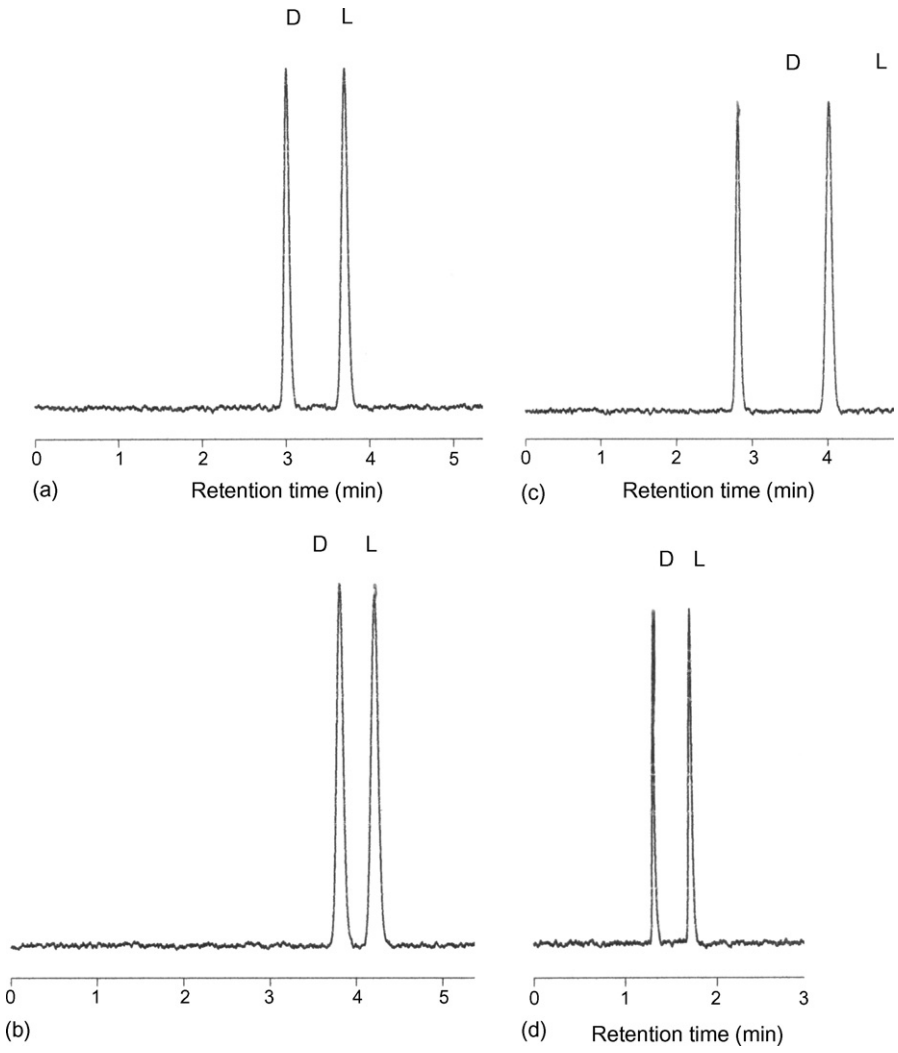

Fig. 4. Chromatographic enantioseparation of (a) dan-nor; (b) dan-tryp; (c) flu; (d) nap. Mobile phase: methanol/phosphate buffer (M/15) (pH 5.6) (0.25–0.75) (v/v), $T = 25\,^{\circ}C$.

the R-group of the enantiomer and the methyl group of the chiral selector. Thus, dan-ala presented the lowest K association constant (≅35) followed by dan-val (≅51) and dan-leu which contained a second $-CH_2-$ group (≅76). In the arylalkanoic acid series, flu ($\log P = 3.52$) exhibited a higher K value (≅315) than ibu ($\log P = 2.76$, $K = 210$). As well, it appears that besides the hydrophobic character, the shape of the R substituent participated also to the overall association mechanism. This is exemplified by the fact that in the dansyl amino acid series, dan-nor ($K \cong 110$) was more bound to the selector than the dan-tryp ($K \cong 59$). Among the arylalkanoic acids, carp, flob and flur presented the highest association constant due to the presence of one chloro group for car, and one and two fluoro groups for flob and flu on the aromatic ring which stabilized the complex. K was linked with the temperature of the experiment, T, following the van't Hoff equation [29], $\ln K = -\Delta H^{\circ}/RT + \Delta S^{\circ}/R$. ΔH° and ΔS° were, respectively, the enthalpy and entropy of association of the enantiomer with the chiral selector. The values of ΔH° and ΔS° obtained for each enantiomer from the linear plots, $\ln K$ versus $1/T$ between 25 °C and 45 °C ($r^2 \geq 0.997$) are given in Table 1. The negative enthalpies indicated that it was energetically more favourable for the enantiomer to be associated with the chiral selector than to be free in the bulk solvent. This was classically accompanied by negative entropies due to the loss of the degree of freedom of the enantiomer when it was included in the chiral selector [5,17,29,30]. This association mechanism was enthalpically driven and can be described by the replacement of weak enantiomer-bulk solvent interactions by strong enantiomer-chiral selector van der Waal's (London forces) and polar interactions [17]. From a chiral discrimination point of view, for the aliphatic dansyl amino acids (dan-ala, dan-nor, dan-leu), the enantioselectivity remained relatively constant around 1.20. For the aromatic dansyl amino acids (dan-phe, dan-try), a weak decrease of the enantioselectivity was observed (around 1.10) demonstrating that a suitable R-chain orientation is required for enantioselective binding to the active site. For the arylalkanoic acid derivatives, the nap molecule presented the highest separation (1.40). Flob, flu and ibu presented an intermediate separation around 1.30. No separation of sul and eto enantiomers was observed.

Table 2
Association constant (K) of D-leucine and D-naproxen and enantioselectivity (α) of the enantiomer pair leucine and naproxen for the three different organic modifiers, i.e., THF, propan-2-ol and methanol

Organic modifier (OM)	Association constant (K)		Enantioselectivity (α)	
	D-Leucine	D-Naproxen	Leucine	Naproxen
THF (HBD = 0)	210	298	1.68	1.98
Propan-2-ol (HBD = 0.33)	144	224	1.58	1.86
Methanol (HBD = 0.43)	121	205	1.54	1.82

Mobile phase: phosphate buffer (pH 5.6, M/15)–organic modifier mixture (0.90/0.10) (v/v), $T = 25\,^{\circ}C$.

3.1. Effects of organic modifier on the solute retention and enantioselectivity

The influence of the nature of the organic modifier on the retention and enantioselectivity of some solute molecule were studied. Firstly, the hydrogen bonding donor (HBD) parameter of the modifier was analysed by addition of the same quantity of THF (HBD = 0.00), propan-2-ol (HBD = 0.33), methanol (HBD = 0.43) in the mobile phase [31]. The HBD values were usually estimated using a statistical analysis which combines electrostatic and steric energy components and predicts with reasonable accurancy and computational efficiency the hydrogen bond strength for a wide variety of compounds [32–36]. In the dansyl amino acid series dansyl-leucine was used as test solute and in the arylalkanoic series naproxen was used. As can be seen in Table 2 the K values decreased as the HBD of the organic modifier increased. As well, the enantioselectivity decreased (Table 2). This result demonstrated well a competition effect for the binding with the chiral selector between the solute molecule and the organic modifier and this effect was maximal for the organic modifier with the highest HBD value. As well, it seems that the size of the organic modifier molecule also influenced both the enantioselectivity and the association. The size of these molecules increased in the order methanol (Mw = 32) < propan-2-ol (Mw = 60) < THF (Mw = 72). The small size organic modifier molecule seems to interact with the cycle more easily confirming the importance of this criterion. When the size of the organic modifier decreased and its HBD increased, a substantial amount of OM can interact with the cycle leading to a competition with the solute-molecule complexation (Table 2) and a decrease of the eantioselectivity (Table 2).

4. Conclusion

In this paper, a new chiral selector derived from a cyclic hexapeptide is evaluated for the enantiomer separation of a series of arylalkanoic and dansyl amino acids. This novel chiral selector demonstrated to be effective in the separation of a great number of enantiomer pairs. It was also clearly demonstrated that both association and enantioselectivity mechanisms of the analytes were dependent on their molecular structure. The change of the organic modifier in the mobile phase allowed to modify the solute retention and enantioselectivity.

References

[1] S.C. Stisnon, Chem. Eng. News 73 (1995) 44.
[2] F. Gasparrini, D. Misiti, W. Still, C. Villani, H. Vennemers, J. Org. Chem. 62 (1997) 8221.
[3] W.H. Pirkle, T.C. Pachapsky, J. Am. Chem. Soc. 108 (1986) 352.
[4] W.H. Pirkle, J.M. Finn, J. Org. Chem. 46 (1981) 2936.
[5] D.S. Hage, J. Chromatogr. 3 (2002) 768.
[6] T. Fornstedt, G. Gotmar, M. Andersson, G. Guiochon, J. Am. Chem. Soc. 121 (1999) 1164.
[7] S.C. Jacobson, S. Golshan-Shirazi, G. Guiochon, J. Am. Chem. Soc. 112 (1990) 6492.
[8] J. Hermansson, J. Chromatogr. 325 (1985) 379.
[9] M. Hilton, D.W. Armstrong, J. Liq. Chromatogr. 14 (1991) 3673.
[10] G. Dotsevi, Y. Sogaah, D.J. Gram, J. Am. Chem. Soc. 97 (1975) 1259.
[11] T. Kubota, C. Yamamoto, Y. Okamoto, J. Am. Chem. Soc. 122 (2000) 4056.
[12] K.B. Lipkowitz, G. Pearl, B. Coner, M.A. Peterson, J. Am. Chem. Soc. 119 (1997) 600.
[13] A. Berthod, S.C. Chang, D.W. Armstrong, Anal. Chem. 64 (1992) 395.
[14] A. Peter, G. Torok, D.W. Armstrong, G. Toth, D. Tourvé, J. Chromatogr. A 828 (1998) 177.
[15] D.W. Armstrong, Y. Liu, K.H. Ekborg-Ott, Chirality 7 (1995) 474.
[16] D.W. Armstrong, S. Chen, Y. Zhou, C. Bagwill, J.R. Chen, Anal. Chem. 66 (1994) 1473.
[17] L. Ismaili, C. Andre, L. Nicod, J.L. Mozer, J. Millet, B. Refouvelet, S. Makki, J.F. Robert, A. Xicluna, Y.C. Guillaume, J. Liq. Chromatogr. Relat. Technol. 26 (6) (2003) 855.
[18] S.J. Wen, T.S. Hu, Z.J. Yao, Tetrahedron 61 (2005) 4931.
[19] T. Teshima, T. Nakai, M. Kitazawa, T. Shiba, Tetrahedron Lett. 28 (40) (1987) 4705.
[20] T. Shiba, T. Teshima, T. Nakai, M. Kitazawa, Tetrahedron Lett. 44 (3) (1988) 787.
[21] A.N.K. Lau, L.L. Miller, B. Zinger, J. Am. Chem. Soc. 105 (1983) 5278.
[22] K.L. Kaestle, M.K. Anwer, T.K. Audhya, G. Goldstein, Tetrahedron Lett. 32 (3) (1991) 327.
[23] D.H. Rich, S.R. Lehrman, M. Kawai, J. Med. Chem. 24 (6) (1981) 706.
[24] M. Falorni, G. Giacomelli, F. Nieddu, M. Taddei, Tetrahedron Lett. 38 (26) (1997) 4663.
[25] N. Subasinghe, M. Schulte, M.Y.M. Chan, R.J. Roon, J.F. Koerner, L.J. Rodney, J. Med. Chem. 33 (1990) 2734.
[26] A.G. Myers, J.L. Gleason, T. Yoon, D.W. Kung, J. Am. Chem. Soc. 119 (1997) 656.
[27] G. Tous, A. Bush, A. Tous, F. Jordan, J. Med. Chem. 33 (6) (1990) 1620.
[28] W.C. Still, M. Kahn, A. Mitra, J. Org. Chem. 43 (1978) 2923.
[29] W. Melander, D.E. Cambell, C. Horvath, J. Chromatogr. 158 (1978) 215.
[30] L.C. Sander, L.R. Field, Anal. Chem. 42 (1980) 209.
[31] K. Sarmini, E. Kenndler, J. Chromatogr. A 792 (1997) 3.
[32] A. Salichs, M. Lopez, V. Segarra, M. Orozco, F.J. Luque, J. Comput. Aided Mol. Des. 16 (2002) 569.
[33] M.J. Kamlet, J.L.M. Abboud, R.W. Taft, Prog. Phys. Org. Chem. 13 (1981) 485.
[34] M.J. Kamlet, J.L.M. Abboud, M.H. Abraham, R.W. Taft, J. Org. Chem. 48 (1983) 2877.
[35] M.H. Abraham, P.L. Grellier, J.L.M. Abboud, R.M. Doherty, R.W. Taft, Can. J. Chem. 66 (1988) 2673.
[36] C. Laurence, P. Nicolet, M.T. Daleti, J.L.M. Abboud, R. Notario, J. Phys. Chem. 98 (1994) 5807.

Available online at www.sciencedirect.com
ScienceDirect
Talanta 71 (2007) 1728–1733
Talanta
www.elsevier.com/locate/talanta

Determination of chromium(VI) and lead in water samples by on-line sorption preconcentration coupled with flame atomic absorption spectrometry using a PCTFE-beads packed column

Aristidis N. Anthemidis *, Salome-Juliette V. Koussoroplis

Laboratory of Analytical Chemistry, Department of Chemistry, Aristotle University, Thessaloniki 54124, Greece

Received 9 June 2006; received in revised form 25 July 2006; accepted 1 August 2006
Available online 7 September 2006

Dedicated to Professor John A. Stratis for his 35 years contribution in analytical chemistry.

Abstract

A new time-based flow injection on-line solid phase extraction method for chromium(VI) and lead determination using flame atomic absorption spectrometry was developed. The use of hydrophobic poly-chlorotrifluoroethylene (PCTFE)-beads as absorbent in on-line preconcentration system was evaluated. Effective formation of ammonium pyrrolidine dithiocarbamate complexes and subsequently retention in PCTFE packed column, was achieved in pH range 1.0–1.6 and 1.5–3.2 for Cr(VI) and Pb(II) ions, respectively. The sorbed analyte was efficiently eluted with isobutyl-methyl-ketone for on-line FAAS determination. The proposed packing material exhibited excellent chemical and mechanical resistance, fast kinetics for adsorption of Cr(VI) and Pb(II) permitting the use of high sample flow rates at least up to 15 mL min^{-1} without loss of retention efficiency. For a preconcentration time of 90 s, the sample frequency was 30 h^{-1}, the enhancement factor was 94 and 220, the detection limit was 0.4 and 1.2 $\mu g\,L^{-1}$, while the precision (R.S.D.) was 1.8% (at 5 $\mu g\,L^{-1}$) and 2.1% (at 30 $\mu g\,L^{-1}$) for chromium(VI) and lead, respectively. The applicability and the accuracy of the developed method were estimated by the analysis spiked water samples and certified reference material NIST-CRM 1643d (Trace elements in water) and NIST-SRM 2109 (chromium(VI) speciation in water).

Keywords: Chromium; Lead; Polychlorotrifluoroethylene; Solid phase extraction; Atomic absorption spectrometry; On-line

1. Introduction

Nowadays, it is well known that the toxicological and biological properties of many elements depend upon their chemical forms. Chromium(III) is considered an essential element controlling glucose lipid and protein metabolism in mammals, while chromium(VI) is definitely highly toxic for biological systems, with mutagenic and potential carcinogenic properties [1]. In addition, there is an increasing interest in determination hazardous substances at trace level, such as heavy metals, because of persistent and bio-accumulative effect in the environment and living organisms. Determination of trace amount of lead in natural water samples plays an important role in the environmental pollution monitoring the environmental pollution. Due to the constant interest for monitoring of toxic elements such as Cr(VI) and lead, extended reviews about the analytical methodologies for their determination are recently published [2,3].

Although, flame atomic absorption spectrometry (FAAS) is one of the most popular techniques, with significant precision and accuracy, a preconcentration and/or separation step prior the final measurement, is usually required, in order to bring the analyte concentration into the dynamic range of the detector or to isolate the analyte from the desirable matrix constituents. The hyphenation of flow injection (FI) on-line solid phase extraction (SPE) with FAAS has proved to be a powerful tool for trace elements determination in a variety of matrices in terms of the enhanced sensitivity, efficient matrix removal, high sampling frequency and low cost of equipment [4].

On-line column preconcentration/separation is based predominantly on the incorporation of mini-columns packed with

* Corresponding author.
E-mail address: anthemid@chem.auth.gr (A.N. Anthemidis).

0039-9140/$ – see front matter © 2006 Elsevier B.V. All rights reserved.
doi:10.1016/j.talanta.2006.08.003

various polar or non-polar sorbent materials. The nature and the properties of the packing materials are of prime importance for effective retention of analyte [5], while some basic requirements for them should be met, like fast and quantitative adsorption, effective elution, negligible swelling and shrinking, regeneration ability, high capacity, accessibility and high chemical resistibility [4].

Several methods have been developed for FI on-line column preconcentration of Cr(VI) and lead for atomic spectrometric determination. These procedures mainly utilize various packing materials like: octadecyl functional groups bonded on silica gel, C_{18} [6–10]; ion-exchange resins, cellex-T [11] cellex-P [12], chelating Sepharose® [13]; activated alumina [14,15]; activated carbon [16]; C60-fulerenes [17]; polyurethane foam [18–20]; polymers amberlite XAD-16 [21], XAD-2 [22], chromosorb-102 [23]; and polytetrafluoroethylene (PTFE) as turnings [24,25], as beads [26] as grafted fiber [27] and as knotted reactor [28,29].

Polychlorotrifluoroethylene, PCTFE (Neoflon® or Kel-F®) is a hydrophobic porous, non-reactive and solvent-resistance polymer, which has been used as packing material for reverse phase column chromatography [30]. Although, it has been reported in batch procedures that PCTFE can effectively adsorb some metal complexes, which can be easily eluted with hydrochloric acid or methanol without any swelling or shrinking effect [31,32], it has not be used for FI-FAAS on-line preconcentration systems.

Various chelating agents containing sulphur, nitrogen or oxygen donor atoms as weak Lewis bases were reported for lead and chromium determination [10,33]. Ammonium pyrrolidine dithiocarbamate (APDC), which is usually employed for metal determination in FAAS, has proved to be suitable for the determination of lead with on-line sorbent extraction and FAAS [16]. Although, it is well known that Cr(III) reacts with APDC ligand under mild conditions to give the complex tris[pyrrolidine-1-dithioato-*S*,*S*′]-Cr(III) [6], the extraction of Cr(III) by APDC-IBMK system under the conditions usually employed for the extraction of Cr(VI) has been found to be inefficient, due to the difficulty of displacing by APDC the coordinated water from the strongly hydrated Cr(III) ion [34,35]. On the other hand, Cr(VI) is reduced easily and quickly by APDC to Cr(III), which subsequently forms complexes easily extracted. This differentiation on complex formation of Cr(III) and Cr(VI) with APDC can be easily applied in on-line preconcentration systems for chromium speciation [6].

In the present work the performance of APDC/PCTFE-beads/IBMK scheme for on-line preconcentration and determination of chromium(VI) and lead was investigated. The applicability of PCTFE as packing material in FI-FAAS systems for trace metal preconcentration and separation was evaluated. All main analytical parameters such as sample acidity, ligand concentration, sample loading and elution flow rate and the preconcentration time were examined thoroughly. The effect of potential interferents occurring in environmental samples also studied. The developed method was applied for chromium(VI) and lead determination in natural water samples and certified reference materials.

2. Experimental

2.1. Instrumentation

A Perkin-Elmer, Norwalk, Connecticut, USA model 5100 PC flame atomic absorption spectrometer equipped with a deuterium arc background corrector was used as a detector. A chromium hollow cathode lamp (Perkin-Elmer), operated at 30 mA and a lead electrodeless discharge lamp (EDL) operated at 10 W, were used as light sources. The wavelength was set at 357.9 nm resonance line and at 283.3 nm for chromium and lead determination, respectively. The monochromator spectral bandpass was set at 0.7 nm and a 0.2 s time-constant was used for peak height evaluation. The flame composition was optimized, in order to compensate for the effect of IBMK, which serves as additional fuel. A flow spoiler was used into the spray chamber for all measurements. The nebulizer free uptake rate was 5.6 mL min^{-1}. An Orion EA 940 pH-meter was employed for the pH measurements.

The flow injection system, which is shown schematically in Fig. 1, was coupled to the nebulizer system of the above spectrometer with a short PTFE capillary 12 cm length, 0.35 mm i.d., to minimize the analyte dispersion. The manifold consisted of two peristaltic pumps (Watson Marlow, Cornwall, England model 205U/BA) and an injection valve two-position six-port (Labpro, Reodyne, USA). Peristaltic pump tubing of "Tygon" type was adopted to deliver the aqueous solutions, while due to the incompatibility of organic solvents with the peristaltic tubes, a displacement bottle (Tecator, Hoganas, Sweden) was used for the IBMK transportation. PTFE tubing of 0.5 mm i.d. was used for all connections.

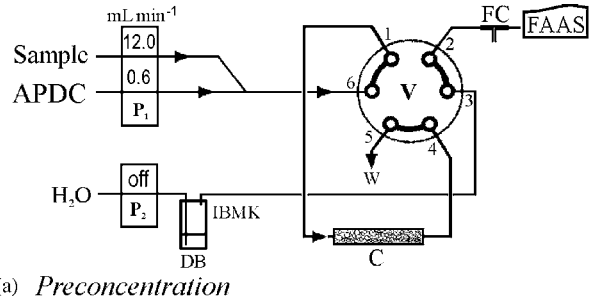

(a) *Preconcentration*

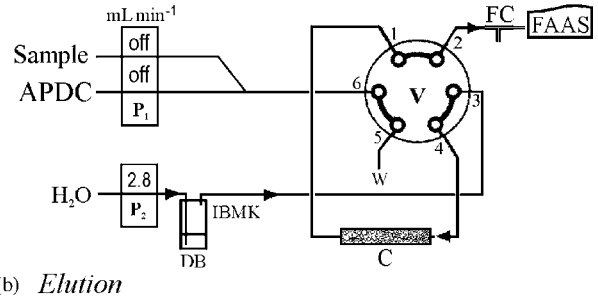

(b) *Elution*

Fig. 1. Schematic diagram of the FI-manifold and the two operation sequences, for chromium(VI) or lead determination by FAAS. (a) Preconcentration and (b) elution steps. APDC: 0.08% (m/v) APDC aqueous solution; P1 and P2: peristaltic pumps; V: injection valve; DB: displacement bottle for IBMK transportation; C: PCTFE-beads packed column; FC: flow compensation adapter; W: waste.

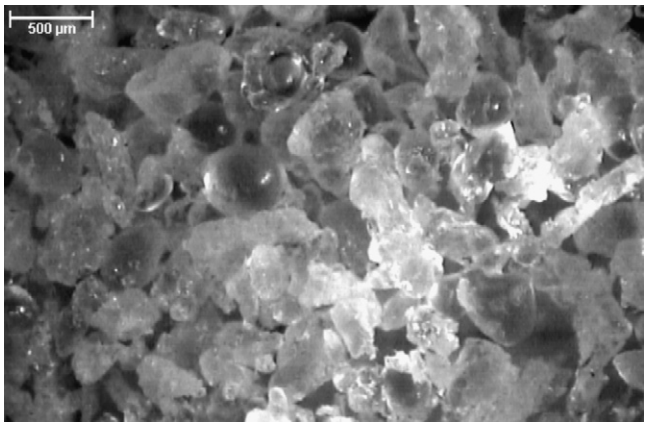

Fig. 2. Image of the PCTFE-beads fraction 100–600 μm, by optical microscope.

A special adapter to the nebulizer (Fig. 1) called flow compensation (FC) in the shape "T" was used in order to compensate the lack of nebulizer free uptake flow rate. The benefit of FC unit was the very good reproducibility of the recorded signal especial at elution flow rate lower than 2 L min^{-1}. In addition, no gas bubbles are produced in the tubing, during the step 1, where the peristaltic pump P2 is inactive as it is described in Section 2.3.

The preconcentration column (C) was made from a glass tube, with an effective length of 70 mm and inner diameter of 3.5 mm. An amount of 950 mg, fraction 100–600 μm (Fig. 2) of PCTFE beads were firmly packed into the column. The ends of each side of the column were plugged with glass wool for keeping the packing material in place. The PCTFE-beads were washed thoroughly by 2.0 mol L^{-1} HNO_3 followed by ethanol and finally with water. As it is proved from the present study, the performance of the column was stable at least over 500 preconcentration cycles.

2.2. Reagents and samples

All chemicals were of analytical reagent grade and were provided by Merck (Darmstadt, Germany). Ultra-pure quality water was used throughout which was produced by a Milli-Q system (Millipore, Bedford. USA). Working standard solutions of chromium(VI) and lead(II) were prepared by stepwise dilution of 1000 mg L^{-1} stock standard solution (Titrisol, Merck) to the required μg L^{-1} levels. The acidity of the standards was adjusted with dilute HNO_3. The chelating reagent, 0.08% (m/v) APDC was prepared fresh daily by dissolving the appropriate amount of ammonium pyrrolidine dithiocarbamate in water. Isobutyl methyl ketone (IBMK) was used after saturation with water, without any other purification. The poly-chlorotrifluoroethylene (PCTFE) powder (Aldrich, Steinheim, Germany) was sieved to obtain the PCTFE-beads fraction between 100 and 600 μm.

Two standard reference materials were used in order to validate the accuracy of the developed method: NIST CRM 1643d (National Institute of Standard and Technology, Gaithersburg, MD, USA) containing trace elements in water and NIST SRM 2109 (Cr(VI) standard reference solution). The SRM 2109 is a standard reference solution with a certified Cr(VI) content of 1000 mg L^{-1}, which was properly diluted (three steps dilution) to a final Cr(VI) concentration of 20.0 μg L^{-1}. Natural water samples were collected from Axios River, Volvi Lake, and seawater from Thermaikos Gulf, which were located in Northern Greece. All water samples were filtered through 0.45 μm membrane filters, acidified to ca. pH 1.6 with dilute HNO_3 and stored at 4 °C in acid-cleaned polyethylene bottles, in order to determine the "dissolved metal" fraction.

2.3. Operational procedure

The on-line FI-manifold of the developed method for the metal preconcentration and determination and the operation sequences are presented in Fig. 1 and Table 1, respectively. The FI-procedure runs through a cycle of two steps. A complete cycle of the operation lasts 120 s. In the preconcentration step (Fig. 1a), the injection valve V is in the "load position" and pump P1 is activated for 90 s. The pump P2 is inactive and the nebulizer aspirates air through the flow compensation adapter (FC). The on-line complex formed is subsequently retained on the surface of the PCTFE-beads in the column. During the elution step, the injection valve V is in the "injection position". The pump P1 is stopped, while pump P2 propels the IBMK through the column in order to elute the sorbed complex and to transport into the nebulizer of spectrometer. For minimum dispersion, the eluent IBMK pumped through the column in reverse direction than that of the sample. The peak height of the transient signal was proportional to metal concentration in the sample, and was used for all measurements. The recorded peaks were sharp and the baseline was stable. Five replicate measurements per sample were made in all instances.

3. Results and discussion

3.1. Optimization of experimental parameters

In order to improve the performance characteristics of the on-line preconcentration procedure for Cr(VI) and Pb(II) determination, all chemical and flow variables were investigated in

Table 1
Operation sequences of the FI-FAAS on-line solid phase extraction preconcentration system for chromium(VI) and lead determination

Step	Valve position	Pumps		Delivered medium	Flow rate (mL min^{-1})	Time (s)	Operation
		P1	P2				
1	Load	ON	OFF	Sample	12.0	90	Preconcentration
				0.08% (m/v) APDC	0.6		
2	Injection	OFF	ON	IBMK	2.8	30	Elution

detail, using the FI-FAAS manifold shown in Fig. 1. Standard solutions of 20.0 μg L^{-1} Cr(VI) and 50.0 μg L^{-1} Pb(II) and a preconcentration period of 90 s were used for each study.

The sample acidity and the APDC concentration affect significantly the on-line complex formation and its adsorption on the sorbent surface. The effect of the pH was studied within the range of 0.1–5.3 and it was achieved through adjusting the concentration of nitric acid or ammonia in the sample solution. The sample solution and the effluent in step 1 had the same pH value, indicating that the influence of the APDC solution on the acidity of the system was not significant. As shown Fig. 3, optimum absorption signal occurred within the pH range of 1.0–1.6 and 1.5–3.2 for Cr(VI) and Pb(II), respectively. Hence, the sample solution was adjusted to pH 1.6 for the on-line preconcentration in further experiments. This fact enables the use of the method directly in water samples after common acid preservation without any laborious precise pH adjustment.

APDC concentration was examined from 0.001 to 0.2% (m/v) at fixed 0.6 mL min^{-1} flow rate. For all studied metals the maximum absorbance was recorded in the range of 0.05–0.2% (m/v). Therefore a 0.08% (m/v) APDC solution in water was adopted for further study. The preconcentration of Cr(III) has been found to be inefficient, while in absence of the chelating agent, no detectable amounts of the two analytes could be retained in the PCTFE-beads packed column.

Organic solvents like IBMK, methanol and ethanol have been proved more effective as eluents at on-line preconcentration systems using hydrophobic packing materials, than acidic or alkaline solutions. In addition, IBMK is practically immiscible with water, less polar solvent than alcohols and also contributes in the rising of the flame temperature. Hence, IBMK produces lower dispersion, better elution of the retained complexes and higher atomization of the analyte. Preliminary experiments between ethanol and IBMK as eluents showed that the last one produced higher and sharpest signals, while the baseline was stable. Thus, IBMK was chosen as eluent, while the elution time was fixed at 50 s for complete elution. The flame composition of the FAAS nebulizer was adjusted properly to have an acetylene–air mixture of 2.0–9.0 L min^{-1}, during this study. The effect of IBMK flow rate was studied within the range 2.5–6.0 mL min^{-1}. Maximum absorbance was achieved within the range 2.5–3.5 mL min^{-1} for all analytes, while above 3.5 mL min^{-1} the absorbance slightly decreases, mainly due to the higher dispersion. Thus, 2.8 mL min^{-1} flow rate of IBMK was used in further experiments as a compromise between the eluent consumption and sampling frequency. At this flow rate the necessary elution time was 30 s for complete elution.

The effectiveness of the on-line time-based preconcentration systems is influenced both by the loading flow rate and the reaction (complex formation) rate. At fixed 0.6 mL min^{-1} APDC flow rate, the effect of the sample flow rate was studied in the range 2.5–15 mL min^{-1}. The absorbance was found to increase linearly up to 12 mL min^{-1} and practically linear into the whole examined range, proving that the kinetic of the complex formation was very fast and the contact time for complete sorption was sufficient. This is a significant advantage over other on-line preconcentration column or knotted reactors, because different loading flow rates can be used with proportional sensitivity. At 90 s preconcentration time a flow rate of 12.0 mL min^{-1} was selected for high sensitivity.

The influence of preconcentration time (loading time) was investigated in the range from 15 to 180 s. As it is shown in Fig. 4, the absorption increased linearly up to 180 s for Cr(VI) and up to 120 s for Pb(II). For longer time, the analytical signal increases with lower rate, probably due to a partial leaching of the complexes. Finally, a 90 s preconcentration time was chosen for all metals as a compromise between medium sample consumption, sufficient sensitivity and high sampling frequency.

3.2. Interference studies

Generally, ammonium pyrrolidine dithiocarbamate is a chelating agent for many transition metals. Thus, interferences from coexisting ions should be considered. The effect of potential interferents occurring in environmental water samples on the on-line determination of chromium(VI) and lead were tested using the optimized on-line preconcentration system for 90 s preconcentration time. The recovery of 10 μg L^{-1} Cr(VI) and

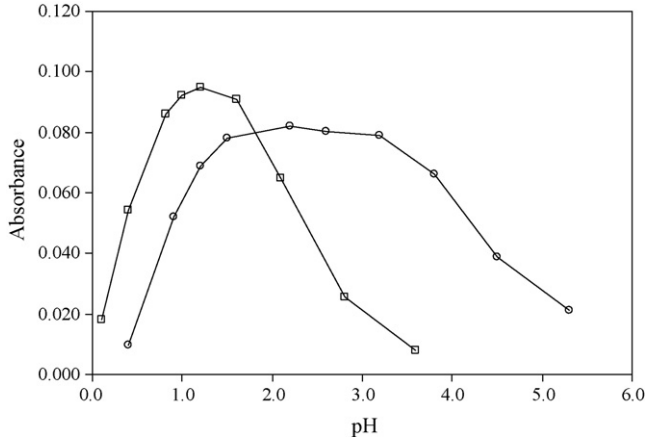

Fig. 3. Effect of sample acidity on the absorbance of 20.0 μg L^{-1} Cr(VI) (□) and 50.0 μg L^{-1} Pb(II) (◯). All other conditions as in Table 1.

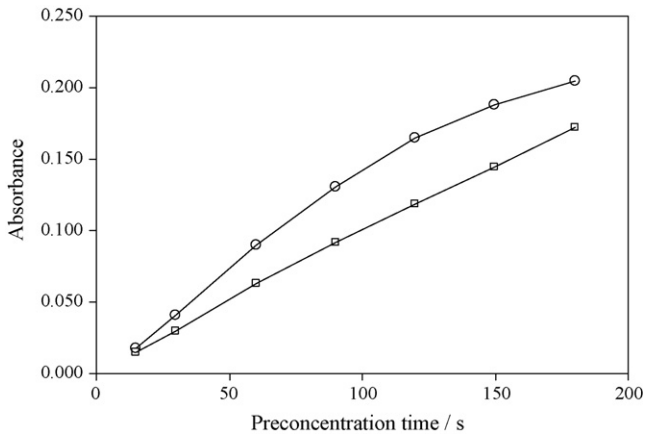

Fig. 4. Effect of preconcentration time on the absorbance of 20.0 μg L^{-1} Cr(VI) (□) and 80.0 μg L^{-1} Pb(II) (◯). All other conditions as in Table 1.

Table 2
Analytical performance of the FI on-line solid phase extraction FAAS method for chromium(VI) and lead determination

Parameter	Chromium(VI)	Lead
Preconcentration time (s)	90	90
Sampling frequency (h^{-1})	30	30
Enhancement factor	94	220
Linear range ($\mu g\,L^{-1}$)	1–50	3–150
Regression equation, $n=5$	$A=0.0047[Cr(VI)]+0.0014$	$A=0.0017[Pb(II)]+0.0022$
Correlation coefficient, r	0.9995	0.9993
Detection limit, 3 s ($\mu g\,L^{-1}$)	0.4	1.2
Precision, R.S.D., $n=10$ (%)	1.8 (5.0 $\mu g\,L^{-1}$)	2.1 (30.0 $\mu g\,L^{-1}$)

30 $\mu g\,L^{-1}$ Pb(II) was tested with individual interferents added. Taking as criterion for interference the deviation of the recovery more than ±5%, the obtained results showed that the tolerance concentrations for each interference were the following, Al(III) at 10 $mg\,L^{-1}$, Cd(II) at 0.2 $mg\,L^{-1}$, Co(II) at 1.0 $mg\,L^{-1}$, Cr(III) at 10.0 $mg\,L^{-1}$, Cu(II) at 1.0 $mg\,L^{-1}$, Fe(III) at 10.0 $mg\,L^{-1}$, Hg(II) at 0.5 $mg\,L^{-1}$, Mn(II) at 10.0 $mg\,L^{-1}$, Ni(II) at 0.5 $mg\,L^{-1}$ for Cr(VI), Ni(II) at 2.0 $mg\,L^{-1}$ for Pb(II), Zn(II) at 2.0 $mg\,L^{-1}$, Cr(VI) at 5.0 $mg\,L^{-1}$ for Pb(II) and Pb(II) at 2.0 $mg\,L^{-1}$ for Cr(VI), do not interfere. High concentrations of alkali and alkaline earth metals, which are usually found in natural water, were tested. Na^+ and K^+ up to 1500 $mg\,L^{-1}$, Ca^{2+}, Mg^{2+}, Ba^{2+} up to 500 $mg\,L^{-1}$ and NaCl up to 30 $g\,L^{-1}$ did not cause any interference.

Table 3
Analytical results for the determination of chromium(VI) and lead in the certified reference materials and water samples (determination in "dissolved metal" fraction)

Analyte	Sample ($\mu g\,L^{-1}$)	Certified value	Added	Found[a]	Recovery (%)
Cr(VI)	SRM 2109	20.0		19.3 ± 0.8	96
	River water		–	3.2 ± 0.3	
			10.0	12.9 ± 0.7	97
	Lake water		–	$<c_L$	
			10.0	9.8 ± 0.5	98
	Seawater		–	1.3 ± 0.3	
			10.0	11.5 ± 0.9	102
Pb	CRM 1643d	18.15 ± 0.64		17.6 ± 0.9	97
	River water		–	7.1 ± 0.5	
			10.0	16.7 ± 0.8	96
	Lake water		–	4.9 ± 0.4	
			10.0	14.7 ± 0.5	98
	Seawater		–	3.2 ± 0.6	
			10.0	12.7 ± 0.8	95

[a] Mean ± S.D. based on three replicate determinations.

Table 4
Comparison of the characteristic data between selected on-line solid phase extraction methods and the developed one for Cr(VI) and Pb(II) determination with FAAS

Reference	Analyte	Sorbent material	Reagent	Eluent	PT (s)	SC (mL)	f (h^{-1})	c_L ($\mu g\,L^{-1}$)	s_r (%)	EF
This work	Cr	PCTFE-beads	APDC	IBMK	90	18.0	30	0.4	1.8	94
[14]		Activated alumina	–	NH_4OH	35	3.0	55	0.8	1.3	25
[18]		PUF	APDC	IBMK	60	12.0	36	2.0	3.6	28
[25]		PTFE-turnings	APDC	IBMK	180	37.8	18	0.8	3.2	80
[29]		KR-MSP	APDC	EtOH	180	36.0	12	0.4	2.1	59
This work	Pb	PCTFE-beads	APDC	IBMK	90	18.0	30	1.2	2.1	220
[8]		C-18 silica gel	DDPA	EtOH	60	3.6	40	11	<6	36
[16]		Activated carbon	APDC	IBMK	120	6	25	10	2.3	50
[18]		PUF	APDC	IBMK	60	12.0	36	1.8	3.4	131
[19]		PUF loaded	TAM	HCl	120	11.6	27	2.2	2.4	45
[22]		Amberlite XAD-2	BTAC	HCl	120	4.5	–	3.7	4.4	27
[23]		Chromosorb -102	NH_4-DDC	EtOH	120	4.4	25	2.5	2.5	25
[24]		PTFE-turnings	APDC	IBMK	180	39	15	0.8	2.6	330
[27]		PTFE-fiber grafted	Acrylic acid	HNO_3	45	7.5	55	0.26	1.9	49
[28]		KR-MSP	APDC	HCl	120	28.8	24	8	1.4	57

TAM: 2-(2-thiazolylazo)-5-dimethylaminophenol; BTAC: 2-(2-benzothiazolylazo)-2-*p*-cresol; NH_4-DDC: ammonium diethyl-dithiocarbamate. EF: enhancement factor; PT: preconcentration time; f: sampling frequency; c_L: detection limit; s_r: precision (R.S.D.); SC: sample consumption.

3.3. Analytical performance of the FI-FAAS method

The characteristics data on the performance of the on-line column preconcentration coupled with FAAS under the optimum conditions for the determination of chromium(VI) and lead are listed in Table 2. The calculation of the enhancement factor was based on the ratio of the slope of the calibration curve obtained with on-line preconcentration to the slope without preconcentration (using aqueous standards solutions in batch mode). The obtained batch slopes using FAAS were 5×10^{-5} and 7×10^{-6} L μg^{-1} for Cr(VI) and Pb, respectively. The accuracy of the proposed method was estimated by analyzing the standard reference solution SRM 2109 and the certified water reference materials CRM 1643d (trace elements in water) for chromium(VI) and lead determination, respectively. The proposed method was applied also to the analysis of local natural water samples (river, lake and seawater) and was validated by spiking the samples with known amounts of Cr(VI) or Pb(II). The obtained results are presented in Table 3, and the recoveries were varied in the range 95–102%.

For comparative purposes, the performance characteristics of the proposed method and other selected on-line solid phase extraction preconcentration FAAS methods reported in the literature are given in Table 4. The proposed method shows good sensitivity (c_L) and precision (s_r) with reasonable preconcentration time (PT) over other online preconcentration methods.

4. Conclusions

The use of PCTFE in the shape of beads as column packing material for FI-FAAS preconcentration and determination of trace chromium(VI) and lead, was successfully performed. The chemical inertness, the excellent swelling and shrinking resistance, the hydrophobic nature and the fast kinetics of the proposed sorbent material make it very attractive for on-line column preconcentration systems. A high sample loading flow rate in conjunction with longer preconcentration time resulted in a more pronounced improvement in retention efficiency. The proposed method proved to be simple, rapid and accurate for chromium and lead determination.

References

[1] M.J. Marqués, A. Salvador, A. Morales-Rubio, M. de la Guardia, Fresenius J. Anal. Chem. 367 (2000) 601.
[2] M. Miro, J.M. Estela, V. Cerda, Talanta 63 (2004) 201.
[3] M.J. Marques, A. Salvador, A. Morales-Rubio, M. de la Guardia, Fresenius J. Anal. Chem. 367 (2000) 601.
[4] Z. Fang, Flow Injection Atomic Absorption Spectrometry, John Wiley & Sons Ltd., West Sussex, England, 1995.
[5] V. Camel, Spectrochim. Acta Part B 58 (2003) 1177.
[6] C.M. Andrle, N. Jakubowski, J.A.C. Broekaert, Spectrochim. Acta B 52 (1997) 189.
[7] T.P. Rao, S. Karthikeyan, B. Vijayalekshmy, C.S.P. Iyer, Anal. Chim. Acta 369 (1998) 69.
[8] A.P. Fernandes, M. de Moraes, J.A.G. Neto, Atom. Spectrosc. 24 (2003) 179.
[9] S.P. Quinaia, J.B.B. da Silva, M.D.E. Rollemberg, A.J. Curtius, Talanta 54 (2001) 687.
[10] R.L. Ma, F. Adams, Spectrochim. Acta Part B 51 (1996) 1917.
[11] A.M. Naghmush, K. Pyrzynska, M. Trojanowicz, Anal. Chim. Acta 288 (1994) 247.
[12] A.M. Naghmush, K. Pyrzynska, M. Trojanowicz, Talanta 42 (1995) 851.
[13] X. Long, M. Miro, E.H. Hansen, J. Anal. Atom. Spectrom. 20 (2005) 1203.
[14] M. Sperling, S. Xu, B. Welz, Anal. Chem. 64 (1992) 3101.
[15] M.J. Marques, A. Morales-Rubio, A. Savador, M. de la Guardia, Talanta 53 (2001) 1229.
[16] Y.P. de Pena, M. Gallego, M. Valcarcel, Talanta 42 (1995) 211.
[17] M. Gallego, Y.P. de Pena, M. Valcarcel, Anal. Chem. 66 (1994) 4074.
[18] A.N. Anthemidis, G.A. Zachariadis, J.A. Stratis, Talanta 58 (2002) 831.
[19] S.L.C. Ferreira, W.N.L. dos Santos, M.A. Bezerra, V.A. Lemos, J.M. Bosque-Sendra, Anal. Bioanal. Chem. 375 (2003) 443.
[20] V.A. Lemos, S.L.C. Ferreira, Anal. Chim. Acta 441 (2001) 281.
[21] R.G. Wuilloud, G.M. Wuilloud, J.C.A. de Wuilloud, R.A. Olsina, L.D. Martinez, Atom. Spectrosc. 23 (2002) 44.
[22] S.L.C. Ferreira, V.A. Lemos, R.E. Santelly, E. Ganzarolli, A.J. Curtius, Microchem. J. 68 (2001) 41.
[23] L. Elci, Z. Arslan, J.F. Tyson, Spectrochim. Acta Part B 55 (2000) 1109.
[24] A.N. Anthemidis, G.A. Zachariadis, J.-S. Kougoulis, J.A. Stratis, Talanta 57 (2002) 15.
[25] G.A. Zachariadis, A.N. Anthemidis, P.G. Bettas, J.A. Stratis, Talanta 57 (2002) 919.
[26] W. Som-Aum, S. Liawruangrth, E.H. Hansen, Anal. Chim. Acta 463 (2002) 99.
[27] Z.-H. Wan, Z.-P. Wang, Z.-P. Zhang, L.-W. Liu, X.-P. Yan, Anal. Chim. Acta 514 (2004) 151.
[28] Y. Li, Y. Jiang, X.-P. Yan, Anal. Chem. 74 (2002) 1075.
[29] Y. Li, Y. Jiang, X.-P. Yan, W.-J. Peng, Y.-Y. Wu, Talanta 64 (2004) 758.
[30] Y. Shijo, H. Yoshida, T. Kitamura, E. Yoshimoto, N. Uehara, Anal. Sci. 12 (1996) 761.
[31] C. Akita, K. Matsumoto, K. Terada, Anal. Sci. 5 (1987) 473.
[32] T. Yamaguchi, Z. Liping, K. Matsumoto, K. Terada, Anal. Sci. 8 (1992) 851.
[33] M. Llobat-Estelles, A.R. Mauri-Aucejo, M.D. Lopez-Catalan, Fresenius J. Anal. Chem. 371 (2001) 358.
[34] K.S. Subramanian, Anal. Chem. 60 (1988) 11.
[35] T. Tande, J.E. Pattersen, T. Torgrimsen, Chromatographia 9 (1980) 997.

Available online at www.sciencedirect.com
ScienceDirect
Talanta 71 (2007) 1512–1519
Talanta
www.elsevier.com/locate/talanta

Solid-phase extraction system for Pb (II) ions enrichment based on multiwall carbon nanotubes coupled on-line to flame atomic absorption spectrometry

Adriano Francisco Barbosa [a], Mariana Gava Segatelli [b], Arnaldo César Pereira [c], Antônio de Santana Santos [c], Lauro Tatsuo Kubota [c], Pedro Orival Luccas [a], César Ricardo Teixeira Tarley [a,*]

[a] *Departamento de Ciências Exatas, Unifal - MG, Alfenas/MG 37130-000, Brazil*
[b] *Departamento de Química Inorgânica, Instituto de Química, Unicamp, Campinas/SP 13083-970, Brazil*
[c] *Departamento de Química Analítica, Instituto de Química, Unicamp, Campinas/SP 13083-970, Brazil*

Received 21 March 2006; received in revised form 31 May 2006; accepted 13 July 2006
Available online 21 August 2006

Abstract

The present paper proposes the application of multiwall carbon nanotubes (MWCNTs) as a solid sorbent for lead preconcentration using a flow system coupled to flame atomic absorption spectrometry. The method comprises the preconcentration of Pb (II) ions at a buffered solution (pH 4.7) onto 30 mg of MWCNTs previously oxidized with concentrated HNO_3. The elution step is carried out with 1.0 mol L^{-1} HNO_3. The effect of the experimental parameters, including sample pH, sampling flow rate, buffer and eluent concentrations were investigated by means of a 2^4 full factorial design, while for the final optimization a Doehlert design was employed. Under the best experimental conditions the preconcentration system provided detection and quantification limits of 2.6 and 8.6 μg L^{-1}, respectively. A wide linear range varying from 8.6 up to 775 μg L^{-1} ($r > 0.999$) and the respective precision (relative standard deviation) of 7.7 and 1.4% for the 15 and 200 μg L^{-1} levels were obtained. The characteristics obtained for the performance of the flow preconcentration system were a preconcentration factor of 44.2, preconcentration efficiency of 11 min^{-1}, consumptive index of 0.45 mL and sampling frequency estimated as 14 h^{-1}. Preconcentration studies of Pb (II) ions in the presence of the majority foreign ions tested did not show interference, attesting the good performance of MWCNTs. The accuracy of the method was assessed from analysis of water samples (tap, mineral, physiological serum and synthetic seawater) and common medicinal herbs submitted to the acid decomposition (garlic and Ginkgo Biloba). The satisfactory recovery values obtained without using analyte addition method confirms the feasibility of this method for Pb (II) ions determination in different type of samples.

Keywords: Multiwall carbon nanotubes; On-line preconcentration; Lead; FAAS; Multivariated optimization

1. Introduction

Nowadays the trace metal determination currently has been performed in association with solid-phase preconcentration/separation techniques, basically aiming the enrichment of metallic species and/or matrix elimination [1,2]. Other techniques for the preconcentration/separation include co-precipitation, liquid–liquid extraction and extraction in micellar environment; however, solid-phase extraction presents good advantages including high enrichment factor, ease regeneration of solid-phase, and moreover, it can be easily combined with flow injection systems [3–5]. Therefore, systems based on flow solid-phase preconcentration confer an increase in the analytical frequency as well as in the sample/reagent consumption. The solid sorbents can be commonly divided into two categories for the preconcentration of metallic ions. In the first, one can be cited the modified octadecyl silica (C_{18}), polyurethane foam, activated carbon, among others, are the most used as sorbents capable to adsorb complexed metallic ions or as solid supports in the incorporation of chelating reagents [6–8]. The second category comprises those sorbents, in which do not require a previous complexation of the metallic ions, such as alumina and ion

* Corresponding author. Tel.: +55 35 3299 1483; fax: +55 35 3299 1262.
E-mail address: ctarleyquim@yahoo.com.br (C.R.T. Tarley).

0039-9140/$ – see front matter © 2006 Elsevier B.V. All rights reserved.
doi:10.1016/j.talanta.2006.07.026

exchange resins [9,10]. Indeed, the literature reports an expressive number of solid sorbents; however, the development of novel solid-phase preconcentration systems has been growing. The great interest in the field of flow solid-phase preconcentration comprises the investigation of sorbents with excellent performance, including large specific surface area, high chemical resistance and, of course, high adsorptive capacity. In this way, simpler flow preconcentration procedures could be developed without using chelating agents as well as additional lines in the flow system. In this context, carbon nanotubes (CNTs), considered a new form of carbon, are fascinating new functional materials, which may provide attractive features for the development of flow solid sorbent preconcentration procedures. Carbon nanotubes were discovered in 1991 [11] and consist of a sheet of graphite rolled into a cylinder, with unique size, shape, and remarkable physical properties. Currently, it is known that CNTs grow by several techniques; possess few nanometers in diameter and several microns of length, promoting the formation of single wall carbon nanotubes (SWNTs) and/or multiwall carbon nanotubes (MWCNTs) [12]. Carbon nanotubes have a large application, such as reinforcement composite [13], gas adsorption [14], as catalyst supports [15] and in the electrochemistry, for instance, in the biosensors preparation as transducer, stabilizer and immobilization matrix [16]. In addition, the large specific surface area and hexagonal arrays of carbon atoms suggest a good characteristic for adsorption processes. Nevertheless, to the best of our knowledge, the application of CNTs in field of preconcentration especially for metallic species is still limited. According to the literature data, the few publications focusing on the use of CNTs for metals ions preconcentration are directed to the trace rare earth elements and cadmium, manganese and nickel determination with further determination by ICP OES [17,18].

Based on these facts mentioned above, the present work is directed to investigate the performance of MWCNTs for lead preconcentration using a flow solid-phase preconcentration system coupled to FAAS. In order to optimize the experimental parameters as well as to maximize the analytical signal and reduce the number of assays, a multivariate optimization procedure was adopted. It was carried by using a 2^4 full factorial design followed by a Doehlert design. The lead determination by proposed method was carried out in tap and mineral waters, physiological serum solution, synthetic seawater samples, garlic and Ginkgo Biloba samples.

2. Experimental

2.1. Apparatus

Spectrometric measurements were carried out with a Shimadzu AA-6800 flame atomic absorption spectrometer equipped with deuterium lamp for background correction. The hollow cathode lamp for lead was operated at 10 mA and the wavelength was set at 283.3 nm. The burner height was adjusted to about 6 mm for optimum sensitivity and the flame composition operated at an acetylene flow rate of 3.0 L min^{-1} and air flow rate of 10.0 L min^{-1}.

A peristaltic pump from Ismatec Model IPC with Tygon tubes was used to propel all sample and reagent solutions while a home-made injector commutator made of Teflon® (PTFE, polytetrafluoro ethylene) was used to select the preconcentration/elution steps. The transport lines were made of PTFE tube of 0.5 nm bore.

The mini-column (6.0 × 1.0 cm i.d.), employed for packing the MWCNTs was made of polyethylene containing glass wool placed at both ends of mini-column aiming to prevent sorbent losses during the system operation. The mini-column was not completely filled with MWCNTs in order to avoid overpressure into the mini-column. The sample pH was measured by a Handylab 1 Schott pHmeter.

Sample decomposition was performed in a microwave oven (Milestone Microwave Laboratory System).

2.2. Reagents

Analytical grade chemical reagents were used as well as ultra pure water from a Millipore Milli-Q purification system. In order to avoid contamination from laboratory glassware, it was kept overnight in a 10% (v/v) HNO_3 solution.

The Pb (II) standards solutions were prepared by appropriated dilution from a 1000 mg L^{-1} lead solution (Merck, Darmstadt), immediately prior using.

Citrate, acetate and phosphate buffer solutions were prepared from their respective sodium salts purchased from Merck without further purification.

The pH of the buffer solutions was adjusted with sodium hydroxide and/or nitric acid solutions. Ultra-pure HNO_3 and 30% (v/v) H_2O_2 (Merck) were used for the sample decomposition procedures. Nitric acid used through the work was purified from a sub-boiling system (Milestone Microwave Laboratory System).

MWCNTs (95% of purity) were kindly provided from CNT Co., Ltd. (Korean). Prior to use, this material was oxidized with concentrated HNO_3 according to the literature with minor modification [12], in order to create binding sites onto MWCNTs surface [19]. The treatment was carried out by dispersion in 30 mL of concentrated HNO_3 of 500 mg of MWCNTs being further refluxed for 1 h at 120 °C. Afterwards, the material was washed with ultra pure water until remove the acid excess (neutral pH of solution), dried at 100 °C and stored until use.

2.3. On-line preconcentration procedure

The schematic diagram of on-line preconcentration is shown in Fig. 1. The manifold was operated in the time-based mode. Aliquots of 20 mL of samples previously buffered (pH 4.7) with 0.003 mol L^{-1} acetate buffer were preconcentrated during 4 min at a flow rate of 5.0 mL min^{-1} onto 30 mg of MWCNTs. During preconcentration, the eluent solution (1.0 mol L^{-1} HNO_3) flows in the system towards to the flame atomic absorption spectrometer. After this stage, by switching the injector commutator to the elution position, the eluent solution at a flow rate of 5.0 mL min^{-1} desorbs in countercurrent the Pb (II) ions retained onto MWCNTs, which is delivered to the FAAS nebulizer. The

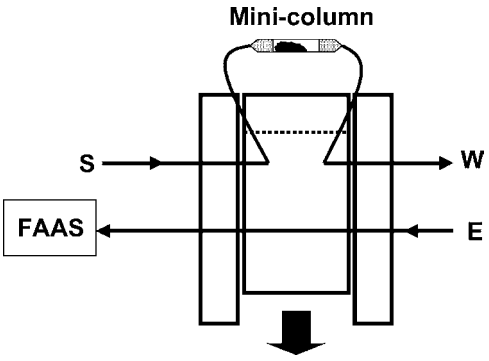

Fig. 1. Diagram of preconcentration system. S = sample, W = waste, E = eluent 1.0 mol L^{-1} HNO_3.

measurements were taken as peak height of the transient signals, in which were proportional to the Pb (II) ions concentration in the sample.

2.4. Sample preparation

Water samples including tap, mineral water, physiological serum and synthetic seawater were spiked with known amount of Pb (II) followed by pH adjusting with buffer solution. Tap water was colleted from Unifal-MG campus, while mineral water and physiological serum was from local supermarkets and drugstores, respectively. The synthetic seawater composition was based on literature: 27.9 mg L^{-1} NaCl; 1.4 g L^{-1} KCl; 2.8 g L^{-1} $MgCl_2$; 0.5 g L^{-1} NaBr; 2.0 g L^{-1} $MgSO_4$ [20]. Ginkgo Biloba was obtained from local drugstore and garlic samples were obtained from supermarkets.

Garlic and Ginkgo Biloba decomposition was performed using microwave oven. Garlic samples were dried (100 °C) at constant weight, triturated and homogenized mechanically with a mortal before sample decomposition. After that, 400 mg for garlic or 350 mg for Ginkgo Biloba samples were accurately weighted into Teflon flasks and 10 mL of concentrated HNO_3 and 4 mL of H_2O_2 were added. The steps of microwave assisted sample decomposition were carried out as follow: 7 min at 502 W and 15 min at 708 W. After finished the sample decomposition, the solutions were heated on a hot plate almost to dryness. The residues previously cooled at room temperature were dissolved in distilled/deionised water and transferred to calibrated flasks of 100 mL. Finally, an aliquot of 50 mL was transferred to calibrated flask of 250 mL followed by pH adjusting to intended value with buffer solution. Blank solutions were prepared for each sample.

2.5. Optimization study

The optimization study for the on-line preconcentration system was carried out in order to determine the best flow and chemical variables associated to the performance of the system in terms of sensitivity as well as sampling frequency. In this way, the multivariate screening of the variable was investigated by means a 2^4 full factorial design conducted in duplicates. Table 1 shows the variables studied and their levels employed.

Table 1
Variables and their levels employed in the 2^4 full factorial design

Variables	Levels	
	(−) Low	(+) High
pH	2.6	6.0
Preconcentration flow rate (PFR) (mL min^{-1})	2.5	5.0
Buffer concentration (BC) (mol L^{-1})	0.01	0.1
Eluent concentration (EC) (mol L^{-1})	0.1	1.0

These experiments were performed in a random order by preconcentration of 10 mL of Pb (II) solution at a concentration of 200 μg L^{-1}. Other important variables in the system, such as mass of MWCNTs and flow rate of eluent were previously fixed. Preliminary studies of MWCNTs amount indicate that higher mass than 30 mg could lead to a leakage in the mini-column due to resulting overpressure in the preconcentration stage. Thus, this amount was used throughout work. The eluent flow rate was set at 5.0 mL min^{-1} in order to match with the flow rate of FAAS nebulizer. Taking into account those significant variables from the full factorial design, the final optimization was further carried out using Doehlert design in duplicate, whose design comprises seven assays. From this design, it was possible to apply the response surface method (RSM) to optimize the levels of the variables. All data were processed using the STATISTICAL package program (Version 6.0).

3. Results and discussion

3.1. Optimization study of the on-line preconcentration procedure

The 2^4 full factorial design used in the attempt to evaluate the effect of the variables in the on-line preconcentration procedure is shown in Table 2. As can be seen, both peak height and effi-

Table 2
2^4 full factorial design used in the variables screening related to the on-line lead preconcentration using MWCNTs as sorbent

Runs	pH	PFR	BC	EC	Response (peak height)	Efficiency of sensitivity
1	−	−	−	−	0.038/0.039	0.0095/0.0098
2	+	−	−	−	0.049/0.048	0.0123/0.0120
3	−	+	−	−	0.030/0.034	0.0150/0.0170
4	+	+	−	−	0.034/0.038	0.0170/0.0190
5	−	−	+	−	0.007/0.008	0.0018/0.0020
6	+	−	+	−	0.047/0.046	0.0118/0.0115
7	−	+	+	−	0.008/0.010	0.0040/0.0050
8	+	+	+	−	0.032/0.031	0.0160/0.0155
9	−	−	−	+	0.054/0.058	0.0135/0.0145
10	+	−	−	+	0.066/0.068	0.0165/0.0170
11	−	+	−	+	0.035/0.036	0.0175/0.0180
12	+	+	−	+	0.045/0.047	0.0225/0.0235
13	−	−	+	+	0.021/0.022	0.0053/0.0055
14	+	−	+	+	0.050/0.049	0.0125/0.0123
15	−	+	+	+	0.008/0.007	0.0040/0.0035
16	+	+	+	+	0.041/0.038	0.0205/0.0190

PFR = preconcentration flow rate; BC = buffer concentration; EC = eluent concentration.

Table 3
Effects calculated to the 2^4 full factorial design

	Effects (absorbance)	Effects (efficiency of sensitivity)
Main effects		
A (pH)	0.0196 ± 0.0002	0.00706 ± 0.00009
B (PFR)	−0.0122 ± 0.0002	0.00432 ± 0.00009
C (BC)	−0.0184 ± 0.0002	−0.00652 ± 0.00009
D (EC)	0.0092 ± 0.0002	0.00290 ± 0.00009
Two factor interaction		
AB	−0.0024 ± 0.0002	0.00156 ± 0.00009
AC	0.0108 ± 0.0002	0.00394 ± 0.00009
AD	0.0008 ± 0.0002	0.00069 ± 0.00009
BC	0.0028 ± 0.0002	−0.00122 ± 0.00009
BD	−0.0042 ± 0.0002	−0.00040 ± 0.00009
CD	−0.0032 ± 0.0002	−0.00102 ± 0.00009
Three factor interaction		
ABC	−0.0008 ± 0.0002	0.00106 ± 0.00009
ABD	0.0032 ± 0.0002	0.00131 ± 0.00009
ACD	−0.0012 ± 0.0002	−0.00018 ± 0.00009
BCD	0.0016 ± 0.0002	0.00015 ± 0.00009
Four factor interaction		
ABCD	0.0018 ± 0.0002	0.00060 ± 0.00009

PFR = preconcentration flow rate; BC = buffer concentration; EC = eluent concentration.

ciency of sensitivity were investigated as analytical response. The efficiency of sensitivity is a paramount parameter that takes into account the time required in the preconcentration step. Thus, it was calculated as the ratio of the peak height to the time (in minutes) during the preconcentration step.

Table 3 reports the main effects as well as those interaction effects followed by error (uncertainty of effect). It can be verified that either using peak height or efficiency of sensitivity the main effects are higher than their error, in which could provides an indicative of significance of variables. From the error of effects can be built a confidence interval using *t*-distribution with a required confidence level. In this way, the supposition was confirmed by multiplying the error by critical t_{16} (2.120) with 95% confidence interval [21]. The results obtained when using peak height as analytical response show an error of 0.000424, while the value for efficiency of sensitivity was 0.000190. As these values are lower than main effects, it is possible to point out that, in fact, all variables are statistically significant. In addition, the majority of interaction effects are also significant.

The interpretation of variables effects demonstrates that due to positive effect of the pH and eluent concentration, the increase on their levels confers improvements in both analytical responses. As it was not verified memory effect after each preconcentration step, 1.0 mol L^{-1} HNO_3 solution was selected for the further experiments. The results related to pH effect in the Pb (II) ions sorption are consistent with literature, whereas during treatment of MWCNTs with boiled concentrated HNO_3, many free oxygen atoms are produced onto their surface, thus resulting in hydroxyl, carbonyl and carboxyl groups [19].

The second more important variable, buffer concentration, presents a negative effect. An increase in the buffer concentration probably provokes competition on the solid-phase, thus decreasing the sorption rate of Pb (II) ions onto MWCNTs and consequently the analytical response. The influence of preconcentration flow rates, as expected, provides opposite effects on both analytical responses. Taking into account the peak height, at a higher preconcentration flow rate the efficiency of mass transport of Pb (II) ions onto MWCNTs is decreased due to slow kinetic sorption. On the other hand, the dependence of the efficiency of sensitivity on the preconcentration flow rate is almost linear with the increase in the level of variable. According to these results, the preconcentration flow rate at 5.0 mL min^{-1} was chosen for subsequent experiments since it provided a reasonable sampling frequency. Higher preconcentration flow rate were not checked because it would imply in leakage in the mini-column.

Table 4
Doehlert design used in the optimization of on-line lead preconcentration procedure using MWCNTs as sorbent

Runs	pH	Buffer concentration (mol L^{-1})	Absorbance (peak height)
4	0 (5.6)	0 (0.003)	0.062
4	0 (5.6)	0 (0.003)	0.059
4	0 (5.6)	0 (0.003)	0.061
5	1 (7.2)	0 (0.003)	0.015
2	0.5 (6.4)	0.866 (0.005)	0.027
3	−1 (4.0)	0 (0.003)	0.059
6	−0.5 (4.8)	−0.866 (0.001)	0.054
7	0.5 (6.4)	−0.866 (0.001)	0.024
1	−0.5 (4.8)	0.866 (0.005)	0.059

The first number represents the coded values while the values between parentheses are the real values.

The optimum values for the sample pH and buffer concentration were obtained using Doehlert design built with coded values (Table 4). In this optimization, peak height was adopted as analytical response since preconcentration flow rate was fixed as already commented. From Doehlert design, both linear and quadratic models for analytical response were evaluated. Linear model is represented by following equation:

$$\text{Absorbance (peak height)} = 0.0467 - 0.0250\,\text{pH} + 0.0023\,\text{BC} \quad (1)$$

The analysis of variance (ANOVA) of linear model is given in Table 5. The $MS_{regression}/MS_{residues}$ ratio of 5.8909 is only little high than the 95% critical $F_{2,6}$ value of 5.14, in which would indicates that this model shows significant regression at this confidence level. Nevertheless, if one considers the MS_{lof}/MS_{pe} ratio of 104.13, which is larger than the critical $F_{4,2}$ value of 19.25, it is possible to stress that linear model clearly presents lack of fit.

The ANOVA of quadratic model (Eq. (2)) is shown in Table 6. As can be observed, the $MS_{regression}/MS_{residues}$ ratio of 28.67 is higher than that ratio obtained for the linear model (5.8909). In addition, the tabled critical $F_{5,3}$ value of 9.01 when compared to the $F_{calculated}$ value (28.67), indicates the significance of the model. Even though MS_{lof}/MS_{pe} ratio of 23.43 is closed to the $F_{critical}$ 18.51, the quadratic model is more adequate for

Table 5
Analysis of variance of linear model

Variation source	Sum of squares (SS)	Degree of freedom (DF)	Mean of squares (MS)	$F_{calculated}$	$F_{critical}$
Regression	0.0018911	2	0.0009455	5.8909	5.14
Residues	0.0009629	6	0.0001605		
Lack of fit (lof)	0.0009583	4	0.0002395	104.13	19.25
Pure error (pe)	0.0000046	2	0.0000023		
Total	0.002854	8			

% of explained variance: 66.25; maximum % of explained variance: 99.83.

Table 6
Analysis of variance of quadratic model

Variation source	Sum of squares (SS)	Degree of freedom (DF)	Mean of squares (MS)	$F_{calculated}$	$F_{critical}$
Regression	0.0027955	5	0.0005591	28.67	9.01
Residues	0.0000585	3	0.0000195		
Lack of fit (lof)	0.0000539	1	0.0000539	23.43	18.51
Pure error (pe)	0.0000046	2	0.0000023		
Total	0.002854	8			

% of explained variance: 97.94; maximum % of explained variance: 99.83.

the experimental results as observed from Fig. 2.

$$\text{Absorbance (peak height)} = 0.0607 - 0.0250\,\text{pH} + 0.0023\,\text{BC} - 0.0230\,\text{pH}^2 - 0.0183\,\text{BC}^2 - 0.0012\,\text{pH}\,\text{BC} \quad (2)$$

Using the quadratic model, a response surface was built (Fig. 3) whose presence of maximum points was confirmed from Lagrange's criterion [22]. The criterion permits to identify optimum conditions of an optimization problem by calculating the Hessian determinant of analytical response (R), in this case, absorbance (peak height). The Hessian determinant is given by

$$H = \begin{vmatrix} \dfrac{\partial^2 R}{\partial A^2} & \dfrac{\partial^2 R}{\partial A \partial B} \\ \dfrac{\partial^2 R}{\partial B \partial A} & \dfrac{\partial^2 R}{\partial B^2} \end{vmatrix}$$

Simplifying, the Hessian determinant leads to the following expression (Eq. (3))

$$H = \left(\frac{\partial^2 R}{\partial A^2}\right)\left(\frac{\partial^2 R}{\partial B^2}\right) - \left(\frac{\partial^2 R}{\partial A \partial B}\right)\left(\frac{\partial^2 R}{\partial B \partial A}\right) \quad (3)$$

According to Lagrange's criterion there is a maximum point above the surface response when $H(A_0, B_0) > 0$ and $\partial^2 R/\partial A^2$ and $\partial^2 R/\partial B^2 < 0$, where A = pH and B = BC (buffer concentration), in this case. Therefore, according to the calculation of the Hessian determinant (1.44×10^{-6}) and $\partial^2 R/\partial A^2$ (-0.046) and $\partial^2 R/\partial B^2$ (-0.0366) it is possible to emphasized the presence of a maximum point. In order to found this value the quadratic model was resolved as function of pH and buffer concentration as follow:

$$\frac{\partial ABS}{\partial \text{pH}} = -0.0250 - 0.046\,\text{pH} - 0.0012\,\text{BC} = 0 \quad (4)$$

$$\frac{\partial ABS}{\partial \text{BC}} = 0.0023 - 0.0366 \cdot \text{BC} - 0.0012 \cdot \text{pH} = 0 \quad (5)$$

This way, a maximum point at -0.530 and 0.079 for pH and BC was achieved. Converting these coded values for the

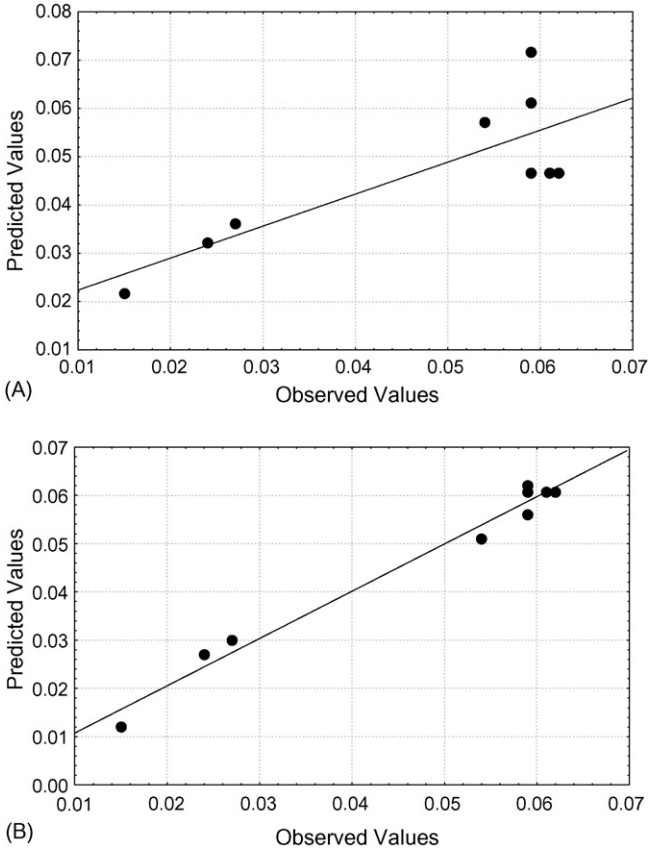

Fig. 2. Comparison of forecasts of two models with respect to the experimental values. (A) Linear model and (B) quadratic model.

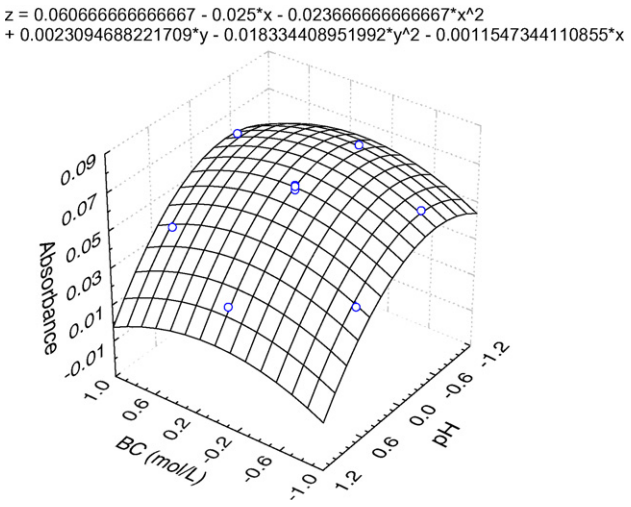

Fig. 3. Response surface obtained from Doehlert design displayed in Table 4.

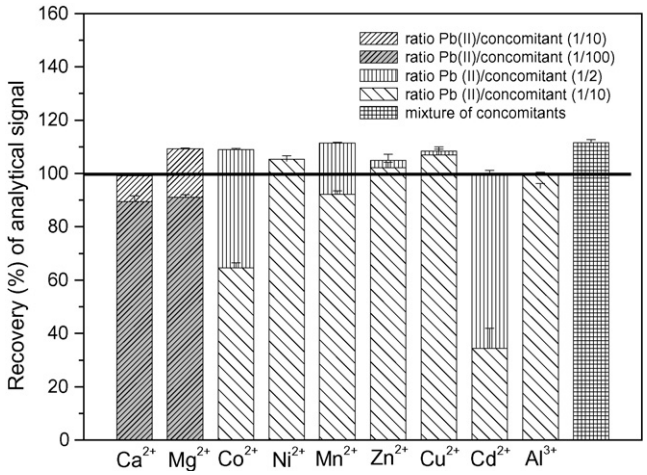

Fig. 4. Interference studies in the preconcentration of 200 μg L^{-1} Pb (II) solution using foreign ions.

real values, using the expression below (Eq. (6)), the respective optimum values for pH and buffer concentration were 4.7 and 0.003 mol L^{-1}.

$$C_i = \left\{ \frac{X_i - X_i^0}{\Delta X_i} \right\} \alpha \quad (6)$$

where C_i is the coded value used in the building of Doehlert design, X_i the real value of variables, X_i^0 the real value of variable at the central point, ΔX_i the difference between each variable at the real value and α is the variation between each coded value.

After establishing the best conditions using multivariated optimization, studies aiming increase the sensitivity was performed by using a longer preconcentration time. A linear relationship was observed between preconcentration time and analytical signal (peak height) varying from 2 up to 4 min. Hence, as a compromise between sensitivity, sampling frequency, consumption of sample/reagent and acetylene fuel, 4 min of preconcentration time was chosen, allowing a sampling frequency of 14 h^{-1}.

3.2. Interference studies

As already mentioned, the retention of Pb (II) onto MWCNTs surface exhibits a typical cationic sorption behaviour. Therefore, even though their high surface area as well as high volume of pores, the presence of foreign ions still could provoke accentuated competition for those sorption sites of sorbent. Thus, it was investigated the effects of foreign ions in the Pb (II) preconcentration. As can be seen in Fig. 4, it can be deducted that major divalent cations Ca (II) and Mg (II) have no significance influence in the Pb (II) sorption. In the same way, the behaviour of other concomitant cations and coexisting ions [ratio Pb/concomitants (1/2)] makes possible to note that there is no interference. The only significant effect in the Pb (II) sorption was observed in sorption experiments for concomitant ions Co (II) and Cd (II) at 10-fold excess, whereas a respective decrease of ca. 40 and 60% in the recovery signal was verified. A possible explanation for the results might be related to the high affinity of both Co (II) and Cd (II) ions for sites of MWCNTs, thus causing a displacement of Pb (II) retained in the solid phase.

3.3. Figures of merit and validation of the on-line preconcentration procedure

The on-line preconcentration procedure provided an analytical linear curve varying from 15 up to 775 μg L^{-1} with good correlation coefficient ($r > 0.999$). With a preconcentration time of 4 min at a flow rate of 5.0 mL min^{-1}, a sensitivity enhancement of 44.2 based on calculation of preconcentration factor (PF) was obtained. PF was calculated by ratio of slopes of analytical curve with ($Y = 0.00694 + 6.04 \times 10^{-4}$ [Pb (II)]) and without ($Y = 0.0349 + 1.367 \times 10^{-5}$ [Pb (II)]) preconcentration step. Preconcentration efficiency (PE), on the other hand, provides a better evaluation of the on-line preconcentration performance. The value of PE establishes the sensitivity enhancement using a preconcentration time of 1 min. Hence, the PE was found to be 11 min^{-1}. Consumptive index (CI) obtained in the proposed method was found to be 0.45 mL. It represents the volume expressed in milliliters necessary to attain a unit of PF. The limits of detection (2.6 μg L^{-1}) and quantification (8.6 μg L^{-1}) were calculated according to IUPAC [23], which was, respectively, based on 3 and 10 times the standard deviation of 10 measurements of the blank solution. The repeatability assessed by eight preconcentration cycles using 15 and 200 μg L^{-1} was 7.7 and 1.4%, respectively. As can be observed from Table 7, a brief comparison of the proposed method with those already reported shows that the solid-phase extraction system for lead enrichment using MWCNTs on-line coupled to FAAS, presents a large linear range, a similar or lower limit of detection as well as the possibility of interference-free determination of lead ions in different type of samples, unlikely of some methods [31–33]. In addition, the values of PF, PE and CI obtained, most used as a criteria for the evaluation of the performance of an on-line preconcentration indicates a satisfactory efficiency of the proposed method [35]. The highlight of proposed method is related to its simplicity, does not requiring additional lines of chelating agents

Table 7
Features of different on-line preconcentration systems for lead determination by FAAS and evaluation with the proposed method using MWCNTs as solid sorbent

Sorbent	Chelating agent	Eluent	PF	CI (mL)	CE (min^{-1})	LD ($\mu g\,L^{-1}$)	Linear range ($\mu g\,L^{-1}$)	Ref.
Activated carbon	APDC	MIBK	42	0.142	21	10	15–365	[24]
Activated carbon	Dithizone	MIBK	90	0.166	18	2	5–80	[24]
C_{18}	DDTP	Ethanol	37	0.270	7.4	6	50–250	[25]
PUF	DDTP	Ethanol	15	0.666	3	13	50–500	[25]
Activated carbon	DDTP	Ethanol	14	0.714	5.6	14	100–1000	[25]
PUF	BTAC	HCl	26	0.269	26	1.0	10–500	[26]
C_{18}	DDC	MIBK	60	0.133	30	3.0	20–100	[27]
Amberlite-XAD-2	BTAC	HCl	27	0.166	13.5	3.7	3.7–300	[28]
Chromosorb 102	DDC	Ethanol	25.4	0.173	12.7	2.0	50–600	[29]
Amberlite XAD-2	BTAC	HCl	60	0.20	30	1.7	–	[30]
Chitosan	8-Hydroxyquinoline	HNO_3	26.5	0.37	18.9	1.7	10–1000	[31]
Rice husks treated with NaOH	–	HNO_3	46	0.52	11.5	14.1	0–2000	[32]
Vermicompost	–	HNO_3	62	0.258	15.5	8.8	29.4–2000	[33]
PUF	TAM	HCl	45	0.31	22.5	2.2	1–150	[34]
MWCNTs	–	HNO_3	44.2	0.45	11	2.6	8.6–775	This work

PF = preconcentration factor; CI = consumptive index; CE = concentration efficiency; LD = limit of detection; APDC = ammonium pyrrolidinedithiocarbamate; DDTP = ammonium diethyldithiophosphate; BTAC = 2-(2-benzothiazolylazo)-2-*p*-cresol; DDC = diethyldithiocarbamate; TAM = 2-(2-thiazolylazo)-5-dimethylaminophenol; MIBK = methyl isobutyl ketone.

Table 8
Evaluation of recoveries values for Pb (II) ions determination in water samples and medicinal herbs

Samples	Pb (II) ions added ($\mu g\,L^{-1}$)	Pb (II) ions found[a] ($\mu g\,L^{-1}$)	Recovery (%)
Tap water	0	Not detected	–
	30.0	29.0 ± 0.7	96.7
Mineral water	0	Not detected	–
	30.0	28.8 ± 1.0	96.0
Physiological solution	0	Not detected	–
	30.0	27.2 ± 1.2	90.6
Synthetic seawater	0	Not detected	–
	30.0	28.6 ± 3.0	95.3
Ginkgo Biloba ($\mu g\,g^{-1}$)	0	64.3 ± 3.9	–
	57.0	117.4 ± 5.6	96.8
Garlic ($\mu g\,g^{-1}$)	0	Not detected	–
	50.0	46.7 ± 4.5	93.4

Not detected = below of limit of detection.
[a] The results are expressed as mean value ± standard deviation based on three replicates ($n = 3$).

and absence of organic solvent as eluent, in which this feature is in accordance with current concept of clean chemistry.

In order to check the feasibility of the analytical system, lead determination in water and common medicinal herbs samples was carried out after on-line preconcentration onto MWCNTs without using analyte addition method. Good recovery results after spiking ranging from 90.6 to 96.8% are shown in Table 8 and reflect the accuracy of the method and the suitability and reliability of the MWCNTs for lead preconcentration in water and organic samples (garlic and Ginkgo Biloba) submitted to acid decomposition. An interesting data is related to the possibility of lead determination in samples with high salt content, such as seawater, because there is very important meaning to monitor the contamination degree of lead in seawater samples. Also, it is important to note that the level of lead obtained in Ginkgo Biloba by proposed method exceeded the maximum recommended limit of 10 $\mu g\,g^{-1}$ according to World Health Organization (WHO) [36]. Thus, the method can successfully be applied for quality control of these products, since in most countries the quality control is not always enforced.

4. Conclusions

In this paper was shown the analytical performance of MWCNTs for on-line lead preconcentration in water samples and medicinal herbs. MWCNTs represent a potentially significant advancement in the field of on-line preconcentration and analytical separations due to their high surface area, thus making possible the free-interference preconcentration of lead ions in different matrices. The proposed method was significant with respect to the good performance of preconcentration system including satisfactory preconcentration factor and preconcentration efficiency, thus resulting in a low limit of detection. Moreover, it could be shown that the method is characterized by simplicity, precision and mainly by absence of chelating agents and additional lines in the flow system as well as organic solvent

used as eluent, most common in solid-phase preconcentration system that use modified octadecyl silica (C_{18}) or fullerene as sorbents, although high preconcentration factors and low sample consumption are achieved using these conventional adsorbents. Finally, these features indicate that the propose method can be a suitable alternative for lead determination in different type of samples, expanding in the same time, the applicability of MWCNTs in analytical purposes.

Acknowledgments

The authors thank the CNPq, FAPESP and CAPES for financial support and fellowships.

References

[1] M.G. Pereira, M.A.Z. Arruda, Microchim. Acta 141 (2003) 115.
[2] A. Fisher, P.S. Goodall, M.W. Hinds, S.M. Nelms, D.M. Penny, J. Anal. At. Spectrom. 18 (2003) 1497.
[3] T.C. Duan, H.T. Chen, X.J. Zeng, J. Anal. At. Spectrom. 17 (2002) 410.
[4] A.R. Ghiasvand, S. Shadabi, E. Mohagheghzadeh, P. Hashemi, Talanta 66 (2005) 912.
[5] L.M. Coelho, M.A.Z. Arruda, Spectrochim. Acta B 60 (2005) 743.
[6] R. Ma, W. Van Mol, F. Adams, Anal. Chim. Acta 285 (1994) 33.
[7] C.R.T. Tarley, M.A.Z. Arruda, Anal. Sci. 20 (2004) 961.
[8] K. Jankowski, A. Jackowska, P. Kukasiak, Anal. Chim. Acta 540 (2005) 197.
[9] J. Yin, Z.C. Jiang, G. Chang, B. Hu, Anal. Chim. Acta 540 (2005) 333.
[10] M.T.S. Cordero, E.I.V. Alonso, A.G. de Torres, J.M.C. Pavon, J. Anal. At. Spectrom. 19 (2004) 398.
[11] S. Iijima, Nature 8 (1991) 354.
[12] L. Yan-Hui, D. Jun, L. Zhaokun, D. Zechao, Z. Yuefeng, X. Cailu, W. Dehai, W. Bingqing, Carbon 41 (2003) 2787.
[13] H.D. Wagner, O. Lourie, Y. Feldman, R. Tenne, Appl. Phys. Lett. 72 (1998) 188.
[14] A.C. Dillon, K.M. Jones, T.A. Bekkedahl, C.H. Kiang, Nature 386 (1997) 377.
[15] J.M. Planeix, N. Coustel, B. Coq, V. Brotons, P.S. Kumbhar, J. Am. Chem. Soc. 116 (1994) 7935.
[16] K.A. Joshi, M. Prouza, M. Kum, J. Wang, J. Tang, R. Haddon, W. Chen, A. Mulchandani, Anal. Chem. 78 (2006) 331.
[17] P. Liang, Y. Liu, L. Guo, Spectrochim. Acta B 60 (2005) 125.
[18] P. Liang, Y. Liu, L. Guo, J. Zeng, H. Lu, J. Anal. At. Spectrom. 19 (2004) 1489.
[19] J. Zhijie, W. Zhengyuan, L. Ji, W. Bingqing, W. Dehai, Carbon 37 (1999) 903.
[20] M. Zougagh, P.C. Rudner, A.G. de Torres, J.M.C. Pavon, J. Anal. At. Spectrom. 15 (2000) 1589.
[21] B.B. Neto, I.S. Scarminio, R.E. Bruns, Como Fazer Experimentos: Pesquisa e Desenvolvimento na Ciência e na Indústria, Unicamp (Ed.), Campinas, 2001, pp. 109–393.
[22] C.R.T. Tarley, W.N.L. Dos Santos, C.M. Dos Santos, M.A.Z. Arruda, S.L.C. Ferreira, Anal. Lett. 37 (2004) 1437.
[23] G.L. Long, J.D. Winefordner, Anal. Chem. 55 (1983) 712.
[24] Y.P. de Pena, M. Gallego, M. Valcárcel, Talanta 42 (1995) 211.
[25] S.P. Quináia, J.B.B. da Silva, M.C.E. Rollemberg, A.J. Curtis, Talanta 54 (2001) 687.
[26] V.A. Lemos, S.L.C. Ferreira, Anal. Chim. Acta 441 (2001) 281.
[27] R.L.K.C. Leandro, R.E. Santelli, Talanta 43 (1996) 977.
[28] S.L.C. Ferreira, V.A. Lemos, R.E. Santelli, E. Ganzarolli, A.J. Curtis, Microchem. J. 68 (2001) 41.
[29] L. Elçi, Z. Arslan, J.F. Tyson, Spectrochim. Acta B 55 (2000) 1109.
[30] V.A. Lemos, J.S. Santos, L.S. Nunes, Sep. Sci. Technol. 40 (2005) 1401.
[31] A.O. Martins, E.L. Silva, M.C.M. Laranjeira, V.T. Fávere, Microchim. Acta 150 (2005) 27.
[32] C.R.T. Tarley, S.L.C. Ferreira, M.A.Z. Arruda, Microchem. J. 77 (2004) 163.
[33] M.D. Pereira, M.A.Z. Arruda, Microchim. Acta 146 (2004) 215.
[34] S.L.C. Ferreira, W.N.L. dos Santos, M.A. Bezerra, V.A. Lemos, J.M. Bosque-Sendra, Anal. Bioanal. Chem. 375 (2003) 443.
[35] Z. Fang, S. Xu, S. Zhang, Anal. Chim. Acta 35 (1987) 200.
[36] WHO, Monographs on Selected Medicinal Plants, vol. 1, World Health Organization, Geneva, 1999.

Available online at www.sciencedirect.com
ScienceDirect
Talanta 71 (2007) 1804–1812
Talanta
www.elsevier.com/locate/talanta

Time-of-flight ion mobility spectrometry and differential mobility spectrometry: A comparative study of their efficiency in the analysis of halogenated compounds

H. Borsdorf [a,*], E.G. Nazarov [b], R.A. Miller [b]

[a] *Department of Analytical Chemistry, UFZ Centre for Environmental Research Leipzig-Halle, PF500135, D-04301 Leipzig, Germany*
[b] *Sionex Corporation, 8-A Preston Court, Bedford, MA 01730, USA*

Received 4 May 2006; received in revised form 14 August 2006; accepted 21 August 2006
Available online 5 October 2006

Abstract

The ion mobilities of halogenated aromatics which are of interest in environmental chemistry and process monitoring were characterized with field-deployable ion mobility spectrometers and differential mobility spectrometers. The dependence of mobility of gas-phase ions formed by atmospheric-pressure photoionization (APPI) on the electric field was determined for a number of structural isomers. The structure of the product ions formed was identified by investigations using the coupling of ion mobility spectrometry with mass spectrometry (APPI–IMS–MS) and APPI–MS. In contrast to conventional time-of-flight ion mobility spectrometry (IMS) with constant linear voltage gradients in drift tubes, differential mobility spectrometry (DMS) employs the field dependence of ion mobility. Depending on the position of substituents, differences in field dependence were established for the isomeric compounds in contrast to conventional IMS in which comparable reduced mobility values were detected for the isomers investigated. These findings permit the differentiation between most of the investigated isomeric aromatics with a different constitution using DMS.

Keywords: Ion mobility spectrometry; Differential mobility spectrometry; Isomeric compounds

1. Introduction

Differential mobility spectrometry (DMS) has been developed as a method for detecting and identifying organic compounds [1]. The small analytical region and other technical parameters (low power requirements, size and weight, ambient pressure, air as drift gas) of the devices allow DMS spectrometers to be miniaturized [2]. The spectrometers can therefore be used as field-portable sensors or detectors for gas chromatography [3].

The development of DMS results from demands for the further miniaturization of ion mobility spectrometers. However, the miniaturization of drift tubes in conventional time-of-flight ion mobility spectrometry (IMS) with a corresponding reduction in the length and width of the drift region has reduced the sensitivity and resolution of ion mobility spectrometers. These limitations result from more significant wall charging or neutralization and non-homogeneous electric fields with a decreasing inner diameter of the drift tube [4]. These developments have prompted the introduction of new methods of ion separation based upon field dependent mobilities where ions are exposed to strong electric fields. Such instruments are commercially available as micro-fabricated differential mobility spectrometers (DMS) [1] or high-field asymmetric waveform ion mobility spectrometers (FAIMS) [5].

The principal of ion filtering using DMS is based on the field dependence of ion mobility that occurs when the density-scaled electric field (E/N, where E is the electric field strength and N the neutral gas density) exceeds 40 Townsend (1 Townsend (Td) = 10^{-17} V cm^{-2}). The first step in determining ion mobilities is therefore the formation of ions from neutral sample molecules at atmospheric pressure. ^{63}Ni ionization sources, corona or partial discharge ionization, photoionization, laser ionization, surface ionization, electrospray ionization and some other techniques are commonly used as ionization methods [6–8]. The ions formed are pushed from the ionization region and moved between two parallel plates with a constant flow of

* Corresponding author. Tel.: +49 341 235 2316; fax: +49 341 235 2625.
E-mail address: helko.borsdorf@ufz.de (H. Borsdorf).

0039-9140/$ – see front matter © 2006 Elsevier B.V. All rights reserved.
doi:10.1016/j.talanta.2006.08.017

gas, commonly air or nitrogen. The asymmetric radio-frequency (RF) field or separating field between the electrodes (commonly with a peak amplitude between 12,000 and 30,000 V cm^{-1}) and a frequency of 0.7–1.5 MHz cause an oscillating motion of ions along the narrow gap formed by the electrodes, eventually leading to collisions and losses on the electrodes. This oscillation of ions results from the alternation between high-field and low-field values of ion mobilities during each RF cycle. Selected ions can be maintained in the drift gas flow or restored to the center of the gap using a low DC voltage (commonly between 0 and 400 V cm^{-1}) which is superimposed on the high-voltage asymmetric field. Depending on the strength of the DC voltage (or compensation voltage), certain ions can be selected to pass between the electrodes and reach the detectors. A compensation voltage is characteristic for an ion at given conditions of temperature, moisture, and separating field. The compensation voltage is therefore swept over a range of voltages and the spectra obtained display the compensation voltage versus the intensity of the ion current. The theoretical background of DMS is extensively described in recent publications [1,9–11].

The attractions of this new method for ion characterization include the simplification of the analyzer, since ion shutters and the aperture grid before the detector are eliminated. Moreover, ions are moved through the analyzer by gas flow alone so positive and negative ions can be simultaneously detected. Furthermore, information from the DMS spectrum complements conventional IMS by providing the field dependence of ion mobility.

DMS is successfully used in a number of different fields including environmental analysis [12–14], health science [15], homeland security [16] and bioanalytics [17–19] and can be used as individual units [20] or coupled with separation techniques for the analysis of complex mixtures [3,21,22] or as a separation technique for mass spectrometry [23,24].

In contrast to this approach, traditional IMS is based on determining the drift velocities attained by gaseous ions in a weak electric field ($E < 1000$ V cm^{-1}) and at ambient pressure. The ions formed are gated into the drift tube via an electronic shutter grid which is briefly opened at a given time interval of a few microseconds and, during this time, permits the transfer of an ion swarm into the drift tube. The ions move through the electric field gradient, whereupon any energy gained from the electrical field is dissipated by collisions with neutral molecules of the supporting gas atmosphere. In contrast to DMS, with typical field strengths of more than 40 Td, about 1 Td is applied in conventional IMS drift tubes (1 Td = 268 V cm^{-1} at conditions with $T = 0$ °C and $p = 760$ Torr). The ions traverse the drift tube in a few milliseconds and the drift velocities are determined using the supporting electronics. The speed of movement of the ion swarm, or the drift velocity (v_d), is proportional to the strength of the electric field (E) with the constant of proportionality being the mobility (K) of the ions [6,7].

In conventional IMS with low electric fields, the motion of the ions is affected by diffusion processes, the electric field, the gas density and ion-neutral interactions. Using high electric fields, additional processes can be expected in the drift channel of the differential mobility spectrometer. The formation and dissociation of ion clusters can become a repeatable process at high frequency in field-dependent methods. Moreover, deformation and variation of the cross-section in high electric fields have been described. Different reaction courses can be expected for different ions depending on the strength of the electric field [25–27].

The different measuring conditions described for traditional time-of-flight IMS and DMS motivated us to investigate possible differences in the ion mobility spectra obtained with both methods of ion separation using the same ionization technique (APPI). The product ions formed using this ionization source were identified using an atmospheric pressure photoionization (APPI)–(IMS)–MS (mass spectrometry) coupling. For testing the separation efficiency between substances with similar properties, we applied both methods for the different structural isomers (*ortho*-, *meta*- and *para*-disubstituted compounds) of fluorotoluene, fluoroaniline, difluorobenzene, chlorotoluene, chloroaniline, chlorofluorobenzene, dichlorobenzene, bromotoluene, bromofluorobenzene and dibromobenzene. Because isomeric compounds have the same mass, possible differences in the ion mobility spectra can be attributed to their different structure. Moreover, the substances investigated here are important analytes in environmental chemistry and process monitoring in industry. The necessity for the identification of different isomers results from differences in risk potential. According the safety data sheets, the *o*-disubstituted isomers are mostly classified as more hazardous to the environment in comparison with the other isomers. Although the separation of large isomers is described literature using high resolution IMS as laboratory instruments with drift tubes of 20 cm and more [28–30], our approach includes the comparison of capability of IMS and DMS for isomeric ion separation using field-deployable and transportable spectrometers.

2. Experimental

The DMS measurements were undertaken using a SIONEX SDP-1 spectrometer (Sionex Corporation, Bedford). The spectrometer was coupled with a gas chromatograph (GC HP 5890, Agilent, Palo Alto). The GC was equipped with a 30 m SE-54 capillary column (0.32 mm inner diameter, 1 μm film thickness). The initial temperature was 40 °C (0.5 min). Subsequently, the temperature was increased at 10 °C min^{-1} to 220 °C. The final temperature was held for 10 min. Between 100 and 500 ng of each substance were injected (split/splitless injector, 220 °C, split ratio 1:20). The carrier gas flow from the GC (about 3 mL min^{-1} nitrogen) was additionally rarefied with 250 mL min^{-1} of nitrogen: therefore maximum concentrations of 6 ng mL^{-1} were transferred to DMS. Nitrogen with moisture of approximately 30 ppm$_V$ was used as carrier gas.

The DMS spectra display the compensation voltage versus the intensity of ion current and were obtained at different RF fields: (600 V = 12 kV cm^{-1}, 800 V = 16 kV cm^{-1}, 1000 V = 20 kV cm^{-1}, 1200 V = 24 kV cm^{-1}, 1350 V = 27 kV cm^{-1}, 1500 V = = 30 kV cm^{-1}). The electric field of the drift channel was provided with an asymmetric square waveform with a frequency of around 1.3 MHz.

The IMS measurements were performed with RAID 1 ion mobility spectrometers (BRUKER, Leipzig, Germany). The spectrometers are equipped with a membrane inlet and operated with a bi-directional flow system. The operational parameters used to obtain the spectra were: temperature of inlet system, 80 °C; carrier gas flow rate, 25 L h^{-1}; drift gas flow rate, 25 L h^{-1}; electric field, 245 V cm^{-1}; temperature of drift tube, 80 °C; drift tube length, 58 mm; pressure, atmospheric pressure. Air was used as the carrier gas and drift gas. The samples were introduced using permeation vessels. The details of the sample introduction system used for IMS and its function were described previously [31]. Series of measurements with increasing concentrations were carried out for each compound in order to estimate any concentration correlation of the ion mobility spectra. However, no significant changes in the number and position of product ion peaks within the ion mobility spectra with increasing concentrations (up to 200 ng mL^{-1}) were found for any substance.

The drift velocity (v_d) was calculated from the drift time and the length of the drift tube and is proportional to the strength of the electric field (E) and the mobility coefficient (K). The mobility of ions was normalized to temperature and pressure and reported as reduced mobility (K_o [cm^2 V s^{-1}]).

Both the RAID 1 ion mobility spectrometer and the DMS were equipped with a photoionization (PI) source. The PI source was equipped with a krypton lamp providing 10.0 eV (80%) and 10.6 eV (20%) photons and operated in similar conditions in these two devices. The same gas-phase chemistry can therefore be expected for the formation of product ions.

Two different techniques were used to identify the product ions formed. The photoionization source was directly used as the ion source of a triple quadrupole mass spectrometer API-*III* from PE-SCIEX (Toronto, Canada). Furthermore, ion mobility spectrometry–mass spectrometer coupling was used. A simplified drift tube with stainless steel drift rings and Teflon insulating rings was attached to the mass spectrometer. Coupling these techniques usually entails adjusting the operational parameters of the ion mobility spectrometer due to the small sample amount which can be transferred to the mass spectrometer and the necessary compatibility of the electric fields between the two devices. For these reasons, the measurements were taken with a longer shutter pulse (2.2 ms) and a modified electric field design within a higher concentration range of compounds.

The Connolly surfaces [32] and volumes of the molecules were calculated on the basis of optimized molecular geometries with the CERIUS^2 software suite (Accelrys Inc., San Diego, USA). Geometry optimization was performed using the semi-empirical AM1 method [33] integrated into the SPARTAN 5.0 suite (Wavefunction, Inc., Irvine, USA). The surfaces and volumes of neutral sample molecules were calculated as a rough approximation of the collisional cross-section. We assumed that the geometry of benzene rings only alters insignificantly if $[M]^+$ ions are formed or that all the molecules investigated change in a comparable manner. The dipole moments were calculated after geometry optimization using AM1 method for the radical cations, with the Hyperchem 5 software (Hypercube Inc., Gainesville, USA). The charge distribution was calculated for the radical cations using the density functional theory (DFT method/B3-LYP) at the 6-31G(d,p) level integrated into the Hyperchem 7.5 software (Hypercube Inc.).

3. Results and discussion

The most likely ionization pathway using PI at atmospheric pressure provides positive product ions related to M^+ for aromatic hydrocarbons. The formation of clustered ions and additional ion-molecule reactions are considerably minimized in comparison to ^{63}Ni ionization or discharge ionization and the spectra obtained using PI are therefore not so complex [34]. For this reason, we performed our measurements with PI. Ionization sources with identical PI discharge lamps were used for both techniques, IMS and DMS. As can be seen from Table 1, the ionization energies of investigated aromatic compounds are below 10 eV and permit direct ionization using the PI source used.

3.1. Mass spectrometric identification of product ions

For the identification of the product ions formed, the PI source (partly combined with IMS) was coupled to a mass spectrometer. The experimental details are described in previous publications [35,36]. Although there is always a problem in transferring ions from the high pressure of the mobility spectrometer to the vacuum of the mass spectrometer, and ions, especially weakly bound cluster ions, may be collisionally decomposed in the interface region, or adiabatic cooling may encourage ion-neutral association, only this coupling permits information regarding the structure of the product ions formed.

We investigated the 1,2-disubstituted compounds using the APPI–(IMS)–MS coupling. The results in Table 1 show the preferred formation of $M^{\bullet+}$ product ions which appear as a base peak in nearly all mass spectra of compounds investigated. Furthermore, clustered product ions were found with lower relative abundances in comparison to $M^{\bullet+}$ ions for halogenated toluenes and halogenated anilines. These additional peaks appear at a mass difference of M + 16 for the investigated halogenated toluenes. This mass difference of 16 indicates the formation of $MO^{\bullet+}$ ions. The ionization mechanisms providing these ions have been described in the literature for benzene and toluene [37] using APPI–MS. An exceptional behaviour was observed for 2-bromotoluene where the molecular ion peak is detectable with a relative abundance of 60%. The base peak appears at $m/z = 122$ and does not show the typical isotopic pattern of bromine-containing substances. The formation of these ions therefore results from the cleavage of bromine due to the lower bond strengths. The bond strength of C_6H_5–Br (81 kcal mol^{-1}) is lower than C_6H_5–Cl (96 kcal mol^{-1}) or C_6H_5–F (126 kcal mol^{-1}) [38]. The mass spectra of halogenated anilines (Table 1) differ from those obtained for halogenated toluenes. In addition to the $M^{\bullet+}$ ions, peaks with a mass difference of M + 18 can be detected for the halogenated anilines and the attachment of water can therefore be supposed due to this mass difference.

The ions of low intensity observed for toluenes and anilines, other than the molecular ions, must be due to the further reaction

Table 1
Physicochemical properties of compounds investigated and results of APPI–(IMS)–MS measurements

Substance	Molecular weight	Dipole moment [D]	Ionization energy [eV]	Surface [Å^2]	Volume [Å^3]	Results of APPI–(IMS)–MS investigations (*ortho*-disubstituted isomers)
2-Fluorotoluene	110	2.47	8.91	132.854	110.226	$M^{\bullet+}$ (100%), $(M+16)^{\bullet+}$ (64%), technique: APPI–IMS–MS
3-Fluorotoluene	110	2.42	8.91	135.916	111.909	
4-Fluorotoluene	110	2.60	8.79	133.432	109.888	
2-Fluoroaniline	111	3.99	8.29	128.210	105.362	$M^{\bullet+}$ (100%), $(M+18)^{\bullet+}$ (79%), technique: APPI–IMS–MS
3-Fluoroaniline	111	6.63	8.32	129.057	105.822	
4-Fluoroaniline	111	7.04	8.09	129.025	105.435	
1,2-Difluorobenzene	114	4.31	9.29	126.324	100.772	$M^{\bullet+}$ (100%), technique: APPI–MS
1,3-Difluorobenzene	114	2.90	9.33	121.965	98.830	
1,4-Difluorobenzene	114	0.00	9.16	123.954	99.528	
2-Chlorotoluene	126	3.15	8.72	142.127	120.473	$M^{\bullet+}$ (100%), $(M+16)^{\bullet+}$ (35%), technique: APPI–IMS–MS
3-Chlorotoluene	126	3.35	8.76	143.631	120.028	
4-Chlorotoluene	126	3.32	8.69	142.602	118.732	
2-Chloroaniline	127	4.54	8.20	133.424	112.161	$M^{\bullet+}$ (100%), $(M+18)^{\bullet+}$ (24%), technique: APPI–IMS–MS
3-Chloroaniline	127	7.68	8.10	136.789	114.266	
4-Chloroaniline	127	8.16	7.99	138.877	115.000	
2-Chlorofluorobenzene	130	4.40	9.17	126.539	104.765	$M^{\bullet+}$ (100%), technique: APPI–MS
3-Chlorofluorobenzene	130	3.17	9.22	129.385	106.893	
4-Chlorofluorobenzene	130	0.62	9.10	130.728	107.364	
1,2-Dichlorobenzene	146	4.27	9.06	141.344	117.955	$M^{\bullet+}$ (100%), technique: APPI–MS
1,3-Dichlorobenzene	146	2.30	9.10	137.372	115.336	
1,4-Dichlorobenzene	146	0.00	8.92	142.982	118.154	
2-Bromotoluene	170	6.28	8.56	146.076	125.082	$M^{\bullet+}$ (60%), $[(M–Br)+32]^{\bullet+}$ (100%), technique: APPI–IMS–MS
3-Bromotoluene	170	6.96	8.73	146.836	124.219	
4-Bromotoluene	170	6.83	8.68	146.166	122.790	
2-Bromofluorobenzene	174	7.06	9.12	132.163	110.396	$M^{\bullet+}$ (100%), technique: APPI–MS
3-Bromofluorobenzene	174	6.18	9.18	132.830	110.832	
4-Bromofluorobenzene	174	4.09	9.01	133.610	111.195	
1,2-Dibromobenzene	234	7.01	8.98	149.124	126.794	$M^{\bullet+}$ (100%), technique: APPI–MS
1,3-Dibromobenzene	234	4.61	9.01	146.275	124.734	
1,4-Dibromobenzene	234	0.00	8.82	150.968	127.398	

IE: ionization energies were obtained from: http://webbook.nist.gov/); surfaces and volumes of molecules were calculated using CERIUS^2 software; the dipole moments were calculated for radical cations using Hyperchem 5 software.

of the molecular ions. Complex chemistry has been observed in the reactions of the analytes with air molecules [37]. However, the single large peak in each mobility spectrum from photoionization in the IMS and DMS analyzer, obtained under drier and more controlled conditions than those used in the APPI–MS experiments, is due to the molecular ion.

Only the molecular ion peaks ($M^{\bullet+}$) were detected for dihalogenated aromatics (1,2-difluorobenzene, 1,2-dichlorobenzene, 1,2-dibromobenzene, 2-bromofluorobenzene and 2-chlorofluorobenzene) using PI–IMS–MS. Although the ion identification was performed using MS in combination with IMS, the formation of identical ions can be expected using DMS because the ion formation in the APPI source is not affected by the method of ion separation and identical ion sources were used for all investigations.

3.2. Results of IMS measurements

The reduced mobility values of positive product ions obtained using traditional time-of-flight IMS are summarized in Table 2. As can be seen from these results, the positive spectra consist of one major product ion peak. These peaks obviously result from the formation of product ions related to M^+ as shown using the mass spectrometric investigations. With the exception of 2-chloroaniline, the structural isomers of the compounds investigated show comparable reduced mobility values within the typical variation in reduced mobility of about 0.01 cm^2 V s^{-1}. These differences mainly arise from the standard deviation in drift time of 0.06 ms using the experimental conditions described above. No significant differences in ion mobility spectra were therefore established for the separate *ortho*-, *meta*- and *para*-disubstituted isomers of each compound, and IMS does not permit the differentiation between the structural isomers.

As known from the theory of ion mobility, ion mobility is influenced by the operational parameters used as well as the mass of analytes (m) and their collisional cross-section. The collisional cross-section (Ω_D) includes structural parameters (physical size and shape) and the resultant electronic factors describing the ion-neutral interaction forces [6]. The influence of ionic mass on ion mobility can be described by mass-to-mobility

Table 2
Reduced mobility values obtained by time-of-flight IMS and compensation voltages detected using DMS depending on the RF field

Substance	PI–IMS ($cm^2\ V\ s^{-1}$)	Compensation voltage (CV) detected using DMS depending on RF field with a peak amplitude of [$V\ cm^{-1}$]					
		12,000	16,000	20,000	24,000	27,000	30,000
Isomers of fluorotoluene (molecular weight: 110)							
2-Fluorotoluene	1.97	−1.63	−3.27	−5.86	−9.38	−13.61	−18.54
					−5.86	−6.08	−7.50
3-Fluorotoluene	1.97	−1.63	−3.27	−5.62	−9.14	−13.14	−17.37
					−5.62	−5.65	−7.03
4-Fluorotoluene	1.97	−1.63	−3.27	−5.62	−9.38	−13.61	−18.31
					−6.09	−7.03	−7.73
Isomers of fluoroaniline (molecular weight: 111)							
2-Fluoroaniline	1.91	−0.82	−1.58	−2.73	−4.64	−6.17	−7.32
3-Fluoroaniline	1.89	−1.20	−1.96	−3.49	−5.02	−6.17	−7.32
4-Fluoroaniline	1.89	−1.20	−2.35	−3.49	−5.41	−6.55	−7.70
Isomers of difluorobenzene (molecular weight: 114)							
1,2-Difluorobenzene	1.99	−1.20	−2.35	−3.49	−4.64	−5.41	−5.41
1,3-Difluorobenzene	2.00	−1.20	−2.35	−3.11	−4.26	−5.02	−5.02
1,4-Difluorobenzene	2.00	−1.58	−2.35	−3.49	−4.64	−5.41	−5.79
Isomers of chlorotoluene (molecular weight: 126)							
2-Chlorotoluene	1.89	−1.20	−1.96	−3.11	−4.64	−5.41	−5.79
3-Chlorotoluene	1.89	−1.20	−1.96	−2.73	−3.88	−4.64	−5.02
4-Chlorotoluene	1.88	−1.20	−2.35	−3.49	−5.02	−5.79	−6.55
Isomers of chloroaniline (molecular weight: 127)							
2-Chloroaniline	1.84	−0.82	−1.20	−1.96	−3.88	−5.02	−5.79
3-Chloroaniline	1.80	−0.82	−1.20	−2.35	−3.49	−4.64	−5.41
4-Chloroaniline	1.81	−1.20	−1.96	−3.11	−4.64	−5.41	−6.55
Isomers of chlorofluorobenzene (molecular weight: 130)							
2-Chlorofluorobenzene	1.92	−1.58	−2.73	−3.88	−5.41	−6.55	−7.32
3-Chlorofluorobenzene	1.91	−1.58	−2.35	−3.49	−5.02	−6.17	−6.55
4-Chlorofluorobenzene	1.91	−1.58	−2.73	−4.26	−5.79	−6.55	−6.94
Isomers of dichlorobenzene (molecular weight: 146)							
1,2-Dichlorobenzene	1.84	−1.20	−1.96	−3.11	−4.26	−5.41	−5.79
1,3-Dichlorobenzene	1.83	−1.20	−1.96	−2.92	−3.88	−4.64	−5.02
1,4-Dichlorobenzene	1.82	−1.20	−2.35	−3.49	−4.64	−5.41	−5.79
Isomers of bromotoluene (molecular weight: 170)							
2-Bromotoluene	1.82	−0.82	−1.58	−2.73	−3.88	−4.64	−5.41
3-Bromotoluene	1.81	−0.82	−1.58	−2.35	−3.11	−3.69	−4.07
4-Bromotoluene	1.81	−1.20	−1.96	−3.11	−4.26	−5.02	−5.41
Isomers of bromofluorobenzene (molecular weight: 174)							
2-Bromofluorobenzene	1.84	−1.20	−1.96	−3.11	−4.26	−5.41	−6.17
3-Bromofluorobenzene	1.84	−1.20	−1.96	−3.11	−4.26	−5.02	−5.41
4-Bromofluorobenzene	1.85	−1.58	−2.35	−3.49	−5.02	−5.79	−6.55
Isomers of dibromobenzene (molecular weight: 234)							
1,2-Dibromobenzene	1.72	−0.82	−1.58	−2.35	−3.11	−3.88	−4.26
1,3-Dibromobenzene	1.70	−0.82	−1.20	−1.96	−2.35	−2.73	−3.11
1,4-Dibromobenzene	1.70	−0.82	−1.58	−2.35	−3.11	−3.88	−4.26

correlation lines, which are known for different chemical families. These mass-to-mobility correlation lines demonstrate to a sufficient approximation that mass effects are the dominating parameters. Structural differences are of minor importance, but cannot be ruled out. As known from the literature for ^{63}Ni ionization, structural differences can entail errors in the correlation between ionic mass and ion mobility of between 5 and 20% [39] within comparable chemical families.

Considering the mass dependence of reduced mobility values (Fig. 1a), a considerable dispersion of the values around the regression line can be established. In addition to mass effects, the drift time is therefore considerably affected by properties determining the collisional cross-section. Although the radical cations of halogenated anilines have the lowest ionic mass in comparison with the corresponding dihalogenated benzenes and halogenated toluenes, these compounds have the lowest

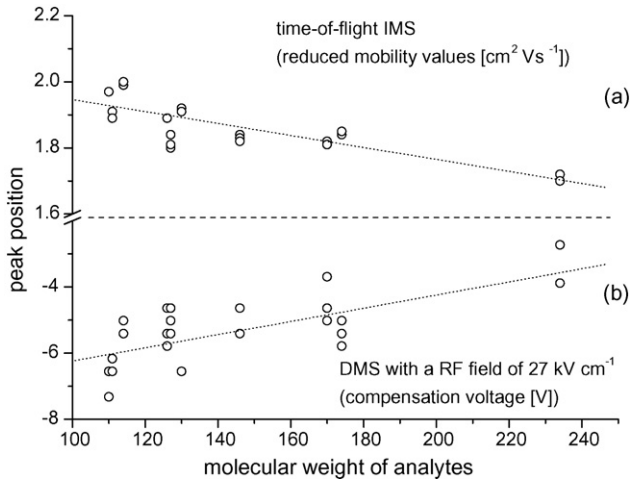

Fig. 1. Peak positions of isomeric compounds depending on their molecular weight (upper frame (a) reduced mobility values obtained using IMS, in bottom frame (b) compensation voltages detected using DMS).

drift velocity. Concerning the fluorine containing substances, a decreasing drift velocity was found in the order difluorobenzene (molecular weight: 114; $K_0 = 2.00\,cm^2\,V\,s^{-1}$) > fluorotoluene (molecular weight: 110; $K_0 = 1.97\,cm^2\,V\,s^{-1}$) > fluoroaniline (molecular weight: 111; $K_0 = 1.90\,cm^2\,V\,s^{-1}$) while for chlorine containing substances the highest drift velocity was established for chlorotoluene (molecular weight: 126; $K_0 = 1.89\,cm^2\,V\,s^{-1}$) in comparison with dichlorobenzene (molecular weight: 146; $K_0 = 1.83\,cm^2\,V\,s^{-1}$) and chloroaniline (molecular weight: 127; $K_0 = 1.82\,cm^2\,V\,s^{-1}$). The difference in reduced mobility values between bromotoluene (molecular weight: 170; $K_0 = 1.81\,cm^2\,V\,s^{-1}$) and dibromobenzene (molecular weight: 234; $K_0 = 1.71\,cm^2\,V\,s^{-1}$) is $0.1\,cm^2\,V\,s^{-1}$. Therefore, the calculation of ionic mass using the derived mass-to-mobility correlation line (logarithm of ionic mass versus reduced mobility values: $\log m = -1.0664\,K_0 + 4.1379$; $R^2 = 0.7328$) of these compounds entails errors of up to 30%. Unfortunately, our attempts to interpret these differences by consulting some individual structural parameters were not successful. The differences in Connolly surfaces and volumes (Table 1) do not correlate with the different drift times. In addition to mass effects and the physical size and shape, the electronic factors due to the different substituent effects therefore have an evident influence on drift behavior. If $M^{\bullet+}$ product ions are formed for all substances, the longer drift time of anilines evidently results from a stronger interaction of ions with the drift gas molecules. These stronger interactions can obviously be ascribed to the substituent effect of the amino group. Considering the dipole moments calculated for radical cations (Table 1), enhanced values were established for the isomers of fluoraniline and chloroaniline in comparison with the corresponding dihalogenated compounds and halogenated toluenes. However, we cannot demonstrate a well-defined correlation.

Negative product ions were only observed for the isomers of dibromobenzene. These product ion peaks were detected at $2.50\,cm^2\,V\,s^{-1}$ for all isomers of dibromobenzene and are obviously formed by the cleavage of bromine from the molecule due to dissociative electron attachment.

3.3. Results of DMS measurements

The results of the measurements using DMS are summarized in Table 2. The data show the detected values of compensation voltage depending on the RF field. With the exception of the isomers of fluorotoluene, spectra with one major peak were obtained for all substances. As can be seen from the data in Table 2, only a small influence of ionic mass and structure on the compensation voltage detected can be established using low asymmetric RF electric fields. The isomeric compounds provide similar values of compensation voltage using RF fields of 12 and $16\,kV\,cm^{-1}$. This phenomenon is well-established and can be explained by the non-significant changing of the alpha-parameter of ions in low-field conditions [25]. The short drift region (1.5 cm) and the short residence time (~1–2 ms) provide only small differences in the drift behavior for the compounds investigated and the additional processes caused by the high electric field (clustering–declustering mechanisms, deformation and variation in cross-section) are not significant up to field strengths of $16\,kV\,cm^{-1}$ for these substances. However, differences in compensation voltage can be observed with increasing asymmetric RF electric fields. The observed significant shifts in the compensation voltage are illustrated in Fig. 2 for the spectra of 1,4-dichlorobenzene and 4-bromotoluene depending on the RF field. As can be seen from these spectra, the detection of ions at higher asymmetric RF electric fields requires more negative compensation voltages. Considering the compensation voltages detected at RF fields of 27 and $30\,kV\,cm^{-1}$ (Table 2), distinct differences between the isomeric compounds were established. These differences are illustrated in Fig. 1 in comparison to traditional time-of-flight IMS. DMS (Fig. 1b) permits the differentiation between most isomeric compounds investigated, while IMS provides fewer signals for each ionic mass (Fig. 1a). Obviously, the structure of ions formed has a more distinct influence on ion trajectories in highly asymmetric RF electric fields in comparison with IMS and causes differences in field dependence for isomeric aromatic compounds. However, the more distinct influence of structural features on DMS spectra leads to a considerable dispersion of data points for each ionic mass and a correlation between ionic mass and detected compensation voltage cannot be derived. Nevertheless, the enhanced structural influence on DMS spectra can be utilized for the differentiation of isomeric compounds by deviating correlation lines between the detected compensation voltage and the RF field used. Such correlation lines are shown in Fig. 3 for the structural isomers of bromofluorobenzene and chlorotoluene by way of example. Depending on the ionic mass and structure, different shapes of regression lines were found which permit the differentiation of most of the isomers investigated.

With the exception of fluoroaniline, the structural isomers with a substitution in 1,3-position (*meta*-disubstituted substances) provide more positive values of compensation voltage in comparison with 1,2- (*ortho*) and 1,4- (*para*) disubstituted compounds; the differences in compensation voltage vary between 0.5 and 1.5 V. Therefore, the 1,3-disubstituted isomers can be clearly differentiated from the other isomers while the 1,2- and 1,4-disubstituted isomers cannot be differentiated for each

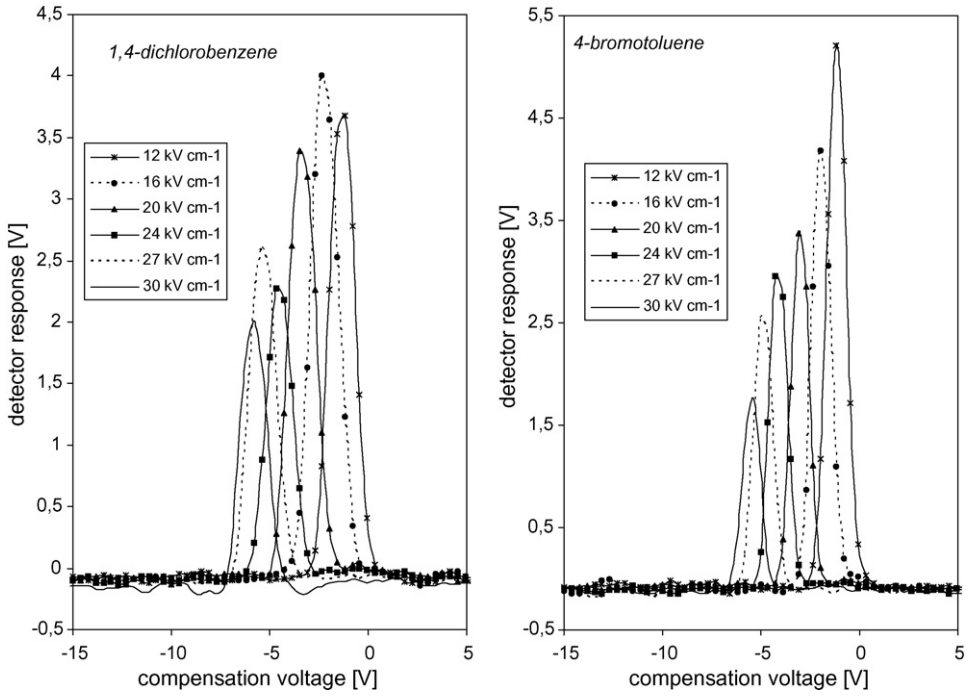

Fig. 2. Ion mobility spectra (PI–DMS) depending on the strength of RF field.

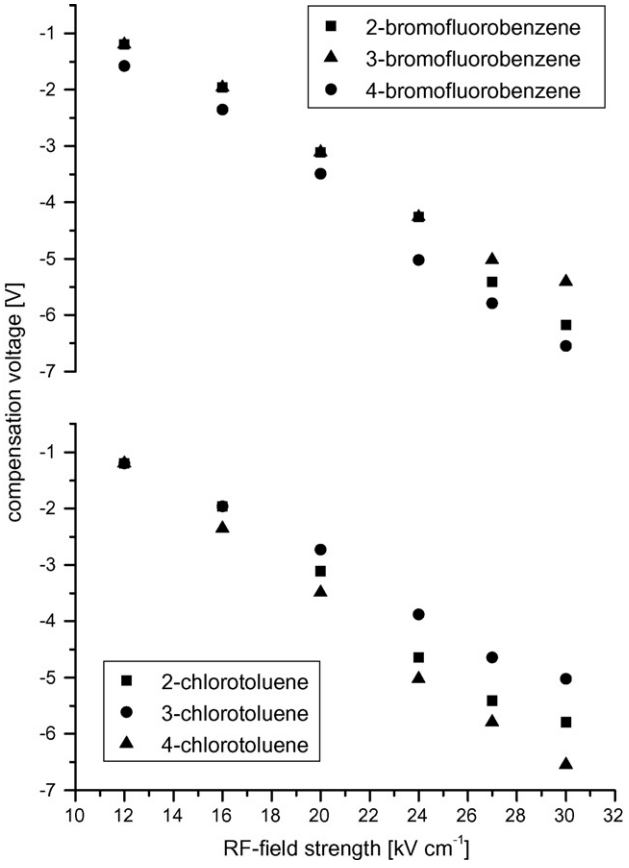

Fig. 3. Dependence of detected compensation voltage (PI–DMS) on the RF field.

compound. The detection of 1,3-disubstituted substances at more positive values of compensation voltage indicates more intensive interactions within the high electric field; probably this shift implies a higher level of clustering. However, there is no correlation between the deviating behaviour of 1,3-disubstituted compounds with the properties of the substances shown in Table 1. Therefore, we calculated the charge distribution within the $M^{\bullet+}$ ions with *ab initio* calculations using the density functional theory (DFT) method. However, we cannot explain the deviating behavior of structural isomers using these data. Although we found differences in charge distribution depending on the position of substituents, we cannot correlate these properties with the above-mentioned processes in the high electric field.

While nearly all the isomers investigated provide one major product ion peak and the most positive compensation voltage was detected for the 1,3-disubstituted substances, a deviating behavior was observed for the isomers of fluorotoluene and fluoroaniline. In addition to product ion peaks which were detected in the range between −17.37 and −18.54 V for the isomers of fluorotoluene, peaks with a comparatively low relative abundance (5–20%) were found between −7.03 and −7.73 V for these isomers. The ions with the more positive compensation voltage are detectable at RF fields above 1200 V (24 kV cm^{-1}). However, the detected compensation voltage of these ions is comparable with those obtained for the single peaks of the other substances investigated at the same RF field (between −3.11 and −7.32 V). As known from the literature [2], the occurrence of ions at more negative values of compensation voltage indicates a lower ionic mass and these ions can therefore be attributed to fragment ions. However, the formation of fragment ions must be caused by processes in the high electric field of the drift channel

and not within the ion source, due to the above-mentioned bond energies. Such phenomena were recently described in the literature [22] for investigations using DMS. In contrast to all the other structural isomers, 3-fluoroaniline provides similar compensation voltages in comparison with the 2-fluoroaniline and does not provide the most positive compensation voltage.

As described above, the stronger influence of structure on the compensation voltage provide only a weak correlation between the detected compensation voltage and the ionic mass. However, the measurements using traditional time-of-flight IMS have also shown that the ionic mass is not the dominating parameter and a more distinct influence of electronic structure on the drift behavior was established. The correlation between the reduced mobility values and compensation voltages (Fig. 4) indicate a similar dependence of drift behavior on the physicochemical properties of substances for both methods of ion separation. Fig. 4 shows this correlation for 1,4-disubstituted compounds by way of example. The peak with the more positive compensation voltage was used for 4-fluorotoluene. Comparable correlations were also obtained for the other isomers using RF fields of 27 and 30 kV cm^{-1} in DMS. A correlation between the peak positions of ions in IMS and DMS is clearly recognizable. However, a deviating behavior was observed for the isomers of difluorobenzene.

Obviously, fluorine-containing substances generally have a different behavior in high electric fields in comparison with chlorine-containing and bromine-containing substances. Although we cannot attribute this deviating behavior to certain properties, the different substituent effects can be supposed as the possible cause. The influence of substituents is essentially influenced by their electronegativity. Fluorine has the highest electronegativity (4.42) in comparison to chlorine (3.54) and bromine (3.24). These differences are reflected in the calculated charge distribution of ions where a stronger localization of the positive charge was established for fluorine containing compounds. These differences in charge distribution can be responsible for different mechanisms of formation and dissociation of ions and ion clusters.

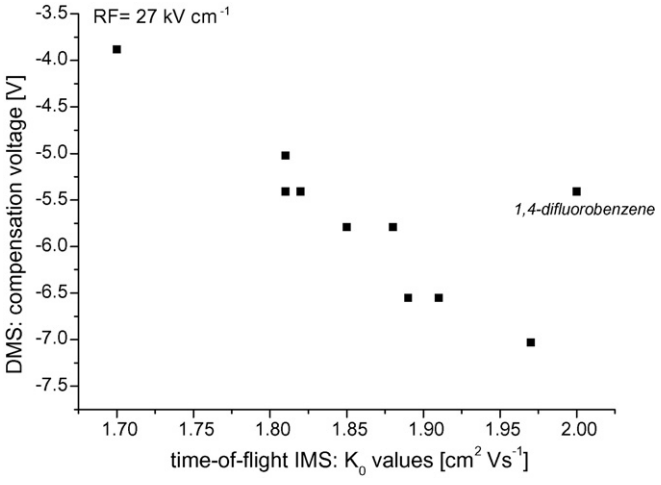

Fig. 4. Correlation between the reduced mobility values obtained using time-of-flight PI–IMS and compensation voltages detected using PI–DMS with an RF field of 27 kV cm^{-1} (*para*-disubstituted compounds).

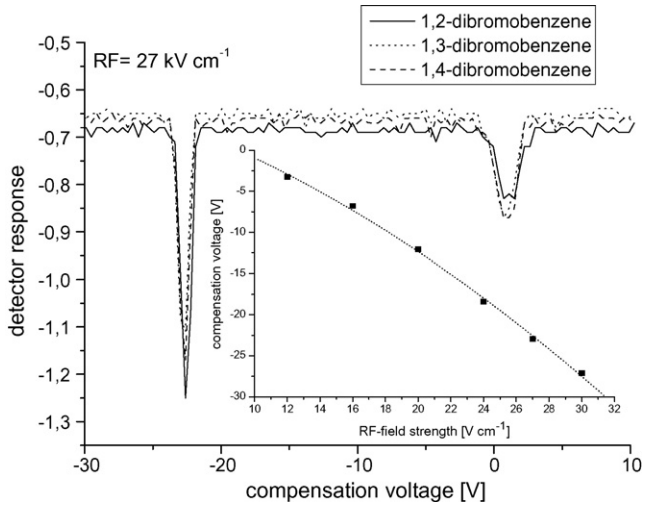

Fig. 5. Negative DMS spectra of dibromobenzene and field dependence of negative product ions (bromine).

One attraction of DMS is the simultaneous detection of positive and negative product ions. Regarding the substances investigated, negative product ions were found for all isomers of dibromobenzene and bromofluorobenzene while no negative ions were observed for bromotoluene and all chlorinated and fluorinated substances. These negative product ions appear at the same value of compensation voltage for the isomers of both compounds and show a shift to more negative values with a stronger asymmetric RF electric field (−3.24 V at 12 kV cm^{-1}; −6.79 V at 16 kV cm^{-1}; −12.10 V at 20 kV cm^{-1}; −18.41 V at 24 kV cm^{-1}; −22.93 V at 27 kV cm^{-1}; −27.12 V at 30 kV cm^{-1}). The field dependence of these product ions and the negative DMS spectra of dibromobenzene are shown in Fig. 5. The occurrence of these product ions at the same value of compensation voltage indicate the formation of comparable product ions which can be attributed to the formation of bromine due to dissociative electron attachment reactions during ionization. Although bromine has the lowest bond energy to the aromatic ring, it is noticeable that these ions can only be observed if the second substituent has electron-withdrawing properties.

4. Conclusion

The field dependence of compensation voltage on the structure of ions permits the distinction between different isomeric compounds with another constitution in contrast to conventional IMS. However, the separation efficiency of ion filtering by DMS strongly depends on the RF field used. While comparable signals are detected using low RF fields, differences in compensation voltage can be observed with increasing RF fields. The differences in DMS spectra observed for the investigated isomeric aromatic hydrocarbons can be attributed to the different behavior of ions formed in the high electric field of the drift channel. Therefore, information from the DMS spectrum complements conventional IMS by providing the relationship between the compensation voltage detected and the electric field strength. The simultaneous detection of positive and negative ions using

DMS permits fast additional information for substances forming negative ions.

Acknowledgements

Dr. H. Borsdorf would like to acknowledge the support of the Sionex Corporation by their provision of the DMS. Furthermore, the authors would like to thank the Deutsche Forschungsgemeinschaft (DFG) for kindly funding this work. Thanks to Prof. H.-J. Hofmann (University of Leipzig, Institute of Biochemistry, Leipzig, Germany) and Prof. J. Stone (Queen's University Kingston, Department of Chemistry, Ontario, Canada) for their support in carrying out the molecular modeling.

References

[1] I.A. Buryakov, E.V. Krylov, L.A. Makas, E.G. Nazarov, V.V. Pervukhin, U.K. Rasulev, Sov. Tech. Phys. Lett. 17 (1991) 446.
[2] R.A. Miller, G.A. Eiceman, E.G. Nazarov, A.T. King, Sens. Actuators B 67 (2000) 300.
[3] G.A. Eiceman, E.G. Nazarov, R.A. Miller, E. Krylov, A.M. Zapta, Analyst 127 (2002) 466.
[4] J. Xu, W.B. Whitten, J.M. Ramsey, Anal. Chem. 72 (2000) 5787.
[5] R. Guevremont, Can. J. Anal. Sci. Spectrosc. 49 (2004) 105.
[6] G.A. Eiceman, Z. Karpas, Ion Mobility Spectrometry, CRC Press, Boca Raton, 2005, p.136.
[7] R.H.St. Louis, H.H. Hill, Trends Anal. Chem. 21 (1990) 321.
[8] J.I. Baumbach, G.A. Eiceman, Appl. Spectrosc. 53 (1999) 388A.
[9] R.A. Miller, E.G. Nazarov, G.A. Eiceman, A.T. King, Sens. Actuators A 91 (2001) 201.
[10] G.E. Spangler, R.A. Miller, Int. J. Mass Spectrom. 214 (2002) 95.
[11] E. Krylov, Int. J. Mass Spectrom. 225 (2003) 39.
[12] B. Ells, D.A. Barnett, R.W. Purves, R. Guevremont, J. Environ. Monit. 2 (2000) 393.
[13] G.A. Eiceman, E.G. Nazarov, B. Tadjikov, R.A. Miller, Field Anal. Chem. Technol. 4 (2000) 297.
[14] G.A. Eiceman, E. Krylov, B. Tadjikov, R.G. Ewing, E.G. Nazarov, R.A. Miller, Analyst 129 (2004) 297.
[15] M.A. McCooeye, M. Zoltan, B. Ells, D.A. Barnett, R.W. Purves, R. Guevremont, Anal. Chem. 74 (2002) 3071.
[16] G.A. Eiceman, E. Krylov, N.S. Krylova, E.G. Nazarov, R.A. Miller, Anal. Chem. 76 (2004) 4937.
[17] H. Schmidt, F. Tadjimukhamedov, I.V. Mohrenz, G.B. Smith, G.A. Eiceman, Anal. Chem. 76 (2004) 5208.
[18] G.A. Eiceman, B. Tadjikov, E. Krylov, E.G. Nazarov, R.A. Miller, J. Westbrook, P. Funk, J. Chromatogr. A 917 (2001) 205.
[19] K. Venne, E. Bonneil, K. Eng, P. Thibault, Anal. Chem. 77 (2005) 2176.
[20] G.E. Spangler, Field Anal. Chem. Technol. 4 (2000) 255.
[21] C.A. Veasey, C.L.P. Thomas, Analyst 129 (2004) 198.
[22] G.R. Lambertus, C.S. Fix, S.M. Reidy, R.A. Miller, D. Wheeler, E.G. Nazarov, R. Sacks, Anal. Chem. 77 (2005) 7563.
[23] R. Guevremont, J. Chromatogr. A 1058 (2004) 3.
[24] D.S. Levin, P. Vouros, R.A. Miller, E.G. Nazarov, J.C. Morris, Anal. Chem. 78 (2006) 96.
[25] E. Krylov, E.G. Nazarov, R.A. Miller, B. Tadjikov, G.A. Eiceman, J. Phys. Chem. A 106 (2002) 5437.
[26] G.A. Eiceman, N. Krylova, E. Krylov, J.A. Stone, Int. J. Ion Mobility Spectrom. 6 (2003) 43.
[27] N. Krylova, E. Krylov, G.A. Eiceman, J.A. Stone, J. Phys. Chem. A 107 (2003) 3648.
[28] L.M. Matz, H.H. Hill, Anal. Chim. Acta 457 (2002) 235.
[29] G.R. Asbury, H.H. Hill, J. Microcolumn Sep. 12 (2000) 172.
[30] L.M. Matz, H.H. Hill, Anal. Chem. 73 (2001) 1664.
[31] H. Borsdorf, H. Schelhorn, J. Flachowsky, H.-R. Döring, J. Stach, Anal. Chim. Acta 403 (2000) 235.
[32] L. Connolly, J. Appl. Crystallogr. 18 (1985) 499.
[33] M.J.S. Dewar, E.G. Zoebisch, E.F. Healy, J.J.P. Steward, J. Am. Chem. Soc. 107 (1985) 3902.
[34] H. Borsdorf, G.A. Eiceman, Appl. Spectrosc. Rev. 41 (2006) 323.
[35] H. Borsdorf, E.G. Nazarov, G.A. Eiceman, Int. J. Mass Spectrom. 232 (2004) 117.
[36] H. Borsdorf, J.A. Stone, G.A. Eiceman, Int. J. Mass Spectrom. 246 (2005) 19.
[37] M. Tubaro, E. Marotta, R. Seraglia, P. Traldi, Rapid Commun. Mass Spectrom. 17 (2003) 2423.
[38] D.R. Lide (Ed.), CRC Handbook of Chemistry and Physics, 73rd ed., CRC Press, Boca Raton, 1992.
[39] J. Stach, Analytiker Taschenbuch 16 (1997) 119.

Available online at www.sciencedirect.com
ScienceDirect
Talanta 71 (2007) 1703–1709
Talanta
www.elsevier.com/locate/talanta

PARAFAC and MCR-ALS applied to the quantitative monitoring of the photodegradation process of polycyclic aromatic hydrocarbons using three-dimensional excitation emission fluorescent spectra Comparative results with HPLC

Marta V. Bosco, M. Soledad Larrechi *

Department of Analytical and Organic Chemistry, Faculty of Chemistry, Rovira i Virgili University, Campus Sescelades, Marcel.li Domingo s/n, 43007 Tarragona, Spain

Received 6 April 2006; received in revised form 31 July 2006; accepted 1 August 2006
Available online 22 December 2006

Abstract

Two methods were developed for the simultaneous quantitative monitoring of photodegradation process of dibenz[*a*,*h*]anthracene (DibA), benz[*a*]anthracene (BaA), benz[*a*]pyrene (BaP) and benz[*k*]fluorantene (BkF) using excitation–emission fluorescence spectroscopy. Parallel factor analysis (PARAFAC) and multivariate curve resolution-alternating least squares (MCR-ALS) were satisfactory applied to the data obtained during this process. The results achieved were statistically compared by means of the joint interval test of slope and intercept, with the data obtained using the reference methodology, high performance liquid chromatography (HPLC) method. There are not significant differences between the methodologies proposed and the standard one, and may be a good alternative to the traditional methods of analysis for monitoring the degradation of these pollutants.

Keywords: Polycyclic aromatic hydrocarbons; PARAFAC; MCR-ALS; Photodegradation; Excitation–emission matrix

1. Introduction

Polycyclic aromatic hydrocarbons (PAHs) are one of the largest groups of chemical carcinogens and mutagens [1]. Demand for determining trace concentrations of these substances and removing them from the natural environment is constantly increasing [2].

Several methods based on the chemical destruction of very stable PAHs have been proposed and tested. Photodegradation is a particularly important methodology in this field, in which major progress is being made in oxidative methods for degrading organic compounds dissolved or dispersed in aquatic media [3,4]. The effectiveness of these methods is evaluated in terms of the time that the polluting agent takes to disappear, which is verified by analytical determination throughout the photodegradation process.

PAHs in complex mixtures are usually determined by gas chromatography (GC) [5] or high resolution liquid chromatography (HPLC) with either UV–visible diode array detectors (DAD) [4,6,7] or fluorescence detectors [8]. Several authors have recently described the use of full excitation–emission fluorescence spectra (EEM, excitation–emission matrix) for identifying and quantifying PAHs in aqueous solutions in combination with the additional information resources provided by such powerful chemometric tools as parallel factor analysis (PARAFAC) [9] or partial least squares regression (PLSR) [10].

One problem that is hindering the wider application of fluorescence spectroscopy for environmental monitoring is the intrinsic lack of selectivity in excitation and emission fluorescence measurements and several studies have discussed how best to increase the selectivity of these methods [11,12]. Recently, several authors have argued that data sets obtained from kinetic experiments help to increase the selectivity of spectroscopic determinations in the application of PARAFAC model [13].

In the optimization of the catalytic process at laboratory level, the ability to analyze multicomponent mixtures without a

* Corresponding author. Tel.: +34 977 559 559; fax: +34 977 558 446.
E-mail address: mariasoledad.larrechi@urv.net (M.S. Larrechi).

0039-9140/$ – see front matter © 2006 Elsevier B.V. All rights reserved.
doi:10.1016/j.talanta.2006.08.009

previous separation is particularly attractive because it would be a fast way of evaluating the effectiveness of a photodegradation process.

In this paper, we present the results of monitoring the photolysis process of a mixture of four analytes: dibenz[*a*,*h*]anthracene (DibA), benz[*a*]anthracene (BaA), benz[*a*]pyrene (BaP) and benz[*k*]fluorantene (BkF). PARAFAC [14,15] and multivariate curve resolution-alternating least squares (MCR-ALS) [16] were applied to the emission–excitation data collected. These results were compared with the ones obtained with HPLC. They were also analyzed in kinetic terms and the percentage of degradation, the degradation constant and the half life of each analyte, all habitual parameters in this area of study, were determined.

In the bibliographic review that we made, we found no studies similar to this one.

Previous studies on calibration with fluorescence excitation–emission matrices of PAHs and multivariate curve resolution methods have used prediction error as the most common means of measuring whether these methodologies were successful. A simultaneous study, using the two analytical techniques, HPLC with univariate calibration, and fluorescence with curve resolution methods, is necessary if their advantages and disadvantages are to be evaluated. It may be useful for drafting a protocol for using these methodologies in the quantitative monitoring of photodegradation processes. The ability of these methodologies in more complicated situations in which other PAHs may interfere will be studied in future work.

2. Experimental

2.1. Materials

All the reagents used were of analytical quality. The PAHs dibenz[*a*,*h*]anthracene (DibA, 97%), benz[*k*]fluorantene (BkF, 98%) benz[*a*]anthracene (BaA, 99%) and benz[*a*]pyrene (BaP, 97%) were obtained from Aldrich. The standard solutions were prepared by weighing the appropriate amount of reagent and dissolving it in acetonitrile (ACN). The pH was adjusted with phosphoric acid (Aldrich 85%). The solvents used for the photodegradation were ethanol (EtOH), acetonitrile (ACN) and Milli-Q quality water. They were obtained from Merck and were HPLC quality.

2.2. Instrumental

The photodegradation studies were carried out in a cylindrical annular batch reactor. The reactor consisted of an immersion quartz tube (2.5 cm i.d. and 38 cm long) which holds a low pressure mercury vapor lamp (LPML) of 15 W (Heraeus Noblelight, Germany). The light source emitted by the LPML is predominantly at 254 nm. The quartz tube was placed in a Pyrex glass outer reactor (0.7 l capacity). An Orion pH-meter was used to check the pH of the reacting mixture.

The spectrofluorimetric data were acquired on an Aminco–Bowman Series 2 Luminescence spectrometer (SLM Aminco, Rochester, NY, USA) equipped with a 150 W continuous xenon lamp and a PMT detector.

HPLC analyses were performed on an Agilent 1100 Series Fluorescence Detector (Germany) equipped with a programmable fluorescence detector. Chromatographic data were collected and recorded on an HP Chemstation Version A.06.01.

2.3. Photolysis experiments

The degradations were carried out in a cylindrical reactor, such as the one described in Section 2.2. The degradation mixture consisted of a solution containing the four analytes (DibA, BkF, BaA and BaP) at a concentration of 100 $\mu g\,l^{-1}$, the solvent volume ratio of water:alcohol:ACN was 50:40:10 and the pH was 2.5. The ACN was added to minimize the adsorption of the PHAs on the walls of the reactor. The total volume of the solution was 500 ml. The photodegradation was carried out at ambient temperature with stirring throughout the reaction (120 min).

Five-millilitre samples were taken through the reactor's sampling valve and the filtered solutions were kept in darkness. In the first 30 min, samples were taken every 2 min, and then every 10 min up to the 120 min of reaction time. A total of 25 samples were taken throughout the experiment.

2.4. Measurements

All solutions (individual standards and samples) were measured in the same conditions. Three-dimensional excitation–emission spectra were recorded between 360 and 450 nm in the emission domain and between 230 and 297 nm in the excitation domain, both at regular steps of 3 nm. The scanning rate of the monochromators was maintained at 30 $nm\,s^{-1}$. The excitation and emission monochromator slit widths were set to 4 nm. All measurements were made in a 10 mm quartz cell at 590 V. The fluorescence spectra were exported in ASCII format from the Instrument Software to MATLAB [17]. This information was then processed with the PARAFAC algorithm, obtained from the N-way toolbox [18] and with the MCR-ALS algorithm [19].

The analyses with HPLC were carried out with a 250 mm × 4 mm Tracer PAH C-18 reverse-phase column from Teknokroma (Barcelona, Spain) with a particle size of 5 μm. A 20 μl loop was used to directly inject the sample. A linear elution gradient programme was performed from 75% (v/v) ACN in water to 95% for 23 min at a flow rate of 1.5 $ml\,min^{-1}$. For

Table 1
Fluorescence detection conditions used to analyse PAHs

Time (min)	Wavelength (nm)		Analyte
	Excitation	Emission	
0	286	387	BaA
14	295	410	BkF/BaP
19.50	296	396	DibA

more sensitive detection of the PAHs, optimum excitation and emission wavelengths had to be used for each component and a wavelength detection program was developed for this purpose (Table 1).

3. Results and discussion

By way of example, Fig. 1 shows the EEM data matrix at time zero and the EEM matrices of each analyte at 100 ppb.

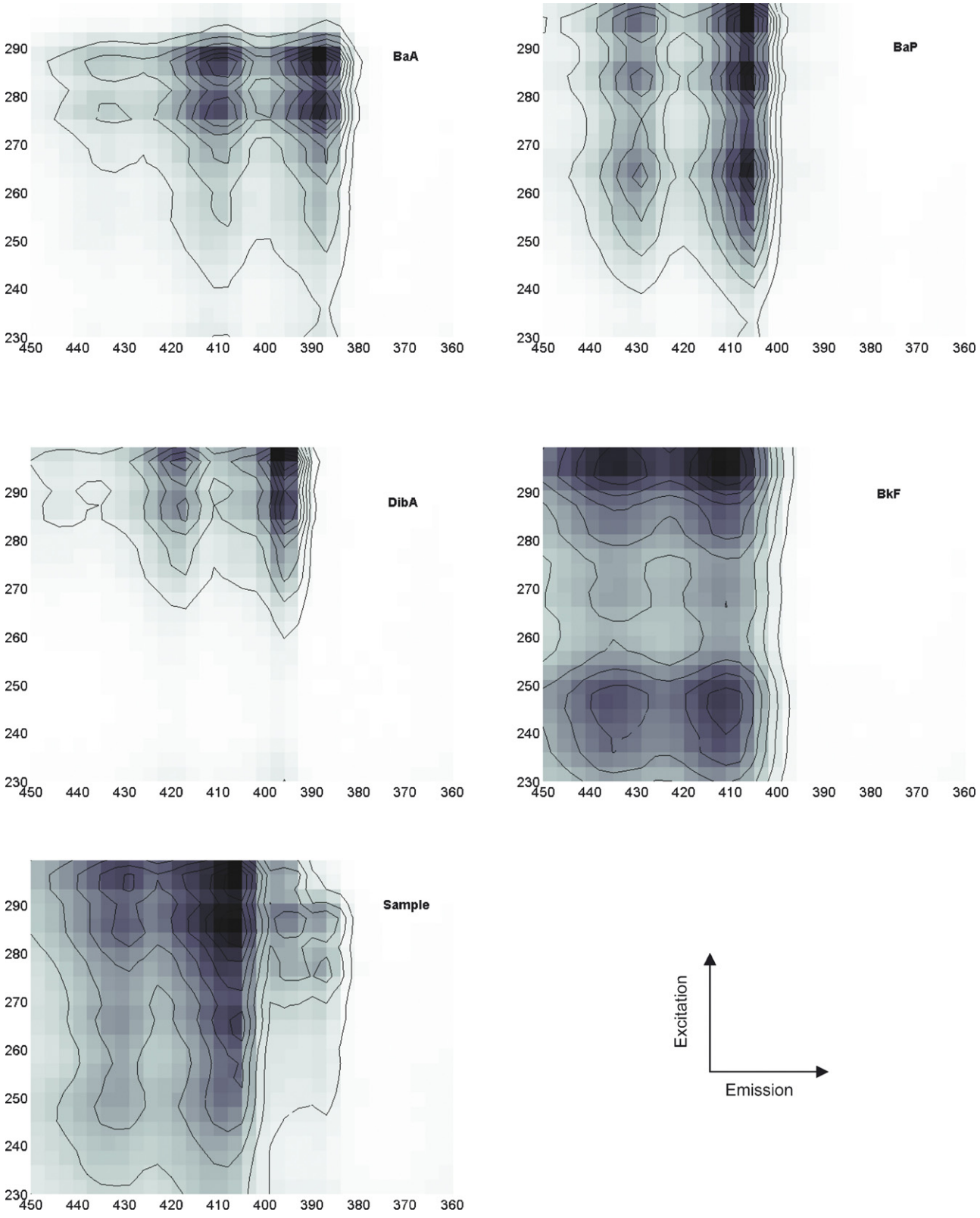

Fig. 1. EEM matrices for BaA, BkF, DibA and BaP at 100 ppb, and the EEM data matrix of a sample at time zero of the photoreaction.

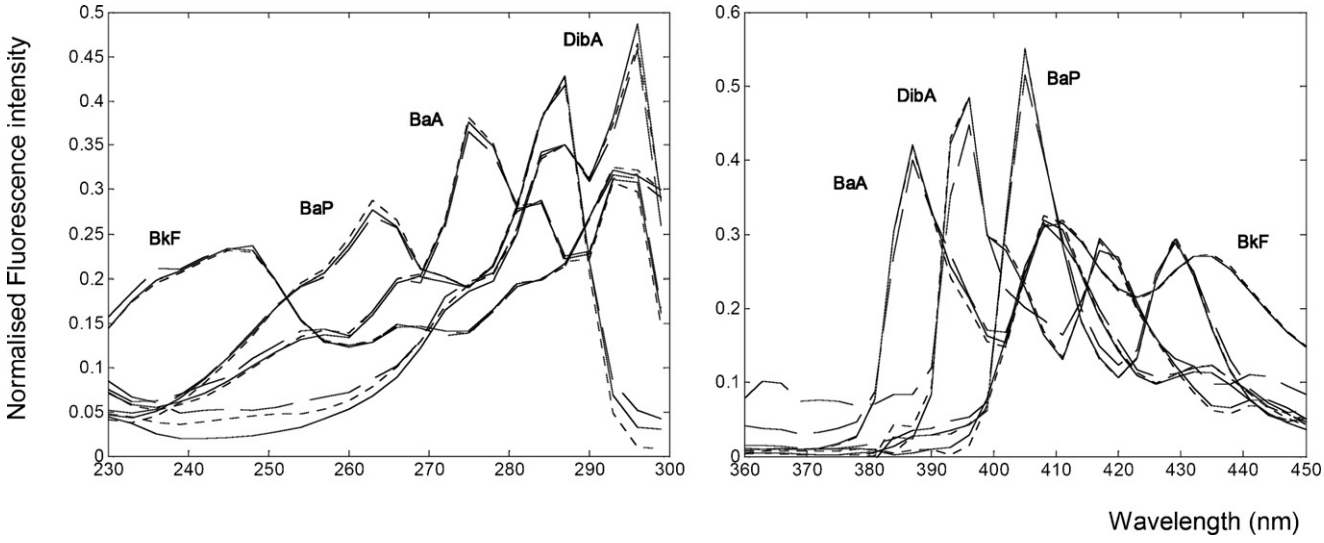

Fig. 2. Excitation and emission spectra obtained by PARAFAC (solid line), MCR-ALS (dotted lines) and the pure spectra of the analytes (broken lines).

The time required to obtain this signal is less than 2 min. The signal recorded is not specific to any analyte in any zone of the spectrum. The sensitivities of each compound at the same concentration were very different: the most sensitive analyte was BkF, then BaP, BaA and DibA. The spectra-overlap and the maximum peaks of absorbance are straits. For this reason, when HPLC uses a fluorescent detector the wavelength must be changed during the elution chromatographic process.

The differences and the simililarities of the spectra are evaluated by the value of the correlation coefficients (r) [20]. A value of $r = 1$ indicates that the spectra are completely overlapped. Table 2 shows the emission and excitation correlation coefficients (r) between the pure analytes of 100 ppb.

Then, we applied PARAFAC with non-negativity constraints to the data cube for the samples of all the photodegradation experiments.

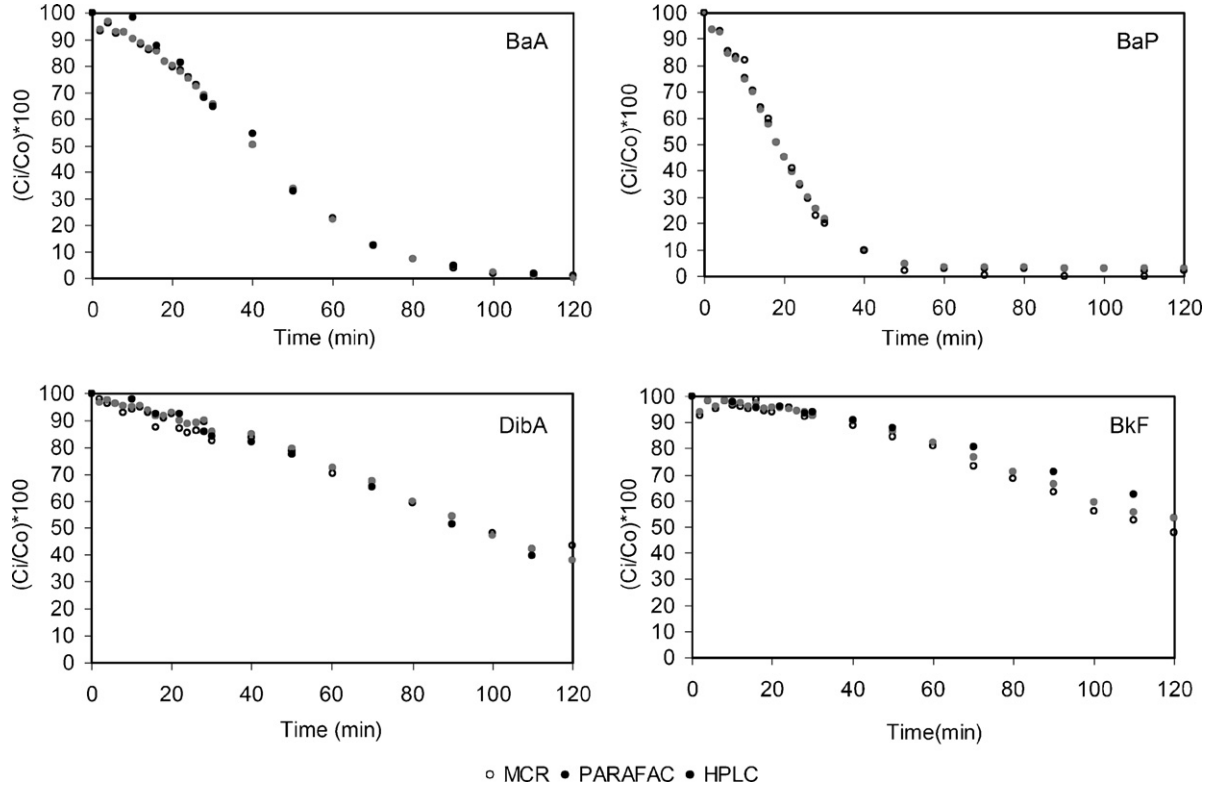

Fig. 3. Relative concentration of each analyte calculated using PARAFAC (grey points), MCR-ALS (white points) and HPLC (black points), throughout the experiment.

Table 2
Emission and excitation correlation coefficients (r) between the analytes

	B[a]A (Ex/Em)	Dib[a,h]A (Ex/Em)	B[a]P (Ex/Em)
Dib[a,h]A	0.7973/0.8273		
B[a]P	0.8649/0.7212	0.8962/0.6891	
B[k]F	0.7484/0.6911	0.8650/0.7153	0.8951/0.8879

Table 3
%Fit and core consistency for PARAFAC models using 1–5 factors

No. of factors (F)	1	2	3	4	5
%Fit	97.47	99.03	99.58	99.88	99.93
Core consistency	100	98.59	96.91	92.69	−1265

A four-factor model gave us a %fit of 99.88 and a core consistency of 92.69 (Table 3). This information indicates that intermediate fluorescent compounds do not appear in the process of photodegradation.

Fig. 2 shows the excitation and emission spectra obtained by PARAFAC and the pure spectra.

The high values of the correlation coefficients (Table 4A) between the pure spectra of each analyte (Fig. 2, broken lines) and the emission and excitation spectra obtained by applying the four-factor PARAFAC model (Fig. 2, solid line) suggest that the spectra retrieved by PARAFAC are representative of the analytes in the samples.

Fig. 3 shows the relative values of the concentration of each analyte calculated using the PARAFAC model developed, throughout the experiment. They are calculated by means of a linear relationship between the value of the score at time zero and the corresponding value at each time for each analyte [21].

For applied MCR-ALS, the EEM were arranged in an excitation-column-wise augmented data matrix [16] built with the 25 photodegradation samples and the standard matrices (each matrix consists of 31 emission vectors and 24 excitation vectors). The number of chemical species in this EEM was first estimated by singular value decomposition, since it was assumed that chemical components were associated with the largest singular values. Once again, four chemical species were found in the rank analysis.

The MCR-ALS method used non-negativity for both spectral modes, a three-way data structure (equal shape and synchronization) and non-normalization constraints in. Excitation spectra were used as initial estimates. The highest percentage of variance explained (r^2) was 99.94. Table 4B shows the correlation coefficients between the excitation and emission spectra obtained (Fig. 2, dotted lines) and the pure spectra (Fig. 2, broken lines) of the analytes at 100 ppb. For the purposes of this calculation, the emission spectrum obtained by MCR-ALS was considered to be the one corresponding to a photodegradation time of zero.

Table 4
Correlation coefficients for the emission and excitation spectra for the four-factor PARAFAC (A) and MCR-ALS (B) model

	B[a]A	B[a]P	B[k]F	Dib[a,h]A
(A) PARAFAC correlation coefficients				
$r_{Emission}$	0.9972	0.9934	0.9998	0.9956
$r_{Excitation}$	0.9986	0.9990	0.9960	0.9913
(B) MCR-ALS correlation coefficients				
$r_{Emission}$	0.9990	0.9999	0.9996	0.9957
$r_{Excitation}$	0.9956	0.9995	0.9983	0.9881

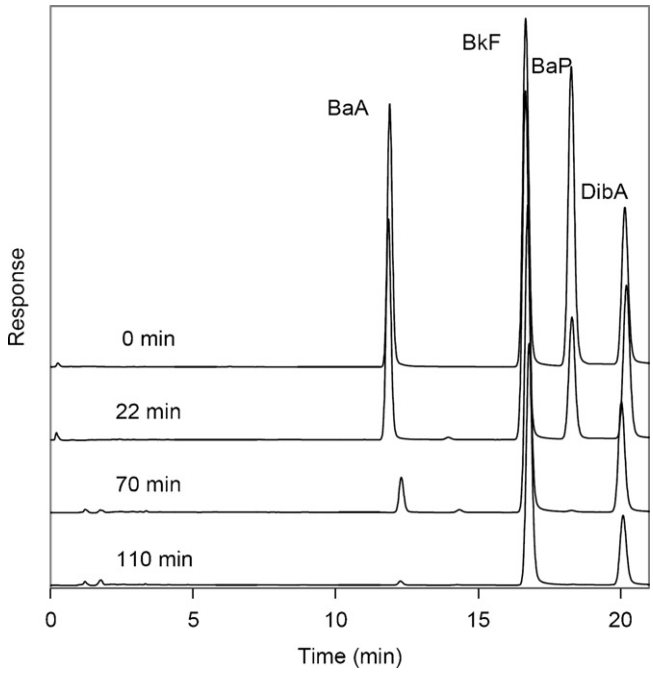

Fig. 4. The chromatograms of some of the samples taken at 0, 22, 70 and 110 min of the photodegradation.

Fig. 3 shows the relative values of the concentration of each analyte calculated using the MCR-ALS methodology. The quantification was performed by comparing the areas below the emission spectra of the analyte in the standard and in each sample obtained during the photodegradation process [16].

The chromatograms of some of the samples taken during the irradiations are presented in Fig. 4. The intensities of the peaks of the analytes of interest were observed to decrease with time, and no other peaks appeared to denote the presence of any intermediates. PAHs concentrations were determined from a calibration curve of fluorescence peak area versus concentration of PAH injected onto the HPLC. The correlation coefficients for each calibration line were 0.9984 for BaP, 0.9959 for BaA, 0.9975 for BkF and 0.9969 for DibA. The data found have been represented in Fig. 3.

As can be seen in Fig. 3, BkF that shows a difference between the three methods, although it can be seen that the results found with PARAFAC and MCR-ALS are more similar to one another than the results obtained by HPLC.

The presences of bias for both methods, regressed against to HPLC, were studied by means of the joint interval test of slope and intercept (Fig. 5). It is possible to see that the results obtained with PARAFAC present not significant differences at a significance level of $\alpha = 5\%$, while MCR-ALS (Fig. 5b) is comparable at a significance level of $\alpha = 1\%$.

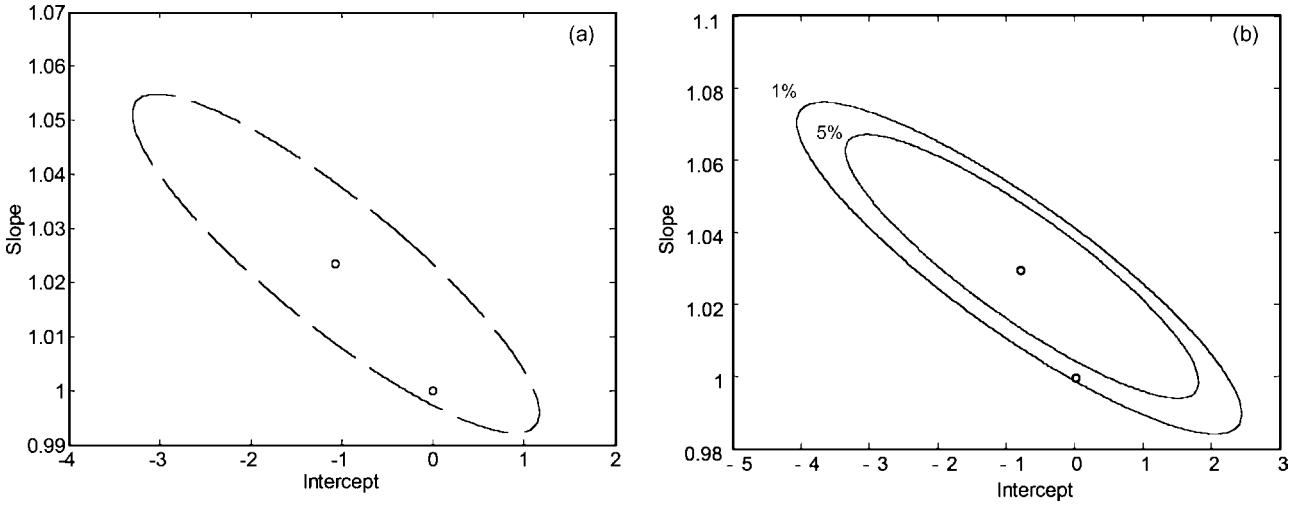

Fig. 5. Joint interval test for the slope and the intercept for: (a) PARAFAC and (b) MCR-ALS.

Table 5
PAHs photodegradation rate constants (k) and half-lives ($t_{1/2}$) calculated on the basis of analytical data

	PARAFAC		MCR-ALS		HPLC	
	$k \times 10^{-3}$ (s^{-1})	$t_{1/2}$ (min)	$k \times 10^{-3}$ (s^{-1})	$t_{1/2}$ (min)	$k \times 10^{-3}$ (s^{-1})	$t_{1/2}$ (min)
BaP	61.1	3.49	61.7	3.48	75.0	3.28
BaA	33.8	4.09	37.5	3.98	39.4	4.08
DibA	7.6	5.57	7.1	5.64	8.2	5.49
BkF	5.1	5.97	5.8	5.84	4.2	6.17

In photodegradation studies, the rate constants and the half-lives of analytes are used to measure the success of the process and these values are listed in Table 5 for the three methods. They were calculated assuming that the degradation normally fits pseudo first order kinetics [4,7,22].

It can be observed that the values of k found by the three methods are of the same order of magnitude. When the absolute differences between the times that the analyte concentration takes to decrease by one-half ($t_{1/2}$), are analysed, it is observed that the greatest differences are for BaP and BkF, but are in no case higher than the 0.33 min that we can assume to not be significant.

A bibliographic review of the values of k and $t_{1/2}$ [4,22–24] for these analytes in similar conditions shows results that agree with the ones that we have found here. So, fluorescence in conjunction with MCR-ALS or PARAFAC was successfully used to monitor the decomposition of PAHs in dilute aqueous solutions and the results are similar to the ones obtained by means of HPLC in a situation such as the one considered.

A more extensive discussion about the goodness of this methodology in comparison with HPLC would require further experimental work that analyzes the effect of concentration on the resolution of the analytes.

4. Conclusions

The results obtained by our methodology present no significant differences with the habitual methodology and it may be a good alternative to the traditional methods of analysis for monitoring the degradation of pollutants. The analysis times are very short and no solvents are used so no residues are generated.

PARAFAC and MCR-ALS can be successfully applied to excitation–emission spectra matrices to semiquantitatively determine the concentration of BaA, BaP, DibA and BkF throughout the degradation process in the aqueous medium. This should be useful for establishing a protocol for using these analytical methodologies to monitor the degradation reactions of fluorescent analytes in a situation such as the one considered.

Acknowledgements

The authors would like to acknowledge the economic support provided by the MCyT (project no. BQU 2003-01142) and the IGSOC (International Graduate School of Catalonia) for providing M.V. Bosco's doctoral fellowship.

References

[1] M.L. Lee, M.V. Novotny, K.D. Bartle, Analytical Chemistry of Polycyclic Aromatic Compounds, Academic Press, New York, 1981.
[2] P. Kubát, S. Civiš, A. Muck, J. Barek, J. Zima, J. Photochem. Photobiol. A: Chem. 132 (2000) 33.
[3] O. Legrini, E. Oliveros, A.M. Braun, Chem. Rev. 93 (1993) 671.
[4] M.P. Fasnacht, N.V. Blough, Environ. Sci. Technol. 36 (2002) 4364.
[5] Y.-J. An, E.R. Carraway, Water Res. 36 (2002) 309.
[6] M.P. Fasnacht, N.V. Blough, Environ. Sci. Technol. 37 (2003) 5767.
[7] A. Kot-Wasik, D. Dabrowska, J. Namieśnik, J. Photochem. Photobiol. A: Chem. 168 (2004) 109.

[8] F.J. Rivas, F.J. Beltrán, B. Acedo, J. Hazard. Mater. B75 (2000) 89.
[9] K.S. Booksh, A.R. Muroski, M.L. Myrick, Anal. Chem. 68 (1996) 3539.
[10] J.L. Beltrán, R. Ferrer, J. Guiteras, Anal. Chim. Acta 373 (1998) 311.
[11] R.D. JiJi, G.G. Andersson, K.S. Booksh, J. Chemom. 14 (2000) 171.
[12] R.D. JiJi, G.A. Cooper, K.S. Booksh, Anal. Chim. Acta 397 (1999) 81.
[13] Y.-C. Kim, J.A. Jordan, M.L. Nahorniak, K.S. Booksh, Anal. Chem. 77 (2005) 7679.
[14] R. Bro, Chemom. Intell. Lab. Syst. 38 (1997) 149.
[15] R. Bro, Multiway Analysis in the Food Industry: Models, Algorithms, and Applications, Ph.D. Thesis, University of Amsterdam, 1998.
[16] J. Saurina, C. Leal, R. Compañó, M. Granados, R. Tauler, M.D. Prat, Anal. Chim. Acta 409 (2000) 237.
[17] The Mathworks, MATLAB, Version 6.1, South Natick, MA, 1999.
[18] C.A. Andersson, R. Bro, The N-way toolbox for MATLAB, Version 2.11, http://www.models.kvl.dk/source/nwaytoolbox, 2004.
[19] R. Tauler, http://www.ub.es/gesq/mcr/mcr.htm.
[20] M. Garrido, I. Lázaro, M.S. Larrechi, F.X. Rius, Anal. Chim. Acta 515 (2004) 65.
[21] M.V. Bosco, M. Garrido, M.S. Larrechi, Anal. Chim. Acta 559 (2006) 240.
[22] K.M. Lehto, E. Vuorimaa, H. Lemmetyinen, J. Photochem. Photobiol. A: Chem. 136 (2000) 53.
[23] G.K.-C. Low, G.B. Batley, C.I. Brockbank, J. Chromatogr. 392 (1987) 199.
[24] J. Sabaté, J.M. Bayona, A.M. Solanas, Chemosphere 44 (2001) 119.

Available online at www.sciencedirect.com
ScienceDirect
Talanta 71 (2007) 1710–1719
Talanta
www.elsevier.com/locate/talanta

A multisyringe flow-through sequential extraction system for on-line monitoring of orthophosphate in soils and sediments

Janya Buanuam [a], Manuel Miró [b,*], Elo Harald Hansen [c], Juwadee Shiowatana [a], José Manuel Estela [b], Víctor Cerdà [b]

[a] *Department of Chemistry, Faculty of Science, Mahidol University, Rama VI Road, Bangkok 10400, Thailand*
[b] *Department of Chemistry, Faculty of Sciences, University of the Balearic Islands, Carretera de Valldemossa km. 7.5, E-07122 Palma de Mallorca, Illes Balears, Spain*
[c] *Department of Chemistry, Technical University of Denmark, Kemitorvet, Building 207, DK-2800 Kgs. Lyngby, Denmark*

Received 16 May 2006; received in revised form 29 July 2006; accepted 1 August 2006
Available online 15 September 2006

Abstract

A fully automated flow-through microcolumn fractionation system with on-line post-extraction derivatization is proposed for monitoring of orthophosphate in solid samples of environmental relevance. The system integrates dynamic sequential extraction using 1.0 mol l^{-1} NH_4Cl, 0.1 mol l^{-1} NaOH and 0.5 mol l^{-1} HCl as extractants according to the Hieltjes–Lijklema (HL) scheme for fractionation of phosphorus associated with different geological phases, and on-line processing of the extracts via the Molybdenum Blue (MB) reaction by exploiting multisyringe flow injection as the interface between the solid containing microcolumn and the flow-through detector. The proposed flow assembly, capitalizing on the features of the multicommutation concept, implies several advantages as compared to fractionation analysis in the batch mode in terms of saving of extractants and MB reagents, shortening of the operational times from days to hours, highly temporal resolution of the leaching process and the capability for immediate decision for stopping or proceeding with the ongoing extraction. Very importantly, accurate determination of the various orthophosphate pools is ensured by minimization of the hydrolysis of extracted organic phosphorus and condensed inorganic phosphates within the time frame of the assay. The potential of the novel system for accommodation of the harmonized protocol from the Standards, Measurement and Testing (SMT) Program of the Commission of the European Communities for inorganic phosphorus fractionation was also addressed. Under the optimized conditions, the lowest detectable concentration at the 3σ level was $\leq$0.02 mg P l^{-1} for both the HL and SMT schemes regardless of the extracting media. The repeatability of the MB assay was better than 2.5% and the dynamic linear range extended up to 7.0 mg P l^{-1} in NH_4Cl and NaOH media and 15 mg P l^{-1} whenever HCl is utilized as extractant for both the HL and SMT protocols.

Keywords: Multisyringe flow injection; Microcolumn sequential extraction; Orthophosphate; Soil; Sediment

1. Introduction

Assessment of the bioavailability of macronutrients and trace elements in environmentally significant solid substrates is a key issue for ecology and environmental management. It is now widely accepted that the accessibility of the various elements for biota uptake depends strongly on their specific chemical forms and binding sites. A commonly used technique for identification of the phase associations of elements in solid phases is based on the application of sequential extractions [1–5]. These methods involve the rational use of a series of moderately selective reagents for releasing of targeted species from particular mineralogical fractions into the liquid phase under simulated natural and/or anthropogenic modifications of the environmental conditions. Sequential extraction procedures have been traditionally performed in a batchwise fashion. Yet, in the last decade, it has been realized that the conventional, manual procedures cannot mimic environmental scenarios accurately because naturally occurring processes are always dynamic, rather than static as they are identified by the traditional equilibrium-based approaches.

Recent trends have been focused on the development of alternative methods aimed at mimicking environmental events more correctly than their classical extraction counterparts [6]. Several

* Corresponding author. Tel.: +34 971 259576; fax: +34 971 173426.
E-mail address: manuel.miro@uib.es (M. Miró).

0039-9140/$ – see front matter © 2006 Elsevier B.V. All rights reserved.
doi:10.1016/j.talanta.2006.08.007

attempts have been made on the characterization and evaluation of dynamic (non-steady-state) partitioning methods, mostly exploiting continuous-flow or flow injection systems, where fresh portions of leaching agents are continuously provided to small containers or columns containing the solid material [7–18]. Dynamic approaches should be regarded as appealing avenues for fractionation assays not only because they alleviate the shortcomings of batch procedures including analyte re-adsorption and limited information on the size of actual available pools, but at the same time result also in improved precision and sample throughput. Furthermore, the overall leaching process may be monitored as a function of the exposure time, giving rise to a more realistic insight into the extractability of elements from different geological reservoirs. As a consequence of the development of flow-based extraction approaches, on-line leachate measurements are readily applicable, as deduced from current trends in the field [9,12–14,16,18,19]. However, most of the works capitalize on hyphenated analytical methods based on coupling of the miniaturizated column extraction manifold to continuously operating atomic spectrometers, such as flame atomic absorption spectrometry, inductively coupled plasma-mass spectrometry or inductively coupled plasma-atomic emission spectrometry, whereby the on-line generated extracts are directly injected into the detection system without any further treatment [9,13,14,16,18,19].

As a result of the precise fluidic control via syringe pumps, the second generation of flow injection (FI), namely, sequential injection (SI) analysis [20] has opened for new avenues in miniaturisation of sample processing including fractionation of solid samples [21]. While most FI-procedures employ continuous, uni-directional pumping of solutions, SI is based on exploiting programmable, bi-directional discontinuous flow as coordinated and controlled by a computer. Despite the well-recognized advantages of SI-microcolumn extraction as compared to its FI counterpart in terms of ruggedness, reagent consumption, precise handling of extracts and selection of the fractionation mode [6,22,23], automated post-column derivatization, which may be indispensable for macronutrient monitoring, is inherently hindered in SI due to the requirements of aspiration of the overall solutions into a holding coil [24].

To circumvent the above drawbacks, a hybrid flowing stream approach, the so-called multisyringe flow injection (MSFI) analysis [25–27], is here proposed as the interface between the microcolumn system and detector for on-line microfluidic manipulation of leachates and reagents. To the best of our knowledge, MSFI, which compiles the advantageous features of FI and SI systems, has not been exploited for dynamic fractionation assays so far.

The hyphenated MSFI-microcolumn set-up has been assembled for automated flow-through partitioning and accurate determination of the content of bioavailable forms of orthophosphate in soils and sediments utilizing the Molybdenum Blue method for extract processing. Although environmental solids contain both organic and inorganic forms of phosphorus [28,29], the latter are most relevant as a consequence of the well-known contribution to euthrophication [30]. In the terrestrial environment, phosphorus is an essential nutrient to support the plant growth; yet, direct uptake of organic forms is regarded to be unlikely. For the very same reason, it is essential that the analytical approach used ensures that distinction between readily available inorganic phosphorus and organic bound phosphate reliably can be accomplished.

In this communication, the potential of the MSFI set-up for accommodation of two sequential extraction schemes involving different operationally defined extracting conditions is assessed. In this context, the Hieltjes–Lijklema (HL) procedure [31] and the harmonized protocol from the Standards, Measurement and Testing (SMT) program of the European Commission [32] were selected and conducted in a dynamic fashion. Careful optimization of the chemical variables for the derivatization reactions is regarded to be crucial for appropriate performance of the analyzer due to the extreme pH conditions of the extracts obtained on-line in the various partitioning steps, not only to attain the desired selectivity, especially in regard to the presence of silicon, but also ensure the distinction between orthophosphate and organic-bound phosphorus.

2. Experimental

2.1. Instrumentation

The flow manifold devised for dynamic microcolumn fractionation and on-line spectrophotometric determination of orthophosphate is shown in Fig. 1. It comprises a 5000-step syringe pump (SP) (Crison Instruments, Alella, Barcelona, Spain) for handling of the leaching reagents and performance of fractionation analysis; a 10-port multiposition selection valve (SV, Valco Instruments, Houston, TX) for selection of the appropriate extractant, and a multisyringe piston pump (MSP, MicroBu 2030, Crison Instruments) for on-line post-column derivatization of the extracts. The automatic SP is furnished with a 5 ml syringe (Hamilton, Switzerland) and a three-way solenoid valve at its head (SP1), which allows connection with the manifold or the carrier (water) reservoir. The central port of the SV is connected to SP via a holding coil (HC; used to house the selected extractant), which consists of a 1.42 m long PTFE tubing (1.5 mm i.d.), with an inner volume of 2.5 ml.

The MSP is equipped with four syringes (S1-S4) of 5, 2.5, 2.5 and 2.5 ml, respectively, whose pistons are connected in block to the same stepper motor. The solenoid commutation valves (V1–V4) (N-Research, Caldwell, NJ) placed at the head of the syringes permit the connection of the liquid drivers with the manifold (On) or with reagent reservoir (Off) regardless of the motion of the piston pump. This module also incorporates two additional discrete three-way solenoid valves (V5 and V6) for effecting soil extraction and on-line extract analysis under optimum experimental conditions.

All the connections including the extract loop and knotted reactors (KR) are made from PTFE tubing of 0.87 mm i.d. The length of the extractant loop, KR1 and KR2 are 42, 65 and 51 cm, respectively, corresponding to ca. 250, 385 and 300 μl, respectively.

A diode-array spectrophotometer (Hewlett-Packard HP8452A) equipped with a flow-through cell (18 μl inner

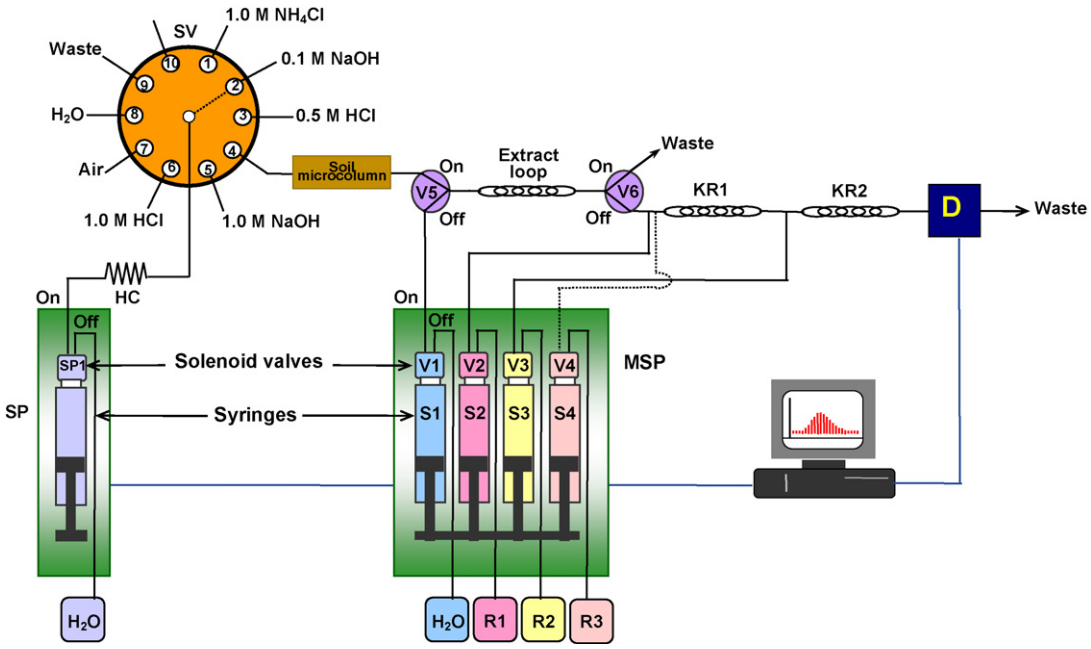

Fig. 1. Schematic diagram of the hybrid flow-through microcolumn extraction/MSFI system for automated fractionation and on-line determination of orthophosphate. R1: 6 g l^{-1} ammonium molydate + 0.125% (w/v) oxalic acid in 0.3 M H_2SO_4 (for HL scheme) or 6 g l^{-1} ammonium molydate + 0.25% (w/v) oxalic acid in 1.0 M H_2SO_4 (for NaOH-P in SMT); R2: 0.15 g l^{-1} $SnCl_2$ + 0.94 g l^{-1} $N_2H_4{\cdot}H_2SO_4$ in 0.25 M H_2SO_4; R3: 6 g l^{-1} ammonium molybdate in water (for HCl-P in SMT). SP: syringe pump; MSP: multisyringe pump; SV: selection valve, V: solenoid valve, KR: knotted reactor, D: detector.

volume, 1 cm optical path) is used as a detector. The analytical and reference wavelengths for monitoring of the Molybdenum Blue (MB) complex and minimization of Schlieren effects, respectively, are set at 690 and 530 nm. The transient spectrophotometric signals are acquired via an HP–IB interface at a frequency of 1.00 Hz. Instrumental control and data acquisition are performed using the software package AutoAnalysis 5.0 (Sciware, Spain).

2.2. Flow-through microcolumn assembly

The design of the extraction microcolumn has been described in detail in a previous work [22]. Made of PEEK, it comprises a central dual-conical shaped sample container for facilitating fluidized-bed like mixing conditions. The entire unit is assembled with the aid of filter supports and caps at both ends. The membrane filters (Fluoropore™, Millipore, 13 mm diameter with 0.45 and 1.0 μm pore sizes for sediment and soil samples, respectively) used at both ends of the extraction microcolumn allowed solutions and leachates to flow freely through but retained the particulate matter. Solid amounts up to 300 mg can be automatically processed without clogging effects as reported elsewhere [19].

2.3. Reagents, solutions and samples

All chemicals were of analytical-reagent grade and used as received. Solutions were prepared with double distilled water. A stock standard solution of orthophosphate (100 mg P l^{-1}) was prepared from KH_2PO_4 (Merck). Working solutions were prepared by stepwise dilution of the stock phosphorus solution. A stock standard solution of silicon (10 g Si l^{-1}) was prepared from $Na_2SiO_3{\cdot}5H_2O$, and diluted standards were used for the investigation of the effect of silicate on the analytical readouts.

The chemical extractants used in both the HL and SMT sequential extraction schemes are summarized in Table 1 along with the geological phosphorus fractions released.

The reagent utilized in the HL scheme (R1) for post-column formation of molybdophosphoric acid was composed of 6 g l^{-1} ammonium molybdate (Panreac) in 0.3 M H_2SO_4 (Merck) containing 0.125% (w/v) oxalic acid (Probus). For the determination of HCl and NaOH extractable phosphorus in the SMT scheme, a solution of 6 g l^{-1} ammonium molybdate was prepared in water (R3) and in 1.0 M H_2SO_4 containing 0.25% (w/v) oxalic acid (R1), respectively. A solution containing 0.15 g l^{-1} $SnCl_2$ (Scharlau) and 0.94 g l^{-1} hydrazine sulphate (Sigma) in 0.25 M H_2SO_4 (R2) was employed for on-line reduction of the molyb-

Table 1
Leaching reagents and corresponding phosphorus fractions in two extraction procedures

Procedure	Step I	Step II	Step III
Hieltjes–Lijklema	1.0 M NH_4Cl, pH 7 (Labile P)	0.1 M NaOH (Fe and Al-bound P)	0.5 M HCl (Ca-bound P)
SMT	1.0 M NaOH (Fe and Al-bound P)	1.0 M HCl (Ca-bound P)	

dophosphoric acid to the blue-coloured MB complex regardless of the fractionation scheme and extraction medium.

Two certified reference materials, namely SRM 2704 and SRM 2711, from the National Institute of Standards and Technology (NIST) were used for traceability studies. The SRM 2704 is a sediment collected from the Buffalo River in the area of the Ohio Street Bridge, NY, with a particle size distribution of 38–150 μm while the SRM 2711 is a pasture soil collected in the till layer of a wheat field (Montana, MT) with particle size <74 μm. The conical microcolumn was packed, in both cases, with 50 mg solid samples, the estimated free column volume being 250 μl.

2.4. Dissolution of solid residues and samples

Residues leftover after the sequential extraction schemes, and extracts collected downstream following post-column derivatization, were digested for quantitation of fixed and total released phosphorus, respectively. The microwave digestion procedure used can be regarded as a modified version of the EPA Method 3051 [33], named microwave-assisted acid digestion for sediments, sludges, soils, and oils. Hence, digestions were performed in a closed-vessel microwave system (Milestone, model MLS-1200 Mega, Italy) using 1.0 ml of concentrated HNO_3 (65%, Scharlau) and 3.0 ml of concentrated HCl (30%, Scharlau). The microwave digestion program consists of five steps each lasting 5 min. The power program applied is detailed as follows: 250 W/400 W/650 W/250 W/0 W. After cooling, if needed, the digests were filtered through 0.45 μm cellulose acetate filters (Minisartfilters, Sartorius, Göttinger). The clear digests were made up to 50 ml and the content of orthophosphate was determined by spectrophotometry using a batchwise standard addition method.

The pseudo-total (aqua regia) phosphorus content in the NIST 2711 was determined using the microwave digestion conditions detailed above.

2.5. General procedure for flow-through sequential extraction

The programmable flow-through fractionation assays were conducted with the aid of SP and SV. In the HL scheme, firstly, the HC was flushed with carrier (water), whereupon a 100 μl air plug from port 7 of SV and 2.0 ml of 1.0 M NH_4Cl from port 1 were consecutively aspirated into HC. Afterward, V5 and V6 were turned 'On' and SP was set to dispense 250 μl of 1.0 M NH_4Cl (which matches the free column volume) from HC through the microcolumn at a flow rate of 3.0 ml min^{-1}, allowing dynamic extraction to take place. The resulting leachate was stored into the extract loop and subsequently swept into the MSFI network for post-column derivatization and on-line determination of orthophosphate using a multicommutation protocol. The program was initially designed for eight cycle runs (equivalent to 2.0 ml of extractant volume) but the operational sequence proceeds until quantitative stripping of labile phosphorus forms.

Prior to continuing with the ensuing HL extraction step, a washing protocol is implemented by aspiration of 100 μl of air and 2.0 ml of H_2O from port 7 and 8, respectively, into HC, and using the same procedure described above for flow-through extraction. Thereafter, the next extractant (viz., 0.1 M NaOH or 0.5 M HCl) is aspirated repeatedly from the respective valve port and delivered to the soil containing microcolumn until completion of the phosphorus extraction.

For the SMT protocol, the dynamic fractionation was performed using an identical operational sequence with 1.0 M NaOH and 1.0 M HCl as leaching reagents.

2.6. Multicommutation protocol for on-line post-column derivatization

Two different multicommutation flow modalities for on-line injection of MB reagents, the so-called merging zones and sandwich-based approaches, were assayed. In both cases, switching of solenoid valves was effected during a single forward displacement of the piston bar of the MSFI pump. Both operational procedures are thoroughly described in the following:

2.6.1. Merging zones mode

As the name implies, the multicommutation protocol was programmed to merge the extract with the two reagent zones for development of the MB reaction as detailed in Table 2. After collection of the leachate in the extract loop, V1 and V2 were switched to 'On' while V5 and V6 were synchronously switched to 'Off'. As a result, the orthophosphate zone merged with a well-defined plug of ammonium molybdate to yield the heteropolyacid species in KR1. Subsequently, V3 was activated to 'On', whereby the reaction zone reaching the next confluence point overlapped with the reducing $SnCl_2$ segment to form the blue-coloured MB complex in KR2. The interdispersed zones were finally delivered downstream to the flow-through diode-array spectrophotometer by the carrier contained in S1, and the blue complex was monitored at 690 nm. Whenever the analysis

Table 2
Multicommuted merging zone protocol for on-line post-column derivatization

Multicommutation step	Solenoid valve position					Reagent (μl)		Carrier (μl)	Total flow rate (ml min^{-1})
	V1	V2	V3	V4	V5	R1	R2		
Merging of the extract and R1	On	On	Off	Off	Off	80	–	160	6.75
Delivery of the reaction zone to KR2	On	Off	Off	Off	Off	–	–	160	4.50
Merging of the reaction zone with R2	On	Off	On	Off	Off	–	120	240	6.75
Delivery of the MB zone to detector	On	Off	Off	Off	Off	–	–	2600	4.50

Table 3
Multicommuted sandwich-type protocol for on-line post-column derivatization

Multicommutation step	Solenoid valve position					Reagent (μl)		Carrier (μl) (S1)	Total flow rate (ml min^{-1})
	V1	V2	V3	V4	V5	R1	R2		
Fronting zone of R1	Off	On	Off	Off	Off	25	–	–	2.25
Simultaneous delivery of extract and R1	On	On	Off	Off	Off	80	–	160	6.75
Delivery of the rear end of extract into MSFI network	On	Off	Off	Off	Off	–	–	90	4.50
Tailing zone of R1	Off	On	Off	Off	Off	40	–	–	2.25
Injection of R2	On	Off	On	Off	Off	–	160	320	6.75
Delivery of the MB zone to detector	On	Off	Off	Off	Off	–	–	2440	4.50

was completed, all valves were returned to their original position for starting the following fractionation assay.

2.6.2. Sandwich-based mode

The multicommutation protocol involves the injection of two zones of molybdate which are stacked at each end of the leachate plug. The automated MSFI-multicommuted protocol using a sandwiched-based injection is summarized in Table 3. The method started when V2 was activated to 'On' and S2 was set to dispense 25 μl of molybdate into KR1. Thereafter, the combined extract/reagent zone was dispensed downstream. A second plug of molybdate (namely, 40 μl) was injected at the rear end of the leachate for sandwiching of the phosphorus containing segment. The reduction of molybdophosphoric acid to the Molybdenum Blue complex was performed in a merging zone fashion. To this end, 160 μl of $SnCl_2$ were injected at the front end of the interdispersed zone, and the transient signal of the MB complex was recorded by the detector.

3. Results and discussion

3.1. Configuration of the flow network for post-column phosphorus derivatization

3.1.1. Implementation of the HL sequential extraction scheme

In this three-step partitioning scheme, 1.0 M NH_4Cl, 0.1 M NaOH and 0.5 M HCl are used as leaching reagents for consecutive extraction of phosphorus pools associated with different geological phases. The flow system was devised aimed at monitoring the orthophosphate, released on-line, via the MB method. Preliminary experiments were carried out for optimization of the MSFI configuration attending the variable chemical composition of the extracts, the volume of which was maintained at 250 μl. Two different reagent injection modalities, namely, the merging zones and the sandwich-type approaches, were assayed as described under Experimental. The merging zones was finally selected over the sandwich mode because the axial interdispersion between segments is not favored in a knotted coil [34,35], thus rendering double peak profiles.

The effect of MB reagent volumes (viz., ammonium molybdate and tin(II) chloride) on the analytical readouts was investigated taking into consideration the different sizes of the various syringes. The analytical sensitivity improved by 75% when increasing the size of the molybdate plugs from 40 to 80 μl, and remained constant up to 130 μl. This might be attributed to the compensation of the better radial mixing of the reagent and extract plugs with the higher dilution of the extract for volumes above 80 μl. Reagent volumes above 130 μl are unnecessary for the present design because they lead to undue dilution. Similar trends were obtained for the optimization of tin(II)chloride volume. To prevent excessive consumption of reagents, the multicommutation protocol was programmed to merely inject 80 μl ammonium molybdate and 120 μl tin(II) chloride per assay.

The influence of the flow rate on the on-line MB derivatization reaction was evaluated over the range from 3.0 to 5.0 ml min^{-1} (for S1) for the three extractant media of the HL scheme. The higher the flow rate the lower was the yield for MB formation, which is not surprising considering the relative slow reaction rate of the derivatization reaction. In fact, the peak height dropped by 20% when increasing the flow rate from 3.0 to 4.5 ml min^{-1}. Yet, the higher the flow rate the lower is the yield of the competitive reaction for generation of the interfering molybdosilicate species and the better is the analytical throughput. Taking into account the variable sensitivity of the MB method in the various leachate solutions (see below) and the stripping of silicate from solid substrates in alkaline medium, the flow rate was fixed to 4.5 ml min^{-1} for processing of the extracts obtained in the first two steps of the HL method. Regarding the apatite-phosphate fraction, it should be born in mind that the kinetics of formation of molybdophosphoric acid are not favoured in the acidic leachate medium. Therefore, a flow rate of 3.0 ml min^{-1}, that can be programmed automatically, was utilized for monitoring of the orthophosphate released in the last step of the HL scheme.

3.1.2. Implementation of the SMT sequential extraction scheme

Within the framework of the Standards, Measurement and Testing Programme of the European Commission, a batch extraction protocol for fractionation of phosphorus in environmental solids was harmonized in order to improve the reproducibility among laboratories [32]. The so-called SMT protocol was originally designed to obtain five phosphorus fractions, namely, total phosphorus (TP), inorganic phosphorus (IP), organic phosphorus (OP), apatite phosphorus (Ca-bound P) and non-apatite phosphorus (Al and Fe-bound P). It should be taken into account that some of the SMT partitioning steps are performed in a single rather than sequential manner and that the calcination of the solid residue as demanded for the TP and OP assays cannot be effected in an on-line fashion. Consequently,

the potential implementation of the SMT fractionation assays related to the measurement of the inorganic (apatite + non-apatite) phosphorus fractions was ascertained. These two fractions are regarded as the most relevant ones for assessing the readily available phosphorus for plant uptake.

The SMT protocol is characterized for endorsing more aggressive leachants as compared with the HL scheme. The immediate consequence is that the optimal MSFI operational conditions for the HL fractionation as detailed above cannot be extrapolated directly to the SMT partitioning. The use of 1.0 M rather than 0.1 M NaOH for leaching of phosphorus associated to hydrous oxides of Al and Fe (non-apatite phosphorus) facilitates the concomitant release of large amounts of silicate. Actually, a 20% increase in the analytical signals was detected whenever the molybdate reagent for HL containing 0.125% (w/v) oxalic acid in 0.3 M H_2SO_4 was utilized for analyzing a 1.0 mg P l^{-1} standard containing 200 mg Si l^{-1} in 1.0 M NaOH. It is known that the interference of silicate on the orthophosphate MB determination can be minimized by increasing both the acidity of the reaction medium and the concentration of the masking organic acid [36–39]. The effect of the concentration of sulphuric acid was thus evaluated from 0.3 to 1.5 M while that of oxalic acid from 0.125 to 0.25% (w/v). Yet, since the acidity has opposite effects on the selectivity and sensitivity of the molybdophosphate formation [36–38], the molybdate reagent was finally prepared in a 1.0 M H_2SO_4 medium containing 0.25% (w/v) oxalic acid. Under these experimental conditions, silicate was tolerated up to 400 mg Si l^{-1} at the 10% interference level.

As to the SMT apatite fraction, the method's sensitivity using the HL reagent decreased dramatically as a result of the slow development of the reaction for molybdophosphoric acid formation under strong acidic conditions. Therefore, the heteropolyacid forming reagent was prepared in distilled water and the reaction flow rate was affixed at 3.0 ml min^{-1}. No appreciable increase of blank signals was detected, thus indicating that the acidity of the extractant suffices for preventing the self-reduction of molybdate. No oxalic acid was here added because of the negligible stripping of silicate from solids at low pH [40].

Although different reagents are needed for monitoring of the inorganic phosphorus in the HL and SMT extracts, a single MSFI assembly was arranged with no need for neither manual manipulations of reagents and leachates nor the changing of the composition of the carrier solutions for the various assays as demanded in previous flow systems for analyzing phosphorus containing soil solutions [40,41]. These facts emphasize the flexibility of MSFI for automated performance of derivatization reactions regardless of the variable chemical composition of the extracts in both fractionation schemes.

Fig. 2 illustrates the extraction patterns as obtained by on-line MSFI analysis of minute volumes of leachate (namely, 250 μl) for SRM 2704 and SRM 2711 following microcolumn extraction using both the HL and the SMT schemes. The extractograms give rise to valuable knowledge on: (i) the extraction kinetics, (ii) the content of phosphorus in available pools, (iii) the efficiency of the leachants and (iv) the actual extractant volumes for quantitative release of orthophosphate. The SMT extractograms show sharp leaching profiles while those of HL depict a gradual stripping of the nutrient species as a result of the milder leachants used. This is especially noticeable in the HCl extraction step in SRM 2704 where the amount of calcium bound phosphate leached in the first 2.0 ml in SMT is twofold higher to that of HL for the same extractant volume.

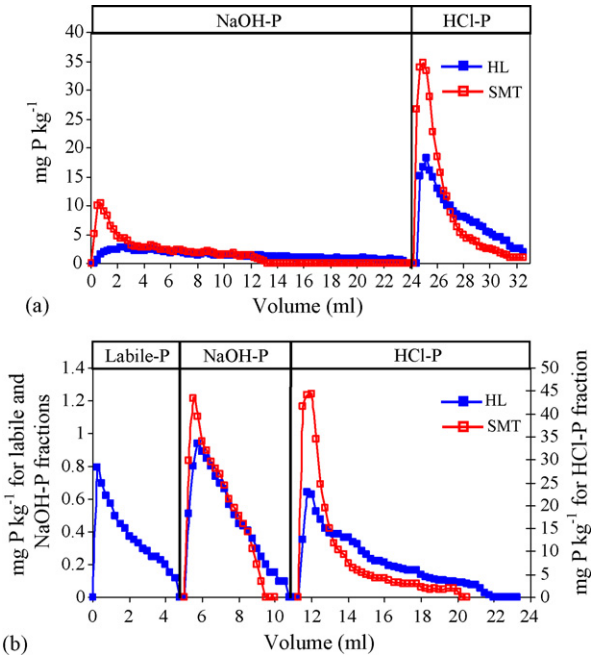

Fig. 2. Comparison of the on-line MSFI extraction profiles of orthophosphate in (a) SRM 2704 and (b) SRM 2711 as obtained by the application of HL and SMT protocols in a dynamic fashion. The labile phosphorus in 1.0 M NH_4Cl was <LOD for SRM 2704. The concentration of orthophosphate is given as mg P kg^{-1} sample.

The analytical results for SRM 2704 and SRM 2711 also evidence that different types of samples, in this case, agricultural soil and river sediment, behave differently under the same extraction conditions (see extraction patterns for the Al and Fe-bound phosphate in Fig. 2). This is attributed to the particular phosphorus soil phase associations existing in each kind of solid, thus, revealing the difficulty for setting a universal extraction protocol for dynamic fractionation of macronutrients.

3.2. Analytical performance of the MSFI analyzer

Under the optimized chemical and physical variables, the dynamic linear range of the multicommutated MB method was established over the range 0.05–7.0 mg P l^{-1} for the NH_4Cl and NaOH extraction media in the HL scheme, and 0.35–15 mg P l^{-1} for the 0.5 M HCl medium. For the NaOH and HCl steps in SMT, the regression lines extended from 0.1 to 7.0 and from 0.5 to 15 mg P l^{-1}, respectively. The limit of detection (LOD) assessed from three times the standard deviation of either the blank or a 50 μg P l^{-1} standard solution were 0.01, 0.01 and 0.02 mg P l^{-1} for NH_4Cl, NaOH and HCl steps in HL, respectively. In SMT, LODs of 0.02 and 0.01 mg P l^{-1} for 1.0 M NaOH and 1.0 M HCl were, respectively, obtained. Repeatability was estimated from 10 consecutive injections of a 1.0 mg P l^{-1} standard solution in each extracting medium. Relative standard deviations (R.S.D.)

Table 4
Comparison of the extraction/determination parameters for the HL scheme in SRM 2711 for three different procedures applied to phosphorus fractionation and extract analysis

Parameters	MSFIA (this work)		SI-MCE/FIA [42]		Batch [31]	
	Amount (mg)	Volume (μl)	Amount (mg)	Volume (μl)	Amount (mg)	Volume (μl)
1. Reagent consumption per extract analysis						
Ammonium molybdate	0.5	80	7.2	600	6.0	150
Reducing agent[a]	0.02	120	0.2	600	5.3	300
Masking agent[b]	0.1	80	2.4	1000	0.1	300
2. Extractant volume (ml)						
NH_4Cl fraction	4.5		25		2×50	
NaOH fraction	6		30		50	
HCl fraction	11		30		50	
3. Analysis time per extract (min)	0.77		0.74		20	
4. Operational time for overall fractionation and extract analysis per sample (h)	2.8		2.7		45.3	

[a] Tin(II) chloride was used as a reducing reagent for MSFIA and SI-MCE/FIA, while ascorbic acid was employed for batchwise analysis.
[b] Oxalic acid was employed as a masking agent for MSFIA, and tartaric acid for the SI-MCE/FIA and batch approaches.

of 1.0, 0.9 and 2.4% were obtained for the NH_4Cl, NaOH and HCl solutions in HL, respectively, and 1.0 and 2.2% for the NaOH and HCl media in SMT, respectively.

In Table 4, the analytical performance of the on-line MSFI analyzer for HL fractionation and orthophosphate determination is critically compared with that of the batchwise method [31] and an SI-microcolumn extraction (SI-MCE) system with further off-line analysis of the extracts by flow injection analysis [42]. A distinguishing feature of the MSFI-multicommutation set-up with respect to the FI and batch systems is the minimum consumption of reagents. Thus, in the proposed system, the consumption of MB chemicals is reduced more than 15-fold as regards to former methods. This is a consequence of the time-based injection of well-defined volumes of solutions at the precise instant for development of the reactions as effected via activation of the solenoid valves. Whenever not needed, the MB reagents are delivered to their respective reservoirs in lieu of being propelled downstream as occurs in continuous, forward-flow assemblies. Therefore, discontinuous-flow based MSFI analyzers might be viewed as environmental-friendly chemical processors.

The slightly higher operational time in MSFIA versus SI-MCE/FIA for fractionation/determination of orthophosphate has its origin in the different number of extracts analysed, that is, 86 extracts in the proposed on-line system as compared with merely 27 using the former FI set-up. Yet, the potential of the flow-through hyphenated MSFI system for handling of minute fractions of extract, that is $\leq$250 μl versus $\geq$5000 μl for methods involving fraction collection, ensures a unrivaled temporal resolution that yields a detailed insight into the leaching kinetics of phosphorus from the different soil/sediment compartments, as illustrated in Fig. 3. Hence, the content of inorganic phosphorus in readily mobilisable reservoirs can be more accurately estimated. At the same time, the sample mass to extractant volume ratio for each sequential extraction step can be calculated with improved accuracy, thereby avoiding the usage of any surplus of reagent for quantitative leaching of phosphorus in the various geological phases. According to Fig. 3 and data presented in Table 4, the leachant volumes used in the MSFI on-line fractionation system are three to four times lower to those required whenever off-line measurements are applied.

3.3. Accuracy of the proposed flow-through microcolumn extraction-multisyringe flow injection system for orthophosphate fractionation

The SRM 2704 river sediment and SRM 2711 Montana soil were utilized to evaluate the reliability and accuracy of the developed flow-through microcolumn hyphenated method. The amount of extractable orthophosphate in both standard reference materials resulting from the application of dynamic partitioning is listed in Tables 5 and 6 along with the certified total phosphorus content and the pseudo-total (aqua regia) phosphorus concentrations. The amount of extractable phosphorus for both solid substrates determined on-line by summation of all fractions plus residue is much lower than the certified values, while

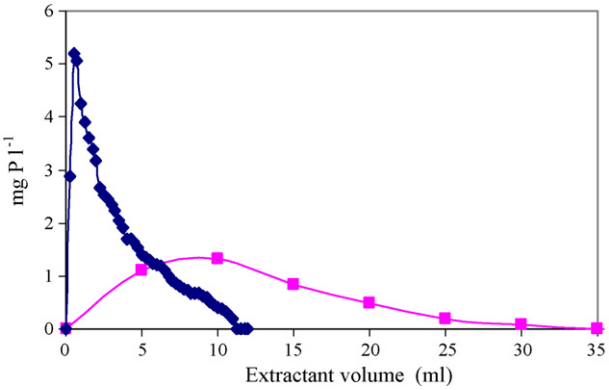

Fig. 3. Comparison of orthophosphate extractograms for the HCl step in the HL scheme for SRM 2711 as obtained by using off-line MB detection (5 ml per subfraction) and on-line MSFI spectrophotometric analysis (250 μl per subfraction).

Table 5
Comparison of extractable amounts of phosphorus in SRM 2711 (mg kg^{-1}) as obtained by using the Hieltjes–Lijklema and SMT sequential extraction schemes with on-line and off-line MB detection modes

Fractions	Hieltjes–Lijklema			SMT	
	On-line (MSFIA)	Off-line[a] (MWD)	Off-line[b] (SI-MCE) [42]	On-line (MSFIA)	Off-line[a] (MWD)
(1) Labile P	7 ± 1	36 ± 2	45 ± 5		
(2) Al and Fe-bound P	13.1 ± 0.4	84 ± 6	93 ± 10	11 ± 1	105 ± 2
(3) Ca-bound P	324 ± 45	370 ± 25	373 ± 18	365 ± 9	384 ± 9
(4) Residue	215 ± 14	215 ± 14	288 ± 43	202 ± 9	202 ± 9
Summation (1 + 2 + 3 + 4)	559 ± 47	705 ± 29	799 ± 48	578 ± 13	690 ± 13

Results are expressed as the mean of five fractionation assays ± S.D.; pseudo-total P: 700 ± 30 mg P kg^{-1}; certified value: 860 ± 70 mg P kg^{-1}; MWD: microwave digestion; SI-MCE: sequential injection-microcolumn extraction.
[a] The concentration of orthophosphate in the extracts is determined by batchwise MB standard addition.
[b] The concentration of orthophosphate in the extracts is determined by FIA-MB.

a good agreement, with maximum deviations of 8%, is obtained between the summation of fractions for SRM 2704 and SRM 2711 following acidic microwave digestion of the extracts collected downstream (after on-line detection) and the endorsed and pseudo-total concentrations, respectively.

According to the MB chemistry, only dissolved orthophosphate can react with MB reagents for generation of the reduced blue-coloured complex. Therefore, the on-line MSFI extraction system with spectrophotometric monitoring detects merely the extractable, reactive inorganic phosphorus. However, in the off-line assays, the extracts that may contain other phosphorus compounds, such as organic phosphorus and condensed inorganic phosphates (see below), can be degraded under microwave digestion into orthophosphate, thus providing information on the total phosphorus released. As a result, the total phosphorus content after appropriate processing of the MSFI extracts is not significantly different at the 0.05 significance level to the certified or pseudo-total phosphorus concentrations in both SRM materials, as shown in Tables 5 and 6.

3.4. Comparison of on-line and off-line modes for phosphorus determination in soil/sediment extracts

The phosphorus fractionation results using the on-line hyphenated MSFI assembly for SRM 2711 were contrasted with those previously obtained by sequential injection microcolumn extraction (SI-MCE) and fraction collection prior to off-line FI analysis [42]. As shown in Table 5, the extractable phosphorus monitored spectrophotometrically is severely affected by the mode of extract processing. It should be stressed that even though the HL and SMT schemes were originally designed for inorganic phosphorus fractionation, soil organic phosphorus can be concurrently released by the extracting reagents themselves. In fact, the most commonly accepted schemes for soil organic phosphorus fractionation [43,44] involve alkaline and acid extractions with 0.1–0.5 M NaOH and >0.1 M HCl, respectively, thus matching the chemical conditions for HL and SMT extractions. NaOH creates electrostatic repulsions by increasing the negative charge of both organic and mineral components [45] while HCl dissolves salts of some organic phosphate esters that are relatively insoluble in alkaline solution [43].

Furthermore, several organic phosphates are instable in alkaline and acid conditions, and therefore might be hydrolyzed under the fractionation conditions to free phosphate, thus leading to the overestimation of the content of readily accessible orthophosphate. The effects of alkaline and acid hydrolysis for a wide range of soil organic phosphorus compounds have been found to be markedly influenced by the nature of the phosphorus species [44,46,47]. The extraction of fast hydrolysable phosphorus forms (e.g., phosphatidyl choline) may hence explain the discrepancy in Table 5 between the on-line and off-line (SI-MCE) data for NaOH and HCl extracts in the HL scheme. Regarding the NH_4Cl extracts in HL, the contribution from organic phosphorus hydrolysis should here be negligible because organic substances cannot be leached under mild extraction media. Yet, common sources of readily hydrolysable phosphorusin soils, that might

Table 6
Comparison of extractable amounts of phosphorus in SRM 2704 (mg kg^{-1}) as obtained by using the Hieltjes–Lijklema and SMT sequential extraction schemes with on-line and off-line MB detection modes

Fractions	Hieltjes–Lijklema		SMT	
	On-line (MSFIA)	Off-line[a] (MWD)	On-line (MSFIA)	Off-line[a] (MWD)
(1) Labile P	<LOD	<LOD		
(2) Al and Fe-bound P	114 ± 14	103 ± 6	164 ± 18	177 ± 14
(3) Ca-bound P	310 ± 43	595 ± 17	288 ± 18	664 ± 21
(4) Residue	232 ± 26	232 ± 26	171 ± 5	171 ± 5
Summation (1 + 2 + 3 + 4)	656 ± 52	930 ± 32	623 ± 26	1012 ± 26

Results are expressed as the mean of five fractionation assays ± S.D.; certified value: 998 ± 28 mg P kg^{-1}; LOD: limit of detection.
[a] The concentration of orthophosphate in the extracts is determined by batchwise MB standard addition.

be released in the first extraction step of HL, are the condensed inorganic phosphates (e.g., pyrophosphate and polyphosphates) [44].

It should be noted that the hydrolysis of organic phosphorus and condensed inorganic phosphates in off-line based fractionation analysis might occur not only during the timeframe of the extraction but to a significant extent during the residence period prior to actual phosphorus determination. As opposed to batch partitioning and dynamic methods involving off-line or at-line analysis of phosphorus containing fractions, the novel multisyringe flow approach leads to a substantial shortening of the assay protocol, thus minimizing the potential decomposition of hydrolyzable phosphorus compounds. Each microvolume of extract leaving the microcolumn is readily treated on-line with MB reagents, while the released organic species in the batchwise method and SI-MCE system with off-line analysis remain in intimate contact with the extracting reagent for >15 and 3 h, respectively. Therefore, the flow-through MSFI fractionation analyzer with MB detection should be regarded as a unique tool for accurate monitoring of mobilisable orthophosphate in environmental solid substrates, even though organic phosphorus may be leached with the extracting reagents.

4. Conclusion

Multisyringe flow injection analysis has been presented as an appealing analytical tool for on-line processing of the extracts generated in flow-through dynamic fractionation assays. Prominent features of the assembled analytical set-up involving multicommutated post-column injection of reagents are the considerable saving of chemicals, the high temporal resolution of the leaching processes, the accurate evaluation of sample mass to leachant volume ratios, and the improved reliability, robustness and automation with respect to methods with off-line analysis of extracts.

The intrinsic versatility of the MSFI analyzer has been exploited for the accommodation in a single set-up of two well-accepted schemes for fractionation of inorganic phosphorus, i.e., the HL and SMT protocols, even though the chemical composition of the extracts resulting from both schemes is significantly different. As a consequence of the most aggressive extractants utilized in the SMT protocol, higher leachable contents and sharper extraction profiles were encountered as compared to the HL scheme. However, SMT does not give information on the labile inorganic phosphorus, which is regarded to be the readily available fraction for plant uptake. Furthermore, the extreme chemical conditions adopted in this scheme are unlikely to mimic the changes in the chemical properties of the solid occurring under environmental scenarios.

The flow-through microcolumn system hyphenated with spectrophotometric detection has been also proven unique for accurate monitoring of available orthophosphate in the extracts due to the minimization of the potential hydrolysis of extracted organic and condensed phosphorus into orthophosphate.

Further research is aimed at expanding the flexibility of the multisyringe flow injection analysis system for monitoring of ultratrace levels of pollutants, viz., heavy metals and metalloids, in solid substrates following dynamic fractionation and on-line solid-phase extraction for isolation and pre-concentration of the targeted species.

Acknowledgments

Janya Buanuam is grateful for financial support granted by the Royal Golden Jubilee Ph.D. Program of the Thailand Research Fund and to the Postgraduate Education and Research Program in Chemistry (PERCH) of the Higher Education Development Project of the Commission on Higher Education (Thailand). Manuel Miró is indebted to the Spanish Ministry of Education and Science for contract sponsorship through the *Ramón y Cajal* research program. The authors are grateful to the Spanish Ministry of Education and Science for financial support through projects CTQ2004-03256 and CTQ2004-01201. Special thanks are also due to Anders Sølby (DTU workshop) for construction of the extraction microcolumn.

References

[1] F.M.G. Tack, M.G. Verloo, Intern. J. Environ. Anal. Chem. 59 (1995) 225.
[2] G. Rauret, Talanta 46 (1998) 449.
[3] A.V. Filgueiras, I. Lavilla, C. Bendicho, J. Environ. Monit. 4 (2002) 823.
[4] C. Gleyzes, S. Tellier, M. Astruc, Trends Anal. Chem. 21 (2002) 451.
[5] J. Hlavay, T. Prohaska, M. Weisz, W.W. Wenzel, G.J. Stingeder, Pure Appl. Chem. 76 (2004) 415.
[6] M. Miró, E.H. Hansen, R. Chomchoei, W. Frenzel, Trends Anal. Chem. 24 (2005) 759.
[7] W. Tiyapongpattana, P. Pongsakul, J. Shiowatana, D. Nacapricha, Talanta 62 (2004) 765.
[8] J. Shiowatana, N. Tantidanai, S. Nookabkaew, D. Nacapricha, J. Environ. Qual. 30 (2001) 1195.
[9] D. Beauchemin, K. Kyser, D. Chipley, Anal. Chem. 74 (2002) 3924.
[10] P.S. Fedotov, A.G. Zavarzina, B.Ya. Spivakov, R. Wennrich, J. Mattusch, K. de P.C. Titze, V.V. Demin, J. Environ. Monit. 4 (2002) 318.
[11] H. Kurosaki, S.M. Loyland-Asbury, J.D. Navratil, S.B. Clark, Environ. Sci. Technol. 36 (2002) 4880.
[12] L.-M. Dong, X.-P. Yan, Talanta 65 (2005) 627.
[13] M. Jimoh, W. Frenzel, V. Müller, H. Stephanowitz, E. Hoffmann, Anal. Chem. 76 (2004) 1197.
[14] M. Jimoh, W. Frenzel, V. Müller, Anal. Bioanal. Chem. 381 (2005) 438.
[15] J. Shiowatana, N. Tantidanai, S. Nookabkaew, D. Nacapricha, Environ. Int. 26 (2001) 38.
[16] M. Schreiber, M. Otto, P.S. Fedotov, R. Wennrich, Chemosphere 61 (2005) 107.
[17] P.S. Fedotov, R. Wennrich, H.-J. Stärk, B.Ya. Spivakov, J. Environ. Monit. 7 (2005) 22.
[18] P.S. Fedotov, E.Yu. Savonina, R. Wennrich, B.Ya. Spivakov, Analyst 131 (2006) 509.
[19] R. Chomchoei, M. Miró, E.H. Hansen, J. Shiowatana, Anal. Chem. 77 (2005) 2720.
[20] C.E. Lenehan, N.W. Barnett, S.W. Lewis, Analyst 127 (2002) 997.
[21] M. Miró, E.H. Hansen, Anal. Bioanal. Chem. 382 (2005) 878.
[22] R. Chomchoei, E.H. Hansen, J. Shiowatana, Anal. Chim. Acta 526 (2004) 117.
[23] R. Chomchoei, M. Miró, E.H. Hansen, J. Shiowatana, Anal. Chim. Acta 536 (2005) 183.
[24] M. Miró, E.H. Hansen, Trends Anal. Chem. 25 (2006) 267.
[25] M.A. Segundo, L.M. Magalhaes, Anal. Sci. 22 (2006) 3.
[26] B. Horstkotte, O. Elsholz, V. Cerdà, J. Flow Injection Anal. 22 (2005) 99.
[27] M. Miró, V. Cerdà, J.M. Estela, Trends Anal. Chem. 21 (2002) 199.
[28] A. Barbanti, M.C. Bergamini, F. Frascari, S. Miserocchi, G. Rosso, J. Environ. Qual. 23 (1994) 1093.

[29] P. Pardo, J.F. López-Sánchez, G. Rauret, Anal. Bioanal. Chem. 376 (2003) 248.
[30] B.Ya. Spivakov, T.A. Maryutina, H. Muntau, Pure Appl. Chem. 71 (1999) 2161.
[31] A.H.M. Hieltjes, L. Lijklema, J. Environ. Qual. 3 (1980) 405.
[32] V. Ruban, J.F. López-Sánchez, P. Pardo, G. Rauret, H. Muntau, Ph. Quevauviller, J. Environ. Monit. 1 (1999) 51.
[33] US-EPA method 3051, Microwave Assisted Acid Digestion of Sediments, Sludges, Soils, and Oils, Code of Federal Regulations, 1991, Title 40, Part 136, Paragraph 33.
[34] B. Kalberg, G.E. Pacey, Flow Injection Analysis: A Practical Guide, Techniques and Instrumentation in Analytical Chemistry, vol. 10, Elsevier, 1989, p. 49.
[35] J. Ruzicka, E.H. Hansen, Flow Injection Analysis, 2nd ed., Wiley/Interscience, New York, 1988, pp. 105–106.
[36] T. Fujiwara, K. Kurahashi, T. Kumamaru, H. Sakai, Appl. Organometall. Chem. 10 (1996) 675.
[37] J.-Z. Zhang, C.J. Fisher, P.B. Ortner, Talanta 49 (1999) 293.
[38] S.-C. Pai, C.-C. Yang, J.P. Riley, Anal. Chim. Acta 229 (1990) 115.
[39] C.X. Galhardo, J.C. Masini, Anal. Chim. Acta 417 (2000) 191.
[40] W. Tiyapongpattana, Application of Continuous Flow Technique for Sequential Extraction and for Determination of Phosphorus in Soil and Sediment, Master thesis, Mahidol University, Bangkok, Thailand, 2002.
[41] N. Amornthammarong, P. Anujaravat, K. Sereenonchai, P. Chisuwan, P. Sastranurak, P. Wilairat, D. Nacapricha, Talanta 68 (2005) 480.
[42] J. Buanuam, M. Miró, E.H. Hansen, J. Shiowatana, Anal. Chim. Acta 570 (2006) 224.
[43] G. Anderson, in: A.D. McLaren, G.H. Peterson (Eds.), Soil Biochemistry, vol. 1, Marcel Dekker, New York, 1967, pp. 67–90.
[44] B.L. Turner, B.J. Cade-Menun, L.M. Condron, S. Newman, Talanta 66 (2005) 294.
[45] E.W. Russell, Soil Conditions and Plant Growth, 11th ed., Longman Scientific & Technical, Harlow, UK, 1988.
[46] M.I. Makarov, L. Haumaier, W. Zech, Soil Biol. Biochem. 34 (2002) 1467.
[47] B.L. Turner, N. Mahieu, L.M. Condron, Soil Sci. Soc. Am. J. 67 (2003) 497.

Available online at www.sciencedirect.com
ScienceDirect
Talanta 71 (2007) 1690–1695
Talanta
www.elsevier.com/locate/talanta

Near infrared reflectance spectroscopy as a tool for the control of sheep leather defatting

R. Cantero [b], T. Canals [b], H. Iturriaga [a,*]

[a] *Departament de Química, Unitat de Química Analítica,Universitat Autònoma de Barcelona, E-08193 Bellaterra, Spain*
[b] *EUETII, L'Escola d'Adoberia, Universitat Politècnica de Catalunya, Barcelona, Spain*

Received 16 January 2006; received in revised form 26 July 2006; accepted 1 August 2006
Available online 15 September 2006

Abstract

The fat content is one of the variables to be controlled by the tanning industry with a view to obtaining leather for various commercial purposes. Ensuring the production of quality leather products frequently entails using some defatting treatment, particularly when the raw skin is rich in natural fat. The official method for determining fat in leather, IUC 4, is rather slow; also, it uses polluting reagents and involves powdering samples for Soxhlet extraction with low-polarity solvents. The combination of NIR diffuse reflectance spectroscopy as implemented with a fibre-optic probe and multivariate calibration is probably the best choice for the direct determination of fat in leather and the monitoring of leather defatting.

In this work, a method for the determination of fat in leather and the control of the defatting process in an expeditious manner and with no sample treatment was developed. Defatting tests were conducted on leather specimens from lambs of various breeds and origins in order to span as wide as possible a range of variability in their properties and natural fat content. The NIR spectra used to construct the calibration matrices were recorded directly on the leather samples prior to and after defatting. Fat contents were determined by partial least-squares regression (PLSR), using the values obtained with the official method as references. Notwithstanding the complex nature of leather, the calibration models used provided good external predictions: the largest overall relative error, obtained by using a single calibration matrix for natural and defatted specimens, was 10%. The proposed method is therefore an advantageous alternative to the official method.

Keywords: Control leather defatting; NIR; Multivariate analysis

1. Introduction

The increasing demand for environmental friendliness and expeditiousness in control analyses has raised the need to replace polluting and slow procedures with faster, environmentally benign alternatives. The classical methods of analysis employed by the tanning industry usually entail the prior separation of the different components of the specimen to be analysed; this hinders automation of the process and results in a low throughput. The use of spectroscopic techniques is proposed as an alternative in different studies [1–7].

The tanning industry uses various types of leather of variable origin and containing also variable amounts of fat. Ensuring quality in a finished leather product entails minimizing the fat content in the raw material. Defatting treatments are intended to remove most natural fat from leather or distribute it evenly throughout so that it will not interfere with the tanning process.

Fat is unevenly distributed in leather; in fact, it is present at higher concentrations in some body regions such as the neck, spine and butt; also, the distribution of fat is only relatively symmetric with respect to the spine. Finally, no two leather specimens contain the same amount of fat, even if they come from animals of the same breed and origin [8].

For the above-described reasons, fat in leather is among the parameters most frequently determined in quality control analyses by the tanning industry. The official method for this purpose uses an extraction process that exploits the solubility of fat in low-polarity solvents [9]. The term "fat" as used by the tanning industry encompasses a wide variety of substances; some are scarcely polar or non-polar, whereas others (e.g. fatty acids) contain some polar group in their structures. A non-polar solvent extracts most fatty substances from leather; some polar compounds and others that bind easily to leather remain in it after extraction, however. The solvents used may also extract other,

* Corresponding author. Tel.: +34 93 5811012; fax: +34 93 5812379.
E-mail address: hortensia.iturriaga@uab.es (H. Iturriaga).

0039-9140/$ – see front matter © 2006 Published by Elsevier B.V.
doi:10.1016/j.talanta.2006.08.005

non-fat substances. As a result, the amount of fat determined is only an estimate of that actually present in leather [10]. A number of authors have studied the conditions required to thoroughly extract fat from leather [11–13] and concluded that accurately determining its fat content is very difficult. Other authors have proposed alternative techniques such as the use of supercritical fluid extraction combined with on-line piezoelectric detection but with little success [14].

The shortcomings of the official method of analysis and the need to use fast analytical procedures led us to explore the potential of NIR spectroscopy for controlling the defatting of sheep skin during the manufacturing of tanned leather from it.

The NIR spectroscopy–multivariate analysis couple is emerging as a powerful tool for process control [15] in such varied fields as biotechnology; earth science; mineralogy; environmental monitoring; and the chemical, agricultural food, clinical chemical, medical, petrochemical, pharmaceutical, polymer, surface analysis and leather tanning [16–20] industries.

In this work we are trying to establish a method that will enable both to determine fat and to control the degreasing process in sheepskins by using NIR diffuse reflectance spectroscopy and by the chemiometric treatment of information. When diffuse reflectance measurements are carried out, the use of a fibre optic sound allows to register the NIR spectre directly on the skin without any previous treatment on the sample. This results in considerable time savings and avoids the use of polluting chemicals.

2. Experimental

2.1. Apparatus and software

Mechanical boiler methacrylate rolls from Salvador Moret (Valencia, Spain) were used to depickle and repickle leather specimens. Simplex rolls from Inoxvic C.B. (Barcelona, Spain) equipped with temperature control and an alternating rotation mechanism were used to conduct laboratory defatting tests. Soxhlet extractor for sample fat extraction with methylene chloride.

Near infrared spectra were recorded on a NIRSystems 6500 spectrophotometer from Perstop Analytical (Silver Spring, MD) equipped with a reflectance detector and an AP6641 ANO4P fibre-optic probe. The instrument was originally governed by the software NSAS v. 3.52 and is currently controlled via Vision v. 2.22; both allow NIR spectra to be acquired and processed.

Powdered leather samples were homogenized in a Turbula® Type T2C shaker from WAB (Basel, Switzerland).

Data were processed using the PLS1 algorithm in Unscrambler v. 7.5, from CAMO (Trondheim, Norway).

2.2. Reagents

The universal reagents used included sodium chloride, sodium bicarbonate, sodium sulphide, calcium hydroxide, formic acid and freshly distilled methylene chloride. The specific reagents employed were Remolgan (oxyethylenated fatty alcohol) and Relugan GTW (glutaraldehyde).

2.3. Skin processing

The operations required to dehair the skins, which were preserved by pickling, are summarized in Table 1.

As noted earlier, the defatting operation is intended to remove as much natural fat as possible from the leather or to distribute it evenly in it so that it will not interfere with the leather production process. Table 2 describes the steps of the defatting process.

2.4. Samples

The leather specimens used were obtained from lambs of various breeds and origin in order to span as wide as possible a natural fat content range. The initial set consisted of nine skins of which three were from Australian, three from Spanish entrefino and three from Spanish merino lambs. All were hair-on and pickled. Three other, dehaired, pickled skins from Russian lambs were subsequently incorporated to the study.

Table 1
Steps of the dehairing process

Depickling (1)	Unhairing (2)	Repickling (3)	Drying (4)
500% H_2O	Prepare Na_2S–$Ca(OH)_2$ paste	500% H_2O	Hang samples
50% NaCl	Apply to skin (on flesh side)	50% NaCl	Dry 2 days
Rotate to complete dissolution	Allow to stand for 3–4 h	Rotate to complete dissolution	
Load skin specimens	Unhairing	Load skin samples	
Rotate 10 min	Place samples in a bath containing 500% H_2O and 0.5% Na_2S	Rotate 30 min	
Stop 1 h	Allow to stand overnight	3% HCOOH	
Rotate 1 min	Wash with abundant water (rotate)	Rotate 3 h	
3% $NaHCO_3$	Repeat washing operation three times	Allow to stand overnight (pH 3.5)	
Rotate 15 min		Empty bath and hand-squeeze skin	
Stop 2 h			
Check pH (6.5–7)			
Empty bath			
Wash with abundant water (rotate 10 min)			
Repeat washing operation three times			
Empty bath and hand-squeeze skin			

The proportions used in steps 1 and 2 are referred to salted raw skin weight; those employed in step 3, to dehaired skin weight.

Table 2
Steps of the defatting process

Soaking (5)	Pre-tanning (6)	Defatting (7)	Washing (8)	Repickling (9)	Drying (10)
400% H_2O	5% Relugan GTW	100% H_2O at 40 °C	200% H_2O at 40 °C	500% H_2O	Hang samples
60 g NaCl/L	Rotate 30 min	Remolgan ROI[a]	Rotate 20 min	50% NaCl	Dry 2 days
Rotate to complete dissolution	1–2% $NaHCO_3$	Rotate 30 min	Empty bath	Rotate 10 min	
Load samples	Rotate 2 h	200% H_2O at 40 °C	200% H_2O at 30 °C	2% HCOOH	
Allow to stand for 1–2 h	Empty bath	Rotate 20 min	Rotate 20 min	Rotate 3 h	
0.1% Remolgan ROI		Empty bath	Empty bath	Allow to stand overnight	
Rotate 1 h			200% H_2O at 20 °C	Empty bath	
			Rotate 20 min		
			Empty bath		

Proportions are referred to pelt weight.
[a] The proportion of surfactant (X) applied to the different samples in order to span a broad enough fat concentration range was 5–15%. Some samples required repeating the defatting step (7) and the subsequent washing operations.

Each skin was dehaired if required and top, bottom and side portions were cut off to obtain a rectangular piece that was split into samples approximately 45 g in weight for the tests and defatting process (see Fig. 1).

The 12 skins were used to prepare a total of 31 samples that differed between one another since, as noted in the introduction, each individual skin need not be uniform throughout. Each sample was designated with a letter and two digits. The letter denoted the race of the animal (*viz*. m for merino, e for entrefino, a for Australian and r for Russian lambs), the first digit the number assigned to each skin and the second that given to each sample from the same skin.

The amount of extractable fat in each sample prior to and after defatting was determined using the official method and the NIR spectra for the sample (both as such and after powdering).

Difference in fat content along the spine were offset as follows: each sample was used to obtain one strip at the top and another at the bottom that were ground jointly according to the IUC 3 standard [21]. The powder thus obtained was used to record a NIR spectrum and quantify natural fat, using the official method for this purpose (IUC 4) [9].

The remaining, central portion of each sample was used to directly record a NIR spectrum for the leather prior to defatting. Then, the portion was defatted to record a new NIR spectrum and determine extractable fat using the official method.

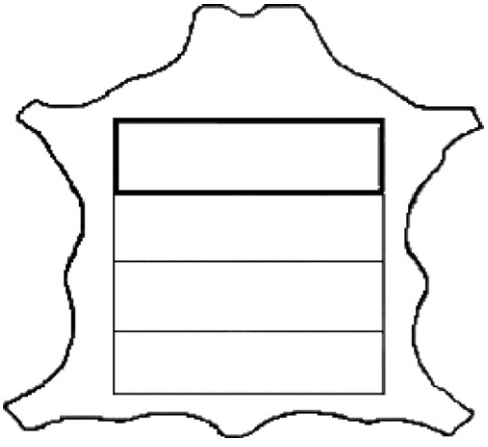

Fig. 1. Scheme of the sampling procedure.

2.5. Reference method (IUC 4)

The fat content in leather is determined by extraction, which is facilitated by the solubility of fat in low-polarity solvents. In order to maximize efficiency, the process is performed in a continuous manner in a Soxhlet extractor at a high temperature.

An amount of 5 ± 0.01 g of powdered leather was used to evenly fill a cellulose cartridge and covered with a thin cotton layer. The extraction flask was dried by heating at 102 ± 2 °C for 30 min in the presence of two glass beads, and weighed after cooling in a desiccator. The leather powder was extracted with methylene chloride and, after at least 30 applications, the solvent containing the extract was distilled. Then, the flask was dried at 102 ± 2 °C for 4 h; if any water drops were visible, a volume of 1–2 mL of ethanol was added to facilitate thorough moisture removal. At that point, the flask was allowed to cool in a desiccator and weighed. This was followed by redrying in a stove for 1 h, cooling and weighing. The process was repeated to weight constancy. All analyses were carried out in duplicate.

2.6. Recording of NIR spectra

Near infrared reflectance spectra were recorded with a fibre-optic probe over the wavelength range 1100–2500 nm, using an average of 32 scans. Their first and second derivatives were then calculated.

The spectrum for each leather sample was obtained as the average of 12 recordings made by placing the fibre-optic probe at different points on the surface. That for each powdered sample was the average of three recordings obtained following homogenization of the powder.

Figs. 2 and 3 show the spectra directly recorded on the surface of four leather samples from the four lamb breeds studied.

2.7. Processing of data

In this work, we studied leather samples prior to and after defatting, and also the two as a whole. In addition, samples were examined as such and after powdering.

The determination of leather fat was based on the use of partial least-squares regression (PLSR) for calibration.

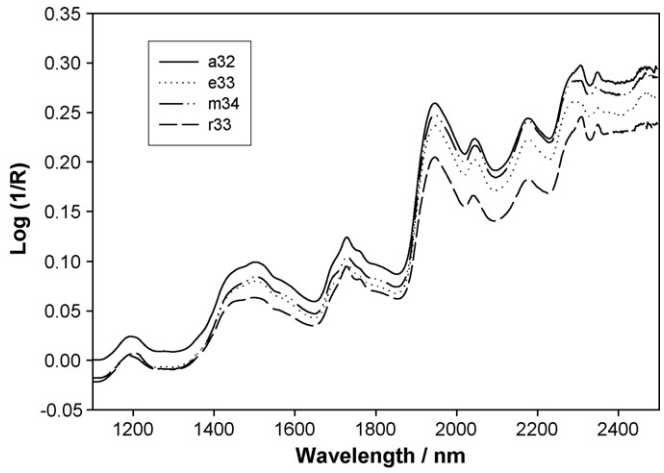

Fig. 2. NIR spectra for samples a32, e33, m34 and r33 as recorded directly on the leather surface prior to defatting.

The values provided by the official methods were used as references.

Spectra were recorded over the wavelength range 1100–2200 nm. Both absorbance, first-derivative and second-derivative data were examined.

Each data matrix was split into a calibration set and an external prediction set. The data used were centred and unscaled. Models were constructed by cross-validation, using as many segments as samples were included in the calibration set to calculate the mean square error of cross-validation (MSECV).

The number of PLS factors used in each calibration model was chosen in terms of the variation of MSECV in the region around the minimum in order to avoid overfitting.

The relative error of prediction for the external set, RSEP, was calculated from

$$\mathrm{RSEP}\,(\%) = \sqrt{\frac{\sum_{i=1}^{n}(c_{\mathrm{REF}(i)} - c_{\mathrm{NIR}(i)})^2}{\sum_{i=1}^{n} c_{\mathrm{REF}(i)}^2}} \times 100$$

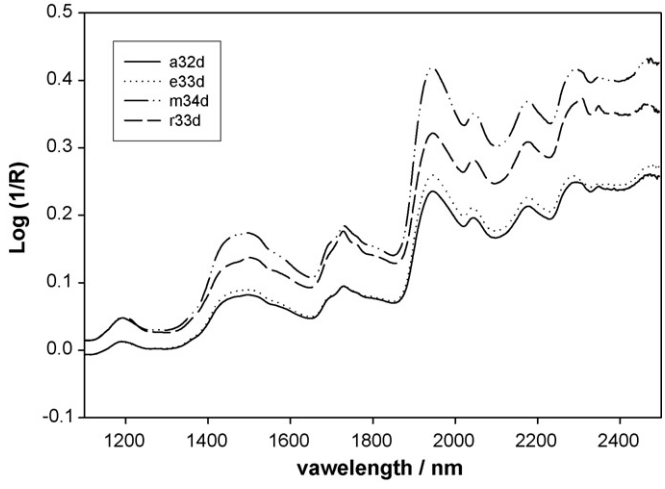

Fig. 3. NIR spectra for defatted samples a32d, e33d, m34d and r33d as recorded directly on the leather surface.

where c_{REF} is the reference concentration and c_{NIR} that calculated using the NIR model.

The percent leather fat contents provided by the PLSR method were plotted against those obtained with the reference method and data points fitted to a straight line. Once the regression line was obtained, the slope and intercept test was used to check for the absence of statistically significant differences between the responses of both methods at a significance level $p < 0.05$.

3. Results and discussion

The ability to record and chemometrically process multivariate analytical signals in a fraction of a second has allowed a number of industrial processes to be revisited. In this work, we established consistent, robust calibration sets with a view to the on-line decoding of the relevant information contained in analytical signals (specifically, the NIR spectra for natural and defatted sheep skin).

Constructing an appropriate calibration set entails using a minimum number of skin specimens from different sheep races. Each specimen was used to obtain natural samples of variable characteristics that were employed to construct the different data matrices for powdered and unpowdered natural and defatted skin.

As a rule, NIR signals and the reference analytical data matrices are incorporated into the internal library for the control analytical system. If, as was the case in this work, the quantitative control parameter is more responsive to a given chemical species present in variable proportions, choosing an appropriate calibration matrix and number of PLS components for it and the external prediction set requires carefully examining the binary plots of scores and loadings, and the total residual variance curve. Also, because the reference method was applied to a powdered sample and the aim was to control the fat content in natural and defatted skin, appropriate data matrices representing such situations must be examined with a view to confirming whether a single calibration matrix can be used to determine the fat content in both natural and defatted samples.

Table 3 shows the results provided by the reference method in the determination of the fat content in each sample prior to and after defatting. For each sample set, the reference values were used to select the calibration model best predicting the results for the samples in the external sets.

Each calibration model was constructed using the sample set selected via a PCA scatter plot. The development of a model consisted in check different spectral pretreatments, as well its combination with different spectral ranges. Once the calibration model was defined, its predictive ability was tested using the sample set not used during its development. The calibration models used were chosen in terms of predictive ability as reflected in their calibration and prediction errors, % RSE.

Fig. 4 shows the score plot obtained by a principal component analysis from second derivative spectra, with the selected cali-

Table 3
Results provided by the reference method (IUC 4)

Sample	Extractable matter prior to defatting (% fat)	%Surfactant applied	Extractable matter after to defatting (% fat)
a21	8.3	15	6.6
a22	9.2	10	5.3
a23	8.2	5	4.0
a31	8.6	10	5.9
a32	9.3	15	5.8
a34	7.3	10	3.1
e11	5.7	15	5.0
e12	5.8	5	4.3
e13	5.7	15	4.9
e22	5.7	10	4.8
e23	5.7	10	3.9
e24	5.0	5	4.1
e32	6.4	10 + 10	4.4
e33	6.7	5 + 5	4.1
m11	7.4	5 + 5	4.7
m13	8.2	5	5.8
m15	7.3	5	5.0
m21	6.8	5 + 5	5.4
m22	6.1	15	5.1
m31	6.3	5	3.8
m32	5.6	5 + 5	4.5
m33	5.1	10	4.5
m34	5.6	10	3.3
r12	9.1	5	6.3
r13	9.0	5 + 5	4.5
r14	8.0	15	5.6
r21	7.4	15	6.4
r31	9.3	10 + 10	6.7
r32	12.2	5 + 5	8.2
r33	12.1	10 + 10	8.1
r34	10.3	5	8.3

bration and prediction sets, for the test series with unpowdered all-samples. Fig. 5 shows the variation of MSECV as a function of the number of PLS factors for the entire body of samples (undefatted and defatted). Table 4 shows the selected models and the results they provided. The errors made in predicting the calibration samples were always comparable to the prediction errors

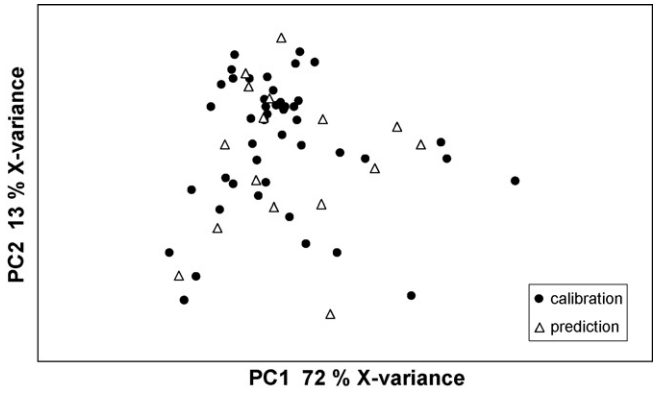

Fig. 4. PCA scatter plot from second derivative for the test series with unpowdered all-samples.

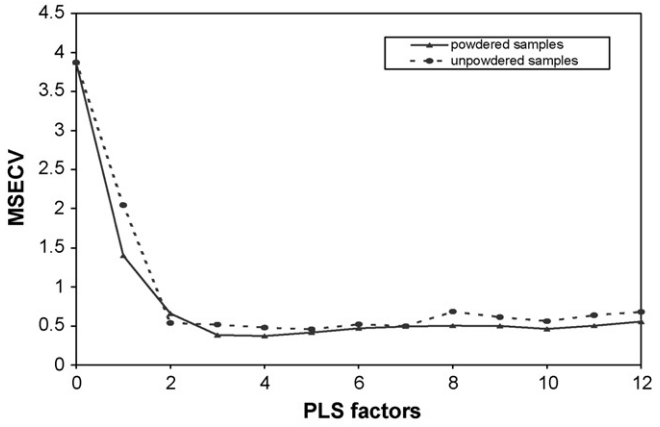

Fig. 5. Variation of MSECV with the number of PLS factors used as calculated from second-derivative spectra. Measurements were made on samples prior to and after defatting.

for the external samples; this confirms the absence of overfitting in the models.

Table 5 shows the figures of merit of the plots of NIR versus reference results for the calibration and prediction samples. Based on the slope and intercepts obtained, the differences between the two methods were not statistically significant, evaluated with joint confidence region test at the $p < 0.05$ level.

Despite the complex nature of leather as a substrate, the multivariate treatment applied to the NIR spectra provided good results in all cases, the quantitation errors obtained being acceptable for the tanning industry.

The results were quite good, even in the third test series, which involved the analysis of all types of samples and where spectra were recorded directly on the leather. Consequently, the proposed method allows the fat content in undefatted and defatted leather to be accurately determined by directly recording NIR spectra with a fibre-optic probe and using a single calibration set encompassing all possible variability among leather samples. In summary, our method allows the highly expeditious, reliable determination of the fat content in leather and the efficiency of defatting procedures.

Table 4
Relative standard errors for the calibration and prediction external sets

Sample state	Spectral mode	PLS components	RSEP (%)	RSEP (%)
Non-defatted leather[a]				
Powdered	Second-derivate	2	8.1	11.6
Unpowdered	Second-derivate	4	7.1	7.4
Defatted leather[a]				
Powdered	Second-derivate	3	9.0	9.5
Unpowdered	Second-derivate	4	9.7	10.5
All samples[b]				
Powdered	Second-derivate	3	8.3	11.8
Unpowdered	Second-derivate	4	8.3	9.9

[a] Calibration set 21 samples; prediction external set 10 samples.
[b] Calibration set 46 samples; prediction external set 16 samples.

Table 5
Regression parameters for NIRS vs. the reference method

Sample state	Set	Concentration range (%)	Slope	Intercept	*R*
Non-defatted leather					
Powdered	Calibration	5.0–12.2	0.89 ± 0.15	0.84 ± 1.16	0.942
	Prediction	5.2–12.1	0.64 ± 0.15	2.27 ± 1.20	0.962
Unpowdered	Calibration	5.0–12.2	0.91 ± 0.14	0.65 ± 1.04	0.955
	Prediction	5.2–12.1	0.78 ± 0.17	1.67 ± 1.38	0.966
Defatted leather					
Powdered	Calibration	3.1–8.3	0.87 ± 0.16	0.67 ± 0.87	0.934
	Prediction	3.3–8.1	0.93 ± 0.30	0.53 ± 1.63	0.930
Unpowdered	Calibration	3.1–8.3	0.85 ± 0.17	0.78 ± 0.92	0.922
	Prediction	3.3–8.1	1.18 ± 0.33	−0.99 ± 1.77	0.947
All samples					
Powdered	Calibration	3.1–12.2	0.92 ± 0.08	0.51 ± 0.54	0.959
	Prediction	3.8–12.1	0.81 ± 0.15	0.87 ± 1.07	0.949
Unpowdered	Calibration	3.1–12.2	0.92 ± 0.08	0.52 ± 0.55	0.958
	Prediction	3.8–12.1	0.98 ± 0.18	−0.02 ± 1.24	0.953

4. Conclusions

The mutual symbiosis of industrial activity, scientific research and technological development helps meet social needs and raise social living standards. Industry is competitive and control analyses call for fast determination methods; however, the increasing environmental awareness questions the use of polluting reagents in such methods.

For a number of industries, the technology of choice for developing fast analytical methods requiring no reagents is NIR spectroscopy in conjunction with chemometric processing of the information it provides.

NIR spectroscopy is especially suitable for implementing control analyses in the leather tanning industry. As shown in this work, this technique allows leather fat to be determined and the defatting process to be monitored competitively with any existing method for this purpose.

A fibre-optic probe allows the diffuse reflectance spectrum for a leather specimen to be acquired within a few seconds. Also, the associated chemometric treatment of the information it contains allows a reliable fat content to be determined virtually immediately after the spectroscopic measurement.

In fact, the proposed method allows leather fat to be determined within a few minutes as opposed to more than 5 h in the official method (IUC 4), to which it is therefore an advantageous alternative.

Acknowledgement

The authors are grateful to Spain's MCyT for funding this research within the framework of Project BQU2003-04247.

References

[1] M. Marjoniemi, JSLTC 79 (1995) 41.
[2] M. Marjoniemi, E. Mäntysalo, JALCA 87 (1992) 249.
[3] D.C. Shelly, E.M. Brown, JALCA 94 (1999) 315.
[4] M. Blanco, T. Canals, J. Coello, J. Gené, H. Iturriaga, S. Maspoch, JSLTC 80 (1996) 110.
[5] M. Blanco, T. Canals, J. Coello, J. Gené, H. Iturriaga, S. Maspoch, Anal. Chim. Acta 419 (2000) 209.
[6] M. Blanco, T. Canals, J. Coello, J. Gené, H. Iturriaga, J. Jumilla, S. Maspoch, JSDC 113 (1997) 311.
[7] M. Blanco, T. Canals, J. Coello, J. Gené, H. Iturriaga, S. Maspoch, K. Mora, JSLTC 83 (1999) 96.
[8] J.M. Adzet et al., *Química Técnica de Teneria*, Igualada, 1985, p. 207.
[9] JSLTC 49 (1965) 10.
[10] J.M. Adzet, et al., Tecnología del Cuero, vol. 4, Ed. Cícero, Barcelona, 1995, p. 303.
[11] G. Lampard, JSLTC 78 (1994) 119.
[12] D.H. Stamp, JALCA 69 (1974) 290.
[13] M. Tomaselli, A. Cozzolino, C. Liccardi, CPMC 71 (4) (1995) 47.
[14] L. Manganiello, A. Marsal, A. Rios, M. Valcárcel, Analyst 126 (2001) 938.
[15] J. Workman, M. Koch, D.J. Veltkamp, Anal. Chem. 75 (2003) 2859.
[16] M.J. Donkin, J. Pearce, JSLTC 79 (1995) 8.
[17] M. Blanco, T. Canals, J. Coello, J. Gené, H. Iturriaga, S. Maspoch, D. Rey, Proceedings of the XXV IULTS Congress, Science in Leather SLP-7, 1999, p. 109.
[18] M. Blanco, T. Canals, J. Coello, R. Gasca, J. Gené, H. Iturriaga, S. Maspoch, JSLTC 83 (1999) 204.
[19] D. Plate, Leder Häute Markt 2 (2000) 25.
[20] D. Plate, H. Geissler, Leder Häute Markt 6 (2003) 30.
[21] JSLTC 49 (1965) 8.

Available online at www.sciencedirect.com
ScienceDirect
Talanta 71 (2007) 1752–1756
Talanta
www.elsevier.com/locate/talanta

A method to construct polyelectrolyte multilayers film containing gold nanoparticles

Hongjun Chen [a,b], Shaojun Dong [a,b,*]

[a] *State Key Laboratory of Electroanalytical Chemistry, Changchun Institute of Applied Chemistry, Chinese Academy of Sciences, Changchun, Jilin 130022, PR China*
[b] *Graduate School of the Chinese Academy of Sciences, Beijing 100039, PR China*

Received 29 March 2006; received in revised form 7 August 2006; accepted 8 August 2006
Available online 26 September 2006

Abstract

Gold nanoparticles in polyelectrolyte multilayers film can be easily prepared by repeating immersion of a substrate in poly(diallyl dimethylammonium) chloride (PDDA)-$AuCl_4^-$ complexes solution followed by reduction Au^{3+} through heating. UV–vis spectroscopy, cyclic voltammetry (CV) and tapping-mode atomic force microscopy (AFM) are used to confirm the successful construction of the polyelectrolyte multilayers film and the formation of gold nanoparticles. The multilayers film shows electrocatalytic activity to dioxygen reduction.

Keywords: Poly(diallyl dimethylammonium) chloride; Polyelectrolyte; Gold nanoparticles; Atomic force microscopy; Electrocatalysis

1. Introduction

In recent years, metal nanoparticles are of fundamental interest and technological importance because of their unique electronic, catalytic and optical properties stemming from their small size and large surface area relative to their volumes [1]. The metal nanoparticles in the form of thin films deposited on suitable substrates will be most useful in many cases. Except for overcoming the metal nanoparticles aggregation, the encapsulated nanoparticles thin films may also have a tremendous influence on their catalytic activity and selectivity [2].

The layer-by-layer (LBL) assembly method with accurately controlling film thickness and formation of films on a wide variety of surfaces has been applied to the preparation of the three-dimensional superstructure [3]. The driving forces in construction such superstructure include ligand–metal ion–ligand bridges [4], covalent bonding [5] and electrostatic interaction between oppositely charged polyelectrolytes [6]. This method has been used extensively to construct composite films containing binary inorganic colloids or nobel metal nanoparticles [7–9]. Cohen et al. demonstrated that inorganic nanoparticles could be synthesized within polyelectrolyte multilayers thin film with molecular level control over the spatial location of the particles and particles size [8]. Bruening et al. synthesized polyelectrolyte multilayers film embedding noble metal nanoparticles and its application in catalysis and selective hydrogenation [9]. Our group has reported a simple preparation method of polymer multilayers film containing Pd nanoparticles and its high catalytic activity for the reduction of dissolved oxygen and oxidation of hydrazine compounds in aqueous solution [10].

In this paper, we demonstrate that gold nanoparticles can be synthesized within poly(diallyl dimethylammonium) chloride (PDDA) multilayers film simply through LBL adsorption of PDDA-$AuCl_4^-$ complex [11] and finally reduction of the Au^{3+} by heating. To our knowledge, PDDA used as polyelectrolyte to synthesis polyelectrolyte–metal nanoparticle composite multilayers film and also as a reducing agent to synthesis metal nanoparticles have not been reported. Through UV–vis spectroscopy, CV and AFM measurements, the polyelectrolyte multilayers film containing gold nanoparticles have been successfully constructed and show the electrocatalysis for the dioxygen reduction.

* Corresponding author. Fax: +86 431 5689711.
E-mail address: dongsj@ciac.jl.cn (S. Dong).

0039-9140/$ – see front matter © 2006 Elsevier B.V. All rights reserved.
doi:10.1016/j.talanta.2006.08.014

2. Experimental part

2.1. Chemicals

PDDA (50 wt% in water, M_w ~20000) and poly(sodium 4-styrenesulfonate) (PSS, M_w ~70000) were purchased from Aldrich. $HAuCl_4$, potassium dihydrogen phosphate and dipotassium hydrogen phosphate were obtained from Beijing Chemical reagent Co. (Beijing, China). All chemicals, unless mentioned otherwise, were of analytical grade and used as received. All aqueous solutions were made with deionized water, which was further purified with a Milli-Q system (Millipore).

2.2. Electrochemistry

CV was performed with a CHI 600 electro-chemical workstation (CH Instrument Co., USA) in a conventional three-electrode electrochemical cell with the modified indium tin oxide (ITO) glass or glassy carbon (GC) plate (diameter 1 cm, purity 99.99%) as the working electrode, a large platinum foil as the auxiliary electrode, and Ag/AgCl (saturated KCl) as the reference electrode. CV was performed in quiescent solution. Prior to use, ITO glass was previously sonicated in acetone for 5 min, followed by rinsing with water, ultrasonic agitation in concentrated NaOH in 1:1 (v/v) of water to ethanol, rinsing further with water, immersion in $CHCl_3$ for 10 min, and drying according to the literature [12]. The GC plate was polished with 1.0, 0.3 and 0.05 μm alumina slurry successively and sonicated in water for about 5 min after each polishing step. Finally, the plate was sonicated in H_2O and ethanol, washed with ethanol, and dried with a high-purity nitrogen stream immediately before use.

2.3. Preparation procedure of multilayers film containing gold nanoparticles

An ITO glass (or GC plate) was firstly immersed into PDDA (2 wt% in water, containing 0.5 M NaCl) for 30 min. After being washed in water and drying in a nitrogen stream, the ITO glass (or GC plate) with the PDDA monolayer was immersed into PSS (2 mg mL^{-1}, containing 0.5 M NaCl) for 30 min. After being washed in water and dried in a nitrogen stream, the ITO glass (or GC plate) with the PSS/ PDDA precursor layer was immersed into PDDA-$AuCl_4^-$ complex solution (2 wt% PDDA in water, containing 0.1 wt% $HAuCl_4$ and 0.5 M NaCl) for 30 min. This step was repeated to obtain the desired number of layers of PDDA-$HAuCl_4$ with the intermediate water washing and drying in a nitrogen stream.

After the ITO glass (or GC plate) with the (PDDA-$HAuCl_4)_n$/PSS/PDDA layers was heated to 200 °C for 0.5 h, the multilayers of (PDDA-$Au^0)_n$/PSS/PDDA film on ITO glass (or GC plate) was obtained.

2.4. Instrumentation

UV–vis spectra were collected on a CARY 500 Scan UV–vis–near infrared (UV–vis–NIR) spectrophotometer. Tapping-mode AFM was conducted on a SPA400 equipped with a SPI3800N controller microscope instrument (made in Japan, Seiko Instruments, Inc.).

3. Results and discussion

To investigate the multilayers film construction, UV–vis spectroscopy of (PDDA-$HAuCl_4)_n$ and (PDDA-$Au^0)_n$ multilayers film on ITO were performed, which demonstrate that LBL deposition occurs. Fig. 1 shows the UV–vis absorption spectra of 4–11 layers of (PDDA-$HAuCl_4)_n$ films on the PSS/PDDA-coated ITO slide, respectively. The linear increase in absorbance with the number of layers suggests a regular deposition of the film (Fig. 1, *inset*). The absorbance of (PDDA-$HAuCl_4)_n$ films at 330 nm, which is likely due to the ligand-to-metal charge transfer of the $AuCl_4^-$ ions [13], is shifted to the longer wave as compared with that of the $HAuCl_4$ solution (319 nm) due to the interaction between $HAuCl_4$ and PDDA [14]. Heat-induced reduction yields gold nanoparticles occurred in the multilayers film. (as shown in Fig. 1 curve i and the inset photograph). The disappearance of the absorbance at 330 nm and the appearance of the absorbance at 544 nm, which is the characteristic absorbance of gold nanoparticles, confirm the formation of gold nanoparticles embedded in the multilayers film through heating. The red color of the ITO glass (*inset*) also provides a clear evidence for the formation of gold nanoparticles [15]. It is noted that the anion of $AuCl^{4-}$ was reduced by PDDA through heating, PDDA used as reducing agent for this reaction [16]. If without PDDA, no gold nanoparticles were synthesized in the same situation, which prove PDDA as reducing agent. But only through heating, this reaction can be occurred.

The UV–vis absorption spectroscopy was used to further investigated the change in surface plasmon absorption of the synthesized gold nanoparticles in (PDDA-$Au^0)_n$ films after LBL construction. Here, when the (PDDA-$Au^0)_n$ films increased from 1 to 8 layers on the PSS/PDDA-coated ITO slide, obvious

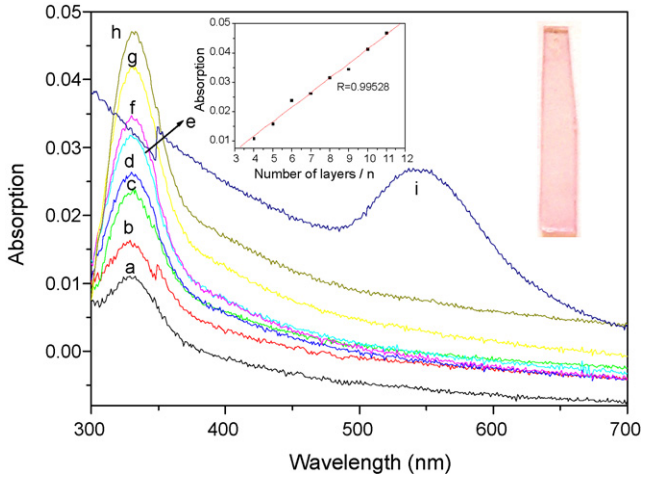

Fig. 1. UV–vis absorption spectra of multilayers film (PDDA-$HAuCl_4)_n$ with n = 4–11 (from curve a to h) and (PDDA-$Au^0)_{11}$ (i) on PSS/PDDA-coated ITO glass, respectively. The inset shows the relationship of absorbance at 330 nm vs. the number of layers and the photograph of (PDDA-$Au^0)_{11}$ on PSS/PDDA-coated ITO glass.

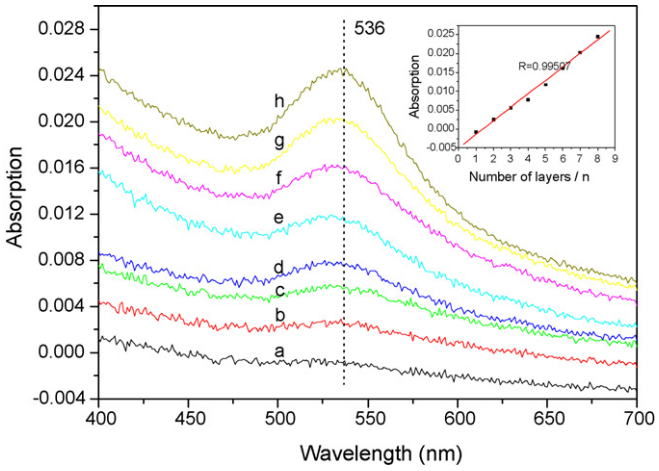

Fig. 2. UV–vis absorption spectra of multilayers film $(PDDA\text{-}Au^0)_n$ with $n = 1$–8 (from curve a to h) on PSS/PDDA-coated ITO glass, respectively. The inset shows the relationship of absorbance at 536 nm vs. the number of layers.

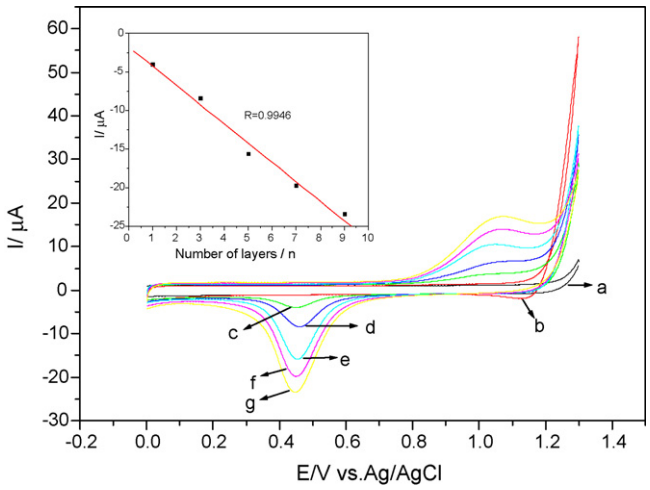

Fig. 3. Cyclic voltammograms of blank ITO glass (a) PSS/PDDA-coated ITO glass (b) and $(PDDA\text{-}Au^0)_n$/PSS/PDDA-coated ITO glass with $n = 1$, 3, 5, 7 and 9 (from curve c to curve g) in pH 7.0 PBS, respectively. Scan rate: 50 mV s^{-1}. The inset shows the relationship of the cathodic current vs. the number of layers.

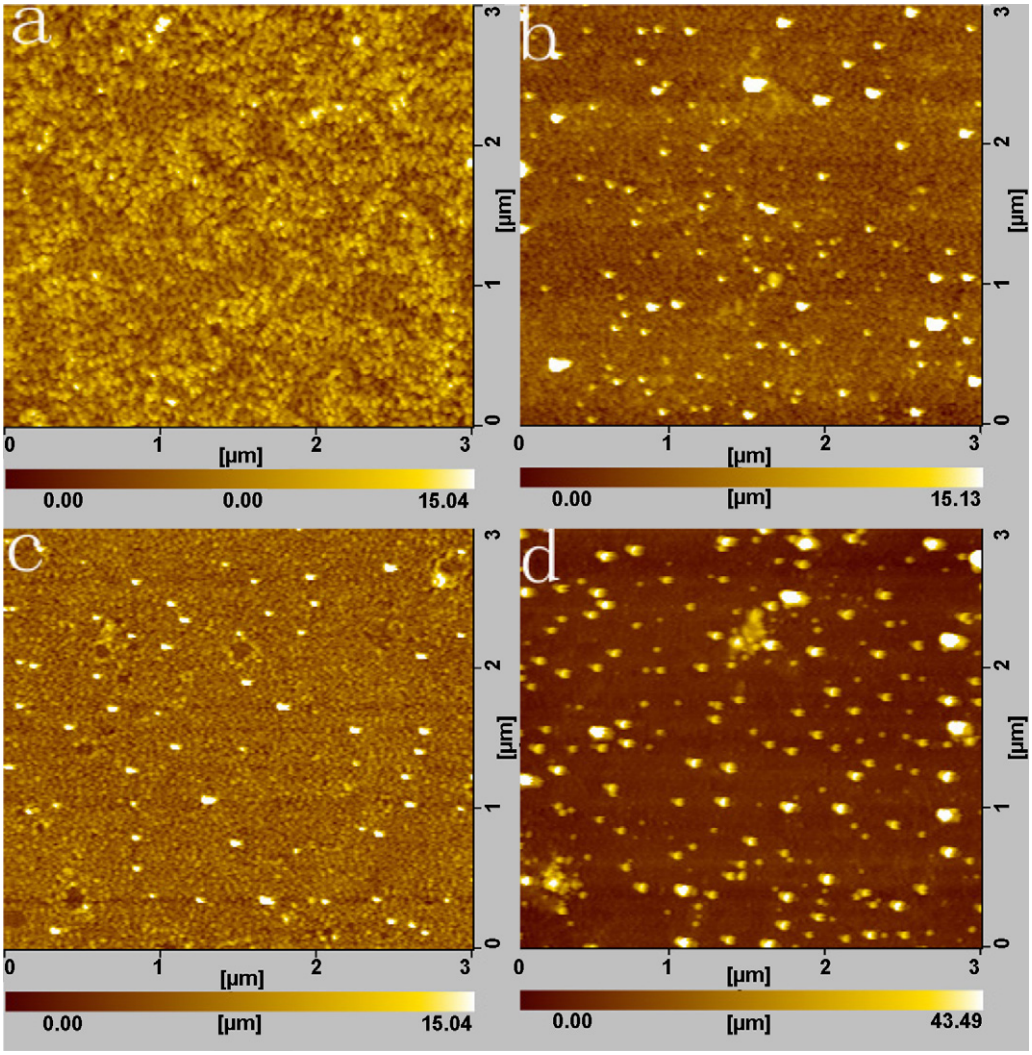

Fig. 4. Tapping-mode AFM images of multilayers film $(PDDA\text{-}HAuCl_4)_4$ on a PSS/PDDA-coated ITO glass before (a) and after (b) heating induced reduction and multilayers film $(PDDA\text{-}Au^0)_1$ (c) and $(PDDA\text{-}Au^0)_9$ (d) on a PSS/PDDA-coated ITO glass.

absorbance increase and red-shift of the surface plasmon band are observed as shown in Fig. 2. The absorbance increase and red-shift of the surface plasmon band with increasing number of layers indicate the number and size of the synthesized gold nanoparticles increased [15]. The evenly changed spectral responses of the surface plasmon band demonstrate uniform growth of $(PDDA\text{-}Au^0)_n$ films (Fig. 2, *inset*).

Because the gold nanoparticles in multilayers film have their characteristic redox peaks in CV, electrochemical measurements can be used to monitor the increase of the multilayers film. Fig. 3 shows cyclic voltammograms of the $(PDDA\text{-}Au^0)_n$ multilayers film with $n = 1$, 3, 5, 7 and 9. There is an oxidation peak at about 1.1 V and a reduction peak at about 0.44 V in pH 7.0 phosphate buffer solution (PBS) in the potential region from 0 to 1.3 V. Because the bare ITO (Fig. 3, curve a) and PSS/PDDA-coated ITO (Fig. 3, curve b) have no current response in this potential region, the redox peaks are attributed to the oxidation and subsequent reduction of gold nanoparticles [17]. The redox current of the gold nanoparticles is regularly enhanced with the number of layers, and the good linear relationship of the cathodic peak current of the multilayers film to the number of layers indicates the uniform growth of the film (Fig. 3, *inset*).

AFM was used to investigate the surface morphology of $(PDDA\text{-}HAuCl_4)_n$ multilayers film and the formation of gold nanoparticles in the film. The AFM images of $(PDDA\text{-}HAuCl_4)_4$ multilayers film assembled on ITO slide before (a) and after (b) exposure to heating are shown in Fig. 4. Before heating, the $(PDDA\text{-}HAuCl_4)_4$ multilayers film exhibits a relative smooth surface morphology, with a root-mean-squared (RMS) roughness of ~2.1 nm. After the multilayers film was reduced by heating, gold nanopartiles with the average diameter about 20 nm can be seen clearly and the RMS roughness increases to ~2.5 nm. Compared with one layer (Fig. 4c) and nine layers (Fig. 4d) of the reduced multilayers film, the number of gold nanoparticles increases and the average diameter of the gold nanoparticles enlarge from about 12 to about 35 nm. The increase of diameter of the gold nanoparticles is probably because heating promotes aggregation of Au atoms [9]. Because of the magnification of the AFM tip convolution effects, the real diameter of gold nanoparticles is smaller than the observed ones.

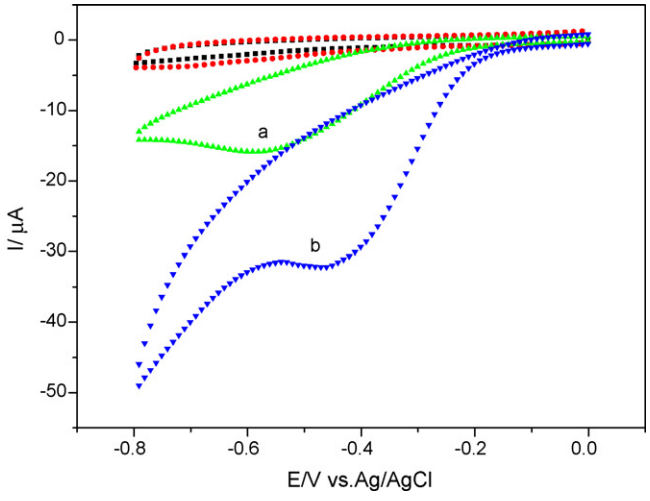

Fig. 5. Cyclic voltammograms obtained for the O_2 reduction at bare GC plate (a) and $(PDDA\text{-}Au^0)_9$ multilayers film on a PSS/PDDA-coated GC plate (b) in air-saturated 0.1 M PBS, respectively. The square and circle lines correspond to the bare and modified GC plate, respectively, in N_2-saturated 0.1 M PBS. Potential scan rate: 50 mV s^{-1}.

The preliminary catalysis experiments are also carried out using $(PDDA\text{-}Au^0)_9$ multilayers film for O_2 reduction. Fig. 5 shows the cyclic voltamograms obtained for the reduction of O_2 with bare (curve a) and $(PDDA\text{-}Au^0)_9$ multilayers film (curve b) modified GC electrodes in air-saturated pH 7.0 PBS. The catalytic features of the $(PDDA\text{-}Au^0)_9$ multilayers film modified GC electrode can be reflected from comparing these two curves, a significant positive shift of O_2 reduction peak potential from −0.6 to −0.45 V and an increase in the peak current. This proves that the $(PDDA\text{-}Au^0)_9$ multilayers film can catalysis O_2 reduction.

4. Conclusion

In conclusion, the assembly of multilayers film can be constructed using the $PDDA\text{-}AuCl_4^-$ complexes solution by LBL technique. Through heating induced reduction, the gold nanoparticles formed in the multilayers film, which show electrocatalytic activity for dioxygen reduction.

Acknowledgement

This work was supported by the National Natural Science Foundation of China (nos. 20427003, 20575064).

References

[1] (a) G. Schmid, L.F. Chi, Adv. Mater. 10 (1998) 515;
(b) P.K. Sudeep, B.I. Ipe, K.G. Thomas, M.V. George, S. Barazzouk, S. Hotchandani, P.V. Kamat, Nano Lett. 2 (2002) 29;
(c) H. Weller, Angew. Chem. Int. Ed. 37 (1998) 1658;
(d) B.C. Gates, Chem. Rev. 95 (1995) 511.
[2] (a) H. Bonnemann, R.M. Richards, Eur. J. Inorg. Chem. (2001) 2455;
(b) S. Dante, R. Advincula, C.W. Frank, P. Stroeve, Langmuir 15 (1999) 193.
[3] (a) A.A. Mamedov, J. Ostrander, F. Aliev, N.A. Kotov, Langmuir 16 (2000) 3941;
(b) N.A. Kotov, I. Dekany, J.H. Fendler, J. Phys. Chem. 99 (1995) 13065;
(c) D.L. Feldheim, K.C. Grabar, M.J. Natan, T.E. Mallouk, J. Am. Chem. Soc. 118 (1996) 7640;
(d) R. Blonder, L. Sheeney, I. Willner, Chem. Commun. (1998) 1393;
(e) T. Cassabneau, J.H. Fendler, J. Phys. Chem. B 103 (1999) 1789.
[4] F.P. Zamborini, J.F. Hicks, R.W. Murray, J. Am. Chem. Soc. 122 (2000) 4514.
[5] M.D. Musick, C.D. Keating, M.H. Keefe, M.J. Natan, Chem. Mater. 9 (1997) 99.
[6] (a) G.J. Kellogg, A.M. Mayer, W.B. Stockton, M. Ferreira, M.F. Rubner, S.K. Satija, Langmuir 12 (1996) 5109;
(b) G. Decher, Science 277 (1997) 1232.
[7] (a) A.A. Mamedov, A. elov, M. Giersig, N.N. Mamedova, N.A. Kotov, J. Am. Chem. Soc. 123 (2001) 7738;
(b) J.W. Ostrander, A.A. Mamedov, N.A. Kotov, J. Am. Chem. Soc. 123 (2001) 1101.
[8] (a) T.C. Wang, M.F. Rubner, R.E. Cohen, Langmuir 18 (2002) 3370;
(b) S. Joly, R. Kane, L. Radzilowski, T. Wang, A. Wu, R.E. Cohen, E.L. Thomas, M.F. Rubner, Langmuir 16 (2000) 1354;
(c) T.C. Wang, M.F. Rubner, R.E. Cohen, Chem. Mater. 15 (2003) 299.

[9] (a) S. Kidambi, M.L. Bruening, Chem. Mater. 17 (2005) 301;
(b) J. Dai, M.L. Bruening, Nano Lett. 2 (2002) 497;
(c) S. Kidambi, J. Dai, J. Li, M.L. Bruening, J. Am. Chem. Soc. 126 (2004) 2658.
[10] J. Liu, L. Cheng, Y. Song, B. Liu, S. Dong, Langmuir 17 (2001) 6747.
[11] A.B.R. Mayer, S.H. Hausner, J.E. Mark, Polym. J. 32 (2000) 15.
[12] I. Prieto, M.T. Martin, D. Mobius, L. Camacho, J. Phys. Chem. B 102 (1998) 523.
[13] (a) J.A. Peck, C.D. Tait, B.I. Swanson, G.E. Brown, Geochim. Cosmochim. Acta 55 (1991) 671;
(b) L. Longenberger, G. Mills, J. Phys. Chem. 99 (1995) 475.
[14] M.Q. Zhao, R.M. Crooks, Angew. Chem. Int. Ed. 38 (1999) 364.
[15] W. Cheng, S. Dong, E. Wang, J. Phys. Chem. B 108 (2004) 19146.
[16] H. Chen, Y. Wang, Y. Wang, S. Dong, E. Wang, Polymer 47 (2006) 763.
[17] (a) A. Yu, Z. Liang, J. Cho, F. Caruso, Nano Lett. 3 (2003) 1203;
(b) L.D. Burke, V.J. Cunnane, J. Electroanal. Chem. 210 (1986) 69;
(c) L.D. Burke, P.F. Nugent, Gold Bull. 31 (1998) 39.

Available online at www.sciencedirect.com
ScienceDirect
Talanta 71 (2007) 1757–1761
Talanta
www.elsevier.com/locate/talanta

Ferric nanoparticle-based resonance light scattering determination of DNA at nanogram levels

Yongqiang Cheng [a], Zhengping Li [a,*], Yuqin Su [a], Yongshan Fan [b]

[a] *College of Chemistry and Environment Science, Hebei University, Baoding 071002, PR China*
[b] *Biological Science and Technology Department, Tangshan Teachers College, Tangshan 063000, PR China*

Received 27 April 2006; received in revised form 8 August 2006; accepted 8 August 2006
Available online 8 September 2006

Abstract

A novel assay of DNA has been proposed by using ferric nanoparticles as probes coupled with resonance light scattering (RLS) detection. At pH 7.40, the RLS intensity of ferric nanoparticles can be greatly enhanced by the aggregation of positively charged ferric nanoparticles through electrostatic interaction with negatively charged DNA. The enhanced intensity of RLS at 452 nm is proportional to the concentration of DNA in the range of 0.01–0.8 μg ml^{-1} for calf thymus and salmon sperm DNA and in the range of 0.005–0.3 μg ml^{-1} for *E. coli* K12 genomic DNA. Detection limits are 3.6 ng ml^{-1} for calf thymus DNA, 4.4 ng ml^{-1} for salmon sperm DNA, and 1.9 ng ml^{-1} for *E. coli* K12 genomic DNA, respectively. Compared with the chromophores previously used in RLS assay, the ferric nanoparticles have offered several advantages in easy preparation, good photostability and high sensitivity without being modified or functionalized.

Keywords: Ferric nanoparticles; Resonance light scattering; DNA

1. Introduction

The detection and quantitation of DNA have been essential in biochemistry, clinical diagnosis and environment application [1,2]. Due to the simplicity and the high sensitivity, the resonance light scattering (RLS) technique has been greatly developed for determination of DNA since it was first introduced to analytical chemistry in 1996 [3,4]. This technique is usually based on the enhanced RLS signals resulting from the aggregations or assembly of chromophores on DNA templates by using a common spectrofluorimeter through simultaneously scanning the excitation and emission monochromators with the same wavelength [5]. Nevertheless, the chromophores used, such as water-soluble porphyrins [6,7], organic dyes [8–10], surfactants [11,12] and drugs [13,14], generally suffer from difficult synthesis, toxic and expensive employment. Accordingly, it is desirable to exploit new materials for determination of DNA with RLS technique.

Recently, nanoparticle-based bioassays are particularly attractive due to their unique size-dependent optical, electronic, and catalytic properties [15,16]. It now appears clear that nanoparticles involving quantum dots and metallic nanoparticles will overcome many of the significant chemical and spectral limitations of organic dyes [17]. Therefore, various nanoparticle-based approaches have been continuously reported for determination of DNA, such as electrochemical [18], colorimetric [19], fluorimetric [20,21] and surface enhanced resonance Raman scattering [22] assays. Owing to the specific size effect of the nanoparticle, it may especially match the RLS technique in detecting the biomolecules if the theory of RLS is taken into account. There are a few reports that the nanoparticles are employed in RLS technique for detecting proteins. Zhu et al. [23] have established the light scattering method for determination of proteins based on the quenching of the RLS of colloidal silver chloride in the presence of proteins. The functionalized HgS nanoparticles have also been applied to determine γ-globulin at nanogram level by its enhancement effect on the RLS [24]. However, both methods had high background and the response signals of proteins were weak. So, these methods have to be performed under rigid experimental conditions. Up to now, to the best of our knowledge, nanoparticle-based RLS determination of DNA has not been reported.

* Corresponding author. Fax: +86 3125079525.
E-mail address: lzpbd@mail.hbu.edu.cn (Z. Li).

0039-9140/$ – see front matter © 2006 Elsevier B.V. All rights reserved.
doi:10.1016/j.talanta.2006.08.008

In this paper, ferric nanoparticles have been applied for determination of DNA coupling with the RLS technique. Ferric nanoparticles, which were used to detect the anionic sites of cell surface [25], can be easily obtained in the size of 3–5 nm and kept their positive charges in a wide range of pH 1.8–7.6 in sodium cacodylate buffer solution. While small amount DNA is added to ferric nanoparticle solution, the ferric nanoparticles with positive charge may conjugate to DNA with negative charge by electrostatic attraction and form large aggregates. As a result of aggregation of ferric nanoparticles, the greatly enhanced RLS has been observed. The enhanced intensity of RLS at 452 nm is proportional to the concentration of DNA, so DNA at nanogram levels can be determined. The method is sensitive, simple and low consumption of the reagents.

2. Experimental

2.1. Apparatus

The RLS spectra and the intensity of RLS were measured with a Hitachi F-4500 spectrofluorometer (Tokyo, Japan) equipped with a quartz cell (1 cm × 1 cm). UV–vis absorption spectra were obtained with a UV-2501PC spectrophotometer (Shimadzu, Japan). A pHS-3C digital pH meter (Shanghai, China) was used to measure the pH values of the solutions. Transmission electron microscopy (TEM) images of the nanoparticles were acquired on a JEM-1200EXII transmission electron microscope (Tokyo, Japan).

2.2. Reagents

Stock solutions of DNA (100 μg ml^{-1}) were prepared by directly dissolving commercial calf thymus DNA (ctDNA, Sigma) and salmon sperm DNA (ssDNA, Sigma) in doubly deionized water and were stored at 0–4 °C. Working standard solutions were obtained by appropriate dilution of the stock solutions. Sodium cacodylate ($C_2H_6AsO_2Na{\cdot}3H_2O$) and ferric chloride ($FeCl_3{\cdot}6H_2O$) was purchased from Amresco and Tian Da Chemical Factory (Tianjin, China), respectively. *E. coli* K12 strain was purchased from National Institute for the Control Pharmaceutical and Biological Products (Beijing, China).

E. coli K12 genomic DNA (K12-gDNA) was prepared according to the following procedure: 0.1 ml *E. coli* K12 strain was cultured overnight in 5 ml Luria-Bertni (LB) medium with gentle shaking at 37 °C. Then, K12-gDNA was extracted from 1 ml fresh bacterial solution using TaKaRa MiniBest bacterial genomic DNA extract kit (TaKaRa Biotechnology Co., Ltd., Dalian, China). The concentration of K12-gDNA was calculated according to the optical density at 260 nm (OD_{260}) and the standard of purity of K12-gDNA was determined by OD_{260}/OD_{280} = 1.8–2.0. K12-gDNA working solution was diluted to 2 μg ml^{-1} and was stored at 0–4 °C for use. K12-gDNA samples with different purities were prepared followed by the same procedure as described above.

According to the previously described method [25], 0.01 mol l^{-1} ferric colloid solution was prepared by droping 10 ml of 0.1 mol l^{-1} $FeCl_3$ to 90 ml of boiling water with stirring and then diluting it to 100 ml after cooling to room temperature. The 2.0×10^{-3} mol l^{-1} ferric nanoparticle working solution was prepared by mixing 20 ml of 0.01 mol l^{-1} ferric colloid solution with 6 ml of 0.1 mol l^{-1} sodium cacodylate buffer solution. And that the solution was adjusted to pH 7.40 by 0.2 mol l^{-1} NaOH solution and was finally diluted to 100 ml with doubly deionized water. The prepared ferric nanoparticle solution is water-soluble, transparent and purple-red. The diameter of nanoparticles is about 5 nm (Fig. 1a).

All other reagents were of analytical reagent grade without further purification. Doubly deionized water was used throughout except preparation of K12-gDNA using sterilized deionized water.

2.3. Procedures

In a series of 10 ml volumetric flasks, 1.5 ml of 2.0×10^{-3} mol l^{-1} ferric nanoparticle solution containing

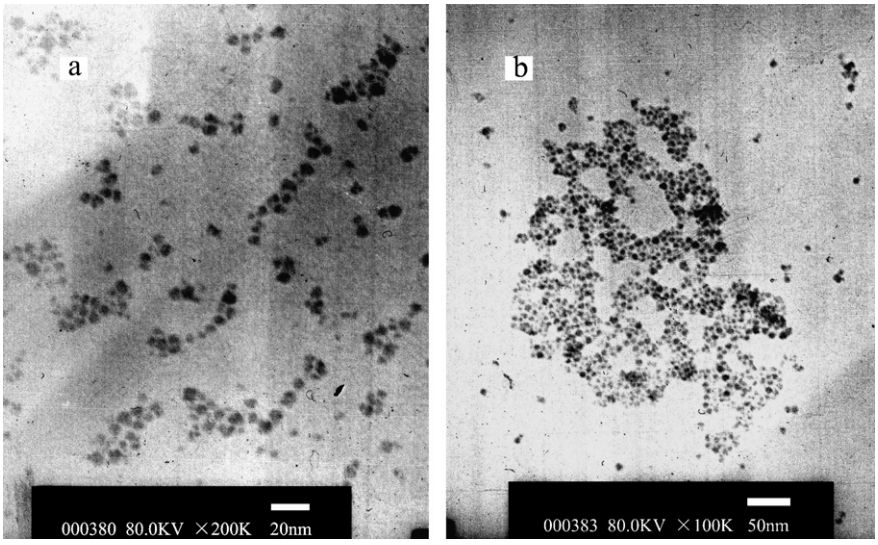

Fig. 1. TEM images of (a) ferric nanoparticles and (b) DNA + ferric nanoparticles.

6.0×10^{-3} mol l^{-1} sodium cacodylate buffer (pH 7.40) and an appropriate volume of DNA solution or samples were added and diluted to the mark with water. The mixture was mixed thoroughly and incubated about 40 min at room temperature. All RLS spectra were obtained by scanning simultaneously the excitation and emission monochromators of F-4500 spectrofluorometer with the same wavelength from 200 to 700 nm. The intensity of RLS was measured at 452 nm with silt width at 5 nm for the excitation and emission.

3. Results and discussion

3.1. Spectral characteristics

TEM images (Fig. 1a) show that the diameter of ferric nanoparticles is about 5 nm. The ferric nanoparticles can be aggregated by the addition of DNA solution (Fig. 1b). The aggregation can be ascribed to the assembly of the ferric nanoparticles on DNA molecules, which act as templates, through the electrostatic interaction between positively charged ferric nanoparticles and negatively charged DNA at pH 7.40.

Fig. 2 shows that the light scattering signal of ferric nanoparticles is very weak. The light scattering is only Rayleigh scattering because the 5 nm size of ferric nanoparticles is smaller than 1/20 of the incident wavelengths over the wavelength range 200–700 nm [26]. An enhanced RLS signals centered wavelength at 452 nm, however, can be observed for the aggregation of ferric nanoparticles by the addition of DNA. Furthermore, the enhanced extent of the light scattering differs for different DNA. This indicates the enhance extent of RLS relates to the length of DNA. These spectral features can be elucidated by the theory of resonance Rayleigh scattering.

According to Pasternack [5,27], when light passes through a solution of aggregates, the extent to which the aggregates absorb and scatter light depends on its size, shape, and index of refractive relative to the surrounding medium including real and imaginary parts. The absorption depends on the first power of

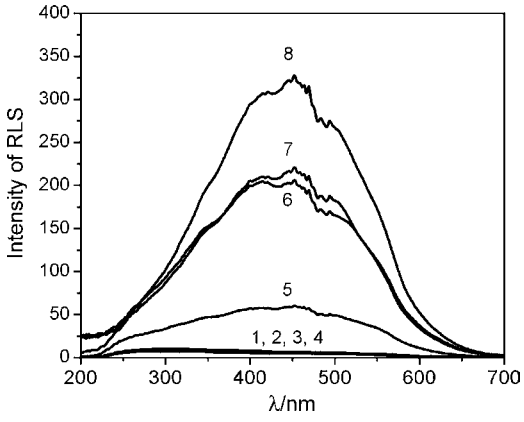

Fig. 2. The resonance light scattering spectra. (1) ctDNA (0.5 μg ml^{-1}); (2) ssDNA (0.5 μg ml^{-1}); (3) K12-gDNA (0.5 μg ml^{-1}); (4) ctDNA + $C_2H_6AsO_2Na$ (3.0×10^{-4} mol l^{-1}); (5) ferric nanoparticles; (6) ferric nanoparticles + ctDNA (0.1 μg ml^{-1}); (7) ferric nanoparticles + ssDNA (0.1 μg ml^{-1}); (8) ferric nanoparticles + K12-gDNA (0.1 μg ml^{-1}). Concentration of ferric nanoparticles: 3.0×10^{-4} mol l^{-1}, pH 7.40.

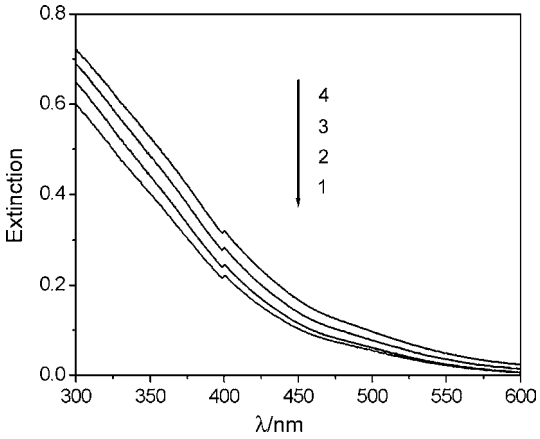

Fig. 3. The extinction spectra of ferric nanoparticles and different concentrations of ctDNA: (1) 0.0; (2) 0.1; (3) 0.3; (4) 0.5 μg ml^{-1}. Ferric nanoparticles: 3.0×10^{-4} mol l^{-1}, pH 7.40.

the polarizability, which in turn depends linearly on the volume of the aggregates. Thus, a solution with a fixed concentration of the aggregation component will exhibit no change in absorbance as aggregation occurs [27]. However, if the solution that scatters appreciable light is measured in a spectrophotometer, it is the extinction that is measured and not absorption [28]. Therefore, consideration must be given both to the absorption of the sample and also to the scattering. As shown in Fig. 3, the extinction spectrum of ferric nanoparticles should be mainly ascribed to the absorption because the light scattering intensity of ferric nanoparticles is very weak. However, the extinction values of the conjugates of ferric nanoparticles with DNA gradually increase with increasing the concentration of DNA. If the absorbance values of ferric nanoparticle and the conjugates of ferric nanoparticles with DNA remain constants as described above, the increased extinction values should be ascribed to the contributions of the enhanced light scattering resulted from the formation of the ferric nanoparticle-DNA aggregates.

The amount of scattering depends on the square of the volume of the aggregate, and it increases as a consequence of aggregation. Thus, the larger the aggregate, the greater the scattering. With the increasing of the concentration of DNA, the size of the ferric nanoparticle-DNA aggregates is increasingly large so that the RLS of the aggregates are strongly enhanced (Fig. 2). Furthermore, compared Fig. 2 with Fig. 3, the extent of the enhanced RLS is obviously greater than that of the enhanced extinction. Therefore, RLS is extremely sensitive to detect the aggregation even at low concentration of DNA interacted with ferric nanoparticles. The absorption band of ferric nanoparticle is in the wavelength of 300–600 nm and the absorbance gradually decreases with increasing of the wavelength. According to the RLS theory, the enhanced RLS should be observed in the absorption band. Because the absorption of ferric nanoparticles is strong at less than 450 nm, the maximum RLS is observed at 452 nm.

3.2. Optimization of the general procedure

The pH of solution plays an important role in the aggregation of ferric nanoparticles. Fig. 4 shows that the RLS intensity

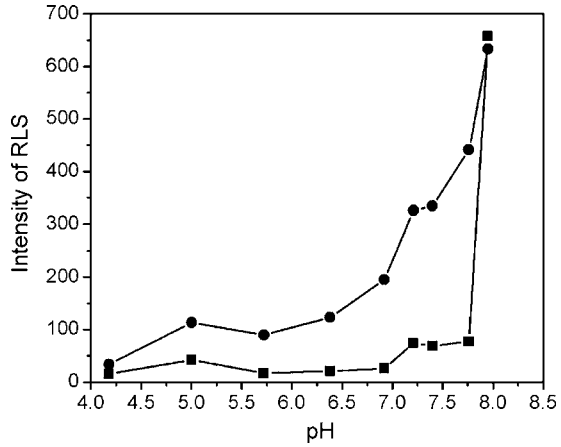

Fig. 4. Effect of pH on RLS intensity of ferric nanoparticles (■) and ferric nanoparticles + ctDNA (●): concentration of ferric nanoparticles is 3.0×10^{-4} mol l^{-1} and ctDNA is 0.2 μg ml^{-1}.

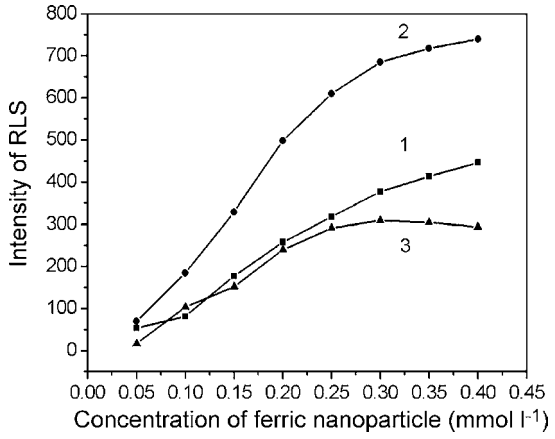

Fig. 5. Effect of the concentration of ferric nanoparticles on RLS intensity. (1) Ferric nanoparticles; (2) ferric nanoparticles + ctDNA (0.2 μg ml^{-1}); (3) differences of RLS intensity between 2 and 1.

of both ferric nanoparticles and ferric nanoparticle-DNA aggregates are increasingly strengthened with increasing pH value. However, the enhanced RLS intensity reaches its maximum in the range of pH 7.40–7.76. When pH value is greater than 7.76, the blank of the ferric nanoparticles increases suddenly resulted from precipitation of the ferric nanoparticles, which indicates that the ferric colloids have been destroyed. Therefore, pH 7.40 was chosen for use considering the stability of reaction system.

The concentration of ferric nanoparticles affects the sensitivity of the RLS assay (Fig. 5). Both RLS intensities of ferric nanoparticles and ferric nanoparticle-DNA aggregates increase with increasing concentration of ferric nanoparticles. However, the differences of the RLS intensities between them reach the maximum when the concentration of ferric nanoparticles is at 3.0×10^{-4} mol l^{-1}. Therefore, a ferric nanoparticle concentration of 3.0×10^{-4} mol l^{-1} was recommended for subsequent work.

The RLS intensities of ferric nanoparticles are stable in at least 120 min at room temperature, while the RLS intensities of ferric nanoparticle-DNA aggregates increase weakly within 40 min and keep stable at least from 40 to 120 min. So the RLS intensity was measured after the system had incubated for 40 min at room temperature. The effect of ionic strength was also examined by the addition of NaCl. The results indicate that the ionic strength has little effect on the assay, which proves that the interaction of ferric nanoparticles with DNA is very strong.

3.3. Interference of coexisting foreign substances

The influence of foreign ions, nucleotides and proteins were tested according to the standard procedure. It was found that these foreign substances had little effects on the determination of DNA under the permission of ±5% error. As Table 1 shows, most of metallic ions can be allowed with high concentrations. Proteins, nucleotides, anionic surfactant (SDS) and phosphate can be allowed with relatively low concentration. However, the allowed concentration of these ions is still higher than the concentration present in biological fluids.

3.4. Calibration and detection limits

Under optimal conditions, the calibration curves for ctDNA, ssDNA and K12-gDNA are constructed according to above standard procedure. There are good linear relationships between the

Table 1
Tolerance of foreign substances[a]

Substances	Concentration ($\times 10^{-6}$ mol l^{-1})	Change of I_{RLS} (%)	Substances	Concentration ($\times 10^{-6}$ mol l^{-1})	Change of I_{RLS} (%)
Ca^{2+}, Cl^-	2000	−3.0	NH_4^+, Cl^-	4000	4.7
Cd^{2+}, Cl^-	3.0	4.9	Zn^{2+}, Cl^-	20	2.8
Co^{2+}, Cl^-	7.5	4.7	Bovine serum albumin	0.1[b]	2.4
Cr^{3+}, NO_3^-	2.0	4.8	Human serum albumin	0.3[b]	3.1
Cu^{2+}, SO_4^{2-}	25	−3.3	Human γ-globulin	1.0[b]	4.8
CTMAB	5.0	1.0	dATP	0.12	5.0
Mn^{2+}, SO_4^{2-}	2.5	3.0	dCTP	0.12	5.0
K^+, Cl^-	2000	−2.8	dGTP	0.12	5.0
Na^+, Cl^-	2500	−1.0	dTTP	0.12	5.0
Mg^{2+}, Cl^-	5.0	−4.2	SDS	0.2	4.5
Na^+, HPO_4^{2-}	0.4	−0.8			

[a] Concentrations: ferric nanoparticles, 3.0×10^{-4} mol l^{-1}; ctDNA, 0.1 μg ml^{-1}; pH 7.40.
[b] Represented by μg ml^{-1}.

Table 2
Analytical parameters for the determination of nucleic acids

Nucleic acids	Linear range ($\mu g\,ml^{-1}$)	Linear regression equation (C, $\mu g\,ml^{-1}$)	Detection limit (3σ, $ng\,ml^{-1}$)	Correlation coefficient (r)
ctDNA	0.01–0.8	$\Delta I_{RLS} = -9.78 + 1137.3C$	3.6	0.9995
ssDNA	0.01–0.8	$\Delta I_{RLS} = -11.9 + 782.9C$	4.2	0.9988
K12-gDNA	0.005–0.3	$\Delta I_{RLS} = 9.3 + 2420.6C$	1.9	0.9998

Table 3
Analytical results for the determination of *E. coli* K12 genomic DNA samples

Sample number	Found value ($\mu g\,ml^{-1}$)	Standard added ($\mu g\,ml^{-1}$)	Recovery value ($\mu g\,ml^{-1}$)	Recovery (%, $n=5$)	R.S.D. (%, $n=5$)
1	0.070	0.060	0.131	96.3–103.8	2.1
		0.120	0.195	97.0–104.6	4.2
2	0.055	0.060	0.120	100.2–108.5	3.7
		0.120	0.169	94.5–102.2	5.1

Ferric nanoparticles 3.0×10^{-4} mol l^{-1}; pH 7.40.

enhanced RLS intensity (ΔI_{RLS}) and the DNA concentrations in the range of 0.01–0.8 $\mu g\,ml^{-1}$ for ctDNA and ssDNA, and 0.005–0.3 $\mu g\,ml^{-1}$ for K12-gDNA. All the analytical parameters are presented in Table 2.

3.5. Sample determination

The present method was applied to quantify genomic DNA samples extracted from *E. coli* K12 bacteria with different purity. The samples were diluted 40-fold with sterilized deionized water before the determination. From Table 3, it can be seen that the results of determination for two samples are satisfied with the different standard added K12-gDNA. Therefore, the determination of DNA by this method is practical.

4. Conclusions

The proposed RLS method is simple, rapid and sensitive for the determination of nanogram-level DNA as a result of the aggregation of ferric nanoparticle directed by DNA. The ferric nanoparticles have several advantages over conventional small organic dyes when used to detect biomolecules in several aspects: (1) ferric nanoparticles are easily prepared with small size by using a simple procedure; (2) the ferric nanoparticles are photostable and biocompatible; (3) the ferric nanoparticles can directly conjugate with DNA through electrostatic interaction without being modified or functionalized. Therefore, it can couple with the polyanion of DNA to form the aggregates, which result in the strong enhancement of RLS, so that determination of DNA at nanogram level can be carried out successfully. The experiment approach provides an easy method of expanding the applications of nano-materials in analytical chemistry and analytical biochemistry.

Acknowledgments

This work was supported by the National Natural Science Foundation of China (NSFC-20375011), program for New Century Excellent Talents in University (NCET-05-0258), the National Science Foundation of Hebei province (B2006000967), and the Youth Science Foundation of Hebei University.

References

[1] C.A. Foy, H.C. Parkes, Clin. Chem. 47 (2001) 990.
[2] J.C. Cho, J.M. Tiedje, Appl. Environ. Microbiol. 68 (2002) 1425.
[3] C.Z. Huang, K.A. Li, S.Y. Tong, Anal. Chem. 68 (1996) 2259.
[4] C.Z. Huang, Y.F. Li, Anal. Chim. Acta 500 (2003) 105.
[5] R.F. Pasternack, C. Bustamante, P.J. Collings, A. Giannetto, E.J. Gibbs, J. Am. Chem. Soc. 115 (1993) 5393.
[6] R. Yang, K.A. Li, K. Wang, F. Liu, N. Li, F.L. Zhao, Spectrochim. Acta A 59 (2003) 153.
[7] C.Z. Huang, K.A. Li, S.Y. Tong, Bull. Chem. Soc. Jpn. 70 (1997) 1843.
[8] C.Z. Huang, K.A. Li, S.Y. Tong, Anal. Chem. 69 (1997) 514.
[9] Y. Liu, C.Q. Ma, K.A. Li, S.Y. Tong, Anal. Chim. Acta 379 (1999) 39.
[10] C.Z. Huang, Y.F. Li, X.D. Liu, Anal. Chim. Acta 375 (1998) 89.
[11] R.T. Liu, J.H. Yang, X. Wu, C.X. Sun, Anal. Chim. Acta 441 (2001) 303.
[12] R.T. Liu, J.H. Yang, X. Wu, Spectrochim. Acta A 58 (2002) 1935.
[13] Z.P. Li, K.A. Li, S.Y. Tong, Talanta 55 (2001) 669.
[14] C. Liu, X.T. Chen, S.Q. Li, X.M. Chen, Chin. J. Chem. Anal. 30 (2002) 1218.
[15] C.M. Niemeyer, Angew. Chem. Int. Ed. 40 (2001) 4128.
[16] A.G. Wu, W.L. Cheng, Z. Li, J.G. Jiang, E. Wang, Talanta 68 (2006) 693.
[17] G.P. Sharron, H. Lin, J.N. Michael, Curr. Opinion Chem. Biol. 7 (2003) 609.
[18] N.N. Zhu, A.P. Zhang, P.G. He, Y.Z. Fang, Electroanalysis 16 (2004) 1925.
[19] S.H. Liu, Z.H. Zhang, Y.B. Wang, F.K. Wang, M.Y. Han, Talanta 67 (2005) 456.
[20] L.Y. Wang, L. Wang, F. Gao, Z.Y. Yu, Z.M. Wu, Analyst 127 (2002) 977.
[21] Y.Y. Zhou, G.R. Bian, L.Y. Wang, L. Dong, L. Wang, J. Kan, Spectrochim. Acta Part A 61 (2005) 1841.
[22] K. Faulds, L. Stewart, W.E. Smith, D. Graham, Talanta 67 (2005) 667.
[23] C.Q. Zhu, D.H. Li, Q.Z. Zhu, H. Zheng, Q.Y. Chen, H.H. Yang, J.G. Xu, Fresenius J. Anal. Chem. 366 (2000) 863.
[24] L.Y. Wang, L. Wang, L. Dong, Y.L. Hu, T.T. Xia, H.Q. Chen, L. Li, C.Q. Zhu, Talanta 62 (2004) 237.
[25] S. Seno, T. Tsujii, T. Ono, S. Ukita, Histochemistry 78 (1983) 27.
[26] G.A. Miller, J. Chem. Phys. 82 (1978) 616.
[27] R.F. Pasternack, P.J. Collings, Science 269 (1995) 935.
[28] P.J. Collings, E.J. Gibbs, T.E. Starr, O. Vafek, C. Yee, L.A. Pomerance, R.F. Pasternack, J. Chem. Phys. B 103 (1999) 8474.

Available online at www.sciencedirect.com
ScienceDirect
Talanta 71 (2007) 1569–1579
Talanta
www.elsevier.com/locate/talanta

Identification of lead pigments in nanosamples from ancient paintings and polychromed sculptures using voltammetry of nanoparticles/atomic force microscopy

Antonio Doménech-Carbó [a,*], María Teresa Doménech-Carbó [b], Xavier Mas-Barberá [b]

[a] *Departament de Química Analítica, Universitat de València, Dr. Moliner 50, Burjassot, 46100 València, Spain*
[b] *Departament de Conservació i Restauracióde Bens Culturals, Institut de Restauració del Patrimoni, Universitat Politécnica de València, Camí de Vera 14, 46022 València, Spain*

Received 27 December 2005; received in revised form 17 July 2006; accepted 24 July 2006
Available online 12 September 2006

Abstract

Voltammetry of nanoparticles coupled with atomic force microscopy was used to identify lead pigments in nanosamples proceeding from works of art. Upon mechanical attachment of few nanograms of sample to a graphite plate, well-defined voltammetric responses were obtained for lead orange, lead yellow, lead white, litharge, minium, Naples yellow, and tin–lead yellow, allowing for an unambiguous identification of such pigments. Atomic force images provide evidence for the occurrence of pigment-characteristic reduction processes accompanied by metal deposition on the graphite substrate. Electrochemical parameters are used for pigment identification. Application to the method for identifying lead pigments in different model binder + pigment specimens and pictorial samples from the canvas painting collection (anonymous, 17th century) of the Saint Joseph Church in Taormina (Italy), the frescoes painted by Antonio Acisclo Palomino y Velasco (1698) in the vault of the *Sant Joan del Mercat* church in València (Spain) and an anonymous polychromed sculpture (16th century) representing a Martyr Saint from Alacant (Spain) is described.

Keywords: Voltammetry of nanoparticles; Atomic force microscopy; Lead pigments; Archaeometry

1. Introduction

Identification of the pigments used by the artists in the past is an obvious target in scientific examination of archaeological artefacts and works of art [1]. Pigment identification in pictorial samples is achieved by polarized light microscopy (PLM), Fourier transform infrared spectroscopy (FT-IR), X-ray diffraction (XRD) [2] and Raman spectroscopy [3]. Scanning electron microscopy (SEM/EDX) and FT-IR transmission or reflectance microscopy are the most used microscopy techniques [4], but in general pigment identification is favoured by a judicious combination of the aforementioned techniques [5,6].

Pigment identification in real pictorial samples, however, is made difficult by: (i) the presence of potentially interfering species such as vernishes and organic bindings, (ii) the strong fixation of the pigments to the substrate, thus causing the need of a frequently uneasy extraction procedure and eventually, (iii) the alteration of pigments and/or other species existing in pictorial layers.

In the search for highly sensitive methods for analyzing works of art, we have previously described the possibility of applying voltammetric methods for identifying pigments in pictorial samples [7–9]. This methodology derives from classical works on carbon paste electrodes [10–14] and is directly based in the voltammetry of microparticles approach developed by Scholz et al. [15–18].

In this context, electrochemical scanning atomic force microscopy devices offer the possibility of analyzing pictorial samples at the nanogram level. Electrochemical scanning atomic force microscopy yields information on the topography and surface reactivity which is of considerable interest in a wide variety of contexts, from polymer to nanostructured layers and thin metal oxide films [19].

The current report presents an intersection of the voltammetry of microparticles approach with atomic force microscopy devoted to the identification of lead pigments in pictorial

* Corresponding author.
E-mail address: antonio.domenech@uv.es (A. Doménech-Carbó).

0039-9140/$ – see front matter © 2006 Elsevier B.V. All rights reserved.
doi:10.1016/j.talanta.2006.07.053

samples at the nanoscopic level. The most used lead pigments in traditional colour palettes [20–24], namely, lead white ($2PbCO_3{\cdot}Pb(OH)_2$), lead–tin yellow ($PbSnO_4$), minium (Pb_3O_4), Naples yellow (lead antimoniate), and PbO pigments litharge and massicot, and those used in the last 150 years, namely chrome yellow and chrome orange (two lead cromates, $PbCrO_4$) [21,22,24], have been studied upon immobilization of pictorial nanosamples to a graphite plate in contact with acetic/acetate buffer (pH 4.8) using an electrochemical scanning atomic force microscopy device. The solid state electrochemistry of microparticulate lead oxides has been extensively studied by Scholz et al. in combination with *in situ* XRD and AFM data [15,16,25–27].

It should be noted, however, that the pigments are accompanied in pictorial samples by bindings and other materials, namely, proteinaceous materials and drying oils, either alone or mixed together so that complex matrix effect can appear. Proteinaceous tempera (milk or casein, egg and animal glue) have been used since antiquity, whereas drying oils began to be used in Europe some time before 13th [28,29]. Moreover, to obtain particular chromatic effects the artists often used *tempera grassa*, which consists of an emulsion of oil and egg and, less frequently, oil and casein or gelatine [28,29].

It is known that several pigments undergo chemical alteration during the ageing of paint. Oil paint films undergo crosslinking reactions, oxidation of unsaturated acids and hydrolysis of glyceride bonds [30]. Proteinaceous materials undergo hydrolysis reactions followed by oxidation, crosslinking, condensation, and dehydration of aminoacids [31]. Following Erhardt et al. [30], hydrolysis has been recognized as the main chemical reaction in paint films both at short and long time scales. Hydrolysis may yield saturated fatty acids (which lack the functional groups that react during the crosslink process), unsaturated fatty acids and short-chain fatty or diacids formed by scission reactions of unsaturated fatty acids. The acids groups formed by hydrolysis may react with metal ions from pigments to produce carboxylate salts, whose presence has been reported in pigmented linseed oil paints [24,32–34]. Boon et al. [33,34] establish that pigment alteration results in the physical change of the paint layer to a hardened, brittle system. These authors describe this hardened system as a polyanionic network in which the several carboxylic acid groups are stabilized by metal ions whose most probable source are the pigments. Accordingly, pigment particles can be surrounded by an ionomeric layer resulting form the reaction of pigments and the products of oil hydrolysis, carboxylate salts (referred to as soaps in the case of fatty acids) [33,34] or free carboxylic acids [30], being considered the main components of the paint layer.

Proteins are rather stable and undergo little chemical change under normal conditions of temperature and humidity [28]. Moisture, however, produces slow hydrolysis of the peptide linkages and eventually permits the action of fungi and bacteria [28]. Ageing yields possibly some changes in protein structure [35,36], while exposure to light, particularly ultraviolet, can produce the breaking of crystalline and peptide linkages [37]. Protein and aminoacids can form complex species with metal cations. In fact, complexation interferes seriously the chromatographic determination of binders in pictorial samples [38–40].

In this work, monitoring the electrochemical response of nanosamples of: (i) pristine lead pigments and $PbCO_3$, $PbCl_2{\cdot}2H_2O$, and $PbSO_4$, taken as model compounds, (ii) model paint specimens consisting of pigment + oil and pigment + oil + protein reproducing traditional preparations and (iii) pictorial samples from different work of arts, is combined with atomic force microscopy imaging in order to identify the different lead pigments. Real pictorial samples proceed from canvas paintings and wall paintings have been studied. It is also studied a sample from polychromed sculpture, a type of work of art where inorganic pigments were also used extensively.

In order to validate the reliability of the voltammetry of nanoparticles/atomic force microscopy (VNP/AFM) methodology, these results were compared with those obtained from microsamples of pigments and synthetic specimens using conventional voltammetry of microparticles, PLM, SEM/EDX, XRD, and FT-IR.

2. Experimental

2.1. Materials and reagents

Commercially available pigments used for blank probes were lead(II) oxide (PbO, litharge, Merck), minium (Pb_3O_4, Probus), lead white ($2PbCO_3{\cdot}Pb(OH)_2$, Sigma–Aldrich, Steinheim, Germany). Massicot (PbO), Naples yellow ($Pb_3[SbO_4]_2$), and lead–tin oxide ($2PbO{\cdot}SnO_2$), all of Kremer, Farbmühle, D-88317 Aichstten/Allgäu, Germany, were supplied by AP Fitzpatrick, London, England. Chrome orange ($7PbCrO_4$ $PbMoO_4{\cdot}2PbSO_4$), produced by Winsor & Newton Ltd., Harrow Wealdstone, Middlesex HA3 5RH, UK, was supplied by Viguer S.L. Productos de Arte y Conservación, València, Spain. Chrome yellow ($PbCrO_4$) from Charbonnel, 13 quai Montebello, 75005 Paris, France, was supplied by RCM Productos de Conservación, Barcelona, Spain. Linseed oil natural cold pressed (Kremer) supplied by AP Fitzpatrick, London, England, bovine gelatine supplied by Sigma–Aldrich (Steinheim, Germany) and ox-gall used in Fine Art works supplied by Dr. Luis Angel de La Fuente (Bilbao, Spain) were used for preparing model paint specimens. Chrome yellow is currently unavailable due to its carcinogenic nature.

Acetic acid (Panreac) and sodium acetate (Merck) were used for electrolyte preparation. $PbCO_3$, $PbCl_2{\cdot}2H_2O$, and $PbSO_4$ (all supplied by Merck) were used as model compounds. Acetic acid (Panreac) plus sodium acetate (Merck) in total concentration 0.50 M were used in nanopure water for electrolyte preparation.

2.2. Instrumentation and procedures

A Multimode AFM (Digital Instruments VEECO Methodology Group, USA) with a NanoScope IIIa controller and equipped with a J-type scanner (maximum scan size of 150 μm × 150 μm × 6 μm) was used. The topography of the samples was studied in contact mode. An oxide-sharpened silicon nitride probe Olympus, VEECO Methodology Group,

model NP-S has been used with a V-shaped cantilever configuration. The spring constant is 0.06 N/m and the tip radius of curvature is 5–40 nm. For electrochemical measurements the AFM was coupled to a Digital Instruments Universal Bipotentiostat (VEECO Methodology group, USA). All measurements were performed at room temperature in solutions previously deaerated with argon during 15 min.

A platinum wire was used as pseudoreference electrode for the *in situ* AFM experiments. The potential of this electrode remained close to 0.25 V versus AgCl (3 M NaCl)/Ag. A platinum wire counterelectrode completed the three-electrode arrangement. All potentials in text are referred to AgCl (3 M NaCl)/Ag reference electrode.

A light microscope Leica DMR (25–400×) was used for selecting the samples to be analyzed and for morphological examination of them.

For performing the VNP/AFM study specimens were prepared by fixing the samples on a graphite plate. Selected grains of the sample were transferred to the surface of the graphite plate with the help of a microscalpel. For all samples, several images were recorded at different locations to verify the repeatability of the observed features.

Complementary experiments with conventional techniques were performed in order to validate pigment identification via VNP/AFM. Examination of samples with light microscope, X-ray diffraction spectrometer, FT-IR spectroscope and scanning electron microscope coupled to an energy dispersive X-ray microanalyzer, and a gas chromatography–mass spectrometer was performed using the equipment already described [7–9].

2.3. Model paint specimens and samples

A series of model paint specimens were prepared by mixing the pigments with the appropriate amount of linseed oil [20]. Thus, pictorial dispersions at 14% (w/w) were obtained and then spread as a thin layer (average thickness, 50–80 μm) on glass slides. The model paint specimens were stored at room temperature (24 ± 2 °C) during 4 weeks and afterwards analyzed.

Similarly to the above model oil paint specimens, a second series of model paint specimens was prepared by mixing the pigments with the appropriate amount of a previously prepared aqueous solution (70 g/L) of bovine gelatine [20]. The resulting pictorial dispersions at 14% (w/w) were obtained and processed as above.

A third series of model paint specimens was prepared by mixing the pigments with the appropriate amount of the above mentioned bovine gelatine aqueous solution and linseed oil. A few drops of ox-gall were also added in order to stabilize the emulsion which reproduces the traditional *tempera grassa* binders prepared by combination of drying oil and a proteinaceous material. The weight percentage of lipids and proteins in the model paint were 24% and 7%, respectively.

Other three series of model paint specimens prepared as previously described which have been naturally aged in the laboratory since 1992 have been analyzed by the proposed VNP/AFM method in order to study the influence of the ageing on the electrochemical response of the specimens. Storage room conditions were 22 °C and 65% RH.

Pictorial samples were extracted, using a microscalpel, from the paintings representing the Betrothal of the Virgin (sample S-1) and the reponse during the Egypt escape (S-2), which are included in the canvas painting collection (anonymous, 17th century) of the Saint Joseph church in Taormina (Italy). Amounts of sample ranging from 10 to 50 ng were estimated. A third sample (S-3) was extracted from the frescoes painted by Antonio Acisclo Palomino y Velasco in 1698 in the vault of the *Sant Joan del Mercat* church in València (Spain). The fourth sample (S-4) was extracted from an anonymous polychromed sculpture (16th century) representing a Martyr Saint from Alacant (Spain).

3. Results and discussion

3.1. VNP at AFM cell of pigments

Fig. 1 shows the cyclic voltammetric curves recorded at AFM cell for: (a) litharge, (b) massicot, (c) Naples yellow, (d) lead white, (e) tin–lead yellow, (f) chrome orange, and (g) chrome yellow. For litharge, two overlapping peaks at −550 and −660 mV are recorded, whereas for massicot, a weak peak at −520 mV precedes the main reduction peak at −630 mV. For Naples yellow, lead white and tin–lead yellow, a well-defined, isolated reduction peak was recorded at −615, −755, and −650 mV. Chrome orange and chrome yellow also present a well-defined cathodic peak at potentials of −640 and −780 mV, respectively. Similar, well-defined responses were obtained for model compounds.

In the subsequent anodic scan, litharge, lead white, tin–lead yellow, chrome orange and chrome yellow exhibit a single stripping oxidation peak close to the precedent cathodic one, while massicot and Naples yellow present several overlapping peaks. On increasing the potential scan rate, the cathodic peaks are in general ill-defined, whereas anodic peaks become more pronounced. In some cases (see Fig. 1d–g), a reduction current precedes the anodic stripping peak during the anodic scan. This signal appears in the region of potentials where the reduction of Pb^{2+} ions in solution occurs and exhibits a typical crossover profile.

This electrochemical response can be described in terms of the initial reduction of the solid to lead metal. Following Scholz and Meyer [17] the reduction process for lead oxide can be represented as:

$$PbO\,(s) + 2H^+ + 2e^- \rightarrow Pb\,(s) + H_2O \quad (1)$$

This process involves a solid state transformation of lead oxide to lead metal, eventually coupled by a reductive process via formation of Pb^{2+} in solution:

$$PbO\,(s) + 2H^+ + 2xe^- \rightarrow (1-x)Pb^{2+}\,(aq) + xPb\,(s) + H_2O \quad (2)$$

further reduced to Pb metal:

$$Pb^{2+}\,(aq) + 2e^- \rightarrow Pb\,(s) \quad (3)$$

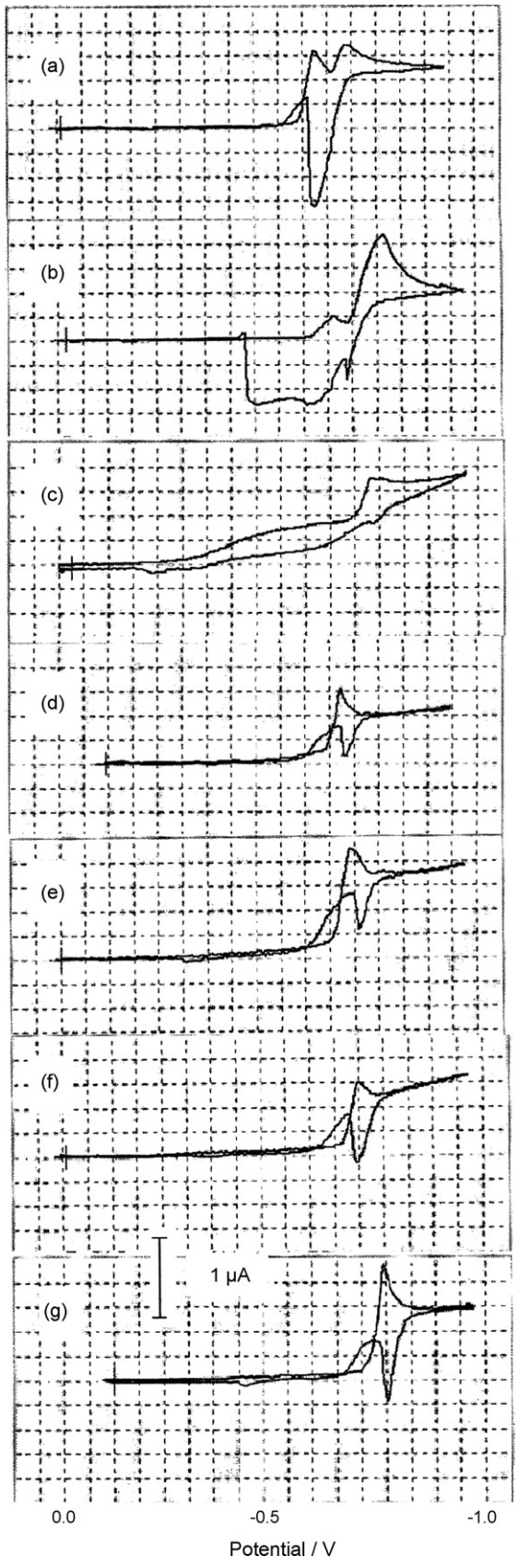

Fig. 1. CVs at the AFM cell for nanosamples of: (a) litharge, (b) massicot, (c) Naples yellow, (d) lead white, (e) tin–lead yellow, (f) chrome orange, and (g) chrome yellow. Electrolyte: 0.50 M acetic/acetate buffer and pH 4.85. Potential scan rate 5 mV/s.

On scanning the potential in the positive direction after the reductive step, lead metal, presumably consisting of different type of deposits, is oxidized to Pb^{2+} (aq) via a typical stripping process that can be represented as the inverse of Eq. (3). Accordingly, the cathodic crossover signal can be attributed to the reduction of Pb^{2+} ions in solution phase at the Pb-plated electrode surface, denoting that the electrochemical pathway represented by Eq. (2) is operative.

A further electrochemical oxidation of Pb^{2+} (aq) to PbO_2 (s) was not observed because that process occurs at potentials more positive (+1.0 V at platinum electrodes in acidic media) [41] than those used here.

The aforementioned differences in the voltammetric responses are accompanied by differences in the morphology of the metal deposits. Typical atomic force micrographs recorded at the beginning of the experiment (open circuit conditions) and just after the reduction peak are shown in Fig. 2

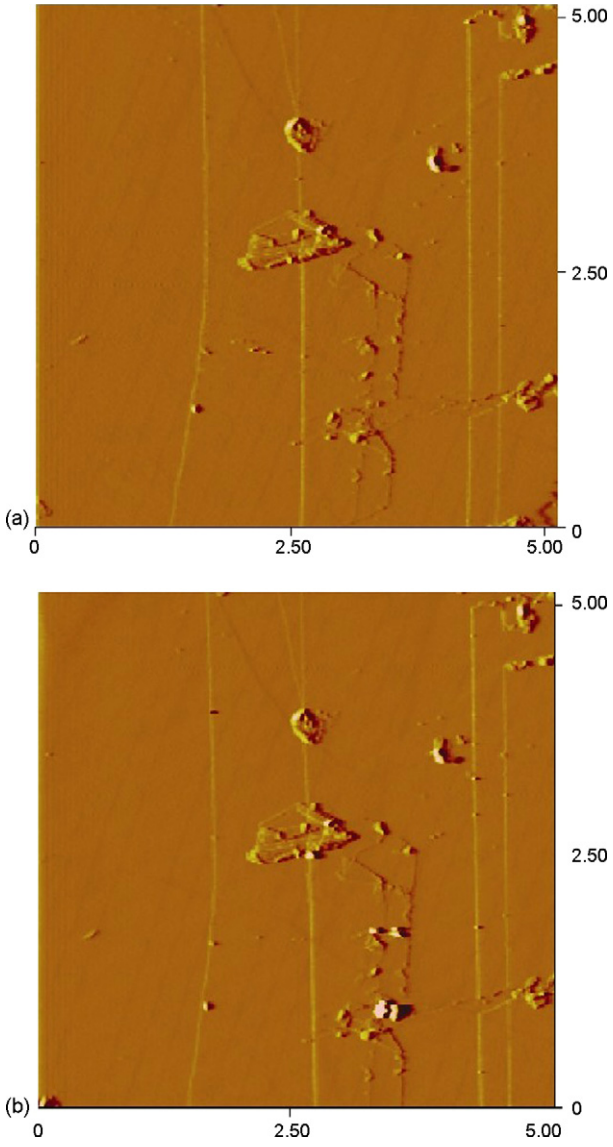

Fig. 2. Atomic force micrographs of Naples yellow deposited on a graphite plate: (a) at open circuit; (b) after scanning the potential from 0.0 to −0.90 V at 5 mV/s.

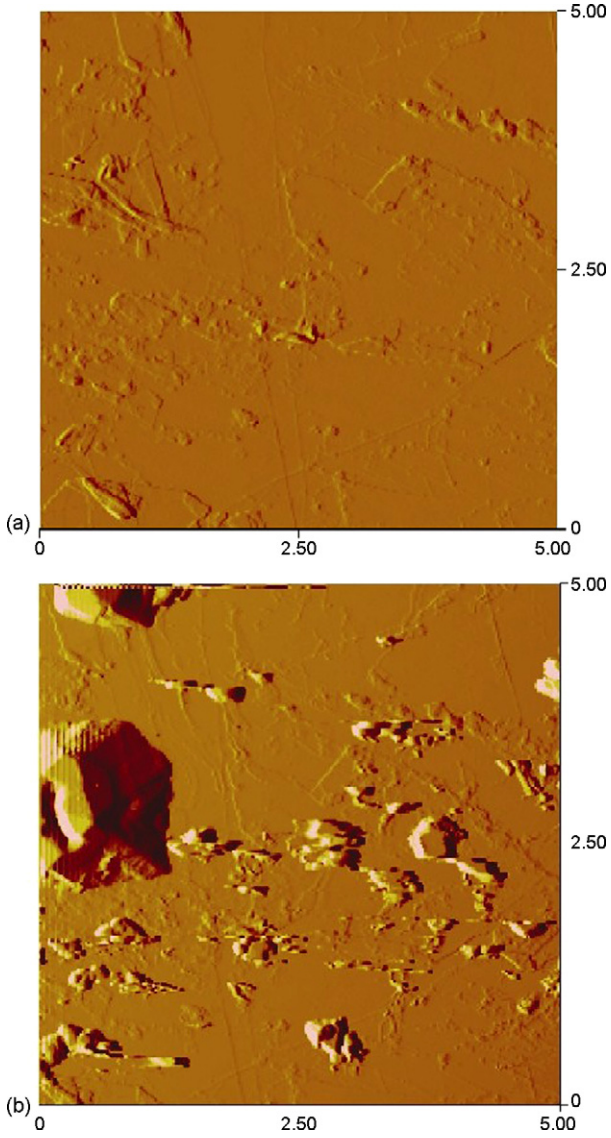

Fig. 3. Atomic force micrographs of minium deposited on a graphite plate: (a) at open circuit; (b) after scanning the potential from 0.0 to −0.90 V at 5 mV/s.

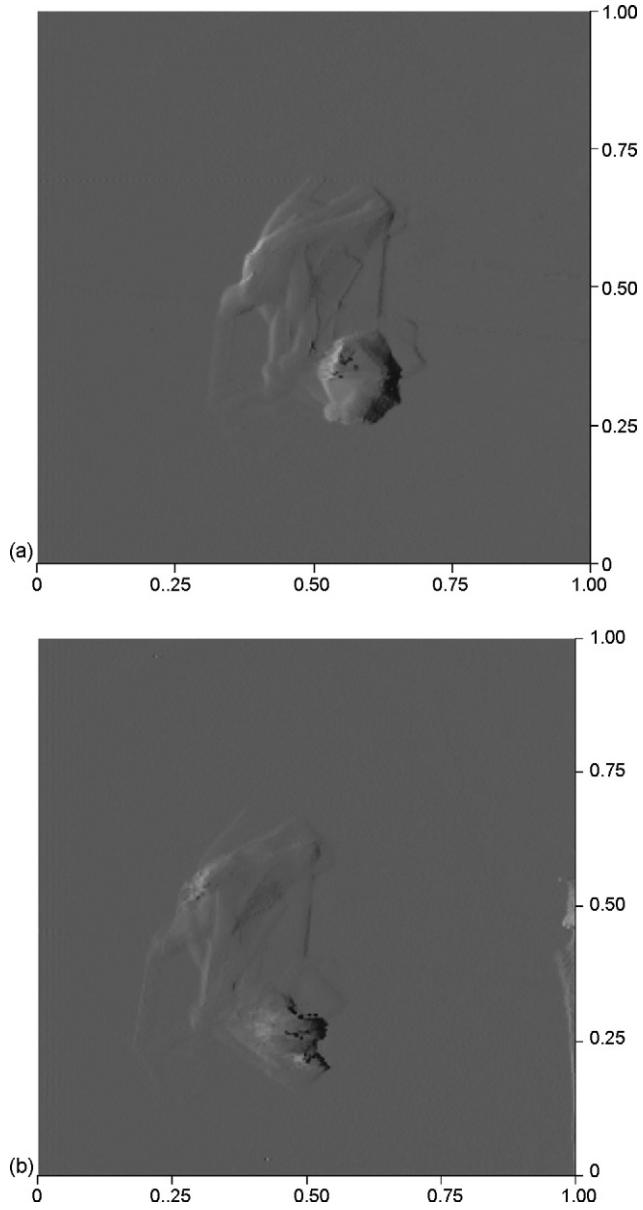

Fig. 4. Atomic force micrographs of minium deposited on a graphite plate: (a) at open circuit; (b) after scanning the potential from 0.0 to −0.70 V at 1.0 mV/s.

for Naples yellow and Fig. 3 for minium. In the initial micrographs (Figs. 2a and 3a), few irregular particles of the pigment appear over the "flat" electrode surface. The second micrograph for Naples yellow (Fig. 2b) corresponds to the situation after scanning the potential from 0.00 to −0.90 V at a sweep rate of 1 mV/s. Here, pigment particles are accompanied by few particles of lead metal deposited just in lateral faces of pigment crystals. This type of lead deposition was also observed for litharge, massicot, chrome yellow, chrome orange, and tin–lead yellow. For minium and lead white, however, lead deposits consisted of irregular bulky aggregates in the vicinity of the particles of pigment, as depicted in Fig. 3b for minium.

Topographic AFM obtained here data agree with those reported by Hasse and Scholz [27] who studied the electrochemical reduction of crystals of litharge with edge lengths between 100 and 500 nm deposited on polycrystalline gold electrodes in contact with 0.10 M KCl. Upon application of potential pulses of 1 s from 0 to −0.695 V, a reduction of ca. 20% of the volume of the particles was estimated, close to the theoretical reduction from PbO to Pb (23%). A similar situation was observed for several of our studied materials. On prolonging the potential towards more negative values, topographic profiles for litharge, massicot, tin–lead yellow, Naples yellow, chrome yellow and chrome orange produced deposits of lead metal located in one side of the initial particle as can be seen in Fig. 4. This feature suggests that the reduction process described by Eq. (1) did not start at the entire three-phase electrode/particle/electrolyte junction; i.e., the epitactic growth of the lead crystal occurs only on one side of the lead oxide crystal [27]. Deposits for minium and lead white, however, consisted on bulky aggregates surrounding entirely the initial particles of the lead material. The formation of such lead deposits can be associated, as previously discussed, to the occurrence of a significant lead deposition via Pb^{2+} in

solution (Eqs. (2) and (3)). Consistently, although lead crystals were mainly deposited in the neighbourhood of the lead oxide crystals, some lead deposits were formed far from lead oxide particles.

3.2. VNP at AFM cell for model paint specimens and samples

In order to test the influence of binding media in the proposed methodology for pigment identification, the voltammetric response of a series of synthetic pictorial specimens was obtained at the AFM cell. The effect of the binders in the VNP response at low potential scan rates of the studied pigments in the AFM cell is illustrated in Fig. 5, corresponding to: (a) lead white + linseed oil, (b) lead white + bovine gelatine. All CVs exhibit significant differences with that of the pristine pigment, depicted in Fig. 1d. For lead white + linseed oil (Fig. 5a), the voltammogram consists of a broad cathodic peak at −725 mV, followed by an anodic stripping peak at −505 mV. In contrast, for lead white + bovine gelatine (Fig. 5b), a monotonically rising current appears in the cathodic region followed, in the reverse scan, by a current increase that determines the appearance of a crossover preceding the prominent anodic stripping peak at −505 mV. For lead white + linseed oil + bovine gelatine specimens, a intermediate response was obtained, the CV consisting of a broad cathodic peak at −970 mV accompanied by a crossover preceding the tall anodic peak at −605 mV.

In contrast, CVs recorded at relatively high potential scan rates become essentially identical for all synthetic specimens of the same pigment. This can be seen in Fig. 6, where the

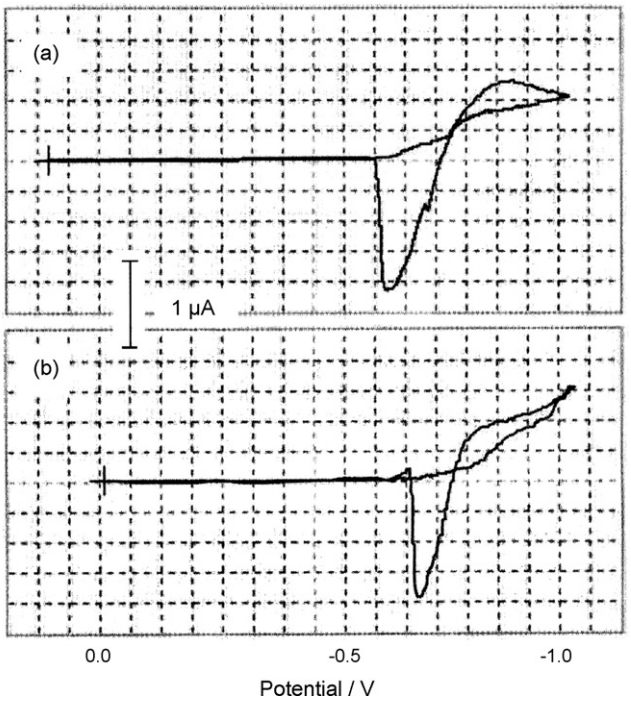

Fig. 5. CVs at the AFM cell recorded for: (a) lead white + linseed oil specimen; (b) lead white + bovine gelatine specimen. Electrolyte: 0.50 M acetic/acetate buffer and pH 4.85. Potential scan rate 100 mV/s.

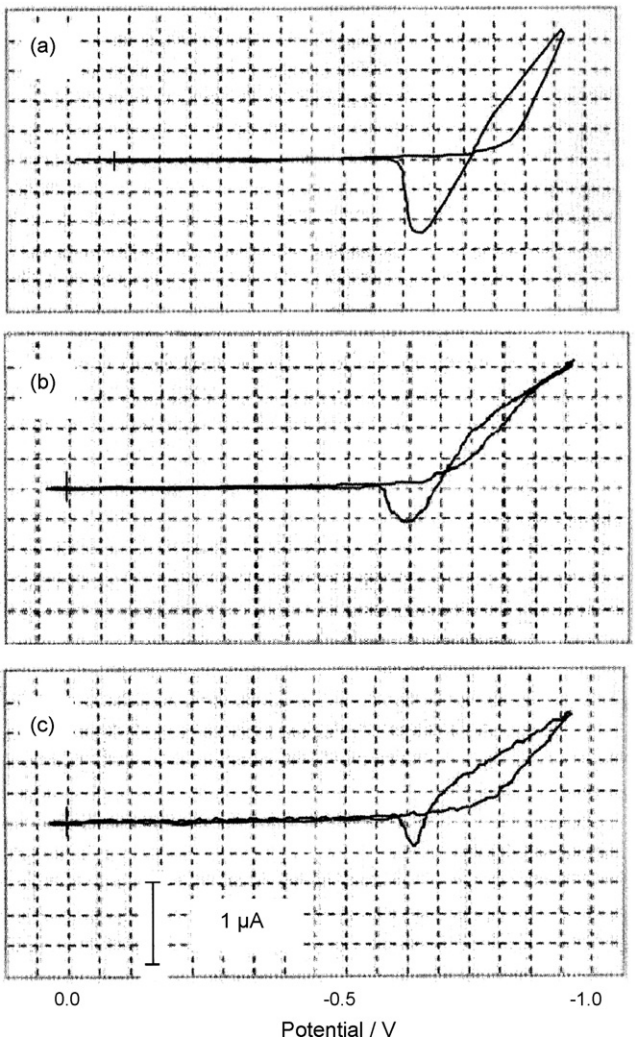

Fig. 6. CVs at the AFM cell recorded for: (a) lead white; (b) model lead white + linseed oil specimen; (c) model lead white + bovine gelatine specimen. Electrolyte: 0.50 M acetic/acetate buffer and pH 4.85. Potential scan rate 100 mV/s.

CVs at 100 mV/s of model specimens for: (a) lead white, (b) lead white + linseed oil, and (c) lead white + bovine gelatine, are shown. It can be seen that the morphology of all three voltammograms was almost identical, with only small variations in the peak potentials. Similar features were obtained for all other tested lead pigments on comparing the CVs at 100 mV/s for the pristine pigments with those recorded for pigment + linseed oil, pigment + bovine gelatine and, pigment + linseed oil + bovine gelatine specimens. In general, with except small shifts of the cathodic signals and, eventually, a 'cleaning' of the anodic region of the voltammograms, where secondary stripping peaks are significantly decreased, the shape of the CVs was essentially indistinguishable for all the specimens prepared with each one of the pigments.

Typical voltammograms for model paint specimens of the studied pigments are shown in Fig. 7. Here, linseed oil + pigment mixtures for: (a) litharge, (b) massicot, (c) minium, (d) Naples yellow, (e) tin–lead yellow, (f) chrome orange, and (g) chrome yellow are depicted. The CV of lead white + linseed oil specimen

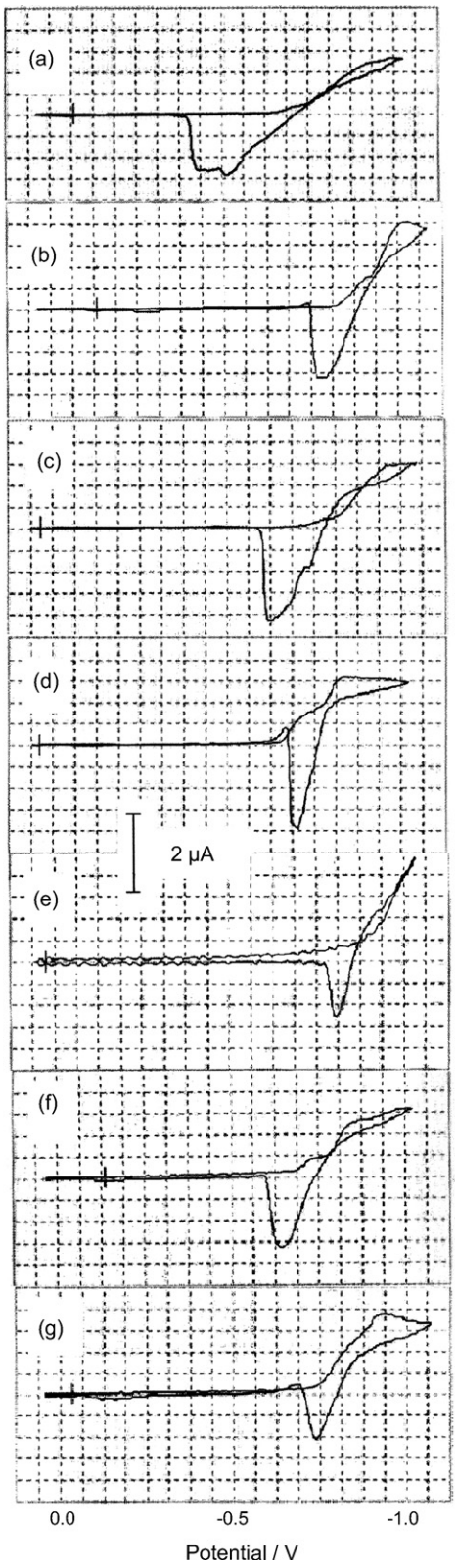

Fig. 7. CVs at 100 mV/s in the AFM cell of model linseed oil + pigment specimens of: (a) litharge, (b) massicot, (c) minium, (d) Naples yellow, (e) tin-lead yellow, (f) chrome orange, and (g) chrome yellow. Electrolyte: 0.50 M acetic/acetate buffer and pH 4.85. Potential scan rate 100 mV/s.

(Fig. 6b) completes the scope of synthetic pictorial specimens with the same composition. Similar voltammetric response was recorded for real samples S-1–S-4.

3.3. Modelling VNP of paint specimens

The reduction of sparingly soluble lead compounds to lead metal can be interpreted in terms of the model developed by Lovric et al. [42–45] for describing voltammetry of nonconducting solids. The redox reaction is initiated at the particle/electrolyte/electrode three-phase junction and expands via electron hopping and ion insertion/hopping through the particle. In the studied cases, the situation is complicated because the progress of the reaction requires proton insertion and the formation of a second solid phase consisting of lead metal. Thus, reduction processes presumably involve two competing mechanisms: a solid-to-solid transformation described by Eq. (1), and a reductive dissolution pathway involving intermediate species in solution, as represented by Eq. (2).

Following Hasse and Scholz [27], PbO is converted into Pb metal without a morphological disintigration but as a process in which the initial crystal is continuously shrunk and reconstructed into the metal crystal. Lead oxide forms upon reduction first to a small heap of amorphous lead that recrystallizes to lead crystal. A reaction layer containing lead atoms, hydroxide ions and water molecules is formed so that lead atoms move towards the growing lead/crystal interface. This situation can be described in terms of a system with moving interfaces [46,47] or a diffuse heterophase interface [48].

Additionally, formation of the deposit of lead metal involves nucleation and growth of metal aggregates. Accordingly, the overall electrochemical process can be controlled not only by the kinetics of the proton insertion and/or electron transfer process, but also by the kinetics of the nucleation and nuclei growth involved in the formation of lead metal.

The above factors can influence significantly the voltammetric profile. As can be seen in Fig. 1, for chrome yellow, chrome orange, Naples yellow, and tin-lead yellow, the separation between the cathodic peak and the anodic one is close to the expected value for a reversible couple. In contrast, litharge and massicot, and specially minium, exhibit relatively large separations between the cathodic peak and the stripping oxidation peak. This feature can be rationalized in terms of: (i) the existence of significant differences in the kinetics of the nucleation process during lead deposition for the different pigments, and (ii) the existence of partial miscibility gaps between the parent lead pigment and lead metal, as theoretically discussed by Lovric et al. [49,50].

To describe the influence of the binder in the voltammetric pattern of lead pigments one can propose a simplified model based on the previously mentioned description of the electrochemistry of lead compounds [17,25–27] and current ideas on pigment-binder interactions [30–40]. Thus, it is assumed that pigment grains are embedded in a binding matrix so that the particles of pigment are at least partly surrounded by an ionomeric layer resulting from different pigment-binding medium interaction. A schematic representation is depicted in Fig. 8. Here, two

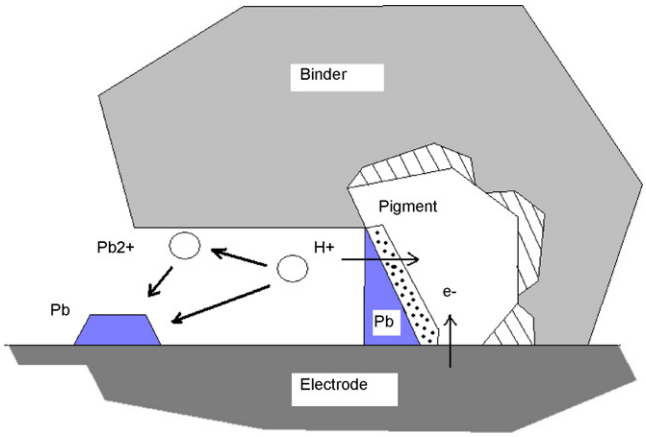

Fig. 8. Schematic representation of redox processes involving a pigment grain surrounded by the binder and in contact with the electrode surface. Ionomeric layer surrounding the pigment particle is marked by dotted lines. The mobile interface where charge transport occurs is marked by dark points.

kinds of Pb deposits (far from the pigment particle, and in the vicinity of the particle/electrode/electrolyte interface) are represented. The pointed region adjacent to the pigment/electrolyte interface corresponds to the amorphous reaction layer constituted by lead atoms, hydroxide ions and water molecules previously described.

Accordingly, one can propose three main processes affecting the electrochemical response of pigments:

(a) As a result of the presence of an ionomeric layer with lead-containing compounds, not only the pristine pigment but also such lead-containing compounds can be electrochemically reduced. For PbO this can be represented as:

$$PbO\,(s) + 2H^+ + \{binder\} \rightarrow \{Pb^{2+}\text{-binder}\} + H_2O \quad (4)$$

$$\{Pb^{2+}\text{-binder}\} + 2H^+ + 2xe^- \rightarrow xPb\,(s) + (1-x)Pb^{2+} + \{2H^+\text{-binder}\} \quad (5)$$

(b) By forming a barrier for charge diffusion, thus lowering the rate of the overall electrochemical process described by Eqs. (1) and (2).

(c) By interacting with Pb^{2+} ions released during the electrochemical reduction of pigments described by Eq. (2) and then modifying the subsequent reduction of such ions. Using again PbO as a model compound, this can be represented as:

$$PbO\,(s) + \{binder\} + 2H^+ + 2xe^- \rightarrow xPb\,(s) + (1-x)\{Pb^{2+}\text{-binder}\} + H_2O \quad (6)$$

Taking into account the foregoing set of considerations, the voltammetric response of pictorial specimens can be tentatively described. It should be noted that the reduction of lead-containing solids to lead metal involves the topotactic destruction/construction of different lattices (Eq. (1)) or a coupled reductive-dissolution crystallization pathway (Eq. (2)). Thus, at relatively large experimentation times (i.e., at low potential scan rates), charge diffusion along solid particles and their surrounding ionomeric layer act as the rate-determining factors. On the contrary, at short experimentation times (i.e., at relatively high potential scan rates), the growth of the mobile interface in the Pb-compound/Pb system controls the rate of the overall electrochemical process.

In the presence of oil binders, the proceses (a) and (b) are probably the most important factors influencing the observed electrochemistry. Then, at low potential scan rates charge transfer across the ionomeric layer can reasonably be taken as the rate-determining process. This diffusion is slower than that for the pure pigment and the reduction peak of the pigment vanishes. As a result, the electrochemical reduction occurs mainly via the processes described by Eqs. (5) and (6). At sufficiently negative potentials, reduction of Pb^{2+} ions in solution over the Pb-plated electrode occurs, thus determining the appearance of a characteristic crossover in the CVs.

In the case of protein binders, again at low potential scan rates, processes (b) and (c) are presumably the prevailing factors conditioning the electrochemistry of paint samples. Now, voltammetric reduction peaks appear, but peak potentials are shifted because of the Pb-binding interaction described by means of Eq. (6). Reduction of Pb^{2+} ions is now likely inhibited by effect of the coordination of such ions by the protein.

On the contrary, at high potential scan rates, the growth of the mobile interface in the Pb-compound/Pb system acts as a rate-determining process. Then, the overall electrochemical process is governed by the properties of that interface and, consequently, the voltammetric response becomes binder-insensitive. Accordingly, voltammograms at relatively high potential scan rates can be considered as characteristic of the pigment and essentially independent of the surrounding binding media.

3.4. Application to pigment analysis

In order to identify lead pigments in paint specimens and samples, a series of voltammetric parameters were taken. Prior data indicate that CVs recorded in the AFM cell at relatively high potential scan rates provide highly pigment-dependent, matrix-insensitive profiles, whereas CVs at low potential scan rates are sensitive to the type of binding media in the paint sample. However, the peak potentials of model paint specimens are often shifted few mV (typically between 0 and 80 mV) with respect to those determined for pristine pigments. It should be noted that all the studied pigments and model compounds display similar values for the involved electrochemical parameters, so that it is difficult to discern between different pigments on the basis of typical voltammetric parameters (peak potentials, half-wave potentials).

Accordingly, shape-characteristic parameters were defined on the basis of criteria used by Sybrandt and Perone [51], for pattern recognition in CV curves. Such parameters were:

(a) Potential separation between the potentials onset potentials ($E'_{onset} - E_{onset}$). These potentials are defined by prolonging the almost-linear regions in the ascendant (initial cathodic scan voltammogram) and descendant (subsequent

Table 1
Voltammetric parameters for pristine lead white pigment and different lead white-based specimens

Modifier	E_{pc} (mV)	E_{pa} (mV)	E_{onset} (mV)	E'_{onset}(mV)	$(E_{onset} - E'_{onset})$ (mV)	$(E_{3/4} - E_{1/4})$ (mV)	$(E_{pa} - E_{onset})$	αn_a
Lead white	−710	−515 ± 5	−670 ± 5	−590 ± 5	80 ± 10	65 ± 5	155 ± 10	1.52 ± 0.04
Id. + linseed oil	−650	−505 ± 5	−645 ± 5	−555 ± 5	90 ± 10	70 ± 5	140 ± 5	1.02 ± 0.04
Id. aged	−660	−525 ± 5	−660 ± 5	−540 ± 5	80 ± 10	70 ± 5	135 ± 10	1.02 ± 0.05
Id. + bovine gelatine	−680	−505 ± 5	−635 ± 5	−545 ± 5	90 ± 10	65 ± 5	130 ± 10	1.10 ± 0.06
Id. aged	−680	−515 ± 5	−640 ± 5	−550 ± 5	90 ± 10	60 ± 5	125 ± 10	0.98 ± 0.05
Id. + linseed oil + bovine gelatine	−690	−510 ± 5	−640 ± 5	−555 ± 5	95 ± 10	60 ± 5	130 ± 10	1.08 ± 0.05

From CVs recorded at 100 mV/s in the AFM cell. Electrolyte: 0.50 M acetic/acetate buffer and pH 4.85.

anodic scan) branches of the main reduction wave. The intersections of those linear branches can be prolonged to intersect the potential axis, thus defining potentials E_{onset} (ascendant branch) and E'_{onset} (descendent branch).

(b) Separation between the potentials for which current is 3/4 and 1/4 of the peak current in the main reduction wave, $E_{3/4} - E_{1/4}$. This parameter, representing the 'mean' inclination of the current/potential curve, is of interest for characterizing voltammetric processes displaying highly overlapping peaks [51].

(c) Separation between the onset potential of the ascendant region of the main reduction wave and the anodic peak potential measured in the subsequent anodic scan, $E^0_{onset} - E_{pa}$.

(d) Apparent charge transfer coefficient, an_a, that can be calculated [8] from the slope of the reduced Tafel plots of $\ln(i/i_p)$ versus E in the rising portion of the voltammetric curves.

Using these shape-characteristic parameters, consistent pigment-dependent values were obtained. This can be seen in Table 1, where voltammetric parameters for lead-white-based specimens are shown. Here, similar values of the aforementioned shape-dependent parameters are obtained.

Accordingly, and although several overlaps exist between the involved parameters for different pigments, characteristic pigment-dependent values were obtained, as can be seen in Table 2, thus enabling for a characterization of each one of the studied pigments.

Remarkably, two-dimensional diagrams constructed from different pairs of such parameters exhibit pigment-characteristic grouping of data points. This can be seen in Fig. 9 where it is presented a $(E_{3/4} - E_{1/4})$ versus $(E'_{onset} - E_{onset})$ diagram constructed from CVs recorded suing the VNP/AFM cell at a potential scan rate of 100 mV/s. Representative points for each pigment in that diagram are clearly separated from one to another and a minimal dispersion was obtained for synthetic samples, pristine pigments and real samples.

Application to real samples is illustrated in Table 1 and Fig. 9. Here, the data point for sample S-2 is within the minium zone of the diagram, whereas samples S-1 and S-4 are within the lead white region. The point representative of sample S-3 falls in the region defined by pristine pigment and paint specimens of Naples yellow. Similar results were also obtained for other pairs of variables. Application of the principal component analysis using all four electrochemical parameters confirmed such assignments.

Interestingly, CVs recorded at low potential scan rates can also be used for obtaining information on the type of binder. Thus, oil-containing binders yield cathodic peak vanishing and produce catalytic currents with typical crossovers in the CV. Protein binders produce peak potential shifts and increases in general the separation between cathodic and anodic peaks. Development of electroanalytical procedures for the identi-

Table 2
Voltammetric parameters for characterizing lead pigments

Modifier	E_{pc} (mV)	E_{pa} (mV)	E_{onset} (mV)	E'_{onset} (mV)	$(E_{onset} - E'_{onset})$ (mV)	$(E_{3/4} - E_{1/4})$ (mV)	$(E_{pa} - E_{onset})$	αn_a
Chrome orange	−660 ± 5	−460 ± 5	−575 ± 5	−540 ± 10	40 ± 10	55 ± 5	115 ± 10	0.93 ± 0.06
Chrome yellow	−710 ± 10	−520 ± 5	−495 ± 10	−570 ± 10	−80 ± 10	65 ± 5	25 ± 20	0.85 ± 0.06
Lead white	−680 ± 10	−510 ± 10	−645 ± 15	−550 ± 10	85 ± 10	65 ± 5	135 ± 10	1.1 ± 0.2
Litharge	−700 ± 10	−365 ± 10	−480 ± 10	−540 ± 10	−55 ± 5	170 ± 5	120 ± 10	0.72 ± 0.04
Massicot	−620 ± 10	−435 ± 10	−460 ± 15	−515 ± 5	−50 ± 10	120 ± 5	40 ± 10	0.59 ± 0.04
Minium	−690 ± 10	−400 ± 50	−550 ± 30	−550 ± 20	10 ± 10	140 ± 5	150 ± 20	0.65 ± 0.05
Naples yellow	−650 ± 10	−450 ± 15	−565 ± 10	−510 ± 10	55 ± 10	145 ± 5	120 ± 20	0.63 ± 0.03
Tin–lead yellow	−750 ± 10	−620 ± 10	−665 ± 10	−615 ± 5	60 ± 10	40 ± 10	125 ± 10	1.01 ± 0.08
S-1	−690 ± 10	−500 ± 5	−645 ± 5	−550 ± 5	95 ± 10	65 ± 5	145 ± 10	1.02 ± 0.05
S-2	−690 ± 10	−450 ± 5	−570 ± 5	−565 ± 5	5 ± 10	130 ± 10	120 ± 10	0.66 ± 0.03
S-3	−670 ± 10	−415 ± 5	−585 ± 5	−525 ± 5	60 ± 10	140 ± 5	170 ± 10	0.64 ± 0.03
S-4	−680 ± 10	−510 ± 5	−635 ± 5	−550 ± 5	85 ± 10	65 ± 5	125 ± 10	1.03 ± 0.05

Mean values recorded for pristine pigments and different pigment-based model specimens. From CVs recorded at 100 mV/s in the AFM cell. Electrolyte: 0.50 M acetic/acetate buffer and pH 4.85.

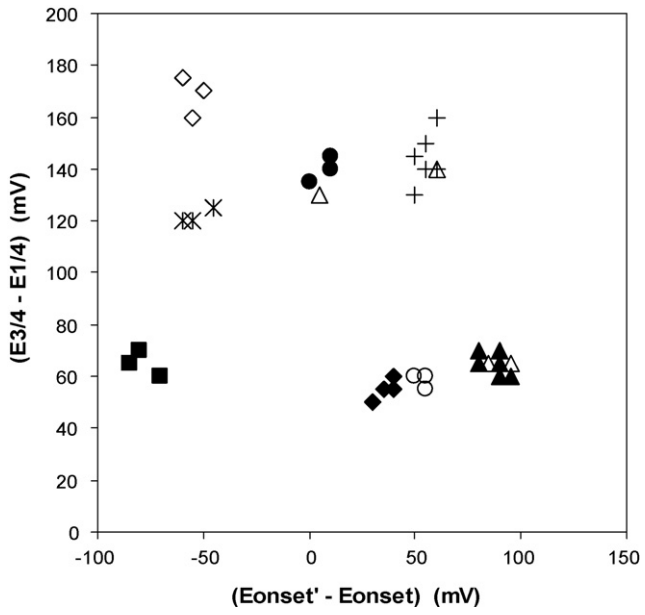

Fig. 9. Representation of $E_{3/4} - E_{1/4}$ vs. $(E'_{onset} - E_{onset})$ for lead pigments, model paint specimens and real samples. Data from CVs recorded in the AFM cell for nanosamples attached to a graphite plate. Electrolyte: 0.50 M acetate buffer. Potential scan rate 100 mV/s. Solid rhombs: chrome orange; solid squares: chrome yellow; solid triangles: lead white; rhombs: litharge; stars: massicot; solid circles: minium; crosses: Naples yellow; circles: tin–lead yellow. Real samples are marked by triangles.

fication of pigment plus binder mixtures is under research currently.

4. Conclusions

Using voltammetry of nanoparticles at the atomic force microscopy cell provides well-defined voltammetric responses for samples of a series of lead model compounds, model paint specimens and real pictorial samples proceeding from ancient pictures and polychromed sculptures.

VNP/AFM data for the reduction of lead-based materials can be interpreted in terms of two competing mechanisms involving the epitactic growth of lead crystal on the crystals of the parent lead compound and a reduction/dissolution/crystallization pathway.

The presence of binding media acompanying lead pigments produces significant modifications in the voltammetric response. Under selected experimental conditions, binder influence can be minimized so that lead pigments can be identified in samples from VNP/AFM data. In these conditions, identification of lead pigments from nanosamples can be achieved by using several diagnostic criteria based on pattern recognition procedures.

The reported methodology enables for an unambiguous identification of lead pigments in real samples from works of art, being illustrative of the capabilities of solid state electrochemistry for providing analytical information in the fields of archaeometry, conservation and restoration.

Acknowledgements

Financial support is gratefully acknowledged from the I + D Generalitat Valenciana projects GV04B/144 and GV04B/197 and the MEC projects CTQ2004-06754-C03-01 and 02, which are also supported by FEDER founds. The authors whish to thank Dr. José Luis Moya López (Atomic Force Microscope) and Mr. Manuel Planas Insausti (Electron microscopy) for technical assistance. The authors whish to express their gratitude to Professor Dr. Pilar Roig Picazo, director of the Mural Paintings Conservation Project at Sant Joan del Mercat Church. Financial support in this project is kindly acknowledged to the Council of València, Lubasa, and Fundación de la Comunidad Valenciana de Aguas de València S.A. The authors would like to express also their gratitude to Dr. Maria Pia Demma, director of the Scientific Reserach Department of the Centro Regionale per la Progettazione e il Restauro di Sicilia. Finnancial support in this project is kindly acknowledged to this institution.

Appendix A. Supplementary data

Supplementary data associated with this article can be found, in the online version, at doi:10.1016/j.talanta.2006.07.053.

References

[1] J.C. Shearer, D.C. Peters, G. Hoepfner, T. Newton, Anal. Chem. 55 (1983) 874A.
[2] F. Rassineux, D. Beaufort, T. Merceron, A. Bouchet, A. Meunier, Analusis 15 (1987) 333.
[3] S.E.J. Villar, H.G.M. Edwards, Anal. Bioanal. Chem. 382 (2005) 283.
[4] R. Cournoyer, J.C. Shearer, D.H. Anderson, Anal. Chem. 49 (1977) 22.
[5] G.E. De Benedetto, F. Catalano, F. Sabbatini, P.G. Zambonin, Fresenius' J. Anal. Chem. 362 (1998) 170.
[6] L. Sabbatini, M.G. Tarantino, P.G. Zambonin, G.E. De Benedetto, Fresenius' J. Anal. Chem. 366 (2000) 116.
[7] A. Doménech, M.T. Doménech, M. Moya, J.V. Gimeno, F. Bosch, Anal. Chim. Acta 407 (2000) 275.
[8] A. Doménech, M.T. Doménech, J.V. Gimeno, F. Bosch, M.C. Saurí, S. Sánchez, Analyst 126 (2001) 1764.
[9] A. Doménech, M.T. Doménech, J.V. Gimeno, F. Bosch, M.C. Saurí, M.J. Casas, Fresenius' J. Anal. Chem. 369 (2001) 576.
[10] T. Kuwana, W.G. French, Anal. Chem. 58 (1964) 2979.
[11] F.A. Schultz, T. Kuwana, J. Electroanal. Chem. 10 (1965) 95.
[12] Kh.Z. Brainina, R.P. Lesunova, Zh. Analit. Khimyi 29 (1974) 1302.
[13] D. Bauer, M.Ph. Gaillochet, Electrochim. Acta 19 (1974) 597.
[14] M. Lamache, D. Bauer, Anal. Chem. 51 (1979) 1320.
[15] F. Scholz, L. Nitschke, G. Henrion, Naturwiss 76 (1989) 71.
[16] F. Scholz, L. Nitschke, G. Henrion, F. Damaschun, Naturwiss 76 (1989) 167.
[17] F. Scholz, B. Meyer, in: A.J. Bard, I. Rubinstein (Eds.), Electroanalytical Chemistry, vol. 20, Marcel Dekker, New York, 1998, pp. 1–87.
[18] T. Grygar, F. Marken, U. Schröder, F. Scholz, Collect. Czech. Chem. Commun. 67 (2002) 163.
[19] A.J. Bard, F.R.F. Fan, M.V. Mirkin, in: A.J. Bard (Ed.), Electroanalytical Chemistry, vol. 18, Marcel Dekker, New York, 1994, pp. 243–373.
[20] R. Mayer, The Artist's Handbook of Materials and Techniques, 2nd ed., Hermann Blume, Madrid, 1993.
[21] R. Ashok (Ed.), Artist's Pigments. A Handbook of their History and Characteristics, vol. 2, National Gallery of Art, Washington, DC, 1993.
[22] R.J. Gettens, G.L. Stout, Painting Materials. A Short Enciclopedia, Dover, New York, 1966.
[23] C. Cennini, Il libro dell'arte, Akal, Madrid, 1988 (14th century).

[24] R.L. Feller (Ed.), Artists' Pigments. A Handbook of their History and Characteristics, vol. 1, National Gallery of Art, Washington, DC, 1986.
[25] N. Zakharchuk, S. Meyer, B. Lange, F. Scholz, Croat. Chem. Acta 73 (2000) 667.
[26] B. Meyer, B. Ziemer, F. Scholz, J. Electroanal. Chem. 392 (1995) 79.
[27] U. Hasse, F. Scholz, Electrochem. Commun. 3 (2001) 429.
[28] J.S. Mills, R. White, The Organic Chemistry of Museum Objects, Butterworth, London, 1994.
[29] M. Matteini, A. Moles, La Chimica nel Restauro, Nardini, Firenze, 1989.
[30] D. Erhardt, C.S. Tumosa, M.F. Mecklenburg, Stud. Conservat. 50 (2005) 143.
[31] C. Genester, C. Pons, Anal. Bioanal. Chem. 382 (2005) 269.
[32] R.J. Meilunas, J.G. Bentsen, A. Steinberg, Stud. Conservat. 35 (1990) 33.
[33] J.J. Boon, S.L. Peulvé, O.F. van den Brink, M.C. Duursma, D. Rainford, in: T. Bakkenist, R. Hoppenbrouwers, H. Dubois (Eds.), Early Italian Painting Techniques and Analysis, Limburg Conservation Institute, 1996, pp. 35–56.
[34] J.D.J. van den Berg, K.L. vand der Berg, J.J. Boon, in: J. Bridgland (Ed.), Preprints of the 12th Triennial Meeting of the ICOM Committee for Conservation, James & James, London, 1999, pp. 248–253.
[35] J. van der Weerd, A. van Loon, J.J. Boon, Stud. Conservat. 50 (2005) 3.
[36] V.J. Birstein, V.M. Tulchinovosky, ICOM Committeee for Conservation, Report 6th Triennial Meeting, Otawa, 1988, pp. 81/1–9.
[37] C.H. Nichols, Develop. Polym. Photochem. 1 (1980) 125.
[38] M.P. Colombini, F. Modugno, A. Giacomelli, J. Chromatogr. A 846 (1999) 101.
[39] S. Kuckova, I. Nemec, R. Hynek, J. Hradilova, T. Grygar, Anal. Bioanal. Chem. 384 (2005) 275.
[40] D.A. Scott, L.S. Dodd, J. Furihata, S. Tamimoto, J. Keeney, M.R. Schilling, R. Cowan, Stud. Conservat. 49 (2004) 177.
[41] H.A. Laitinen, N.H. Watkins, Anal. Chem. 47 (1975) 1352.
[42] M. Lovric, F. Scholz, J. Solid State Electrochem. 1 (1997) 108.
[43] M. Lovric, F. Scholz, J. Solid State Electrochem. 3 (1999) 172.
[44] K.B. Oldham, J. Solid State Electrochem. 2 (1998) 367.
[45] U. Schröder, K.B. Oldham, J.C. Myland, P.J. Mahon, F. Scholz, J. Solid State Electrochem. 4 (2000) 314.
[46] R.H. Doremus, J. Non Cryst. Solids 19 (1975) 137.
[47] Z. Boksay, G. Bouquet, S. Dobos, Phys. Chem. Glasses 9 (1968) 69.
[48] A.P. Sutton, R.W. Balluffi, Interfaces in Crystalline Materials, Clarendon Press, Oxford, 1995.
[49] F. Scholz, M. Lovric, Z. Stojek, J. Solid State Electrochem. 1 (1997) 134.
[50] M. Lovric, M. Hermes, F. Scholz, J. Solid State Electrochem. 4 (2000) 394.
[51] L.B. Sybrandt, S.P. Perone, Anal. Chem. 44 (1972) 2331.

Available online at www.sciencedirect.com
ScienceDirect
Talanta 71 (2007) 1720–1727
Talanta
www.elsevier.com/locate/talanta

Ag selective electrode based on glassy carbon electrode covered with polyaniline and thiacalix[4]arene as neutral carrier

G.A. Evtugyn *, I.I. Stoikov, S.V. Beljyakova, R.V. Shamagsumova, E.E. Stoikova, A.Yu. Zhukov, I.S. Antipin, H.C. Budnikov

A.M. Butlerov Chemistry Institute, Kazan State University, Kremlevskaya Street 18, Kazan 420008, Russian Federation

Received 22 May 2006; received in revised form 25 July 2006; accepted 1 August 2006
Available online 7 September 2006

Abstract

Potentiometric sensor based on glassy carbon electrode covered with polyaniline and neutral carrier, e.g. thiacalix[4]arene containing pyridine fragments in the substituents in the lower rim has been developed and applied for determination of Ag^+ ions in the range from 1.0×10^{-2} to 5.0×10^{-7} M with the response time of 12 s. The presence of thiacalixarene in the surface layer improves the reversibility and selectivity of the signal towards transient metal ions. The potentiometric selectivity coefficients were determined for various measurement conditions. As shown, the pH control and the use of NaF as a masking agent fully eliminate the interfering effect of Hg^{2+} and Fe^{3+} ions, respectively. The reaction of Ag^+ with thiacalixarene was proved by the investigation of the extraction of picrate complexes of transient metals in the organic phase. The potentiometric sensor developed was successfully used for the potentiometric determination of silver sulfathiazole (Argosulfan™).

Keywords: Potentiometric sensor; Polyaniline; Calixarene; Host–guest complexation; Silver determination

1. Introduction

Electroconducting polymers are widely applied in the solid-state ion selective electrodes [1,2]. Due to mixed ionic and electronic conductivity, these materials generate electric response to the changes in the content of the potential determining species. The incorporation of conducting polymer into the surface coating of the ion-selective sensor simplifies its manufacture due to the elimination of internal filling and stabilizes the response due to the suppression of the effect of dissolved oxygen and plastic membrane leaching [3]. The thickness, conductivity and charge of the surface layer obtained in electropolymerization are easily controlled by the electrolysis parameters and reaction media content. This makes it possible to change the operational characteristics and analytical performance of the sensors in accordance with the particular tasks of their application. Due to these advantages, the application of electroconductive polymers offers broad opportunities for developing ion-selective electrodes, which are of great importance in chemical, environmental and clinical analysis.

Polyaniline (PANI) [3–6], polythiophene derivatives [7–9] and polypyrrole [10–14] are mainly investigated in the potentiometric sensor development. Generally, the electropolymerized polymer is used either as a solid redox mediator between the transducer and ion-exchangeable component or as an immobilization matrix entrapping the components with intrinsic ionic/electron conductivity. In accordance with this, the sensor potential changes either with the redox potential of the electroconductive polymer or with the number of charged complexes formed by a neutral carrier and guest species on the surface.

Neutral carriers on the calixarene platform are intensively investigated to obtain selective and sensitive recognition response toward various analytes. Simple and cost-effective synthesis, variety of substituents introduced into the lower and upper rims as well as complexation abilities toward inorganic [15–19] and organic [20,21] ions make calixarenes promising components of ion-selective membranes and solid-contact sensors. Most calixarene-based sensors have been developed for selective detection of alkali and alkali-earth metals. Besides, the introduction of soft donor atoms of sulfur and nitrogen into the functional groups of calixarene substituents results in the pri-

* Corresponding author.
E-mail address: Gennady.Evtugyn@ksu.ru (G.A. Evtugyn).

0039-9140/$ – see front matter © 2006 Elsevier B.V. All rights reserved.
doi:10.1016/j.talanta.2006.08.004

mary detection of soft transient metals (Ag, Pb and Hg) over alkali and earth-alkali metals. Thus, di-substituted arylamide [18] and tetrasubstituted carboxyphenyl azo [19] derivatives of calix[4]arene were successfully used as neutral carriers for lead detection while thiazole azo derivatives showed selective recognition of Hg(II) ions [22].

The potentiometric sensors for Ag^+ determination received the bulk of attention. Besides providing a simple and reliable analysis of silver in pharmaceutical industry and semiconductors and photomaterials, Ag^+–calixarene interactions are considered a suitable model for the investigation of electrostatic and π-electron donating supramolecular interactions with soft metal ions [23]. Di- and tetrasubstituted calix[4]arenes with thioetheric groups were used in the assembly of PVC based membrane sensors [24]. The selectivity coefficients $\log K_{Ag/M}$ varied from −2 (Hg^{2+}) to −5 (Cu^{2+}) with the lowest detectable Ag^+ concentration of $10^{-4.5}$ M.

Recently, dimeric calix[4]arene derivatives with four imine groups at the upper rim and different spacers between two calixarene units were employed to prepare Ag^+ selective potentiometric sensors. The electrodes showed near-Nernstian responses to Ag^+ ions in the concentration range from 1.0×10^{-1} to 1.0×10^{-5} M with the limit of detection of about 10^{-6} M [25].

The sensitivity of Ag^+ detection was increased by introducing N-containing heterocycles into the thioether chain [26–29]. The use of pyrimidine group in the thiaamyloxy substituent of calix[4]arene decreased the limit of detection of Ag^+ to 1×10^{-8} M, although the selectivity toward other transient metal ions appeared worse than in the previous case. The 1,3-bis(2-benzothiazolyl)thioalkoxycalix[4]arenes in PVC membrane potentiometric sensors provided nearly Nernstian response toward 10^{-1} to 10^{-5} M of Ag^+, with satisfactory selectivity toward Hg^{2+} ($\log K_{Ag/M} < -2.6$) and other soft metal ions ($\log K_{Ag/M} = -5.5$ to −4.0) [26]. The 1,3-disubstituted calix[4]arene with amidopyridine fragments was incorporated into the PVC membrane and applied for selective detection and liquid membrane transportation of Ag^+ ions in the activity range of 5×10^{-6} to 10^{-2} M in the presence of 250–700 times excessive amounts of transient, alkali and alkali-earth metals [27]. Mono and dibenzothiazolyl substituted calix[4]arenes showed selectivity coefficients $\log K_{Ag/M}$ from −5.8 (Ca^{2+}, Mg^{2+}) to −2 (Hg^{2+}) and limits of Ag^+ detection down to 10^{-5} M [28].

Thiacalixarenes offer promising opportunities for artificial receptor design. The replacement of the CH_2 bridges in calixarene moiety by sulfur heteroatoms changes both the size and flexibility of the calixarene cavity and provides an additional binding site both for metal ion coordination and for potential ligand covalent binding [29]. Thiacalixarene films deposited by vacuum evaporation on gold were used as recognition elements for Cu^{2+} sensing [30]. Sulfonated thiacalixarene derivatives were successfully applied for pre-column concentration of Ni^{2+} in HPLC analysis [31]. However, the potentialities of these complexing agents in developing ion-selective electrodes have not been achieved at the moment. In this report, novel calixarene based receptor for Ag^+ detection, i.e. 5,11,17,23-tetra-*tert*-butyl-25,26,27,28-tetrakis[(2-pyridyl)-carbamoyl-methoxy]-2,8,14,20-tetrathiacalix[4]arene, was investigated in the assembly of the solid-contact potentiometric sensor based on the PANI modified electrode.

2. Experimental

2.1. Chemicals

p-Tert-butylphenol used for synthesis of tetraacid derivative of thiacalix[4]arene was purchased from "EcRos", Russia. Aniline was distilled under vacuum prior to its use in electropolymerization. Silver sulfathiazole (Argosulfan™, EAN: 5904398400020, 2% gel) was purchased from Jelfa S.A., Poland. All other chemicals were analytical-reagent grade. Bidistilled water was used to prepare all the aqueous solutions.

2.2. Synthesis of 5,11,17,23-tetra-tert-butyl-25,26,27,28-tetrakis[(2-pyridyl)-carbamoyl-methoxy]-2,8,14,20-tetrathiacalix[4]arene

Neutral ionophore on thiacalixarene platform **1** was synthesized from the tetraacid derivative of thiacalix[4]arene, i.e. 5,11,17,23-tetra-*tert*-butyl-25,26,27,28-tetrakis (hydroxycarbonylmethoxy)-2,8,14,20-tetrathiacalix[4]arene **2** obtained as described elsewhere [32].

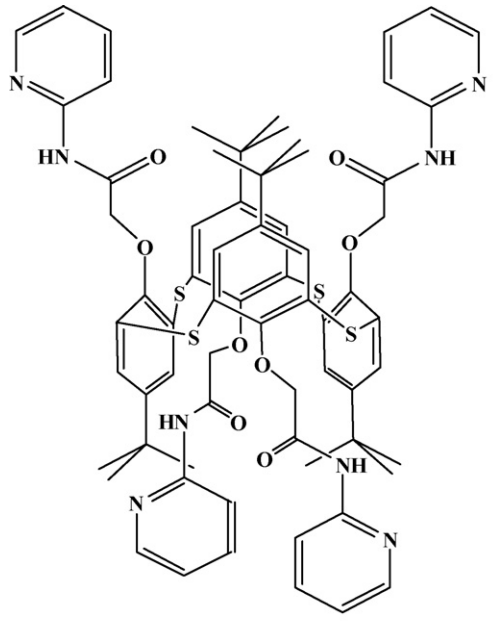

1

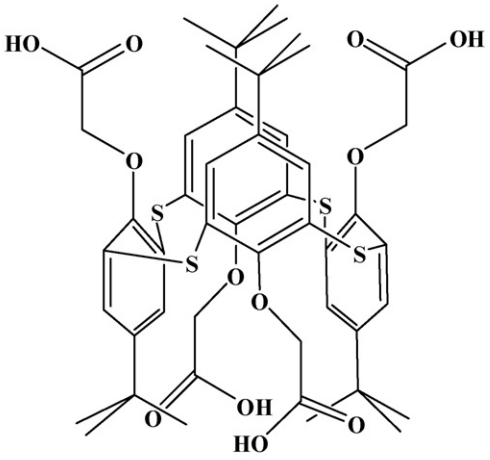

2

The solution of acid 2 (1.00 g, 1.05 mmol) in $SOCl_2$ (10.0 mL, 139 mmol) was stirred at reflux for 1 h. The excess of thionylchloride was evaporated at reduced pressure. The residue was dried in vacuum at 80 °C for 2 h. The reaction mixture was cooled to room temperature, then the solution of triethylamine (4.69 mL, 33.6 mmol) and 2-aminopyridine (3.16 g, 33.6 mmol) in dichloromethane (50 mL) was added. The reaction mixture was stirred overnight at room temperature and then washed with 50 mL of water. The organic layer was dried over 3 Å molecular sieves. The crude product was purified by recrystallization from dichloromethane/methanol to yield the derivative 5,11,17,23-tetra-*tert*-butyl-25,26,27,28-tetrakis[(2-pyridyl)-carbamoyl-methoxy]-2,8,14,20-tetrathiacalix[4]arene **1** (1.06 g, 80%) as a white solid with the m.p. of 272 °C. Elemental analysis: found: C, 64.41; H, 5.70; N, 8.45%. Calc. for $C_{68}H_{72}N_8S_8O_4$: C, 64.94; H, 5.77; N, 8.91%. ^{1}H NMR (300 MHz, $CDCl_3$), δ: 0.73 (s, 36H, *t*-Bu–H), 5.09 (s, 8H, COC–H), 6.96–7.00 (m, 4H, Py–H), 7.61–7.66 (m, 4H, Py–H), 7.66 (s, 8H, Ar–H), 8.24–8.29 (m, 8H, Py–H), 8.94 (br. s, 4H, N–H). ^{13}C NMR (75 MHz, $CDCl_3$), δ: 30.4, 34.0, 68.8, 114.5, 120.0, 126.4, 130.0, 137.9, 148.0, 150.8, 155.4, 168.0. IR in KBr pellet (ν cm^{-1}): 3410 (NH, free), 3295 (NH, bonded), 1720 (CO). MALDI TOF: 1257 ($M+H^+$), 1279 ($M+Na^+$), 1295 ($M+K^+$).

2.3. Picrate extraction

Metal picrates were prepared from appropriate nitrates by pH-titration with picric acid to pH 4.0. Then the aqueous solution of metal picrate complex (3 mL, 2.32×10^{-4} M) was mixed with thiacalix[4]arene **2** dissolved in dichloromethane (3 mL, 2.50×10^{-3} M). The mixture was stirred at 25 °C for 30 min and then left to stay for 60 min for phase separation. The absorbance of the aqueous phase was measured before (A_0) and after the extraction (A_i) at 355 nm with a "Perkin-Elmer Lambda-35" spectrometer. The part of the metal cation extracted (%*E*) was calculated as a ratio $100 \times (A_0 - A_i)/A_0$. The R.S.D. of the extraction value estimated for three runs was about 3%. Extraction experiments were performed at different ligand concentration. The extraction constant K_{ex} and the complex stoichiometry were determined from the dependence of the extraction degree on the ligand and metal concentrations.

2.4. Potentiometric sensor preparation

Glassy carbon electrode of 3 mm in diameter was mechanically polished to a mirror like surface and then rinsed with acetone, KOH and H_2SO_4. After that, the electrode was conditioned in 0.2 M H_2SO_4 at +0.1 V for 3 min followed by the potential cycling between −0.2 and +1.0 V at 40 mV s^{-1} for 10 min. After cleaning, the electrode was placed into the solution of 0.07 M aniline in 0.2 M H_2SO_4 and electropolymerization was performed by scanning the potential between −0.3 and +0.8 V at 50 mV s^{-1}. The quality of the PANI coating was controlled by AFM with the "Solver P47H" ("NT-MDT", Russia). The AFM images were obtained in the tapping mode at room temperature on the air with the scanner 50 μm × 50 μm and conventional silicon cantilevers NSG11 ("NT-MDT"). Five cycles of potential scanning were used in all the cases to obtain a dense continuous polymer film. After the PANI deposition, 10 μL of 1.0×10^{-3} M thiacalix[4]arene solution in chloroform were placed onto the surface and the sensor was left to dry at room temperature. Before measurements, the electrode was conditioned in the supporting electrolyte for 10 min.

2.5. Potentiometric measurements

All the measurements were performed at room temperature 23 ± 2 °C. To avoid the possible effect of internal filling of the reference electrode, a salt bridge filled with 0.1 M $NaNO_3$ was

used in all the potentiometric measurements. The cell set up for the EMF measurement was as follows: glassy carbon, PANI, thiacalix[4]arene **1** |test solution| salt bridge (0.1 M $NaNO_3$)||3 M KCl|AgCl, Ag. In some experiments, the glassy carbon electrode covered with PANI was also used as a reference electrode. It was prepared as described before but contained no thiacalix[4]arene in the surface layer. The potential of the sensor was measured in a stirring solution with the digital ionometer Ecotest-001 ("Econix-Expert", Moscow, Russia) connected to PC. The performance of the electrodes was examined by measuring the EMF of the primary ion solutions in 0.1 HNO_3 or 1.0×10^{-3} M Na_2SO_4 in the concentration range from 10^{-8} to 10^{-1} M. The selectivity coefficients log $K_{Ag/M}$, were determined by the separate solution method with 0.01 M solutions of Ag^+ and interfering ions [33]. Silver sulfathiazole (2% gel) was first dissolved in HNO_3 and then diluted with distilled water.

3. Results and discussion

3.1. The performance of PANI covered glassy carbon electrode

Low selectivity of the PANI potential toward cationic species as well as the narrow range of reversibility conditions are considered the weak point of this material in sensor applications. Indeed, the potential of the glassy carbon electrode covered with electropolymerized aniline depended on the cation concentration and the pH. The characteristics of the potential variations changed with the increase in the number of the potential cycles of polymer deposition. As shown by AFM, a dense uniform PANI film was obtained after ten potential scans in 0.2 M sulfuric acid at the rate of 50–100 mV s^{-1} (Fig. 1). The polymer formed 50–150 nm aggregates on the electrode surface, which were evenly distributed along the electrode surface. Rarely, there appeared bigger conglomerates of the primary aggregates of uncertain morphology.

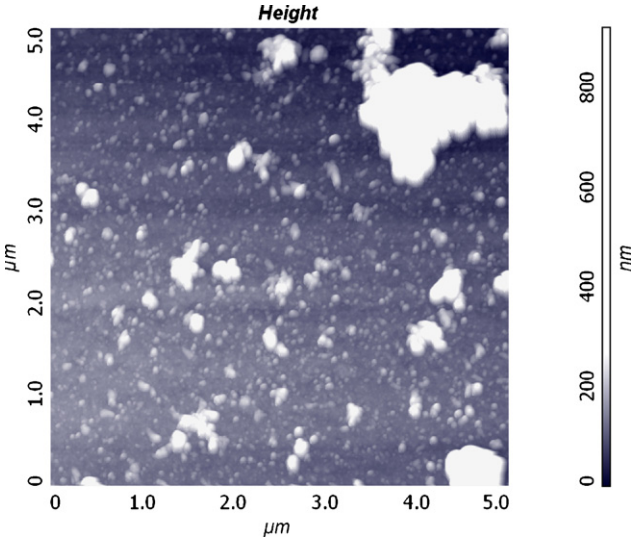

Fig. 1. AFM image of PANI layer obtained with five scans of the potential in 0.2 M sulfuric acid at 50 mV s^{-1}.

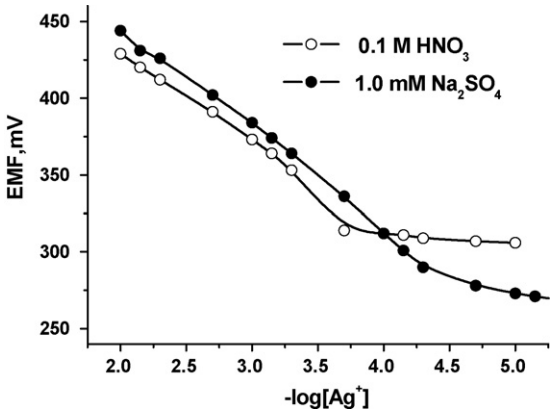

Fig. 2. The determination of Ag^+ ions with PANI covered electrode.

The following increase of the potential scan number results in the larger response time and a lower reversibility of the potential shifts toward pH and ionic content changes. For this reason, 10 cycles of the potential scans were chosen for the PANI electrodeposition in the sensor development. The glassy carbon electrode covered with PANI depended on the Ag^+ concentration in the range of log[Ag^+] from −2.0 to −4.0 in 0.1 M nitric acid and from −2.0 to −4.5 in 1.0×10^{-3} M Na_2SO_4 with nearly Nernstian slope of about 63 ± 3 mV (Fig. 2).

The response time of PANI electrode toward Ag^+ ions did not exceed 3.5–5.0 min and remained stable for at least 15 min. The signal was reproducible both for single and repeated additions of the Ag^+ test solution (R.S.D. 6.4% for the single measurement of 5.0×10^{-4} M $AgNO_3$ with six PANI covered electrodes). The recovery of the potential of PANI electrode after its contact with Ag^+ solution was achieved by its treatment with hydroquinone solution. The addition of EDTA and NaCl did not show the restoration of the initial potential. The results of hydroquinone treatment depended both on the contact period and hydroquinone concentration. In the series of the measurement, recovery cycles performed with the same sensor, the signal toward 5.0×10^{-4} M $AgNO_3$ decreased by 10–15% for each measurement due to the irreversible redox degradation of the polymer film.

Similar changes of the electrode potential were observed after the Fe^{3+} injection, whereas, the effect of Cd^{2+}, Pb^{2+}, K^+ and Na^+ was much lower. The response toward Fe^{3+} ions was observed only in acidic media and corresponded to the hydrolytic stability of the appropriate salt. The potential shifted much slower than that in the presence of Ag^+ with 95% change in 15 min.

All of the above facts indicate that the potential changes of the PANI electrode can be referred to the influence of the Ag^+ and Fe^{3+} ions on the redox status of the polymer, whereas, the effect of the surface charge changes is less significant.

3.2. The effect of thiacalix[4]arene *1* on the sensitivity of Ag^+ determination

The modification of the electrode by thiacalix[4]arene **1** placed from its chloroform solution onto the PANI layer resulted in a significant improvement of the analytical performance of the sensor. As was shown, the addition of 1×10^{-7} mol of **1** per

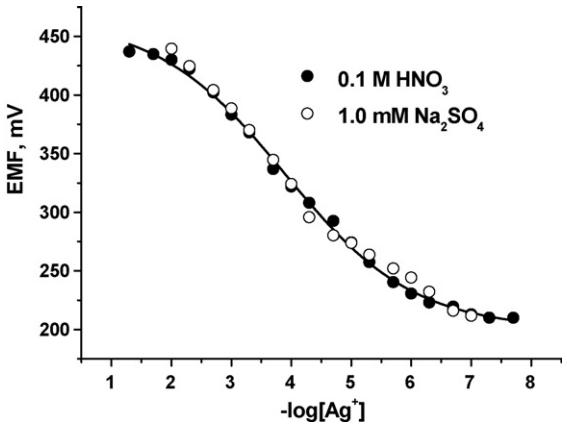

Fig. 3. The determination of Ag^+ ions with the potentiometric sensor based on glassy carbon electrode covered with PANI and thiacalixarene **1** (0.1 μmol per electrode).

electrode provided a most stable stationary potential with minimal drift within the measurement series. Low amounts of the modifier do not provide complete coverage of the PANI surface, whereas, higher loading of thiacalix[4]arene **1** lead to formation of too thick non-conductive layer with less reproducible characteristics. The dependence of the signal on the amounts of thiacalix[4]arene added to the electrode is presented in the figure. The presence of thiacalix[4]arene **1** did not alter the pH-dependence of the sensor potential as well as the response time.

The signal of the PANI-**1** covered sensor depended on the Ag^+ concentration within $\log[Ag^+] = -2.0$ to -6.3 with $10^{-7.6}$ M limit of detection obtained both in 0.1 M HNO_3 and 1.0×10^{-3} M Na_2SO_4 (Fig. 3). The 95% shift of the potential after the injection of 5.0×10^{-4} M $AgNO_3$ was reached in 12 s. The following addition of 0.1 M NaCl effectively suppressed the potential to its initial value (Fig. 4). The sensor recovery can be also obtained with 0.01 M EDTA. The repeated treatment with NaCl and EDTA did not seriously affect the initial potential and the response toward Ag^+ in the series of 15 consecutive measurements performed with the same sensor. The effective recovery of the sensor potential was observed after 2–3 min contact with the complexing agent. After that, the sensor was washed by distilled water and measurement solution (0.1 M HNO_3 or 1.0×10^{-3} M Na_2SO_4) and used again. The R.S.D. of the signal toward 2.0×10^{-4} M $AgNO_3$ was 1.4% and 1.5% for 0.1 M NaCl and 0.01 M EDTA treatment, respectively (six measurements with the same sensor). The R.S.D. of the initial potential measured after the recovery procedure was 1.9% and 7.9%, respectively. Lower reproducibility of the potential recovery observed after the EDTA treatment can be related to the partial accumulation of EDTA onto the positively charged PANI and its less effective removal from the surface layer.

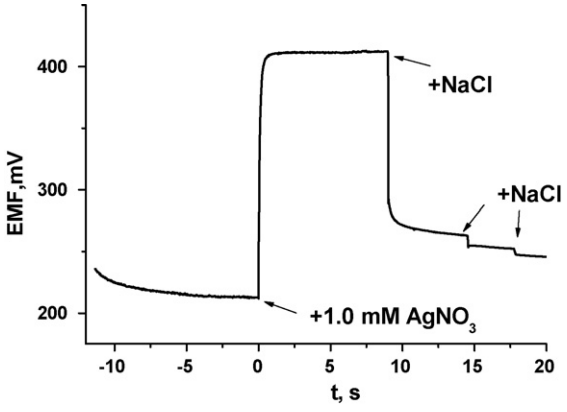

Fig. 4. Dynamic response of potentiometric sensor toward $AgNO_3$ (final concentration 1.0×10^{-3} M) and NaCl (1.0×10^{-2} M). Arrows indicate the time of solution injections.

The influence of complexing agents on the potential recovery as well as a faster and reversible response toward Ag^+ ions in a broader concentration range distinguishes the behavior of the sensor containing thiacalixarene **1** from that of the PANI covered electrode. Probably, the sensor signal toward Ag^+ ions is to a greater extent determined by the host–guest complexation than by PANI redox reactions. The complexation probably involves cooperative interaction of the carbonyl oxygen atoms and of the nitrogen atoms of pyridine fragments with the Ag^+ ion. The structure of the complex (1) corresponds well to the present concepts of calixarene–cation interactions [23].

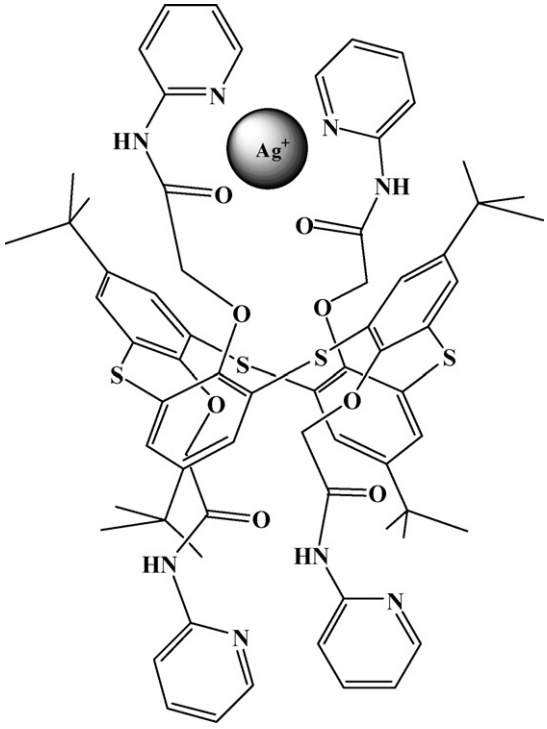

(1)

This was proved by the replacement of Ag/AgCl reference electrode with glassy carbon covered with PANI (Fig. 5). The changes in the sensor potential measured against PANI were rather low and irregular in the range of $\log[Ag^+]$ from -2.0 to -3.5. This agrees with results of Ag^+ determination with the PANI covered electrode (see Fig. 2). At lower Ag^+ concentration, the changes in the sensor potential can be related only to the interactions of thiacalxarene **1** with Ag^+ ions. The host–guest complexation increases the charge of the surface and the sensor potential.

Table 1
Selectivity coefficients $\log(K_{Ag/M})$ of potentiometric sensor with thiacalixarene **1** in the surface layer (values in the brackets refer to the glassy carbon electrode covered with PANI only)

Media content	$-\log(K_{Ag/M})$						
	Na	K	Pb	Cd	Hg^{2+}	Cu^{2+}	Fe^{3+}
0.1M HNO_3 (pH 1.7)	6.18 (2.64)	6.06 (2.82)	7.98 (4.46)	6.53 (2.87)	0.46 (0.25)	4.51 (3.47)	0.13 (−1.71)
1.0×10^{-3} M Na_2SO_4 (pH 5.1)	–	7.22 (5.38)	8.05 (4.72)	6.05 (4.21)	–	5.01 (4.24)	0.55 (−0.85)

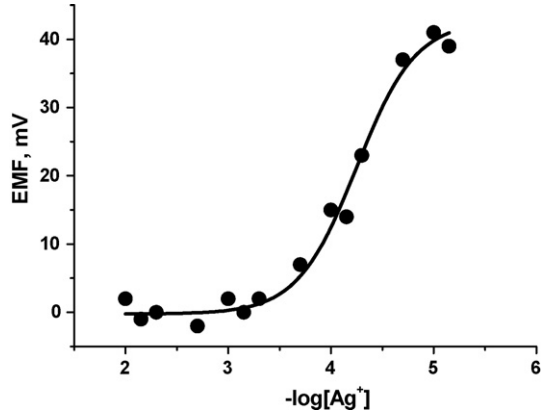

Fig. 5. The potentiometric response toward Ag^+ ions measured against glassy carbon electrode covered with PANI.

3.3. Selectivity of Ag^+ determination

The selectivity coefficients $\log K_{Ag/M}$ determined by the separate solution method are presented in Table 1. Thiacalixarene **1** is shown to significantly improve the selectivity of the response toward Ag^+ against all the other ions investigated. In acidic media the selectivity of the sensor response was found to be lower both for the PANI and PANI-**1** surface layers. In neutral media, the inherent PANI charge is small enough so that the effect of cations (with that of Ag^+ complexation, among them) on the potential is higher than that in acidic media. This corresponds well enough to the pH sensitivity of the selectivity coefficients established for transient metals (Fig. 6).

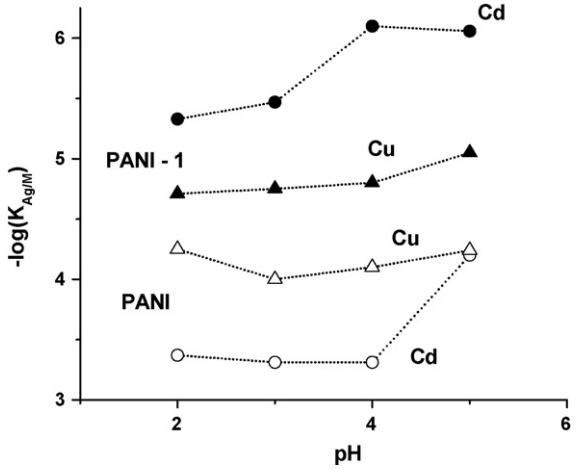

Fig. 6. pH dependence of the potentiometric selectivity coefficients $\log(K_{Ag/M})$ measured with electrodes modified with PANI and PANI–thiacalixarene **1**.

As was established in the mixed run studies, the influence of Fe^{3+} and Hg^{2+} on the sensor signal toward Ag^+ ions is expressed in diminishing linear piece of the calibration curve, whereas, its slope remains about the same within the whole range of the concentrations of interfering ions investigated (see Fig. 7a for Fe^{3+} as an example, the addition of Hg^{2+} gives similar consequences). This corresponds well to the description of the influence of interferences on the potential of an ions-selective electrode (2).

$$\mathrm{EMF} = \mathrm{Const.} + S \log \left[a_{Ag} + \sum K_{Ag/Me} a_{Me}^{1/z_{Me}} \right] \quad (2)$$

where S is the sensitivity of determination, a the ion activity, and z is the charge of the interfering ion M^{z+} ($z = 1$ for Ag^+) [34].

The interfering effect of Hg^{2+} can be easily eliminated by increasing the pH. No response toward Hg^{2+} was observed at pH 3.0 and higher due to the hydrolytic instability of mercury cations. For other transition metals, the increase of the pH

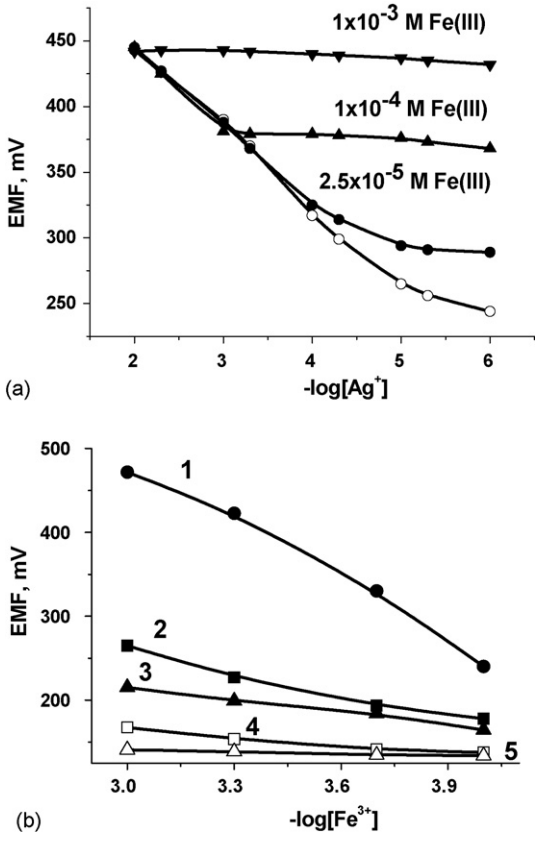

Fig. 7. Interfering effect of Fe^{3+} ions on the Ag^+ signal (a) and masking effect of NaF on the calibration curve of Fe^{3+} (b). [NaF] = 0 (1), 6×10^{-4} M (2), 1×10^{-3} M (3) 5×10^{-3} M (4) 2×10^{-3} M (5). All the measurements were performed on the electrode covered with PANI and thiacalixarene **1**.

from 1.3 to 5.0 improves the selectivity of Ag^+ measurements (Fig. 6).

The Fe^{3+} ion showed the highest interfering effect on the Ag^+ signal due to its ability to oxidize PANI (Fig. 7). The introduction of thiacalixarene **1** in the PANI layer diminished its influence by two orders of magnitude (see Table 1) but the potential shift remained still comparable with that of Ag^+. Sodium fluoride that forms a stable complex with Fe^{3+} ions suppresses both the effect of Fe^{3+} on the PANI and its interference with the Ag^+ signal. Meanwhile, the signal of Ag^+ remained about the same in the presence of the 50–1000 excess of the masking agent. The addition of NaF to its final concentration of 1.0 mM fully eliminated the influence of Fe^{3+} in the whole range of the Ag^+ concentrations determined.

3.4. Picrate extraction investigation

The relative activity of thiacalixarene **1** in the reaction with some transition metal ions was investigated by the liquid–liquid extraction of appropriate picrate salts [35]. The experiments were carried out in a mutually saturated water–dichloromethane system. The extraction equilibrium is described by Eq. (3) where M^+, L, Pic^-, ML^+, and $ML_n^+Pic^-$ denote the metal ion, the ligand (here, thiacalixarene **1**), the picrate anion, the metal complex and the ion-pair, respectively; n is the number of ligands binding to one metal ion. Hereafter, the indices aq and org refer to the species present in aqueous and organic phase, respectively.

$$M^+_{aq} + nL_{org} + Pic^-_{aq} \rightleftarrows ML_n^+Pic^-_{org} \quad (3)$$

The percentage extraction $E\%$ and the extraction degree, α, were calculated in accordance with Eq. (4).

$$E\% = \alpha \times 100\% = \frac{[ML_n^+Pic^-]_{org}}{[Pic^-]_{aq}} \times 100\% \quad (4)$$

The thermodynamic extraction constant, K_{ex}, is given by Eq. (5).

$$K_{ex} = \frac{[ML_n^+Pic^-]_{org}}{[M^+]_{aq}\,[Pic^-]_{aq}\,[L]^n_{org}} \quad (5)$$

The stoichiometry coefficient n of the complexes formed in the organic phase was calculated in accordance with (4) transformed from (6).

$$\log K_{ex} = \log\left(\frac{\alpha}{1-\alpha}\right) - \log[M^+]_{aq} - n \times \log[L]_{org} \quad (6)$$

The plot of $\log(\alpha/(1-\alpha)) - \log[M^+]_{aq}$ *versus* $\log[L]_{org}$ presents a straight line, the slope of which is equal to n. The extraction constant K_{ex} is calculated in accordance with (7) using the intercept values (b) of the line.

$$b = \log K_{ex} + \log[M^+]_{aq} \quad (7)$$

For all the transition metals investigated, the linearity of relationship (6) was proved by experimental data. The results of the extraction investigation are presented in Table 2.

In the organic phase thiacalixarene **1** forms complexes with the stoichiometry 1:1, 1:2 and 1:4 for Ag^+, Hg^{2+} and Fe^{3+}, respectively. Thus, one or two pyridine containing substituents O–CH_2–C(O)NH-*o*-Py participate in binding the metal ions. Negative allosteric effect was observed for Ag^+ along with the absence of the macrocycle pre-organization in the reaction with Fe^{3+} ions. This can be explained from the point of view of Pirson's principle of "hard and soft acids and bases" (HSAB). The Ag^+ ion as a soft acid fits the size and electronic nature of the binding site. This results in the strong reorganization of the whole macrocycle geometry upon complexation, which is not observed for soft-to-intermediate mercury ion. Charge control of the complexation allows the Fe^{3+} ion to interact with podant moieties of thiacalixarene **1** independently. The formation of 1:2 and 1:4 complexes partially compensates for the difference in the complex extraction observed for both transient metals and Ag^+. To be sure, the binding of Fe^{3+} with thiacalixarene **1** adsorbed onto the PANI layer of the electrode can be affected both sterically and electrostatically. The data obtained prove the results of potentiometric determination showing preferable transfer into the surface layer of all the above ions. The pH control and use of masking agents provide for the selective determination of Ag^+ ion in a wide range of its concentration.

Table 2
Extraction constants ($\log K_{ex}$) and stoichiometry coefficient (n = L:M ratio) of transition metal complexes at 25 °C

	Ag^+	Hg^{2+}	Fe^{3+}
$\log K_{ex}$	5.14 ± 0.05	4.29 ± 0.01	4.03 ± 0.02
n	1.08 ± 0.02	0.49 ± 0.01	0.27 ± 0.02

3.5. Silver sulfathiazole determination

Silver sulfathiazole (Argosulfan^{TM}) refers to sulfonamide group of antibiotics that after topical application show strong antibacterial activity and good tolerance. It is purchased for external application as a 2% gel that contains, along with silver thiazole, liquid paraffin, detergents, glycerol, methyl- and propylhydroxybenzoate. As in the case of silver sulfadiazine, Ag^+ ions promote the antibacterial effect of sulfathiazole and diminish its sensitizing activity [36]. Prior to determination, the preparation was diluted when stirring with 0.1 M HNO_3 and then the upper part of the liquid was taken for potentiometric measurements. The potential of the sensor contained PANI and thiacalixarene **1** depended on the concentration of silver sulfathiazole in the range from 1×10^{-6} to 1×10^{-3} M in accordance with Eq. (8).

$$\text{EMF (mV)} = (543 \pm 24) + (46 \pm 5) \times \log C,\ M,\ R = 0.9769,$$
$$\text{S.D.}: 11.04, \quad p\text{-value} = 7.92 \times 10^{-4} \quad (8)$$

Boiling the Argosulfan solution diluted by 0.1 M HNO_3 for 10 min increased the slope of the calibration curve to near-Nernstian value 52 ± 7 mV. Probably, nitric acid oxidized organic ligands of Ag^+ ions and simplified their following interaction with thiacalix[4]arene molecules. Microheterogeneity of the solution contained paraffin emulsion and detergents as well as rather low concentration of the nitric acid decrease the repro-

ducibility of the treatment procedure. The appropriate R.S.D. of the response calculated for 1×10^{-5} M silver sulfathiazole was found to be 12%. In addition to direct potentiometric determination, the Ag^+ ion released from the gel were determined in the aqueous part of the mixture by titration with 1×10^{-3} M NaCl. The titration was performed under stirring by consecutive addition of 50 μL of titrant solution. The accuracy of the end-point detection was found to be 7%.

4. Conclusion

The use of the thiacalixarene neutral carrier without any additional plasticizer significantly improved the analytical performance of the PANI based potentiometric sensor for the determination of silver. As shown, the presence of pyridine containing thiacalixarene changed the mechanism of the signal generations. The low Ag^+ concentrations change the number of positive charges onto the sensor surface due to the host–guest complexation, whereas, in the absence of thiacalixarene the oxidation of the PANI layer occurs. As a result, the selectivity of the response toward transient metals and the reversibility of the response were significantly improved in comparison with the behavior of the PANI covered glassy carbon. The investigation of the extraction of picrate complexes of transient metals showed the formation of the complexes with various stoichiometry to depend on the nature of the metal. However, the choice of the pH and the use of masking agent, NaF, made it possible to fully avoid the interference of the Hg^{2+} and Fe^{3+} ions which compete with Ag^+ for the binding sites of thiacalixarene. The potentiometric sensor can be applied for routine analysis of silver containing pharmaceuticals as was shown with silver sulfathiazole (Argosulfan^{TM}) as an example.

Acknowledgements

Financial support of RFBR (grants 04-03-97511 and 05-03-33162-a), Federal Science Agency of Russian Federation (RI-19.0/001/184 and 2005-IN-12.1/012) is gratefully acknowledged.

References

[1] J. Bobacka, A. Ivaska, A. Lewenstam, Electroanalysis 15 (2003) 366.
[2] R. Buck, Ion Selective Electrodes in Analytical Chemistry, Plenum Press, New York, 1980.
[3] T. Lindfors, A. Ivaska, Anal. Chim. Acta 404 (2000) 111.
[4] T. Lindfors, A. Ivaska, Anal. Chim. Acta 437 (2001) 171.
[5] W.-S. Han, M.-Y. Park, K.-C. Chung, D.-H. Cho, T.-K. Hong, Talanta 54 (2001) 153.
[6] H. Karami, M.F. Mousavi, Talanta 63 (2004) 743.
[7] J. Bobacka, A. Lewenstam, A. Ivaska, Talanta 40 (1993) 1437.
[8] T.A. Bendikov, T.C. Harmon, Anal. Chim. Acta 551 (2005) 30–36.
[9] M. Ocypa, A. Michalska, K. Maksymiuk, Electrochim. Acta 51 (2006) 2298.
[10] A.A. Khan, Inamuddin, M.M. Alam, React. Funct. Polym. 63 (2005) 119.
[11] K.-K. Shiu, F.-Y. Song, K.-W. Lau, J. Electroanal. Chem. 476 (1999) 109.
[12] A. Alumaa, A. Hallik, U. Mäeorg, V. Sammelselg, J. Tamm, Electrochim. Acta 49 (2004) 1767.
[13] R. Toczyłowska, R. Pokrop, A. Dybko, W. Wróblewski, Anal. Chim. Acta 540 (2005) 167.
[14] D.M. Duncan, J.S. Cockayne, Sens. Actuators B 73 (2001) 228.
[15] T. Katsua, K. Ido, K. Takaishi, H. Yokosu, Sens. Actuators B 87 (2002) 331.
[16] A.K. Jain, V.K. Gupta, J.R. Raisoni, Sensors 4 (2004) 115.
[17] A.K. Jaina, V.K. Gupta, L.P. Singh, P. Srivastava, J.R. Raisoni, Talanta 65 (2005) 716.
[18] L. Chen, J. Zhang, W. Zhao, X. He, Y. Liu, J. Electroanal. Chem. 589 (2006) 106.
[19] J. Lu, R. Chen, X. He, J. Electroanal. Chem. 528 (2002) 33–38.
[20] N. Ramamurthy, R.B. Brown, R. Hower, M.E. Meyerhoff, Fresenius J. Anal. Chem. 364 (1999) 41.
[21] J. Radecki, H. Radecka, T. Piotrowski, S. Depraetere, W. Dehaen, J. Plavec, Electroanalysis 16 (2004) 2073.
[22] J. Lu, X. Tong, X. He, J. Electroanal. Chem. 540 (2003) 111; S.M. Lim, H.J. Chung, K.-J. Paeng, C.-H. Lee, H.N. Choi, W.-Y. Lee, Anal. Chim. Acta 453 (2002) 81.
[23] R. Ludwig, N.T.K. Dzung, Sensors 2 (2002) 397.
[24] E. Malinowska, Z. Brzozka, K. Kasiura, R.J.M. Egberink, D.N. Reinhoudt, Anal. Chim. Acta 298 (1994) 245.
[25] R.K. Mahajan, I. Kaur, R. Kaur, V. Bhalla, M. Kumar, Bull. Chem. Soc. Jpn. 78 (2005) 1635.
[26] X. Zeng, L. Weng, L. Chen, X. Leng, Z. Zhang, X. He, Tetrahedron Lett. 41 (2000) 4917.
[27] L. Chen, X. He, B. Zhao, Y. Liu, Anal. Chim. Acta 417 (2000) 51.
[28] L. Chen, H. Ju, X. Zeng, X. He, Z. Zhang, Anal. Chim. Acta 437 (2001) 191.
[29] N. Iki, S. Miyano, J. Incl. Phenom. Macrocycl. Chem. 41 (2001) 99.
[30] M. Ben Ali, R. Ben Chabanne, F. Vocanson, C. Dridi, N. Jaffrezic, R. Lamartine, Thin Solid Films 495 (2006) 368.
[31] H. Matsumiya, T. Ishida, N. Iki, S. Miyan, Anal. Chim. Acta 478 (2003) 163.
[32] N. Iki, N. Morohashi, F. Narumi, T. Fujimoto, T. Suzuki, S. Miyano, Tetrahedron Lett. 40 (1999) 7337.
[33] Y. Umezawa, K. Umezawa, H. Sato, Pure Appl. Chem. 67 (1995) 507.
[34] R.P. Buck, E. Linder, Pure Appl. Chem. 66 (1994) 2527.
[35] R. Lamartine, C. Bavoux, F. Vocanson, A. Martin, G. Senlis, M. Perrin, Tetrahedron Lett. 42 (2001) 1021.
[36] C.L. Fox Jr., S.M. Modak, Antimicrob. Agents Chemother. 5 (1974) 582.

Available online at www.sciencedirect.com
ScienceDirect
Talanta 71 (2007) 1795–1803
Talanta
www.elsevier.com/locate/talanta

AGNES: A technique for determining the concentration of free metal ions. The case of Zn(II) in coastal Mediterranean seawater

J. Galceran [a,*], C. Huidobro [a], E. Companys [a], G. Alberti [b]

[a] *Departament de Química, Universitat de Lleida, Rovira Roure 191, 25198 Lleida, Spain*
[b] *Dipartimento di Chimica Generale, Università di Pavia, via Taramelli 12, 27100 Pavia, Italy*

Received 28 April 2006; received in revised form 4 August 2006; accepted 21 August 2006
Available online 29 September 2006

Abstract

Absence of Gradients and Nernstian Equilibrium Stripping (AGNES) is a recently suggested electroanalytical technique designed for the determination of the free concentration of heavy metals (such as Zn, Cd or Pb) which is here developed and applied to seawater samples. A key improvement for the implementation of AGNES with complex matrices is the development of a new blank, called the shifted blank (presented in this work for the first time), which can be applied to the same sample where the measurement is intended. The careful selection of the required parameters for the determination of the free Zn concentration (or activity) at the nanomolar level is described in detail. The methodology has been validated with a synthetic solution containing Zn and nitrilotriacetic acid (NTA) and then applied, as a first case, to two coastal seawater samples taken close to Barcelona and Tarragona (Catalonia, North-Eastern Spain) finding values in the range of 1–3 nM, representing around 25% of total Zn. This technique can, in the near future, be crucial in helping to elucidate the role of the free zinc(II) concentration in natural waters.

Keywords: Chemical speciation; Zinc; Seawater; Stripping analysis; Heavy metals; FIAM

1. Introduction

Knowledge of the concentration of free metal ions in natural waters is essential for understanding the role and fate of nutrient and pollutant elements [1–5]. Indeed, the Free Ion Activity Model [6] or the Biotic Ligand Model [7,8] highlight the free concentration as more relevant than the total metal concentration, which can be determined with well established techniques. In this context, the implementation and development of a variety of techniques for reliable measurements of free metal ion concentrations (or well-defined labile fractions) can be of interest [9–15].

In the particular case of Zn ion, there has been a long debate on the potential limiting role of Zn(II) concentration in the marine environment [16–20]. A coherent answer to the questions of this debate can only be done by putting together complementary information on the speciation of Zn provided by different techniques.

Some methods to measure total Zn and/or its labile fraction involve a preconcentration step, such as Anodic Stripping Voltammetry [21] or Cathodic Stripping Voltammetry [22,23]. When these kind of methods have been applied to seawater samples, they have usually supported the hypothesis of a very low availability (and limiting role) of Zn, especially in the open ocean, where a large proportion of the total Zn would be bound, mostly to organic ligands. For instance, Donat and Bruland [24,25] determined that >95% of total dissolved Zn is strongly complexed by organic ligands having concentrations of 1.6–2.2 nM and forming complexes with conditional stability constants of 10^{10} to 10^{11}. A number of other reports indicate, however, a much lower proportion of organically complexed zinc [26–28].

As far as we know, there is no standard method for the determination of Zn(II) free concentration, despite intense work such as the search for an ion selective electrode for Zn [29] and many other strategies [30,31]. So, the availability of techniques allowing such determination could be helpful in the solving of an important question for the scientific community.

Recently, we have designed [32] a new stripping technique aiming at the determination of free metal ion concentration,

* Corresponding author. Tel.: +34 973 70 28 26; fax: +34 973 23 82 64.
E-mail address: galceran@quimica.udl.es (J. Galceran).

0039-9140/$ – see front matter © 2006 Elsevier B.V. All rights reserved.
doi:10.1016/j.talanta.2006.08.027

whose name, AGNES, indicates that the stripping step is applied when a special situation has been achieved. One advantage of this new electroanalytical technique is its simple interpretation, in contrast with the difficulties encountered in many current determinations of the "labile metal" concentration whose exact meaning depends on a number of assumptions and ill-unknown parameters. In a further development [33] we have shown that AGNES can determine free Zn concentrations in various synthetic solutions with labile or non-labile complexes. So, we aim here at implementing and developing AGNES methodology for the measurement of Zn in Mediterranean seawater samples, tackling the problem of reducing the limit of detection and the difficulties of a complex matrix.

2. Theoretical background

2.1. Principles of AGNES

AGNES has been presented in detail in previous works [32,33]. We summarize here the principles of this electroanalytical technique for the particular case of Zn. AGNES consists of two stages: deposition or first stage and stripping or second stage. In the simplest potential program (see Fig. 1), only one constant potential E_1 is applied along the deposition time t_1, while stirring is on during a time $t_1 - t_w$.

2.1.1. First stage

A key feature of AGNES is that by the end of the first stage a special situation is reached:

(i) "Absence of Gradients": there are no concentration profiles at either side of the electrode surface. So, the free Zn concentration at the bulk is the same as in the electrode surface and we represent them here as $[Zn^{2+}]$.
(ii) "Nernstian Equilibrium". The couple Zn^{2+}/Zn^0 has reached the equilibrium corresponding to the applied potential (E_1).

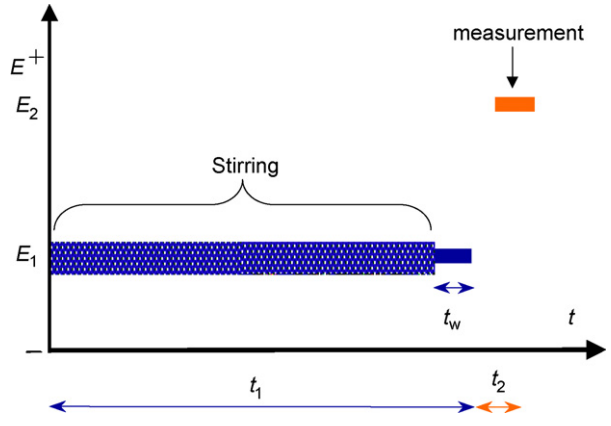

Fig. 1. Schematic potential program for the simplest implementation of AGNES (one potential step along the first stage). The thicker line indicates that stirring is on along most of the deposition time (t_1). One key point of AGNES is that t_1 must be sufficiently long and the required preconcentration factor Y sufficiently small so that equilibrium is reached by the end of the first stage. A second important aspect is that E_2 must correspond to diffusion limited conditions for the reoxidation.

Nernst equation allows to compute the ratio of concentrations at each side of the electrode surface (which we call the preconcentration factor or "gain" Y) as

$$Y = \frac{[Zn^0]}{[Zn^{2+}]} = \exp\left[-\frac{2F}{RT}(E_1 - E^{\circ\prime})\right] \quad (1)$$

where F is the Faraday constant, R the gas constant, T the temperature and $E^{\circ\prime}$ is the standard formal potential (where the activity coefficients are embedded). In the present implementation of AGNES, the preconcentration factor is determined from E_{peak}, the potential peak of a Differential Pulse Polarography (DPP) experiment [32]:

$$Y = \sqrt{\frac{D_{Zn}}{D_{Zn^0}}} \exp\left[-\frac{2F}{RT}\left(E_1 - E_{peak} - \frac{\Delta E_{DPP}}{2}\right)\right] \quad (2)$$

where D_{Zn} and D_{Zn^0} are the diffusion coefficients for the free metal ion and the reduced metal (inside the amalgam) and ΔE_{DPP} is a characteristic parameter of the DPP experiment.

2.1.2. Second stage

The aim of the second stage is the determination of the concentration of Zn^0 in the amalgam. For that purpose, a simple strategy consists in applying a sufficiently less negative potential (E_2) producing a stripping current under diffusion limited conditions. The response function in this implementation of AGNES is the current I at a certain time t_2.

2.1.3. The proportionality factor, h

Due to the linear properties of the diffusion of Zn^0 inside the amalgam [32], there is a direct proportionality between the Faradaic current I_f and the concentration of Zn^0 built up inside the mercury drop. But Eq. (1) indicates another direct proportionality between this Zn^0-concentration and that of free Zn. So, regardless of processes such as electrodic adsorption, complexation or hydrodynamic regimes, the following fundamental relationship between Faradaic current and free metal concentration applies:

$$I_f = h[Zn^{2+}] \quad (3)$$

As the measured current, I, contains components other than the Faradaic one of the analyte (see next section), there is a need to subtract a blank from the total current.

2.2. An improved blank: the "shifted" blank

The subtracted blank in AGNES has been, up to the present date [32,33], determined in a synthetic solution with the same composition of the sample and no added metal. This "synthetic" blank exhibits some limitations: (a) the presence of traces of the analysed metal (via contamination) cannot be avoided (if this trace concentration in the blank is not well determined there will be a loss of accuracy in the determination of low concentrations in the sample) and variations in the contamination concentration leads to a (relatively) high value for the limit of detection (LOD); (b) for natural samples it is very difficult to mimic such complex

matrices via synthetic solutions. So, we develop here a new blank which will be essential in the improving of the LOD of AGNES and suitable for natural samples.

In principle, in any response current I measured with AGNES (either in any blank or in a sample with a given amount of metal) at a certain time t_2, we recognise the following components:

(i) The charging or capacitive current, which we denote I_c.
(ii) The current due to the reduction of O_2, I_{O_2}. Even if N_2 flows through the cell, traces of oxygen are always present.
(iii) The Faradaic current due to non-analyte elements which have been preconcentrated along the first stage and stripped along the second stage, I_{fna}. For instance, when determining Zn, the deposition potential (E_1) will also preconcentrate Cd and if the stripping potential (E_2) was −0.1 V, then the re-oxidating preconcentrated Cd would also contribute to the measured current at t_2.
(iv) The Faradaic current due to the analyte (Zn in this case). We denote it as I_f.

So, the current obtained at t_2, for any given preconcentration factor Y, can be split into

$$I = I_c + I_{O_2} + I_{fna} + I_f \quad (4)$$

Now, assume that we perform two experiments with two different Y-values, being one Y-value negligible in front of the other. For simplicity in the exposition in this section, we take $Y = 500$ and 0.01, but many other combinations would be possible. If we subtract both measured currents,

$$\begin{aligned} I_{Y=500} - I_{Y=0.01} &= (I_{c,Y=500} - I_{c,Y=0.01}) \\ &\quad + (I_{O_2,Y=500} - I_{O_2,Y=0.01}) \\ &\quad + (I_{fna,Y=500} - I_{fna,Y=0.01}) \\ &\quad + (I_{f,Y=500} - I_{f,Y=0.01}) \end{aligned} \quad (5)$$

As detailed in Section 4 (Section 4.1) below, a suitable selection of the potential program parameters allows the neglecting of all the terms in the r.h.s. of previous Eq. (5), except the last one (the one corresponding to the Faradic current). Under such conditions

$$\begin{aligned} I_{Y=500} - I_{Y=0.01} &= I_{f,Y=500} - I_{f,Y=0.01} \\ &= [Zn^{2+}](h_{Y=500} - h_{Y=0.01}) \end{aligned} \quad (6)$$

where we have used the proportionality between Faradaic current and free metal concentration given by the fundamental Eq. (3). If we take into account the proportionality between h and Y (see Appendix in [32]):

$$\begin{aligned} I_{Y=500} - I_{Y=0.01} &= [Zn^{2+}](h_{Y=500} - h_{Y=0.01}) \\ &= [Zn^{2+}]h_{Y=500}\left(1 - \frac{0.01}{500}\right) \\ &\approx [Zn^{2+}]h_{Y=500} \end{aligned} \quad (7)$$

So, the measurement performed at $Y = 0.01$ (i.e. for a Y which is negligible with respect to the Y-value of the main measurement) would act as the blank to be subtracted in order to experimentally access to the proportionality between Faradaic current and concentration. This negligible Y (of the blank) corresponds to a change in the (main) deposition potential E_1 by an amount which can be called ΔE_{shift}. The essence of the new blank consists, as will be detailed in Section 4.1 below, in applying basically the same potential program as in the main measurement, but with the applied potentials shifted a fixed ΔE_{shift} towards less negative potentials. For this reason, we suggest to call it the "shifted blank" and to label its parameters with the subscript "sb".

3. Experimental

3.1. Instrumentation and reagents

Voltammetric measurements were carried out with Eco Chemie Autolab PGSTAT30 and PGSTAT12 potentiostats attached to Metrohm 663VA Stands and to a computer by means of the GPES (Eco Chemie) software package. The working electrode was a Metrohm multimode mercury drop electrode. The smallest drop in our stand was chosen, which according to the catalogue corresponds to a radius around $r_0 = 1.41 \times 10^{-4}$ m.

The auxiliary electrode was a glassy carbon electrode and the reference electrode was Ag/AgCl/3 mol L^{-1} KCl, encased in a 0.1 mol L^{-1} KNO_3 jacket.

A glass combined electrode (Orion 9103) was attached to an Orion Research 920A ion analyser and introduced in the cell to control the pH. A glass jacketed cell and a Teflon (PFA) cell provided by Metrohm were used in all measurements. The vessel was thermostated at 25.0 °C.

To stir the solution, the PTFE tip stirrer of the Metrohm 663VA Stand, which is screwed onto the driving axis, was used. The rotation rate is set on the 663VA Stand and it was fixed at 1500 rpm for all experiments.

All laboratory ware and the equipment for sampling and filtering were extensively washed using the following procedure: they were stored in 3 M nitric acid ultra pure for at least 1 week, then the solution was replaced by fresh 0.1 M nitric acid and they were stored in this solution just before their use. Finally they were rinsed with ultrapure Milli-Q water and air-dried under a cleaned hood.

Zinc standard solutions were prepared by adequate dilution from the Merck 1000 mg L^{-1} stock solution. Potassium nitrate was used as the inert supporting electrolyte and prepared from solid KNO_3 (Merck, Suprapur). Nitrilotriacetic acid (NTA) (Fluka, analytical grade) in the H_3L form, was used as ligand.

KOH and HNO_3 titrisol (Merck) were added to fix the pH to the desired values.

Ultrapure water (Milli-Q plus 185 System, Millipore) was employed in all the experiments. Purified water-saturated nitrogen N_2 (50) was used for deaeration and blanketing of solutions.

3.2. Seawater sample collection

Seawater samples were collected at 50 m from the shore and placed in 5 L plastic bottles. The collections took place on 7

June 2005 (Castelldefels, Barcelona) and on 13 October 2005 (La Rabassada, Tarragona) from beaches located in the western Mediterranean sea in Catalonia, Spain. All of them were surface samples (~0.25 m). After their collection, seawater samples were transferred within a few hours to the laboratory where they were filtered through nitric cellulose Millipore 0.45 μm filters.

The pH of the Castelldefels and Tarragona seawaters were 8.20 and 8.18, respectively, and the temperatures were 21 and 23 °C. The conductivities of Tarragona and Castelldefels seawaters were 48.5 and 49.5 mS cm^{-1}, respectively.

4. Results and discussion

4.1. Selection of the conditions for the shifted blank to be used for the determination of Zn in seawater

The use of the shifted blank procedure requires the cancelling (or neglecting) of components other than the Faradaic current of Zn in Eq. (5). Now, we analyse these components in order to select the best conditions for Eq. (7) to be applied.

(i) The capacitive current, I_c, for this electrode, decays faster than the Faradaic component [34], so that its absolute value (for the main measurement) is expected to be low at the relatively long measuring time t_2 such as 0.25 s. However, specially for low Faradaic currents, I_c can be still relevant at t_2, so we conducted a series of experiments, in synthetic solutions with just traces of Zn, to see how the different potential programs would affect the capacitive current term we want to minimise, i.e. $(I_{c,Y=500} - I_{c,Y=0.01})$.

Fig. 2 shows AGNES currents I_{sb} (at $t_2 = 0.2$ s) measured in a solution with just KNO_3 and in another solution with KNO_3 and EDTA. The presence of EDTA has not a noticeable impact on the currents, despite reducing dramatically the free Zn concentration of an already very low total metal concentration (just from the existence of traces of Zn) and forming very inert complexes. So, we conclude that the changes in the total measured currents are mostly due to the variations in the capacitive component (the oxygen component can be considered practically constant in the range of potentials scanned by E_2 in the figure and EDTA forms complexes with other existing trace metals, so that their Faradaic contribution should also be totally negligible). The key conclusion from Fig. 2 is that I_c depends mostly on the difference in the potentials applied during the first stage (E_1) and the second stage (E_2); when this potential jump between stages ($E_2 - E_1$) increases, I_c increases, as expected from the usual charging model for the capacitive current [34]. When comparing experiments performed at different deposition potentials E_1 corresponding to $Y_{sb} = 0.01$ and 0.0025 (e.g. diamond and square markers for the case without added EDTA and triangles and circles in the solution with added EDTA) we see no relevant impact on the current. The capacitive current term depends, then, on the difference of $E_2 - E_1$, rather than on the particular values of E_1 and E_2. So, we conclude that the term $(I_{c,Y=500} - I_{c,Y=0.01})$ will be minimised when $E_2 - E_1$ is kept fixed for both the main measurement (e.g. at $Y = 500$) and the shifted blank measurement (e.g. at $Y_{sb} = 0.01$).

The suitability of this strategy is shown in Fig. 3 where currents are obtained with a fixed $E_2 - E_1 = 0.1982$ V (this value was chosen given the relatively flat region in Fig. 2). The "shifted blank" currents obtained for $Y_{sb} = 0.01$, $Y_{sb} = 5 \times 10^{-3}$ and 2.5×10^{-3} are essentially constant, regardless the presence or absence of EDTA. The main measurements at $Y = 50$ and 100 are much higher when there is no EDTA (we are measuring the current of the existing traces of Zn), but they fall down to practically the same values of the shifted blanks (around 1 nA) when the added EDTA dramatically reduces the free metal concentrations. So, we observe that the shifted blank yields the current of the main measurement when there is no Faradaic (of the analyte) component in it.

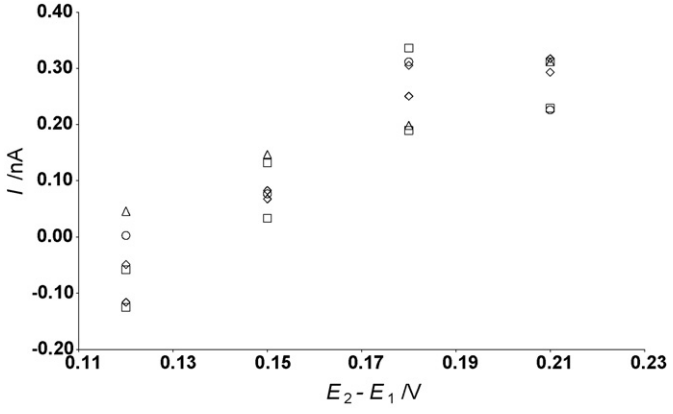

Fig. 2. Currents measured at $t_2 = 0.2$ s for different potential differences $(E_2 - E_1)$ between the first potential step and the second potential step of the implementation of AGNES with only one potential step in the deposition stage (see Fig. 1). Diamonds: $Y = 0.01$; squares: $Y = 0.0025$; triangles: $Y = 0.01$ with added EDTA; circles: $Y = 0.0025$ with added EDTA. The presence or absence of the ligand is not relevant in the measured shifted blank, while the value of $E_2 - E_1$ is a crucial parameter in the shifted blank current.

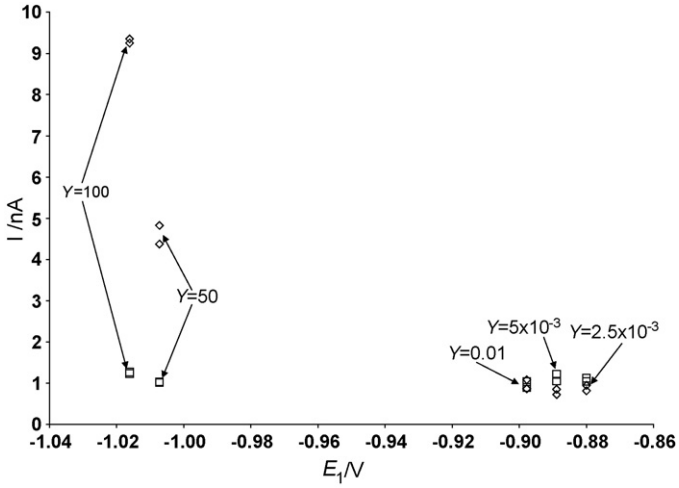

Fig. 3. Current measured at $t_2 = 0.2$ s for different deposition potentials while keeping a fixed $E_2 - E_1 = 0.1982$ V. Diamonds: KNO_3 0.1 M (without any EDTA); squares: same solution after adding EDTA 2×10^{-5} M.

(ii) I_{O_2} could depend on E_1 and E_2 and on the achievement of some steady state regime. We can assume that the concentration profile of O_2 is essentially the steady-state profile for diffusion limited conditions in spherical semi-infinite diffusion after some 20 s from the stopping of the stirring (in the waiting period while we apply E_1) have elapsed. It is also reasonable to assume that this concentration profile is not essentially altered by switching the potential to E_2, because O_2 is totally reduced on the electrode surface at both potentials. So, the measured current will depend on the reduction process at E_2. The well-known O_2 reduction wave exhibits a plateau between −0.8 and −0.2 V. So, the term $I_{O_2,Y=500} - I_{O_2,Y=0.01}$ will be negligible as long as the E_2-values, for both the main measurement and the corresponding shifted blank, fall within this plateau.

(iii) I_{fna} can be minimised if $E_{2,sb}$ is still negative enough for the non-analytes (Cd and Pb, mostly) as to not be stripped back to the solution. This stripping back will be satisfactorily avoided if the time t_1 is insufficient for them to be preconcentrated up to the resulting $Y_{2,sb}$ (for these non-analytes) corresponding to $E_{2,sb}$. As an illustration of these issues, Fig. 4 shows an anodic striping voltamogram of a sample containing Zn and also some traces of Cd and Pb (non-analytes) together with the potentials applied both in the AGNES experiment and the shifted blank (depicted as vertical lines). The relative position of each AGNES potential with respect to a given peak provides a first indication whether the corresponding species is entering or leaving the mercury drop. Regarding this issue (iii), notice how $E_{2,sb}$ is still quite more positive than the peak potential of Cd.

Obviously, a very low concentration of Cd or Pb (as existing in seawater) also renders this condition less important. We checked (data not shown) that the currents of shifted blanks in a solution of KNO_3 0.1 M did not change when varying t_1, this indicating that traces of Cd were not discharged under our conditions and parameters.

Taking into account the previous points, the parameters selected for the shifted blank were a potential program of just one potential step, $E_{1,sb}$ corresponding to $Y_{sb} = 0.01$, such as −0.9070 V, for the deposition stage ($t_1 - t_w = 350$ s; $t_w = 50$ s) and a stripping potential $E_{2,sb}$ so that the potential jump was the same as in the main measurement, i.e. $(E_2 - E_1) = 0.3165$ V leading to $E_{2,sb}$ such as −0.5905 V.

4.2. Optimising the deposition time

A key issue in the implementation of AGNES is the use of a suitable deposition time (and potential program) for the fulfillment of conditions (i) and (ii) stated in Section 2.1.1 by the end of the first stage. This deposition time has to be long enough so that all dynamic processes (diffusion, electron transfer kinetics, complexation kinetics, adsorption kinetics, etc.) have reached the equilibrium state. Previous work [33] showed that the application of two potential steps ($E_{1,a}$ during a time $t_{1,a}$ and $E_{1,b}$ during a time $t_{1,b} + t_w$ as shown in Fig. 5) along the first stage could reduce the overall deposition time (t_1) needed with respect to that of the simplest implementation depicted in Fig. 1. The first potential ($E_{1,a}$) corresponds to diffusion limited conditions and the second one ($E_{1,b}$) corresponds to the desired Y of the experiment.

Preliminary tests in seawater indicated that the AGNES Zn-reoxidation current obtained with $Y = 500$ was sufficiently different from the shifted blank current; so this Y was taken as the target preconcentration factor.

The "recipe" developed in previous work [33] prescribed a ratio of times given by $t_{1,b} = 3 \times t_{1,a}$. Taking into account that the goal of this work is the measurement of one concentration (and not very different from one sampling site to the other) in each solution (i.e. there is no change of ligand concentrations), we decided to optimize the required times of the potential program for the particular conditions of our Mediterranean seawater. The key idea is to apply the first potential step $E_{1,a}$ (in diffusion limited conditions) for a convenient time $t_{1,a}$ so that the desired

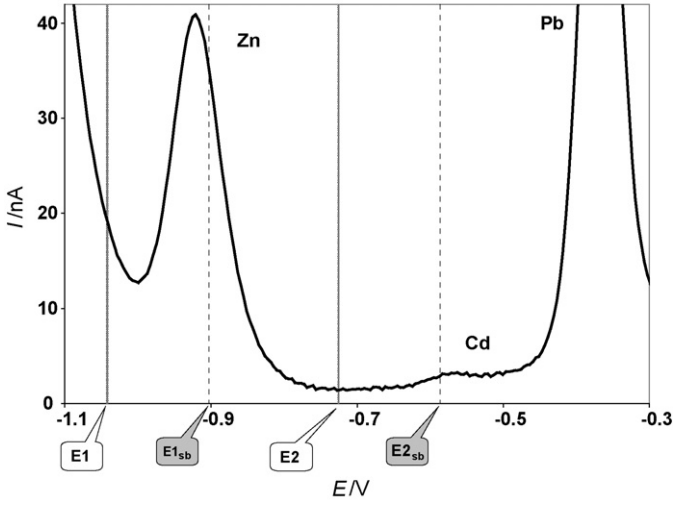

Fig. 4. Anodic stripping voltammogram corresponding to a sample containing Zn, but also traces of Cd and Pb (non-analytes). The difference between potentials in the measurement (E_1 and E_2) must be the same as in the shifted blank ($E_{1,sb}$ and $E_{2,sb}$) and $E_{2,sb}$ should not produce the reoxidation of other non-analytes (Cd and Pb in this work).

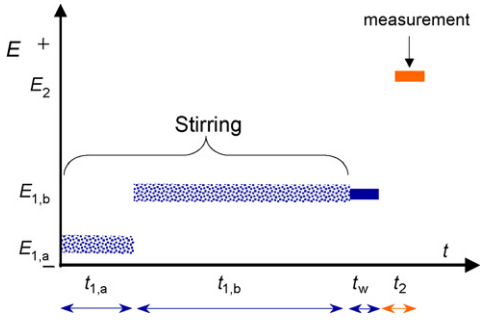

Fig. 5. Potential program for AGNES with two potential steps. The total time of the first stage (t_1) comprises a short period under diffusion limited conditions ($t_{1,a}$), a "fine tunning" pre-concentration period ($t_{1,b}$) with the desired gain Y and a "waiting" period (t_w) without stirring. The aim of this program is to allow for shorter deposition times.

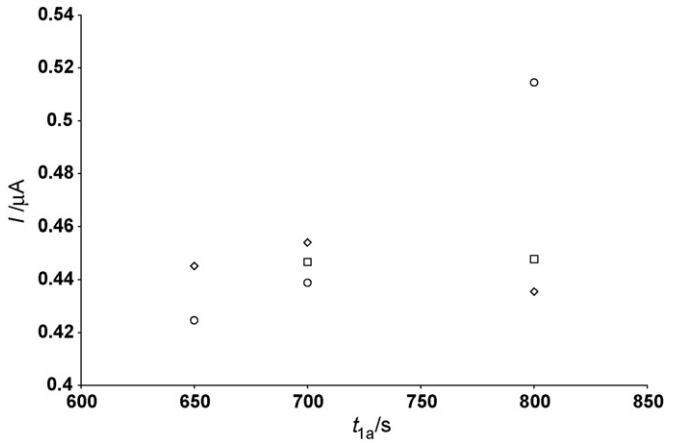

Fig. 6. Currents measured at $t_2 = 0.25$ s for different combinations of $t_{1,a}$ and $t_{1,b}$ in a solution with $[Zn^{2+}] = 3.71 \times 10^{-7}$ M in KNO_3 0.5 M. Markers: open circle $t_{1,b} = 50$ s; open square $t_{1,b} = t_{1,a}$; open diamond $t_{1,b} = 3 \times t_{1,a}$.

number of moles of Zn have practically entered the mercury drop. Thus, a time $t_{1,b}$ (say $t_{1,b} = t_{1,a}$) much lesser than $3 \times t_{1,a}$ can be used for the fine-tuning and stabilization of $[Zn^0]$ to the desired value $Y \times [Zn^{2+}]$.

Fig. 6 shows the last phase of the search for a convenient $t_{1,a}$. When we conducted the experiment with $t_{1,b} = t_{1,a} = 800$ s (see open square) we obtained (within the experimental accuracy) the same current as when applying the "recipe" $t_{1,a} = 800$ s; $t_{1,b} = 2400$ s (see open diamond). In order to decide whether to increase or to reduce $t_{1,a}$, we analysed whether at $t_{1,a} = 800$ s the actual concentration of Zn^0 built up inside the drop was higher or lower than the desired value $Y \times [Zn^{2+}]$. We call "overshoot" [33] to the existence (inside the drop) at $t = t_{1,a}$ of an amount of Zn^0 larger than desired, i.e. $[Zn^0]_{actual} > Y \times [Zn^{2+}]$; this leads to a decaying current for $t_{1,a} < t < t_1$ because the excess of accumulated Zn^0 has to be re-oxidized to reach the prescribed Nernstian equilibrium by $t = t_1$. For samples with high metal concentrations, this overshoot can be easily seen in the evolution of the current along the first stage [33]. We can call "undershoot" the opposite situation where, at $t = t_{1,a}$, we have $[Zn^0]_{actual} < Y \times [Zn^{2+}]$, so that Zn continues to enter the mercury drop for $t > t_{1,a}$. Due to the low Zn concentration in the samples here analysed, the currents in case of "overshoot" or "undershoot" are difficult to be distinguished in the evolution of the currents. So, we decided to probe the "overshoot" or "undershoot" situation by measuring the currents at the second stage (i.e. at $t_2 = 0.25$ s within the second stage) with a very short $t_{1,b} = 50$ s (this usually leaves not enough time for the reaching of conditions (i) and (ii) of Section 2.1.1 by the end of the first stage). As seen on the right of Fig. 6 (open circle), the use of $t_{1,a} = 800$ s with $t_{1,b} = 50$ s produces a current higher than with a $t_{1,b}$ (say 800 or 2400 s) allowing AGNES conditions to be attained: we conclude that with the combination $t_{1,a} = t_{1,b} = 800$ s there has been overshoot, so we can look for a $t_{1,a}$ shorter than 800 s. On the left of Fig. 6, we see that using $t_{1,a} = 650$ s with $t_{1,b} = 50$ s produces a current less than the one obtained with $t_{1,b} = 2400$ s, this indicating that there is undershoot when using $t_{1,a} = 650$ s and that we could try a better $t_{1,a}$ in between 650 and 800 s. We finally found that $t_{1,a} = t_{1,b} = 700$ s was a safe combination exhibiting neither overshoot nor undershoot and fully agreeing with the results from the recipe $t_{1,b} = 3 \times t_{1,a}$.

So, the potential program for the main measurements (i.e. not blanks) applied in this work is:

- $E_{1,a}$ under reduction diffusion limited conditions (with stirring) corresponding to $Y = 10^{10}$ for $t_{1,a} = 700$ s.
- $E_{1,b}$ corresponding to $Y = 500$ for $t_{1,b} = 700$ s (with stirring) and waiting time $t_w = 50$ s (without stirring).
- E_2 corresponding to re-oxidation diffusion limited conditions corresponding to $Y = 10^{-8}$ for 50 s, with the response current being read at $t_2 = 0.25$ s.

4.3. Validation of the determination of free Zn^{2+} in a synthetic solution

Prior to the application of AGNES to real samples, a validation procedure was designed based on the determination of a known low concentration of free Zn (due to known NTA and Zn total concentrations with known pH) in a medium of higher ionic strength than those used with AGNES up to now [33].

The value of h for the medium KNO_3 0.5 M was obtained from AGNES values using a concentration range of Zn between 0.1 and 1 μM. One calibration plot is shown in Fig. 7: in this particular instance an $h = 1.04$ A M^{-1} was found from the linear regression of I versus $[Zn^{2+}]$ data.

The total concentrations of the prepared mixture were 10^{-5} M in NTA and 1.2×10^{-7} M in Zn. The pH of the solution was varied around the interval 5.2–6.1. The difference between the pH values of the validation procedure and that of the seawater sample was considered immaterial, given experimental evidence of h being the same for a large set of pH values. According to the speciation codes VMINTEQ [35] and MEDUSA [36], in this range of pH, with the combination of total concentrations of Zn and NTA here considered, the concentration of free Zn moves around 2–20 nM. The logarithm of the concentrations of

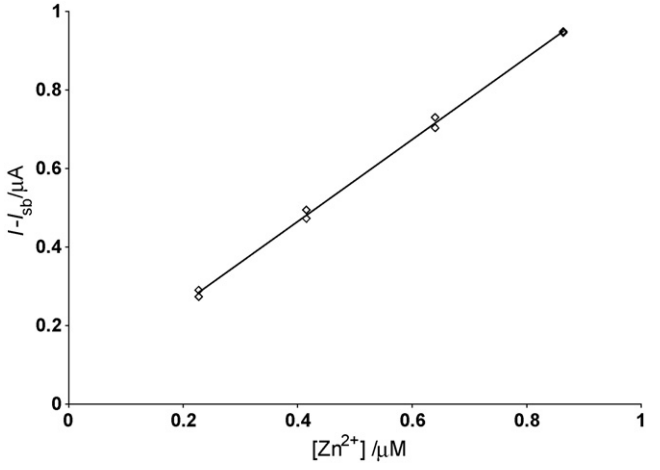

Fig. 7. Calibration plot for Zn^{2+} in KNO_3 0.5 M. Parameters: $t_{1,a} = t_{1,b} = 700$ s; $Y_{1,a} = 10^{10}$; $Y_{1,b} = 500$; $Y_2 = 10^{-8}$. From the slope we derive $h = 1.04$ A M^{-1} to be used in a speciation test on Zn + NTA (see Fig. 8).

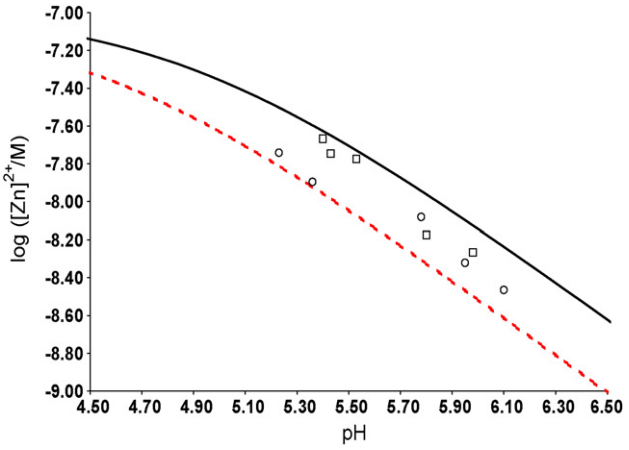

Fig. 8. Theoretical and experimental free Zn concentrations in a synthetic solution of Zn + NTA at different pH-values. Continuous line: MEDUSA calculations; dashed line: MINTEQ calculations; circle and square markers are experimental results obtained with AGNES in two different experiments carried out different days.

free Zn obtained with AGNES (in two different days) at each pH is shown in Fig. 8 with markers. The slight disagreement (around 0.2 log units) between the replicates of different days can be mainly ascribed to small differences in the prepared sample and uncertainties in pH measurements. The continuous line represents the computed values obtained considering the complexation equilibria Zn/NTA and the hydrolysis of Zn at the ionic strength used with the code MEDUSA. The dashed line corresponds to the theoretical values predicted by MINTEQ for the same mixture at the same pH-range. Differences between MEDUSA and MINTEQ can be traced to be mainly due to differences in: (i) the computation of the activity coefficients (MINTEQ uses Davies' equation while MEDUSA uses equations by Helgeson, Kirkham and Flowers [37]) and (ii) the value of the stability constant for the complex ZnNTA (MINTEQ takes $\log K_{ZnNTA} = 12.01$ while MEDUSA takes 11.84). Considering the difficulties in theoretically ascertaining the free metal concentration [38], the experimental results can be accepted as satisfactory.

4.4. Determination of free Zn^{2+} in seawater samples

From the experience gained in the previous results, the parameters used for AGNES aiming at probing the seawater samples were: (i) for measurement $t_{1,a} = t_{1,b} = 700$ s; $Y = 500$; $t_2 = 0.25$ s; $Y_2 = 10^{-8}$, (ii) for the shifted blank $t_{1,sb} = 400$ s; $Y_{sb} = 0.01$; $t_2 = 0.25$ s; $Y_{2,sb} = 2 \times 10^{-13}$. For each speciation determination the required h-value was determined in a calibration, conducted within a few days proximity, in a medium with a similar ionic strength to that corresponding to the seawater. For this purpose, a concentration of background electrolyte KNO_3 0.7 M was used.

An estimation of the limit of detection (LOD) and the limit of quantification (LOQ) of this implementation of AGNES (basically defined by $Y = 500$ and the shifted blank) was obtained carrying out 10 repetitions of shifted blanks in a solution of KNO_3 0.7 M without any added Zn (notice that, from the 0.005 ppm maximum impurities given by the manufacturer, one estimates up to 5 nM in Zn for this solution which could have been taken for the "classical blank"). The same kind of experiment was performed also in seawater, in order to compare the results. Table 1 gathers the average value of the current, the standard deviation (S.D.) and the values of LOD and LOQ (computed, respectively, from the ratios 3 × S.D./slope of the calibration curve and 10 × S.D./slope of the calibration curve) [39]. These results show the high sensitivity and the good precision of the AGNES measurement even in a natural complex matrix as seawater, provided a low blank, such as the shifted one developed here, can be accepted. It is also important to highlight that the capability to determine free Zn concentration at so low concentration, renders AGNES a very promising technique for speciation analysis, especially if one takes into account that better limits would be obtained with larger Y-values.

Table 1
Limit of detection (LOD) and limit of quantification (LOQ) for AGNES procedure with $Y = 500$ in KNO_3 0.7 mol L^{-1} and in a seawater sample (Castelldefels sample)

	I_{sb} (average/nA)	I_{sb} (S.D./nA)	LOD (nM)	LOQ (nM)
KNO_3 0.7 M	2.0	0.1	0.20	0.65
Seawater	1.61	0.09	0.18	0.59

Results of the application of AGNES to the sample from Castelldefels are gathered in Table 2. Measurement currents around 5.6 nA and blank currents around 0.8 nA lead to difference currents around 4.8 nA. Applying Eq. (3), with $h = 1.53$ A M^{-1} from its corresponding calibration at $I = 0.7$ M, one finally reaches the average of this determination of $[Zn^{2+}]$ as 3.1(4) nM.

In order to check whether an intermetallic [21,22,40,41] amalgam complex between Cu^0 and Zn^0 could affect the response from AGNES current at $t_2 = 0.25$ s, we performed an experiment with Castelldefels seawater as usual and obtained a current $I = 4.89$ nA. After the additions of Cu up to a total concentration of 5 nM, the new currents in the two replicates were 4.94 nA and 5.30 nA. If there was an interference due to the formation of an intermetallic complex, there would be a substantial decrease of the current of Zn^0-reoxidation, which did not appear in our experiment. So, we concluded that for the level of Cu and Zn concentrations present in our seawater, the

Table 2
Results obtained applying AGNES to the seawater sample collected in Castelldefels

Experiment (n replicates)	I (nA)	$I - I_{sb}$ (nA)	$[Zn^{2+}]$ (nM)	pH
1 (3)	6.0 (6)	5.2 (5)	3.4 (3)	8.7
2 (5)	5.2 (3)	4.4 (4)	2.8 (2)	8.9

Free Zn^{2+} concentrations, $[Zn^{2+}]$, calculated with Eq. (3) with an h value of 1.53 A M^{-1} obtained in a calibration experiment with $KNO_3 = 0.7$ M. Number between brackets indicates the standard deviation and refers to the last significant digit. Parameters used: (i) for measurement $t_{1,a} = t_{1,b} = 700$ s; $Y = 500$; $t_2 = 0.25$ s; $Y_2 = 10^{-8}$, (ii) for the shifted blank $t_{1,sb} = 400$ s; $Y_{sb} = 0.01$; $t_2 = 0.25$ s; $Y_{2,sb} = 2 \times 10^{-13}$.

Table 3
Results obtained applying AGNES to the sea water sample collected in Tarragona (La Rabassada)

Experiment (*n* replicates)	I (nA)	$I - I_{sb}$ (nA)	$[Zn^{2+}]$ (nM)	pH
1 (6)	2.3 (2)	2.0 (2)	1.4 (2)	8.9
2 (5)	2.0 (2)	1.64 (8)	1.17 (5)	8.9
3 (6)	2.8 (3)	1.44 (9)	1.0 (7)	8.9

Free Zn^{2+} concentrations, $[Zn^{2+}]$, calculated with Eq. (3) with an h value of 1.40 A M^{-1} obtained in a calibration experiment with KNO_3 = 0.7 M. Parameters used: (i) for measurement $t_{1,a} = t_{1,b}$ = 700 s; Y = 500; t_2 = 0.25 s; $Y_2 = 10^{-8}$, (ii) for the shifted blank t_1 = 400 s; Y_{sb} = 0.01; t_2 = 0.25 s; $Y_{2,sb} = 2 \times 10^{-13}$.

used preconcentration factor and deposition time, there is not evidence of the formation of intermetallic Cu–Zn. Results for the sample from La Rabassada are gathered in Table 3. One can see a very similar structure to the results of Castelldefels. Measurement currents span from 2.0 to 2.8 nA yielding concentrations from 1.0 to 1.4 nM via the corresponding h-value of 1.40 A M^{-1}. The resulting average is 1.2 nM with a standard deviation 0.2 nM.

Total Zn concentrations were determined by Anodic Stripping Voltammetry and Square Wave Stripping Voltammetry in samples acidified to pH 1.5. The average value for Castelldefels sample was 10.6(6) nM. This means that the free fraction in Castelldefels is about 29% of the total. The average value for La Rabassada sample was 9(1) nM. So, the free fraction in La Rabassada seawater was around 21% of the total Zn.

The high values of total concentrations are consistent with the general trend of higher concentration in coastal waters than in open ocean ones [16,18,42,43]. Regarding the fraction of free Zn over total, our results differ from several authors who have found that Zn in seawater is more than 95% complexed by organic matter [18,24,25,27,44]. However, there exist some other reports finding -as we have done- a much lower organic fraction. For instance, Lewis et al. [27] found ca 28% of total Zn was free or weakly bound according to their pseudopolarographic method; [28] found 30% of total Zn as organically bound in seawater; [26] reported 26% of organically bound in South Atlantic surface waters. Caution must, thus, be exercised because of the particularity of the speciation of any sample from a given location, depth, season, etc. [18,43,45], which hinders a proper comparison between different experimental techniques with just literature data. In any case, one should keep in mind that different experimental techniques are – in fact – measuring different fractions of any metal in a given complex matrix [15].

5. Summary and perspective

AGNES is a recent electroanalytical technique designed to quantify the free metal activity (or concentration) [32]. The first stage consists in the preconcentration of the reduced metal inside the amalgam up to a level prescribed by the preconcentration factor (Y) which is controlled by the applied potential via Nernst Eq. (1). The second stage consists in the measurement of the preconcentrated metal via stripping. In the current implementation there is a proportionality factor (h) between the Faradaic intensity current (I) and the concentration of the free metal ion in the solution (3).

The development of the shifted blank strategy, introduced for the first time in this work, allows a crucial lowering of the limit of detection of AGNES with respect to the "synthetic" blanks, where it was hard to obtain a synthetic reproduction of a complex matrix (such as seawater) free from trace amounts of the analyte. In essence, the shifted blank consists in the application of an analogous potential program to that of the main measurement, but with the potential values shifted towards a region where the analyte is not appreciably preconcentrated along the first stage. Thus, the shifted blank fundamentally evaluates the capacitive current for the same potential jump between the two stages of AGNES in the same sample where the measurement is intended.

The two-pulse strategy (i.e. the application of two potential steps along the first stage, see Fig. 5), described in a previous work [33], has been specifically optimised for our particular setup with Zn^{2+} and Y = 500, so that an important reduction of the deposition time has been achieved ($t_{1,a} = t_{1,b}$).

The developed methodology has been applied to the system NTA + Zn (with changing pH, see Fig. 8) in a validation phase. The results obtained by AGNES are in good agreement with theoretical predicted concentrations by two independent speciation codes.

Two Mediterranean seawater samples have been analysed with the described strategies. The sample from Castelldefels yielded a free Zn(II) concentration of 3.1 nM (see Table 2) from a determined total of 10.6 nM, while the sample from La Rabassada (Tarragona) yielded $[Zn^{2+}]$ = 1.2 nM (see Table 3) from a total of 9.2 nM. The results of this first implementation of AGNES to measure seawater indicate that Zn in Mediterranean coastal waters is much more available than in reported estimations corresponding to open oceans [24,25], but similar to a few other measurements [26–28,46].

AGNES has been shown to determine free Zn in these seawater samples. We have begun by tackling Zn due to the lack of a standard procedure to measure its free concentration and its intrinsic interest, but AGNES can also be a useful tool in the determination of free metal concentrations in seawater for a series of elements (such as Cu, Cd or Pb). Further work, with Zn and other metals, should address other aquatic systems of environmental interest where an even lower limit of detection is required.

Acknowledgements

The authors gratefully acknowledge support of this research by the Spanish Ministry of Education and Science (DGICYT: Projects BQU2003-9698 and BQU2003-07587) and from the "Comissionat d'Universitats i Recerca de la Generalitat de Catalunya".

References

[1] M.A. Anderson, F.M.M. Morel, R.R.L. Guillard, Nature 276 (1978) 70.
[2] W.G. Sunda, S.A. Huntsman, Limnol. Oceanogr. 37 (1992) 25.

[3] J. Buffle, G. Horvai, In Situ Monitoring of Aquatic Systems. Chemical Analysis and Speciation. IUPAC Series on Analytical and Physical Chemistry of Environmental Systems, John Wiley & Sons, Chichester, 2000.
[4] J. Galceran, H.P. van Leeuwen, in: H.P. van Leeuwen, W. Koester (Eds.), Physicochemical Kinetics and Transport at Chemical–Biological Surfaces. IUPAC Series on Analytical and Physical Chemistry of Environmental Systems, John Wiley, Chichester, UK, 2004, p. 147 (Chapter 4).
[5] G.E. Batley, S.C. Apte, J.L. Stauber, Aust. J. Chem. 57 (2004) 903.
[6] A. Tessier, J. Buffle, P.G.C. Campbell, in: J. Buffle, R.R. DeVitre (Eds.), Chemical and Biological Regulation of Aquatic Systems, Lewis Publishers, Boca Raton, FL, 1994, p. 197 (Chapter 6).
[7] P.G.C. Campbell, O. Errecalde, C. Fortin, W.R. Hiriart-Baer, B. Vigneault, Comp. Biochem. Physiol. C 133 (2002) 189.
[8] P.R. Paquin, J.W. Gorsuch, S. Apte, G.E. Batley, K.C. Bowles, P.G.C. Campbell, C.G. Delos, D.M. Di Toro, R.L. Dwyer, F. Galvez, R.W. Gensemer, G.G. Goss, C. Hogstrand, C.R. Janssen, J.C. McGeer, R.B. Naddy, R.C. Playle, R.C. Santore, U. Schneider, W.A. Stubblefield, C.M. Wood, K.B. Wu, Comp. Biochem. Physiol. C 133 (2002) 3.
[9] M.L. Tercier-Waeber, F. Confalonieri, G. Riccardi, A. Sina, S. Noel, J. Buffle, F. Graziottin, Mar. Chem. 97 (2005) 216.
[10] M. Pesavento, R. Biesuz, C. Gnecco, E. Magi, Anal. Chim. Acta 449 (2001) 23.
[11] R. Biesuz, G. Alberti, G. D'Agostino, E. Magi, M. Pesavento, Mar. Chem. 101 (2006) 180.
[12] M. Pesavento, R. Biesuz, F. Dalla Riva, G. Alberti, Polyhedron 21 (2002) 1343.
[13] L. Tomaszewski, J. Buffle, J. Galceran, Anal. Chem. 75 (2003) 893.
[14] L. Sigg, F. Black, J. Buffle, J. Cao, R. Cleven, W. Davison, J. Galceran, P. Gunkel, E. Kalis, D. Kistler, M. Martin, S. Noel, Y. Nur, N. Odzak, J. Puy, W. Van Riemsdijk, E. Temminghoff, M.L. Tercier-Waeber, S. Toepperwien, R.M. Town, E. Unsworth, K.W. Warnken, L.P. Weng, H.B. Xue, H. Zhang, Environ. Sci. Technol. 40 (2006) 1934.
[15] E.R. Unsworth, K.W. Warnken, H. Zhang, W. Davison, F. Black, J. Buffle, J. Cao, R. Cleven, J. Galceran, P. Gunkel, E. Kalis, D. Kistler, H.P. van Leeuwen, M. Martin, S. Noel, Y. Nur, N. Odzak, J. Puy, W. Van Riemsdijk, L. Sigg, E. Temminghoff, M.L. Tercier-Waeber, S. Toepperwien, R.M. Town, L.P. Weng, H.B. Xue, Environ. Sci. Technol. 40 (2006) 1942.
[16] L.E. Brand, W.G. Sunda, R.R.L. Guillard, Limnol. Oceanogr. 28 (1983) 1182.
[17] F.M.M. Morel, J.R. Reinfelder, S.B. Roberts, C.P. Chamberlain, J.G. Lee, D. Yee, Nature 369 (1994) 740.
[18] M.J. Ellwood, C.M.G. van den Berg, Mar. Chem. 68 (2000) 295.
[19] M.J. Ellwood, Mar. Chem. 87 (2004) 37.
[20] D.W. Crawford, M.S. Lipsen, D.A. Purdie, M.C. Lohan, P.J. Statham, F.A. Whitney, J.N. Putland, W.K. Johnson, N. Sutherland, T.D. Peterson, P.J. Harrison, C.S. Wong, Limnol. Oceanogr. 48 (2003) 1583.
[21] A.L.B. Marques, G.O. Chierice, Talanta 38 (1991) 735.
[22] C.M.G. van den Berg, Talanta 31 (1984) 1069.
[23] K.W. Cha, C.I. Park, S.H. Park, Talanta 52 (2000) 983.
[24] K.W. Bruland, Limnol. Oceanogr. 34 (1989) 269.
[25] J.R. Donat, K.W. Bruland, Mar. Chem. 28 (1990) 301.
[26] C.M.G. van den Berg, S. Dharmvanij, Limnol. Oceanogr. 29 (1984) 1025.
[27] B.L. Lewis, G.W. Luther, H. Lane, T.M. Church, Electroanalysis 7 (1995) 166.
[28] K. Hirose, Y. Dokiya, Y. Sugimura, Mar. Chem. 11 (1982) 343.
[29] A.R. Fakhari, M. Shamsipur, K. Ghanbari, Anal. Chim. Acta 460 (2002) 177.
[30] R.B. Thompson, E.R. Jones, Anal. Chem. 65 (1993) 730.
[31] J. Van den Bergh, B. Jakubowski, P. Burba, Talanta 55 (2001) 587.
[32] J. Galceran, E. Companys, J. Puy, J. Cecília, J.L. Garcés, J. Electroanal. Chem. 566 (2004) 95.
[33] E. Companys, J. Cecília, G. Codina, J. Puy, J. Galceran, J. Electroanal. Chem. 576 (2005) 21.
[34] A.J. Bard, L.R. Faulkner, Electrochemical Methods, Fundamentals and Applications, Wiley, New York, 1980.
[35] J.D. Allison, D.S. Brown, K.J. Novo-Gradac, MINTEQA2/PRODEFA2, A Geochemical Assessment Model for Environmental Systems: Version 3.0 User's Manual, Environmental Protection Agency, Office of Research and Development, Washington, DC, US, 1991.
[36] Puigdomenech I. Medusa: Make Equilibrium Diagrams Using Sophisticated Algorithms, Royal Institute of Technology KTH, Stockholm, Sweden, 2001.
[37] E.H. Oelkers, H.C. Helgeson, Geochim. Cosmochim. Acta 54 (1990) 727.
[38] D.R. Turner, in: A. Tessier, D.R. Turner (Eds.), Metal Speciation and Bioavailability in Aquatic Systems, John Wiley & Sons, Chichester, 1995, p. 149, Chapter 4.
[39] L.A. Currie, Pure Appl. Chem. 67 (1995) 1699.
[40] M.S. Shuman, G.P. Woodward, Anal. Chem. 48 (1976) 1979.
[41] E.Y. Neiman, L.G. Petrova, V.I. Ignatov, G.M. Dolgopolova, Anal. Chim. Acta 113 (1980) 277.
[42] F. Elbaz-Poulichet, C. Guieu, N.H. Morley, Mar. Pollut. Bull. 42 (2001) 623.
[43] K. Kremling, P. Streu, Deep Sea. Res. Part I 48 (2001) 2541.
[44] J. Buffle, Complexation Reactions in Aquatic Systems. An Analytical Approach, Ellis Horwood Limited, Chichester, 1988.
[45] E.P. Achterberg, C. Colombo, C.M.G. van den Berg, Continental Shelf Res. 19 (1999) 537.
[46] E. van Veen, S. Comber, M. Gardner, J. Environ. Monit. 4 (2002) 116.

Available online at www.sciencedirect.com
ScienceDirect
Talanta 71 (2007) 1624–1628
Talanta
www.elsevier.com/locate/talanta

Determination of nanomolar concentrations of phosphate in natural waters using flow injection with a long path length liquid waveguide capillary cell and solid-state spectrophotometric detection

Laura J. Gimbert [a,b,*], Philip M. Haygarth [b], Paul J. Worsfold [a]

[a] School of Earth, Ocean and Environmental Sciences, University of Plymouth, Drake Circus, Plymouth, Devon PL4 8AA, UK
[b] Cross Institute Programme for Sustainable Soil Function (SoilCIP), Institute of Grassland and Environmental Research (IGER), North Wyke Research Station, Okehampton, Devon EX20 2SB, UK

Received 19 May 2006; received in revised form 10 July 2006; accepted 24 July 2006
Available online 30 August 2006

Abstract

A flow injection manifold incorporating a 1 m liquid waveguide capillary cell and a miniature fibre-optic spectrometer for the determination of low phosphorus concentrations in natural waters is reported. The limit of detection (blank + 3 S.D.) was 10 nM using the molybdenum blue chemistry with tin(II) chloride reduction. The sensitivity of the flow injection manifold was improved by 100-fold compared with a conventional 1 cm flow cell. The response was measured at 710 nm and background corrected by subtracting the absorbance at 447 nm. Interference from silicate was effectively masked by the addition of 0.1% (m/v) tartaric acid and results were in good agreement ($P = 0.05$) with a segmented flow analyser reference method for freshwater samples containing 1 μM phosphate.

Keywords: Flow injection; Phosphate; Liquid waveguide capillary cell; Solid-state spectrophotometry; Natural waters

1. Introduction

Phosphorus (P) is an essential element for all life including plant growth and photosynthesis in algae [1–3], and excessive phosphorus concentrations can result in eutrophication of natural waters. Phosphorus exists in different forms in natural waters, soil leachates, and agricultural runoff with the most commonly measured fractions being dissolved reactive phosphorus, total dissolved phosphorus and total particulate phosphorus [4–7]. The dissolved fraction, operationally defined as the fraction that passes through a conventional 0.2 or 0.45 μm membrane, contains inorganic and organic compounds such as orthophosphate, inositol phosphates, nucleic acids, phospholipids, phosphoamides, phosphoproteins, sugar phosphates and condensed phosphates [4,5,8,9]. The particulate fraction, operationally defined as the material retained by the membrane, comprises material of biological origin (animal, plant, bacterial), weathering products (primary and secondary minerals), and authigenic minerals formed by direct precipitation of inorganic phosphorus or sorption to other precipitates [8,10–12]. Both the dissolved and particulate fractions will also have phosphorus associated with colloidal material, defined as the 0.001–1 μm fraction [13–15].

There are a number of different methods for the determination of P species [11], with spectrophotometric methods the most widely used for phosphate, often in conjunction with flow injection analysis (FIA). Motomizu and Li recently reviewed trace and ultra trace methods for P determination with FIA [16] and concluded that detection based on chemiluminescence was the most sensitive with a limit of detection of 1 nM [17]. Spectrophotometric methods for the determination of phosphate are usually based on the Murphy and Riley molybdenum blue reaction [11,18–20], but sensitivity is limited by the use of conventional 1 cm path length cells:

$$PO_4^{3-} + 12MoO_4^{2-} + 27H^+ \rightarrow H_3PO_4(MoO_3)_{12} + 12H_2O \quad (1)$$

* Corresponding author at: School of Earth, Ocean and Environmental Sciences, University of Plymouth, Drake Circus, Plymouth, Devon PL4 8AA, UK. Tel.: +44 1752 232402; fax: +44 1752 233009.
E-mail address: lgimbert@plymouth.ac.uk (L.J. Gimbert).

0039-9140/$ – see front matter © 2006 Elsevier B.V. All rights reserved.
doi:10.1016/j.talanta.2006.07.044

$$H_3PO_4(MoO_3)_{12} \xrightarrow{\text{reduction}} \text{phosphomolybdenum blue} \quad (2)$$

An additional challenge with the molybdenum blue chemistry is the interference from related species, particularly silicate (Si). The silicomolybdenum blue complex has a broad absorbance band (λ_{max} 790 nm) that overlaps the 710 nm typically used for phosphomolybdenum blue detection [21]. Silicate interference can be reduced or eliminated using lower temperatures (silicomolybdenum blue complex formation is favoured at higher temperatures, i.e. 40–65 °C) or by reducing the pH [19,22]. Masking agents such as tartaric acid can also be effective provided that they are added before the molybdophosphate or molybdosilicate species have formed [17,23].

Zhang and Chi [24] obtained a limit of detection of 0.5 nM phosphate using a gas-segmented continuous flow analyser and a 2 m liquid waveguide capillary cell (LWCC) with the molybdenum blue method using ascorbic acid as the reductant. This system was applied to seawater [24] and river water samples [25]. The Beer–Lambert law states that absorbance is proportional to the path length of the cell (flow or static) but long path length cells normally suffer from serious attenuation of the light source. However, with a LWCC attenuation is minimised by the light being totally internally reflected [24] using a Teflon AF fluoropolymer which has a refractive index lower than that of water (∼1.33). A capillary of fused silica coated with Teflon AF enables light travelling through the capillary to be totally internally reflected at the AF–silica interface provided that the incident angle, on going from the optically more dense medium (water) to the less dense medium (AF–clad silica tubing) exceeds the critical angle [26]. The refractive index (schlieren) interference using segmented flow analysis with a LWCC has been quantified using samples of different salinities and measuring the absorbance. When the refractive index at the sample/carrier interface does not match, the absorbance measurements require a correction for the refractive index interference [24]. The effect of potential matrix interferences such as silicate in natural waters has not been reported with LWCCs.

There are generic attractions in combining FIA with a LWCC flow cell, including enhanced sensitivity compared with conventional flow cells and a more rapid response and portability compared with segmented flow analysers. However, combining the two has significant challenges including refractive index effects and long-term stability.

The aim of this work was therefore to optimise a flow injection manifold incorporating a 1 m LWCC for the sensitive detection of phosphate in natural waters using the molybdenum blue chemistry. Tin(II) chloride was used as the reductant rather than ascorbic acid due to the faster kinetics [4,18,27]. The effect of silicate interference on the FIA-LWCC manifold was significantly reduced by the addition of tartaric acid and the accuracy determined by comparative analysis of freshwater samples using an air-segmented analyser.

2. Experimental

2.1. Reagents and solutions

All glassware and bottles were cleaned overnight in nutrient free detergent (Neutracon®, Decon Laboratories, UK), rinsed three times with ultra-pure water (Elga Maxima®, 18.2 MΩ), soaked in 10% (v/v) HCl for 24 h, again rinsed three times with ultra-pure water and dried at room temperature.

All solutions and reagents were prepared with ultra-pure water and all reagents were of AnalaR grade (VWR International, Dorset, UK) or equivalent, unless otherwise stated. A 3 mM PO_4-P stock solution was prepared by dissolving 0.4393 g of potassium dihydrogen orthophosphate (oven dried for 1 h at 105 °C) in 1 L of ultra-pure water. Working standards in the range 0.01–1 μM were prepared by dilution of the stock solution.

Two reagents were prepared, ammonium molybdate (10 g ammonium molybdate and 35 mL sulphuric acid in 1 L ultra-pure water), and tin(II) chloride (0.2 g tin(II) chloride, 2 g hydrazinium sulphate and 28 mL sulphuric acid in 1 L ultra-pure water). Tartaric acid solution (1%, w/v) was prepared by dissolving 1 g in 100 mL ultra-pure water and diluting to the appropriate concentration as required. The silicate standards were prepared by dilution of a silicate SpectrosoL® solution (1000 mg L^{-1}) to give working standards in the range 0.5–2.0 mg Si L^{-1}.

2.2. Instrumentation and procedures

The flow injection manifold used in this work is shown in Fig. 1. The starting conditions were based on the method used by Hanrahan et al. [28] and are summarised in Table 1. The manifold was re-optimised after incorporation of a long path length 1 m LWCC. A peristaltic pump (MiniPuls 2, Gilson, Villiers-le-Bel, France) was used to propel the ammonium molybdate and tin(II) chloride reagent streams at flow rates of 0.30 mL min^{-1}. A second peristaltic pump (Mini S840, Ismatec, Surrey, UK)

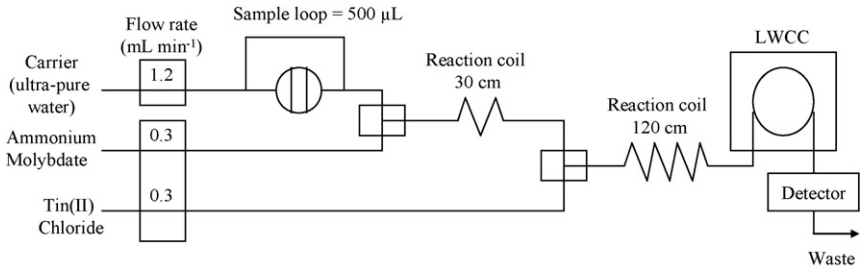

Fig. 1. FIA-LWCC manifold for the determination of PO_4-P with optimised flow rates and reaction coil lengths. One peristaltic pump was used for the carrier and one for the reagents. A third peristaltic pump was used to fill the sample loop.

Table 1
Summary of FIA manifold starting conditions [28] and final conditions for the key physical parameters

Parameter	Starting conditions	Final conditions
Sample volume (μL)	130	500
Flow rate of carrier (mL min^{-1})	0.58	1.2
Flow rate of ammonium molybdate (mL min^{-1})	0.86	0.3
Flow rate of tin(II) chloride (mL min^{-1})	0.58	0.3
Reaction coil A (cm)	30	30
Reaction coil B (cm)	30	30
Reaction coil C (cm)	90	120

was used for the ultra-pure water carrier stream at a flow rate of 1.2 mL min^{-1}, and a third peristaltic pump (Mini S820, Ismatec, Surrey, UK) was used to fill the sample loop. All tubing used in the manifold was 0.8 mm i.d. PTFE tubing (Fisher Scientific, UK) which is standard in FIA.

Sample (500 μL) was injected into the carrier stream using a Rheodyne rotary injection valve. The carrier with sample passed through a reaction coil of 30 cm length before merging with the ammonium molybdate reagent using a T piece, passed through a second reaction coil of 30 cm length before merging with tin(II) chloride reagent at a second T piece and flowing through another reaction coil of 120 cm length before entering the LWCC. The LWCC was of 1 m path length, 550 μm internal diameter and 250 μL internal volume (World Precision Instruments, Sarasota, FL, USA). A miniature fibre-optic spectrometer (S2000-FL, Ocean Optics, Dunedin, FL, USA) and a miniature tungsten halogen lamp (LS-1 Ocean Optics Inc., Orlando, USA) were connected using two fibre-optic cables of 400 μm diameter to the LWCC. The spectrometer was connected via a Serial A/D converter SAD-500 module to a computer through a RS-232 interface. The absorbance at 710 nm was measured and processed by subtracting the absorbance at a non-absorbing wavelength (447 nm) using a FIAlab for Windows 5.0 software program (FIAlab Instruments, WA, USA).

3. Results and discussion

3.1. Optimisation of the FI manifold

The parameters of the FI manifold were optimised to take into account the longer path length of the flow cell (1 m). The sample loop volume was increased from 130 to 500 μL so that the sample zone completely filled the LWCC [29]. A suitably large volume, in this case double the volume of the cell, is important to avoid refractive index interference (schlieren effect) as the sample flows through the LWCC [30]. When the initial conditions shown in Table 1 were used with the LWCC an unstable baseline was observed and hence the flow rates of the carrier and reagent streams and reaction coil lengths were changed to ensure complete mixing of sample and reagent. The carrier flow rate was increased from 0.58 to 1.20 mL min^{-1} to make the manifold compatible with typical mobile phase flow rates for HPLC and hence provide the capability for the manifold to be used for post-column detection. This was then kept constant while the flow rates of the ammonium molybdate and tin(II) chloride reagents were optimised. The optimum flow rate for both reagents was 0.30 mL min^{-1} to give reasonable analysis times without compromising peak shape. This was because higher flow rates (>0.50 mL min^{-1}) resulted in a much noisier baseline (and double peaks) due to pressure fluctuations within the 1 m path length of the LWCC whereas lower reagent flow rates (<0.25 mL min^{-1}) resulted in broad peaks of low peak height. The length of reaction coils A and B were kept at 30 cm whereas reaction coil C was increased to 120 from 90 cm.

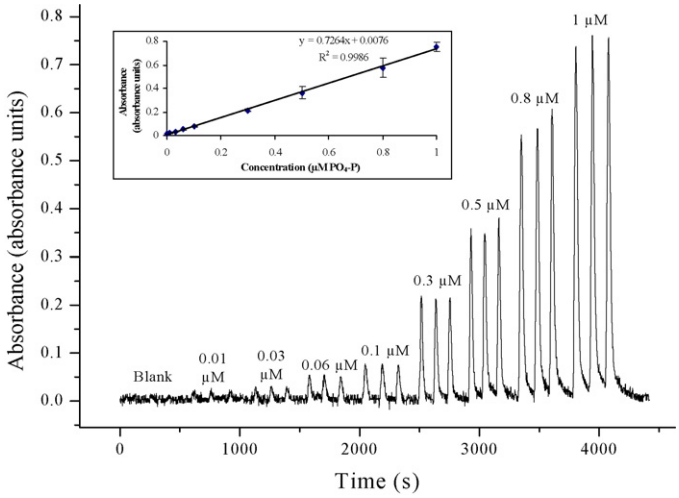

Fig. 2. Typical detector trace and calibration using standards in the range 0.01 to 1 μM PO_4-P obtained using the LWCC of 1 m path length. Error bars ± 3 S.D., $n = 3$.

For long-term storage it is essential that the LWCC is cleaned thoroughly, filled with ultra-pure water and sealed at both ends. During the optimisation process it was observed that the LWCC gave the best day-to-day performance when sequentially flushed at the end of each day with 1 M NaOH (10 mL), 1 M HCl (10 mL) and ultra-pure water (30 mL). Cleaning with organic solvents such as methanol is not recommended as this can result in erratic detector response.

3.2. Analytical figures of merit

A calibration graph was obtained over the concentration range 0.01 to 1 μM PO_4-P ($R^2 = 0.9986$, $n = 3$). The regression equation was $y = 0.7264x + 0.0076$ (y: absorbance (absorbance units) and x: concentration (μM)), and a limit of detection of 10 nM was achieved (calculated from the mean of the blank plus three times the standard deviation of the blank). A typical detector trace and calibration are shown in Fig. 2. The baseline noise was of the order of 0.010–0.015 absorbance units with blanks typically 0.0030–0.0044 absorbance units above the baseline noise. Reproducibility was good with R.S.D.s <7% for three replicate injections. In 1 h, six samples or standards can be analysed in triplicate with baseline resolution giving a total of 18 injections.

For comparison a calibration was also carried out using the same manifold but replacing the LWCC with a conventional 1 cm flow through cell; the regression equation was $y = 0.0125x - 0.004$ (y: absorbance (absorbance units) and x: concentration (μM)) with a limit of detection of 1 μM and a linear range of 2–30 μM ($R^2 = 0.9987$, $n = 3$). The detection limit was lowered from 1 μM to 10 nM (i.e. 100-fold) using the 100 cm LWCC and suggests that a 2 m cell (also commercially available) would give a detection limit of 5 nM. This is still a factor of 10 higher than that reported by Zhang and Chi [24] using a segmented flow analyser but it should be stressed that this is a high throughput FIA manifold that also incorporates a low cost solid-state detector.

3.3. Interferences

Silicate is the major potential interferent when determining phosphorus in freshwaters and agricultural runoff waters and its effect was investigated by injecting a 2 mg L^{-1} Si standard. This concentration was chosen as freshwaters typically contain concentrations of 2 mg L^{-1} Si or lower [17]. The result was a response equivalent to 0.07 μM PO_4-P and therefore silicate seriously interfered at lower phosphate concentrations. To reduce the interference from silicate, two approaches were investigated. Firstly, sulphuric acid was added to the carrier stream at increasing concentrations from 0.2 to 1.0 M to increase the acidity because a lower pH favours the formation of the phosphomolybdenum blue complex over the silicomolybdenum blue complex. A blank (ultra-pure water), 0.1 μM PO_4-P standard and a 2 mg L^{-1} Si standard were injected in triplicate at each increase in sulphuric acid added to the carrier. Results showed that on increasing the concentration of acid up to 0.6 M the peak height for the 0.1 μM PO_4-P and 2 mg L^{-1} Si standards increased as well as the signal for the blank (see Fig. 3A). When the acid concentration was increased from 0.6 to 1.0 M the peak heights for the standards and the blank decreased. Hence, increasing the acidity of the carrier did not reduce the silicate interference.

The second approach used 0.06–1% (m/v) tartaric acid as a masking agent, which was added to both the carrier and the standards to match viscosities and hence avoid any refractive index effects. A 0.1 μM PO_4-P standard and a 2 mg L^{-1} Si standard were injected in triplicate and the peak heights measured. Concentrations above 0.2% (m/v) tartaric acid resulted in a decrease in peak height for both the standards until no response was seen with a tartaric acid concentration of 1.0% (m/v). The optimum result was obtained using 0.1% (m/v) tartaric acid as the peak

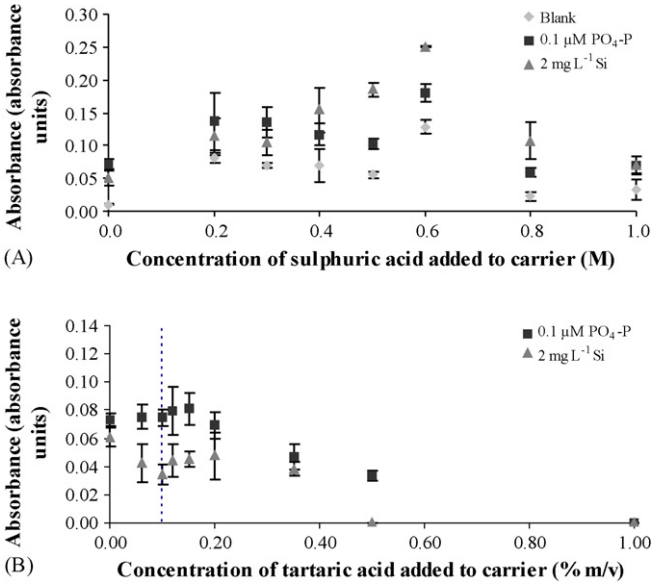

Fig. 3. Silicate interference study: (A) effect of adding increasing concentrations of sulphuric acid (0.2–1 M) to the carrier and (B) effect of adding tartaric acid (0.06–1%, m/v) to the carrier and standards. Error bars ± 3 S.D., $n = 3$. Dashed line shows optimum tartaric acid concentration.

height for the 0.1 μM PO_4-P standard did not decrease compared with the response with no tartaric acid, whereas the response for the 2 mg L^{-1} Si standard was significantly reduced and calculated to be equivalent to only 0.035 μM PO_4-P (see Fig. 3B). Furthermore, silicate standards in the range 0.5–1.5 mg L^{-1} were also analysed and no detector response was observed.

A calibration was carried out using the modified method to reduce silicate interference and a regression equation of $y = 0.6165x + 0.0103$ (y: absorbance (absorbance units) and x: concentration (μM)) was obtained with a linear range of 0.03–1 μM ($R^2 = 0.9987$, $n = 3$) and a limit of detection of 11 nM.

3.4. Application to freshwaters

An intercomparison experiment was carried out between the FIA-LWCC manifold and an automated segmented flow analyser (Skalar SAN^{plus}) as the reference method. Freshwater samples were collected from the River Plym, Plymouth, UK (NGR SX 519 569) and filtered through a cellulose nitrate membrane (0.45 μm pore size, 47 mm dia., Whatman, Maidstone, Kent). Tartaric acid (0.1%, m/v) was added to the samples prior to analysis with the FIA-LWCC manifold whereas no masking agent was added to the samples analysed using the reference method.

Table 2
Determination of phosphate in freshwater samples from the River Plym using the FIA-LWCC method and an automated segmented flow analyser reference method

Freshwater sample	FIA-LWCC method		Segmented flow analyser reference method	
	Mean concentration (μM)	R.S.D. % ($n = 3$)	Mean concentration (μM)	R.S.D. % ($n = 3$)
1	0.901	2.6	0.958	0.9
2	0.894	2.7	0.896	1.2
3	0.867	2.2	0.885	0.7
4	0.928	2.6	0.948	1.4

Results from this intercomparison experiment are shown in Table 2. For each of the four freshwater samples analysed there was good agreement, and a paired t-test showed no significant difference at $P = 0.05$ as the critical value of $|t|$ was 3.18 and the calculated value of $|t|$ was 2.08. Silicate concentrations in these freshwater samples were in the range 1–1.5 mg L^{-1} Si. Therefore, the addition of tartaric acid effectively masks silicate without compromising the phosphorus detection chemistry.

4. Conclusions

A 1 m LWCC with molybdenum blue chemistry has been used for the determination of low phosphate concentrations and a limit of detection of 10 nM was achieved using tin(II) chloride as the reductant. The effect of silicate interference with the phosphorus analysis has been examined and the addition of a masking agent (tartaric acid) minimised the response from any silicate in the sample. An intercomparison experiment showed good agreement between the proposed method and a reference method which suggests that this manifold is suitable for the analysis of freshwater samples with a detection limit of 11 nM phosphate.

Acknowledgements

The authors would like to thank the Natural Environment Research Council (NERC) for research grant NE/C514107/1 and the Institute of Grassland and Environmental Research for a subcontract from Defra project PE0120 in support of this work. IGER is supported by the Biotechnology and Biological Sciences Research Council.

References

[1] T.C. Daniel, A.N. Sharpley, J.L. Lemunyon, J. Environ. Qual. 27 (1998) 251.
[2] P.M. Haygarth, S.C. Jarvis, Adv. Agron. 66 (1999) 195.
[3] R.W. McDowell, A.N. Sharpley, L.M. Condron, P.M. Haygarth, P.C. Brookes, Nutr. Cycl. Agroecosyst. 59 (2001) 269.
[4] K. Robards, I.D. McKelvie, R.L. Benson, P.J. Worsfold, N.J. Blundell, H. Casey, Anal. Chim. Acta 287 (1994) 147.
[5] O. Broberg, G. Persson, Hydrobiologia 170 (1988) 61.
[6] I.D. McKelvie, B.T. Hart, T.J. Caldwell, R.W. Cattrall, Analyst 114 (1989) 1459.
[7] M.D.R. Vaz, A.C. Edwards, C.A. Shand, M. Cresser, Talanta 39 (1992) 1479.
[8] H. Holtan, L. Kamp-Nielsen, A.O. Stuanes, Hydrobiologia 170 (1988) 19.
[9] E.M. Thurman, Organic Geochemistry of Natural Waters, Martinus Nijhoff/Dr. W. Junk Publishers, Dordrecht, The Netherlands, 1985.
[10] W. Maher, L. Woo, Anal. Chim. Acta 375 (1998) 5.
[11] I.D. McKelvie, D.M.W. Peat, P.J. Worsfold, Anal. Proc. Anal. Commun. 32 (1995) 437.
[12] F.H. Denison, P.M. Haygarth, W.A. House, A.W. Bristow, Int. J. Environ. Anal. Chem. 69 (1998) 111.
[13] P.M. Haygarth, A.N. Sharpley, J. Environ. Qual. 29 (2000) 10.
[14] P.M. Haygarth, M.S. Warwick, W.A. House, Water Res. 31 (1997) 439.
[15] M. Hens, R. Merckx, Water Res. 36 (2002) 1483.
[16] S. Motomizu, Z.-H. Li, Talanta 66 (2005) 332.
[17] M. Yaqoob, A. Nabi, P.J. Worsfold, Anal. Chim. Acta 510 (2004) 213.
[18] O. Broberg, K. Pettersson, Hydrobiologia 170 (1988) 45.
[19] C. Ciavatta, L.V. Antisari, P. Sequi, J. Environ. Qual. 19 (1990) 761.
[20] J. Murphy, J.P. Riley, Anal. Chim. Acta 27 (1962) 31.
[21] D.M.W. Peat, I.D. McKelvie, G.P. Matthews, P.M. Haygarth, P.J. Worsfold, Talanta 45 (1997) 47.
[22] J.-Z. Zhang, C.J. Fischer, P.B. Ortner, Talanta 49 (1999) 293.
[23] P.R. Freeman, I.D. McKelvie, B.T. Hart, T.J. Cardwell, Anal. Chim. Acta 234 (1990) 409.
[24] J.-Z. Zhang, J. Chi, Environ. Sci. Technol. 36 (2002) 1048.
[25] L. Guo, J.-Z. Zhang, C. Guéguen, Glob. Biogeochem. Cycle 18 (2004) GB1038.
[26] T. Dallas, P.K. Dasgupta, Trends Anal. Chem. 23 (2004) 385.
[27] T.A.H.M. Janse, P.F.A. Van Der Wiel, G. Kateman, Anal. Chim. Acta 155 (1983) 89.
[28] G. Hanrahan, M. Gledhill, P.J. Fletcher, P.J. Worsfold, Anal. Chim. Acta 440 (2001) 55.
[29] Liquid Waveguide Capillary Cell Instruction Manual, World Precision Instruments, Inc., Sarasota, FL, USA.(2004).
[30] A.C.B. Dias, E.P. Borges, E.A.G. Zagatto, P.J. Worsfold, Talanta 68 (2006) 1076.

Available online at www.sciencedirect.com
ScienceDirect
Talanta 71 (2007) 1774–1781
Talanta
www.elsevier.com/locate/talanta

Electrochemical determination of dopamine and ascorbic acid at a novel gold nanoparticles distributed poly(4-aminothiophenol) modified electrode

Anantha Iyengar Gopalan [a,b,c], Kwang-Pill Lee [a,b,*], Kalayil Manian Manesh [a], Padmanabhan Santhosh [a], Jun Heon Kim [a,b], Jae Soo Kang [a]

[a] *Advanced Analytical Science and Nanomaterials Lab, Department of Chemistry Education, Kyungpook National University, Daegu 702-701, South Korea*
[b] *Nano Practical Application Center, Daegu 704-230, South Korea*
[c] *Department of Industrial Chemistry, Alagappa University, Karaikudi-630 003, India*

Received 11 April 2006; received in revised form 19 August 2006; accepted 19 August 2006
Available online 4 January 2007

Abstract

A modified electrode is fabricated by embedding gold nanoparticles into a layer of electroactive polymer, poly(4-aminothiophenol) (PAT) on the surface of glassy carbon (GC) electrode. Cyclic voltammetry (CV) is performed to deposit PAT and concomitantly deposit Au nanoparticles. Field emission transmission electron microscopic image of the modified electrode, PAT-Au_{nano}-ME, indicates the presence of uniformly distributed Au nanoparticles having the sizes of 8–10 nm. Electrochemical behavior of the PAT-Au_{nano}-ME towards detection of ascorbic acid (AA) and dopamine (DA) is studied using CV. Electrocatalytic determination of DA in the presence of fixed concentration of AA and vice versa, are studied using differential pulse voltammetry (DPV). PAT-Au_{nano}-ME exhibits two well defined anodic peaks at the potential of 75 and 400 mV for the oxidation of AA and DA, respectively with a potential difference of 325 mV. Further, the simultaneous determination of AA and DA is studied by varying the concentration of AA and DA. PAT-Au_{nano}-ME exhibits selectivity and sensitivity for the simultaneous determination of AA and DA without fouling by the oxidation products of AA or DA. PAT and Au nanoparticles provide synergic influence on the accurate electrochemical determination of AA or DA from a mixture having any one of the component (AA or DA) in excess. The practical analytical utilities of the PAT-Au_{nano}-ME are demonstrated by the determination of DA and AA in dopamine hydrochloride injection and human blood serum samples.

Keywords: Gold nanoparticles; Conducting polymer; Cyclic voltammetry; Differential pulse voltammetry; Ascorbic acid; Dopamine; Real samples

1. Introduction

Dopamine, DA, belongs to the family of excitatory chemical neurotransmitter [1]. DA plays an important role in the function of central nervous, renal, hormonal and cardiovascular system. In the extra-cellular fluid of the central nervous system, the basal DA concentration is very low (0.01–1 μM) [2]. A major problem in its electrochemical determination is the coexistence of ascorbic acid (AA) in relatively high concentrations. Usually, the concentration of DA is in the range from 10^{-8} to 10^{-6} M. The concentration of AA in biological systems is as high as 10^{-4} M, while using conventional solid electrodes for the determination of DA, the main and foremost difficulty is the interference of AA, which is oxidized almost at the same potential as DA. As a result, an overlapping voltammetric response for the oxidation of mixture of DA and AA is obtained. Also, a large overpotential and fouling by oxidation products are the additional difficulties in the determination of DA [3,4]. Therefore, it is important to widen the potential range in which oxidation of AA and DA occurs. This warrants the use of modified electrode for this purpose.

Conducting polymers with entrapped metal nanoparticles [5,6] receive interest due to the probable electronic interactions between the nanoparticles and groups in the polymer. The porous structure of conducting polymer allows to disperse the metal particles into the polymer matrix and generates additional electrocatalytic sites. Gold nanoparticles anchored

* Corresponding author. Tel.: +82 539 505 901; fax: +82 539 528 104.
E-mail address: kplee@knu.ac.kr (K.-P. Lee).

0039-9140/$ – see front matter © 2006 Elsevier B.V. All rights reserved.
doi:10.1016/j.talanta.2006.08.026

into certain substrates show catalytic activity for many reactions [7,8]. In particular, Au nanoparticles protected via self-assembly (in two or three dimensional lattices) are showing promise for the construction of nanodevices and nanocircuits [9,10]. Recently, Au nanoparticles entrapped into the matrix like amine terminated self-assembled monolayer, poly(3,4-ethylenedioxythiophene), sulfohydryl-terminated monolayer, carbon fiber electrode [11–14] have been widely used for the voltammetric sensing of DA and (or) AA.

4-Aminothiophenol (AT) has attracted significant attention in making 2D/3D assembly of nanoparticles via covalent or electrostatic interactions [15]. The difference in reactivity between the thiol and amine ends of AT [16] has been effectively utilized to design molecular assemblies leading to unique morphologies and chemical manipulations. In addition, the presence of phenyl group in AT enhances the electrical coupling between the electrode and nanoparticles. Self-assembled monolayer assembly of AT on Au electrode has been used for the selective determination of DA and AA [17].

In the present work, a new kind of modified electrode was fabricated by distributing Au nanoparticles into a conductive polymer matrix, poly(aminothiophenol), PAT over the surface of GC electrode. A simple, one-pot electrochemical approach was used for the fabrication of the modified electrode, PAT-Au_{nano}-ME. PAT-Au_{nano}-ME showed excellent selectivity for the electrochemical determination of AA and DA and the details are presented.

2. Experimental

2.1. Chemicals used

β-Cyclodextrin (CD), AT, $HAuCl_4$, AA, DA and H_2SO_4 were of analytical grade samples and used as received. For real sample analysis, human blood serum samples from single donor were obtained from Innovative Research, Inc, USA. Double-distilled water was used for the preparation of reagent solutions. Aqueous solutions of AA and DA were prepared afresh at the time of experiments in phosphate buffer (pH 7).

2.2. Preparation of inclusion complex

Inclusion complex of CD with AT was prepared by adopting the procedure detailed in the literature [18]. In a typical synthesis, 0.0626 g of AT was dissolved in 10 mL of ethanol and added to an aqueous solution containing 0.5676 g of CD in 40 mL of water. A homogenous solution was obtained after stirring. After distilling off the solvent, under reduced pressure, a white powder, CD/AT-IC was collected. The powder was washed with acetone to remove the excess of AT and dried.

2.3. Fabrication of PAT-Au_{nano} modified electrode

A suspension was prepared by dissolving 50 mg of the inclusion complex (CD/AT-IC) in 10 mL of *N*,*N*′-dimethylformamide. Five microliter of the suspension was dropped on the surface of GC electrode and kept at 60 °C for 12 h in nitrogen atmosphere to evaporate the solvent. The electrode was washed with water and stored. Electrochemical deposition of Au particles into the GC/CD/AT-IC electrode surface was performed in 0.5 M H_2SO_4 solution containing 2.0×10^{-4} M $HAuCl_4$ by applying a repetitive potential scan between 1000 and −100 mV (versus SCE) at a scan rate of 50 mV s^{-1} for 100 cycles. Poly(aminothiophenol), PAT, and Au particles were simultaneously formed on the surface of GC electrode. Thus, the modified electrode (PAT-Au_{nano}-ME) was fabricated. The steps involved in the fabrication of PAT-Au_{nano}-ME are illustrated in Scheme 1.

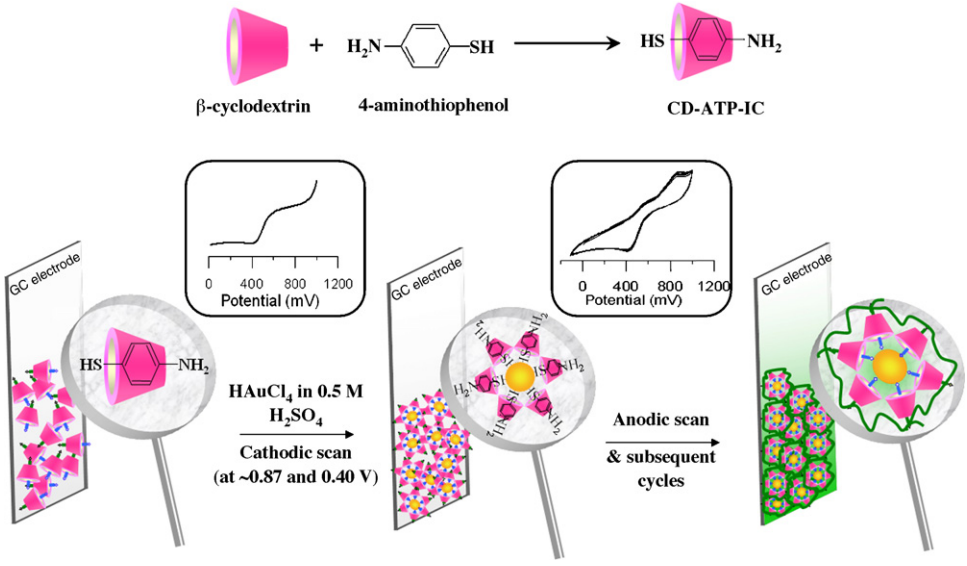

Scheme 1. Fabrication of PAT-Au_{nano}-ME through a cyclic electrochemical process.

2.4. Characterization

The morphology of PAT-Au_{nano}-ME was investigated by means of field emission transmission electron microscope (FETEM) (JEOL, JEM-2000EX) with a field emission electron gun operated at 200 kV. X-ray diffraction pattern of the sample was collected by employing a D8-Advanced Bruker AXS diffractometer using Cu Kα radiation.

2.5. Electrochemical measurements

Electrochemical measurements were performed in a cell consists of PAT-Au_{nano}-ME as working electrode, SCE and platinum wire as reference and auxiliary electrodes, respectively, using EG & G PAR 283 Electrochemical Analyzer. Cyclic voltammetry was used for the fabrication of the modified electrode and for following the electrochemical behavior of the modified electrode towards the detection of AA and DA. Simultaneous determination of AA and DA was performed using differential pulse voltammetry (DPV) at a scan rate of 50 mV s^{-1} with pulse amplitude of 25 mV, pulse rate of 0.5 s and pulse width of 60 ms.

3. Results and discussion

3.1. Fabrication of PAT-Au_{nano}-ME

The modification consists of the formation of electroactive PAT by the oxidation of AT present in the layer of CD/AT-IC on GC surface and deposition of Au nanoparticles by the reduction of $HAuCl_4$ from the electrolyte solution. Importantly, PAT on the modified electrode plays dual role; as a conducting matrix and a stabilizer for Au nanoparticles. The -SH groups present in PAT stabilize the Au nanoparticles and prevent from aggregation. Scheme 1 represents the methodology of fabrication of PAT-Au_{nano}-ME.

Fig. 1 represents the CVs of CD/AT-IC coated GC electrode recorded in a solution containing 2.0×10^{-4} M $HAuCl_4$ (in 0.5 M H_2SO_4) by scanning the potential from 1000 to −100 mV at a scan rate of 50 mV s^{-1}. The mechanism of formation of PAT-Au_{nano} is as follows. At the first cycle, during the cathodic scan of potential, two reduction waves were noticed at ∼870 and ∼400 mV. These two waves correspond to adsorption of $AuCl_4^-$ and reduction of $AuCl_4^-$ to Au particles, respectively. In the subsequent anodic scan, a peak at ∼750 mV was observed which corresponds to the formation of AT radical cation from the oxidation of AT in the self assembled monolayers (Scheme 1) [19,20]. On the subsequent potential scans, two anodic peaks, at ∼670 and ∼900 mV, were observed and that are attributed to the formation of polaronic and bipolaronic forms of PAT. The peak current values for the polaronic and bipolaronic transitions of PAT showed continuous increase with increase in number of potential cycles. These observations inform the simultaneous formation of electroactive PAT and Au nanoparticles on the GC electrode.

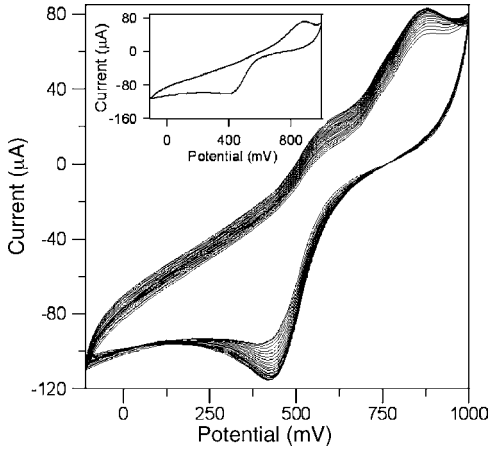

Fig. 1. Cyclic voltammograms of CD/AT-IC coated GC electrode in the 0.5 M H_2SO_4 solution containing 2.0×10^{-4} M $HAuCl_4$; scan rate: 50 mV s^{-1} (inset shows the first cycle).

3.2. Characterization of PAT-Au_{nano}-ME

3.2.1. FETEM analysis

Fig. 2 shows the FETEM image of PAT-Au_{nano}. Spherically shaped Au particles having an average size of about 8–10 nm can be seen. FETEM image also indicates that the Au nanoparticles are uniformly distributed in the entire region of the surface of electrode. Generally, Au nanoparticles tend to aggregate to form bigger metallic particles. The type and structure of catalyst support influence the agglomeration of Au nanoparticles [21–23]. In present study, Au nanoparticles are uniformly distributed since the -SH functional groups present in PAT helps to anchor the Au nanoparticles (Scheme 1). Further, the interactions between -SH groups and Au nanoparticles prevent them from aggregation [24–26].

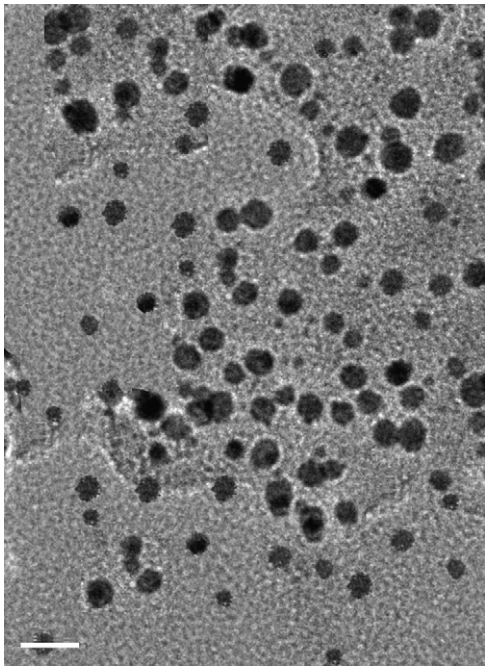

Fig. 2. FETEM image of PAT-Au_{nano}; scale bar: 20 nm.

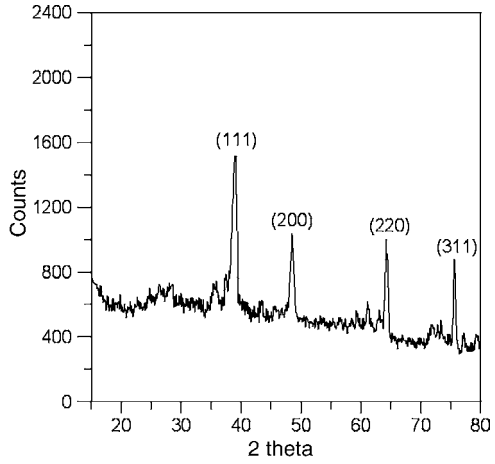

Fig. 3. XRD profile of PAT-Au_{nano}.

3.2.2. XRD analysis

Crystalline structure and size of the Au nanoparticles present in PAT-Au_{nano} were examined by XRD analysis (Fig. 3). Peaks observed around 38.0°, 48.2°, 64.5° and 77.4° are attributed to (1 1 1), (2 0 0), (2 2 0) and (3 1 1) facets of the fcc crystal structure of Au [27]. From the full width measured at the half-maximum of the peak at $2\theta = 38°$, the average crystallite size of the Au particles was evaluated to be ~10 nm using Scherer's equation [28].

3.3. Electrochemical behavior of AA and DA at PAT-Au_{nano}-ME

CVs recorded for the oxidation of AA (1.5×10^{-4} M) at the bare GC electrode (Fig. 4A(i)) and PAT-Au_{nano}-ME (Fig. 4A(ii)) in aqueous phosphate buffer (pH 7) are presented. Oxidation of AA occurs at a lower potential (153 mV) at PAT-Au_{nano}-ME in comparison to oxidation at bare GC electrode (376 mV). The enhanced electrocatalytic activity of PAT-Au_{nano}-ME for AA arises probably due to electrostatic binding between protonated amine/imine groups in PAT and carboxylic groups in AA prior to oxidation. Enhanced anodic current was noticed at PAT-Au_{nano}-ME in comparison to the current values noticed at the bare GC electrode. An increase of nearly 20% current for the oxidation of AA was noticed at PAT-Au_{nano}-ME than at bare GC electrode.

Electrochemical oxidation of DA at the bare GC electrode (Fig. 4B(i)) and PAT-Au_{nano}-ME (Fig. 4B(ii)) was followed in the aqueous phosphate buffer (pH 7) containing 1.0×10^{-4} M DA. Oxidation of DA occurs at a lesser potential (300 mV) with PAT-Au_{nano}-ME in comparison to the bare GC electrode (326 mV). Here again, PAT-Au_{nano}-ME exhibits enhanced electrocatalytic oxidation of DA with a shift of 26 mV. Also, a much higher peak current for the oxidation of DA was noticed at PAT-Au_{nano}-ME than at bare GC electrode (Fig. 4B). It is envisaged that self-assembled Au nanoparticles on the surface of PAT reduces electrode fouling and accelerate the rate of electron transfer for the oxidation of DA [11,13].

Independent studies on oxidation of AA and DA inform that PAT-Au_{nano}-ME electro-catalyzes the oxidation of AA and DA.

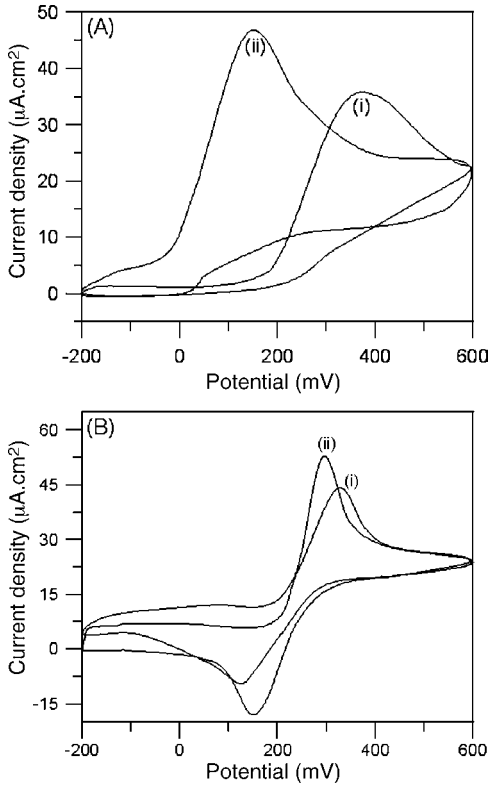

Fig. 4. Cyclic voltammograms of (A) 1.5×10^{-4} M AA and (B) 1.0×10^{-4} M DA at bare GC electrode (i) and PAT-Au_{nano}-ME (ii) in phosphate buffer (pH 7). Scan rate: 50 mV s^{-1}.

Further, it is inferred that oxidation of AA and DA occur at closer potentials (376 mV for AA and 326 mV for DA) on bare GC electrode. However, oxidation of AA and DA occurs at potentials (153 mV for AA and 300 mV for DA) with a difference of 150 mV on PAT-Au_{nano}-ME. Hence, it is inferred that PAT-Au_{nano}-ME can be used for the simultaneous electrochemical determination of AA and DA.

The morphology of the PAT-Au_{nano}-ME after the detection of AA or DA was analyzed by FETEM. There is no apparent change in the morphology of PAT-Au_{nano}-ME after using the electrode for the detection of AA or DA. This indicates that PAT-Au_{nano}-ME is not susceptible for fouling by the oxidation products or by pH or ionic strength of the electrolyte medium.

The focus of the present study is to electrochemically oxidize DA without having concurrent influence from AA. Hence, experiments were performed to understand the electrocatalytic behavior of PAT-Au_{nano}-ME for the mixture of AA and DA. Previous reports inform that there is a shift in the potential for the oxidation of AA and DA in each other's presence [29–32]. Voltammetric pulse techniques have been established to be very sensitive in the detection of micromolar amounts of this analyte [33]. More electrochemical methods such as differential pulse voltammetry can be used for obtaining better resolved voltammetric characteristics for mixture of components. We employed DPV to understand the inter-dependence in the electrochemical signals on the oxidation of AA or DA in the mixture. Further, DPV was used for the simultaneous determination of AA and DA in the mixture.

3.4. Factors influencing the electrochemical response of AA and DA

3.4.1. Influence of solution pH

The effect of pH in the electrolytic solution on the determination of AA and DA in the mixture at the PAT-Au_{nano}-ME was studied in the range of pH 4–8.5 using DPV. The peaks corresponding to the oxidation waves of AA and DA appeared with larger differences in potentials, as the pH was changed from 4 to 6.5. It was found that at a pH of 7.0 the peak separation was maximum. Hence, the phosphate buffer with a pH of 7 was chosen as the supporting electrolyte for the selective determination of AA or DA in the mixture.

3.4.2. Influence of the potential scan rate and potential pulse amplitude

The effect of the scan rate on the current response of DPV at the PAT-Au_{nano}-ME in phosphate buffer (pH 7) was investigated. The ratio of peak current to peak half width ($j_p / W_{1/2}^{-1}$ A cm^{-2} V^{-1}) showed a linear increase with the scan rate between 10 and 50 mV s^{-1}. On the other hand, when the scan rate is higher than 50 mV s^{-1}, the increase of the peak current values was accompanied by broadening and distortion of the peaks. From these results, the scan rate of 50 mV s^{-1} was chosen as it gives the best voltammetric profile with higher sensitivity and subsequently used throughout the present study. The current values of peak were also found to vary with pulse amplitude (10–75 mV) applied on DPV at a scan rate of 50 mV s^{-1} at the PAT-Au_{nano}-ME. The use of a pulse amplitude larger than 25 mV led to an increase in the capacitive current. In this sense, the best voltammetric sensitivity was obtained with 25 mV and therefore, this value was chosen for further studies.

3.5. Electrochemical determination of AA and DA in the mixture at PAT-Au_{nano}-ME

Sensitivity and selectivity of PAT-Au_{nano}-ME for the simultaneous determination of AA and DA were evaluated for a mixture of AA and DA at the PAT-Au_{nano}-ME. Fig. 5 shows the DPVs recorded for a mixture of AA (15 μM) and DA (10 μM) at the bare GC electrode (line (i)) and PAT-Au_{nano}-ME (line (ii)) in phosphate buffer. A poor current response with a broad overlapped peak around 380 mV was observed for the oxidation of AA and DA at the bare GC electrode (Fig. 5(i)). Almost, it was impossible to distinguish the peak potential for the independent oxidation of AA and DA at the bare GC electrode. Hence, bare GC electrode could not effectively discriminate the voltammetric signals from AA and DA.

On the other hand, two well-defined anodic peaks around the potential of 75 and 400 mV were observed for the oxidation of AA and DA, respectively, at the PAT-Au_{nano}-ME (Fig. 5(ii)). It is interesting to note that oxidation of AA occurs at a less positive potential (75 mV) in the mixture in comparison to the oxidation peak noticed at 153 mV for a electrolyte solution contain AA alone. However, the oxidation peak potential of DA in the mixture was shifted to more positive potential (400 mV) in comparison to the oxidation potential (300 mV) noticed for simple DA. Thus, oxidation of AA and DA occur with a difference in potential of 325 mV (400–75 mV) at PAT-Au_{nano}-ME. Presence of PAT and Au nanoparticles in the modified electrode favors preferential electrostatic interactions with negatively-charged ascorbate anions. Thus, AA is expected to preconcentrate at the surface of PAT-Au_{nano}-ME prior to oxidation. Subsequently, oxidation of AA becomes facile and occurs at a less positive potential (75 mV). On the other hand, the existence of protonated amine/imine nitrogen in PAT excludes DA from the electrode site due to electrostatic repulsion between amine sites in PAT and DA. As a result, oxidation of DA occurs at a much more positive potential (400 mV). This causes a large separation of potential (325 mV) for the oxidation of AA and DA. The larger potential difference in the oxidation potentials of AA and DA makes the simultaneous determination of AA and DA as feasible from the mixture.

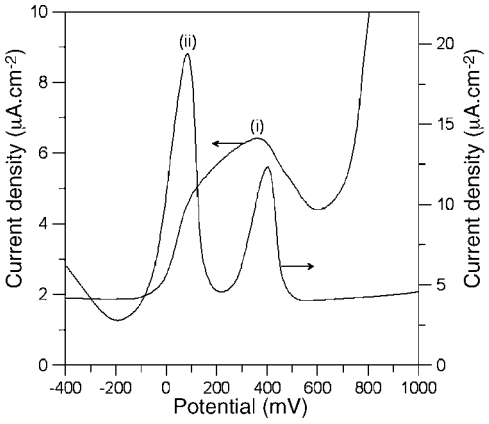

Fig. 5. DPVs of 15 μM AA and 10 μM DA mixture at (i) bare GC electrode and (ii) PAT-Au_{nano}-ME in phosphate buffer (pH 7). Scan rate: 50 mV s^{-1}, Pulse amplitude: 25 mV, pulse rate: 0.5 s, pulse width: 60 ms.

Generally, for a given concentration of DA, a comparatively large oxidation current was noticed in the presence of AA at conventional electrode. This is due to the fact that oxidation product of DA, dopamine-*o*-quinone, catalytically reacts with AA and reduces the dopamine-*o*-quinone back to DA [34–36]. Therefore, determination of concentration of DA could not be done accurately in the presence of AA. However, in the present investigation, oxidation of AA occurs ahead of DA due to the preferential preconcentration of AA at PAT-Au_{nano}-ME. Hence, in addition to the wider potential difference (325 mV) for the oxidation of AA and DA at PAT-Au_{nano}-ME, the interference from oxidation product of DA is minimized. Thus, the combined presence of PAT and Au nanoparticles in PAT-Au_{nano}-ME helps in the simultaneous determination of AA and DA.

3.5.1. Selective determination of DA in the presence of fixed concentration of AA

DPVs recorded for different concentrations of DA (15–45 μM) at PAT-Au_{nano}-ME keeping a constant concentration of AA (12.5 μM) are presented (Fig. 6). There is an increase

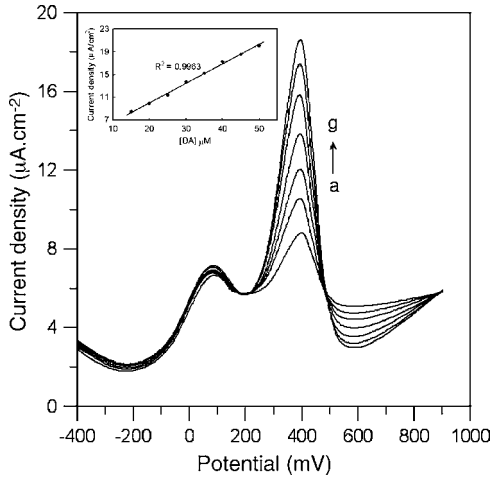

Fig. 6. DPVs of 12.5 μM AA at PAT-Au_{nano}-ME in phosphate buffer (pH 7) in the different concentrations of DA (a–g: 15, 20, 25, 30, 35, 40 and 45 μM). Scan rate: 50 mV s^{-1}, Pulse amplitude: 25 mV, pulse rate: 0.5 s, pulse width: 60 ms. Inset shows the calibration curve.

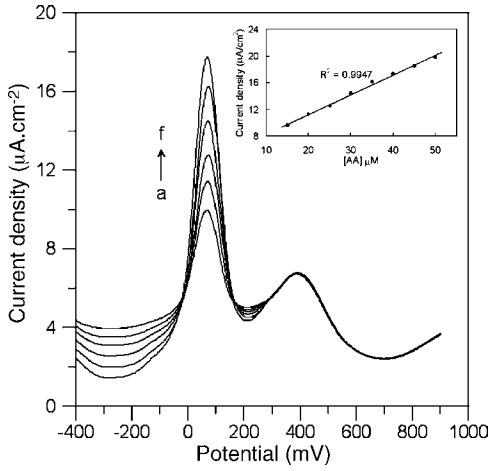

Fig. 7. DPVs of 12.5 μM DA at PAT-Au_{nano}-ME in phosphate buffer (pH 7) in the different concentrations of AA (a–f: 20, 25, 30, 35 40 and 45 μM). Scan rate: 50 mV s^{-1}, pulse amplitude: 25 mV, pulse rate: 0.5 s, pulse width: 60 ms. Inset shows the calibration curve.

in the voltammetric peak current corresponding to the oxidation of DA with the increase of the concentration of DA. The current response with concentration of DA seems to be linear with a correlation coefficient of 0.9963 in the concentration range: 15–50 μM (Fig. 6, inset). Further, DPVs were recorded at PAT-Au_{nano}-ME, while changing the concentration of DA from 0.01 to 1 μM in the presence of 0.1 mM AA (∼1000 times higher concentration than DA). It is observed that the peak current for DA was increased linearly with the increase in DA concentration between 0.01 and 1 μM with the correlation coefficient of 0.9983. It is to be noted that in the presence of AA at millimolar level (0.1 mM), the PAT-Au_{nano}-ME can sense the increase of DA at micromolar concentration (0.01–1 μM) which is close to the physiological condition. Thus, the selective and sensitive detection of DA in the presence of high concentration of AA is achievable at this electrode.

3.5.2. *Selective determination of AA in the presence of a fixed concentration of DA*

Fig. 7 shows the DPVs recorded for increasing concentration of AA (20–45 μM) for a fixed concentration of DA (12.5 μM). The current for the oxidation of AA shows an increasing trend with an increase in the concentration of AA and no significant changes is observed in the oxidation current of DA. Also, the oxidation current of AA shows linearity with the concentration of AA (Fig. 7 (inset)). These results suggest that the PAT-Au_{nano}-ME can effectively be utilized for the determination of AA in the presence of DA.

3.5.3. *Simultaneous determination of AA and DA in the mixture*

DPV experiments were performed (Fig. 8) while changing the concentration of AA and DA simultaneously at the micromolar levels. The peak current values were proportional to the concentration of AA and DA in the mixture. As can be seen from the inset of Fig. 8, the oxidation current of AA increases linearly with its concentration between 10 and 50 μM. For the regression plot of i_p versus AA concentration, the slope is 0.4 μA μM^{-1}, the y-intercept is 2.3 μA, and correlation (r^2) is 0.9967. At the same time, the calibration plot of DA is linear between 10 and 50 μM with slope, intercept and correlation of 0.22 μA μM^{-1}, 5.5 μA and 0.9954, respectively. Further, the oxidation potentials of AA and DA are not influenced much (Fig. 8). Hence, it is confirmed that for the oxidation of AA or DA at PAT-Au_{nano}-ME, the other component does not give any interference to the electrochemical signal. Interestingly, ΔE_a does not change with concentration of AA and DA in the mixture.

3.6. *Interference study*

It is well known that uric acid (UA) coexists with DA in the extracellular fluid of the central nervous system and its concentration is much higher than that of DA. Hence, UA and AA are the two important interfering substances for the electrochemical

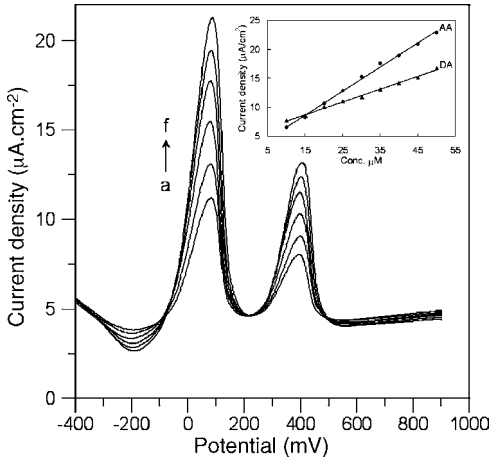

Fig. 8. DPVs of AA and DA mixtures at PAT-Au_{nano}-ME in phosphate buffer (pH 7). AA contents from a–f are 20, 25, 30, 35, 40 and 45 μM, respectively. DA contents from a–f are 10, 15, 20, 25, 30 and 35 μM, respectively. Scan rate: 50 mV s^{-1}, pulse amplitude: 25 mV, pulse rate: 0.5 s, pulse width: 60 ms. Inset shows the calibration curves.

Table 1
Determination of DA in dopamine hydrochloride injection ($n = 5$)

Dopamine					Ascorbic acid			
Content (mg mL^{-1})	Added (mg mL^{-1})	Found (mg mL^{-1})	R.S.D. (%)	Recovery (%)	Added (mg mL^{-1})	Found (mg mL^{-1})	R.S.D. (%)	Recovery (%)
	0	09.98	1.3	–	10	9.91	1.5	99.5
	0.5	10.46	1.8	98	13	12.87	1.2	98.1
10	1.0	10.93	2.5	96.5	15	15.01	0.8	100
	1.5	11.51	2.0	101	18	17.98	2.1	97.6
	2.0	11.94	2.8	97.4	20	19.92	2.3	102
	0	09.99	2.3	–	10	9.95	1.0	97.9
	0.5	10.51	3.0	95	13	12.99	1.5	99.4
10	1.0	11.07	1.8	91	15	14.89	2.5	99.8
	1.5	11.49	1.6	96	18	17.94	1.7	96.7
	2.0	11.98	2.0	93	20	20.08	1.1	98.2

detection of DA. The interference from AA and UA was investigated. Fig. 9 shows the DPV of 25 μM AA + 25 μM DA + 25 μM UA in phosphate buffer (pH 7). Well defined anodic peaks at 10, 210 and 475 mV for the oxidation of AA, DA and UA, respectively were observed at the PAT-Au$_{nano}$-ME. However, the oxidation of AA and UA does not modify or influence the current response of the oxidation of DA. Interference studies were also performed with other compounds. In the case of 25 μM DA, no interference could be observed for glucose (2 0 0), glutamic acid (2 0 0), citric acid (1 0 0), tartaric acid (1 0 0), NaCl (5 0 0) and KCl (5 0 0), where the data in the brackets were the concentration ratios. These results indicate that selective and sensitive determination of DA is possible at PAT-Au$_{nano}$-ME.

3.7. Reproducibility, repetition and stability

We have checked the reproducibility and stability of the PAT-Au$_{nano}$-ME for a period of operation. The performance of PAT-Au$_{nano}$-ME for the detection of DA was tested in phosphate buffer (pH 7) for a longer period. Over the first 2 days, the signal showed a 2% decrease of its initial response, over 10 days, the current response decreased by about 5% and in the following 15 days, the decrease was 10%. PAT-Au$_{nano}$-ME retains 90% of its original activity after 15 days and continued to exhibit excellent response to both AA and DA. Thus, PAT-Au$_{nano}$-ME does not tend to foul by the oxidation products of AA or DA and exhibits high sensitivity for the simultaneous determination of AA and DA. Further, it was found that the anodic peak currents for the oxidation AA and DA in the mixture remain unchanged after successive measurements at PAT-Au$_{nano}$-ME. For instance, peak current values of 20.22, 19.38 and 17.19 μA (for AA) and peak currents values of 12.70, 12.19 and 11.46 μA (for DA) were observed for the 1st, 3rd and 30th measurements, respectively. These results indicated that PAT-Au$_{nano}$-ME electrode is stable and the measurement can be repeated for the selective determination of AA or DA.

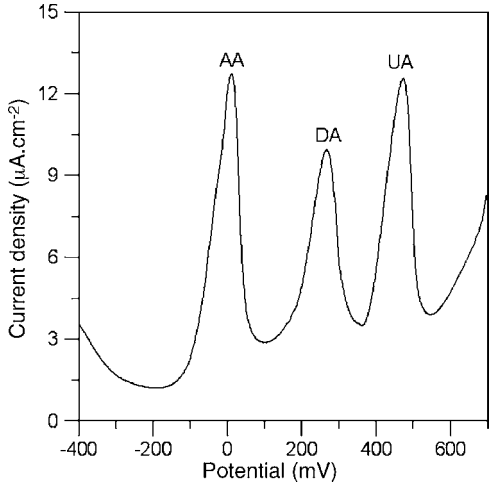

Fig. 9. DPV of 25 μM AA, 25 μM DA and 25 μM UA mixtures at PAT-Au$_{nano}$-ME in phosphate buffer (pH 7). Scan rate: 50 mV s^{-1}, pulse amplitude: 25 mV, pulse rate: 0.5 s, pulse width: 60 ms.

3.8. Real sample analysis

3.8.1. Determination of DA and AA in the mixture

The PAT-Au$_{nano}$-ME was applied to the determination of DA and AA in dopamine hydrochloride injection sample. DOPADIC®—dopamine hydrochloride injection solution (concentration of DA 200 mg mL^{-1}, 5 mL per injection) was diluted to 10 mL with water. 1 mL of this diluted solution or some amount of standard DA or AA (from vitamin C tablet) solutions were injected into each of a series of 5 mL volume flasks and made up to volume with phosphate buffer (pH 7). An aliquot of 2 mL of this solution was placed in an electrochemical cell for the determination of DA and AA using DPV method. The results are listed in Table 1.

3.8.2. Determination of DA in human blood serum

Most of the previously reported modified electrodes were reported on the detection of DA in dopamine hydrochloride injection [37–39]. Few reports are available for the determination of DA in human blood serum [40]. At PAT-Au$_{nano}$-ME, DA was not detected in human blood serum. However, when the DA standard solution was spiked, the presence of AA, UA and some other interfering substances, such as albumin and glucose did not interfere with the determination of DA (Table 2). PAT-

Table 2
Determination of DA in human blood serum ($n = 5$)

Samples	Added ($\mu M L^{-1}$)	Found ($\mu M L^{-1}$)	R.S.D. (%)	Recovery (%)
1	0.3	0.32	2.3	101
2	0.6	0.57	2.4	98
3	0.9	0.89	2.0	96

Au_{nano}-ME responds well for the recovery of spiked DA with high sensitivity and selectivity in comparison to other reported methods. This implies a promising feature for the applicability of the PAT-Au_{nano}-ME for the selective and sensitive determination of DA in the real samples.

4. Conclusions

A newer modified electrode, PAT-Au_{nano}-ME, was fabricated by embedding Au nanoparticles into conducting PAT matrix on the GC electrode and used for the simultaneous determination of AA and DA. PAT-Au_{nano}-ME shows two well-defined anodic peaks for the oxidation of mixture of AA and DA with a larger peak potential difference of 325 mV. The combined presence of PAT and Au nanoparticles provide synergic influence for the simultaneous oxidation of AA and DA with a wider potential difference ($\Delta E_a \approx 325$ mV). Stable electrochemical response for a longer period (>15 days) and minimum interference form the oxidation product of AA or DA were observed at PAT-Au_{nano}-ME. Thus, PAT-Au_{nano}-ME seems to be a promising electrode for the simultaneous determination of AA and DA.

Acknowledgements

This work was supported by Korean Research Foundation Grant (KRF-2006-J02402). The authors acknowledge Korea Basic Science Institute (Daegu) and Kyungpook National University Center for Scientific Instrument.

References

[1] R.M. Wightman, C. Amatore, R.C. Engstrom, P.D. Hale, E.W. Kristensen, W.G. Kubr, L.J. May, Neuroscience 25 (1988) 513.
[2] A.J. Downard, A.D. Roddick, A.M. Bond, Anal. Chim. Acta 317 (1995) 303.
[3] L.A. Pachla, D.L. Reynolds, P.T. Kissinger, J. Assoc. Anal. Chem. Intl. 68 (1985) 1.
[4] V.S. Ijeri, P.V. Jaiswal, A.K. Srivastava, Anal. Chim. Acta 439 (2001) 291.
[5] S. Tian, J. Liu, T. Zhu, W. Knoll, Chem. Mater. 16 (2004) 4103.
[6] L. Zhang, M. Wan, J. Phys. Chem. B 107 (2003) 6748.
[7] P. Santhosh, A. Gopalan, K.P. Lee, J. Catal. 238 (2006) 177.
[8] M. Valden, X. Lai, D.W. Goodman, Science 281 (1998) 1647.
[9] L.O. Brown, J.E. Hutchison, J. Phys. Chem. B 105 (2001) 8911.
[10] R.L. Whetten, J.T. Khoury, M.M. Alvarez, S. Murthy, I. Vezmar, Z.L. Wang, P.W. Stephens, C.L. Cleveland, W.D. Luedtke, U. Landman, Adv. Mater. 8 (1996) 428.
[11] C.R. Raj, T. Okajima, T. Ohsaka, J. Electroanal. Chem. 543 (2003) 127.
[12] S.S. Kumar, J. Mathiyarasu, K.L. Phani, J. Electroanal. Chem. 578 (2005) 95.
[13] L. Zhang, X. Jiang, J. Electroanal. Chem. 583 (2005) 292.
[14] L. Lu, X. Wang, X. Lin, Anal. Sci. 20 (2004) 1131.
[15] A. Gole, S.R. Sainkar, M. Sastry, Chem. Mater. 12 (2000) 1234.
[16] S. Wang, S. Sato, K. Kimura, Chem. Mater. 15 (2003) 2445.
[17] L. Zhang, J. Jia, X. Zou, S. Dong, Electroanalytical 16 (2004) 1413.
[18] A. Harada, J. Li, M. Kamachi, Nature 356 (1992) 325.
[19] M.O. Finot, G.D. Braybrook, M.T. McDermott, J. Electroanal. Chem. 466 (1999) 234.
[20] M. Okamura, T. Kondo, K. Uosaki, J. Phys. Chem. B 109 (2005) 9897.
[21] H.Y. Huang, W.F. Chen, P.L. Kuo, J. Phys. Chem. B 109 (2005) 24288.
[22] M. Haruta, N. Yamada, T. Kobayashi, S. Iijima, J. Catal. 115 (1989) 301.
[23] N.M. Gupta, A.K. Tripathi, J. Catal. 187 (1999) 343.
[24] M. Brust, M. Walker, D. Bethell, D.J. Schiffrin, R. Whyman, J. Chem. Soc. Chem. Commun. (1994) 801.
[25] N.R. Jana, X. Peng, J. Am. Chem. Soc. 125 (2003) 14280.
[26] W.A. Hayes, C. Shannon, Langmuir 12 (1996) 3688.
[27] T. Shimizu, T. Teranishi, S. Hasegawa, M. Miyake, J. Phys. Chem. B 107 (2003) 2719.
[28] L.V. Azaroff, Elements of X-ray Crystallography, McGraw-Hill, New York, 1968, p. 549.
[29] X.L. Wen, Y.H. Jia, Z.L. Liu, Talanta 50 (1999) 1027.
[30] A. Dalmia, C.C. Liu, R.F. Savinell, J. Electroanal. Chem. 430 (1997) 205.
[31] P.R. Roy, T. Okajima, T. Ohsaka, J. Electroanal. Chem. 561 (2004) 75.
[32] P. Alivisatos, Nat. Biotechnol. 22 (2004) 47.
[33] K. Wu, S. Hu, J. Fei, W. Bai, Anal. Chim. Acta 489 (2003) 215.
[34] C.R. Raj, K. Tokuda, T. Ohsaka, Bioelectrochemistry 53 (2001) 183.
[35] M.A. Dayton, A.G. Ewing, R.M. Wightman, Anal. Chem. 52 (1980) 2392.
[36] J.B. Justice, J.A. Jaramillo, J. Electrochem. Soc. 131 (1984) 106C.
[37] Y. Zhang, Y. Cai, S. Su, Anal. Biochem. 350 (2006) 285.
[38] G. Jin, Y. Zhang, W. Cheng, Sens. Actuators B 107 (2005) 528.
[39] H. Zhao, Y. Zhang, Z. Yuan, Anal. Chim. Acta 441 (2001) 117.
[40] Y. Zhao, Y. Gao, D. Zhan, H. Liu, Q. Zhao, Y. Kou, Y. Shao, M. Li, Q. Zhuang, Z. Zhu, Talanta 66 (2005) 51.

Available online at www.sciencedirect.com
ScienceDirect
Talanta 71 (2007) 1520–1523
Talanta
www.elsevier.com/locate/talanta

Enzymatic reverse FIA method for total phenols determination in urine samples

Marcos Grünhut, Miriam E. Palomeque, Adriana G. Lista *, Beatriz S. Fernández Band *

FIA Laboratory, Department of Chemistry, Universidad Nacional del Sur, Av. Alem 1253, 8000 Bahía Blanca, Buenos Aires, Argentina

Received 4 May 2006; received in revised form 13 July 2006; accepted 14 July 2006
Available online 2 October 2006

Abstract

A reverse flow injection spectrophotometric enzymatic method is proposed to quantify total phenols in urine samples. The polyphenol oxidase (PPO; EC 1.14.18.1) obtained as a crude extract from sweet potato root (*Ipomoea batatas*) was used as enzymatic catalyze. The detection limit, the sample throughput and relative standard deviation were 7.7 mg l^{-1} of total phenols, 49 h^{-1} and 0.9%, respectively. The method was applied to real samples and a recovery study was carried out in order to its validation.

Keywords: Reverse FIA method; Polyphenol oxidase; Urine samples

1. Introduction

Phenols can be absorbed into the human body through the skin and the digestive and respiratory system [1]. Phenolic compounds are released in urine, such as sulphate and/or glucoronide conjugates. The amount of these conjugates is due to the kind and concentration of phenols that the individuals have been exposed [2]. Phenol compounds are frequently monitored in human urine and other biological samples to obtain an indication of occupational exposure or exposure to environmental contamination [3,4]. High-pressure liquid chromatography [5,6] and spectrometry [7,8] are techniques usually used. Nevertheless, each technique has diverse disadvantages such as high cost, the use of organic solvents and sometimes the analysis is prolonged a long time.

Moreover, several enzymatic methods using crude extracts as enzymatic source have been developed to determine phenols and polyphenols in different matrixes. The extraction of enzymes from natural products presents low cost and enables to perform highly selective analyses [9–11]. A crude extract of sweet potato root (*Ipomoea batatas* (L.) Lam.) was used as the enzymatic source of polyphenol oxidase (PPO). PPO (EC 1.14.18.1) catalyses the *ortho*-hidroxylation of phenols and the oxidation of catechols to *ortho*-quinones in presence of oxygen [12,13], that have a strong absorption at 410 nm.

Flow injection methodologies has been widely used to perform enzymatic method [14,15]. In this work a reverse flow injection system was developed for the enzymatic spectrophotometric determination of total phenols in urine samples using a natural source of PPO.

2. Experimental

2.1. Apparatus

Centrifugation of extracts was conducted in a refrigerated-automatic Sorvall (USA) centrifuge, provided with a type SS-34 rotor.

Spectrophotometric measurements were carried out by using a Hewlett-Packard model 8452 A UV–vis diode array spectrophotometer (Germany), with a Hellma 178-010-QS flow cell (inner volume of18 μl).

A Gilson Minipuls 3 (France) peristaltic pump and a Rheodyne 5041 injection valve were used.

The reaction coils, sampling loop and flow lines were made of PTFE tubing (0.5 mm i.d.).

A Spectronic 20 Genesis^{TM} model 4001/4 (USA) was used for enzymatic activity, and creatinine determination.

* Corresponding authors. Tel.: +54 291 4595160; fax: +54 291 4595160.
E-mail addresses: alista@criba.edu.ar (A.G. Lista), usband@criba.edu.ar (B.S.F. Band).

0039-9140/$ – see front matter © 2006 Elsevier B.V. All rights reserved.
doi:10.1016/j.talanta.2006.07.032

An Orion model 710 A pH meter with an Orion-Ross® model 81-02 electrode was used to carry out the pH measurements.

2.2. Reagents and solutions

All reagents were of analytical grade. To prepare all solutions an ultra pure water (18 MΩ) was used.

A 0.1 M phosphate buffer solution of pH 7 was prepared.

A 0.55 g l^{-1} catechol stock solution used as substrate was daily prepared by dissolving 0.0275 g of catechol (Anedra, Argentine) in 50 ml of the buffer solution. Standard solutions were prepared from the stock solution by appropriate dilution whit buffer solution.

Dowex 1 × 8 100–200 mesh (Fluka AG, Germany) strong basic, quaternary ammonium anion exchange resin was used as a protective and stabilizer agent during the preparation of the sweet potato extract.

The 0.015% sodium azide (Sigma–Aldrich, USA) solution was prepared.

For the acid hydrolysis of the urine sample 12 M HCl (Cicarelli, Argentine) was used. Then, a 4.0 M NaOH solution (Cicarelli, Argentine) was added to the hydrolyzed urine samples up to pH 7.

Wiener lab. kit (Argentine) for creatinine determination was used.

Sweet potato roots (*I. batatas* (L.) Lam.) acquired from a market place were washed, hand-peeled, chopped and frozen at −18 °C until they were used.

2.3. Methods

2.3.1. Extraction of PPO from the sweet potato root

An amount of 25 g of *I. batatas* L. previously frozen was cut into small pieces and placed in a liquefier and added 100 ml of 0.1 M phosphate buffer (pH 7.0) and 2.5 g of Dowex 1 × 8. It was homogenized for 3 min at 4–6 °C. The homogenate was rapidly filtered through two layers of cheesecloth and centrifuged at 14,500 rpm for 60 min, at 2–6 °C. The resulting supernatant was separated and stored at 4 °C in refrigerator with previous addition of 0.015% sodium azide solution. This crude extract was then used as enzymatic source in the FIA procedure.

2.3.2. Measurement of PPO activity

The PPO activity, that is natural present in the crude extract of the *I. batatas*, was determined. The *o*-quinones were obtained when different volumes of PPO (0.04–0.2 ml) were mixed with 2.8 ml of 0.05 M catechol and buffer phosphate to 5.0 ml. The classical spectrophotometric method was used for the absorption measurements of the pigments at 410 nm.

One unit of PPO activity is defined as the amount of enzyme that causes an increase of 0.001 absorbance units per minute, under the conditions above described [16].

2.3.3. Total protein determination

The protein concentration was determined by triplicate. The Biuret method [17], using bovine serum albumin as standard, was applied.

2.3.4. Sampling of urines

Urine samples (100 ml) were obtained during a work shift from 10 laboratory-workers (7 women and 3 men). The samples were immediately refrigerated until further treatment.

2.3.5. Hydrolysis of urine samples

About 6 ml of urine were introduced into a Hach® tube and 0.6 ml of 12 M HCl was added. The hydrolysis was carried out heating between 100 and 110 °C during 90 min. The hydrolyzed urine was cooled at room temperature and then, 4 M NaOH was added up to pH 7. Finally, the hydrolyzed sample was diluted with buffer solution to 10 ml and total phenols were determined by the proposed method.

On the other hand, the same samples were spiked with different concentrations of catechol standard solution before doing the hydrolysis. These samples were used for the recovery study.

2.3.6. Creatinine determination

The concentration of creatinine in urine was determined to give all the analysis results as mg of phenol/g creatinine [18]. The method is based on the Jaffé reaction. The complex absorbance was measured at 510 nm.

2.3.7. FIA system and procedure

A two-channel reverse FIA manifold with spectrophotometric detection was developed (Fig. 1). An injected volume

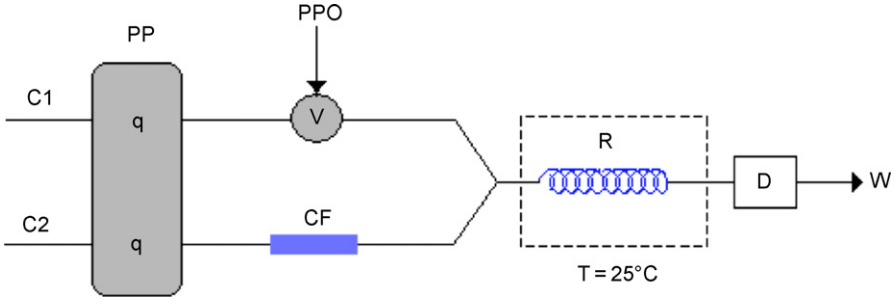

Fig. 1. Flow injection system for the determination of total phenols. C1, carrier solution (pH 7.0); C2, sample; PPO, polyphenol oxidase; PP, peristaltic pump; *q*, flow rate; V, injection valve; CF, cotton filter; R, tubular coiled reactor; D, detector; W, waste.

(300 μl) of PPO solution was inserted in a 0.1 mol l^{-1} phosphate buffer carrier solution C1 at a flow rate of 1.1 ml min^{-1}. The sample stream that was flowing through the channel C2 (flow rate of 1.1 ml min^{-1}) was filtered on-line by passing through a tubular cotton filter (CF). This stream merged with the PPO stream in the R reactor (thermostatized at 25 °C) where the catalyzed oxidation took place and went forward to the flow cell. The absorbance was measured at 410 nm. The baseline was obtained while the sample solution was continuously flowing through the system.

3. Results and discussion

3.1. Enzymatic and specific activity

The crude extracts were obtained from different commercial sweet potatoes root along one semester. The sweet potatoes used were gathered in the period spring–summer where the temperature varies between 24 and 40 °C. The enzymatic and specific activity in the crude extract were always determined and the results are shown in Table 1. The obtained values were optimum, and they have been improved with regard to the cited in the literature [19]. Therefore, the conditions for the obtaining of crude extract are satisfactory. The azide solution was used as antimicrobial agent to extend the preservation of the extract. So, it can be preserved without enzymatic activity variation for 3 months, in the refrigerator at 4 °C.

3.2. Sampling of urines

The recommended collection of urine samples was random type. However, the recommendation is not to take the first urine morning samples, because there are a lot of interferents that produce wrong values in the total phenol determination.

3.3. Hydrolysis of urine samples

From total of phenolic compounds that are released in the urine, a minimum fraction is present as free phenols and the remainder as water-soluble sulfates and/or glucuronides [2]. Therefore an acid hydrolysis of these conjugates is necessary to determine different phenols in urine samples [2,8].

Table 1
Determination of enzymatic and specific activity

Crude extract	Enzymatic activity (unit ml^{-1})	Total protein (mg ml^{-1})	Specific activity (unit mg^{-1} protein)
1	5225	2.87	1820
2	4112	2.65	1552
3	6047	3.34	1810
4	4329	2.76	1568
5	5541	2.80	1979
Mean	5051	2.88	1746
S.D.	816	0.27	328

S.D., standard deviation.

Table 2
Optimization of FIA parameters

Parameters	Studied ranges	Optimum values
Injected volume (μl)	50–600	300
Reactor length (cm)	150–750	500
Flow rate (ml min^{-1})	0.8–2.2	1.1

The optimal conditions for acid hydrolysis are not well established in the literature. Thus, in this work the most important variables for this purpose were studied. The optimum values were: time 90 min, 100–110 °C of temperature and 6 M of HCl.

3.4. Optimization of variables

The hydrodynamic parameters of the system: injected reagent volume, reactor length and flow rate, were optimized by univariate method in order to achieve a compromise between sensitivity, sample throughput and reproducibility. The studied ranges and optimum values were showed in Table 2.

The only chemical variable optimized was the enzyme concentration. This concentration was tested between 300 and 1200 UE ml^{-1}, and the optimum value was 800 UE ml^{-1}.

3.5. Analytical parameters

The calibration graph was linear between 11 and 132 mg l^{-1} of catechol. The regression line was $A = (0.0039 \pm 0.0001)C + (0.1737 \pm 0.0080)$, where A is the absorbance and C is the concentration in mg l^{-1} of cathecol, with a $R^2 = 0.998$. The detection limit [20] and the sample throughput were 7.7 mg l^{-1} of catechol and 49 h^{-1}, respectively. The precision of the method, represented by the repeatability (%R.S.D.) was 0.9% and it was calculated from 10 independent measurement of a standard containing 30 mg l^{-1} of catechol.

3.6. Analytical application to real samples

The proposed method was applied to determine total phenols in urine samples. The concentrations of total phenols are shown in Table 3, where these values were also expressed as a function

Table 3
Determination of total phenols in urine samples

Samples	mg total phenols l^{-1} urine	mg creatinine l^{-1} urine	mg total phenols mg creatinine
1	37.9[a]	1.72	22.0
2	n.d.	0.68	n.d.
3	22.4	1.40	16.0
4	25.5	2.61	9.80
5	28.8[a]	1.43	20.1
6	14.4	0.73	19.7
7	26.1	1.42	18.4
8	35.4[a]	1.65	21.4
9	17.8	1.74	10.2
10	44.1[a]	1.68	26.2

n.d., not detected.
[a] Explained in text.

Table 4
Recovery study in urine samples

Samples	Added (mg catechol l^{-1} urine)	Found (mg catechol l^{-1} urine)	Recovery (%)
1	22.0	21.8	98.9
2	22.0	20.0	90.1
3	44.0	40.3	91.3
4	44.0	44.5	101.2
5	44.0	43.7	99.3
6	44.0	42.6	96.8
7	44.0	43.4	98.7
8	44.0	42.2	96.0
9	66.0	60.3	91.4
10	66.0	61.2	92.7

of mg of creatinine in order to compare the results of the real samples. The threshold value for total phenols in urine is 20 mg l^{-1}, for non-exposed workers to benzene and phenol [4]. As can be seen in Table 3 the samples 1, 5, 8, and 10 are clearly up to the threshold value. These samples were taken from laboratory-workers that were exposed by respiratory route during 4–6 h to different phenolics compounds (phenol, *ortho*-nitrophenol, *para*-nitrophenol, 4-chlorophenol, 1,3,5-trichlorophenol). This suggests that the high values founded in the analyzed samples can be associated to the previous exposure to the different phenolic compounds.

A recovery study was carried out to validate the method. For that purpose different concentrations of catechol were added to the urine samples before hydrolyzing them. Table 4 lists the obtained results. Recoveries of 91.4–101.2% evidence the good accuracy of the proposed method.

4. Conclusion

The proposed continuous method can be used as a rapid screening and quantitative determination of total phenols in urine samples. This method is fast, simple, inexpensive and with high sample throughput by comparing with other conventional method. Moreover, with the FIA reverse configuration, the consumption of the enzyme is low and this represents an important advantage.

The method was validated by means of spiked samples.

The enzymatic and specific activity was improved and the preservation of the extract was increased by adding azide solution as antimicrobial agent.

Acknowledgements

M. Grünhut and B.S. Fernández Band acknowledge CONICET (Consejo Nacional de Investigaciones Científicas y Técnicas) for support.

All authors are gratefully acknowledged to Universidad Nacional del Sur.

References

[1] K. Schmid, P. Lederet, T. Göen, Int. Arch. Occup. Environ. Health 69 (1997) 399.
[2] H. Kontsas, C. Rosenberg, P. Pfäffli, P. Jäppinen, Analyst 120 (1995) 1745.
[3] G.A. Khoschsorur, W. Petek, Anal. Sci. 16 (2000) 589.
[4] C.D. Klassen, M.O. Amdur, J. Doull, Casarett and Doull's Toxicology, the Basic Science of Poisons, 5th ed., McGraw-Hill, New York, 1998.
[5] B.L. Lee, H.Y. Ong, C.Y. Shi, C.N. Ong, J. Chromatogr.: Biomed. Appl. 619 (1993) 259.
[6] J.M. Wada, S. Kinoshita, Y. Itayama, N. Kuroda, K. Nakashima, J. Chromatogr. B 721 (1999) 179.
[7] S. Waidyanatha, N. Rothman, G. Li, M.T. Smith, S. Yin, S.M. Rappaport, Anal. Biochem. 327 (2004) 184.
[8] M.A. Crespín, M. Gallego, M. Valcárcel, J. Chromatogr. B 773 (2002) 89.
[9] V.S. Bezerra, J.L. de Lima Filho, M. Montenegro, A.N. Araújo, V. Lins da Silva, J. Pharm. Biomed. Anal. 33 (2003) 1025.
[10] I.C. Vieira, O. Fatibello-Filho, L. Angnes, Anal. Chim. Acta 398 (1999) 145.
[11] O. Fatibello-Filho, K.O. Lupetti, I.C. Vieira, Talanta 55 (2001) 685.
[12] S.G. Burthon, Catal. Today 22 (1994) 459.
[13] K. K. Lerch, in: H. Sigel (Ed.), Copper Monoxygenases: Tyrosinase, Dopamine b-Monoxygenase, Copper Proteins, vol. 13, issue 5, Marcel Dekker, New York, 1981.
[14] C. Martıǐn, E. Domıǐnguez, J. Pharm. Biomed. Anal. 19 (1999) 107.
[15] E.R. Kiranas, M.I. Karayannis, S.M. Tzouwara-Karayanni, Talanta 45 (1998) 1015.
[16] E.J. Lourenco, J.S. Leão, V.A. Neves, J. Sci. Food Agric. 52 (1990) 249.
[17] O.H. Lowry, N.J. Rosebrough, A.L. Farr, R.J. Randall, J. Biol. Chem. 193 (1951) 265.
[18] H.P. Seelig, H. Wüst, Ärztl. Lab. 15 (1969) 34.
[19] I.C. Vieira, O. Fatibello-Filho, Anal. Chim. Acta 366 (1998) 111.
[20] J.N. Miller, J.C. Millar, Estadística y Quimiometría para Química Analítica, Pearson Educación, SA, Madrid, 2002.

Available online at www.sciencedirect.com
ScienceDirect
Talanta 71 (2007) 1734–1740
Talanta
www.elsevier.com/locate/talanta

Immobilization and voltammetric detection of human interleukine-2 gene on the pencil graphite electrode

M.S. Hejazi [a], E. Alipour [b], M.H. Pournaghi-Azar [b,*]

[a] *Faculty of Pharmacy & Drug Applied Research Center, Tabriz University of Medical Sciences, Tabriz, Iran*
[b] *Electroanalytical Chemistry Laboratory, Faculty of Chemistry, University of Tabriz, Tabriz, Iran*

Received 1 May 2006; received in revised form 2 August 2006; accepted 2 August 2006
Available online 15 September 2006

Abstract

The immobilization and differential pulse anodic voltammetry (DPAV) of a 20-mer oligonucleotide related to the human interleukine-2 (hIL-2) using renewable pencil graphite electrode (PGE) is described. The influences of electrochemical pretreatment of PGE on the ability of the electrode in hIL-2 adsorption, and conditions of hiIL-2 immobilization on PGE including immobilization potential and time, sodium chloride concentration as well as stirring of the solution were studied and optimum conditions were suggested. Accordingly, the electrochemical pretreatment of the polished PGE by electrostatic procedure at 1.80 V for 5 min in 0.50 M acetate buffer solution of pH 4.8 is proposed as the optimum pre-treatment procedure. Similarly, the obtained optimum conditions for immobilization of hIL-2 on the activated PGE was an immobilization duration of 5 min at applied potential of 0.50 V. Trace levels of hIL-2 was readily detected following only 5 min immobilization period with detection limit of 6 nM.

Keywords: Human interleukine-2 DNA; Differential pulse voltammetry; Guanine oxidation; Label-free DNA determination; Pencil graphite electrode

1. Introduction

Interleukine-2 (IL-2) is an immune system cytokine secreted by activated T cells [1]. This cytokine stimulates T-cells proliferation and differentiation and consequently promotes immune response against bacteria and viruses [2]. IL-2 is produced as a recombinant protein [3–8] and is available in the market as an anticancer drug [9,10]. This recombinant protein is mainly extracted from recombinant bacteria transfected with plasmids containing IL-2 encoding cDNA. Additionally, various recombinant viruses such as adenoviruses, retroviruses and lentiviruses which contain IL-2 encoding cDNA have been developed by different investigators [11,12]. These viruses have been utilized in gene therapy protocols for treatment of human diseases including various cancers. Some of these viruses have been used in vivo studies demonstrating promising results which offer their routine consume in the near future [13]. Considering that the detection of recombinant DNAs and microorganisms needs time-consuming and expensive techniques, developing an electrochemical method for determination of IL-2 encoding cDNA could be a promising approach for detection of recombinant DNAs (e.g., plasmids encoding human IL-2) as well as detection of recombinant microorganisms (e.g., recombinant bacteria used for industrial IL-2 production and recombinant viruses utilized for gene therapy protocols).

Guanine was reported to be the most redox active nitrogenous base in DNA strands [14]. This activity is conducted with reduction of guanine residue at mercury electrode [15–18] or its oxidation in solid electrodes [19–24]. On the basis of a literature investigation, the label-free monitoring, based on guanine moiety oxidation signal of probe or target on conventional carbon electrodes in electrochemical DNA biosensor, seems to be a simple, less time consuming and more applicable strategy in comparison with the others [21,22,25,26]. Wang et al. used chronopotentiometric signal of guanine oxidation of DNA adsorbed on carbon paste [19] and pencil lead electrodes for evaluating DNA hybridization event [20]. A catalytic guanine oxidation protocol with an indium tin oxide electrode using ruthenium complexes as oxidation catalysts were reported [21,22]. Palecek and co-workers [23] monitored the oxidation signal of guanine moiety in DNA and PNA strands by applying

* Corresponding author. Fax: +98 411 3340191.
E-mail address: pournaghiazar@tabrizu.ac.ir (M.H. Pournaghi-Azar).

0039-9140/$ – see front matter © 2006 Published by Elsevier B.V.
doi:10.1016/j.talanta.2006.08.010

chronopotentiometry and voltammetry at pyrolytic graphite electrode. Erdem et al. reported a differential pulse voltammetric determination of DNA, and oligonucleotides using graphite-epoxy composite (GEC) electrode [24]. They found that the guanine (and also adenine) moieties are more easily oxidized on GEC electrode compared to other carbon-based transducers. They also proposed a novel label-free hybridization genosensor for the specific detection of a sequence related with salmonella spp. based on guanine signal. Kizek et al. reported voltammetric study of two single-stranded isomeric end-labeled–SH deoxyoligonucleotides on mercury electrode [27]. Wang et al. demonstrated and characterized the enhanced detection of the guanine nucleobases at multi-wall carbon nanotubes (MWCNT) modified glassy carbon electrodes, and exploited the improved purine response for amplifying trace measurements of nucleic acids [26]. The MWCNT modified glassy carbon electrodes were also used by Hu and coworkers for the sensitive determination of adenine and guanine, either as free bases or as residues of DNAs [28]. Pedano et al. described the use of carbon nanotubes paste electrodes (CNTPE) prepared by dispersion of carbon nanotubes within mineral oil for studying the adsorption and electrooxidation of nucleic acids [29]. Considering the difficulties with the analysis of longer DNA molecules Palecek et al. described a label-free detection of DNA and RNA based on the determination of adenines (at ppb levels, by cathodic stripping voltammetry) released from the nucleic acids by acid treatment [30].

Polymerase chain reaction (PCR) amplified real samples of lysteria mono cytogen were monitored by using guanine signal after electrochemical enrichment on plastic composite electrodes [31]. PCR samples were tested to detect factor V leiden mutation with the help of guanine oxidation signal on CPE [32]. Double stranded DNA and 23-mer oligonucleotides were directly adsorbed at polycrystalline Au electrodes, then cyclic voltammetry and SWV were employed to detect guanine oxidation signal at 0.73 V [33].

In this work, the use of pencil lead graphite as a low cost and renewable electrode for DPAV of hIL-2 encoding DNA is described. The special emphasis is given to both monitoring the influence of some experimental variables upon the adsorptive behavior and further DPA voltammetric measurements of the electrode.

2. Experimental

2.1. Chemicals

The pencil graphite was available as pencil lead from Rotring Co. Ltd. (Germany, R 505210 N of type H). Pencil leads are commonly composed of natural graphite, a polymeric binder and clay with different percents depending on desired durability or other physical properties. All leads had a diameter of 2.0 mm and were used as-received. A 20-mer oligonucleotide corresponding to sense strand of human IL-2 gene denoted as hIL-2 was supplied (as lyophilized powder) from MWG-BIOTECH, with the following sequence: (hIL-2): 5′-GGA GGA AGT GCT AAA TTT AG-3′.

The hIL-2 stock solution (16 μM) was prepared with TE buffer solution (10 mM Tris–HCl, 1 mM EDTA, pH 8.00) and kept frozen. More diluted solutions of the hIL-2 were prepared using 0.50 M acetate buffer (pH 4.80) solution containing 20 mM NaCl. The distilled, deionized and sterilized water was used in all solution preparation. Each measurement consisted of the accumulation/determination cycle carried out on a fresh PGE surface. All the experiments were performed at room temperature in an electrochemical cell.

2.2. Apparatus

Electrochemical experiments were performed using AUTOLAB PGSTAT 30 electrochemical analysis system and GPES 4.7 software package (Eco Chemie., The Netherlands). The utilized three-electrode system was composed of a PGE (surface area of 0.037 cm^2) as the working electrode, a saturated calomel electrode (SCE) as the reference electrode and a platinum wire as the auxiliary electrode.

2.3. Procedure

2.3.1. Preparation of the working electrode

The body of pencil lead was tightly coated with Teflon band and the surface was polished on a weighing paper to a smoothed finish before each use. Electrical contact with the lead was achieved by soldering a copper wire to the metallic holder of the working electrode. The pencil lead was fixed vertically and immersed in the solution in which the contact was only achieved via cross section of the lead.

2.3.2. Activation of PGE and immobilization of hIL-2 on the PGE

The electrochemical activation of the surface of polished PGEs was carried out at 1.80 V of imposed potential in 0.50 M acetate buffer solution (pH 4.80) without stirring for 5 min. Following activation of the PGE as mentioned above, the hIL-2 was subsequently pre-concentrated on the activated electrode by applying 0.50 V to the electrode for 5 min in 0.50 M acetate buffer solution containing 2 μM hIL-2 and 20 mM NaCl with 200 rpm stirring. The electrode was then rinsed with sterilized and deionized water for 10 s.

2.3.3. Electrochemical measurement

The electrochemical measurement was carried out using differential pulse anodic voltammetry (DPAV) in 0.5 M acetate buffer (pH 5) solution and sweeping the electrode potential between 0.50 and 1.15 V using a pulse amplitude of 50 mV. The raw data were treated using the Savitzky and Golay filter (level 2) of the GPES software, followed by the GPES software moving average baseline correction, using a ‘peak width’ of 0.01. Repetitive measurements were carried out following renewing the PGE surface by cutting or polishing.

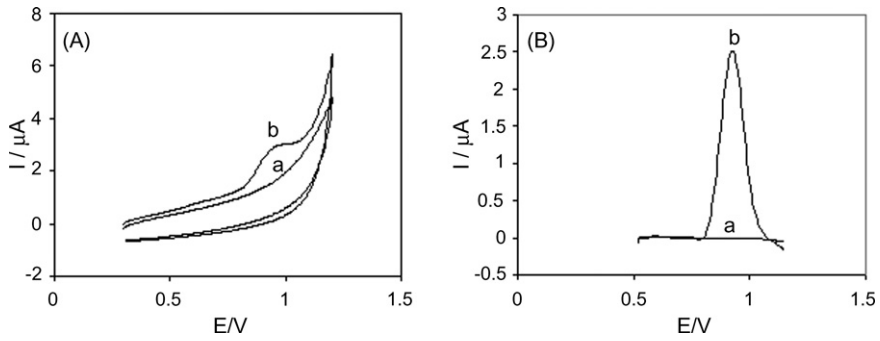

Fig. 1. (A) Cyclic voltammograms and (B) differential pulse anodic voltammograms of accumulated hIL-2 oligonucleotide at: (a) non-activated PGE and (b) activated PGE. Electrochemical activation potential: 1.70 V. hIL-2 concentration in accumulation solution: 5 μM. Other PGE activation, hIL-2 accumulation and voltammetric conditions as discribed in Section 2.3.

3. Results and discussion

3.1. Preliminary investigation

To get some information about the electrochemical system used in the present study and selecting a simple and sensitive electrochemical technique, a primary investigation starting by cyclic voltammetry at experimental conditions reported previously for carbon paste electrode (CPE) [34] seems to be useful. Fig. 1A, a shows a cyclic voltammogram obtained in 20 mM Tris–HCl buffer (pH 7.00) with scan rate of 50 mV s^{-1} from 0.3 to 1.2 V after about 5 min accumulation of hIL-2 at 0.50 V on a non-activated PGE in a 5 μM hIL-2 solution. No anodic peak related to the oxidation of guanine residue was observed. On the other hand, in accumulation of hIL-2 on the activated PGE at positive imposed potential of 1.70 V used for CPE activation [32,34] for 5 min, a discernible oxidation peak appeared due to guanine oxidation and no peak is observed in the cathodic region (Fig. 1Ab). In contrast, a dramatic improvement in the detection of the oxidation of guanine residues is obtained using differential pulse anodic voltammetry (Fig. 1B). The advantages of the differential pulse anodic voltammetry analysis are obvious, so this technique was used for all the measurements.

3.2. Influence of different experimental conditions

3.2.1. Influence of medium exchange

In order to obtain information about the strength of the interaction between the adsorbed hIL-2 layer and the surface of PGE, the voltammetric measurement was performed in the absence and presence of 5 μM hIL-2. The results showed that the difference between the intensity of the signals obtained with and without medium exchange is rather small (1.5%), indicating that hIL-2 is strongly adsorbed on PGE. This strong interaction makes it possible to perform the voltammetric measurements in a blank solution and avoids the probable interference of some compounds present in the accumulation.

3.2.2. Influence of electrochemical pretreatment of PGE

3.2.2.1. Effect of pretreatment potential. Considering that the electrochemical pretreatment is usually required to activate the surface of the PGE [35], and as the electrochemical pretreatment is commonly conducted either at negative and positive potentials [36], first we have started this study by potentiostatic method. In order to find an optimum pretreatment potential, the polished PGE was pretreated at different potentials within a wide range (i.e., from −2 to 2.5 V), then accumulation of hIL-2 was conducted as described in Section 2.3.3. On the basis of the results obtained from the differential pulse voltammetric response of the accumulated hIL-2 on the electrodes, it is obvious that the electrochemical pretreatment of the PGE at imposed potentials in the region between −2 and 1 V had no effect on the activity of the electrode for adsorption of hIL-2, but its activity improved as the potentials exceeded 1 V, until reached to its maximum value at 1.80 V, and then decreased at more positive potentials (Fig. 2A). Note that at positive potentials higher than 2 V and at negative potentials lower than −1.5 V, the oxidation or reduction of supporting electrolyte ions or solvent itself began to occur yielding gaseous products. But at this potential range (from −2 to 2.5 V) damaging of the electrode was not observed.

3.2.2.2. Effect of electrochemical procedure. Based on the results obtained from potentiostatic procedure, the potentiodynamic activation of the PGE was also carried out at the same solution conditions by scanning the electrode potential between 1.50 and 2.00 V with scan rate of 50 mV s^{-1} for 15 cycles. The results obtained from this study confirmed that in both cases the pretreatment of the PGE surface has a positive effect on the adsorption of hIL-2. But this effect is more pronounced with potentiostatic procedure (2.38 ± 0.27 μA for potentiostatic and 0.53 ± 0.07 μA for potentiodynamic procedures). In addition, the results clearly demonstrated that the state of the PGE surface is critical when it is used for the accumulation of hIL-2 and a fresh surface or freshly polished surface must be provided in order to get the reproducible responses.

3.2.2.3. Effect of pretreatment time. Similarly, the effect of PGE activation time on the accumulation of hIL-2 was studied using DPV measurements of guanine signals following activation of PGE in different activation periods. The accumulation of hIL-2 on the electrode was performed according to the procedure described in Section 2.3.3. Fig. 2B displays the response for hIL-2 versus activation time. It is clear that the hIL-2 oxidation signal is increased with increasing the activation time and nearly

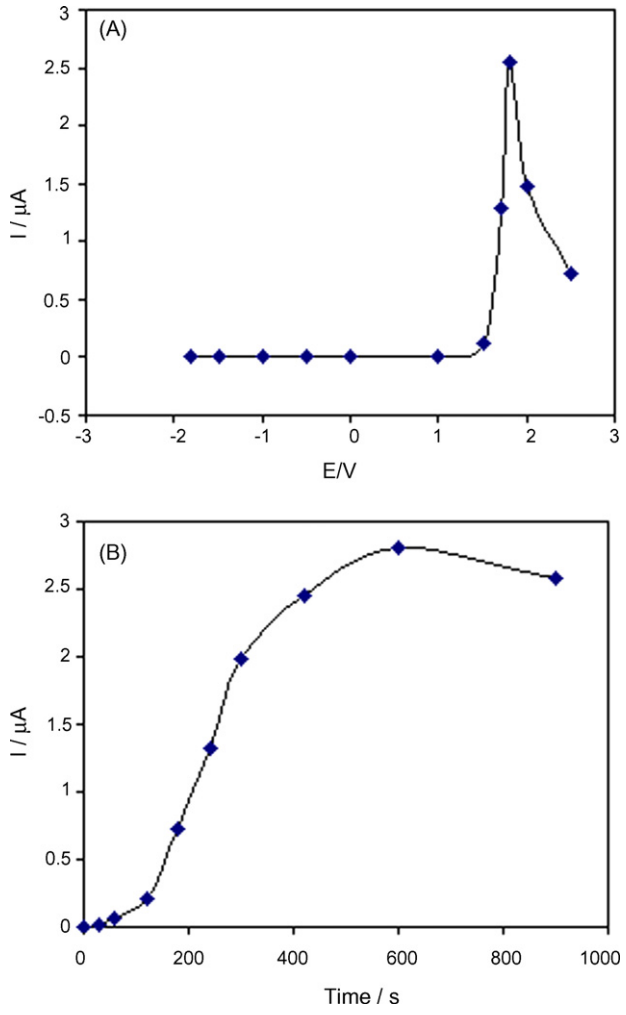

Fig. 2. (A) Variations of DPA voltammetric signal of the immobilized hIL-2 on the activated PGE vs. activation potentials and (B) variations of DPA voltammetric signal vs. activation times. hIL-2 concentration in solution: 2 μM. Other conditions for PGE activation, hIL-2 immobilization and DPAV measurements as described in Section 2.3.

leveled off after 10 min. These results showed that a moderate time (5 min) is sufficient for activation of the PGE surface in order to accumulate the considerable amount of hIL-2.

3.2.2.4. Effect of background electrolyte. The influence of some buffer solutions such as Tris–HCl (pH 7) or acetate (pH 4.8) and phosphate (pH 7) commonly used in similar studies on the CPE [19,34] upon the activation of PGE was investigated. The voltammetric measurements were performed following the procedure as described in Section 2 and the results are illustrated in Fig. 3. As seen in Fig. 3, the lowest signal is obtained using Tris–HCl (pH 7.00) buffer and the voltammogram related to phosphate buffer is less shaped. On the other hand, a systematic study involving the effect of concentration and pH of the acetate buffer solution upon pretreatment of PGE, showed that the variation of the acetate buffer concentration between 0.1 and 0.5 M as well as variations of its pH between 4 and 6 has less effect on the results obtained. So, a 0.5 M acetate buffer solution of pH 4.8 was used for all experiments.

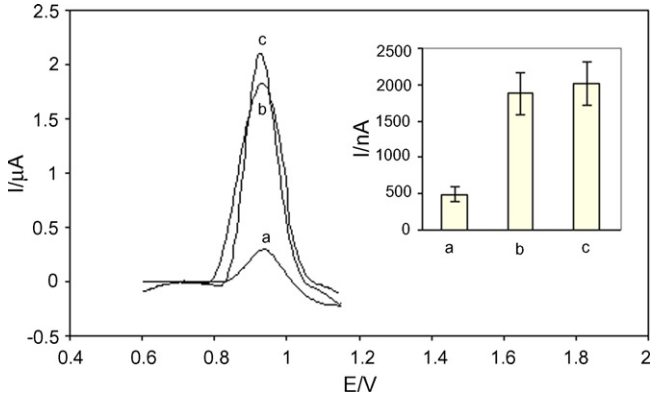

Fig. 3. Effect of buffer kind upon the accumulation of 12.5 mg/L hIL-2 oligonucleotide. Electrolytes: (a) 0.50 M acetate buffer (pH 4.80) solution, (b) 0.50 M phosphate buffer (pH 7.00) solution and (c) 0.50 M Tris–HCl buffer (pH 7.00) solution. Electrochemical activation time: 5 min. hIL-2 concentration: 5 μM, accumulation and DPAV measurement conditions as described in Section 2.3.

3.2.3. Influence of kind of pencil lead and the electrode surface polishing

A systematic study, based on the transducing the DPA voltammetric measurement of the adsorbed hIL-2 layer on the electrode, showed that the pencil leads type H displays the smallest background signal and most favorable signal-to-background characteristic. Note that polishing the electrode surface provides a reproducible surface area and subsequently a more repetitive experiments that confirmed by statistic analysis of the data. Also the polishing strategy allows one lead to be used for several times. These can be provided by a type H pencil lead (2 mm in diameter).

3.2.4. Optimization of hIL-2 immobilization conditions on the PGE

3.2.4.1. Effect of immobilization potential. One of the important factors affecting the immobilization of hIL-2 on the electrode is the imposed potential to the electrode during the accumulation. The influence of the imposed potential was investigated on the basis of DPAV response of hIL-2. The measurement was performed following immobilization of hIL-2 on the PGE at different potentials ranged between −0.80 and 0.80 V (Fig. 4A). The results showed that imposing a positive potential to the PGE, favored the accumulation of hIL-2 DNA on the electrode and maximum voltammetric signal was observed at 0.50 V. A potential of 0.50 V was, therefore, selected for most subsequent works.

3.2.4.2. Effect of immobilization time. The effect of hIL-2 immobilization time on the activated PGE was investigated. In order to obtain the optimum immobilization time, immobilization of the hIL-2 was conducted for different time durations. The results obtained from the voltammetric measurements revealed that the guanine oxidation signal elevated as the accumulation time increased from zero to about 300 s and remained constant between 300 and 600 s (Fig. 4B). Therefore, 300 s was suggested as optimum time for the accumulation of the hIL-2 on the PGE.

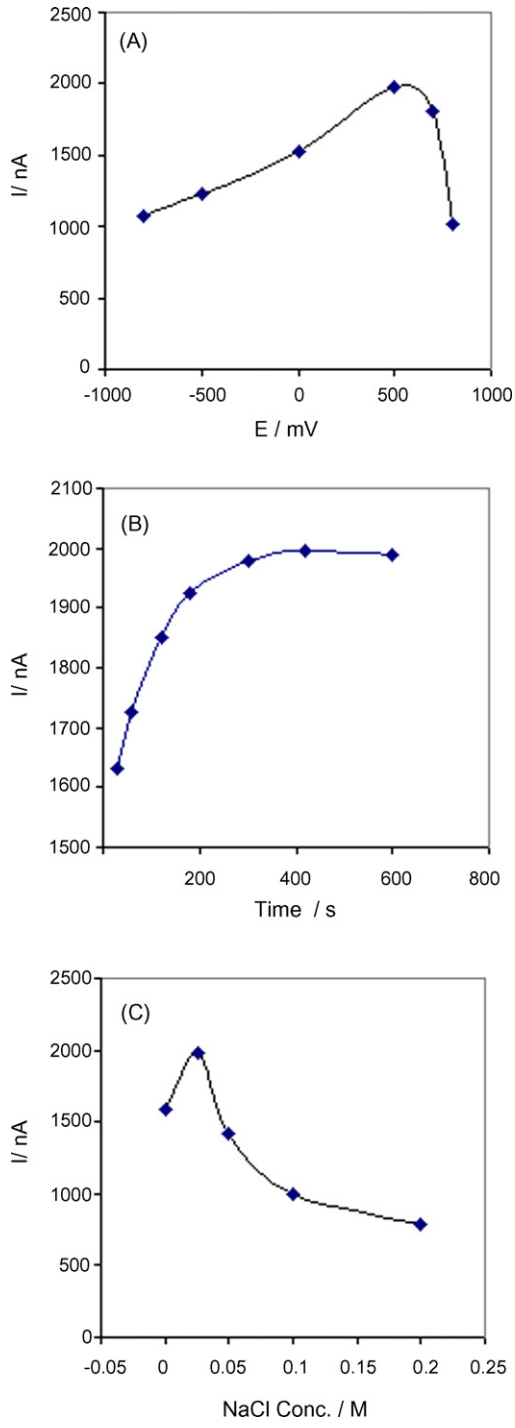

Fig. 4. (A) Variations of DPAV response of immobilized hIL-2 oligonucleotide on the activated PGE vs. immobilization potential, (B) variation of DPAV response of hIL-2 oligonucleotide immobilized on the activated PGE vs. immobilization time and (C) effect of the NaCl concentration in the immobilization buffer solution upon the immobilization of hIL-2 oligonucleotide on the activated PGE. hIL-2 concentration: 2 μM, other experimental conditions as described in Section 2.3.

3.2.4.3. Effect of sodium chloride concentration. Fig. 4C illustrates the influence of sodium chloride present in the solution upon the adsorption of hIL-2 on the activated PGE. As seen in Fig. 4C the DPAV signal increases at the beginning with the concentration of NaCl up to 0.02 M and decreases thereafter. When the concentration of NaCl increases, more than one effect has to be considered. One is the increase of ionic strength itself, responsible for the decrease in the signal, while the others are the specific effect of the anion on the oligonucleotide conformation in solution as well as the interaction of the anion with the surface of the electrode [37]. The effect of NaCl on the voltammetric response of hIL-2 is more pronounced when the time of immobilization and consequently the time of interaction between the chloride and hIL-2 increases (results are not shown). Thus the suppressing effect of the chloride on the voltammetric response of the hIL-2 is indicative of a specific interaction with the nucleic acid itself as well as an interaction with surface of PGE.

3.2.4.4. Effect of stirring of the solution. In order to increase the adsorption rate, stirring of the solution during the accumulation of analyte seems to be effective. To prevent the perturbation of the adsorption rules; optimization of stirring speed is suggested. We observed that the accumulation amount of hIL-2 on the electrode enhanced as stirring speed increased, until reached

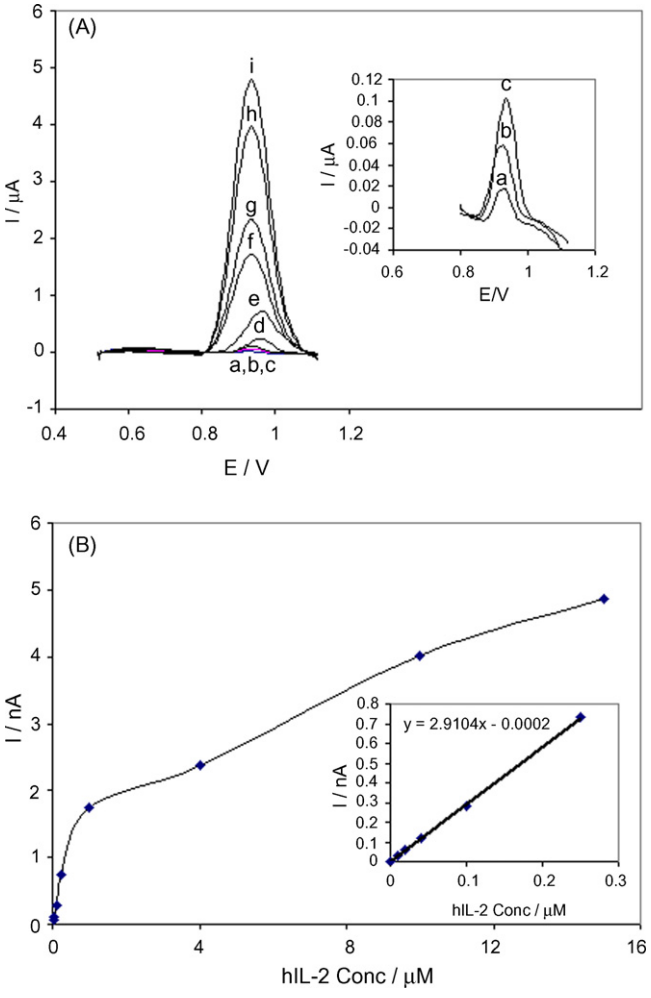

Fig. 5. (A) Differential pulse anodic voltammograms of different hIL-2 concentrations: (a) 0.01, (b) 0.02, (c) 0.04, (d) 0.10, (e) 0.25, (f) 1.00, (g) 4.00, (h) 10.00, (i) 15.00 μM. (B) Variation of DPAV response vs. hIL-2 concentration. *Inset*: related calibration graph at concentration range 0.01–0.25 μM. Experimental conditions described in Section 2.3.

Table 1
Comparison of detection limit of presented sensor with some similar studies

Electrode type	Detection limit ($\mu g\,l^{-1}$)	Detection signal	References
PGE[a]	36	Guanine oxidation	Present method
CNT/GC[b]	40	Guanine oxidation	[26]
Plastic composite electrode	60	Guanine oxidation	[31]
GC[c]	60	Guanine oxidation	[37]
CPE[d]	67	Guanine oxidation	[38]
CPE	120	Guanine oxidation	[19]
PGE	500	Guanine oxidation	[39]
CNTSPE[e]	2000	Guanine oxidation	[40]
SPE[f]	10	Oxidation of α-naphthol as enzymatic reaction product	[41]
GC	500	Methylene blue reduction	[42]
PGE	1140	Methylene blue reduction	[43]
CPE	20000	Reduction of $Co(phen)_3^{3+}$	[44]

[a] Pencil graphite electrode.
[b] Carbon nanotube modified glassy carbon electrode.
[c] Glassy carbon electrode.
[d] Carbon paste electrode.
[e] Carbon nanotube modified screen printed electrode.
[f] Screen printed electrode.

to a maximum value at about 200 rpm and then decreased at more stirring speed. This may be attributed to more distribution of the solution that may perturb the adsorption isotherms governed in the system. Therefore, 200 rpm was suggested as optimum stirring speed for the accumulation of the hIL-2 on the PGE.

3.3. Analytical performance

Fig. 5A displays DPA voltammograms obtained after immobilization of increasing level of hIL-2 (0.01–10 μM). Well defined peaks over a flat background were obtained. Fig. 5B shows the plot of the voltammetric response versus hIL-2 concentration. The calibration graph is shown in inset of Fig. 5B for hIL-2. A linear dependence between DPAV signal and hIL-2 concentration up to 0.25 μM was observed. The regression equation is $I\,(\mu A) = 2.9104C\,(\mu M) - 0.0002$. The detection limit estimated as three times of the ratio between the blank signal and the sensitivity, is 6 nM (36 $\mu g\,l^{-1}$). The detection limits of some similar electrochemical DNA sensors (based on label as well as label-free detection strategies) are given in Table 1. As seen in Table 1 the proposed sensor in the present work has a low detection limit that is comparable with the others.

4. Conclusion

The effective immobilization of a 20-mer of sense strand oligonucleotide related to human IL-2 gene on treated PGE surface was achieved. The results recommend that the PGE to be a very useful, inexpensive and renewable material for the immobilization of hIL-2 under controlled potential. Very dilute solutions of probe can be used to get full coverage of the PGE to detect the voltammetric signal of guanine at variance with other reports. Trace levels of hIL-2 can be easily immobilized and monitored on the activated electrode by differential pulse voltammetry following a short immobilization period in optimized experimental conditions.

The strong interaction of the hIL-2 with surface of the PGE makes the modified PGE, as a useful tool for further developments of a label-free biosensor for the detection of hybridization events. Related work is being done at present in our laboratory.

References

[1] R.J. Robb, Immunol. Today 5 (1984) 203.
[2] A. Weinberg, M. Kondard, T. Mergian, J. Virol 62 (1987) 2120.
[3] H.F. Seow, M.J. Mucha, L. Hurst, J.S. Rothel, P.R. Wood, Vet. Immunol. Immunopathol. 56 (1997) 107.
[4] R. Devos, G. Plaetinck, H. Cheroutre, G. Simons, W. Degrare, J. Tavenier, E. Remaut, W. Fiers, Nucleic Acids Res. 11 (1983) 4307.
[5] D.P. Cerretti, K. McKereghan, A. Larsen, M. Cantrell, D. Anderson, S. Gillis, D. Cosman, P.E. Backer, P. Natl. Acad. Sci. USA 83 (1986) 3223.
[6] D.P. Williams, D. Regier, D. Akiyoshi, F. Genbouff, J.R. Murphy, Nucleic Acids Res. 16 (1988) 10453.
[7] J. Robbens, A. Raeymaekers, L. Steidler, W. Fiers, E. Remaut, Protein. Expr. Purif. 6 (1995) 481.
[8] Y. Lin, Q. Ya-Li, B. Wei-Cheng, Y. Xiao-Lan, H. Hong-Liang, C. Huan-Chun, Eur. Cytokine Netw. 15 (3) (2004) 240.
[9] G. Bertram, Katzung Basic & Clinical Pharmacology, ninth ed., The McGraw-Hill Companies, Inc., USA, 2004, p. 928.
[10] D.G. Cada, T.R. Covington, S.K. Hebel, D.A. Hussar, L. Lasagna, B.R. Olin, J.R. Selevan, R.W. Sloan, D.S. Tatro, T.L. Whitsett, Drug Facts and Comparison, 54th ed., Facts and Comparisons, USA, 2000, p. 1946.
[11] M. Liu, B. Acres, J.M. Balloul, N. Bizourne, S. Paul, P. Slos, P. Squiban, Proc. Natl. Acad. Sci. USA 101 (2004) 14567.
[12] C. Kittel, B. Ferko, M. Kurz, R. Voglauer, S. Sereinig, J. Romanova, G. Stiegler, H. Katinger, A. Egorov, J. Virol. 79 (16) (2005) 10672.
[13] W. Jia, Q. Zhou, Curr. Gene Ther. 5 (1) (2005) 133.
[14] S. Steenken, S.V. Jovanovic, J. Am. Chem. Soc. 119 (1997) 617.
[15] L. Trnkova, M. Studniekova, E. Palecek, Bioelectrochem. Bioenerg. 7 (1980) 643.
[16] E. Palecek, F. Jelen, L. Trnkova, Gen. Physiol. Biophys. 5 (3) (1986) 315.
[17] M. Studniekova, L. Trnkova, J. Zetek, Bioelectrochem. Bioenerg. 21 (1989) 83.
[18] E. Palecek, Electroanalysis 8 (1996) 7.
[19] J. Wang, G. Rivas, J.R. Fernandes, J.L. Lopez Paz, M. Jiang, R. Waymire, Anal. Chim. Acta 375 (1998) 197.
[20] J. Wang, A.-N. Kawde, A. Erdem, M. Salazar, Analyst 126 (2001) 2020.
[21] M.E. Napier, C.R. Loomis, M.F. Sistare, J. Kim, A.E. Eckhardt, H.H. Thorp, Bioconjugate Chem. 8 (1997) 906.
[22] I.V. Yang, H.H. Thorp, Anal. Chem. 73 (2001) 5316.
[23] M. Tomschik, F. Jelen, L. Havran, L. Trnkova, P.E. Nielsen, E. Palecek, J. Electroanal. Chem. 476 (1999) 71.
[24] A. Erdem, M.I. Pividori, M.D. Valle, S. Alegret, J. Electroanal. Chem. 567 (2004) 29.
[25] K. Kerman, Y. Matsubara, Y. Morita, Y. Takamura, E. Tamiya, Sci. Tech. Adv. Mater. 5 (2004) 351.
[26] J. Wang, A.N. Kawde, M. Musameh, Analyst 128 (2003) 912.
[27] R. Kizek, L. Havran, T. Kubicarova, B. Yosypchuk, M. Heyrovsky, Talanta 56 (2002) 915.
[28] K. Wu, J. Fei, W. Bai, S. Hu, Anal. Bioanal. Chem. 376 (2003) 205.
[29] M.L. Pedano, G.A. Rivas, Electrochem. Commun. 6 (2004) 10.
[30] E. Palecek, S. Billova, L. Havran, R. Kizek, A. Miculkova, F. Jelen, Talanta 56 (2002) 919.
[31] J. Schulein, B. Grabl, J. Krause, C. Schulze, C. Kugler, P. Muller, W.M. Bertling, J. Hassmann, Talanta 56 (2002) 875.

[32] D. Ozkan, A. Erdem, P. Kara, K. Kerman, B. Meric, J. Hassmann, M. Ozsoz, Anal. Chem. 74 (2002) 5931.
[33] E.E. Ferapontova, E. Dominguez, Electroanalysis 15 (2003) 629.
[34] B. Meric, K. Kerman, D. Ozkan, P. Kara, S. Erensoy, U.S. Akarca, M. Mascini, M. Ozsoz, Talanta 56 (2002) 837.
[35] R.L. Mc Creery, K.K. Cline, in: P. Kissinger, W.R. Heineman (Eds.), Laboratory Techniques in Electroanalytical Chemistry, second ed., Marcel Dekker, 1996 (Chapter 10).
[36] R.C. Engstrom, Anal. Chem. 54 (1982) 2310.
[37] M.L. Pedano, G.A. Rivas, Biosens. Bioelectron. 18 (2003) 269.
[38] B. Meric, K. Kerman, D. Ozkan, P. Kara, M. Ozsoz, Electroanalysis 14 (18) (2002) 1245.
[39] J. Wang, A.N. Kawde, Anal. Chim. Acta 431 (2001) 219.
[40] Y. Ye, H.X. Ju, Biosens. Bioelectron. 21 (2005) 735.
[41] J. Wang, D. Xu, A. Erdem, R. Polsky, M.A. Salazar, Talanta 56 (2002) 931.
[42] H.F. Teh, H. Gong, X.D. Dong, X. Zeng, A.L.K. Tan, X. Yang, S.N. Tan, Anal. Chim. Acta 551 (2005) 23.
[43] M.H. Pournaghi-azar, M.S. Hejazi, E. Alipour, Anal. Chim. Acta 570 (2006) 144.
[44] J. Wang, J.R. Fernandez, L.T. Kubota, Anal. Chem. 70 (1998) 3699.

Available online at www.sciencedirect.com
ScienceDirect
Talanta 71 (2007) 1684–1689
Talanta
www.elsevier.com/locate/talanta

Ascorbate amperometric determination using conducting copolymers from aniline and *N*-(3-propane sulfonic acid)aniline

Jorge Yánez Heras, Ana F. Forte Giacobone, Fernando Battaglini *

INQUIMAE, Departamento de Química Inorgánica, Analítica y Química Física, Facultad de Ciencias Exactas y Naturales, Universidad de Buenos Aires, Ciudad Universitaria, Pabellón 2, C1428EHA Buenos Aires, Argentina

Received 30 May 2006; received in revised form 28 July 2006; accepted 30 July 2006
Available online 7 September 2006

Abstract

The sequential electrochemical polymerization of aniline and *N*-(3-propane sulfonic acid)aniline (PSA) is proposed to construct a sensor able to detect ascorbate at physiological conditions. Compared to poly(aniline) modified electrode, a device with improved conducting and electrochemical properties at neutral pH is obtained. The electrochemical copolymerization of the same starting materials is also carried out. For a PSA:aniline ratio of 10:90, a polymer with a similar electrochemical behavior to the one grown in the sequential mode is observed.

The detection of ascorbate was tested for both configurations at pH 7.2, the modified electrode is able to determine ascorbate at 0 mV versus Ag/AgCl; an optimized sensor constructed by sequential polymerization can easily detect ascorbate concentrations with a detection limit of 2.2 μM. Uric acid and dopamine does not interfere in the ascorbate determination.

Keywords: Poly(aniline); *N*-(3-Propane sulfonic acid)aniline; Ascorbate; Amperometric detection

1. Introduction

Ascorbate is a relevant biomolecule involved in the immune response, wound healing and the absorption of iron [1]; its concentration can be used to assess the stress in human as well as in plants [2,3]. It is present in many fruits and vegetables, and used in pharmaceutical preparations; therefore, its determination is important in many areas.

Ascorbic acid can be electrocatalytically oxidized at polyaniline electrodes; its detection using conducting polymer modified electrodes has been recently reviewed [4]. It has been shown that, in a slightly acidic solution, the anodic peak for electro-oxidation of ascorbic acid shifts from 0.36 V versus Ag/AgCl at a bare platinum electrode to 0.13 V versus Ag/AgCl at a polyaniline modified electrode [5]. Also, polyaniline modified electrodes can be used for ascorbate determination at neutral pH; an autocatalytic mechanism has been proposed to explain the ability of polyaniline to electrocatalyze the oxidation of ascorbate at pH conditions where PANI is present in its undoped and non-conducting form [6]. For this type of modified electrode, an operating potential window of 0.1–0.3 V was used and a 50 μM limit of detection was achieved, this detection limit is likely due to PANI protonation dependence with the analyte.

Poly(aniline) behaves as a conductor only in the half-oxidized form (emeraldine) when it is protonated. Above pH 5, the emeraldine deprotonates becoming an insulator. For a poly(aniline) film, the deprotonation of the emeraldine form is associated with the egress of both, protons and the associated anions from the film. This is only possible if the anions are small and mobile, for example chloride or bisulfate anions. If instead of mobile ions, long chain polymeric counter ions are used, they become trapped within the poly(aniline) film, and the overall process changes. As a consequence of this change, the conductivity of poly(aniline) can be maintained at a much higher pH [7]. This strategy has been used with several negatively charged polymers [8–12]. In particular, Bartlett and Wallace presented a poly(vinylsulfonate)/polyaniline composite electrode able to oxidize ascorbate at neutral pH using a working potential of 0.14 V versus Ag/AgCl [10].

Another approach that may aid the detection at neutral pH would be to modify the N atom in the backbone with an alkyl sulfonate group. Our group have modified PANI with 3-propane sultone to obtain a copolymer, poly(aniline-co-*N*-propane sulfonic acid aniline), with good conducting and electrochemical

* Corresponding author. Tel.: +54 11 45763358; fax: +54 11 45763341.
E-mail address: battagli@qi.fcen.uba.ar (F. Battaglini).

0039-9140/$ – see front matter © 2006 Elsevier B.V. All rights reserved.
doi:10.1016/j.talanta.2006.07.057

properties at physiological pH [13]. The synthesis of this copolymer involves two steps, the aniline electrochemical polymerization, followed by the chemical reaction between propane sultone and the PANI modified electrode. This second step could be troublesome if the reaction has to be carried out on small dimension electrodes. To overcome this drawback, it would be convenient to bind the propane sulfonate moiety to the polymer by electrochemical means.

To achieve that goal, the synthesis of *N*-(3-propane sulfonic acid)aniline (PSA) from propane sultone and aniline was carried out. The new aniline derivative was electrochemical polymerized in different conditions, in contrast to previous works in which propane sultone is reacted with PANI in solution [14] or in heterogeneous phase [13].

Through the electrochemical polymerization of PSA with aniline, the construction of modified electrodes able to work at physiological pH was achieved. The construction was carried out in a sequential order, first the electrochemical polymerization of aniline followed by the electrochemical polymerization of PSA. The modified electrode obtained presents an improved conducting behavior at neutral pH compared with PANI modified electrodes. Also, the copolymerization from a solution containing PSA and aniline in a molar ratio of 10:90 is able to produce a modified electrode with improved properties compared to polyaniline at neutral pH.

The modified electrodes are used as amperometric sensors for the detection of ascorbate. They are able to work at 0 mV versus Ag/AgCl with a limit of detection of 2.2 μM in the case of the sequential electrochemical polymerization. Furthermore, the presence of other electroactive compounds, like uric acid or dopamine, does not interfere in the ascorbate determination. In the case of uric acid, no signal is observed. For dopamine a signal at higher potentials is obtained, which is easily distinguishable from the ascorbate signal.

2. Experimental

2.1. Reagents

Aniline and propane sultone were from Aldrich. All other reagents used were analytical grade. Aniline was distilled prior to use.

2.2. Equipment

Electrochemical measurements were performed using a PINE Instruments AFRDE 5 bipotentiostat. Signals were recorded in a computer using a LabPC 1200 data acquisition card (Texas Instruments). A Ag/AgCl electrode was used as reference and Pt as the counter electrode. Three millimeter diameter glassy carbon electrodes and home-built dual carbon band electrodes [13] were used as working electrodes.

2.3. Conductivity measurements

The resistance of the polymers synthesized on the band electrodes was measured modifying a technique presented by Wrighton and co-workers [13,15]. A cell of two working electrodes, the dual carbon bands (WE), one reference electrode and one counter electrode is used. The two carbon bands are 12 μm apart from each other, separated by an insulating gap. The polymer grows on both WE until the two bands are joined by it. Then, the modified electrodes are immersed in a solution at a given pH. One of the WE (let us say WE1) is kept at a constant potential with respect to the reference, while the potential of the other WE (WE2) is swept up and down by 20 mV with respect to WE1. The current flowing through the cell is the result of the electrochemical process plus the current that flows between the two WE due to the potential difference between them. By analogy with a physical transistor, the current flowing between the two working electrodes is called the "drain current", the potential of WE1 with respect to the reference is the "gate voltage", and the potential of WE2 referred to WE1 is the "drain voltage". The current measured in any of the working electrodes is the sum of the current produced by a redox process and the current forced to flow between the two WE by the drain voltage (drain current). For such small potential changes (20 mV), the contribution to the current produced by the redox processes can be neglected with respect to the drain current. The current flowing through the polymer can be assumed to be the result of electronic conduction of the film, which is inversely proportional to the resistance. A source of error in the determination is the capacitive current, which can be avoided by stopping the voltage sweep in the positive (or negative) limit until the value of the current is constant.

2.4. Hydrodynamic techniques

A wall jet cell was made in acrylic, with a 0.5 mm nozzle and 1 mm nozzle to electrode distance. A 3 mm diameter glassy carbon electrode was employed. The counter electrode was part of the stainless steel outlet tubing, and the reference electrode was a Ag/AgCl electrode placed downstream. The working potential was set at 0 mV versus Ag/AgCl. The sample (10 mL) circulated continuously through the cell at 1.5 mL min^{-1}. For the flow injection system, a 200 μL loop was used with the same flow rate.

2.5. Synthesis of PSA

The synthesis of PSA was carried by dissolving 0.7 g of propane sultone in 2.5 mL of aniline under stirring at 30 °C. After a few minutes a white precipitate is formed and the product is recrystalized from methanol/acetone, giving a white powder. ^{1}H NMR; 500 MHz, D_2O; δ values were 2.15 (m, 2H), 2.95 (t, 2H), 3.55(t, 2H) and 7.5(m, 5H). M^+: 215.

2.6. Polymerization

Sequential polymerization was carried out by cyclic voltammetry between −0.2 and 0.85 V versus Ag/AgCl at 50 mV s^{-1}. The first step was carried out by cycling the electrode in a solution of 0.09 M aniline in 1.8 M H_2SO_4 for five times, unless stated otherwise; then, the electrode was rinsed with water and

immersed in a solution of 0.01 M PSA in 1.8 M H_2SO_4 and cycled at 50 mV s^{-1}; the number of cycles for this step is indicated in each experiment.

Electrochemical copolymerizations were carried out by cyclic voltammetry between −0.2 and 0.85 V versus Ag/AgCl at 50 mV s^{-1}, from a solution of PSA and recently distilled aniline in 1.8 M H_2SO_4 with a total concentration of co-monomers equal to 0.1 M.

The growth of the polymer on dual band electrodes was carried out by immersing the electrode in a 0.52 M aniline in 1.8 M H_2SO_4 solution at fixed potential of 0.8 V versus Ag/AgCl for 3 min. The union of the band was checked by conductance measurements in acid medium and then, the electrochemical polimerization of PSA was carried out.

2.7. Ascorbate detection

The determination of ascorbate was carried out in different ways. Cyclic voltammetry at 2 mV s^{-1} was used to establish the response and sensitivity to ascorbate and the effect of potential interferences of the different modified electrodes prepared. The results of these studies were used to choose the type of sensor and the working potential for the determinations carried out in the hydrodynamic techniques.

3. Results and discussion

3.1. Sensor construction and properties

The reaction of aniline with propane sultone produces the aniline derivative (Scheme 1) in a few minutes. The compound is soluble in water and methanol giving a colorless solution. The electrochemical response of this compound in acid medium is depicted in Fig. 1. It presents peak currents at 0.52 and 0.7 V and the signal increases with continuous cycling until the 8th cycle; then, the current begins to decay and the solution turns green, like emeraldine, which can be attributed to the formation of a soluble polymer.

Copolymerization of PSA with aniline was carried out from solutions with the following ratios of PSA:aniline: 75:25, 50:50, 25:75 and 10:90. The electrochemical polymerization of the three first solutions leads to cyclic voltammetries with peaks at 0.52 and 0.7 V, similar to the pure PSA. The growth rate of the polymer depends on the ratio of PSA:aniline; the higher is the proportion of PSA, the faster is the growth rate of the polymer. In all the cases the signal increases until the 12th cycle. However, unlike pure PSA, the signal remains stable, suggesting that the joint polymerization of PSA and aniline produces a

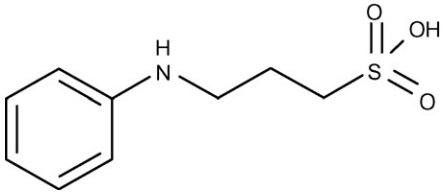

Scheme 1. Structure of *N*-(3-propane sulfonic acid)aniline (PSA).

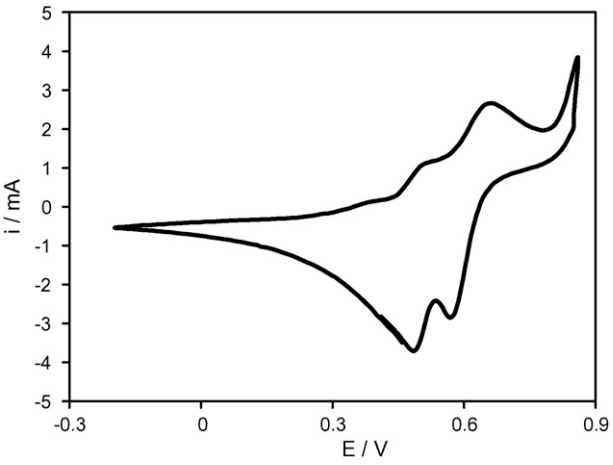

Fig. 1. Cyclic voltammetry of electropolymerized PSA on a glassy carbon electrode in 1.8 M sulfuric acid at 50 mV s^{-1}.

polymer that remains anchored to the electrode surface. In none of these cases, the typical current peak for the first oxidation process of PANI, at 0.24 V, is observed.

When a solution with a PSA:aniline ratio equal to 10:90 is used, the voltammogram shows two peaks in the first scans at 0.52 and 0.7 V versus Ag/AgCl; then, a peak at 0.25 V begins to grow faster than the others. The electrochemical response of this polymer after 20 scans is shown in Fig. 2. The presence of a broad new peak compared to the typical voltammogram of PANI indicates the incorporation of PSA as part of the electrically conducting polymer.

In the sequential polymerization method, PANI was grown by cycling the potential five times at 50 mV s^{-1} between −0.20 and 0.85 V (Fig. 3, gray line). Then, the electrode was immersed in a 10 mM PSA solution in 1.8 M sulfuric acid and cycled four times between the same potentials (Fig. 3, thin black line). It can be observed that the peak current at 0.25 V increases from 60 μA to practically 80 μA and a broad anodic peak around 0.5 V develops. If cycling is continued, after 7 cycles (Fig. 3, bold black line), the first anodic peak shifts to a higher potential

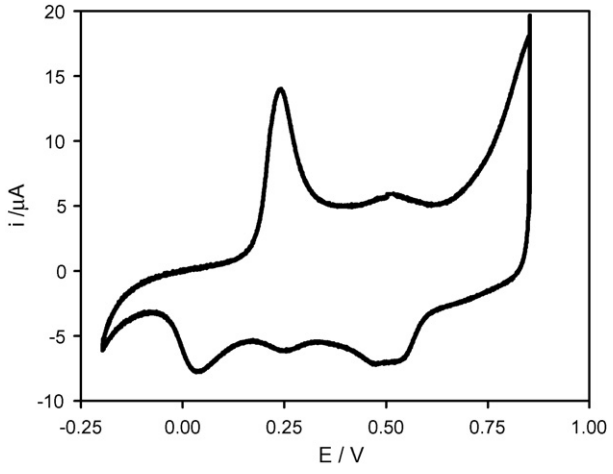

Fig. 2. Cyclic voltammetry in 1.8 M sulfuric acid of the polymerization product obtained from a solution containing 90 mM aniline and 10 mM PSA in 1.8 M H_2SO_4. Sweep rate: 10 mV s^{-1}.

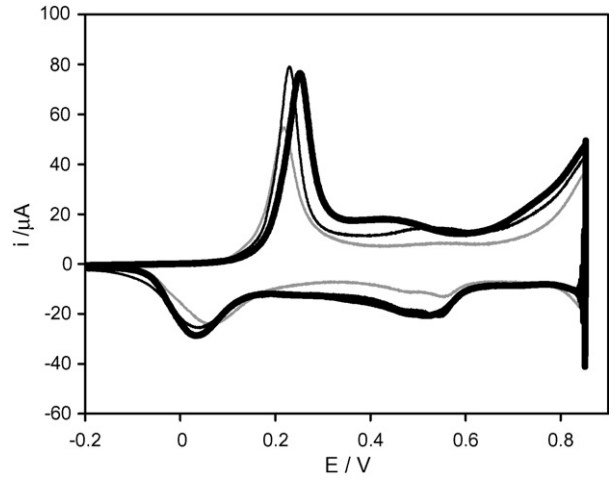

Fig. 3. Cyclic voltammetries in 1.8 M H_2SO_4 of PANI modified electrode (gray line), PANI + 4 cycles of PSA (thin black line) and PANI + 7 cycles of PSA (bold black line). Sweep rate: 10 mV s^{-1}.

but it does not increase further, suggesting that the oxidation process becomes slightly slower. In addition, a broader peak is observed in the range of 0.4–0.6 V. If the cycling of the potential in presence of PSA continues after 15 cycles, the first anodic peak does not change, while the broad peak between 0.4 and 0.6 increases and the voltammogram shows a larger capacitive response (data not shown).

The modified electrodes obtained either by copolymerization from a PSA:aniline solution (10:90) or by sequential polymerization, show a quasi-reversible behavior at pH 7.2. In both cases, the electrodes show a stable signal; the peak currents are around 70% of the original values for both types of electrodes after 40 min of cycling between −0.2 and 0.6 V at 50 mV s^{-1}. Fig. 4 depicts the quasi-reversible response of an electrode modified in sequential order (PSA 7 cycles). The resistance of the same polymer grown between two band electrodes can also be observed;

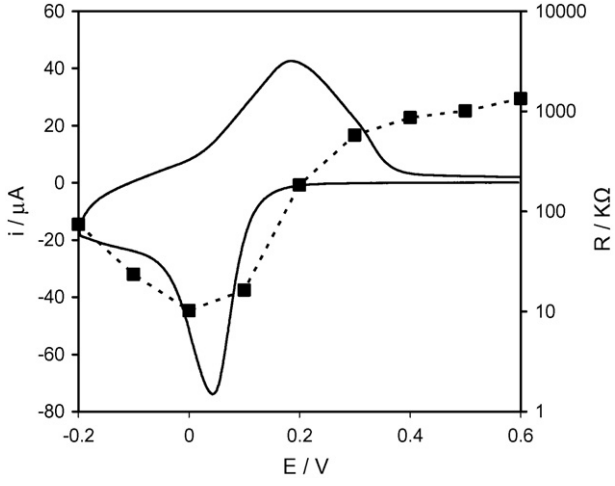

Fig. 4. Cyclic voltammetry of a modified electrode by subsequent polymerization of aniline and PSA (7 cycles) in 0.1 M phosphate buffer pH 7.2 at 10 mV s^{-1} (currents on left axis); and resistance behavior of the same polymer in 0.1 M phosphate buffer pH 7.2, grown between two band electrodes at a distance of 12 μm (right axis).

the conducting potential region follows the oxidation process for the formation of emeraldine. The maximum conductivity of this polymer decreases 25 times from acid to neutral medium.

3.2. Ascorbate determination

The equilibrium potential of the couple ascorbate–dehydroascorbate is −0.139 V versus Ag/AgCl, but oxidation at bare glassy carbon or platinum electrodes requires potentials of 0.4 and 0.6 V, respectively. These high over potentials result in electrode fouling, poor reproducibility and low selectivity when these materials are used for analytical applications. Due to these problems several groups have developed modified electrodes to catalyze the electrochemical oxidation of ascorbate; among them, Bartlett and Wallace have shown that it is possible to oxidize ascorbate at lower potentials using a polyaniline–polyvinylsulfonate composite coated electrode [10].

For all the electrode configurations presented in this work, a catalytic response to the presence of ascorbate can be observed. As an example, Fig. 5 shows a cyclic voltammogram in buffer at pH 7.2, for a modified electrode constructed in a sequential mode (dotted line). When ascorbic acid is added to a final concentration of 125 μM, a new peak at 25 mV appears due to its oxidation (solid line), while the cathodic wave of PANI dramatically decreases due to its reduction by ascorbate.

Cyclic voltammetry was also used to study the sensitivity of the ascorbate response for the different electrode configurations. The electrode modified by copolymerization of aniline and PSA shows the poorest response and worst linear range (white squares in Fig. 6). The response improves in the case of the electrodes modified by subsequent polymerizations. In all of them, PANI was grown by cycling the potential five times between −0.2 and 0.85 V at 10 mV s^{-1}; then, different amounts of PSA were polymerized. The best sensitivity and linear range is observed in those electrodes where the polymerization of PSA was carried

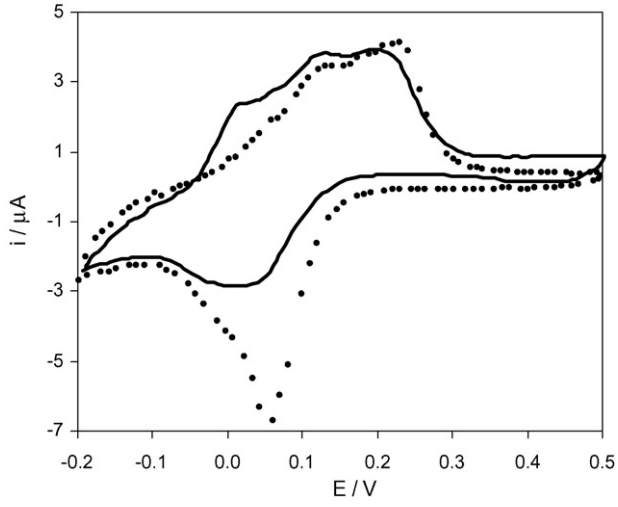

Fig. 5. Cyclic voltammetry for a modified electrode by subsequent polymerization of aniline and PSA (7 cycles) in 0.1 M phosphate buffer pH 7.2 (dotted line), in the presence of 125 μM ascorbate (solid line). Sweep rate: 2 mV s^{-1}.

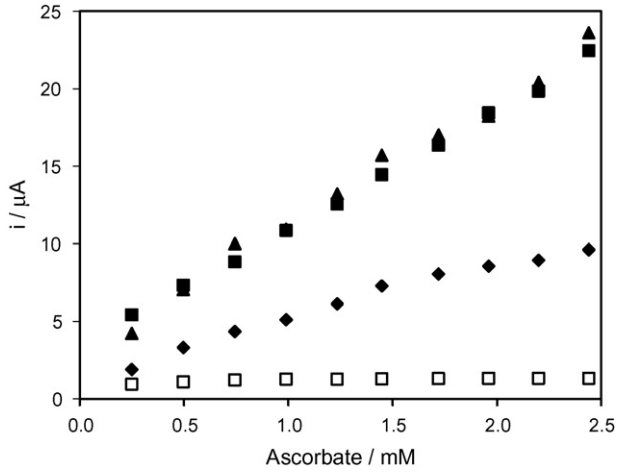

Fig. 6. Ascorbate response for different electrode configurations: copolymer from aniline and PSA (90:10) (white squares); PANI + 4 PSA cycles (diamonds); PANI + 7 PSA cycles (black squares); PANI + 15 PSA cycles (triangles). The values plotted are the currents observed at 20 mV vs. Ag/AgCl from a cyclic voltammetry at 2 mV s^{-1}.

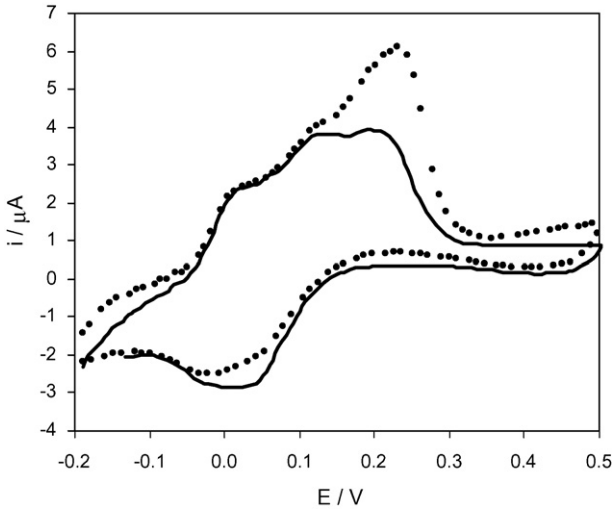

Fig. 7. Cyclic voltammetry for a modified electrode by subsequent polymerization of aniline and PSA (7 cycles) in the presence of 125 µM ascorbate (solid line) and 125 µM dopamine (dotted line). Sweep rate: 2 mV s^{-1}.

out by 7 and 15 cycles (circles and triangles in Fig. 6). It can be observed for the last two electrodes that the response is practically the same. This is probably due to the fact that the addition of PSA to the polymer does not scale linear with the number of cycles. As it is was stated before, after 7 cycles the peak corresponding to 0.25 V does not increase further, indicating that the electroactive part of the polymer that takes part in the ascorbic detection remains the same.

The effect of possible interferences was studied, the response to ascorbate in the presence of uric acid and dopamine was determined. The modified electrode constructed by the polymerization of aniline (5 cycles) followed by the polymerization of PSA (7 cycles) was used in these experiments. The presence of uric acid did not affect the response of the modified electrode in a working potential range from −0.2 to 0.5 V, in spite of uric acid presents an oxidation peak potential at 0.4 V on a bare carbon electrode. A similar result was obtained by O'Connell et al. [16] using only polyaniline. These authors suggested that the polyaniline layer is acting as a permselective membrane avoiding the oxidation of uric acid on the electrode surface. In Fig. 7, the cyclic voltammogram for ascorbate at pH 7.2 (solid line) is compared to the response for ascorbate plus dopamine, at the same concentrations (dotted line). Dopamine is oxidized at higher potentials, with no effect on the ascorbate signal, allowing the possibility of simultaneous determination of both species, e.g. by means of square wave voltammetry [17].

A similar modified electrode than the one used for the interferences studies was tested for ascorbate determinations at low concentrations. In this case the working potential was fixed at 0 mV. The electrode was part of a wall jet cell with the sample continuously circulating. The calibration curve presents a linear range from 5 to 50 µM (Fig. 8). Table 1 shows the equation obtained for the calibration graph and the regression coefficient. The detection limit was calculated on the basis of 3σ (σ being the residual standard deviation of the intercept), yielding a value of 2.2 µM.

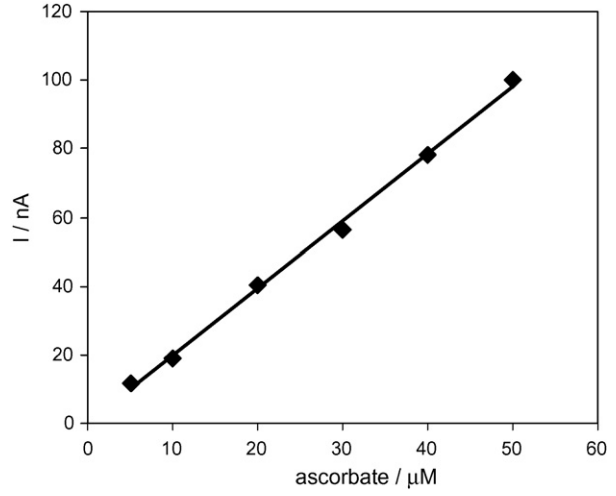

Fig. 8. Ascorbate amperometric response in a flow system. Applied potential: 0 mV vs. Ag/AgCl, flow rate 1.5 mL min^{-1}. Sensor constructed by consecutive electrochemical polymerization of aniline and PSA (7 cycles).

The response in a flow injection system with a 200 µL loop was also studied. For this experiment PANI was grown by cycling the electrode three times at 10 mV s^{-1}, and then in presence of PSA four times more. The sensor, constructed in these conditions, shows good stability at pH 7.2 and the time response is faster than for the other electrodes previously shown, since a

Table 1
Parameters for the calibration curve shown in Fig. 8

Parameter	Value
Slope (nA μM^{-1})	1.96
Intercept (nA)	2.7
Correlation coefficient	0.9970
Limit of detection (µM)	2.2
Linear range (µM)	5–50

thinner layer is used. Using this system and a linear range up to 100 μM was obtained.

4. Conclusions

The sequential polymerization of aniline and PSA produces a polymer with improved conducting and electroactive properties compared to PANI at pH 7. These properties make them very suitable to determine ascorbate at physiological conditions, which reacts with the polymer at lower potentials compared to glassy carbon, platinum or other modified electrodes presented in the literature. The low potential value for the ascorbate oxidation allows its determination in presence of uric acid and dopamine.

In contrast to our previous report where PANI was chemically modified with propane sultone [13], these modified electrodes can be built completely by electrochemical means. Therefore their size can be severely reduced and they can be part of an array of different modified electrodes. For the last, the construction of the modified electrode would not even require the handling of small volumes, since it will only need to impose the right potential to the element of the array which is going to be modified.

Acknowledgements

The financial support of Universidad de Buenos Aires and ANPCyT is acknowledged.

References

[1] R. Berkow, A.J. Fletcher (Eds.), El Manual Merck de Diagnóstico y Terapéutica, 9th ed., Mosby/Doyma Libros, Barcelona, Spain, 1996, p. 1091 (in Spanish).
[2] P.L. Conklin, E.H. Willlams, E.L. Last, Proc. Natl. Acad. Sci. U.S.A. 93 (1996) 9970–9974.
[3] I. Koshiishi, T. Imanari, Anal. Chem. 69 (1997) 216–220.
[4] A. Malinauskas, R. Garjonyte, R. Mazeikiene, I. Jureviciute, Talanta 64 (2004) 121–129.
[5] S.L. Mu, J.Q. Kan, Synth. Meth. 132 (2002) 29–33.
[6] I. Jurevciute, K. Brazdziuviene, L. Bernotaite, B. Salkus, A. Malinauskas, Sens. Actuators B 107 (2005) 716–721.
[7] P.N. Bartlett, Y. Astier, J. Chem. Soc., Chem. Commun. (2000) 105–112.
[8] J. Liu, S. Tian, W. Knoll, Langmuir 21 (2005) 5596–5599.
[9] O.A. Raitman, E. Katz, A.F. Bückmann, I. Willner, J. Am. Chem. Soc. 124 (2002) 6487–6496.
[10] P.N. Bartlett, E.N.K. Wallace, Phys. Chem. Chem. Phys. 3 (2001) 1491–1496.
[11] P.N. Bartlett, E. Simon, Phys. Chem. Chem. Phys. 2 (2000) 2599–2606.
[12] P.N. Bartlett, E.N.K. Wallace, J. Electroanal. Chem. 486 (2000) 23–31.
[13] D. Raffa, K.T. Leung, F. Battaglini, Anal. Chem. 75 (2003) 4983–4987.
[14] S.A. Chen, G.-W. Hwang, J. Am. Chem. Soc. 117 (1995) 10055–10062.
[15] E.W. Paul, A.J. Ricco, M.S. Wrighton, J. Phys. Chem. 89 (1985) 1441–1447.
[16] P.J. O'Connell, C. Gormally, M. Pravda, G.G. Guilbault, Anal. Chim. Acta 431 (2001) 239–247.
[17] P.R. Roy, T. Okajima, T. Ohsaka, Bioelectrochemistry 59 (2003) 11–19.

Available online at www.sciencedirect.com
ScienceDirect
Talanta 71 (2007) 1524–1529
Talanta
www.elsevier.com/locate/talanta

Application of thiophene-2-carbaldehyde-modified mesoporous silica as a new sorbent for separation and preconcentration of palladium prior to inductively coupled plasma atomic emission spectrometric determination

Mohammad Reza Jamali [a], Yaghoub Assadi [b,*], Farzaneh Shemirani [a], Masoud Salavati-Niasari [c]

[a] *School of Chemistry, University College of Science, University of Tehran, Tehran, Iran*
[b] *Department of Analytical Chemistry, Faculty of Chemistry, Iran University of Science and Technology, Tehran, Iran*
[c] *Department of Chemistry, Faculty of Science, University of Kashan, Kashan, Iran*

Received 15 May 2006; received in revised form 17 July 2006; accepted 17 July 2006
Available online 22 August 2006

Abstract

A new and efficient method was described for an easy synthesis of functionalized mesoporous silica (MCM-41) using thiophene-2-carbaldehyde. This new chemically bonded analytical reagent was used as an effective sorbent for the solid phase extraction of palladium(II) ion from aqueous solutions. Conditions for effective adsorption of trace levels of palladium concentration were optimized with respect to different experimental parameters in batch process. Thiourea solution could efficiently elute adsorbed palladium(II) ion from the surface of the sorbent which then was determined by inductively coupled plasma atomic emission spectrometer (ICP-AES).

Common coexisting ions did not interfere with the separation and determination. The preconcentration factor was 100 (1 ml elution volume) for a 100 ml sample volume. The limit of detection of the proposed method is 0.2 ng ml^{-1}. The maximum sorption capacity of sorbent under optimum conditions has been found to be 5 mg of palladium per gram of sorbent. The relative standard deviation under optimum conditions was 3.2% ($n = 10$). Accuracy and application of the method was estimated by using test samples of natural and synthetic water spiked with different amounts of palladium(II) ion.

Keywords: Preconcentration; Palladium; Modified mesoporous silica (MCM-41); Solid phase extraction; ICP-AES

1. Introduction

Noble metals, particularly palladium, find an extensive use in the electrical industry as contacts in telephone relay and printed circuits as girds for electronic tubes and electrodes for high quality spark plugs. Palladium affects the environment to an increasing degree as a new pollutant, especially by the technical use of catalysts containing active palladium metal [1]. This metal may enter the environment and interact with complexing materials, such as humic substances [2]. Palladium has no biological role and all palladium compounds should be regarded as highly toxic and carcinogenic. However, palladium chloride was formerly prescribed as a treatment for tuberculosis without too many bad side effects. There is currently much discussion about its bioavailability and toxicology [3]. Thus, due to its increasing use, on the one hand, and the toxicity of Pd(II) compounds to mammals, fish and higher plants, on the other hand, the separation and determination of palladium is of special interest in environmental analysis.

Low concentration of Pd in industrial (μg g^{-1} level) and environmental samples (ng g^{-1} level) together with the complexity of the matrix cause much interference during the determination of palladium. Therefore, the application of highly sensitive techniques, ICP-AES [4,5], ICP-MS [6,7], GF AAS [8,9], coupled with a separation and enrichment procedure is necessary [10–12].

Liquid–liquid extraction has been widely used for separation and preconcentration of palladium [13–15]. Because of some disadvantages of solvent extraction methods such as emulsion formation, different extracting efficiencies and low sensitivity, much interest has been recently focused on repairing conventional solvent extraction methods for isolating

* Corresponding author. Tel.: +98 21 77491204; fax: +98 21 77491204.
E-mail address: y_assadi@iust.ac.ir (Y. Assadi).

0039-9140/$ – see front matter © 2006 Elsevier B.V. All rights reserved.
doi:10.1016/j.talanta.2006.07.034

environmental pollutants with solid phase extraction (SPE) techniques.

SPE has been demonstrated to be a very effective preconcentration method when applied prior to spectrometric determination. The analytes are partitioned between a solid and liquid phase based on the affinity to the solid phase. Compared with liquid–liquid extraction, methods utilizing solid sorbents are simpler and faster, reduce organic solvent consumption and yield higher enrichment factors [16–18]. Different solid phase extractors such as Amberlite XAD resins [19,20], polyurethane foam [21], activated carbon [22] and silica gel [23,24] with chelating groups have been the most widely used collectors. In spite of these collectors, the synthesis of adsorbents for removal palladium ions from water and wastewater samples is a continuing research objective of environmental pollution control processes [25–29].

Recently, a new family of ordered mesoporous materials has been obtained. These ordered mesoporous materials show a large BET (a method for determination of surface area by the physical adsorption of gas molecules on a solid surface) surface area, high pore porosity, controllable and narrowly distributed pore sizes and an ordered pore arrangement [30,31]. They are synthesized with surfactants, used as template and can be functionalized later on with different organic groups [32–36]. The development of functionalized mesoporous materials for adsorption applications has generated a considerable interest. Among the variety of adsorption applications, the preparation of highly effective adsorbents for heavy metal ions trapped by the grafting or incorporation of ligands into mesoporous materials is clearly one of the most promising methods for environmental clean-up [34–39]. In particular, materials whose surfaces have been functionalized with groups containing sulfur and nitrogen as active donor atoms have high selectivity for platinum metals [40]. For this purpose, we used thiophene-2-carbaldehyde in order to react with amine group of 3-aminopropyl triethoxy silane (APS) to produce a sorbent that have S and N as active donor atoms. In this study, we report the synthesis of this new sorbent and its application as a selective sorbent for separation, preconcentration and determination of palladium by inductively coupled plasma atomic emission spectrometry.

2. Experimental

2.1. Apparatus

A Shimadzu (model: 7000, Kyoto, Japan) inductively coupled plasma atomic emission spectrometer (ICP-AES) equipped with the mini-torch-type and conventional pneumatic concentric nebulizer was used for the determination of palladium. The operation conditions and analytical wavelength are summarized in Table 1.

Separation of sorbent was assisted using a centrifuge (centurion scientific model: K 240R, West Sussex, U.K.).

The pH values were measured with a Metrohm pH-meter (model: 713, Herisau, Switzerland) supplied with a glass-combined electrode.

Table 1
ICP-AES operating conditions for axial view

Parameters	Values
Incident power (W)	1000
Plasma gas (Ar) flow rate ($l\,min^{-1}$)	8.0
Auxiliary gas (Ar) flow rate ($l\,min^{-1}$)	0.6
Nebulizer gas (Ar) flow rate ($l\,min^{-1}$)	0.6
Sample uptake flow rate ($ml\,min^{-1}$)	1
Observation position (mm)	8.0
Integration time (s)	5
Wavelength (nm)	340.458

2.2. Reagents and solutions

All reagents used were of analytical grade. All solutions were prepared using doubly distilled water. Organic solvents were of HPLC grade and were purchased from Aldrich (Chemical Co., Milwaukee, WI, USA). Thiophene-2-carbaldehyde and 3-aminopropyl triethoxy silane were purchased from Merck (Darmstadt, Germany).

Stock solution of palladium ($1000\,mg\,l^{-1}$) was prepared by dissolving an appropriate amount of metallic Pd in aqua regia. Working solutions were prepared from the stock solution by serial dilutions with doubly distilled water. A stock standard acetic acid/acetate buffer solution ($0.1\,mol\,l^{-1}$, pH 4.0) was prepared by dissolving an appropriate amount of sodium acetate in doubly distilled water and neutralizing to pH 4.0 with hydrochloric acid.

The pipettes and vessels used for trace analysis were kept in 10% nitric acid for at least 24 h and subsequently washed four times with deionized water before use.

2.3. Preparation of MCM-41 and aminopropyl modified MCM-41 (APS-MCM-41)

Mesoporous molecular sieve MCM-41 was prepared according to the reported method [41]. Modification of the prepared MCM-41 was performed as follows (Scheme 1A): MCM-41 (2.0 g) was suspended in dry toluene (70 ml), then (3-aminopropyl)triethoxysilane (APS) (1.0 g) was added under dry nitrogen atmosphere, and the mixture was refluxed for 12 h. The solid was filtered, washed with dichloromethane and ethanol and dried. It was then soxhlet extracted with a mixture of ethanol and dichloromethane (1:1) to remove the silylating reagent residue, and later it was vacuum dried at 343 K. The characterization of APS-MCM-41 was performed using FT-IR spectroscopy and X-ray diffraction. In the X-ray diffraction pattern of the prepared material the peak (1 0 0) of the parent MCM-41 was preserved but the other peaks disappeared because of the incorporation of organic groups inside the channels of MCM-41. In addition, nitrogen sorption analysis of the prepared material showed a great surface area ($753\,m^2\,g^{-1}$) indicating the preservation of the mesoporosity of the material.

2.4. Preparation of Thio-APS-MCM-41

For the preparation of MCM-41 containing thiophene-2-carbaldiminato group (Scheme 1B), APS-MCM-41 (2.0 g) was

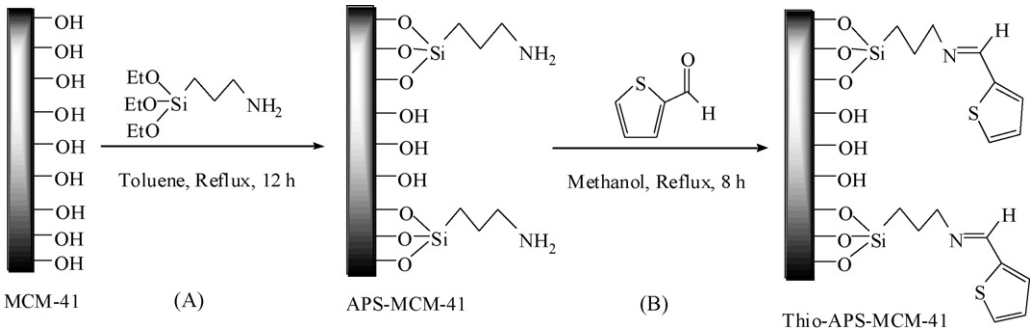

Scheme 1. (A) Preparation of APS-MCM-41 and (B) preparation of Thio-APS-MCM-41.

suspended in 100 ml of methanol, and to this mixture, excess of thiophene-2-carbaldehyde (1.07 g, 9.58 mmol) was added and refluxed for 8 h. The solid was filtered, dried and then soxhlet extracted with ethanol then dried under vacuum at 343 K. FT-IR spectrum shows that the thiophene-2-carbaldiminato group was covalently grafted to the silica successfully (characteristic C=N stretching at 1650 cm^{-1}) after the condensation process. In addition, X-ray diffraction showed the preservation of the support material during the modification.

2.5. Procedure

A batch-wise process was employed for the extraction and preconcentration of palladium. Extraction was performed in test tubes containing Pd^{2+} in 10 ml acetate buffered solution (pH 4.0). Fifty milligrams modified MCM-41 (Thio-APS-MCM-41) was added into the solution. After that, the mixture was shaken manually for an appropriate time to extract palladium completely from the solution. Finally, test tubes were placed in centrifuge and separation of sorbent was achieved by centrifugation for 2.0 min at 3500 rpm. The bulk aqueous phase was removed with a pipette and any residual aqueous phase was easily decanted. The back extraction was performed using 1.0 ml of 1.0 mol l^{-1} thiourea solution. The palladium concentration was determined by ICP-AES.

3. Results and discussion

Some preliminary experiments were carried out in order to investigate the extraction of palladium by the modified MCM-41 and non-modified MCM-41 from solution. The results showed that non-modified MCM-41 cannot extract Pd^{2+} from solution but modified MCM-41 can extract it quantitatively.

3.1. Effect of pH

The effect of pH on the extraction of Pd^{2+} from water samples was studied in the pH range of 1.0–8.0. The higher pH values were not studied because functionalized mesoporous silicates were not stable in alkali solutions due to the breaking of the Si–O–Si bonds by hydroxide ions attack [42]. pH of the solution was adjusted at the required value by adding 1.0 mol l^{-1} sodium hydroxide and/or 1.0 mol l^{-1} nitric acid. As can be seen in Fig. 1, extraction was nearly constant and quantitative in the pH range of 2–8.0. At lower pH (<2), the nitrogen atoms in Thio-APS-MCM-41 are protonated, so the stability of complex formation between the sorbent and Pd^{2+} is reduced. Therefore, the extraction of palladium decreased. Hence, pH of 4.0 was chosen as the optimum pH for extraction.

3.2. Choice of eluent

In order to choose the most effective eluent for desorbing palladium ion from the sorbent surface aliquots of 10 ml of 0.1 μg ml^{-1} palladium ion solution was contacted with 50.0 mg of modified MCM-41. A series of selected eluent solution such as nitric acid, hydrochloric acid, acetic acid, sodium thiosulfate and thiourea was used. A total of 10.0 ml of 0.1 mol l^{-1} of the above mentioned eluents were used for desorbing the adsorbed palladium ion. The amount of palladium ion back-extracted into the liquid phase by each eluent was measured using ICP-AES. Percent recoveries of palladium ion were calculated for each sample. The results (Fig. 2) showed that recovery was the best when thiourea was used as eluent. Also, higher concentrations of hydrochloric and nitric acid (0.5 and 1.0 mol l^{-1}) solutions were tested and the results showed the recovery of palladium was not quantitative. Therefore, thiourea was selected as eluent.

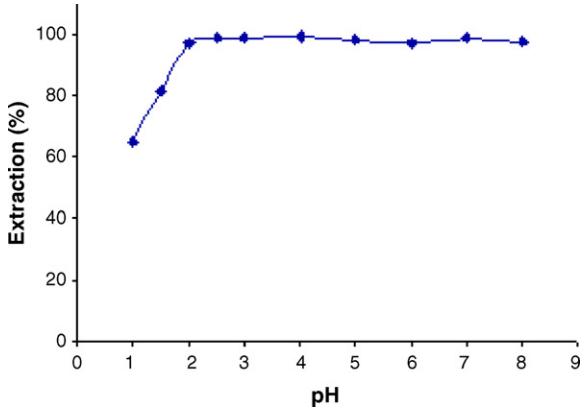

Fig. 1. Effect of pH on the extraction of palladium. Experimental conditions: source, 10 ml of 0.1 μg ml^{-1} Pd^{2+} solution; amount of sorbent, 50.0 mg.

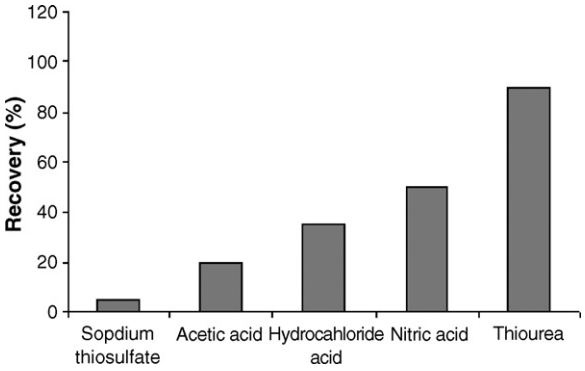

Fig. 2. Effect of nature of eluent on the recovery of palladium. Experimental conditions: source, 10 ml of 0.1 μg ml^{-1} Pd^{2+} solution at pH 4.0; sorbent 50.0 mg.

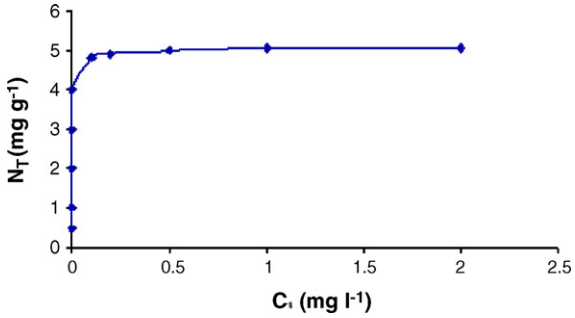

Fig. 3. Adsorption isotherm of palladium ion on sorbent.

3.3. Effect of eluent concentration

The influence of the concentration of thiourea on desorption of palladium ion was studied. For desorbing 1.0 μg palladium ion, already adsorbed on 50.0 mg of sorbent, 1.0 ml of different concentration of eluent (thiourea) have been used. At a concentration of more than 0.7 mol l^{-1}, thiourea desorbs (recovery of almost 100%) palladium ion completely from the sorbent surface. A concentration of 1.0 mol l^{-1} of thiourea was selected for further studies.

3.4. Effect of the sample volume

In order to explore the possibility of concentrating low concentrations of palladium from large volumes, the maximum applicable volume must be determined. For this purpose, the effect of the sample solution volume on the recovery was studied by keeping the total amount of Pd^{2+} uptake constant (1.0 μg). The quantitative recoveries were obtained for sample volume of ≤100 ml. Therefore, the concentration factor was 100 for Pd^{2+} since the final elution volume was 1.0 ml.

3.5. Effect of the amount of Thio-APS-MCM-41

To test the effect of the amount of modified MCM-41 on quantitative retention of analyte different amounts of sorbent (range from 2.0 to 200.0 mg) were added into the solution following the experimental method. The results showed that the extraction of Pd^{2+} was quantitative by using only 10.0 mg of modified MCM-41.

Subsequent extraction experiments were carried out with 50.0 mg of Thio-APS-MCM-41 in order to achieve higher capacity and to account for other extractable species.

3.6. Adsorption capacity

The capacity of the sorbent is an important factor that determines how much sorbent is required to remove a specific amount of metal ions from the solution quantitatively. For investigation of adsorption isotherm of palladium ion, the same volumes of palladium ion solution with different concentrations of palladium ion were contacted with 0.1 g of sorbent in the batch mode. Then, the concentration of the remaining palladium in the solution was determined by ICP-AES. The adsorption isotherm that is the number of microgram absorbed per gram of adsorbent (N_f) versus the equilibrium concentration of cation (C_s) is shown in Fig. 3. According to these results, the maximum amount of palladium that can be sorbed by Thio-APS-MCM-41 was found to be 5 mg g^{-1} at pH 4.0.

3.7. Effect of equilibrium time

In order to investigate the effect of shaking time on the extraction efficiency, extraction for a series of solutions containing 1.0 μg Pd^{2+} were carried out. The results showed that the shaking time (from 20 to 300 s) has no effect on the extraction efficiency of palladium and the extraction was quantitative.

Although the extraction process can be continued during the centrifugation, however, the results showed that extraction was quantitative and very fast in all cases. Thus, the mixtures have been shaken for 20 s to reach equilibrium in the subsequent experiments.

3.8. Effect of ionic strength

The influence of ionic strength on the extraction of palladium was studied in the potassium nitrate solution with various concentrations from 0.01 to 1.0 mol l^{-1}. Results have shown that ionic strength has no considerable effect upon extraction efficiency up to 1.0 mol l^{-1} of KNO_3. These observations showed the specific tendency of Thio-APS-MCM-41 for Pd^{2+} and the possibility of using this method for separation of palladium from highly saline solutions.

3.9. Effect of coexisting ions

The effects of common coexisting ions in natural water samples on the recovery of palladium were studied. In these experiments, 10 ml of solutions containing 0.1 μg ml^{-1} of palladium and various amounts of interfering ions were treated according to the recommended procedure. An ion was considered to interfere when its presence produced a variation in the extraction recovery of sample more than ±5%. The results showed that, in excess of 10,000-fold Li^+, K^+, Na^+, Ca^{2+}, Mg^{2+}, Ba^{2+}, Sr^{2+} and 1000-fold Cl^-, Br^-, SO_4^{2-}, Ag^+, Co^{2+}, Cd^{2+}, Ni^{2+}, Zn^{2+},

Mn^{2+}, Pb^{2+}, Al^{3+}, Cr^{3+}, Fe^{3+} and Pt^{4+} ions had no significant interferences in the extraction and determination of palladium. As can be seen, Thio-APS-MCM-41 has shown a high tolerance limit for alkali and alkaline earth metals. This is particularly useful for the analysis of palladium in natural water samples, for example, seawater, which contain large amounts of alkali and alkaline earth metal ions.

3.10. Reusability and stability of Thio-APS-MCM-41

Reusability is one of the key parameters to assess the effectiveness of a sorbent. A series of sorption/desorption experiments were performed to understand the reusability of the synthesized Thio-APS-MCM-41. After sorption, the sorbent was treated with 1.0 mol l^{-1} thiourea to desorb Pd^{2+} and this sorption/desorption procedure was repeated five times. After each desorption step, the sorbent was washed with doubly distilled water to remove thiourea and condition sorbent. It was determined that there was no decrease in sorption capacity after five consecutive uses of 50.0 mg of modified MCM-41.

On storing for a year under dark and dry conditions, the stability of sorbent was excellent and adsorption capacity did not change significantly.

3.11. Real sample analysis and analytical performance

To assess the capability of the method for real samples with different matrices containing varying amounts of diverse ions, the method was applied to the separation, preconcentration and determination of palladium from 100 ml of water samples. According to the results, the concentration of palladium in analyzed water samples was below the LOD of the method. The suitability of the proposed method for the analysis of natural water samples was checked by spiking samples with 5.0 and 10.0 ng ml^{-1} of palladium. Good recoveries (97–102%) were achieved for all analyzed samples. The data obtained with the proposed method were presented in Table 2. The results indicate that the proposed method can be reliably used for the determination of palladium in various matrices.

The limit of detection (LOD) and the limit of quantification (LOQ) were calculated as the amount of analyte necessary to yield a signal equal to three times (3σ) and ten times (10σ) the standard deviation of the blank signals, respectively. Using sample volume of 100 ml a LOD of 0.2 μg l^{-1} and a LOQ of 1.0 μg l^{-1} were obtained for the determination of palladium. Ten replicate extraction and measurement of 1.0 μg of Pd^{2+} ion in 100 ml water solution gave a R.S.D. of 3.2%. Calibration graph was obtained using preconcentration of 100 ml of standard solutions buffered at pH 4.0 with 50 mg of sorbent. For this purpose, standard solutions containing palladium ion in the range of 1–1000 μg l^{-1} were examined by the proposed procedure and it was observed that calibration curve were linear in this range. The regression equation was $I = 0.0034C$ (μg l^{-1}) + 0.0008 and the correlation coefficient was 0.9988.

Table 2
Determination of Pd^{2+} in water samples

Sample	Pd^{2+} spiked (ng ml^{-1})	Pd^{2+} detected (ng ml^{-1})	Recovery (%)
Sample 1[a]	5.0	4.9 (3.1)[b]	98
	10.0	9.8 (3.5)	98
Sample 2[c]	5.0	5.0 (2.8)	100
	10.0	9.9 (3.2)	99
Tap water[d]	0.0	n.d.[e]	—
	5.0	5.1 (2.9)	102
	10.0	9.9 (3.3)	99
River water[f]	0.0	n.d.	—
	5.0	5.0 (3.1)	100
	10.0	10.1 (3.6)	101
Sea water[g]	0.0	n.d.	—
	5.0	4.9 (3.2)	98
	10.0	9.7 (3.8)	97

[a] Cu^{2+}, Co^{2+}, Cd^{2+}, Fe^{3+}, Ni^{2+}, Cr^{3+}, 5000 ng ml^{-1} of each cation; K^+ and Li^+, 10,000 ng ml^{-1} of each.
[b] R.S.D of three replicate experiments.
[c] Cu^{2+}, Co^{2+}, Cd^{2+}, Fe^{3+}, Ni^{2+}, Cr^{3+}, 2500 ng ml^{-1} of each cation; K^+ and Li^+, 5000 ng ml^{-1} of each.
[d] From drinking water system of Tehran.
[e] Not detected.
[f] Tajan river water, Sari, Iran.
[g] Caspian sea water.

4. Conclusion

Synthesis of a new sorbent through the functionalization of MCM-41 with thiophene-2-carbaldehyde has been described and shown to be an alternative and efficient route for separation/preconcentration purpose in the determination of palladium in various water samples. This sorbent has high capacity, good stability and fast adsorption and desorption kinetics.

High preconcentration factor was obtained easily by this method. The proposed method can be applied to environmental and/or other samples having Pd levels higher than the detection limit of the method. In future, an attempt to use a flow-injection technique with on-line sample separation/preconcentration for Pd is predicted not only to enhance the sensitivity but also to decrease the analysis time.

Acknowledgements

The author thanks the research council at the University of Tehran and Iran University of Science and Technology for financial support.

References

[1] S. Daniel, J.M. Gladis, T.P. Rao, Anal. Chim. Acta 488 (2003) 173.
[2] T. Hees, B. Wenclawiak, S. Lusting, P. Schramel, M. Schwarzer, M. Schuster, D. Verstraete, R. Dams, E. Hemers, Environ. Sci. Pollut. Res. 5 (1998) 105.
[3] S.D. Lee, Biochemical Aspects of Environmental Pollutants, Ann Arbor Science Publishers, Ann Arbor, 1980.
[4] P. Kovacheva, R. Djingova, Anal. Chim. Acta 464 (2002) 7.
[5] Y. Wu, B. Hu, Z. Jiang, Sh. Chen, J. Anal. At. Spectrom. 17 (2002) 121.

[6] K. Benkhedda, B. Dimitrova, H.G. Infante, E. Ivanova, F.C. Adoms, J. Anal. At. Spectrom. 18 (2003) 1019.
[7] M. Moldovan, M.M. Gómez, M.A. Palacios, Anal. Chim. Acta 478 (2003) 209.
[8] K. Boch, M. Schuster, G. Risse, M. Schwarzer, Anal. Chim. Acta 459 (2002) 257.
[9] P. Anderson, C.M. Davidson, D. Littlejohn, M.A. Ure, C.A. Shand, M.V. Cheshire, Anal. Chim. Acta 327 (1996) 53.
[10] B. Godelewska-Zylkiewicz, Microchim. Acta 147 (2004) 189.
[11] L. Bencs, K. Ravindra, R.V. Grieken, Spectrochim. Acta B 58 (2003) 1723.
[12] K.H. Ek, G.M. Morrison, S. Rauch, Sci. Total Environ. 334–335 (2004) 21.
[13] M. Schuster, Fresenius J. Anal. Chem. 342 (1992) 791.
[14] A.P. Paiva, Solvent Extr. Ion Exch. 18 (2000) 223.
[15] Z. Marczenko, in: M. Masson (Ed.), Separaction and Spectrophotometric Determination of Elements, John Wiley & Sons, New York, 1986.
[16] S. Mitra, Sample Preparation Techniques in Analytical Chemistry, John Wiley & Sons, Inc., Hoboken, New Jersey, 2003.
[17] E.M. Thuman, M.S. Mills, Solid Phase Extraction Principles Practice, Wiley, New York, 1998.
[18] N.J.K. Simpson (Ed.), Solid Phase Extraction: Principles, Strategies and Applications, Marcel Dekker, New York, 2000.
[19] A. Tunceli, A.R. Turker, Anal. Sci. 16 (2000) 81.
[20] I.A. Kovalev, L.V. Bogacheva, G.I. Tysin, A.A. Formanovsky, Y.A. Zolotov, Talanta 52 (2000) 39.
[21] S.W. Kang, S.S. Lee, J. Korean Chem. Soc. 27 (1983) 268.
[22] C. Chakrapani, P.L. Mahanta, D.S.R. Murty, B. Gomathy, Talanta 53 (2001) 1139.
[23] P. Liu, Q. Pu, Z. Su, Analyst 125 (2000) 147.
[24] S. Toaliglu, T. Oymak, S. Kartal, Anal. Chim. Acta 511 (2004) 255.
[25] Q. Pu, Z. Su, Z. Hu, X. Chang, M. Yang, J. Anal. At. Spectrom. 13 (1998) 249.
[26] M.M. Hassanien, K.S. Abou-El-Sherbini, Talanta 68 (2006) 1550.
[27] M. Muzikar, C. Fontas, M. Hidalgo, T. Havel, V. Salvado, Talanta 70 (2006) 1081.
[28] Y. Wu, Z. Jiang, B. Hu, J. Duan, Talanta 63 (2004) 585.
[29] S. Zhang, Q. Pu, Q. Sun, Z. Su, Anal. Chim. Acta 452 (2000) 223.
[30] C.T. Kresage, M.E. Leonowicz, W.J. Roth, J.C. Vartuli, J.S. Beck, Nature 359 (1992) 710.
[31] J.S. Beck, J.C. Vortuli, W.J. Roth, M.E. Leonowicz, C.T. Kresge, K.D. Schmitt, C.T.W. Chu, D.H. Olson, E.W. Sheppad, S.B. McCullen, J.B. Higgins, J.L. Schlenker, J. Am. Chem. Soc. 114 (1992) 10834.
[32] L. Mercier, T.J. Pinnavaia, Adv. Mater. 9 (1997) 500.
[33] S.R. Hall, C.E. Fowler, B. Lebeow, S. Mann, Chem. Commun. (1999) 201.
[34] M. Algarra, M.V. Jimenez, E. Rodriguez-Castellon, A. Jimenez-Lopez, J. Jimenez-Jimenez, Chemosphere 59 (2005) 779.
[35] Y. Shiraishi, G. Nishimura, T. Hirai, I. Komasawa, Ind. Eng. Chem. Res. 41 (2002) 5065.
[36] D. Perez-Quintanilla, I. del Hierro, M. Fajardo, I. Sierra, J. Environ. Monit. 8 (2006) 214.
[37] D. Perez-Quintanilla, I. del Hierro, M. Fajardo, I. Sierra, J. Hazard. Mater. 134 (2006) 245.
[38] O. Kaftan, M. Acikel, A.E. Eroglu, T. Shahwan, L. Artok, C. Ni, Anal. Chim. Acta 574 (2005) 31.
[39] P. Trens, M.L. Russell, L. Spjuth, M.J. Hudson, J. Liljenzin, Ind. Eng. Chem. Res. 41 (2002) 5220.
[40] E. Lachowicz, B. Rozanska, F. Teixidor, H. Meliani, M. Barboiu, N. Hovnanian, J. Membr. Sci. 210 (2002) 279.
[41] Q. Cai, W.Y. Lin, F.S. Xiao, W.Q. Pang, X.H. Chen, B.S. Zou, Microporous Mesoporous Mater. 32 (1999) 1.
[42] M.V. Landau, S.P. Varkey, M. Herskowitz, O. Regev, S. Pevzner, T. Sen, Z. Luz, Microprous Mesoporous Mater. 33 (1999) 149.

Available online at www.sciencedirect.com
ScienceDirect
Talanta 71 (2007) 1669–1674
Talanta
www.elsevier.com/locate/talanta

The electrocatalytic examination of cephalosporins at carbon paste electrode modified with CoSalophen

E.S. Jamasbi [a], A. Rouhollahi [a,*], S. Shahrokhian [b], S. Haghgoo [c], S. Aghajani [d]

[a] *Chemistry Department, Faculty of Science, K.N. Toosi University of Technology, Tehran 15418, Iran*
[b] *Chemistry Department, Sharif University of Technology, Tehran 11365-9516, Iran*
[c] *Quality Control Lab Ministry of Health & Medical Education, Iran*
[d] *Office No. 1529, Ministry of Jahad-e-Agric, Main Building-Keshavarz Bul, Tehran, Iran*

Received 15 April 2006; received in revised form 26 July 2006; accepted 27 July 2006
Available online 25 September 2006

Abstract

The electrocatalytic oxidation of cephalexin and cefazolin has been studied at a carbon paste electrode modified with cobalt salophen (CoSal) by cyclic voltammetry. The selectivity of the carbon paste modified with CoSal in detecting cephalexin and cefazolin was examined. To suggest the electrocatalytic mechanism for electro-oxidation of cefazolin, the electrochemical behavior of ceftriaxone was investigated which has a thiol group out of the beta lactam ring. The electrocatalytic oxidation of these antibiotics is shown to be irreversible at the CoSal modified electrode. Scan rate dependence of cefazolin, which is a sulfur-containing compound, has been examined. The results indicated that the electrocatalytic oxidation of the compounds is diffusion controlled. The responses of the modified electrode were compared with those of unmodified electrode and it has shown that the modified electrode has better sensitivity than unmodified electrode to the detection of cefazolin. The overall number of electrons contributed to the oxidation of cefazolin is obtained 1 by chronoamperometry; the number of electron involved in the rate-determining step was 1. The results of differential pulse voltammetry (DPV) using the modified electrode with high sensitivity were applied for the determination of cefazolin in human synthetic serum samples. The linear range was obtained from 1×10^{-5} to 1×10^{-3} M for DPV determination of cefazolin in buffered solutions (pH 3.0).

Keywords: Cephalosporins; Carbon paste electrode; Modified electrode; Cobalt salophen; Cyclic voltammetry; Chronoamperometry; Differential pulse voltammetry

1. Introduction

Cephalosporins are widely used in clinical therapy for the treatment of sever detection because of their antibacterial and pharmacokinetic properties [1–5]. Up to now several methods have been reported to study cephalosporins such as spectrophotometric [6–8] and chromatographic [9–13] techniques. However, the detection of these sulfur-containing compounds by spectrophotometry is not effective, because these sulfur-containing groups do not absorb light [14] and derivatization of sulfur-containing compounds is sophisticated [15,16]. So applying a simple and easy technique has been urgently desired to detect cephalosporins. Electrochemical methods, due to rapidity, simplicity and high sensitivity in analysis, have been considered to study of the compounds such as cephalosporins and cepfamycins [17].

Although the electrochemical study of sulfur-containing compounds has been reported using carbon, platinum, mercury and gold as a working electrodes [18,19], but the sever detection conditions can damage the electrode and cause fluctuating background currents [14]. To reduce these problems, some researchers used the modified electrodes. Transition metal complexes are well known as electron mediators in the electrocatalytic oxidation of sulfhydryl compounds. Application of Schiff base complexes of cobalt in the matrix of carbon paste electrode has been reported for the sensitive electrochemical detection of sufhydryl compounds, e.g. cysteine [20], penicillamine [21], propylthiouracil [22] and captopril [23]. Carbon paste electrode modified with cobalt phthalocyanin is used for voltammetric detection of some sulfhydryl compounds [24,25]. In these investigations, the modified carbon paste elec-

* Corresponding author. Tel.: +98 21 22853308; fax: +98 21 22853650.
E-mail addresses: rouhollahi@kntu.ac.ir (A. Rouhollahi), shaghgoo@hotmail.com (S. Haghgoo).

0039-9140/$ – see front matter © 2006 Published by Elsevier B.V.
doi:10.1016/j.talanta.2006.07.058

trodes show efficient ability to catalyze the electrode process via significant decreasing of its overpotential, which is due to the selective interaction of the electron mediator with the target analyte [26]. The electrode is capable to considerable enhancement in the selectivity of electro-analytical methods [20].

In the present work, the electrochemical behavior of cefazolin is examined using the carbon paste electrode modified with CoSal. In order to compare the selectivity of electrode to detect the cephalosporins, the electro-oxidation of cephalexin is also studied. On the other hand, the electrocatalytic oxidation of ceftriaxone was investigated to obtain the electrocatalytic mechanism of the antibiotics in which a thiol group is out of the beta lactam ring.

2. Experimental

2.1. Preparation of electrodes

Cobalt salophen (CoSal) as electron mediator is prepared by the previously reported procedure [27]. The experimental conditions to prepare the carbon paste electrode modified with cobalt salophen have been described elsewhere [20]. The carbon paste electrode was prepared by mixing graphite powder with appropriate amount of mineral oil (Nujol) and thorough hand mixing in a mortar and pestle (∼75%:25%, w/w). A portion of the composite mixture was packed into the end of a Teflon tube (ca. 2.5 mm i.d.). Electrical contact was made by forcing a copper pin down into the Teflon and into the back of the composite. The modified electrode was prepared by mixing unmodified composite with CoSal (2%, w/w) and then the composite was dissolved in dichloromethane. The mixture was stirred by a magnetic stirrer till the solvent evaporated, completely. Then, the modified composite was then air dried for 24 h and used in the same way as unmodified electrode.

2.2. Instruments

All experiments were carried out using Autolab potentiostat (PGSTAT30) with a three-electrode glass cell. A silver/silver chloride as a reference electrode, a Pt wire as an auxiliary electrode and the carbon paste electrode (CPE) (unmodified or modified with CoSal) was used as the working electrode. The pH of buffered solutions in all voltammetric experiments were controlled by a pH meter model 744 Metrohm.

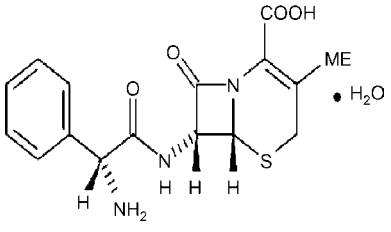

Scheme 1. Structure of cephalexin.

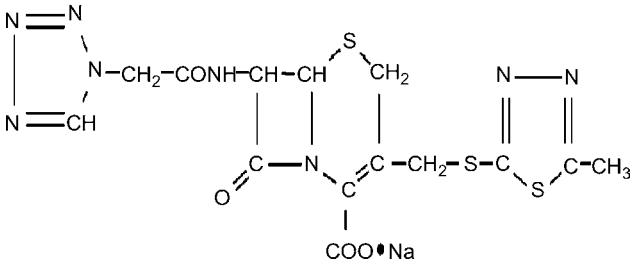

Scheme 2. Structure of cefazolin.

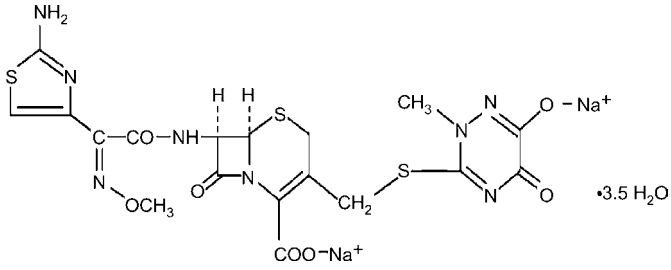

Scheme 3. Structure of ceftriaxone.

2.3. Reagents

All chemical reagents were of analytical grade of Merck, cephalexin (Turkey-fako), cefazolin (India-fortice) and ceftriaxone (Italy, Exir). Doubly distilled deionized water was used to prepare the solutions. The structures of cephalexin, cefazolin and ceftriaxone are shown in Schemes 1–3, respectively.

3. Results and discussion

3.1. Cyclic voltammetric studies

The previous research showed that CoSal (as a Schiff base complex) electrode is widely used to detect of biological thiols and has more catalytic effect in decreasing the anodic overpotential of analyte process and enhancement the anodic peak current [20]. In this research, the modified electrode is used to study the electrochemical behavior of cephalexin and cefazolin, the antibiotics belong to the first generation of cephalosporins and the selectivity of the modified electrode to detect these sulfur-containing compounds was examined.

The cyclic voltammograms of cefazolin using modified (A) and unmodified (B) electrodes carried out in 10 mM cefazolin and 0.1 M phosphate buffer solution (pH 3.0) as a supporting electrolyte (Fig. 1). As can be seen, the direct oxidation of cefazolin using unmodified electrode shows a very weak voltammetric wave. On the other hand, by using the modified electrode, the anodic peak current is considerably enhanced and a well-resolved oxidation wave, with respect to the background signal, is observed. These results revealed that the modified electrode is capable to catalyze effectively the electro-oxidation of cefazolin. A similar investigation is performed on cefazolin solutions using the modified carbon paste electrode. Fig. 2 shows the cyclic voltammogram of cephalexin using the CoSal-modified electrode taken in 10 mM solution of antibiotic

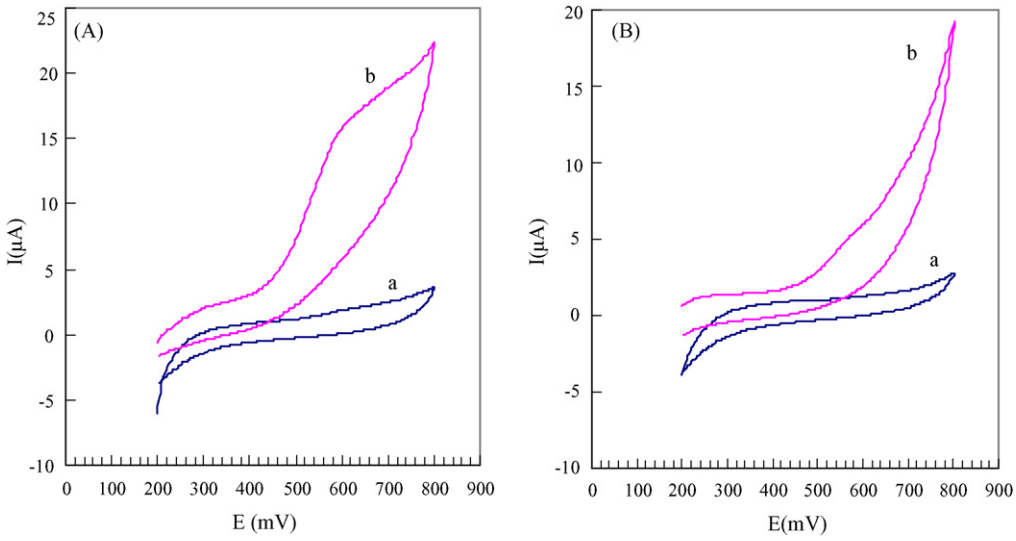

Fig. 1. Cyclic voltammograms of cefazolin on the modified electrode (A) and unmodified electrode (B) in 0.1 M phosphate buffer solution (pH 3.0) in the presence (a) and absence (b) of 10 mM cefazolin. Scan rate, 100 mV s^{-1}.

containing 0.1 M phosphate buffer solution (pH 3) as the supporting electrolyte. As can be seen, the direct oxidation of cephalexin, using modified electrode was poorly defined wave. On the other hand, a comparison between the cyclic voltammograms of cephalexin and cefazolin on the modified electrode (Figs. 1 and 2) confirms that the electrode modified with CoSal is capable to detect cefazolin rather than cephalexin selectively and effectively.

Results of the present work and also our previous works on the application of phthalocyanine and Schiff base complexes of cobalt have been shown that the values of a modifier of less than 2% (w/w) causes to a considerable decrease in the peak current along with the broadening of peaks and also positive shift in peak potential [20,21]. On the other hand, values of the modifier more than 2% (w/w) increase background (capacitive) current in conjunction with a graduate decrease in peak current. Therefore, a value of ∼2% (w/w) of CoMSal is used as the optimum value of the modifier in the matrix of CPE.

A series of cyclic voltammograms for the modified electrode taken in various concentrations of cefazolin at a sweep rate 100 mV s^{-1} is shown in Fig. 3. These results show that in 0.1 M

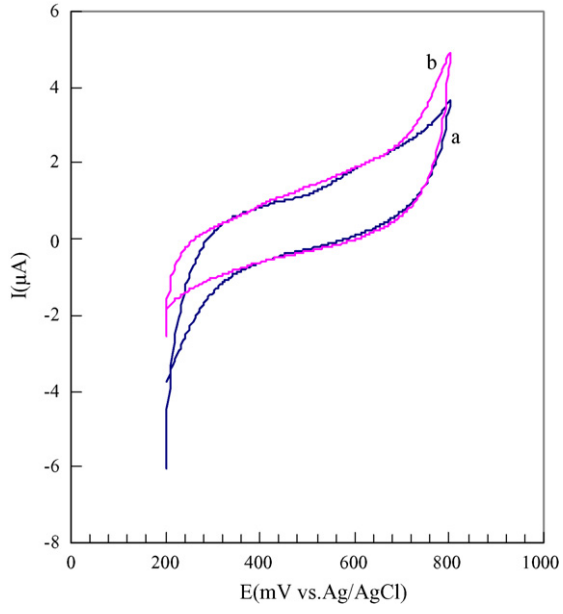

Fig. 2. Cyclic voltammogram of cephalexin on the modified electrode in 0.1 M phosphate buffer solution (pH 3.0) in the (a) absence and (b) presence of 10 mM cephalexin. Scan rate, 100 mV s^{-1}.

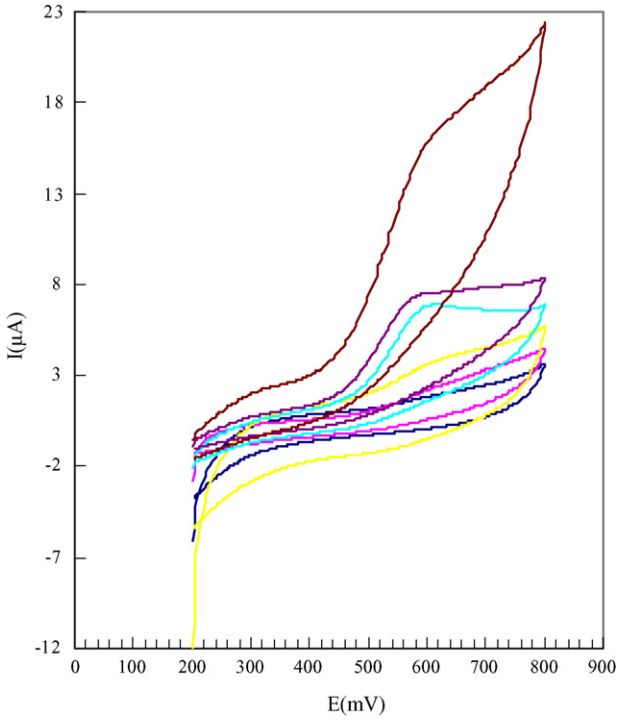

Fig. 3. Cyclic voltammogram for carbon paste electrode modified with CoSal in 0.1 M phosphate buffer solution (pH 3.0) for a series of cefazolin concentrations: up to down, 10, 7.5, 5.0, 2.5, 1.0 and 0 mM (background electrolyte). Potential sweep rate, 100 mV s^{-1}.

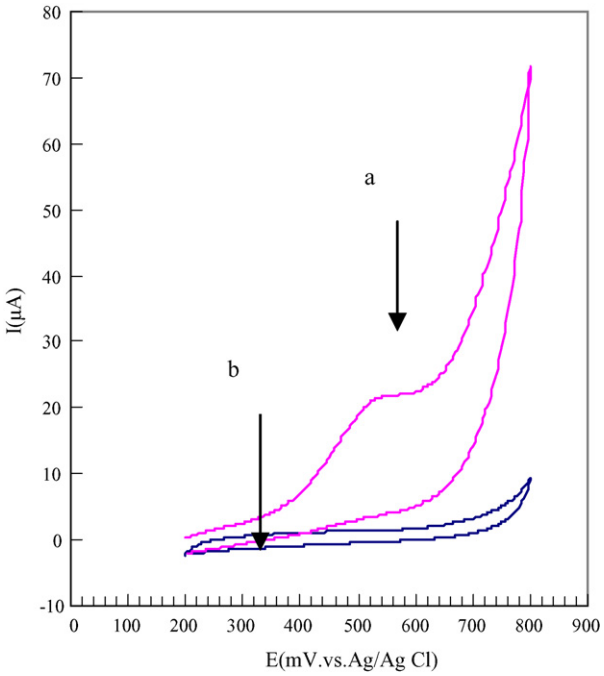

Fig. 4. Cyclic voltammograms of ceftriaxone for modified electrode vs. Ag/AgCl in 0.1 M phosphate buffer solution (pH 3.0) in the presence (b) and absence (a) of 10 mM ceftriaxone. Scan rate, 100 mV s^{-1}.

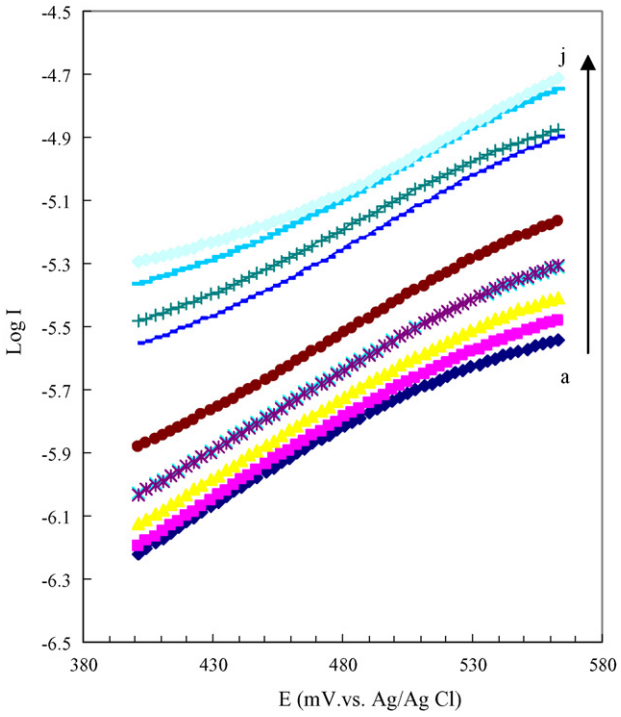

Fig. 5. Polarization curves for 10 mM cefazolin in 0.1 M phosphate buffer solution (pH 3.0) at modified electrode at various sweep rates: (a) 2 mV s^{-1}, (b) 4 mV s^{-1}, (c) 6 mV s^{-1}, (d) 8 mV s^{-1}, (e) 10 mV s^{-1}, (f) 25 mV s^{-1}, (g) 50 mV s^{-1}, (h) 100 mV s^{-1}, (i) 200 mV s^{-1} and (j) 300 mV s^{-1}.

phosphate buffer solution (pH 3.0) as a supporting electrolyte, the voltammetric response (anodic peak current) increases with the concentration of cefazolin. The potential sweep rate dependence of peak current was investigated and a linear relationship is observed with the square root of the sweep rate, revealing the diffusion-controlled process in the electro-oxidation at the surface of modified electrode.

The current function ($I_p/C\upsilon^{1/2}$) for the electrocatalytic oxidation of cefazolin at the surface of CoSal-modified electrode decreases with the square root of potential sweep rate. This behavior can be explained as an evidence for the catalytic pathway in the mechanism [28]. To suggest the electrocatalytic mechanism of cefazolin, the electro-oxidation of ceftriaxone was investigated which is a sulfur-containing compound with the thiol group out of the ring. The cyclic voltammogram of ceftriaxone shows a well-defined anodic peak in the potential range of Fig. 4. It can be concluded that the electrocatalytic oxidation of cefazolin occurs in its thiol group which exists out of the beta lactam ring.

3.2. Polarization measurements

To elucidate the mechanism and the rate determination step in a multi-step reaction, the Tafel plot and its slope were used. The results of polarization studies ($\log I$ versus E) for electrocatalytic oxidation of cefazolin were obtained in various sweep rates. These results that are obtained from two ranges of potential sweep rates are shown in Fig. 5. By considering a value of 0.58 for α in these irreversible systems, it is concluded that one electron transferred in the rate determination step of reaction. To determine the number of electrons in the overall reaction, the following equation (for irreversible and diffusion-controlled reactions) is used [28].

$$I_p = 3.01 \times 10^5 n[(1-\alpha)n_a]^{1/2} A C_{ox} D^{1/2} V^{1/2}$$

By considering $(1-\alpha)n_a = 0.58$, $D = 5.5 \times 10^{-5}$ cm^2 s^{-1} (obtained by chronoamperometry) and the geometric area of

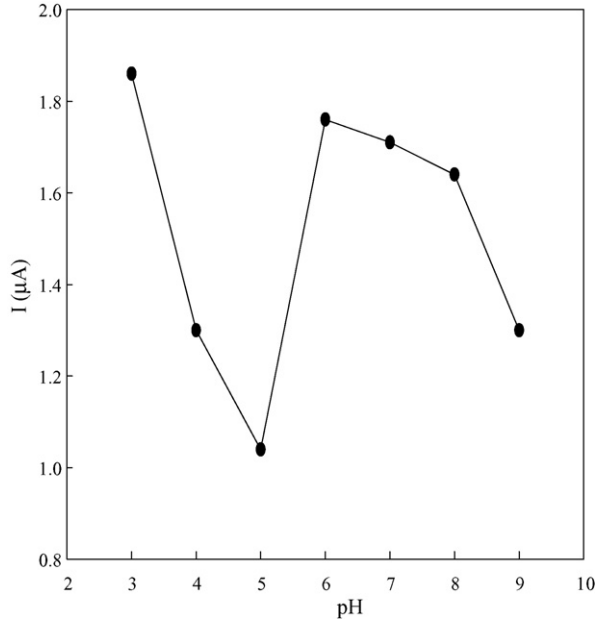

Fig. 6. The effect of pH for 10 mM cefazolin at a CoSalophen-modified electrode. Sweep rate, 100 mV s^{-1}.

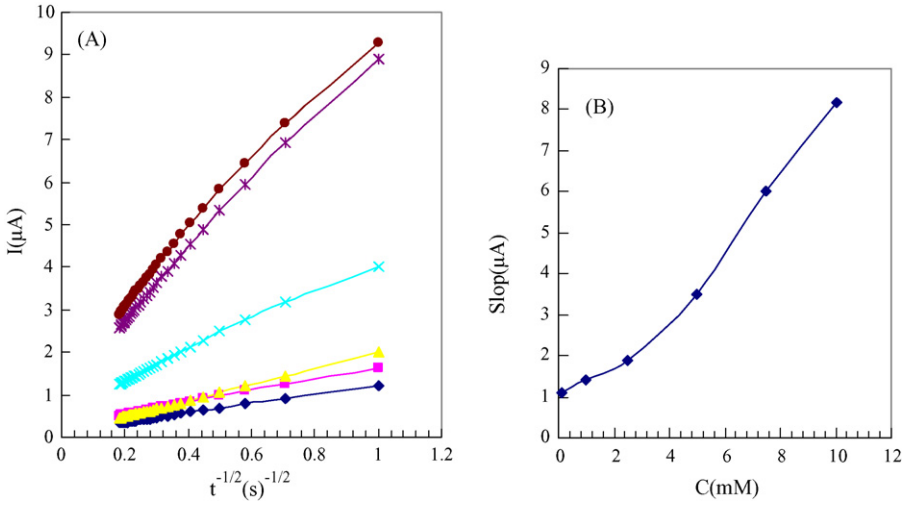

Fig. 7. (A) Plot of I vs. $t^{-1/2}$ obtained from chronoamperograms of carbon paste modified electrode in 0.1 M phosphate buffer solution (pH 3.0) at modified electrode for various concentrations of cefazolin: (a) 2 mV s^{-1}, (b) 4 mV s^{-1}, (c) 6 mV s^{-1}, (d) 8 mV s^{-1}, (e) 10 mV s^{-1}, (f) 25 mV s^{-1}, (g) 50 mV s^{-1} and (h) 100 mV s^{-1}. (B) The slop of straight against the cefazolin concentration.

electrode (A) as 0.125 cm^2, it was found that one electron contribute in the overall reaction.

3.3. Effect of pH

The pH effect on the oxidation of antibiotics is examined. The studies showed that by increasing the pH from 3 to 5, the peak current is decreased. Previous studies on phthalocyanine complexes of cobalt show that the most electrocatalytic activity is observed in more acidic solutions, where a redox couple of cobalt with a higher oxidation state exists (Co(III)/Co(II)) [27]. On the other hand, in solutions with pH higher than 5, due to the deprotonation of cefazolin and formation of its carboxylate anions, electrostatic attraction with positively charged CoSalophen may be caused to enhance the interaction with cephazolin. In solutions with pHs greater than 6, the decreasing of the catalytic activity of Co(III)/Co(II) redox system together with the axial coordination of hydroxide anion with the central metal of the complex catalyst, caused to lowered the catalytic current for cephazolin. The results of the effect of pH on the catalytic current for cefazolin are shown in Fig. 6.

3.4. Chronoamperometric studies

Chronoamperometric studies were investigated to obtain the diffusion coefficient for cefazolin in this mechanism. Fig. 7A shows the plot of I versus $t^{-1/2}$ in which the slopes of the resulting straight lines were plotted versus the cefazolin concentration (Fig. 7B), by using the slops and cottrell equation [28], the

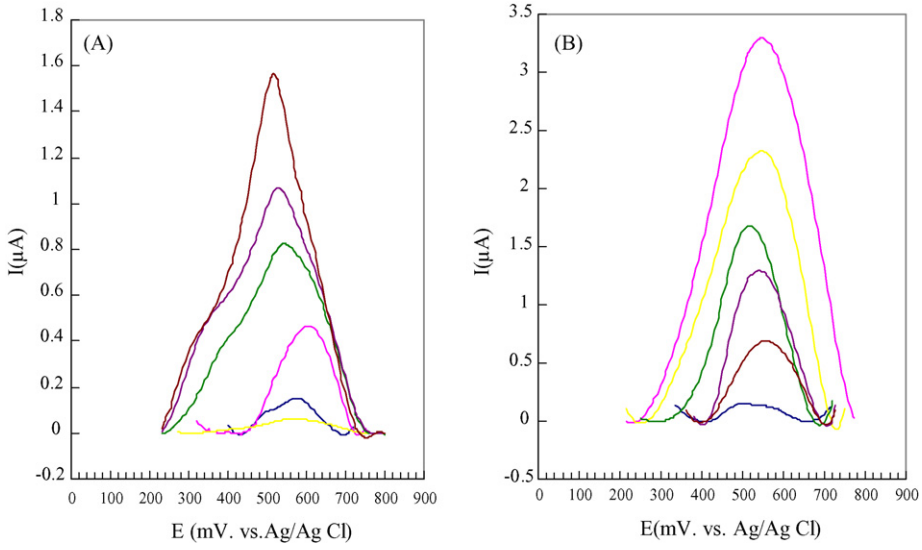

Fig. 8. (A) Differential pulse voltammograms of solutions containing (down to up): 0.01, 0.05, 0.1, 0.5 and 1 mM cefazolin in 0.1 M phosphate buffer solution (pH 3.0) at modified electrode. (B) Differential pulse voltammograms of cefazolin spiked to human synthetic serum containing 0.1 M phosphate buffer. Various concentrations of cefazolin from down to up are: 0.01, 0.05, 0.1, 0.5 and 1 mM.

diffusion coefficient was calculated as 5.5×10^{-5} cm^2 s^{-1} for cefazolin.

3.5. Differential pulse voltammetry studies

Differential pulse voltammetry (DPV) is a very sensitive and rapid method with low detection limit to detect the trace amount of cefazolin. Fig. 8A shows differential pulse voltammograms of cefazolin for CoSal-modified electrode in 0.1 M phosphate buffer solution with pH 3.0. A linear range from 1×10^{-5} to 1×10^{-3} M is obtained for cefazolin. Fig. 8B shows the result of DPVs for various concentration of cefazolin spiked to the human synthetic serum in which, each component was chosen close to its normal level in the real human serum. Voltammetric calibration curves for the peak current versus cefazolin concentration in phosphate buffer and synthetic serum show similar linear range between 1×10^{-5} and 1×10^{-4} M.

The slope of calibration curve for the variation of peak current versus cefazolin concentration in a background of 0.1 M phosphate buffer solution (pH 3.0) was 1.1371 μA M^{-1}, and in the background of human synthetic serum (containing the same buffer) was 1.096 μA M^{-1}. These results show that there is an excellent recovery for the cefazolin spiked to the synthetic serum; revealing that the complicated matrix of serum sample does not interfere with the voltammetric determination of cefazolin. The voltammetric detection limit for cefazolin using this electrode is obtained as 1×10^{-6} M; 0.4 ppm (based on the linear calibration curve) and slope variation for six replicates is 2.5%. The resulted detection limit is lower than dosage uptake by the patients in daily uses.

4. Conclusions

The electrocatalytic oxidation of cephalosporins at the carbon paste electrode modified with CoSal performed with a reasonable selectivity and good sensitivity. The response of the modified electrode is highly dependent on the structure of the sulfur-containing compounds. Cefazolin and ceftriaxone have the thiol group out of the beta lactam ring, so formation of the dimmer is possible for them during the electro-oxidation at the modified electrode. However, for cephalexin, which does not have the thiol group out of the beta lactam ring, formation of the dimmer is impossible. DPV is applied successfully for the determination of cefazolin in complex matrix of human synthetic serum samples and very good recoveries are resulted using the modified electrode.

Acknowledgements

The authors gratefully acknowledge the support of this work by K.N. Toosi University of Technology Research Council, Chemistry Department, Sharif University of Technology and Quality Control Lab Ministry of Health & Medical Education. Also, we wish to thank Dr. Jalal Hoseini for reviewing the manuscript and his useful comments.

References

[1] P. Garzone, J.A. Lyon, V.L. Yu, Drug. Intell. Clin. Pharm. 17 (1983) 507.
[2] P. Garzone, J.A. Lyon, V.L. Yu, Drug. Intell. Clin. Pharm. 17 (1983) 615.
[3] D.S. Reeves, M.J. Bywater, D.W. Bullock, H.A. Holt, J. Antimicrob. Chemother. 6 (1980) 647.
[4] T. Kamimura, Y. Matsumoto, N. Okada, Y. Mine, M. Nishida, S. Goto, S. Kuwahara, Antimicrob. Agents Chemother. 16 (1979) 540.
[5] K.P. Fu, H.C. Neu, Antimicrob. Agents Chemother. 17 (1980) 583.
[6] A.B.C. Yu, C.H. Nightingale, D.R. Flanagan, J. Pharm. Sci. 66 (1977) 213.
[7] R.H. Barbhaiya, P. Turner, J. Pharm. Pharmacol. 28 (1976) 791.
[8] D. Agbaba, S. Eric, K. Karlijikovic-Rajic, S. Vladimirov, D. Zivanov-Stakic, Spectrosc. Lett. 30 (1997) 309.
[9] B. Calahorra, M.A. Companero, B. Sadaba, J.R. Azanza, Biomed. Chromatogr. 13 (1999) 272.
[10] I.N. Valassis, M. Parissi-poulon, P. Macheras, J. Chromatogr. 13 (1999) 272.
[11] M. Ip, C. Au, S. Cheung, C. Chan, A. Caeng, J. Antimicrob. Chemother. 42 (1998) 121.
[12] J. Dokladalova, G.T. Quericia, J.P. Stankewich, J. Chromatogr. 276 (1983) 129.
[13] S. Eric-Jovanovic, D. Agbaba, D.Z. Inov-Staki, S. Vladimorov, J. Pharm. Biomed. Anal. 18 (1998) 893.
[14] G.S. Owens, W.R. LaCourse, Current Separations 14 (1996) 82.
[15] N. Adam, J.R. Kramer, Aqua Geochem. 5 (1999) 1.
[16] L. Gallo-Martinez, A. Sevillano-Cabeza, P. Campins-Falco, F. Bosch-Reig, Anal. Chim. Acta 370 (1998) 115.
[17] P. Zuman, V. Kapetanovic, M. Aleksic, Anal. Lett. 33 (2000) 2821.
[18] F.G. Banica, A.G. Fogg, J.C. Moreira, Analyst 119 (1994) 2343.
[19] M. Heyrovsky, S. Vavricka, J. Bioelectrochem. Bioenerg. 48 (1999) 43.
[20] S. Shahrokhian, M. Karimi, Electrochim. Acta 50 (2004) 77.
[21] S. Shahrokhian, A. Souri, H. Khajehsharifi, J. Electroanal. Chem. 565 (2004) 95.
[22] S. Shahrokhian, M.J. Jannat-Rezvani, Microchim. Acta 151 (2005) 73.
[23] S. Shahrokhian, M. Karimi, H. Khajehsharifi, Sens. Actuators B 109 (2005) 278.
[24] M.K. Halbert, R.P. Baldwin, Anal. Chem. 57 (1985) 591.
[25] X. Qi, R.P. Baldwin, J. Electrochem. Soc. 143 (1996) 1283.
[26] I. Svancara, K. Vytras, J. Barek, J. Zima, Crit. Rev. Anal. Chem. 31 (2001) 311.
[27] D.A. Atwood, J.A. Jegier, D. Rutherford, Inorg. Chem. 5 (1996) 63.
[28] A.J. Bard, L.R. Faulkner, Electrochemical Methods, Fundamental and Applications, 2nd ed., John Wiley, New York, 2001.

Available online at www.sciencedirect.com
ScienceDirect
Talanta 71 (2007) 1476–1480
Talanta
www.elsevier.com/locate/talanta

Electrogenerated chemiluminescence from CdS nanotubes and its sensing application in aqueous solution

Gui-Fen Jie, Bo Liu, Jian-Jun Miao, Jun-Jie Zhu *

Key Laboratory of Analytical Chemistry for Life Science, School of Chemistry and Chemical Engineering, Nanjing University, Nanjing 210093, PR China

Received 9 May 2006; received in revised form 24 June 2006; accepted 9 July 2006
Available online 14 August 2006

Abstract

Electrogenerated chemiluminescence (ECL) of CdS nanotubes in aqueous solution and its sensing application were studied by entrapping the CdS nanotubes in carbon paste electrode. Two ECL peaks were observed at −0.9 V (ECL-1) and −1.2 V (ECL-2), respectively, when the potential was cycled between 0 and −1.6 V. The electrochemically reduced nanocrystal species of CdS nanotubes could collide with the oxidized species in an annihilation process to produce the peak of ECL-1. The electron-transfer reaction between the reduced CdS nanocrystal species and oxidant coreactants such as $S_2O_8^{2-}$, H_2O_2, and reduced dissolved oxygen led to the appearance of the ECL-2 peak. Based on the enhancing effect of H_2O_2 on ECL-2 intensity, a novel CdS ECL sensor was developed for H_2O_2 detection. The sensor exhibited a detection limit of 0.1 μM and a linear range from 0.5 μM to 0.01 mM. The relative standard deviations of five replicate determinations of 5 μM H_2O_2 was 2.6%. In addition, the ECL spectrum in aqueous solution also exhibited two peaks at 500 and 640 nm, respectively.

Keywords: Electrogenerated chemiluminescence; CdS nanotubes; H_2O_2 detection

1. Introduction

Semiconductor nanocrystals (NCs) have been extensively studied because of their unique size-dependent electronic, optical and electrochemical properties [1]. Highly luminescent semiconductor NCs have gained increasing attention in light-emitting devices and tagging applications [2–6]. Due to the controllable merits of electrochemical method, the spectroelectrochemical behavior of semiconductor NCs has been extensively carried out [7,8]. As reported, an electron injection by applying cathodic potential to the nanoparticle layers composing of CdSe or CdSe/CdS core-shell NCs can dramatically enhance the efficiency of chemiluminescence and allow the achievement of efficient and stable ECL from CdSe nanoparticle layers in aqueous solution [9]. Recent research indicated that the electrochemically reduced and oxidized Si NCs [10] or CdSe NCs [11] could react with coreactants to produce ECL. The electron-transfer reaction between electrochemically formed nanocrystal species and coreactants implies that NCs have great potential for developing novel ECL sensors.

ECL has many promising advantages such as simplicity, high sensitivity, rapidity and easy controllability, and it has been proved to be a useful technique for analytical applications including organic analysis, immunosensors, DNA-probe assays and enzymatic biosensors [12]. In this paper, following the ECL studies on CdS nanoparticles [13] and CdS nanotubes in the mixed solution of 0.1 M $K_2S_2O_8$ and 0.1 M KOH [14], an alternative approach to study the ECL properties of CdS nanotubes in pH 8.0 phosphate buffer solution (PBS) was proposed, which is more suitable for analytical applications in biological system. Based on the electron-transfer reaction between electrochemically reduced CdS nanocrystal species and coreactant H_2O_2, a new CdS ECL sensor for H_2O_2 determination was developed.

The accurate and rapid determination of H_2O_2 is of practical importance in chemical, biological, clinical and other fields [15,16] Although H_2O_2 can be detected by many enzyme-based biosensors [17,24], the enzymes cannot promise a complete long-term stability of the sensors due to their inherent instability. Here, a novel CdS-based ECL sensor for H_2O_2 detection provides a more effective way with better stability and higher

* Corresponding author. Tel.: +86 25 83594976; fax: +86 25 83317761.
E-mail address: jjzhu@netra.nju.edu.cn (J.-J. Zhu).

0039-9140/$ – see front matter © 2006 Elsevier B.V. All rights reserved.
doi:10.1016/j.talanta.2006.07.029

sensitivity. As expected, the hydrophobicity of paraffin used for preparing the carbon paste resulted in the formation of a clear O/W interface between immobilized CdS nanotubes and aqueous solution, which suggested a new fabrication method to study the ECL behavior of nanocrystals in aqueous system. Using carbon paste to immobilize CdS nanocrystals not only provided an easy renewable modified electrode surface, but also could retain the ECL features of CdS for more than several months.

2. Experimental

2.1. Reagents

The CdS nanotubes were synthesized following the reference [14]. H_2O_2 (30%, w/v, solution) and $K_2S_2O_8$ were purchased from Shanghai Chemical Reagent Company (Shanghai, China). 0.1 M phosphate buffer solution (PBS) (pH 8.0) containing 0.01 M $K_2S_2O_8$ and 0.1 M KCl was used as the electrolyte in the measuring system. High-purity nitrogen was used for air-free condition. All other chemicals were of analytical grade. Doubly distilled water was used throughout.

2.2. Modified electrode preparation

The carbon paste electrode (CPE) was fabricated as follows: graphite powder (60 mg) and the CdS nanotubes (20 mg) were thoroughly mixed in ethanol solvent by ultrasonic dispersion. After drying under stirring, a homogenized graphite/CdS mixture was achieved. Subsequently, paraffin oil was added to the mixture (oil/mixture = 1:4, w/w) and mixed fully until a homogeneous paste was obtained. The prepared paste was packed into a glass tube with a 4 mm inner diameter and electrical contact was established with a copper rod through the back of the homemade electrode. Prior to each experiment, the electrode surface was polished with weighing paper and rinsed with redistilled water.

2.3. Instrumentation and measurements

Electrogenerated chemiluminescence studies were performed using a Model MPI-A from Electrochemiluminescence Analyzer Systems (Xi'An Remax Electronic Science & Technology Co. Ltd., Xi'An, China). The spectral width of the photomultiplier tube (PMT) used in Model MPI-A Electrochemiluminescence Analyzer was 200–800 nm and the voltage of the PMT was set at 800 V in the process of detection. A CHI 660 electrochemical analyzer (Shanghai Chenhua, China) was used for electrochemical experiments. A conventional three-electrode configuration was used. An Ag/AgCl reference electrode and a platinum wire counter electrode were used for all measurements, respectively. The CPE with the CdS nanotubes was used as the working electrode. The UV absorption spectra were acquired in a Ruili 1200 photospectrometer (Peking Analytical Instrument Co., Peking, China). Photoluminescence (PL) and ECL spectra were obtained on AMINCO Bowman Series 2 Luminescence Spectrometer (SLM Inc., USA).

3. Results and discussion

3.1. PL and UV characterizations for CdS NCs

As reported [14], the CdS nanotubes with diameter of about 100–140 nm are composed of numerous compacted nanocrystals. The average size of these nanocrystals is estimated to be about 7 nm. Fig. 1 shows the photoluminescence (PL) and UV (inset) spectra from the CdS in ethanol solution. The PL emission peak at 616 nm and the absorption peak at 490 nm indicated the existence of quantum size effect for the CdS nanoparticles [18].

3.2. Electrochemical and ECL behaviors of CdS nanotubes in CPE

Cyclic voltammograms (CVs) and ECL curves of the CdS nanotubes are shown in Fig. 2. In the CVs (inset A), the anodic and the cathodic peaks (curve c) were observed at −0.85 V (A1) and −1.2 V (C1), respectively, in pH 8.0 PBS containing 0.1 M KCl and 0.01 M $K_2S_2O_8$. In the curve b, the peak A1 did not appear at the blank carbon paste electrode, which implied that the peak A1 was attributed to the oxidation of CdS nanotubes. The peak C1 appeared in both curve a and curve b was assigned to the reduction of $S_2O_8^{2-}$, because this peak was not found in the absence of $S_2O_8^{2-}$ (curve a). In the ECL curves, upon the potential scan with an initial negative direction, two light emission peaks occurred at −0.9 and −1.2 V defined as ECL-1 and ECL-2, respectively, corresponding to the two CV peaks. No light emission was observed on bare CPE in the same condition, suggesting the ECL processes were due to the existence of CdS nanotubes. Therefore, the ECL peaks indicated that the CdS nanocrystals immobilized in CPE could be oxidized or reduced by charge injection during potential cycling and participated in relevant ECL processes. According to the previous report [13], electrogenerated reduced species ($CdS^{\bullet -}$) can col-

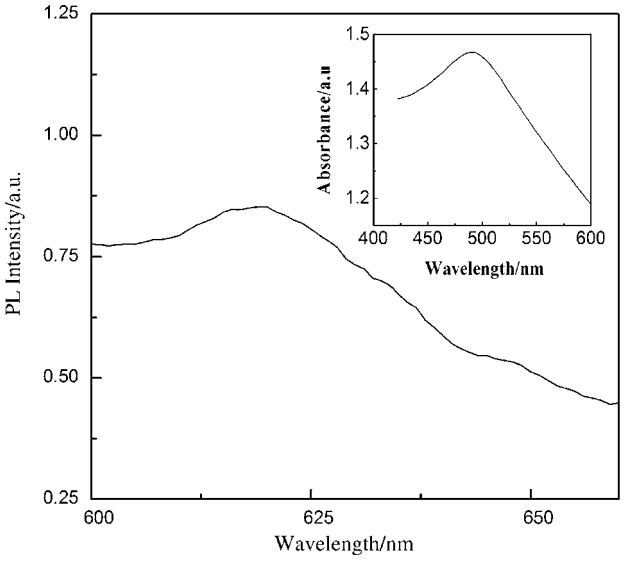

Fig. 1. Photoluminescence and UV (inset) spectra of CdS nanotubes in ethanol solution. Excitation wavelength: 350 nm.

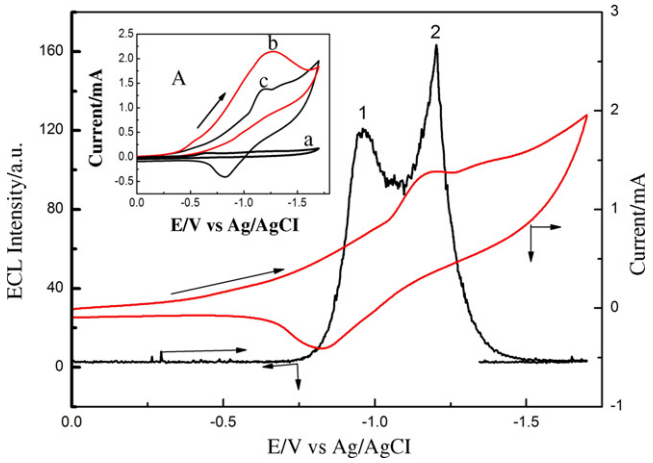

Fig. 2. Cyclic voltammograms and ECL curves of the CdS CPE in 0.1 M pH 8.0 PBS containing 0.1 M KCl and 0.01 M $K_2S_2O_8$; inset (A): cyclic voltammograms of (a) blank CPE in 0.1 M pH 8.0 PBS containing 0.1 M KCl; (b) the same as (a) but containing 0.01 M $K_2S_2O_8$; (c) CdS CPE in 0.1 M pH 8.0 PBS containing 0.1 M KCl and 0.01 M $K_2S_2O_8$; scan rate: 40 mV/s.

lide with oxidized species ($CdS^{\bullet+}$) in an annihilation process to produce excited states (CdS*), which generated the luminescence (ECL-1) [10]. The coincidence between peak potential of ECL-1 and A1 indicates that ECL-1 is generated only from the CdS nanocrystals [13]. The mechanisms are as follows:

ECL-1:

$$CdS^{\bullet-} + CdS^{\bullet+} \rightarrow CdS^* + CdS \quad (1)$$

$$CdS^* \rightarrow CdS + h\nu \quad (2)$$

In this case, electrogenerated species should be stable enough to allow reaction (1) to compete with decomposition reaction [19]. This can be correlated to the aggregation morphology of the CdS nanocrystals and the addition of the coreactant ($S_2O_8^{2-}$), which help to overcome the poor stability of electrogenerated species. After ECL-1, as the negative scan potential reached −1.2 V, $S_2O_8^{2-}$ was reduced and generated a strong oxidant $SO_4^{\bullet-}$. $SO_4^{\bullet-}$ can react with the electrogenerated species ($CdS^{\bullet-}$) to generate higher intensity light emission (ECL-2). Here the coreactants can also be dissolved oxygen or H_2O_2. When dissolved oxygen was removed from the solution by bubbling high-purity nitrogen for 30 min, the intensity of ECL-2 decreased dramatically; whereas the intensity can be enhanced by adding H_2O_2 in the deoxygenated solution. The corresponding ECL processes are as follows [20]:

ECL-2:

$$CdS\ NCs + ne \rightarrow nCdS^{\bullet-} \quad (3)$$

$$S_2O_8^{2-} + e^- \rightarrow SO_4^{2-} + SO_4^{\bullet-} \quad (4)$$

$$CdS^{\bullet-} + SO_4^{\bullet-} \rightarrow CdS^* + SO_4^{2-} \quad (5)$$

$$CdS^* \rightarrow CdS + h\nu \quad (6)$$

or

$$O_2 + H_2O + 2e \rightarrow OOH^- + OH^- \quad (7)$$

$$2CdS^{\bullet-} + OOH^- + H_2O \rightarrow 3OH^- + 2CdS^* \quad (8)$$

$$2CdS^{\bullet-} + H_2O_2 \rightarrow 2OH^- + 2CdS^* \quad (9)$$

$$CdS^* \rightarrow CdS + h\nu \quad (10)$$

3.3. Effect of various factors

The factors influencing CdS ECL, such as scan rate, potential range and the pH value were all investigated.

With the increase of scan rate, the ECL intensities increased and reached the maximum values at 40 mV/s. The increase in emission intensity might be due to the formation of more reduced CdS nanocrystal species in unit time. When the scan rate was higher than 40 mV/s, the emission signal became unstable and decreased slowly, this was because the electrochemical process was irreversible, and high scan rate was unfavorable to the electrochemical reduction of CdS NCs. For the reasons showed above, 40 mV/s was chosen in our experiments.

When the switching potential was selected as 1.0, 0.8, 0, −1.2, −1.4 and −1.6 V, respectively, the ECL intensities were enhanced only with more negative scan potential, revealing that more CdS NCs could be reduced to $CdS^{\bullet-}$ species at more negative applied potential. Then the ECL experiments were conducted between 0 and −1.6 V.

The dependence of ECL intensity from CdS nanotubes on pH value is shown in Fig. 3, the ECL-2 intensity increased with the increase of pH values from 6.0 to 9.0, indicating pH played an important role in the cathodic ECL-2 process. Recent research demonstrated that ECL feature of semiconductor NCs was very sensitive to their surface states [21], and increasing pH values could alter surface states of CdS nanocrystals in the solution due to the adsorption of Lewis bases [22,23], which resulted in the enhanced ECL intensity. In addition, since the pH of the biological systems is ~7.4, given attention to both the high ECL intensity and the potential analytical applications, the ECL measurements were performed in 0.1 M pH 8.0 PBS.

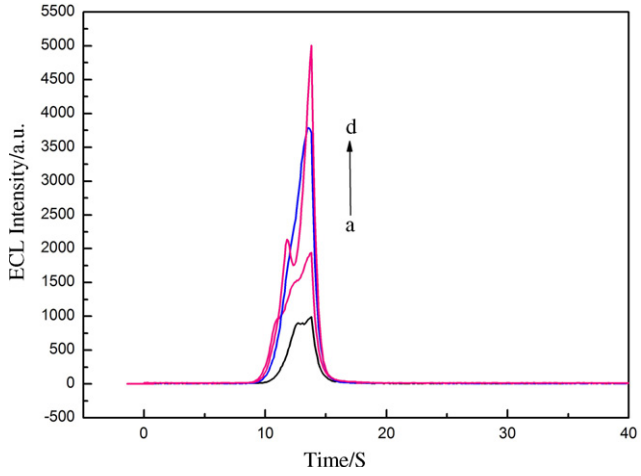

Fig. 3. Effect of pH on ECL of the CdS CPE in 0.1 M PBS containing 0.1 M KCl and 0.01 M $K_2S_2O_8$. (a) pH 6, (b) pH 7, (c) pH 8, (d) pH 9.

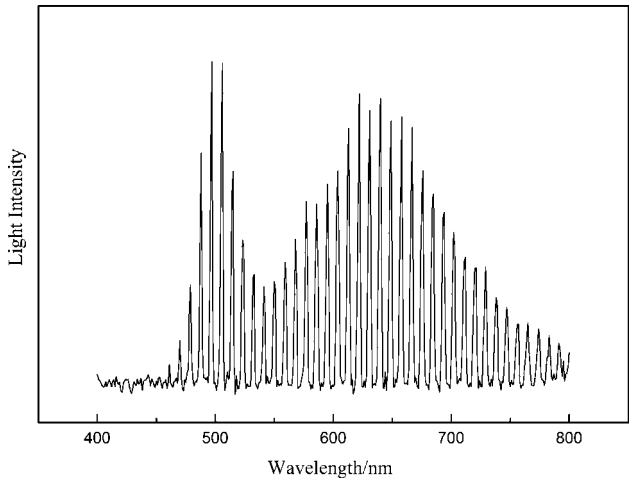

Fig. 4. ECL spectrum of the CdS CPE in 0.1 M pH 8.0 PBS containing 0.1 M KCl and 0.01 M $K_2S_2O_8$ by potential steps between +1.0 and −1.6 V at the step time of 0.5 s.

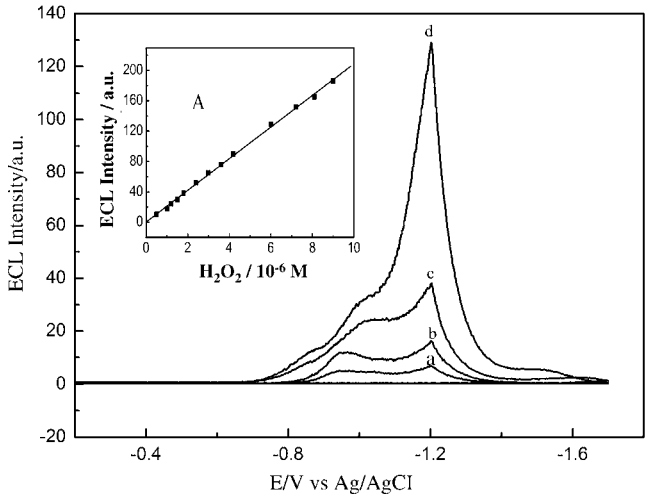

Fig. 5. Effect of hydrogen peroxide concentration on ECL-2 intensity of CdS CPE in 0.1 M pH 8.0 PBS containing 0.1 M KCl and 0.01 M $K_2S_2O_8$. (a) 0 μM; (b) 1 μM; (c) 3.6 μM; (d) 12 μM H_2O_2. Inset A: calibration curve for H_2O_2 detection.

3.4. ECL spectrum

As shown in Fig. 4, the ECL spectrum was obtained from the CdS CPE in 0.1 M pH 8.0 PBS containing 0.1 M KCl and 0.01 M $K_2S_2O_8$ by potential stepping between +1.0 and −1.6 V at a step time of 0.5 s, a sharp peak at 500 nm and a broad one at 640 nm were observed, respectively. According to the luminescence mechanism of CdS nanocrystals [24], the peak at 500 nm was attributed to band gap luminescence (350–500 nm) and the one at 640 nm was due to surface state luminescence (500–700 nm). Compared with the PL spectrum (Fig. 1), the peak at 640 nm is ∼24 nm red-shifted, suggesting the strong role of surface states on the NCs in electrochemical and ECL processes [10,11].

3.5. Sensing application of the CdS CPE for ECL detection of H_2O_2

Fig. 5 shows the ECL sensing response of the modified CPE to hydrogen peroxide in pH 8.0 PBS containing 0.1 M KCl and 0.01 M $K_2S_2O_8$ by bubbling high-purity nitrogen for 30 min. Under optimized conditions, hydrogen peroxide could obviously enhance the intensity of ECL-2 (curves b–d), a linear relation between the intensity of ECL-2 and hydrogen peroxide concentration was obtained from 5.0×10^{-7} to 1.0×10^{-5} M with a correlation coefficient of 0.9993 (inset A). The detection limit was 1.0×10^{-7} M, which was lower than those of the biosensor for H_2O_2 detection [25].

3.6. Stability and selectivity of the CdS ECL sensor

The CdS nanotubes modified CPE showed good stability. After the electrode was stored under dark conditions at room temperature for 2 months, the ECL-2 response only decreased 4.2%. The effects of some interferences on H_2O_2 determination with this ECL sensor were also investigated in the same experimental conditions, the addition of K^+, Cl^-, and NO_3^- slightly increased the ECL intensity at concentrations lower than 0.1 M, showing little interference with H_2O_2 determination.

Although the detection of CdS ECL sensor for hydrogen peroxide at the present stage was not so efficient as that of luminol-enzyme based ECL system [26], improved performance would be achieved by extensively optimizing the size, structure and surface states of semiconductor NCs influencing CdS ECL features. The further optimized ECL sensor of CdS nanocrystal should possess greater potential than those sensors based on PL of QDs or ECL from luminol for determination of many analytes [12,26].

4. Conclusions

In summary, electrogenerated chemiluminescence of CdS nanotubes in aqueous solution exhibited two ECL peaks, which corresponded to two different mechanisms. The first peak (ECL-1) is generated via an annihilation process between reduced and oxidized species. The second one (ECL-2) is attributed to the electron-transfer reaction between electrochemically reduced CdS nanocrystal species ($CdS^{\bullet -}$) and coreactants. Based on the reaction of $CdS^{\bullet -}$ with the coreactant H_2O_2, a novel and sensitive CdS ECL sensor was fabricated for H_2O_2 detection. The CdS ECL spectrum also showed two peaks, confirming that the ECL of CdS nanotubes could emit two kinds of visible light, which suggests a potential use in spectroelectrochemical assay.

Acknowledgments

This work is supported by the National Natural Science Foundation of China (Grants 20325516 and 20575026) and Jiangsu Scientific Project (BK2004210). This work is also supported by NSFC for Creative Research Group (20521503).

References

[1] A.P. Alivisatos, Science 271 (1996) 933.
[2] P. Reiss, J. Bleuse, A. Pron, Nano Lett. 2 (2002) 781.
[3] C.M. Strohsahl, H. Du, B.L. Miller, T.D. Krauss, Talanta 67 (2005) 479.
[4] M. Shingyoji, D. Gerion, D. Pinkel, J.W. Gray, F. Chen, Talanta 67 (2005) 472.
[5] Y. Ma, C. Yang, N. Li, X. Yang, Talanta 67 (2005) 979.
[6] W. Vastarella, R. Nicastri, Talanta 66 (2005) 627.
[7] M. Shim, C. Wang, P. Guyot-Sionnest, J. Phys. Chem. B 105 (2001) 2369.
[8] B.L. Wehrenberg, P. Guyot-Sionnest, J. Am. Chem. Soc. 125 (2003) 7806.
[9] S.K. Poznyak, D.V. Talapin, E.V. Shevchenko, H. Weller, Nano Lett. 4 (2004) 693.
[10] Z. Ding, B.M. Quinn, S.K. Haram, L.E. Pell, B.A. Korgel, A.J. Bard, Science 296 (2002) 1293.
[11] N. Myung, Z. Ding, A.J. Bard, Nano Lett. 2 (2002) 1315.
[12] K.A. Fähnrich, M. Pravda, G.G. Guilbault, Talanta 54 (2001) 531.
[13] T. Ren, J.Z. Xu, Y.F. Tu, S. Xu, J.J. Zhu, H.Y. Chen, Electrochem. Commun. 7 (2005) 5.
[14] J.J. Miao, T. Ren, D. Lin, J.J. Zhu, H.Y. Chen, Small 1 (2005) 1.
[15] R.C. Matos, E.O. Coelho, C.F. Souza, F.A. Guedes, M.A.C. Matos, Talanta 69 (2006) 1208.
[16] R.F. Pupo Nogueira, M.C. Oliveira, W.C. Paterlini, Talanta 66 (2005) 86.
[17] B.Q. Wang, B. Li, Z.X. Wang, G.B. Xu, Q. Wang, S.J. Dong, Anal. Chem. 71 (1999) 1935.
[18] X.W. Zhou, X.P. Li, Y. Lin, X.R. Xiao, Chin. J. Semicond. 15 (1994) 858.
[19] A.J. Bard, L.R. Faulkner, Electrochemical Methods, Fundamentals and Applications, second ed., Wiley, New York, 2001.
[20] H. Cui, G.Z. Zou, X.Q. Lin, Anal. Chem. 75 (2003) 324.
[21] N. Myung, Y. Bae, A.J. Bard, Nano Lett. 3 (2003) 1053.
[22] R.J. Brainard, A.B. Ellis, J. Phys. Chem. B 101 (1997) 2533.
[23] G.Z. Zou, H.X. Ju, Anal. Chem. 76 (2004) 6871.
[24] K. Dou, J.L. Zhao, C.M. Jin, L.D. Sun, S.H. Huang, J.Q. Yu, Chin. J. Lumin. 16 (1995) 278.
[25] H. Yao, N. Li, S. Xu, J.Z. Xu, J.J. Zhu, H.Y. Chen, Biosens. Bioelectron. 21 (2005) 372.
[26] S. Kulmala, J. Suomi, Anal. Chem. Acta 500 (2002) 21.

Available online at www.sciencedirect.com
ScienceDirect
Talanta 71 (2007) 1494–1499
Talanta
www.elsevier.com/locate/talanta

Quantum dot-based immunosensor for the detection of prostate-specific antigen using fluorescence microscopy

Kagan Kerman [a,*], Tatsuro Endo [b], Masatoshi Tsukamoto [a], Miyuki Chikae [a], Yuzuru Takamura [a], Eiichi Tamiya [a]

[a] *School of Materials Science, Japan Advanced Institute of Science and Technology (JAIST), 1-1 Asahidai, Nomi City, Ishikawa 923-1292, Japan*
[b] *Department of Mechano-Micro Engineering, Interdisciplinary Graduate School of Science and Engineering, Tokyo Institute of Technology, 4259 Nagatsuta-cho, Midori-ku, Yokohama 226-8502, Japan*

Received 18 May 2006; received in revised form 11 July 2006; accepted 11 July 2006
Available online 22 August 2006

Abstract

A sensitive optical method based on quantum dot (QD) technology is demonstrated for the detection of an important cancer marker, total prostate-specific antigen (TPSA) on a disposable carbon substrate surface. Immuno-recognition was carried out on a carbon substrate using a sandwich assay approach, where the primary antibody (Ab)-protein A complex covalently bound to the substrate surface, was allowed to capture TPSA. After the recognition event, the substrate was exposed to the biotinylated secondary Abs. After incubation with the QD streptavidin conjugates, QDs were captured on the substrate surface by the strong biotin-streptavidin affinity. Fluorescence imaging of the substrate surface illuminated the QDs, and provided a very sensitive tool for the detection of TPSA in undiluted human serum samples with a detection limit of 0.25 ng/mL. The potential of this method for application as a simple and efficient diagnostic strategy for immunoassays is discussed.

Keywords: Quantum dot; Immunoassay; Prostate-specific antigen; Fluorescence microscopy

1. Introduction

Semiconductors with all three dimensions in the ∼1–10 nm size range are referred to as "quantum dots" (QDs) [1–3]. These luminescent nanocrystals behave like a transitional stage between bulk semiconductors and single atoms [4,5]. QDs have become the ultimate tools for scientific research of three dimensionally confined systems. The quantum confinement of electron and hole carriers at dimensions smaller than the bulk Bohr exciton radius enables QDs with size-dependent tunable properties [6]. QDs can be prepared in homogeneous size and shape to allow emission with narrow bandwidths [7]. Moreover, a substantial enhancement in the QD photoluminescence quantum yield occurs, when their inorganic core is over-coated with a thin layer of a wider band-gap semiconducting material [8]. Especially, the use of appropriate surface-capping ligands allows their dispersion in a wide variety of solvents, including water, which enables a surface suitable for bioconjugation [9].

During the last few years, intensive work has been directed toward the synthesis and use of photoluminescent quantum dots for biochemical applications as labels in bioanalysis and diagnostics, as tags for protein and DNA-based assays, or as bio-compatible labels for in vivo imaging studies [10,11]. Recent advances have shown that QDs can be conjugated with biomolecules, such as peptides, antibodies (Abs), nucleic acids for use in clinical and biochemical research [12–14]. Different approaches have been reported for the linkage between the biomolecules and QDs. Bruchez et al. [4] coated the surface of QD with silica, and then linked biomolecules onto the silica surface. Chan and Nie [5] directly linked proteins to the QD surface via mercaptoacetic acid and showed that transferrin-coated QDs could undergo receptor-mediated endocytosis into HeLa cells. Self-assembled QD bioconjugates were prepared by using engineered poly-histidine terminated proteins [15].

Adaptor molecules have been self-assembled on the QD surface and constituted the link between QDs and biomolecules. The advantages of avidin as "natural" bridge between QDs

* Corresponding author.
E-mail address: kkerman@jaist.ac.jp (K. Kerman).

0039-9140/$ – see front matter © 2006 Elsevier B.V. All rights reserved.
doi:10.1016/j.talanta.2006.07.027

and antibodies were reported by Goldman et al. [16]. Lingerfelt et al. [17] reported the preparation of QD-biotin conjugates and their use in immunochromatograhic assays. The detection of immunoglobulin G (IgG) was carried out on a glass chip using a sandwich assay approach in connection with the QD-labeled secondary antibody [18]. A sandwich immunoassay for the detection of staphylococcal enterotoxin B (SEB) was run using polyclonal sheep anti-SEB antibody (SEB-pAb)–QD conjugate and microtiter plates coated with monoclonal SEB antibody (SEB-mAb) [16]. Sapsford et al. [19] used glass slides coated with a monolayer of neutravidin (NA) as the template, QDs with maltose binding protein (MBP) and avidin coordinated to their surface were attached to the glass slides in discrete patterns using an intermediary bridge of biotinylated MBP or antibody linkers. Su and Li [20] reported the immunomagnetic separation and detection of *E. coli* O157:H7. After magnetic separation, the immuno-complexes were labeled with QDs via biotin-streptavidin conjugation. The peak intensity of the fluorescence emission was proportional to the initial cell concentration of *E. coli* O157:H7 in the range of 10^3–10^7 CFU/mL with a detection limit at least 100 times lower than that of the FITC-based method. Pegylated and streptavidin-conjugated QDs were used as effective detection elements for reverse-phase protein microarrays [21]. Hahn et al. [22] have also used QDs in a simple fluorometric assay to detect single cells of the pathogenic *E. coli* O157:H7 serotype. Other examples included both direct and indirect immunoassays with QDs in microarrays, spironolactone determination, uric acid biosensor, and Western blotting [23–27].

PSA is an intracellular glycoprotein (34 kDa, kallikrein-like protease) synthesized only by the prostate gland. PSA is a normal constituent of prostatic tissue, and is also found in metastatic prostatic carcinoma, prostatic fluid, and seminal plasma [28]. PSA in serum exists both as free PSA (fPSA) and α_1-antichymotrypsin complexed with PSA (ACT-PSA) [29–31]. Total PSA (TPSA) is defined as the combination of both fPSA and ACT-PSA. The cut-off limit for TPSA between prostate hyperplasia and cancer is 4 ng/ml [32]. The objective of this report was the exploration of the possible application of QD-labeled biomolecules in a sandwich-type immunoassay for TPSA detection on a screen-printed carbon substrate in connection with fluorescence imaging.

2. Experimental

2.1. Reagents

Quantum dot 525 Streptavidin conjugates (QD) and incubation buffer were obtained from Invitrogen (USA). Monoclonal antibody to total prostate-specific antigen (TPSA-mAb) was purchased from Scripps Laboratories (San Diego, CA) and Rohto Pharmaceutical Co., Ltd. (Osaka, Japan). The purified protein of TPSA, was obtained from Chemicon International (Temecula, CA). Recombinant human chorionic gonadotropin (hCG) was obtained from Rohto Pharmaceutical Co., Ltd. (Osaka, Japan).

N-hydroxysulfosuccinimide (NHS) and 1-ethyl-3-(3-dimethylaminopropyl) carbodiimide (EDC) were purchased from Aldrich. All other chemical reagents were supplied by Wako Pure Chemicals Co. (Tokyo, Japan) and were used as received. The planar screen-printed carbon substrates consisted of a carbon working electrode, a carbon counter electrode, and Ag/AgCl reference electrode, were provided from BioDevice Technology Ltd. (Ishikawa, Japan). The length and width of the strip was 11 and 3 mm, respectively, and the geometric working area was 2.64 mm^2. Ultra-pure water (18.3 MΩ-cm) that was obtained from Milli-Q purification system (Millipore, MA, USA), was used for the preparation of all solutions and cleaning of substrates. The present work with human serum samples was carried out in accordance to the ethical standard of the Helsinki Declaration of 1975, as revised in 1996.

2.2. Method

All carbon substrates were first rinsed with water and blot dried before use. The substrates were then electrochemically activated by applying 1.70 V for 1 min, which caused the formation of carboxylic groups on the carbon surface. Then, the substrates were immersed into 100 μL of 50 mM phosphate buffer solution (PBS, pH 7.4) containing 5 mM EDC and 8 mM NHS for 1 h. After the covalent activation process and rinsing with water, an aliquot (20 μL) of 100 μg/mL Protein A in acetate buffer (3 mM acetic acid and 7 mM sodium acetate, pH 4.8) was pipetted onto the surface and kept for 1 h at room temperature to couple Protein A lysine residues covalently to the functionalized substrates. The modified substrates were then extensively rinsed with water and conditioned overnight at 4 °C before use. No loss of IgG binding activity was observed over a 3-day storage period. Then, an aliquot (20 μL) of a desired amount of mAb in PBS was pipetted onto the surface, and allowed to interact with the Fc fragment of the Abs for 30 min at room temperature to yield the sensing interfaces.

The unbound mAb was washed away with blank PBS. The unreacted covalent-active surface groups were subsequently passivated by reaction with 1 mM ethanolamine under the similar conditions for 1 h as reported by Lieber and co-workers [33].

The target Ag, TPSA, was pipetted (20 μL) onto the surface, and incubated for 30 min at room temperature. After rinsing the substrates with PBS, the biotinylated secondary TPSA-mAbs at 12.5 μg/mL diluted in PBS were introduced (20 μL) to the substrate surface, and incubated for 1 h. The QD 525 Streptavidin Conjugate (Invitrogen, USA) was diluted to the appropriate concentration (1:50) with QD Incubation Buffer (Invitrogen, USA). The substrates were rinsed with PBS, and the prediluted QD solution was added (20 μL) onto each substrate, and incubated for 30 min. After the incubation with QDs, the substrates were rinsed with PBS.

The fluorescence from QDs attached on the surface of the substrate was magnified by a Leica MZFL III microscope (Wetzlar, Germany) and imaged using a charge-coupled device (CCD) camera detector (ZVS-3C75DE, Carl Zeiss Inc., Switzerland) and its GFP3 filter set (excitation at 470 nm with a band width of 40 nm; emission at 525 nm with a band width of 50 nm) in connection with AquaCosmos 2.5 image acquisition software

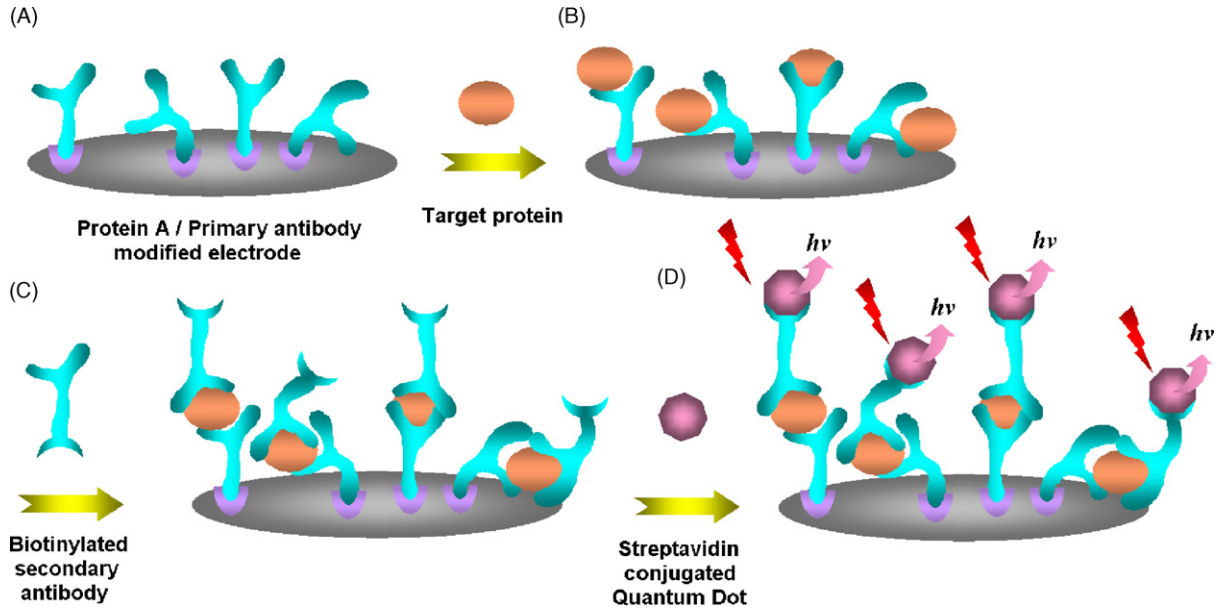

Scheme 1. Quantum dot (QD)-based sandwich-type immunoassay. Protein A/TPSA-mAb modified surface (A) is exposed to the target Ag (TPSA) (B). Then, the electrode is exposed to the biotinylated secondary Abs (C). After incubation with the QD streptavidin conjugates, QDs are captured on the surface by the strong biotin-streptavidin affinity. Fluorescence scanning of the electrode surface illuminates the QDs, with an emission at 525 nm (D).

(Hamamatsu Photonics Inc., Japan). The images were then analyzed using IP Lab 3.5.5 software (Scanalytics Inc., VA, USA).

3. Results and discussion

The immunoassay was conducted by following the typical procedure for sandwich-type assays as shown in Scheme 1. The primary TPSA-mAbs were immobilized on the substrate surface through the binding of their Fc portions with Protein A covalently immobilized on the carbon surface (Scheme 1A). Then, TPSA was captured as a result of the immuno-recognition event (Scheme 1B). Then, the biotinylated secondary TPSA-mAbs were attached to the TPSA molecules on the surface (Scheme 1C). Streptavidin-coated QDs bound to the biotinylated secondary TPSA-mAbs with high affinity (Scheme 1D). Since the biotinylated secondary TPSA-mAbs recognized TPSA specifically, they led to the extensive attachment of the streptavidin-coated QDs on the substrate surface. The substrates with the immobilized TPSA became bright, while the substrates without TPSA remained dark. In this way, TPSA could be determined in a simple format using the fluorescence imaging. QD-based detection systems have a high possibility of realizing simple sandwich assay systems, because the ELISA requires labeling of the secondary Abs with external reagents; such as enzymes and/or fluorescent dyes. This labeling procedure may cause structural change in the epitope and suppression in its specific recognition ability. Furthermore, the enzymatic and fluorescence dye labeling procedures are time-consuming and cause a high background signal. However, the application of streptavidin-coated QDs greatly simplifies the labeling procedure, while not affecting the binding efficiency of the secondary Abs.

We spiked the serum sample of a healthy female with the known concentrations of TPSA. The images obtained with several spiked concentrations of TPSA are shown in Fig. 1. The limit of detection was achieved at 0.25 ng/mL as observed in Fig. 1A. As the amount of TPSA captured on the surface increased, the fluorescence response of the substrates increased as displayed in Fig. 1A–D. The number of attached QDs and their intensity values increased linearly with the increasing concentration of TPSA in a wide range of 0.25–100 ng/mL. According to the fluorescence intensity results, there was 12.5 ng/μm^2 of primary TPSA-mAb on the electrode. We also determined that 90% ($\pm$10) of the fractions were active. Only a negligible amount, which was 0.75% ($\pm$0.25) of the mAbs, eluted off during the incubation period with TPSA, and this elution did not significantly affect our results.

Surface fluorescence intensity dependency of the QD streptavidin conjugates are shown in Fig. 2. The biotinylated secondary TPSA-mAbs captured the streptavidin conjugated QDs, and the fluorescence images of QDs confirmed the presence of target protein on the substrate. We observed that the number of QDs increased with the increasing concentration of TPSA on the substrate surface. The fluorescence images provided a limit of detection at 0.25 ng/mL TPSA, which is comparable to the previously reported QD-based immunoassays [18]. Undiluted serum samples were also employed in the target Ag step. The serum samples belonged to consenting adult patients with prostate cancer. The ELISA indicated that PC #1 and #2's serum samples contained 100 and 25 ng/mL TPSA, respectively. Accordingly, we observed ~4-fold higher fluorescence response with higher number of attached QDs on the substrates prepared with the serum sample of PC #1.

Control experiments were performed for checking the unspecific adsorption of QDs onto the substrate surface. First, primary

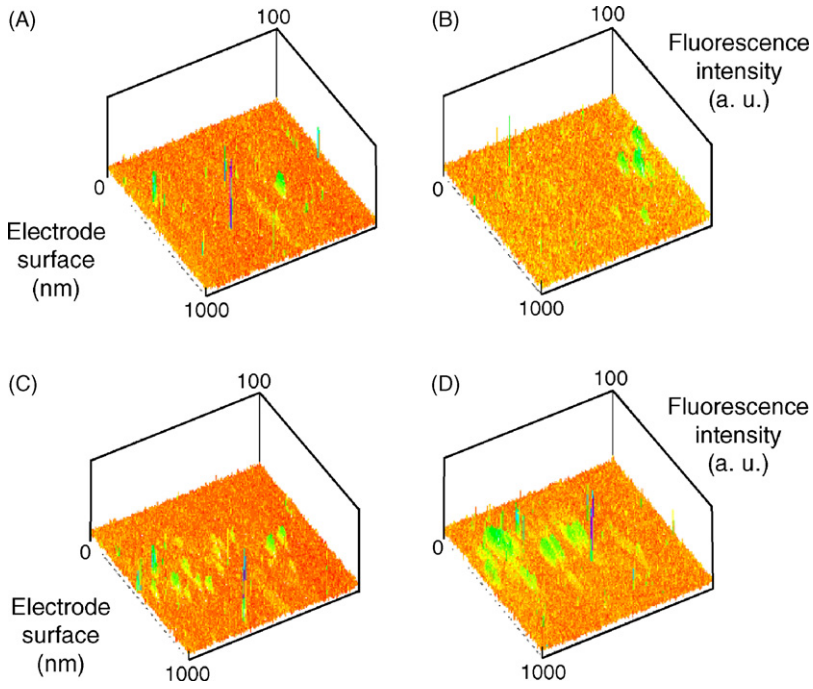

Fig. 1. Surface fluorescence intensity images for the QD streptavidin conjugates with TPSA spiked into healthy female human serum samples at (A) 0.25 ng/mL, (B) 0.5 ng/mL, (C) 1 ng/mL, (D) 2 ng/mL. Other conditions were as described in Section 2.2.

TPSA-mAb was immobilized on the substrate, then, 10 ng/mL TPSA was applied to the surface in 20 μL PBS. However, no biotinylated secondary TPSA-mAb was attached to the Ags. After the interaction with the streptavidin-coated QDs, no fluorescence was observed from the substrate as shown in Fig. 3A. Since there was no biotinylated target for the streptavidin-coated QDs to bind, they could be washed away from the surface easily.

Specificity experiments involved the exposure of the primary TPSA-mAb immobilized on the surface to a different Ag, human chorionic gonadotropin (hCG). A high concentration of hCG at 100 ng/mL was applied onto the primary TPSA-mAb-coated substrate surface, and allowed to react for 30 min at room temperature. The conjugates were then exposed to the biotinylated secondary TPSA-mAb for 1 h. After the interaction with the streptavidin-coated QDs, the substrates were imaged as shown in Fig. 3B. No fluorescence enhancement was observed, since hCG could not bind to the primary TPSA-mAbs immobilized on the surface.

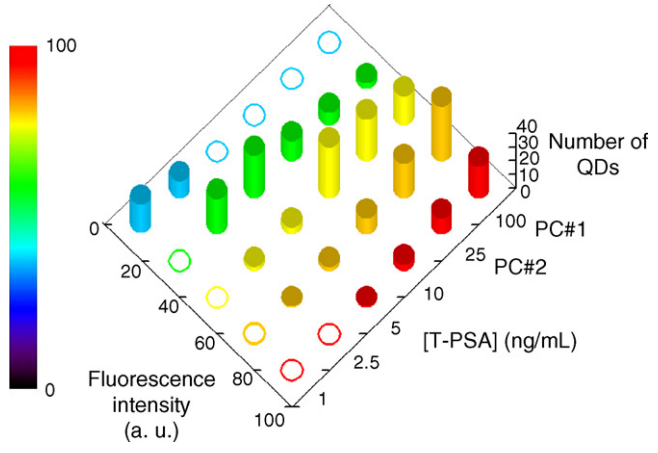

Fig. 2. Plot for the fluorescent intensity and number dependence of QDs on the target antigen (TPSA) concentration for the sandwich-type immunoassay at the substrate surface with the spiked samples in a healthy female human serum, and real serum samples from prostate cancer patient #1 (PC #1) with 100 ng/mL TPSA, and prostate cancer patient #2 (PC #2) with 25 ng/mL TPSA. Other conditions were as described in Section 2.2.

Fig. 3C shows the high fluorescence intensity observed when the serum sample of a consenting adult with prostate cancer. The undiluted serum sample in 20 μL volume was applied on the substrate surface. After the incubation with QDs and rinsing, a high fluorescence response was observed indicating the successful attachment of QDs to the biotinylated secondary TPSa-mAbs on the surface (Figs. 3C and 2, PC #1). The result was in agreement with the expected specificity for the sandwich immunoassays, while providing new opportunities for future immunosensing applications using QDs.

The QD aggregation owing to the non-optimal surface chemistry leading to the loss of colloidal stability in the biolabeling procedure is an important problem for QD-based biosensor applications [34]. In this report, the application of the streptavidin-coated QDs onto the surface of the substrate without any prior conjugations provided a more efficient condition for streptavidin-biotin affinity reaction. When the streptavidin-coated QDs were conjugated with the biotinylated secondary TPSA-mAbs before application to the substrate surface, the aggregation of the QDs lowered the binding efficiency of the secondary TPSA-mAbs to the target Ag, and caused low reproducibility. We anticipate that our reported method here will accelerate the application of QD-based immunoassays and biosensors with various applications.

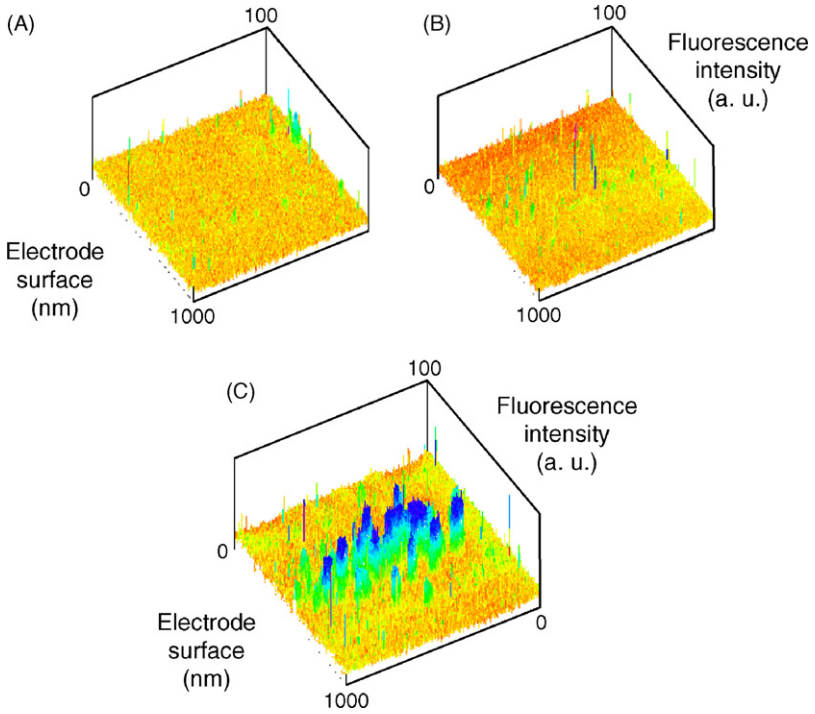

Fig. 3. Surface fluorescence intensity images for the QD streptavidin conjugates (A) without incubation with the biotinylated secondary TPSA-mAb, (B) with 100 ng/mL hCG as the target antigen in the place of TPSA, (C) with the serum sample of a prostate cancer patient (PC #1). Other conditions were as described in Section 2.2.

4. Conclusions

QDs in immunology are promising nanomaterials especially owing to their unique photophysical properties. In this report, we applied QD strpetavidin conjugates in a model immunoassay system for the detection of TPSA cancer marker from the spiked and undiluted serum samples. The applicability of this simple method to serum samples from cancer patients and the low detection limit are promising results. In our laboratory, the application of a multiplexed immunoassay on a disposable carbon-based microarray using different QDs with varying emission wavelengths is under progress.

References

[1] I.L. Medintz, H.T. Uyeda, E.R. Goldman, H. Mattoussi, Nat. Mater. 4 (2005) 435–446.
[2] E.R. Goldman, I.L. Medintz, H. Mattoussi, Anal. Bioanal. Chem. 384 (2006) 560–563.
[3] J.M. Costa-Fernandez, Anal. Bioanal. Chem. 384 (2006) 37–40.
[4] M. Bruchez, M. Moronne, P. Gin, S. Weiss, A.P. Alivisatos, Science 281 (1998) 2013–2016.
[5] W.C.E. Chan, S. Nie, Science 281 (1998) 2016–2018.
[6] C.B. Murray, C.R. Kagan, M.G. Bawendi, Annu. Rev. Mater. Sci. 30 (2000) 545–610.
[7] C.B. Murray, D.J. Norris, M.G. Bawendi, J. Am. Chem. Soc. 115 (1993) 8706–8715.
[8] X. Peng, M.C. Schlamp, A.V. Kadavanich, U. Banin, A.P. Alivisatos, J. Am. Chem. Soc. 119 (1997) 7019–7029.
[9] P. Alivisatos, Nat. Biotechnol. 22 (2004) 47–52.
[10] R.E. Bailey, A.M. Smith, S. Nie, Physica E 25 (2004) 1–12.
[11] A.M. Smith, S. Nie, Analyst 129 (2004) 672–677.
[12] M. Han, X. Gao, J.Z. Su, S. Nie, Nat. Biotechnol. 19 (2001) 631–635.
[13] J.K. Jaiswal, H. Mattoussi, J.M. Mauro, S.M. Simon, Nat. Biotechnol. 21 (2003) 47–51.
[14] X. Gao, Y. Cui, R.M. Levenson, L.W.K. Chung, S. Nie, Nat. Biotechnol. 22 (2004) 969–976.
[15] E.R. Goldman, I.L. Medintz, A. Hayhurst, G.P. Anderson, J.M. Mauro, B.L. Iverson, G. Georgiou, H. Mattoussi, Anal. Chim. Acta 534 (2005) 63–67.
[16] E.R. Goldman, E.D. Balighian, H. Mattoussi, M.K. Kuno, J.M. Mauro, P.T. Tran, G.P. Anderson, J. Am. Chem. Soc. 124 (2002) 6378–6382.
[17] B.M. Lingerfelt, H. Mattoussi, E.R. Goldman, J.M. Mauro, G.P. Anderson, Anal. Chem. 75 (2003) 4043–4049.
[18] B. Sun, W. Xie, G. Yi, D. Chen, Y. Zhou, J. Cheng, J. Immunol. Meth. 249 (2001) 85–89.
[19] K.E. Sapsford, I.L. Medintz, J.P. Golden, J.R. Deschamps, H.T. Uyeda, H. Mattoussi, Langmuir 20 (2004) 7720–7728.
[20] X.-L. Su, Y. Li, Anal. Chem. 76 (2004) 4806–4810.
[21] D. Geho, N. Lahar, P. Gurnani, M. Huebschman, P. Herrmann, V. Espina, A. Shi, J. Wulfkuhle, H. Garner, E. Petricoin, L.A. Liotta, K.P. Rosenblatt, Bioconjugate Chem. 16 (2005) 559–566.
[22] M.A. Hahn, J.S. Tabb, T.D. Krauss, Anal. Chem. 77 (2005) 4861–4869.
[23] E.R. Goldman, A.R. Clapp, G.P. Anderson, H.T. Uyeda, J.M. Mauro, I.L. Medintz, H. Mattoussi, Anal. Chem. 76 (2004) 684–688.
[24] M. Shingyoji, D. Gerion, D. Pinkel, J.W. Gray, F. Chen, Talanta 67 (2005) 472–478.
[25] J. Liang, S. Huang, D. Zeng, Z. He, X. Ji, X. Ai, H. Yang, Talanta 69 (2006) 126–130.
[26] F. Zhang, C. Li, X. Li, X. Wang, Q. Wan, Y. Xian, L. Jin, K. Yamamoto, Talanta 68 (2006) 1353–1358.
[27] R. Bakalova, Z. Zhelev, H. Ohba, Y. Baba, J. Am. Chem. Soc. 127 (2005) 9328–9329.
[28] S. Knoll, F.R. Vogel, L. Niessen, Lett. Appl. Microbiol. 34 (2002) 144–148.

[29] S. Wesseling, C. Stephan, A. Semjonow, M. Lein, B. Brux, P. Sinha, S.A. Loering, K. Jung, Clin. Chem. 49 (2003) 887–894.
[30] C. Fernandez-Sanchez, C.J. McNeil, K. Rawson, O. Nilsson, Anal. Chem. 76 (2004) 5649–5656.
[31] S.P. Balk, Y.-J. Ko, G.J. Burbley, J. Clin. Oncol. 21 (2003) 383–391.
[32] F. Oberpenning, S. Hetzel, C. Weining, B. Brandt, G.A. Angelis, A. Heinecke, M. Lein, P. Fornara, H. Schmid, L. Hertle, A. Semjonow, Eur. Urol. 43 (2003) 478–484.
[33] G. Zheng, F. Patolsky, Y. Cui, W.U. Wang, C.M. Lieber, Nat. Biotechnol. 23 (2005) 1294–1301.
[34] M. Seydack, Biosens. Bioelectron. 20 (2005) 2454–2469.

Available online at www.sciencedirect.com
ScienceDirect
Talanta 71 (2007) 1642–1651
Talanta
www.elsevier.com/locate/talanta

The definition of basic TEDS of IEEE 1451.4 for sensors for an electronic tongue and the proposal of new template TEDS for electrochemical devices

Jeong-Do Kim [a], Dong-Jin Kim [a,*], Hyung-Gi Byun [b], Yu-Kyung Ham [a], Woo-Suk Jung [a], Dong-Won Han [c], Jun-Seok Park [c], Hyo-Lin Lee [d]

[a] *Department of Electronics Engineering, Hoseo University, San 29-1 Sechul, Beabang Asan City, Chungnam 336-795, Republic of Korea*
[b] *School of Information and Communication Engineering, Kangwon National University, Samcheok, Kangwondo 245-711, Republic of Korea*
[c] *Electronics and Telecommunications Research Institute, Republic of Korea*
[d] *McScience Co., Republic of Korea*

Received 16 June 2006; received in revised form 26 July 2006; accepted 26 July 2006
Available online 7 September 2006

Abstract

It is important to define a standard method to store basic sensor information, such as the type and the structure of sensors for an electronic tongue system and there is no such method defined in the IEEE 1451.4 transducer electronic data sheet (TEDS) so far. The major challenge is to choose a suitable standard template that can be used with sensors for electronic tongues. However, the standard templates provide an imprecise specification when used with sensing devices for electronic tongues. In this paper, we present definitions of the basic TEDS of IEEE 1451.4 for sensors for an electronic tongue system and propose a new template TEDS for IEEE 1451.4 for potentiometric devices.

Keywords: IEEE 1451.4 TEDS; Electronic tongue; New template TEDS

1. Introduction

A sensor senses the surrounding environment and converts the sensed information into a signal. The converted signal should be communicated to other devices such as microprocessors. It is very important for a sensor to communicate with other devices that receive information from sensors.

In 1993, the IEEE P1451.4 standard for plug-and-play systems between sensors and microprocessors was proposed by the National Institute of Standards and Technology (NIST) and the Institute of Electrical and Electronic Engineers (IEEE). In 1997, the IEEE 1451.2 standard defined the communication protocol and a format the transducer electronic data sheet (TEDS) between a sensor and microprocessor [1]. Further, in 2004, the IEEE 1451.4 TEDS was standardized based on the IEEE 1451.2 TEDSs [2]. The IEEE 1451.4 TEDS structure is flexible and extensible to handle a wide range of sensor type and it is very compact allowing the saving of memory. In fact, while the IEEE 1451.2 TEDS requires 1376 bits to describe one sensor, the IEEE 1451.4 TEDS requires only about 256 bits [3]. Recently, many companies such as National Instrument and Honeywell Sensotec are proposing methods to use the IEEE 1451.4 TEDSs [4,5]. The IEEE 1451.4 standard, which comprises an accelerometer is commercialized by Wilcoxon Inc. [6]. The communication protocol that includes an IEEE 1451.4 TEDS is implemented by the Korea Research Institute of Standards and Science (KRISS) in Korea. The IEEE 1451.4 TEDS has 17 standard template TEDSs according to the type of sensor structure and measurement circuit [4,5].

Electronic tongue (E-tongue) uses sensing principles, such as methods like potentiometry or voltammetry, optical method and quartz crystals. Electrochemical techniques such as potentiometry and voltammetry are most important techniques. These two techniques require at least two electrodes. One electrode responds to the target molecule and is called the working elec-

* Corresponding author. Tel.: +82 41 534 6778; fax: +82 41 534 6778.
E-mail address: xjr1@nate.com (D.-J. Kim).

0039-9140/$ – see front matter © 2006 Elsevier B.V. All rights reserved.
doi:10.1016/j.talanta.2006.07.049

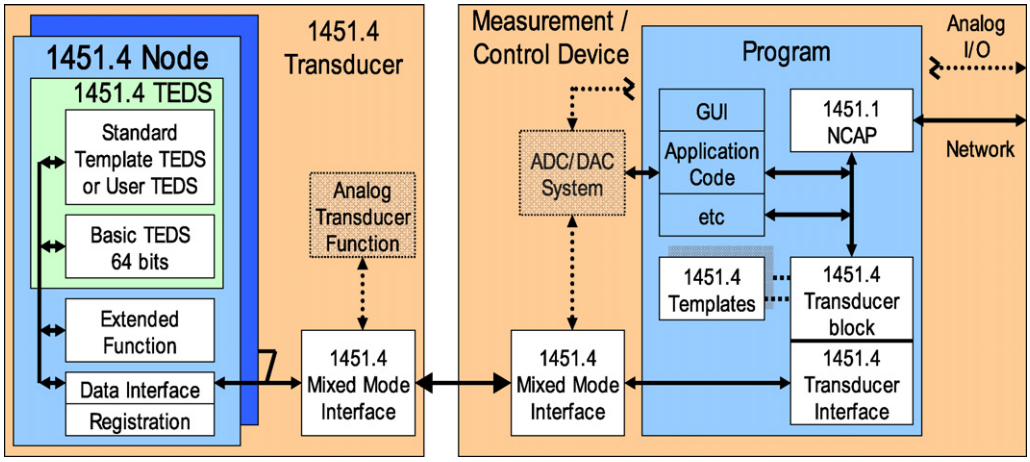

Fig. 1. Block diagram of the IEEE 1451.4 TEDS data system [2].

trode, the second electrode is of constant potential and is called the reference electrode.

Moreover, new concepts pertaining to taste sensors for E-tongues were published in 1990. These comprised multichannel ion-selective liquid membranes based on the potentiometric method [7,8].

In an E-tongue, a different array setup has to be selected for different applications because sensing devices have limited sensitivity and selectivity for a certain compound.

It is important to define a standard way to store basic sensor information, such as the type and structure of the sensor, relating to E-tongues in the basic TEDS since there is none defined in the IEEE 1451.4 so far. A solution to standardize gas sensors and electronic olfactory systems was presented by Ulivieri et al. [3].

In this paper, we codify the version letter and version number in the basic TEDS to indicate the type of sensor for the E-tongue. However, even though the sensor information for an E-tongue is defined, it does not allow automatic configuring of the electronic interface. This facility is offered by the standard templates. The major challenge is to choose a suitable standard template that is universally accepted and that can be used with the sensors for E- tongues. However, the standard templates, provide an imperfect specification for the sensing devices for E-tongues.

In this paper, we propose a template TEDS for potentiometric devices, which are popular sensing device in E-tongues, and also present a virtual instrument for the automatic creation of the TEDS.

2. The IEEE 1451.4

2.1. Overview of IEEE 1451.4

The purpose of the IEEE 1451 standards for a smart transducer interface for sensors and actuators is to define a set of common interfaces for connecting transducers to microprocessor-based systems. At present, the IEEE 1451 family standard is divided into seven parts named IEEE 1451.0–4, IEEE P1451.5, and IEEE P1451.6, where P standards for "proposal" since some parts are not yet approved [3,9].

The IEEE 1451.2 was first approved in 1997 [1], but it has been under revision since 2004. This standard defines a 10-wire bus and the related protocol. The main innovation introduced by the IEEE 1451.2 is the definition of a TEDS, which is a data structure stored in a small amount of nonvolatile memory that is physically associated with the transducer. The IEEE 1451.4 defines a mixed-mode interface (MMI) for analog transducers and defines the TEDSs to be associated with the analog transducers; these TEDSs are different from those of the IEEE 1451.2 [3,9,10].

The block diagram of the TEDS data system in Fig. 1 shows a hierarchy of functions; this hierarchy is necessary to house the TEDS data within a physical memory and to allow the accessibility of that data via a data transmission protocol. Note that Fig. 1 illustrates all parts of a fully implemented IEEE 1451.4-compliant TEDS system: the TEDS is contained within a node located inside a transducer, which contains an MMI. The TEDS data are available to a measurement/control device containing the 1451.4 transducer interface and transducer block and a template library, to fit into the IEEE 1451.1 network capable application processor (NCAP) object model. The NCAP is constructed by means of a common control network information object model for smart sensors and actuators. The NCAP object model is described fully in IEEE Std 1451.1-1999 [10].

2.2. Mixed-mode interface of IEEE 1451.4 standard

The IEEE 1451.4 MMI connects the transducer conforming to this standard and NCAP or data acquisition system for both analog signals and digital TEDS data. This standard is defined by two classes, namely, classes 1 and 2 interfaces [3].

Class 1 MMI is defined for the sequential transmission of either a transducer signal or digital TEDS data on a single connection. Class 1 shall allow a transducer signal and power, or digital TEDS data and power, to make alternate use of the same connection. Class 1 transducers utilize the existing analog standard by adding the TEDS to a switch that is controlled by the

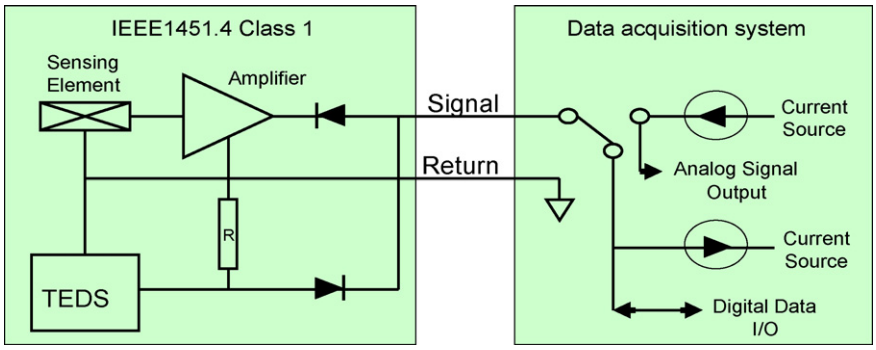

Fig. 2. IEEE 1451.4 class 1 MMI tow-wire interface [2,3].

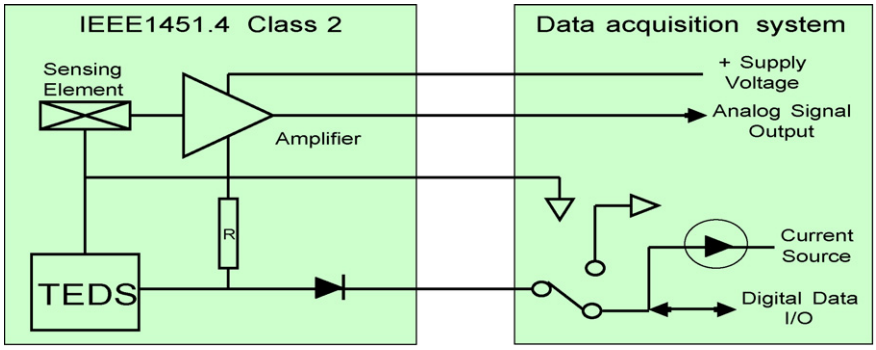

Fig. 3. IEEE 1451.4 class 2 MMI multi-wire interface [2,3].

direction of the current as sketched in Fig. 2. By reversing the direction of the current, the data acquisition system switches the sensor into digital TEDS mode [2,3].

Class 2 MMIs use separate connections for transducer signals and digital TEDS data. These allow simultaneous access to a transducer signal and digital TEDS data, and class 2 connections may share a common return. Fig. 3 illustrates an example of the IEEE 1451.4 based class 2 multi-wire interface. Other front ends such as a multi-wire interface with a bridge sensor or with a 4–20 mA sensor are supported by the class 2 interface as well [2,3].

2.3. IEEE 1451.4 TEDS

In 2004, IEEE 1451.4 was established for adding plug-and-play capabilities to analog transducers. The underlying mechanism for the plug-and-play identification is the standardization of a TEDS. A TEDS contains the critical information needed by an instrument or measurement system to identify, characterize, interface, and properly use the signal from an analog sensor.

The TEDS information consists of basic TEDS, standard template TEDS, calibration TEDS template, and user data [2,4,5].

The basic TEDS includes the manufacturer ID, model number, version letter, and serial number of the sensor. The standard template TEDS records the type of the sensor and actuator, sensitivity of the sensor, range of measurement, bandwidth, etc. Moreover the calibration TEDS template comprises the date of last calibration, correction engine coefficients, etc. Consequently, a TEDS contains the critical information required to use the sensors. The content of a standard TEDS for IEEE 1451.4 is illustrated in Table 1 [2,4,5].

The basic TEDS has the first 64 bits in the IEEE 1451.4 standard TEDS and stores data in a nonvolatile memory. These data have to describe the manufacturer and product information for the sensor and actuator. The manufacturer ID is an enumeration of manufacturers. These ID assignments will also be available in an American standard code for information interchange (ASCII) text file available from the IEEE. Moreover, the assignment of the remainder of the basic TEDS is left to the discretion of the manufacturer. The basic TEDS is shown in Table 2 [4,5].

The standard template TEDS is shown in Table 3. This defines the template ID according to the general classification of sensors. Templates 25 through 39 are sensor type templates that contain the properties required for specific types of sensors (transducers). Templates 40, 41, and 42 are calibration templates and can

Table 1
Standard TEDS contents [4,5]

Basic TEDS (64 bits)
Selector (2 bits)
Template ID (8 bits)
Standard template TEDS (ID = 25–39)
Selector (2 bits)
Template ID (8 bits)
Calibration TEDS template (ID = 40–42)
Selector (2 bits)
Extended end selector (1 bit)
User data

Table 2
Contents of the basic TEDS [2,4,5]

	Bit length	Allowable range
Manufacturer ID	14	17–16381
Model number	15	0–32767
Version letter	5	A–Z (data type, Char 5)
Version number	6	0–63
Serial number	24	0–16777215

Table 3
Standard template TEDS [2,4,5]

Type	Template ID	Name of template
Transducer type template	25	Accelerometer and force
	26	Charge amplifier (without attached accelerometer)
	27	Charge amplifier (without attached force transducer)
	28	Microphone with built-in preamplifier
	29	Microphones (capacitive)
	30	High-level voltage output sensors
	31	Current loop output sensors
	32	Resistance sensors
	33	Bridge sensors
	34	LVDT/RVDT
	35	Strain gage
	36	Thermocouple
	37	Resistance temperature detectors (RTDs)
	38	Thermistor
	39	Potentiometric voltage divider
Calibration template	40	Calibration table
	41	Calibration curve (polynomial)
	42	Frequency response table

be used with one of the transducer-type templates. Each template ID is classified according to the type of sensor, sensing circuit, output signal, operation temperature, etc. A classified template ID has specific information for individual sensors such as the level of output signal for sensing, resolution of the analog-to-digital converter (ADC), etc.

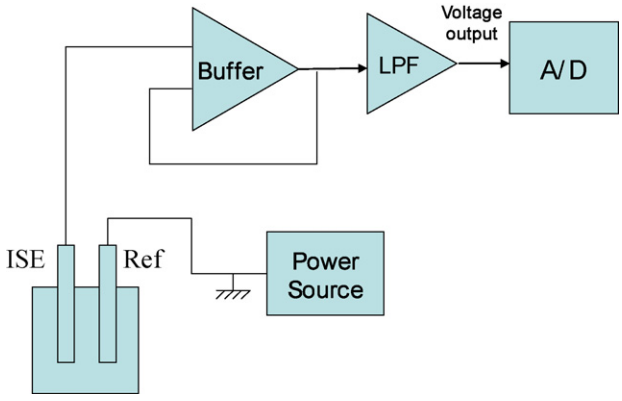

Fig. 4. A typical measurement circuit for potentiometry techniques.

3. Sensors for E-tongue system [11]

3.1. Electrochemical devices

There are several measurement principles that have potential uses in an E-tongue system. The most important ones are based on electrochemical techniques such as potentiometry, voltammetry, and conductometry. The two basic electrochemical principles are potentiometry and voltammetry. Potentiometric and voltammetric devices require at least two electrodes: a working electrode that responds to the target molecule and a reference electrode that has a constant potential [7,12].

Potentiometry measures the potential of electrodes across an ion-selective membrane at zero current flow. Different types of membrane materials with different recognition properties have been developed. The selective determination of various species is possible by using ion-selective electrodes (ISE) and is based on the selective reaction or complexation of the analyte with a species that is present within the electrode. By using different types of ion-selective membranes, sensor arrays with overlapping selectivities can be obtained. In the early 1970s, ion-selective field-effect transistors (ISFETs), in which the ion-selective material was directly integrated with solid-state electronics, were developed. The company which is called Alpha

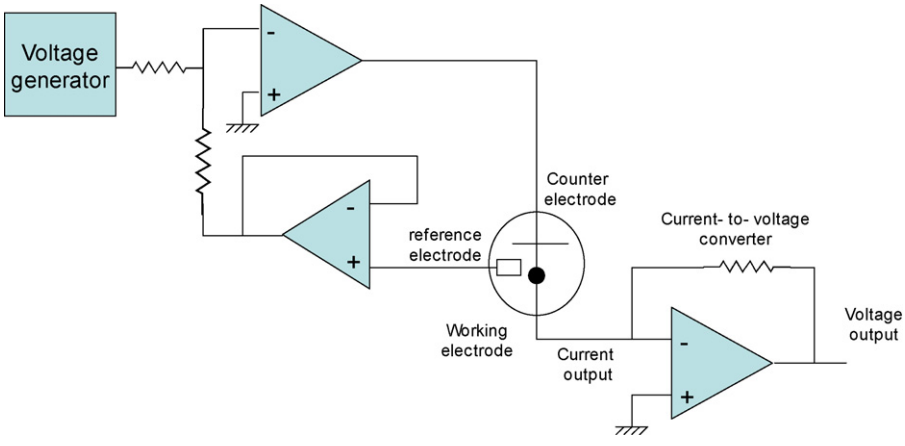

Fig. 5. A typical measurement circuit for voltammetry techniques.

MOS [13], has commercialized an E-tongue that consists of different types of ISFETs.

Fig. 4 shows a typical measurement circuit for the potentiometry technique, which provides voltage as the output signal.

In voltammetric techniques, the electrode potential is used to drive an electron transfer reaction, and the resulting current is measured. The magnitude of the electrode potential determines whether the target molecules lose or gain electrons. Voltammetric methods can thus measure any chemical species that is electroactive: they also provide a high sensitivity, a wide linear range, and require simple instrumentation [7,12]. Many types of voltammetric methods exist. The specific type depends on the type of the potential profile employed and the point where the current is measured. Five types of voltammetric techniques are commonly used: cyclic voltammetry, amperometry, linear-sweep voltammetry, differential-pulse voltammetry, and stripping voltammetry.

Fig. 5 illustrates the circuit for voltammetry techniques, which provides a voltage output throughout the current-to-voltage (*C*/*V*) converter.

The conductivity or impedance measurements of polymers such as polythiophene or polypyrrole have also been described as a useful application of the E-tongue system. These systems offer a very simple measurement technique in which voltage is measured obtaining impedance: because of the membrane properties, the system are versatile and can be miniaturized [7,12] (Figs. 6 and 7).

Table 4
Basic TEDS for electronic tongue

	Length in bits	Allowable range
Manufacturer ID	14	16382
Model number	15	0–32767
Version letter	5	Reserved
Version number	6	Reserved
Serial number	24	

Recently, many studies on sensor arrays using microelectrochemical biosensors and DNA sensors have been reported. These sensor arrays are designed by applying potentiometric, voltammetric, conductometric and acoustic methods.

3.2. Other devices (piezoelectric devices, optical devices)

In piezoelectric devices, piezoelectric crystals generate a voltage with a stable oscillation across them when an alternating current is applied using an external oscillatory circuit. This resonant frequency changes with the crystal mass [7,12].

With regard to optical devices, a multichannel taste sensor based on a fiber optic evanescent field absorption sensor was recently described [7,12].

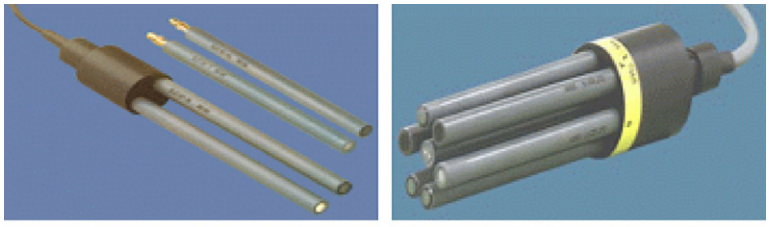

Fig. 6. (a) Electrode and (b) electrodes.

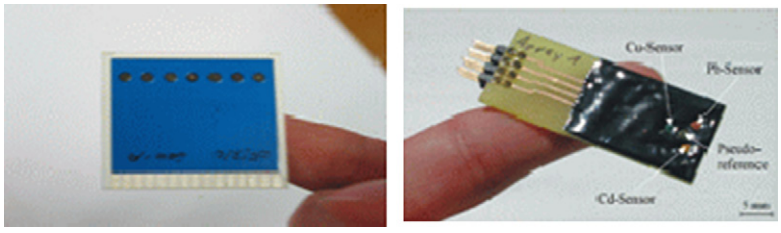

Fig. 7. Specially designed electrodes.

Table 5
Proposal of version letter-type of sensor

Version letter	Type of electronic tongue sensor	Version letter	Type of electronic tongue sensor
L	Ion-sensitive lipid membranes	C	Electroconductive polymer sensor
S	Ion-selective electrodes	V	Voltammetric electrode
F	Ion-selective field effect transistors	O	Optic sensor
M	Surface potential mapping method	P	Piezoelectric sensor

Table 6
Version number for active materials corresponding to E-tongue sensors

Version Number		Type of Sensor (Version Letter)							
		L	S		F	M	C	V	O	P
000 000		No description								
000 001 : 000 111		R	R		R	R	R	R	R	R
001 XXX			Solid-state membrane							
010 XXX			PVC membrane							
011 XXX			Glass membrane							
100	000	R	Metal electrode	No-description	R	R	Polypyrrol (polymeric material)	Platinum (working electrode)	R	R
	001			Platinum			Polyaniline	Gold		
	010			Silver			Polythiophene	Iridium		
	011			Gold			R	Rhodium		
	100			Antimony				Palladium		
	101			Mercury				Rhenium		
	110			Glassy carbon				R		
	111			Others						
101 XXX			pH electrode				R	R		
110 XXX			R							
111 XXX										

R: reserved.

4. Proposal of IEEE 1451.4 TEDS for E-tongue system

4.1. Definition of IEEE 1451.4 basic TEDS for E-tongue system

The basic TEDS for sensors of the E-tongue system is important to codify the proposal and is shown in Table 4.

The manufacturer ID is an enumeration of manufacturers. Several IDs have been assigned to early adopters, and future assignments will be managed by the IEEE [5]. In this paper, the manufacturer ID assigned is 16382, which is reserved for a user-defined template for academic experiments.

To indicate the type of E-tongue sensor and its sensing materials, we proposed the version letter and number given in Tables 5 and 6 in the basic TEDS. The version letter proposed correspondence letter type can be associated with the type of sensors for the E-tongue system, which is illustrated in Table 5. The proposed active materials corresponding to the E-tongue sensors and their version number are shown in Table 6 [14–17].

4.2. A proposal for a new template TEDS of IEEE 1451.4 for potentiometric devices

To define the IEEE 1451.4 TEDS an E-tongue system, we should apply a potentiometric voltage divider template with an

Table 7
The structure of the template TEDS

Field (section)	Contents
Basic information on system	See Table 8
Information on sensor	See Table 11
Limitation of sensor	See Table 12
Information on reference electrode	See Table 13
Information on calibration	See Table 16

Table 8
Proposal for a template TEDS-basic information on system

Field	Property/command	Description	Access	Bits	Data type (and range)
Basic information on system	Template	Template ID		8	Integer (ID = 44)
	Select case—version letter (see Table 5)		ID	5	Char 5
	Select case—version number (see Table 6)		ID	6	Select case
	Select ion species and sensing element (see Table 10)		ID	6	Select case

Table 9
An example of basic information on system

Field	Description	Access	Bits	Data
Basic information on system	Template ID		8	Integer (ID = 44)
	Ion selective electrode	ID	5	"S"
	Platinum electrode MSB 3 bit 0b**011xxx**: metal electrode LSB 3 bit 0b**xxx011**: platinum element	ID	6	0b011001
	Type of wire	ID	6	0b010111

Table 10
Types of ion species and sensing elements [14–17]

Case	Ion species/sensing element	Case	Ion species/sensing element	Case	Ion species/sensing element
0	Ammonium (NH_4^+)	10	Iodide (I^-)	20	Thiocyanate (SCN^-)
1	Barium (Ba^{2+})	11	Lead (Pb^{2+})	21	Sulphate (SO_4^{2-})
2	Bromide (Br^-)	12	Mercury (Hg^{2+})	22	Plate
3	Cadmium (Cd^{2+})	13	Nitrate (NO_3^-)	23	Wire
4	Calcium (Ca^{2+})	14	Nitrite (NO_2^-)	24	2 Wire
5	Carbonate (CO_3^-)	15	Perchlorate (CLO_4^-)	25	Ring
6	Chloride (Cl^-)	16	Potassium (K^+)	26	Rod
7	Copper (Cu^{2+})	17	Silver (Ag^+)	27	Disc
8	Cyanide (CN^-)	18	Sodium (Na^+)	28	Cup
9	Fluoride (F^-)	19	Sulfide (S^{2-})	29∼	Others

assigned ID of 39 from the standard template TEDS described in Table 3 of Section 2. However, template ID 39 cannot describe all the information for the electrodes because it is only defined for measured signals.

Therefore, the standard template TEDS of IEEE 1451.4 has to be defined and modified for an E-tongue system. The template TEDS proposed for the E-tongue system is classified into five fields. The structure of the template TEDS proposed for E-tongue system is shown in Table 7.

The first field describes the basic information of the sensor and is shown in Table 8. We define a new template ID (44), which is assigned according to IEEE standards and is not used at present. The template ID 44 has basic information regarding the sensor for the E-tongue system described in Table 8. Table 9 presents information for ISE for the new template: the ISE is a metal electrode element using a platinum wire.

Table 10 describes the ion species and sensing elements for the ISE.

The second field is shown in Table 11 and describes the output voltage, sensor resistance, response time, etc.

Table 12 describes the limitation of sensors, which is the third field. It presents information that includes the

Table 11
Proposal for a template TEDS-information on sensor

Field	Property/command	Description	Access	Bits	Data type (and range)	Unit
Information on sensor	%MinElecVal	Minimum electrical value	CAL	32	ConRes (−1000 to −1, step 1)	mV
	%MaxElecVal	Maximum electrical value	CAL	32	ConRes (1–1000, step 1)	mV
	%MapMeth	Mapping method	ID		Assign = 0 "linear"	–
	%MimLinearRan	Linear measuring range (min)	ID	16	ConRes (2–10000, step 1)	ppm
	%MaxLinearRan	Linear measuring range (max)	ID	16	ConRes (2–10000, step 1)	ppm
	%SensorImped	dc resistance (at 25)	ID	12	ConRelRes (0.1–10, ±1%)	MΩ
	%PreConTime	Preconditioning time	ID	5	ConRes (1–10, step 0.5)	min
	%StableReadT	Time for stable reading after immersion	ID	5	ConRes (1–10, step 0.5)	min
	%PotentialDrift	Potential drift (in 1000 ppm)	ID	7	ConRes (0.1–10, step 0.1)	mV/day
	%RespTime	Sensor response time	ID	6	ConRes (1–60, step 1)	s

Table 12
Proposal for a template TEDS-limitation of sensor

Field	Property/command	Description	Access	Bits	Data type (and range)	Unit
Limitation of sensor	%MinTempRan	Minimum temperature range	ID	8	ConRes (−20 to 125, step 1)	°C
	%MaxTempRan	Maximum temperature range	ID	8	ConRes (−20 to 125, step 1)	°C
	%MinOptPH	Minimum optimal pH[a]	ID	4	ConRes (0–15, step 1)	pH
	%MaxOptPH	Maximum optimal pH	ID	4	ConRes (0–15, step 1)	pH
	%MinSamVol	Minimum feasible sample volume	ID	4	ConRes (1–10, step 1)	mol
	%DetctLimit	Minimum detection limit[b]	ID	7	ConRes (0.1–10, step 0.1)	ppm

[a] Optimal pH = measured pH.
[b] Detection limit = minimum value measured in units of ppm.

Table 13
Proposal for a template TEDS—information on reference electrode

Field	Property/command	Description	Access	Bits	Data type (and range)	Unit
Information on reference electrode	%RefElectrode	Type of reference electrode	ID	4	See Table 14	–
	%MinTempSam	Minimum temperature of reference electrode	ID	8	ConRes (−20 to 125, step 1)	°C
	%MaxTempSam	Maximum temperature of reference electrode	ID	8	ConRes (−20 to 125, step 1)	°C
	%MinPHSam	Minimum pH of reference electrode	ID	4	ConRes (0–15, step 1)	pH
	%MaxPHSam	Maximum pH of reference electrode	ID	4	ConRes (0–15, step 1)	pH
	%RefLiquid	Reference liquid	ID	4	See Table 15	–
	%MolRefLiquid	Mole of reference liquid	ID	10	ConRes (0–10, step 0.01)	mol
	%JuncPotential	Junction potential of electrode	ID	10	ConRes (0–1, step 0.001)	V

Table 14
Types of reference electrode [14–17]

Case	Type of reference electrode
0	Ag/AgCl
1	Calomel
2	Hg/Hg_2SO_4 (chloride free)
3∼	Others

Table 15
Reference liquids [14–17]

Case	Reference liquid
0	Ag/AgCl
1	KCl
2	LiCl
3	K_2SO_4 (chloride free)
4∼	Others

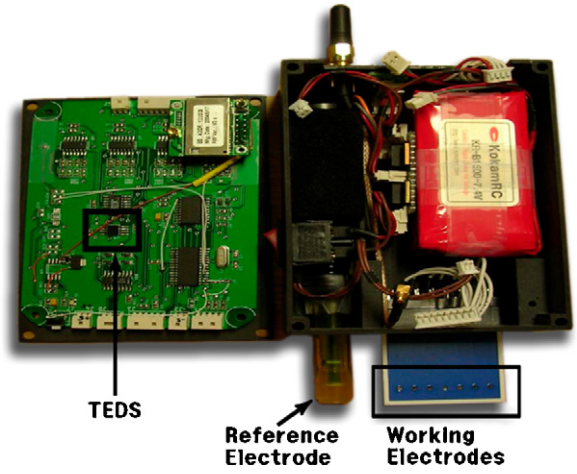

Fig. 8. Electronic tongue system.

temperature and pH ranges and concentration limit for samples.

Table 13 shows the fourth field and presents information on the reference electrode and liquid used for the E-tongue system. Tables 14 and 15 show the types of reference electrodes and liquids.

Finally, the fifth field provides information on the calibration of the sensor, which includes the time of last calibration and time interval between successive calibrations, etc. (Table 16).

Table 16
Proposal of template TEDS—information of calibration

Field	Property/command	Description	Access	*Bits*	Data type (and range)
Information on calibration	%CalDate	Calibration data	CAL	16	DATE
	%CalInitials	Calibration Initials	CAL	15	CHR 5
	%CalPeriod	Calibration period	CAL	12	UNINT
	%MeasID	Measurement location ID	USR	11	UNINT
	%SenModel	Sensor model	USR	–	Sensor model number
	%UsrData	User data (comment)	USR	–	Hoseo University

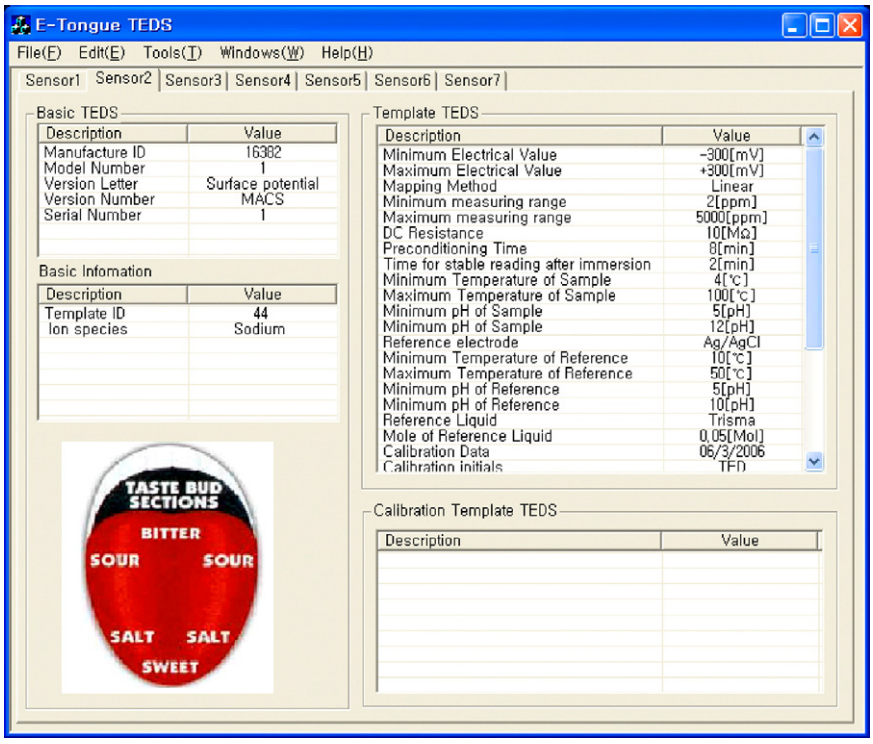

Fig. 9. Program for reading the TEDS.

5. Experimental result for the proposed method applicable to the E-tongue system

The proposed method for the TEDS is implemented for the E-tongue system, which has been developed using an ISE. A reference electrode and seven working electrodes are arranged in an array. The ion species that are used in the working electrodes are sodium, potassium, calcium, chloride, nitrate, and ammonium. Fig. 8 shows the E-tongue system developed using the TEDS, and Fig. 9 illustrates the program to read the TEDS information for an E-tongue system.

6. Conclusions

Sensors and actuators will become small, intelligent, and wireless in accordance to market demands. Apart from their functions such as the conversion of mobility and optical, chemical, and biological phenomenons to electrical signals, sensors also have to possess logic control, wired/wireless communication, cognitive, and judging abilities. At present, capabilities of a sensor are beyond that of traditional sensors: these capabilities are widening the use of sensors to intelligent home networks, telemedicine systems, environment monitoring systems, etc. The IEEE 1451 standard, which is for a smart sensor, is applicable to standard E-tongue system for the future development.

In this paper, we adapted the IEEE 1451.4 TEDS to E-tongue system. However, it was difficult to provide information on the E-tongue system using IEEE 1451.4 TEDS, which can only provide information on a single sensor.

Therefore, we proposed a solution to standardize sensors by using an array for the E-tongue system. The proposed method considered only the most usable array of ISE and associated system. Future work will be devoted to the implementation of a more general system throughout experimental trails.

References

[1] Institute of Electrical, Electronics Engineers Inc., IEEE Std 1451.2-1997, Standard for a Smart Transducer Interface for Sensors and Actuators—Transducer to Microprocessor Communication Protocols and Transducer Electronic Data Sheet (TEDS) Formats, Institute of Electrical and Electronics Engineers Inc., Piscataway, NJ, 1997.
[2] Institute of Electrical Electronics Engineers Inc., IEEE Std 1451.4-2004, Standard for a Smart Transducer Interface for Sensors and Actuators—Mixed-Mode Communication Protocols and Transducer Electronic Data Sheet (TEDS) Formats, Institute of Electrical and Electronics Engineers Inc., New York, NY, USA, 2004.
[3] N. Ulivieri, C. Distante, T. Luca, S. Rocchi, P. Siciliano, Sens. Actuators B 114 (1) (2006) 141–151.
[4] National Instrument, IEEE 1451.4 Sensor Templates Overview, http://zone.ni.com/devzone/.
[5] National Instrument, IEEE 1451.4 Standard Overview, http://zone.ni.com/devzone/.
[6] http://www.wilcoxon.com/.
[7] F. Winquist, C. Krantz-Rulcker, I. Lundstrom, MRS Bull. 29 (10) (2004) 726–731.
[8] J.D. Kim, H.G. Byun, D.J. Kim, Y.K. Ham, W.S. Jung, C.O. Yoon, Talanta 70 (2006) 546–555.
[9] P. Doyle, D. Heffernan, D. Duma, Microprocess. Microsyst. 28 (1) (2004) 1–12.
[10] V. Kochan, K. Lee, R. Kochan, A. Sachenko, Comput. Std. Interface 28 (2005) 141–149.
[11] J.W. Gardner, P.N. Bartlett, Electronic Tongues Principles and Applications, Oxford University Press, 1998.

[12] F. Winquist, C. Krantz-Rulcker, I. Lundstrom, in: T.C. Pearce, S.S. Schiffman, H.T. Nagle, J.W. Gardner (Eds.), Handbook of Machine Olfaction: Electronic Nose Technology, Wiley, 2003, pp. 267–289.
[13] http://www.alphamos.com/.
[14] http://www.nico2000.net/.
[15] http://www.radiometer-analytical.com/.
[16] http://www.astisensor.com/.
[17] http://www.thermo.com/.

Available online at www.sciencedirect.com
ScienceDirect
Talanta 71 (2007) 1487–1493
Talanta
www.elsevier.com/locate/talanta

An ion-imprinted silica-supported organic–inorganic hybrid sorbent prepared by a surface imprinting technique combined with a polysaccharide incorporated sol–gel process for selective separation of cadmium(II) from aqueous solution

Feng Li, Hongquan Jiang, Shusheng Zhang *

College of Chemistry and Molecular Engineering, Qingdao University of Science and Technology, Qingdao 266042, China

Received 11 May 2006; received in revised form 28 June 2006; accepted 10 July 2006
Available online 23 August 2006

Abstract

Ion-imprinting concept and polysaccharide incorporated sol–gel process were applied to the preparation of a new silica-supported organic–inorganic hybrid sorbent for selective separation of Cd(II) from aqueous solution. In the prepared shell/core composite sorbent, covalently surface coating on the supporting silica gel was achieved by using a Cd(II)-imprinting sol–gel process starting from an inorganic precursor, γ-glycidoxypropyltrimethoxysiloxane (GPTMS), and a functional biopolymer, chitosan (CS). The sorbent was prepared through self-hydrolysis of GPTMS, self-condensation and co-condensation of silanol groups (Si-OH) from siloxane and silica gel surface, in combination with in situ covalent cross-linking of CS with partial amine shielded by Cd(II) complexation. Extraction of the imprinting molecules left a predetermined arrangement of ligands and tailored binding pockets for Cd(II). The prepared sorbent was characterized by using X-ray energy dispersion spectroscopy (EDX), X-ray diffraction (XRD), and scanning electron microscopy (SEM). Batch experiments were conducted to study the sorption performance by removal of Cd(II) when present singly or in binary system, an aqueous Cd(II) and Zn(II) mixture. The ion-imprinted composite sorbent offered a fast kinetics for the sorption of Cd(II) and the maximum capacity was 1.14 mmol g^{-1}. The uptake capacity of the imprinted sorbent and the selectivity coefficient were much higher than that of the non-imprinted sorbent. The imprinted sorbent exhibited high reusability. The prepared functional sorbent was shown to be promising for the preconcentration of cadmium in environmental and biological samples.

Keywords: Cadmium; Chitosan; Imprinting; Sol–gel; Sorbent; Selective

1. Introduction

Heavy metal ion contamination remains a serious environmental problem and presents a threat to living systems especially to human health [1,2]. Cadmium is widely used in several industries including metallurgy, surface treatment, dye synthesis or battery production. Due to its severe toxicity to animals and humans, even at low concentrations, cadmium is known to be one of the most toxic heavy metal elements. Consequently, cadmium removal has been given great priority in the last decade [3–9]. Owing to the co-existence of various heavy metal ions in industrial effluents or other water resources, selective removal of toxic metal ions attracts much attention in both industries and researches. Sorption based on suitable sorbent possessing selectivity toward the offending heavy metals, is inherently attractive and more popular for selective removal of metal ion from aquatic environment, especially from dilute aqueous solutions [3,5,7]. Therefore, development of novel solid sorbents for selective cadmium clean-up in environmental and biological samples is of great significance.

Currently, biopolymers represent an interesting and attractive alternative as cheap and more effective sorbents. Amongst them, polysaccharides deserve particular attention [10]. As a natural polysaccharide, chitosan remains a focus of study owing to a set of its unique characteristics such as hydrophilicity, non-toxicity, biocompatibility and gel forming property [11–13]. Noteworthily, high concentration of amino and hydroxy groups in the polyaminoglucosan chain endows the material with an

* Corresponding author. Tel.: +86 532 84022750; fax: +86 532 84023927.
E-mail address: shushzhang@qust.edu.cn (S. Zhang).

0039-9140/$ – see front matter © 2006 Elsevier B.V. All rights reserved.
doi:10.1016/j.talanta.2006.07.023

excellent capacity to bind heavy metal ions. The applications of chitosan to wastewater treatment have been well documented [14,15]. Moreover, chitosan could selectively bind several transition metal ions in the presence of alkaline and alkaline-earth metal [16]. Therefore, much attention has been drawn to this biopolymer or its derivatives for selective sorption. To overcome the inherent drawbacks of pure chitosan power and flake, e.g., swelling, solubility in acidic conditions, unsatisfying mechanical property and mass transfer resistance, using the emulsion cross-linking method to synthesize cross-linked particles/beads is explored as a conventional way to develop chitosan-based sorbents for dynamic metal ion sorption. Though such particles/beads have enhanced mechanical and diffusion properties and can be reused in sorption, the method turns out to be ineffective and results in large consumption of organic reagents arising from difficult emulsification and tedious washing procedures [15,17]. Recently, coating chitosan on preformed microparticle, e.g., silica gel, followed by chemical cross-linking has shown a successful method [18,19]. The essence lies in the combination of the functionality of chitosan and advantages of silica gel, e.g., large surface area and excellent mechanical resistance. Moreover, coating of cross-linked chitosan could enhance stability of silica in alkaline solutions [18].

Molecular imprinting has become a powerful method for the preparation of materials with the ability to recognize a specific chemical species [20]. Due to the interaction between monomers and templates, the imprinted materials possess predetermined arrangement of ligands and tailored binding pockets, which show affinity for the template molecule over other structurally related compounds [20]. Metal ion-imprinting, employing metal coordination between template and functional monomer, is one of the important types of molecular imprinting [5,7]. Chitosan-based sorbent prepared by ion-imprinting possesses high selectivity and avoids problem of mass transfer [21,22]. By shielding amine groups in the cross-linking process, decreased sorption capacity caused by the loss of binding sites could be overcome in ion-imprinted chitosan [21–23]. However, the cross-linking agents used in their work, e.g., glutaraldehyde (GA) and ethylene glycol diglycidy1 ether (EGCE), are not preferred due to the physiological toxicity and the lack of biodegradability of the cross-linked beads [24].

Sol–gel technology offers simple and convenient methodology to the production of advanced materials with molecular level uniformity [5,7,25–28]. Incorporation of polysaccharide into inorganic network by polysaccharide-manipulated sol–gel process is potentially related to the biomineralization processes [29,30]. As functional biomaterials, chitosan-based organic–inorganic hybrid materials possess many advantages over conventional cross-linked chitosan materials, e.g., low toxicity and high biocompatibility [31,32]. However, chitosan-based hybrid materials used in most of researches only utilize the compatibility generated by formation of hydrogen bonds. Very recently, a novel method for incorporating chitosan into inorganic network through cross-linked organic–inorganic hybridization is proposed by Liu and Shirosaki [33–35]. In situ cross-linking of chitosan and simultaneous formation of chitosan–silica hybrid are revealed by a set of investigation, e.g., ^{29}Si NMR, scanning and transmission electronic microscopy. In addition, the hybrid membrane has been proved to show high hydrophilicity and good cytocompatibility.

This work attempts to present a new approach to prepare new chitosan-based composite sorbent based on ion-imprinting and polysaccharide incorporated sol–gel coating process. Covalently surface coating through sol–gel process in chitosan–Cd(II) solution at room temperature resulted in silica-supported functional material. The preparation methodology, its main characteristic features and application to selective sorption of Cd(II) from aqueous solution are described and discussed in detail.

2. Experimental

2.1. Instrumentation

Scanning electron microscopy (SEM) images were obtained at 5.0 kV on the field emission scanning electron microscope (SIRION, USA) after gold plating. X-ray energy dispersion spectroscopy (EDX) measurements were conducted with a GENENIS 4000 energy dispersive X-ray micro analyzer (EDAX, USA). X-ray diffraction (XRD) was performed on Siemens D 5005 powder X-ray diffractometer. X-rays of 1.5408 Å wavelength were generated by a Cu K source. The angle of diffraction varied from 5° to 40° to identify the change in the crystal structure. A So1AAR S2 atomic absorption spectrometer (Thermo Electron Co., UK) was used to measure the concentration of metal ions in aqueous solution.

2.2. Chemicals

Chitosan (CS), with 98% deacetylation and an average molecular weight of 6×10^4 g mol^{-1} (Yuhuan Biomedical Corp., China) and γ-glycidoxypropyltrimethoxysiloxane (GPTMS, Alfa aesar) were used to functionalize silica gel (100–200 mesh, Qingdao Ocean Chemical Co., China). Ninhydrin reagent solution (ninhydrin, hydrindantin, dimethyl sulfoxide, and lithium acetate at pH 5.2, Sigma) was used to determine the non-hybrid chitosan. Cadmium and zinc were used in the $CdCl_2{\cdot}2.5H_2O$ and $ZnCl_2$ form, respectively (Merck Germany). All the other chemicals used were in analytical grade. Doubly deionized water (DDW) was used throughout this work.

2.3. Preparation of the ion-imprinted composite sorbent

Silica gel was heated up at 110 °C for 1 h to activate the surface. A portion of $CdCl_2{\cdot}2.5H_2O$ was added to CS solution dissolved in 0.1 mol l^{-1} acetic acid aqueous solution (Cd/aminoglucosan 2:1, mole/mole). After stirring for 1 h, certain amount of GPTMS was added to the transparent solution. The mixture was stirred for 4 h and then bathed in an ultrasonic bath for 20 min before the activated silica gel was added. The amount of coated CS was controlled at 120 mg/g silica gel. The wet bead was allowed to evaporate at room temperature to complete the cross-linking reaction and gelation. The dry product was thoroughly washed with DDW to remove non-bound

Cd(II). The consequent Cd(II)-complexed composite bead was filtered and treated with a 0.1 mol l^{-1} HCl to completely leach the coordinated Cd(II). The acid-treated sorbent was rinsed several times with DDW and then recovered using 0.1 mol l^{-1} NaOH to ensure complete H^+ neutralization. The resulting sorbent with Cd(II) cativities was filtered, washed with DDW, and dried under vacuum. For comparison, the non-imprinted sorbent was also prepared as a blank in parallel but without the addition of Cd(II).

2.4. Determination of non-hybrid chitosan

The ninhydrin test was used to determine the non-hybrid chitosan released from the prepared materials. Different siloxane ratios, 0% and 2%, were used, respectively. For comparison, the concentrations of CS and Cd(II) in the coating solution for each material were uniform. After non-bound Cd(II) removal, all beads were shaken separately in 1 mol l^{-1} acetic acid aqueous solution overnight. Extracted chitosan was measured using ninhydrin reagent [36,37].

2.5. Sorption experiments

The effect of pH on the sorption of Cd(II) was tested by equilibrating 1 g of the prepared sorbent with 10 ml of the buffer solutions containing 30 mmol l^{-1} of Cd(II) under different pH conditions for 1 h. The pH of the solutions was adjusted using the following buffers: sodium acetate/hydrochloric acid for pH 2–3, and sodium acetate/acetic acid for pH 4–6.5. Uptake kinetics of Cd(II) to the prepared sorbent was performed by adding 1 g sorbent to 10 ml of 30 mmol l^{-1} Cd(II) solution at pH 6.0. Samples were regularly collected at appropriate time intervals, separated and analyzed for Cd(II) content. To measure the sorption capacity, 1 g of Cd(II)-imprinted or non-imprinted sorbent was equilibrated with 10 ml of various concentrations of Cd(II) solutions buffered at pH 6.0. Competitive loading of Cd(II) and Zn(II) by Cd(II)-imprinted and non-imprinted sorbents was examined in Cd(II)/Zn(II) binary aqueous solutions at pH 6.0. A 1 g portion of Cd (II)-imprinted or non-imprinted sorbent was equilibrated with 10 ml of the buffered solutions containing 30 mmol l^{-1} of Cd(II) and 30 or 60 mmol l^{-1} of Zn(II), respectively.

In all the above batch experiments, the mixtures were centrifugally separated. The cadmium concentration in the sorbent was determined by mass balance between liquid and solid phases. The amount of Cd(II) adsorbed was calculated by the following Eq. (1):

$$Q = \frac{(C_0 - C_e)V}{m} \quad (1)$$

where C_0 and C_e represent initial and equilibration concentration of Cd(II), respectively, V is the volume of solution, m is the weight of the sorbent.

2.6. Reuse of the Cd(II)-imprinted sorbent

The Cd(II) ion recognized on the sorbent was stripped by being washed with 0.5 mol l^{-1} HCl. The acid-treated sorbent was rinsed several times with DDW and then regenerated using 0.1 mol l^{-1} NaOH. The sorbent was used to remove Cd(II) through eight extraction/regeneration cycles.

3. Results and discussion

3.1. Preparation of the ion-imprinted composite sorbent

The sol–gel coating technology appears to be universal in nature. Silica gel has been known as a good supporting material because of its large surface area and excellent mechanical resistance. Silanol groups (Si-OH) on its surface are responsible for chemical modifications. Polysaccharide-manipulated sol–gel process has received particular attention considering its acceleration and catalytic effect on the silica polymerization processes [29,30]. The new silica-supported composite sorbent was prepared using Cd(II)-imprinting sol–gel coating. In the original blend of CS and Cd(II), Cd(II) coordinated to chitosan resulting in CS arrangement around the template Cd(II) with a specific geometry. When the epoxy-siloxane with trimethoxy anchor groups was added, silanol groups were in situ generated through acid-catalyzed self-hydrolysis. Then, the self-condensation and co-condensation between silanols from siloxane and silica gel surface, and addition of non-coordinated amino groups in CS chains to epoxy rings in siloxane took place simultaneously. Such polymerization created covalent coating with structural order on the surface of silica gel and the domain for templating Cd(II) was frozen in the gel along with solvent evaporation. The specificity of a particular ligand toward target metal ions is usually the result of a conventional acid–base interaction between the ligand and the metal ion. Although chitosan-functionalized sorbents can exhibit interactions with soft Lewis acids, e.g., Cd(II), Hg(II), Zn(II), and Ag(I), specific interactions with a given metal ion might consider the stereochemical interactions between the ligand and metal ion, which results in the selectivity of the material. This is especially remarkable for the cross-linked polymer network with the restricted diffusion of molecules and reduced polymer chain flexibility [38]. Doyle group investigated the structure of the potassium channel, which exhibited molecular basis of K^+ conduction and selectivity [39]. Potassium was at least 10,000 times more permeant than Na^+, indicating strong energetic interactions between K^+ ions and the pore. Currently, the interaction mechanism between chitosan and metal ion still tantalizes the chemists. Terreux et al. [40] used molecular modeling to study the interactions between one Cu(II) and one or several glucosamine residues. By computed parameters, e.g., the geometries and the interaction energies, they evidenced that the most stable interactions involved the free amino site and the participation of the heterocyclic O site was less favored. Moreover, the glucosamine could not act as a bidentate ligand and *N*-acetyl glucosamine was not coordinating with Cu(II). In our procedure, Cd(II) complexation to chitosan might result in a stable conformation for chitosan chain, which was fixed by the following chitosan cross-linking and gelation. After Cd(II) removal, the imprinted material with a predetermined arrangement of ligands and tailored binding pocket for Cd(II), therefore, was obtained.

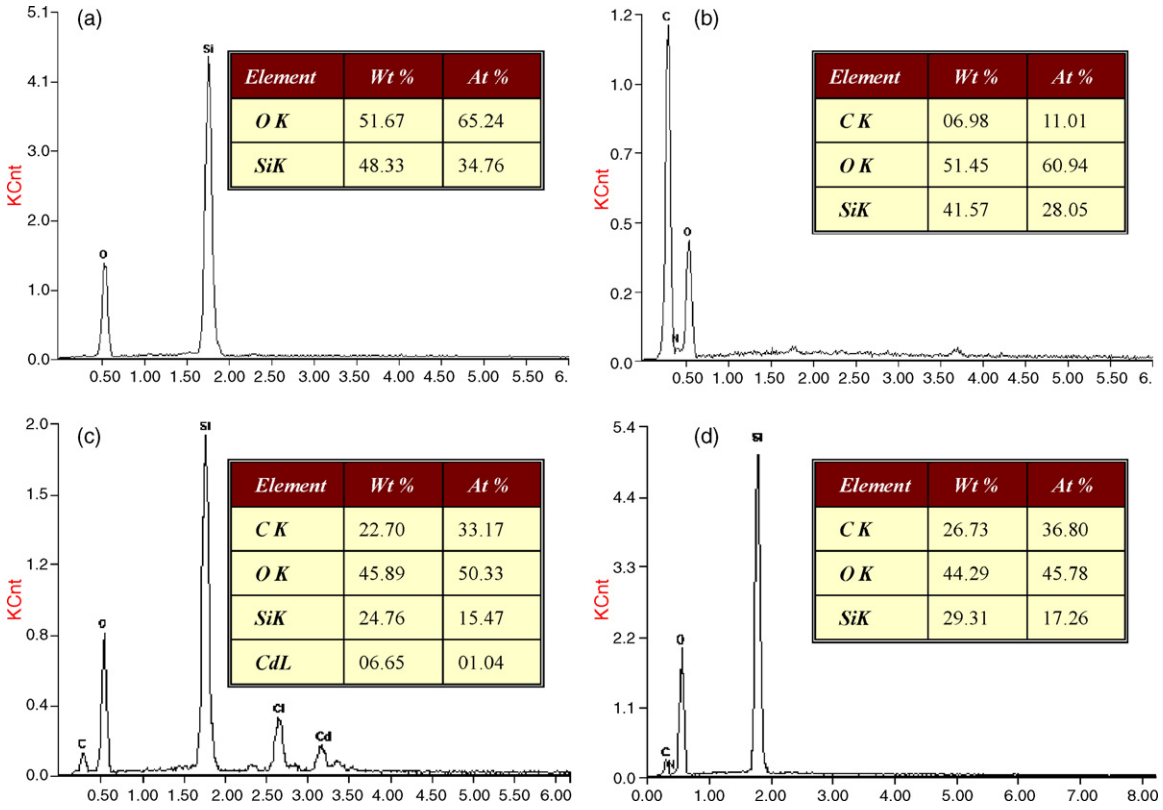

Fig. 1. X-ray energy dispersion spectroscopy of silica gel (a), GPTMS-modified silica gel (b) and Cd(II)-complexed composite bead (c), and Cd(II)-imprinted composite sorbent (d).

The transfer of the elemental distribution on silica gel was investigated with X-ray energy dispersion spectroscopy (EDX), which gave a qualitative evaluation of surface modification in the preparation procedure. EDX of pure silica gel, GPTMS-modified silica gel, Cd(II)-complexed bead and the prepared ion-imprinted sorbent were illustrated in Fig. 1. For the supporting silica gel, only Si, O signals appeared in accordance with its composition of element (Fig. 1a), while the element species and percentage of each element changed greatly after coating. The appearance of the C signal for GPTMS-modified silica gel, which was prepared with only addition of GPTMS in the coating solution, well established the affinity between silica gel and GPTMS for covalent linkage (Fig. 1b). For Cd(II)-complexed composite bead (Fig. 1c), the appearance of cadmium firmly confirmed the interaction between Cd(II) and chitosan. After coordinated Cd(II) leaching, the final Cd(II)-imprinted composite sorbent mainly showed signals of C, Si, O (Fig. 1d).

3.2. Determination of non-hybrid chitosan

To evaluate the hybrid status, chitosan extracted from ion-imprinted or non-imprinted sorbents using 1 mol l^{-1} acetic acid aqueous solution was measured by ninhydrin test. For comparison, sorbent prepared using the identical procedure but without adding of GPTMS was also investigated. As expected, the extraction rate for such sorbent was 100% resulting from no cross-linking of chitosan. However, almost no released chitosan was detected for both Cd(II)-imprinted and non-imprinted

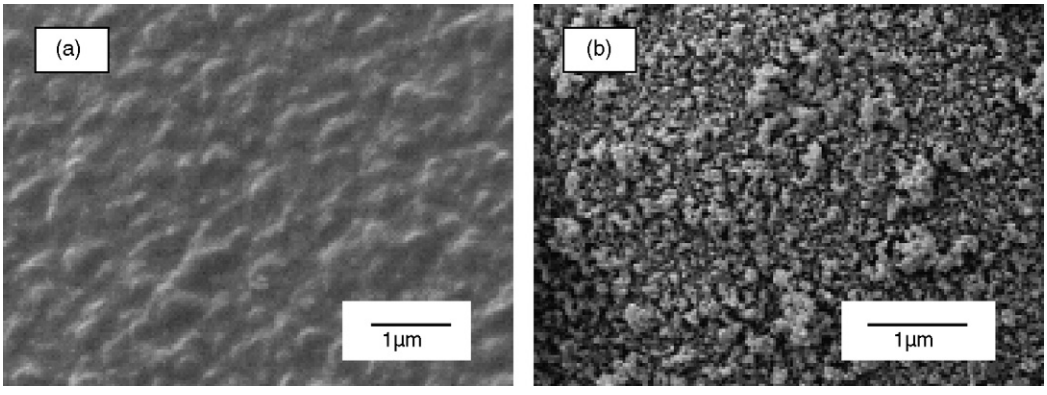

Fig. 2. SEM image (5.0 kV) of non-imprinted composite sorbent (a) and Cd(II)-imprinted composite sorbent (b).

composite sorbents. The phenomenon indicated the effective hybridization between siloxane and chitosan, which might be ascribed to the homogenous cross-linking and compatibility between polysaccharide and siloxane.

3.3. Characteristics of the ion-imprinted sorbent

Fig. 2 represented the surface morphology of the ion-imprinted composite sorbent and the non-imprinted sorbent. The non-imprinted sorbent exhibited a dense and slightly rough surface (Fig. 2a), while a significantly different morphology was observed on the surface of Cd(II)-imprinted sorbent (Fig. 2b). It was monoliths with nanocomposites arranged together, which might possess geometrical distribution of legends and avoid problem of mass transfer.

The crystallinity of CS could significantly influence the sorption properties by controlling the accessibility to sorption sites. Cross-linked materials usually had reduced crystalline domains in the polysaccharide and then increased sorption capacity [12,15]. Fig. 3 showed the XRD pattern of pure CS, supporting silica gel and ion-imprinted sorbent. There are two strong peaks in the diffractogram of CS at $2\theta = 11.4^\circ$ and 20.2° (Fig. 3a). XRD patterns of the ion-imprinted sorbent (Fig. 3b) mainly showed the characteristic of the supporting silica gel (Fig. 3c). However, a slight shift could be found compared with silica gel, indicating the hybridization between CS and GPTMS. To avoid the perturbation of high quantity of silica gel, the coating solution was cast on a clean glass plate and the scraped power was analyzed. As shown in Fig. 3d, it displayed no peak for crystallization regions compared with pure CS indicating significant decrease of crystallization. As compared to heterogeneous cross-linking after phase-inversion, CS cross-linking and organic–inorganic hybridization in homogenous condition was expected to increase hydrophilicity and enhance metal binding capacity resulting from more destruction of crystallization [18,19,33].

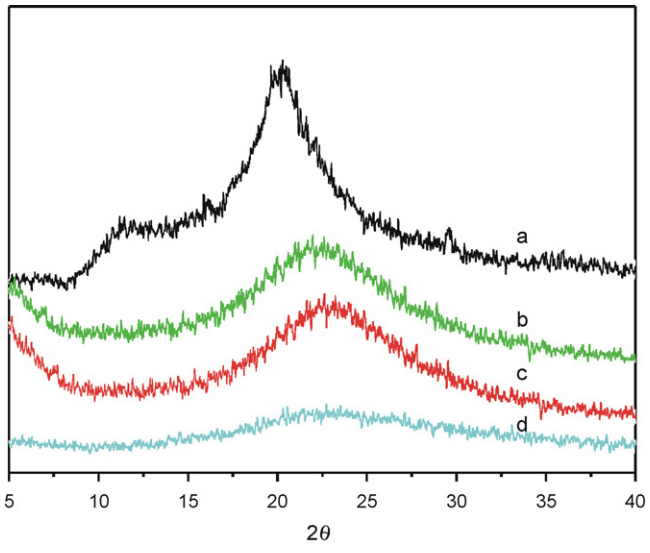

Fig. 3. X-ray diffraction patterns of chitosan (a), Cd(II)-imprinted composite sorbent (b), silica gel (c), and Cd(II)-imprinted hybrid material without silica gel supporting (d).

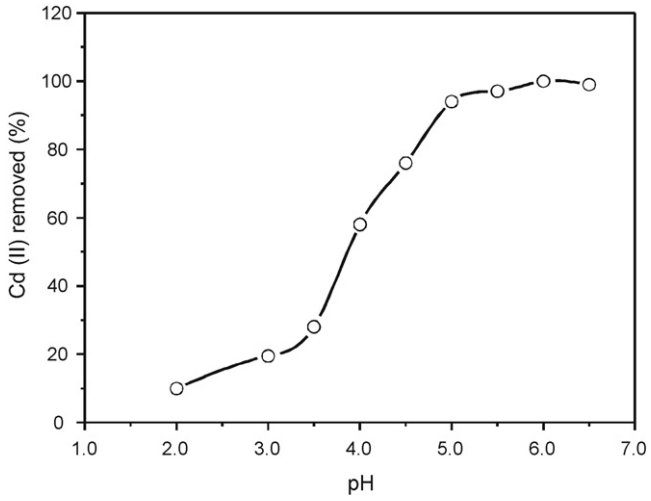

Fig. 4. Effect of pH on the uptake of 30 mmol l^{-1} Cd(II) onto 1 g of the Cd(II)-imprinted sorbent for 1 h.

3.4. Cd(II) sorption to the sorbent

The effect of pH on Cd(II) sorption onto Cd(II)-imprinted composite sorbent was studied by varying the pH between 3.0 and 6.5, as shown in Fig. 4. The sorption of Cd(II) increased as the pH increased, from a low value of 10.5% at pH 2.0 to its maximum of 99.2% at pH 6.0. As chitosan chelated Cd(II) ions mainly by the amine groups, the protonation of amine at low pH minimized the extent of Cd(II) sorption. When the pH increased, protonation weakened and the sorbent surface became less positively charged, therefore, Cd(II) sorption was more favorable. To avoid Cd(II) removal by precipitation, pH 6.0 was chosen for further sorption performance.

The uptake kinetics of Cd(II) sorption to the Cd(II)-imprinted composite sorbent was investigated. As shown in Fig. 5, the Cd(II) uptake by Cd(II)-imprinted composite sorbent was successful and rapid. The sorption occurred primarily within 20 min and then the equilibrium was achieved. The sorption capacity of the imprinted and non-imprinted sorbent for Cd(II) was

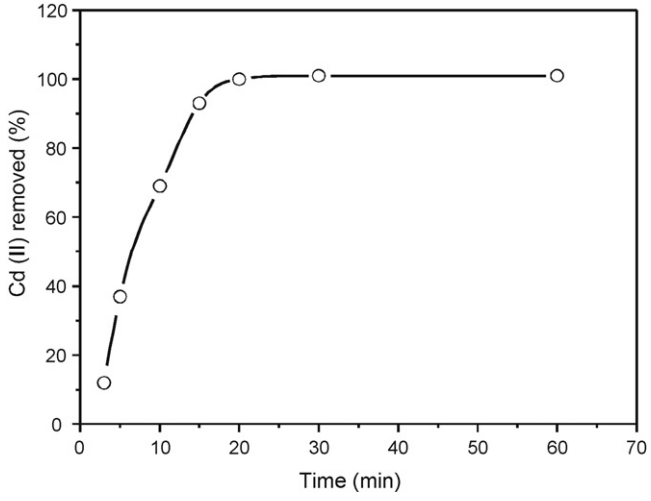

Fig. 5. Uptake kinetics for 30 mmol l^{-1} Cd(II) onto 1 g of the Cd(II)-imprinted sorbent at pH 6.0.

Table 1
Competitive sorption of Cd(II) and Zn(II) by Cd(II)-imprinted composite sorbent and non-imprinted composite sorbent at pH 6.0 (mean ± σ, $n = 3$)

Sorbent	Initial concentration (mmol l^{-1})		Uptake (%)		Capacity (mmol g^{-1})		K_d[a] (ml g^{-1})		k[b]	k'[c]
	Cd(II)	Zn(II)	Cd(II)	Zn(II)	Cd(II)	Zn(II)	Cd(II)	Zn(II)		
Cd(II)-imprinted	30	0	99.1 ± 0.3		0.2973 ± 0.0009		1101			
	30	30	98.4 ± 0.4	31.8 ± 0.3	0.2952 ± 0.0012	0.0954 ± 0.0009	615	5	113	120
	30	60	96.3 ± 0.4	20.1 ± 0.4	0.2889 ± 0.0012	0.1206 ± 0.0024	260	3	87	79
Cd(II)-non-imprinted	30	0	97.4 ± 0.5		0.2922 ± 0.0015		375			
	30	30	60.3 ± 0.6	61.2 ± 0.6	0.1809 ± 0.0018	0.1836 ± 0.0018	15	16	0.94	
	30	60	44.9 ± 0.3	39.4 ± 0.5	0.1347 ± 0.0009	0.2364 ± 0.0030	8	7	1.1	

[a] K_d, distribution coefficient.
[b] k, selectivity coefficient, $K_d(Cd)/K_d(Zn)$.
[c] k', relative coefficient, $k' = k_{imprinted}/k_{non\text{-}imprinted}$.

1.14 and 0.58 mmol g^{-1}, respectively, whereas the initial silica gel exhibited no sorption for Cd(II). Obviously, the capacity of imprinted sorbent was larger than that of non-imprinted sorbent, which was attributed to the surface morphology caused by the Cd(II)-imprinting. As known, morphology of the materials played an important role for its sorption performance, e.g., kinetics and sorption capacity, due to the decision in the legend density and mass diffusion resistance. The Cd(II) sorption capacity was slightly higher than the imprinted sorbent also prepared by sol–gel process, which might caused by different concentration of functional legends and density of the products.

The sorption selectivity of the Cd(II)-imprinted and non-imprinted sorbents was investigated by studying competitive loading of Cd(II) and Zn(II) in their binary mixture. The Zn(II) ion was chosen as the competitive species with Cd(II) for their same charge and similar binding ability to chitosan. Table 1 summarized parameters of the percentage uptake, sorption capacity, distribution coefficient (K_d), selectivity coefficient of the sorbent toward Cd(II) (k), and the relative selectivity coefficient (k'). The k value for the imprinted sorbent showed significant increase compared with that of the non-imprinted sorbent. Therefore, competitive sorption between Cd(II) and Zn(II) was apparent for the binary mixture and the imprinted sorbent showed the superiority of Cd(II) sorption. Formation of the Cd(II)–CS complex ultimately built template-selective recognition sites with functional ligands in a orderly stereochemical arrangement. However, in the non-imprinted sorbent, the functional ligand arranged random and disorderly, resulted in unremarkable selectivity performance.

3.5. Recycling of the sorbent

To make the sorbent economically competitive, ions adsorbed must be released from the sorbent in order to reuse the material. Adsorbed Cd(II) ions could be stripped by the addition of 0.1 mol l^{-1} HCl, which introduced protons that competed with the metal ions for binding sites and made amine groups finally protonation. The acid-treated sorbent could be regenerated using 0.1 mol l^{-1} NaOH. Afterwards, the sorption ability was resumed. In test of sorbent recycling, the ion-imprinted sorbent was used to remove Cd(II) through eight extraction/regeneration cycles. The capacity of the prepared imprinted sorbent through eight cycles was found to be 92 ± 4% of the fresh sorbent. In the CS-coated procedures previously reported, the matrices were prepared by coating of non-cross-linked CS on silica gel followed by CS deposition using phase-inversion method [18,19]. Deposited CS could easily strip because interaction between CS and silica gel was mainly non-covalent hydrogen bonding. Moreover, sorption capacity usually remarkably decreased in the initial reused process due to the incomplete CS cross-linking in heterogeneous condition, whereas, only very slight decrease of sorption capacity occurred in recycling studies of our silica-supported organic–inorganic sorbent. The covalently bounded coating and unique CS treatment in homogenous condition, e.g., cross-linking and organic–inorganic hybridization endowed the sorbent with stable performance for recycling.

4. Conclusions

The successful preparation of ion-imprinted sol–gel coating materials demonstrated the feasibility of the direct formation of the functional sorbent with selective recognition for Cd(II) ion. The prepared sorbent using such covalently surface coating possesses good mechanical and diffusion properties. The method is simple and mild. All procedures are performed in aqueous medium without addition of any organic solvents, which is essential from environmental and economical point of view. This methodological study and application of this cost-efficient sorbent in the preconcentration and separation of toxic metal ions will be an important field.

Acknowledgements

This research was supported by the National Natural Science Foundation of China (No. 20475030), the Program for New Century Excellent Talents in Universities (No. NCET-04-0649), and Doctoral Found of QUST (No. 0022178).

References

[1] L.Q. Ma, G.N. Rao, J. Environ. Qual. 26 (1997) 259.
[2] C.J. Koester, S.L. Simonich, B.K. Esser, Anal. Chem. 75 (2003) 2813.
[3] Y.P. DePena, M. Gallego, M. Valcarel, J. Anal. Atom. Spectrom. 12 (1997) 453.

[4] J. Munoz, J.R. Baena, M. Gallego, M. Valcarel, J. Anal. Atom. Spectrom. 17 (2002) 716.
[5] Y.K. Lu, X.P. Yan, Anal. Chem. 76 (2004) 453.
[6] V.A. Lemos, P.X. Baliza, Talanta 67 (2005) 564.
[7] G.Z. Fang, J. Tan, X.P. Yan, Anal. Chem. 77 (2005) 1734.
[8] F.A.C. Amorim, S.L.C. Ferreira, Talanta 65 (2005) 960.
[9] A.C. Davis, P. Wu, X.F. Zhang, X.D. Hou, B.T. Jones, Appl. Spectrosc. Rev. 41 (2006) 35.
[10] G. Crini, Prog. Polym. Sci. 30 (2005) 38.
[11] X.Z. Ye, Q.H. Yang, Y. Wang, N.Q. Li, Talanta 47 (1998) 1099.
[12] P.K. Dutta, J. Dutta, M.C. Chattopadhyaya, V.S. Tripathi, J. Polym. Mater. 21 (2004) 321.
[13] S.K. Mehta, A.K. Malik, B. Singh, A.L.J. Rao, Talanta 67 (2005) 725.
[14] C.L. Lasko, M.P. Hurst, Environ. Sci. Technol. 33 (1999) 3622.
[15] A.J. Varma, S.V. Deshpande, J.F. Kennedy, Carbohyd. Polym. 55 (2004) 77.
[16] H. Benaissa, B. Benguella, Environ. Pollut. 130 (2004) 157.
[17] V.R. Sinha, A.K. Singla, S. Wadhawan, R. Kaushik, R. Kumria, K. Bansal, S. Dhawan, Int. J. Pharm. 274 (2004) 1.
[18] Q.H. Shi, Y. Tian, X.Y. Dong, S. Bai, Y. Sun, Biochem. Eng. J. 16 (2003) 317.
[19] F.N. Xi, J.M. Wu, J. Chromatogr. A 1057 (2004) 41.
[20] C. Alexander, H.S. Andersson, L.I. Andersson, R.J. Ansell, N. Kirsch, I.A. Nicholls, J. O'Mahony, M.J. Whitcombe, J. Mol. Recognit. 19 (2006) 106.
[21] Z.Y. Cao, H.C. Ge, S.L. Lai, Eur. Polym. J. 37 (2001) 2141.
[22] J.Y. Yun, H.L. Choi, T.I. Son, Y.M. Kim, W.J. Kim, D.K. Moon, J. Ind. Eng. Chem. 11 (2005) 957.
[23] N. Li, R.B. Bai, Ind. Eng. Chem. Res. 44 (2005) 6692.
[24] K.S. McCain, D.C. Hanley, J.M. Harris, Anal. Chem. 75 (2003) 4351.
[25] N.I. Kovtyukhova, T.E. Mallouk, T.S. Mayer, Adv. Mater. 15 (2003) 780.
[26] A. Salimi, K. Abdi, Talanta 63 (2004) 475.
[27] J.H. Shin, S.W. Weinman, M.H. Schoenfisch, Anal. Chem. 77 (2005) 3494.
[28] Z.H. Zhang, L.H. Nie, S.Z. Yao, Talanta 69 (2006) 435.
[29] J.S. Chang, Z.L. Kong, D.F. Hwang, K.L.B. Chang, Chem. Mater. 18 (2006) 702.
[30] Y.A. Shchipunov, T.Y. Karpenko, Langmuir 20 (2004) 3882.
[31] S.S. Silva, R.A.S. Ferreira, L.S. Fu, L.D. Carlos, J.F. Mano, R.L. Reis, J. Rocha, J. Mater. Chem. 15 (2005) 3952.
[32] Y. Liu, H.J. Lu, W. Zhong, P.Y. Song, J.L. Kong, P.Y. Yang, H.H. Girault, B.H. Liu, Anal. Chem. 78 (2006) 801.
[33] Y.L. Liu, Y.H. Su, J.Y. Lai, Polymer 45 (2004) 6831.
[34] Y.L. Liu, Y.H. Su, K.R. Lee, J.Y. Lai, J. Membr. Sci. 251 (2005) 233.
[35] Y. Shirosaki, K. Tsuru, S. Hayakawa, A. Osaka, M.A. Lopes, J.D. Santos, M.H. Fernandes, Biomaterials 26 (2005) 485.
[36] R.T. Lee, Y.C. Lee, Biochemistry 19 (1980) 156.
[37] L. Yang, W.W. Hsiao, P. Chen, J. Membr. Sci. 197 (2002) 185.
[38] M. Ruiz, M.A. Sastre, A. Maria, E. Guibal, React. Funct. Polym. 45 (2000) 155.
[39] D.A. Doyle, J.M. Cabral, R.A. Pfuetzner, A.L. Kuo, J.M. Gulbis, S.L. Cohen, B.T. Chait, R. Mackinnon, Science 280 (1998) 69.
[40] R. Terreux, M. Domard, C. Viton, A. Domard, Biomacromolecules 7 (2006) 31.

Available online at www.sciencedirect.com
ScienceDirect
Talanta 71 (2007) 1675–1678
Talanta
www.elsevier.com/locate/talanta

Study on DNA damage induced by CdSe quantum dots using nucleic acid molecular "light switches" as probe

Jiangong Liang [a,b], Zhike He [a,*], Shusheng Zhang [a], Shan Huang [a], Xinping Ai [a], Hanxi Yang [a], Heyou Han [b,*]

[a] *College of Chemistry and Molecular Sciences, Wuhan University, Wuhan 430072, PR China*
[b] *College of Science, Huazhong Agricultural University, Wuhan 430070, PR China*

Received 22 April 2006; received in revised form 22 July 2006; accepted 27 July 2006
Available online 1 September 2006

Abstract

The calf thymus DNA (ctDNA) damage induced by water-soluble CdSe quantum dots (QDs) was investigated using nucleic acid molecular "light switches" as probe. It was found that little ctDNA was damaged by CdSe QDs without UV irradiation. However, under UV irradiation, ctDNA was nicked by CdSe QDs very clearly. The mechanism of ctDNA damage was also discussed. The results strongly suggested that the ctDNA damage caused by CdSe QDs was not due to photo-induced liberation of Cd^{2+}, but due to the production of free radicals and reactive oxygen species.

Keywords: DNA; Damage; Quantum dots; Nucleic acid molecular "light switches"

1. Introduction

Quantum dots (QDs) are nanocrystals of inorganic semiconductors that are restricted in three dimensions to a somewhat spherical shape, typically with a diameter of 2–8 nm (on the order of 200–10,000 atoms) [1]. They have unique optical and electronic properties such as bright fluorescence, board excitation spectrum, narrow/symmetric emission spectrum and high photostability [2–4]. In 1998, Alivisatos, Nie and co-workers demonstrated the first applications of QDs for biology [5,6]. Since those foundational papers, the use of QDs has been demonstrated in biology and medicine as fluorescent probes and more recently in analytical chemistry [7–13].

As QDs have some harmful constituents such as cadmium or selenium, which are toxic to many cells or DNA, the potential toxic effects of them have recently become a topic of considerable importance and discussion. Dubertret et al. reported the effects of CdSe/ZnS core-shell QDs on the development of individual cells of early stage Xenopus embryos [14]. They found CdSe/ZnS core-shell QDs have little effect on cell viability, morphology, function, or development over the duration of the experiments at their concentrations optimized for labeling efficiency. However, at higher concentrations, CdSe/ZnS core-shell QDs had noticeable effect on embryo development. They thought that these abnormalities may result from changes in the osmotic equilibrium of the cells due to the injected CdSe/ZnS core-shell QDs. Bhatia and co-workers probed the cytotoxicity of CdSe QDs using primary hepatocytes as a liver model [15]. They found cytotoxicity of CdSe QDs correlated with the liberation of free Cd^{2+} ions due to deterioration of the CdSe lattice. Yamamoto and co-workers developed several novel surface-modified QDs using carboxylic acids, polyalcohols, and amines and evaluated their cytotoxicity in mammalian cells [16]. They believed the cytotoxicity of QDs was caused by the surface-covering molecules of QDs but not by the nanocrystalline particle itself. Parak and his co-workers investigated the effect of different organic shells on cytotoxicity [17]. They found that the aggregation of CdSe QDs plays an important role for cytotoxic effects in addition to the release of toxic Cd^{2+} ions from the particles. Lovrić et al. examined the subcellular localization and toxicity of CdTe QDs [18]. The results showed that QD-induced cytotoxicity is in part dependent on QD size and is characterized by chromatin condensation and membrane blebbing. In addition, cytotoxicity of QDs could be significantly reduced by treatment of cells with *N*-acetylcysteine or bovine serum albumin. Green and How-

* Corresponding authors. Tel.: +86 27 87162672; fax: +86 27 68754067.
E-mail addresses: zhkhe@whu.edu.cn (Z. He), hyhan@mail.hzau.edu.cn (H. Han).

0039-9140/$ – see front matter © 2006 Elsevier B.V. All rights reserved.
doi:10.1016/j.talanta.2006.07.048

man reported DNA damage in plasmid nicking assays with water-soluble CdSe/ZnS core-shell QDs [19]. They suggested a nicking mechanism based on observed free radical generation.

Nucleic acid molecular "light switch" means some ruthenium complexes, which show no fluorescence in aqueous solution at ambient temperatures, but display intense fluorescence in the presence of double-helical DNA, to which the complexes bind avidly [20,21]. Our group had synthesized a series of derivatives of nucleic acid molecular "light switch" and used them in the double stranded DNA detection, single-mismatch oligonucleotide analysis and so on [22–25].

In this paper, we investigate ctDNA damage induced by water-soluble CdSe QDs using nucleic acid molecular "light switches" $Ru(bipy)_2(dppx)^{2+}$ (dppx = 7,8-dimethyldipyrido [3,2-a: 2′,3′-c]phenazine) as probe. Compared with previous methods to the research of toxicity of QDs, our method is very simple and quick, which can also be used to investigate DNA damage induced by other nanoparticles.

2. Experimental

2.1. Apparatus

The absorption spectra were acquired on a TU-1900 UV–vis spectrometer (Beijing, China). All fluorescence measurements were made with Perkin-Elmer model LS-55 luminescence spectrometer equipped with a 20 kW xenon discharge lamp as a light source. The UV lamp of ChemiDoc XRS (Bio-Rad) was used as irritation source, which could provide a stable 254, 302 and 365 nm UV light.

2.2. Reagents

Hexane, methanol and CdO were purchased from Shanghai Reagent Factory and used as received without further purification. Selenium (Se), dioctylamine, tributylphosphine (TBP) and tri-*n*-octylphosphine oxide (TOPO) were purchased from Aldrich (Milwaukee, WI). The ctDNA was purchased from HuaMei biochemical Co. (China). Solution of ctDNA in 5.0×10^{-2} mol/L NaCl gave a ratio of UV absorbance at 260 and 280 nm of 1.8–1.9, indicating that the DNA was sufficiently free of protein. The concentration of ctDNA was calculated according to the extinction coefficient at 260 nm (1OD = 50 μg/mL). $[Ru(bpy)_2dppx]^{2+}$ was prepared by our laboratory [22]. All other chemicals used were of analytical-reagent grade. Doubly deionized water was used throughout the experiment.

2.3. Procedure

CdSe QDs were synthesized and purified according to procedure reported by Qu and Peng with some modifications [26]. Briefly, CdO and stearic acid were heated to 150 °C under Ar flow. After CdO completely dissolved, the mixture was allowed to cool to room temperature, TOPO and hexadecylamine were added, and the mixture was heated to 310 °C under Ar flow. At this temperature, the Se solution in TBP and dioctylamine was swiftly injected into the reaction flask. The reaction was stopped 3 min after the injection, and heat was immediately removed. After purification by precipitation, centrifugation, and decantation, the vacuum-dried CdSe QDs were redispersed in chloroform and kept in the dark for future use. Water-soluble CdSe QDs were synthesized according to the scheme reported by Chan et al. [6] with minor modifications. Glacial mercaptoacetic acid was added to chloroform solvated CdSe QDs prepared above until the solution become cloudy. Then, the CdSe QDs were centrifuged out. Afterward, double deionized water was added to the pellet and pH was adjusted to 10–11 by dropwise addition of 1 mol/L NaOH solution. Next, acetone (50:50, v/v) was added to the aqueous solution to precipitate out the mercapto-conjugated CdSe QDs. The as-prepared precipitate was dried in air until they were ready to be used. The QD solution concentrations were estimated from the absorption spectra using the molar absorptivity at the first absorption maximum for QDs of this size reported by Schmelz et al. ($\sim 1 \times 10^5\ M^{-1}\ cm^{-1}$) [27].

For a typical DNA damage experiment, 1.0 mL 5.0 μg/mL of ctDNA, 1.0 mL 0.5 mol/L of NaCl, 2 mL 0.2 mol/L of Tris buffer solution (pH 7.2) and 200 μL 9.0×10^{-6} mol/L of CdSe QDs were added to a calibrated 5 mL test tube. After 90 min UV irritation, 150 μL 1.0×10^{-4} mol/L of $[Ru(bipy)_2dppx]^{2+}$ and doubly deionized water were added to the mark.

3. Results and discussion

3.1. Effect of the concentration of $Ru(bipy)_2(dppx)^{2+}$ on the reaction between $Ru(bipy)_2(dppx)^{2+}$ and ctDNA

Fig. 1 shows the typical excitation and emission spectra of $Ru(bipy)_2(dppx)^{2+}$ before and after adding ctDNA. $Ru(bipy)_2(dppx)^{2+}$ has no excitation and emission band. While in the presence of ctDNA, the maximum excitation occurred at the wavelength of 455 nm and a strong emission appeared at 600 nm. The influence of $Ru(bipy)_2(dppx)^{2+}$ concentration was studied in the range of 0–5.0×10^{-6} mol/L. It was found that the emission intensity increased with the increase of the concentration of $Ru(bipy)_2(dppx)^{2+}$, when the concentration of $Ru(bipy)_2(dppx)^{2+}$ was higher than 2.0×10^{-6} mol/L, the fluorescence intensity reached a plateau. So 3.0×10^{-6} mol/L $Ru(bipy)_2(dppx)^{2+}$ was used in the subsequent study.

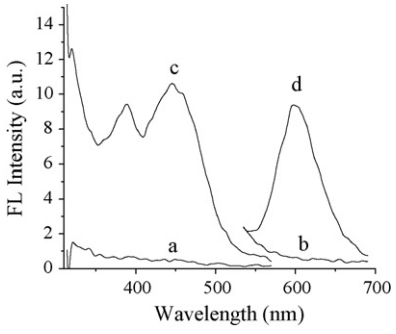

Fig. 1. Excitation and emission spectra of $Ru(bipy)_2(dppx)^{2+}$ and $Ru(bipy)_2(dppx)^{2+}$-DNA; pH 7.2; (a) and (b) 3.0×10^{-6} mol/L $Ru(bipy)_2(dppx)^{2+}$; (c) and (d) 1.0 μg/mL ctDNA + 3.0×10^{-6} mol/L $Ru(bipy)_2(dppx)^{2+}$.

3.2. Effect of time on the reaction between $Ru(bipy)_2(dppx)^{2+}$ and ctDNA

The experiments demonstrated that the reaction finished within 5 min and the fluorescence signals were stable more than 3 h. We recorded the fluorescence intensity after the system had reacted for 10 min.

3.3. Study on ctDNA damage induced by CdSe QDs

Ling et al. [22–25] had studied the interference of coexisting substances such as protein, bases, RNA and metal ions on the detection of DNA. It was found that high concentration of these coexisting substances had no influence on the fluorescence of $Ru(bipy)_2(dppx)^{2+}$-DNA. The fluorescence of water-soluble CdSe QDs is very weak due to the strong quench by mercaptoacetic acid [3]. The emission maximum is obtained at 552 nm, which do not overlap with the fluorescence of $Ru(bipy)_2(dppx)^{2+}$-DNA. So CdSe QDs do not interfere with the determination of ctDNA damage. The proposed method can be used to detect DNA damage induced by CdSe QDs.

The experimental results in Fig. 2 clearly reveal that UV irradiation is a determining factor for the ctDNA damage induced by CdSe QDs. As shown in Fig. 2b, the fluorescence intensity of $Ru(bipy)_2(dppx)^{2+}$-DNA had a slight decrease after adding 3.6×10^{-7} mol/L of CdSe QDs. UV irradiation of the ctDNA in the absence of CdSe QDs also provoked a slight but non-significant decrease of the fluorescence of $Ru(bipy)_2(dppx)^{2+}$-DNA (Fig. 2c). However, treatment of ctDNA with CdSe QDs and subsequent UV irradiation provoked a statistically significant decrease of the fluorescence of $Ru(bipy)_2(dppx)^{2+}$-DNA (Fig. 2d). According to decrease of the fluorescence of $Ru(bipy)_2(dppx)^{2+}$-DNA, we calculated that 70% ctDNA was damaged by CdSe QDs.

Fig. 3 indicates the effect of UV irradiation time on the ctDNA damage. To avoid the damage of $Ru(bipy)_2(dppx)^{2+}$ under UV irradiation, $Ru(bipy)_2(dppx)^{2+}$ was added to the system after UV irradiation in each experiment. A marked increase in ctDNA damage was observed with the increase of the UV irradiation

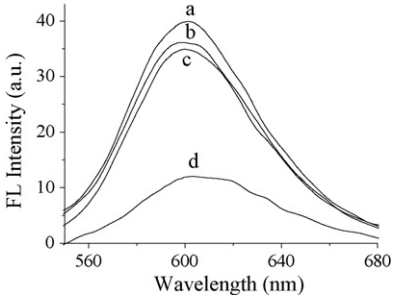

Fig. 2. The emission spectra of $Ru(bipy)_2(dppx)^{2+}$-DNA before and after treatment with CdSe QDs and/or UV irradiation. (a) 1.0 μg/mL ctDNA + 3.0×10^{-6} mol/L $Ru(bipy)_2(dppx)^{2+}$; (b) 1.0 μg/mL ctDNA + 3.6×10^{-7} mol/L CdSe QDs + 3.0×10^{-6} $Ru(bipy)_2(dppx)^{2+}$; (c) 1.0 μg/mL ctDNA of treatment with 90 min UV irradiation + 3.0×10^{-6} mol/L $Ru(bipy)_2(dppx)^{2+}$; (d) 1.0 μg/mL ctDNA + 3.6×10^{-7} mol/L CdSe QDs treatment with 90 min UV irradiation + 3.0×10^{-6} $Ru(bipy)_2(dppx)^{2+}$.

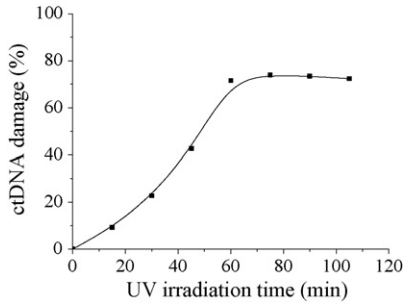

Fig. 3. The effect of UV irradiation time on the ctDNA damage at pH 7.2. The concentrations of CdSe QDs and $Ru(bipy)_2(dppx)^{2+}$ were 3.6×10^{-7} mol/L and 3.0×10^{-6} mol/L, respectively. The concentration of ctDNA was 1.0 μg/mL. $Ru(bipy)_2(dppx)^{2+}$ were added to the system after UV irradiation in each experiment.

time. When the irradiation time was more than 60 min, ctDNA damage reached a plateau. Fig. 4 shows the influence of UV irradiation time on the absorbance spectra of CdSe QDs. A blue-shift in the absorbance spectra is observed because of a decrease in the size of the CdSe QDs, which is in agreement with previous studies [28]. It has been postulated that O_2 molecules oxidize Se atoms located on the surface of the QDs to form SeO_2 [15,29]. These SeO_2 molecules desorb from the surface, leaving behind "dangling" reduced Cd atoms. Thus, prolonged exposure of CdSe QDs to an oxidative environment can cause the decomposition of the CdSe nanocrystal, thereby leading to desorption of Cd^{2+} ions or CdSe complexes from the CdSe QDs [15]. After 60 min UV irradiation, the CdSe QDs had decompounded completely, so no more ctDNA damage was observed.

3.4. The possible mechanism of ctDNA damage

There are at least two potential reasons for the observed ctDNA damage of CdSe QDs with UV irradiation: (i) CdSe nanocrystals mediate the UV-induced local generation of free radicals and reactive oxygen species; and/or (ii) UV induces the liberation of free Cd^{2+} ions [16–19]. A liberation of free Cd^{2+} ions was detected by ICP-MS for 3.6×10^{-7} mol/L of CdSe QDs after 90 min UV irradiation. It was found that 1.7×10^{-5} mol/L Cd^{2+} was released from CdSe QDs. However, in our experiments, it was found that even 5.0×10^{-5} mol/L Cd^{2+} ions did not manifest damage to ctDNA either with 90 min UV irradiation or not. It indicates the reason for the ctDNA damage induced

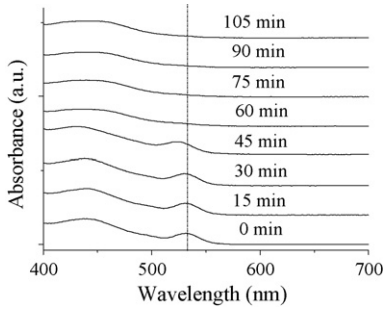

Fig. 4. The influence of UV irradiation time on the absorbance spectra of 3.6×10^{-7} mol/L of CdSe QDs at pH 7.2.

by CdSe QDs is not the UV induced the liberation of free Cd^{2+} ions. Several groups have already reported the possibility of the generation of free radicals and reactive oxygen species during UV illumination of CdSe QDs [19,28,30–35]. According to the results they reported, we thought free radicals and reactive oxygen species play an important role on the ctDNA damage induced by CdSe QDs, which is similar to the DNA nicking from TiO_2 [36].

Green and Howman have investigated the interaction of water-soluble CdSe/ZnS QDs with supercoiled DNA [19]. They found 29% DNA was damaged by QDs even in the dark and suggested the ZnS cap slowly oxidises in the presence of air and water giving SO_2 that desorbs into solution, producing the free radical $SO^{\bullet 2-}$. In our study, no significant DNA damage was found in the dark, which may contribute to two reasons: (i) The toxicity of CdSe QDs is different from that of CdSe/ZnS QDs; (ii) Surface ligands play a critical role in the toxicity of QDs, and different kinds of surface ligands may lead to different toxicity of QDs [17].

4. Conclusion

In conclusion, ctDNA damage caused by water-soluble CdSe QDs was studied using nucleic acid molecular "light switches" as probe. The results strongly suggested that ctDNA damage induced by CdSe QDs was not photo-induced liberation of Cd^{2+}, but the production of free radicals and reactive oxygen species. The proposed method could also be used to investigate DNA damage induced by other nanoparticles.

Acknowledgements

The authors acknowledge the support from National Natural Science Foundation of China (20275028), the National Key Basic Research and Development Program (973 Program 2002CB211800) and 863 Program (2002AA2Z2004). We thank Professor Bin Hu and Doctor Linbo Xia for their assistance with the ICP-MS. We also thank the Editor and anonymous reviewer for several constructive suggestions.

References

[1] A.M. Smith, S.M. Nie, Analyst 129 (2004) 672.
[2] X. Michalet, F.F. Pinaud, L.A. Bentolila, J.M. Tsay, S. Doose, J.J. Li, G. Sundaresan, A.M. Wu, S.S. Gambhir, S. Weiss, Science 307 (2005) 538.
[3] J. Liang, S. Huang, D. Zeng, Z. He, X. Ji, X. Ai, H. Yang, Talanta 69 (2006) 126.
[4] Q. Ma, X.G. Su, X.Y. Wang, Y. Wan, C.L. Wang, B. Yang, Q.H. Jin, Talanta 67 (2005) 1029.
[5] M. Bruchez Jr., M. Moronne, P. Gin, S. Weiss, A.P. Alivisatos, Science 281 (1998) 2013.
[6] W.C.W. Chan, S. Nie, Science 281 (1998) 2016.
[7] X.Y. Wu, H.J. Liu, J.Q. Liu, K.N. Haley, J.A. Treadway, J.P. Larson, N.F. Ge, F. Peale, M.P. Bruchez, Nat. Biotechnol. 21 (2003) 41.
[8] X. Gao, Y. Cui, R.M. Levenson, L.W.K. Chung, S. Nie, Nat. Biotechnol. 22 (2004) 969.
[9] M. Han, X. Gao, J.Z. Su, S. Nie, Nat. Biotechnol. 19 (2001) 631.
[10] Q. Lu, S. Hu, D. Pang, Z. He, Chem. Commun. (2005) 2584.
[11] W.J. Jin, M.T. Fernández-Argüelles, J.M. Costa-Fernández, R. Pereiro, A. Sanz-Medel, Chem. Commun. (2005) 883.
[12] F. Zhang, C. Li, X. Li, X. Wang, Q. Wan, Y. Xian, L. Jin, K. Yamamoto, Talanta 68 (2006) 1353.
[13] J. Weng, X. Song, L. Li, H. Qian, K. Chenb, X. Xu, C. Cao, J. Ren, Talanta, in press.
[14] B. Dubertret, P. Skourides, D.J. Norris, V. Noireaux, A.H. Brivanlou, A. Libchaber, Science 298 (2005) 1759.
[15] A.M. Derfus, W.C.W. Chan, S.N. Bhatia, Nano Lett. 4 (2004) 11.
[16] A. Hoshino, K. Fujioka, T. Oku, M. Suga, Y.F. Sasaki, T. Ohta, M. Yasuhara, K. Suzuki, K. Yamamoto, Nano Lett. 4 (2004) 2163.
[17] C. Kirchner, T. Liedl, S. Kudera, T. Pellegrino, A.M. Javier, H.E. Gaub, S. Stölzle, N. Fertig, W.J. Parak, Nano Lett. 5 (2005) 331.
[18] J. Lovrić, H.S. Bazzi, Y. Cuie, G.R.A. Fortin, F.M. Winnik, D. Maysinger, J. Mol. Med. 83 (2005) 377.
[19] M. Green, E. Howman, Chem. Commun. (2005) 121.
[20] Y.X. Jiang, X.H. Fang, C.L. Bai, Anal. Chem. 76 (2004) 5230.
[21] J. Wang, Y.X. Jiang, C.S. Zhou, X.H. Fang, Anal. Chem. 77 (2005) 3542.
[22] L.S. Ling, Z.K. He, G.W. Song, D. Yuan, Y.E. Zeng, Anal. Chim. Acta 403 (2000) 209.
[23] L.S. Ling, Z.K. He, G.W. Song, Y.E. Zeng, C. Wang, C.L. Bai, X.D. Chen, P. Shen, Anal. Chim. Acta 436 (2001) 207.
[24] L.S. Ling, Z.K. He, F. Chen, Y.E. Zeng, Talanta 59 (2003) 269.
[25] L.S. Ling, Z.K. He, F. Chen, H.S. Zhang, Y.E. Zeng, Chin. Chem. Lett. 14 (2003) 300.
[26] L.H. Qu, X.G. Peng, J. Am. Chem. Soc. 124 (2002) 2049.
[27] O. Schmelz, A. Mews, T. Basché, A. Herrmann, K. Müllen, Langmuir 17 (2001) 2861.
[28] J. Aldana, Y.A. Wang, X.G. Peng, J. Am. Chem. Soc. 123 (2001) 8844.
[29] A.P. Alivisatos, J. Phys. Chem. 100 (1996) 13226.
[30] R. Bakalova, H. Ohba, Z. Zhelev, T. Nagase, R. Jose, M. Ishikawa, Y. Baba, Nano Lett. 4 (2004) 1567.
[31] B.I. Ipe, M. Lehnig, C.M. Niemeyer, Small 1 (2005) 706.
[32] A.C. Samia, X. Chen, C. Burda, J. Am. Chem. Soc. 125 (2003) 15736.
[33] J. Lovric, S.J. Cho, F.M. Winnik, D. Maysinger, Chem. Biol. 12 (2005) 1227.
[34] R. Balakova, H. Ohba, Z. Zhelev, M. Ishikawa, Y. Baba, Nat. Biotechnol. 22 (2004) 1360.
[35] J.M. Tsay, X. Michalet, Chem. Biol. 12 (2005) 1159.
[36] G. Wakefield, S. Lipscomb, E. Holland, J. Knowland, Photochem. Photobiol. Sci. 3 (2004) 648.

Available online at www.sciencedirect.com
ScienceDirect
Talanta 71 (2007) 1455–1463
Talanta
www.elsevier.com/locate/talanta

Determination of phenolic acids in strawberry samples by means of fast liquid chromatography and multivariate curve resolution methods

Sílvia Mas [a], Gemma Fonrodona [b], Romà Tauler [a,*], Jose Barbosa [b]

[a] *Department of Enviromental Chemistry, IIQAB-CSIC, Jordi Girona 18-26, 08034 Barcelona, Spain*
[b] *Department of Analytical Chemistry, Universitat de Barcelona, Diagonal 647, 08028 Barcelona, Spain*

Received 10 January 2006; received in revised form 16 June 2006; accepted 6 July 2006
Available online 12 September 2006

Abstract

Use of Multivariate Curve Resolution Alternating Least Squares (MCR-ALS) is evaluated in the analysis of nine phenolic acids, both in standards mixture samples and in strawberry juice samples, by liquid chromatography with diode array detection (LC-DAD). Chromatographic coelution problems either because of unknown matrix interferences or because of the increase of organic modifier to reduce chromatographic analysis times are investigated. pH (4.25) and proportion of organic modifier in acetonitrile–water ratios (11:89, v/v) used as mobile phases have been optimized for separation of mixture of nine phenolic acids. Results obtained in the resolution and quantitation of phenolic acids in standards mixture samples and strawberry samples at two proportions of organic modifier (11:89 and 40:60 acetonitrile–water (v/v) ratios) show that the proposed MCR-ALS approach reduces analysis times and solvent expenses and improves determinations in case of strong coelution. Limits on the use of MCR-ALS are investigated in the analysis of phenolic acids in strawberry samples.

Keywords: Phenolic acids; MCR-ALS; LC-DAD; Coelution

1. Introduction

During the last decades, the scientific community has recognized the value of vegetables and fruits, not only as a nutrient source, but also as a good for vitaminical deficiencies prevention. For many years, beneficial effects of some fruits and plants have been known. Their consume provides reduction of heart diseases, free radicals and hypertension, improvement on weight control and even reduction of the risk of some cancers (cervix, ovary, prostate, liver, kidney, etc.) [1]. Many of these beneficial effects are attributed to phenolic acids present in vegetables and fruits. These phenolic acids are bioactive compounds and they are widely distributed in the vegetal world. They take part in the diary diet and they influence the health. It has been demonstrated that they act as antioxidants, anti-inflammatories, antihistaminics and anti-tumorals. Moreover, phenolic acids have been associated with color, sensory qualities and nutritional and conservation properties of aliments [2].

In order to establish separation methodologies and determine phenolic acids in biological samples, liquid chromatography (LC) is at present the method of choice because of its versatility, precision and sensitivity [3–5]. Molecular UV–vis absorption spectroscopy is one of the most useful tools currently employed in the determination of compounds when it is combined with LC. Absorption spectra can be combined with retention parameters for the possible identification of unknown compounds, to measure purity of the elution band in question and to perform quantitative sample analysis. In this context, mass spectrometry detection is also being used at present as a very powerful tool to perform identification and quantitation of unresolved mixtures of phenolic acids [6].

In this study, the proportion of organic modifier and the pH of the hydro-organic mobile phase are optimized in order to separate a series of nine phenolic acids. Relationships between the retention parameters of the compounds and Reichardt's E_T^N scale of solvent polarity have been used to optimize the proportion of organic modifier in the mobile phase [7]. Relationships between the capacity factor and the pH measured in the different acetonitrile–water mixtures have also been used to optimize the pH of the mobile phase and pK_a values of the studied phenolic

* Corresponding author. Tel.: +34 93 400 61 40; fax: +34 93 204 59 04.
E-mail address: rtaqam@iiqab.csic.es (R. Tauler).

0039-9140/$ – see front matter © 2006 Elsevier B.V. All rights reserved.
doi:10.1016/j.talanta.2006.07.030

acids are estimated using chromatographic data at the optimized mobile phase [7].

Although chromatographic methods allow in general obtaining good peak resolutions, in many circumstances they require long time for routine analyses. The increase of organic modifier in the mobile phase produces a reduction in elution times, and therefore time and costs of analysis decrease. However, the problem is, in many cases, the coelution of some of the compounds under analysis. In order to solve this problem, coupling LC with diode array detection and Multivariate Curve Resolution by Alternating Least Squares (LC-DAD and MCR-ALS) [8] is proposed as a complementary tool to traditional chromatographic approaches. In the study of natural samples by LC-DAD methods, frequently encountered problems are interference substances and coelutions between two or more compounds. In these cases, the application of multivariate curve resolution (MCR) methods can be also useful to improve the resolution of the peaks that coelute in those samples [9–12]. In this work, phenolic acids have been analyzed in strawberry juice samples by means of fast liquid chromatography with multivariate curve resolution (LC-DAD and MCR-ALS) after method optimization using standard samples containing phenolic acid mixtures.

2. Experimental

2.1. Chemicals and reagents

Analytical reagent grade chemicals were used unless otherwise indicated. Gallic acid, *p*-hydroxybenzoic acid, protocatechuic acid, vanillic acid, benzoic acid, ferulic acid, *p*-coumaric acid, sinapic acid and caffeic acid were purchased from Sigma and used without further purification.

Formic acid 98% (Merck, for analysis), phosphoric acid 85% (Merck, for analysis), potassium bromide (Merck, for spectroscopy), potassium hydrogen phthalate (dried at 110 °C before use, Fluka), sodium hydroxide (Merck, titrisol 1 mol L^{-1}) were used. Acetonitrile (Merck) HPLC grade and MilliQ water, with a conductivity <0.05 μS cm^{-1}, was obtained using MilliQ water purification system (Millipore, Mosheim, France).

Stock samples of phenolic acids were prepared in water at concentrations of approximately 200 mg L^{-1}. Working samples were diluted with the corresponding mobile phase to 10 mg L^{-1}. Samples were passed through a 0.45 μm nylon filter membrane (MSI) before injection. Working samples were analyzed before 3 weeks and the stock samples were used within 2 months of their preparation. Both stock and working samples were stored in a refrigerator at 4 °C in darkness.

2.2. Apparatus

Chromatographic equipment consisted of an Agilent Technologies 1100 Series Model liquid chromatograph, an injection valve with a 20 μL sample loop, a degasser system, a quartet pump and a Hewlett-Packard diode-array detector (DAD). The whole chromatographic system was controlled by Chemstation software for LC 3D Rev. A. 08.03(847) running on a personal computer. Chromatograms and spectra were obtained, respectively, with a resolution of one measurement per second and 1 nm.

A LiChrospher 100 RP-18 column (Merck) (250 mm × 4 mm, i.d. 5 μm) and a LiChrospher 100 RP-18 precolumn (Merck) (4 mm × 4 mm, i.d. 5 μm) were used at ambient temperature. Emf measurements used to evaluate the pH of the mobile phase were performed using a Model 2002 potentiometer (±0.1 mV) (Crison Instruments, Barcelona, Spain) with an Orion 8102 Ross combination pH electrode (Orion Research, Boston, MA, USA). All solutions were thermostatized externally at 25 ± 0.1 °C. The electrode was stabilized in the appropriate acetonitrile–water mixture prior to emf measurement. Measurements were performed in triplicate to verify stability and reproducibility of the potentiometer system. Potassium hydrogen phthalate solutions (0.05 mol kg^{-1}) dissolved in the appropriate acetonitrile–water medium were used as primary standard buffer [13].

2.3. Optimization of the chromatographic separation

Throughout this study, the mobile phases initially assayed were acetonitrile–water at 10:90, 11:89, 12:88, 20:80, 25:75, 30:70, 35:75 and 40:60 (v/v) with 0.1% formic acid and phosphoric acid. In previous studies, different kinds of buffer were used [14], but better peak symmetry and resolution were observed when formic acid was used. In this work, at low pH values up to pH 5.5, the buffer capacity of formic acid was sufficient for adjusting the pH, while at higher pH values phosphoric acid was preferred because of its appropriate pK_a values. The pH of the mobile phase was adjusted between 3.76 and 6.50 with sodium hydroxide. The flow-rate was maintained at 1 mL min^{-1}. For each compound and for every mobile phase composition the retention time values, t_R, were determined from three different injections. Retention factors were calculated as $k = (t_R - t_0)/t_R$, where t_0 is the retention time of potassium bromide (hold-up time). Retention factors were established for each mobile phase composition and studied pH.

In order to optimize the proportion of organic modifier the normalized E_T^N scale of solvent polarity proposed by Reichardt.

$$\log k = C + eE_T^N \quad (1)$$

See references [7] and [15–17] for more details.

The relationships between the retention factor and the pH measured in the different acetonitrile–water mixtures were used to optimize the pH of the mobile phase. The retention behaviour of all studied compounds can be described by Eq. (2). This equation allows obtaining pK_a values, from non-linear least-squares fit of experimental data [18].

$$k = \frac{k_{HA} + k_{A^-} K_a/\gamma a_{H^+} a_{H^+}}{1 + K_a/\gamma a_{H^+} a_{H^+}} \quad (2)$$

where k is the retention factor of each compound, k_{HA} the retention factor of neutral form, k_A the retention factor of ionic form, K_a the dissociation constant of the compound and γa_{H^+} is the activity coefficient which was calculated by Debye–Hückel expression [19].

Achieving a good resolution between all the analytes of interest is the main goal of any chromatographic separation. In terms of fundamental chromatographic parameters the resolution, R_s, between two adjacent peaks can be expressed by

$$R_s = (1/4)\sqrt{N}\left[\frac{\alpha-1}{\alpha}\right]\left[\frac{k}{1+k}\right] \quad (3)$$

where N is the theoretical plates number. Although the selectivity term $[(\alpha-1)/\alpha]$ is generally regarded as the most important in LC, full attention must be given to all the terms in Eq. (3).

2.4. Extraction and hydrolysis of strawberry samples

In a previous work [7], extraction of phenolic acids in strawberry samples was investigated. Hydrolysis at low temperature in complete darkness was found to be the optimal conditions for the extraction procedure. This is justified by the fact that phenolic acids exhibit great sensitivity to light and temperature, which easily induces phenolic decomposition [20]. Firstly, the strawberries were crushed in a food processor. The sample (5 g of juice) was spiked with the adequate volume of a standard solution of the series of nine phenolic acids to have them at a concentration of 4 mg L^{-1} each. Then the sample was rinsed with 25 mL of methanol into a bottle. Ascorbic acid (80 mg) was added as antioxidant. To this mixture 10 mL of 6 mol L^{-1} HCl was added by careful mixing and the solution was sonicated for 2 min. The mixture was set in a water bath in darkness at 35 °C. After 16 h, water was added to the sample extract to have a final volume of 100 mL. Prior to injection the mixture (20 μL) was filtered.

3. Chemometric procedure

Every chromatographic run gives a new data matrix, $\mathbf{D}_k$ ($k = 1, 2, \ldots, N$), which can be described assuming a bilinear model (based on the multiwavelength extension of Beer's absorption law):

$$\mathbf{D}_k = \mathbf{C}_k\mathbf{S}^T + \mathbf{E}_k \quad k = 1, 2, \ldots, N \quad (4)$$

Rows of matrix $\mathbf{D}_k$ are the spectra recorded at different elution times and columns of matrix $\mathbf{D}_k$ are the chromatographic elution profiles recorded at different wavelengths. $\mathbf{C}_k$ is the matrix of the elution profiles of the resolved compounds during a particular chromatographic run in the analysis of sample k and $\mathbf{S}^T$ is the matrix of corresponding resolved pure spectra. Resolved elution profiles allow quantitation (see below) and resolved spectra allow then identification of the coeluted compounds. Finally, $\mathbf{E}_k$ is the residuals matrix with the unmodelled absorbance data values.

For all data matrices a certain amount of background signal (absorption by mobile phase whose composition and relative concentration change along the chromatographic run) was detected. To subtract the initial background absorption, the spectrum at the first initial elution time (where it is supposed that there is no elution of the compounds of interest and only the solvent contribute to the signal) was subtracted from subsequent spectra at all other elution times. Doing this, all the chromatograms started at zero.

The main goal of curve resolution methods is the determination of $\mathbf{C}_k$ and $\mathbf{S}^T$ matrices from the only analysis of the experimental data matrix $\mathbf{D}_k$. First, the number of eluted compounds present in a particular peak cluster is estimated from the "chemical rank" associated whit the data matrix $\mathbf{D}_k$. The chemical rank is defined as the mathematical rank in absence of experimental noise. This determination is performed by singular value analysis of matrix $\mathbf{D}_k$ [21]. Singular values associated with eluted compounds are assumed to be larger than singular values associated with noise and experimental undeterminations. Secondly, initial estimates of pure spectra of these components are obtained from techniques based on the detection of "purest" variables [22] and from previous spectra estimates obtained in the analysis of phenolic acid standards. These initial spectra estimations are then iteratively optimized by a constrained alternating least squares regression procedure. At each iteration, a new estimation of the matrix of spectra $\mathbf{S}^T$, and of the matrix of concentration profiles $\mathbf{C}_k$, are obtained by solving alternatively the two least-squares matrix equations:

$$\mathbf{C}_k = \mathbf{D}_k(\mathbf{S}^T)^+ \quad (5)$$

$$\mathbf{S}^T = (\mathbf{C}_k)^+\mathbf{D}_k \quad (6)$$

where $(\mathbf{S}^T)^+$ and $(\mathbf{C}_k)^+$ are the pseudoinverse of the $\mathbf{S}^T$ and $\mathbf{C}_k$ matrices, respectively [21]. At each iteration of this ALS optimization, different constraints are applied (non-negativity, unimodality and selectivity). See references [23–25] for more details of the MCR-ALS method and software implementation.

When a single chromatographic run is analyzed, quantitative estimations of relative concentrations between different components within the same chromatographic run are only possible if some assumptions about their spectra/signal contribution are applied. Otherwise, such estimations are scale ambiguous and no quantititative information can be derived (intensity/scale ambiguity [23]) directly from the analysis of a single chromatographic run.

3.1. Quantitation for standards mixture samples (calibration curve method)

Multivariate curve resolution can be easily extended to the simultaneous analysis of several chromatographic runs [9–11,23] and to recover relative quantitative information. Relative quantitative information for one particular compound is directly derived from the comparison of its MCR-ALS resolved elution profile in the different chromatographic runs.

In order to perform the quantitation of standards at 11:89 and 40:60 acetonitrile–water (v/v) ratios, calibration curves at 4, 10, 16 and 20 mg L^{-1} concentrations were built up for each phenolic acid except for benzoic acid, which was at concentrations of 8, 20, 32 and 40 mg L^{-1}. Three consecutive injections of every standards mixture samples of phenolic acids were made to evaluate the repeatability of retention times and of the peak areas of each compound. Limits of detection (LOD) and limits of

quantitation (LOQ) were calculated following the methodology described in ref. [26].

At optimal separation conditions of 11:89 acetonitrile–water (v/v) ratio, a good peak resolution was obtained for all phenolic acids and the quantitation was performed by univariate data analysis. In this case, the areas were obtained directly from Chemstation LC 3D software at only one wavelength (the system operates at 280 nm for hydroxybenzoic acids and at 320 nm for hydroxycinnamic acids). On the other hand, in the case of 40:60 acetonitrile–water (v/v) ratio, many of the phenolic acid compounds were coeluted. In order to perform their quantitative analysis in mixtures, peak areas were obtained from elution profiles resolved by the MCR-ALS method. Simultaneous analysis of the multiple data matrices corresponding to chromatograms of the different standards mixture samples at the four concentration levels (4, 10, 16 and 20 mg L^{-1}), together with data matrices corresponding to the different pure standard samples, was performed using the MCR-ALS method. Concentrations of the analytes in unknown samples are then obtained by inverse regression using the areas of their MCR-ALS resolved elution profiles.

3.2. Evaluation of the recovery of extraction method (comparison of areas)

In order to evaluate phenolic acids recoveries of the previously established extraction method, samples were adequately spiked with known amounts (4 mg L^{-1}) of the compounds of interest. This recovery evaluation is then roughly estimated by comparison of peak areas of phenolic acids in the strawberry sample with peak areas of pure standard samples whose concentration was 10 mg L^{-1}.

4. Results and discussion

4.1. Optimization of chromatographic separation conditions

Fig. 1 shows changes in chromatographic resolution, $R_{i–j}$, and selectivity, $\alpha_{i–j}$, for adjacent chromatographic peaks at each percentage of organic modifier in the different assayed mobile phases at pH 4.25 (acetonitrile–water 10:90, 11:89, 12:88, 20:80, 25:75, 30:70, 35:65 and 40:60, v/v). Dot symbols represent experimental values and lines represent selectivity and resolution values obtained using Eq. (1). Fig. 1 shows that a good chromatographic separation of phenolic acids can be expected when the acetonitrile content of the mobile phase is 10–12% (v/v). With a lower percentage of organic modifier ratios, longer retention times were obtained and with a higher percentage of organic modifier ratios, some phenolic acids were poorly resolved. The composition of 11:89 acetonitrile–water (v/v) in the mobile phase resulted to be optimal with appropriate selectivity, resolution and retention time.

Changes in selectivity and resolution values between adjacent pairs of chromatographic peaks at 11:89 acetonitrile–water (v/v) ratio and at different pH (3.75, 4.25, 4.75, 5.25, 6.00 and 6.50) values were also studied (figure is not show). An optimal

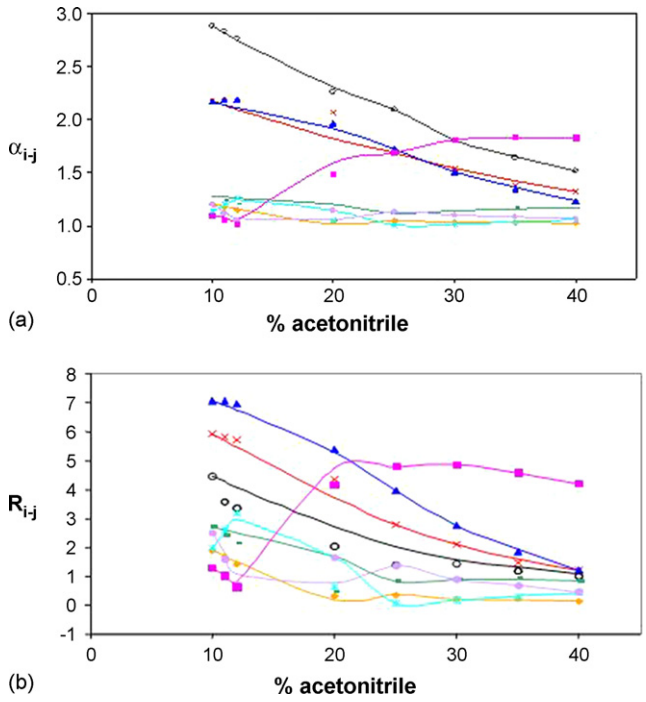

Fig. 1. Plot of selectivity, $\alpha_{i–j}$ (a) and resolution, $R_{i–j}$ (b) vs. percentage of acetonitrile for pairs of studied polyphenolic acids: gallic acid/protocatechuic (◯), protocatechuic acid/*p*-hydroxybenzoic acid (✕), *p*-hydroxybenzoic acid/vanillic acid (▬), vanillic acid/caffeic acid (◆), caffeic acid/*p*-coumaric acid (▲), *p*-coumaric acid/benzoic acid (✳), benzoic acid/ferulic acid (●), ferulic acid/sinapinic acid (■). Acetonitrile–water percentages were: 10:90, 11:89, 12:88, 20:80, 25:75, 30:70, 35:65 and 40:60 (v/v), with 0.1% (v/v) formic acid and pH adjusted with NaOH.

pH value of 4.25 in the mobile phase was chosen, since at this pH, all chromatographic resolution values were higher than 1. As a conclusion, for the separation of the series of nine polyphenolic acids investigated in this work, the optimal conditions for chromatographic separation and determination were a mobile phase composed of acetonitrile–water at 11:89 (v/v) ratio with an isocratic elution at pH 4.25 (with formic acid buffer).

In Table 1, pK_a values of phenolic acids estimated at 11:89 acetonitrile–water (v/v) ratio are listed. These values were calculated by a non-linear least-squares fit of the experimental data

Table 1
pK_a values and retention parameters obtained in the analysis of phenolic acids pure standard samples using 11:89 acetonitrile–water (v/v) ratio

Phenolic acids	pK_a [a]	k_{HA} [a]	k_{A^-} [a]
Gallic acid	4.63 (0.03)	0.83 (0.02)	0.00 (0.01)
Protocatechuic acid	4.67 (0.06)	2.3 (0.1)	0.03 (0.04)
p-Hydroxybenzoic acid	4.72 (0.05)	4.9 (0.1)	0.1 (0.1)
Vanillic acid	4.65 (0.06)	6.2 (0.2)	0.1 (0.1)
Caffeic acid	4.75 (0.08)	6.9 (0.3)	0.2 (0.2)
p-Coumaric acid	4.70 (0.09)	15.5 (0.8)	0.4 (0.5)
Benzoic acid	4.3 (0.1)	24 (1)	1.1 (0.5)
Ferulic acid	4.73 (0.08)	20.4 (0.9)	0.6 (0.5)
Sinapic acid	4.7 (0.1)	21 (1)	0.6 (0.6)

[a] See Eq. (2) and reference [18] for this parameter evaluation. Values in parenthesis are the standard deviation among replicate estimations of the parameters using Eq. (2).

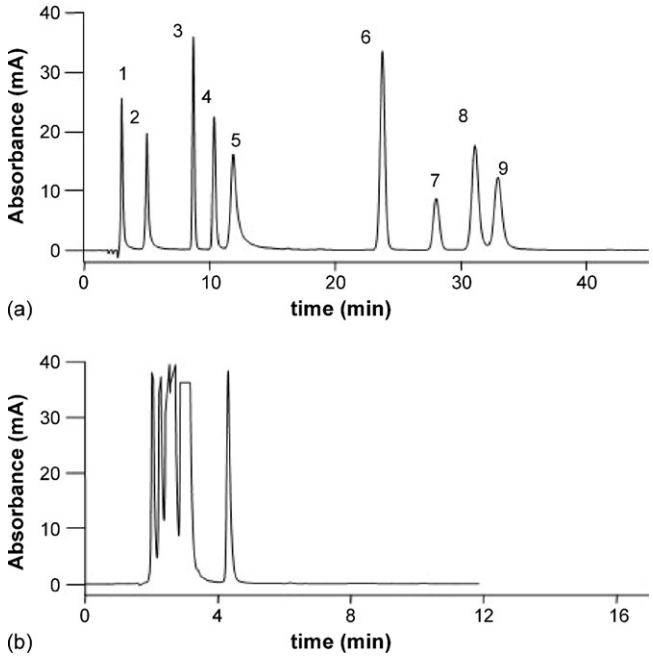

Fig. 2. (a) Chromatogram of a standards mixture sample of phenolic acids with the optimized mobile phase of 11:89 acetonitrile–water (v/v) ratio, containing 0.1% (v/v) formic acid and pH 4.25. Gallic acid (1), protocatechuic acid (2), *p*-hydroxybenzoic acid (3), vanillic acid (4), caffeic acid (5), *p*-coumaric acid (6), benzoic acid (7), ferulic acid (8) and sinapic acid (9). (b) Chromatogram of a standards mixture sample of phenolic acids, with a mobile phase of 40:60 acetonitrile–water (v/v) ratio, containing 0.1% (v/v) formic acid and pH 4.25. Due to strong coelutions, identification of the nine compounds was not possible directly.

using Eq. (2) [18]. Retention factor values for the neutral and ionic forms of the different cinnamic and benzoic acid species are also given in Table 1.

4.2. Resolution and quantitation of phenolic acids in standards mixture samples at 11:89 and 40:60 acetonitrile–water (v/v) ratios by LC-DAD and MCR-ALS

In Fig. 2a, separation of a standards mixture sample of nine phenolic acids at the optimal conditions previously established (at 11:89 acetonitrile–water (v/v) ratio with isocratic elution at pH 4.25) is shown. This optimal separation was achieved in 35 min. The same analysis with less time but lower resolution was attempted then at 40:60 acetonitrile–water (v/v) ratio and at pH 4.25. Much shorter retention times were then obtained (5 min), but in this case some of the compounds appeared strongly coeluted.

In Fig. 2b, the chromatogram obtained at these conditions is shown. MCR-ALS was applied to resolve coeluted compounds in Fig. 2b. It was initialized using pure spectra previously known from individual analysis of standards. After MCR-ALS optimization (see Section 3) elution profiles matrix ($\mathbf{C}_k$) as well the pure spectra matrix ($\mathbf{S}^T$) were obtained. Obviously, this resolution can only be possible if UV-spectra of coeluted compounds are different, even though their retention times were very similar and the chromatographic resolution extremely poor. Indeed, some of the phenolic acids investigated in this work had very similar UV-spectra. In spite of this, MCR-ALS resolution of nearly all compounds in their standards mixture samples was achieved (Fig. 3a). For instance, it is remarkable that MCR-ALS allowed the resolution of protocatechuic acid and of vanillic acid with chromatographic resolution values lower than 0.1 units. Table 2 gives chromatographic resolution values for peak pairs of coeluted compounds in the experimental chromatogram. These resolution values were calculated using ALS resolved elution profiles and the equation given in Table 2 caption. Fig. 3a shows as an example, the resolution of a standards mixture sample of phenolic acids at 10 mg L^{-1} concentration, 40:60 acetonitrile–water (v/v) ratio and pH 4.25. Once the resolution of coeluted peaks was achieved, quantitation of different phenolic acids in their mixtures was attempted.

Table 2
Chromatographic resolutions obtained in the analysis of standards mixture sample at 40:60 acetonitrile–water (v/v) ratio and pH 4.25

Pairs of compounds	Resolution values[a]
Gallic acid/protocatechuic acid	0.4
Protocatechuic acid/caffeic acid	0.3
Caffeic acid/*p*-hydroxybenzoic acid	0.3
p-Hydroxybenzoic acid/vanillic acid	<0.1
Vanillic acid/sinapic acid	0.4
Sinapic acid/*p*-coumaric acid	0.1
p-Coumaric acid/ferulic acid	0.2

[a] Chromatographic resolution is evaluated using equation: $R_s = 2\Delta t_{AB}/w_A + w_B$, where Δt_{AB} is the time difference between the two maxima of resolved peaks and w_A and w_B are the respective resolved peak widths.

In order to perform resolution and quantitation of phenolic acids in standards mixture samples at 11:89 and 40:60 acetonitrile–water (v/v) ratios, calibration curves at different concentration values of the phenolic compounds were built up using the procedure previously described in the chemometric procedure section. Intercept, slope and correlation coefficients of the calibration curves, LOD values, LOQ values and relative errors for each phenolic acid are given in Table 3. In the case of 11:89 acetonitrile–water (v/v) ratio, peak areas were obtained directly from Chemstation LC 3D software while in the case of 40:60 acetonitrile–water (v/v) ratio, peak areas were obtained from elution profiles resolved by MCR-ALS. All phenolic acids were investigated at both acetonitrile–water mixture ratios except benzoic acid because this compound was not coeluted at 40:60 acetonitrile–water (v/v) ratio and the area of its peak could be obtained directly in both cases (11:89 and 40:60 acetonitrile–water (v/v) ratios). In Fig. 3b, resolution and quantitation of the three replicate chromatographic runs corresponding to different standards mixture samples of the phenolic acids at 4, 10, 16 and 20 mg L^{-1} are given. Chromatographic runs of the pure standard acids at 10 mg L^{-1} were also includes in the MCR-ALS analysis.

Good linear relationships between peak areas and concentrations were found in all cases (see Table 3). Relative errors for the concentrations of the nine considered analytes in standards mixture samples were always below 10%. In the case of protocatechuic acid and caffeic acids relative errors were higher than for the other compounds, probably due to experimental

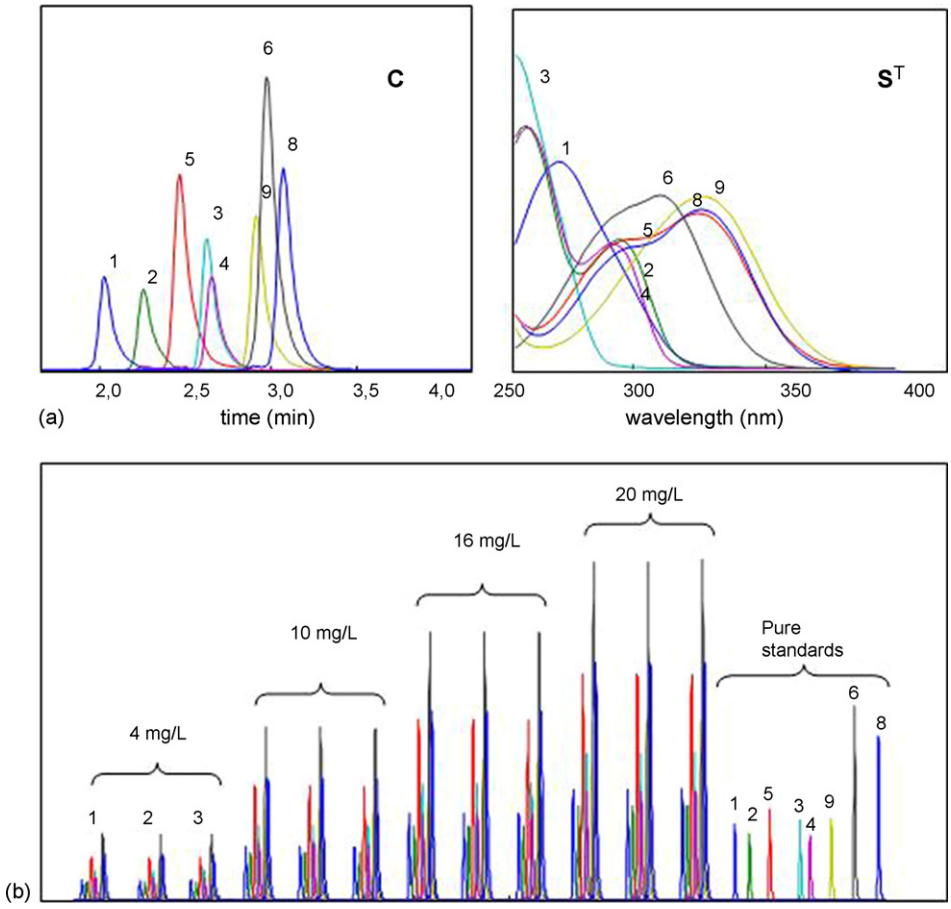

Fig. 3. (a) MCR-ALS resolution of a standards mixture sample of phenolic acids at 40:60 acetonitrile–water (v/v) ratio, for the chromatogram shown in Fig. 2b. Resolved elution and spectra profiles are shown. Each number corresponds to a phenolic acid. Identification numbers for the resolved compounds are given in the caption of Fig. 2a. (b) MCR-ALS resolution and quantitation of four triplicate standards mixture samples of the phenolic acids at 40:60 acetonitrile–water (v/v) ratio and at concentrations of 4, 10 (Fig. 2b), 16 and 20 mg L^{-1}. Eight chromatographic runs of the pure standard samples were also used for optimal MCR-ALS resolution.

Table 3
Figures of merit obtained in the analysis of standards mixture samples and concentration recoveries of the different polyphenolic acids after extraction and chromatographic analysis of strawberry samples using a mobile phase of 11:89 acetonitrile–water (v/v) ratio and pH 4.25

Phenolic acids	LOD and LOQ (mg L^{-1})[a]		Calibration curves (correlation coefficient[b], intercept and slope)		Relative errors[c]		MCR-ALS recovery (%)[d]
	11:89	40:60	11:89	40:60	11:89	40:60	
Gallic acid	1.3 and 4.6	0.4 and 1.2	0.9969, −8.9 and 30.2	0.9999, -6×10^{-4} and 6×10^{-3}	3.5	2.5	103 (4)
Protocatechuic acid	0.8 and 2.5	0.6 and 2.0	0.9991, −20.8 and 31.6	0.9994, -9×10^{-4} and 5×10^{-3}	1.9	8.9	68.7 (<0.1)
p-Hydroxybenzoic acid	0.6 and 1.9	0.3 and 0.9	0.9995, 5.9 and 41.9	0.9999, -9×10^{-4} and 1.4×10^{-3}	1.9	1.4	97 (1)
Vanillic acid	0.6 and 2.0	0.5 and 1.7	0.9994, 4.5 and 32.7	0.9999, 9×10^{-4} and 8×10^{-3}	1.5	1.5	103 (3)
Caffeic acid	0.9 and 2.9	0.2 and 0.6	0.9987, −54.8 and 58.8	0.9999, 1.1×10^{-3} and 6×10^{-3}	2.2	7.6	65 (2)
p-Coumaric acid	0.5 and 1.7	0.4 and 1.2	0.9996, 16.1 and 92.2	0.9998, 8×10^{-4} and 1×10^{-2}	1.3	2.2	94 (3)
Benzoic acid	0.8 and 2.8	0.8 and 2.5	0.9997, −12.2 and 68.6	0.9998, 0.153 and 7.147	1.1	0.9	103 (3)
Ferulic acid	0.6 and 2.0	0.2 and 0.7	0.9994, −16.4 and 52.3	0.9999, 2×10^{-4} and 2.1×10^{-2}	1.5	0.5	66 (2)
Sinapic acid	0.5 and 1.6	0.3 and 0.8	0.9996, −1.3 and 14.2	0.9999, 1.3×10^{-3} and 1.5×10^{-2}	1.2	0.7	35 (2)

[a] See reference [26] for the methodology followed to estimate LOD and LOQ.

[b] Correlation coefficients obtained between areas of directly integrated peaks (11:89, v/v) or of MCR-ALS resolved elution profiles (40:60, v/v) and the concentration of the considered compounds in the analysis of standard mixture samples.

[c] %Error is the error in quantitation evaluated by means of equation: $\%\text{Error} = \sqrt{\sum_i (c_i - \hat{c}_i)} / \sqrt{\sum_i c_i^2}$, where c_i is the known concentration of the analyte in the standard i and $\hat{c}_i$ is the calculated concentration of it using the calibration equation.

[d] Concentration recoveries values were estimated from the comparison between MCR-ALS calculated concentrations and experimental actual ones. In parenthesis, standard deviation among recoveries obtained for three replicate in the analysis of each phenolic acid.

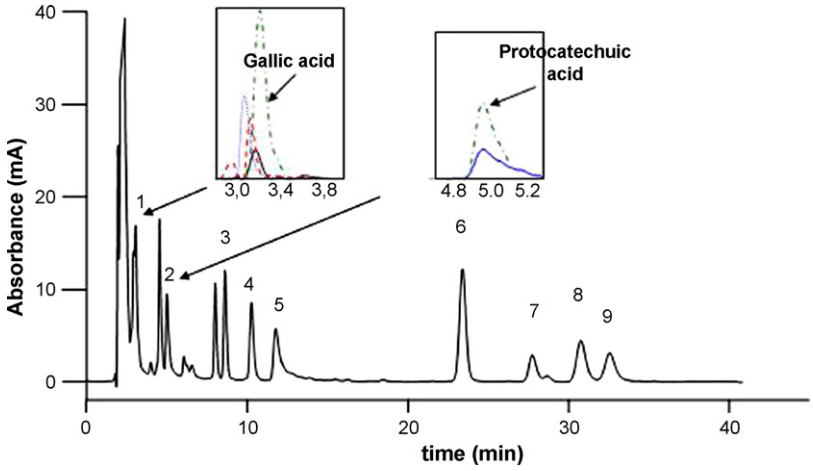

Fig. 4. Chromatogram of a strawberry sample spiked with the different phenolic acids under study at a concentration of 4 mg L^{-1}, with the optimized mobile phase of 11:89 acetonitrile–water (v/v) ratio and pH 4.25. Identification numbers for the resolved compounds are given in the caption of Fig. 2a. MCR-ALS resolution of gallic acid and caffeic acid in the presence of matrix interferences are inserted.

errors caused by dissolution problems during the preparation of these two substances in their standards mixture samples (lower systematic concentration values were always estimated for them). Using either optimal chromatographic condition (11:89 acetonitrile–water (v/v) ratios) or fast chromatographic condition (40:60 acetonitrile–water (v/v) ratios) similar quantitative results were obtained. In the second case (fast chromatography), however, a clear save of time (from 35 to 5 min) and of solvent consumption (approximately the half) were achieved, making this second approach worth to considerer as an alternative strategy of chromatographic analysis in spite of the coelution problems encountered in this case.

4.3. Resolution and quantitation of phenolic acids in spiked strawberry samples at 11:89 and 40:60 acetonitrile–water (v/v) ratios by LC-DAD and MCR-ALS

In order to validate the proposed MCR-ALS method in the analysis of strawberry samples, determination of phenolic acids at 11:89 and 40:60 acetonitrile–water (v/v) ratios was attempted. In a preliminary analysis, and after following the extraction method previously established [27], the concentration of these phenolic acids resulted to be too low, close or lower than their detection limit. These results would indicate that the concentration of these compounds in natural strawberry samples was probably influenced by factors like conservation, maturation and soil [14]. In order to check the application of the previously described MCR-ALS method and to evaluate the recovery of the previously established extraction method, samples were spiked by the compounds of interest before their analysis (see Section 2).

First, resolution and quantitation of spiked strawberry samples at 11:89 acetonitrile–water (v/v) ratio were attempted. Matrix interferences, such as flavonoids and anthocyanidines were expected to be present [14]. In Fig. 4, a chromatogram of a spiked strawberry sample at 11:89 acetonitrile–water (v/v) ratio, at pH 4.25 is shown. The inserted figure in the chromatogram shows MCR-ALS resolved elution profiles in the presence of matrix interferences for the determination of gallic and protocatechuic acids. In order to obtain their area and calculate their recovery, the augmented data matrix formed with three chromatographic runs of the spiked strawberry samples together with the pure standard samples at 10 mg L^{-1} was analyzed by MCR-ALS. It is remarkable the resolution achieved for the protocatechuic acid whose peak was totally embedded in the unknown interference peak.

In Table 3, concentration recovery values of phenolic acids in strawberry samples after their sample extraction and LC-DAD analysis at 11:89 acetonitrile–water (v/v) ratio, together with their standard deviation values are given. As a conclusion, the established extraction method together with MCR-ALS resolution gave reproducible results with low standard deviation values and was suitable for the analysis of many of the compounds under study like gallic, *p*-hydroxybenzoic, vanillic, *p*-coumaric and benzoic acid with recovery values higher than 95%. However, for the analysis of protocatechuic, caffeic, ferulic and sinapic acid, results were not good enough, probably due to the difficulties encountered in the extraction and manipulation of these compounds due to their sensitivity to light and temperature [20].

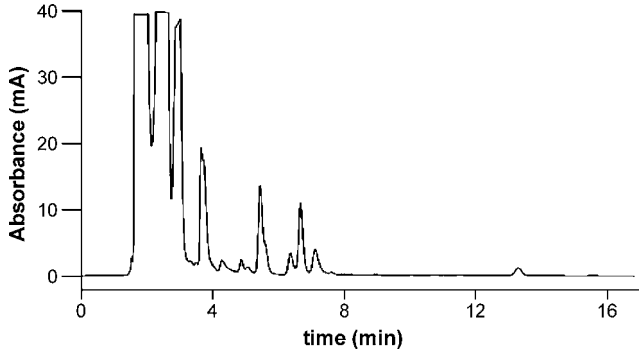

Fig. 5. Chromatogram of a strawberry sample spiked with the different phenolic acids under study at a concentration of 4 mg L^{-1}, with a mobile phase of 40:60 acetonitrile–water (v/v) ratio, containing 0.1% (v/v) formic acid and pH 4.25. Due to strong coelutions identification of the nine compounds was more difficult.

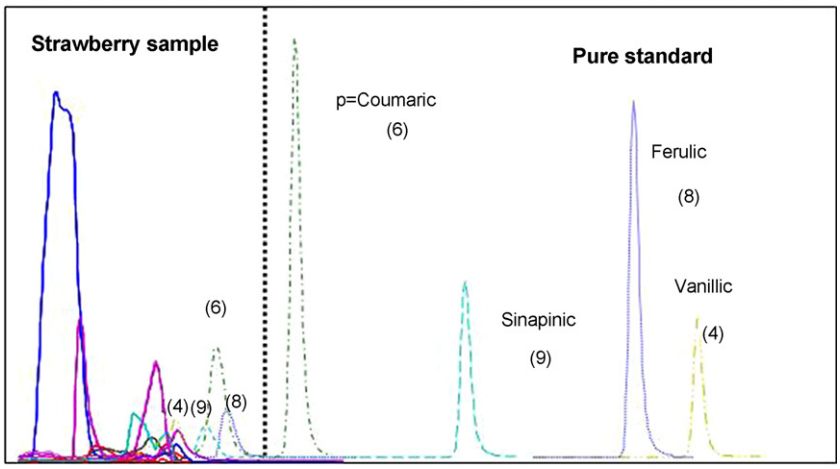

Fig. 6. MCR-ALS resolution of *p*-coumaric, ferulic, sinapic and vanillic acid in LC-DAD analysis of spiked strawberry samples at 40:60 acetonitrile–water (v/v) ratio.

Attempts to achieve MCR-ALS resolution and quantitation of spiked strawberry samples in their LC-DAD analysis at 40:60 acetonitrile–water (v/v) ratio were only successful for some of the investigated compounds. Phenolic acids, which appeared already coeluted in the standards mixture samples were now also coeluted with major matrix interferences. Therefore, their resolution in strawberry samples at this solvent ratio was the more difficult case investigated in this work. In Fig. 5, a chromatogram of a spiked strawberry sample at 40:60 acetonitrile–water (v/v) ratio, is given.

When MCR-ALS was simultaneously applied to the augmented data matrix formed by the strawberry sample extract data matrix together with the data matrices corresponding to chromatographic runs of the different pure standard samples *p*-coumaric acid, sinapic acid, ferulic acid and caffeic acid were properly resolved (Fig. 6) but they were quantified with errors higher than 10%. The sample matrix complexity and the similarity among the UV spectra of the phenolic acid compounds considered in this work marked the limits of the proposed chromatographic and MCR-ALS methods.

5. Conclusions

MCR-ALS has been shown to be a very powerful approach to solve strong coelution problems encountered in the analysis of phenolic acids in complex mixtures and natural samples. Using the advantages of the proposed combined mathematical and chromatographic resolution method, cost, time and solvent expenses were reduced and determinations improved. In this work, LC determination of mixtures of nine phenolic acids is investigated for fast LC analysis of standards mixture samples. However, some limitations were found in the determination of phenolic acids in strawberry samples because of the complexity of the sample matrix and because of the lack of selectivity of UV detection of the investigated compounds. As an alternative, in future works, the incorporation of MS detection in LC is planned to provide more selective information to advantageously resolve, identify and quantify these strong coelutions. In its present development stage, the proposed method is specially useful for research purposes. A more practical and user-friendly implementation of the proposed method would require its incorporation in commercial LC software as a data analysis option.

Acknowledgements

This research was supported by the Spanish MCYT (BQU2003-00191). Sílvia Mas acknowledges a PhD grant UAC 2005-0071 from the Ministerio de Ciencia y Tecnología (Associated Unit between University of Barcelona and CSIC).

References

[1] C.-T. Ho, F. Shahidi (Eds.), Phenolic Compounds in Foods and Natural Health Products, American Chemical Society, Washington, DC, 2005.
[2] J.A. Maga, Crit. Rev. Food Sci. Nutr. 10 (1978) 323–372.
[3] A. Schieber, P. Keller, R. Carle, J. Chromatogr. A 910 (2001) 265–273.
[4] A. Escarpa, M.C. González, J. Chromatogr. A 897 (2000) 161–170.
[5] A. Cert, W. Moreda, M.C. Pérez, J. Chromatogr. A 881 (2000) 131–148.
[6] R.J. Robbins, J. Agric. Food Chem. 51 (2003) 2866–2877.
[7] N. Sanli, G. Fonrodona, D. Barrón, G. Ozkan, J. Barbosa, J. Chromatogr. A 975 (2002) 299–309.
[8] E. Peré-Trepat, A. Hildebrandt, D. Barceló, S. Lacorte, R. Tauler, Chemometrics Intell. Lab. Syst. 74 (2004) 293–303.
[9] R. Tauler, D. Barceló, Trends Anal. Chem. 12 (1993) 319–327.
[10] R. Tauler, B.R. Kowalski, S. Fleming, Anal. Chem. 65 (1993) 2040–2047.
[11] R. Tauler, A.K. Smilde, J.M. Henshaw, L.W. Burgess, B.R. Kowalski, Anal. Chem. 66 (1994) 3337–3344.
[12] G. Durand, V. Bouvot, D. Barceló, J. Chromatogr. A 607 (1992) 319–327.
[13] J. Barbosa, I. Marqués, D. Barrón, V. Sanz-Nebot, Trends Anal. Chem. 18 (1999) 543–549.
[14] S. Häkkinen, Flavonols and phenolic acids in berries and berry products, Ph.D. thesis, University of Kuopio, Finland, 2000.
[15] V. Sanz-Nebot, B. Andón, J. Barbosa, J. Chromatogr. B 796 (2003) 379–393.
[16] V. Sanz-Nebot, I. Toro, J. Barbosa, J. Chromatogr. A 933 (2001) 45–56.
[17] J. Barbosa, R. Bergés, V. Sanz-Nebot, Chromatography 51 (2000) 417–427.
[18] Cs. Hovarth (Ed.), HPLC—Advances and Perspectives, Academic Press, New York, 1983.
[19] J. Barbosa, G. Fonrodona, I. Marqués, S. Buti, I. Toro, Trends Anal. Chem. 16 (1997) 104–111.
[20] A. Escarpa, M.C. González, Crit. Rev. Anal. Chem. 31 (2001) 57–139.

[21] G.H. Golub, Ch.F. Van Loan, Matrix Computations, second ed., The John Hopkins University Press, London, 1989.
[22] W. Winding, Chemom. Intell. Lab. Syst. 16 (1992) 1–16.
[23] R. Tauler, A. Smilde, R. Kowalski, J. Chemom. 9 (1995) 31–58.
[24] R. Tauler, Chemom. Intell. Lab. Syst. 30 (1995) 133–146.
[25] Multivariate Curve Resolution Website http://www.ub.es/gesq/mcr/mcr.htm.
[26] L. Cuadros-Rodríguez, A. García-Campaña, F. Alés-Barrero, C. Jiménez-Linares, M. Román-Ceba, J. Assoc. Off. Anal. Chem. 78 (1995) 471–477.
[27] G. Zgorka, K. Glowniak, Phytochem. Anal. 10 (1999) 268–271.

Available online at www.sciencedirect.com
ScienceDirect
Talanta 71 (2007) 1449–1454
Talanta
www.elsevier.com/locate/talanta

Development and characterization of ion selective electrode for the assay of antimony

G.A.E. Mostafa

Microanalytical Laboratory, Applied Organic Chemistry Department, National Research Center, Dokki, Cairo, Egypt

Received 3 December 2005; received in revised form 18 April 2006; accepted 12 May 2006
Available online 14 September 2006

Abstract

The construction and general performance characteristics of two novel potentiometric carbon paste electrodes (CPE) responsive to antimony are described. These sensors are based on the use of the ion associate complexes of tetraiodoantimonate (TIA) anion with cetylpyridinium (CP) and triphenyl tetrazolium (TPT) counter cations as ion exchange site in a carbon paste matrix. The two sensors exhibits fast, stable and near-Nernstian for the mono charged TIA anion over the concentration range 1×10^{-3} to 10^{-6} M at 25 °C in the pH range 4–10 with anionic slope of 58.0 ± 0.5 and 55.0 ± 0.7 per concentration decade for TIA-CP and TIA-TPT, respectively. The lower detection limits are 4 and 5×10^{-6} M and response time are 20 and 30 s in the same order of both electrodes. Selectivity coefficients for antimony relative to a number of different cations and anions were investigated. There is negligible interference from many inorganic cation and anion except for Hg^{2+}, Cd^{2+}, and Bi^{3+}; however, their effect were eliminated by EDTA. The determination of 1.0–120.0 μg/ml of antimony in aqueous solutions shows an average recovery of 99.0 and 97.5% with relative standard deviation of 2.0% for both electrodes at 40 μg/ml. The determination of antimony in wastewater and some antibilharzial compounds using the proposed electrodes gave results that compare favorably with those obtained by the atomic absorption spectrometric method. Precipitation titrations involving cetylpyridinium chloride as titrant are monitored with both electrodes with inflection point of 180 and 100 mV for TIA-CP and TIA-TPT, respectively.

Keywords: Antimony; Carbon paste electrode; Potentiometry

1. Introduction

Antimony is ubiquitously present in the environment as a result of natural processes and human activities. It exists mainly as Sb(III) and Sb(V) in environmental, biological and geochemical samples. Antimony and its compounds are considered to be priority pollutants interest by the USEPA and the EU [1]. According to European community standard [2], the maximum admissible concentration of antimony in surface and drinking water is 10 μg/l. In addition to its industrial application, the derivatives of antimony are utilized in therapeutic agents against several major tropical parasitic diseases. As the toxicity and physiological behavior of antimony, has paid for more accurate, precise and selective methods for the determination of antimony.

Spectrophotometry [3,4], hydride generation atomic absorption spectrometry [5], hydride generation-atomic using different detectors, e.g. fluorescence [6,7], fourier transform infrared spectrometry [8], graphite furnace atomic absorption spectrometry [9] electrothermal atomic absorption spectrometry [10], fluorescence [11], anodic stripping voltammetry [12], and inductively coupled plasma mass spectrometry [13] have been reported for determination of antimony. However, some of these methods involve several manipulation steps and required sophisticated instruments. On the other hand, most of electrochemical methods reported for selective determination of antimony are mainly voltammetry [14–16]. Potentiometric ion selective electrodes have found vast application in diverse fields of analysis being of low cost, selective, sensitive and simply applicable over a wide range of experimental conditions [17–22] with no reports that describe an ion selective electrode for antimony. The present work describes the construction, potentiometric characterization and analytical application of a new modified carbon paste electrode selective for antimony based on the use of TIA-CP and TIA-TPT ion association complex as electroactive material.

E-mail address: gamal_most@yahoo.com.

0039-9140/$ – see front matter © 2006 Elsevier B.V. All rights reserved.
doi:10.1016/j.talanta.2006.05.095

2. Experimental

2.1. Apparatus

All potentiometric measurements were carried out at $25 \pm 1\,^{\circ}C$ unless otherwise stated using an Orion pH/mV meter (model 330) and a combined Ross glass pH electrode (Orion 81-02) was used for pH measurements. An Orion double junction Ag/AgCl reference electrode (model 90-02) containing 10% (w/v) potassium nitrate in the outer compartment was used.

2.2. Reagents and materials

All chemicals used were of analytical reagent grade unless otherwise stated and doubly distilled water was used throughout. Dioctylphthalate (DOP), potassium iodide, potassium antimony tartrate, and graphite powder were obtained from Aldrich Chemical Company. Cetylpyridinium chloride (CPC) and 2,3,5-triphenyl-2-*H*-tetrazolium chloride (TPTC) were obtained from Across Organics. The stock solution of 1×10^{-1} M antimony(III) was prepared by dissolving 3.249 of potassium antimony tartrate in 100 ml of doubly distilled water containing two drops of hydrochloric acid. Phosphate buffer of pH 8.0 was prepared by mixing 50.0 ml of 0.1 M potassium dihydrogen phosphate with 46.1 ml of 0.1 M of sodium hydroxide in a 100 ml measuring flask and completed to the mark with distilled water. A stock solution of 1×10^{-2} M of antimony (tetraiodoantimonate(III)) was prepared by diluting 10 ml of 1×10^{-1} M antimony(III) in excess amount of 0.5 M KI, acidified ~1.2 M H_2SO_4 in a 100 ml measuring flask and complete to the mark with water. The standard antimony solution were prepared (1×10^{-2} to 1×10^{-5} M) by diluting the appreciate amount in double distilled water. One percent EDTA solution was prepared.

2.3. Preparation of the antimony carbon paste electrode

Upon the addition of 50 ml (1×10^{-2} M of antimony in 5×10^{-1} M KI in acidic solution) to 50 ml of 1×10^{-2} M CPC or TPTC a white and a yellow precipitate of TIA-CP and TIA-TPT ion pairs were formed. The precipitates were filtered through Whatman filter paper No. 41, thoroughly washed with doubly distilled water and dried at 50 °C. The sensing electrode were prepared by mixing 10 mg portions of the ion associate complex, with 250 mg graphite powder, and 100 μl DOP in glass Petri dishes and the result paste were used for sensor construction as previously described [23]. Electrode bodies were made from a disposable 1 ml polyethylene syringes the tip of which had been cut off with a cutter. These bodies were filled with approximately amount of such chemical modified carbon paste (CMCP). Smooth surface was obtained by applying manual pressure to the piston while holding the electrode surface a smooth solid support. A fresh electrode surface has been obtained by squeezing out a small amount of paste and scraping off the excess against a conventional paper then polishing the electrode on a smooth paper to obtain a shiny appearance. The electrical connection was made with a copper wire. The electrochemical cell used for potential measurements was: Ag/AgCl ||test solution|| CMCPE. The indicator electrode was conditioned by soaking in a 1×10^{-2} M aqueous tetraiodoantimonate solution for 1 h and stored in the same solution when not in use.

2.4. Procedure

The newly constructed ISEs were calibrated by immersion in conjunction with the reference electrode in a 50 ml beaker containing 9.0 ml of phosphate buffer solution of pH 8. Then 1.0 ml aliquot of TIA solution of different concentration ranging from 1×10^{-2} to 1×10^{-5} M was added with continuous stirring. The potential was recorded after stabilization to ±0.2 mV and the e.m.f. was plotted as function of log[TIA]. The resulting graph was used for subsequent determination of unknown antimony concentration.

2.5. Determination of antimony in antibilharzial compounds

For determination of antimony in potassium antimony tartrate and stibophen (antibilharzial compounds), a portion of the powder containing an appreciable amount of antimony was weight, dissolved in water or acidified with 0.1 M HCl. Excess of iodide concentration was added to give the final concentration 0.5 M in acidic medium of ~1.2 M H_2SO_4 and the solution was transferred to 25 ml measuring flask, completed to the mark with distilled water. The solution was transferred to measuring cell containing 10 ml of phosphate buffer pH 8.0 and the e.m.f. of the electrode systems was measured. The concentration of antimony was calculated from the previous calibration graph as in procedure. Alternatively, the standard addition technique was used for the determination of antimony by mentoring the potential of the sample after treatment with both iodide and acid solution as in pervious procedure. Then the test sample was measured in phosphate buffer solution (pH 8.0) and the potential was measured before and after addition of standard known concentration of TIA (Fig. 1).

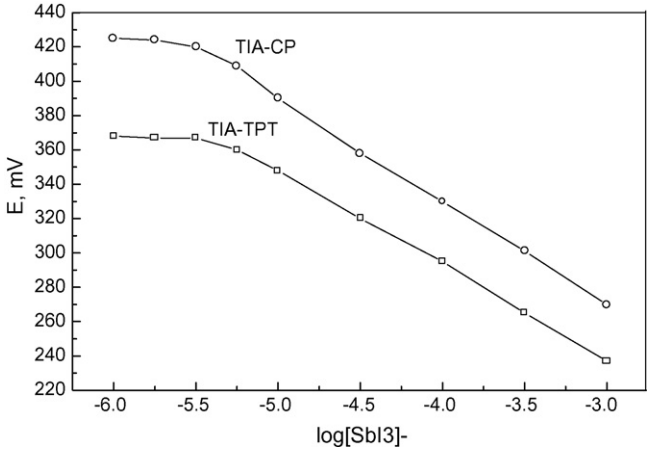

Fig. 1. Calibration graph of TIA using the proposed electrodes.

3. Results and discussion

The procedure is based on the formation of yellow tetraiodoantimonate (III) acid ($HSbI_4$) when antimony(III) in sulfuric acid solution is treated with excess of potassium iodide [24]. Upon addition of CPC or TPTC to solution containing TIA, sparingly soluble complex of SbI_4-CP or SbI_4-TPT have been respectively instantaneously formed. The dry powders of the formed ion pairs are used for the construction of new ion selective electrodes. The elemental analysis data agree with the composition of 1:1. This mean that the trivalent antimony Sb(III) can be determined as tetraiodoantimonate (SbI_4^-) [24] i.e. behave as monocharged anion.

3.1. Sensor characteristics

Cetylpyridinium and triphenyl tetrazolium cation were tested as ion pair agent for the preparation of electroactive ion associate complexes of antimony. Sensors incorporating the composition of electroactive material and dioctylphathalate as solvent mediator in graphite powder matrix were evaluated according to IUPAC recommendations [25], the results are shown in Table 1. Electrodes incorporating TIA-CP and TIA-TPT ion associate show calibration slopes of 58.0 ± 0.5 and 55.0 ± 0.7 mV/concentration decade. The lower limit of detection was 4 and 5×10^{-6} M in the same order of both electrodes. The response times for both electrode at 1×10^{-4} M were 15 and 20 s for TIA-CP and TIA-TPT, respectively. The correlation coefficient (r), intercept (mV) and working acidity range (pH) were (0.999 and 0.998), (-115 ± 0.6 and -85.0 ± 0.6) and 4–10 and 5–9 for TIA-Cp and TIA-TPT respectively.

3.2. Effect of pH and the response time

The pH effect of the antimony test solution (1×10^{-3}, 1×10^{-4}, and 1×10^{-5} M) on the sensors potential were investigated by following the potential variation over the pH range 1–12. The electrode response for different antimony concentrations was tested at various pH values, each time being adjusted by using hydrochloric acid or sodium hydroxide. Potential against pH plots (Fig. 2a and b) reveal that within the pH range 4–10 and 5–9 for TIA-CP and TIA-TPT respectively, the potential did not vary by more than ±0.5 mV over the pH range.

The average response time is defined [25], as the time required for the electrode to reach a stable potential within ±1 mV of the final equilibrium value, after successive immersion of the electrode in different antimony solutions. Each having a 10-fold difference in concentration or after rapid 10-fold increases in concentration by addition of TIA. This time was found to be 15 s for concentration of $\geq 1 \times 10^{-4}$ M and 30 s for concentration $\leq 1 \times 10^{-5}$ M. The two sensors exhibit a day-to-day reproducibility is ±0.6 mV for the same solution and the useful lifetime of the sensor is 4 weeks during which the potential slope is reproducible to within ±1 mV. A fresh electrode surface was obtained by squeezing out a small amount of paste, and polishing the electrode on a smooth filter paper.

Table 1
Response characteristics of the modified carbon paste electrodes

Parameter	Value	
	TIA-CP	TIA-TPT
Slope (mV/decade)	-58.0 ± 0.5	-55.0 ± 0.7
Intercept (mV)	-115 ± 0.6	-85.0 ± 0.6
Correlation coefficient (r)	0.999	0.998
Lower detection limit (M)	4×10^{-6}	5×10^{-6}
Response time for1×10^{-4} M solution (s)	15 ± 0.5	20 ± 0.6
Working pH range	4–10	5–9

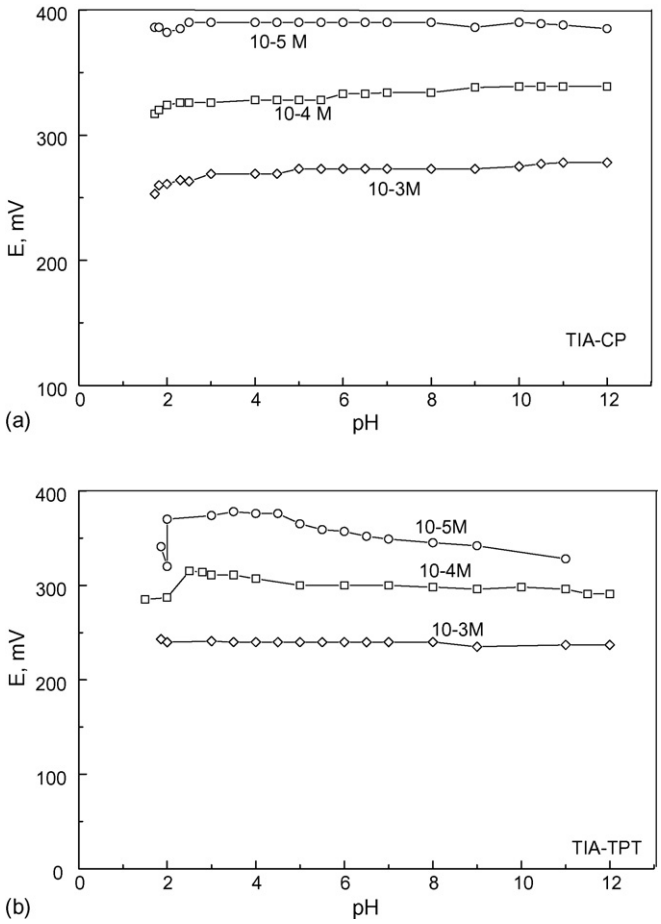

Fig. 2. (a) Effect of pH on the response of TIA-CP electrode using three series of TIA solution (1×10^{-3}, 1×10^{-4}, and 1×10^{-5} M). (b) Effect of pH on the response of TIA-TPT electrode using three series of TIA solution (1×10^{-3}, 1×10^{-4}, and 1×10^{-5} M).

3.3. Effect of ion pair composition

It is known that the potentiometric sensitivity and linearity for a given ion-pair depend significantly on its membrane composition. To study the optimization of the amount of modifier in the electrode, three different composition of the modifier were 2.5, 5.0, 10.0% were prepared, in which the amount of carbon powder and solvent mediator are kept constant, the results obtained are summarized in Table 2. From these results, it is clear that the composition one of the modifier was found to have a Nernstian slope, and wide range of linearity, while

Table 2
General characteristic of some different composition of the modified carbon paste electrodes

Carbon paste electrode	Modified (%)	Slope	Range of determination (M)	Lower limit of detection (M)	Correlation coefficient (r)
TIA-CP	2.5	58.0 ± 0.7	1×10^{-3} to 6×10^{-6}	4×10^{-6}	0.999
TIA-TPT		55.0 ± 0.7	1×10^{-3} to 5×10^{-6}	5×10^{-6}	0.999
TIA-CP	5.0	55.0 ± 0.7	1×10^{-3} to 6×10^{-6}	5×10^{-6}	0.998
TIA-TPT		53.0 ± 0.7	1×10^{-3} to 6×10^{-6}	5×10^{-6}	0.998
TIA-CP	7.5	54.0 ± 0.9	1×10^{-3} to 7×10^{-6}	6×10^{-6}	0.998
TIA-TPT		53.0 ± 0.9	1×10^{-3} to 7×10^{-6}	6×10^{-6}	0.997

electrodes containing higher ratio of the modifier showed less linearity in their response On the other hand, it has been found that, electrode containing zero percentage of the modifiers showed a negligible response. However, increasing the amount of the modifier up to 2.5% has lead to increasing the electrode response; more increase in the modifier percentage more than 2.5% has lead to a decrease again in the electrode response. Therefore, in all incoming studies a carbon paste ion selective electrode were prepared by using a casting solution of the composition 2.5:65:32.5 (w/w/w) ion pair, graphite powder, and dioctylphthalate as solvent mediator, respectively.

3.4. Effect of potassium iodide concentration

The negative charge TIA is formed in solution contains excess of iodide in acidic solution. Thus, the influence of iodide concentration on the response of the electrodes was investigated. The response of the proposed electrodes increased with increasing the concentration of iodide solution (0.4 M) to give a Nernstian slope of about 58.0 ± 0.5 and 55.0 ± 0.6 mV for TIA-CP and TIA-TPT, respectively. Again with increasing the iodide concentration gave no change in the electrode response until it reached to 1 M, where the slope began to decrease. Therefore, 0.5 M of KI was chosen as the optimum amount of KI.

3.5. Effect of diverse ions

The influence of the presence of some different anions and the cations forming iodo complexes similar to the Sb^{3+} ion on the response of antimony sensors were investigated. The selectivity coefficients ($K^{pot}_{A,B}$) were determined by both separate and mixed solution method [25,26] in a phosphate buffer solution of pH 8. Table 3 shows, on the one hand reasonable selectivity by both sensors with many common anions and metal halides. Except for mercury, cadmium and bismuth, are significant interfere, however, their effect were eliminated by addition of 1 ml of 1% EDTA. At the same time to prevent the interferences form other substances, which liberate iodine with potassium iodide, their effect will be reduced with sulfuric acid.

3.6. Validity of the proposed method

3.6.1. Precision and accuracy of the method

The precision of the method was checked by the analysis of five replicate of sample that expressed as the R.S.D.% at the limit of quantification range was less than 2.5%. Also the accuracy was expressed in the term of % deviation of the measured concentration from the actual concentration. The results obtained are within the acceptance range of less than 2.5%.

Table 3
Potentiometric selectivity coefficients of some common species, using the proposed modified carbon paste electrodes

Interferent (J)	$K^{pot}_{Sb(III)+j}$	
	TIA-CP	TIA-TPT
Cu^{2+}	1.5×10^{-4}	1.3×10^{-4}
Hg^{2+}	0.7	0.7
Cd^{2+}	0.6	0.7
Bi^{3+}	0.7	0.8
Pb^{2+}	2.4×10^{-3}	2.5×10^{-3}
Tl^{+}	1.3×10^{-2}	1.3×10^{-2}
Ag^{+}	3×10^{-2}	3×10^{-2}
Zn^{2+}	2.3×10^{-3}	1.3×10^{-4}
Fe^{3+}	1.4×10^{-2}	1.4×10^{-2}
Acetate	1.4×10^{-3}	3.5×10^{-3}
Citrate	1.4×10^{-3}	1.5×10^{-3}
Tartrate	2.3×10^{-4}	3.5×10^{-4}
Benzoate	2.2×10^{-4}	2.2×10^{-4}
Phosphate	1.2×10^{-4}	1.3×10^{-4}
Carbonate	2.2×10^{-4}	6.8×10^{-4}
Thiocyanate	4.5×10^{-3}	1.4×10^{-3}
Chloride	2.2×10^{-3}	2.2×10^{-3}
Nitrate	2.2×10^{-4}	3.6×10^{-4}

* All metal was tested as metal iodide.

3.6.2. Ruggedness

The ruggedness of the potentiometric method was evaluated by caring out the analysis using standard working solution, same electrode and same conditions on the different days. The R.S.D. of less than 2.5% were observed for repetitive in 3 day time

Table 4
Determination of antimony in spiked wastewater samples by direct potentiometry using the proposed electrodes and flame atomic absorption spectrometry

Wastewater sample[a]	Added (μg/ml)	Found (μg/ml)[b]		Found (μg/ml)[b] FAAS
		TIA-CP	TIA-TPT	
Sample 1	10	10 ± 2	10 ± 2	10 ± 2
Sample 2	50	50 ± 2	49 ± 2	49 ± 2
Sample 3	100	99 ± 2	98 ± 2	99 ± 2

[a] Wastewater samples were collected from River Nile near Mansoura City.
[b] Average of the mean of five determinations ±R.S.D.

Table 5
Determination of antimony in some antibilharzial compounds by direct potentiometry using the proposed electrodes and flame atomic absorption spectrometry

Compounds (antimony, %)	The proposed method					
	Sb-CPC		Sb-TPT		FAAS	
	F%	R% ± R.S.D.	F%	R% ± RSD	F%	R% ± R.S.D.
Potassium antimony tartrate (37.47%)	37.0	99 ± 2	36.8	98 ± 2	36.9	98 ± 2
Stibophen (15.86%)	15.55	98 ± 2	15.71	99 ± 2	15.55	98 ± 1.5

Average of the mean of five determinations ±R.S.D. F%: found %.

periods. The result indicates that the method is capable of producing results with high precision on different days.

3.7. Determination of antimony

For verifying the feasibility of the developed method, we carried out the determination of antimony(III) in water. The analysis of 1–120 μg/ml antimony solutions (in five replicate) by direct potentiometric or calibration graph method gave an average recovery of (99.0 and 97.5%) with relative standard deviation of 2.0%, for TIA-CP and TIA-TPT electrode respectively at 40 μg/ml. Alternatively, the standard addition technique was used for the determination of antimony by monitoring the potential of the sample after treating with iodide and acidic solution as in pervious procedure in phosphate buffer (pH 8.0) and recorded the e.m.f. before and after the addition of known concentration of TIA [25].

3.7.1. Determination of antimony in wastewater

The proposed method has been investigated for the direct determination (calibration graph) of antimony in wastewater sample and spiked wastewater gave good results that compared favorably with those obtained by AAS [27]. The results obtained are shown in Table 4 with an average recovery of 99 and 98% and a mean standard deviation of 2 at 50 μg/ml for TIA-CP and TIA-TPT electrode, respectively.

3.7.2. Determination of antimony in some antibilharzial compounds

The method was applied for the determination of antimony in some antibilharzial compounds, e.g. potassium antimony tartrate, and stibophen. The results obtained are in Table 5 (calculated by both calibration graph and standard addition method) with an average recovery of 98.0 and 99.0% and relative standard deviation of 1.6% were obtained with ($n = 5$) for TIA-CP and TIA-TPT, respectively. The results were compared with the data obtained by AAS [27]. The result indicates that the content of antimony in various dosage forms is in good agreement with those obtained by AAS.

In addition, the developed electrodes in conjunction with an Ag/AgCl reference electrode has been examined as an end point indicator electrode for some potentiometric reactions. Titration of antimony (TIA) with CPC as a titrant has been performed and it is clear that the TIA reacts with CPC in 1:1 molar ratio. The titration curves were symmetrical with a very well defined potential jump of about 180 and 100 mV for CP and TPT electrode respectively indicating the high sensitivity of the electrodes (Fig. 3).

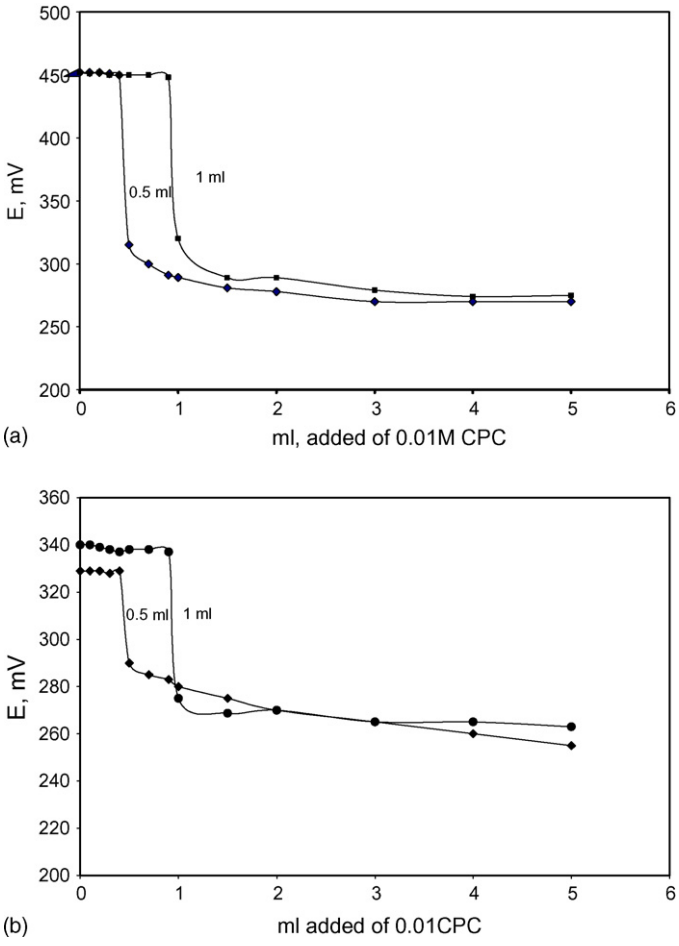

Fig. 3. (a) Typical potentiometric titration curves of 0.5 and 1 ml of 1×10^{-2} M TIA with 1×10^{-2} CPC using TIA-CP electrode. (b) Typical potentiometric titration curves of 0.5 and 1 ml of 1×10^{-2} M TIA with 1×10^{-2} M CPC using TIA-TPT electrode.

4. Conclusion

Experimental comparison of two ion-pair complexes of antimony for use as electroactive materials in potentiometric sensors, reveals that the TIA-CP and TIA-TPT carbon paste electrodes display good performance characteristics. In general the developed electrodes described in this work offer a simple, accurate, selective and specific tool for quantitative determination of antimony in different matrices. The developed electrodes have

also been used as indicator electrode for the determination of antimony using the potentiometric titration.

References

[1] M. Filella, N. Belzile, Y.-W. Chen, Earth-Sci. Rev. 57 (2002) 125–176.
[2] Council directive relating to the quality of water intended for Human consumption (80/778/EEC), Council of the European Comminutes, 1980.
[3] A. Abbaspour, M. Najafi, M.A. Kamyabi, Anal. Chim. Acta 505 (2004) 301–305.
[4] X. Huang, W. Zhang, S. Han, Y. Yin, G. Xu, X. Wang, Talanta 45 (1997) 127–135.
[5] J.Y. Cabon, C.L. Madec, Anal. Chim. Acta 504 (2004) 209–215.
[6] N.V. Semenova, L.O. Leal, R. Forteza, V. Cerdà, Anal. Chim. Acta 530 (2005) 113–120.
[7] E. Fuentes, H. Pinochet, I. De Gregori, M. Potin-Gautier, Spectrochim. Acta B: At. Spectrosc. 58 (2003) 1279–1289.
[8] M. Gallignani, C. Ayala, M.R. Brunetto, M. Burguera, J.L. Burguera, Talanta 59 (2003) 923–934.
[9] T. Kubota, A. Kawakami, T. Sagara, N. Ookubo, T. Okutani, Talanta 53 (2001) 1117–1126.
[10] I. Koch, C.F. Harrington, K.J. Reimer, W.R. Cullen, Talanta 44 (1997) 771–780.
[11] Q. Wei, J. Yang, Y. Zhang, G. Chang, B. Du, Talanta 58 (2002) 419–426.
[12] F. Quentel, M. Filella, Anal. Chim. Acta 452 (2002) 237–244.
[13] S.E. Bulska, A. Hulanicki, Z. Fijalek, Spectrochim. Acta B: At. Spectrosc. 55 (2000) 793–800.
[14] S.B. Khoo, J. Zhu, Anal. Chim. Acta 373 (1998) 15–27.
[15] A.M. Bond, S. Kratsis, O. Michael, G. Newman, Anal. Chim. Acta 372 (1998) 307–314.
[16] R.D. Sekharan, R. Raghavan, L.K. Agrawal, Talanta 43 (1996) 1069.
[17] A.K. Singh, P. Saxena, A. Panwar, Sens. Actuators B: Chem. 110 (2005) 377–381.
[18] S.S. Badawy, Y.M. Issa, A.A. Mutair, J. Pharm. Biomed. Anal. 39 (2005) 117–124.
[19] I.S. da Silva, E.M. Richter, C.L. do lago, I.G.R. Gutz, A.A. Tanaka, L. Angnes, Talanta 67 (2005) 651–657.
[20] A.K. Jain, A.K. Singh, S. Mehtab, P. Saxena, Anal. Chim. Acta 551 (2005) 45–50.
[21] M.M. Hassanien, Kh.S. Abou-El-Sherbini, G.A.E. Mostafa, Talanta 59 (2003) 383–392.
[22] M.N. Abbas, G.A.E. Mostafa, A.M.A. Homoda, Talanta, 53 (20001) 425–432.
[23] M.N. Abbas, G.A.E. Mostafa, Anal. Chim. Acta 478 (2003) 329–335.
[24] G.H. Jeffery, J. Bassett, R.C. Denney, Vogle'S Textbook of Quantitative Chemical Analysis, 5th ed., England, 1989, p. 680.
[25] IUPAC Analytical Chemistry Division, Commission on Analytical Nomenclature, Pure Appl. Chem. 66 (1994) 2527.
[26] T.S. Ma, S.S.M. Hassan, Organic Analysis Using Ion Selective Electrodes, vols. 1–2, Academic Press, London, 1982.
[27] Standard Methods for the Examination of Water and Wastewater, 20th ed., American Public Health Association, Washington DC, 1998, pp. 3–20.

Available online at www.sciencedirect.com
ScienceDirect
Talanta 71 (2007) 1587–1593
Talanta
www.elsevier.com/locate/talanta

Selenium speciation in cow milk obtained after supplementation with different selenium forms to the cow feed using liquid chromatography coupled with hydride generation-atomic fluorescence spectrometry

Óscar Muñiz-Naveiro [a], Raquel Domínguez-González [a], Adela Bermejo-Barrera [a], Pilar Bermejo-Barrera [a,*], José A. Cocho [b], José M. Fraga [c]

[a] *University of Santiago de Compostela, Department of Analytical Chemistry, Nutrition and Bromatology, Faculty of Chemistry, Avda. de las Ciencias s/n, E-15782 Santiago de Compostela, Spain*
[b] *Laboratory of Metabolic and Nutritional Disorders, University Clinical Hospital, E-15706 Santiago de Compostela, Spain*
[c] *Department of Pediatrics, Faculty of Medicine, University Clinical Hospital, E-15782 Santiago de Compostela, Spain*

Received 8 February 2006; received in revised form 21 July 2006; accepted 24 July 2006
Available online 1 September 2006

Abstract

The purpose of this paper is to develop an easy and quick on-line selenium speciation method (LC-UV-HG-AFS) in cow milk obtained after different supplementation to cow feed. This study focuses on selenium speciation in cow milk after the use of different selenium species (organic selenium as selenised yeast and inorganic selenium as sodium selenite) in the supplementation of forages. Separation was carried out on a μBondapack C_{18} column with the positively charged ion-pairing agent tetraethylammonium chloride in the mobile phase. The optimization of pre-reduction conditions was carried out; this step was done with UV irradiation and a heating block to improve the reduction of the different Se-compounds. Variables such as exposure time, hydrochloric acid concentration and temperature were studied. The detection limits for $SeCyst_2$, Se(IV), SeMet and Se(VI) were 0.4, 0.5, 0.9 and 1.0 $\mu g\,l^{-1}$, respectively. The proposed method was applied to cow milk samples. The milk samples obtained after an organic supplementation of feeding as selenised yeast present three species of selenium, SeCyst2, Se(IV) and SeMet, while only SeCyst2 and Se(IV) are present in milk samples obtained after an inorganic supplementation of feeding.

Keywords: Selenium speciation; LC-UV-HG-AFS; Cow milk; Enzymatic digestion

1. Introduction

Selenium (Se) is an important trace element for human health, necessary for the formation and function of at least 13 proteins and component of glutathione peroxidase (GSHPx) enzyme, mainly in the form of selenocysteine [1–4]. Its anti-carcinogenic effect, especially in the case of prostate cancer and some gastric cancers has been reported in recent years [5–8]. Nevertheless, the bioavailability and chemoprotective activity of Se are species dependant [9]. Each species is absorbed by humans in a different way. Dietary studies have shown that selenium in amino acids are absorbed more readily by the body than an inorganic forms of the element [10]. Recently, several authors have aimed their efforts to achieve an increase in selenium concentration in daily products, which shows the importance of selenium species determination in foodstuffs. As an example, it is well-known that cow milk occupies a special place in the human diet, since it is drunk by people from childhood until old age.

Selenium content in milk, which is generally in low selenium content [11,12], varies substantially depending on regional conditions, such as natural selenium levels in soils and natural waters, in cereals, plants, etc. The possibility that selenium supplementation of food might protect against the development of cancer in humans, has generated great interest in Se speciation in milk in order to establish how this supplementation has influence in the presence of the various chemical forms of selenium.

Selenium speciation has been studied by different techniques: high performance liquid chromatography-electrothermal atomic absorption spectrometry (HPLC-ETAAS) [13], liquid chromatography-inductively coupled plasma mass spectrome-

* Corresponding author. Tel.: +34 600 942 346; fax: +34 981 595 012.
E-mail address: pbermejo@usc.es (P. Bermejo-Barrera).

0039-9140/$ – see front matter © 2006 Elsevier B.V. All rights reserved.
doi:10.1016/j.talanta.2006.07.040

try (LC-ICP-MS) [14,15], liquid chromatography-electro spray mass spectrometry (LC-ES-MS) [16], and high performance liquid chromatography coupled to hydride generation-atomic fluorescence spectrometry (HPLC-HG-AFS) [17–22]. UV radiation and microwave treatment were used in hydride generation to transform the different species present in the sample into selenium(IV). UV radiation was applied to water reference materials [18], dietetic supplements [21], rain water, oysters and selenised yeast [22]. The microwave treatment was used with different redox mixtures, obtaining good results for yeast [19], urine reference material [20], etc.

The aim of the present study is to develop an analytical method to perform the selenium speciation in milk using an anion exchange separation coupled to hydride generation-atomic fluorescence spectrometry (LC-HG-AFS) for the speciation of selenite, selenate, selenocystine and selenomethionine in milk, that can be applied for routine quality control purposes.

2. Experimental

2.1. Apparatus

Enzymatic digestion was carried out in a Boxcult incubator (J.P. Selecta S.A., Barcelona, Spain) equipped with a Rotabit orbital-rocking platform shaker with temperature control.

A L8-Beckman ultracentrifuge (Beckman, Palo Alto, CA) with a rotor SW-40 was used to obtain the sample to inject in the chromatographic system. The sample was filtered through an acetate cellulose syringe filter, 25 mm, 0.22 μm (Albet, Barcelona, Spain) previously to inject in the chromatographic system.

A LC system, Waters model 625 LC with a six-port Rheodyne (Cotati, CA, USA) sample injection valve was used with a μBondapack C_{18} column, at particle diameter 10 μm, 300 mm × 3.9 mm.

An UV-cracker (PSA, Orpington, Kent, UK) used as the photoreactor, coupled with a heating block was used in the selenium reduction stage. The heating block used in this study was made from a commercial unit (Multi-bloc, Pselecta, Afora, Barcelona, Spain) designed for tubes and we made a new one to introduce the iron cylinders. The PTFE-tube was coiled around the cylinders and placed into the heating block.

A hydride generation system (Millenium Excalibur PS Analytical, Orpington, Kent, UK) with two peristaltic pumps and a gas–liquid separator was used in the hydride generation procedure.

A Millenium Excalibur AFS detector (PSA, Orpington, Kent, UK) with a Se-boosted hollow cathode lamp (Photron, Cambridge, UK) (current intensities: primary, 20.0 mA; boost, 25.0 mA) was used. The signal from the spectrometer was recorded by the software CSW32, Chromatography Station for Windows (Data Apex Ltd., 2002, Prague, Czech Republic).

2.2. Reagents

All solutions were prepared using ultra pure water (resistivity 18 MΩ cm) from a Milli-Q purification system (Millipore Co., Bedford, MA, USA). All reagents used were analytical grade.

The 0.8% (w/v), sodium tetrahydroborate solution was prepared daily by dissolving sodium tetrahydroborate in 0.1 M sodium hydroxide solution (Panreac Química SA, Barcelona, Spain).

The 5 M hydrochloric acid solution was prepared daily by diluting from the concentrated acid 35% (w/v) (Panreac Química SA, Barcelona, Spain).

Nutral Vacas A.R. (NUTRAL S.A., Madrid, Spain) was used for forage supplementation with inorganic selenium as sodium selenite.

SEL-PLEX (Alltech Biotechnology, Barcelona, Spain) was used for forage supplementation with organic selenium as selenised yeast (90% selenomethionine).

The mobile phase was a tetraethylammonium chloride solution prepared daily from the commercial product (Merck Darmstadt, Germany).

Stock selenium solutions of 1000 μg ml^{-1} were prepared by dissolving sodium selenite (Aldrich, Milwaukee, USA) and sodium selenate (Sigma, St. Louis, MO, USA) from the commercial products using water and seleno-DL-cystine and seleno-DL-methionine (Sigma) using 0.5% (v/v) hydrochloric acid. Diluted solutions were prepared with Milli-Q water immediately before use.

Pronase E and lipase solutions were prepared by dissolving from the commercial products (Sigma–Aldrich Co., St. Louis, MO, USA) in a buffer solution. Phosphate buffer solution was prepared from analytical grade ammonium dihydrogenphosphate (Aldrich, Milwaukee, USA) and pH was adjusted by adding dropwise 2 M sodium hydroxide (Panreac, Barcelona, Spain).

All gases, N_2, H_2, Ar and He, were of the highest purity and purchased from Air Liquid (Madrid, Spain).

2.3. Samples

The different milk samples were obtained after supplementation of Total Mix Rations (TMR) fed to cows with different selenium sources.

Two cow farms were selected on the basis of the most homogeneous characteristics (site, size, operation mode, equipment, etc.). Both farms belong to a co-operative and follow the same protocols with regard to feed, milk collection, veterinary controls, etc. There were no over seven-month-pregnant nor nursing cows included in the milk producing herd. The two farms chosen for study had a milk production of 1740 and 1200 l per day, respectively.

The number of cows involved in the experiment was 60 (farm 1), and 40 (farm 2). During the study, in order to know the influence of the intake of Se using different selenium chemical forms, organic selenium as selenised yeast, at different levels of the concentration, and inorganic selenium were added as supplementation. Feeding was the same in both farms. The food composition was changed every two weeks by increasing the organic selenium level of supplementation. The different organic selenium levels studied were 0.0, 0.2, 0.3, 0.4 and 0.5 μg g^{-1}

and inorganic selenium level studied was 0.3 μg g^{-1}, which is traditional in feeding in Spanish farms. In both farms, milk samples were collected one week and two weeks after beginning the new feeding (following the procedure described above). Samples were stored at −20 °C until treatments were performed.

The TMR was prepared so as to provide the same nutrition input (17% crude protein content, 22–25% starch, 1.7 Mcal kg^{-1} referred to dry matter). To prepare the TMR, the forage (the mixture of maize, grass and alfalfa) from each farm was mixed with a concentrate mixture (cereals, soy, Se supplement) from the milk company in a mixing carriage prior to the TMR being deposited in the manger.

2.4. Enzymatic digestion

Selenium in food is not only present as inorganic species, organic species with covalent bonds with proteins and peptides are also present. Different procedures to extract selenium amino acids have been described. Nowadays the extraction method mostly used is enzymatic digestion. Viñas et al. [21] use protease from *Bacillus licheniformis* to obtain the free amino acids. Pronase E and lipase were chosen for the enzymatic digestion by Gilon et al. [23] and Simon et al. [22]. In this study a solution of Pronase E and lipase was prepared in 50 ml of phosphate buffer (25 mM) with 100 mg of lipase and 100 mg of pronase E at pH 7.0. Five millilitre of enzymatic solution was added to 10 ml of milk sample to perform the enzymatic digestion in a Boxcult incubator at 37 °C for 24 h. After proteolysis the samples were ultracentrifuged for 60 min at 31,000 rpm (160,000 × *g*) with 1 min acceleration and 1 min deceleration times at 4 °C. The sample (enzymatic digested) was taken out with a micropipette from the middle of the ultracentrifuge tube. A fraction of these samples were frozen until perform selenium determination in the enzymatic digest and another fraction was used to inject in the LC system and perform the chromatographic separation of Se-species.

2.5. Chromatographic separation procedure

An effective, repeatable and consistent separation of SeCys2, SeMet, Se(IV) and Se(VI) was carried out using an isocratic LC system. The reversed-phase chromatography on a μBondapack C_{18} column, at particle diameter 10 μm, 300 mm × 3.9 mm, with the positively charged ion-pairing agent tetraethylammonium chloride was applied because it allows the use of an aqueous mobile phase avoiding the use of organic solvents that suppress the formation of selenium hydride. To degas the mobile phase He was used.

The samples (100 μl of enzymatic digest) were injected through the injection valve into the LC system after filtering through a 0.22 μm membrane syringe filter. This allowed separation of all four Se-species, in less than 15 min with good resolution.

2.6. Reduction selenium species procedure

Only selenium(IV) can form selenium hydride. Therefore, all selenium compounds have to be transformed to this oxidation state prior to hydride generation. This step is very important to obtain a good analysis of the selenium species by HG-AFS. In this work a new procedure, use of the UV irradiation coupled to a block heating, was developed to carry out this stage.

At the column outlet an UV-cracker (PSA) was used as a photoderivatization step to transform selenium species in selenite. The sample remained in this part of the system for 2.30 min. Because this reduction process is not satisfactory for all the selenium compounds, a heating block was introduced in the system to end the reduction. The UV cracker was located between the chromatographic column and the heating block. This heating system consisted in 10 m of 0.8 mm PTFE-tube, coiled around two iron cylinders placed in the heating block. The heating system was an electric resistance with a thermostat. The electric resistance consisted in two iron blocks and two iron cylinders. The thermostat allowed the control of temperature of the heating system between room temperature and 200 °C. The solution from the UV-cracker was mixed with the HCl and the result was heated in the heating block (180 °C). Using this system, reduction for all species was obtained. After leaving the heating block, 2 m of 0.8 mm PTFE-tube was introduced into an ice-bath to cool down the sample stream before the hydride generation stage. The instrumental set-up is shown in Fig. 1.

2.7. Se-species determination procedure

Se was determined by HG-AFS. Hydride generation was carried out by adding 5 ml min^{-1} $NaBH_4$ (0.8% (w/v)) in 1% (w/v) NaOH. An Ar flow of 250 ml min^{-1} was used to carry the Se-hydrides to the gas–liquid separator. An H_2 stream (60 ml min^{-1}) was used to obtain a good diffusion flame. In order to dry the Se-hydride a permapure system was used with a 2.5 l min^{-1} N_2 flow. The primary current of the discharge hollow cathode lamp was set at 20 mA and the boosted current at 25 mA.

3. Results and discussion

3.1. Optimization of experimental parameters

3.1.1. Optimal conditions for the reduction step

The optimisation of reduction step conditions was the first assay performed. UV light was used to convert the selenium species into Se(IV), the specie needed for hydride formation.

Aliquots of 10 μg l^{-1} of Se(IV) and SeCyst2 and 20 μg l^{-1} of Se(VI) and SeMet were injected into the LC system and the fluorescence signal was measured after the reduction step. The chromatogram obtained using UV irradiation in the reduction step presents only three peaks.

The selenate signal was not observed under these conditions and the seleno-methionine signal was very poor (Fig. 2A). Therefore, an extra heating block was added to the system. The efficiency of this system was studied with and without the heating block. Similar responses were obtained for selenite, while for SeCyst2 and SeMet an important increase in the peak height was observed, and the peak of selenate was detected in these

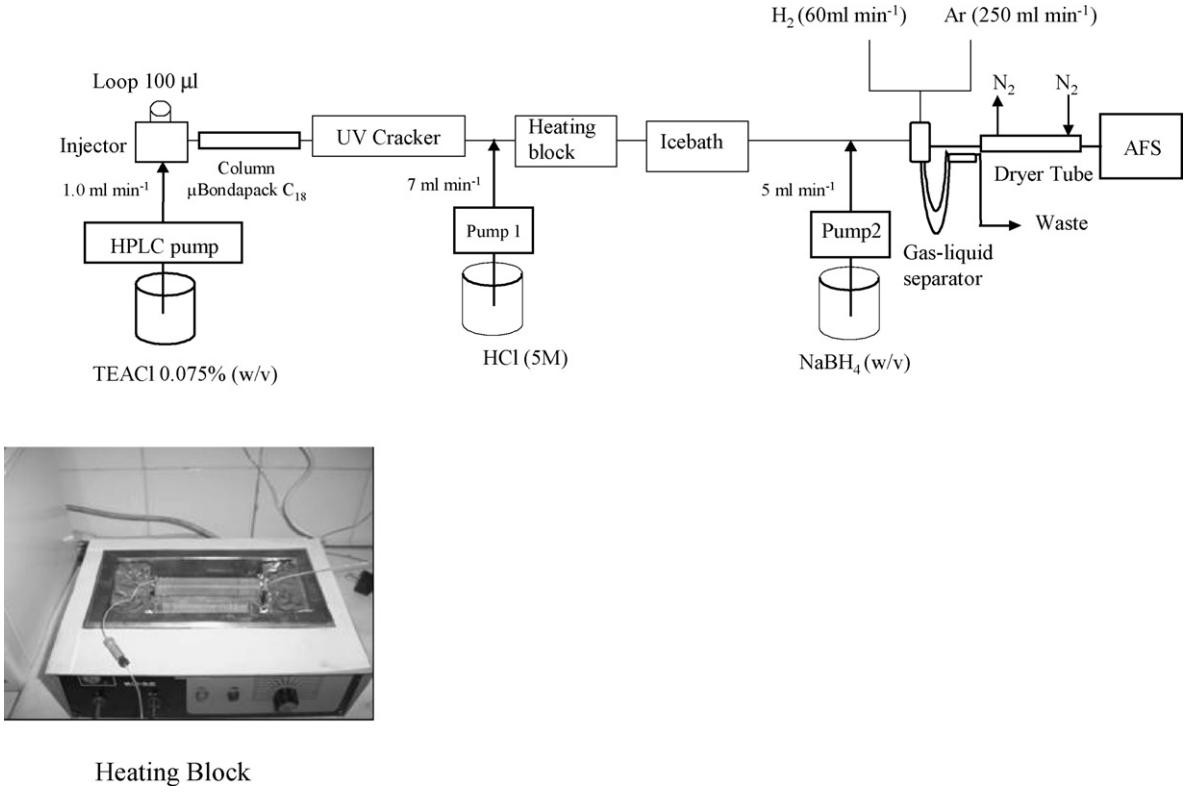

Fig. 1. Instrumental diagrams for Se-speciation in milk by HPLC-UV-HG-AFS.

conditions (Fig. 2B). The heating temperature was optimized in the 100–200 °C range (Fig. 3). The connection of the UV-cracker upstream from the heating block improved the sensitivity of the selenoamino acids more than when the heating block was placed before UV lamp. The advantage of this arrangement is, firstly, the selenoamino acids are destroyed with UV radiation and, secondly, the selenium is changed to selenite with the help of HCl and heat (180 °C). With this configuration an ice bath was necessary to cool down the sample stream to reduce the vapour that has negative effects on the hydride generation and interferes with the hydrogen flame. Under these conditions, the reduction mixture was not necessary and the Se-compounds were transformed into Se(IV) using HCl, UV irradiation and heat. The HCl concentration was also optimized and it was observed that the concentration of hydrochloric acid had an important influence in the results obtained for reduction of selenate and selenoamino acids. The optimum value found was 5 M. This HCl solution was also used as carrier solution for hydride generation. All optimized parameters for pre-reduction conditions are summarized in Table 1.

3.1.2. Optimal conditions for chromatographic separation

Reversed-phase chromatography was optimized using as mobile phase water (pH 6) at a flow rate of 1 ml min^{-1}. Using this column, selenite and selenate eluted together at the void time and only the selenoamino acids were retained, being eluted in the order SeCyst2 and SeMet. Due to this reason ion-pair reagent (tetraethylammonium chloride) was studied for the separation of Se(IV) and Se(VI). The concentration of tetraethylammonium chloride (TEACl) in mobile phase system was optimised regarding resolution and peak shapes. For this purpose, in TEACl a concentration range of 0.05–0.2% (w/v) was tested; the optimum concentration value of TEACl in the reversed-phase system was 0.075% (w/v).

The most important impact of the ion-pair reagent presence was the separation of Se(IV) and Se(VI) and the different

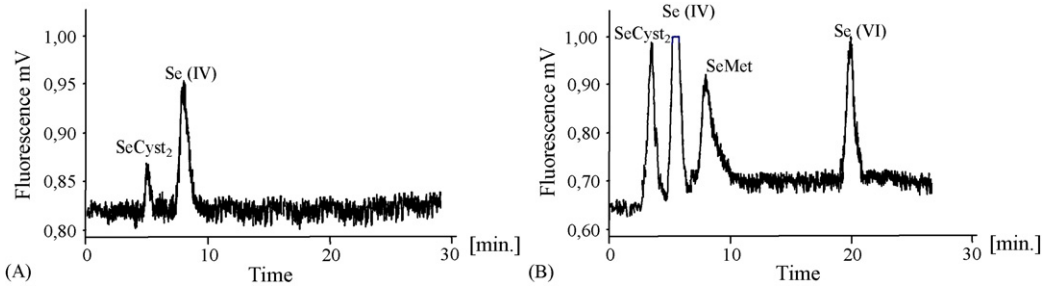

Fig. 2. Chromatograms obtained Se-species standard studied with the initial reduction conditions (A) and optimal reduction conditions (B).

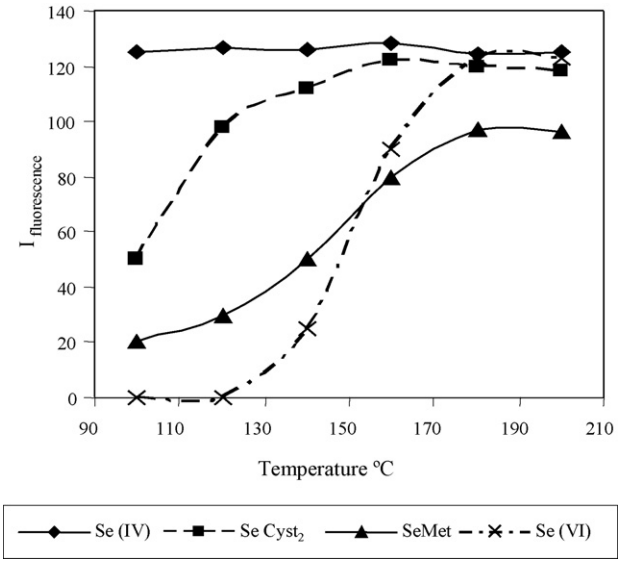

Fig. 3. Effect of block heating temperature in the signal response of different seleno species.

selenoaminoacids. The study of the mobile phase pH was necessary to obtain the ion-pair formation. The pH was studied in the 4–7 range and 4.5 was the optimum value to obtain a satisfactory separation (Fig. 4).

All optimized parameters for pre-reduction conditions are summarized in Table 1.

3.2. Analytical performance

Calibration is plotted for the peak area versus standard concentration for three different solutions injected with increasing

Table 1
Instrumental settings and HPLC conditions

Pre-reduction parameters	
UV source power	78 VA
Reaction coil UV	8 m
Heating block T	180 °C
Reaction coil heating block	10 m
HCl	5 M HCl
HCl flow rate	7.0 ml min^{-1}
HPLC parameters	
Column	μBondapack C18
Dimensions	300 mm × 3.9 mm 10 μm
Mobile phase	Tetraethylammonium chloride 0.75% (w/v)
pH	4.5
Flow rate mobile phase	1.0 ml min^{-1}
Injected volume	100 μl
HG parameters	
Carrier solution	HCl 5 M
Reductant solution	0.8% (w/v) NaHB4
AFS parameters	
Primary current	20 mA
Boosted current	25 mA
H_2 flow rate	60 ml min^{-1}
Ar gas flow rate	250 ml min^{-1}
Drying N_2 flow rate	2.5 l min^{-1}

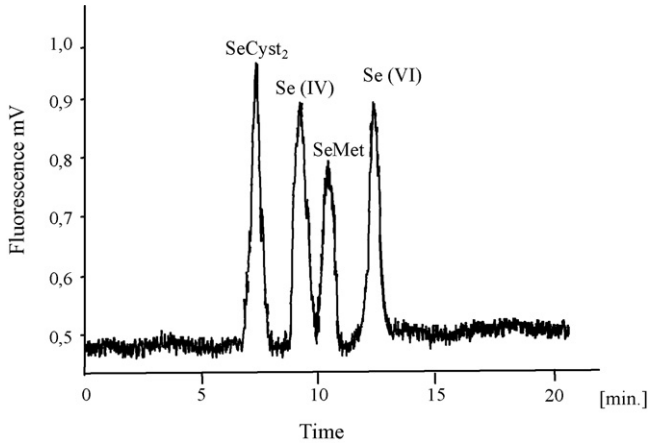

Fig. 4. Chromatogram obtained for the four Se-species standard studied by on-line HPLC-UV-HG-AFS with optimal conditions.

concentrations between 5 and 30 μg l^{-1} for each Se-specie. The linearity of the response (peak area versus concentration) is verified in the whole range investigated. The correlation coefficients R^2 are always >0.997. The slopes and R^2 for the four Se-species are shown in Table 2.

The limit of detection (LOD) and the limit of quantification (LOQ), defined as 3 S.D./*m* and 10 S.D./*m*, respectively, where S.D. is the standard deviation of the blank ($n = 7$) and *m* is the slope of calibration graph, are listed in Table 2. The detection limits obtained were adequate for selenium speciation analysis in milk samples.

Repeatability and reproducibility of the method were evaluated under the optimized conditions. Repeatability was obtained by independent trials of the same method, in the same laboratory, by the same operator in a short period of time; under these conditions three different injections of a mixture containing all the Se-species studied at concentration of 10 μg l^{-1} each were performed, and the average value of the retention times and the standard deviations were calculated. The method repeatability results are shown in Table 3. Repeatability was lower than 5% for all the Se-compounds. The new mixture was analyzed three times by different operators on different days. The average retention times obtained using the two mixtures were compared and the standard deviation and the R.S.D.% were calculated. The reproducibility results are shown in Table 3, in all cases R.S.D. < 5% were obtained.

There are no reference materials available for Se-species in milk or in a similar matrix. Therefore, the analytical recovery

Table 2
Calibration parameters (slope and correlation coefficient of calibration graph) and detection (LOD) and quantification (LOQ) limits for the different Se-compounds by on-line HPLC-UV-HG-AFS

Se-specie	HPLC-UV-HG-AFS			
	Slope (*m*)	Correlation coefficient	LOD	LOQ
SeCyst2	625	0.998	1.1	3.5
Se(IV)	646	0.998	0.9	3.0
SeMet	303	0.997	2.9	9.7
Se(VI)	545	0.997	1.7	5.5

Table 3
Validation parameters for repeatability and reproducibility evaluation ($n = 6$)

	Day 1		Day 2		Reproducibility	
	tr_1 (min)	R.S.D. (%)	tr_2 (min)	R.S.D. (%)	Mean (min)	R.S.D. (%)
SeCyst2	6.61	2.1	6.41	2.2	6.51	3.2
Se(IV)	7.78	0.9	7.62	0.8	7.70	1.1
SeMet	9.26	2.9	9.38	3.2	9.32	4.8
Se(VI)	20.2	1.2	20.2	1.3	20.2	2.3

Table 4
Recovery of Se-compounds from milk sample containing standard of Se-species

Se-species	Sample concentration ($\mu g\,l^{-1}$)	Added concentration ($\mu g\,l^{-1}$)	Recovery %
SeCyst2	7.2	10	96
		20	98
Se(IV)	8.8	10	95
		20	96
SeMet	12.0	10	93
		20	95
Se(VI)	[a]	10	92
		20	93

[a] Value lower than LOD (1.7 $\mu g\,Se\,l^{-1}$).

Table 5
Total selenium concentrations in milk and enzymatic hydrolizates

$[Se]_{Supplementation\ level}$ $\mu g\,g^{-1}$	[Se] milk $\mu g\,l^{-1}$	[Se] enzymatic hydrolizates $\mu g\,l^{-1}$
Organic Se 0.5	38.3 ± 0.3	31.8 ± 0.2
Organic Se 0.4	35.4 ± 0.4	29.1 ± 0.3
Organic Se 0.3	32.3 ± 0.4	26.5 ± 0.3
Organic Se 0.2	29.1 ± 0.3	24.4 ± 0.2
Inorganic Se 0.3	20.2 ± 0.3	17.1 ± 0.1
No supplementation	20.3 ± 0.4	16.8 ± 0.3

The results are expressed as mean ± standard deviation ($n = 12$).

was studied for different milk samples at the different levels to evaluate the accuracy of the method proposed. The different concentrations of four standard Se-species were added to each milk sample and were subjected to the whole procedure. The recovery results are shown in Table 4, recovery values obtained were between 92% and 98%.

The analytical method presented in this study has been demonstrated as a sensitive, repeatable, reproducible, and accurate method for Se speciation (SeCyst2, Se(IV), SeMet and Se(VI)) in cow milk samples.

3.3. Applications

The proposed procedure was applied to six cow milk samples obtained after using different cow feeds. The selenium extracted and the total selenium in the six cow milk samples were determined according to the procedures presented in a previous work [24] by HG-AAS. The results for total selenium in milk and enzymatic hydrolizates with regard to different cow feeds are listed in Table 5. The dependence of total selenium levels in cow milk and enzymatic hydrolizates on the type and levels of Se supplementation of cow feed used was evident. There were no statistically differences between the selenium content in milk obtained after a no supplementation process and a supplementation with inorganic selenium. In a previous selenium bioavailability study [25] same correlations were found after an *in vitro* with dialysis procedure. The selenium dialisability increased in function of organic selenium used as supplement of cow feed and there were no statistical significant differences in selenium bioavailability between milk obtained after organic and inorganic selenium supplementation at levels below 0.5 μg Se/g forage was used. These results made recommended the use of selenium organic as selenised yeast to supplement cow fed not only to obtain cow milk with higher content in selenium but to obtain higher content in bioavailable selenium.

The analytical recovery study show (Table 4) that the extraction procedure based on enzymatic digestion gave good Se recoveries (80–85%).

The milk samples obtained after an organic supplementation of feeding as selenised yeast present three selenium species,

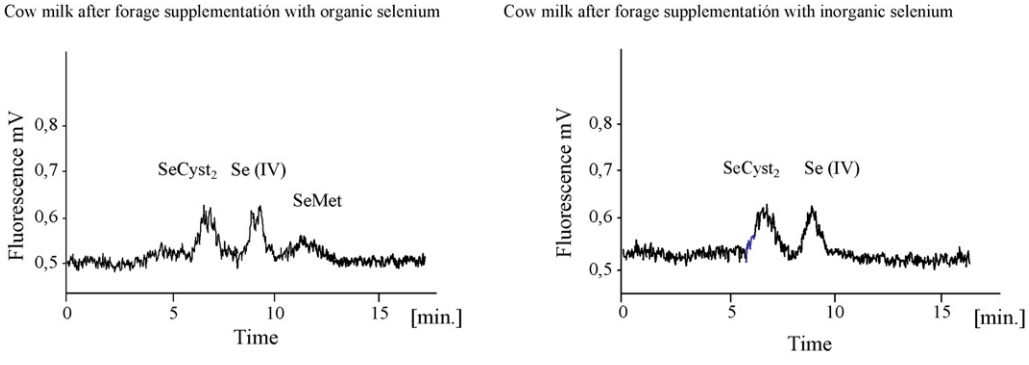

Fig. 5. Chromatograms obtained for the cow milk samples after a supplementation with different selenium forms to cow feed by on-line HPLC-UV-HG-AFS.

Table 6
Selenium species concentrations by HPLC-UV-HG-AFS

$[Se]_{Supplementation\ level}$ $\mu g\,g^{-1}$	[SeCyst2] $\mu g\,l^{-1}$	[Se(IV)] $\mu g\,l^{-1}$	[SeMet] $\mu g\,l^{-1}$	[Se(VI)] $\mu g\,l^{-1}$
Organic Se 0.5	10.3 ± 0.6	7.6 ± 0.4	8.5 ± 0.7	<LOD
Organic Se 0.4	9.6 ± 0.7	7.8 ± 0.5	7.9 ± 0.6	<LOD
Organic Se 0.3	8.2 ± 0.8	7.5 ± 0.6	<LOD	<LOD
Organic Se 0.2	7.9 ± 0.5	7.1 ± 0.5	<LOD	<LOD
Inorganic Se 0.2	7.1 ± 0.6	6.4 ± 0.4	<LOD	<LOD
No supplementation	6.5 ± 0.5	5.9 ± 0.6	<LOD	<LOD

The results are expressed as mean ± standard deviation ($n = 6$). $LOD_{Met} = 2.9\ \mu g\,l^{-1}$ and $LOD_{Se(VI)} = 1.7\ \mu g\,l^{-1}$.

SeCyst2, selenite and SeMet, while only SeCyst2 and selenite are present in milk samples obtained after an inorganic supplementation of feeding (Fig. 5). At higher levels of organic Se supplementation the content in milk of SeCyst2, Se(IV) and Se(VI) increased (Table 6). The differences are higher for SeCyst2. For Se(VI) we could not notice any change in Se levels because these were below LOD. The lowest Se-species concentrations were in cow milk from no supplemented and inorganic Se supplemented cow feed.

Acknowledgments

The authors gratefully acknowledge the support FEIRACO Sociedad Cooperativa Gallega, and Council for Innovation, Industry and Commerce of the Regional Government of Galicia, Spain, for project PGIDIT03TALDE.

References

[1] L. Campanella, T. Ferri, R.A. Morabito, Analusis 17 (1989) 507.
[2] M.R. Calomme, K. Van den Branden, D.A. Vanden Berghe, J. Appl. Bacteriol. 79 (1995) 331.
[3] P. Whanger, J. Trace Elem. Exp. Med. 13 (2001) 367.
[4] S. Mark, Y.L. Qiao, S. Dawsey, Y.P. Wu, H. Katki, E. Gunter, J. Fraumeni, W. Blot, Z.W. Dong, P. Taylor, J. Natl. Cancer Inst. 92 (2000) 1753.
[5] E. Klein, I. Thompson, S. Lippman, P. Goodman, D. Albanes, P. Taylor, C. Coltman, Urol. Oncol. 21 (2003) 59.
[6] F. Fernandez-Banares, E. Cabre, M. Esteve, M.D. Mingorance, A. Abad-Lacruz, M. Lachica, A. Gil, M.A. Gassull, Am. J. Gastroenterol. 97 (2002) 2103.
[7] G.N. Schrauzer, Cell. Mol. Life Sci. 57 (2000) 1864.
[8] H. Ganther, Carcinogenesis 20 (1999) 1657.
[9] S.M. Bird, P.C. Uden, J.F. Tyson, E. Block, E. Denoyer, J. Anal. At. Spectrom. 12 (1997) 785.
[10] A. Vonderheide, K. Wrobel, S. Kannamkumarath, C. B'Hymer, M. Montes-Bayon, C. Ponce de Leon, J. Caruso, J. Agric. Food Chem. 50 (2002) 5722.
[11] J.A. Milner, J. Pediatr. 117 (1990) S147.
[12] M.P. Rayman, Br. J. Nutr. 92 (2004) 557.
[13] M. Potin-Gautier, C. Boucharat, A. Astruc, M. Astruc, Appl. Organomet. Chem. 7 (1993) 593.
[14] V. Diaz-Huerta, M.L. Fernandez-Sanchez, A. Sanz-Medel, J. Anal. At. Spectrom. 19 (2004) 644.
[15] P. Moreno, M.A. Quijano, A.M. Gutiérrez, M.C. Pérez-Conde, C. Cámara, J. Anal. At. Spectrom. 16 (2001) 1044.
[16] M. Montes-Bayón, E.G. Yanes, C. Ponce de Leon, K. Jayasimhulu, A. Stalcup, J. Shann, J.A. Caruso, Anal. Chem. 74 (2002) 107.
[17] I. Ipolyi, Z. Stefanka, P. Fodor, Anal. Chim. Acta 435 (2001) 367.
[18] M. Vilanó, R. Rubio, J. Anal. At. Spectrom. 15 (2000) 177.
[19] E. Dummont, K. de Cremer, M. Van Hulle, C.C. Chéry, F. Vanhaecke, R. Cornelis, J. Anal. At. Spectrom. 19 (2004) 167.
[20] J.L. Gómez-Ariza, D. Sanchez-Rodas, M.A. Caro de la Torre, I. Giraldez, E. Morales, J. Chromatogr. A 889 (2000) 33.
[21] P. Viñas, I. López-García, B. Merino-Meroño, N. Campillo, M. Hernández-Córdoba, Anal. Chim. Acta 535 (2005) 49.
[22] S. Simon, A. Barats, F. Pannier, M. Potin-Gautier, Anal. Bioanal. Chem. 383 (2005) 562.
[23] N. Gilon, A. Astruc, M. Astruc, M. Potin-Gautier, Appl. Organomet. Chem. 9 (1995) 623.
[24] O. Muñiz-Naveiro, R. Domínguez-González, A. Bermejo-Barrera, J.A. Cocho, J.M. Fraga, P. Bermejo-Barrera, Anal. Bioanal. Chem. 381 (2005) 1145.
[25] O. Muñiz-Naveiro, R. Domínguez-González, A. Bermejo-Barrera, P. Bermejo-Barrera, J.A. Cocho, J.M. Fraga, Anal. Bioanal. Chem. 385 (2006) 189.

Available online at www.sciencedirect.com
ScienceDirect
Talanta 71 (2007) 1788–1794
Talanta
www.elsevier.com/locate/talanta

Indirect thermal lens detection for capillary electrophoresis

D.A. Nedosekin [a,*], S.N. Bendrysheva [a], W. Faubel [b], M.A. Proskurnin [a], U. Pyell [c]

[a] *Analytical Chemistry Division, Chemistry Department, M.V. Lomonosov Moscow State University, Vorob'evy Hills d. 1 Str. 3, 119992 Moscow, Russia*
[b] *Research Center Karlsruhe, Institute of Technical Chemistry, Water Technology and Geotechnology Division, Karlsruhe, Germany*
[c] *Chemistry Department, University of Marburg, Marburg, Germany*

Received 9 February 2006; received in revised form 10 August 2006; accepted 21 August 2006
Available online 18 September 2006

Abstract

Thermal lens detection with a 325.0 nm He–Cd excitation laser is used for thermooptical indirect detection in combination with the capillary electrophoretic separation of organic anions. The optimization of indirect thermooptical detection is discussed. With Mordant Yellow 7 (an azo dye) chosen as a probe ion limits of detection for 1-heptane-, 1-pentane-, 1-butane-, 1-propanesulfonic, and acetic acid at a level of $n \times 10^{-7}$ M were achieved with a separation electrolyte containing 50 μM of the probe ion and 5 mM Tris pH 9.90. A further increase in the detection sensitivity (twofold decrease in the limit of detection) was obtained with a separation electrolyte containing a volume fraction of 20% acetonitrile.

Keywords: Capillary electrophoresis; Indirect thermooptical detection; Thermal lens detection; Alkanesulfonic acids; Organo-aqueous separation electrolyte

1. Introduction

The high sensitivity and spatial resolution of laser based thermooptical methods of analysis predetermined the method expansion into the field of flow analysis [1,2]. The combination of photothermal detection with separation techniques such as capillary zone electrophoresis (CZE) [3–7], separation in microfluidic channels [8,9], and liquid chromatography [10,11] takes advantage of a sensitivity increase compared to conventional detection techniques. Thermal lens detection provides not only a detection sensitivity level comparable to or even better than that of laser-induced fluorescence detection but also has the advantage that it can be applied for a larger number of analytes, while laser-induced fluorescence detection is restricted to those substances having a sufficiently large fluorescence quantum yield [1,3,4,12].

Two different approaches to the combination of thermal lensing and CZE are to be named: the first one is the use of thermal lens microscopy [5–7] and the second one is the use of a crossed-beam thermal lens detector [3,4]. These approaches provide close levels of the detection sensitivity [2,5], however, thermal lens microscopy cannot be used in the capillary, requiring a microchip interface to be used for the detection [5,6]. The near-field crossed-beam thermal lens detector, on the other hand, can be directly used for the detection in the capillary and proved to be very efficient for the CZE needs [2].

The difficulty common for all laser based photothermal spectrometry methods, however, is the need to apply lasers emitting at the absorption band of the analyte [1,2]. A high cost associated with the most promising UV lasers and the power instability of the gas lasers still are the problems to be solved. Besides the search for new non-laser based excitation sources [1,9] there are ways to overcome this drawback with the use of the indirect detection technique [12] which is well known in CZE in combination with UV–vis or with laser-induced fluorescence detection [13–19].

The information on the use of the indirect mode in thermal lens detection is rather scare, in spite of the fact that the indirect detection makes it possible to detect substances which do

* Corresponding author. Tel.: +7 095 939 3514; fax: +7 095 939 4675.
E-mail address: tanarek@mail.ru (D.A. Nedosekin).

0039-9140/$ – see front matter © 2006 Published by Elsevier B.V.
doi:10.1016/j.talanta.2006.08.016

not absorb at the wavelength of the excitation laser. Firstly, the application of the thermal lens spectrometry detection in the indirect mode for CZE was described by Ren et al. [20] and Hu et al. [21]. Indirect thermooptical detection was used for the determination of amino acids [20] and several metal cations [21] with methylene blue as a probe ion (excitation laser wavelength 632.8 nm). However, a high level of adsorption of the cationic probe ion on the negatively charged capillary surface and the use of the same excitation and probing laser wavelength reduced the sensitivity of the measurements due to light scattering. In spite of these drawbacks, detection limits at the level of 5×10^{-6} M for lysine and 2×10^{-7} M for Cu(II) were achieved [20,21].

The thermal lens detector designed for capillary electrophoresis with the use of a He–Cd excitation laser (325.0 nm) and a diode probe laser (681.9 nm) described previously [22] increases the sensitivity of direct detection by a factor 10–30 compared to the sensitivity of a conventional UV absorbance detector. However, it is reasonable to expect that the detection in the indirect mode could be less sensitive as the baseline noise in the thermooptical detection is a function of the baseline signal [22]. Thus, an optimization strategy similar to that used for indirect laser-induced fluorescence detection [18] should be applied.

In this paper, the description of the optimization of indirect detection for the separation of model compounds employing a mode-mismatched dual-laser crossed-beam thermal lens detector is presented. The most suitable approach for thermooptical detection in combination with CZE [2–4] was selected employing a UV excitation laser (325.0 nm) which was not previously used in an indirect mode. The comparison of conventional UV–vis indirect detection and indirect thermooptical detection is made.

2. Materials and methods

2.1. Reagents

Following reagents were used: Alizarin Yellow GG (dye content 50%, Aldrich, Germany); Mordant Yellow 7 (dye content 65%, Aldrich); Naphthol Yellow S (p.a., Fluka, Germany); 9,10-anthraquinone-1,5-disulfonic acid (p.a., Fluka); 4-nitrophenol (p.a., Fluka); Tris (p.a., Fluka); histidine (p.a., Fluka); lysine (p.a., Fluka); glycine (p.a., Fluka). Deionised high-purity water (Milli-Q plus 185 (18.0 MΩ), Millipore, Bedford, MA, USA) was used for sample preparation. Sample solutions of alkanesulfonic acids and acetic acid (p.a., Fluka) were prepared in water.

Photometric measurements were performed using a Philips PU 8720 UV/VIS (the Netherlands) spectrophotometer. The pH value of the running buffer was measured by an inoLab pH Level 1 pH-meter (Germany).

2.2. CZE unit

A SpectraPhORESIS 100 capillary electrophoresis system (ThermoQuest, USA) was used. It was possible to couple it both with the thermal-lens detector and a conventional UV-detector (TSP SPECTRA UV100, USA). Separations were carried out in fused-silica capillaries (Polymicro technologies, Phoenix, AZ, USA), i.d. 75 μm, o.d. 360 μm and 71.6 cm total length (41.3 cm to detector). The protection coating at the 5 mm wide zone of the detection window was removed with warm concentrated sulfuric acid (accuracy is required), because this procedure gives a better quality of the capillary rather than the use of flame or a blade, resulting in a better laser beam diffraction picture at the pinhole plane. Sample injection was performed by applying vacuum (200 mbar) for 1 s at the detection side.

2.3. Thermal lens indirect detection

The near-field thermal lens detector used in our experiments had a (crossed) dual-beam mode-mismatched optical scheme design [3,4,22]. At this configuration, the excitation beam and the probe beam cross at right angles within the inner volume of the capillary. The pathways of the excitation and probe beams through the capillary and the main elements of the optical scheme are shown in Fig. 1. For excitation a He–Cd laser is used (excitation wavelength, λ_e, 325 nm, P_e, 50 mW, IK3552R-G Kimmon Electronic Co. Ltd. Tokyo, Japan). The spot size at the waist is 7.7 μm. The laser beam is modulated by a mechanical chopper (frequency range from 40 to 95 Hz), reflected at a right angle by a mirror and focused into the capillary by the focusing Lens 1. The probe laser beam (Toshiba TOLD 1050, Schaeffer & Kirchhoff, Germany, a laser diode, wavelength, λ_p 682 nm) is focused by the achromatic Lens 2, passes through the capillary, and changes its divergence dependent on the thermooptical element created in the capillary. The laser power at the sample, P_p, is 30 mW; the beam waist in the capillary is 75 μm. The beam center passes through the pinhole and reaches the photo diode. The photo diode signal is amplified by a laboratory made lock-in amplifier and translates to a PC by ADC-DAC. The synchronization of the measurements was implemented by an in-house written software.

2.4. Data treatment

The analytical thermal lens signal θ is defined as following:

$$\theta = 2.303 E_0 P_e A, \quad (1)$$

where P_e is the excitation power (W), A the absorbance of the sample, and E_0 is the enhancement factor of thermal lensing for unit excitation power.

$$E_0 = -\frac{dn/dT}{\lambda_p k}. \quad (2)$$

Here, λ_p is the probe laser wavelength, dn/dT is the temperature gradient of the medium refractive index, and k is the thermal conductivity of the medium [1,23].

The instrumental and the analytical signal are related to each other by:

$$\vartheta = KB\theta, \quad (3)$$

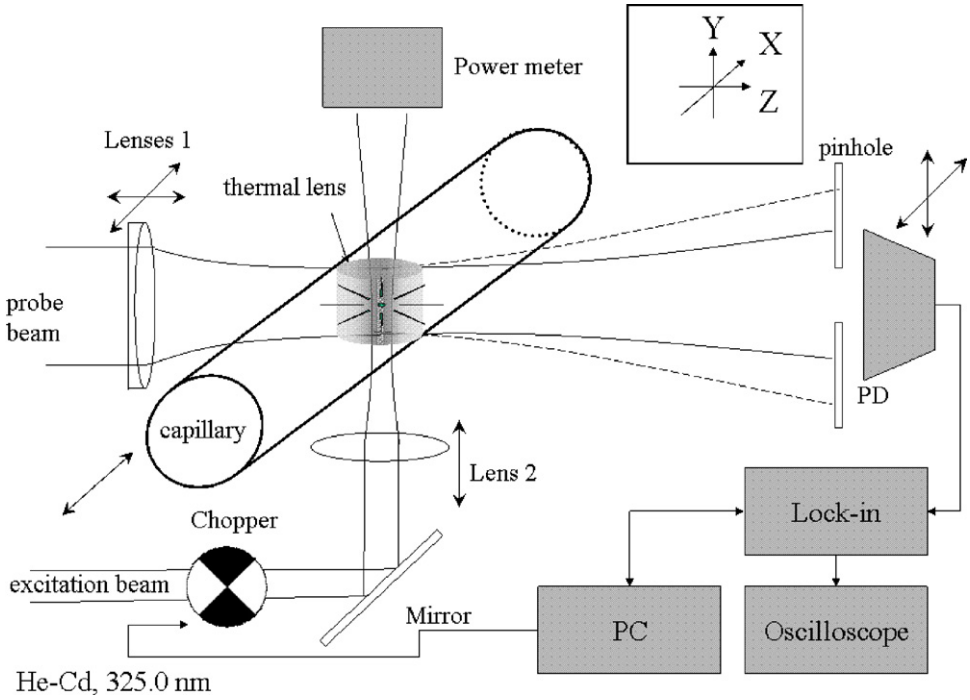

Fig. 1. Optical scheme of the near-field thermal lens detector [22].

where K is a constant which depends on the lock-in amplifier and B is the spectrometer configuration parameter [1].

3. Results and discussion

The limit of detection (LOD) for indirect photometric detection of ionic analytes is given by [12,16,19]:

$$c_{\min} = \frac{c_p}{RD_r} = \frac{N_{BL}}{R\varepsilon_p l}, \tag{4}$$

where $c_{\min}$ is the LOD (molar concentration), c_p is the probe ion molar concentration, R is the transfer ratio (the number of probe ions displaced by one analyte ion), D_r is the dynamic reserve (background signal-to-noise ratio), N_{BL} is the background noise, ε_p is the molar absorbance coefficient of the probe ion, and l is the detection cell pathlength.

In general, in the case of indirect thermooptical detection the baseline noise is a function of the probe ion concentration and excitation laser power, i.e. it is a function of signal value, $N_{BL} = f(c_p, P_e)$. Thus, expressing the analytical thermal lens signal θ by replacing A in Eq. (1) with $c_p\varepsilon_p l$, and D_r in Eq. (3) with ϑN_{BL}^{-1} and taking in consideration that $N_{BL} = \text{const}\, c_p P_e$, the LOD for an analyte ion can be given as:

$$c_{\min} = \frac{c_p}{R}\frac{N_{BL}}{\vartheta} = \frac{\text{const} c_p}{2.303KBRE_0\varepsilon_p l} \tag{5}$$

From this equation it is obvious that the use of a highly absorbing dye as a probe ion decreases the LOD [16,19]. And increasing the probe ion background signal increases the baseline noise so that $c_{\min}$ is inversely proportional to the probe ion concentration [12]. On the other hand, this might increase the electrophoretic dispersion during separation, i.e. reduce the separation efficiency correspondingly decreasing the peak height [12,16].

Thus, with the use of a highly sensitive detector such as the thermooptical detector, new optimum conditions for the composition of the separation electrolyte are to be found. Direct application of the techniques developed for indirect photometric detection is inefficient [18]. Also it should be noted that thermooptical detection provides a further increase in the sensitivity of analysis in case of improvements in the spectrometer configuration [1,3,22] by reducing the fraction of scattered light and by employing organo-aqueous separation buffers increasing the enhancement factor E_0 described in Eq. (2) by improving the thermooptical properties of the medium [1].

3.1. Detection mode optimization

The optimization of the optical scheme of the thermal lens detector and consideration of the detector sensitivity for direct detection mode is described elsewhere [3,22]. However, indirect detection demands additional considerations concerning the dependence of the detector noise on the separation conditions and on the parameters of the signal acquisition.

The analysis of the TL detector 'baseline signal'-to-'baseline noise' ratio dependent on the chopper frequency and on the electrolyte velocity (separation voltage) (Fig. 2) shows that the optimum detection conditions are reached with higher chopper frequencies and are relatively independent from the separation voltage and hence the electrolyte flow velocity.

These findings strongly deviate from results obtained for the direct TL detection where better signal-to-noise ratios were obtained with lower chopper frequencies compared to results

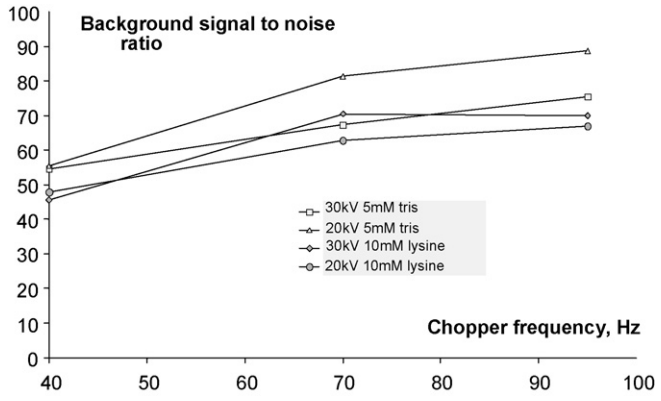

Fig. 2. Dynamic reserve dependent on the chopper frequency for different separation voltages (electroosmotic flow velocities). The data were calculated from a horizontal part of the electropherogram taking 500 data points. Probe ion: Mordant Yellow 7, 50 μM; buffer: Tris 5 mM or lysine 10 mM.

obtained with maximum chopper frequency of 95 Hz [22]. This fact corroborates the assumption that parameters providing the improvement of TL direct detection are not accessible in indirect detection because of the proportionality of the noise of the signal to the signal height.

3.2. Choice of the background electrolyte

The detection sensitivity is expected to be (at a constant transfer rate) directly proportional to the molar absorptivity of the probe ion at the wavelength of the excitation laser ($\lambda_e = 325.0$ nm) (see Eq. (5) [1,16,19,24]. The following acidic dyes and acids were tested: Alizarin Yellow GG, Mordant Yellow 7, Naphthol Yellow S, 9,10-anthraquinone-1,5-disulfonic acid, and 4-nitrophenol. The analytes to be separated and detected are alkanesulfonic acids and acetic acid. The following parameters were taken into consideration for the selection of the probe ion [12]: (a) molar absorptivity at the pH of the separation electrolyte; (b) effective electrophoretic mobility (which should match the effective electrophoretic mobility of the analytes at the pH of the separation electrolyte); (c) photostability; (d) disposition towards adsorption onto the capillary walls. Adsorption onto the walls should be minimized in order to avoid baseline disturbances.

The stability of these dyes in the excitation laser beam was tested experimentally in a standard quartz cell (1 cm length) exposed in the dark to the unfocused laser irradiation for 5 h. The change of the absorption spectra was monitored by a spectrophotometer. For all dyes investigated no significant changes were observed.

From the listed probe ions, Mordant Yellow 7 (MY7, see Fig. 3) was selected as the most suitable one. This dye possesses a high molar absorptivity ($\varepsilon_{325} \sim 1.2 \times 10^4$ L mol^{-1} cm^{-1}). At the pH of the optimized separation electrolyte (pH 9.9) the sulfonic acid group, the carboxylic acid group, and the phenolic group can be expected to be fully dissociated. The high negative charge of this dye in alkaline solution is assumed to prevent adsorption of the dye molecule onto the negatively charged fused-silica capillary walls.

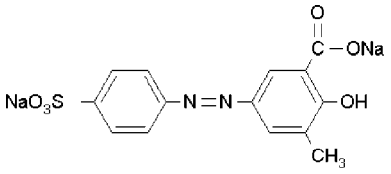

Fig. 3. Mordant Yellow 7 dye.

The background electrolyte should provide a sufficient electric conductivity of the solution, some buffering capacity at the selected pH and a low level of competition with the probe ion for analyte displacement [12,24]. Lysine, glycine, histidine, Na_2HPO_4, and Tris-based buffer electrolytes were tested, and 5 mM Tris (not titrated with HCl) was chosen for further experiments. With low Tris concentrations there is a low electric current minimizing Joule heating which is reported to result in peak broadening and baseline distributions [12,24]. Tris-based buffers (5 mM, pH 9.90) provided the most stable baseline with a minimal noise and insignificant probe ion adsorption on the walls. These BGE conditions allowed the separation and detection of the anions selected within 10 min using a counter-EOF separation under positive voltage.

3.3. Optimization of the probe ion concentration

As it was mentioned above, the use of indirect thermooptical detection in combination with CZE demands the optimization of the probe ion concentration [19–21]. With a given buffer and an optimized detector scheme, a decrease in the baseline noise can be achieved at low probe ion concentrations, however, causing excessive electrophoretic dispersion in the case of a analyte-probe ion-mobility-mismatch.

The empirical optimization of the probe ion concentration (and thus the minimization of the LOD) is very time consuming. Therefore, we employed a semiempirical optimization scheme. Eq. (5) can be presented in the following way:

$$c_{\min(c_{\text{probe}})} = N_{\text{BL}(c_{\text{probe}})} H_{(c_{\text{probe}})} \text{const}, \quad (6)$$

where $H_{(c_{\text{probe}})}$ is the parameter reflecting the ratio of electrophoretic dispersion for the analytes in the capillary with a decrease of the probe ion concentration, const is the constant overall parameter for the selected optical scheme geometry and buffer composition. The parameter H was measured experimentally as follows: $H_{(c_{\text{probe}})} = h_{\max}/h_{(c_{\text{probe}})}$, here $h_{(c_{\text{probe}})}$ is the peak height for the analyte under investigation obtained for the selected concentration of the probe ion and $h_{\max}$ is the peak height in the case of minimal electrophoretic dispersion observed experimentally. For the selected range of the probe ion concentrations, the criterion of the minimal electrophoretic dispersion is the achievement of the separation conditions where the analyte peak reaches the maximum height and is independent from the probe ion concentration. Thus, the H parameter equals to 1 in the case of minimal peak broadening, and $H > 1$ in the case of significant electrophoretic dispersion, increasing the detection limits.

Fig. 4 shows the relative noise of the baseline signal N_{BL} value (the maximum noise value corresponds to the highest probe ion

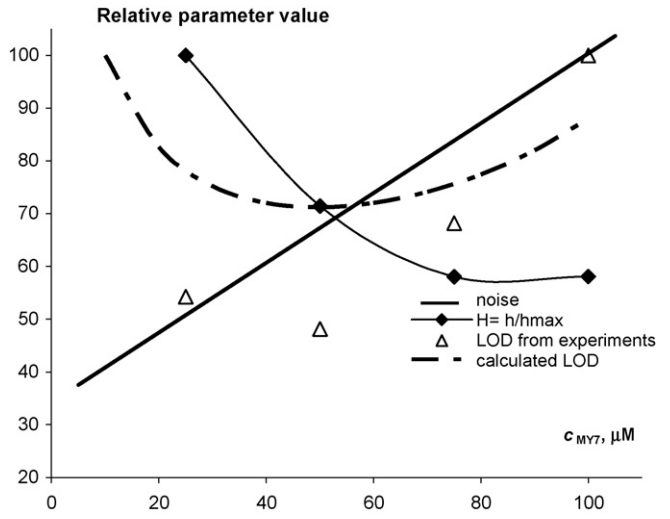

Fig. 4. Dependence of detection limits for acetate on the probe ion concentration, indirect TLS detection, and aqueous separation electrolyte. Separation electrolyte: Mordant Yellow 7, varied concentrations; Tris 5 mM; pH 9.9. Separation voltage: 30 kV. All parameters are given as a relative value (normalized on the maximum value) in order to improve the readability of the graph.

concentration and was taken as 100%) and the $H_{(c_{probe})}$ parameter for acetate (10 μM) as a function of the probe ion (Mordant Yellow 7) concentration. According to Eq. (6) the LOD can be obtained by multiplying these values. The dependence of LODs presented in Fig. 4 by the dotted line was obtained semiempirically from the trends of the noise and dependence of the peak height on the probe ion concentration. This approach is effective, because it is possible to obtain the detailed function of the noise for the detection system on the basis of only a few experiments.

Based on this approach, the concentration of Mordant Yellow 7 of 50 μM was selected for further experiments making necessary only four test runs with varied probe ion concentrations. The dynamic range calculated from the background thermal lens signal divided by the corresponding noise of the background signal (signals were measured with a separation electrolyte containing 50 μM Mordant Yellow 7 and 5 mM Tris, separation voltage 30 kV, and calculation of baseline noise taking 200 data points) equals to 80. In photometric indirect detection the dynamic range reaches 500 [25].

3.4. Electromigration dispersion and calibration graph linearity

In the case of low electrolyte concentration, which has to be employed in indirect thermooptical detection, the local electric field strength in the sample zone differs from that in the buffer zone [12,24]. This discontinuity results in peak fronting or tailing according to the respective analyte/probe ion electrophoretic mobility ratio. In Fig. 5, an electropherogram is presented demonstrating the separation and indirect TL detection of different alkanesulfonic acids (10 μM). Peak fronting caused by electrophoretic dispersion can be observed for each component of the mixture. However, in the case of acetate there

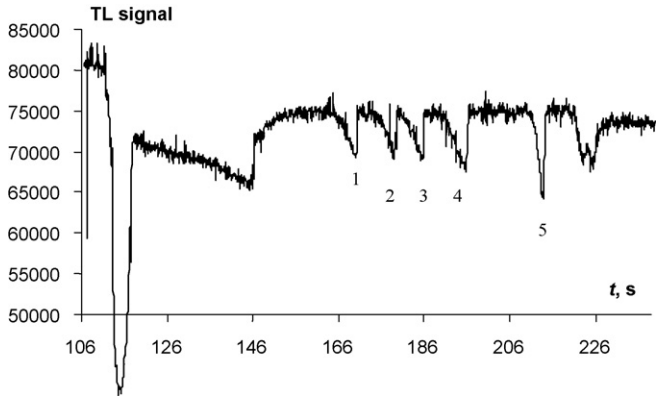

Fig. 5. Electropherogram of an equimolar (10 μM) anion mixture: (1) 1-heptanesulfonic acid; (2) 1-pentanesulfonic acid; (3) 1-butanesulfonic acid; (4) 1-propanesulfonic acid; (5) acetic acid. Separation electrolyte: Mordant Yellow 7 50 μM, Tris 5 mM, pH 9.9.

Table 1
Limits of detection (S/N = 3) for thermal lens detection of model mixture components (for experimental conditions see Fig. 5) ($n = 8$, $P = 0.95$)

Mixture component	LOD (μmol L^{-1})
CH_3COOH	0.5 ± 0.1
$C_3H_7SO_3H$	0.7 ± 0.1
$C_4H_9SO_3H$	1.1 ± 0.2
$C_5H_{11}SO_3H$	0.8 ± 0.1
$C_7H_{15}SO_3H$	0.8 ± 0.1

is a less pronounced peak fronting indicating the similarity of the acetate and the probe ion effective electrophoretic mobilities at the conditions given. The ratio of the analyte/probe ion electrophoretic mobilities mismatch causes the increase in the LOD calculated for the analytes selected (see Table 1) except the acetic acid.

Due to electrophoretic dispersion there is no linear dependence of the peak height on the analyte concentration (see Fig. 6). The calibration graphs for C_3–C_7 alkanesulfonic acids and acetic acid were calculated from the respective peak areas. The linearity range for the calibration graphs at the conditions selected

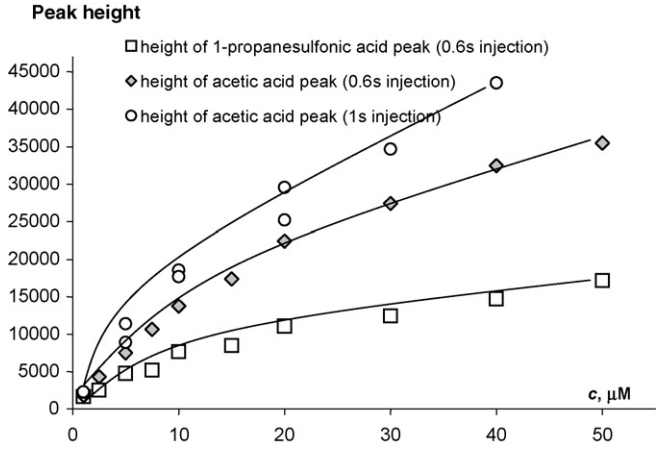

Fig. 6. Dependences of the peak height on the concentration of the analyte in the injected sample. For further experimental parameters refer to Fig. 5.

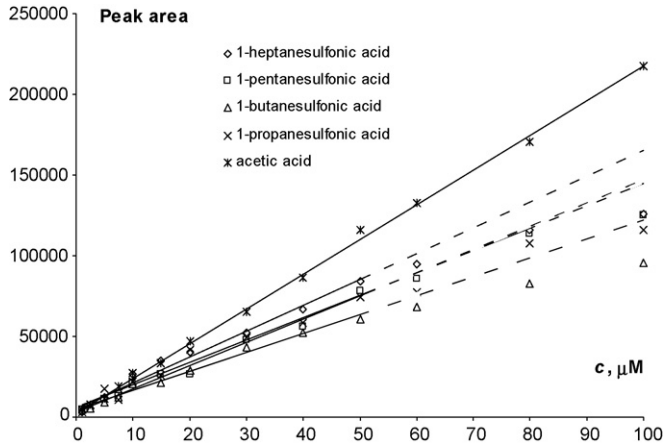

Fig. 7. Calibration graph for anionic analytes. For further experimental parameters refer to Fig. 5.

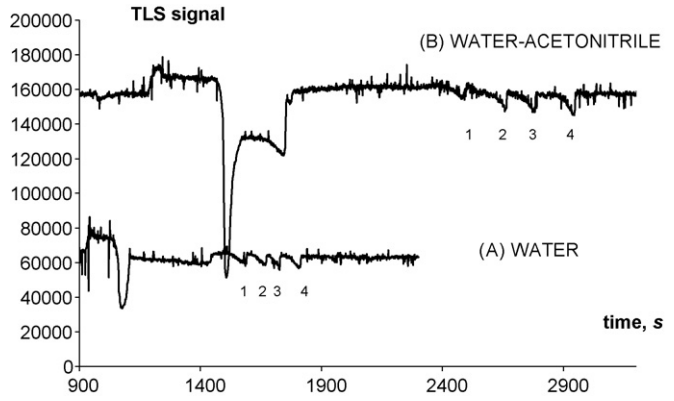

Fig. 8. Electropherograms for a sample containing 10 μM of (1) 1-heptanesulfonic acid; (2) 1–pentanesulfonic acid; (3) 1–butanesulfonic acid; (4) 1–propanesulfonic acid. Separation electrolyte: Mordant Yellow 7 50 μM, Tris 5 mM, pH 9.9, in (A) water and (B) 20% (v/v) acetonitrile; separation voltage: 30 kV.

is in the range 1–100 μM for acetic acid, and 1–50 μM for the alkanesulfonic acids (see Fig. 7).

3.5. Indirect detection in organo-aqueous separation electrolytes

The use of organo-aqueous solutions is well known in conventional thermooptical spectroscopy and allows increasing of the detection sensitivity changing the thermooptical properties of the medium, Eq. (2), [1]. In CZE with conventional photometric UV detection organo-aqueous media have been used to improve the separation selectivity [12,26]. It should be also mentioned that the analyte and/or probe ion absorbance coefficients can be also affected by the composition of the separation electrolyte [26]. Thus, a positive impact on the detection sensitivity via a change in the thermooptical properties of the medium can be counteracted by a negative impact on separation parameters.

For further comparison, acetonitrile–water mixtures were selected as solvent mixtures because of their advantageous thermooptical properties and the low viscosity of acetonitrile. At the pH chosen (9.90) the molar absorptivity of Mordant Yellow 7 at 325 nm is the same for solutions of the dye in acetonitrile–water mixtures (10–40%) and in water. Electropherograms for a sample containing several alkanesulfonic acids employing an aqueous separation electrolyte and a separation electrolyte containing water and acetonitrile are given in Fig. 8. Under the conditions optimized for the aqueous separation electrolyte and thermooptical detection, the use of the separation electrolyte containing 20% acetonitrile (v/v) decreased the electroosmotic flow velocity by 25% and increased the baseline signal for a factor of 2.6 with an increase in the baseline noise for a factor of 1.3. The choice of the probe ion concentration was done according to the procedure described in Section 3.1 (see Fig. 9). The optimum concentration of Mordant Yellow 7 calculated from this data is in the range 35–55 μM; thus, the MY7 concentration of 50 μM was kept for further experiments. The D_r factor calculated for these conditions was about 160 (a solution of MY7, 50 μM; Tris, 5 mM; Acetonitrile, 20%; separation voltage, 30 kV; 200 data points).

In order to estimate the influence of acetonitrile added to the separation medium on the separation efficiency, UV detection under the same conditions was implemented. The comparison of LODs for 1-propanesulfonic acid obtained with TLS and UV detection in water and in water–acetonitrile is presented in Table 2.

The LODs in the case of UV–vis detection both in water and in the water–ACN mixture are very close to each other. The small difference observed can be attributed to a decrease in the electroosmotic flow velocity and to an increase in the vacuum injected sample volume [12,26]. However, in the case of the thermal lens detection the LOD for the water–acetonitrile mix-

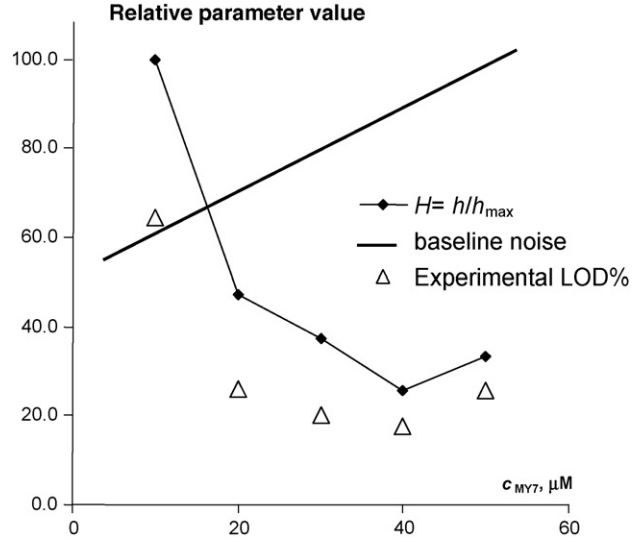

Fig. 9. Detection limit for acetate dependent on the probe ion concentration for indirect TLS detection employing a water–acetonitrile 20% mixture as separation medium. Separation electrolyte: Mordant Yellow 7, varied molar concentration; Tris 5 mM; pH 9.9; ACN 20% (v/v); separation voltage: 30 kV. All parameters are given as a relative value (normalized on the maximum value) in order to improve the readability of the graph. For further experimental parameters refer to Fig. 5.

Table 2
Limits of detection (S/N = 3) for 1-propanesulfonic acid with TLS and UV indirect detection (for experimental conditions see Fig. 8) ($n = 8$ for H_2O and $n = 6$ for ACN/H_2O, $P = 0.95$).

	Medium	LOD (μmol L^{-1})
TLS	H_2O	0.7 ± 0.1
	ACN/H_2O (20:80, v/v)	0.4 ± 0.1
UV	H_2O	6 ± 0.1
	ACN/H_2O (20:80, v/v)	7 ± 0.1

ture is two times lower than that for water. From these data, it can be concluded that the decrease in the LODs for TLS detection was achieved only because of the increase in E_0 which is increasing the dynamic range (see Eqs. (4) and (5)). However, a more detailed study of the impact of the thermooptical properties of the separation medium on the LOD in indirect thermal lens detection (e.g. with water–acetonitrile mixtures) is needed and will be studied in future work.

4. Conclusions

A procedure for the optimization of method parameters for a method employing indirect thermal lens detection combined with CZE is developed. With the use of the proposed semiempirical approach, the concentration of the probe ion corresponding to a minimum LOD for a mixture of alkanesulfonic acids was optimized. Selecting Mordant Yellow 7 in alkaline solution as a probe ion provided limits of detection for the model mixture components at the level of $n \times 10^{-7}$ M. These values are by an order of magnitude better than those obtained with UV detection at the same detection wavelength and identical composition of the separation electrolyte. It was shown that limits of detection in indirect TLS detection can be further reduced by improving the thermal lens enhancement factor E_0 via use of organic–aqueous separation electrolytes.

The data achieved show that the thermal lens detector can be used for the determination of analytes non-absorbing at the wavelength of the excitation laser. However, it should be noted that the LOD obtained in this work for the alkanesulfonic acids selected are of the same order of magnitude as those published recently for indirect photometric UV–vis detection of alkanesulfonic acids [19]. Thus, advantages of direct TLS detection over direct UV–vis detection in capillaries [3,4] cannot directly be transferred to indirect detection due to differences in the baseline noise characteristics.

References

[1] S.E. Bialkowski, Photothermal Spectroscopy Methods for Chemical Analysis, Wiley Interscience, New York, 1996.
[2] T. de Beer, N.H. Velthorst, U.A.Th. Brinkman, C. Gooijer, J. Chromatogr. A 971 (2002) 1.
[3] B.S. Seidel, E. Steinle, W. Faubel, H.J. Ache, SPIE 2836 (1996) 283.
[4] B.S. Seidel, W. Faubel, H.J. Ache, J. Biomed. Opt. 2 (1997) 326.
[5] K. Uchiyama, A. Hibara, K. Sato, H. Hisamoto, M. Tokeshi, T. Kitamori, Electrophoresis 24 (2003) 179.
[6] K. Uchiyama, M. Tokeshi, Y. Kikutani, A. Hattori, T. Kitamori, Anal. Sci. 21 (2005) 49.
[7] M. Yamauchi, M. Tokeshi, J. Yamaguchi, T. Fukuzawa, A. Hattori, A. Hibara, T. Kitamori, J. Chromatogr. A 1106 (2006) 89.
[8] T. Kitamori, M. Tokeshi, A. Hibara, K. Sato, Anal. Chem. 76 (2004) 52.
[9] E. Tamaki, A. Hibara, M. Tokeshi, T. Kitamori, Lab on a Chip 5 (2005) 129.
[10] M. Sikovec, M. Novic, M. Franko, J. Cromatogr. A 739 (1996) 111.
[11] M. Sikovec, M. Novic, Vida Hudnik, M. Franko, J. Cromatogr. A 706 (1995) 121.
[12] H. Engelhardt, W. Beck, T. Schmitt Kapillarelektrophorese, Vieweg. Braunschweig. Wiesbaden. (1994).
[13] W.G. Kuhr, E.S. Yeung, Anal. Chem. 60 (1988) 2642.
[14] Y. Xue, E.S. Yeung, Anal. Chem. 65 (1993) 2923.
[15] M.C. Breadmore, P.R. Haddad, J.S. Fritz, J. Chromatogr. A 920 (2001) 31.
[16] J.E. Melanson, C.A. Boulet, C.A. Lucy, Anal. Chem. 73 (2001) 1809.
[17] C. Johns, M. Macka, P.R. Haddad, Electrophoresis 23 (2002) 43.
[18] N. Ragozina, M. Putz, W. Faubel, U. Pyell, Electrophoresis 24 (2003) 567.
[19] C. Johns, M.J. Shaw, M. Macke, P.R. Haddad, Electrophoresis 24 (2003) 557.
[20] J. Ren, B. Li, Ya. Deng, J. Cheng, Talanta 42 (1995) 1891.
[21] Yo. Hu, J. Cheng, Ya. Deng, Analyst 122 (1997) 1089.
[22] M.A. Proskurnin, S.N. Bendrysheva, N. Ragozina, S. Heissler, W. Faubel, U. Pyell, Appl. Spectrosc. 59 (2005) 1470.
[23] M. Fischer, J. Georges, Anal. Chim. Acta 322 (1996) 117.
[24] P. Doble, M. Macka, P.R. Haddad, J. Chromatogr. A 804 (1998) 327.
[25] Y. Ma, R. Zhang, J. Chromatogr. 625 (1992) 341.
[26] C. Schwer, E. Kenndler, Anal. Chem. 63 (1991) 1801.

Available online at www.sciencedirect.com
ScienceDirect
Talanta 71 (2007) 1813–1816
Talanta
www.elsevier.com/locate/talanta

Investigation of the stability of selenoproteins during storage of human serum by size-exclusion LC–ICP-MS

Òscar Palacios *, Ryszard Lobinski

Equipe de Chimie Analytique Bio-inorganique, CNRS UMR5034, Hélioparc, 2 av. pr. Angot, F-64053 Pau, Spain

Received 9 May 2006; received in revised form 12 August 2006; accepted 21 August 2006
Available online 27 September 2006

Abstract

The stability of selenium-containing proteins in human serum was investigated by size-exclusion chromatography–ICP-MS under non-denaturating conditions. The peak characteristic to glutathione peroxidase (GSHPx) (tetramer) was the most affected; peaks of the GSHPx monomer and of selenite were found to appear with time. No trace of selenite was present in fresh samples, which suggest that the presence of this species in serum may be an artifact of storage. The mass balance of selenium species indicates that some of selenium is lost as a function of the storage time.

Keywords: Selenium; Selenoproteins; Degradation; Size-exclusion–ICP-MS; Human serum

1. Introduction

Selenium (Se) is an essential trace element, which shows putative cancer chemopreventive properties [1–4]. Most of the selenium present in humans is known to be protein-bound and to occur in the form of two amino acids [5]. One of them, selenocysteine, is genetically encoded and referred to as the 21st amino acid [6]. It is considered biologically active and normally present in serum mostly in glutathione peroxidase (GSHPx) and selenoprotein P (Sel P) [7]. The other aminoacid, selenomethionine, occurs mostly in albumin [7,8] and is considered inactive because of being biologically indistinguishable from methionine.

The importance of selenium spurs interest in its speciation in serum and in the development of adequate analytical techniques. HPLC–ICP-MS appears as the most common approach to the determination of Se species [9–13], providing high sensitivity and selectivity. Selenium speciation was measured in a multi-elemental array by size-exclusion chromatography (SEC)–ICP high resolution MS [14]. SEC–ICP-MS of a human serum sample yielded three signals; however, none of them co-related with the glutathione peroxidase activity [15]. A combination of affinity chromatography with SEC with on-line ICP-MS detection was reported to separate the three major Se-containing proteins (albumin, glutathione peroxidase and selenoprotein P) found in human plasma [16]. Low molecular species have not been included. The results reported were often limited to a few chromatograms and were not taking into account the possible degradation of any species during storage or experimental processing. We recently reported a method based on the coupling of SEC with ICP collision cell MS, which allowed a fast screening of the Se distribution in cow blood and human serum [17,18].

Because of the difficulties with speciation analysis and the poor availability of standards, quality control procedures have been given little attention. The stability of the most common selenoproteins GSHPx and Sel P during storage and analysis is largely unknown. The selenium atom in SeCys, being more active and accessible [19], is expected to be more prone to oxidation than SeMet [20,21]. Ma et al. observed the conversion of selenocysteine to dehydroalanine [21] as a consequence of the oxidation to selenoxide and further elimination of selenenic acid. Other authors observed the depletion of plasma selenium and GSHPx activity in HIV-infected persons and the appearance of low molecular mass selenocompounds [22].

* Corresponding author. Present address: Department of Physical and Analytical Chemistry, University of Oviedo, c/Julián Clavería 8, 33006 Oviedo, Spain. Tel.: +34 985103069; fax: +34 985103125.
E-mail addresses: palaciososcar@uniovi.es, o_palacios_b@yahoo.com (Ò. Palacios).

0039-9140/$ – see front matter © 2006 Elsevier B.V. All rights reserved.
doi:10.1016/j.talanta.2006.08.018

The storage of serum and plasma in view of the subsequent analysis has been in the core of interest for many years [23]. The methods to monitor the sample stability included the measuring of the concentration or activity of certain proteins [24–26] or hormones [27] without taking into account other factors, such as, e.g. the metal speciation or the selenium status. A recent study emphasized the necessity of controlling a number of pre-analytical variables to maintain the integrity of the analytes [28].

The objective of this research was to investigate the stability of selenium speciation in human serum during sample storage. SEC–ICP-MS was chosen as an analytical tool for this purpose because of the high tolerance to the serum matrix and speed of analysis. It allows the simultaneous monitoring of the different Se-related proteins in serum as well as the identification of signals due to other selenized species as selenite, selenate and free selenomethionine.

2. Experimental

2.1. Instrumentation

The chromatographic separations were performed by a Series 1100 HPLC pump (Agilent Technologies, Tokyo, Japan) fitted with an autosampler and variable volume sample loop. The detection was carried out using an ICP-MS instrument, Agilent model 7500ce (Agilent Technologies, Tokyo, Japan) equipped with an octopole collision–reaction cell. The exit of the SEC column was directly connected to a Micromist nebulizer (Glass Expansion, Romainmotier, Switzerland) by means of PEEK tubing. The nebulizer was fitted to a double pass Scott spray chamber.

2.2. Chemicals and samples

Glutathione peroxidase, dithiotreitol (DTT), iodoacetamide, hydrogen peroxide and analytical reagent grade chemicals were purchased from Sigma–Aldrich (Saint-Quentin Fallavier, France) unless stated otherwise. Water (18.2 MΩ cm) was purified with a Milli-Q system (Millipore, Bedford, MA). A selenium standard solution (1000 mg Se L^{-1} as H_2SeO_3 in 2% HNO_3) was obtained from Merck Eurolab (Fontenay-sous-Bois, France). The hydrogen (N55 purity) collision cell gas was from Air Liquide (Paris, France). Two human serum samples used were: control serum (61 ± 4 ng g^{-1} Se) from a healthy volunteer and Se-rich (149 ± 7 ng g^{-1} Se) serum from a person on a selenium supplemented diet. Both samples were divided into a number of aliquots stored frozen in Eppendorf vials at −20 °C.

2.3. Analytical method

A number of sera aliquots were thawed at different days, in a way that on the day of the measurement a series of samples thawed for the different times were available. All the samples were stored under the same conditions (4 °C or room temperature) and analyzed the same day. A serum sample, diluted twice with the LC mobile phase, was injected on a Superdex G-75 HR 10/30 size-exclusion column (SEC) (Pharmacia Biotech, Uppsala, Sweden), using 50 mM ammonium acetate buffer (pH 7) at 0.6 mL min^{-1}. The signals for the different Se isotopes (76, 77, 78, 80 and 82) were measured. Derivatization of GSHPx with iodoacetamide was done as already described elsewhere [29].

3. Results and discussion

3.1. Degradation of selenoproteins during storage

Fig. 1 shows the evolution of the distribution of selenium among the different species during storage of a serum sample at 4 °C as a function of time. The elution volumes characteristic of the different species were obtained by injection of the different standards; selenoprotein P (prepared as described elsewhere [18]), GSHPx tetramer, albumin, GSHPx monomer, selenate,

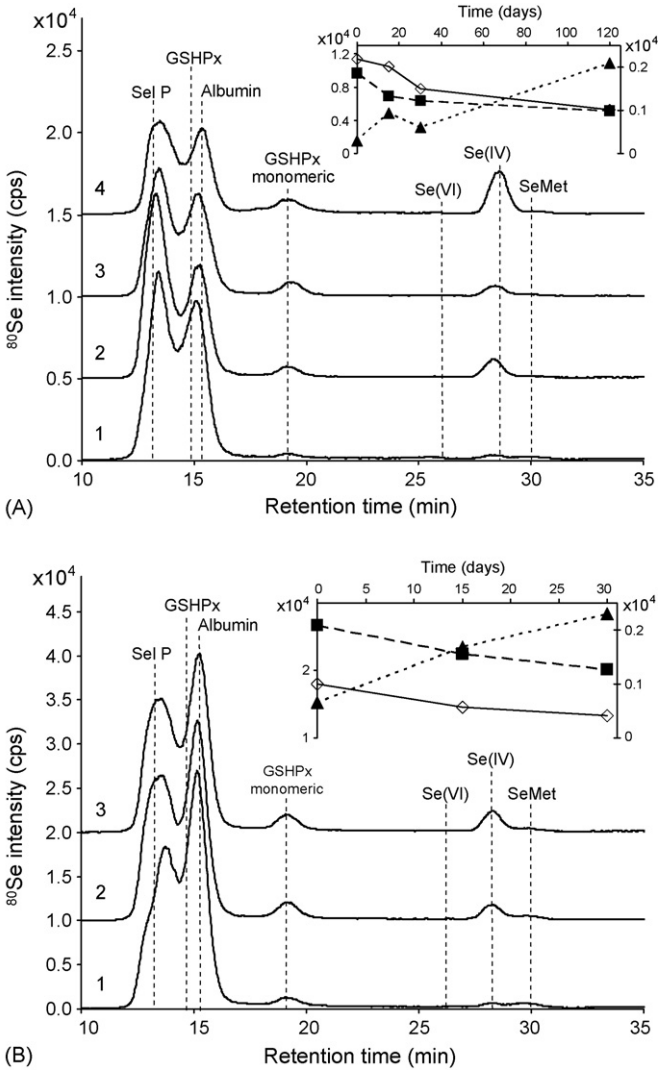

Fig. 1. Effect of storage time (at 4 °C) on the stability of selenium speciation. Size-exlcusion–ICP-MS chromatograms of: (A) control serum; (B) serum of a supplemented individual. (1) Freshly thawed; (2) after 15 days; (3) after 1 months; (4) after 4 months. For the sake of clarity the chromatograms were set off. The insets show the changes of the intensity of selenoprotein P (solid line), GSHPx (+ selenoalbumin) (dashed line) and Se(IV) (dotted line, in a different scale). Markers show the elution volumes of standard selenium species.

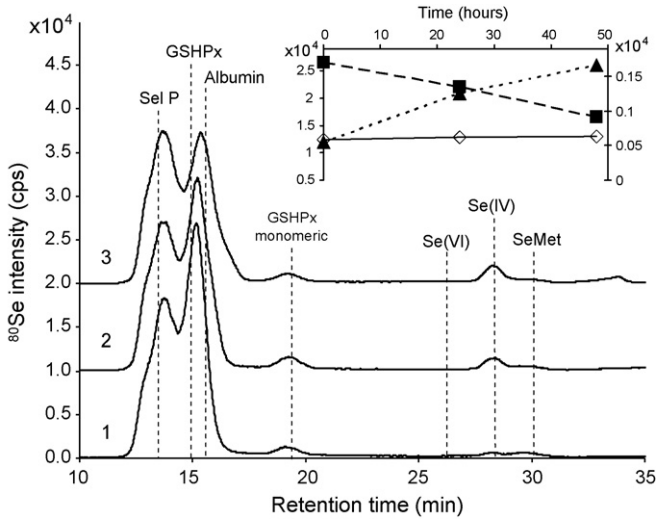

Fig. 2. Effect of storage time (at room temperature) on the stability of selenium speciation. Size-exclusion–ICP-MS chromatograms of serum from a supplemented individual. (1) Freshly thawed; (2) after 24 h; (3) after 48 h. For the sake of clarity, the chromatograms were set off by 10,000 cps from each other. The inset shows the changes of the intensity of selenoprotein P (solid line), GSHPx (+ selenoalbumin) (dashed line) and Se(IV) (dotted line, in a different scale). Markers show the elution volumes of standard selenium species.

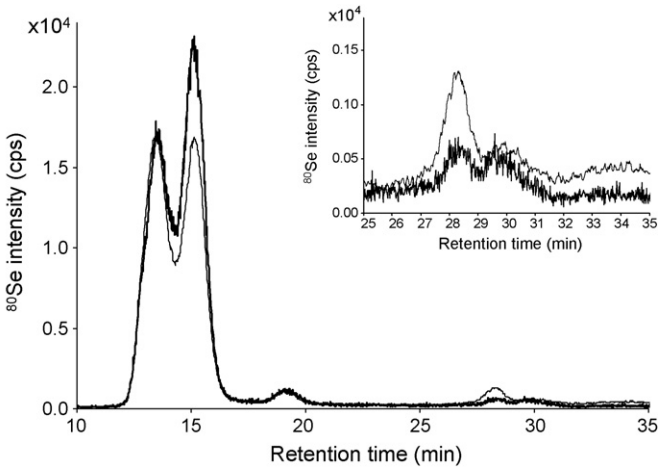

Fig. 3. Effect of addition of H_2O_2 (at room temperature) on the stability of selenium speciation. Size-exclusion–ICP-MS chromatograms of serum from a supplemented individual freshly thawed (thick line) and after 1 h incubation with 0,15% H_2O_2 (thin line). The inset shows a zoom of the signal recorded between 25 and 35 min.

selenite and selenomethionine. As it can be seen from the figure, the elution profiles for the control serum and Se-rich serum are similar except that in the latter case the contribution of Se-albumin is distinctly higher.

The analysis of the evolution of the elution profiles as a function of storage time indicates a gradual loss of selenium from the protein fraction, especially from the peak where albumin and GSHPx are coeluting. This loss is partly compensated by the appearance of the peak of selenite, which suggests the degradation of SeCys from the "true" selenoproteins, possibly according to the mechanism proposed elsewhere by Ma et al. [16]. The hypothesis that Se is lost preferentially from SeCys-containing proteins is corroborated by the observation that in the control serum where the ratio of selenoproteins/Se-albumin is three times higher, the loss of selenium is faster. All these observations point out that selenium is preferentially lost from GSHPx than from Sel P, which is also substantiated by the appearance of the peak of the monomer of GSHPx. Note that the selenium mass balance before and after storage shows the possibility of the formation and losses of volatile species that are not seen in the chromatogram.

3.2. Effect of the storage temperature of the loss of selenium

The loss of selenium from the protein fraction was found to be much faster when Se-rich serum was kept at room temperature instead of at 4 °C. Fig. 2 shows that after 48 h as much selenium was lost as after 1 month of storage at +4 °C. The loss of selenium form GSHPx is not compensated by the increase of the selenite signal, which suggests that some selenium (about 10%) is lost by volatilization. The serum profiles (not shown) recorded for different aliquots of the same sample after storage at −20 °C during more than 1 year did not show any differences. No symptoms of degradation of selenoproteins were noticed.

3.3. Effect of oxidating agents on the stability of selenoproteins in serum

The above results indicate that the protein affected the most by loss of selenium is GSHPx, which indicates oxidation as a likely mechanism. In order to corroborate this hypothesis a solution of diluted H_2O_2 was added to Se-rich serum (0.15% H_2O_2, v/v in the final solution). The peak of GSHPx/albumine was found to diminish rapidly whereas the Sel P peak remained constant (Fig. 3). An increase in the Se(IV) peak was also observed. In order to obtain a definitive proof for the oxidative degradation of GSPx as a source of selenium loss, the stability of a GSHPx standard was investigated.

3.4. Stability of GSHPx during storage

Fig. 4 (chromatograms 1–3) shows that the degradation of GSHPx at 4 °C was taking place in a similar way as observed for serum, with small increase of the signals related to monomeric GSHPx and inorganic Se(IV). About 75% of selenium was lost after 30 days of storage. The incomplete mass balance (Fig. 4B) indicates the possibility of loss of selenium via volatilization [30,31]. The degradation was much less pronounced in the presence of a reducing agent already, used as antioxidant, DTT (chromatogram 4), confirming thus that the loss is taking place by oxidation of the SeCys present in GSHPx. The derivatization of selenocysteine by reaction with iodoacetamide assured the definitive stabilization of GSHPx (chromatogram 5), mainly as the monomeric form, due to the denaturing step needed in the derivatization procedure. The acetilation of selecysteine avoids the oxidation of selenium and thus, its loss as selenite.

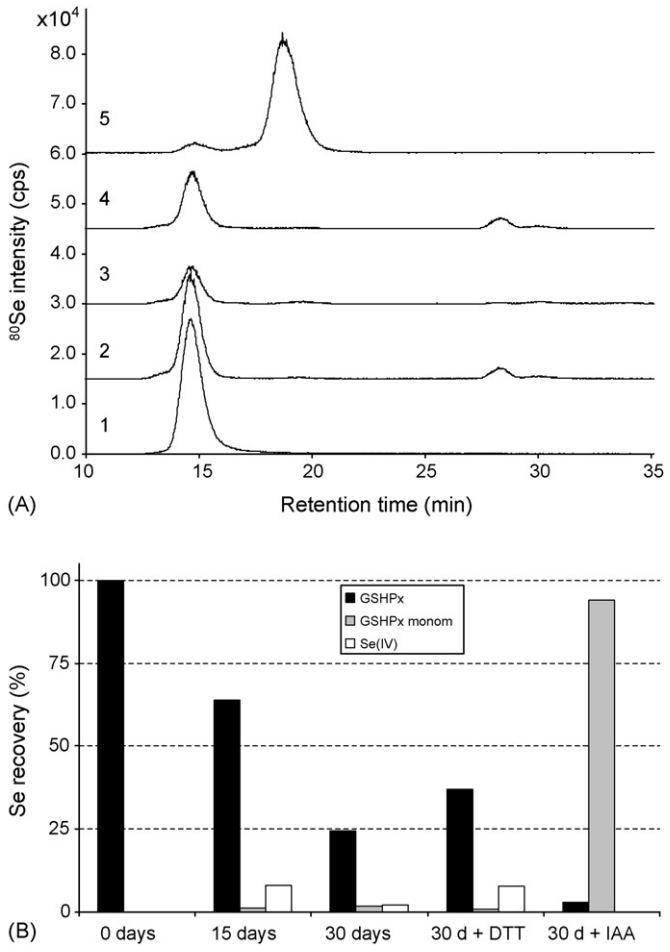

Fig. 4. Effect of storage time (at 4 °C) on the stability of glutathione peroxidase solution. (A) Size-exlusion–ICP-MS chromatogram. (1) Freshly thawed; (2) after 15 days; (3) after 30 days; (4) after 30 days in the presence of 20 mM DTT; (5) after 30 days derivatized with iodoacetamide (IAA). For the sake of clarity, the chromatograms were set off. (B) Recovery of the different selenium species from the column.

4. Conclusions

The results demonstrate the oxidative degradation of Sel P and GSHPx during storage of serum. The degradation products include selenite(IV) and unidentified volatile species. As the GSHPx measurement procedures often include an addition of an oxidizing agent, care should be taken to avoid losses of selenium and the related activity. Se(IV) reported in literature as a selenium species present in serum may be only due to inappropriate sample storage procedure.

Acknowledgements

The authors thank Dr. Sven Moesgaard (PharmaNord, Denmark) for providing the Se supplemented human serum. A CNRS postdoctoral fellowship to O. Palacios is also acknowledged.

References

[1] C. Ip, J. Nutr. 128 (1998) 1845.
[2] G.N. Schrauzer, Cell. Mol. Life Sci. 57 (2000) 1864.
[3] P.R. Rayman, Lancet 356 (2000) 233.
[4] M. Birringer, S. Pilawa, L. Flohé, Nat. Prod. Rep. 19 (2002) 693.
[5] G.F. Combs Jr., L.C. Clark, B.W. Turnbull, Biofactors 14 (2001) 153.
[6] V.N. Gladyshev, Identity, evolution and function of selenoproteins and selenoprotein genes, in: D.L. Hatfield (Ed.), Selenium, its Molecular Biology and Role in Human Health, Kluwer Academic Publishers, Boston, 2001, pp. 99–114.
[7] T. Plecko, S. Nordmann, M. Rükgauer, J.D. Kruse-Jarres Fresenius, J. Anal. Chem. 363 (1999) 517.
[8] G.N. Schrauzer, J. Nutr. 130 (2000) 1653.
[9] R. Lobinski, J.S. Edmonds, K.T. Suzuki, P.C. Uden, Pure Appl. Chem. 72 (2000) 447.
[10] P.C. Uden, Anal. Bioanal. Chem. 373 (2002) 422.
[11] J. Szpunar, Analyst 125 (2000) 963.
[12] A. Sanz-Medel, M. Montes-Bayón, M.L. Fernández Sánchez, Anal. Bioanal. Chem. 377 (2003) 236.
[13] J. Szpunar, R. Lobinski, A. Prange, Appl. Spectrosc. 57 (2003) 102A.
[14] J. Wang, R.S. Houk, D. Dreessen, D.R. Wiederin, J. Biol. Inorg. Chem. 4 (1999) 546.
[15] H. Koyama, Y. Kasanuma, C.Y. Kim, A. Ejima, C. Watanabe, H. Nakatsuka, H. Satoh, Tohoku J. Exp. Med. 178 (1996) 17.
[16] H. Koyama, K. Omura, A. Ejima, Y. Kasanuma, C. Watanabe, H. Satoh, Anal. Biochem. 267 (1999) 84.
[17] O. Palacios, J. Ruiz Encinar, G. Bertin, R. Lobinski, Anal. Bioanal. Chem. 383 (2005) 516.
[18] O. Palacios, J. Ruiz Encinar, D. Schumloffel, R. Lobinski, Anal. Bioanal. Chem. 384 (2006) 1276.
[19] C. Jacob, G.I. Giles, N.M. Giles, H. Sies (Eds.), Angew. Chem., Int. 42 (2003) 4742.
[20] J. Ruiz Encinar, D. Schaumloeffel, Y. Ogra, R. Lobinski, Anal. Chem. 76 (2004) 6635.
[21] S. Ma, R.M. Caprioli, K.E. Hill, R.F. Burk, J. Am. Soc. Mass Spectrom. 14 (2003) 593.
[22] V.N. Gladyshev, C.T. Stadtman, D.L. Hatfield, K. Jeang, Proc. Natl. Acad. Sci. U.S.A. 96 (1999) 835.
[23] (a) L.G. Menendez, A.L. Fernandez, A. Enguix, C. Ciriza, J. Amador, Ann. Clin. Biochem. 38 (2001) 252;
(b) B.Y. Chan, K.A. Buckley, B.H. Durham, J.A. Gallagher, W.D. Fraser, Clin. Chem. 49 (2003) 2083;
(c) M. Jung, S. Klotzek, M. Lewandowski, M. Fleischhacker, K. Jung, Clin. Chem. 49 (2003) 1028;
(d) J. Perman, C. Fagerlund, J. Hulthe, Scand. J. Clin. Lab. Invest. 64 (2004) 753;
(e) D. Ulmert, C. Becker, J.A. Nilsson, T. Piironen, T. Bjoerk, J. Hugosson, G. Berglund, H. Lilja, Clin. Chem. 52 (2006) 235.
[24] F.C. Ballantyne, B. Morrison, D. Ballantyne, Clin. Chim. Acta 87 (1978) 455.
[25] A. Raabe, O. Kopetsch, U. Gross, M. Zimmermann, P. Gebhart, Clin. Chem. Lab. Med. 41 (2003) 700.
[26] K.D. Huinink, K. Venema, H. Roelofsen, J. Korf, Analyst 130 (2005) 1168.
[27] M.J. Evans, J.H. Livesey, M.J. Ellis, T.G. Yandle, Clin. Biochem. 34 (2001) 107.
[28] R.E. Banks, A.J. Stanley, D.A. Cairns, J.H. Barrett, P. Clarke, D. Thompson, P.J. Selby, Clin. Chem. 51 (2005) 1637.
[29] J. Ruiz-Encinar, D. Schaumloffel, Y. Ogra, R. Lobinski, Anal. Chem. 76 (2004) 6635.
[30] S.C. Apte, A.G. Howard, J. Anal. At. Spectrom. 1 (1986) 379.
[31] K. Johansson, A. Olin, J. Chromatogr. 598 (1992) 105.

Available online at www.sciencedirect.com
ScienceDirect
Talanta 71 (2007) 1616–1623
Talanta
www.elsevier.com/locate/talanta

Fractionation analysis of manganese and zinc in beers by means of two sorbent column system and flame atomic absorption spectrometry

Pawel Pohl *, Bartlomiej Prusisz

Analytical Chemistry Division, Faculty of Chemistry, Wroclaw University of Technology, Wybrzeze Stanislawa Wyspianskiego 27, 50-370 Wroclaw, Poland

Received 10 May 2006; received in revised form 21 July 2006; accepted 24 July 2006
Available online 30 August 2006

Abstract

In the present article, a method of operational fractionation of Mn and Zn in beer using flame atomic absorption spectrometry was developed. The proposed fractionation scheme was based on use of a hydrophobic adsorbing resin Amberlite XAD7 (first column, 2 g resin bed) connected in a series with a strong cation exchanger Dowex 50Wx4 (second column, 1 g resin bed). After passing the samples of beers through the columns, distinct groupings of Mn and Zn species retained on the sorbents, i.e., hydrophobic fraction of polyphenols bound metal species and cationic metal species fraction, respectively, were determined in respective eluates obtained after complete recovery of Mn and Zn species with 10 ml of 2.0 mol l^{-1} HNO_3 (first column) and 10 ml of 4.0 mol l^{-1} HCl (second column). In addition, the effluents collected were analyzed prior to the evaluation of the third, residual fraction, presumably attributed to any hydrophilic anionic and inert metal species. The established fractionation patterns for Mn and Zn were discussed in reference to likely associations of metals with endogenous food bioligands and possible availability of the distinguished metal species classes. The quality of the results was proved by the recovery experiments.

Keywords: Beer; Operational fractionation; Amberlite XAD7; Dowex 50Wx4; Flame atomic absorption spectrometry

1. Introduction

Assessment of mineral composition of beer, including determination of major and trace metals, is of special importance and notice regarding evident influence of metals on beer quality, nutritional value and brewing process control [1–7]. For example, some metals may be harmful above certain concentration (Cd, Hg, Pb), some of them are regarded to affect quality of foam and flavor (Cu, Mn), other are essential and have advantageous effect on human health (Fe, Zn). In regard to health and/or disease implications, the nutritional content claims of trace metals are strictly regulated [3].

Information of total content of trace metals, typically originated from natural raw by-products and water used for manufacturing, brew processing and containers, is documented to be a valuable parameter applied to differentiation and classification of beer brands [6,7]. In reference to the determination of the total metal quantities, methods of beer analysis usually require degassing and further destruction of the organic matter before instrumental measurements by means of different atomic spectrometry techniques. Normally, it implies a wet digestion procedure in concentrated H_2SO_4 [5] or HNO_3 [1,2,6–8] with admixture of H_2O_2, performed in an open vessel system or using a temperature programmable microwave oven. Much rarely, a direct injection of samples to different atomizers or plasma emission sources is chosen [2–4,7]. In this case, a reasonably high dilution of beer aliquots is necessary due to serious physical and chemical matrix interferences. However, it has been established that, regardless of the execution of the mineralization procedure in a pressurized microwave oven, there is still some remaining organic matter in the samples that can have an effect on the analyte responses [5]. As a consequence, a standard addition technique is recommended as a reliable method of determination of metals in beer samples.

Although the studies devoted to the multivariate characterization and prediction of nutritional worth of beers in relation to their total mineral composition are obviously valuable, it should be emphasized that the effect of metals present in beers does not depend on their concentrations but foremost on the type of different metal species resulted from complexing of metals by

* Corresponding author. Tel.: +48 71 320 3445; fax: +48 71 328 4330.
E-mail address: pawel.pohl@pwr.wroc.pl (P. Pohl).

0039-9140/$ – see front matter © 2006 Elsevier B.V. All rights reserved.
doi:10.1016/j.talanta.2006.07.039

endogenous bioligands existing in beverages and food products of natural origin [9–14].

Beer contains various classes of natural compounds, including polydentate polyphenolics, proteins, amino acids or other organic species, that have a capacity of binding the metals through donor nitrogen, oxygen and sulfur atoms. Hence, metals can be present as non-complexed cations as well as complexed forms of different stability and, in a consequence, of different bioavailability and toxicity to human organisms [15–19]. Accordingly, for better understanding of health implications and nutritional value of widely consumed variety of beers, it is essential to develop simple and versatile methods enabling speciation or fractionation of metals in that kind of beverages.

To the best of our knowledge, very few research works have been dedicated to partitioning of metal groupings in beer. So far, charge of Cu, Fe and Mn species in bottled beer has been established by means of a non-elution approach, applying cation and anion exchange cartridges [20]. Besides, size exclusion was subjected in the cited paper for the estimation of possible metal associations with ligands of different molecular weight. A strong cation exchanger was used as well to evaluate the amount of broadly meant cationic fraction of Cd, Co, Cu, Ni and Zn comprising free cations, stable cationic complexes as well labile metal species in canned beer [21].

In the present study, a two sorbent column protocol, based on the retention of distinct metals species on a hydrophobic Amberlite XAD7 adsorbent followed by a strong cation exchanger Dowex 50Wx4, was developed for the operational fractionation of Mn and Zn, in various canned and bottled Polish beers. Initially, sorption and desorption properties of Mn(II) and Zn(II) cations as well as metal complexes with ethylenediaminetetraacetic and tannic acids toward applied sorbents were systematically investigated. The contents of metals under discussion in respective hydrophobic and cationic metal species fractions were measured by FAAS method in the eluates obtained by subsequent solvent elution. The concentrations of studied metals in third, residual metal species fraction were determined by the assessment of metal amounts in the effluents remained after passing the samples through the columns. The total concentrations of Mn and Zn in analyzed beers were established after a wet digestion in the mixture of HNO_3 and H_2O_2. The validity of the devised procedure of metal partitioning and analysis of the classified metal fractions was verified performing the recovery test. Fractionation patterns of Mn and Zn in analyzed beer samples were discussed in terms of likely bioavailability of distinguished metal groupings.

2. Experimental

2.1. Instrumentation

A Perkin-Elmer 1100B flame atomic absorption spectrometer equipped with a deuterium lamp background corrector was applied. The instrument had a single slot 10-cm titanium burner head for air–acetylene flame and a burner assemblage including a plastic mixing chamber with a flow spoiler, a stainless steel nebulizer, and a drain safety siphon interlock. Working parameters used for measurements of Mn and Zn concentrations were consistent with the manufacturer recommendations. Air and acetylene flow rates used were 8.0 and 2.5 l min^{-1}, respectively, for both analytes. Prominent analytical line wavelengths and spectral band widths were selected for determinations, i.e., 279.5 and 0.2 nm for Mn, 213.7 and 0.7 nm for Zn. Hollow cathode lamps for Mn and Zn were operated at 20 and 15 mA, correspondingly. A "hold" mode was used for data signal processing. At each read cycle, three replicate readings were performed, integrated at 0.1 s intervals over the pre-selected integration time of 1.0 s.

For calibration, the technique of standard addition was used to determine the analytes' concentrations in sample solutions achieved after mineralization, as well as effluents and eluates collected. If necessary, the samples were diluted to match the linear range of analytical curves established for both metals.

2.2. Reagents

All solutions were prepared using analytical-reagent grade chemicals and re-distilled water. Standard stock solutions of Ca, Mg, Mn and Zn at concentrations of 1000 μg ml^{-1} were purchased from Merck (Germany). Other reagents, namely concentrated nitric acid (HNO_3), concentrated hydrochloric acid (HCl), 30% (m/v) solution of hydrogen peroxide (H_2O_2), as well as solid sodium hydroxide (NaOH), potassium dihydrogen phosphate (KH_2PO_4), potassium hydrogen phthalate ($C_8H_5O_4K$), disodium salt of ethylenediaminetetraacetic acid ($C_{10}H_{14}N_2Na_2O_8{\cdot}2H_2O$, EDTA) and tannic acid ($C_{76}H_{52}O_{46}$, TA) were obtained from POCH (Poland). Two-component 0.10 mol l^{-1} buffering solutions giving pH values of 4.0, 4.5, 5.0, 5.5 (mixtures of NaOH and $C_8H_5O_4K$) and 6.0 (mixture of NaOH and KH_2PO_4) were prepared following the prescription given by Bower and Bates [22]. Four-element solutions (volume of 100 ml) containing 0.15 and 0.50 μg ml^{-1} of Zn(II) and Mn(II), respectively, and the admixture of main mineral matrix components, i.e., Ca(II) and Mg(II) at concentrations selected as the average values found in the literature devoted to the analysis of different beer brands, that is 70 and 150 μg ml^{-1}, correspondingly, were prepared by dilution of the respective stock solutions. To adjust the solutions to appropriate pH values, 20 ml of distinct two-component buffers were added, and finally, the flasks were completed with water to the volume. About 100-ml solutions containing complexes of Mn (0.15 μg ml^{-1}) and Zn (0.50 μg ml^{-1}) with EDTA or TA were obtained by addition of 10 ml of a 0.10 mol l^{-1} EDTA solution or 10 ml of a 1000 μg ml^{-1} TA solution, respectively, to the solutions comprising proper volumes of metal stock solutions and buffers. The resulted solutions contained Ca and Mg at concentrations corresponding to 70 and 150 μg ml^{-1} as well. Finally, the solutions were made up with water to the volume, mixed well and let to equilibrate for 24 h.

2.3. Procedures

Pyrex glassware (volumetric flasks and vessels), a Supelco filtration apparatus, consisted of a 250-ml glass reservoir, a

tapered funnel base and a 1000-ml flask, as well as Supelco liquid chromatographic columns (300 mm in length, 10 mm of internal diameter) with coarse frits and Teflon stopcocks were kept before use in a 10% (m/v) solution of HNO_3 for 24 h. After that, they were successively washed with re-distilled water and air dried.

2.3.1. Resin preparation

An adsorbing Amberlite XAD7 resin, non-ionic macroreticular acrylic ester polymer (20–60 mesh of a particle size, 450 $m^2\,g^{-1}$ of the surface area) was obtained from Sigma–Aldrich (Germany). A styrene divinylobenzene copolymer based, gel type, Dowex 50Wx4 strong cation exchanger (200–400 mesh of a particle size, the functionality maintained by sulfonic acid groups) was purchased from Supelco (USA). Both sorbents were packed into the columns as water slurries using portions of the resins as received at amounts of 2.0 and 1.0 g, respectively, for Amberlite XAD7 and Dowex 50Wx4.

Before use, the resin beds were pre-conditioned. The Amberlite XAD7 was initially washed with 25 ml of a methanol–water solution (1 + 1). Then, the adsorbent beds were flushed with 10 ml of a 1.0 mol l^{-1} NaOH solution, followed by rinsing with 50 ml of water. After that, 10 ml of a 2.0 mol l^{-1} HCl solution were passed and to finish, 50 ml portions of water were used for washing the resin beds until the effluents reached neutrality.

The treatment subjected to Dowex 50Wx4 resulted at first in washing the cation exchanger beds with water (25 ml), then in rinsing with 10 ml of 2.0 mol l^{-1} solution of HCl. Next, washing with another 25-ml portions of water was proceeded, and 10 ml of 1.0 mol l^{-1} solution of NaOH were passed through the resin beds. Finally, the excess of NaOH was removed by flushing the resin beds with 25 ml of water. The flow rate of water and solutions used for conditioning treatment was maintained at 1.0 ml min^{-1} by means of a two-channel programmable peristaltic pump, type 306 (UniPan, Poland).

2.3.2. Optimization study

At the outset, some factors related to sorption and desorption properties of Mn(II) and Zn(II) cations and their complexes with EDTA and TA toward the adsorbent and the strong cation exchanger used were examined.

In case of Amberlite XAD7, sorption of free metal cations of Mn and Zn and their anionic complexes with EDTA or TA were studied at different solution pHs (from 4.0 to 6.5). Hence, 100-ml solutions of Mn (0.15 μg ml^{-1}) and Zn (0.50 μg ml^{-1}), containing matrix elements (Ca and Mg, respectively, at 70 and 150 μg ml^{-1}), added EDTA or TA to final concentration of 0.010 mol l^{-1} or 100 μg ml^{-1}, respectively, and buffered to the pH ranged from 4.0 to 6.5, were loaded onto the adsorbent columns at the flow rate of 1.0 ml min^{-1}. The effect of the flow rate on the sorption efficiency of Mn and Zn complexes with TA was studied using the analytes' solutions buffered to pH of 4.5. The flow rate settings were corresponded to 0.50, 1.0 and 2.0 ml min^{-1}. Each time, the column effluents were collected (about 10 ml) and analyzed by F-AAS in order to evaluate the amounts of metals sorbed by the resin.

The influence of the concentration of HCl and HNO_3 in the solutions used for stripping of the complexes of Mn and Zn with TA from the adsorbent was examined at 0.50, 1.0 and 2.0 mol l^{-1}. For that purpose, the analytes' solutions (pH of 4.5) were driven through the columns at 1.0 ml min^{-1}, and afterward, 10 ml of tested acid solutions were used for the elution, passing them through the adsorbents at the same flow rate. The recovery efficiencies for Mn and Zn were assessed with respect to the concentrations found in the respective eluates collected (10 ml) and considering the amounts of metals retained during the loading step.

In case of Dowex 50Wx4, the recovery of both metal cations from the resin was studied using the solutions of HCl and HNO_3 at concentrations of 1.0, 2.0 and 4.0 mol l^{-1}. For that reason, four-element, 100-ml solutions of Mn(II), Zn(II), Ca(II) and Mg(II) at concentrations of 0.15, 0.50, 70 and 150 μg ml^{-1}, respectively, and adjusted to pH of 4.5 were passed through the cation exchange resin beds at the flow rate of 1.0 ml min^{-1}. The respective eluents (10 ml) were used to retrieve the analytes, then, the relevant 10-ml eluate fractions were collected and subjected to the analysis by means of F-AAS on the content of Mn and Zn. The eluting solutions were driven through the columns with the flow rate set to 1.0 ml min^{-1}. In all cases, the recoveries of both metals were calculated by comparison of the concentrations found in the eluates with their concentrations in loaded solutions. In addition, for selected 4.0 mol l^{-1} HCl solution, the influence of the flow rate at which the eluent is passed through the resin beds was investigated on the recovery efficiencies of Mn and Zn at 2.0 and 4.0 ml min^{-1}.

To examine the effect of the solution pH (at the flow rate of 1.0 ml min^{-1}) as well as the influence of the flow rate at which the analyte solutions (buffered to pH of 4.5) are loaded onto the columns on the retention efficiencies of Mn and Zn on Dowex 50Wx4 resin, four-element, 100-ml working solutions comprising Mn(II), Zn(II), Ca(II) and Mg(II) cations at concentration corresponding to 0.15, 0.50, 70 and 150 μg ml^{-1}, respectively, were passed through the columns. After that, 10 ml of 4.0 mol l^{-1} HCl solution were used for the elution at the flow rate of 1.0 ml min^{-1} and the respective 10-ml portions of eluates were collected. The concentrations of Mn and Zn in the eluates were determined using the F-AAS method and the retention efficiencies for both analytes were assessed.

During loading and elution, the flow rates of all solutions passed through the columns were controlled using the two-channel programmable peristaltic pump. The recovery and the retention efficiencies were calculated as mean values obtained for three independent replicates. Relevant column blanks were proceeded and taken into consideration in all calculations.

2.4. Samples and sample treatment

2.4.1. Total metal concentration

Six canned pasteurized and three bottled non-pasteurized Polish Pils-type beers available at the market were analyzed. The pH of beers was varied from 4.0 to 4.4. After opening, beers were degassed by filtration through 0.45 μm nylon 66 membrane filters (Supelco, USA); the filtrates were immediately subjected

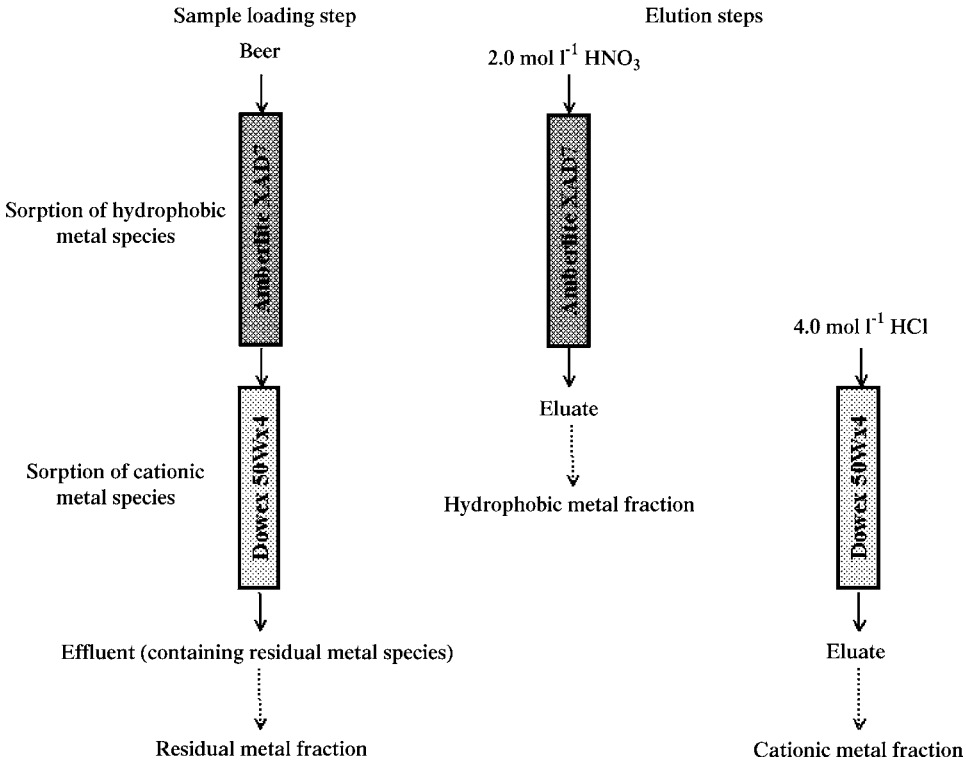

Fig. 1. Scheme of Amberlite XAD7–Dowex 50Wx4 column system used for fractionation of Mn and Zn in beer.

to further treatment. The total concentrations of Mn and Zn in resulted filtrates were determined using F-AAS method after a wet digestion in an open vessel system. For that purpose, a dependable procedure proposed earlier by Matsushige and Oliveira [8] was adopted. In this case, 25-ml sample portions were piped into 250-ml beakers, next 10 ml of concentrated HNO_3 were added and heated on a hot plate under covering. After about 90–120 min of heating, when the samples' volume was reduced to approximately 1 ml, the beakers were let to cool and 5 ml of 30% (m/v) H_2O_2 were added. Digestion was continued for further 30 min to evaporate the solutions again. Finally, the resulted aliquots were transferred quantitatively to 25-ml volumetric flasks and topped with water to the volume. For each beer analyzed, three separate samples along with adequate blind sample were prepared.

2.4.2. Operational fractionation

For the operational fractionation of Mn and Zn species, degassed beer samples (100 ml) were driven at the flow rate of 1.0 ml min^{-1} through the two sorbent column system consisted of the adsorbent Amberlite XAD7 (first column) connected with the strong cation exchanger Dowex 50Wx4 (second column). After passing the analyzed samples through the columns, they were split up and the elution was carried on using 10 ml of 2.0 mol l^{-1} HNO_3 (first column) and 10 ml of 4.0 mol l^{-1} HCl (second column), passed through the resin beds at the flow rate of 1.0 ml min^{-1}. The respective eluates (volume of 10 ml) achieved for both columns, along with the effluents originated from loading the samples through the system (approximately 10 ml) were analyzed by the F-AAS method to ascertain the concentrations of metals of interest in the metal species fractions distinguished through the proposed fractionation protocol, i.e., the fraction of hydrophobic metal species mostly attributed to complexes of Mn and Zn with polyphenolic compounds, the cationic metal species fraction comprising free ions, stable cationic complexes of metals with organic acids and the residual metal species fraction probably ascribed to inert or negatively charged stable complexes of metals with low molecular mass ligands (see Fig. 1).

3. Results and discussion

Studying sorption and desorption behavior of Dowex 50Wx4 and Amberlite XAD7 toward different species of manganese and zinc (free cations, simple anionic complexes and metals bound to polyphenols), the concentrations of the analytes in question as well as the addition of two main macrocomponents (Ca, Mg) were selected considering the average concentrations of Mn, Zn, Ca and Mg found in the literate devoted to the characterization of mineral content of different beer brands [6,7]. Tannic acid was chosen as a model compound representing the polyphenolic substances capable of complexing Mn and Zn in natural alcoholic products [23].

3.1. Sorption and desorption properties of Amberlite XAD7

The Amberlite XAD7, macroreticular, non-ionic, acrylic ester polymer resin of the moderate adsorption area, was chosen for sorption of the hydrophobic complexes of Mn and Zn with polyphenolic compounds. Contrary to formerly published paper [10], in which Amberlite XAD7 was used for the frac-

tionation of Al in tea infusions and was reported to sorb Al^{3+} ions, in the present work, the resin applied was not observed to retain simple cations of Mn^{2+} and Zn^{2+} in the studied pH range (from 4.0 to 6.5). It was expected that such discrepancy could be explained only by the difference in the type of the resin matrix polymers [24]. In contrast to the acrylic ester polymer resin applied herein, the resin used in the paper cited above was based on a styrene divinylobenzene copolymer. As it was reported previously [23–25], such SDB frameworks contain different polar impurities having a cation exchange capacity. Therefore, a special treatment with In(III) or Bi(III) salts is typically required for initial conditioning of that kind of resins in order to block the active sites of ion exchange.

It was also found that stable anionic complexes of Mn(II) and Zn(II) with low molecular weight ligand, that is EDTA, were not sorbed by the resin at studied pH (range from 4.0 to 6.5).

Later, it was established that Mn and Zn were retained from the solutions in the form of hydrophobic complexes with TA with the average efficiency of $53 \pm 3\%$ and $38 \pm 2\%$, respectively, and it was assumed that the complexation efficiency of metal cations in question by tannic acid was of that magnitude. Unfortunately, available in the literature data, adequate for comparison of this experimental evidence of complexation of Mn and Zn by TA, is unique. Very recent results devoted to the recovery of different metal cations, including Mn^{2+} and Zn^{2+}, by TA immobilized on an activated carbon [26], have indicated rather relatively low affinity of this polyphenolic acid toward divalent cations of Mn and Zn, and poor binding property of metals under discussion; under optimal conditions, only 45% of Mn and 49% of Zn were bound by TA on the activated carbon. Other works [27,28] tended to the conclusions that interactions of TA are not so strong as those of humic acids and that the complexing of metals by TA at pH lower than its pK_a value (8.68) may be possibly attributed to physical and/or chemical absorption of metal ions to tannic acid keeping them as bound ions.

The sorption efficiencies of Mn and Zn complexes with TA evaluated by passing the solutions through the adsorbents at the flow rates of 0.50 or 1.0 ml min^{-1}, respectively, were of the same magnitude, i.e., 53% for Mn and 38% for Zn. At higher flow rate setting (2.0 ml min^{-1}), the retention of metal-tannic acid complexes decreased about 3% on average. Due to the mesh size of the resin, for the sample loading and the elution, the flow rate of 1.0 ml min^{-1} was chosen for further investigations.

Taking into account the complexation efficiency of Mn and Zn by TA, it was found that the quantitative release of metal-tannin complexes from the resin was achieved using 10 ml of 2.0 mol l^{-1} HNO_3 solution ($100 \pm 1\%$ for Mn and $101 \pm 2\%$ for Zn). Other HNO_3 solutions (0.50 and 1.0 mol l^{-1}) as well as the solutions of HCl at concentrations corresponded to 0.50, 1.0 and 2.0 mol l^{-1} resulted in retrievals of Mn and Zn lower than 85%.

3.2. Sorption and desorption properties of Dowex 50Wx4

The Dowex strong cation exchangers, possessing a reasonably high exchange capacity, have been recognized so far as very useful in partitioning of metals and distinguishing of broadly meant fraction of the cationic species of determined metals [9,10,21,23]. Typically, moderately concentrated solutions of HCl or HNO_3 were used in these studies for retrieval of the metals retained by that kind of resins.

In the present study, researching the effect of the concentration of HCl and HNO_3 solutions at 1.0, 2.0 and 4.0 mol l^{-1}, respectively, on the recoveries of Mn and Zn, it was established that 4.0 mol l^{-1} solution of HCl was adequate for the exhaustive desorption of both metals with the efficiency of $99 \pm 3\%$ for Mn and $99 \pm 2\%$ for Zn. In case of zinc, very corresponding results ($99 \pm 5\%$) were obtained using the solution of HCl at concentration of 2.0 mol l^{-1}. Unfortunately, under these conditions, the recovery efficiency obtained for Mn was slightly lower, i.e., $94 \pm 4\%$. Use of 1.0 mol l^{-1} HCl solution was ineffective, the recoveries achieved for both metals were not quantitative ($82 \pm 2\%$ and $86 \pm 2\%$, respectively, for Mn and Zn). Appling HNO_3 solutions as the eluents, the recoveries established for Mn varied from $59 \pm 6\%$ (for the concentration of 1.0 mol l^{-1}) to $84 \pm 1\%$ (4.0 mol l^{-1}). For Zn, the corresponded recoveries were from $64 \pm 4\%$ to $87 \pm 3\%$. The application of much concentrated solutions of HNO_3 was neglected due to a possible corrosion of the integrated burner-chamber system of the spectrometer and the nebulizer.

Considering the height of the resin beds used for Dowex 50Wx4, the influence of the flow rate with which the selected eluent (4.0 mol l^{-1} HCl solution) is percolated through the column was also studied and observed to have a significant impact on the recoveries of Mn and Zn. For higher flow rates settings, i.e., 2.0 and 4.0 ml min^{-1}, the recovery efficiencies determined were lower than the respective ones attained using the flow rate of 1.0 ml min^{-1}. As a result, the recoveries of Mn under these conditions diminished to $91 \pm 1\%$ and $84 \pm 1\%$, respectively. In case of Zn, it was $96 \pm 1\%$ and $90 \pm 2\%$, correspondingly.

Although the pH of beers analyzed in the present contribution was varied on average from 4.0 to 4.4, the influence of the solution pH on the sorption properties of the exchanger used was examined in the range from 4.0 up to 6.5. It was ascertained that both metals were quantitatively retained by the resin within studied pH range. The average retention efficiency, calculated as mean of the retention efficiencies assessed for the individual pH settings, were equal to 100% and 99% for Mn and Zn, respectively, with the precision of 5% (propagated standard deviation obtained for separate results).

Studding the behavior of the exchanger toward the complexes of Mn and Zn with EDTA, it was established that Dowex 50Wx4 did not retain stable anionic complexes of these metals. The recoveries of Mn and Zn found on the basis of the concentrations determined in the column effluents obtained after passing the solutions of the analytes with the admixture of EDTA and buffered to the pH changed from 4.0 to 6.5 were very close to 100%.

Unfortunately, it was also found that the cation exchanger completely retained both metals from the solutions with the addition of TA (at pH ranged from 4.0 to 6.5). Possibly, in contact with the functional groups of the cation exchanger, tannin complexes of Mn and Zn dissociated, and cations of Mn^{2+} and

Zn^{2+} were sorbed by the resin. Previously, Chelex 100 chelating resin was reported to retain partially organic complexes of Al with tannic and gallic acids (metal sorption of 76% and 68%, respectively) [10].

It should be also pointed out that despite excellent sorption and desorption properties of Dowex 50Wx4 toward Mn and Zn, due to a low selectivity of this exchanger, Ca^{2+} and Mg^{2+} present in working solutions as matrix constituents were also retained and recovered along with the analytes. However, the concentrations of both matrix elements, selected in the study at level of 70 and 150 μg ml^{-1}, respectively, for Ca and Mg, did not affect the retention and the recovery of Mn and Zn under the conditions examined, as well as measurements of the metal concentrations by FAAS.

Concluding, Dowex 50Wx4 cation exchanger was decided to follow Amberlite XAD7 adsorbent in the two-column system devised for partitioning of Mn and Zn species. For elution of the Mn and Zn species from the cation exchange resin beds, the solution of 4.0 mol l^{-1} HCl was preferred (10 ml, at 1.0 ml min^{-1}).

3.3. Fractionation of manganese and zinc in beers

So far, the experimental evidence of metal partitioning in beer has been occasionally reported in the literature [20]. An unique protocol based on the application of different resins was described formerly for the fractionation of selected metals in wine samples [23]. In the present contribution, a simple and versatile procedure utilizing two sorbent columns (Amberlite XAD7-Dowex 50Wx4) was proposed and evaluated prior to the classification of Mn and Zn groupings into hydrophobic, cationic and residual metal species fractions.

3.3.1. Fractionation pattern of Mn

As can be seen in Table 1, the concentration of Mn in Polish beers varied from 0.12 to 0.24 μg ml^{-1} and was consistent with the literature data reported for other lager beers [6,7]. The amount of the hydrophobic metal fraction, containing foremost the species of manganese complexes with polyphenolic substances, was relatively low and within the range 3–8% of the total metal concentration. The exception was low price *Piast* beer for which the contribution of the fraction of Mn bound to polyphenols was lower than 0.3%. Unfortunately, the results concerning the concentration of Mn in that fractionation could not be compared with the literature data due to lack of the appropriate contributions devoted to the subject. Nevertheless, this fraction was regarded as hardly bioavailable to humans [18].

The quantity of Mn in the cationic metal species fraction was differentiated as it varied from less than 60% to over 100% in relation to the total concentration. In low grade beers such as *Piast*, *Karpackie* and *Perla*, this fraction was predominant as accounted for over 90%. On the other hand, in two well recognized and awarded in Europe Polish beer brands that is *Zywiec* and *Tyskie Gronie*, the donation of the cationic metal fraction was the lowest and equal to 58% on average. Low contribution of the cationic manganese fraction was also characteristic for non-pasteurized bottled brands *Mocne dobre* and *Ksiazece* being produced by local brewery and popular in the region.

Former study [20], attempted to differentiate Mn species according to molecular size by means of a size exclusion column and charge using a cation exchange cartridge, concluded that Mn was present in beer principally in non-complexed forms, most likely as free Mn^{2+} cations; one separate signal was observed on a size exclusion chromatogram at the volume very close to the retention volume of the column. In the present study, except for mentioned low price brands *Piast*, *Karpackie* and *Perla*, there was a considerable amount of Mn found in the residual metal fraction, i.e., from 22% for *Ksiaz* to 42% for *Tyskie* compared with the total metal content, indicating that Mn was present in beers not only as simple cations and polyphenolic complexes but also probably in the form of low molecular mass, hydrophilic, neutral or negatively charged metal species. Bearing in mind the natural organic substances present in beers, it can be expected that this residual metal species fraction obtained after passing the samples through the Amberlite XAD7 adsorbent linked with Dowex 50Wx4 strong cation exchanger might be attributed to

Table 1
Results (in μg ml^{-1}, mean value ± 1 S.D., $n = 3$) of total Mn concentration (*A*), contents of hydrophobic fraction (*B*), cationic fraction (*C*) and residual fraction (*D*) in different Polish beer brands

Beer brand	Brewing company	*A*	*B*	*C*	*D*	$E^{\#} = B + C + D$
Canned and pasteurized						
Piast	Browary Dolnoslaskie Piast	0.118 ± 0.004	<0.0004	0.120 ± 0.020	<0.004	<0.124 ± 0.020
Tyskie	Tyskie Browary Ksiazece	0.142 ± 0.007	0.009 ± 0.001	0.081 ± 0.001	0.060 ± 0.010	0.150 ± 0.010
Ksiaz	Browary Dolnoslaskie Piast	0.158 ± 0.010	0.013 ± 0.002	0.113 ± 0.002	0.035 ± 0.005	0.161 ± 0.006
Zywiec	Grupa Zywiec	0.140 ± 0.005	0.011 ± 0.001	0.082 ± 0.002	0.044 ± 0.001	0.137 ± 0.002
Karpackie	Browar Van Pur	0.149 ± 0.003	0.005 ± 0.001	0.134 ± 0.002	0.011 ± 0.005	0.150 ± 0.005
Perla	Browary Lubelskie Perla	0.235 ± 0.010	0.018 ± 0.001	0.217 ± 0.004	0.007 ± 0.001	0.242 ± 0.004
Perla[a]	Browary Lubelskie Perla	0.484[b]	0.041 ± 0.006	0.445 ± 0.006	0.007 ± 0.001	0.493 ± 0.009
Bottled and non-pasteurized						
Mocne dobre	Browar Slaski 1209	0.188 ± 0.010	0.015 ± 0.003	0.111 ± 0.002	0.065 ± 0.005	0.191 ± 0.006
Zywe	Browar Amber	0.245 ± 0.010	0.011 ± 0.001	0.163 ± 0.004	0.070 ± 0.010	0.244 ± 0.011
Ksiazece	Browar Slaski 1209	0.127 ± 0.010	0.010 ± 0.002	0.078 ± 0.013	0.039 ± 0.002	0.127 ± 0.013

[a] Spiked sample with Mn^{2+} (0.249 μg ml^{-1}) and Zn^{2+} (0.020 μg ml^{-1}).
[b] Expected value.
[#] Propagated S.D. is given.

Table 2
Results (in μg ml^{-1}, mean value ± 1 S.D., $n = 3$) of total Zn concentration (*A*), contents of hydrophobic fraction (*B*), cationic fraction (*C*) and residual fraction (*D*) in different Polish beer brands

Beer brand	Brewing company	*A*	*B*	*C*	*D*	$E^{\#} = B + C + D$
Canned and pasteurized						
Piast	Browary Dolnoslaskie Piast	0.021 ± 0.004	<0.0004	0.018 ± 0.004	<0.004	<0.022 ± 0.004
Tyskie	Tyskie Browary Ksiazece	0.022 ± 0.003	0.003 ± 0.001	0.011 ± 0.001	0.008 ± 0.005	0.022 ± 0.005
Ksiaz	Browary Dolnoslaskie Piast	0.027 ± 0.003	0.004 ± 0.001	0.013 ± 0.002	0.010 ± 0.003	0.027 ± 0.003
Zywiec	Grupa Zywiec	0.027 ± 0.002	0.003 ± 0.001	0.016 ± 0.001	0.009 ± 0.001	0.028 ± 0.002
Karpackie	Browar Van Pur	0.025 ± 0.002	0.003 ± 0.001	0.015 ± 0.001	0.009 ± 0.001	0.027 ± 0.002
Perla	Browary Lubelskie Perla	0.021 ± 0.003	0.003 ± 0.001	0.013 ± 0.002	0.007 ± 0.001	0.0023 ± 0.002
Perla[a]	Browary Lubelskie Perla	0.041[b]	0.005 ± 0.001	0.029 ± 0.001	0.008 ± 0.002	0.042 ± 0.002
Bottled and non-pasteurized						
Mocne dobre	Browar Slaski 1209	0.037 ± 0.005	0.005 ± 0.001	0.010 ± 0.001	0.020 ± 0.001	0.035 ± 0.001
Zywe	Browar Amber	0.034 ± 0.001	0.004 ± 0.001	0.019 ± 0.001	0.010 ± 0.001	0.033 ± 0.002
Ksiazece	Browar Slaski 1209	0.019 ± 0.002	<0.0004	0.016 ± 0.001	<0.004	0.020 ± 0.001

[a] Spiked sample with Mn^{2+} (0.249 μg ml^{-1}) and Zn^{2+} (0.020 μg ml^{-1}).
[b] Expected value.
[#] Propagated S.D. is given.

neutral or anionic complexes of Mn with such polydentate ligands as amino acids [15,17], organic acids being of primary origin (citric, malic) or secondary products of alcoholic fermentation (pyruvic, lactic, ketoglutaric, succinic, citramalic, fumaric) [19]. It cannot be excluded that simple complexes of Mn^{2+} with mentioned organic acids might be cationic and contribute in this way to the cationic fraction.

Both, cationic and residual metal fractions were regarded as containing the most bioavailable forms of Mn according to the possible metal associations presumed above.

3.3.2. Fractionation pattern of Zn

The concentration of Zn in Polish beers was ranged from 0.019 to 0.037 μg ml^{-1} (see Table 2). Contrary to manganese, zinc was previously acknowledged to be more willingly complexed by the polyphenolic and flavonoid species [20,23]. Apparently, the contribution of the fraction of Zn bound to polyphenols in analyzed beers was about two times higher than the respective donation of this metal fraction established for Mn. Except for two low price beers *Piast* and *Ksiazece*, for which the concentration of the fraction of polyphenolic complexes of Zn was lower than 2% on average, the amount of this fraction changed from 11% to 15%.

The abundance of the cationic Zn species fraction, presumably ascribed to the presence of free Zn(II) cations and other stable cationic complexes with low molecular mass bioligands, including amino acids, alpha-hydroxy and non-hydroxy acids, and/or labile complexes of this metal [21,23], varied from 27% (*Mocne dobre*) to almost 62% (*Perla*) of its total amount. Only in mentioned low price brands *Piast* and *Ksiazece*, the cationic metal fraction contributed to 85% on average, while the residual metal fraction was lower than 20%. For other beers studied the contribution of the residual metal fraction was about 1.3–1.9-fold lesser than the respective donation of the cationic fraction. The exception was bottled non-pasteurized beer *Mocne dobre* for which the concentration of Zn in the residual fraction was about two times higher than that in the respective cationic fraction.

Likewise for manganese, the metal species of the cationic and residual fractions distinguished were considered as the most bioavailable to humans.

3.3.3. Recovery test

In contrast to previously published work in which relatively low sample volumes were used for the fractionation analysis of wine (from 1 to 8 ml) [23], in the present study larger sample volume was taken to concentrate the metal groupings in the analyzed samples as well as to let the samples to equilibrate with the sorbents used, *nota bene*, at the amounts corresponded to those in mentioned work.

To verify that the selected sample volume (100 ml) did not saturate the sorbents and that the fractions were not overestimated, the recovery test was performed. For that purpose, 100-ml portions of beer *Perla* were spiked simultaneously with 250 μl of 100 μg ml^{-1} solution of Mn (addition of 0.249 μg ml^{-1}) and 20 μl of 100 μg ml^{-1} solution of Zn (addition of 0.020 μg ml^{-1}) and the resulted sample solutions were left for 24 for equilibration. Then, the spiked samples were passed through the devised two sorbent column system in order to separate the metal species and determine the respective metal fraction contributions (see Tables 1 and 2 where the expected total concentrations and found contents of Mn and Zn in different metal fractions are given).

It was found that for Mn, 9.2 ± 2.4% of added Mn^{2+} was retrieved from the fraction of metal bound to polyphenols. The remainder, that is over 90% of Mn^{2+}, was determined in the cationic metal fraction, probably as Mn^{2+}. No increase in the manganese concentration was found in the last residual metal fraction. Corresponding results were reported previously in Ref. [20] where added Mn^{2+} was recovered in its cationic form.

In contrast to manganese, added Zn^{2+} was divided among all classified metal fractions, i.e., 10 ± 5% in the fraction of metal complexes with polyphenols, 80 ± 5% in the cationic matal fraction and the remainder in the residual metal fraction.

The total recoveries established were equal to 102 ± 2% for Mn and 102 ± 5% for Zn proving the reliability and the accurateness of the whole proposed fractionation procedure developed

for partitioning of Mn and Zn in beers. In addition, relative to the total metal quantities, sums of metal concentrations in the separated fractions were in the range from 98% to 105% for Mn and from 95% to 110% for Zn what also confirmed the truthfulness of the fractionation scheme applied to different beer brands.

4. Conclusions

The analytical scheme of the fractionation of Mn and Zn in beers has been proposed and evaluated. Distinct metal species were extracted to solid phase of the Amberlite XAD7 adsorbing resin (hydrophobic metal fraction), followed by the strong cation exchanger Dowex 50Wx4 (cationic metal fraction). The residual metal fraction was assessed on the basis of the metal content found in the effluents resulted from passing the samples through the columns connected in a series. The whole procedure, low-cost and easy in operation, enables the determination of the distribution of Mn and Zn among defined chemical species classes, i.e., hydrophobic, high molecular weight species of metal complexes with polyphenolic and flavonoid compounds, the sum of free metal cations and stable cationic metal complexes with low molecular weight species and finally the residual metal species, most likely being anionic and neutral metal associations either with low molecular mass ligands. In comparison to previously described in the literature one column fractionation protocols, the proposed procedure was a significant extension since it simultaneously employs two different sorption mechanisms to the metal species classification.

The metal groupings distinguished through the fractionation protocol devised are operationally defined and relate to the sorption behavior of Mn and Zn species toward the adsorbent and the cation exchanger applied. However, with respect to the total content analysis, the information retrieved on the abundance of different metal fractions in analyzed beers yields useful knowledge about metal bioavailability, beverage safety, authenticity and nutrition.

Acknowledgment

P. Pohl acknowledges receiving the fellowship of the Alexander von Humboldt Foundation in 2006.

References

[1] A. Onate-Jaen, D. Bellido-Milla, M.P. Hernandez-Artiga, Food Chem. 97 (2006) 361.
[2] M. Llobat-Estelles, A.R. Mauri-Aucejo, R. Marin-Saez, Talanta 68 (2006) 1640.
[3] A. Asfaw, G. Wibetoe, Microchim. Acta 152 (2005) 61.
[4] C.C. Nascentes, M.Y. Kamogawa, K.G. Fernandes, M.A.Z. Arruda, A.R.A. Nogueira, J.A. Nobrega, Spectrochim. Acta Part B 60 (2005) 749.
[5] D. Bellido-Milla, A. Onate-Jaen, J.M. Palacios-Santander, D. Palacios-Tejero, M.P. Hernandez-Artiga, Microchim. Acta 144 (2004) 183.
[6] A. Alcazar, F. Pablos, M.J. Martin, A.G. Gonzalez, Talanta 57 (2002) 45.
[7] D. Bellido-Milla, J.M. Moreno-Perez, M.P. Hernandez-Artiga, Spectrochim. Acta Part B 55 (2000) 855.
[8] I. Matsushige, E. de Oliveira, Food. Chem. 47 (1993) 205.
[9] A. Ruszczynska, K. Pyrzynska, E. Bulska, Chem. Anal. (Warsaw) 49 (2004) 19.
[10] S.B. Yasar, S. Gucer, Anal. Chim. Acta 505 (2004) 43.
[11] S.B. Erdemoglu, K. Pyrzynska, S. Gucer, Anal. Chim. Acta 411 (2000) 81.
[12] Y. Ozdemir, S. Gucer, Food Chem. 61 (1998) 313.
[13] K.E. Odegard, W. Lund, J. Anal. Atom. Spectrom. 12 (1997) 403.
[14] O. Abollino, M. Aceto, M.C. Bruzzoniti, E. Mentasti, C. Sarzanini, Anal. Chim. Acta 375 (1998) 299.
[15] A. Khatib, E.G. Wilson, H.K. Kim, A.W.M. Lefeber, C. Erkelens, Y.H. Choi, R. Verpoorte, Anal. Chim. Acta 559 (2006) 264.
[16] M. Nardini, A. Ghiselli, Food Chem. 84 (2004) 137.
[17] S. Cortacero-Ramirez, M. Hernainz-Bermudez de Castro, A. Segura-Carretero, C. Cruces-Blanco, A. Fernandez-Gutierrez, Trends Anal. Chem. 22 (2003) 440.
[18] S. Gorinstein, A. Caspi, M. Zemster, S. Trakhtenberg, Nutr. Res. 20 (2000) 131.
[19] L. Montanari, G. Perretti, F. Natella, A. Guidi, P. Fantozzi, Food Sci. Technol. 32 (1999) 535.
[20] R. Svendsen, W. Lund, Analyst 125 (2000) 1933.
[21] P. Pohl, B. Prusisz, Anal. Chim. Acta 502 (2004) 83.
[22] V.E. Bower, R.G. Bates, J. Res. Natl. Bur. Stand. 55 (1955) 197.
[23] I. Karadjova, B. Izgi, S. Gucer, Spectrochim. Acta Part B 57 (2002) 581.
[24] K. Terada, in: Z.B. Alfassi, C.M. Wai (Eds.), Preconcentration Techniques for Trace Elements, CRC Press, Boca Raton, 1992 (Chapter 7).
[25] P. Burba, Fresen. J. Anal. Chem. 348 (1994) 301.
[26] A. Ucer, A. Uyanik, S.F. Aygun, Sep. Purif. Technol. 47 (2006) 113.
[27] B.H. Cruz, J.M. Diaz-Cruz, C. Arino, M. Esteban, Electroanalysis 12 (2000) 1130.
[28] A.R.S. Ross, M.G. Ikonomou, K.J. Orians, Anal. Chim. Acta 411 (2000) 91.

Available online at www.sciencedirect.com
ScienceDirect
Talanta 71 (2007) 1500–1506
Talanta
www.elsevier.com/locate/talanta

Determination of ammonium using a microplate-based fluorometric technique

Patrick Poulin, Émilien Pelletier*

Institut des Sciences de la Mer de Rimouski (ISMER), Université du Québec à Rimouski, 310 allée des Ursulines, Rimouski, Que., Canada G5L 3A1

Received 8 April 2006; received in revised form 12 July 2006; accepted 12 July 2006
Available online 1 September 2006

Abstract

The determination of ammonium (NH_4^+) in concentrations ranging from nanomolar to micromolar in fresh and brackish waters often loaded in high suspended particulate matter and dissolved organic acids is presented. The newly described microplate-based fluorometric technique is allowing quick automated readings of different groups of samples with different background fluorescence and matrix effects. The lowest detectable concentration was estimated to 5 nM using the average detected blank ±3S.D. and the practical detection limit (LOD) determined with successive calibration curves was 50 nM with an excellent repeatability. High loading of suspended particular matter, coloured organic acids, and salinity changes were not interfering with the accurate determination of ammonium. To illustrate its robustness and efficiency, this technique has been applied to water samples taken from rivers, saltmarshes and estuaries, spanning a large range of ammonium levels and chemical properties. Measurements of ammonium on reddish turbid waters sampled in south shore of St. Lawrence Estuary showed ammonium concentrations between 0.05 ± 0.01 and 3.89 ± 0.03 μM, indicating a significant source of ammonium from terrestrial and saltmarsh ecosystems.

Keywords: Ammonium; Microplate technique; Spectrofluorometry; Brackish waters; Estuaries

1. Introduction

Nitrogen availability is one of the major factors regulating primary production in coastal environments [1]. The marine geochemical cycling of nitrogen and fluxes of inorganic nitrogen species (NO_3^-, NO_2^-, NH_4^+) and dissolved organic nitrogen (DON) in coastal environments are essential to biological processes and marine life in oceans [2]. Easily assimilated and preferentially used by phytoplankton species, ammonium is introduced into coastal systems by bacterial mineralization [3]. In addition, discharge of waste waters increases ammonium in rivers and saltmarshes [4] makes ammonium an efficient marker of anthropogenic pollution in coastal waters. To understand how in situ production and terrestrial supplies of ammonium affect aquatic biochemical processes and global nitrogen cycling in coastal environments, accurate determination of ammonium in micromolar or even sub-micromolar concentration is needed. However, precise and accurate determination of ammonium in fresh and brackish waters is often a difficult task because of the high variability of physical and chemical proprieties of coastal waters and related problems resulting from sample conservation and contamination.

In recent years, the use of orthophthadialdehyde (OPA) reagent which could solve various matrix effects and interference problems often encountered with other methods was developed [5–7]. Considering its excellent sensitivity, low detection limit and ubiquity of applications, the OPA-sulfite-NH_3 reaction is attractive as a reliable method for the measurement of ammonium in nearshore marine environments where salinity, suspended particulate matter and water colour change rapidly from one sample to another. Following a well established mechanism, OPA forms a complex with ammonium which exhibits an intense fluorescent signal [8]. Moreover, the specificity of the reaction has been improved by adding sulphite which contributes to eliminate possible interferences from dissolved amino acids and primary amines [9].

In this paper, we describe an application of the OPA method using a microplate florescence reader in an attempt to provide a

* Corresponding author. Fax: +1 418 723 1842.
E-mail address: Emilien_Pelletier@uqar.qc.ca (É. Pelletier).

0039-9140/$ – see front matter © 2006 Elsevier B.V. All rights reserved.
doi:10.1016/j.talanta.2006.07.024

robust method working in a large range of ammonium concentrations with unfiltered coloured samples showing variable ionic strength and pH. The method has been assessed by determining ammonium in a series of low salinity and reddish turbid samples from rivers, saltmarshes and estuaries of eastern Canada.

2. Experimental

2.1. Reagents and solutions

Working reagent (WR) consisting of a solution of OPA and sodium sulphite in a sodium borate buffer is prepared following published instructions [7]. Only freshly ultra-pure deionised water was used to prepare WR, standards and blanks. High purity of water is a determining factor in the success of this method.

The OPA solution is prepared first by dissolving 1.0 g of orthophthadialdehyde (Sigma, P-1378) into 25 mL of high-grade pure ethanol (BDH, B-90169). The solution has been protected from light and refrigerated in a brown glass bottle due to the light sensitivity of OPA. It is suggested to prepare only the required volume of OPA solution for preparation of the working solution and avoid long-term storage of OPA solution.

The sodium sulphite solution is prepared by adding 1.0 g of sodium sulphite (A.C.S. grade Na_2SO_3 from Sigma, S-4672) to 125 mL deionised water. This solution is stable for at least 1 month when stored in a dark glass bottle at ambient temperature.

The borate buffer solution is prepared by dissolving 30.0 g of sodium tetraborate hydrate (A.C.S. grade $Na_2B_4O_7{\cdot}10H_2O$ from Sigma, S-9640) into 1 L of deionised water. This solution remained stable for months when stored in a glass bottle at ambient temperature.

The working reagent solution was prepared by mixing 500 mL of sodium borate buffer solution, 2.5 mL of sodium sulphite solution and 25 mL of OPA solution in a carefully precleaned glass bottle. A rest period of at least 24 h is required to optimise the WR complexion ability and decrease the blank response [7]. WR remained stable for months when stored at 4 °C in the dark.

To ensure high sensitivity and low variability within replicates and because the reactivity of the WR changes slowly with time, a new calibration curve is performed for each new series of four samples corresponding to the preparation of one microplate as shown hereafter. Each calibration curve is calculated by using five standard solutions in a range of expected ammonium concentrations (usually between 0.25 and 2.00 μM) from successive dilutions of a 50 μM ammonium solution prepared with freshly deionised water using high purity ammonium hydroxide (Sigma, A-6899) or ammonium salts (Aldrich, 326372) [5].

2.2. Instrumentation

All measurements were performed using a microplate fluorescence reader (Spectra Max Gemini®, Molecular Devices Sunnyvale, CA) operated at ambient temperature. The reader is equipped with a dual monochromator allowing a precise selection (±1 nm) of optimum wavelengths. Ammonium readings in raw fluorescence unit (RFU) were obtained at $\lambda_{ex} = 360$ nm and $\lambda_{em} = 430$ nm. Microplate-based technique combines fast and automated multiple readings and the use of small samples. Although reacting and transferring small samples increase the analytical error, the possibility of increasing the number of replicates on the same microplate without increasing significantly the working load compensates for the loss of precision on single reading. Preliminary work using 96-well microplates and 200-μL samples showed standard errors >10% and a practical detection limit above 100 nM which were considered as unsatisfactory for the purpose of our current research on nitrogen cycle in coastal waters. Thus, disposable polystyrene 48-well microplates (Costar® type from Corning) allowing larger sample volumes were adopted for all ammonium determinations. Microplates were not reused and fluorescence must be read within 5 min after the microplate preparation.

2.3. Sample collection and preservation

Small Pyrex bottles (10 mL) with ground-glass joint and glass stopper or ODB type bottles (60–125 mL) were pre-washed with HCl 10% solution, thoroughly rinsed with deionised water, and then dried in oven. Bottles were rinsed twice with water to be sampled, fully filled and kept capped in dark on an ice bath until analysis. Such precautions made unnecessary the addition of WR to samples during the field work [7] and simplified the overall field procedure. Dosage has been performed within 2 h after sampling to minimize possible effects of bacterial and plankton metabolism. Incubation at 2, 6 and 12 °C of freshly sampled sediment cores collected in the impacted Pointe-au-Père saltmarsh showed a quantitative reduction of labelled $^{15}NO_3^-$ to $^{15}NH_4^+$ within a few hours in the overlying water column indicating a rapid change in nitrogen species in these brackish waters (unpublished results). Filtration of samples is not recommended because of inherent well-documented problems resulting from adsorption of ammonium on filters and degassing losses [10,11]. Since the fluorescence OPA method has been found almost unaffected by suspended particles [12], all samples were analysed without previous filtration.

2.4. Sample preparation and incubation with working reagent

The reaction between OPA and ammonium ions is slow at ambient temperature and an optimum incubation period of 4 h has been determined from a kinetic study detailed below (Fig. 1a). Attempts of direct incubation in polystyrene microplates indicated a slow but quantitative reaction of WR with plastic surface (Fig. 1b). Plastic microplates could contain additive products rich in terminal reduced nitrogen used as antioxidant compounds to stabilize polymer structure [13]. These products seem to remain available for a slow chemical reaction with WR solution and induce a background fluorescence signal. Thus, incubation has to be carried out in glass tubes.

Accurate determination of ammonium in natural waters has to take in account background fluorescence and matrix effect from dissolved and particulate organic matter. The matrix

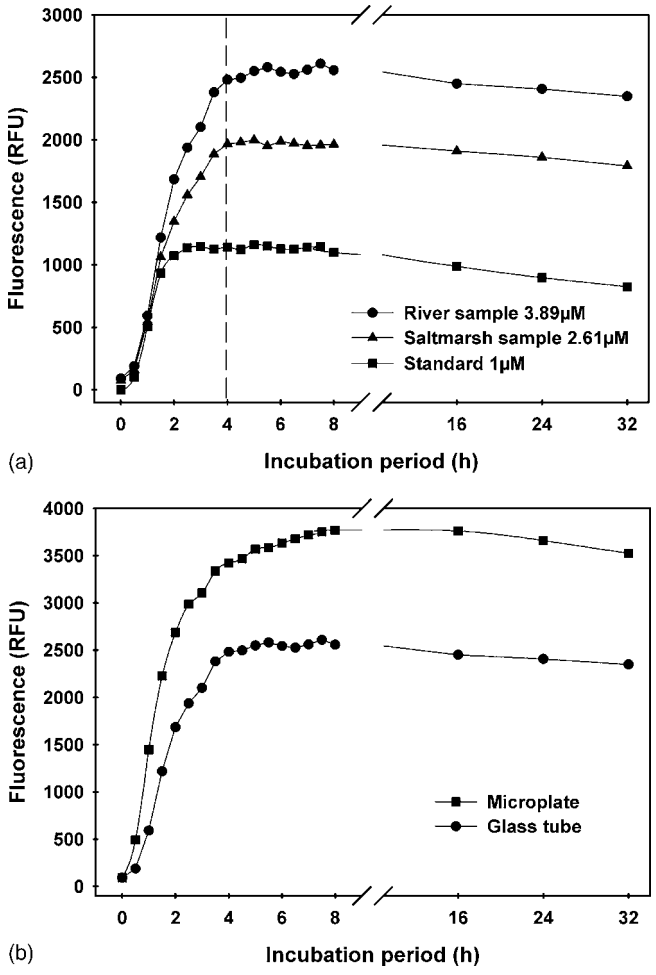

Fig. 1. (a) Time course of the reaction of OPA with ammonium at room temperature (22 °C). Field samples were collected in a small river and a saltmarsh in the provincial park of Bic close to Rimouski. Samples were incubated in 25 mL borosilicate test tubes. Aliquots were transferred into microplate following given time intervals for fluorescence reading. (b) Time course of the ammonium/OPA reaction at room temperature (22 °C). Incubation carried directly in polystyrene microplates was compared with incubation in glass tubes followed by reading in microplates. Natural freshwater samples were collected from Rimouski River.

effect (ME) is related to unidentified natural substances that may alter the intensity of the fluorescence response of ammonium reacted with OPA whereas background fluorescence is attributed to existing compounds naturally fluorescent at determined wavelengths. Sample replicates doped with known amount of ammonium were prepared to evaluate the matrix effect.

For each natural sample, duplicate 4.00 mL samples were transferred into two disposable 6-mL borosilicate test tubes. In one of the tube, ammonium standard solution (100 μL, 50 μM NH_4^+) was added as a known surrogate together with 1.00 mL of WR. In the remaining tube only 1.00 mL of WR was added. Tubes were tightly stopped to avoid evaporation and air contamination, manually shaken for a few seconds and incubated in complete darkness for 4 h at 22 °C. To evaluate possible contamination or degradation of reagents, blank determination (4.00 mL of freshly deionised water and 1.00 mL of WR solution) was conducted for each series of four samples. Exposure of standards and samples to the ambient air and light could induce a significant drift of the analytical results.

Standard 1 0.25 µM	Standard 3 0.75 µM	Standard 5 2.00 µM	BK	Sample A	Sample B	Sample C	Sample D
Standard 1 0.25 µM	Standard 3 0.75 µM	Standard 5 2.00 µM	BK	Sample A	Sample B	Sample C	Sample D
Standard 1 0.25 µM	Standard 3 0.75 µM	Standard 5 2.00 µM	Sample A BG	Sample A	Sample B	Sample C	Sample D
Standard 2 0.50 µM	Standard 4 1.00 µM	BK	Sample B BG	Sample A-add	Sample A-add	Sample A-add	Sample A-add
Standard 2 0.50 µM	Standard 4 1.00 µM	BK	Sample C BG	Sample A-add	Sample A-add	Sample A-add	Sample A-add
Standard 2 0.50 µM	Standard 4 1.00 µM	BK	Sample D BG	Sample A-add	Sample A-add	Sample A-add	Sample A-add

Fig. 2. A typical 48-well microplate scheme showing standards in triplicate on the left side, reagents background blanks (BF in five wells) and sample background blanks (BG) in the middle. Samples and samples with surrogate to determine matrix effect (ME) are located on the right side of the plate. The reading of the whole plate takes 30 s.

2.5. Microplate preparation

Following the incubation period, samples in glass tubes were transferred into wells of flat-bottomed 48-well microplate for fluorescence determination (Fig. 2). Five standard solutions and four samples (1.00 mL each) were triplicately added into microplate wells. Five wells were left for reagent blank (BK) and four wells for the determination of background fluorescence (BG). Solution used in determining BK was transferred into five consecutive microplate wells whereas BG was evaluated by mixing 200 μL of borate buffer solution with 800 μL of each sample directly in the microplate well without WR addition. Repeated BG readings for the same sample showed a very low variability and thus only one reading was preserved in routine analysis.

2.6. Calculation method (adapted from Ref. [7])

The fluorescence signal attributed to the ammonium content in samples (i.e. F_{NH_4} and F_{NH_4ADD}) can be calculated by subtracting blank and background readings (RF_{BK} and RF_{BG}) from raw fluorescence obtained for samples (Eq. (1a) and (1b)):

$$F_{NH_4} = RF_{NH_4} - RF_{BK} - RF_{BG} \quad (1a)$$

$$F_{NH_4ADD} = RF_{NH_4ADD} - RF_{BK} - RF_{BG} \quad (1b)$$

The matrix effect can be calculated for each sample with known F_{NH_4} and F_{NH_4ADD} values using Eq. (2), where F_{STD5} and F_{STD4} are fluorescence values of standards 5 and 4, respectively, after subtraction of RF_{BK}:

$$\%ME = \left\{ \frac{[(F_{STD5} - F_{STD4}) - (F_{NH4ADD} - F_{NH4})]}{[F_{STD5} - F_{STD4}]} \right\} \times 100 \quad (2)$$

Table 1
Examples of ammonium determination ($n = 3$) in field samples with various physical and chemical properties

Sample ID	Sampling temp. (°C)	Salinity	pH	SPM (mg L^{-1})	RF_{NH_4} (RFU ± S.D.)	RF_{BK} (RFU)	RF_{BG} (RFU)	F_{NH_4} (RFU ± S.D.)	ME (% ± S.D.)	COR_{NH_4} (μM ± S.D.)	Precision (%)
Rimouski River	0.7	0.1	7.64	5.64	302.1 ± 1.6	165.8 ± 3.4	50.0	86.3 ± 3.4	20.0 ± 0.5	0.05 ± 0.01	20.0
Metis River	0.7	0.0	6.66	4.87	1343.5 ± 6.7	98.1 ± 2.0	58.5	1186.9 ± 6.7	24.1 ± 0.7	1.31 ± 0.02	1.4
Bic River	0.6	0.1	7.90	3.24	2571.1 ± 5.5	98.1 ± 2.0	32.3	2113.7 ± 5.5	40.2 ± 0.6	3.89 ± 0.03	0.8
Ste. Anne River	9.8	0.3	7.61	3.78	1619.4 ± 0.8	239.0 ± 3.3	104.2	1366.2 ± 3.3	34.0 ± 0.5	2.25 ± 0.01	0.4
Bic Saltmarsh	9.4	18.0	7.74	12.66	1965.6 ± 4.4	239.0 ± 3.3.	19.9	1706.7 ± 4.4	24.9 ± 0.5	2.61 ± 0.02	0.8
Pointe-au-Père Saltmarsh	10.9	15.4	8.04	13.11	784.7 ± 5.4	239.0 ± 3.3	26.2	519.4 ± 5.4	19.6 ± 0.6	0.34 ± 0.01	2.9
St. Lawrence River	8.79	0.8	8.14	15.21	2307.9 ± 4.6	184.6 ± 8.3	9.9	2113.4 ± 8.3	26.7 ± 1.0	3.08 ± 0.04	1.3
St. Lawrence Estuary (10 m depth)	3.3	28.1	8.09	3.12	958.3 ± 1.3	213.3 ± 13.2	37.6	707.4 ± 13.2	9.9 ± 1.9	0.88 ± 0.04	4.5

As the difference in ammonium concentrations between these two standards is 1.0 μmol and the amount of ammonium added to the sample replicate is also 1.0 μmol, a lower reading of F_{NH_4ADD} will induce a positive % ME. After F_{NH_4} has been corrected for background and the ME contribution has been determined, the accurate concentration of ammonium in the sample (COR_{NH_4}) can be calculated from ammonium values (CAL_{NH_4}) obtained from the standard curve followed by the correction for ME using as shown in Eq. (3):

$$COR_{NH_4} = CAL_{NH_4} + (\%\,ME \times CAL_{NH_4}) \quad (3)$$

3. Results and discussion

3.1. Incubation period

The optimum incubation period of 4 h was determined according to the reaction kinetic of a standard solution and field samples with OPA over a 32-h period at ambient temperature (Fig. 1a). Fluorescence intensity increases abruptly at the very beginning of the reaction, and then a plateau is reached in approximate 3 h for standards and 4 h for samples. Published instructions from Ref. [7] suggested a 2 h incubation period which is considered not optimal when examining curves of Fig. 1. The reaction between OPA and ammonium is slower in field samples than standard samples. A longer incubation time provides a better reproducibility of the results. The length of the plateau depends on the maximum quantity of fluorescent product and its chemical stability, which extends to about 6 h. Incubations of tubes at 30, 40 and 50 °C in thermostatic bath have been tested and results indicate a good preservation of reproducibility of the method while reducing time to reach the plateau to less than 2 h for all temperatures tested. A warm incubation can be a viable option when reaction time has to be drastically reduced, but keeping in mind inconveniences introduced by a temperature regulated device and possible side-reactions modifying the accuracy of the method.

3.2. Background fluorescence (RF_{BG})

The RF_{BG} of natural waters results from the presence of self-fluorescent substances and can be quantitatively evaluated using an aliquot of each sample in which WR solution is replaced by free-OPA borate buffer solution that does not react with ammonium to form the fluorescent complex. The intensity of this signal may be significant and reaches >10% of the RF signal in some natural waters (Table 1). Highly productive waters containing high levels of chlorophyll and pigments might exhibit high RF_{BG} values. Variation in background fluorescence depends on the origin of the samples and RF_{BG} must be systematically determined and subtracted from measured RF for each sample.

3.3. Matrix effect

Some samples, particularly those from rivers draining peat bogs and saltmarshes, are heavily loaded with reddish humic substances exhibiting a strong ME. These substances reduce the

fluorescence intensity produced by the reaction between OPA and ammonium. Unidentified natural dissolved substances have a quenching effect on the fluorescent complex. The ME correction becomes very significant in turbid or strongly coloured water samples, reaching more than 40% of the RF signal in some extreme cases (Table 1). Even if ME cannot be eliminated by a chemical reaction, this effect can be adequately corrected by adding a known amount of ammonium to each sample and determining % ME [7].

3.4. Influence of salinity

Low salinity effect is a determining factor in the choice of a method dedicated to ammonium determination in nearshore environments. The low ion strength effect (3%) exhibited by the OPA method compared with other methods has already been discussed [6]. We reassessed this salt effect for the microplate technique by repetitively determining 1.00 μM of ammonium standards prepared with artificial seawater solution of salinity ranging from 0 to 35 over 5 successive days (Fig. 3). Deviation (%) relative to the response of freshwater reference was calculated and was found not exceeding 1.8% on average at salinity 35. The deviation is more important in low salinity from 0 to 5 than in the higher salinity range. From a mechanistic point of view, it seems that the fluorescent isoindole formed by the reaction of OPA and ammonium [14] is almost not sensitive to the ionic strength of the solution. Furthermore, the addition of a borate buffer to WR brings the pH value of the reaction medium close to 9.0 which maintains carboxylic acids in neutral forms and reduces surface adsorption on suspended particles and glass tubes. Considering the low deviation observed within the entire salinity range, the present method does not require correction for salt effect as long as the precision of ±2% is acceptable. Thus blank and STD solutions were prepared with pure deionised water and salinity effect was neglected.

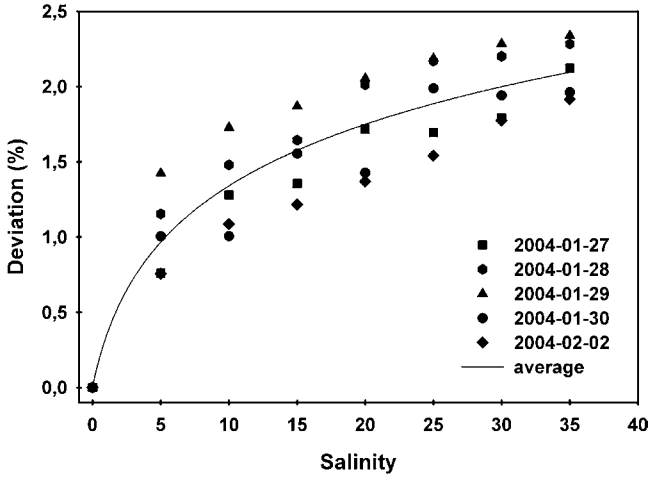

Fig. 3. Influence of salinity on the fluorescence signal obtained for ammonium (1.00 M) in five successive determinations over the entire range of salinity (0–35). Deviation is calculated against the response obtained for the same ammonium concentration in deionised freshwater used as reference.

3.5. Limit of detection and analytical reproducibility

The performance of the OPA method heavily relies on the purity of deionised water used for reagent, standard and blank preparations. Moreover, contamination sources from airborne particles and handling are critical factors to be considered in all steps of the protocol, especially in field conditions. Calibration curves calculated with standard solutions from 0 to 10.00 μM are shown in Fig. 4. In all cases, the linear regression provided $R^2 = 0.99$ or better and exhibited no significant variability

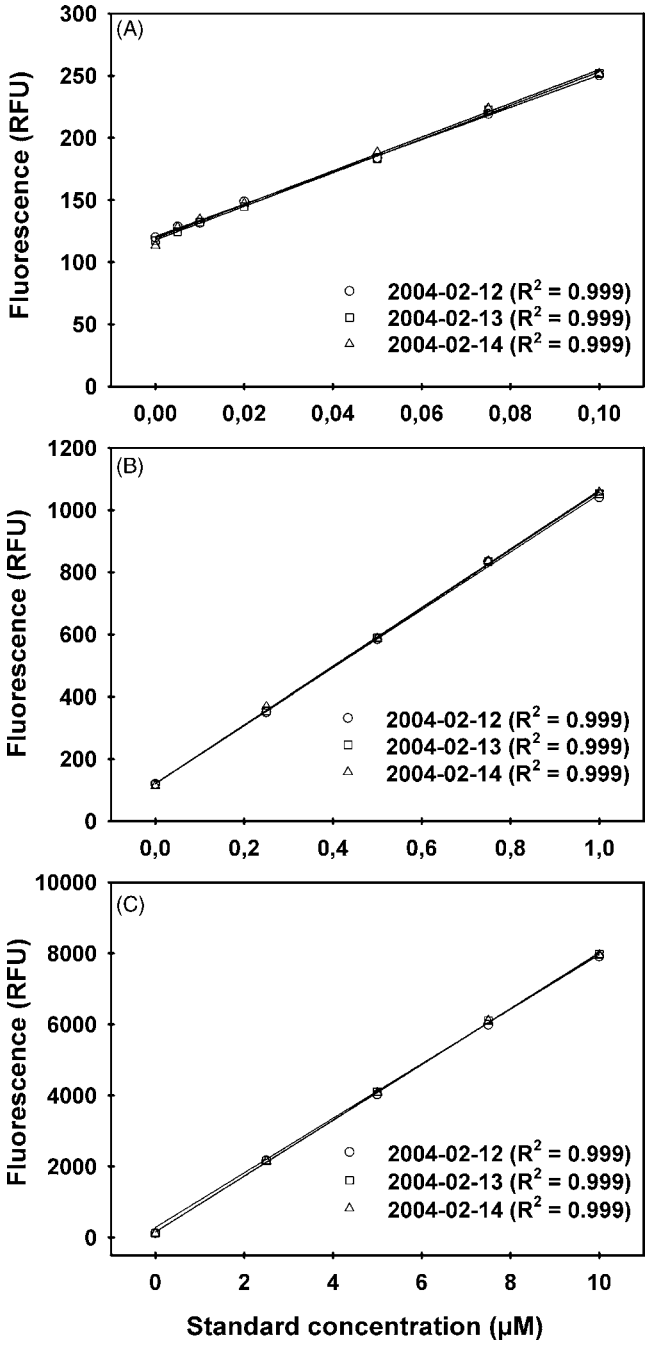

Fig. 4. Standard curves obtained following a 4 h incubation at 22 °C. (A) Low, (B) medium, (C) high ammonium concentrations. Measurements were repeated in triplicate over 3 consecutive days.

Table 2
Determination of the practical limit of detection (LOD) of the method according to Ref. [16] and using five calibration curves obtained in 5 successive days

Standard curve (0.25–2.00 μM)	Correlation coefficient (R^2)	Intercept (a) (RFU)	Slope (b) (RFU μM^{-1})	Standard deviation ($S_{y/x}$)	LOD ($y–a=3S_{y/x}$) (μM)
A	1.000	100.45	872.70	9.91	0.03
B	0.999	77.38	891.27	15.81	0.05
C	0.999	59.33	865.62	18.86	0.07
D	1.000	74.17	820.71	10.04	0.04
E	0.999	44.01	880.33	18.80	0.06

Table 3
Comparison of analytical characteristics of ammonium determination procedures

Method	LOD (μM)	Working range and linearity (μM)	Apparatus	Sample volume (mL)	Toxic reagents	References
IPB	0.007	0.007–0.7	Spectrophotometer UV–vis	5	Phenol Nitroprusside	[17]
ISE	0.2	0.25–10	Electrode	125	*n*	[18]
CSV	0.004	0.010–3	Electrodes potentiostat	6	*n*	[19]
IEC	0.125	0.5–500	Liquid chromatograph	0.1	Organic solvents	[20]
Roth's	0.001	Not reported	Fluorometer	0.1	OPA, *O*-diacetylbenzene, 2-mercaptoethanol	[8]
OPA	0.002	0.005–250	Fluorometer	~5	OPA	[6,7,12,15]
Microplate-based OPA	0.005	0.05–10	Microplate fluorescence reader	8	OPA	This paper

between successive runs over 3 days. The average analytical blank fluorescence contribution was evaluated to 117 ± 3 RFU. This residual fluorescence seems to correspond to ammonium remaining in deionised water or from handling and air contamination. The lowest detectable concentration was estimated to 5 nM using the average detected blank ±3S.D. This result can be compared to recently published results [15] where a LOD of 7 nM (blank + 3S.D.) was obtained using a flow-injection apparatus operated at 70 °C with OPA reagent. Using the slope of calibration curves instead of the average blank value and following the calculation method recommended by Miller and Miller [16], the practical limit of detection (LOD) of the OPA method using a microplate-based technique was 0.05 μM (Table 2). A well planed work schedule allows the analysis of 16 samples per hour.

Table 3 presents and compares the OPA-microplate-based technique with existing ammonium determination methods using spectrophotometry with idenophenol blue (IPB) [17], voltametry with ions selective electrodes (ISE) [18] or cathodic stripping techniques (CSV) [19], ion-exclusion chromatography (IEC) [20] and spectrofluorometry with OPA reagent [6,7,12,15]. Most methods can reach a LOD below 0.01 μM, but their common problem is either their lack of applicability to fresh, brackish and marine waters or their excessive sensitivity to coloured waters and suspended particulate matter. Using OPA-based methods, authors [6,7,12,15] developed a sensitive and robust method for ammonium in a very large range of water samples with highly variable properties. The improved OPA technique using microplate reader provides a LOD comparable to the best methods and offers the advantages of a semi-automated method (simple, fast, precise and highly reproducible with almost no interferences). The commercial availability of not expansive microplates using inert material not reacting with OPA would allow the incubation directly in microplates and reduce the work load by 50%.

3.6. Field examples

The microplate technique was tested on water samples collected from rivers, saltmarshes along the St. Lawrence Estuary over a period of 24 months providing a large spectrum of different chemical and physical properties (Table 1; Fig. 5). In all cases, samples were analysed in triplicate. Standard deviation (S.D.) with values <±0.05 μM showed the good reproducibility of this technique for determining COR_{NH_4}. The contribution of blank fluorescence under field conditions may be high (30.5% for Pointe-au-Père saltmarsh) and can reach >50% of total raw fluorescence when ammonium concentration is particularly low as shown by the Rimouski River sample (Table 1). Fluorescence generated by natural products (RF_{BG} values) cannot be neglected especially for those with sub-micromolar concentrations as illustrated by the samples of Ste Anne River reaching 104 RFU and the Rimouski River where RF_{BG} represented up to 16% of the

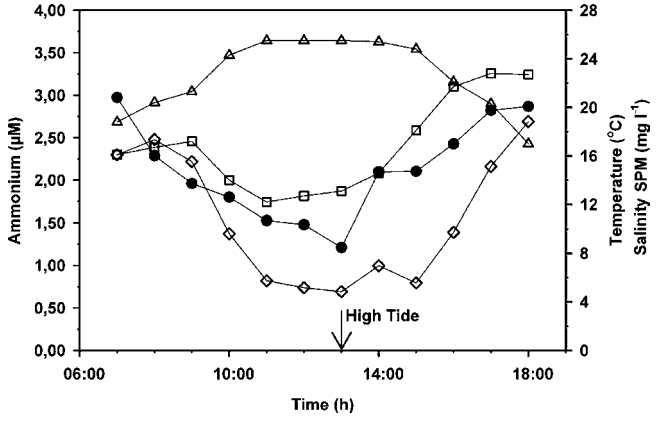

Fig. 5. Ammonium concentration determined during a complete tidal cycle in the Pointe-au-Père saltmarsh. Symbols stand for ammonium (●); temperature (□); salinity (△) and suspended particular matter (◊).

total RF value. The matrix effect remains low for seawater samples (<15%) but reaches 30–40% of the fluorescence signal in rivers with a strong background value. The precision, calculated from S.D. of each field analysis in triplicate, averaged ±2.2% for ammonium concentrations higher than 0.3 μM, but increased to ±20% with concentrations close to the practical LOD in the Rimouski River sample.

Ammonium concentrations were measured in the Pointe-au-Père saltmarsh over a complete tidal cycle (Fig. 5). This impacted littoral environment dominated by *Spartina alterniflora* is affected by municipal sewage and receives natural reddish turbid waters from surrounding peat bogs. Parameters including temperature, salinity and suspended particular matter concentration (SPM) were measured during one tidal cycle in July 2004 and compared with ammonium measurement. Results show ammonium concentrations vary from 2.97 μM at low tide to 1.21 μM at high tide (Fig. 5) with no particular interferences from salinity, temperature and SPM.

4. Conclusion

By adapting the OPA method [6] to a microplate technique, we intended to reduce the sample volume to less than 10 mL, reduce the working load for multiple replicates and increase the robustness of the method for organically loaded samples containing self-fluorescing molecules and humic substances generating a strong matrix effect. As precise and accurate measurements of the reagent blank, sample background and matrix effect are integrated to the automated microplate reading, this technique reduced the variability of the fluorescence signal by using a calibration curve for each group of four samples. Providing an excellent repeatability, low detection limit, low reagent toxicity and waste, this technique was applied with success to natural waters coastal with high contents in particulate and dissolved organic matter and variable salinity.

Acknowledgements

Authors acknowledge J. Campredon, K. Belzile, and G. Canuel for their technical support during laboratory development of the method and field work. This research was supported by the Canada Research Chairs program (E.P.) and the Natural Sciences and Engineering Research Council of Canada (NSERC Discovery grant).

References

[1] R.A. Herbert, FEMS Microbiol. Rev. 23 (1999) 563.
[2] T.H. Blackburn, J. Sorensen, Nitrogen Cycling in Coastal Marine Environment, Wiley, 1988.
[3] R.M. Maier, I.L. Pepper, C.P. Gerba, Environmental Microbiology, Academic Press, 2000.
[4] B.D. Nedwell, L.F. Dong, A. Sage, G.J.C. Underwood, Estuar. Coast. Shelf Sci. 54 (2002) 951.
[5] R. Kérouel, A. Aminot, Mar. Chem. 52 (1996) 173.
[6] R. Kérouel, A. Aminot, Mar. Chem. 57 (1997) 265.
[7] M. Holmes, A. Aminot, R. Kérouel, B.A. Hooke, B.J. Peterson, Can. J. Fish. Aquat. Sci. 56 (1999) 1801.
[8] M. Roth, Anal. Chem. 43 (1971) 880.
[9] Z. Genfa, P.K. Dasgupta, Anal. Chem. 61 (1989) 408.
[10] A.D. Eaton, V. Grant, Limnol. Oceanogr. 24 (1979) 397.
[11] H.-H. Schierup, B. Riemann, Archiv. Hydrobiol. 86 (1979) 204.
[12] A. Aminot, R. Kérouel, R.D. Birot, Water Res. 35 (2001) 1777.
[13] W.L. Hawkins, Polymer Stabilisation, Wiley-Interscience, 1972.
[14] P. de Montigny, J.F. Stobaugh, R.S. Givens, R.G. Carlson, K. Srinivasachar, L.A. Sternson, T. Higuchi, Anal. Chem. 59 (1987) 1096.
[15] R.J. Watson, E.C. Butler, L.A. Clementson, K.M. Berry, J. Environ. Monit. 1 (2005) 37.
[16] J.C. Miller, J.N. Miller, Statistics for Analytical Chemistry, second ed., Ellis Horwood, 1988.
[17] L. Solorzano, Limnol. Oceanogr. 14 (1969) 799.
[18] C. Garside, G. Hull, S. Murray, Limnol. Oceanogr. 23 (1978) 1073.
[19] A.-M. Harbin, C.M.G. van den Berg, Anal. Chem. 65 (1993) 3411.
[20] M. Mori, K. Tanaka, M.I.H. Helaleh, Q. Xu, M. Ikedo, Y. Ogura, S. Sato, W. Hu, K. Hasebe, J. Chromatogr. 977 (2003) 191.

Available online at www.sciencedirect.com
ScienceDirect
Talanta 71 (2007) 1599–1609
Talanta
www.elsevier.com/locate/talanta

Analysis of interferents by means a D-optimal screening design and calibration using partial least squares regression in the spectrophotometric determination of Cr(VI)

B.D. Real [a], M.C. Ortiz [a,*], L.A. Sarabia [b]

[a] *Department of Chemistry, University of Burgos, Pza Misael Bañuelos s/n, 09001 Burgos, Spain*
[b] *Department of Mathematics and Computation, Faculty of Sciences, University of Burgos, Pza Misael Bañuelos s/n, 09001 Burgos, Spain*

Received 25 February 2006; received in revised form 14 July 2006; accepted 24 July 2006
Available online 6 September 2006

Abstract

Using a central composite design, the signal of the process for the spectrophotometric determination of hexavalent chromium ($\lambda = 543$ nm) is maximised and its variability minimised using as complexing agent 1,5-diphenylcarbazide in sufficiently acid medium. To analyse the interference of various analytes (Mo(VI), V(V), Fe(III) and Mn(VII)) on the Cr(VI) as a function of concentration of interferent, a factorial design was prepared at three levels of each (zero, medium and high concentration), which implies performing 81 determinations. However, a D-optimal design with just nine experiments is sufficiently good to estimate the model proposed.

The interference of these metals makes it impossible to determine Cr(VI) when they are present in the sample. To avoid prior separation steps, a multivariate regression by partial least squares, PLS, is proposed to calibrate the Cr(VI) in the presence of these analytes varying the concentration of the Cr(VI) between 0.1 and 0.9 $\mu g\,ml^{-1}$ and that of the interferents between 3 and 5 $\mu g\,ml^{-1}$. The average errors obtained were 4.5% and 3.29% fitted and in prediction, respectively, with a standard error in prediction (RMSEP) of 0.016% presenting absence of both constant and proportional bias.

The detection limit with the PLS regression in the presence of interferents is 0.1 $\mu g\,ml^{-1}$ with a probability of false positive equal to 5% and less than 5% for false negative. The capability of detection is similar to that obtained with the univariate calibration (absorbance at 543 nm) in absence of interferents.

With the PLS regression it is possible to discriminate 0.085 $\mu g\,ml^{-1}$ of Cr(VI) in a sample with 0.5 $\mu g\,ml^{-1}$ of Cr(VI) with probabilities of false compliance and false non-compliance equal to 0.05. For the univariate calibration without interferents, it was established at 0.0971 $\mu g\,ml^{-1}$ of Cr(VI) for the same nominal concentration.

In relation to interference of V(V), Fe(III) and Mn(VII), the PLS calibration could be an efficient alternative to the separation step for Cr(VI) spectrophotometric determination using 1,5-diphenylcarbazide.

Keywords: Chromium(VI); 1,5-Diphenylcarbazide; Screening D-optimal design; Response surface design; Interferents; Mo(VI); V(V); Fe(III); Mn(VII); Partial least squares; Spectrophotometry; Multivariate limit of detection; Multivariate analytical sensitivity

1. Introduction

Chromium in aqueous medium is found mainly in two states of oxidation: Cr(III) and Cr(VI). The biological effects of the metal in the two oxidation states are markedly different. The trivalent form is relatively non-toxic and is regarded as an essential trace element even as character therapeutic. Its contributes to protecting the human cognitive function [1] and the combination of Cr(III) with niacin decreases total cholesterol and total lipid levels in serum significantly [2]. In contrast, Cr(VI) is of relatively high toxicity and has been shown to be carcinogenic. Public concern has been expressed in relation to possible exposure of drinking water consumers to hexavalent chromium. A reduction in the concentration is of interest and a focus on Cr(VI) generates a requirement for analytical methodology suitable for monitoring purposes.

Several techniques available for the determination of chromium speciation include electrochemical methods and

* Corresponding author. Fax: +34 947 258 831.
E-mail address: mcortiz@ubu.es (M.C. Ortiz).

0039-9140/$ – see front matter © 2006 Elsevier B.V. All rights reserved.
doi:10.1016/j.talanta.2006.07.050

methods involving separation of species and subsequent determination of the separated fractions using an analytical technique for total metal.

Spectrophotometry is widely employed for laboratory analysis because of its low cost, easy automation and is not time-consuming. The Cr(VI) does not have absorption bands in the UV–vis and so a chromogenic agent is added: leucomethylene blue [3], cyclam [4], iodide [5], variamine blue [6], *p*-amino-*N*,*N*-dimethylaniline [7] but diphenylcarbazide (DPC) in acid medium is the most commonly used. The DPC oxidises to diphenylcarbazone (DPCO) and this reduces the Cr(VI) to Cr(III) [8] forming the complex Cr(III)–DPCO which has an intense pink colour with an absorption band at 543 nm. This methodology for the determination of Cr(VI) is well established [9] and is even used as a post-column reaction in the determination of Cr(VI) by ion-chromatography [10], as solid reagent in flow injection spectrophotometric determination of Cr(VI) [11] or as portable field method for determination of insoluble or total Cr(VI) in workplace air [12]. The determination of chromium with DPC enables the speciation of chromium without a previous separation step, because this reaction is selective for Cr(VI) [13] and total chromium can be determined after the oxidation of Cr(III).

The reaction of the Cr(VI) with the DPC is selective and non-specific so in the determination other metals present in the sample may interfere, other metals which also react with the DPC in the same conditions of acidity. This problem is common to all the methods based on the use of a chromogenic reagent and in the bibliography consulted either tolerance limits are established for the interferents or the authors propose preconcentration steps of the Cr(VI) [14–16], or others [15,17] depending on the technique used later for the determination. The use of solid-phase extraction (SPE) enables the simultaneous preconcentration and removal of interferents. It is thus proposed as a step prior to the spectrophotmetric determination of the Cr(VI) with DPC, see Refs. [12,17,18] and the bibliography cited therein. However, the retention is not always complete for all the interferents. For example, in Ref. [18] it is shown that Mo(VI) and V(V) are retained but Fe(III) is not well retained by the solid phase and is eluted with the chromium.

These difficulties motivated a chemometric approach to spectrophotometric determination of Cr(VI) in acid medium with DPC in presence of the most frequent interferents according to the bibliography consulted: molybdenum as Mo(VI) [18–20], vanadium as V(V) [18–20] potentially dangerous for the health, iron as Fe(III) [18,20] and manganese as Mn(VII) [21] causing the deterioration of pipes.

After this introduction, the paper is divided into three sections—Section 2: experimental, Section 3: results and discussion and Section 4: conclusions.

Initially the analytical signal of the complex Cr(III)–DPCO is optimised. In general it is as important to determine those experimental conditions which maximise the signal as to determine those which minimise its variability. This is done in Section 3.1 through the analysis of the response surfaces obtained with a central composite design. Section 3.2 looks at the stability of diphenylcarbazide using ANOVA when the storage conditions and preparation time are varied.

The effect of the four interferents on the absorbance of the complex Cr(III)–DPCO is studied in Section 3.3. For this analysis three levels of each interferent were considered (zero concentration, average and high). Using a D-optimal screening design, the experimental effort can be markedly reduced. By using three levels it is possible to analyse in detail the interference caused by each analyte.

That it is impossible to make determinations of Cr(VI) using the maximum absorbance in the presence of interferents is shown in Section 3.4, comparing two calibrations, with and without interferents and describes the multivariate analysis of the interferent using a partial least squares regression. In order to build the calibration, a design similar to a central composite design is used such that each of the four analytes Cr(VI), Mn(VII), V(V) and Fe(III) is at five different levels. The PLS model for the calibration of the content in Cr(VI) is peculiar because only two latent variables are necessary despite there being four analytes in the calibration samples. The position of the scores on the plane of the two latent variables allows one to qualitatively analyse the effect of the interferents.

Section 3.5 evaluates some figures of merit. Of particular interest are: (i) the capability of detection evaluating the probability of false positive and false negative and (ii) the analytical sensitivity evaluating the probability of false non-compliance and false compliance. Both figures of merit allow one to compare the univariate calibration with completely specific signals (without interferents) with the PLS multivariate calibration with non-specific signals (with the three interferents). The trueness and precision are also established.

In this paper several very different chemometric techniques are used. Instead of describing them in a common theory section, each is introduced in the section in which it is used to make reading of the corresponding results easier. The technical details should be consulted in the bibliography.

This paper shows that proper use of experimental design allows one to analyse a complex problem of interferents the effect of which is not clear. Furthermore, the previous separation step of the Cr(VI) can be substituted by a multivariate calibration which also allows one to analyse the interferent of each analyte and its global effect on the analytical signal. This paper is part of a conceptual current of papers on the usefulness of chemometrics eloquently expressed by Wold and Sjöström [22].

2. Experimental

2.1. Chemicals

The reagents used were: $K_2Cr_2O_7$ (Fluka, 99.5%) to obtain Cr(VI), sym-diphenylcarbazide ($C_{13}H_{14}N_4O$) (Fluka, 97% for HPLC) and H_2SO_4 (Merck, 96% purity for quality analysis 96%).

To study the interferents: ammonium molybdato ($(NH_4)_6Mo_7O_{21}\cdot 4H_2O$) (May & Baker), ammonium metavanadato (NH_4VO_3) (Panreac, >99%), iron nitrate(III)

($(Fe(NO_3)_3)\cdot 9H_2O$) (Merck, analysis purity) and potassium permanganate ($KMnO_4$) (Panreac, >99%).

The standard solutions were prepared with deionised water through a Milli-Q system of Millipore.

2.2. Apparatus and software

The measurements were taken with a visible ultraviolet spectrophotometer, Varian Cary 50 with a xenon lamp, which enables one to cover the complete spectrum in the range of 200–800 nm.

The experimental designs and their results were analysed with the NEMRODW programme [23], while the PLS calibration models were done with Q-PARVUS 3.0 [24]. The ANOVA and the validation of the linear regressions were done with STATGRAPHICS [25]. The detection of outliers in the regressions by least squares was done with PROGRESS [26].

2.3. Standards and sample solutions

Stock standard solution (205 $\mu g\,ml^{-1}$) of Cr(VI) was prepared from $K_2Cr_2O_7$. Diphenylcarbazide stock solution (2×10^{-3} M) was prepared daily in 10% (v/v) acetonitrile solution [19] (Merck, isocratic grade for liquid phase chromatography), placing it in an opaque recipient. The H_2SO_4 (9×10^{-3} M) was prepared from H_2SO_4 concentration 96% and density 1.84 $g\,ml^{-1}$.

Stock standards solutions (1 $mg\,ml^{-1}$) of interferents were prepared from the compounds mentioned above, subjecting the solutions to ultrasound to aid the process of dissolving and placing them in amber glass bottles to avoid contact with light.

3. Results and discussion

3.1. Optimization

The first stage of the experiment was to search for the conditions for which the absorbance of the complex formed by the Cr(III) and the DPCO was maximum and its standard deviation minimum. The experimental factors considered are: (i) concentration of H_2SO_4 since the formation of the complex requires a sufficiently acid medium capable of oxidising the DPC to DPCO and (ii) concentration of DPC, since if it is insufficient it cannot reduce all the Cr(VI) to Cr(III). In Ref. [19] it has been shown that the joint reaction of the Cr(III) with the DPC and the DPCO does not take place.

A central composite design with three replicates at the centre point has been chosen in order to be able to analyse the lack of fit of the estimated surface from the experimental data. The design used allows one to fit a quadratic model:

$$y = b_0 + b_1x_1 + b_2x_2 + b_{11}x_1^2 + b_{22}x_2^2 + b_{12}x_1x_2 + \varepsilon \qquad (1)$$

where x_1 and x_2 are the concentrations of H_2SO_4 and DPC, respectively, in codified units; b_i and b_{ij} the coefficients to be determined and ε is the random error associated with the response. As is known, the central composite design has optimum properties to estimate a quadratic model such as that of Eq. (1), and these have been evaluated using NEMRODW [23]. Particularly the variance inflation factor, VIF, lies between 1.00 and 1.09. VIF is an index greater than or equal to 1 which must be less than 4 for the design to give sufficiently precise estimations of the coefficients. The variance of the response predicted by the model at a point, u, within the experimental domain depends on the so-called variance function, d(u), and should be as small as possible (never greater than 1). For the central composite design used the maximum value of this function is 0.33 for the centre point and 0.62 for the other eight design points.

To a sample of Cr(VI) with 0.5 $\mu g\,ml^{-1}$ the different quantities of H_2SO_4 and DPC were added according to the experimental design proposed, as shown in Table 1. The complete design was repeated three times.

In order for the complex with its characteristic pink colour to form, 10 min must elapse before determining the absorbance at 543 nm.

The responses to optimise were: (i) the mean absorbance (analytical signal) of the complex Cr(III)–DPCO; (ii) the variability of the replicated measurements ($n = 3$) through the standard deviation of the absorbance.

The problem with maximising the signal and minimising its variation is interesting when one is going to use an analytical signal for quantitative purposes, because many figures of merit depend on the variability of the signal. Recent applications of optimisation of various analytical responses can be seen in Refs.

Table 1
Matrix of experiments of the central composite design and experimental responses obtained for a fixed concentration of chromium of 0.5 $\mu g\,ml^{-1}$

Run	Codified values		True values		Responses ($n = 3$)	
	x_1	x_2	H_2SO_4 (mM)	DPC (mM)	Average absorbance	Standard deviation
1	−1.00	−1.00	0.54	0.48	0.2102	0.0083
2	1.00	−1.00	2.34	0.48	0.4987	0.0053
3	−1.00	1.00	0.54	0.96	0.3695	0.0067
4	1.00	1.00	2.34	0.96	0.5248	0.0014
5	−1.41	0.00	0.17	0.72	0.2555	0.0073
6	1.41	0.00	2.71	0.72	0.5101	0.0055
7	0.00	−1.41	1.44	0.38	0.3972	0.0075
8	0.00	1.41	1.44	1.06	0.5102	0.0054
9	0.00	0.00	1.44	0.72	0.5337	0.0003
10	0.00	0.00	1.44	0.72	0.5155	0.0013
11	0.00	0.00	1.44	0.72	0.5222	0.0010

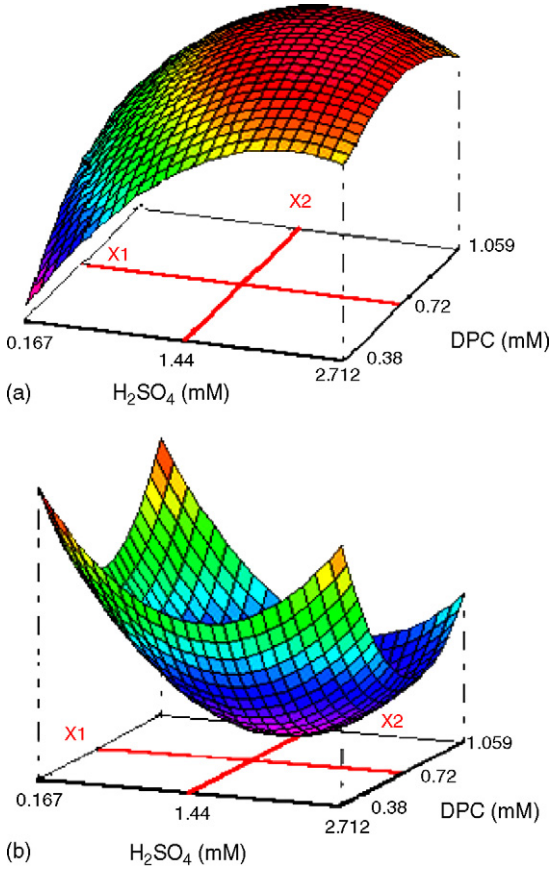

Fig. 1. Response surface fitted for the average of absorbances (a) and for the standard deviation (b). Experimental factors: concentration (mM) of DPC and of H_2SO_4.

[27–30]. Table 1 shows the experimental matrix of the design in codified variables and the real variables and in the last two columns the experimental responses.

3.1.1. Absorbance

Experimental data were fitted to the model in Eq. (1) by least squares. The absolute value of standardized residuals are lower than 2.5 and they are normally distributed. The regression explains significantly the experimental variation of the absorbance because the p-value is 0.0004 less than 0.05. As there are three replicates of the central point the lack of fit can be tested, the p-value is 0.14 so there is not lack of fit and the model is statistically valid to explain the absorbance as function of the H_2SO_4 and DPC concentrations. This is corroborated also by the coefficient of determination, R^2, that is 0.987.

The equation of the adjusted response surface is the following:

$$y = 0.524 + 0.100x_1 + 0.043x_2 - 0.075x_1^2 - 0.039x_2^2 + 0.033x_1x_2 \quad (2)$$

The optimum is reached inside the experimental domain, as can be seen in Fig. 1(a). The coordinates of the optimum are $x_1 = 0.606$ and $x_2 = 0.291$ in codified variables, that corresponding in real units to 1.98×10^{-3} and 7.9×10^{-4} M for H_2SO_4 and DPC, respectively.

3.1.2. Standard deviation

Experimental standard deviation data were fitted also to the model in Eq. (1) by least squares. The analysis of the standardized residuals shows that there is not outlier data. The regression explains significantly the experimental variation because the p-value is 0.012 less than 0.05. Also there is not lack of fit, p-value equal to 0.11, and the model is statistically valid to explain the standard deviation as function of the H_2SO_4 and DPC concentrations. Finally the coefficient of determination, R^2, is 0.914.

The equation of the fitted response surface is the following:

$$y = 0.87 \times 10^{-3} - 1.3 \times 10^{-3}x_1 - 1.05 \times 10^{-3}x_2 + 2.50 \times 10^{-3}x_1^2 + 2.53 \times 10^{-3}x_2^2 - 0.58 \times 10^{-3}x_1x_2 \quad (3)$$

In Fig. 1(b) it can be seen that the stationary point for the standard deviation model is a minimum inside the experimental domain and close to the maximum of the absorbance.

In codified values the position of the minimum is (x_1, x_2) = (0.300, 0243) that in real units is equal to 1.71×10^{-3} and 7.8×10^{-4} M for H_2SO_4 and DPC, values very similar those for the maximum absorbance.

Unless otherwise indicated, in the following section the concentrations of H_2SO_4 (1.98×10^{-3} M) and DPC (7.9×10^{-4} M) obtained for the mean of absorbance will be used. At this point in the experimental domain, the estimated value of the standard deviation, 0.0008 ± 0.0006, is significantly equal to the minimum value 0.0005 ± 0.0007.

3.2. Study of the stability of diphenylcarbazide

Several authors, by example Ref. [13], states that diphenylcarbazide is not stable in aqueous medium. With time it acquires a pale pink colour which absorbs in the visible and may interfere with the signal of the complex. In this paper, the study of its stability was carried out with the concentrations H_2SO_4 (1.98×10^{-3} M) and DPC (7.9×10^{-4} M) from the optimum in Section 3.1. Two factors were considered: (i) how the samples were stored (three levels; refrigerated (4 °C) and in darkness, at room temperature in darkness, at room temperature in sunlight). (ii) The time elapsed between its preparation and measurement (five levels). Table 2 shows the absorbance at 543 nm. Two-way

Table 2
Measurements of absorbance for the diphenylcarbazide in aqueous medium with sulphuric acid

Time (h)	Storage		
	Without light at 4 °C	Without light at room temperature (20 °C)	With light at room temperature (20 °C)
1/6	0.1216	0.1067	0.1086
5	0.1816[a]	0.1129	0.1072
24	0.1099	0.1113	0.1089
48	0.1069	0.1125	0.1079
72	0.1069	0.1119	0.1145

[a] Data considered outlier.

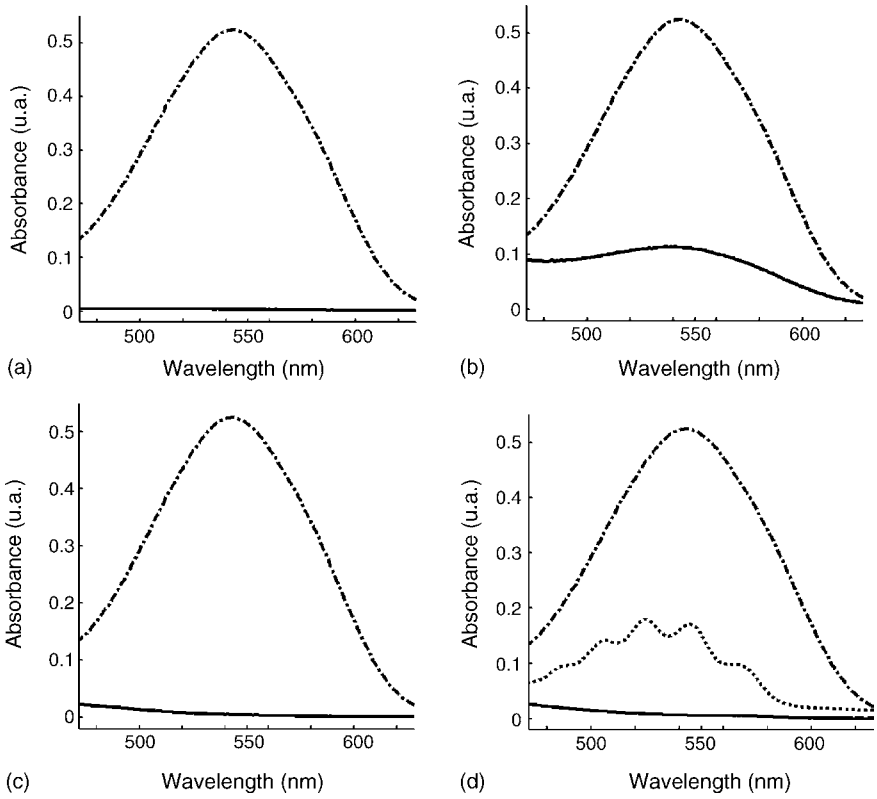

Fig. 2. Spectra of the four interferents and of the Cr(III)–DPCO recorded between 472 and 628 nm. The dotted and dashed line is the absorbance spectra of the Cr(III)–DCPO in all the cases. The continuous line shows the spectrum of the complex I-DPCO where I: Mo(V) in (a), V(V) in (b), Fe(II) in (c) and Mn(II) in (d). Graph (d) also represents the absorbance of the Mn(VII) with a dotted line. The concentrations used were: 0.5 μg ml^{-1} of Cr(VI) and 40 μg ml^{-1} of Mo(VI), V(V), Fe(III) and Mn(VII).

ANOVA was done [25] and neither of the two factor "storage" and "time" are significant (p-values 0.81 and 0.94, respectively). Based on this, the experimental procedure was continued as follows: samples protected from light, at room temperature and the colorimetric measurement taken 10 min after preparation of the samples.

3.3. Interferents

Industries such as plating, tanning, paint and pigment production and metallurgy are the principal producers of hexavalent chromium in aqueous medium and this cation can generally be found in their waste waters together with other substances from different transition elements and which may act as interferents in the reduction of the Cr(VI) to Cr(III) with the DPC. Hence the need to analyse its effect on the signal of the complex Cr(III)–DPCO. Fig. 2 shows the spectra of the complexes formed by these anions with the diphenylcarbazide.

3.3.1. Experimental methodology: D-optimal screening design at three levels

In the study of interferents using experimental design it is common to consider each of them at two levels: absent (zero concentration) and present in the sample to analyse. When the determination of an analyte is based on the formation of a complex, it is reasonable to think that the effect of an interferent depends on its concentration in the sample problem. That is why the effect over the complex Cr(III)–DPCO of the four interferents (Mo(VI), V(V), Fe(III) and Mn(VII)) will be analysed through a screening design at three concentration levels (low, 0 μg ml^{-1}; middle, 3 μg ml^{-1} and high, 5 μg ml^{-1}). The aim of the screening study [31] is not to obtain complete information about the behaviour of the colorimetric signal when the factor changes but to get an initial idea of the effects and discriminate the non-active interferents. Those factors concluded to be non-significant are omitted in the PLS-calibration step.

For this task several options are possible. We have used a D-optimal design because it is a general methodology to adapt the experimental design to each analytical problem [32,33].

Below we briefly describe the steps followed in the selection of the design to ease later interpretation of the results, but for a more thorough explanation readers should consult the monographs on this subject.

Define the factors to be analysed and their levels establishing all the possible candidate N_C experiments, in this paper, $N_C = 81$.

(i) Propose a model and in particular establish the number of its coefficients (p). The mathematical model of the response, y, as a function of one factor, x_1, at three levels (A, B and C) can be expressed as follows:

$$y = b_0 + b_{1A}x_{1A} + b_{1B}x_{1B} + b_{1C}x_{1C} \quad (4)$$

Unlike the model in Eq. (1), in which the variables are continuous, now the variables are indicators, that is x_{1A}

takes the value of 1 if the factor is in level 1 or the value of 0 if the factor is in level 2 or 3. x_{1B} is 1 if the factor is in level 2 or 0 if the factor is in level 1 or 3. The same for x_{1C}. The coefficients b_{1A}, b_{1B} and b_{1C} that estimate the effect of factor level are not independent, in fact there are only two independent coefficients and it can be proved [31] that $b_{1A} + b_{1B} + b_{1C} = 0$ and $x_{1A} + x_{1B} + x_{1C} = 1$. Taking into account the interdependence of the variables in Eq. (4), one of them can be removed so that the model will be reduced and expressed with respect to a reference state in the following way:

$$y = b_0 + b_{1A}x_{1A} + b_{1B}x_{1B} \quad (5)$$

The new coefficients, b, are now independent and can be estimated by least squares. They can be defined as the variation of the response when the factor varies from the level 3 to either the level 1 (b_{1A}) or 2 (b_{1B}). In other words the change from the average or the response value predicted at level 3 (maximum concentration of interferent). The third coefficient, b_{1C}, the effect of level 3 in Eq. (4) is estimated by $-(b_{1A} + b_{1B})$.

According to Eq. (5), the following mathematical model is proposed to explain the variation of the response due to the presence of four interferents:

$$y = b_0 + b_{1A}x_{1A} + b_{1B}x_{1B} + b_{2A}x_{2A} + b_{2B}x_{2B} + b_{3A}x_{3A} + b_{3B}x_{3B} + b_{4A}x_{4A} + b_{4B}x_{4B} \quad (6)$$

where b_0 is the intercept, and the coefficients b_{iA} and b_{iB} are defined considering level 3 as the reference [23]. The reduced model, Eq. (6), has nine independent coefficients so can be estimated with only nine experiments extracted from the complete factorial design.

(ii) Verify the coherence between the model and the information obtained in the $N_C = 81$ candidate points. In this case for all the coefficients of Eq. (8) one has VIF = 1.30 and $\max(d(u)) = 0.11$.

(iii) Construct various experimental matrices with information of sufficiently good quality for different values of the number of experiments, N. Make N vary between the minimum value possible (p) and a pre-set maximum N_m smaller or equal to N_C. That is, $p \leq N \leq N_m \leq N_C$. For each N, the election of the N experiments from the full factorial design (81 experiments) is done through an exchange algorithm because it would be tedious (practically impossible) to evaluate the determinant of all possible N-experiment combinations with the 81 experiments (this number, $C_{81,N}$, ranges between 2.16×10^{11} and 1 for $N = 9$ and 81, respectively). Let ξ_N be a matrix which contains N candidate points. Each row represents an experiment and each column a variable. The matrix of moments $M(\xi_N)$, is defined by:

$$M(\xi_N) = \frac{X^t X}{N} \quad (7)$$

The exchange algorithm method [31] based on the D-optimality criterion is an iterative procedure which progressively replaces experiments. Briefly, for a N the method consists of exchanging experiments from an initial design, ξ_{N_0}, and evaluating the determinant of the matrix of moments of the new candidate design, ξ_{N_1}. If $|M(\xi_{N_1})| > |M(\xi_{N_0})|$ the replacement of the experiment is accepted and the algorithm continues until the determinant of the matrix of moments stops increasing. This final matrix, ξ_N^*, is the D-optimal design with N experiments. As N is fixed, ξ_N^* is the best information matrix X^tX. Theory and comparative analysis of several algorithms for building D-optimal designs can be found in Chapter 7 of Ref. [34] and literature there cited. Once the designs have been obtained ξ_N^* ($p \leq N \leq 81$) to decide the minimum number, N, necessary, additional quality criteria are used.

D-optimal designs were obtained [23]. It was chosen the experimental matrix that had the highest D- and G-efficiency (0.6137 and 100%, respectively) and an acceptable $d_{max} = 1$. Of greater interest is that this design provides sufficiently precise estimations for the coefficients of the model (VIF = 1.33).

The design is completed with four replicates in absence of interferents to obtain an estimation of the variability in the absorbance. The variance inflation factors (VIF) remain acceptable. With this screening design VIFs are 1.53 and 1.28 for b_{iA} and b_{iB} ($i = 1$–3), respectively, which means that the estimation of one effect is accurate.

3.3.2. Analysis of the effect of possible interferents

Table 3 shows the nine experiments of design and the four replicates carried out in the absence of interferents. Each row corresponds to a sample with 0.5 μg ml^{-1} of Cr(VI) and the concentration of each of the interferents in accordance with the D-optimal design. The last column shows the results obtained when their absorbance is recorded at 543 nm.

The second and third columns of Table 4 show the coefficients of the model of Eq. (6) and their significance. They are considered significant those coefficients whose p-value is less than 0.05. Of greater interest is the analysis of the significant effects, that is the three coefficients which accompany the variables indicating the level of the interferent according to the model in Eq. (4). The reference used to interpret the effects of the three levels is a hypothetical average level, since their sum is equal to zero as we pointed out before. The effects and their p-values are shown in the fourth and fifth columns of Table 4.

The most relevant effects are for the V(V) and the Fe(III) which are significant for the three concentration levels. For both cations there is an increase in the absorbance when going from the hypothetical average reference level to the low level (absence of interferent) since both b_{2A} and b_{3A} are positive while there is a reduction of absorbance when moving both to the middle concentration level (b_{2B} and b_{3B} are negative) and to the high level (b_{2C} and b_{3C} are also negative), that is, the two interferents compete with the Cr(VI) withdrawing DPCO from the medium bringing about a reduction in the quantity of Cr(III)–DPCO formed such that its absorbance is reduced as the concentration of either of the two cations increases.

The absorbance decreases significantly when the Mn(VII) is not in solution (b_{4A} is negative) and increases, although not now significantly, as the concentration of this interferent in the

Table 3
Matrix of experiments of the D-optimal design chosen to study the effects of the four interferents

Sample	Factors ($\mu g\,ml^{-1}$)				Response adsorbance
	Mo(VI), x_1	V(V), x_2	Fe(III), x_3	Mn(VII), x_4	
Matrix of D-optimal experiments					
1	3	0	0	0	0.438
2	5	3	3	0	0.195
3	0	5	5	0	0.159
4	5	5	0	3	0.327
5	0	0	3	3	0.375
6	3	3	5	3	0.287
7	0	3	0	5	0.314
8	3	5	3	5	0.288
9	5	0	5	5	0.394
Replicates					
10	0	0	0	0	0.483
11	0	0	0	0	0.462
12	0	0	0	0	0.453
13	0	0	0	0	0.459

The amount of each interferent added to a sample with 0.5 $\mu g\,ml^{-1}$ of Cr(VI) is noted in $\mu g\,ml^{-1}$ and the corresponding response obtained. The factors were codified according to Eq. (6).

sample increases. The absorbance increases due to the fact that the Mn(VII) in aqueous solution absorbs in the same region of the visible as the Cr(III)–DPCO complex and although the MnO_4^- also reacts with the DPCO reducing it to Mn^{2+}, which does not absorb in the range in which the Cr(III)–DPCO complex absorbs, it does not compete significantly with the Cr(VI) for the DPCO.

Finally it is observed that for the Mo(VI) only the move from the hypothetical reference level to the middle level is significant (the p-value of coefficient b_{1B} is 0.033). However, alternative analyses of the effects (graphs of normality and the Bayesian approach [31]) do not show this coefficient to be significant. The effects do not show any pattern either of increases or decreases with concentration as occurs with the other three interferents. Consequently, it can be stated that the Mo(VI) does not affect the response of the Cr(III)–DPCO complex.

Table 4
Estimated coefficients of the model (Eq. (6)) fitted to the experimental data of Table 3 and the estimated effects of the interferents on the absorbance according to their concentration

	Coefficient	p-Value	Effect	p-Value
b_0	0.316	<0.0001[a]	0.316	<0.0001[b]
b_{1A}	−0.011	0.1330	−0.011	0.1330
b_{1B}	0.022	0.0329[a]	0.022	0.0329[b]
b_{1C}	–	–	−0.011	0.1700
b_{2A}	0.108	0.0002[a]	0.108	0.0002[b]
b_{2B}	−0.050	0.0025[a]	−0.050	0.0025[b]
b_{2C}	–	–	−0.058	0.0016[b]
b_{3A}	0.065	0.0008[a]	0.065	0.0008
b_{3B}	−0.030	0.0133[a]	−0.030	0.0133[b]
b_{3C}	–	–	−0.036	0.0079[b]
b_{4A}	−0.030	0.0100[a]	−0.030	0.0104[b]
b_{4B}	0.014	0.1040	0.014	0.1040
b_{4C}	–	–	0.016	0.0680

The first subindex identifies the factor (1, Mo(VI); 2, V(V); 3, Fe(III); 4, Mn(VII)) and the second the level (A, 0 $\mu g\,ml^{-1}$; B, 3 $\mu g\,ml^{-1}$; C, 5 $\mu g\,ml^{-1}$).
[a] Significant coefficient, of the mathematical model at the 5% significance level.
[b] Significant effect at the 5% significance level.

3.4. Calibration

3.4.1. Univariate calibration of chromium: the effect of interferents

Two calibration lines are built for the Cr(III)–DPCO complex; the first in absence of interferents and the second in the presence of V(V), Fe(III) and Mn(VII). In both seven standards were measured in duplicate in the optimum conditions of H_2SO_4 and DPC and with concentrations of Cr(VI) between 0.1 and 0.9 $\mu g\,ml^{-1}$. In the second 5 $\mu g\,ml^{-1}$ of each interferent were added to each calibration standard. Finally the absorbance of each sample was determined at 543 nm.

The regression by least mean squares, LMS, allows one to detect the outlier data [26], its utility in chemical analysis is described in Ref. [35]. As no standardised residual (in absolute value) is greater than 2.5 it must be accepted that none of the data is outlier. The calibration line for the chromium complex in the absence of interferents has a slope of 0.9439 ± 0.0456, an intercept of -0.0145 ± 0.0263 and a residual standard deviation s_{yx} of 0.0225. The calibration line in the presence of interferents has a slope of 0.2211 ± 0.0361, an intercept of 0.3352 ± 0.0207 and a residual standard deviation s_{yx} of 0.0179. The coefficient of determination is 0.994 and 0.936 for the calibration in absence and presence of interferents, respectively.

The two regressions were validated to check that the linear model is suitable by carrying out the necessary hypothesis tests both for the functional part and for the residuals. The conclusion in both cases was that the linear model proposed was acceptable since for a significance probability set at 0.05 the two linear models explain the experimental variability observed without existence of lack of fit, with independent, non-correlated residuals, normally distributed.

However, the calibration in presence of interferents showed constant bias (its intercept is significantly different from zero) and what is more proportional bias since its slope is significantly different from that of the calibration without interferents. As a result it is impossible to determine the quantity of Cr(VI) in presence of V(V), Fe(III) and Mn(VII) using a univariate signal: the maximum absorbance.

3.4.2. Multivariate calibration of chromium: qualitative analysis

In the problem of the determination of Cr(VI) in presence of interferents, calibration by a partial least squares regression, PLS [36,37] is an option to model the effect of its presence on the sample. Put another way, the regression by partial least squares must provide qualitative information as to the effect of the interferents, whose effect is to increase or decrease the signal of the complex Cr(III)–DCPO. As Martens [38] has pointed "when combined with proper interactive computer graphics, the soft multivariate bilinear modelling method of PLS regression provides cognitive access to the relevant and reliable information in data".

To do the PLS regression, make mixtures of Cr(VI), V(V), Fe(III) and Mn(VII) according to a central composite design. The design consists of 27 samples: $16 = 2^4$ from the factorial part plus eight samples of the star and three replicates at the center point. Therefore, each analyte participates in the mixtures at five concentration levels, between 0.1 and 0.9 $\mu g\,ml^{-1}$ for the Cr(VI) and between 3 and 5 $\mu g\,ml^{-1}$ for the remaining analytes.

A PLS model [24] was done taking as predictor variables the 79 absorbances measured every 2 nm from 628 to 472 nm for the 27 samples and as variable response the concentration of Cr(VI). The data were autoscaled. As a criterion to determine the number of latent variables we used the complete crossvalidation with six cancelation groups. The spectra have similar projections in the space spanned by the latent variables and their residuals are significantly equal at the 95% level. But the sample with 0.3, 4.5, 4.5 and 3.5 $\mu g\,ml^{-1}$ of Cr(VI), V(V), Fe(III) and Mn(VII), respectively, have a standardised residual of 3.30 greater than 2.5, therefore the sample must be considered outlier and the PLS regression is redone with the rest.

The PLS regression needs only two latent variables with an average relative error (in absolute value) of 3.95%. The explained (98.8%) and crossvalidated (98.5%) variances of the response are very similar which indicates a stable regression model. Despite the fact that in the samples there are four analytes only two latent variables are needed, that is, the effect of the three interferents can only be seen in signals in one way.

Fig. 3 shows the projection of the 26 samples on the space spanned by the first two latent variables. They have been codified with four digits: the first refers to the concentration of the Cr(VI), the second to that of the V(V), the third to that of the Fe(III) and the fourth to that of the Mn(VII). Each digit varies from 1 to 5 according to the concentration, this being: 0.1, 0.3, 0.5, 0.7 or 0.9 $\mu g\,ml^{-1}$ for the Cr(VI) and 3.0, 3.5, 4.0, 4.5 or 5.0 $\mu g\,ml^{-1}$ for the remaining analytes. On the first latent variable (which accounts for 96.7% of the variance of the spectra and explains 98.1% of the variance of the Cr(VI)) the samples are ordered from lower to higher scores as the concentration of the Cr(VI) increases; five different regularly spaced sample groups can be seen corresponding to the five concentration levels of Cr(VI).

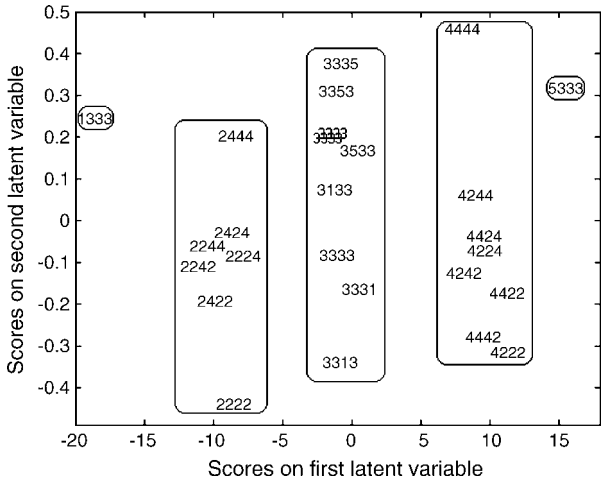

Fig. 3. Scores of the samples in the plane formed by the first two latent variables of the PLS calibration model. See text for the codification.

On the second latent variable which only accounts for 1.42% of the spectra variance and only explains 0.34% of the concentration of the Cr(VI) the samples are ordered from smaller to greater signal according not only to the quantity of intereferent but also to the type of interference. For example, samples 2422, 2242 and 2224 have 0.3 $\mu g\,ml^{-1}$ of Cr(VI) and 4.5 $\mu g\,ml^{-1}$ of V(V), Fe(III) and Mn(VII), respectively (each of them has the other two interferents at the same level 2 or 4 $\mu g\,ml^{-1}$). The scores of these samples in the second latent variable reproduce the effect on the absorbance of the complex Cr(III)–DPCO: the interference of the V(V) and of the Fe(III) is translated into a more important reduction in the absorbance for the V(V); this agrees with the magnitude of the effects shown in Table 4. On the contrary, the increase in Mn(VII) leads to an increase in the signal. The same effect can be seen in samples 3533, 3353 and 3335 or in 4422, 4242 and 4224. The PLS regression allows for a qualitative analysis of the interferents.

It also shows that the effect of the analytes V(V), Fe(III) and Mn(VII) present in the sample depends on the concentration of the Cr(VI). One only has to look at the samples with 0.3 and 0.7 $\mu g\,ml^{-1}$ of Cr(VI) (those which have a first digit of 2 or 4, respectively in Fig. 3) have the same relative position in the second latent variable according to the interferent present but with a greater score for higher concentrations of Cr(VI). Remember that the sample corresponding to code 2422 was eliminated.

The loadings in the first latent variable are positive and their magnitude is practically constant between 492 and 614 nm, decreasing outside this interval. Clearly this is a size effect linked to the absorbance band of the Cr(VI) in agreement with the analysis of the scores of the calibration samples. The loadings of the second latent variable have a negative sign for wavelengths

between 512 and 610 nm, their magnitude decreasing at the ends of this region. Outside it, the loadings are positive and increase as they move away from the central area of the spectrum. With these signs, the effect of the interferents which may increase or decrease the signal is modelled.

3.4.3. Multivariate calibration of chromium with interferents: quantitative analysis

In order to establish the quantitative performance the 27 samples were randomly divided into a training set (18 samples) and a prediction set (nine samples). As before, the data were autoscaled and a complete crossvalidation with six cancelation groups was used to determine the number of latent variables. Two latent variables were obtained and the same sample corresponding to code 2422 had a standardised residual above 2.5. The calibration model was therefore redone with the remaining 17 samples. Again only two latent variables are necessary and the correlation between the loadings of the first latent variable of the two PLS is 0.996 and for the loadings of the second 0.999.

The mean error, in absolute value, with this calibration is 4.5% $\mu g\,ml^{-1}$ in fitting and 3.3% $\mu g\,ml^{-1}$ in prediction. The residual mean square error in prediction, RMSEP, obtained is 0.016 $\mu g\,ml^{-1}$.

3.5. Figures of merit

3.5.1. Limit of detection

The capability of detection or minimum detectable net concentration has been defined [39–41] for a given probability of false positive, α, as "the true net concentration of the analyte in the material to be analysed which will lead, with probability $1-\beta$, to the correct conclusion that the concentration in the analysed material is different from that in the blank material". The application of this figure of merit to the chemical analysis with zero-order signals and univariate calibration models is detailed in the second part of the standard ISO 11843 and also this procedure is accepted by 657/2002/EC European norm [42]. These norms establish the capability of detection as a unilateral Neyman–Pearson test. The details and a version for personal computer can be seen in Ref. [43]. Formally the capability of detection is stated as follows:

- null hypothesis, the concentration of the analyte in the sample is 0, $x_0 = 0$;
- alternative hypothesis, the concentration of the analyte in the sample is greater than 0, $x_0 > 0$;
- α is defined as the probability of false positive, that is, to admit that the analyte is present when it is not true;
- β, the probability of false negative or probability to accept that the analyte is not present when it is

$$x_d = \frac{\Delta(\alpha, \beta) w_0 s}{b_1} \tag{8}$$

where $\Delta(\alpha, \beta)$ is the critical value of a noncentral t distribution which depends on the probabilities α and β. s is the residual standard deviation of the regression and b_1 the estimated slope. w_0 (Eq. (9)) is a function of the position of the standards, x_i, in the calibration curve and is inversely proportional to the number of replicates of the sample, K, and to the number of standards in the calibration model, I:

$$w_0^2 = \frac{1}{K} + \frac{1}{I} + \frac{\bar{x}^2}{\sum_{i=1}^{I}(x_i - \bar{x})^2} \tag{9}$$

In the case of first and higher-order signals the capability of detection can also be determined evaluating both probabilities α and β. The generalisation [44] is based on the mathematical proof that the capability of detection as is defined by ISO and IUPAC for univariate calibration signal versus concentration is invariant for linear transformations in the response (the signal). As a consequence, one obtains the same capability of detection using the regression estimated concentration versus true concentration. This approach can be used with signals of any order and any calibration method [45]. This unified procedure to establish the capability of detection of analytical procedures allows for comparisons. In this work, once it has been checked that the PLS calibration enables one to quantify the Cr(VI) in the presence of the three interferents, its capability of detection will be compared with that obtained with the univariate calibration of Cr(VI) without interferents considered as the reference. The capability of detection of the Cr(VI) with the univariate calibration is 0.094 $\mu g\,ml^{-1}$ for the probabilities $\alpha = \beta = 0.05$ and $K = 1$.

The capability of detection is also estimated with the multivariate PLS calibration with 17 standard samples. The LMS regression does not detect outliers and a regression line (estimated concentration versus true concentration) is obtained with a slope of 0.9753 ± 0.0556, an intercept of 0.0105 ± 0.0299 and the residual standard deviation s_{yx} is 0.0207. The regression is validated by checking the normality and independence of the residuals. The capability of detection is estimated at 0.089 $\mu g\,ml^{-1}$ also setting α and β at 0.05 and for $K = 1$. This capability of detection must be considered equal to that obtained with the univariate signal in absence of interferents.

Due to the fact that in both calibrations the limit reached is below the calibration standard with the lowest concentration, the capability of detection must be established at 0.1 $\mu g\,ml^{-1}$ of Cr(VI), which is the standard with the lowest concentration, for a probability of false positive equal to 0.05 there is a risk of false negative below 0.05.

3.5.2. Capability of discrimination (multivariate analytical sensitivity)

The capability of discrimination or minimum discriminable net concentration, d, as the smallest concentration of analyte that can be distinguished from the nominal concentration x_0 with a probability fixed at $1 - \beta$. This definition is a generalisation of the capability of detection to the case of sample concentrations close to the fixed nominal concentration.

For a nominal concentration, x_0, the bilateral hypothesis test is posed as follows:

Table 5
Values of the slope (b_1), intercept (b_0) and standard residual deviation (s_{yx}) for the two calibrations obtained with the RLS regression

Type of calibration	RLS regression			Nominal concentration, Cr(VI), x_0 ($\mu g\,ml^{-1}$)	Capability of discrimination ($\mu g\,ml^{-1}$)
	b_1	b_0	s_{yx}		
Univariate	0.944	−0.0145	0.0225	0.5	9.71×10^{-2}
				0.7	9.86×10^{-2}
Multivariate	0.975	0.0105	0.0207	0.5	8.50×10^{-2}
				0.7	8.74×10^{-2}

Capability of discrimination ($\mu g\,ml^{-1}$), $d = |x - x_0|$, of the two analytical procedures studied as a function of nominal concentration (x_0) for $K = 1$ and $\alpha = \beta = 0.05$.

- null hypothesis, the concentration of the analyte in the sample is x_0;
- alternative hypothesis, the concentration of the analyte in the sample is not x_0;
- α is defined as the probability of false non-compliance, that is, to admit that the analyte concentration is not x_0 when it is really x_0;
- β, the probability of false compliance or probability to accept than the concentration of the analyte is x_0 when it is not.

Finally, the capability of discrimination is expressed as:

$$d = |x - x_0| = \frac{\Delta(\alpha, \beta) w_{x_0} s}{b_1} \tag{10}$$

w_{x_0} is defined as in Eq. (9) but in relation to the nominal concentration x_0:

$$w_{x_0}^2 = \frac{1}{K} + \frac{1}{I} + \frac{(x_0 - \bar{x})^2}{\sum_{i=1}^{I} (x_i - \bar{x})^2} \tag{11}$$

The capability of discrimination is a concept closely linked with the analytical sensitivity since it allows one to select from several procedures that which leads to a better determination (discrimination) of concentrations when these are distant from the limit of detection. In Ref. [46] one can read the details of this approach which can be applied to calibrations with first order and higher order signals.

With the calibration lines found in the previous section for a α and β set at 0.05, we proceeded to evaluate their capability of discrimination to be able to compare the univariate analytical sensitivity (without interferents) and the multivariate (with interferents). Table 5 shows the results obtained for $K = 1$, and for the different levels of nominal concentration of Cr(VI). It is observed that with the multivariate calibration the sensitivity is somewhat smaller, $9.71 \times 10^{-2}\,\mu g\,ml^{-1}$ versus $8.50 \times 10^{-2}\,\mu g\,ml^{-1}$ for the nominal concentration $x_0 = 0.5$ and $9.86 \times 10^{-2}\,\mu g\,ml^{-1}$ versus $8.74 \times 10^{-2}\,\mu g\,ml^{-1}$ for the concentration $x_0 = 0.5\,\mu g\,ml^{-1}$.

It is also important to underline that the evaluation of the multivariate capability of discrimination is not based fundamentally on the study of the estimated calibration slope, b_1, but also on the analysis of the standard residual deviation, s_{yx}, since the lower is this value, the lower will be the quantity which the procedure is capable of discriminating for the same probabilities α and β [46].

4. Conclusions

The methodology of experimental designs has been of great utility in improving the procedure for the determination of Cr(VI) using as complexing agent 1,5-diphenylcarbazide by UV–vis spectroscopy:

(i) Through analysis of response surfaces we have found that the concentrations 1.98×10^{-3} M of H_2SO_4 and 7.9×10^{-4} M of DPC lead to greater and more precise absorbance.
(ii) An ANOVA was used to show the stability of 1,5-diphenylcarbazide.
(iii) A D-optimal screening design at three levels enabled us with only nine experiments to evaluate the effect of the interferents Mo(VI), V(V), Fe(III) and Mn(VII) on the absorbance of the complex Cr(VI)–DPCO. The presence of both chemical (due to the competition by DPC for the cations) and physical (due to the absorption of the Mn(VII) at similar wavelengths) interferences has been illustrated.

It has been shown to be impossible to determine hexavalent chromium with the univariate signal in the presence of interferents, while a PLS calibration allows for their quantification without a prior separation of the interferents. There is an average error, in absolute value, of 3.3% in prediction and 4.5% in fitting. The RMSEP is $0.016\,\mu g\,ml^{-1}$ in the range of 0.1–0.9 $\mu g\,ml^{-1}$.

The multivariate PLS calibration maintains the capability of detection ($0.1\,\mu g\,ml^{-1}$ with probability of false positive of 5% and less than 5% for false negative) reachable with the univariate signal without interferents and also the analytical sensitivity, established as the minimum net quantity discriminable with probability of false non-conformity and false conformity of 5%. With the PLS calibration this quantity is 8.50×10^{-2} and $8.74 \times 10^{-2}\,\mu g\,ml^{-1}$ for a concentration of Cr(VI) of 0.5 and $0.7\,\mu g\,ml^{-1}$, respectively, it is also significantly equal to that reachable in the case of specific univariate signals.

The PLS calibration shows neither constant nor proportional bias because the intercept 0.0105 ± 0.0299 and slope 0.9753 ± 0.0556 of the regression of the concentration calculated with PLS as compared with the real concentration are

significantly equal to 0 and 1, respectively. As a consequence the procedure is true.

Acknowledgements

Financial support, with FEDER funds, from the Spanish Ministerio de Educación y Ciencia (DGI) (project CTQ2004-07216/BQU) and Junta de Castilla y León (BU 06/04) are gratefully acknowledged.

References

[1] C. Smorgon, E. Mari, A.R. Tai, E.D. Nora, Arch. Gerontol. Geriat. 9 (2004) 393.
[2] S. Bolkent, R. Yanardag, M.M. Doler, Biol. Trace Elem. Res. 101 (2004) 219.
[3] S.K. Lee, W.Y. Choi, Chem. Lett. 34 (2005) 816.
[4] M.A. Zaitun, Int. J. Environ. Anal. Chem. 85 (2005) 399.
[5] M. Telepcakova, V. Andruch, I.S. Balogh, Chem. Pap. Chem. Zvesti 59 (2005) 109.
[6] B. Narayana, T. Cherian, J. Brazil. Chem. Soc. 16 (2005) 197.
[7] F.Q. Guo, L.F. Huang, Y.Z. Liang, Chin. J. Anal. Chem. 31 (2003) 1250.
[8] M. Gardner, S. Comber, Analyst 127 (2002) 153.
[9] Standard Methods for the Examination of Water and Wastewater, 19 ed., American Public Health Association, Washington, DC, 1995.
[10] P. Pastore, G. Favaro, A. Ballardin, D. Danieletto, Talanta 63 (2004) 941.
[11] F.J. Andrade, M.B. Tudino, O.E. Troccoli, Analyst 121 (1996) 613.
[12] K.J. Hazelwood, P.L. Drake, K. Ashley, D. Marcy, J. Occup. Environ. Hyg. 1 (2004) 613.
[13] P. Salinas-Hernández, A. Rojas-Hernández, M.T. Ramírez-Silva, Spectrochim. Acta, Part A 59 (2003) 2667.
[14] S. Hoshi, K. Konuma, K. Sugawara, M. Uto, K. Akatsuka, Talanta 47 (1998) 659.
[15] M.J. Marqués, A. Salvador, A. Morales-Rubio, M. de la Guardia, Fresenius J. Anal. Chem. 367 (2000) 601.
[16] M. Dogutan, H. Filik, I. Tor, Talanta 59 (2003) 1053.
[17] M.J. Marqués, A. Salvador, A. Morales-Rubio, M. de la Guardia, Fresenius J. Anal. Chem. 362 (1998) 239.
[18] M. Llobat-Estellés, A.R. Maurí-Aucejo, ·M.D. López-Catalán, Fresenius J. Anal. Chem. 371 (2001) 358.
[19] A. Padarauskas, A. Judzentiene, E. Naujalis, V. Paliulionyte, J. Chromatogr. A 808 (1998) 193.
[20] H. Abdollahi, Anal. Chim. Acta 442 (2001) 327.
[21] K. Kargosha, M. Noorzifar, Anal. Chim. Acta 413 (2000) 57.
[22] S. Wold, M. Sjöström, Chem. Intell. Lab. Syst. 44 (1998) 3.
[23] NEMRODW, D. Mathieu, J. Nony, R. Phan-Tan-Luu, Ver. 2000, Marseille, France, 2000.
[24] Q-PARVUS 3.0, M. Forina, S. Lanteri, C. Armanino, Dipartamento de Chimica e Tecnologie Farmaceutiche ed Alimentati, Genova, Italy, 2001.
[25] STATGRAPHICS Plus for Windows, Ver. 2.1, Statistical Graphics Corp., 1994.
[26] P.J. Rousseeuw, A.M. Leroy, Robust Regression & Outliers Detection, John Wiley and Sons Inc., Hoboken, NJ, 2001.
[27] M.E. Rueda, L.A. Sarabia, A. Herrero, M.C. Ortiz, Anal. Chim. Acta 479 (2003) 173.
[28] M.E. Rueda, M.C. Ortiz, L.A. Sarabia, A. Herrero, Anal. Chim. Acta 498 (2003) 119.
[29] M.C. Ortiz, A. Herrero, S. Sanllorente, C. Reguera, Talanta 65 (2004) 246.
[30] I. García, L.A. Sarabia, M.C. Ortiz, J.M. Aldama, Anal. Chim. Acta 544 (2005) 26.
[31] G.A. Lewis, D. Mathieu, R. Phan-Tan-Luu, Pharmaceutical Experimental Design, Marcel Dekker, New York, 1999.
[32] P.F. De Aguiar, B. Bourguignon, M.S. Khost, D.L. Massart, R. Phan-Tan-Luu, Chem. Intell. Lab. Syst. 30 (1995) 199.
[33] I. García, L.A. Sarabia, M.C. Ortiz, J.M. Aldama, J. Chromatogr. A 1085 (2005) 190.
[34] J.P. Gauchi, in: J.J. Droesbeke, J. Fine, G. Saporta (Eds.), Plans d'expériences, Technip, Paris, 1997, p. 325.
[35] M.C. Ortiz, L.A. Sarabia, A. Herrero, Talanta 70 (2006) 499–512.
[36] S. Wold, H. Martens, H. Wold, in: A. Ruhe, B. Kagstrom (Eds.), Proceedings Conference on Matrix Pencils, Lecture Notes in Mathematics, Springer-Verlag, Heidelberg, 1983, pp. 286–293.
[37] T. Naes, T. Isaksson, T. Fearn, T. Davies, A User-Friendly Guide to Multivariate Calibration and Classification, NIR Publications, Chichester, UK, 2002.
[38] H. Martens, Chem. Intell. Lab. Syst. 58 (2001) 85.
[39] International Standard Organization (ISO) 11843-2, Capability of detection: methodology in the linear calibration case, ISO, Geneva, Switzerland, 2000.
[40] L.A. Currie, Anal. Chim. Acta 391 (1999) 127.
[41] J. Inczédy, T. Lengyel, A.M. Ure, A. Gelencsér, A. Hulanicki, IUPAC, Compendium of Analytical Nomenclature, Blackwell, Oxford, 1998.
[42] Implementing council directive 96/23/EC concerning the performance of analytical methods and the interpretation of results, 2002/657/EC Commission Decision of August 12, 2002.
[43] M.C. Ortiz, L.A. Sarabia, TRAC Trend Anal. Chem. 13 (1994) 1.
[44] M.C. Ortiz, L.A. Sarabia, A. Herrero, M.S. Sánchez, B. Sanz, M.E. Rueda, D. Giménez, M.E. Meléndez, Chem. Intell. Lab. Syst. 69 (2003) 21.
[45] M.C. Ortiz, L.A. Sarabia, I. García, D. Giménez, E. Meléndez, Anal. Chim. Acta 559 (2006) 124.
[46] M.B. Sanz, L.A. Sarabia, A. Herrero, M.C. Ortiz, Anal. Chim. Acta 489 (2003) 82.

Available online at www.sciencedirect.com
ScienceDirect
Talanta 71 (2007) 1536–1540
Talanta
www.elsevier.com/locate/talanta

Characterization of lipid components of *Melanorrhoea usitata* lacquer sap

Rong Lu, Yukio Kamiya, Tetsuo Miyakoshi *

Department of Applied Chemistry, School of Science and Technology, Meiji University, 1-1-1 Higashi-Mita, Tama-ku, Kawasaki-shi 214-8571, Japan

Received 15 June 2006; received in revised form 18 July 2006; accepted 18 July 2006
Available online 28 August 2006

Abstract

The lipid component of *Melanorrhoea usitata* lacquer sap isolated by acetone was analyzed and compared to synthesized ω-phenylalkylcatechols and ω-phenylalkylphenols. In addition, laccol and urushiol analogues synthesized in our laboratory were used as standard materials to analyze the lipid component of the Myanmar lacquer sap. The GC and GC/MS measurements confirmed the results of Kumanotani and Du that neither ω-phenylalkylcatechol nor ω-phenylalkylphenol exist in the lacquer saps from *Rhus vernicifera* and *R. succedanea*.

Keywords: Lipid; *Melanorrhoea usitata*; GC/MS; Laccol; Urushiol

1. Introduction

Lacquer is a natural polymer that has been used in Asian countries for thousands of years [1,2]. There are three kinds of lacquer trees growing in Asia, *Rhus vernicifera* in China, Japan, and Korea, *R. succedanea* in Vietnam and Taiwan, and *Melanorrhoea usitata* in Burma and Thailand. The constituents and properties of the lacquers vary not only by species but also by the age of the tree, location, and season of collection [3,4]. The constituents are urushiol (60–70%), water (20–30%), plant gum (4–10%), the enzyme laccase (1.5–2%), and water-insoluble glycoprotein (3–5%) [5].

The lacquer sap obtained from *M. usitata* contains compounds with various structures, 3- or 4-substituted catechol and phenol derivatives and resorsinol derivatives, in comparison to the saps from *R. vernicifera* and *R. succedanea* [6,7]. The characteristic materials that are not found in the sap of *R. vernicifera* and *R. succedanea* are the ω-phenylalkylcatechols and the ω-phenylalkylphenols, which were characterized by Kumanotani and co-workers [8], Du and Oshima [9], and Sargent and Wangchareontrakul [10] in 1989, but their results have not been confirmed.

In this study, we attempted to clarify the structure of the lipid components by applying a method that we have reported previously [11,12]. As shown in Scheme 1, the structures of synthesis of the specific phenol components, the ω-phenylalkylcatechols and the ω-phenylalkylphenols, have been determined. In addition, the lipid components of the saps derived from *M. usitata* were also analyzed by gas chromatography (GC) and gas chromatography/mass spectrometry (GC/MS). The structures and compositions of the lipid components were identified primarily by comparing the retention times in the GC analysis of the ω-phenylalkylcatechols and the ω-phenylalkylphenols as standards that were synthesized in this study and the phenol components (urushiols and laccols) that were previously synthesized as standards [11,12].

2. Experimental

2.1. Materials, GPC, GC, and GC/MS conditions

The native sap obtained from Myanmar was used for the GC and GC/MS analyses. The monomeric components were separated by GPC. GPC was carried out using a LC-908 (Jai Co., Ltd.) equipped with a refractive index detector, UV detector (254 nm), and GPC column (TSK-gel G1000H6 × 2, 60 cm × 21.5 mm i.d.; TOSOH) with flow rate of 3.5 ml/min and $CHCl_3$ as the eluent. The GC was conducted using a SHI-

* Corresponding author. Tel.: +81 44 934 7203; fax: +81 44 934 7203.
E-mail address: miya@isc.meiji.ac.jp (M. Tetsuo).

0039-9140/$ – see front matter © 2006 Elsevier B.V. All rights reserved.
doi:10.1016/j.talanta.2006.07.033

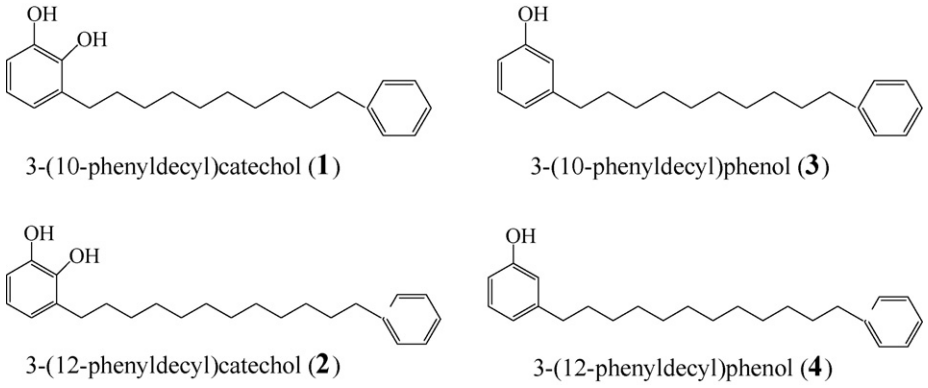

Scheme 1. Structure of synthesized lipid components in this study.

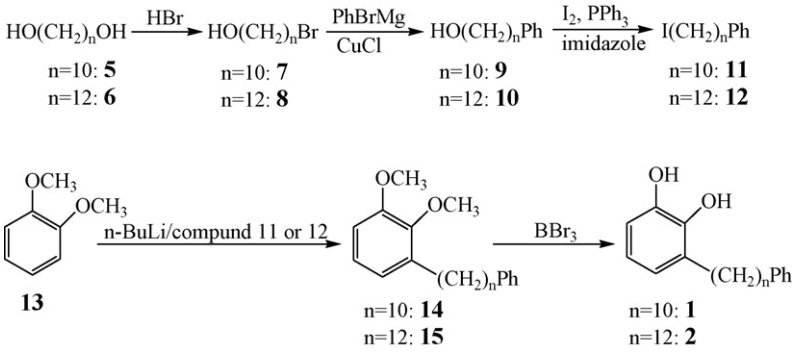

Scheme 2. Synthesis of 3-(ω-phenylalkyl)catechol.

MADZU GC-17A instrument equipped with a flame-ionization detector. The GC/MS was carried out using an HP6890 (Hewlett-Packard, Ltd.) instrument and mass spectrometer in the EI-mode (70 eV). A DB-17 column (J&W Scientific) was used: DB-17 [methylphenyl(50%)silicone], 30 m × 0.25 mm i.d., and the thickness of the liquid phase film (d_f) = 0.25 μm. The carrier gas was He and the samples were injected in the split mode (splitting ratio 50:1). The GC and GC/MS were programmed for a temperature increase from 2 °C to 80 °C, then held at 80 °C for 20 min.

2.2. *Synthesis of* ω*-phenylalkylcatechols and* ω*-phenylalkylphenols*

As shown in Scheme 1, the ω-phenylalkylcatechols **1** and **2** were synthesized by reacting 3-lithioveratrole derived from veratrole with 1-phenyl-10-iododecane and 1-phenyl-12-iododododecane, followed by de-protection of the methoxyl group as shown in Scheme 2. The 1-phenyl-10-iododecane and 1-phenyl-12-iododecane were synthesized from 1,10-decanediol and 1,12-dodecanediol by halogenation using HBr and the cross-coupling reaction with PhMgBr, followed by iodination of the hydroxyl group, respectively [13].

The ω-phenylalkylphenols **3** and **4** were synthesized by the cross-coupling reaction of the Grignard reagents from 3-bromoanisole and bromobenzene using 1,10-dibromodecane and 1,12-dibromododecane, followed by de-protection of the methoxyl group, as shown in Scheme 3. 1,10-Dibromodecane and 1,12-dibromododecane were synthesized from 1,10-decanediol and 1,12-dodecanediol by a well-known method, i.e., halogenation of a hydroxyl group using CBr_4.

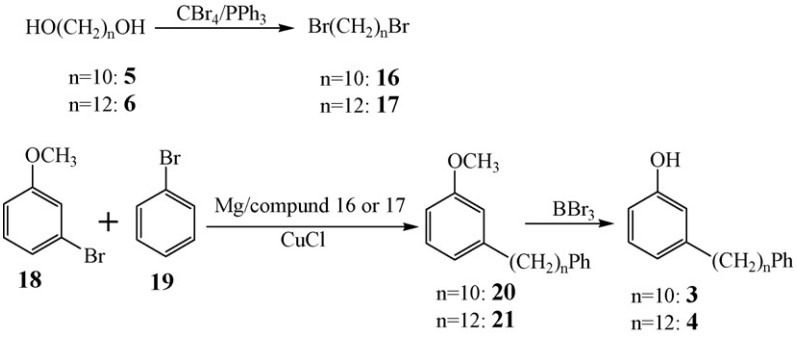

Scheme 3. Synthesis of 3-(ω-phenylalkyl)phenol.

During the reaction of the cross-coupling compound **18** and **19**, and the dibromoalkane **16** or **17**, a diphenylalkane and a di(3-methoxyphenyl)alkane, were produced as the by-products. However, when considering the total yield, this reaction was acceptable because this synthetic route was shorter than that shown in Scheme 2, and had a higher total yield. The other standards used in this study also were synthesized in our laboratory previously [14,15].

3. Results and discussion

3.1. Analysis of lipid components from M. usitata

The native lacquer sap was mixed with acetone (sap:acetone = 1:3, v/v) to extract the lipid components. The filtered acetone solution was evaporated to give the crude lipid components. The residue (100 mg) was dissolved in 2 ml of chloroform, and the resulting solution was chromatographed on a GPC column (TSK-gel G1000H6 × 2, 60 cm × 21.5 mm i.d.; TOSOH) to obtain monomeric and oligomer lipid fractions.

The monomeric fraction was analyzed by gas chromatography (GC) and gas chromatography/mass spectrometry (GC/MS). The results of analysis using a DB-17 [methylphenyl(50%)silicone] column for GC and GC/MS were acceptable because of no overlapping peaks in the chromatogram occurred. In the gas chromatogram of the monomeric lipid from Myanmar (Fig. 1), the presence of ω-phenylalkylcatechols and ω-phenylalkylphenols was confirmed by the corresponding mass spectra (Fig. 2), respectively.

The molecular ion peaks at *m/z* 310 and *m/z* 388 were ω-phenylalkylphenols (peaks **e** and **p**), while those at *m/z* 326 and 354 were the ω-phenylalkylcatechols (peaks **g** and **u**). The all mass spectra of these components exhibited the characteristic tropylium cation fragment at *m/z* 91, which decomposed further to the cyclopentadienyl cation at *m/z* 65 as a specific fragment peak in the mass spectra. This is derived from the

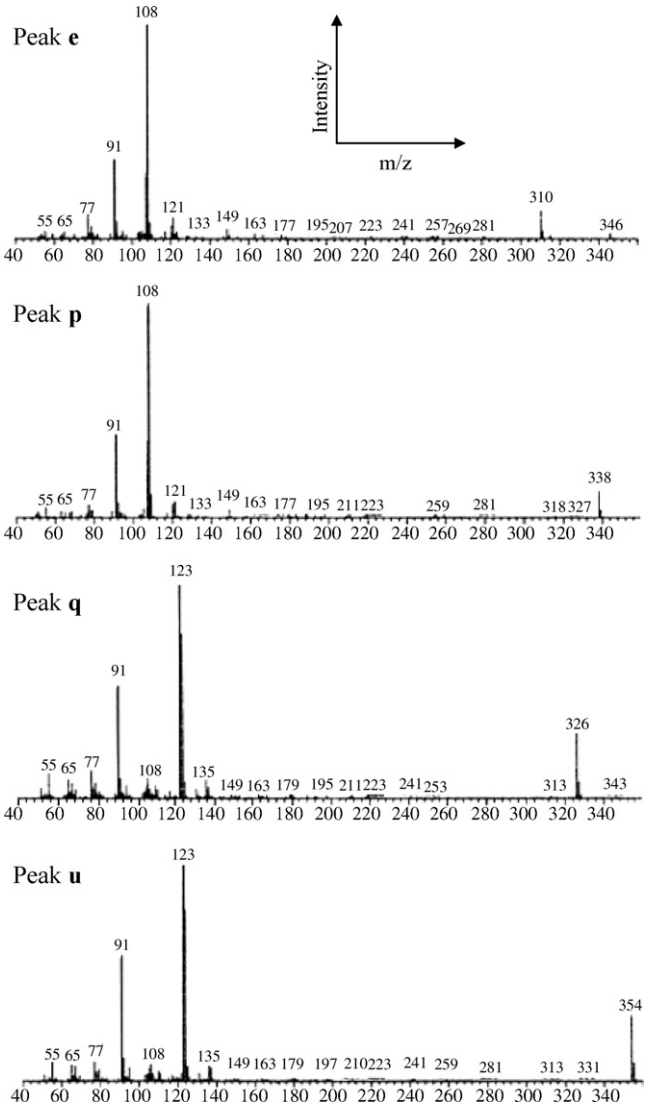

Fig. 2. Mass spectra of Myanmar lacquer lipid component (*X*-axis is *m/z* and *Y*-axis is the signal intensity).

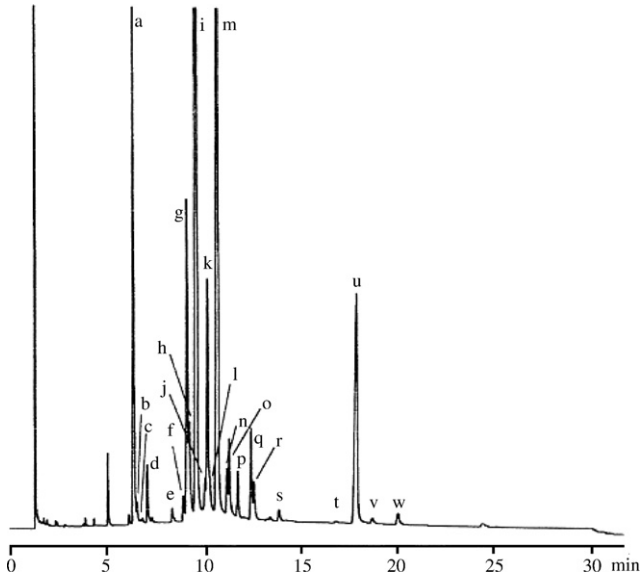

Fig. 1. GC chromatogram of Myanmar lacquer lipid component.

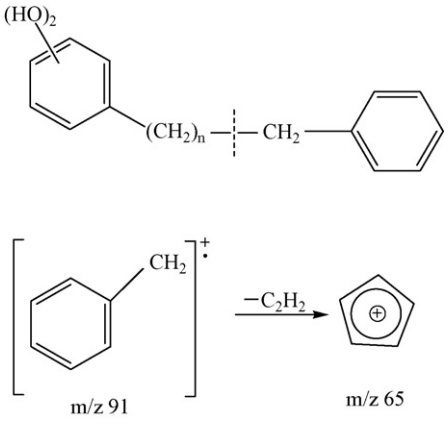

Scheme 4. Formation of fragment peak (*m/z* 91).

Table 1
Structure and composition of lipid components of *Melanorrhoea usitata* lacquer sap

Peak no.	*m/z*	Retention time (min)	Content (%)	Structure
a	320	6.59	12.78	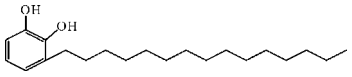
b	328	6.65	1.01	Heptadecadienylphenol
c	318	6.80	0.32	Pentadecadienylphenol
d	320	7.34	1.77	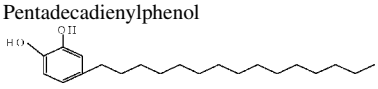
e	310	8.63	0.26	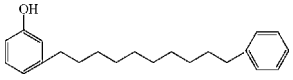
f	348	9.18	0.59	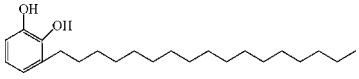
g	346	9.37	4.50	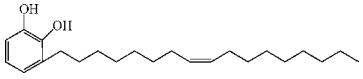
h	346	9.49	2.19	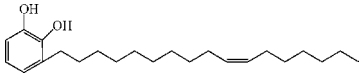
i	344	9.83	26.12	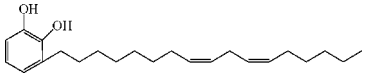
j	344	10.29	0.65	Heptadecadienylcatechol
k	346	10.41	3.97	Heptadecenylcatechol
l	346	10.55	1.12	Heptadecenylcatechol
m	344	10.94	27.34	Heptadecadienylcatechol
n	344	11.45	1.13	Heptadecadienylcatechol
o	344	11.58	1.85	Heptadecadienylcatechol
p	338	12.02	0.33	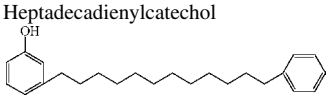
q	326	12.76	1.81	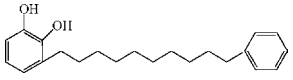
r	344	12.92	1.14	Heptadecadienylcatechol
s	326	14.29	0.30	4-(12-Phenyldodecyl)phenol
t	Unknown	17.23	0.14	Unknown
u	354	18.30	10.03	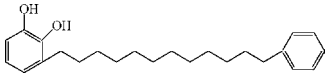
v	354	19.20	0.23	4-(12-Phenyldodecyl)catechol
w	354	20.60	0.45	ω-Phenyldodecylresorsinol

terminal alkylphenol group of ω-phenylalkylcatechols and ω-phenylalkylphenols, as shown in Scheme 4.

The other components in the chromatogram were identified as compounds derived from the laccols and urushiols according to the mass spectra. Structural identification of the lipid components was carried out by comparison of the retention times of the GC analysis with the components **1–4** synthesized and other compounds, such as 3-pentadecylcatechol, 3-heptadecylcatechol, 8*Z*-3-(8-heptadecenyl)catechol, 10*Z*-3-(10-heptadecenyl)catechol, and 3-[(8*Z*,11*E*)-8,11-heptadecadienyl]catechol, which were synthesized in our previous study. 4-Pentadecylcatechol was easily synthesized by the reaction of 1-iodopentadecane with veratrole, followed by de-protection of the hydroxyl groups of catechol. The analyzed results in Fig. 1 are summarized in Table 1.

The structure and compositions of approximately 70% of the lipid components were characterized and quantified in this study. The trienyl components were identified in the lacquer saps from *R. vernicifera* and *R. succedanea*, but not confirmed in the saps from the *M. usitata*. The absence of the ω-phenylalkylcatechols and the ω-phenylalkylphenols in the lacquer saps from *R. vernicifera* and *R. succedanea* was confirmed.

4. Conclusion

The synthesis of the specific lipid components of *M. usitata* lacquer sap, i.e., ω-phenylalkylcatechols and ω-phenylalkylphenols, was carried out. The sap from the *M. usitata* lacquer tree was analyzed by comparison with the synthesized lipid components **1–4**, the laccol and urushiol analogues, syntheses of which were outlined in our laboratory. The results showed that the percent composition (approximately 70% total) of the lipids in the sap from the *M. usitata* was identified. Neither ω-phenylalkylcatechols nor ω-phenylalkylphenols were present in the lacquer saps from *R. vernicifera* and *R. succedanea,* as confirmed in this study.

Acknowledgements

We thank Professor Shigeo Sugihara of Meiji University, Tokyo, for valuable discussions and suggestions. This work was partly supported by the Academic Frontier Project for Private Universities: a matching funds subsidy from MEXT, 2006–2010, and the Research Project Grant B from the Institute of Science and Technology, Meiji University.

References

[1] E.J. Kidder, Ancient Peoples and Places, Thames & Hudson, Japan, 1959.
[2] Y. Kuraku, N.S. Brommelle, P. Smith (Eds.), Getty Conservation Institute, California, 1988, p. 45.
[3] J. Kumanotani, Prog. Org. Coat. 26 (1995) 163.
[4] O. Vogl, J. Bartus, M. Qin, J.D. Mitchell, in: K.P. Ghiggino (Ed.), Progress in Pacific Polymer Science, vol. 3, Springer-Verlag, Berlin, 1994, p. 423.
[5] R. Oshima, J. Kumanotani, Carbohydr. Res. 127 (1984) 43.
[6] Y. Du, R. Oshima, J. Kumanotani, J. Chromatogr. 284 (1984) 463.
[7] J. Bartus, W. Simonic, C. Garner, T. Nishiura, T. Kitayama, K. Hatada, O. Vogl, Polym. J. 26 (1994) 67.
[8] Y. Du, R. Oshima, H. Iwatsuki, J. Kumanotani, J. Chromatogr. 295 (1984) 179.
[9] Y. Du, R. Oshima, J. Chromatogr. 318 (1985) 378.
[10] M.V. Sargent, S. Wangchareontrakul, J. Chem. Soc. Perkin Trans. I 431 (1989).
[11] Y. Kamiya, T. Miyakoshi, J. Oleo Sci. 50 (2001) 865.
[12] Y. Kamiya, W. Sato, T. Miyakoshi, J. Oleo Sci. 51 (2002) 473.
[13] R. Lu, Y. Kamiya, T. Miyakoshi, J. Anal. Appl. Pyrolysis, in press.
[14] T. Miyakoshi, H. Kobuchi, N. Niimura, Y. Yoshihiro, Bull. Chem. Soc. Jpn. 64 (1991) 2560.
[15] Y. Kamiya, Y. Niimura, T. Miyakoshi, Bull. Chem. Soc. Jpn. 73 (2000) 2621.

Available online at www.sciencedirect.com
ScienceDirect
Talanta 71 (2007) 1580–1586
Talanta
www.elsevier.com/locate/talanta

Fractionation metallothionein-like proteins in mussels with on line metal detection by high performance liquid chromatography–inductively coupled plasma-optical emission spectrometry

Sandra Santiago-Rivas, Antonio Moreda-Piñeiro, Adela Bermejo-Barrera, Pilar Bermejo-Barrera *

Department of Analytical Chemistry, Nutrition and Bromatology, Faculty of Chemistry, University of Santiago de Compostela, Avenida das Ciencias, s/n. 15782 Santiago de Compostela, Spain

Received 2 February 2006; received in revised form 17 July 2006; accepted 24 July 2006
Available online 1 September 2006

Abstract

A rapid method for the determination of Al, Ba, Cu, Fe, Mn, Sr and Zn binding metallothionein-like proteins (MLPs) in mussels (*Mytilus galloprovincialis*) by inductively coupled plasma-optical emission spectrometry was developed. The method uses a short column (8 mm × 75 mm) anion exchange high performance liquid chromatography (HPLC) with inductively coupled plasma-optical emission spectrometric (ICP-OES) detection. Working in isocratic mode (75 mM Tris–HCl at pH 7.4, flow rate at 0.8 ml min^{-1}), two major MLPs isoforms (MLP-1 and MLP-2) can be separated in ten minutes. The distribution of basal metals binding MLPs was assessed by on line HPLC and ICP-OES, while the basal contents of metals binding MLPs were obtained after off line HPLC and ICP-OES (collection of the two major fractions and multi-element determination by ICP-OES). The calculated LODs were 81, 6, 10, 13, 30, 9 and 123 ng g^{-1} for Al, Ba, Cu, Fe, Mn, Sr and Zn binding MLP-1 and MLP-2, respectively. The repeatability of the over-all method (five different mussel cytosols prepared from the same mussel sample and subjected to the off line HPLC–ICP-OES procedure twice) was from 11.2 for Cu to 16.2% for Zn. The method was finally applied to different raft mussels from Ría de Arousa estuary in order to know basal levels of elements binding MLPs.

Keywords: Metallothionein-like proteins; Trace elements; Mussel; High performance liquid chromatography; Inductively coupled plasma-optical emission spectrometry

1. Introduction

There are several metal-binding proteins in living organisms, mainly enzymes (metalloenzymes) and metal-binding proteins which transport metals or acts as metal store in the body. Most of them play crucial roles in the optimal healthy status of the living organisms, but also in some pathological disorders [1]. Metallothioneins, MTs, are non-enzymic metal-binding proteins characterized by low molecular weight, high content of cysteine residues, lack of aromatic amino acids and high resistance to heat. These proteins have been described as physiologically multifunctional because they are involved in the transport, storage and detoxification of metals. Their sulphydryl-rich primary structure confers them with a high capacity for metal binding, mainly copper, cadmium and zinc [2]. These metal-binding proteins, firstly discovered in mammalians, have been observed in a wide range of marine invertebrates [3]. Therefore, MTs isolated from invertebrates are preferably called as metallothionein-like proteins (MLP) rather than metallothioneins.

MLPs in mollusks can be considered as a kind of stress proteins which are particularly responsive to heavy metals, although some recent studies have concluded that the biosynthesis of MLPs can be induced by hydrocarbons [4] and herbicides [5], which reduce the metal (Cu, Zn and Cd) content in MLPs and increase the total protein content. These results suggest that MTs and MLPs induction may not be considered as specific biomarkers of metal exposure, although most of the MTs and MLPs induction in living organisms is attributed to heavy metals [6] and there is a well-established relationship between MLPs and Cd, Cu and Zn [7,8].

* Corresponding author. Tel.: +34 981 591079; fax: +34 891 595012.
E-mail address: pbermejo@usc.es (P. Bermejo-Barrera).

0039-9140/$ – see front matter © 2006 Elsevier B.V. All rights reserved.
doi:10.1016/j.talanta.2006.07.038

Isolation procedures based on ion exchange properties and electrophoresis has led to the recognition of a variety of forms of metallothioneins which were subsequently shown to differ in amino acid composition and sequence. In mammalians, there are at least two major isometallothioneins (metallothioneins isoforms) numbered according to the order in which they elute from anion exchanger as metallothionein-1 (MT-1) and metallothionein-2 (MT-2) [9]. Advances in high performance liquid chromatography (HPLC) combined with sensitive spectrometric detectors have aided the resolution of not only differently charged MT isoforms but also other polymorphic variants not separated by classical chromatographic procedures. Thus, several MT subisoforms have been reported, mainly MTs subisoforms isolated from mammalians [10–13].

Beside anion exchange-HPLC and capillary electrophoresis separation procedures, size exclusion and reversed phase-HPLC combined with element or molecular mass spectrometric techniques have been widely used for the identification, characterization and determination of metal-binding proteins [1], and specially, MTs and MLPs [2,14]. These hyphenated HPLC and, mainly, inductively coupled plasma-mass spectrometry (ICP-MS) are commonly used to perform multielement trace-element speciation in metal-binding proteins. Some developments and applications of speciation of metals binding MTs have been carried out for standard MTs isolated from rabbit liver [13,15], rat liver [16,17], human liver [18,19] and for MLPs in mussels [7,8,20].

In this work, on line and off line anion exchange-HPLC–ICP-OES procedures have been developed to determine basal levels of Al, Ba, Cu, Fe, Mn, Sr and Zn binding MLPs in mussel (*Mytilus galloprovincialis*). One of the main aims of the current work has been the optimization of an isocratic anion exchange, HPLC separation of MTs-like proteins, which has led the resolution of the two major MLPs isoforms (MLP-1 and MLP-2) in 10 min. The distribution pattern of these elements among different MLPs isoforms, mainly MLP-1, has been analyzed for different raft mussel from unpolluted areas in Ría de Arousa estuary.

2. Experimental

2.1. Instrumentation

An Optima 3300 DV inductively coupled plasma optical emission spectrometer (Perkin-Elmer, Norwalk, USA) with a GemCone nebulizer on a cyclonic spray chamber and an autosampler AS 91 (Perkin-Elmer) was used in the current study. The chromatographic system consisted of a Waters 515 HPLC pump (Waters, Milford, MA, USA) and a Rheodyne 7125 (Cotati, CA, USA) injector with a loop volume of 200 μl. A Waters 486 absorbance detector (Waters) was used for metallothioneins-like proteins UV detection, using Millennium (Waters) software for data acquisition. A Protein-Pak DEAE-5PW anion exchange 8 mm × 75 mm glass column was obtained from Waters. A Lab Blender Stomacher 400 (Seward Med. Ltd., London, UK) was used to blend and homogenize fresh mussel samples. During the blending process samples were contained in Stomacher closure bags 6041/CLR (Seward). A centrifuge Centromix (Selecta, Barcelona, Spain) and refrigerated centrifuge Laborzentrifugen 2K15 (SIGMA, Osterode, Germany) were used to separate the solid biological material from the cytosolic extract. An ORION 720A plus pH-meter with a glass–calomel electrode (ORION, Cambridge, UK) was also used.

2.2. Reagents

Ultra-pure water, resistance 18 MΩ cm, was obtained from a Milli-Q water purification device from Millipore Co. (Bedford, MA). Rabbit liver metallothioneins MT-1 and MT-2 were purchased from Sigma–Aldrich (Stemheim, Switzerland). Al, Ba, Cd, Cu, Fe, Mn, Sr and Zn stock standard solutions (1000 mg l^{-1}) were supplied by Merck (Poole, Dorset, UK). Hydrogen peroxide 33% was from Panreac (Barcelona, Spain). Nitric acid 70.0% and hydrochloric acid 37% were from J.T. Baker B.V. (Deventer, Holland). The extracting solution was made from Tris–hydroxymethyl–aminomethane (Sigma–Aldrich), 2-mercaptoethanol (2-MCE) (Sigma–Aldrich), phenylmethylsulfonyl fluoride (PMSF) (Sigma–Aldrich) and sodium chloride (Merck).

2.3. Procedure for cytosol preparation

Mussels (*M. galloprovincialis*) were collected from mussel rafts at Ría de Arousa estuary (Galicia, NW Spain) at different sampling sites. After removal of abductor and foot muscles, the soft tissues (muscle and gill) were subjected to an optimized cytosolic preparation method [21] based on a modified protocol of the methods reported by Roesijadi and Fowler [3]. The method consists in weighting around 5.0 g of soft tissue into a Stomacher bags and adding 25 ml of an extracting solution (Tris–HCl (pH 7.4), 0.01 mM phenylmethylsulfonyl fluoride (PMSF), 5 mM 2-mercaptoethanol (2-MEC) and 25 mM NaCl). The mixture was blended at high speed for 5 min, and it was transferred to centrifuge tubes and centrifuged at 3500 rpm for 30 min. The pellets were separated by decantation and the extracts were transferred into a second centrifuge tube and they were warmed in a water-bath at 60 °C for 15 min. A second centrifugation step at 4 °C and 15300 r.p.m. for 30 min was carried out to separate the tertiary structure proteins which have suffer denaturalization at high temperature. Mussel cytosolic extracts, obtained by decantation, were made up to 25 ml and stored in polyethylene bottles at −20 °C before measurements.

2.4. Anion exchange chromatography on line UV–vis spectrometry–ICP-OES

A 75 mM Tris–HCl (pH 7.4) buffer solution was used as a mobile phase at a flow rate of 0.8 ml min^{-1} (isocratic mode). This mobile phase was previously de-gassed for 15 min in an ultrasonic water-batch. The mussel cytosols were filtered through a 0.45 μm filter, and a 200 μl sample loop was filled. Anion exchange conditions and ICP-OES operating parameters are given in Table 1.

Table 1
Anion exchange chromatographic conditions and data acquisition parameters

Injection volume (μl)	200
Flow rate (ml min^{-1})	0.8
Mobile phase composition	75 mM Tris–HCl, pH 7.4
Anion exchange column	ProteinPak DEAE-5PW 8 × 75 mm glass column
Elution mode	Isocratic
Data acquisition	*UV spectrometric detection*
Wavelength (nm)	254
ICP-OES detection	
Forward power (W)	1300
Gas flows (l min^{-1})	
Nebuliser	0.85
Auxiliary	1.0
Coolant	15.0
Nebuliser type	GemCone (cyclonic chamber)
Wavelengths (nm)	Al, 396.153; Ba, 455.403; Cu, 324.752; Fe, 238.204; Mn, 257.610; Sr, 421.552; Zn, 202.548

2.5. Anion exchange chromatography off line ICP-OES

MLP-1 and MLP-2 isoforms fractions (eluted volume of 1.6 ml, chromatographic time between 3.0 and 5.0 min for MLP-1 and within the 6.4–8.4 min range for MLP-2) were collected and they were directly analyzed by ICP-OES (Table 1) using an aqueous calibration.

3. Results and discussion

3.1. Anion exchange chromatography and UV spectrometric detection: optimization of MLP-1 and MLP-2 chromatographic separation

The optimization of the anion exchange chromatographic separation of MLPs isoforms (mobile phase composition and flow rate) has been carried out using UV detection at 254 nm. A Tris–HCl buffer system at pH 7.4 was selected as mobile phase because it is the same medium in which the MLPs are dissolved after cytosol preparation. In addition, according to Ødegård and Luna, similar pHs of the sample solution and the mobile phase allow better separations of metal-binding biomolecules [22]. Therefore, different Tris–HCl buffer solutions at pH 7.4 and at different ionic strengths (Tris–HCl buffer concentrations between 2.0 and 200.0 mM) were tested as a mobile phases. For all these experiments, individual standard rabbit liver MT isoforms or mixtures of MT isoforms (10 mg l^{-1}) as well as mussel cytosols were used. Buffer concentration has the following effect on the separation of MLPs by anion exchange-HPLC. The retention time of the two MLP isoforms are similar a buffer concentration 150–200 mM, and therefore poorly resolved. Resolution improves when buffer concentration is in the range 20–75 mM. It is illustrated on Fig. 1(a and b). At low buffer concentration, i.e. 2, 5 10 and 20 mM Tris–HCl, four subisoforms from MLP-1 were resolved (Fig. 2(a and b)) however, MLP-2 was not eluted within 10 min under the low buffer concentrations (Fig. 2(a and b)). Results agree with those previously reported by Farrarello et al. [13], whose have separated different rabbit liver MT-1 and MT-2 by anion exchange chromatography with gradient elution. They have found partial resolution of MT-1 subisoforms when working with low buffer concentrations.

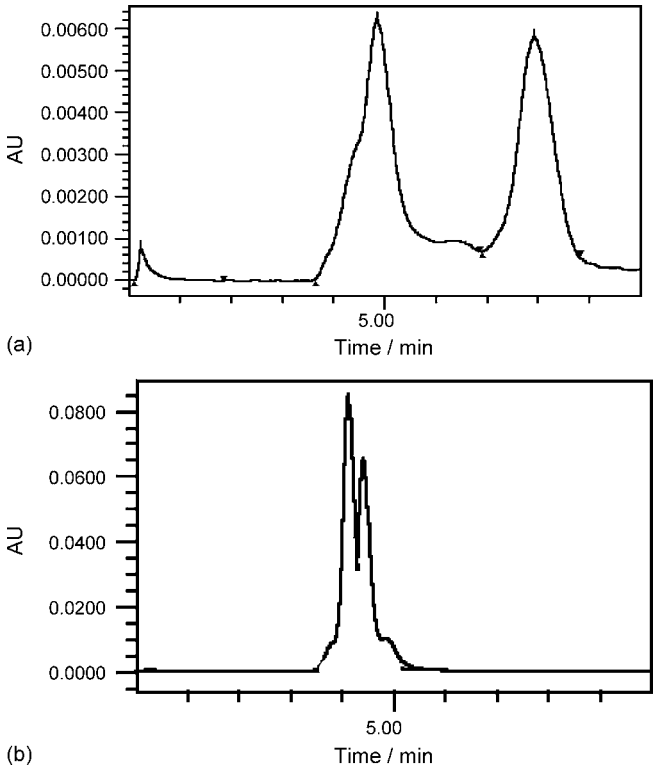

Fig. 1. Anion exchange chromatographs with UV detection (254 nm) for 10 mg l^{-1} standard MT-1 and MT-2 isoforms (rabbit liver) for Tris–HCl buffer concentrations of 75.0 (a) and 200 mM (b).

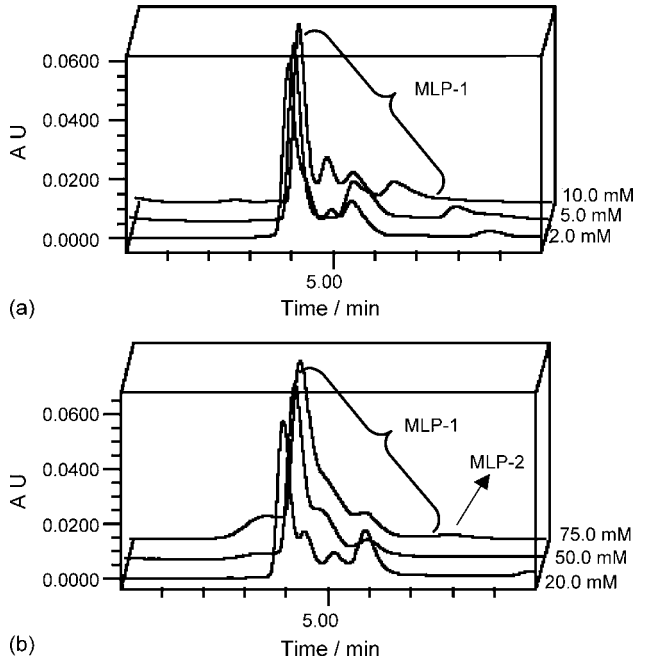

Fig. 2. Anion exchange chromatographs with UV detection (254 nm) for MLP-1 and MLP-2 isoforms from mussel cytosols in function of the Tris–HCl buffer concentration: 2.2, 5.0 and 10.0 mM (a) and 20.0, 50.0 and 75.0 mM (b).

When using a buffer concentration of 75 mM three different subisorform from MLP-1 and a small signal corresponded to MLP-2 isoform (7.40 min as retention time) were observed. Therefore, a compromise between MLP-1 and MLP-2 resolution (poor resolution when increasing the buffer concentration) and partial resolution of MLP-1 subisoforms at low buffer concentrations has been considered and a buffer concentration of 75 mM has been chosen.

After studying the mobile phase flow rate between 0.4 and 1.2 ml min^{-1}, a flow rate fixed at 0.8 ml min^{-1} was finally selected. Under these conditions (Fig. 3(a and b)), the MLP-1 isoform elutes from column at 4.01 min and offer a partial resolution of two subisoforms, while the MLP-2 isoform elutes at 7.40 min. It can be seen in Fig. 3(b) that the amount of MLP-2 isoform in the analyzed mussel cytosol is low. It must be said that the retention time for rabbit liver MT-1 and mussel MLP-1 are slight different and a value of 4.84 ± 0.01 min was achieved for six replicates of rabbit liver MT-1. However, retention times for rabbit liver MT-2 and MLP-2 are the same (around 7.40 min). The repeatability of the retention times for both MLP-1 and MLP-2 isoforms was established after performing eleven anion exchange chromatographic separations for a mussel cytosol. Mean retention times for both MLP isoforms were 4.01 ± 0.02 and 7.40 ± 0.05 min for MLP-1 and MLP-2, respectively. The resolution (R), measured as $2(t_{m2} - t_{m1})/(w_1 - w_2)$, was 1.05 ± 0.02.

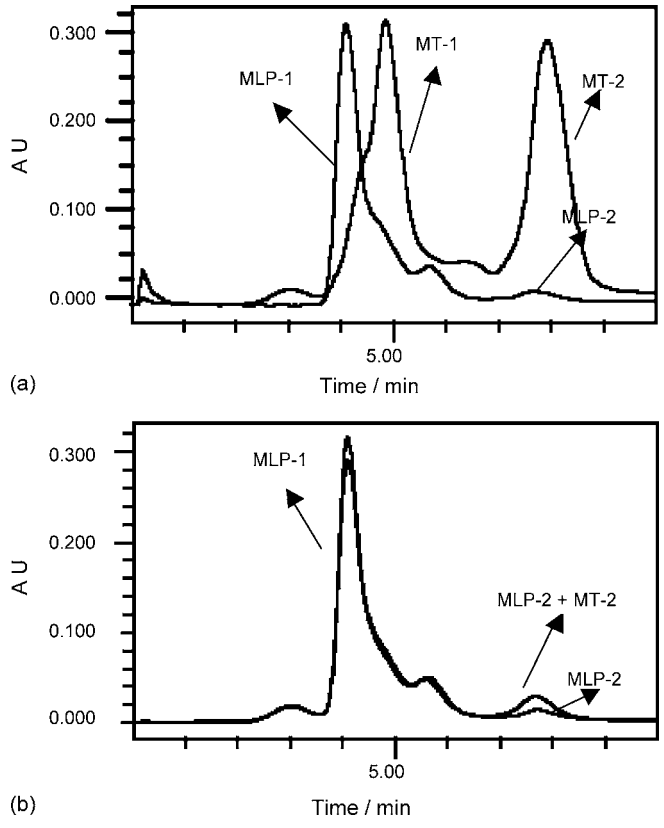

Fig. 3. Anion exchange chromatographs with UV detection (254 nm) under optimised conditions for a mussel cytosol and a mixture of 10 mg l^{-1} of standard rabbit liver MT-1 and MT-2 isoforms (a) and for a mussel cytosol and a mussel cytosol spiked with 5 mg l^{-1} of standard rabbit liver MT-2 (b).

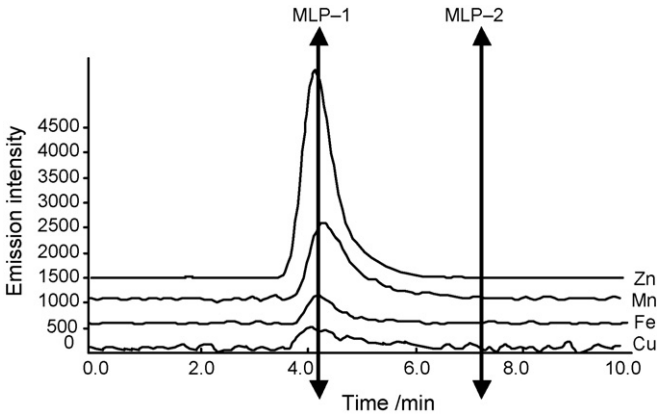

Fig. 4. Anion exchange chromatographs with ICP-OES detection for Cu (324.752 nm), Fe (238.204 nm), Mn (257.610 nm) and Zn (202.548 nm) binding MLPs in mussel cytosols.

3.2. Anion exchange chromatography on line ICP-OES

Anion exchange-HPLC was on line coupled with ICP-OES as a first multi-elemental survey of trace metals associated with MLPs in mussel cytosols. The elution profiles of Cu, Fe, Mn and Zn were directly obtained (Fig. 4) and as it can be seen, all elements investigated are mainly bound to MLP-1 isoform (the amount of MLP-2 is low in mussel cytosols and the concentration of elements associated with must be also low). Similar elution profiles of Al, Ba and Sr (not plotted) were obtained. However, negligible signals were recorded for Cd. Negligible signals for Cd were obtained because of the use of ICP-OES as detector. A more sensitive detector, such as ICP-MS, ICP-OES would be desirable in order to assess low Cd levels binding MLPs. Fig. 5 shows some chromatographs when monitoring Cd, Cu, S and Zn lines for a mixture of 10.0 mg l^{-1} standard rabbit liver MT-1 and MT-2. It can be seen two peaks for these elements related to the two MT isoforms, proving the feasibility of the separation method. This is possible because the MT isoforms from rabbit liver were isolated from Cd-exposed animals.

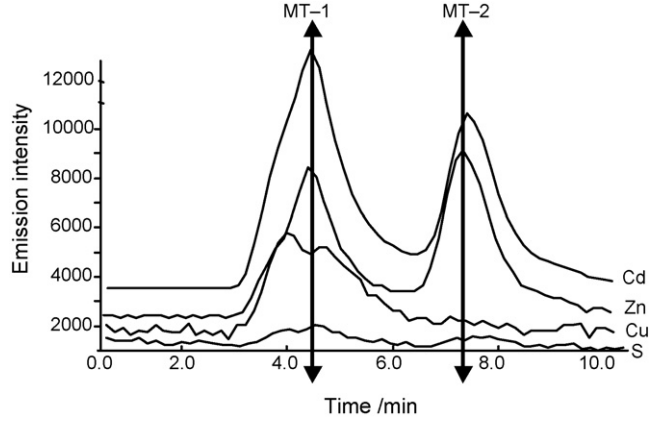

Fig. 5. Anion exchange chromatographs with ICP-OES detection for Cd (238.204 nm), Cu (324.752 nm), S (257.610 nm) and Zn (202.548 nm) binding standard rabbit liver MT isoforms.

Table 2
Repeatability of the retention times and peak height for six replicate injections of a mussel cytosol by anion exchange-HPLC–ICP-OES

	MLP-1 isoform			
	Retention time for MLP-1: 4.01 ± 0.02 min			
	Retention time (min)		Peak height/height units	
	$\bar{x}$ ± S.D.	R.S.D. (%)	$\bar{x}$ ± S.D.	R.S.D. (%)
Al	4.03 ± 0.15	4	1280 ± 68	5
Ba	4.05 ± 0.13	3	1352 ± 72	5
Cu	4.03 ± 0.18	4	779 ± 51	6
Fe	3.98 ± 0.11	3	627 ± 12	2
Mn	4.08 ± 0.08	2	1674 ± 78	5
Sr	4.07 ± 0.11	3	143255 ± 4727	3
Zn	3.98 ± 0.11	3	4048 ± 98	2

The repeatability of the retention times for each metal associated with MLP-1 was calculated. A same mussel cytosol was injected six times and the metal profiles were obtained. Results are shown in Table 2 where it can be seen that good precision is achieved for all cases. Retention times for element binding MLP-1 were close to the retention time of MLP-1 (UV–vis detection).

3.3. Anion exchange chromatography off line ICP-OES

As the shape of the metal-MLPs in mussel cytosols is unknown, a direct coupling anion exchange-HPLC–ICP-OES can not give information about the concentration of metal binding MLPs because of standards metal-MLPs complexes are not available. Therefore, an off line anion exchange-HPLC–ICP-OES procedure was developed to quantify metals binding MLPs. This has implied the collection of the different fractions eluted from anion exchange column and the analysis of them by ICP-OES under optimum conditions. Two different fractions were collected, the first fraction was corresponded to the MLP-1 isoform (retention time of 4.01 ± 0.02 min), that means an eluted volume of 1.6 ml when the mobile flow rate is 0.8 ml min^{-1} (times between 3.01 and 5.01 min). The second fraction was the MLP-2 isoform (retention time of 7.40 ± 0.05 min). The eluted volume of this fraction is 1.6 ml too and it implies times between 6.40 and 8.40 min. All these fractions were directly measured under optimum ICP-OES operating conditions (Table 1).

3.3.1. Calibration: matrix effects

Aqueous calibration, aqueous calibration matched with 75.0 mM Tris–HCl buffer solution at pH 7.4 and the standard addition technique were established for each element. The metal concentration levels were until 2000 μg l^{-1} for Al, Cu, Fe, Mn and Zn, and until 100 μg l^{-1} for Ba and Sr. The three calibration types were obtained three times for all elements, and the mean slopes were not found statistically significant different at a 95.0% of confidence interval (*t*-test). That means that there are not matrix effect and an aqueous calibration can be used to quantify metal binding MLPs.

3.3.2. Limit of detection and precision

The limit of detection (LOD) and the limit of quantification (LOQ) defined as follows

$$\mathrm{LOD} = 3\frac{\mathrm{S.D.}}{m}; \qquad \mathrm{LOQ} = 10\frac{\mathrm{S.D.}}{m}$$

where S.D. is the standard deviation corresponding to eleven replicates measurements of a blank (mobile phase), and *m* is the slope of the aqueous calibration graph, were calculated. The calculated LODs, referred to the wet mussel weight, were 81, 6, 10, 13, 30, 9 and 123 ng g^{-1} for Al, Ba, Cu, Fe, Mn, Sr and Zn, respectively, while the calculated LOQs, also referred to the wet mussel tissue, were 270, 20, 33, 43, 100, 30 and 410 ng g^{-1} for Al, Ba, Cu, Fe, Mn, Sr and Zn, respectively.

The repeatability of the over-all method was assessed by determining the amount of elements binding MLP-1 and MLP-2 isoforms in a mussel sample which was prepared as cytosol four times. Each cytosol was analyzed twice by the off line HPLC–ICP-OES method and results, expressed as relative standard deviation (R.S.D.), were 7, 13, 11, 12, 15, 6 and 16% for metal concentrations of 1.54, 0.37, 0.15, 0.40, 0.12, 6.4 and 0.16 μg g^{-1} of Al, Ba, Cu, Fe, Mn, Sr and Zn binding MLP-1 isoform, respectively.

3.3.3. Accuracy

Since there are not certified reference materials with certified concentrations for metals binding MTs or MLPs, validation of method was carried out by studying the analytical recovery. However, the performance of the analytical recovery implies the use of standards (metals binding MLPs), which are not available from mussels (there are only available MT-1 and MT-2 standards from rabbit liver with indicative values of Cd, Cu and Zn binding to MTs). Therefore, before performing analytical recovery studies, different volumes of MLP-1 and MLP-2 were isolated from mussel cytosols by anion exchange chromatography. The pools of the isolated MLP-1 and MLP-2 were used as standards for spiking fresh mussel tissue. Firstly, the amount of metal binding MLP-1 and MLP-2 were determined by the off line HPLC–ICP-OES method. Table 3 lists the concentrations of metals binding MLP-1 (the concentrations of metals binding MLP-2 were lower than the LODs). For spiking, volumes of 2.0 and 3.0 ml of the isolated MLP-1 isoform were added to different 5.0 g soft tissues subsamples directly into Stomacher bags and the MLPs extraction procedure, described in Section 2.3, was carried out. After cytosolic preparation, the mussel extracts were analyzed by the off line HPLC–ICP-OES method and the analytical recovery, defined as follows, was calculated.

$$\text{Analytical recovery}(\%) = \frac{[]_{\text{measured}}}{[]_{\text{added}}} \times 100$$

where $[]_{\text{measured}}$ is the concentration of metal binding MLP-1 determined after off line HPLC–ICP-OES and $[]_{\text{added}}$ is the concentration of metal binding MLP-1 added. Similarly, a mussel cytosol without spiking was prepared and the metals binding MLP-1 were determined. Each volume of metals binding MLP-1 "standard" and the mussel cytosol without spiking were prepared three times, and each cytosol was analyzed twice by the off line

Table 3
Mean analytical recoveries ($n = 6$) of the method

	Metal binding MLP-1 (mg l^{-1} [a])	Metal binding MLP-1 added (mg l^{-1})		Metal binding MLP-1 measured (mg l^{-1})		Analytical recovery (%)	
		2.0 ml[b]	3.0 ml[b]	2.0 ml[b]	3.0 ml[b]	2.0 ml	3.0 ml
Al	0.134	0.011	0.016	0.009	0.012	82	75
Ba	0.0092		0.0011	–[c]	0.0008	–[c]	76
Cu	0.053	0.004	0.006	0.003	0.004	75	60
Fe	0.393	0.031	0.047	0.034	0.037	108	79
Mn	0.063	0.005	0.008	0.005	0.007	100	96
Sr	0.172	0.014	0.021	0.015	0.018	110	86
Zn	0.566	0.045	0.068	0.029	0.045	64	66

[a] Concentration of metal binding MLP-1 in the MLP-1 "standard solution".
[b] Concentration of metal binding MLP-1 added (2.0 or 3.0 ml made up 25 ml after cytosol preparation).
[c] Not determined.

HPLC–ICP-OES method. Therefore, data in Table 3 are related to six independent determinations. Results indicate that analytical recoveries higher than 60% are obtained for all elements and they are close to 100% for Fe, Mn and Sr binding MLP-1. These implies good accuracy for the mussel cytosol preparation and off line HPLC–ICP-OES methods. Poor analytical recovery for some elements (Cu and Zn) can be attributed to the complexity of the experiment and the degradation of Cu and Zn binding MLPs during the experiment (spiking fresh mussel tissue with metal-binding MLPs, previously isolated from another mussel tissue). According with Wolf et al. [18,19], some metal binding MLPs, especially Zn-MLPs, are easily degraded by temperature and other environmental conditions. Since mussel tissue spiked with metals binding MLPs are subjected to a 60 °C treatment at some point of the cytosolic preparation procedure, degradation of some metal-MLPs complexes can be occurred.

Table 4
Levels of metal binding MLPs expressed as $\bar{x} \pm$ S.D. for four measurements

Element	Sample code	Concentration as μg g^{-1} (wet weight)	
		MLP-1 isoform	MLP-2 isoform
Al	1	<LOD (<0.08)	<LOD (0.270)
	2	0.70 ± 0.08	0.42 ± 0.05
	3	1.21 ± 0.11	0.81 ± 0.09
	4	0.85 ± 0.07	0.59 ± 0.07
	5	1.47 ± 0.15	0.72 ± 0.06
Ba	1	1.75 ± 0.13	0.99 ± 0.09
	2	1.65 ± 0.14	1.01 ± 0.08
	3	0.025 ± 0.002	0.88 ± 0.07
	4	0.029 ± 0.001	<LOD (0.02)
	5	0.056 ± 0.002	<LOD (0.02)
Cu	1	0.20 ± 0.02	0.19 ± 0.04
	2	0.12 ± 0.02	0.043 ± 0.008
	3	0.11 ± 0.03	0.070 ± 0.006
	4	0.14 ± 0.02	0.037 ± 0.005
	5	0.11 ± 0.03	<LOD (0.033)
Fe	1	0.43 ± 0.06	0.34 ± 0.05
	2	0.45 ± 0.08	<LOD (0.043)
	3	0.50 ± 0.06	<LOD (0.043)
	4	0.61 ± 0.05	<LOD (0.043)
	5	0.43 ± 0.06	<LOD (0.043)
Mn	1	0.21 ± 0.04	<LOD (0.100)
	2	0.15 ± 0.03	<LOD (0.100)
	3	0.067 ± 0.003	<LOD (0.100)
	4	0.17 ± 0.03	<LOD (0.100)
	5	0.086 ± 0.005	<LOD (0.100)
Sr	1	4.26 ± 0.23	0.27 ± 0.05
	2	4.60 ± 0.21	0.38 ± 0.06
	3	4.14 ± 0.18	0.46 ± 0.07
	4	5.29 ± 0.29	0.40 ± 0.06
	5	4.43 ± 0.17	0.33 ± 0.07
Zn	1	0.21 ± 0.03	<LOD (0.41)
	2	0.58 ± 0.08	<LOD (0.41)
	3	1.33 ± 0.10	0.63 ± 0.08
	4	0.68 ± 0.07	<LOD (0.41)
	5	0.91 ± 0.08	0.56 ± 0.07

3.4. Application

The developed method was applied to mussels (*M. galloprovincialis*) collected from mussel rafts at five different sampling sites along the Ría de Arousa estuary (Galicia, NW Spain). For each site a composite sample of about 30 mussels was prepared by pooling together specimens of different size, with shell lengths ranging from 3 to 7 cm. Each composite sample was prepared twice as mussel cytosol, and each mussel cytosol was chromatographied also twice. Table 4 lists the concentrations of metals binding MLP-1 and MLP-2 isoforms. It can be seen that all elements are mainly binding MLP-1 isoform, although low levels of Al, Ba, Fe and Sr have been found associated to MLP-2 isoform. Metals concentrations lower than the LODs of the method have been found for some samples, mainly for metals binding MLP-2 isoform.

4. Conclusions

The use of anion exchange-HPLC working in isocratic mode results in a fast MLPs chromatographic separation in mussel cytosols. Under optimum conditions (75 mM Tris–HCl buffer solution at pH 7.4 and flow rate at 0.8 ml min^{-1}) two MLP isoforms can be separated in 10 min, which is a short chromatographic time when comparing to previously published works (between 30 and 60 min). The hyphenation of HPLC and ICP-OES allows the determination of basal levels of Al, Ba, Cu, Fe, Mn, Sr and Zn binding MLPs in mussels, although more highly sensitive detection techniques are needed to measure basal lev-

els of other elements binding MLPs, such as Cd. However, the HPLC–ICP-OES method results feasible to determine basal levels of elements binding to MTs from rabbit liver.

Acknowledgements

The authors would like to thank the "Unidade de Control de Moluscos-Instituto de Acuicultura" at the University of Santiago de Compostela for providing mussel samples. S. S.-R would like to thank financial support provided by "Consellería de Educación e Ordenación Universitaria-Xunta de Galicia" for a doctoral grant.

References

[1] M.B. de la Calle Guntiñas, G. Bordin, A.R. Rodríguez, Anal. Bioanal. Chem. 374 (2002) 369.
[2] M. Nordberg, Talanta 46 (1998) 243.
[3] G. Roesijadi, B.A. Fowler, Meth. Enzymol. 205 (1991) 263.
[4] C. Porte, M. Sole, V. Borghi, M. Martínez, J. Chamorro, A. Torreblanca, M. Ortiz, A. Orbrea, M. Soto, M.P. Cajaraville, Biomarkers 6 (2001) 335.
[5] Y.Y. Mosleh, S. Paris-Palacios, F. Arnoult, M. Couderchet, G. Vernet, Comm. Agric. Appl. Biol. Sci. 68 (2003) 759.
[6] A. Viarengo, B. Burlando, F. Dondero, A. Marro, R. Fabbri, Biomarkers 4 (1999) 455.
[7] C.N. Ferrarello, M.R. Fernández de la Campa, C. Sariego-Muñiz, A. Sanz-Medel, Analyst 125 (2000) 2223.
[8] C.N. Ferrarello, M. Montes-Bayón, M.R. Fernández de la Campa, A. Sanz-Medel, J. Anal. At. Spectrom. 15 (2000) 1558.
[9] K.T. Suzuki, in: M.J. Stillman, C.F. Shaw III, K.T. Suzuki (Eds.), Metallothioneins. Synthesis, structure and properties of metallothioneins, phytochelatins and metal-thiolate complexes, VCH Publishers Inc., Weinheim, 1992, pp. 14–29.
[10] H. Chassaigne, R. Łobiński, Anal. Chem. 70 (1998) 2536.
[11] H. Chassaigne, R. Łobiński, J. Chromatogr. A 829 (1998) 127.
[12] S. Mounicou, K. Połeć, H. Chassaigne, M. Potin-Gautier, R. Łobiński, J. Anal. At. Spectrom. 15 (2000) 635.
[13] C.N. Ferrarello, M.R. Fernández de la Campa, H. Goenaga-Infante, M.L. Fernández-Sánchez, A. Sanz-Medel, Analysis 28 (2000) 351.
[14] A. Prange, D. Schaumlöffel, Anal. Bioanal. Chem. 374 (2002) 441.
[15] B. Deng, W.-T. Chan, Electrophoresis 22 (2001) 2186.
[16] K. Poleć, J. Szpunar, O. Palacios, P. González-Duarte, S. Atrian, R. Łobiński, J. Anal At. Spectrom. 16 (2001) 567.
[17] K. Poleć, O. García-Arribas, M. Pérez-Calvo, J. Szpunar, B. Ribas-Ozonas, R. Łobiński, J. Anal At. Spectrom. 15 (2000) 1363.
[18] C. Wolf, U. Rösick, P. Brätter, Fresenius'J. Anal. Chem. 368 (2000) 839.
[19] C. Wolf, U. Rösick, P. Brätter, Anal. Bional. Chem. 372 (2002) 491.
[20] K.A. High, B.A. Methven, J.W. McLaren, K.W.M. Siu, J. Wang, J.F. Klaverkamp, J.S. Blais, Fresenius'J. Anal. Chem. 351 (1995) 393.
[21] R. Santamaría-Fernández, S. Santiago-Rivas, A. Moreda-Piñeiro, A. Bermejo-Barrera, P. Bermejo-Barrera, S.J. Hill, At. Spectrosc. 25 (2004) 37.
[22] K.E. Ødegård, W. Luna, J. Anal. At. Spectrom. 12 (1997) 403.

Available online at www.sciencedirect.com
ScienceDirect
Talanta 71 (2007) 1696–1702
Talanta
www.elsevier.com/locate/talanta

Determination of methylmercury and inorganic mercury in water samples by slurry sampling cold vapor atomic absorption spectrometry in a flow injection system after preconcentration on silica C_{18} modified

Susana Río Segade [a,*], Julian F. Tyson [b]

[a] *Estación de Viticultura y Enología de Galicia, Ponte San Clodio s/n, Leiro, 32427-Ourense, Spain*
[b] *Department of Chemistry, University of Massachusetts, Amherst, MA 01003, USA*

Received 31 March 2006; received in revised form 30 July 2006; accepted 1 August 2006
Available online 15 September 2006

Abstract

A novel method for preconcentration of methylmercury and inorganic mercury from water samples was developed involving the determination of ng l^{-1} levels of analytes retained on the silica C_{18} solid sorbent, previous complexation with ammonium pyrrolidine dithiocarbamate (APDC), by slurry sampling cold vapor atomic absorption spectrometry (SS-CVAAS) in a flow injection (FI) system. Several variables were optimized affecting either the retention of both mercury species, such as APDC concentration, silica C_{18} amount, agitation times, or their determination, including hydrochloric acid concentration in the suspension medium, peristaltic pump speed and argon flow-rate. A Plackett–Burman saturated factorial design permitted to differentiate the influential parameters on the preconcentration efficiency, which were after optimized by the sequential simplex method. The contact time between mercury containing solution and APDC, required to reach an efficient sorption, was decreased from 26 to 3 min by the use of sonication stirring instead of magnetic stirring. The use of 1 mol dm^{-3} hydrochloric acid suspension medium and 0.75% (m/v) sodium borohydride reducing agent permitted the selective determination of methylmercury. The combination of 5 mol dm^{-3} hydrochloric acid and 10^{-4}% (m/v) sodium borohydride was used for the selective determination of inorganic mercury. The detection limits achieved for methylmercury and inorganic mercury determination under optimum conditions were 0.96 and 0.25 ng l^{-1}, respectively. The reliability of the proposed method for the determination of both mercury species in waters was checked by the analysis of samples spiked with known concentrations of methylmercury and inorganic mercury; quantitative recoveries were obtained.

Keywords: Preconcentration; Mercury speciation; Water samples; Flow injection; Slurry sampling cold vapor atomic absorption spectrometry

1. Introduction

Mercury species, usually present in natural water samples, are inorganic mercury and methylmercury. Mercury speciation in these samples is of great environmental importance nowadays due to the high toxicity of mercury compounds and their low concentrations, especially when methylmercury is present. Cold vapor (CV) atomic absorption spectrometry (AAS) is one of the most attractive techniques for total mercury determination in environmental and biological samples due to its high sensitivity and reliability [1]. However, this determination at trace amounts requires a preliminary preconcentration step in order to achieve quantifiable levels.

Although different approaches have been proposed for mercury determinations at trace levels by CVAAS, the recent developments in the field of the preconcentration of mercury compounds from several samples are focused to on-line solid-phase extraction (SPE) in flow injection (FI) systems by the use of a minicolumn. A diversity of combinations between solid sorbent and complexing agent have been employed for preconcentration of both inorganic mercury and methylmercury: (i) on-line formation of mercury diethyldithiocarbamates on silica C_{18} and quantitative elution of the retained chelates with ethanol [2,3]; (ii) chelation with dithiophosphoric acid diacyl ester (DDTP), adsorption of the corresponding chelates on a C_{18} column and elution with ethanol [4]; (iii) sorption of the mercury complexes formed with ammonium pyrrolidine

* Corresponding author. Tel.: +34 988 488033; fax: +34 988 488191.
E-mail address: evegadoc2@cesga.es (S.R. Segade).

0039-9140/$ – see front matter © 2006 Elsevier B.V. All rights reserved.
doi:10.1016/j.talanta.2006.08.006

dithiocarbamate (APDC) on silica C_{18}, which were after eluted with a methanol–acetonitrile–water mixture [5].

Several complexing solid sorbents have been applied to on-line preconcentration of mercury species from natural water samples using different detection techniques [2,3,6,7]. Thus, sulphydryl cotton permitted to retain methylmercury, ethylmercury and inorganic mercury, which were then eluted with 3 mol dm^{-3} hydrochloric acid [6,7]. Emteborg et al. [8] incorporated a microcolumn of dithiocarbamate resin in a FI system to preconcentrate mercury species, being used acidic thiourea as eluent. On the other hand, mercury compounds were preconcentrated on a column containing 2-mercaptobenzimidazol loaded on silica gel and then quantitatively eluted with 0.05 mol dm^{-3} potassium cyanide or 2 mol dm^{-3} hydrochloric acid for inorganic mercury or methylmercury, respectively [9].

Several authors have also proposed off-line enrichment of mercury species on complexing resins. Emteborg et al. [10–12] introduced in natural water samples the complexing resin, prepared by immobilization of dithiocarbamate functional groups on macroporous hydroxyethylmethacrylate spheres, and the suspension was stirred, whereafter the samples were filtered. Mercury species were extracted with acidified thiourea. Determination of inorganic mercury and organomercury compounds was also carried out after preconcentration on dithizone-anchored poly(ethylene glycol dimethacrylate–hydroxyethylmethacrylate) microbeads, when the desorption medium was a mixture of copper sulphate and acidic potassium bromide for organomercury species or dilute nitric acid for inorganic mercury [13]. However, the possibility of direct determination of mercury compounds adsorbed on solid sorbent by slurry sampling (SS) has been investigated. One of the most important advantages of the SS technique is the elimination of the desorption step. So, total mercury was determined in natural gas liquid and condensate using activated carbon by electrothermal (ET)AAS [14]. Phenylmercury was selectively preconcentrated from water samples by living *Escherichia coli* and the amount of organomercury specie retained was determined directly in the biomass slurry by CVAAS [15].

Inorganic mercury and total mercury were quantitatively extracted and, afterwards, determined in biological and environmental solid samples by FI-CVAAS using 10^{-4} and 0.75% (m/v) sodium borohydride reducing agent, respectively [16]. Then, this methodology was successfully applied to mercury speciation analysis in fish tissue samples by slurry sampling technique [17]. In the last work, methylmercury was selectively determined when solid samples were suspended in a selective extraction medium for this mercury specie, such as 1 mol dm^{-3} hydrochloric acid, and sodium borohydride concentration was equal to or less than 0.1% (m/v) due to its inability to reduce mercury occluded into the solid particles. Selective determination of inorganic mercury required the suspension of the solid samples in hydrochloric acid concentrations higher than 4 mol dm^{-3} and the use of reducing agent concentrations equal to or less than 0.05% (m/v) because of its inability to reduce methylmercury.

The low concentrations of the most commonly found mercury species in environmental waters (methylmercury and inorganic mercury) led to investigate the possible determination of both mercury species by slurry sampling technique in a FI-CVAAS system after preconcentration on a solid sorbent. In this sense, the present work combines the advantages of enrichment and the slurry sampling techniques for mercury speciation at ng l^{-1} concentrations. The introduction of slurried sorbents into FI systems has not been previously reported for mercury speciation analysis by cold vapor generation technique. In this work, silica C_{18} and APDC were the solid sorbent and complexing agent, respectively. The reaction of mercury species with complexing agents is highly dependent on the sample pH. Nevertheless, previous studies tested little effect of pH values varying from 3 to 9 on mercury recovery. The preconcentration parameters were after optimized by the sequential simplex method. Furthermore, the advantages of the use of ultrasonic energy during sorption step were investigated in order to facilitate the solid-phase extraction process and to reduce the time involved. Following sorption, the solid sorbent was suspended in hydrochloric acid concentrations ranging from 1 to 5 mol dm^{-3}, containing Triton X-100 as dispersing agent. Although the differentiation between total mercury and inorganic mercury was based on sodium borohydride reducing agent concentration (10^{-4} and 0.75% (m/v) for inorganic mercury and total mercury determinations, respectively), the possibility of separate determination of methylmercury and inorganic mercury was also studied. The proposed methodology was applied to the analysis of spiked water samples.

2. Experimental

2.1. Instrumentation

A Perkin-Elmer flow injection mercury system (FIMS) Model 400 (Überlingen, Germany), equipped with a flow injection analysis system (FIAS) and an autosampler Model AS-91, was used for all mercury determinations. This system consisted of two peristaltic pumps (P_1 and P_2), a flow-meter, a cylindrical gas–liquid separator partially filled with glass beads, a six-way injection valve equipped with a sample loop and a quartz cell (25 cm length with quartz windows). The slurry was injected into the system during certain time, while it was being stirred, and transported in an acid carrier to the chemifold where it was mixed with the sodium borohydride reducing agent along a reduction coil of 5.0 cm (R_1). Then, mercury vapor was purged from the liquid-phase along a stripping coil of 15 cm (R_2) with an argon stream of 40 ml min^{-1}, before its entrance into the gas–liquid separator and then swept into the quartz cell.

The peristaltic pumps, injection time and data acquisition were controlled through Perkin-Elmer AAWinLab Atomic absorption spectroscopy software (Norwalk, CT, USA). The FIAS program used for all mercury determinations is shown in Table 1. The sample loop (500 μl) was filled by means of pump P_2. The acid carrier, reducing agent and waste solution from the gas–liquid separator were pumped using peristaltic pump P_2 through Tygon tubes and the waste solution from the injection valve was pumped with a peristaltic pump P_1 also through a Tygon tube. The flow injection manifold is shown in Fig. 1. Acid carrier flow-rates were 5.5 and 9.5 ml min^{-1} for inorganic mercury and total mercury determination, respectively.

Table 1
FIAS 400 program for mercury determination

Step	Time (s)	P_1 speed (rpm)	P_2 speed (rpm)	Valve position	Read
Prefill	15	100	120	Fill	No
1	10	100	120	Fill	No
2	15	0	120	Inject	Yes
3	0	–	–	Fill	No

Reducing agent flow-rates were 4.0 and 6.5 ml min^{-1} for inorganic mercury and total mercury determination, respectively. The manifold tubing was made of 1.0 mm i.d. Teflon (FEP). An integration time of 20 s and peak height measurement mode were used.

A Fisher Scientific magnetic stirrer (Fair Lawn, NJ, USA), a Sonics and Materials sonication probe Model VC50S (Danbury, CT, USA) with 20 kHz and 50 W, a Fisher Scientific centrifuge and a Fisher Scientific pHmeter Model 915 were used for enrichment purposes. MultiSimplex KB software (Karls Krona, Sweden) was used for the optimization of preconcentration method.

2.2. Reagents, standards and samples

All solutions were prepared in deionized water produced by a Barnstead E-Pure system and the chemicals used were of analytical-reagent grade. The 10^{-4} and 0.75% (m/v) solutions of sodium borohydride reducing agent for inorganic mercury and total mercury determination was prepared daily by dissolution of the appropriate amount of the solid reagent (Alfa Aesar, Ward Hill, MA, USA) in a 0.001 and 1.0% (m/v) sodium hydroxide solution, respectively. The carrier was 3.0% (v/v) hydrochloric acid. The stock standard solution of mercury nitrate (1000 mg l^{-1}), was supplied by Alfa Aesar. The stock standard solution of methylmercury chloride (100 mg l^{-1}), was prepared by dissolving the appropriate amount of the solid reagent from Strem Chemicals (Newburyport, MA, USA) in a minimum volume of methanol and diluting it to volume with deionized water. The working standard solutions for each individual mercury species were prepared daily by appropriately diluting the 10 mg l^{-1} (as Hg) standard solutions, prepared weekly, with dilute hydrochloric acid. All standards were stored at 4 °C away from light before use.

Drinking and pond water samples were filtered through 0.45 μm membranes from Millipore (Bedford, MA, USA).

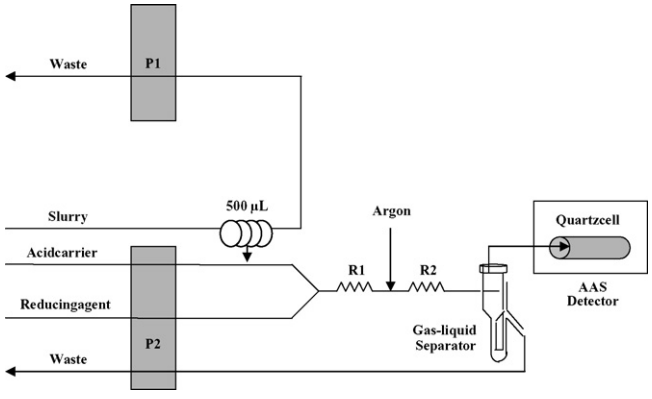

Fig. 1. Flow injection manifold used for mercury determinations. P_1 and P_2 are peristaltic pumps; R_1 and R_2 are reaction coils.

2.3. Preconcentration procedure

A sample volume of 90 ml was introduced in a polyethylene centrifuge tube. Then, pH was adjusted to values comprised between 3 and 9, and the appropriate amount of APDC was added in order to achieve a concentration of 0.0041 mol dm^{-3}. The mixture was magnetically stirred during 26 min or sonicated during 3 min at 50% power in order to improve the complexes formation. Then, 37.4 mg of silica C_{18} were suspended and the resulting suspension was magnetically stirred for 30 min to achieve an efficient retention of mercury species on solid sorbent. The solid particles were separated by centrifugation during 5 min at 5000 rpm. Then, they were slurried in 10 ml of 1 or 5 mol dm^{-3} hydrochloric acid (containing 0.02% (v/v) Triton X-100 as dispersing agent) for methylmercury determination or inorganic and total mercury determination, respectively. The slurries were magnetically stirred for 10 min to obtain a homogeneous dispersion and maintained under magnetic stirring during the injection into the FI system. Blanks were prepared with the same reagents undergoing a similar treatment.

2.4. Plackett–Burman design

The Plackett–Burman fractional factorial design was used to estimate the influence of some variables on preconcentration efficiency of mercury species. The concentration used of methylmercury and inorganic mercury was 0.5 μg l^{-1}. A design for seven factors (Table 2) was selected using as many columns as variables studied. Therefore, only eight experiments were carried out by three replicates. The variables investigated with their factor designators and the lower (−) and upper (+) levels for each one of them are shown in Table 3. The response was concentration recovered of inorganic mercury and total mercury using 10^{-4} and 0.75% (m/v) sodium borohydride reducing agent, respectively. A variable was considered as significant when the difference between the mean value of the results obtained for upper and lower levels was higher than the double of the mean standard deviation.

Table 2
Plackett–Burman design

Experiment	A	B	C	D	E	F	G
1	+	+	+	−	+	−	−
2	+	+	−	+	−	−	+
3	+	−	+	−	−	+	+
4	−	+	−	−	+	+	+
5	+	−	−	+	+	+	−
6	−	−	+	+	+	−	+
7	−	+	+	+	−	+	−
8	−	−	−	−	−	−	−

2.5. Sequential simplex method

Only the significant variables were after optimized by using the sequential simplex method. The optimal experimental conditions were: maximum recovery for methylmercury and inorganic mercury using 5 mol dm^{-3} hydrochloric acid, maximum recovery for methylmercury when 1 mol dm^{-3} hydrochloric acid was used and minimum recovery for inorganic mercury using 1 mol dm^{-3} hydrochloric acid. The response variables evaluated were the concentration recovered of methylmercury and inorganic mercury for a 0.5 $\mu g\,l^{-1}$ standard aqueous solution. The experiments were performed in three replicates.

3. Results and discussion

3.1. Factor screening

The main effect of the different factors for inorganic mercury and total mercury determination by SS in a FI-CVAAS system after preconcentration on silica C_{18} modified with APDC complexing agent was checked using a Plackett–Burman saturated factorial design. As shown in Table 3, the first four factors were related to the enrichment procedure, the other three to determination of mercury retained. So, it was possible to detect the most significant variables by performing few experiments (k factors were studied in $k+1$ runs). The results obtained are shown in Fig. 2, which indicated: agitation time with APDC, silica C_{18} amount, agitation time with silica C_{18}, P_2 speed and argon flow-rate were significant variables for methylmercury determination as total mercury (using 0.75% (m/v) sodium borohydride reducing agent; see Fig. 2a); APDC concentration, hydrochloric acid concentration and argon flow-rate gave significant effects for inorganic mercury determination as total mercury (using 0.75% (m/v) sodium borohydride reducing agent; see Fig. 2b); and silica C_{18} amount, hydrochloric acid concentration and P_2 speed were significant variables for inorganic mercury determination (using 10^{-4}% (m/v) sodium borohydride reducing agent; see Fig. 2c). However, hydrochloric acid concentration, P_2 speed and argon flow-rate were fixed at 1 or 5 mol dm^{-3} for methylmercury or inorganic mercury determination, 120 rpm and 40 ml min^{-1}, respectively, due to the similar influence observed in all figures: positive for hydrochloric acid concentration in inorganic mercury determination and P_2 speed; or negative for hydrochloric acid concentration in methylmercury determination and argon flow-rate.

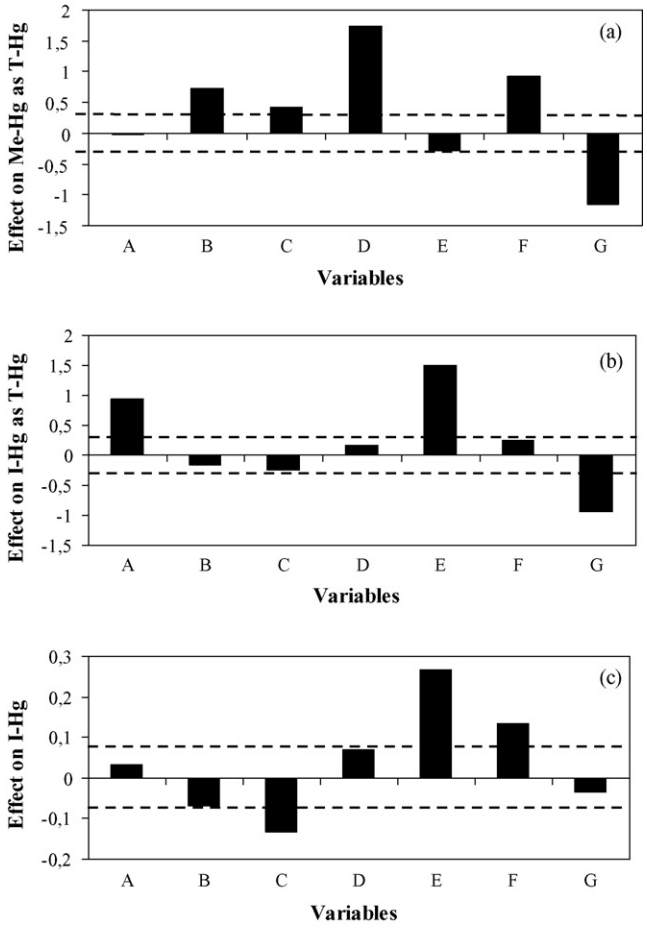

Fig. 2. Effect of the different variables in the determination of methylmercury as total mercury (a), inorganic mercury as total mercury (b) and inorganic mercury (c) by SS in a FI-CVAAS system after preconcentration on silica C_{18} modified with APDC complexing agent, using a Plackett–Burman saturated factorial design. The effect was calculated as the difference between the mean value of the results obtained for upper and lower levels. Dashed lines show double of the mean standard deviation.

Table 3
Variables studied for mercury species preconcentration

Variable	Factor	Lower level (−)	Upper level (+)
APDC concentration (mol dm^{-3})	A	0.001	0.005
Agitation time with APDC (min)	B	0	30
Silica C_{18} amount (mg)	C	10	50
Agitation time with silica C_{18} (min)	D	1	30
Hydrochloric acid concentration (mol dm^{-3})	E	1	5
P_2 speed (rpm)	F	75	120
Argon flow-rate (ml min^{-1})	G	40	75

3.2. Optimization of the experimental conditions

The sequential simplex method was used to optimize the influential variables that were not previously selected, including APDC concentration, agitation time with APDC, silica C_{18} amount and agitation time with silica C_{18}. The step size and reference value for each variable are presented in Table 4. The simplex progressed towards the optimum recovery for

Table 4
Step size and reference value of the optimized variables

Variable	Step size	Reference value
APDC concentration (mol dm^{-3})	0.0020	0.0050
Agitation time with APDC (min)	10	15
Silica C_{18} amount (mg)	20.0	20.0
Agitation time with silica C_{18} (min)	20	30

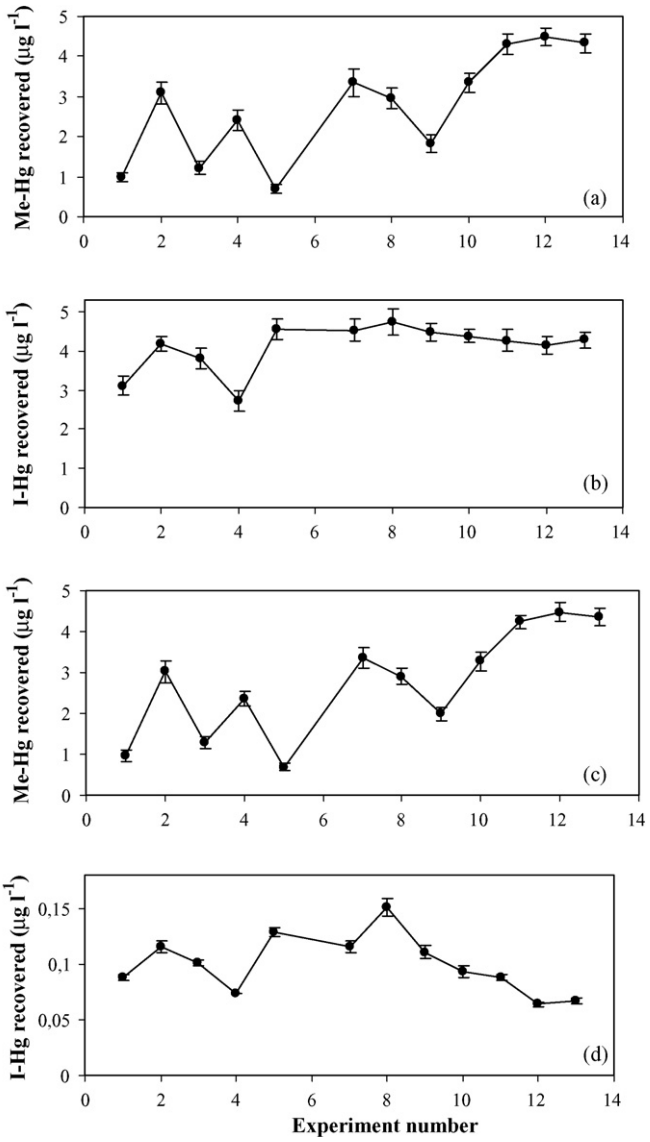

Fig. 3. Evolution of concentration recovered along the sequential simplex method of methylmercury using 5 mol dm^{-3} hydrochloric acid (a), inorganic mercury using 5 mol dm^{-3} hydrochloric acid (b), methylmercury using 1 mol dm^{-3} hydrochloric acid (c) and inorganic mercury using 1 mol dm^{-3} hydrochloric acid (d). Mercury concentration was determined by SS in a FI-CVAAS system involving 0.75% (m/v) sodium borohydride reducing agent, after preconcentration on silica C_{18} modified with APDC complexing agent.

methylmercury and inorganic mercury using 1 and 5 mol dm^{-3} hydrochloric acid. Fig. 3 shows the evolution of the responses along 12 experiments. The experiment 6 was not carried out because the software proposed to avoid silica C_{18}. The simplex stopped when three consecutive experiments led to no significantly different response. The greatest similitude found between the evolution of both variables studied and response values corresponded to: (i) methylmercury recovery and silica C_{18} amount; (ii) inorganic mercury recovery and APDC concentration. Taking into account the response values obtained, the optimized experimental variables were 0.0041 mol dm^{-3} APDC with a magnetic stirring time of 26 min and 37.4 mg of silica C_{18} with magnetic stirring for 30 min. Methylmercury and inorganic mercury form charged complexes with the chloride ion $MeHgCl_2^-$ and $HgCl_4^{2-}$, respectively. So, an increase of hydrochloric acid concentration promotes the $HgCl_4^{2-}$ formation. Furthermore, an incomplete desorption of methylmercury using 1 mol dm^{-3} hydrochloric acid should be compensated with a little attack of 0.75% (m/v) sodium borohydride reducing agent on methylmercury retained on the solid particles. Previous studies, developed in our laboratory, revealed that the complexes formed between methylmercury and APDC are more easily reducible (36%) than those corresponding to inorganic mercury.

3.3. Ultrasound-assisted sorption step

Magnetic and sonication stirrings were compared in order to reduce the time involved in the sorption step, including complexation reaction between mercury species and APDC complexing agent and, afterwards, retention on silica C_{18} of the complexes formed. First, the power and time of sonication were optimized for the complexes formation phase. The concentration recovered of inorganic mercury was quantitative for sonication power and sonication time values of 50% and 3 min, respectively. Inorganic mercury recovery increased with sonication time for times less than 3 min and sonication powers comprised between 50 and 75%. However, the use of sonication times higher than 3 min had an opposite effect. On the other hand, this recovery also increased when the sonication power was increased from 30 to 50%, while it decreased when the sonication power was increased from 50 to 75%. Although no significant effect was found for methylmercury when both sonication parameters were modified, the concentration recovered of methylmercury was also quantitative in all experiments. Therefore, sonication power and sonication time values of 50% and 3 min, respectively, were selected for further studies.

The power and time of sonication were also optimized for the effective retention of the complexes on silica C_{18}. Sonication power had an opposite effect for methylmercury and inorganic mercury determinations. While concentration recovered of inorganic mercury decreased when sonication power was increased, concentration recovered of methylmercury increased when sonication power was increased from 30 to 50% and it decreased for power values higher than 50%. Nevertheless, all recoveries investigated were less than 32%. Furthermore, the sonication time had no effect on the recoveries studied. So, magnetic stirring was selected for the performance of this second phase of the sorption step in further experiments.

3.4. Analytical figures of merit

The analytical performance of the proposed off-line preconcentration and slurry sampling methodology in a FI-CVAAS system was evaluated using the optimum experimental conditions. Linear calibration curves were achieved by the treatment of a series of methylmercury and inorganic mercury standards of up to 1.0 μg l^{-1}, because of the enrichment was not efficient when higher mercury concentrations were used. So, recoveries of 58.9 ± 2.8, 72.8 ± 2.8, 55.5 ± 2.4 and 78.9 ± 4.4% were found for the determination of 2 μg l^{-1} methylmercury as total

mercury (using 5 mol dm^{-3} hydrochloric acid and 0.75% (m/v) sodium borohydride reducing agent), inorganic mercury as total mercury (using 5 mol dm^{-3} hydrochloric acid and 0.75% (m/v) sodium borohydride reducing agent), methylmercury (using 1 mol dm^{-3} hydrochloric acid and 0.75% (m/v) sodium borohydride reducing agent) and inorganic mercury (using 5 mol dm^{-3} hydrochloric acid and 10^{-4}% (m/v) sodium borohydride reducing agent), respectively. The slopes obtained for the calibration lines, expressed as mean value ± standard deviation ($n = 3$), were 0.149 ± 0.006, 0.146 ± 0.004, 0.145 ± 0.006 and 0.199 ± 0.010 l μg^{-1} for the determination of methylmercury as total mercury, inorganic mercury as total mercury, methylmercury and inorganic mercury, respectively. The correlation coefficient (r) was always higher than 0.9997. As expected, the slopes of the calibration lines for total mercury determination obtained with methylmercury and inorganic mercury standards were not significantly different (t-test, $P = 0.05$). Furthermore, the slope of the calibration line for inorganic mercury determination was greater than that corresponding to total mercury and methylmercury determination. The detection limit based on the amount necessary to yield a net signal equal to three times the standard deviation of the blank was 2.6, 2.6 and 0.48 ng l^{-1} for total mercury, methylmercury and inorganic mercury, respectively. The best detection limit corresponded to inorganic mercury determination because of the use of a little concentration of sodium borohydride. The precision, expressed as the relative standard deviation ($n = 10$) for a 0.50 $\mu g\, l^{-1}$ mercury standard was less than 3% for all mercury determinations.

It should be noted that the detection limits obtained by the proposed method are comparable to those reported for other preconcentration approaches of mercury species based on: (i) on-line SPE in FI systems by the use of a minicolumn filled with complexing solid sorbent, with detection limits of 16 ng l^{-1} [2] or 10 ng l^{-1} [4] when CVAAS was used as detection technique; and 6 ng l^{-1} for methylmercury determination [6], or 0.07 and 0.05 ng l^{-1} for inorganic mercury and methylmercury determination, respectively [9], when CVAFS was the detection technique employed; (ii) off-line enrichment on complexing resins; (iii) retention on solid sorbent and slurry sampling technique with a detection limit of 2000 ng l^{-1} for total mercury determination by ETAAS [14], or 50 ng l^{-1} for phenylmercury determination by CVAAS [15]. As can be seen the lowest detection limits not only corresponded to the use of more sensitive detection techniques, such as CVAFS, but also to the great sample volume required (1 l).

With the aim of decreasing the detection limits, the effect of different sample volumes containing the same amount (45 ng) of both analytes on the recovery of mercury species was investigated. The results obtained offered the use of sample volumes of up to 270 and 180 ml for methylmercury and inorganic mercury determination, respectively, achieving recoveries higher than 92%. Therefore, the detection limits decreased to 0.96 and 0.25 ng l^{-1} for methylmercury and inorganic mercury determination, respectively.

3.5. Determination of methylmercury, inorganic mercury and total mercury in spiked water samples

The developed method was applied to the analysis of water samples. As the concentration of methylmercury and inorganic mercury was not detectable in these samples, the accuracy of the proposed method for mercury speciation in water samples was checked by the analysis of deionized water in the presence of interfering ions (0.1 mg l^{-1} of Al^{3+}, Co^{2+}, Cr^{3+}, Cu^{2+}, Fe^{3+}, Mn^{2+}, Ni^{2+}, Pb^{2+} and Zn^{2+}; 10 mg l^{-1} of K^+ and Mg^{2+}; 50 mg l^{-1} of Ca^{2+}; 100 mg l^{-1} of Na^+; 25 mg l^{-1} of Cl^- and $SO_4{}^{2-}$; and, finally, 300 mg l^{-1} of $HCO_3{}^-$), drinking water and pond water samples; all of them spiked with different concentrations of methylmercury and inorganic mercury (30–90 ng l^{-1}). The results obtained can be seen in Table 5, showing that the recovery values were greater than 95% for methylmercury, inorganic mercury and total mercury determinations. The relative

Table 5
Determination of methylmercury, inorganic mercury and total mercury in spiked water samples

Mercury added (ng l^{-1})	Me-Hg recovered (ng l^{-1})[a]	I-Hg recovered (ng l^{-1})[a]	T-Hg recovered (ng l^{-1})[a]
Deionized water containing interfering ions			
0	<LOD	<LOD	<LOD
30 (Hg^{2+}) + 30 ($MeHg^+$)	30 ± 3	29 ± 2	62 ± 4
60 (Hg^{2+}) + 60 ($MeHg^+$)	58 ± 4	59 ± 2	115 ± 7
90 (Hg^{2+}) + 90 ($MeHg^+$)	87 ± 4	86 ± 4	176 ± 8
Drinking water			
0	<LOD	<LOD	<LOD
30 (Hg^{2+}) + 30 ($MeHg^+$)	30 ± 3	30 ± 2	60 ± 5
60 (Hg^{2+}) + 60 ($MeHg^+$)	58 ± 5	58 ± 3	119 ± 9
90 (Hg^{2+}) + 90 ($MeHg^+$)	87 ± 5	87 ± 5	173 ± 12
Pond water			
0	<LOD	<LOD	<LOD
30 (Hg^{2+}) + 30 ($MeHg^+$)	29 ± 3	30 ± 2	59 ± 6
60 (Hg^{2+}) + 60 ($MeHg^+$)	58 ± 4	58 ± 3	116 ± 8
90 (Hg^{2+}) + 90 ($MeHg^+$)	86 ± 6	87 ± 5	172 ± 10

[a] Mean value ± standard deviation ($n = 3$).

standard deviations for three replicate samples submitted to the same spiking, treatment and detection procedures were less than 10%. Therefore, both the accuracy and precision were satisfactory.

4. Conclusions

The direct introduction of slurried solid sorbent into a FI system for mercury speciation analysis by CV generation technique combined with AAS has successfully permitted the determination of ng l^{-1} levels of methylmercury and inorganic mercury in water samples, previously complexed with APDC and retained on silica C_{18}. All variables involved in the steps of mercury preconcentration and slurry analysis were optimized by the sequential simplex method, which provided a viable option for this purpose when the experimental parameters to optimize were previously chosen by a Plackett–Burman saturated factorial design. On the other hand, sonication stirring resulted to be a valuable alternative to magnetic stirring for achieving efficient complexation between mercury species and APDC in much less time. Thus, the time-consuming step was sorption of the complexes on the silica C_{18} sorbent. The detection limits obtained for methylmercury and inorganic mercury were comparable to the majority of the previously reported, including those related to other more sensitive detection techniques, such as CVAFS. The main advantage of this method is its inexpensive instrumentation along with a relatively good sensitivity and precision. The applicability of the proposed methodology to the determination of both mercury species in water samples was demonstrated.

Acknowledgments

Two grants supplied by Xunta de Galicia and Universidad de Vigo are gratefully acknowledged by S. Río Segade.

References

[1] B. Welz, M. Sperling, Atomic Absorption Spectrometry, 3rd ed., Wiley, Weinheim, 1999.
[2] M. Fernández García, R. Pereiro García, N. Bordel García, A. Sanz Medel, Talanta 41 (1994) 1833.
[3] R. Martínez Blanco, M. Tagle Villanueva, J.E. Sánchez Uría, A. Sanz-Medel, Anal. Chim. Acta 419 (2000) 137.
[4] A.C.P. Monteiro, L.S.N. de Andrade, R.C. de Campos, Fresenius J. Anal. Chem. 371 (2001) 353.
[5] X. Yin, W. Frech, E. Hoffmann, C. Lüdke, J. Skole, Fresenius J. Anal. Chem. 361 (1998) 761.
[6] J. Wei, C.W. McLeod, Talanta 39 (1992) 1537.
[7] M.L. Mena, C.W. McLeod, P. Jones, A. Withers, V. Minganti, R. Capelli, P. Quevauviller, Fresenius J. Anal. Chem. 351 (1995) 456.
[8] H. Emteborg, D.C. Baxter, W. Frech, Analyst 118 (1993) 1007.
[9] H. Bagheri, A. Gholami, Talanta 55 (2001) 1141.
[10] S. Hänström, C. Briche, H. Emteborg, D.C. Baxter, Analyst 121 (1996) 1657.
[11] H. Emteborg, D.C. Baxter, M. Sharp, W. Frech, Analyst 120 (1995) 69.
[12] H. Emteborg, H.-W. Sinemus, B. Radziuk, D.C. Baxter, W. Frech, Spectrochim. Acta B 51 (1996) 829.
[13] B. Salih, R. Say, A. Denizli, O. Genc, E. Piskin, Anal. Chim. Acta 371 (1998) 177.
[14] J. Shiowatana, A. Siripinyanond, W. Waiyawat, S. Nilmanee, Atom. Spectrosc. 20 (1999) 224.
[15] L.C. Robles, J.C. Feo, A.J. Aller, Anal. Chim. Acta 423 (2000) 255.
[16] S. Río Segade, J.F. Tyson, Spectrochim. Acta 58B (2003) 797.
[17] S. Río Segade, J.F. Tyson, J. Anal. Atom. Spectrom. 18 (2003) 268.

Available online at www.sciencedirect.com
ScienceDirect
Talanta 71 (2007) 1679–1683
Talanta
www.elsevier.com/locate/talanta

A combination of modified particle swarm optimization algorithm and support vector machine for gene selection and tumor classification

Qi Shen [a,b,*], Wei-Min Shi [a], Wei Kong [a], Bao-Xian Ye [a]

[a] *Chemistry Department, Zhengzhou University, Zhengzhou 450052, China*
[b] *State Key Laboratory of Chemo/Biosensing and Chemometrics, College of Chemistry and Chemical Engineering, Hunan University, Changsha 410082, China*

Received 26 April 2006; received in revised form 6 July 2006; accepted 27 July 2006
Available online 1 September 2006

Abstract

In the analysis of gene expression profiles, the number of tissue samples with genes expression levels available is usually small compared with the number of genes. This can lead either to possible overfitting or even to a complete failure in analysis of microarray data. The selection of genes that are really indicative of the tissue classification concerned is becoming one of the key steps in microarray studies. In the present paper, we have combined the modified discrete particle swarm optimization (PSO) and support vector machines (SVM) for tumor classification. The modified discrete PSO is applied to select genes, while SVM is used as the classifier or the evaluator. The proposed approach is used to the microarray data of 22 normal and 40 colon tumor tissues and showed good prediction performance. It has been demonstrated that the modified PSO is a useful tool for gene selection and mining high dimension data.

Keywords: Particle swarm optimization; Support vector machine; Gene selection; Gene expression data

1. Introduction

The development of microarray technology is creating a wealth of gene expression data and brings about a revolution in biological and medical research [1]. Thousands even tens of thousands of genes expression levels could be monitored simultaneously in microarray technology [2,3]. In the analysis of gene expression profiles, the number of tissue samples with genes expression levels available is usually small compared with the number of genes. This can lead either to possible overfitting and dimensional curse or even to a complete failure in analysis of microarray data. Most of the genes monitored in microarray may not be relevant to classification and these genes may potentially degrade the prediction performance of data analysis by masking the contribution of the relevant genes [4–7]. The selection of genes that are really indicative of the tissue classification concerned is becoming one of the key steps in microarray studies. The benefit gained from gene selection in microarray data analysis is not only the stability of the analysis model, but also the biological interpretability of relationship between the genes and a complex biological phenomenon. Large numbers of features also increase computational complexity and cost. Therefore, reducing the dimensionality of the gene expression information is a key step in developing a successful gene expression-based data analysis system.

Various clustering, classification, and prediction techniques have been used to analyze and understand the gene expression data resulted from DNA microarray, such as Fisher discriminant analysis, artificial neural networks and support vector machine (SVM). SVM has been found useful in handling classification tasks in case of the high dimensionality and sparsity of data points and has been recommended as an popular approach to efficiently treating this particular data structure [8–11]. However, there is increasing evidence that gene selection is also essential for successful SVM analysis of microarray data and the lack of gene selection also can spoil the SVM performance [12,13]. Results of SVM analysis might not be improved when using excess of genes. It has been recognized that the elimina-

* Corresponding author: Tel.: +86 371 67767957; fax: +86 371 67763220.
E-mail address: shenqi@zzu.edu.cn (Q. Shen).

0039-9140/$ – see front matter © 2006 Elsevier B.V. All rights reserved.
doi:10.1016/j.talanta.2006.07.047

tion of uninformative genes which do not contribute to model formulation is of importance in microarray data analysis even in situations when SVM is applied.

For the gene selections, one can use filtering approach such as t test and nonparametric scoring, as well as some more sophisticated methodologies such as genetic algorithms (GAs) and evolution algorithm (EAs) [14–19]. Among them, GAs and EAs are optimization techniques simulating biological systems which are classified as a category of the research of so-called artificial life. Particle swarm optimization (PSO) algorithm [20–22], a relatively new optimization technique in this category, can also be used as an excellent optimizer which originated as a simulation of simplified social system. Similar to GAs and EAs, PSO is a population based optimization tool, which search for optima by updating generations. However, unlike GAs and EAs, PSO has no evolution operators such as crossover and mutation. Compared to GAs and EAs, the advantages of PSO are that PSO is easy to implement and there are few parameters to adjust. Most versions of PSO have operated in continuous and real-number space. A modified discrete PSO algorithm has been proposed in our previous study [23–25] to select variables in partial least squares modeling and shown satisfied performance. In the present paper, we have combined the modified discrete PSO and support vector machines (SVM) for tumor classification. The modified discrete PSO is applied to select genes, while SVM is used as the classifier or the evaluator. The formulation and corresponding programming flow chart are presented in details in the paper. The proposed approach is used to the microarray data of 22 normal and 40 colon tumor tissues and showed good prediction performance. It has been demonstrated that the modified PSO is a useful tool for gene selection and mining high dimension data.

2. Methods

2.1. Support vector machines

SVM is used here for classifying tumor and normal tissues. SVM is a kind of learning machine based on statistical learning theory and is a popular tool in pattern recognition. The most remarkable characteristics of SVMs are the absence of local minima, the sparseness of the solution, and the use of the kernel-induced feature spaces. The basic idea of applying SVMs to pattern classification can be outlined as follows. First, map the input vectors into a feature space either linearly or non-linearly, which is relevant to the selection of the kernel function. Then, within the feature space, seek an optimized linear division; i.e. construct a hyperplane which can separate two classes with the least error and maximal margin. The SVM training process always seeks a global optimized solution and avoids overfitting, so it has the ability to deal with a large number of features. A complete description to the theory of SVMs for pattern recognition is given in the book by Vapnik [26]. In this study, linear kernel function is included in the SVM procedure.

2.2. Modified particle swarm optimization for gene selection

PSO [20–22] developed by Eberhart and Kennedy in 1995 is a stochastic global optimization technique inspired by social behavior of bird flocking. The algorithm models the exploration of a problem space by a population of individuals or particles. In PSO, each single solution is a particle in the search space. Each individual in PSO flies in the search space with a velocity which is dynamically adjusted according to the flying experience of its own and its companions. In PSO algorithm, a population of particles is updated on a basis of information about each particles previous best performance and the best particle in the population. PSO is initialized with a group of random particles. Each particle is treated as a point in a D-dimensional space. The ith particle is represented as $\mathbf{x}_i = (x_{i1}, x_{i2}, \ldots, x_{iD})$. The best previous position of the ith particle that gives the best fitness value is represented as $\mathbf{p}_i = (p_{i1}, p_{i2}, \ldots, p_{iD})$. The best particle among all the particles in the population is represented by $\mathbf{p}_g = (p_{g1}, p_{g2}, \ldots, p_{gD})$. Velocity, the rate of the position change for particle i is represented as $\mathbf{v}_i = (v_{i1}, v_{i2}, \ldots, v_{iD})$. In every iteration, each particle is updated by following the two best values.

For a discrete problem expressed in a binary notation, a particle moves in a search space restricted to 0 or 1 on each dimension. In binary problem, updating a particle represents changes of a bit that should be in either state 1 or 0 and the velocity represents the probability of bit x_{iD} taking the value 1 or 0.

According to information sharing mechanism of PSO, a modified discrete PSO [22] was proposed as follows. The velocity v_{iD} of every individual is a random number in the range of (0, 1). The resulting change in position then is defined by the following rule:

$$\text{If}\,(0 < v_{iD} \le a), \quad \text{then} \quad x_{iD}(\text{new}) = x_{iD}(\text{old}) \tag{1}$$

$$\text{If}\left(a < v_{iD} \le \frac{1+a}{2}\right), \quad \text{then} \quad x_{iD}(\text{new}) = p_{iD} \tag{2}$$

$$\text{If}\left(\frac{1+a}{2} < v_{iD} \le 1\right), \quad \text{then} \quad x_{iD}(\text{new}) = p_{gD} \tag{3}$$

where a is a random value in the range of (0, 1) named static probability. In this study static probability a equals to 0.5. Though the velocity in the modified discrete PSO is different from that in continuous version of PSO, information sharing mechanism and updating model of particle by following the two best positions is the same in two PSO versions. To circumvent convergence to local optima and improve the ability of the modified PSO algorithm to overleap local optima, 10% of particles are forced to fly randomly not following the two best particles:

$$\text{If}\,(0 < v_{iD} \le 0.1) \ \text{and} \ \text{for}\,(0 < b \le \beta) \quad \text{then} \quad x_{iD}(\text{new}) = 1 \tag{4}$$

$$\text{If}\,(0 < v_{iD} \le 0.1) \ \text{and} \ \text{for}\,(\beta < b \le 1) \quad \text{then} \quad x_{iD}(\text{new}) = 0 \tag{5}$$

$$\text{If}\,(0.1 < v_{iD} \leq 1) \quad \text{then} \quad x_{iD}(\text{new}) = x_{iD}(\text{old}) \tag{6}$$

where b is a random value in the range of (0, 1), β is selection probability. In random flying operator, 10% of particles were randomly selected, and each site of the selected particles has a probability of 0.1 to vary the value in a stochastic manner. In this study selection probability β equals to 0.01 to avoid the large number of genes contained in subsets. For microarray data analysis, 1% of genes were randomly selected. If the minimum error criterion is attained or the number of cycles reaches a user-defined limit, the algorithm is terminated.

2.3. Classification modeling by the combination of modified discrete PSO and support vector machines (PSOSVM)

Though SVM has the ability to avoid overfitting, and deal with a large number of features, there is increasing evidence that feature selection is also essential for successful SVM analysis. The efficient scheme is to combine the gene selection with SVM analysis. SVM is used as the classifier and the modified discrete PSO is applied to select features. In the modified discrete PSO, each particle is encoded to a string of binary bits associated with the number of genes, which makes up of a SVM classifier with all its features. A bit "0" in a particle represents the uselessness of corresponding gene. The classification modeling by particle swarm optimization and support vector machine (PSOSVM) is described as follows:

- Step 1. Randomly initialize all the initial binary strings **IND** in modified discrete PSO with an appropriate size of population. **IND** is strings of binary bits corresponding to each gene in SVM.
- Step 2. Calculate the fitness function of the individual corresponding to models in training set. If the best object function of the generation fulfills the end condition, the training is stopped with the results output, otherwise, go to the next step.
- Step 3. Update the **IND** population according to the modified discrete PSO.
- Step 4. Go back to the second step to calculate the fitness of the renewed population. The PSOSVM scheme is presented in Fig. 1.

In this study, a cross-validation (CV) resampling approach is used to construct the learning and test sets. We evaluated the classification accuracy of the prediction models derived from the four datasets by using a leave-half-out CV (LHOCV) procedure. Briefly, the two-class samples are randomly split into two data sets of approximately equal size, respectively. The training data set, which is a random combination of the subsets for the two classes, is used to derive a classification model that is then applied to predict the total remaining subsets. The LHOCV produces four pairs of learning and test sets. Each individual is evaluated by the averaged value over the four pairs.

In PSOSVM, the performance of each particle is measured according to a pre-defined fitness function. The fitness is defined as the reciprocal of averaged classification accuracy over LHOCV that is evaluated using a linear SVM.

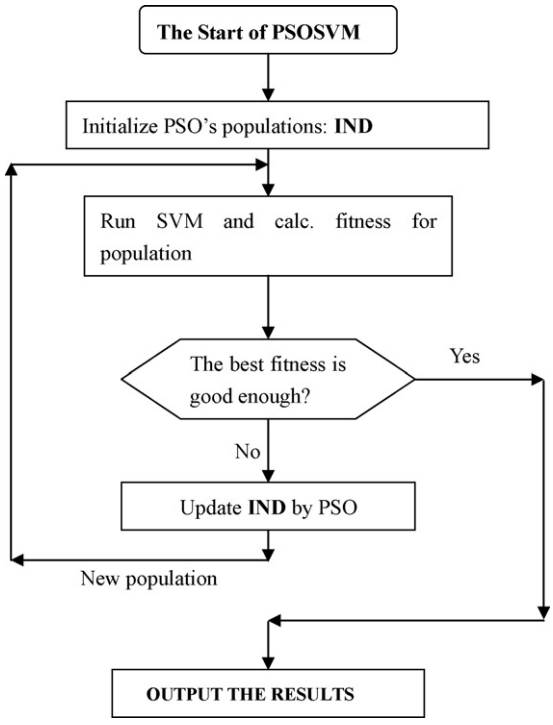

Fig. 1. The chart of the PSOSVM scheme.

The modified PSO, SVM algorithm was written in Matlab 5.3 and run on a personal computer (Intel Pentium processor 4/1.5 GHz 256 MB RAM).

3. Data set

Alon [27] analyzed the gene expressions of colon tissue. In the present study, the colon data was used to test the performance of PSOSVM in gene selection of microarray data analysis. The colon data set consists of expression profiles of 2000 genes using an Affymetrix oligonucleotide array from 22 normal and 40 colon tumor tissues and these data are publicly available at http://www.microarray.princeton.edu/oncology/. The gene expression data are scaled into (0.0, 1.0) for analysis. Among 62 colon samples, 50 randomly selected samples were used as training set and the remaining 12 samples as the prediction set. For colon dataset, we first applied t test filtering algorithm to select 400 top-ranked informative genes and then applied PSOSVM search methods on these 400 genes.

4. Results and discussion

At the beginning, SVM classifier with all 2000 genes was carried out for colon cancer dataset. Using all initial 2000 genes, the accuracy of classification for training set and test set were 1 and 0.8333, respectively. Using all 2000 genes does not offer good predictive ability and there is an obvious symptom of overfitting. Inclusion of excess of the gene variables in the modeling process will degrade the performance of SVM analysis. This might arise from the sensitivity of SVM to irrelevant variables that do not contribute to classification and prediction. So the modified PSO

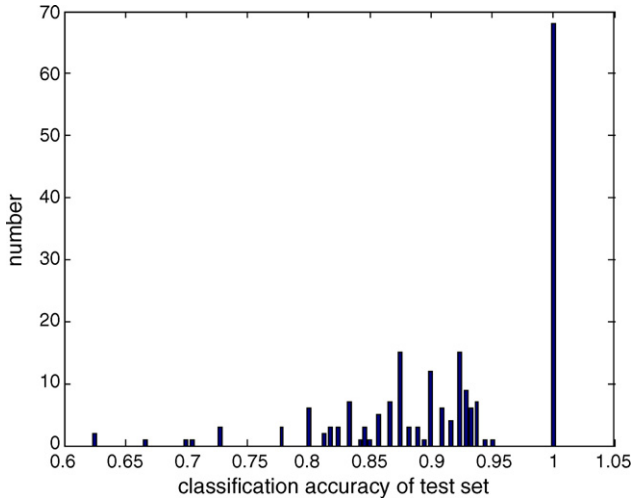

Fig. 2. Distribution of classification accuracy over 200 runs of partition samples using the best four-gene model.

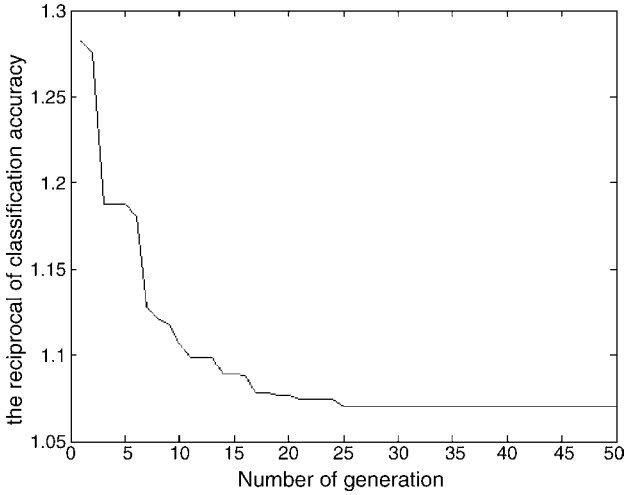

Fig. 3. Convergence curves for PSOSVM.

algorithm is employed to select the genes strongly contributing to classification for SVM modeling. In the present work, the population size of PSO is selected as 50 and PSOSVM was stopped after 50 iterations. In PSOSVM, the prediction performances of the classification models derived by selected variables were evaluated by using a LHOCV procedure.

The best model with maximum classification accuracy contains four genes during the PSOSVM search. The four genes are No. 377, 765, 1495 and 1582. The best model gives the classification accuracy 94.00% for training set and 91.67% for test set. Two samples reported are false positives and the number of false negatives reported by the best model is also equal to 2. The four-gene model provides the sensitivity 95% and specificity 91%. The classification accuracy by the next best model which contains five genes are 95.1 and 90% for training and test set, respectively. Using only five or four genes, the PSOSVM method provided 91% accuracy of classification for test set for colon cancer. By removing redundant genes the test error was reduced.

Even the classification accuracy of the prediction models were evaluated by using LHOCV procedure, it should be noted that the classification accuracy of a model at each iteration is not necessarily the same because of the variation partition of training and tests sets. The reliability of a classification model is an essential issue in microarray data analysis. To evaluate accurately the predictive ability and reliability of models derived by these selected optimal sets of genes by PSOSVM, the total tissue samples were randomly partitioned into training and tests sets 200 times and then averaged the classification accuracy for each selected set of genes. Fig. 2 shows the distribution of classification accuracy for test set over 200 runs of partition samples using the best four-gene model. As shown in Fig. 2, classification accuracy larger than 91.5% is about 111 times in 200 runs and the highest accuracy (100%) appear 68 times. By resampling a large number of learning samples, the average classification accuracy achieved 91.8%. It can be seen that the classification model using the selected four genes is stable and reliable.

In comparing with SVM analysis by all genes, it shows that better results are obtained from classification analysis including only selected genes than from SVM analysis including all variables. The predictive ability of SVM model was much improved in classification accuracy by the PSOSVM analysis from 83 to 91.7%. One notices that the use of the modified PSO search helps us to select 4 or 5 genes from 2000 descriptors. These selected genes carry more or less information related to tumor classification. In this way, PSOSVM maximally extracts information from the original data set for microarray data analysis.

As shown in Fig. 3 the maximum classification accuracy can be obtained in about 25 cycles during the PSOSVM algorithm and fitness value drops quickly in the PSOSVM algorithm. Information sharing in PSO is among the global best position, and the corresponding personal best positions. This is a very unique attribute for the PSO algorithm. It seems that it is due to the introduction of this unique attribute that the PSO algorithm generally exhibits a high convergence rate.

Fig. 4 shows the relationship between classification accuracy and the number of genes in a selected optimal gene set

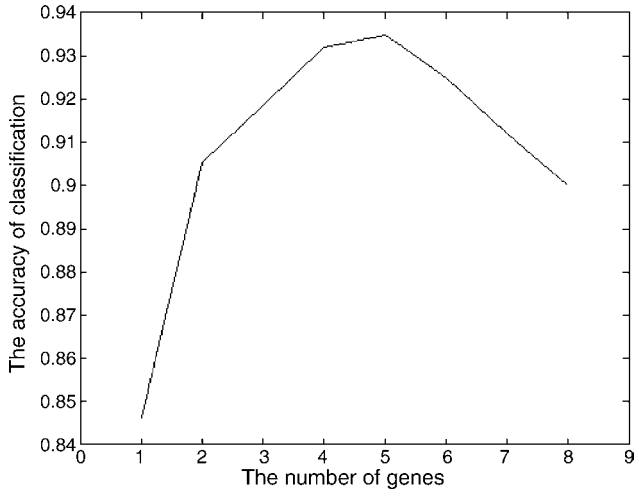

Fig. 4. The relationship between classification accuracy and the number of genes selected using PSOSVM.

using PSOSVM. For colon dataset, four or five genes are an optimal number for classification by SVM. As the number of genes exceeds 5, the accuracy of classification decreases. The more genes are selected, the small the classification accuracy became. This may be because more irrelevant genes were included to build the classification model and thus degraded the prediction performance. It indicates the necessity of excluding irrelevant genes or selecting relevant genes in microarray analysis.

In the modified discrete PSO, the performance of each particle is measured according to a pre-defined fitness function. In PSOSVM the fitness is defined as the reciprocal of averaged classification accuracy over LHOCV that is evaluated using a linear SVM. Other classification methods such as the Fisher liner discriminant analysis (LDA) instead of SVM can also be used to evaluate the fitness in the modified PSO. The best model with maximum classification accuracy contains three genes using LDA as fitness. The three genes are No. 377, 493 and 1964. The best model gives the classification accuracy 94.00% for training set and 75% for test set. By resampling learning samples 200 times, the average classification accuracy achieved 90.43 and 89.38% for training and test set.

When the modified PSO search terminates, one may count the number of times a particular gene descriptor appears in 100 individual combinations. When one lists the descriptors by order of decreasing numbers of times of appearance, the top descriptors or the most frequently appeared feathers are obtained. Gene 377 (Z50753) related to uroguanylin precursor is shown to be important in classification analysis of colon dataset. Gene 377 is markedly low expression in colon samples and it may play an essential role in pathological and treatment of colon cancer [28–30]. Gene 1423 (J02854) corresponding to myosin regulatory light chain occupies an important position. Besides these genes, genes 14, 66, 249, 698, 765 1042 and 1873 also have advantage for classification of colon dataset. It is interesting that most of these top descriptors are high expression in normal tissue and low expression in colon samples. Genes (No. 14, 249 and 377) were also found to be correlated with colon tumor in researches [30,31]. The genetic architecture of the disease is a complex one and we developed a novel approach to hunting for disease relevant genes using an approach with PSOSVM as the feature gene search engine.

5. Conclusion

The selection of genes that are really indicative of the tissue classification concerned is a key step in developing a successful gene expression-based data analysis system. In this paper, the modified discrete PSO was applied to select genes and support vector machine was used for classifier. A new objective function was formulated to determine the appropriate number of genes. Colon data set was used by the proposed PMPSO algorithm. The results have demonstrated that the proposed method is useful for gene selection and classification.

Acknowledgements

The work was financially supported by the National Natural Science Foundation of China (Grant Nos. 20505015, 20475050).

References

[1] D. Schena, R.W. Shalon, P.O. Davis, Science 270 (1995) 467.
[2] Y. Yamaguchi, D. Ogura, K. Yamashita, M. Miyazaki, H. Nakamura, H. Maeda, Talanta 68 (2006) 700.
[3] G.P. Yang, D.T. Ross, W.W. Kuang, P.O. Brown, R.J. Weigel, Nucleic Acids Res. 27 (1999) 1517.
[4] G. Stephanopoulos, D. Hwang, W.A. Schmitt, J. Misra, Bioinformatics 18 (2002) 1054.
[5] S. Biceiato, A. Luchini, C.D. Bello, Bioinformatics 19 (2003) 571.
[6] D.V. Nguyen, D.M. Rocke, Bioinformatics 18 (2002) 1216.
[7] Y.X. Tan, L. Shi, W. Tong, G.G.T. Hwang, C. Wang, Comput. Biol. Chem. 28 (2004) 235.
[8] C.Z. Cai, W.L. Wang, L.Z. Sun, Y.Z. Chen, Math. Biosci. 185 (2003) 111.
[9] E. Byvatov, U. Fechner, J. Sadowski, G.J. Schneider, Chem. Inf. Comput. Sci. 43 (2003) 1882.
[10] H.X. Liu, R.S. Zhang, F. Luan, X.J. Yao, M.C. Liu, Z.D. Hu, B.T. Fan, J. Chem. Inf. Comput. Sci. 43 (2003) 900.
[11] R. Burbidge, M. Trotter, B. Buxton, S. Holden, Comput. Chem. 26 (2001) 5.
[12] J. Weston, S. Mukherjee, O. Chapelle, M. Pontil, T. Poggio, V. Vapnik, Adv. Neural Inf. Process. Syst. 13 (2001) 668.
[13] I. Guyon, J. Weston, S. Barnhill, V. Vapnik, Mach. Learn. 46 (2002) 389.
[14] V.G. Franco, J.C. Peraan, V.E. Mantovani, H.C. Goicoechea, Talanta 68 (2006) 1005.
[15] T. Golub, D. Slonim, P. Tamayo, C. Huard, M. Gaasenbeek, J. Mesirov, H. Coller, M. Loh, J. Downing, M. Caligiuri, Science 286 (1999) 531.
[16] L. Li, W. Jiang, X. Li, K.L. Moser, Z. Guo, L. Du, Q. Wang, E.J. Topol, Q. Wang, S. Rao, Genomics 85 (2005) 16.
[17] Z. Ramadan, D. Jacobs, M. Grigorov, S. Kochhar, Talanta 68 (2006) 1683.
[18] P. Watkins, G. Puxty, Talanta 68 (2006) 1336.
[19] T. Furey, N. Cristianini, N. Duffy, D. Bednarski, M. Schummer, D. Haussler, Bioformatics 16 (2000) 906.
[20] J. Kennedy, R. Eberhart, Proceedings of IEEE International Conference On Neural Networks, 1995, p. 1942.
[21] Y. Shi, R. Eberhart, Proceedings of the IEEE World Congress on Computational Intelligence, 1998, p. 69.
[22] M. Clerc, J. Kennedy, Proceedings of the IEEE Transactions on Evolutionary Computation, vol. 6, 2002, p. 58.
[23] Q. Shen, J.H. Jing, G.L. Shen, R.Q. Yu, Eur. J. Pharm. Sci. 22 (2004) 145.
[24] Q. Shen, J.H. Jing, W.Q. Lin, G.L. Shen, R.Q. Yu, J. Comput. Chem. 25 (2004) 1726.
[25] Q. Shen, J.H. Jing, G.L. Shen, R.Q. Yu, J. Chem. Inf. Comput. Sci. 44 (2004) 2027.
[26] V. Vapnik, Statistical Learning Theory, Wiley, New York, 1998.
[27] U. Alon, Proc. Natl. Acad. Sci. 96 (1999) 6745.
[28] D. Notterman, U. Alon, A. Sierk, A. Levine, Cancer Res. 61 (2001) 3124.
[29] K. Shailubhai, H.H. Yu, K. Karunanandaa, J.Y. Wang, S.L. Eber, Y. Wang, N.S. Joo, H.D. Kim, B.W. Miedema, S.Z. Abbas, Cancer Res. 60 (2000) 5151.
[30] Y. Li, C. Campbell, M. Tipping, Bioinformatics 18 (2002) 1332.
[31] S. Ma, J. Huang, Bioinformatics 21 (2005) 4356.

Available online at www.sciencedirect.com
ScienceDirect
Talanta 71 (2007) 1782–1787
Talanta
www.elsevier.com/locate/talanta

Chromogenic radical based optical sensor membrane for screening of antioxidant activity

Ivana Murković Steinberg *, Stjepan Milardović

University of Zagreb, Faculty of Chemical Engineering and Technology, Marulićev trg 19, HR-10000 Zagreb, Croatia

Received 8 September 2005; received in revised form 16 August 2006; accepted 21 August 2006
Available online 26 September 2006

Abstract

Solid-state optical sensor membranes based on immobilised chromogenic radicals for the assessment of antioxidant activity have been studied. Two stable lipophilic chromogenic radicals, DPPH• (2,2-diphenyl-1-picrylhydrazyl radical) and galvinoxyl radical, GV•, (2,6-di-*tert*-butyl-α-(3,5-di-*tert*-butyl-oxo-2,5-cyclohexadien-1-ylidene)-*p*-tolyloxy radical), were immobilised in plasticised PVC films and screened for suitability as indicators of antioxidative activity. The spectrophotometric characterisation of the polymer films containing immobilised free radicals was performed, and the response of the immobilised free radicals toward standard antioxidants was studied. It has been demonstrated that the immobilised radicals retain their reactivity towards antioxidants and the results suggest that the reactivity of immobilised radicals is comparable to standard solution-based DPPH assays. Polymer films containing immobilised DPPH• radical respond to standard antioxidants in aqueous solutions by changing colour irreversibly from purple (absorption maximum at 520 nm) to yellow. The initial slopes of the response curves to the phenolic antioxidant gallic acid, obtained in the 1–50 mM concentration range, gave a linear calibration plot in a 1 min exposure cuvette test. The polymer films were used to screen antioxidative activity of beverage and food samples known to contain antioxidants, such as black and green tea, coffee, red wine, fruit juice, olive oil and sunflower oil. It has been demonstrated that a rapid and simple qualitative screening test of untreated samples is possible using a test strip based on immobilised DPPH• radical.

Keywords: Antioxidative activity; Immobilised radicals; Polyphenolic antioxidants; DPPH• radical; Plasticised PVC; Screening test

1. Introduction

Understanding the chemistry of free radicals and antioxidants is gaining importance, particularly in the areas of clinical medicine and nutritional science. Free radicals are known to cause damage to lipids, proteins and nucleic acids and are implicated in a number of pathological interactions and degenerative diseases in living organisms, including cancer, Alzheimer's and Parkinson's disease [1]. Antioxidants act as free radical scavengers and can prevent the damage caused by oxidative reactions. Hence, the evaluation of the antioxidative activity of biomedical, cosmetic and food samples provides useful clinical and dietary information.

A number of optical-based tests for the determination of antioxidant activity have been developed [2] based on different chemical and biological mechanisms, including the Trolox Equivalent Antioxidant Capacity (TEAC) [3], Oxygen Radical Absorbance Capacity (ORAC) [4], Ferric Reducing Antioxidant Power (FRAP) [5] and Total Radical Antioxidant Potential (TRAP) [6] assays. In general, the activity of antioxidants present in the sample is related to their free radical scavenging ability or to their reducing power, which is then coupled to chromogenic or fluorogenic detection. Some of these optical assays have been further adapted for use in commercial test kits and instruments using solution-based chemistries, such as the TEAC assay which has been commercialised by Randox Laboratories (San Francisco, CA, USA).

Another optical method widely used to measure radical scavenging capacity of food and plant compounds was introduced by Blois [7], and improved by Brand-Williams et al. [8]. The method is based on the decolourisation of the stable free radical DPPH• in the presence of antioxidants performed as a simple solution-based test. A similar test in homogenous solutions and aqueous dispersions has been reported using the galvinoxyl

* Corresponding author. Tel.: +385 1 45 97 287.
E-mail address: ivana.murkovic@fkit.hr (I.M. Steinberg).

0039-9140/$ – see front matter © 2006 Elsevier B.V. All rights reserved.
doi:10.1016/j.talanta.2006.08.015

radical [9]. The tests are based on the reduction of the chromogenic radicals by an antioxidant, which causes the radicals to change colour, and this change may be monitored spectrophotometrically. These simple, solution-based assays, can provide information on the ability of a compound to donate hydrogen atoms, on the number of electrons available for reaction, and on the reaction mechanism between the radical and the antioxidant. Other techniques have been used for detection, including electron spin resonance spectroscopy [10] and a combined optothermal window and colourimetry method [11].

Optical sensors based on immobilised chemistries are particularly suited to rapid and low-cost screening applications, since they have appropriate sensitivity, and at the same time can be provided in the form of inexpensive test-kits and strips [12].

In the work presented here, we have studied the feasibility of transforming the solution-based, free radical assay for antioxidants into a solid-state optical test strip.

Gallic acid, an antioxidant typically present in wines and green and black teas, has been used as a standard to study the response of films to total phenols and antioxidants. Gallic acid is routinely employed as a standard in the determination of total phenolic content, specifically in the widely used Folin–Ciocalteau analysis procedure for phenolics and antioxidants, where the results are expressed as gallic acid equivalents (GAE).

The response of the polymer film containing immobilised radical molecules has been characterised, and its suitability for screening the antioxidant activity of real samples evaluated. The standard DPPH• test is thus presented here in a novel, chemical sensor format, and its new screening applications proposed.

2. Experimental

2.1. Chemicals

The radicals DPPH• (2,2-diphenyl-1-picrylhydrazyl radical) and galvinoxy radical (2,6-di-*tert*-butyl-α-(3,5-di-*tert*-butyl-oxo-2,5-cyclohexadien-1-ylidene)-*p*-tolyloxy were obtained from Sigma–Aldrich. The antioxidants Trolox (6-hydroxy-2,5,7,8-tetramethylchroman-2-carboxylic acid), ascorbic acid, uric acid, glutathion, ferulic acid, gallic acid and caffeic acid were obtained from Sigma–Aldrich.

Poly(vinylchloride) (PVC, high molecular weight), bis-(2-ethylhexyl)-sebacate (DOS) and tetrahydrofuran (THF) were obtained from Fluka.

2.2. Sensing film preparation

All materials were deposited on a planar support for investigation in a spectrophotometer. Planar sensor films (membranes) were made by spreading a "cocktail" onto a solid transparent polyester support (Mylar^{TM}, 175 μm thick, from Du Pont de Nemours & Co., Brussels), as described in our previous work [13,14]. The technique involves a screen-printing like method using a fixed substrate onto which the viscous cocktail is applied, and spread with a knife blade over the surface and left to dry at ambient conditions.

The cocktail was prepared by dissolving 120 mg PVC, 240 mg DOS (the plasticiser) and 2 mg of the radical in 1.5 mL THF. The sensor films were prepared by spreading the cocktail onto a 1 cm × 4 cm strip of the polyester support, using a custom-made spreading device. The films obtained were transparent and clear, with dye evenly dissolved in plasticiser. From the volume applied, the thickness of the dry membrane (i.e., after evaporation of THF) was estimated to be 2–3 μm.

2.3. Apparatus and measurement procedures

Absorbance measurements were performed using a Varian UV Cary 100 spectrophotometer. The test strips were fixed in 1 cm × 1 cm × 4 cm disposable cuvettes (Brand, Germany) and all measurements were performed in batch mode.

The response of the membrane to antioxidants was investigated in sodium phosphate buffers (0.1 M) at pH 7.4. The film was first exposed to the buffer solution and after recording of the spectrum, the respective antioxidant solution of known concentration was added into the cuvette. The absorption spectrum, or absorbance value at the set wavelength in kinetic response studies, were recorded.

3. Results and discussion

3.1. Sensing scheme and choice of radicals

The ability of antioxidants to scavenge radicals such as DPPH• and GV• (Fig. 1) is used as the basis for optical assays in the assessment of antioxidant activity [7–9]. Although the DPPH• radical may be used for the measurement of antioxidant capacity of biomedical samples, such as blood plasma [15], it has mainly been used for the determination of antioxidant activity of naturally occurring plant foods, such as flavonoids and other polyphenols [16,17]. Galvinoxyl radical has similar properties and has been used for studying antioxidative properties of ascorbic acid, cysteine and glutathione in homogenous solutions and aqueous dispersions [9].

The stable radical DPPH• reacts with antioxidants present in the solution and the reduction in the concentration of DPPH• is followed by monitoring the decrease in its absorbance at the characteristic wavelength during the reaction. In its radical form,

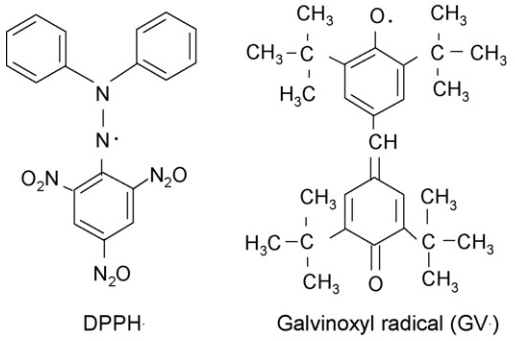

Fig. 1. Chemical structures of DPPH• (2,2-diphenyl-1-picrylhydrazyl radical) and GV• (galvinoxyl radical).

DPPH• absorbs at 520 nm, but upon reduction by an antioxidant (AH), the radical becomes paired with a hydrogen atom from the antioxidant to give the reduced form, DPPHH, which results in decrease of absorbance at 520 nm and a change of colour to yellow. This colour change is irreversible and observable with the naked eye:

$$\underset{\text{purple}}{\text{DPPH}^\bullet} + \text{AH} \rightarrow \underset{\text{yellow}}{\text{DPPHH}} + \text{A}^\bullet \quad (1)$$

Galvinoxyl is a stable phenoxy radical that exhibits characteristic absorption at 430 nm. The same sensing mechanism of radical scavenging described with Eq. (1), can be applied to the GV• radical. However, the colour change induced by exposure to antioxidants is not easily detected by the naked eye.

These two chromogenic radicals were chosen for this study because of their widespread use in well-established procedures for the determination of antioxidants in solutions, together with their sufficient chemical stability and lipophilicity. Both radicals are soluble in plasticiser, which allows preparation of thin films and minimises problems associated with leaching. Also, by using a stable neutral radical, such as DPPH•, there is no need for generation of radicals in situ which makes the test strips simple to use in practice.

3.2. Film composition

Radicals were mixed into the PVC/DOS/THF cocktail and spread onto a transparent polyester support. After evaporation of THF, optically transparent and homogenous films were obtained. The results reported in our previous study were used here for optimal film composition [13,14]. The composition of the plasticised PVC cocktails was typical for preparation of optical sensor films (membranes), with plasticiser/PVC mixed in a 2:1 mass ratio [18]. A film thickness of 2–3 μm and a mass concentration of the radical in the DOS plasticiser of around 1%, were found to be optimal for our purpose.

3.3. Spectral characterisation of the films

The membranes containing free radicals were fixed on a wall of a cuvette and exposed to plain buffer solution and subsequently to the buffer solution containing an antioxidant, such as ascorbate (see Section 2). The corresponding absorption spectra are shown (Figs. 2 and 3). The membrane absorption maxima were found to be at 520 nm for DPPH• radical, and at 430 nm for GV• radical, which corresponds to their ethanol solution values. On exposure to the ascorbate solution, the absorbance of the membranes at the characteristic wavelength decreases. The films containing DPPH• radical showed faster response and higher sensitivity, and had the additional advantage that the change of colour (from purple to yellow) is easily detected with the naked eye. For these reasons, the DPPH• based films were selected for more detailed studies.

Firstly, the pH response of the DPPH• based films was studied. No significant effect of pH values of solutions tested (phosphate and acetate buffers in the pH range 4–8, and 0.01 M HCl and 0.01 M NaOH solutions) on absorbance of the films at the characteristic wavelength of 520 nm was observed within a typical response time window of 1–5 min.

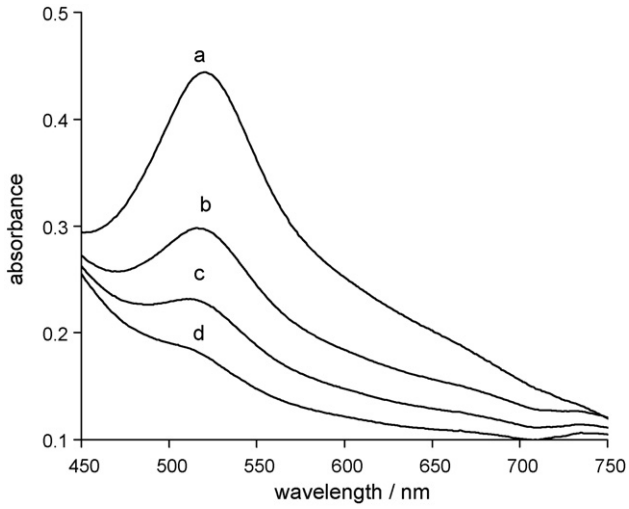

Fig. 2. Absorption spectra of DPPH/PVC/DOS film exposed to (a) phosphate buffer of pH 7.4; (b–d) exposed to 0.1 M solution of ascorbic acid at 1 min intervals.

3.4. Response of DPPH• films to standard antioxidants

The DPPH• films were tested in solutions of standard antioxidants, including ascorbic acid, Trolox, glutathion, uric acid and the phenolic antioxidants: ferulic, gallic and caffeic acid. The dynamic response to antioxidants was monitored as a change in absorbance at 520 nm (absorbance maximum of DPPH• radical in the film) as the membrane was exposed to buffer solutions containing antioxidants. All the antioxidants tested produced visible colour change within 10 min of exposure with 1 mM solutions, however, each with different kinetics of response. Characteristic response curves obtained for the phenolic antioxidants are shown (Fig. 4).

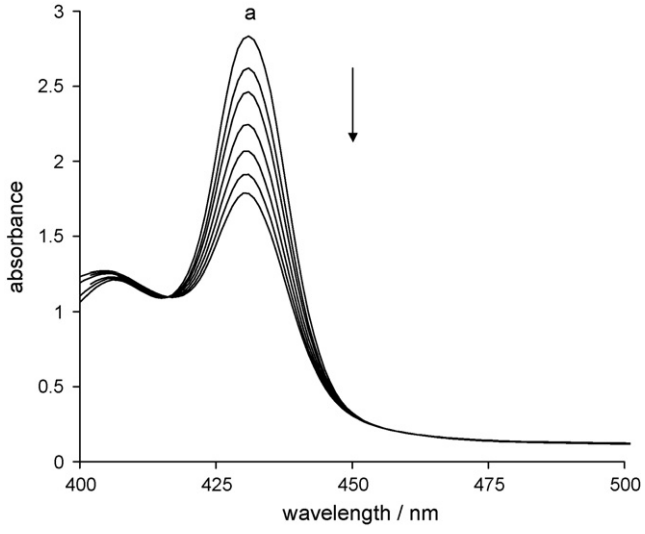

Fig. 3. Absorption spectra of GV/PVC/DOS film exposed to (a) phosphate buffer of pH 7.4; and exposed to 0.1 M solution of ascorbic acid at 5 min intervals. The arrow indicates the direction of change.

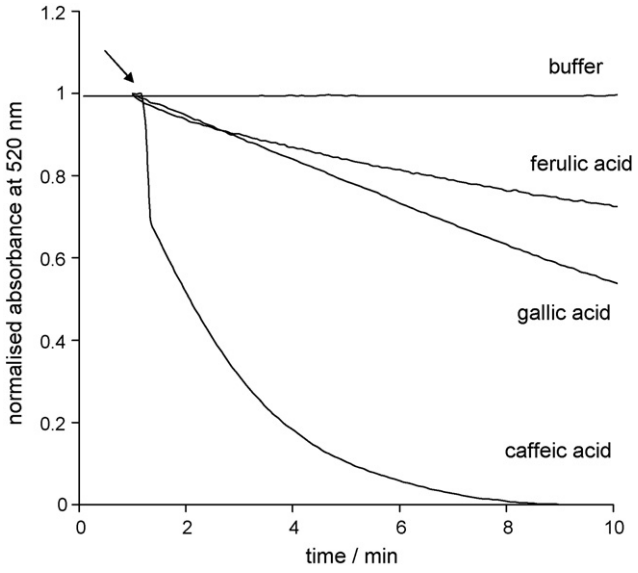

Fig. 4. Response curves of DPPH/PVC/DOS films recorded at 520 nm as a result of exposure to 1 mM solutions of phenolic antioxidants. The arrow indicates the addition of sample.

3.5. Effect of antioxidant concentration on kinetic response

Gallic acid is a phenolic antioxidant typically present in wines and green and black teas. Gallic acid is employed as a standard in the determination of total phenolics content in the widely used Folin–Ciocalteau analysis procedure for phenolics and antioxidants [19], and where the results are expressed as gallic acid equivalents. For this reason, the DPPH• membranes were evaluated using gallic acid as a standard antioxidant.

The kinetics of the membrane response to different concentrations of gallic acid is shown (Fig. 5).

The initial slope of the response curves for an exposure time of 1 min was plotted against the logarithm of the gallic acid concentration (Fig. 6). A sigmoidal curve, typical of optical sensor calibration plots, was obtained for the concentration range between 0.005 and 0.1 M. The linear part of the sigmoidal curve covers approximately the 1–50 mM concentration range ($y = 0.0081x + 0.0254$, $R^2 = 0.9712$) for a 1 min exposure time. The dynamic range can be shifted to either higher or lower concentrations by choosing an appropriate exposure time as evident from the response curves. Also, the saturation point of the membrane depends upon the total concentration of the radical dissolved in the membrane, and this fact can be exploited in order to shift the dynamic range to concentration values needed for any specific application.

3.6. Effects of immobilisation on the response of DPPH• radical

From the results reported here, it is evident that in the immobilised form, the DPPH• radical can be scavenged by antioxidants and used for detection of antioxidant activity. Its reactivity to the phenolic antioxidants is in agreement with the previously reported kinetic classification of radical response to caffeic acid

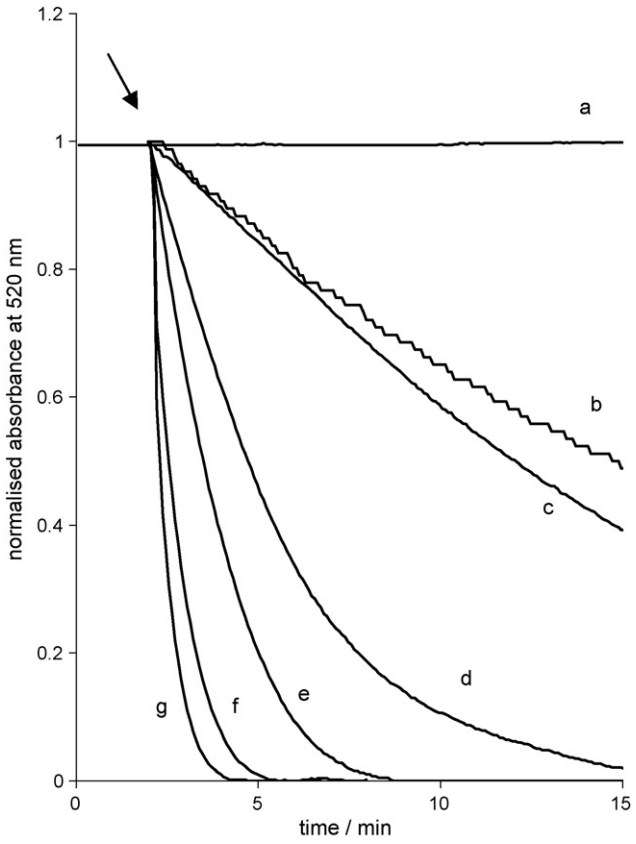

Fig. 5. Response curves of DPPH/PVC/DOS film recorded at 520 nm as a result of exposure to (a) buffer; and different concentrations of gallic acid: (b) 0.1 mM, (c) 1 mM, (d) 2 mM, (e) 5 mM, (f) 10 mM and (g) 50 mM. The arrow indicates the addition of sample.

as rapid-intermediate, gallic acid as intermediate, and ferulic acid as slow. It is also in agreement with the parameter T_{EC50}, introduced for classification of kinetic behaviour of antioxidants in the solution-based DPPH• test [20].

The kinetics of the reaction between the immobilised radical and an antioxidant is the result of two processes; firstly, extraction of the antioxidant into the organic film, followed by chemical reaction with the radical. The polymer film provides extraction, preconcentration and detection of the analyte

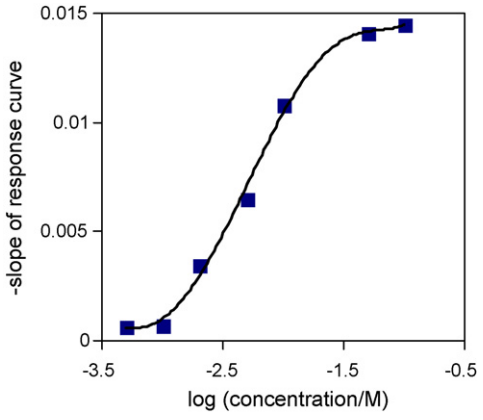

Fig. 6. Calibration plot of DPPH/PVC/DOS film for gallic acid expressed as the initial slope of the response curve for a given concentration.

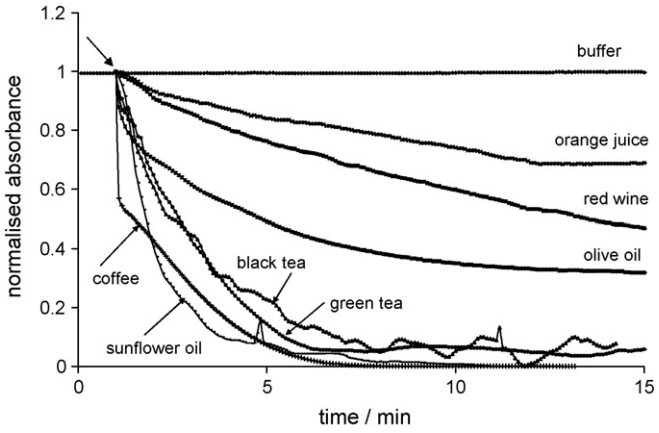

Fig. 7. Response curves of DPPH/PVC/DOS film recorded at 520 nm as a result of exposure to food and beverage samples. The arrow indicates the addition of sample.

in one step. This is especially important for compounds such as flavonoids, since it is known that the partition coefficients, as well as their reaction rate with radicals, can play an important role in defining the antioxidant activity in the lipophilic phase. This characteristic of the membrane offers a useful tool in studying reaction mechanisms and in the assessment of antioxidant activity of plant extracts, in both the lipophilic and aqueous phases [21].

It is known that the absorbance of DPPH• radical is effected by light, oxygen and pH, and this effect can be as drastic as an 80% decrease in 2 h, at pH 10 in acetone, under light [22]. The absorbance of the polymer films described here deteriorates on exposure to ambient light and air at room temperature, with decolouration occurring completely within 1 week. However, when the membranes are kept in phosphate buffer solutions at around pH 7 in the dark, no significant loss in absorbance was noticed within 24 h. So although we have demonstrated that a solid-state DPPH assay is feasible, the specific problem of radical decomposition, which occurs both in solution as well as in the solid-state, has not yet been addressed.

Since the DPPH• radical is not soluble in water, solution-based assays have to be performed either in ethanol or methanol solutions. It has been found that the choice of solvent plays a very important role in hydrogen atom abstraction in the reaction of the DPPH• radical with phenolic compounds, and that reactions in alcohols show abnormally enhanced values of rate constants [23]. It is suggested that popular tests with the DPPH• radical in alcohol solvents generally lead to an overestimation of antioxidant activity of phenols, an effect that can be avoided here with the DPPH• immobilised in a membrane, where a non-polar plasticiser is used as solvent.

3.7. Antioxidant activity of real samples

The response of the DPPH• films was tested with a number of food and beverage samples known to contain antioxidants. The samples were used without pretreatment and the results of the tests are shown (Fig. 7). Coffee, black and green teas, and sunflower oil showed comparable kinetic characteristics and scavenged more than 90% of the radical within 5 min of exposure. All other samples tested caused observable colour change in less than 10 min of exposure, and buffer solution showed no effect.

The total phenolic content in certain Croatian red wines expressed as gallic acid equivalents measured using the Folin–Ciocalteu method has been reported to be around $\gamma = 4000$ mg/L [24]. In addition, a very strong correlation between total phenols in wines and their antioxidative activity as determined by the DPPH method has been demonstrated [25]. The GAE of the wines tested by Piljac et al. [24] corresponds approximately to a molar concentration of 20 mmol/L, a concentration well within the dynamic range of our DPPH films (Fig. 6). It therefore follows that a 1-min exposure time is appropriate for assessing real samples such as wines. Also, from the calibration graphs obtained, we can estimate that the untreated samples of coffee and tea that were tested would show antioxidative activity if expressed as GAE of the DPPH method of around 10 and 6 mM, respectively.

There is no standard method for antioxidant activity determination, and different methods can give different results depending upon the sample matrix or the specific indicator (free radical) used in the test. It is thus generally accepted that there is no single assay available that can provide both accurate and quantitative determination of antioxidant activity, and the interpretation of results obtained with different assays should therefore be made critically [26,27].

The polymer films presented here can easily be adapted for use as optical test strips for screening of the presence of antioxidants (yes/no screening) at concentration ranges typical for food and beverage samples. Our further studies will focus on adapting the sensor membranes for quantitative assessment of antioxidants and the total phenolics content in real samples expressed as gallic acid equivalents.

4. Conclusion

The lipophilic radicals, DPPH• and GV•, were immobilised in plasticised PVC matrices, and it has been demonstrated that these radicals retain their reactivity towards various antioxidants after immobilisation into a polymer support. The DPPH• films showed sufficient sensitivity to detect presence of antioxidants at their typical concentration levels in untreated beverage and food samples, such as black and green tea, coffee, red wine, fruit juice, olive oil and sunflower oil. Generally, the colour changes were observable with the naked eye in less than 5 min.

Unlike the solution-based assay, in its present format the colourimetric test strip containing immobilised chromogenic free radicals cannot be used for quantitative assessment of antioxidant activity. However, the test strip does allow for the qualitative assessment of antioxidative activity of complex mixtures, or the quantitative determination expressed as a gallic acid equivalent. Also, determination of the concentration of a single antioxidant present in a solution is possible, as demonstrated in the case of gallic acid. The solid-state method offers some advantages over solution-based assays, including the potential for use as a rapid, low-cost, easy-to-use screening tool forantioxidative

activity, especially appropriate in the screening of plant extracts of unknown composition. Samples can be assessed without pre-treatment, and the format of the test is suitable for use with coloured or turbid samples, which is not possible with the solution-based DPPH$^{\bullet}$ test.

Acknowledgement

This work was supported by the Ministry of Science and Technology, Republic of Croatia, under project grant number 0125054, which is gratefully acknowledged.

References

[1] B. Halliwell, J.M.C. Gutteridge, Free Radicals in Biology and Medicine, third ed., Oxford University Press, New York, 1999.
[2] R.L. Prior, G.H. Cao, Free Rad. Biol. Med. 27 (1999) 1173.
[3] N.J. Miller, C. Rice-Evans, M.J. Davies, V. Gopinathan, A. Milner, Clin. Sci. 84 (1993) 407.
[4] A.N. Glazer, Method Enzymol. 186 (1990) 161.
[5] I.F.F. Benzie, J.J. Strain, Anal. Biochem. 239 (1996) 70.
[6] D.D.M. Wayner, G.W. Burton, K.U. Ingold, S. Locke, FEBS Lett. 187 (1985) 33.
[7] M.S. Blois, Nature 181 (1958) 1199.
[8] W. Brand-Williams, M.E. Cuvelier, C. Berset, Lebensm. Wiss. Technol. 28 (1995) 25.
[9] J. Tsuchiya, T. Yamada, E. Nike, Y. Kamiya, Bull. Chem. Soc. Jpn. 58 (1985) 326.
[10] Q. Guoa, G. Rimbachb, H. Moinic, S. Webera, L. Packer, Toxicology 179 (2002) 171.
[11] M. Buijnsters, D. Bicanic, M. Chirtoc, M.C. Nicoli, Y. Min-Kuo, Anal. Sci. 17 (2001) 544.
[12] O.S. Wolfbeis (Ed.), Fiber Optic Chemical Sensors and Biosensors, CRC Press, Boca Raton, 1991.
[13] I. Murkovic, A. Lobnik, G.J. Mohr, O.S. Wolfbeis, Anal. Chim. Acta 334 (1996) 125–132.
[14] I. Murkovic Steinberg, A. Lobnik, O.S. Wolfbeis, Sensors Actuat., Part B 90B (2003) 230.
[15] A. Janaszewska, G. Bartosz, Scand. J. Clin. Lab. Inv. 62 (2002) 231.
[16] O.I. Aruoma, Mutat. Res. 523 (2003) 9.
[17] D. Amic, D. Davidovic-Amic, D. Beslo, N. Trinajstic, Croat. Chem. Acta 76 (2003) 55.
[18] K. Seiler, W. Simon, Anal. Chim. Acta 266 (1992) 73.
[19] V.L. Singleton, R. Orthofer, R.M. Lamuela-Raventos, Method Enzymol. 299 (1999) 152.
[20] C. Sanchez-Moreno, J.A. Larrauri, F. Saura-Calixto, J. Sci. Food Agric. 76 (1998) 270.
[21] C.A. Rice-Evans, N.J. Miller, G. Paganga, Free Rad. Biol. Med. 20 (1996) 933.
[22] B. Ozcelik, J.H. Lee, D.B. Min, J. Food Sci. 68 (2003) 487.
[23] G. Litwinienko, K.U. Ingold, J. Org. Chem. 68 (2003) 3433.
[24] J. Piljac, S. Martinez, L. Valek, T. Stipcevic, K. Kovacevic-Ganic, Food Technol. Biotechnol. 43 (2005) 271.
[25] V. Katalinic, M. Milos, D. Modun, I. Music, M. Boban, Food Chem. 86 (2004) 593.
[26] E. Niki, Nutrition 18 (2002) 524.
[27] C. Sanchez-Moreno, Food Sci. Technol. Int. 8 (2002) 121.

Available online at www.sciencedirect.com
ScienceDirect
Talanta 71 (2007) 1741–1751
Talanta
www.elsevier.com/locate/talanta

Determination of phenolic compounds and their antioxidant activity in fruits and cereals

P. Stratil, B. Klejdus, V. Kubáň *

Department of Chemistry and Biochemistry, Mendel University of Agriculture and Forestry, Zemědělská 1, CZ-613 00 Brno, Czech Republic

Received 20 March 2006; received in revised form 28 July 2006; accepted 4 August 2006
Available online 11 September 2006

Abstract

Three methods, FCM (with Folin–Ciocalteu reagent), PBM (Price and Butler) and AAPM (with 4-aminoantipyrine) for assessment of phenolic compounds and three commonly used methods, TEAC (Trolox equivalent antioxidant capacity), DPPH (with diphenyl-picrylhydrazyl radical), and FRAP (ferric reducing antioxidant power) for evaluation of antioxidant capacity, were modified to a semimicroscale (total volume 1 ml) with minimum consumption (to 100 μl) of a sample and thereby applicable for fast screening. Appropriate standards and extracts of 17 kinds of fruit and six kinds of cereal were assessed for total content of phenolic compounds and total antioxidant capacity by each of these methods. The results of analyses of commonly used standards (gallic, caffeic and ferulic acids, (+)-catechin, Trolox, fenol and $FeSO_4$) for these methods and identical plant extract showed different reactivity of principal reagent of the methods with individual standards and therefore with phenolic substances of extracts as well. However, the trends of the measured values of extracts could be compared, though their absolute values differ proportionally. At assessments of phenolic compounds it is important to determine content of ascorbic acid at roughly the same time and correct the obtained values according to its contribution to the increase in absorbance calculated on the basis of absorbance equations, especially for samples with a higher content. The same is true for reducing saccharides; they can significantly "elevate" values of contents of phenolic compounds and antioxidant activities (by even more than 50%), especially in samples of sweeter fruits. The saccharides should therefore be removed or a correction applied reflecting their concentration.

Keywords: Phenolic compounds; Total antioxidant capacity; Fruits; Cereals

1. Introduction

Phenolic compounds widely distributed in the medicinal plants, spices, vegetables, fruits, grains, pulses and other seeds are an important group of natural antioxidants with possible beneficial effects on human health. They can participate in protection against the harmful action of reactive oxygen species, mainly oxygen free radicals. Free radicals are produced in higher amounts in a lot of pathological conditions and are involved in the development of the most common chronic degenerative diseases, such as cardiovascular disease and cancer [1–3].

Even though several plants containing phenolic compounds with important favourable health effects (e.g. silymarin, curcumin, resveratrol, phenolic compounds in *Gingko Biloba*, etc.) are utilized commercially but the consumption is rather rare. Commonly consumed plant foods, like vegetables, fruit, cereals and drinks with lower (or zero) content of alcohol are the most important sources of phenolic compounds from a health standpoint and from the aspect of consumption by the whole population. Relatively little information is however yet known about the content of phenolic compounds and their antioxidant capacity in common plant food.

Methods for assessment of total content of phenolic compounds and determination of their antioxidant capacity are mostly based on oxidizing–reducing properties, possibility of phenolic compounds functioning as reduction agents and offering hydrogen radical or electron [4]. A Folin–Ciocalteu (FCM) method [5] is commonly used only for assessment of the sum of phenolic compounds in plant extracts and juices. Nevertheless two other methods for assessment of phenolic compounds exist, namely the ferricyanide method according to Price and Butler (PBM) [6] and a method using 4-aminoantipyrine (AAPM) [7]. Little is known about their value and about comparative results obtained by them.

* Corresponding author. Tel.: +420 545133285; fax: +420 545212044.
E-mail address: kuban@mendelu.cz (V. Kubáň).

0039-9140/$ – see front matter © 2006 Elsevier B.V. All rights reserved.
doi:10.1016/j.talanta.2006.08.012

On the contrary, over 20 methods are used for assessment of antioxidant capacities [8]. The significance of the measured values and mutual comparison of the results gained by individual method is still an unresolved problem. For the methods based on similar principles of redox reactions (e.g. Trolox equivalent antioxidant capacity (TEAC), Ferric reducing antioxidant power (FRAP) and the method with 2,2 diphenyl-1-picrylhydrazyl (DPPH)) the measured values for similar samples using calibration with the same standard could correlate relatively well (see refs. [9–14]).

The purpose of the present study was to analyse the reactivity of compounds used as standards and known interfering compounds with the above methods and evaluate the influence of the standard selected on the values determined. For further understanding of determined values and possible comparison, concentration of the free and total phenolic compounds were determined by the three spectrophotometric methods (FCM, PBM and AAPM) on the same extracts of selected species of fruits and cereals. Their total antioxidant capacities were simultaneously determined by applying another three commonly used spectrophotometric methods (TEAC, FRAP and DPPH) on the same extracts and the values compared.

2. Materials and methods

2.1. Instruments

A spectrophotometer HELIOS β controlled with a VISION 32 Software (Spectronic Unicam, Cambridge, UK); an ultrasonic bath HD 2070 (model M8 72, Bandelion Sonoplus, Germany), a high-speed Grindomix mill (Retsch, Germany) and a CHRIST ALPHA 1-2 B lyophiliser (Braun Biotech International, Germany) were used for sample preparation.

2.2. Chemicals

Caffeic, ferulic and ascorbic acids (purity ≥99.0% each), 2,2-diphenyl-1-picrylhydrazyl radical (DPPH•, ≈90.0%) and 2,2′-azinobis(3-ethylbenzothiazolin-6-sulfonate) diammonium salts (ABTS, ≈98.0%) were purchased from Sigma–Aldrich Chem. Comp. (USA); gallic acid monohydrate (≥98.0%), Trolox (6-hydroxy-2,5,7,8-tetramethylchromane-2-carboxylic acid, a hydrophilic derivative of tocopherol, purum, ≥99%, for HPLC), Folin–Ciocalteu reagent (FC reagent) and 2,4,6-tris(2-pyridyl)-*s*-triazine (TPTZ, puriss, ≥99.0%) were obtained from Fluka Chemie (Buchs, Switzerland). Methanol and acetonitrile of gradient grade were purchased from Merck (Darmstadt, Germany). Other chemicals of p.a. purity were from Pliva-Lachema (Brno, Czech Republic). All reagents and standard solutions were prepared using Milli Q deionised water (Millipore, Bedford, USA).

2.3. Sample preparation

Samples (17 kinds of fruits and 6 kinds of grains mostly commonly consumed in Czech Republic—Table 1) were purchased from a local market (Delvita stores). Less usual or seasonal fruits (sea-buckthorn and black rowanberry, apricots, peaches, plum, greengage and red current) were gained from own sources and kept frozen at −20 °C until freeze-drying. Edible parts of fruits (20–50 g) were cut into small pieces, lyophilised and dry matter was determined gravimetrically (±1 mg). Lyophilisates were homogenized in a laboratory ultra-mixer and the powder was stored in plastic bottles under nitrogen at −20 °C until analysed [9]. Cereals and products of them, such as flowers, were used in natural state without further dehydration. Vinson et al. [11,13] procedure for extraction of free and total (conjugated) phenolic compounds was modified. Details of this procedure were published in a previous paper [9].

2.3.1. Determination of phenolic compounds in extracts

Performance of Folin-Ciocalteau method according Singleton et al. [5] and Vinson et al. [11] was described in details in our previous paper [9]. PBM procedure was performed according to Waterman and Mole [14] and AAPM according Schoonen and Sales [7]. All three methods were modified to a reaction volume of 1 ml. Reactions and incubations were carried out in plastic test tubes and spectrophotometric measurements were made in cuvettes with 1 cm light pathway (see refs. [9–14] for details).

2.3.2. Determination of ascorbic acid

High-performance liquid chromatographic method with mass spectrometric detection (HPLC/MS) was selected for assessment of ascorbic acid concentration in extracts. Standard solution of ascorbic acid in aqueous methanol (1:1, v/v) was prepared. Ascorbic acid was determined using HP 1100 liquid chromatograph equipped with HP MSD 1100 (Hewlett-Packard), a Waters dC 18 chromatographic column (4.6 mm × 20 mm, 3 μm) at the flow rate 1.5 ml/min and the column thermostat set at 20 °C. Mobile phase consisted of A: 0.01% trifluoroacetic acid, B: acetonitrile (ACN); gradient: $t = 0.0$ min: 1% B; $t = 0.2$ min: 1% B; $t = 3.0$ min: 30% B; $t = 3.5$ min: 50% B; $t = 5.0$ min: 1% B. Specific MS detection: SIM mode (ESI negative), *m/z* 175.0; gain 1.0; fragmentor 70; drying gas 8.0 l/min, nebulizer pressure 60 psi; temperature of drying gas flow 300 °C; capillary voltage 3000 V.

2.3.3. Determination of antioxidant activity/capacity of plant extracts

Three methods, TEAC, FRAP and DPPH• were used for the estimation of antioxidant capacity based on the reaction of specific reagent of each method with electron donating or hydrogen radical (H•) producing antioxidant compounds. Chemistry of these methods described in details Huang et al. [4]. The "total antioxidant power" was interpreted as the total reducing power. The antioxidant capacity was then interpreted as the reducing capacity [14]. Detailed information about the performance of these methods was published in our previous paper [9]. Despite the similar redox mechanism of the methods, the main reagents, originating products and also performance of the methods are different and the interpretation of resulting values often differ considerably in publications. Thus, comparison of published results of individual methods and between publications for the same method is often problematic.

Table 1
Numeration of the samples and comparison of our contents of phenolic compounds determined by FCM and dry weight (DW) with published results of Kähkönen et al. [10] and Vinson et al. [11]

Number		Content of phenolic compounds							
		Total[a], *x*		Free[b], *x*		Total[b], *x*		DW (%)	
		S[c]	[25]	*S*[c]	[10]	*S*[c]	[10]	*S*[c]	[10]
1	Apple Idared	20.5	11.9 + 0.4	38.0		42.2		19.5	18.8
2	Apple Golden Delicious	14.9	12.1 + 0.3	17.7	16.4	30.8	34.1	18.6	
3	Pear Klapp's	19.2		14.0	19.0	39.6	41.4	14.25	15.9
4	Quince		26.0		31.4		53.3		18.14
5	Apricot		52.0		57.4		107.1		19.90
6	Peach		20.2		26.1	9.7	41.6	22.9	18.83
7	Plum		21.8		22.9	39.1	45.0	58.2	18.85
8	Greengage	28.4		27.9		58.5		16.49	
9	Red currant	18.1	12.6 + 0.2	71.0		37.3		15.05	
10	Sea buckthorn	15.8		53.9		32.6		21.17	
11	Black chokeberry (aronia)	66.1		185.6		36.2		20.44	
12	Orange		11.8		17.1	3.6	24.2	18.9	13.42
13	Orange peel	22.8		22.5		46.9		27.22	
14	Mandarine	15.9		18.2		32.7		14.48	
15	Red grapefruit	15.1		22.8	4.2	31.0	7.5	15.47	12.0
16	Lemon		11.2		18.6	2.4	23.0	19.6	12.84
17	Banan		10.2		4.3	12.6	21.0	42.3	27.42
18	Kiwi		9.6		13.6		19.7		17.18
Grains									
19	Peeld barley (groat)								
20	Hulled buckwheat								
21	Oat flakes								
22	Rice, natural								
23	Wheat wholemeal (ashes 1800 mg/100 g)								
24	Wheat smooth flower (ashes 650 mg/100 g)								
25	Wheat semi-smooth flower (ashes 550 mg/100 g)								
26	Wheat course flower (ashes 450 mg/100 g)								
27	Hulled millet								

[a] GE, gallic acid equivalent in mg/g DW.
[b] CE, catechin equivalent in mmol/g DM.
[c] Our results, DW, dry weight; [12]: plum 1435 ± 406; red grapefruit 2206 ± 612 mg CE/g DW.

3. Results and discussion

3.1. Comparison of reactivity of the methods with individual standards

All the used methods (see Table 2) exhibited a strictly linear dependence between absorbance and concentration of all standards (gallic, ferulic and caffeic acids, catechin, Trolox, phenol and iron sulphate) and possible interfering substances (ascorbic acid, glucose, fructose and saccharose). The measured absorption coefficients for TEAC, DPPH and FRAP methods are mentioned in our previous publication [9]. The nearest values of absorption coefficients of analysed standards were for Trolox. Additional study was made for comparison of FCM, PBM and AAPM.

From the comparison of molar absorption coefficients of the different standards used (Table 2; Fig. 1), it follows that the determined values principally depend on three basic factors: (i) the method used, i. e. reactivity of oxidizing substances or radical (reactant); (ii) the standard used; (iii) the individual reactivity of the compounds in the extracts.

Table 2
Determined millimolar absorption coefficients and ratio of absolute values of molar absorption coefficients related to ferulic acid (after/symbol) of all used methods for applied standards

Method	Gallic (3OH)	Caffeic (2OH)	Ferulic (1OH)	Phenol (1OH)	Trolox (1OH)	Ascorbic (2OH)	$FeSO_4$ ($1e^-$)
FCM	0.177/1.22	0.201/1.39	**0.145**	0.092/0.63	0.058/0.40	0.098/0.68	0.028/0.20
PBM	0.952/2.27	0.290/0.69	**0.420**	0.178/0.42	0.179/0.43	0.275/0.65	0.102/0.24
AAPM	0.003/0.03	0.007/0.06	**0.112**	0.120/1.07	0/0	0/0	0/0
TEAC	−1.588/2.54	−0.179/0.29	**−0.624**	−/0.28	−/0.40	−/0.28	−/0.16
FRAP	−/2.13	−/1.52	**0.471**	−/0.00	−/0.84	−/0.60	−/0.42
DPPH	−/5.70	−/1.14	**−0.244**	−/0.00	−/1.04	−/0.60	−/0.65

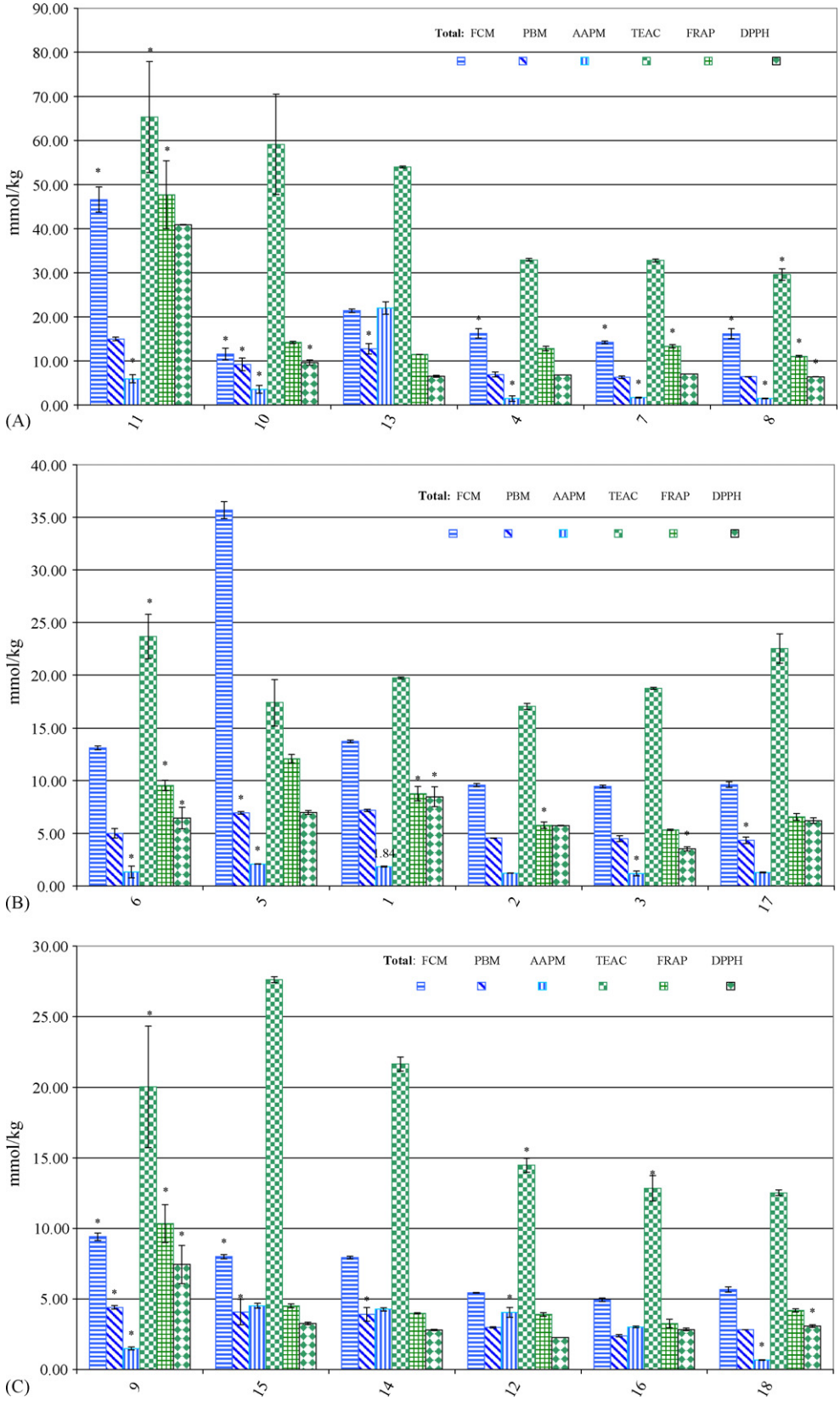

Fig. 1. Content of total phenolic compounds determined by the FC, PB and AAP methods (GE) and antioxidant activity determined by TEAC, FRAP and DPPH methods (TE) in extracts of fruit (mmol/kg fresh mass), $x \pm$ absolute mean deviation, $n = 2$, $^{*}n = 4$.

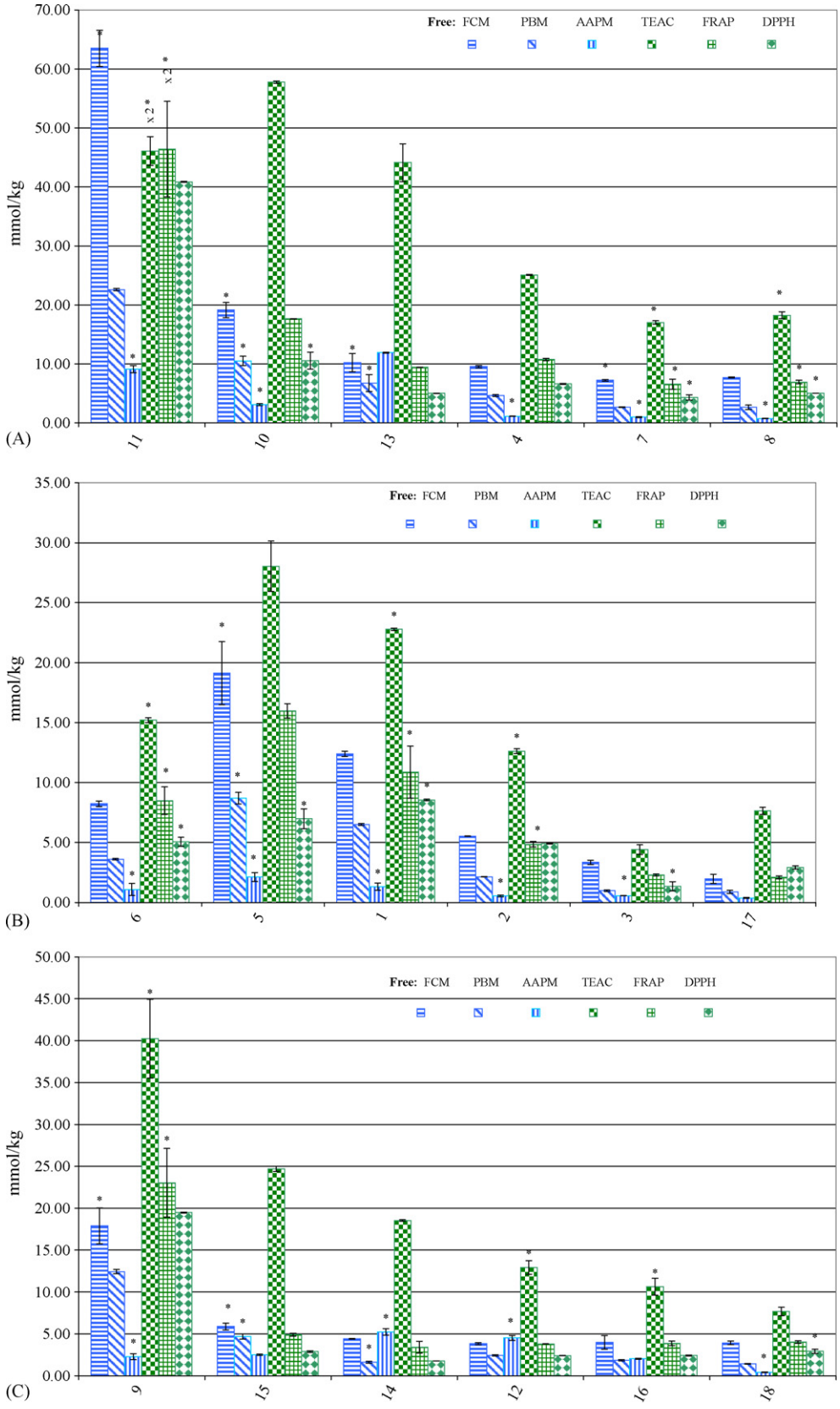

Fig. 2. Content of free phenolic compounds determined by the FC, PB and AAP methods (GE) and antioxidant activity determined by TEAC, FRAP and DPPH methods (TE) in extracts of fruit (mmol/kg fresh mass).

From a simple comparison of determined values of phenolic compound concentrations in a set of fruit extracts determined by the FCM and PBM (Figs. 2 and 3) calibrated on a common standard (gallic acid), it appears that the PBM provide lower values and it should be therefore less reactive. On average 2.36/2.14 times lower values for total/free phenolic compounds, respectively, were obtained by PBM in the set of extracts from the fruits under examination. However, gallic acid reacts relatively little using FCM, whereas very intensely in PBM, so that ratio of their absorption coefficients is 1:5.38. When a phenolic compound is used as a common standard, which has the same absorption coefficient for both the methods, the results would be five times higher for PBM compared those FCM. Therefore, either phenol, which has nearly the same absorption coefficients for FCM, PBM and AAPM methods or caffeic acid, which has very similar absorption coefficients for these methods, could be an ideal common standard for mutual comparison of the values determined by these methods. A decrease of reactivity of individual substances in PBM according to absorbance was: gallic (3OH) > ferulic (1OH + 1OCH_3) > caffeic (2OH) ≈ ascorbic > Trolox (1OH) > $FeSO_4$ > fructose > glucose > saccharose. An amount of rising product evidently did not depend only on the number of OH-groups in molecule, but on the ability of their hydrogen cation dissociation (e.g. higher value for ferulic acid with one OH than for caffeic acids containing two OH).

3.2. Determination of phenolic compounds in extracts

The FCM actually measures a total reducing capacity of a sample. Determination correlates well with redox and antioxidant ability of phenolic compounds. Dissociation of phenolic proton leads to phenolate anion, which is capable of reducing FC reagent. FCM is non-specific to phenolic compounds. Many non-phenolic compounds, in fruits above all ascorbic acid and saccharides can reduce the reagent.

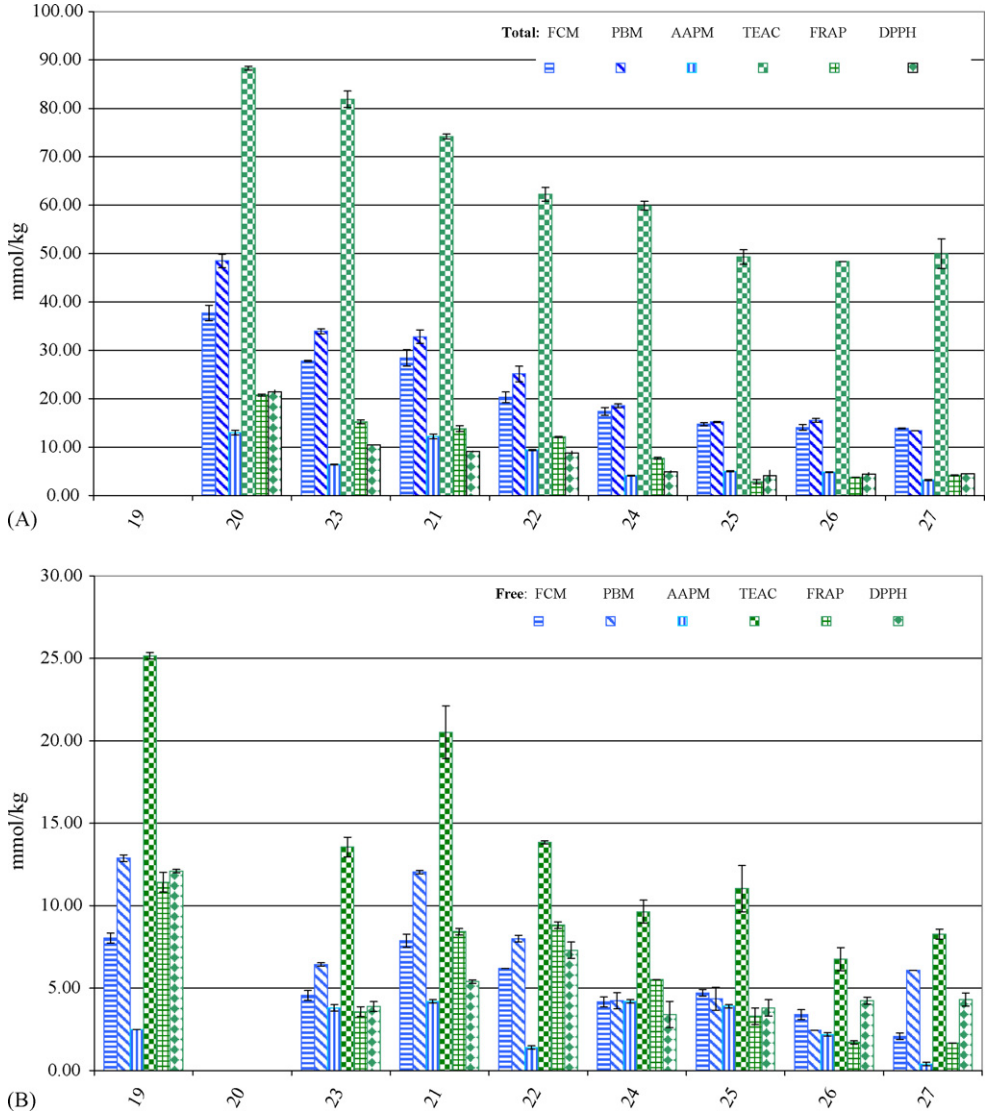

Fig. 3. Content of total/free phenolic compounds determined by the FC, PB and AAP methods (GE) and antioxidant activity determined by TEAC, FRAP and DPPH methods (TE) in extracts of grains (mmol/kg dry weight), $n = 2$.

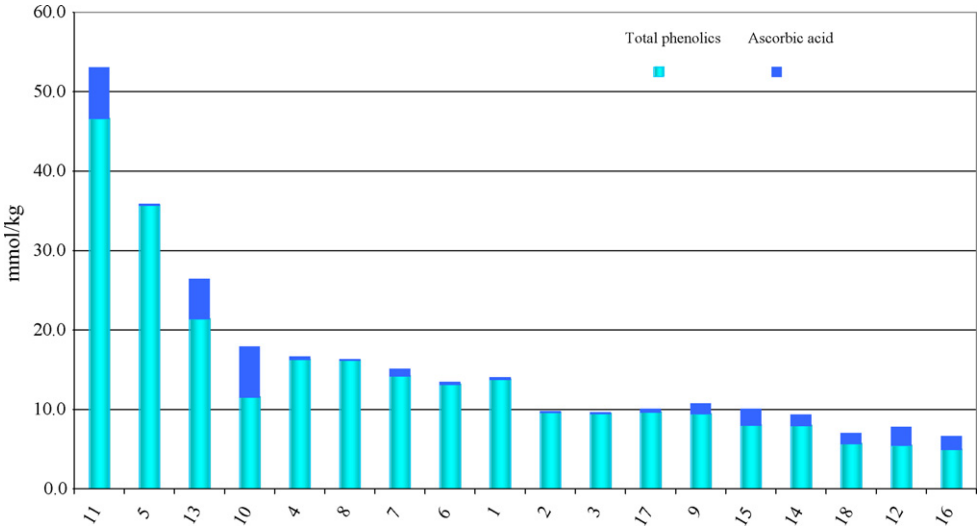

Fig. 4. Participation of total phenolics and ascorbic acid on values determined by the FCM (GA) in mmol/kg fresh mass.

The determined total contents of phenolic compounds and antioxidant activities are presented in Figs. 1–4. Values determined with FCM and PBM on extracts of fruit are corrected for the content of ascorbic acid. Free phenolic compounds determined by FCM considerably predominate (four times) over the conjugated compounds in the majority of fruits (11 kinds of 18). The content of conjugated (total minus free) phenolic compounds ranged from 19.2% (with the exception of one sort of apples of 9.9%) to 79.5% (only for four kinds over 50%). The significantly higher content of free phenolic compounds in comparison with the total has been found in three kinds of samples, red currant, sea-buckthorn and black chokeberry—aronia. The lower values for total phenolic compounds in comparison with free determined in coloured kinds indicate some artefact, a hydrolytic process decomposing or degrading a part of the phenolic compounds or another accompanying reducing substances in these varieties with a high content of anthocyanine pigments. The pigments could be partly hydrolytically degraded or modified to lessen reactive derivatives. In our samples, the hydrolytic process converted red colours to darker yellowish-brown, which indicates that at least part of the anthocyanidins was degraded. Therefore, for anthocyanine coloured fruits other more suitable ways of extraction of total phenolic compounds should be used.

Few published data are suitable for comparison by reason of methodology. Comparing the determined values of Vinson et al. [13], whose results for conjugated phenolic compounds ranged from 31 to 94%, the content of conjugated phenolic compounds was lower in five and higher in three of our samples. It is explainable by fact that the content of phenolic compounds and therefore the ratio of free to conjugated phenolic compounds in fruits depends on several factors, such as variety, season, maturity, vegetative conditions (especially content of nutrients and intensity of solar energy), state of health of the fruit, method of storage, etc. [15–18].

In our samples, the total content of phenolic compounds (mmol/kg fresh mass, FM) in decreasing order was: black chokeberry (aronia) (highest 46.6) > apricot > orange peel > quince > greengage > plum > apple Idared > peach > sea-buckthorn > banana > apple Golden Delicious > Klap's pear > red currant > red grapefruit > mandarin orange > kiwi > orange > lemon (lowest 4.9). In our apples, the concentration of free and total phenolic compounds were (mg of gallic acid equivalent, GAE/100 g FM): 160 and 278 for Golden Delicious variety and 359 and 399 for Idared (red) variety, respectively. Imeh and Khokhar [19] found the concentration of free and total phenolic compounds on the average for Golden Delicious variety 135 and 384, respectively, and 444 mg of total phenolic compounds for Red Delicious variety. The total content of phenolic compounds in Red Delicious variety including skin has been quoted as 290 mg/100 g and in peeled as 220 mg/100 g [20]. The intensely coloured skin could therefore cause significant difference in content of phenolic compounds. As for other fruits, they determined the total concentration of phenolic compounds (without correction to ascorbic acid) using the same method of extraction at 302–458, 385, 535 and 303 mg GAE/100 g FM for pears, peach, plum and kiwi, respectively [19]. Our results were (with the correction to ascorbic acid) 274, 1035, 381 and 164 mg GAE/100 g FM for pears, peach, plum and kiwi, respectively. During maturation, the ratio of phenolic compounds to dry matter mass diminishes and individual phenolic compounds do not behave uniformly. The evident shift from monomeric structures to oligomeric with a tendency to the production of procyanidins (4β,6-epicatechine) at the end of vegetative periods has been observed for flavonol [21].

Fruits and vegetables are usually mentioned as primary sources of phenolic compounds in food but different cereals may be a good source of phenolic compounds as well. The cereals of primary economic and nutritional importance in developed countries include wheat, rye, barley, oat and rice. Corn, millet and sorghum that are more consumed in developing countries, are consumed much less. The total content of phenolic compounds determined by FCM decreased (mostly also with PBM) in sequence from buckwheat hulled > oat flakes > wholemeal

Table 3
Correlation of method for determination of phenolic compounds and antioxidant activity by methods of linear least squares method (Excel)

Total/free	FCM	PBM	AAPM	TEAC	FRAP	DPPH
Fruits						
FCM	–	(18T) ++	(18T) –	(17T) ++	(18T) ++	(18T) ++
PBM	(18F) ++	–	(18T) –	(18T) ++	(18T) ++	(18T) ++
AAPM	(17F) ++	(17F) ++	–	(17T) +	(17T) +	(17T) +
TEAC	(17F) ++	(18F) ++	(17F) +	–	(18T) ++	(18T) ++
FRAP	(18F) ++	(18F) ++	(17F) ++	(17F) ++	–	(18T) ++
DPPH	(18F) ++	(18F) ++	(17F)++	(17F) ++	(18F) ++	–
Cereals						
FCM	–	(7T) ++	(8T) ++	(8T) ++	(8T) ++	(8T) ++
PBM	(7F) ++	–	(8T) ++	(8T) ++	(8T) ++	(8T) ++
AAPM	(8F) –	(8F) –	–	(7T) ++	(8T) ++	(8T) ++
TEAC	(8F) ++	(8F) ++	(8F) –	–	(8T) ++	(8T) ++
FRAP	(8F) ++	(7F) ++	(8F) –	(8F) ++	–	(8T) ++
DPPH	(8F) +	(7F) ++	(8F) –	(8F) +	(8F) ++	–

T/F, total/free phenolic compounds; +, significant (P 0.05–0.01); ++, higly significant ($P < 0.01$); –, no significant ($P > 0.05$).

wheat > natural rice > smooth wheat flour > semi-smooth wheat flour > wheat whole-meal wheat flour > to millet hulled. In contradistinction to fruits, for which the contents of phenolic compounds determined by PBM were mostly significantly lower than the values determined by FCM, most of the values of total and free phenolic compounds determined with PBM were notably higher to those determined with FCM. In contradistinction to fruits, conjugated phenolic compounds predominated in all the types of cereals analysed and they formed 68–85% from the total phenolic compounds.

The concentration of total phenolic compounds determined with PBM decreased in sequence buckwheat hulled > wholemeal wheat > oat flakes > natural rice > smooth wheat flour > whole-meal wheat flour > semi-smooth wheat flour > millet hulled. The values for FCM and PBM correlate highly significantly (Table 3), but FCM values are approximately half the value for PBM.

The values determined by AAPM are lowest because this method is highly selective. It reacts only with a small part of phenolic compounds able to undergo redox reactions. The amount of colour product is directly proportional only to concentration of phenolic compounds able create quinone structures or substances able create imine structures. The results of assay for single extracts are depicted in Figs. 1–4. Generally, the results determined with AAPM are less then half, compared to the values determined with PBM. The lower values for AAPM are due to the fact the only part of the phenolic compounds in extracts of fruit are able to create quinone structure.

Of the individual phenolic compounds analysed only ferulic acid responded comparably to phenol but the reaction with gallic acid was approximately 50 times smaller; gallic and caffeic acids almost did not react and ascorbic acid, Trolox and $FeSO_4$ did not react at all. For saccharides, very little response was found only for glucose and fructose (see Table 2).

The majority of the concentrations in extracts of fruits ranged from (mmol/kg FM//DM) 1–2//4–10, high value in orange peel (22//81)) and lower values in black chokeberry (5.9//29) and in oranges, mandarin, grapefruit and lemon (3–4//23–30). The concentrations for cereals evaluated with AAPM were related to DM and the results are comparable with the values for fruits. However, they are notably higher (3.2–13.0 mmol/kg DM) for the total phenolic compounds as compared with free phenolic compounds (0.4–4.2 mmol/kg DM). The values in cereal extracts were, in decreasing concentration: buckwheat hulled > oat flakes > natural rice > wholemeal wheat > semi-smooth wheat flour > coarse wheat flour > smooth wheat flour > millet. PBM and AAPM are used for assessment of phenolic compounds in foods of plant origin rather rarely, so that published data that we could compare to ours were not found.

The values determined by AAPM would be a measure of pro-oxidizing activity of certain phenolic substances in extracts, considering its ability to react almost exclusively with quinones and semiquinones. These can be reduced easily and therefore have generally pro-oxidative properties. Redox cycling including antioxidizing radicals and their oxidative forms, in the case of polyphenols, semiquinones and quinones, is the most likely the basis for their pro-oxidizing effects [22].

3.3. Antioxidant activity/capacity of extracts

Three most commonly used methods (TEAC, FRAP and DPPH) assess the total antioxidant activities in a hydrophilic medium. Hydrolysed extracts contain superior antioxidants, because it is commonly known that glycosides of phenolic compounds are less active antioxidants than their aglycones [23,24]. Additional hydroxyl group capable of redox reaction can be liberated by hydrolysis. The values of antioxidant activity of individual methods in extracts are depicted in Figs. 1–4.

3.4. Determination with TEAC method

This method gives relatively high values. It is related to high reactivity of the ABTS reagent, which is advantageous. On the other hand, the method is the most problematic of the three methods used. The ABTS reagent itself is relatively unstable

Table 4
Antioxidant activity determined with FRAP method in equivalent $FeSO_4$ (mmol/100 g FM—modified acc. [17])

Fruit/reaction time:	4 min	10 min	30 min	This paper (4 min)
Apple	1.06–1.81	1.39–2.25	1.83–2.89	
Apple, Golden Delicious	1.48	1.86	2.42	0.58
Apple, Red Delicious	1.31	1.61	2.01	0.88 (Idared)
Pear	1.04–1.43	1.28–1.80	1.62–2.25	0.53
Peach	1.07	1.36	1.76	0.96
Plum	1.60	2.04	2.61	1.33
Kiwi	0.93	1.15	1.57	0.42

and slowly deteriorates under reaction conditions, i. e. there is measurable decrease of absorbance during the incubation period. That can increase the measured values [9]. However, this decrease is possible to be subtracted.

The concentration of free phenolic compounds determined by TEAC method, were in decreasing sequence: aronia > sea-buckthorn > orange peel > red currant > apricot > quince > red grapefruit > Idared apple > mandarin > greengage > plum > peach > orange > Golden Delicious apple > lemon > kiwi > banana > Klap's pear. The decreasing sequence for total phenolic compounds is: aronia > sea-buckthorn > orange peel > plum > quince > greengage > grapefruit > peach > banana > mandarin > greengage > Idared apple > pear > apricot > Golden Delicious apple > orange > lemon > kiwi. The antioxidant activity of cereals determined by TEAC in decreasing order for free phenolic compounds was: peeled barley (25.2 mmol/kg DM) > oat flakes > natural rice > wholemeal wheat > semi-smooth wheat flour > smooth wheat flour > millet > coarse wheat flour (6.76) and for total phenolic compounds: buckwheat (88.3) > wholemeal wheat > oat flakes > natural rice > smooth wheat flour > millet > semi-smooth wheat flour ≫ coarse wheat flour (48.3). Essentially the higher content of phenolic compounds and the antioxidant activity of wholemeal flour, in addition to the higher content of vitamins, mineral substances, phospholipids and fibres, can be an additional favourable factor for human health and a significant reason for its preferable consumption instead of white flours.

3.5. Determination with FRAP method

The antioxidant activity rated for total phenolic compounds in fruits were, in decreasing order: aronia > sea-buckthorn > plum > quince > apricot > orange peel > greengage > red currant > peach > Idared apple > banana > Golden Delicious apple > pear > grapefruit > kiwi > mandarin > orange > lemon. The antioxidant capacity for cereals was, in decreasing order: buckwheat > wholemeal wheat flour > oat flakes > natural rice > smooth wheat flour > millet > semi-smooth wheat flower ≈ course wheat flour. Phenolic compounds with known effectiveness (radicals per molecule) of quercetine 1.2, rutine 0.9, myricetine 2.2 and myricitrine 1.9 [26] are predominant in citrus fruits and apples.

There are only few data in the literature, with which it would be possible to compare our results considering the methods of extraction, analysis and samples. Results for several kinds of fruits [19] offer some possibility of comparison (see Table 4).

3.6. Determination with DPPH method

The values of antioxidant activities determined with DPPH method are lowest, despite that this DPPH method gives the same values as the TEAC method. The standard Trolox is most often used [9]. The DPPH method gives several times lower values for extracts than TEAC. This significant difference in values could be explained by a relatively higher stability of the DPPH radical what may result in significantly lower reactivity. This radical will evidently react only with the more reactive phenolic substances. Therefore, it will not detect the less reactive phenolic substances, which still could have antioxidant activity in the human organism.

3.7. Interfering substances

Ascorbic acid and sugars (mono- and disaccharides) belong to the group of most interfering substances in plant extracts. Ascorbic acid significantly reacts with the FC reagent and the determined values reach approximately half the values of gallic acid (Fig. 1). Therefore, a fruit with a high content of ascorbic acid notably "increases" the determined content of phenolic compounds. Assessment of ascorbic acid is complicated because of its rapid reduction to dehydroascorbic acid, which reacts with FC positively as well. Dehydroascorbic acid reacts relatively quickly to further compounds. We determined that the concentration of ascorbic acid solution (the same as used for extraction of phenolics) at laboratory temperature decreased by approximately 70% per day. A very low concentration of ascorbic acid may be already present in extracts after several days of their storage, even at −20 °C. Therefore, ascorbic acid should

Table 5
Determined molar absorption coefficients for particular methods for the reactions with main saccharides in fruits ($\times 10^3$)

Method/saccharide	Glucose	Fructose	Saccharose
FCM	0.6	2.2	0.5
PBM	0.7	2.3	0.6
AAPM	2.3	2.3	0.0
TEAC	−0.2	−0.6	−1.1
FRAP	0.0	0.4	0.0
DPPH	0.0	0.0	0.0

Table 6
Calculated quantitative influence of saccharides to increase of determined contents of phenolic compounds and antioxidant activity of particular methods using measured absorption coefficients

Matter	Tabulated contents of saccharides (%)[a]			Contribution of saccharides to determined values (vol%)							
				FCM		PBM		TEAC		FRAP	
	Glc	Fru	Sach	Free	Total	Free	Total	Free	Total	Free	Total
Apple	1.80	5.00	2.4	22.1	19.9	9.4	8.5	4.6	5.4	1.8	2.6
Pear	2.20	6.00	1.1	68.2	24.8	48.9	11.6	18.3	4.3	9.0	4.0
Apricot	1.90	0.40	4.4	2.6	1.4	1.9	2.4	3.9	6.3	0.2	0.2
Peach	1.50	0.90	6.7	10.1	6.4	6.4	4.5	7.6	4.9	0.6	0.4
Plum	3.50	1.30	1.5	10.8	5.5	9.7	4.1	7.7	4.0	0.8	0.2
Red currant	2.30	1.00	0.2	2.2	3.8	1.0	2.5	1.6	3.2	0.2	0.2
Orange	2.40	2.40	4.7	17.5	13.9	7.3	6.4	7.2	6.4	2.0	2.0
Grapefruit red	2.00	1.20	2.1	7.8	6.2	3.0	3.3	2.9	2.6	1.0	1.0
Lemmon	0.50	0.90	0.2	5.7	4.9	2.7	2.3	1.4	1.2	0.8	0.8
Banana	5.00	3.80	6.6	>90	34.3	86.0	20.4	45.3	15.4	12.2	3.8

[a] [27], Approximate correction according to content of phenolic compounds (100, 200, 500 and 1000 mg/l) were calculated as 5, 5, 4, 3%; 8, 10, 6, 6%; –, 20, 10, 10% for 25, 50 and 100 g/l of saccharides, respectively.

be determined in a as short as possible time from the assessment of phenolic compounds. The contribution of ascorbic acid to increasing concentration of phenolic compounds in analysed extracts of fruit is presented in Fig. 4.

Glucose, fructose and sucrose belong to the most important saccharides present in fruits and vegetables. These sugars react (interfere) with different intensity in the methods used for the assessment of phenolic compounds and in the methods used for the assessment of antioxidant activity, with the exception of the DPPH method, that require donation of hydrogen radical. Molar absorption coefficients for individual methods and sugars (Table 5) express their reactivity for individual methods. It is possible to evaluate their contribution to the FCM reaction by percentual subtraction from the total values in the samples with the higher content without real determination (using published data on their average content). According to Singleton et al., it is possible to express the theoretical quantitative influence of saccharides depending on quantity of phenolic compounds and saccharides [5].

Approximate correction can be estimated according to the note in Table 6. Using the calibration coefficient for FCM, it is possible to estimate that the influence of fructose is approximately 3.5 times that of glucose and perhaps 4.5 times that of saccharose. The estimated influence of saccharides on the increased values for analysed fruits mostly not exceed 5% and often is less than 1%. The proximate influence of saccharides on the determined values by FCM, PBM, TEAC and FRAP calculated from the average content of saccharides and calculated absorption coefficients is presented in Table 6.

However, for several kinds of fruits with relatively higher concentration of saccharides, especially for the FCM, most values exceed 5% and in very sweet kinds of fruit, such as grape, cherry, banana, pear, etc. they may even increase the values of free phenolic compounds by more than 50%. In an alkaline medium endiol reduction agents, easily reducing compounds, are formed from saccharides. Ascorbate is also a reducing agent. Reactions of FCM and AAPM are performed in an alkaline medium at pH 10.0.

Purines like guanine (not guanosine), xanthine and uric acid react with molar yields similar to mono-phenols. Adenine and pyrimidines react very little. The reaction of proteins responds to the content of tyrosine and tryptophane and is insignificant. Cysteine produces molar absorbance approximately one half in comparison to mono-phenols; glutathione reacts similarly [5]. Carotenoids can interfere in some methods [19] but their content in fruits is usually low.

3.8. Correlation of methods used

Because all the used methods for the assessment of phenolic compounds and antioxidant capacity are based on redox properties, there should exist some correlation between content of phenolic compounds (free or total) and antioxidant capacity as measured by the individual methods. These relationships are evident from bars in Figs. 1–4 and values in Table 3. The values of phenolic compounds concentration and the antioxidant activities for free and total phenolic compounds in fruits and cereals, as determined by the FCM, PBM, TEAC, FRAP and DPPH methods, correlate highly significantly. However, the DPPH method showed correlation with the FCM and TEAC methods for free phenolic compounds of cereals. The values determined by AAPM mostly do not, or only non-significantly, correlate with values determined by other methods. This can be explained by lesser reactivity of the DPPH reagent and the very selective reactivity of the AAP reagent. Data in the literature about the relation between concentration of phenolic compounds and antioxidant activity are contradictory. While some authors have observed high correlation [10], others find no direct correlation or only a very weak one.

4. Conclusions

The assessment of phenolic compounds and total antioxidant capacity in extracts of fruits and cereals were investigated by several spectrophotometric methods. Three methods, FCM, PBM and AAPM for the assessment of phenolic compounds,

were modified to a semimicro-scale (total volume 1 ml) with minimum consumption of a sample (down 100 μl) and thereby applicable for fast screening (1 person is able to analyse about 20 extracts per hour with 1 method). The analyses of standards, interferents and identical plant extracts demonstrated different reactivity of the principal reagents of the methods with individual substances. In addition, the trends of the measured values, even if their absolute values differ proportionally, could be compared.

The relatively less commonly used PBM method is the most reactive of the three methods (FCM, PBM and AAPM) used for the estimation of phenolic compounds concentration. The commonly used FCM reacts only with the more reactive phenolic compounds. AAPM has significantly different mechanism of response and reacts only with phenolic substances that are able to create a quinoidal structure and thus with only a smaller part of the total content of phenolic compounds. AAPM might be of informative value about the pro-oxidizing ability of phenolic compounds and could be a measure of pro-oxidizing strength, e.g. in orange peel value four–five times higher than in black chokeberry, grapefruit, mandarin and 10–20 times higher than in the other kinds of fruits determined.

Three most often used methods for estimation of antioxidant capacity, TEAC, FRAP and DPPH were modified and applied for the evaluation of antioxidant capacity to the same set of standards, interferents and plant extracts. The methods enable fast and reproducible assessment of the equivalent antioxidant capacity of selected standard (e.g. Trolox) in semi-microscale, reaction volume 1 ml, with limited sample consumption down 100 μl. The TEAC method is the most reactive and the FRAP method is essentially the least. The DPPH radical (often quoted in publications) is relatively stable and therefore less reactive, so that it reacts only with more reactive reducing (phenolic) substances. Lowermost results obtained using DPPH method evidently correlate with the low reactivity (high stability) of the radical.

Extracts of 17 kinds of fruit and of 6 kinds of cereals were analysed by each of the 6 mentioned methods. In the assay of phenolic compounds, it is important to determine the content of ascorbic acid at virtually the same time and correct the values obtained according to its contribution to increasing absorbance, especially for samples with a high content. Samples with high amounts of saccharides may notably elevate contents of phenolic compounds and antioxidant activities by even more than 50%. They should, therefore, be separated priory to assay or a correction reflecting their content should be applied. Ascorbic acid (not or very little sugars) reacts with principal reagents of the methods used for estimation of antioxidant capacity significantly as well.

The determined values of fruit extracts assessed by different methods highly correlate with the exception of those of AAPM. The latter method is very selective and assays only the phenolic compounds able to create a quinoline structure.

References

[1] G. Block, B. Patterson, A. Subar, Nutr. Cancer 18 (1992) 1.
[2] M.G.L. Hertog, D. Kromhout, C. Aravanis, H. Blacburn, R. Buzina, S. Fidanza, S. Giampaoli, A. Jansen, A. Menotti, S. Nedelijkovic, M. Pekkarinen, B.S. Simic, H. Toshima, E.J.M. Feskens, P.C.H. Hollman, M.B. Katan, Arch. Intern. Med. 155 (1995) 381.
[3] B. Halliwell, J.M.C. Gutteridge (Eds.), In: Free Radical in Biology and Medicine, Oxford University Press, UK, 1999, p. 617.
[4] D. Huang, B. Ou, R.L. Prior, J. Agric. Food Chem. 53 (2005) 1841.
[5] V.L. Singleton, R. Orthofer, R.M. Lamuela-Raventós, Methods Enzymol. 299 (1999) 152.
[6] M.L. Price, L.G. Butler, J. Agric. Food Chem. 25 (1977) 1268.
[7] J.W. Schoonen, M.G.F. Sales, Anal. Bioanal. Chem. 372 (2002) 822.
[8] E.N. Frankel, A.S. Meyer, J. Sci. Food Agric. 80 (2000) 1925.
[9] P. Stratil, B. Klejdus, V. Kubáň, J. Agric. Food Chem. 54 (2006) 607.
[10] M.P. Kähkönen, A.I. Hopia, H.J. Vuorela, J.-P. Rauha, K. Pihlaja, T.S. Kujala, M. Heinonen, J. Agric. Food Chem. 47 (1999) 3954.
[11] J.A. Vinson, Y. Hao, X. Su, L. Zubík, J. Agric. Food Chem. 46 (1998) 3630.
[12] S. Karakaya, S.N. El, A.A. Tas, Int. J. Food Sci. Nutr. 52 (2001) 501.
[13] J.A. Vinson, X. Su, L. Zubik, P. Bose, J. Agric. Food Chem. 49 (2001) 5315.
[14] P.G. Waterman, S. Mole (Eds.), Methods in Ecology, Blackwell Science Publisher, Oxford, 1994, p. 66.
[15] R. Cote, D. Nadeau, Anal. Lett. 26 (1993) 87.
[16] I.F.F. Benzie, J.J. Strain, Methods Enzymol. 299 (1999) 15.
[17] B. Lata, M. Przeradzka, M. Bukowska, J. Agric. Food Chem. 53 (2005) 8970.
[18] M. Leja, A. Mareszek, J. Ben, Food Chem. 80 (2003) 303.
[19] U. Imeh, S. Khokhar, J. Agric. Food Chem. 50 (2002) 6301.
[20] M.V. Eberhardt, C. Yong, I.R. Hei, Nature 405 (2000) 903.
[21] U. Mayer, D. Treutter, C. Santos-Buelga, H. Bauer, W. Feucht, Phytochemestry 38 (1996) 1151.
[22] W. Bors, C. Michel, K. Stettmaier, Methods Enzymol. 335 (2001) 166.
[23] I.B. Afanas'ev, A.I. Dorozhko, A.V. Brodskii, A. Kostyuk, A.I. Potapovitch, Biochem. Pharmacol. 38 (1989) 1763.
[24] J.A. Vinson, Y.A. Dabbagh, M.M. Serry, J.J. Jang, Agric. Food Chem. 43 (1995) 2800.
[25] H. Wang, G. Cao, R.L. Prior, J. Agric. Food Chem. 44 (1996) 401.
[26] P.T. Gardner, D.B. McPhail, A. Crozier, G.G. Duthie, J. Sci. Food Agric. 79 (1999) 1011.
[27] J. Velíšek, Chemie potravin (Chemistry of Foodstufs, in Czech): OSSIS Tabor, 1999.

Available online at www.sciencedirect.com
ScienceDirect
Talanta 71 (2007) 1637–1641
Talanta
www.elsevier.com/locate/talanta

Voltammetric sensing of sugar by an electrode covered with wheat germ agglutinin/chitin film

Kazuharu Sugawara [a,*], Tomoyuki Takayanagi [a], Naoto Kamiya [a], George Hirabayashi [a], Hideki Kuramitz [b]

[a] *Faculty of Education, Gunma University, Maebashi, Gunma 371-8510, Japan*
[b] *Department of Environmental Biology and Chemistry, Faculty of Science, University of Toyama, Toyama 930-8555, Japan*

Received 10 June 2006; received in revised form 25 July 2006; accepted 25 July 2006
Available online 1 September 2006

Abstract

The binding between wheat germ agglutinin (WGA) and *N*-acetylglucosamine at the electrode covered with chitin film was investigated with voltammetry. Chitin, β-1,4-poly-*N*-acetylglucosamine, is one of the biolpolymers which have a high biocompatibility. WGA is immobilized to the surface of chitin film by the affinity of WGA to *N*-acetylglucosamine residue of chitin. To investigate the binding event of WGA on the chitin modified electrode, *N*-acetylglucosamine labeled with an electroactive compound was prepared. The binding causes the changes in the electrode response of labeled sugar. The peak current of labeled sugar decreased due to the specific binding with WGA on the chitin film modified at the electrode. *N*-Acetylglucosamine was successfully determined by using the competitive reaction with labeled sugar to WGA on the chitin film electrode.

Keywords: Wheat germ aggutinin; *N*-Acetylglucosamine; Chitin; Voltammetry

1. Introduction

Chitin, which is β-1,4-poly-*N*-acetylglucosamine, widely exists in exoskeleton of crab, shell skins of the mollusc and cell wall of the fungus. Because chitin has a high biocompatibility, the film and fiber form of chitin have been applied to various fields as an excellent biomaterial [1,2]. In electrochemical application, Ohashi et al. has reported a glucose sensor using a chitin thin film that immobilized glucose oxidase (GOx) on a gold electrode surface [3]. In previous study, we evaluated streptavidin–biotin binding at an electrode covered with chitin film [4]. The immobilization of streptavidin was based on an electrostatic interaction between protonated acetylamide group of chitin and streptavidin with negative charge. Biotin labeled with an electroactive compound was used as a probe to monitor the binding. The interaction between streptavidin and biotin can be evaluated from the changes in the electrode response of labeled biotin.

Lectin, which is one of glycoproteins, combines with specific sugar chain at cell surface [5,6]. It is known that wheat germ agglutinin (WGA) recognizes *N*-acetylglucosamine residue of chitin [7,8]. WGA is a subunit with a molecular weight of 18 kDa and consists of a dimmer with equal subunits at pH 7.0. WGA has two bound *N*-acetylglucosamine per monomer, and the binding constant between WGA and *N*-acetylglucosamine is about $2.5 \times 10^3\ M^{-1}$ [9]. Therefore, WGA is immobilized through *N*-acetylglucosamine residue on chitin surface. The binding hardly causes change of structure in WGA for the immobilization and prepares chitin film with a new function. In addition, this method does not need any chemical modification. When chitin powder is dissolved and is formed to its film, the film can be mounted on an electrode. On the other hand, Anzai et al. has reported multiplayer thin films that consist of concanavalin A (ConA) and native GOx on the surface of a platinum electrode [10]. The concept of this study is similar to the design concept of our electrode.

In this study, the binding between WGA and *N*-acetylglucosamine was investigated at an electrode covered with chitin film. WGA is selectively immobilized at chitin film surface by specific recognition of *N*-acetylglucosamine residue to WGA (Fig. 1). *N*-Acetylglucosamine labeled with an electroactive

* Corresponding author. Tel.: +81 27 220 7282; fax: +81 27 220 7282.
E-mail address: kzsuga@edu.gunma-u.ac.jp (K. Sugawara).

0039-9140/$ – see front matter © 2006 Elsevier B.V. All rights reserved.
doi:10.1016/j.talanta.2006.07.046

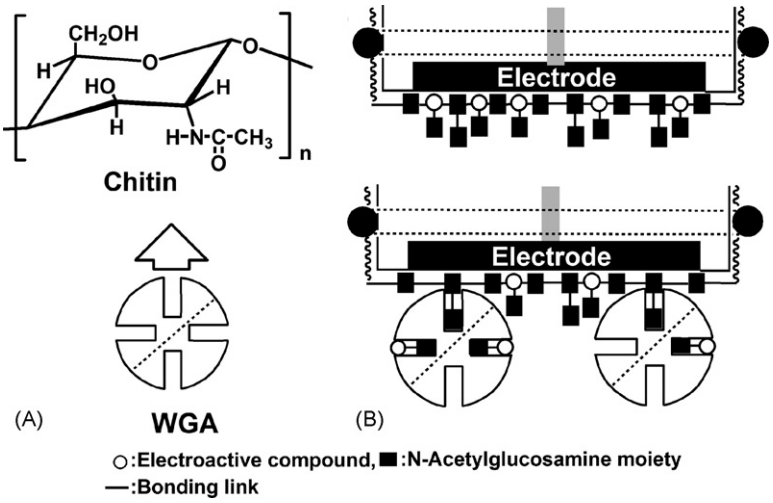

Fig. 1. Principle of WGA immobilization and the WGA–*N*-acetylglucosamine binding at an electrode covered with chitin film.

compound as a probe to evaluate the binding was prepared. The labeled sugar permeates the film and gets to the electrode surface resulting in the electrode response. The peak current of labeled sugar decreases only when the labeled sugar trapped into the binding site of WGA immobilized on the chitin film. *N*-Acetylglucosamine is related to transmission of the signal from the extracellular surface to intracellular [11] and control of the cancer cell growth [12]. IgG sugar chain of a chronic rheumatoid arthritis patient has a high ratio of sugar chain owning *N*-acetylglucosamine on the end. Furthermore, *N*-acetylglucosamine may influence to type 2 diabetes [13]. Therefore, sensing of *N*-acetylglucosamine in living body is important to early recognition and treatment. The WGA/chitin film is an attempt of pseudo-biomembrane formation, and an electrode covered with the film becomes sensor of *N*-acetylglucosamine. In addition, the electrode is powerful as reaction fields that protein-sugar binding occurring at the cell membrane is evaluated.

2. Experimental

2.1. Apparatus

CV-50W analyzer (Bioanalytical Systems Inc. (BAS)) was used for all voltammetric measurements. A working electrode was a glassy carbon electrode (Model No. 11-2012, BAS). The electrode was polished with 1.0, 0.3, and 0.05 μm alumina (Baikoski International Corp., Charlotte, NC), respectively. A counter electrode was a platinum wire, and an Ag/AgCl electrode (Model No. 11-2210, BAS) was a reference electrode. The pH of solution was measured with a Horiba D-21 pH meter. The measurements of visible spectra of the reagents were carried out with a UV 1240 mini spectrophotometer (Shimadzu, Tokyo, Japan).

2.2. Reagents

Chitin powder was purchased from Funakoshi Co. Ltd., Japan. *N*-Acetylglucosamine, daunomycin as an electroactive compound, *N*,*N*-dimethylacetoamide (DMA), 1-methyl-2-pyrrolidone (NMP) reagent were purchased from Wako Pure Industries, Japan. Phosphate buffer (pH 7.0) of 0.1 M with KH_2PO_4 of 0.1 M and NaOH of 0.1 M was used as incubation solution and as a supporting electrolyte in electrochemical measurement. The supporting electrolyte before the measurement was deaerated by high quality nitrogen. All reagents used were of analytical reagent grade.

2.3. Preparations of chitin film and labeled sugar

Chitin (0.075 g) was dissolved with DMA (1.6 g), NMP (1.6 g) and LiCl (0.25 g), and the solution was stirred until the chitin became gel. Then, DMA (3.5 ± 0.1 g) and NMP (3.5 ± 0.1 g) were added to the gel. The gel was made to a homogeneous solution by stirring. The chitin solution was transferred to several Petri dishes (diameter: 3 cm) and evaporated at 55 °C for 24 h. The prepared film was rinsed with pure water to eliminate the organic solvents and stored in pure water. Thickness of the film was about 0.009 mm [6].

Structure of labeled *N*-acetylglucosamine was shown in Fig. 2. Labeled *N*-acetylglucosamine was prepared by Schiff base reaction between daunomycin and *N*-acetylglucosamine for 24 h at 4 °C in 0.1 M phosphate buffer solution (pH 8.5).

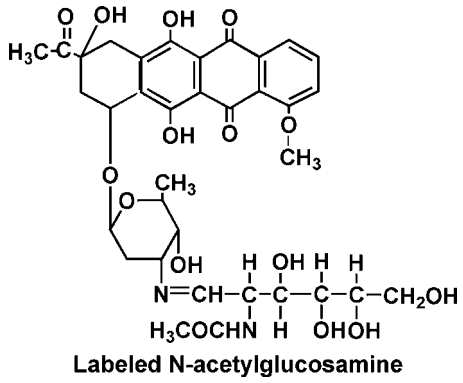

Fig. 2. Structure of labeled *N*-acetylglucosamine.

The solution was spotted on a sheet of thin-layer chromatography (silica gel alumina sheet, MERCK) in 1-propanol:ammonia water = 4:1% (v/v). After developing, the labeled sugar was stripped from the sheet and collected. The reagent was dissolved in ethanol, and the solution was centrifuged to exclude silica gel. Then, the supernatant solution was evaporated, and ethanol and phosphate buffer were added. The concentration of the labeled sugar was determined on the basis of the mole absorbance efficiency (11,000) of daunomycin at 490 nm [13].

2.4. Procedure

Chitin film (1.0 cm × 1.0 cm) was held on to a glassy carbon electrode by a rubber O-ring. To immobilize WGA on the chitin film surface, the electrode was immersed with stirring for 1 h in 0.1 M phosphate buffer (pH 7.0) with WGA. After the immobilization, the electrode was removed to 0.1 M phosphate buffer (pH 7.0) without WGA and incubated in the solution with labeled sugar. Next, a potential at −1.0 V was applied to the electrode for 5 min with stirring. The potential was scanned to a positive direction with differential pulse voltammetry (scan rate: 5 mV s^{-1}; pulse amplitude: 50 mV; sample width: 2 ms; pulse width: 50 ms; pulse period: 200 ms). Detection of *N*-acetylglucosamine was attempted with the competitive reaction to the limited binding sites of WGA between labeled *N*-acetylgulcosamine and free *N*-acetylglucosamine. Voltammetric measurement was carried out with the method mentioned above.

3. Results and discussion

3.1. Voltammograms of labeled N-acetylglucosamine and WGA at a glassy carbon electrode covered with chitin film

Permeability of labeled *N*-acetylglucosamine to the chitin film was investigated (Fig. 3). After a potential at −1.0 V for 5 min was applied to the electrode in 0.1 M phosphate buffer (pH 7.0) with 5×10^{-7} M labeled *N*-acetylglucosamine, measurement was carried out with differential pulse voltammetry. As a result, a peak due to the reoxidization of reduced quinone moiety in the labeled sugar appeared at −0.65 V [14]. The peak current at the electrode covered with chitin film became 70% of that at a plain electrode. Although the electrode response of labeled sugar decreases due to the effect of steric hinderance in chitin film, it is clear that the labeled sugar penetrates the chitin film. Therefore, the WGA-sugar binding at the film surface can be evaluated by using the labeled sugar.

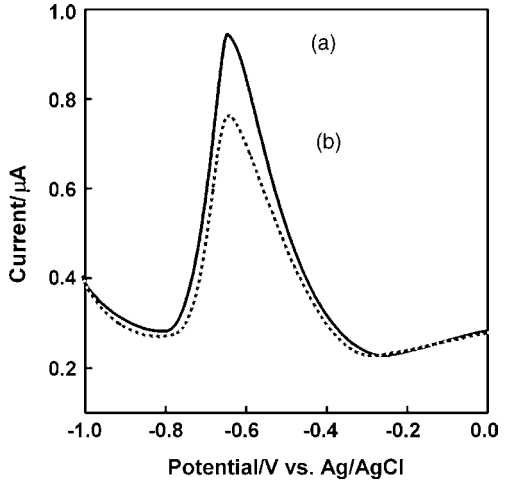

Fig. 3. Voltammograms of labeled *N*-acetylglucosamine at a glassy carbon electrode. (a) Without chitin film; (b) with chitin film. Measurements were carried out with differential pulse voltammetry (DPV, scan rate = 5 mV s^{-1}), after a potential at −1.0 V for 5 min was applied to the electrode in 0.1 M phosphate buffer (pH 7.0) with 5.0×10^{-7} M labeled *N*-acetylglucosamine.

Next, an electrode covered with chitin film was immersed for 1 h in 0.1 M phosphate buffer (pH 5.5) with 5×10^{-7} M WGA. Then, the electrode was removed to 0.1 M phosphate buffer containing only 5×10^{-7} M labeled *N*-acetylglucosamine. After the electrode was incubated for 1 h in the solution, voltammetric measurement was carried out. The peak current of 5.0×10^{-7} M labeled *N*-acetylglucosamine at the electrode with WGA/chitin film decreased to 35% in comparison with the current at an electrode with chitin film which was not immersed in the solution containing WGA (Fig. 4). In contrast, the peak current of 5×10^{-7} M daunomycin was measured at the electrode covered with WGA/chitin film. The peak current was similar to that at an electrode covered with chitin film without WGA. This is because daunomycin does not combine with WGA. When the pH of solution was changed to 7.0, the peak current of labeled *N*-acetylglucosamine decreased. Isoelectric point of WGA is about 9, and the protonation of acetylamide group of chitin film occurs at pH less than 6.5. Consequently, it is expected that WGA is immobilized on the film due to the molecule recognition function and not due to the electrostatic interaction between chitin film and WGA. The peak current of labeled sugar decreased on the basis of the holding of the electroactive moiety in the binding sites of WGA at chitin film.

3.2. The immobilization time of WGA to chitin film and the concentration of the immobilization of WGA

The immobilization time of WGA to the chitin film were examined. The electrode was immersed in 0.1 M phosphate buffer (pH 7.0) with 5×10^{-7} M WGA and removed to 0.1 M phosphate buffer (pH 7.0) without WGA. Labeled *N*-acetylglucosamine of 5×10^{-7} M was added to the solution, and the solution was mixed for 1 h. The peak current decreased with increasing the immobilization time and became constant over 40 min. This is because of the saturation for amount of WGA immobilized to the chitin film surface.

Relationships between the concentration of immobilization WGA and the peak current were shown in Fig. 5. After the electrode was immersed for 1 h in 0.1 M phosphate buffer (pH 7.0) with WGA, the electrode was incubated in other phosphate buffer containing only 5×10^{-7} M labeled *N*-acetylglucosamine. The peak current decreased up to 1.2×10^{-6} M WGA drastically. The concentration of WGA was sufficient in 2.0×10^{-6} M WGA. In contrast, it is clear that the electrode response of daumomycin is not influenced by WGA immobilized to the chitin film.

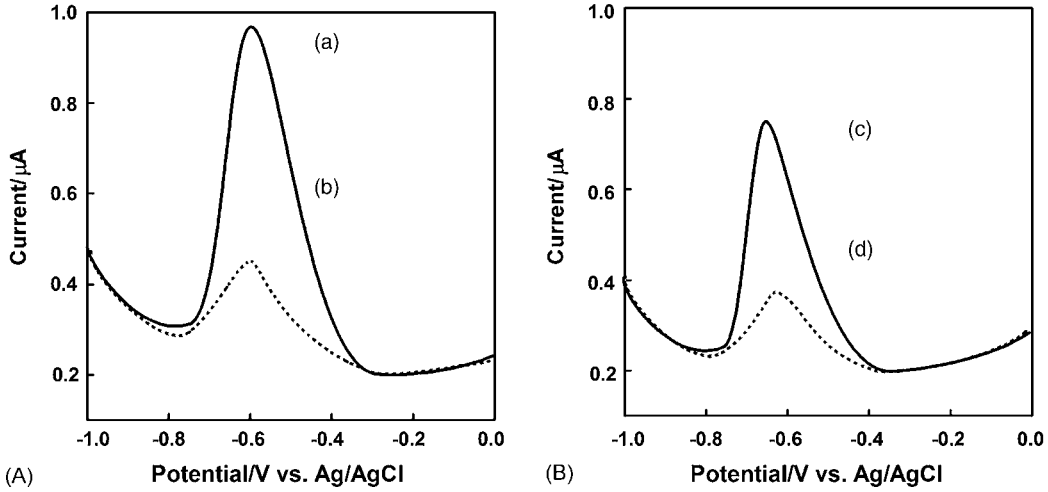

Fig. 4. Voltammograms of labeled *N*-acetylglucosamine and WGA at the electrode covered with chitin film. (A) 0.1 M phosphate buffer (pH 5.5): (a) 5.0×10^{-7} M labeled *N*-acetylglucosamine; (b) 5.0×10^{-7} M labeled *N*-acetylglucosamine + 8.0×10^{-7} M WGA. (B) 0.1 M phosphate buffer (pH 7.0): (c) 5.0×10^{-7} M labeled *N*-acetylglucosamine; (d) 5.0×10^{-7} M labeled *N*-acetylglucosamine + 8.0×10^{-7} M WGA. Measurements were carried out with DPV after a potential at −1.0 V for 5 min was applied to the electrode.

3.3. Voltammograms of labeled mannose and ConA at the electrode covered with chitin film

The immobilization of ConA (isoelectric point 5.0) to the chitin film was attempted. Because mannose combines with ConA, a labeled mannose was prepared. Although ConA has a negative charge in a solution at pH 7.0, acetylamide group of chitin is neutral. Therefore, it is expected that ConA is not immobilized to the film on the basis of electrostatic interaction. The peak current of labeled *N*-acetylglucosamine at the electrode immersed in 0.1 M phosphate buffer with ConA did not change in comparison with that at an electrode with chitin film without ConA. That is, ConA was not immobilized on the chitin film due to the electrostatic interaction and molecular recognition. On the other hand, the immobilization of WGA having positive charge to the neutral chitin film in a solution of pH 7.0 was achieved. This fact also supposes that WGA combines with *N*-acetylglucosamine residue of chitin.

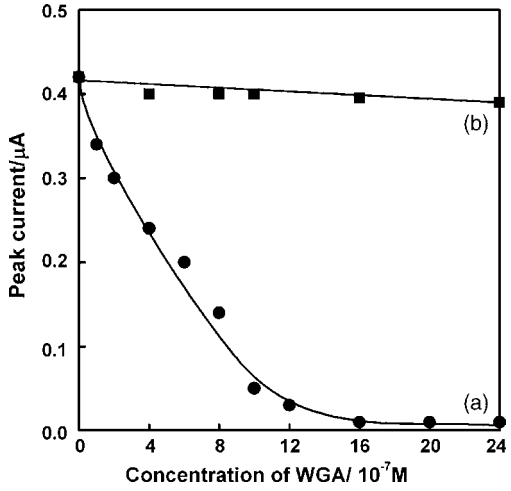

Fig. 5. Immobilization of WGA at the electrode covered with the chitin film. (a) 5.0×10^{-7} M labeled *N*-acetylglucosamine; (b) 5.0×10^{-7} M daumomycin. The electrode was immersed with stirring for 1 h in 0.1 M phosphate buffer (pH 7.0) with WGA. Next, 5.0×10^{-7} M reagent was added to in 0.1 M phosphate buffer (pH 7.0) without WGA, and the electrode was incubated for 1 h with stirring in the solution. Measurements were carried out with DPV, after a potential at −1.0 V for 5 min was applied to the electrode.

3.4. Immobilization amount of WGA at the chitin film

Amount of WGA immobilized on the surface of chitin film was estimated from the following experiments. First, an electrode covered with chitin film was immersed for 1 h in 0.1 M phosphate buffer with 5.0×10^{-7} M WGA. Then, the electrode was removed from the solution, and 5.0×10^{-7} M labeled *N*-acetylglucosamine was added to the solution. After the labeled sugar and WGA which has remained in the solution were mixed for 1 h, the peak current was measured at a plain electrode. Because WGA was immobilized at the chitin film, the concentration of WGA in the solution decreased. Second, 5.0×10^{-7} M labeled sugar and 5.0×10^{-7} M WGA were incubated in 0.1 M phosphate buffer for 1 h. Next, the peak current was recorded at a plain electrode. The peak current mentioned above was larger than that of this operation. The amount of immobilization was calculated on the basis of the peak current. That is, the difference of peak current was referred to the calibration curve of WGA to the peak current of 5×10^{-7} M labeled sugar at a plain electrode. The value became about 8.0×10^{-9} mol/cm^2.

3.5. Detection of N-acetylglucosamine on the basis of competitive reaction

The competitive reaction to the limited binding sites of WGA between *N*-acetylglucosamine and labeled *N*-acetylglucosamine was applied to detection of *N*-acetylglucosamine. The electrode covered with WGA/chitin film was immersed in 0.1 M phosphate buffer with both reagents. The concentration of labeled *N*-acetylglucosamine and WGA were constant, and the con-

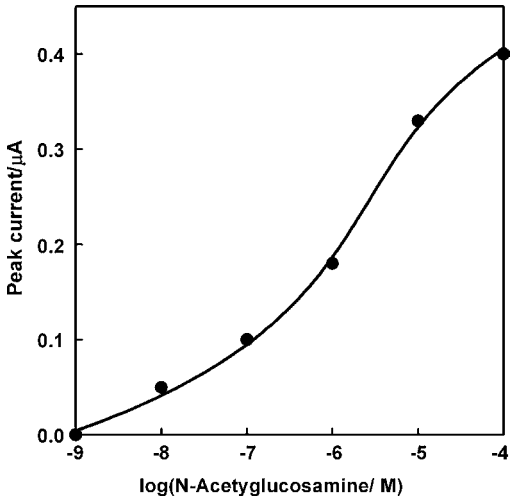

Fig. 6. Detection of *N*-acetylglucosamine based on the competitive reaction. The electrode was incubated for 1 h in 0.1 M phosphate buffer (pH 7.0) with 2.0×10^{-6} M WGA. Next, 5.0×10^{-7} M labeled *N*-acetylglucosamine and a various concentration of biotin were added to in 0.1 M phosphate buffer (pH 7.0) without WGA, and the electrode was incubated with stirring for 1 h in the solution. Measurements were carried out with DPV, after a potential at −1.0 V for 5 min was applied to the electrode.

centration of *N*-acetylglucosamine was changed. When the concentration of *N*-acetylglucosamine increased, the peak current depended on the concentration of *N*-acetylglucosamine (Fig. 6). For the measurements, the relative standard deviation at 1×10^{-7} M labeled sugar was 5.0% ($n = 5$). The detection limit of labeled *N*-acetylglucosamine estimated from three times the standard deviation (3σ) was 10^{-8} M.

4. Conclusions

Because WGA recognizes *N*-acetylglucosamine residue of chitin, immobilization of WGA was immobilized at an electrode covered with chitin film. The binding between WGA and *N*-acetylglucosamine was evaluated by *N*-acetylglucosamine labeled with an electroactive compound at the electrode. Sensing of *N*-acetylglucosamine at the electrode was carried out by the competitive reaction to the binding sites of WGA between free sugar and labeled sugar. Thus, chitin film with a new function was produced and the WGA-sugar binding was monitored. The merit of this method is that WGA is selectively immobilized to chitin film on the basis of molecular recognition. The film is suitable as a reaction fields that binds sugar existing on cell surface and a protein. This method hardly caused change of structure in WGA for the immobilization, and it prepared chitin film with a new function.

Acknowledgements

The authors thank the Ministry of Ministry of Education, Culture, Sports, Science, and Technology of Japan for support of this work under a Grant-in-Aid for Scientific Research (No. 16550068).

References

[1] S. Hirano, Biotechnol. Annu. Rev. 2 (1996) 237–258.
[2] A. Kato, I. Tanaka, M. Arakawa, T. Kondo, Biomater. Med. Dev. Artif. Organs 13 (1985) 61–82.
[3] E. Ohashi, I. Karube, J. Biotechnol. 15 (1995) 13–19.
[4] K. Sugawara, G. Hirabayashi, N. Kamiya, H. Kuramitz, S. Tanaka, Electroanalysis 17 (2005) 1659–1664.
[5] A. Leppanen, S. Stowell, O. Blixt, R.D. Cummings, J. Biol. Chem. 18 (2005) 5549–5562.
[6] R. Fiala, Z. Sulova, A.H. El-Saggan, B. Uhrik, T. Liptaj, I. Dovinova, E. Hanusovska, Z. Drobna, M. Barancik, A. Breier, Biochim. Biophys. Acta 1639 (2003) 213–224.
[7] H.A. Lucero, M.J. Kuranda, D.A. Bulik, Anal. Biochem. 305 (2002) 97–105.
[8] J. Ciopraga, O. Gozia, R. Tudor, L. Brezuica, R.J. Doyle, Biochim. Biophys. Acta 1428 (1999) 424–432.
[9] G. Bains, R.T. Lee, Y.C. Lee, E. Freire, Biochemistry 31 (1992) 12624–12628.
[10] J.-I. Anzai, Y. Kobayashi, T. Hoshi, H. Saiki, Chem. Lett. 28 (1999) 365–366.
[11] R.B. Parekh, R.A. Dwek, D.J. Sutton, D.L. Fernandes, A. Leung, D. Stanworth, T.W. Rademacher, T. Mizuochi, T. Taniguchi, K. Matsuta, F. Takeuchi, Y. Nagano, T. Miyamoto, A. Kobata, Nature 316 (1985) 452–457.
[12] T. Kitada, E. Miyoshi, K. Noda, S. Higashiyama, H. Ihara, N. Matsuura, N. Hayashi, S. Kawata, Y. Matsuzawa, N. Taniguchi, J. Biol. Chem. 276 (2001) 475–480.
[13] K. Vosseller, L. Wells, M.D. Lane, G.W. Hart, Proc. Natl. Acad. Sci. U.S.A. 99 (2002) 5313–5318.
[14] J.M. Kauffmann, O. Chastel, G. Quarin, J. Partriarche, Bioelectrochem. Bioenerg. 23 (1990) 167–175.

Available online at www.sciencedirect.com
ScienceDirect
Talanta 71 (2007) 1507–1511
Talanta
www.elsevier.com/locate/talanta

A green analytical procedure for sensitive and selective determination of iron in water samples by flow-injection solid-phase spectrophotometry

Leonardo S.G. Teixeira [a], Fábio R.P. Rocha [b,*]

[a] *Departamento de Engenharia e Arquitetura, Universidade Salvador, Av. Cardeal da Silva 132, 40220-141, Salvador, BA, Brazil*
[b] *Instituto de Química, Universidade de São Paulo, PO Box 26077, 05513-970 São Paulo, SP, Brazil*

Received 21 March 2006; received in revised form 12 July 2006; accepted 13 July 2006
Available online 14 August 2006

Abstract

A greener analytical procedure based on flow-injection solid-phase spectrophotometry is proposed for iron determination. Iron(II) is reversibly retained on 1-(2-thiazolylazo)-2-naphthol immobilized on C18-bonded silica, yielding a brown complex. The metal ion is eluted as iron(II) with a small volume of a diluted acid solution without removing the immobilized reagent, which can be used for at least 100 determinations. Other chemicals (buffer and reducing agent) were carefully selected taking into account the analytical performance and toxicity. The developed procedure is 10-fold more sensitive in comparison to the analogous procedure based on measurements in solution, being suitable for the determination of iron in water samples with good accuracy and precision. The detection limit (99.7% confidence level), sampling rate and coefficient of variation ($n = 10$) were estimated as 15 $\mu g\,L^{-1}$, 25 measurements per hour and 4.0%, respectively. The proposed procedure involves a reduced effluent generation (3.6 mL per determination) and consumes micro amounts of reagents.

Keywords: Green chemistry; Flow injection analysis; Solid-phase spectrophotometry; Iron; Water

1. Introduction

Green chemistry, defined as the use of chemistry for pollution prevention [1], has been applied mainly in the context of organic and inorganic synthesis, resulting in new synthetic routes, replacement of toxic solvents and minimization of side products [2]. However, several analytical methods currently in use generate large amounts of toxic residues, causing environmental impact. In this sense, the development of greener analytical procedures is widely desirable and this aspect should be taken into account by the analytical chemists [1]. Waste amount and toxicity are parameters as important as any other analytical feature. Several strategies are available to achieve this goal, such as reagent replacement, recycling and waste treatment. However, minimization of both reagent consumption and waste generation is the more general approach. Analytical methodologies can be revisited to drastically minimize waste generation, exploiting automation and miniaturization, for example.

Amounts of iron exist widely in river, tap, pond, well, and underground water and this metallic ion is essential for biological systems [3,4]. There are many spectrophotometric methods for iron determination, but some problems arise when these methods are applied to samples having complex matrices or containing traces of iron, owing to their poor sensitivity and selectivity [5]. Thus, it is important to develop procedures that can be directly applied to these samples and that incorporate aspects of green chemistry.

Conventional spectrophotometry, based on measurement of light transmission through solutions of absorbing species, is a widespread instrumental technique whose scope can be expanded by measurements in solid-phase. This approach, named solid-phase spectrophotometry (SPS), is based on absorbance measurements directly on a solid support on which the analyte is retained, thus avoiding tedious preconcentration and separation analytical steps [6,7]. Measurements can be carried out with conventional spectrophotometers, resulting in simple and low cost procedures. SPS also offers the advantage of *in situ* concentration of the analyte due to its accumulation in a small volume of the solid support, thus resulting in better sensitivity and lower detection limits in comparison to measurements

* Corresponding author. Fax: +55 11 3815 5579.
E-mail address: frprocha@iq.usp.br (F.R.P. Rocha).

0039-9140/$ – see front matter © 2006 Elsevier B.V. All rights reserved.
doi:10.1016/j.talanta.2006.07.025

in solution. Selectivity is also improved due to different retention abilities of the analyte and the interfering substances on the solid support [8,9]. Coupling flow injection with SPS (FI-SPS) makes feasible such measurements without attaining (physical or chemical) equilibrium conditions, thus providing faster and more selective procedures in comparison to those implemented in batch. In addition, small amounts of samples and reagents are employed and, in some situations, reagents immobilized on the solid support can be used for the reversible retention of the analyte, resulting on inherently greener procedures [7,8].

In this work, a greener analytical procedure is proposed for sensitive and selective determination of iron in water samples exploring its retention on 1-(2-thiazolylazo)-2-naphthol (TAN)/C18-bonded silica support in a flow injection system. Elution, buffering and reduction steps are performed with non-toxic chemicals in order to drastically minimize waste toxicity.

2. Experimental

2.1. Apparatus

The flow system was constructed with a lab-made sliding-bar injector, similar to one previously described [10,11], polyethylene tubes (0.7 mm i.d.) and Perspex joint points. Alternatively, the sliding-bar injector can be replaced by two commercially available six-way injection valves coupled in series. An Ismatec IPC-4 peristaltic pump equipped with Tygon tubes was used for fluid propulsion. An UV–vis spectrophotometer (Varian, Cary 1E) equipped with a lab-made 1-mm optical path cell for FI-SPS similar to one previously described [7] was employed for signal measurements. This flow cell consisted of two Perspex blocs separated by a rubber strip (1 mm thickness) and attached with four screws. A 10-mm diameter circular hole was made in the rubber strip to support the C18-bonded silica. In previous experiments, it was observed that higher optical paths caused an excessive attenuation of the radiation beam by absorption and scattering.

2.2. Reagents and solutions

All solutions were prepared with analytical grade chemicals and freshly distilled-deionized water. Iron reference solutions were prepared in the range 50.0–1000 μg L^{-1} by dilution of a 1000 mg L^{-1} stock solution prepared after dissolving metal iron in 5 mL concentrated HCl under heating.

Sodium acetate/acetic acid, hexamine/hydrochloric acid and tris(hydroxymethyl)aminomethane/maleic acid were evaluated as buffer solutions. Ascorbic acid and hydroxylamine solutions were evaluated as reducing agents.

A 0.1 mol L^{-1} HCl solution was employed as eluent. TAN solution was prepared by dissolving 1.0 mg 1-(2-thiazolylazo)-2-naphthol (Merck) in 1.0 mL ethanol and bringing the volume to 100 mL with a 5% (m/v) Triton X-100 solution. Water was used as the carrier stream.

Freshwater samples were collected in polyethylene vessels and filtered through 0.45-μm cellulose acetate membranes (Millipore) before analysis. Sample solutions were prepared containing 0.05 mol L^{-1} acetate buffer pH 5.5 and 0.1% (m/v) ascorbic acid. The blank solution was prepared in freshly distilled-deionized water, containing the same concentrations of buffer and the reducing solutions.

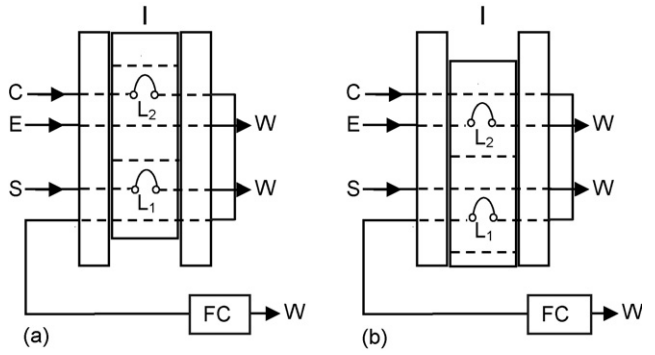

Fig. 1. Flow diagram of the system for iron determination by FI-SPS: (a) sampling position and (b) injection position. I: sliding-bar injector; S: sample; C: carrier stream (H_2O, 1.5 mL min^{-1}), E: eluent (0.1 mol L^{-1} HCl), L_1: 125-cm sample loop (625 μL), L_2: 20-cm eluent loop (100 μL), FC: lab-made flow cell placed at the spectrophotometer optical path, W: waste vessel.

2.3. Flow diagram and procedure

The flow-cell was filled with ca. 35 mg C18-bonded silica (60–100 μm) obtained from Sep-Pak cartridges (Waters). TAN reagent was immobilized on the solid support by pumping the solution through the flow cell at 0.5 mL min^{-1} for 10 min. The cell was then sequentially washed with 0.1 mol L^{-1} HCl and water.

In the flow diagram shown in Fig. 1, sample and eluent aliquots are alternately introduced into the carrier stream. In the sampling position (Fig. 1a), the loop L_1 (625 μL) is filled with buffered sample or reference solutions (S), while the acid eluent aliquot contained in L_2 is transported towards the flow cell by the water carrier stream. Metallic ions retained at the solid support are then eluted and the solid-phase is regenerated previously to the sample injection. By sliding the central bar of the injector to the other resting position (Fig. 1b), the sample aliquot (loop L_1) is inserted into the analytical path and transported by the carrier towards the flow cell. The iron(II)–TAN complex is formed at the solid support, yielding an analytical signal proportional to the metal amount, measured at 780 nm. Simultaneously, the loop L_2 is filled with the eluent solution (0.1 mol L^{-1} HCl). After attaining the signal maximum, the central bar is moved back to the sampling position to start another measurement cycle.

The reference method was based on complex formation between iron(II) and 1,10-phenantroline in ammonium acetate buffer after reduction of iron(III) with hydroxylamine [12]. For achieving the required sensitivity, after sample processing according to the reference method, absorbance measurements were carried out in a 100-cm optical path flow cell constructed with a liquid core waveguide (LCW) based on Teflon AF-2400® [13]. A similar strategy was adopted by Zhang et al. that employed an LCW with 200 cm optical path for iron determination in a gas segmented flow system [14].

3. Results and discussion

3.1. Chemical variables

TAN reacts quickly with iron(II) in aqueous solution to form a brown complex with absorption maxima at 575 and 787 nm [15]. The reaction also occurs instantaneously when the reagent is adsorbed on C18 bonded silica and the formed complex yields slightly different absorption maxima −580 and 780 nm. Measurements at 780 nm can be exploited for selectivity improvement, because other metallic ions (e.g., copper, zinc, nickel and cobalt) react with TAN forming complexes with absorption maxima between 550 and 600 nm [8,9].

Iron retention on C18-TAN is reversible – the complex is decomposed in acid media and iron(II) is eluted without removing the chromogenic reagent from the solid support. This characteristic allows the development of a greener analytical assay also incorporating the advantages of using SPS such as improvements in sensitivity and selectivity.

Eluent, buffer and reducing solutions were carefully selected in order to minimize waste amount and toxicity. It was observed that both ascorbic acid and hydroxylamine solutions could be used for iron(III) reduction with the same efficiency. Ascorbic acid was selected in view of its very low toxicity. The retention of iron(II) on C18-TAN was studied at various pH values for different buffers (Fig. 2). Acetate buffer was selected taking into account the sensitivity and its low toxicity when compared with other solutions evaluated. As higher signals were obtained at pH 6.3, ammonium acetate buffer can be used in view of the buffer capacity.

Different mineral acids can be used for iron elution from the solid support. Hydrochloric acid was selected because it allowed quantitative iron elution without removing the immobilized chromogenic reagent. The effects caused by eluent concentration and volume were evaluated and it was observed that 100 μL of 0.1 mol L^{-1} HCl was sufficient for complete iron elution. Thus, the reversible adsorption of the analyte was assured and no significant change on iron retention efficiency was observed even after 100 measurements. After this, the C18 solid support was replaced and a new aliquot of TAN was pumped through the cell for immobilization of the reagent. By considering the TAN amount on the solid support (ca. 9×10^{-7} mol), the estimated reagent consumption is lower than 1 μg per determination.

A systematic evaluation of the effect of potentially interfering species on iron determination in natural water samples was carried out. This study was performed by adding known amounts of foreign species usually found in water samples to a 500 μg L^{-1} iron solution. The threshold was established ±5% variation in the analytical signal. When the study was carried out at 580 nm, interferences were not observed for the following species up to 50 mg L^{-1}: Al(III), Ba(II), Be(II), Ca(II), Cr(III), Hg(II), Li(II), Mg(II), Mn(II), Mo(VI), Pb(II), Sb(IV), Sn(IV), Ti(IV), V(IV), W(IV), chloride, bromide, iodide, sulfate, nitrate and carbonate. Positive interferences were observed in the presence of Cd(II), Cu(II), Co(II), Ni(II) and Zn(II) even in the same concentration of the analyte. However, with measurements at 780 nm, selectivity was improved and these metallic ions were tolerated up to 2 mg L^{-1}. For higher concentrations (unusual in water samples), negative interferences were observed in view of the competition of the cations by the immobilized reagent.

3.2. Hydrodynamic variables

The flow system was designed to provide the removal of the analyte from the solid support after each sample measurement to avoid saturation of the adsorbent sites. This was carried out by introducing the sample and the eluent aliquots alternately into an inert carrier stream (see Fig. 1). As the total flow rate can affect both the retention efficiency and sampling rate in FI-SPS, the effect of this parameter was studied over the range 0.4–2.1 mL min^{-1} (Fig. 3). Higher sensitivities were obtained when lower flow rates were employed. Flow rates >2.1 mL min^{-1} caused fluid leakage in the joints due to the increase in back-pressure. A flow-rate of 1.5 mL min^{-1} was

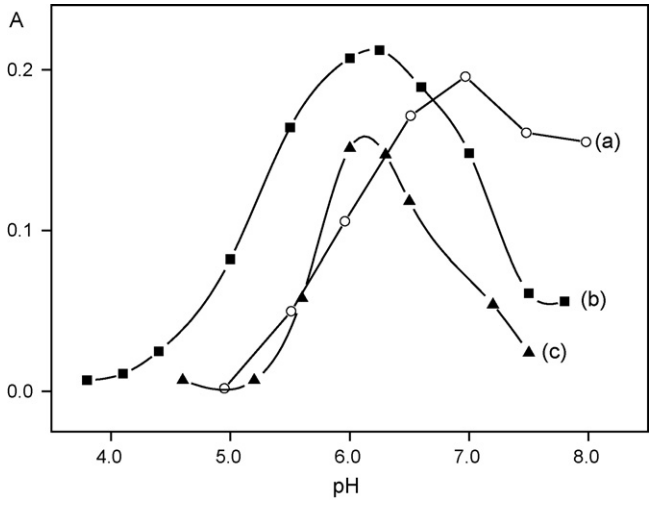

Fig. 2. Effect of the pH on iron(II) retention. (a) Tris(hydroxymethyl)aminomethane/maleic acid; (b) acetate/acetic acid and (c) hexamine/hydrochloric acid buffer. *A*: absorbance measured at solid-phase.

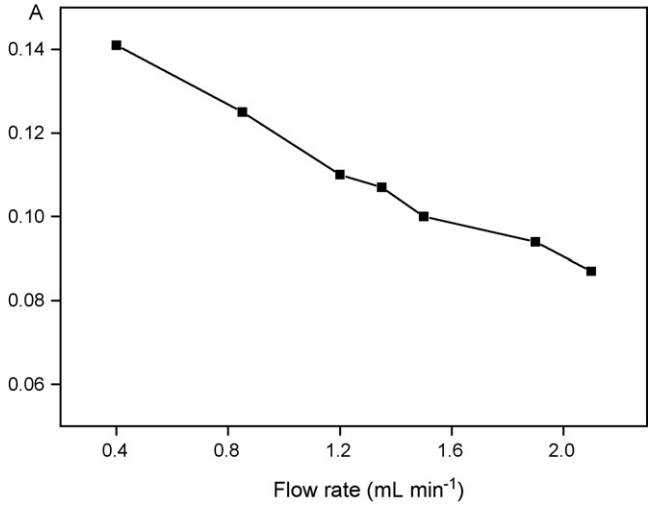

Fig. 3. Effect of the carrier flow rate on the analytical signal. *A*: absorbance measured at solid-phase.

selected as a compromise between sample throughput and sensitivity.

An important advantage of solid-phase spectrophotometry is the potential to improve sensitivity by increasing the sample volume from which the analyte is concentrated in the solid support [7,16]. This alternative can be exploited to adjust the sensitivity of the SPS procedure as function of the iron concentration in the samples and also to obtain analytical curves from a single standard solution. In this experiment, a linear correlation between the absorbance signal and the sample volume was observed in the range 200–800 μL. On the other hand, by increasing the sample volume, an inherent decrease in the sampling rate was also observed. Thus, a 625-μL sample volume was chosen as a compromise between sensitivity and sample throughput.

3.3. Analytical features and application

In the optimized conditions, linear response was observed between 50 and 1000 $\mu g\,L^{-1}$ for a 625-μL sample volume. The calibration curve can be described by the equation: $A = 0.341C + 0.0278$, $r = 0.997$, in which **A** represents the absorbance measured as peak height and **C** the iron concentration in $mg\,L^{-1}$. The flow cell filled with TAN-C18 and equilibrated with water (carrier stream) was employed to zero-setting the spectrophotometer in the single beam mode to establish the baseline. Under this condition, low blank values were measured, as described in the calibration curve equation.

Apparent molar absorptivity was estimated as $1.9 \times 10^5\,L\,mol^{-1}\,cm^{-1}$, which is ca. 17-fold higher than that achieved in the Fe(II)-1,10-phenantroline reference method ($1.1 \times 10^4\,L\,mol^{-1}\,cm^{-1}$) [12] and ca. 10-fold higher than that obtained in the analogous batch procedure with measurements in solution [15], in which higher sample and reagents volumes were employed. The assay presented in this paper uses only small volumes of sample and reagents, showing low sample and reagents consumption (see Table 1) with a waste generation of $90\,mL\,h^{-1}$.

The detection limit at the 99.7% confidence level was estimated as 15 $\mu g\,L^{-1}$, according to the recommendations of IUPAC [17]. Sampling rate and coefficient of variation ($n = 10$) were estimated as 25 measurements per hour and 4.0%, respectively. The FI-SPS procedure was applied to total iron determination in freshwaters from lake, river or weirs. The results shown in Table 2 agreed with those achieved by the modified reference method [12] at the 95% confidence level.

Table 1
Reagent consumption per determination in procedures using TAN as chromogenic reagent for iron determination

Reagent	Consumption	
	Proposed procedure	Conventional spectrophotometry [15]
TAN (μg)	<1.0	1000
Ascorbic acid (mg)	0.6	–
Hydroxylammonium chloride (mg)	–	100
Sodium acetate (mg)	3.6	340
Glacial acetic acid (μL)	0.4	147
Concentrated hydrochloric acid (37.5%) (μL)	0.8	–

Table 2
Mean values and standard deviations ($n = 3$) for total iron determination by the proposed and reference methods [12]

Sample	Iron concentration ($\mu g\,L^{-1}$)	
	FI-SPS	Reference method
Lake water	51 ± 2	53 ± 6
River water	80 ± 1	92 ± 1
Weir water 1	21 ± 1	21 ± 3
Weir water 2	80 ± 1	101 ± 6

4. Conclusions

The developed procedure provides a highly sensitive, selective and simple method for iron determination at $\mu g\,L^{-1}$ level. The proposed FI-SPS procedure was suitable for the determination of iron in water samples, yielding good accuracy and precision. The reversible retention of iron(II) on the C18-TAN solid support was explored to develop a greener analytical procedure, with reduced sample and reagent consumption and minimized waste generation.

As TAN immobilized on C18 does not react with iron(III), this species can be determined by difference from measurements carried out with and without the reducing solution. This strategy can be then adopted for redox speciation of iron that is often required in environmental studies.

Acknowledgements

The authors acknowledge the fellowships and financial support from the Brazilian agencies Conselho Nacional de Desenvolvimento Científico e Tecnológico (CNPq), Financiadora de Estudos e Projetos (FINEP) and Fundação de Amparo à Pesquisa do Estado de São Paulo (FAPESP).

References

[1] P.T. Anastas, Crit. Rev. Anal. Chem. 29 (1999) 167.
[2] P. Tundo, T.C. Williamson, Green Chemistry: Challenging and Perspectives, Oxford University Press, 1998.
[3] S. Ohno, M. Tanaka, N. Teshima, T. Sakai, Anal. Sci. 20 (2004) 171.
[4] S. Kawakubo, A. Naito, A. Fujihara, M. Iwatsuki, Anal. Sci. 20 (2004) 1159.
[5] P.K. Tarafder, R. Thakur, Microchem. J. 80 (2005) 39.
[6] F.R.P. Rocha, L.S.G. Teixeira, Quim. Nova. 27 (2004) 807.
[7] L.S.G. Teixeira, F.R.P. Rocha, M. Korn, B.F. Reis, S.L.C. Ferreira, A.C.S. Costa, Anal. Chim. Acta 383 (1999) 309.
[8] L.S.G. Teixeira, F.R.P. Rocha, M. Korn, B.F. Reis, S.L.C. Ferreira, A.C.S. Costa, Talanta 51 (2000) 1027.
[9] L.S.G. Teixeira, A.C.S. Costa, S. Garrigues, M. de la Guardia, J. Braz. Chem. Soc. 13 (2002) 54.
[10] P.B. Martelli, B.F. Reis, M. Korn, I.A. Rufini, J. Braz. Chem. Soc. 8 (1997) 479.
[11] F.R.P. Rocha, J.A. Nóbrega, Chem. Educator 4 (1999) 179.

[12] L.S. Clesceri, A.E. Greenberg, A.D. Eaton, Standard Methods for the Examination of Water and Wastewater, 20th ed., American Public Health Association, Washington, 1998.
[13] R.H. Byrne, W. Yao, E. Kaltenbacher, R.D. Waterbury, Talanta 50 (2000) 1307.
[14] J.Z. Zhang, C. Kelble, F.J. Millero, Anal. Chim. Acta 438 (2001) 49.
[15] S.L.C. Ferreira, R.M.W. Nano, Talanta 41 (1994) 1937.
[16] L.S.G. Teixeira, E.S. Leão, A.F. Dantas, H.L.C. Pinheiro, A.C.S. Costa, J.B. de Andrade, Talanta 64 (2004) 711.
[17] M. Thompson, H.M. Bee, R.V. Cheeseman, W.H. Evans, D.W. Lord, B.D. Ripley, R. Wood, J.J. Wilson, Analyst 112 (1987) 199.

Available online at www.sciencedirect.com
ScienceDirect
Talanta 71 (2007) 1652–1660
Talanta
www.elsevier.com/locate/talanta

Sequential multiple analyses of atmospheric nitrous acid and nitrogen oxides

Kei Toda [a,*], Yuki Hato [a], Kotaro Mori [a], Shin-Ichi Ohira [a], Takao Namihira [b]

[a] *Department of Environmental Science, Kumamoto University, 2-39-1 Kurokami, Kumamoto 860-8555, Japan*
[b] *Department of Electrical and Computer Engineering, Kumamoto University, 2-39-1 Kurokami, Kumamoto 860-8555, Japan*

Received 26 June 2006; received in revised form 26 July 2006; accepted 26 July 2006
Available online 1 September 2006

Abstract

Sequential injection analysis (SIA) was applied to multi-gas monitoring for atmospheric analysis. HONO, NO_2 or NO was collected in an individual diffusion scrubber in which the channel array was filled with either HCl or triethanolamine solution. All analytes were collected in the form of nitrite ions in the scrubber, and were transferred via a 12-port selection valve into a 2.5-ml syringe. The reagent, 3-amino-1,5-naphthalenedisulfonic acid (C-acid) solution was subsequently introduced into the syringe, and inter-mixed with the nitrite sample, whereafter the mixed solution was transferred to a heated reactor and held for 3 min at 100 °C. After that, the sample/reagent solution was returned to the syringe and alkalinized. Then, the final solution was analyzed using a homemade fluorescence detector. Atmospheric HONO, NO_2 and NO were successfully monitored 3 or 4 times/h. The limits of detection were 0.22, 0.28 and 0.35 ppbv for HONO, NO_2 and NO, respectively. It was demonstrated for the first time that SIA is a good tool for multi-gas atmospheric analysis. These nitrogen–oxygen compounds are interconvertible, and the simultaneous measurement of these gases is important. Especially, HONO is a source of OH radicals which contribute greatly to atmospheric pollution, and indeed atmospheric chemistry. This method allows the three gases to be measured using one system. The NO_2 and NO data obtained by SIA was compared with those obtained using chemiluminescence instrument. SIA has been successfully applied to atmospheric measurements. Interestingly, it was observed that HONO levels rose toward the end of periods of rain.

Keywords: Sequential injection analysis; Atmospheric nitrous acid and nitrogen oxides

1. Introduction

Sequential injection analysis (SIA) was initially proposed as an exciting successor to the commonly known flow injection analysis (FIA) [1]. SIA is a robust and fully automated measurement system, making it highly suitable for semi-continuous atmospheric measurement. However, few atmospheric SI analyses have been reported so far. We first introduced the application of SIA to NO_x gas analysis in 2003. Recently, Dasgupta's group demonstrated a new SIA system, combining the merits of both FIA and SIA, which incorporates two syringe pumps for the measurement of NH_3 [2]. Both aqueous NH_3 and atmospheric NH_3 were successfully measured using the dual syringe pump system. Here, we demonstrate a multi-gas analysis by using a single syringe SIA.

Recently, nitrous acid (HONO) has been considered a noteworthy species in the atmosphere. HONO is widely considered as a major source of OH radicals, which are themselves, responsible for governing a number of chemical and photochemical oxidation reactions in the atmosphere [3]. The irradiation of HONO with UV light results in OH radical formation, together with the production of NO. HONO itself is known to be produced from NO_x and H_2O during heterogeneous reactions occurring on the surfaces of buildings and aerosol particles [3,4]. Indeed, additional HONO formation routes are also believed to exist [5]. Suffice to say, NO_x is considered as both the source and fate of HONO in the atmosphere. Therefore, time variation data of HONO would be more useful if obtained alongside the corresponding data for the nitrogen oxides. Several methods have been used to determine the atmospheric HONO. Some of these include methods that rely on the use of mist chambers [6], Na_2CO_3 denuders [7–10] or Na_2CO_3 impregnated filters [11] in order to collect HONO. In these cases, the collected HONO molecules are extracted into purified water and

* Corresponding author. Tel.: +81 96 342 3389; fax: +81 96 342 3389.
E-mail address: todakei@sci.kumamoto-u.ac.jp (K. Toda).

0039-9140/$ – see front matter © 2006 Elsevier B.V. All rights reserved.
doi:10.1016/j.talanta.2006.07.054

measured using ion chromatography (IC). For those methods without IC, HONO is measured using a scrubbing coil denuder coupled with a colorimetric [12–17] or fluorescence detector [18]. Differential optical absorption spectroscopy (commonly referred to as DOAS) is also used to determine HONO in the atmosphere [4,5,19], however, this method relies on a very long optical path length (several hundreds of meters or kilometers) and requires complicated data processing to eliminate other gas interferences. Of the current methods employed to determine atmospheric HONO, NO_2, and NO, none are particularly simple to use, either directly or simultaneously.

Here, we attempted to determine ppb-levels of HONO, NO and NO_2 by SIA using a single chemistry. Wet scrubbers optimal for SIA were developed. SIA is more robust than conventional flow analysis, but the sensitivity of the technique is generally poor. Hence, here we adopted a fluorometric method based on inexpensive reagents, such as C-acid [20], instead of the more commonly used Griess–Saltzman colorimetric method or 2,3-diaminonaphthalene (DAN) fluorometric method, where DAN is typically 50 times more expensive than the C-acid reagent.

2. Experimental

2.1. Reagents

A fluorescence developing reagent solution was prepared by dissolving C-acid (3-amino-1,5-naphthalenedisulfonic acid disodium salt, purchased from Tokyo Kasei) in 0.1 M HCl to obtain a 10 mM C-acid solution. Fluorescence of the product was activated with 5 M NaOH, and carrier solution was 1.25 M NaOH. For gas collection, two kinds of absorbing solutions were used; 0.5 M HCl for HONO and 0.3% triethanolamine (TEA) for NO_2 and NO.

A HONO elimination filter was prepared by impregnating a filter paper (no. 5A, Ø7 mm) with an aqueous solution comprising 2% Na_2CO_3 and 2% glycerin, which was then dried at 50 °C for 1 h [11]. An extraction column to remove NO_2 was prepared as follows. Molecular sieves (5A, 1/16 in., obtained from Nacalai) were impregnated with 20% TEA aqueous solution. After drying, the molecular sieves were packed in a column with an internal diameter (i.d.) of 13 mm, where the effective length of the column was 100 mm. Oxidation of NO to NO_2 was performed using a $KMnO_4$ impinger. A 2.5% (w/v) $KMnO_4$ in 0.25 M H_2SO_4 solution (20 ml) was placed inside the impinger equipped with a G1 glass ball filter.

Test gases of NO and NO_2 were prepared by two successive dilutions of the standard gases (from 100 ppm cylinders) with purified air. HONO gas was prepared in a similar way to previously reported methods [21–23]. The HONO generation system used in our experiment is shown in Fig. 1. A concentrated HCl solution was placed inside a glass test tube, fitted with a plug through which a Teflon tube was inserted. The tube consisted of a second porous tube (1.8 mm i.d. × 2.3 mm o.d.) with a window (width 1 mm) to work as an HCl permeation device. The entire test tube was then placed in a plastic holder (25 mm i.d. × 284 mm long). HCl gas was generated by passing air at 200 ml min^{-1} through the permeation device holder, which was kept at 15 °C. The HCl gas was passed through an HCl–HONO converter, where 1 g of finely grinded $NaNO_2$ powder was stirred on a filter in a plastic sample tube. The converter was heated at 50 °C. The HONO generation rate was confirmed by collection of two water impingers connected in series and IC measurement. The HONO source gas was diluted with purified air for HONO gas testing.

2.2. Gas sampling

Multi-channel gas scrubbers were fabricated by 3D modeling machine (Modela MDX-15, Roland DG). Channels (1 mm wide) were fabricated in two acryl plates to form 0.2 and 3 mm deep channels for an absorbing solution and sample air, respectively. The two acryl plates were then clamped together so that their respective channel-sides face each other, and a gas permeable membrane was sandwiched between them, as shown in Fig. 2. The membrane used was a porous PTFE flat membrane (pore size 0.45 μm, thickness 30 μm), similar to those employed as

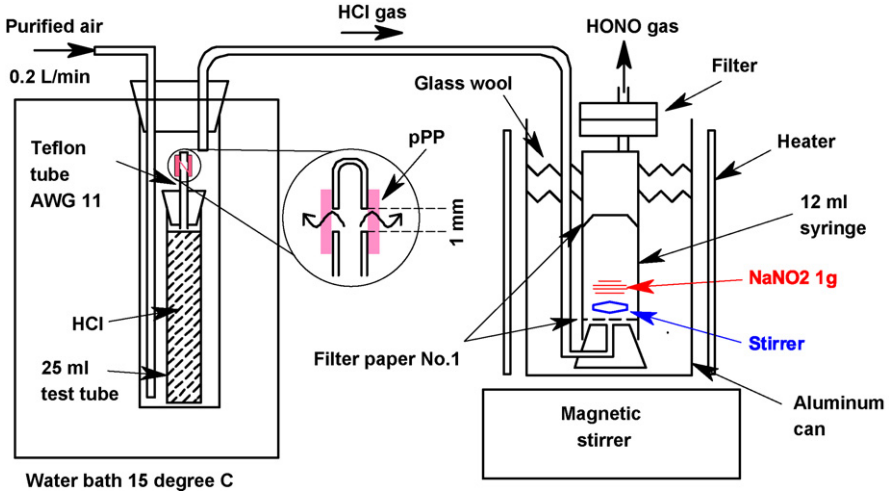

Fig. 1. HONO generation system. Left half is for HCl generation, and the right device converts HCl to HONO. The HCl permeation window (width 1 mm) was composed of porous polypropylene membrane tube (1.8 mm i.d. × 2.3 mm o.d.). The HCl and HONO generators were maintained at 15 and 50 °C, respectively.

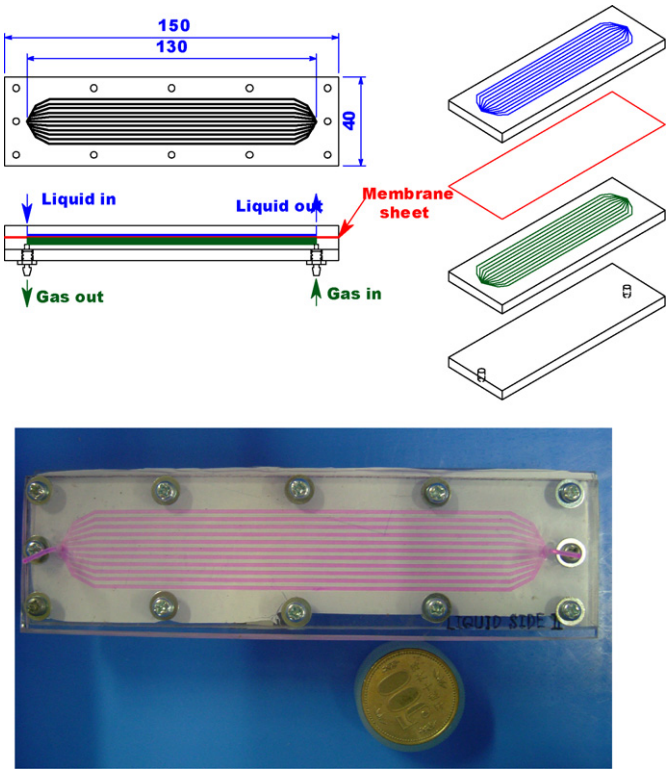

Fig. 2. Multi-channel scrubber. A gas permeable membrane was sandwiched between two acryl plates which had 0.2 and 3 mm deep channels for the absorbing solution and gas sample flows. Line and space widths of the each channel were both 1 mm. The picture shows the liquid bearing channels filled with a colored test solution.

microchannel scrubbers in micro gas analysis systems (μGAS) [24]. An absorbing solution was flowed through the shallower channels (depth 0.2 mm), while a gas sample was passed through the deeper channels (depth 3 mm), so that the target analyte diffused through the membrane to dissolve into the absorbing solution. Three scrubbers are connected in series in the gas sampling line, as shown in Fig. 3, and the sample air was aspirated at a rate of 300 ml min^{-1} using a miniature air pump (CM-15-12, Enomoto Micropump, Tokyo). The first, second and third scrubbers were used to collect HONO, NO_2 and NO, respectively. A filter unit (impregnated with Na_2CO_3) and molecular sieve column (impregnated with TEA) were placed downstream of the first and second scrubbers, in order to remove the remaining HONO and NO_2, respectively. A $KMnO_4$ impinger, employed as a converter, was placed before the third scrubber to oxidize NO to NO_2. The absorbing solutions were placed into drip bags suspended from a pole above the instrument. The height from the solution inlet of the scrubbers to the bottom of the drip bag was set at 50 cm.

2.3. Sequential system

The sequential system used in the current work is shown in Fig. 3 together with the air sampling system. A syringe pump coupled with a 12-port ceramic selection valve (Versa 6, Kloehn, Las Vegas, NV) was utilized in this system. The center port of the selection valve was directly connected to a 2.5-ml syringe. The scrubbers and the reactor were connected to selection valve ports with small Teflon tubes (AWG 30, 0.3 mm i.d., ∼10 cm). The measurement procedure adopted here is as follows (see Table 1 for exact steps). Firstly, the collected HONO sample (300 μl) was aspirated into the syringe. Then, 150 μl of C-acid solution was introduced into the syringe, and the syringe piston was drawn in and out three times to mix the two solutions. The mixture was then transferred to the reactor, which was maintained at 100 °C. After reaction for 3 min, the solution was drawn back into the syringe, and then mixed with 150 μl of 5 M NaOH in the same way as described in the previous mixing. The air contained within the headspace of the syringe was completely expelled from the syringe through a waste port, and the final 300-μl solution was introduced into the detector line. The solution was then forced through a homemade fluorescence detector, with the aid of a 1.25 M NaOH carrier solution (1.8 ml) for 36 s. After the measurement, the reactor was purged with water and

Table 1
Sequence of HONO, NO_2 and NO measurement

	Port no.	Port name	Operation	Notes
1	1, 2 or 3	Scrubber	Aspirate 0.3 ml	Sample introduction
2	6	C-acid	Aspirate 0.15 ml	Addition of C-acid
3	9	Air	Piston position 1.5 ↔1 ml, × 3	Mixing of sample with C-acid
4	4	Reactor	Push out all	Transfer to reactor
5	1, 2 or 3	Scrubber	Aspirate 2 ml	Scrubber refreshment
6	7	5 M NaOH	Aspirate 0.15 ml	NaOH introduction into syringe
7	4	Reactor	Wait 3 min after 4, then aspirate 1 ml	Taking back of sample/reagent to syringe
8	9	Air	Piston position 2 ↔1 ml, × 3	Mixing with NaOH
9	11	Waste	Push out until piston position 0.4 ml	Removal of air
10	5	Detector	Push out all	Introduction of reacted sample into detector line
11	8	1.25 M NaOH	Aspirate 2 ml, then push out 0.2 ml	Carrier preparation
12	5	Detector	Push out all	Fluorescence measurement
13	12	Water	Aspirate 2 ml	
14	4	Reactor	Push out all	Reactor cleaning, repeat 13 and 14 twice
15	9	Air	Aspirate 1.5 ml	
16	4	Reactor	Push out all	Drying of reactor
17	2, 3 or 1			To another cycle for the next gas

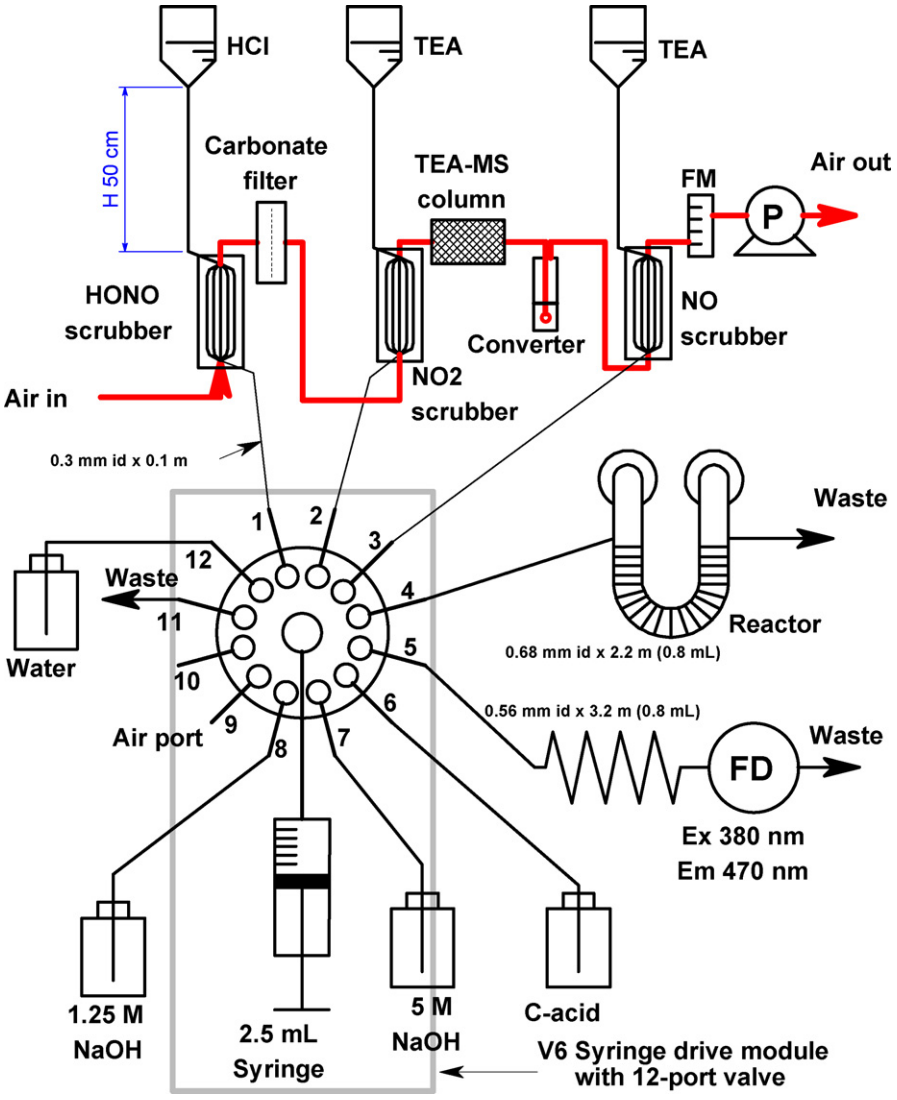

Fig. 3. SIA system diagram. Carbonate filter: Ø47 mm filter paper impregnated with Na_2CO_3/glycerin for removal of HONO, TEA-MS column: a column packed with molecular sieve impregnated with TEA for NO_2 removal, FM: flow meter, P: air pump, FD: fluorescence detector comprising a UV LED and photodiode.

then with air. Next, NO_2 and NO were measured in the same way as HONO by introducing sample solutions from the second and third scrubbers, respectively. The total measurement time for the three gases was within 20 min, and the measurements were repeated automatically.

The fluorescence detector was equipped with a UV-LED (380 nm, $\lambda_{1/2}$ 15 nm, max 700 mA (3.2 W), NCCU001E, Nichia, 300 mA), a photodiode (OPT301, Texas Instruments), and a band pass filter (MIF-S, 475 nm, Ø8 mm × t 3.05 mm from Spectrogon). The flow cell was comprised of a glass tube (1.8 mm i.d. × 3.0 mm o.d.) in which both ends were modified in order to receive Teflon tubing. All parts were incorporated in an opaque resin block. The UV-LED was driven at 100 mA, and the photodiode current was amplified with 100 Mohm feedback resister. The reactor was constructed from a Teflon tube (0.68 mm i.d. × 1.18 mm o.d. × 2.2 m), coiled round a U-shaped heater. The whole system was set in a tower-type computer housing, and driven by a notebook computer fitted with an AD converter card (CBI-3133A, Interface).

2.4. Atmospheric measurements

The developed system was positioned next to a fifth floor laboratory window, and sample air was aspirated from outside. The acquisition and processing of data was performed using software GASANA [25] developed in-house. The absorbing solutions were packed into drip bags and refilled daily. For comparison, a chemiluminescence (CL) instrument (model 42C, Nippon Thermo) was placed next to the SIA system. NO and total NO_x were measured by direct CL measurement and by conversion to NO through a carbon molybdenum converter, respectively.

3. Results and discussion

3.1. Optimization for nitrite measurement

In the present gas measurement system, all target gases were collected as nitrite in the scrubbers. Firstly, the SIA conditions

were optimized for nitrite measurement prior to analyzing the gas samples.

A holding coil, which is usually employed in SIA, was not used in this system. In conventional SIA systems, a three-way valve is placed at the port of a syringe, and a holding coil is set between the selection valve and three-way valve. In the present system, the sample and reagent solutions were introduced into a syringe, and mixed by forcing the piston in and out three times; a sufficient number for mixing 0.45 or 0.6 ml of solution in a 2.5 ml syringe. Note that repeated retraction of the syringe plunger is needed for larger volume mixing. Compared to the holding coil, the solutions were mixed well quickly, because the axial distance/diameter ratio is much smaller than in the holding coil. Hence, more than two kinds of solution can be introduced into the mixer without repeating successive small aspirations.

The determination system comprises two reaction steps; the slow diazonium formation resulting from the reaction between C-acid and nitrite in acidic medium, and the faster alkalinization of the resulting diazonium for fluorescence activation. In this case, a relatively complicated sequence is needed, whereas the reactor and detector can be connected in series, such that the sample passes through both devices in quick succession, which is particularly advantageous if the second reaction is slow. On the other hand, in the present case, the C-acid nitrite mixture was transferred to a reactor, constructed from a Teflon tube coiled around a U-shaped heater. Here, the solution was kept in the reactor for a fixed time, and then aspirated back into the syringe where it was mixed with the alkaline solution. There is no dilution by dispersion usually occur in the holding coil in the conventional SIA, because no carrier solution was used in the above processes. After, the final mixture was flowed through the detector, and the reactor was washed with water and the flushings removed by air in order to avoid dilution of the next sample. The reactor cleaning, with water and air, served as washing of the syringe as well to avoid carrying over.

To accelerate the reaction of C-acid with nitrite, the reactor was set to the maximum possible temperature (100 °C) to avoid boiling. The formation of small bubbles within the reactor was considered harmless in this system, because the mixture was drawn back into the syringe once before detection. The reaction condition was examined using 100, 20 and 10 μM C-acid for 1 μM nitrite, and the results are shown in Fig. 4. The highest concentration of C-acid (100 μM) required only a short reaction time (1.5 min), but the intensity of the blank was not small; it corresponded to a concentration of 0.1 μM of nitrite. The reaction speed was low when the lower concentrations (20 or 10 μM) of C-acid were used, where the blank signal was 2/3 or 1/2, respectively. Atmospheric gas level changes are not particularly fast such that low level measurements are more important than high throughput. In conclusion, a 3-min reaction at 100 °C with 10 μM C-acid was chosen as the optimum reaction conditions.

The HCl concentration in the C-acid solution and NaOH concentration for the second reaction were examined. It was found that the HCl concentration had little effect on the final signal in the range from 0.05 to 2 M. To neutralize the TEA absorbing solution, 0.1 M HCl was added to the C-acid solution. For fluorescence emission, low concentrations of NaOH caused a high blank signal; therefore more concentrated solutions (5 M NaOH) were adopted. In order to eliminate baseline fluctuation resulting from the Schlieren effect caused by the highly concentrated NaOH solution in the sample zone, a NaOH solution having the same concentration (1.25 M) as the final mixture was used for the carrier solution.

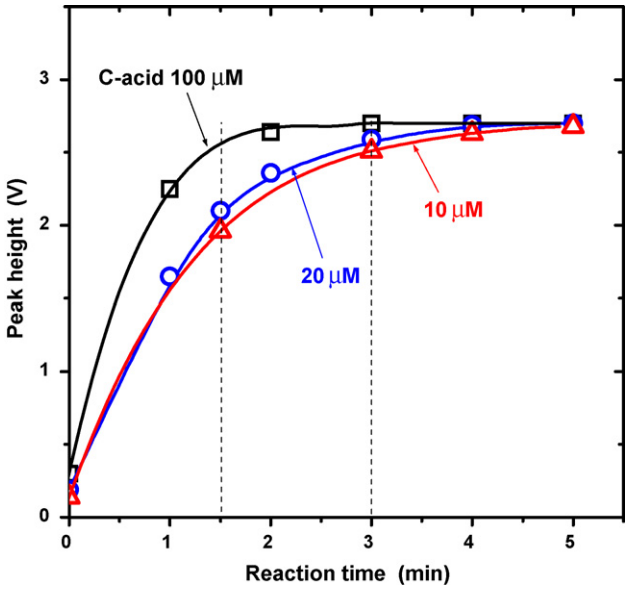

Fig. 4. Peak height for 1 μM nitrite as a function of reaction time, obtained using 10, 20 and 100 μM C-acid solutions.

The response chart obtained for aqueous nitrite in these conditions is shown in Fig. 5. The observed peaks in the chart correspond to the 0, 0.5, 1.0, 1.5 and 2.0 μM nitrite standards. Here, a linear response to the nitrite concentration was obtained

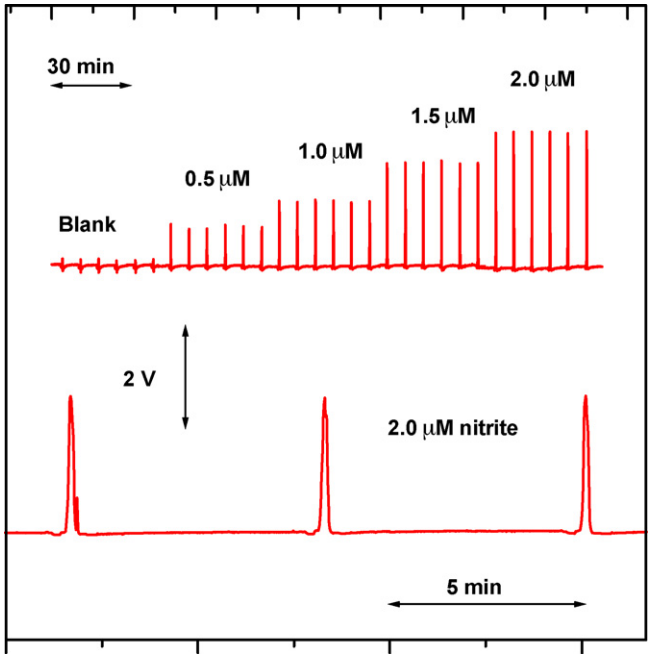

Fig. 5. Response of fluorescence signal to nitrite solutions obtained by the SIA system. The upper shows the responses to nitrite from 0 to 2.0 μM. In the lower data, the three peaks are presented to show the peak shape.

with good repeatability. The limit of detection (LOD), estimated here as 16 nM, was obtained using three times the standard deviation of the blank signals. The LOD obtained here was better than those (0.1–1.5 μM) obtained by SIA with colorimetric reactions [26–28]. This improvement in sensitivity was due to the fluorometry and relatively large sample volume compared to the carrier stream flow. Also, a small axial dispersion in the tube helped enhance the signals.

3.2. Collection of HONO and NO_2

This system was based on the selective collection of HONO and NO_2. In addition, NO was measured after NO_2 removal and following its conversion to NO_2. We have previously employed annular diffusion scrubbers for flow analysis of gases [25,29,30]. In this study, the same annular type scrubber was examined in the early stages, but air was observed to pass through the membrane into the liquid phase during the liquid aspiration step because of high flow resistance within the small porous tube. Hence, the channel scrubber shown in Fig. 2 was developed for SIA gas measurements. Estimated Reynolds number (*Re*) of gas flow was only 10, and the flow in the channels was supposed to be laminar ($Re < 2300$). Therefore, the analyte molecules reached to the membrane surface by diffusion. In this collection, the diffusion in the channels was not rate determining step, and the collection was limited by passing (diffusion) through the membrane that was affected by the absorbing solution. The collection characteristics were examined with respect to the changing pH of the absorbing solution (Fig. 6). The pH was adjusted with HCl, phosphate buffer or NaOH. When a strong alkaline solution was used as the absorber, both HONO and NO_2 were effectively dissolved into the solution. HONO gave a larger signal intensity compared to that of NO_2 due to its greater dissolution characteristics. NO_2 molecules dissolves to form nitrite and nitrate ions [31], whereas dissolved HONO affords only nitrite ions. The quantity of nitrite collected became poorer with decreasing pH in both cases for HONO and NO_2. At the point where the HONO collection factor was decreasing, the pH was found to correspond to the acid dissociation constant of nitrite (pK_a 3.35). However, HONO collection can be performed even in acidic conditions. At pH 0–1, only HONO was collected. Thus, the optimum HONO absorbing solution is considered to be 0.5 M HCl. NO_2 collection was performed with 0.3% TEA, corresponding to 0.02 M of TEA. At low concentration, the TEA performance was better than the NaOH solution. The efficiencies of collection as nitrite in the selective collection conditions were 12% for HONO, 9.0% for NO_2 and 6.0% for NO. These factors include loss in the introducing from the scrubber to the syringe, nitrite formation ratio in the solution $[NO_2^-]/([NO_2^-] + [NO_3^-])$ in the NO_2/NO collections, and conversion rate of NO. Though the collections were not quantitative differently from that by a chromatomembrane cell [32,33], high sensitive measurement was easily performed several days with the multi-channel scrubbers.

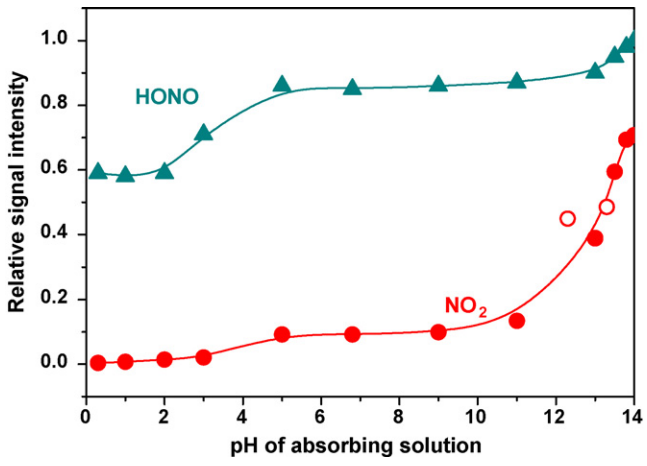

Fig. 6. Effect of pH on the collection of HONO and NO_2. White circles for NO_2 were obtained using TEA solution.

3.3. Removal of HONO and NO_2

Here, not all target gases could be effectively scrubbed clean using the chosen scrubber. Therefore, the remaining gases should be removed prior to being introduced into the next scrubber. Filter papers impregnated with Na_2CO_3 were tested for their ability to remove HONO. After passing HONO (10 ppmv) through the two filters at 300 ml min^{-1} for 30 min, the target analyte was extracted into water with the aid of ultrasonication. This solution was then injected into IC to measure the nitrite concentration. The two carbonate filters were placed in series in the sampling line, and the collection efficiency f was estimated from the ratio of IC signals S_u and S_d, corresponding to the upstream and downstream filters, respectively.

$$f = 1 - \frac{S_d}{S_u} \quad (1)$$

The removing efficiency of HONO at the carbonate filter was 98.9%, while the transferring efficiency of NO_2 was 99.3%. Thus, good selectivity and efficiency were obtained.

NO_2 was eliminated from the mixture by passing it through a column packed with molecular sieves impregnated with TEA. An alkaline impinger was placed downstream of the molecular sieve column, and 17.2 ppmv NO_2 and 9.9 ppmv NO were passed through the column for 15 min at 300 ml min^{-1}. The outgoing gases from the columns were measured following injection of the impinger solution into the IC system. The removing efficiency of NO_2 was 98.3% and the transferring efficiency of NO was 102.6%. Only NO_2 was captured at the TEA column, with no loss of NO. Other columns such as activated carbon, and TEA impregnated filter paper were tested in order to determine their effectiveness as removers. The activated carbon adsorbed NO_2 from the NO/NO_2 mixture, while the remaining NO was oxidized to NO_2 and partially captured. The TEA molecular sieve column, on the other hand, was shown to be a better absorber of NO_2.

3.4. Conversion of NO into NO_2

NO does not dissolve into the absorbing solution. Therefore, NO should be converted into NO_2 before collection. An activated carbon column [34,35], CrO_3 impregnated molecular

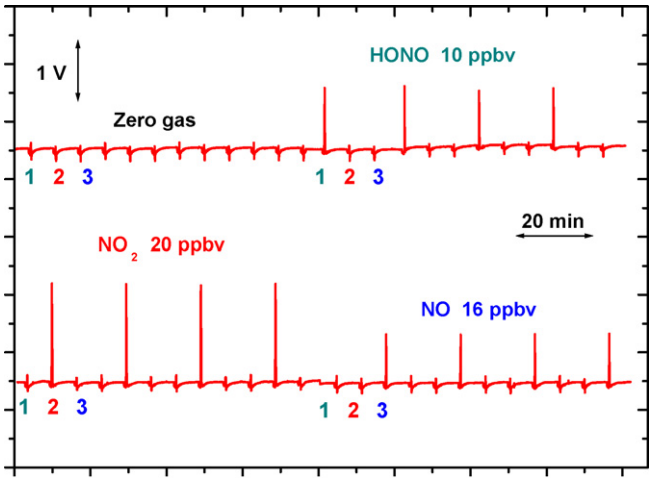

Fig. 7. Response to the test gases. The numbers correspond to the number of the scrubber used. (1) HONO scrubber, (2) NO_2 scrubber, and (3) NO scrubber.

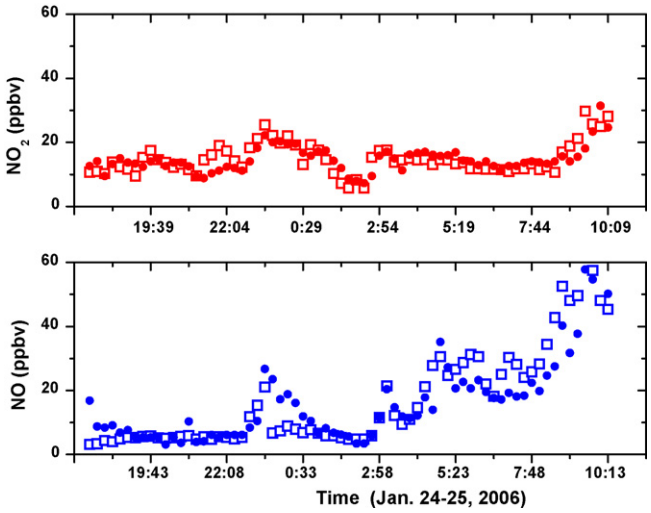

Fig. 8. Comparable measurement of atmospheric NO_2 and NO by SIA (bold circles) and chemiluminescence detection (white squares).

sieve column [36], CrO_3 coated glass beads [37] and CrO_3 impregnated filter paper were examined for their ability to oxidize NO. Activated carbon is sometimes used for detecting ppm-levels of NO. For low level detection, however, there was a noticeable loss in NO concentration in the activated column. The activated carbon is known to adsorb the NO_2 formed in the column, thereby preventing it from being employed as an effective NO detector. The CrO_3 column tended to be affected by the gas humidity or wetness conditions of the packing material. Finally, the classic $KMnO_4$ impinger was employed.

3.5. Gas measurement

In the construction of the SIA system, the scrubbers, eliminators, and NO oxidation converter were all connected in series, as shown in Fig. 3, and sample air was aspirated through these devices. In the present SIA, the total time taken to perform the measurement of one component was 6.5 min. Here, the measurement of all three HONO, NO_2 and NO samples was performed within 20 min, enabling relatively long sampling times to be taken for each component, namely 18.5 min (total −1 min). An example response chart is shown in Fig. 7. The numbering of the peaks corresponds to the scrubber used, namely: scrubber 1 for HONO, scrubber 2 for NO_2 and scrubber 3 for NO. Good repeatability was obtained as shown in Fig. 7. The LODs were 0.22 ppbv for HONO, 0.26 ppbv for NO_2 and 0.35 ppbv for NO.

3.6. Atmospheric measurement

Atmospheric data was obtained using the proposed SIA system. Calibration of the system was performed by the three standard gases individually. The captured data was compared with those performed using the chemiluminescence (CL) system. The atmospheric NO and NO_2 results are shown in Fig. 8. The gas data obtained using both methods agreed well. In this way, the SIA gas measurement system was applicable to real atmospheric NO_x measurements. Further, we tried to detect HONO using the CL system, fitted with a three-way solenoid valve and a filter impregnated with Na_2CO_3. Here, the difference between the detection values obtained after passing through the filter and those obtained after bypassing it, is supposed to correspond to the HONO level. However, this signal was much higher than expected (several ppbv) and fluctuated greatly. Compared to the total NO_x level, the signal change produced after passing though the filter was very small, and the HONO determination was difficult. Also, this signal may contain other NO_y components including HNO_3 and organic nitrates/nitrites. For organics such as peroxyacetylnitrate, ethyl nitrate and ethyl nitrite, 90% of these compounds are known to be converted into NO using either a commercial molybdenum converter at 450 °C [38,39], or HNO_3 [40] and HONO [41]. Thus, HONO could not be measured using the CL system, but it was confirmed that the SIA and CL data for the other gases, NO_2 and NO, agreed well each other.

Fig. 9 shows the atmospheric data obtained during the period from 9 to 17 February 2005 at Kumamoto University. Note that the HONO data are enlarged 10-fold to simplify reading. In the holidays, it was found that all gas levels are essentially quite low due in part to the lower volume of traffic. In good weather, the concentration of all target gases tended to decrease after sunrise. Here, it was observed that fluctuations in the NO level were relatively fast, indicating that NO is largely produced as a result of major traffic congestion. Interestingly, relatively significant HONO levels were observed toward the end of a period of rain; for example, 5 a.m. 10 February, 3 a.m. 16 February and 3 a.m. 17 February. The nitrite collected in rain water by the washout, was released during vaporization. Here, water vaporization is expected to occur continuously in rain, but the released HONO was subsequently recaptured in water drops during periods of rain. In this way, the concentration of HONO appears high only at the end of the period of rain. In addition to the heterogeneous reactions, dew formation and fog mist are also said to be related to HONO generation [14]. The emission of HONO in response to

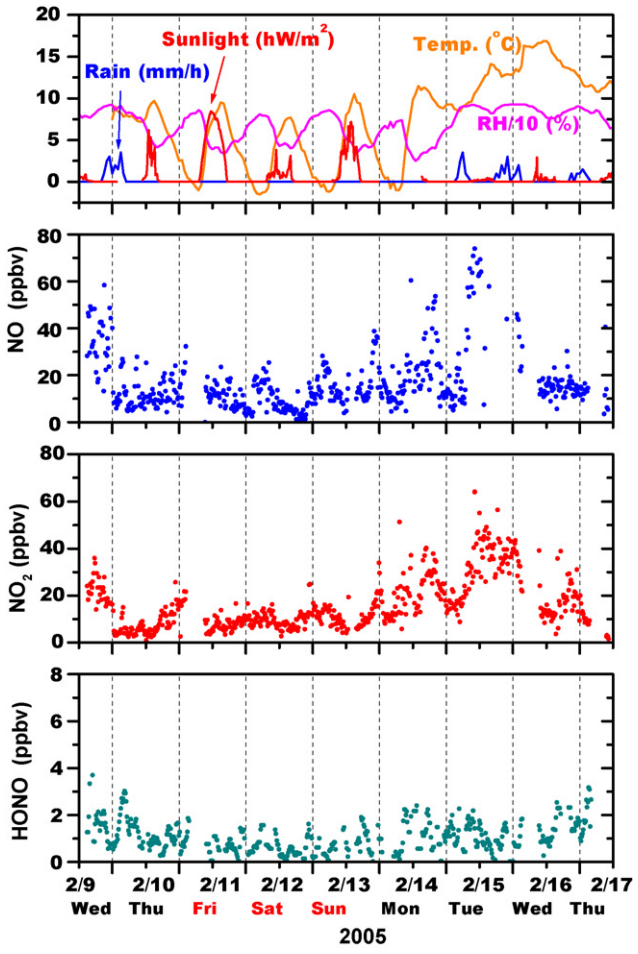

Fig. 9. Results of atmospheric HONO, NO_2 and NO measurement over a 1-week period. Weather data and sunlight data are shown in the top panel.

the end of a rain spell is similar to the amount of HONO released from dew. Here, the relationship between HONO generation and rain was shown for the first time.

4. Conclusions

Sequential analysis is an appropriate measurement technique for atmospheric analysis due to the reliability of the automated analysis. The collection time, which directly impacts on signal intensity, is easily and robustly kept constant. Multi-gases can be analyzed with only one system with a single detector. An optimal gas collection scrubber has been developed for use in SI gas analysis systems. The SIA system is expected to be applied to many gas analyses applications.

Acknowledgements

The authors thank Prof. Dasgupta and Dr. Takeuchi (both of Texas Tech University) for their valuable comments on NO_x and HONO measurements. This work was supported by Grants-in-aid for Basic research (C) (2) No. 15550075 and a Research Grant for Young Scientists No. 168610, from the Japan Society for the Promotion of Science (JSPS), and from the Industrial Technology Research Grant Program operated by the New Energy and Industrial Technology Development Organization (NEDO).

References

[1] J. Ruzicka, G.D. Marshall, Anal. Chim. Acta 237 (1990) 329.
[2] N. Amornthammarong, J. Jakmunee, J. Li, P.K. Dasgupta, Anal. Chem. 78 (2006) 1890.
[3] B.J. Finlayson-Pitts, L.M. Wingen, A.L. Sumner, D. Syomin, K.A. Ramazan, Phys. Chem. Chem. Phys. 5 (2003) 223.
[4] R. Kurtenbach, K.H. Becker, J.A.G. Gomes, J. Kleffmann, J.C. Lörzer, M. Spittler, P. Wiesen, R. Ackermann, A. Geyer, U. Platt, Atmos. Environ. 35 (2001) 3385.
[5] J. Stutz, B. Alicke, A. Neftel, J. Geophys. Res. 107 (D22) (2002) 8192.
[6] A. Neftel, A. Blatter, R. Hesterberg, T. Staffelbach, Atmos. Environ. 30 (1996) 3017.
[7] T.W. Kirchstetter, R.A. Harley, D. Lettlejohn, Environ. Sci. Technol. 30 (1996) 2843.
[8] A. Bari, V. Ferraro, L.R. Wilson, D. Luttinger, L. Husain, Atmos. Environ. 37 (2003) 2825.
[9] Z. Genfa, S. Slanina, C.B. Boring, P.A.C. Jongejan, P.K. Dasgupta, Atmos. Environ. 37 (2003) 1351.
[10] K. Acker, G. Spindler, E. Brüggemann, Atmos. Environ. 38 (2004) 6497.
[11] M. Takeuchi, H. Okochi, M. Igawa, Bull. Chem. Soc. Jpn. 75 (2002) 757.
[12] X. Zhou, H. Oiao, G. Deng, K. Civerolo, Environ. Sci. Technol. 33 (1999) 3672.
[13] G. Huang, X. Zhou, G. Deng, H. Qiao, K. Civerolo, Atmos. Environ. 36 (2002) 2225.
[14] X. Zhou, K. Civerolo, H. Dai, G. Huang, J. Schwab, K. Demerjian, J. Geophys. Res. 107 (2002) 4590.
[15] X. Zhou, Y. He, G. Huang, T.D. Thornberry, M.A. Carroll, S.B. Bertman, Geophys. Res. Lett. 29 (2002) 101029.
[16] J. Heland, J. Kleffmann, R. Kurtenbach, P. Wiesen, Environ. Sci. Technol. 35 (2001) 3207.
[17] J. Kleffmann, R. Kurtenbach, J. Lörzer, P. Wiesen, N. Kalthoff, B. Vogel, H. Vogel, Atmos. Environ. 37 (2003) 2949.
[18] X. Chen, Y. Oro, K. Tanaka, N. Takenaka, H. Bandow, Anal. Sci. 20 (2004) 1019.
[19] M.D. Andrés-Hernández, J. Notholt, J. Hjorth, O. Schrems, Atmos. Environ. 30 (1996) 175.
[20] S. Motomizu, H. Mikasa, K. Toei, Talanta 33 (1986) 729.
[21] A. Febo, C. Perrino, M. Gherardi, R. Sparapani, Environ. Sci. Technol. 29 (1995) 2390.
[22] I. Allegrini, M. Cortiello, A. Febo, C. Perrino, in: G. Restell, G. Angelett (Eds.), Physico-chemical Behavior of Atmospheric Pollutants, Kluwer Academic Publishers, 1990, pp. 140–144.
[23] M. Taira, Y. Kanda, Anal. Chem. 62 (1990) 630.
[24] S. Ohira, K. Toda, Lab Chip 5 (2005) 1374.
[25] S. Ohira, M.A.K. Azad, R. Kuraoka, T. Tanaka, K. Mori, K. Toda, Bunseki Kagaku 55 (2006) 109.
[26] M.T. Oms, A. Cerdá, V. Cerdá, Anal. Chim. Acta 315 (1995) 321.
[27] A. Cerdá, M.T. Oms, R. Forteza, V. Cerdá, Anal. Chim. Acta 371 (1998) 63.
[28] P.C. Pinto, J.L. Lima, M.L. Marques, F.S. Saraiva, Clin. Chim. Acta 337 (2003) 69.
[29] K. Toda, K. Yoshioka, K. Mori, S. Hirata, Anal. Chim. Acta 531 (2005) 41.
[30] N. Teshima, J. Li, K. Toda, P.K. Dasgupta, Anal. Chim. Acta 535 (2005) 189.
[31] S.E. Schwartz, W.H. White, Adv. Environ. Sci. Technol. 12 (1983) 1.
[32] Y. Wei, M. Oshima, J. Simon, S. Motomizu, Talanta 57 (2002) 355.
[33] Y. Wei, M. Oshima, J. Simon, L.N. Moskvin, S. Motomizu, Talanta 58 (2002) 1343.

[34] I. Mochira, Y. Kawabuchi, S. Kawano, Y. Matsumura, M. Yoshikawa, Fuel 76 (1997) 543.
[35] Z. Guo, Y. Xie, I. Hong, J. Kim, Energy Convers. Manage. 42 (2001) 2005.
[36] D. Levaggi, E.L. Kothny, T. Belsky, E. de Vera, P.K. Mueller, Environ. Sci. Technol. 8 (1974) 348.
[37] X. Zhan, D. Li, H. Zheng, J. Xu, Y. Zhou, Talanta 58 (2002) 855.
[38] A.M. Winer, J.W. Peters, J.P. Smith, J.N. Pitts Jr., Environ. Sci. Technol. 8 (1974) 1118.
[39] D. Grosjean, J. Harrison, Environ. Sci. Technol. 19 (1985) 862.
[40] D.W. Joseph, C.W. Spicer, Anal. Chem. 50 (1978) 1400.
[41] A. Febo, C. Perrino, Atmos. Environ. A 25 (1991) 1055.

Available online at www.sciencedirect.com
ScienceDirect
Talanta 71 (2007) 1560–1568
Talanta
www.elsevier.com/locate/talanta

Determination of phosphate/arsenate by a modified molybdenum blue method and reduction of arsenate by $S_2O_4^{2-}$

Susanna Tsang, Frank Phu, Marc M. Baum, Gregory A. Poskrebyshev *,[1]

Oak Crest Institute of Science, 2275 E. Foothill Blvd., Pasadena, CA 91107, United States

Received 1 July 2006; received in revised form 22 July 2006; accepted 22 July 2006
Available online 28 August 2006

Abstract

A modified molybdenum blue method for fast and accurate measurement of arsenate and phosphate in aqueous solution at concentrations below 10 μmol l^{-1} is reported. The modification consists of optimizing the composition of the molybdenum-containing solution (potassium antimony tartrate, ammonium molybdate, sulfuric acid).

Selective reduction of arsenate by sodium dithionite is used to determine phosphate concentrations, and for the speciation of arsenate and arsenite, in an aqueous mixture according to the scheme developed by Johnston and Pilson. Sodium dithionite is used for the first time to achieve complete, fast (<10 min), and selective reduction of arsenate in neutral solution.

These two significant improvements afforded a colorimetric limit for As detection near 1 ppb, which easily meets the requirements imposed by the revised EPA threshold levels for As in drinking water.

Keywords: Molybdenum blue; Arsenate; Phosphate; Arsenite; Reduction; Dithionite

1. Introduction

Arsenic (As) is a known Group A human carcinogen. The association between cancer and other diseases (e.g., hypertension, diabetes) with As levels in drinking water has been the subject of numerous reports [1]. The main sources of As are volcanoes, arsenic-containing minerals, and industrial processes (e.g., smelting, chromated copper arsenate for wood treatment, solid residues from mining extraction and agrochemicals).

The principal sources of human exposure to As consist of food and drinking water, where arsenic is present in both organic and in inorganic forms. Inorganic forms of As generally are more toxic than organic As compounds, but recent toxicology studies showed that some organic As acids (e.g., monomethylarsonic acid, MMA^{III}, and dimethylarsonic, DMA^{III}) formed in human body via methylation [2–4] are as toxic as, or even more toxic than, inorganic As [5]. However, the presence of MMA^{III} and DMA^{III} in water only has been reported in rare cases and their importance in terms of environmental chemistry is less significant than those in the case of inorganic As.

Among its inorganic forms, trivalent arsenic (As^{III}) mainly presented in water as arsenite (H_3AsO_3 or $HAsO_2$) is recognized as the most toxic [6]. The mechanism of inorganic As^{III} toxicity is unclear and several simultaneous pathways for toxicity of As^{III} in human are being considered [7], including the binding of inorganic As^{III} with proteins, the inhibition of enzymes, the formation of MMA^{III}, DMA^{III} and reactive oxygen species, biotransformation, genetic polymorphysm, signal transduction. The toxicity of pentavalent arsenic (As^{V}) mainly presented in water as arsenate (H_3AsO_4) is 25–60 times lower than that of As^{III} [8], primarily due to the replacement of biochemical phosphate (e.g., in ATP) by arsenate.

While food, which contains mainly organic forms of As, is the main source of As exposure, the toxicity of As-containing drinking water is more significant due to the high levels of inorganic As that can be present. Current US EPA regulations require the concentration of inorganic As in drinking water to be below 10 μg l^{-1}, a fivefold reduction from pre-2006 threshold levels [9]. Consequently, the new limit requires compliance As measurements to be five times more sensitive than pre-2006 analyses.

* Corresponding author. Tel.: +1 626 817 0883; fax: +1 626 817 0884.
E-mail address: g.poskrebyshev@oak-crest.org (G.A. Poskrebyshev).
[1] On leave from the Institute of Energy Problem of Chemical Physics, Russian Academy of Science (poskr@yahoo.com).

0039-9140/$ – see front matter © 2006 Elsevier B.V. All rights reserved.
doi:10.1016/j.talanta.2006.07.043

Table 1
Comparison of component concentrations of molybdenum blue method in the final (analyzed) solution

	Murphy and Riley [29]	Murphy and Koroleff [13]	Parsons et al. [14]	Dhar et al. [27]	Lenoble et al. [19]	Present
$[C_6H_8O_6]$ (mM)	4.8	10.9	5.57	6.1	11.4	11.4
$[(NH_4)_6Mo_7O_{24}]$ (mM)	5.4	2.7	3.1	0.24	0.84	3.4
$K(SbO)C_4H_4O_6$ (μM)	68	59	38	80	82.7	20.7
H_2SO_4 (HCl) (M)	0.2	0.1	0.11	0.063 (0.32)	0.216	0.4 to 0.76

The accurate measurement of As in water using expensive, laboratory-based instrumentation (e.g., hydride generation atomic absorption spectrophotometry, HG-AAS; HG inductively-coupled plasma, ICP, AAS; graphite furnace AAS; ICP mass spectrometry, MS) easily can accommodate the more stringent EPA compliance levels. However, these expensive facilities are not always available and it often is desirable to conduct measurements directly in the field (i.e., in situ). Simple, fast, inexpensive, portable, and sensitive methods of aqueous inorganic As determination therefore are in high demand [10] and can be accommodated by the established, colorimetric molybdenum blue method proposed by Osmond [11] combined with the scheme developed by Johnson and Pilson [12] that only requires a small photometer and inexpensive reagents. Because of advances in photonics, and the resulting high sensitivity, this method can be considered as a viable alternative to differential pulse anodic stripping voltammetry (DPASV).

Although the molybdenum blue method is well-established for the determination of phosphate (H_3PO_4) and inorganic As in solution [13,14], it is considered to be unoptimized [15]. Optimization is complicated by two sets of variables. Firstly, the method is based on multi-components solutions, each requiring optimization of its components' concentrations. Secondly, this optimal composition of the reagents also depends on the concentration of arsenate and H_3PO_4 in the solution to be analyzed (i.e., rate of color development and resulting complex stability), and should be optimized for each particular concentration range.

Several modifications of the molybdenum blue method have been reported in literature [16–18]. Most use the established procedure that requires trained personal for preparation of a solution containing ammonium molybdate (AM), potassium antimony tartrate (PAT), sulfuric acid, and ascorbic acid; the mixture is stable for less than 24 h. An alternative and more useful procedure for field application of the molybdenum blue method is described in the ISO norm [18]. In contrast to the classical method, the ISO norm requires the separation of the reagent mixture into two solutions: one solution with AM, PAT and sulfuric acid and a second solution with ascorbic acid. The concentrations of the components in these solutions and amount of solutions added to the sample are specified by Lenoble et al. [19]. The solutions are added consecutively to the water sample to be analyzed. Although this procedure requires close to 1 h for determination of 10 μmol l^{-1} H_3AsO_4 at room temperature, or around 10 min at 50 °C, it does not require highly trained personal [19]. The low rate of color development obtained in this case is due to the low concentration of AM in the final solution, significantly lower than those levels used by other authors (Table 1). Increasing the concentration of AM in the mixture should increasing the rate of color development, and help avoid the heating step, but also requires optimization of the concentrations of other components of the mixture.

Additional improvements to the procedure employ solutions that are stable during relatively long periods of time (∼2 months at 4 °C) and produce a colored complex that is stable for more than 1 day. This improved procedure was used as the starting point for the optimization of the molybdenum blue method in the present work.

A significant drawback of H_3AsO_4 determination in drinking water by the molybdenum blue method is the interference of arsenate with phosphate, and vice versa. Both H_3PO_4 and H_3AsO_4 have analogous physical and chemical properties and generally are present together in water; the concentration of phosphate is usually higher than corresponding As concentrations. Consequently, they form molybdenum complexes (molybdophosphate and molybdoarsenate, respectively) with similar spectra and molar absorptivity ($\varepsilon_{max} \sim 20{,}000\,l\,mol^{-1}\,cm^{-1}$) in the 500–950 nm range [13,14,19].

The Johnson and Pilson scheme is the most common approach for measuring mixed arsenate, arsenite and phosphate in aqueous solution using the molybdenum blue method [12]. The resolution of the absorbance signals requires selective reduction of H_3AsO_4 to H_3AsO_3, which does not produce a colored complex in the presence of molybdate. This approach allows the H_3PO_4 concentration to be determined independently of H_3AsO_4. Oxidation of H_3AsO_3 to H_3AsO_4 enables the total concentration of H_3PO_4 and inorganic arsenic in solution to be determined. The difference between these values corresponds to the total concentration of inorganic As in solution, which can be speciated in terms of As^{III}/As^{V} by measuring untreated solution (no reduction and no oxidation).

A range of oxidizing agents have been used successfully (e.g., H_2O_2, $KClO_n$, KIO_n, where $1 \leq n \leq 4$, $KMnO_4$, and Fe^{2+}/Fe^{3+}) by many authors [19,20]. Among these compounds, KIO_3 is the most common oxidant used for arsenite oxidation. Given the good agreement between the reported results, no optimization of the oxidation chemistry of arsenite is required. However, the final choice of oxidant should be based on practical requirements (e.g., rate of dissolution and oxidation, temperature effects, form and simplicity of delivery, *etc.*).

The H_3AsO_4 reduction scheme described by Johnson and Pilson of is weakest aspect of their method. In this procedure, the reduction of H_3AsO_4 by thiosulfate ($Na_2S_2O_3$) requires the presence of SO_2 (from $Na_2S_2O_5$) that readily evaporates from the acidic solution when exposed to air. The loss of SO_2 from solution leads to the formation

and precipitation of colloidal sulfur that significantly limits the method's usefulness, particularly for field measurements. The reduction of H_3AsO_4 by SO_2 in highly acidic solution reported by Linge and Oldham [21] is not sufficiently fast ($\sim$1 h at Na_2SO_3 concentrations below 1 mol l^{-1}) for field application.

In the past 10 years, a range of new reducing agents have been tested [22], but none fulfill the requirements of the scheme originally described by Johnson and Pilson. Most of these reducing agents reduce H_3AsO_4 to arsine as part of a modified Gutzeit method. Typical reagents include KI in strongly acidic solution (>0.3 mol l^{-1}) and in combination with ascorbic acid, Na_2SO_3, thiourea or tungsten(II) chloride; mercaptoacetic acid; and zinc with sulfamic acid. Arsine is a highly toxic gas and is unsuitable for field measurements by unskilled personnel. In addition, the reduction by KI requires impractical time periods (4–5 h) to reach completion. The use of L-cysteine [22] also has been proposed as a reducing agent, but requires a strongly acidic medium that cannot be combined with the molybdenum blue method without decreasing its sensitivity. Suitable reducing reagents to be used in the Johnson and Pilson method therefore still remain in high demand.

In the present work, the molybdenum blue method is modified to achieve fast and accurate measurements of H_3AsO_4 and H_3PO_4 in solution at concentrations below 10 μmol l^{-1}. The method was modified by optimizing the concentrations of the components in the mixture used for color development of arsenate/phosphate in solutions according to the procedure described in the ISO norm. A new reducing reagent, dithionite, is proposed for the Johnson and Pilson scheme. The modified molybdenum blue method is used to study the completeness of H_3AsO_4 reduction by dithionite and to optimize the conditions for this reaction.

2. Experimental

Reagents: H_2SO_4 (Fisher, $P^V < 1$ ppb), L-ascorbic acid (Acros Organics, $C_6H_8O_6$), $(NH_4)_6Mo_7O_{24}{\cdot}4H_2O$ (Acros Organics), $(K(SbO)C_4H_4O_6)_2{\cdot}H_2O$ (Fisher), $Na_2HAsO_4{\cdot}7H_2O$ (Alfa Aesar), KH_2PO_4 (Acros Organics), $Na_2S_2O_4$ (Fluka) were used as received in the preparation of solutions. All solutions were prepared at room temperature (28 ± 2 °C) using deionized water (Millipore-Q system).

Stock solutions of arsenate and phosphate (100 μmol l^{-1}) were prepared by dissolving of 10 μmol of arsenate/phosphate salts in 100 ml of water and were used for sample preparation. The masses of all solids were measured using an analytical balance.

Sample solutions of arsenate, phosphate and their mixture were prepared by adding an accurately measured aliquot of stock solution into 40 ml of water dispensed in a 50 ml volumetric flask. Prepared solutions were color developed and diluted to the final volume with deionized water. This procedure was used to prepare solutions with different concentrations of phosphate and arsenate.

For accurate measurement of solutions with the same concentration of phosphate or arsenate, an aliquot of stock solution was dispensed into a 250 or 500 ml of solution (final volume), which subsequently were divided into multiple samples (45 ml) in 50 ml volumetric flasks. These solutions were diluted to 50 ml by the color development reagents (3 ml), sulfuric acid (0.5 ml) and deionized water (1.5 ml).

The volume of aliquots used for sample preparation varied from 5 μl to 5 ml.

Arsenate was reduced by sodium dithionite dissolved in the aqueous sample and heated from 5 to 120 min in a thermostat bath (Haake GH) at constant temperatures between 50 and 80 °C. Heated solutions were cooled to room temperature and color developed as described below. The concentration of reductant (sodium dithionite) in solution was varied from 0.4 to 0.8 mmol l^{-1}.

Sample solutions were color developed according to the procedure described below and were measured in a dual-beam spectrometer (Model PC160PLC, Shimadzu) in a 1 cm optical path cell between 400 and 1000 nm and a custom dual-beam photometer (prototype instrument, SpectraSensors, Inc., San Dimas, CA) equipped with a light emitted diode (LED, λ = 775–1000 nm, λ_{max} = 880 nm) and a 4 cm optical path cell. The photometer was used in the determination of low concentrations of H_3AsO_4 and H_3PO_4 in solution.

Color development procedure was carried out using two solutions: (1) ascorbic acid and (2) molybdate [19]. The procedure includes the addition of 2 ml of molybdate solution to the sample with subsequent addition of 1 ml of ascorbic acid solution and bringing sample solution to a final volume of 50 ml.

Aqueous solutions of ascorbic acid were prepared according to Lenoble et al. The concentration of ascorbic acid (=0.57 mol l^{-1}, 10.8 g in 100 ml) was not varied in the present study.

Solutions of molybdate were prepared by adding solid AM and PAT salts to 5.4 M solution of sulfuric acid [19]. The concentration of AM and PAT salts were varied from 21 to 170 mmol l^{-1} and from 0.52 to 2.1 mmol l^{-1}, respectively.

Solutions were acidified by adding sulfuric acid directly to the aqueous sample prior to color development. The concentration of sulfuric acid in the final solution was varied from 0.23 to 0.92 mol l^{-1}.

3. Results and discussion

The molybdenum blue method is modified in the present work to establish an analytical procedure to enable the determination of H_3AsO_4 and H_3PO_4 in aqueous solution at concentrations below 10 μmol l^{-1}. As stated above, the procedure used by Lenoble is thought to be the best existing adaptation of the molybdenum blue method in terms of field measurements. This procedure was tested in the present work for concentrations of arsenate/phosphate below 10 μmol l^{-1} and was compared with the results reported by Lenoble. The UV–vis spectra of molybdoarsenate and molybdophosphate complexes formed according to the Lenoble procedure (H_3AsO_4 and H_3PO_4 concentration = 5 μmol l^{-1}) are presented in Fig. 1 (insets 1 and 2, respectively, curve a). The time dependencies for the formation of molybdoarsenate (SI, Note 1, open black squares) and molyb-

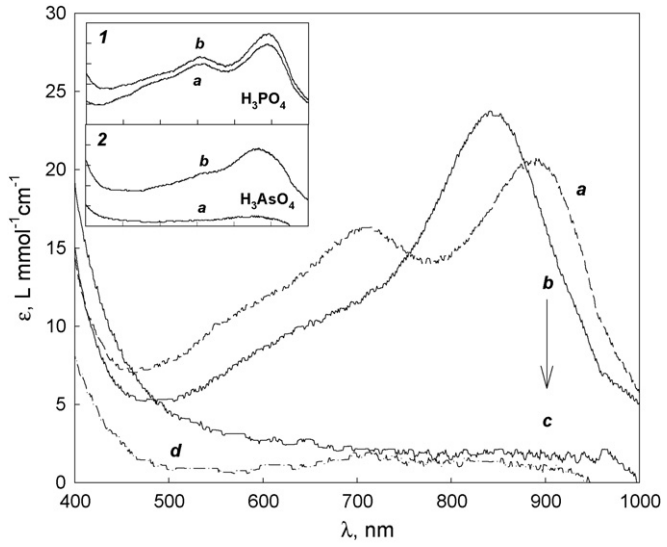

Fig. 1. Spectra of molybdophosphate (curve a) and molybdoarsenate (curve b) complexes obtained from 5 μmol l^{-1} phosphate/arsenate solutions using our modified molybdenum blue method. Spectra c and d are correspond to color developed solutions with reduced arsenate (5 μmol l^{-1}) and without arsenate/phosphate, respectively. Insets 1 and 2, demonstrate spectra of molybdophosphate and molybdoarsenate complexes, respectively, obtained with Lenoble's procedure for solutions at room temperature (curve a) and after 20 min of heating at 70 °C (curve b).

dophosphate (SI, Note 1, closed black circles) complexes were measured in terms of the spectral absorbance at λ = 878 nm. It was observed that H_3PO_4 forms the molybdenum complex significantly faster than H_3AsO_4 under employed conditions; this observation is in accord with previous reports [17].

The spectrum of the molybdophosphate complex shown in Fig. 1 (inset 1, curve a) remains unchanged for 2 h after an aqueous sample containing 5 μmol l^{-1} phosphate was color developed. The observed spectrum of stable molybdophosphate had a molar absorptivity $\varepsilon(P^V) = 19{,}520\,l\,mol^{-1}\,cm^{-1}$ at $\lambda_{max} = 900$ nm, similar those reported previously ($\lambda_{max} = 900$ nm [17]; 895 nm [23]; 880 nm [24]).

In contrast to the molybdophosphate results discussed above, a stable absorbance by the molybdoarsenate complex (i.e., color developed solution with 5 μmol l^{-1} H_3AsO_4) was not observed, even after 5 h of color development. A spectrum of this solution ($\lambda_{max} = 849$ nm) measured at 5 h after color development is presented in Fig. 1 (inset 2, curve a) and was found to be in good agreement with the data reported by Johnson ($\lambda_{max} = 865$ nm [23]) and Karlberg ($\lambda_{max} = 850$ nm [24]) for molybdoarsenate complexes. However, the molar absorptivity ($\varepsilon(As^V) \sim 2400\,l\,mol^{-1}\,cm^{-1}$) of the molybdoarsenate complex measured here is 7–8 times lower than the values reported by Lenoble et al. ($\varepsilon(As^V) = 16{,}600\,l\,mol^{-1}\,cm^{-1}$ at $\lambda_{max} = 870$ nm). This difference in $\varepsilon(As^V)$ suggests that only ca. 10–15% of the H_3AsO_4 in solution forms the corresponding molybdoarsenate complex, even after 5 h of reaction under the employed conditions. Based on these measurements, it is concluded that the method described by Lenoble et al. can provide accurate results in the determination of H_3PO_4 solutions with concentrations below 5 μM but requires more than 1 h for complete color development. At the same time, this method cannot be used for the determination of H_3AsO_4 in solution up to concentrations of 5 μmol l^{-1} without some modification.

It was found previously [16,19] and is supported by the present work, that the method used by Lenoble et al. can be improved for the above low concentrations of analyte by heating the color-developed solution. The effect of temperature (<50 °C) on the formation of molybdoarsenate complexes has been discussed by Lenoble for solutions with an H_3AsO_4 concentration of 10 μmol l^{-1}. However, the importance of heating of color-developed solutions with low concentration of arsenate and phosphate was not stressed in this report.

In the present study, the effect of heating on the formation of molybdophosphate and molybdoarsenate complexes was investigated for solutions with a concentration of a 5 μmol l^{-1} H_3PO_4 and H_3AsO_4. Spectra of color developed solutions with H_3PO_4 (Fig. 1 inset 1, curve b) and H_3AsO_4 (Fig. 1 inset 2, curve b) heated, for 30 and 95 min at 70 °C, respectively, were found to be similar those reported above (Fig. 1, insets 1 and 2, curve a). The time dependencies of formation of these complexes measured at the same temperature are presented under SI (Note 2, in red) and assume 10 times (or more) faster color development than observed at room temperature.

The observed spectra of molybdoarsenate with $\varepsilon(As^V) = 19{,}200\,l\,mol^{-1}\,cm^{-1}$ at $\lambda(As^V)_{max} = 867$ nm and molybdophosphate with $\varepsilon(P^V) = 22{,}400\,l\,mol^{-1}\,cm^{-1}$ at $\lambda(P^V)_{max} = 891$ nm complexes are found to be in agreement with those reported previously [19]. The slightly (~20%) lower values of $\varepsilon(As^V)$ reported by Lenoble compared to those measured for color developed solutions containing H_3AsO_4 heated at 70 °C are attributed to incomplete conversion of H_3AsO_4 to the corresponding molybdoarsenate complex as a result of the shorter times of heating and of the lower temperatures employed in the color development procedure used in Lenoble's work.

Heating of solution of the molybdoarsenate complex over 95 min at 70 °C leads to an irreversible red-shift of λ_{max}. The same effect has been reported by Sjosten and Blomqvist [25] for solutions heated to 110 °C and was explained in terms of thermal decomposition of the complex [19].

The procedure described by Lenoble was found to be consistent and reproducible; heating of solutions at 70 °C improved the procedure for fast determination of low concentrations of H_3PO_4 and H_3AsO_4. However, this procedure still is impractical for field deployment due to the heating step. Further refinement of the method is reported here in terms of concentration optimization of the components in the color development reagent.

According to the procedure described by Lenoble, two solutions should be used in the color development step. One solution contains ascorbic acid and the second contains molybdate and an antimonyl complex. It was shown previously that the concentration of ascorbic acid does not have a significant effect on color development [17] and further optimization of this solution was not carried out in the present study.

It was found in the present work that the method cannot be improved simply by changing the amount of molybdenum containing solution added to analyte. Increasing of the amount of

this solution increases the rate of color development, but also leads to instability of the absorbance signal. It was found that the time of color development for 5 μmol l^{-1} solutions of H_3PO_4 could be reduced to ~10 min when the amount of molybdenum solution added to analyte was double (4 ml) that used by Lenoble et al. (2 ml). However, the resulting absorbance signal was not stable and changed during 2 h [12,23]. The absorbance measured in the end of the experiment also was not proportional to the concentration of phosphate/arsenate. The observed effect was attributed to polymerization/coagulation of molybdate [26] that subsequently precipitates on the walls of the optical cell. On the basis of these observations, it is concluded that the method cannot be optimized without judiciously changing the composition of the molybdenum solution.

The effect of the composition of the molybdenum-containing solution on the rate of color development, and subsequent stability of the resulting molybdoarsenate and molybdophosphate complexes, was investigated here. The molybdenum solution used for color development according to Lenoble's procedure contains three components (PAT, AM and H_2SO_4 with final concentrations in the color developed solution presented in Table 1) that were optimized in the present work for fast measurement of trace levels (below 10 μmol l^{-1}) of H_3AsO_4 and H_3PO_4 in aqueous solution. The two main parameters used in the optimization process are: (1) time of color development (below 5 min for phosphate) and (2) stability[1] of the final complex. Both of these parameters are important for fast and accurate field measurements of low concentrations of H_3AsO_4/H_3PO_4 in aqueous solution.

Optimization of the molybdenum containing solution was carried out by independently varying the concentration of the components (see Lenoble et al., Table 1). The color development procedure was kept same those described by Lenoble et al. (see above). The order for this optimization was defined by the ascending concentration of the component in the final solution, starting from PAT, which is present at the lowest concentration. The amount of sulfuric acid in solution was increased relative to the ISO norm (0.5 ml in 50 ml solution) and was added in advance to the analyte solution to decrease the rate of polymerization/coagulation of the molybdenum complexes thereby stabilizing the resulting signal; the effect of sulfuric acid is discussed in detail below.

Rate of color development and stability of molybdocomplexes were controlled by time dependence of absorbance signal measured at λ = 878 nm. It is found that decreasing the concentration of antimonyl tartrate significantly improves the stability of molybdophosphate/molybdoarsenate complexes, but results in a concomitant decrease in the rate of color development. Conversely, a proportional increase in the concentration of molybdenum ([PAT] × [AM] = 6.9×10^{-8} mol^2 l^{-2}) leads to an increase in the rate of formation of molybdophosphate/molybdoarsenate complexes without significantly decreasing their stability. The optimized concentrations of antimonyl tartrate and molybdate in the final solution are presented in Table 1 and are four times lower and four times higher, respectively, than those reported by Lenoble [19].

The time required for color development to reach completion using our optimized color development procedure was below 5 min for 5 μmol l^{-1} H_3PO_4 and ca. 40 min for the same concentration of H_3AsO_4. The time required for complete color development of a H_3PO_4 and H_3AsO_4 mixture with a total concentration in solution of 5 μmol l^{-1} was found to be below 10 min, even at H_3PO_4 levels four times lower than corresponding H_3AsO_4 concentrations [20]. The time dependence of the formation of molybdocomplexes measured under these conditions is presented under supporting information (SI, Note 1, inset).

The absorbance of molybdocomplexes formed at H_3PO_4/H_3AsO_4 concentrations below 5 μmol l^{-1} using the procedure described here was found to be stable in excess of 2 h. However, an increase in the concentration of either analyte above 10 μmol l^{-1} leads to an easily visualized instability of their molybdenum complexes. We suspect that under these conditions, the complexes rapidly polymerize/coagulate as discussed above.

The final spectra of molybdophosphate (Fig. 1, spectrum a) and molybdoarsenate (Fig. 1, spectrum b) complexes, respectively, with $\varepsilon(P^V) = 20{,}700$ l mol^{-1} cm^{-1} at $\lambda_{max} = 893$ nm and $\varepsilon(As^V) = 23{,}740$ l mol^{-1} cm^{-1} at $\lambda_{max} = 842$ nm obtained using our modified color development procedure closely resemble those reported previously [19] and formed according to the ISO norm standard procedure under heating (Fig. 1, insets 1 and 2, curve b). Spectra of theses complexes formed using the molybdenum blue method modified in the present work have two isobestic points at $\lambda_{i.p.} \approx 756$ and 878 nm that can be used for the determination of the total concentration of H_3PO_4 and H_3AsO_4 in solution.

The effect of acidity on the rate of color development and on the stability of the resulting molybdoarsenate/molybdophosphate complexes has been reported previously [20] and was investigated for our modified molybdenum blue method.

The concentration of sulfuric acid in the molybdenum-containing reagent solution was not modified from Lenoble's recipe (0.23 mol l^{-1} in the final solution, or 5.4 mol l^{-1} in the molybdate reagent solution). In our investigations on the impact of acidity on reaction kinetics/product stability, the amount of sulfuric acid pre-mixed with analyte before color development was varied between 0 and 2 ml. The dependence of absorbance (λ = 878 nm) of color-developed solutions containing 5 μM H_3PO_4 on the concentration of sulfuric acid were measured at 2 min (Fig. 2, open square) and 10 min (Fig. 2, closed circles) after color development. It was found that increasing the concentration of sulfuric acid decreases the rate of color development, but also increases the stability of the chromophore complex by decreasing its rate of polymerization. The molybdenum complex was found to be stable for more than 2 h (SI, Note 2, inset) when the total sulfuric acid concentration (includ-

[1] Instability of the molybdoarsenate and/or molybdophosphate complexes in the present work is defined as a change in absorbance during 1 h that exceeds three standard deviations of the instrument noise (1 S.D. ≈ 0.6 ma.u.) and is thought to be due to polymerization of the molybdenum complexes.

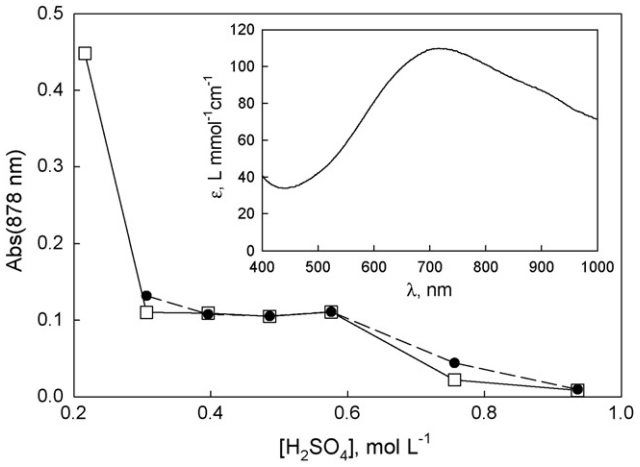

Fig. 2. Dependence of the molybdophosphate complex absorbance on the concentration of sulfuric acid in the final solution measured using Shimadzu spectrophotometer at 2 min (open squares) and 10 min (closed circles) following color development of a 5 μmol l^{-1} phosphate solution. Inset shows a spectrum of the product formed 2 min following color development of a solution containing 0.23 mol l^{-1} of sulfuric acid.

ing H_2SO_4 from molybdenum solution) in the final solution was above 0.42 mol l^{-1} ($[H^+] \approx [H_2SO_4]_o$, $pK_{a_2}(H_2SO_4) = 2$). This value corresponds to a ratio [H^+, mol l^{-1}]/[AM, mol l^{-1}] = 118, which is higher than those reported previously [17,20].

Molybdoarsenate and molybdophosphate complexes rapidly polymerize at sulfuric acid concentrations below 0.42 mol l^{-1}. The spectrum of the product formed in solution with a final sulfuric acid concentration of 0.23 mol l^{-1} over the first 2 min of color development (Fig. 2, inset) was found to be different from that expected for molybdophosphate. This product's spectral response was unstable over the first 2 h and was not proportional to the H_3PO_4 levels in solution. The observed molar absorptivity of this species, assuming the H_3PO_4 concentration in solution exceeded 10^5 l mol^{-1} cm^{-1}, are several times higher than previously reported values and those measured here with our optimized method. In addition, the formation of this complex follows the precipitation of a blue residue on the wall of the optical cell (see above).

Although polymerization/coagulation of molybdenum complexes can be avoided by adding sulfuric acid to the analyte solution, the higher acidity also decreases the rate of color development [12] making it impractically low (>10 min) if the concentration of sulfuric acid in the final solution exceeded 0.6 mol l^{-1}. Heating solutions with a concentration of sulfuric acid above 0.6 mol l^{-1} at 50 and 70 °C leads to the formation of products that resemble those shown in Fig. 2 (inset) and, consequently, heating cannot be used to improve the method without further modifications.

The optimum range of sulfuric acid concentrations in the final solution for low-level H_3PO_4/H_3AsO_4 measurement was found to be several times higher than the levels reported previously (Table 1), excluding only the work of Dhar and colleagues [27]. However, these investigators employed significantly lower concentrations (12 and 4 times, respectively, in the final solution) of AM and PAT than in our modified method. In addition, much of the solution's acidity in Dhar et al.'s work is from hydrochloric acid. By analogy with the effect of fluoride, chloride may lead to a decrease in the rate of color development [17].

Calibration of H_3AsO_4 and H_3PO_4 signals from color developed solutions using our optimized molybdenum blue method was carried out for Shimadzu spectrophotometer at $\lambda_{i.p.}$ = 878 nm and SpectraSensors photometer. The corresponding data for H_3AsO_4 and H_3PO_4 are presented in SI (Note 2 and Note 3, respectively). The linear dependence of absorbance on analyte concentration (r^2 = 0.999) was observed over the entire measurement range (<10 μmol l^{-1}) of H_3AsO_4 (closed circles), H_3PO_4 (open squares) and H_3AsO_4/H_3PO_4 mixtures (open hexagons). All three mixtures exhibited near identical molar absorptivity ε_{878} = 20,000 ± 200 l mol^{-1} cm^{-1} (standard error), as expected from the choice of measurement wavelength (i.e., isobestic point). The equivalent values of ε_{878} measured for these solutions imply that the absorbance observed for aqueous mixtures of H_3AsO_4 and H_3PO_4 at λ = 878 nm is a simple superposition of the individual absorbance contributions from the molybdoarsenate and molybdophosphate complexes.

In contrast, the linear dependence of molar absorptivity on the H_3AsO_4/(H_3AsO_4 + H_3PO_4) ratio was not observed at other wavelengths. Measuring the absorbance below 878 nm will increase [H_3AsO_4] sensitivity of because the molar absorptivity of arsenate is higher than that of phosphate, but this also will increase the uncertainty in the interpretation of the observed absorbance due to non-linearities. However, optimization wavelength for these conditions also can be carried out.

The linear dependence of absorbance on H_3AsO_4 (SI, Note 3, closed circles, $\varepsilon(As^V)$ = 14,300 ± 300 l mol^{-1} cm^{-1}) and H_3PO_4 (SI, Note 3, open squares, $\varepsilon(P^V)$ = 18,400 ± 300 l mol^{-1} cm^{-1}) concentration in individual solutions as well as in their mixture (SI, Note 3, open hexagons) also was observed using the SpectraSensors photometer (SI, Note 3). However, in this case, the measured signal corresponds to the integral absorption of the analyte solution between 775 and 950 nm, corresponding to the emission spectrum (λ_{max} = 880 nm) of the light emitted diode (LED) source. The non-monochromatic nature of the LED source explains the difference between ε_{878} measured using a spectrophotometer and the LED-based photometer.

Using the above rationale, the observed molar absorptivity of H_3PO_4/H_3PO_4 mixtures using the SpectraSensors photometer was not found to be linearly proportional to the mole fraction of H_3AsO_4 (SI, Note 3, inset, open circles) [12]. This observed dependence can be described in terms of a second order polynomial equation:

$$\varepsilon_{obs}\,(\mathrm{l\,mol^{-1}\,cm^{-1}}) = 18,400 - 1069X - 3026X^2 \qquad (1)$$

with a correlation coefficient (r^2) 0.98 (SI, Note 3, inset, solid curve). The largest deviation from linearity (≤5%) (SI, Note 3, inset, dashed line) was observed for solutions with equimolar concentrations of H_3PO_4 and H_3AsO_4.

The molybdenum blue method was optimized in the present work for an H_3PO_4/H_3AsO_4 full-scale of 5 μmol l^{-1}; however, the above results show that the method can be extended

to analyte measurements of 10 μmol l^{-1}. The limit of detection (LOD) for H_3PO_4/H_3AsO_4 of 10 nmol l^{-1} (0.7 ppb As) is defined in the present work as corresponding to two standard deviations of 5 independent measurements of solutions containing 1 μmol l^{-1} H_3PO_4, using the SpectraSensors photometer. The measurement error was found to be significantly higher than that measured with the SpectraSensors instrument when a solution of a stable dye (absorbance corresponds to 2 nmol l^{-1} As) absorbing at 880 nm is used. Based on this observation, the measurement error is mostly attributed to the color developments procedure.

The optimized procedure for the determination of H_3PO_4/H_3AsO_4 over the 0–5 μmol l^{-1} range is described below:

Stock solution of ascorbic acid is prepared according to the ISO norm [18]:

Stock solution of molybdate is prepared by dissolution of 5.2 g ammonium molybdate and 8.8 mg of potassium antimonyl tartrate in 30 ml of 9 mol l^{-1} sulfuric acid and diluted by deionized water to a final volume of 50 ml in a volumetric flask:

Measuring of the analyte solution:

a. 45 ml of analyte solution (V_{sample}) is measured out in a 50 ml volumetric flask (V_{flask});
b. add 0.5 ml of 98% H_2SO_4, shake;
c. wait 45 s and add 2 ml of molybdate *stock solution*, shake;
d. wait 45 s and add 1 ml of ascorbic acid *stock solution*, shake;
e. top up solution to a final volume of 50 ml with deionized water, shake;
f. wait ∼10 min and measure absorbance at 880 nm (C_{meas}).

The analyte concentration is calculated using Eq. (2):

$$C_{sample} = \frac{V_{flask} C_{meas}}{V_{sample}} \quad (2)$$

After establishing a standard procedure for fast and accurate phosphate/arsenate measurement in solution, a new reduction scheme for arsenate was developed.

The reduction of H_3AsO_4 by dithionite was carried out in solutions with natural pH. The concentrations of H_3AsO_4 and dithionite were varied between 0.02 and 1 μmol l^{-1} and 0.4 and 0.8 mmol l^{-1}, respectively. The concentration of arsenate was measured using our modified molybdenum blue method. The amount of dithionite added to the solution was measured gravimetrically.

It is found that increasing the dithionite concentration above 0.8 mmol l^{-1} results in precipitation at room temperature, due to the formation of colloidal sulfur [28]. This precipitate can be removed by heating, but only from solutions that have not been acidified (see below).

At room temperature, dithionite (<0.8 mmol l^{-1}) did not reduce H_3AsO_4, even after 1 h of reaction time in unacidified solution or in solutions containing sulfuric acid concentrations below 0.18 mol l^{-1}. Heating an H_3AsO_4/dithionite unacidified solution in the 50–80 °C temperature range leads to H_3AsO_4 reduction. The time needed for reduction of H_3AsO_4 to reach completion depends on temperature, varying from 1 h to 10 min, respectively. The time dependence of H_3AsO_4 reduction (i.e., absorbance decrease) measured in solution with a background H_3PO_4 concentration of 0.9 μmol l^{-1} using the SpectraSensors prototype photometer at two temperatures is presented under supporting information (Note 4, curves 1 and 2). The dashed lines show the absorbance corresponding to the total H_3AsO_4 and H_3PO_4 levels (SI, Note 4, red) and H_3PO_4 (SI, Note 4, blue) in the initial solution.

The kinetics of H_3AsO_4 reduction at the highest employed temperature (80 °C) were found to be faster than the time resolution of our measurement approach and only solutions with completely reduced H_3AsO_4 (i.e., no H_3AsO_4 signal following color development) were observed. The induction period observed at 50 °C was attributed primarily to the time required for the sample to reach the temperature setpoint. The heating temperature profile at T_{bath} = 50 °C is presented under SI (Note 4, curve 3). However, a portion of the induction period also can be attributed to H_3AsO_4 reduction and formation of colloidal sulfur (see above). The latter leads to H_3AsO_4 independent scattering of light thereby masking a concomitant decrease in absorbance of the color developed solution due to reduction of H_3AsO_4 to H_3AsO_3. Our contention that light extinction by colloidal sulfur at the wavelengths used to measure the molybdophosphate/arsenate complexes is supported by similar results obtained from "reduced" (heated from 10 to 40 min at 50 °C) and subsequently color developed solutions containing the same concentration of phosphate (0.9 μmol l^{-1}) and dithionite (0.8 mmol l^{-1}), but in the presence (0.9 μmol l^{-1}) and absence of H_3AsO_4 (SI, Note 4, closed squares).

Colloidal sulfur was not observed and complete reduction of H_3AsO_4 was obtained when solutions of H_3AsO_4 and dithionite were heated for 20 min at 80 °C. The residual spectrum of color-developed 5 μmol l^{-1} H_3AsO_4 solutions reduced by dithionite over 20 min at 80 °C (Fig. 1, spectrum c) closely resembled the spectrum obtained when H_3AsO_4/H_3PO_4 are omitted from the analyte solution (Fig. 1, spectrum d).

The temperature dependence of the absorbance of color developed solutions measured with the SpectraSensors photometer is shown in Fig. 3 and corresponds to the residual (i.e., unreduced) H_3AsO_4 concentration under the following conditions: 20 min of heating, initial dithionite concentration 0.4 mmol l^{-1} (open squares) and 0.8 mmol l^{-1} (closed circles); H_3PO_4 levels of 0.9 μmol l^{-1}; H_3AsO_4 levels of 0.9 μmol l^{-1}. These data show that the amount of H_3AsO_4 reduced over 20 min of heating increases with temperature and concentration of dithionite. Complete reduction of H_3AsO_4 was observed consistently only with a dithionite concentration of 0.8 mmol l^{-1} at 80 °C; with dithionite concentrations of 0.4 mmol l^{-1} reduction was incomplete even at 80 °C (Fig. 3, dashed line 2). It is believed that the large standard deviations observed below 70 °C are due to dithionite weighing errors (4–7 mg). This assertion is supported by significantly lower errors (open squares) obtained when a 500 ml flask is used for the preparation of the sample solution containing dithionite. However, under these conditions, the solution with the highest dithionite concentration (0.8 mmol l^{-1}) leads to the formation of colloidal sulfur, even before heating.

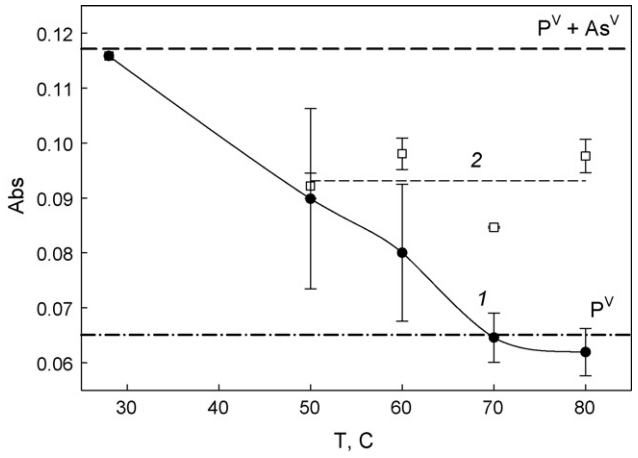

Fig. 3. Temperature dependence of the absorbance (measured using SpectraSensors photometer, $\lambda_{max} = 880$ nm) of color developed, reduced arsenate solutions with equimolar (0.9 μmol l^{-1}) initial concentration of phosphate and arsenate. Solutions were heated during 20 min. Errors bars correspond to 1 S.D. of four independent measurements.

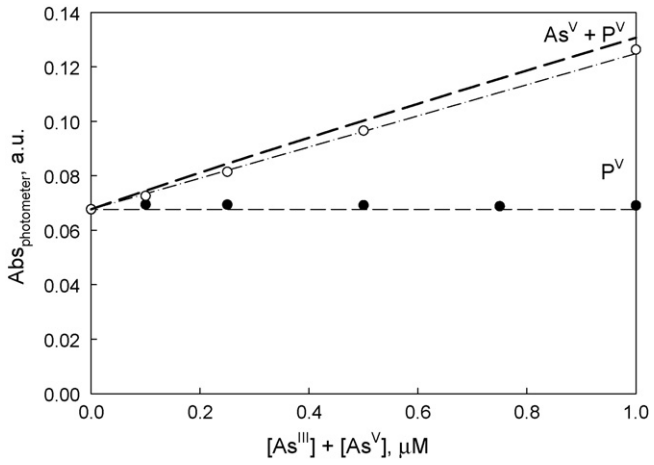

Fig. 4. Dependence of absorbance of solutions (measured using SpectraSensors photometer) that were color developed following 20 min of dithionite-mediated reduction of arsenate at 80 °C (closed circles) and solutions that were not subjected to reduction (open squares) on the concentration of arsenate in the initial mixture in the presence of 0.9 μmol l^{-1} phosphate. Dashed and short dashed lines with dots represent the expected absorbance for phosphate/arsenate aqueous mixture and phosphate solutions, respectively, calculated based on individual molar absorptivity of molybdophosphate and molybdoarsenate complexes. Long dashed line corresponds to the absorbance calculated using Eq. (1).

Cooling a 0.8 mmol l^{-1} dithionite solution to room temperature following 20 min of heating ($T < 70$ °C) often resulted in the formation of colloidal sulfur, which could be eliminated by subsequent heating of this sample. Colloidal sulfur appears to decompose at elevated temperatures [28]. Consequently, heating of the dithionite solution also can be used to prevent the formation of cloudy solutions during the acidification of samples via the color development procedure even if the concentration of dithionite in solution before heating is above its acceptable limit for low pH values.

The reduction of H_3PO_4 under analogous experimental conditions to H_3AsO_4 reduction was not observed, suggesting that dithionite can be used for selective H_3AsO_4 reduction. Consequently, the scheme described by Johnson and Pilson can be adapted using our optimized molybdenum blue method in combination with dithionite as a selective reductant, enabling low-level speciation of inorganic arsenic and H_3PO_4.

The reduction of H_3AsO_4 by dithionite at 80 °C was investigated using an initial solution over a range of H_3AsO_4 concentrations (0.1–1 μmol l^{-1}) and in the presence of 0.9 μmol l^{-1} H_3PO_4. The dependence of absorbance on H_3AsO_4 concentration in the initial solution in the presence/absence of the reducing agent is presented in Fig. 4. This dependence was measured using the SpectraSensors photometer. The absorbance of these solutions is in good agreement with predicted values based on the molar absorptivity of molybdoarsenate/molybdophosphate complexes calculated for H_3PO_4 (Fig. 4, short dashed line) and H_3AsO_4 in the presence of H_3PO_4 (Fig. 4, dashed line with dots and long dashed line). The predicted data presented in Fig. 4 were calculated using linear (Fig. 4, dashed line with dots) and non-linear (Fig. 4, long dashed line) models for the additivity of molybdoarsenate and molybdophosphate spectra. In the latter case, the molar absorptivity of the mixture was calculated according to Eq. (1), using molar absorptivities of 14,300 and 18,400 l mol^{-1} cm^{-1} for molybdoarsenate and molybdophosphate, respectively. In both cases, the difference between calculated and experimental values was found to be below 5% of the measured H_3AsO_4 concentration and was attributed to an uncertainty in the molar absorptivity (SI, Note 3, inset).

The optimized procedure for H_3AsO_4 reduction is described below:

a. 45 ml of analyte is dispensed into a 50 ml volumetric flask;
b. add 5–7 mg of sodium dithionite to the analyte solution;
c. heat solution 20 min at 80 °C;
d. cool solution to room temperature;
e. color develops using our optimized procedure (see above).

4. Conclusion

The molybdenum blue method has been optimized for fast, sensitive, and accurate measurements of H_3PO_4 and H_3AsO_4 in aqueous solution.

The high stability (>2 h) of the absorbance signal following color development according to our procedure eliminates the need for the addition of small amounts of oxidizing agents to color developed solution for signal stabilization used in previous methods [12].

Selective reduction of H_3AsO_4 by dithionite was observed in the 50–80 °C temperature range. Dithionite does not reducing phosphate under these conditions and can replace the reducing system used in the Johnson and Pilson procedure.

The reduction of H_3AsO_4 by dithionite does not require high solution acidity and therefore can be carried at the sample's pH without incurring a loss in sensitivity.

The time required for complete H_3AsO_4 reduction by dithionite is independent of H_3AsO_4 concentration (note: $[H_3AsO_4] \ll$ [dithionite]) [12], but depends on the concentration of dithionite.

Acknowledgements

We thank Dr. Randy May, Dr. Greg Sanger, Dr. Sorhab Zarrabian and Dr. Pedatsure Neta for helpful discussions. The authors gratefully acknowledge SpectraSensors, Inc. for funding this research. We also appreciate the reviewer of this paper for his/her friendly and helpful comments.

Appendix A. Supplementary data

Supplementary data associated with this article can be found, in the online version, at doi:10.1016/j.talanta.2006.07.043.

References

[1] J.V.S. Smith, J. Jankowski, J. Sammut, Appl. Geochem. 18 (2003) 1479.
[2] F. Challenger, Chem. Res. Toxicol. 19 (1945) 315.
[3] W.R. Cullen, K.J. Reimer, Chem. Rev. 89 (1989) 713.
[4] T. Hayakawa, Y. Kobayashi, X. Cui, S. Hirano, Arch. Toxicol. 79 (2005) 183.
[5] G. Jiang, Z. Gong, X.-F. Li, et al., Chem. Res. Toxicol. 16 (2003) 873–880.
[6] S.E. Hrudey, W. Chen, C.G. Rousseaux, Bioavalability in Environmental Risk Assessment, Lewis, Boca Raton, Fl, 1996.
[7] H.V. Aposhian, M.M. Aposhian, Chem. Res. Toxicol. 19 (2006) 1.
[8] N.E. Korte, Q. Fernando, Crit. Rev. Environ. Contr. 21 (1991) 1.
[9] A. Brandsteller, E. Lombi, W.W. Wenzel, D.C. Adriano, Wise Remediation Engineering of Contaminated Soils, Dekker, NY, 2000.
[10] M.M. Rahman, D. Mukherjee, M.K. Sengupta, U.K. Chowdhury, D. Lodh, C.R. Chanda, S. Roy, M. Selim, Q. Quamruzzaman, A.H. Milton, S.M. Shahidullah, M.T. Rahman, D. Chakraborti, Environ. Sci. Technol. 36 (2002) 5385.
[11] N.F. Osmond, Bull. Soc. Chim. Paris 47 (1887) 745.
[12] D.L. Johnson, M.E.Q. Pilson, Anal. Chim. Acta 58 (1972) 289.
[13] J. Murphy, F. Koroleff, Methods of Seawater Analysis, Chimie, Weinheim, 1983.
[14] T.R. Parsons, Y. Maita, C.M. Lalli, A Manual of Chemical and Biological Methods for Seawater Analysis, Pergamon Press, Oxford, 1984.
[15] P.K. Dasgupta, Talanta 58 (2002) 1.
[16] V.I. Bogdanova, Mikrochim. Acta 2 (1984) 317.
[17] S. Blomqvist, K. Hjellstrom, A. Sjosten, Int. J. Environ. Anal. Chem. 54 (1993) 31.
[18] AFNOR, Qualite des eaux. Afnor ed., Paris, 1997.
[19] V. Lenoble, V. Deluchat, B. Serpaud, J.C. Bollinger, Talanta 61 (2003) 267.
[20] R.E. Stauffer, Anal. Chem. 55 (1983) 1205.
[21] K.L. Linge, C.E. Oldham, Anal. Chim. Acta 450 (2001) 247.
[22] H.W. Chen, I.D. Brindle, X.C. Le, Anal. Chem. 64 (1992) 667.
[23] D.L. Johnson, Environ. Sci. Technol. 5 (1971) 411.
[24] A.K. Pettersson, B. Karlberg, Anal. Chim. Acta 354 (1997) 241.
[25] A. Sjosten, S. Blomqvist, Water Res. 31 (1997) 1818.
[26] T. Liu, E. Diemann, H. Li, A.W.M. Dress, A. Muller, Nature 426 (2003) 59.
[27] R.K. Dhar, Y. Zheng, J. Rubenstone, A. van Geen, Anal. Chim. Acta 526 (2004) 203.
[28] R.G. Rinker, S. Lynn, D.M. Mason, W.H. Corcoran, Industr. Eng. Chem. Fundam. 4 (1965) 282.
[29] J. Murphy, J.P. Riley, Anal. Chim. Acta 26 (1962) 31.

Available online at www.sciencedirect.com
ScienceDirect
Talanta 71 (2007) 1464–1469
Talanta
www.elsevier.com/locate/talanta

Characterisation of the surface composition in electrospun nanowebs with static secondary ion mass spectrometry (S-SIMS)☆

P. Van Royen [a,*], E. Schacht [b], L. Ruys [c], L. Van Vaeck [a]

[a] *Department of Chemistry, University of Antwerp, B-2610 Wilrijk, Belgium*
[b] *Department of Org. Chem., Polymer Materials Research Group, B-9000 Gent, Belgium*
[c] *Centexbel-Gent, B-9052 Zwijnaarde, Belgium*

Received 15 September 2005; received in revised form 19 June 2006; accepted 21 June 2006
Available online 22 August 2006

Abstract

Electrospinning is a recently rediscovered method to produce non-woven nanowebs of which the individual polymer fibres have diameters of 50–500 nm. Applications require specific functionalities to be present at the surface. The use of additives in the electrospun solution provides an elegant alternative to functionalised polymers. This study has focused on the use of the static secondary ion mass spectrometry (S-SIMS) to characterise the surface composition of nanofibres electrospun from acetone solutions containing 15% (w/w) of poly(ε-caprolactone) (PCL, molecular weight 40,000) and 0–15 mol% (relative to PCL) cetyltrimethylammonium bromide (CTAB). Specifically, the calibration of the relative signal intensities of structural ions from PCL and CTAB as a function of the local concentrations requires adequate reference samples to be prepared. In general, this step becomes a major bottleneck in nanoscale analysis. A relatively simple method using a combination of spincoating and hand barcoating of solutions has been developed. Its applicability and limitations for monitoring the surface enrichment of CTAB in PCL nanowebs are discussed.

Keywords: Electrospinning; S-SIMS; Poly(ε-caprolactone); Cetyltrimethylammonium bromide

1. Introduction

For many applications the usability of the materials depends on the interactions between its surface and the environment to which it is exposed. Hence, modern material research increasingly focus on tailoring the chemical surface composition of materials with a high specific area per gram. Nanosized objects excel with respect to surface over volume ratio. The use of electrospinning (ES) allows non-woven webs of nanofibres (diameter between 50 and 500 nm) to be produced from various polymers [1]. Already patented in 1943 [2], ES has been resuscitated in the 1980s [3]. The specific area of nanowebs can be as high as 200 $m^2\,g^{-1}$ and, thereby, compares with that of active coal. The use of a functionalised polymer or additives gives the possibility to provide the surface with specific groups. Apart from filtration, a wide range of potential applications relates to the fields of biomedicine and tissue engineering, such as wound dressing, bio-interactive scaffolds, while nanowebs also offer perspectives for novel protective clothing, etc. [1].

In principle, the ES experiment is relatively simple. A flow of up to several ml h^{-1} of polymer solution or melt is injected with a syringe into a strong electric field of typically 20–40 kV over 10–30 cm. The electrostatic forces lead to the formation of a Taylor cone and a liquid jet towards the collector plate. Fast evaporation of the solvent yields a polymer filament that is further elongated and thinned by the electrical field. The strong forces on the ultimately thinned fibre lead to a chaotic lateral movement or "whipping" in the vicinity of the collector. As a result, a non-woven nanoweb is deposited [3–6]. A complete description of the ES physics [6] requires knowledge of, e.g. viscosity, surface tension and dielectric constant in each stage of the dynamic transition from liquid jet to dry fibre. As this information is experimentally inaccessible, ES optimisation is often based on the effect of given process parameters on the morphology of the nanofibres [7,8] while the performance of functionalised nanofibres depends on the presence of specific groups at the surface.

☆ Paper presented at the Colloquium Spectroscopicum International XXXIV (CSI 34) held in Antwerp (Belgium), September 4–9, 2005.

* Corresponding author.
E-mail address: pieter.vanroyen@ua.ac.be (P. Van Royen).

0039-9140/$ – see front matter © 2006 Elsevier B.V. All rights reserved.
doi:10.1016/j.talanta.2006.06.042

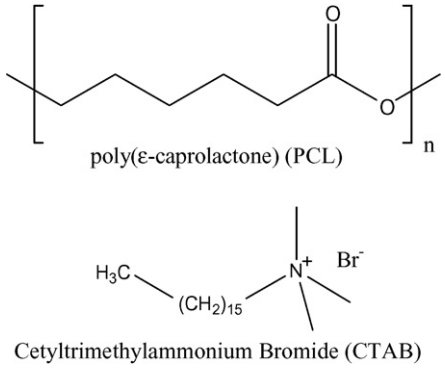

Fig. 1. Structure of (top) poly(ε)caprolactone (PCL) and (bottom) cetyltrimethylammonium bromide (CTAB).

There is a clear need for a chemical analysis method that probes selectively the molecular composition of the outer monolayer of the nanofibres. At present, static secondary ion mass spectrometry (S-SIMS) is virtually the only method meeting the requirements of both molecular characterisation and monolayer information [9–11]. The use of additives to the polymer solution provides an elegant alternative to the electrospinning of functionalised polymers [1]. A current project focuses on the ES of biodegradable poly(ε-caprolactone) (PCL) using cetyltrimethylammonium bromide (CTAB) as additive to tune the concentration of the quaternary ammonium functionalities at the surface [12]. Structures are given in Fig. 1. This system serves as model for scaffolds based nanowebs with bio-interactive receptor sites. The feasibility of S-SIMS for the detection of structural ions from both components in the outer monolayer of nanofibre has been described before [12]. The next step is the correlation of the ion signal intensities to the actual local concentration. This requires calibration by means of adequate reference mixtures of which the analysed volume has a well-known composition. The use of S-SIMS, which specifically detects molecular information from only a monolayer, complicates the task because many commonly used approaches for preparing calibration standards lead to surface enrichment at the level of only one monolayer. As a result, the concentration of components in the probed layer becomes different from those in the bulk. For organic analysis, there is no method for the independent control of the actual composition of the outer monolayer.

To overcome this problem, reference mixtures have been prepared in the form of monolayers and thick layers. The relative signal intensity of CTAB- and PCL-specific ions has been calibrated as a function of the concentration ratio of both components in the electrospun solution. The comparison of the calibration data in both cases is used to delineate the possible error to be associated with surface enrichment during standard preparation.

2. Experimental

The in-house made apparatus for ES consists of a 10 ml syringe with a NE-1000 single syringe pump (New Era Pump Systems Inc., Wantagh, NY, USA), that can deliver a flow rate between 0.7 $\mu l\,h^{-1}$ and 2 $l\,h^{-1}$. The needle of the syringe is connected to the actual injector through a Teflon tube (internal diameter: 1 mm, length: 3 m), providing sufficient electrical insulation to protect the syringe pump. The injector with external and internal diameter of 2 and 1 mm, respectively, protrudes 9 mm from a small metal flange with diameter of 30 mm, which is connected to a high-voltage source (ASH 30 55 type 2053, EME, Glabbeek, Belgium). The distance between the injector and the grounded aluminium collector plate (40 cm × 40 cm) can be varied between 15 and 30 cm. Aluminium foil is deposited on the collector and sample of 1 cm × 1 cm is cut from the central zone for analysis.

The electrospun solutions have been made in acetone with PCL and CTAB at concentrations of 15% (w/w) and 0–15 mol% (relative to PCL), respectively. The additive has been purchased from Janssen Chimica (Beerse, Belgium) and PCL with nominal molecular weight 40,000 from Interox Solvay (Brussels, Belgium). Dissolution of the polymer requires refluxing the PCL in acetone and stirring the hot pasta for 30 min [12]. Injection of the solutions at a flow rate of 5 $ml\,h^{-1}$ and electrospinning during 2 min at a voltage of 20 kV and a 30 cm distance between the injector and collector has yielded an adequate loading of the substrate for S-SIMS analysis.

Morphological examination of the samples has been performed with scanning electron microscopy (SEM) using 20 keV electrons at a beam current of 1 nA in a Jeol JSM-6300 (Jeol Ltd., Tokyo) instrument. Atomic force microscopy (AFM) was conducted on a Nanoscope IIIa instrument (Digital Instruments, Santa Barbara, CA).

Reference mixtures have been made by spincoating (Spincoater G3-8, Pi-KEM, Tamworth, UK) at 4000 rpm during 30 s using an aliquot of 10 μl of an acetone solution containing 10^{-4} M PCL and CTAB in the range of 0–15 mol% (relative to PCL) on a silicon wafer substrate, thoroughly precleaned by ultrasonification in methanol. Thick films were prepared by barcoating. A 'K hand coater' (RK print Coat Instrument Ltd., Litlington, UK) was used to produce layers with a wet film thickness of 24 μm on a silicon wafer. The dry film thickness is of about 100 nm.

Analyses have been carried out in a time-of-flight (TOF) Ion TOF IV instrument (Cameca, Courbevoie, France) equipped with a liquid metal ion gun producing 25 keV Ga^+ primary ions. Positive ion mass spectra have been obtained from 100 μm × 100 μm areas with an acquisition time of 150 s. The total ion dose density has been 3.7×10^{12} ions cm^{-2}. The charge build-up during bombardment of the sample has been compensated using the low energy electron flood gun. To eliminate the effects of occasional anomalies in the fibre loadings, all mass spectra used further on were recorded from sample regions where the secondary ion intensity ratio of the $C_6H_{11}O_2^+$ ions (*m/z* 115) over the sum of $C_6H_{11}O_2^+$ and Al^+ ions is between 0.1 and 0.3.

3. Results and discussion

Throughout this discussion, the concentration of CTAB is expressed in mol%, relative to PCL. Mass resolution figures refer to the full-width at half-maximum (FWHM).

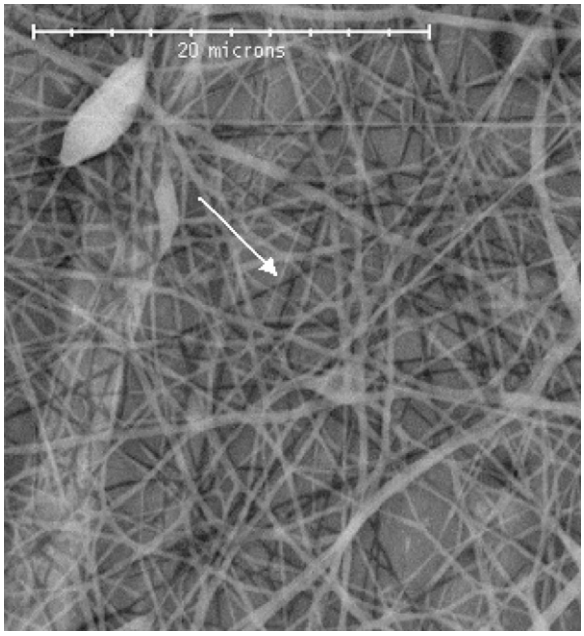

Fig. 2. Electron microscopy of nanofibres made by ES from a 15% (w/w) PCL and 7 mol% (relative to PCL) CTAB in acetone. The arrow indicates a fibre with diameter in the range of 180–220 nm.

3.1. Initial characterisation of nanofibres

Fig. 2 shows the electron micrograph of the nanofibres electrospun on aluminium foil using a solution of PCL with 7 mol% of CTAB. In order to obtain an adequate number of ion counts for the diagnostic ions, ES must be performed during about 2 min, yielding a loosely packed web with several fibres superimposed on top of each other. Application of AFM to samples made under the same conditions but with low surface coverage, has yielded an average diameter between 160 and 220 nm for the thinner fibres.

Fig. 3 shows a positive ion mass spectrum recorded from the nanofibres electrospun from a PCL solution with 7 mol% CTAB. The base peak at *m/z* 27 refers to the Al^+ ions generated from aluminium foil substrate, which is incompletely covered by the nanoweb. The major signals of diagnostic interest for PCL are found at *m/z* 115, 97, 69 and 55. The ions at *m/z* 115 and 97 are assigned to the protonated monomer and fragment corresponding to its dehydration. Subsequent loss of CO or CH_2CO from the ions at *m/z* 97 can explain the signals at *m/z* 69 and 55, respectively. The formation of these protonated monomers and the their fragments from the polymer can be rationalised using the desorption-ionisation (DI)-model [9] and is discussed extensively elsewhere [13]. The structural interpretation of the detected ions in TOF S-SIMS is supported by accurate *m/z* determinations, which allow the deviation between the experimental and theoretical *m/z* to be kept within 35 ppm, at least for monolayer samples on silicon. The mass accuracy in nanofibre measurements is lower, typically within 350 ppm, as a result of the sample morphology. In particular, the roughness of the surface causes a height difference of the points from where the secondary ions are generated. Apart from the decreased mass accuracy, also the mass resolution for the ions at *m/z* 115 goes down from typically 7000 to about 5000 for spincoated layers and nanowebs, respectively. Furthermore, the irregular structure of loosely piled nanofibres hampers the critical tuning of the electron flood gun to compensate the charge build up in the nanowebs during bombardment. The intense signal at *m/z* 284 refer to the intact cations of CTAB while a whole series of diagnostic ions are seen between *m/z* 58 and 268. Again, the principles of the previously developed DI model are found to be entirely adequate to explain the detected structural ions [14].

Because S-SIMS selectively probes the composition of the outer monolayer at the surface, the method has potential to detect the enrichment or depletion of given components at the surface relative to the overall composition in the bulk. Fig. 4 shows the intensity ratio of the CTAB-specific ions at *m/z* 284 to the PCL-specific ions at *m/z* 115 as a function of the concentration of CTAB in the electrospun solutions, all of which contain 15% PCL. The relative intensity of CTAB-ions over PCL-ions show a steep increase up to 3 mol% CTAB, a broad maximum between 5 and 10 mol% CTAB and a sharp decrease for nanowebs from solutions with 12–15 mol% CTAB. On the condition that the ion intensity ratio linearly varies with the local abundance of the two components in the probed monolayer, the data indicates that surface enrichment of CTAB occurs at low concentrations

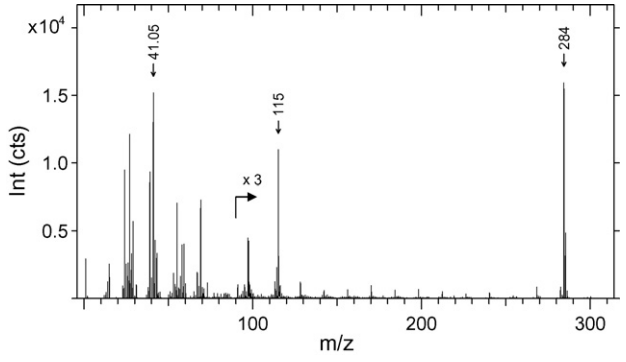

Fig. 3. Positive ion mass spectra are recorded by S-SIMS with Ga^+ primary ions from nanofibres electrospun on aluminium-foil from a 15% (w/w) PCL and 7 mol% CTAB (relative to PCL) solution in acetone.

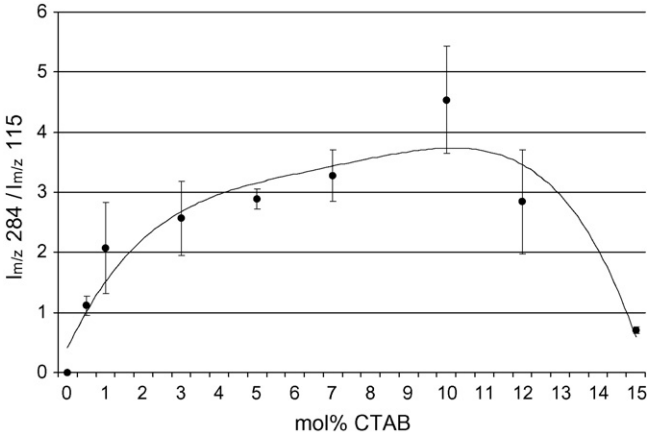

Fig. 4. Intensity ratio of characteristic ions from CTAB (*m/z* 284) over the specific ion of PCL (*m/z* 115) for nanofibres generated by ES as a function of the CTAB concentration (relative to PCL).

and depletion at high concentrations in the electrospun solution. This conclusion would be of high interest to the optimisation of the ES and therefore, motivates careful study of the relationship between the intensity ratio considered and the local concentration of CTAB and PCL. This requires adequate standards samples to be made.

3.2. Problem of calibration standards

In conventional mass spectrometry (MS) using ionisation of the analytes in the gas phase by e.g. electron beams in electron ionisation (EI) MS, the ion yield essentially depends on the structure of the analyte provided that the instrumental conditions are kept constant. The reason is that the energy is transferred to individual molecules in vacuum, that do not undergo further interactions with other analyte or matrix molecules in the source and subsequent flight to the detector. However, the situation becomes more difficult when energetic beams are used to desorb and ionise the analytes from a solid. Specifically, in SIMS, Ga^+ primary ions with high energy penetrate seriously deep in the sample and deposit their energy into the subsurface [16]. The primary ion energy is much higher than the binding energy within molecules. As a result, the energy deposition can be rationalised by a collision cascade type model, involving extensive relocation of individual atoms from sample constituents along the trajectory of the projectile. As a result, a whole series of the ion beam-induced damage processes are known to occur in the subsurface, for instance, atom mixing, segregation and enhanced diffusion, etc. The resulting change of the original composition is especially important in dynamic SIMS, where the relatively fast erosion rate causes ions from increasingly deeper layers to be detected. In contrast, static SIMS limits the analysis time to ensure that a given nanoscopic sample area (diameter typically 10 nm) never is hit twice by a primary ion during analysis. As a result, most of the typical SIMS complications due to ion beam-induced damage effects can be disregarded in S-SIMS. On the other hand, sputtering and ionisation are essentially phenomena occurring at the surface that depend on the way that the primary ion energy in deposited in to the sample, dissipated and redistributed to the ultimate surface region. Hence, also in S-SIMS, composition and physical properties of the sample matrix, i.e. the material surrounding the analyte, can significantly affect the ion yield from a given analyte. For instance, the deposition of an organic monolayer on a noble metal substrate, doped silicon wafer or a non-conducting polymer substrate makes a lot of difference for the ion yield. Apart from that, instrumental parameters must be accounted for. Although the primary ion beam impact angle seems to be of little effect, type and energy of the primary ion, surface charge compensation, surface roughness, etc. must be accounted for. As a result, measurement of adequate reference sample is most commonly used to estimate the relationship between specific analyte ions and the local concentration in a given sample environment.

The relative standard deviation (R.S.D.) of the absolute intensities for PCL and CTAB-specific ions in duplicate samples typically is better than 25%. The same holds true for the relative intensities of PCL over CTAB specific ions. These compares well with the typical R.S.D. of 10–15%, achieved during organic analysis of multicomponent systems on ideal flat "monolayers". The reasonable reproducibility of the mass spectra, recorded from different 100 μm × 100 μm areas in the electrospun samples also suggests that the random orientation of the nanofibres levels out the impact angle variations typical for fibre analysis. As a result, the thickness of the organic matrix deposited on the metal substrate has been considered as the prime factor affecting the ion yield for a given set of instrumental parameters. However, preparation of reference samples for the CTAB-PCL system with a thickness of typically 100 nm and a precisely known surface composition at the level of the outer monolayer is hampered by the inevitable surface enrichment or depletion effects, causing the ultimate surface composition to differ from the bulk. The deposition of the CTAB-PCL mixtures in the form of monolayer on a substrate circumvents the problem and the adequacy of the reference samples can be readily checked by imaging the lateral distribution of components. However, monolayer cause the energy dissipation to occur almost exclusively in the inorganic substrate, unlike in the case of nanofibres, where the 100 nm thick matrix plays a prominent role in the redistribution of the projectile's energy towards the analysed surface.

Hence, we based our approach on (1) the use of spincoating for the preparation of reference mixtures in the form of closed monolayers. Unless domains with different composition nature formed, the component ratio in the surface of the reference sample can be assumed to correspond to that of the spincoated solution; (2) use of barcoating for the preparation of reference mixtures in the form of 100 nm thick layers. Surface enrichment is assessed by comparing the form and slope of the calibration line with that of the one obtained for monolayers.

Spincoating is a suitable method to deposit thin layers on flat substrates in a very reproducible manner. On the other hand, the exact layer thickness depends on experimental factors such as evaporation rate of the solvent, surface tension and viscosity of the solution. Some of these parameters are difficult to control. The extreme dependence of the ion intensities in S-SIMS on the layer thickness can be used to determine the concentration of the solution from which "ideal monolayers" can be spincoated for a given system [15]. Fig. 5 illustrates the secondary ion intensities for the PCL-specific ions at m/z 115 and the CTAB-specific ions at m/z 284 as a function of the concentration of the spincoated solution. The increase of the ion intensities in the low concentration range is explained by incomplete surface coverage. Although the ion intensities from PCL show little effect of the layer thickness when 10^{-3} or 10^{-4} M solutions are spincoated, those from CTAB exhibit a clear maximum for 10^{-4} M concentrations, suggesting that the latter should be used for the preparation of samples in the monolayer range.

Fig. 6 shows the calibration of the intensity ratio for the CTAB-specific ions at m/z 284 over the PCL-specific ions at m/z 115 as a function of the CTAB concentration in the spincoated solution containing 10^{-4} M PCL. The ion intensity ratio correlates linearly with the CTAB concentration with in the range, that is useful for ES, with a linear correlation coefficient of volume (confidence level of 99.9%).

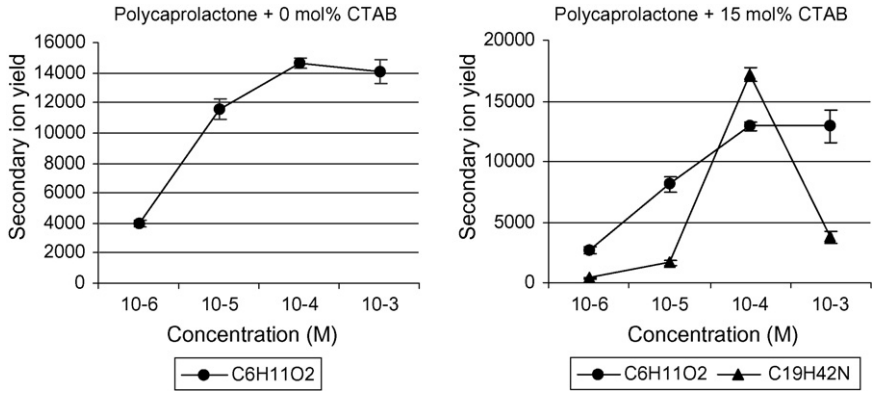

Fig. 5. Intensities for selected positive ions of PCL and CTAB recorded from layers spincoated from different concentrations for solutions of 15% (w/w) PCL with (left) 0 mol% and (right) 15 mol% of CTAB.

Using barcoated reference mixtures with a layer thickness of about 100 nm, the calibration of the signal intensity ratio for the ions from CTAB at *m*/*z* 284 over those from PCL at *m*/*z* 115 as a function of the CTAB concentration in the solution has yielded a significantly different relationship than the spincoated samples. Fig. 7 shows that the calibration now takes the form of a concave curve. Note that the intensity ratio for a given CTAB concentration for a barcoated reference mixture sample lies below that of the spincoated one. An explanation would be that the CTAB becomes depleted from the surface in comparison to PCL. Alternatively, a change in the ion yield when the silicon substrate is replaced by the organic matrix, could be considered to explain the results. The fact that intensity ratios for the barcoated samples approach those of spincoated ones at higher concentrations makes the latter interpretation less likely but further experiments are needed to exclude this possibility.

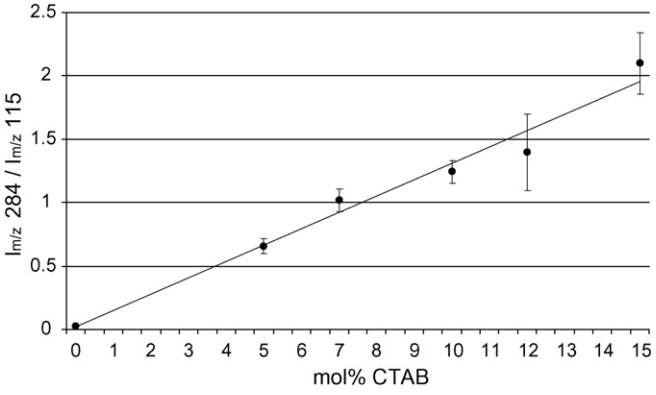

Fig. 6. Calibration of the intensity ratio of CTAB-specific ions at *m*/*z* 284 over PCL-specific ions at *m*/*z* 115 as a function of the CTAB concentration (mol% relative to PCL) using spincoated reference mixtures.

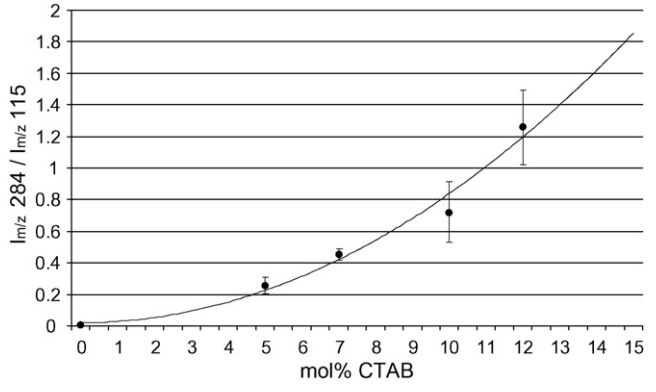

Fig. 7. Calibration of the intensity ratio of CTAB-specific ions at *m*/*z* 284 over PCL-specific ions at *m*/*z* 115 as a function of the CTAB concentration (mol% relative to PCL) using barcoated reference mixtures.

In the meantime it is clear that both calibrations support the evidence for the surface enrichment of CTAB in nanofibres depending on the relative concentration to PCL. Regardless the thickness of the organic matrix in the reference mixtures, the intensity ratio of the signals at *m*/*z* 284 over those at *m*/*z* 115 follows a continuous function that increases with the CTAB concentration. As a result, the drop seen in Fig. 4 for the intensity ratio in nanofibres made from a solution with 12 mol% CTAB must be related to an effective decrease of the local CTAB concentration in the nanofibres. Similarly, the difference in slope associated with the steep rise of the intensity ratio for CTAB concentrations up to 5 mol% and that of the broad maximum between 5 and 10 mol%, can be explained by surface enrichment of CTAB at low concentrations, regardless a linear or concave calibration is involved.

4. Conclusion

It is shown that the combination of spincoating and hand-barcoating can provide an interesting way to overcome the bottleneck of preparing suitable reference mixtures, allowing the signal intensity ratios of different component-specific ions to be calibrated as a function of the relative local concentrations. Specifically, it provides a relatively easy way to assess the importance of surface enrichment effects for given components during the preparation of layers from solutions. Such effects may cause significant differences between the relative composition of the components in the solutions and that in the surface layer, actually analysed in S-SIMS. The approach has been applied to the analytically demanding case of nanofibres. The results support that the trends in the signal intensity ratios of CTAB over PCL specific ions as a function of the additive concentration indeed reflected a substantial surface enrichment as a result of the ES

process. Although further research is needed to verify the reasons for the slightly different form of the calibration functions seen for samples with different thickness of the organic layer, the developed procedure may be useful for S-SIMS applications in nanoscale analysis.

Acknowledgements

The authors would like to thank Solvay for providing PCL. This research was funded by the Flemish Fund for Scientific Research (FWO Vlaanderen) and the Inter University Attraction Pole program (IUAP V).

References

[1] Z.M. Huang, Y.Z. Zhang, M. Kotaki, S. Ramakrishna, Compos. Sci. Technol. 63 (2003) 2223.
[2] A. Formhals, Process and apparatus for preparing artificial threads, US 1975504 (1934).
[3] L. Larrondo, R.S.J. Manley, J. Polym. Sci. Phys. 19 (1981) 909.
[4] J. Doshi, D.H. Reneker, J. Electrostat. 35 (1995) 151.
[5] A. Frenot, I.S. Chronakis, Curr. Opin. Coll.: Interf. Sci. 8 (2003) 64.
[6] M.M. Hohman, M. Shin, G. Rutledge, M.P. Brenner, Phys. Fluids 13 (2001) 2201.
[7] M.M. Demir, I. Yilgor, E. Yilgor, B. Erman, Polymer 43 (2002) 3303.
[8] K.H. Lee, H.Y. Kim, H.J. Bang, Y.H. Jung, S.G. Lee, Polymer 44 (2003) 4029.
[9] L. Van Vaeck, A. Adriaens, R. Gijbels, Mass Spectrom. Rev. 18 (1999) 1.
[10] A. Adriaens, L. Van Vaeck, F. Adams, Mass Spectrom. Rev. 18 (1999) 48.
[11] J.C. Vickerman, D. Briggs (Eds.), ToF-SIMS Surface Analysis by Mass Spectrometry, Surface Spectra and IM Publications, Manchester, UK, 2001, p. 788.
[12] P. Van Royen, L. Van Vaeck, E. Schacht, L. Ruys, Rapid Commun. Mass Spectrom. 20 (2006) 346.
[13] P. Van Royen, A. Taranu, L. Van Vaeck, Rapid Commun. Mass Spectrom. 19 (2005) 552.
[14] R. Van Ham, L. Van Vaeck, A. Adriaens, F. Adams, Anal. Chim. Acta 500 (2003) 259.
[15] D. Van Leyen, B. Hagenhoff, E. Niehuis, A. Benninghoven, Mikrochim. Acta 7 (1989) 1790.
[16] Z. Postawa, B. Czerwinski, M. Szewcyk, E.J. Smiley, N. Winograd, B.J. Garrison, J. Phys. Chem. B 108 (2004) 7831.

Available online at www.sciencedirect.com
ScienceDirect
Talanta 71 (2007) 1546–1552
Talanta
www.elsevier.com/locate/talanta

Direct and rapid determination of sulphate in environmental samples with diffuse reflectance Fourier transform infrared spectroscopy using KBr substrate

Santosh Kumar Verma, Manas Kanti Deb *

Pt. Ravishankar Shukla University, School of Studies in Chemistry, Raipur 492 010, Chhattisgarh, India

Received 9 May 2006; received in revised form 20 July 2006; accepted 20 July 2006
Available online 7 September 2006

Abstract

The feasibility of employing diffuse reflectance Fourier transform infrared spectroscopy (DRS-FTIR) as a sensitive tool in the submicrogram level determination of sulphate (SO_4^{2-}) was checked in this work. This paper presents the development of a new, rapid and precise analytical method for ppb levels of sulphate (SO_4^{2-}) in environmental samples like coarse and fine aerosol particles, dry deposits and soil. The determination of submicrogram levels of sulphate is based on the selection of a quantitative analytical peak at 617 cm^{-1} among the three observed vibrational peaks and preparing calibration curve using different known concentrations of sulphate by diffuse reflectance-Fourier transform infra red spectrometric (DRS-FTIR) technique. Pre-weighed and ground IR grade KBr was used as substrate over which remarkably wide range of known concentration of sulphate was sprayed and dried. The dried sample was analysed by DRS-FTIR. Three calibration curves for three different concentration ranges of sulphate were prepared for samples containing low and relatively higher sulphate contents. The relative standard deviation ($n = 8$) for the sulphate concentration ranges, 2.5–35.5, 25.5–165, 55–1000 μg/0.5 g KBr, as used to prepare calibration curves, were 2.4%, 2.1% and 1.5%, respectively. The relative standard deviation for the sulphate concentration in real samples were found to be in the range, 3.11–5.76% ($n = 16$), 4.05–7.75% ($n = 16$) and 1.48–3.52% ($n = 10$) for aerosol, dry deposits and soil, respectively. The LOD of the method is 0.20 μg/g SO_4^{2-}. The *F*- and *t*-tests were performed to check the analytical quality assurance test. The noteworthy feature of the reported method is the non-interference of any of the associated anions and cations. The results were compared with that of ion-chromatographic method with high degree of acceptability. The method can be applied in wide concentration ranges. A method for sulphate determination was introduced that did not require pretreatment of samples. This method employed the direct determination of the sulphate. The method is reagent less, nondestructive, very fast, repeatable, and accurate and has high sample throughput value.

Keywords: DRS-FTIR; Sulphate determination; KBr substrate; Environmental samples

1. Introduction

The determination of sulphate in a variety of environmental samples at trace levels has been a matter of great concern for analytical chemists over the years. Many techniques including ion-selective electrodes [1,2], turbidimetry [3], electrophoresis [4,5], flow injection analysis [6], ion exchange resin [7], etc. have been reported for the determination of sulphate in samples from different origin. These techniques, however, have their known inherent drawbacks such as poor sensitivity, low sample throughput, high detection limit and requirement of large sample size, dealing with number of chemicals, etc. Ion-chromatographic technique [8] overcomes most of the drawbacks mentioned above. However, the sample throughput is less, as the sample preparation processes such as soil-leaching, dissolution of aerosol in water, and the spectral scan requires atleast half an hour for one sample.

Recently, FTIR has emerged as an important analytical tool for qualitative as well as quantitative analysis of multi-atomic inorganic ions in aerosols. Qualitative and quantitative spectral identification of multi atomic inorganic ions and organic compounds mainly using attenuated total reflectance (ATR)-FTIR and diffuse reflectance Fourier transform infrared spectroscopy (DRS-FTIR) using zinc selenide substrate have been done to

* Corresponding author. Tel.: +91 771 2593367.
E-mail address: debmanas@yahoo.com (M.K. Deb).

0039-9140/$ – see front matter © 2006 Elsevier B.V. All rights reserved.
doi:10.1016/j.talanta.2006.07.056

measure the concentration and chemical composition of aerosols [9–14].

Ion-chromatographic method for analyzing inorganic samples since is a time consuming and destructive analytical process, we evaluate a new reagent-less technique namely diffuse reflectance Fourier transform infrared spectroscopy (DRS-FTIR) as an alternative method for the quantitative analysis of sulphate in environmental samples in this study. In the present investigation, the viability of DRS-FTIR technique for quantitative analysis of sulphate in atmospheric aerosols, dry deposits and soil is assessed with low detection limit and relatively high sample throughput value. The present investigation has shown excellent results with smooth and horizontal baseline peaks for sulphate as potassium sulphate at 617, 983 and 1117 cm^{-1} when KBr substrate is used as background. These peaks are quantitative with excellent correlation coefficient value. The IR peak at 983 cm^{-1} is found to be sharpest among all observed peaks for sulphate but with relatively very weak intensity. Although peak observed at 1117 cm^{-1} is relatively stronger but broader than that observed at 617 cm^{-1}. Therefore, vibrational peak at 617 cm^{-1} has been utilized for quantitative analysis of SO_4^{2-} for the simple reason of sharp and strong IR absorption.

2. Experimental

2.1. Apparatus

Aerosol sampling was performed using a 28.3 actual litre per min (ALPM) eight-stage cascade impactor type aerosol sampler (non viable) (Tisch Air Pollution Monitoring Equipment, USA, model TE 20-800) in the following particle size ranges: stage (0) 9.0–10.0 μm, stage (1) 5.8–9.0 μm, stage (2) 4.7–5.8 μm, stage (3) 3.3–4.7 μm, stage (4) 2.1–3.3 μm, stage (5) 1.1–2.1 μm, stage (6) 0.7–1.1 μm, stage (7) 0.4–0.7 μm, and stage (8) 0–0.4 μm. For collection of dust-fall a glass sampler having 45 cm height and 15 cm diameter with half filled ultrapure water and guard frame was used.

Gravimetric analysis of size-segregated aerosols was done using a Sartorius electronic balance, AG Gottingen, Germany, model CP225D (precision—10 μg).

Diffuse Reflectance, model DRS-8000A, Shimadzu Corporation Analytical and Measuring Instruments Division, Kyoto, Japan and FTIR spectrometer, model 8400S Shimadzu Corporation Analytical and Measuring Instruments Division, Kyoto, Japan, equipped with an L-alanine doped deuterated triglycine sulphate (DTGS) detector was used for the sample scanning. Table 1 shows the detailed information on the instrumental set up used.

Table 1
Instrumental specifications set for the DRS-FTIR analysis of samples for sulphate

Particulars	Description
Instrument	Fourier transform infrared spectroscopy, Model 8400S, Shimadzu Corporation, Kyoto, Japan
DRS attachment	DRS 8000-A, Shimadzu Corporation, Kyoto, Japan
Technique	Diffuse reflectance infrared Fourier transform spectroscopy
Software	IR solution
Sample volume	About 15 mg
Sample form	Solid
Appodization function	Happ-Ganzel
Resolution	4 cm^{-1}
No. of scanning	45
Measurement mode	Absorption
Spectral range (peak identification)	1300–500 cm^{-1}
Spectral range (quantitative analysis)[a]	650–550 cm^{-1}
Beam	Internal
Detector	L-Alanine-doped deuterated triglycine sulfate
Mirror speed	2.8 mm/s

[a] Baseline correction range for all analysis.

2.2. Glasswares

Because of the high sensitivity of the method, special care was taken during handling of all glasswares to avoid contamination. For volumetric measurements calibrated glass apparatus were used. Glassware were cleaned with hot chromic acid and after proper washing, rinsed with Millipore ultrapure water.

2.3. Reagents

To avoid contamination special precautions were taken from reagents and glass apparatus at every stage of experiment.

Infrared spectrometric grade Potassium bromide, Merck KGaA 64271 Darmstadt, Germany, was used in this analysis.

Due to the dominance of sulphate as potassium sulphate in the tested real aerosol samples the standard stock solution of sulphate was prepared by dissolving suitable amount of potassium sulphate, analytical reagent grade, Merck. Appropriate dilutions were made to obtain solutions containing sulphate in the concentration range 2.5–1000 μg/20 μl.

2.4. Sampling of aerosol, dry deposits and soil

Aerosol samples were collected in eight-different stages using eight-different pre-weighed stainless steel substrates having diameter 81 mm. Since the aerosol mass come maximum to few milligrams in all stages, though depending on air quality and sampling period, the sampler was run for a period of 20 h so that analytical amount of the samples could be obtained. The samples such collected in eight-different stages were taken out individually for the gravimetric measurement of the aerosol mass and then for the FTIR analysis of sulphate in each size range.

Dry deposition samples were collected for a period of 30 days according to the usual practice. Airborne solid particulate

matters having diameter greater than 100 μm, with larger settling velocities and having the tendency to settle down because of the gravity and inertia, were collected using a glass jar-type dust collector. Ultrapure water was placed in each of the collectors to avoid sample loss by blowing air. Sample collectors were positioned in guard frames at elevations of 5–15 m above ground level. Samples, after collection, were reduced to 25 ml volume by evaporation and transferred to a pre-weighed 50 ml beaker. Samples were further dried completely and the weight differences were noted. The dried samples were then directly taken for DRS-FTIR scanning using KBr substrate in a proper dilution.

Soil samples were collected from representative areas in and around the city. Surface soil was mixed thoroughly with soil from a depth of 2–3 ft to get a complete homogeneous sample. The samples (~0.1 g) were crushed to fine particles by grinding for 2–5 min in an agate mortar. The moisture content of the samples was removed by drying the samples in an electric oven at 40 °C for not more than 10 min as prolong heating might reduce the actual content of the analyte.

2.5. Sample preparation

In this method there are no special sample preparation procedures were required, samples could be directly put in DRS-FTIR after mixing with KBr and spectra could be obtained. These spectra were used for the both qualitative and quantitative analysis of sulphate in samples.

2.6. Preparation of calibration curves for FTIR determination of sulphate

Calibration curves for the FTIR determination of sulphate were prepared using a series of exactly weighed (0.5 g) and finely ground KBr taken in small test tubes (10 mm outer diameter × 45 mm length, without annular rims). Varied known concentrations of SO_4^{2-} in the range 2.5–35.5, 25.5–165 and 55–1000 μg in a final 20 μL were poured into the pre-weighed KBr substrate with the help of micropipette tips. Then all the standard KBr-matrix was dried in an electric oven at 40 °C for 10 min. After drying KBr-matrix were thoroughly mixed. This dried standard was analyzed by the DRS-FTIR technique. The optimum conditions set for DRS-FTIR analysis of the samples are shown in Table 1.

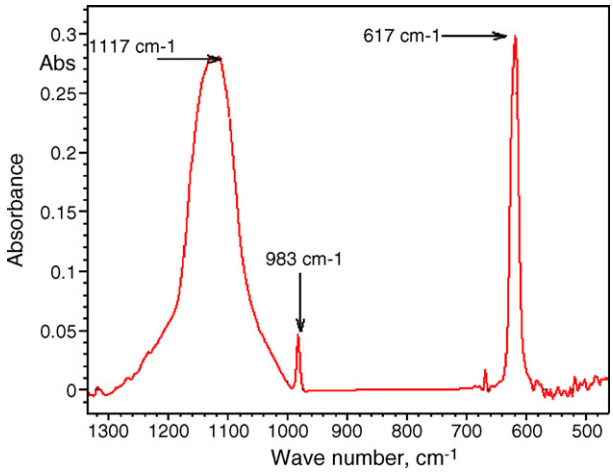

Fig. 1. Qualitative peak(s) at 1117, 983 and 617 cm^{-1} for sulphate, when used as K_2SO_4, obtained at a level 500 μg SO_4^{2-} spiked over 0.5 g KBr.

3. Results and discussion

3.1. Qualitative peak identification of sulphate

DRS-FTIR spectroscopy provides information about the presence of the sulphate without giving any information about mono atomic cations like Na^+ and K^+ associated to sulphate. However, no all the sulphates have the same bands and sometimes other bands are critical for the assignation of a cation. The FTIR spectra were interpreted following the characteristic IR absorption bands for sulphate functional groups as reported in the literatures [15,16]. All the characteristics IR absorption bands were checked by scanning spectra of standard samples of salt of associated cations, i.e. Na_2SO_4, K_2SO_4, $(NH_4)_2SO_4$ and $CaSO_4$ over the entire IR region, 4000–200 cm^{-1}. The present work quantitatively identifies the presence of SO_4^{2-} ion species by the study of spectra of their salt or compound. The smooth and horizontal baseline peaks were observed for sulphate when used as Na_2SO_4, K_2SO_4, and $(NH_4)_2SO_4$ at 617, 983 and 1117 cm^{-1} and when KBr substrate is used as background. However, $CaSO_4$ shows absorption at 660 and 597 cm^{-1} instead of 617 cm^{-1}. The IR peak at 983 cm^{-1} is found to be strongest among all observed peaks for sulphate but with relatively weaker intensity. Although peak observed at 1117 cm^{-1} is relatively stronger but broader than that observed at 617 cm^{-1}. Therefore, vibrational peak at 617 cm^{-1} has been utilized for quantitative analysis of SO_4^{2-}

Table 2
Infrared absorption bands for sulphate and different modes of vibration

Sulphate absorption peaks reported earlier [15,16] (cm^{-1})[a]	Characteristic absorption peaks found in the present work (cm^{-1})[a]	Modes of vibration
1120	1117 (strong and broad)	Asymmetric stretching (ν_3)
983	983 (weak and sharp)	Symmetric stretching (ν_1)
618	617 (strong and sharp)[b]	Bending vibrations (ν_4)
451	–	Bending vibrations (ν_2)

[a] Absorption peaks found for sulphate when used as K_2SO_4.
[b] IR absorption peak chosen for quantitative analysis.

for the simple reason of sharp and strong IR absorption, Fig. 1. Table 2 shows the FTIR absorption bands found in the present work for different modes of vibration of sulphate when used as potassium sulphate.

3.2. Quantitative analytical peak selection for determination of sulphate

The very sharp and suitable for quantification absorption band found at 617 cm^{-1} for the S–O bending vibration (ν_4) was chosen for the quantitative determination of sulphate in the pure compound and in the real samples, Fig. 1. The analyses have been done by calibration curve method. The calibration curve method uses the Lambert–Beer's law and executes the quantification of an unknown sample by acquiring a regression equation which represents the relationship between the peak intensity (peak height or area in the absorbance) of target ion and concentration from spectra of standard samples whose concentrations are already known.

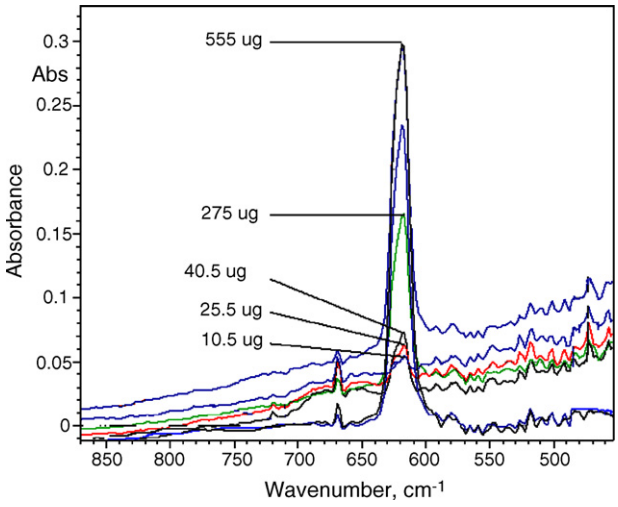

Fig. 2. Linear change in absorbance with increasing SO_4^{2-} concentration, 10.5–555 μg/0.5 g KBr, for DRS-FTIR analysis at the selected analytical peak, 617 cm^{-1}.

3.3. Calibration curves

The possibility of working with large analytical range of sulphate is the magnificence of the DRS-FTIR technique. Owing to the large variability in the sulphate concentration range in environmental samples of different nature, three different calibration curves were prepared. The ratio between the minimum and maximum sulphate concentration range which in the data were observed was 1:400. The corresponding absorbance data were obtained for full range of concentration at 617 cm^{-1} for large number of standard series with as little as 2.5 μg SO_4^{2-}/0.5 g KBr and as high as 1000 μg SO_4^{2-}/0.5 g KBr, Calibration curve no. 1 (CC no. 1). The data obtained was processed by the software Table Curve 2D v5.01.01. This absorbance versus concentration plot shows a straight line with excellent correlation coefficient value of 0.999. The intercept and the slope for this straight line were 0.05254 and 0.000410, respectively. Owing to the variation in concentration of sulphate in the order soil > dry deposition > aerosol, three different standard calibration curves in the ranges 2.5–35.5, 25.5–165 and 55–1000 μg SO_4^{2-}/0.5 g KBr were also prepared for low, moderate and high concentration (CC nos. 2–4). These all three calibration curves also show straight line. The straight line equation $y = a + bx$, where b = slope and a = intercept of the curve obtained for the above three calibration curves have correlation coefficient, slope and intercept values as 0.993, 0.997, 0.999, 0.000654, 0.000412, 0.000406, 0.046112, 0.054549, and 0.055548, respectively. The relative standard deviation ($n = 8$) for the sulphate concentration ranges, 2.5–35.5, 25.5–165, 55–1000 μg/0.5 g KBr were 2.4%, 2.1% and 1.5%, respectively. Fig. 2 shows the linear change in absorbance with increasing sulphate concentration at 617 cm^{-1} using KBr substrate for DRS-FTIR analysis.

The other statistical parameters such as d.f. Adj r^2, Fit Std Err and FStat as obtained for four sets of X–Y data using the software TableCurve 2D have been incorporated in Table 3. TableCurve 2D uses four common goodness of fit statistics. In the following descriptions, SSM is the sum of squares about the mean, SSE is the sum of squared errors (residuals), n is the total number of data values, and m is the number of coefficients in the model. d.f., the degree of freedom, is $n - m$. The details of the statistical terms used with equations are described as follows: coefficient of determination (CD, r-squared), $r^2 = 1 - \mathrm{SSE/SSM}$; degree of freedom adjusted coefficient of determination, $\mathrm{d.f.}r^2 = (1 - \mathrm{SSE}^*(n-1))/(\mathrm{SSM}^*(\mathrm{d.f.}-1))$; fit standard error (root mean square error), $\mathrm{Std\,Err} = \sqrt{\mathrm{SSE/d.f.}}$; F-statistic, $F\text{-stat} = ((\mathrm{SSM} - \mathrm{SSE})/(m-1))/(\mathrm{SSE/d.f.})$. As a fit

Table 3
Statistical data for the different calibration curves prepared for low, moderate and high sulphate concentrations

Calibration curve no.	Concentration range (μg) SO_4^{2}/0.5 g KBr	Statistical data[a] for the x–y plot (concentration vs. absorbance) for the straight line equation, $y = a + bx$							
		Intercept (a)	Slope (b)	Correlation coefficient (r)	CD r^2	d.f. Adj r^2	Fit Std Err	F-statistics	R.S.D. ($n = 8$)
1	2.5–1000	0.052549	0.000410	0.999	0.999	0.999	0.003687	19100.0	1.6
2	2.5–35.5	0.046112	0.000654	0.993	0.986	0.981	0.000976	441.2	2.4
3	25.5–165	0.054549	0.000412	0.997	0.994	0.992	0.001631	1069.2	2.1
4	55–1000	0.055548	0.000406	0.999	0.999	0.999	0.003419	12608.7	1.5

CD = coefficient of determination (r-squared), d.f. Adj r^2 = degree of freedom adjusted coefficient of determination, Fit Std Err = fit standard error (root M.S.E.), Fstat = F-statistic.

[a] Data processed by the software Table Curve 2D v5.01.01.

becomes more ideal, the r^2 values approach 1.0 (0 represent a complete lack of fit), the standard error decreases toward 0, and the F-statistic goes toward infinity. Thus, the data shown in Table 3 verifies the ideal calibration curves.

3.4. Effect of multi-atomic ionic units

The effect of presence of a large numbers of inorganic and organic multi-atomic anionic and cationic species i.e. the inter-ionic effect on the change in the position of spectral band and intensity for standard sulphate was observed. The inter-ionic effect of foreign species was tested at a level of 20 μg SO_4^{2-}/0.5 g KBr. To the test solution varied amount of the foreign species was introduced and the sample was then analyzed as in the procedure. The band position and spectral intensity due to sulphate remained intact even in the presence of atleast 280-fold molar excess of the following tested multi-atomic cationic and anionic species including NH_4^+, CN^-, OH^-, SCN^-, ClO_2^-, ClO_3^-, NO_3^-, ClO_4^-, BrO_3^-, IO_3^-, IO_4^-, HCO_3^-, MnO_4^-, CO_3^{2-}, SeO_3^{2-}, AsO_3^{2-}, MoO_4^{2}, FeO_4^{2-}, CrO_4^{2-}, $Cr_2O_7^{2-}$, SiO_4^{2-}, BO_3^{3-}, PO_4^{3-}, AsO_4^{3-}, formate, acetate, oxalate, succinate, cinnamate and citrate. Mono-atomic cations and anions like Na^+, K^+, Ca^{2+}, Mg^{2+}, Cl^-, Br^-, I^-, F^-, etc. have absolutely no diverse effect in the quantitative determination of sulphate since they do not posses dipole change, however there effect were observed only around 200 cm^{-1}.

3.5. Analysis of the rinses

Although the inter-ionic effect of diverse ions was tested up to an amount 280-fold molar excess with no adverse effect but to see the feasibility of minimizing the possible interference

Table 4
Analysis of sulphate by DRS-FTIR technique in aerosols, dry deposits and soil

Samples	Amount of SO_4^{2-} found					F-value[b] ($S.D._1^2/S.D._2^2$, $S.D._1 > S.D._2$)	t-Value[c] $\pm t = \bar{X}\mu(\sqrt{N}/s)$
	Present method (DRS-FTIR)			Standard method (IC)[a]			
	Concentration	Relative standard deviation ($n = 16$[d,e], 10[f])	DRS-FTIR/IC mean relative discrepancies[g]	Concentration	Relative standard deviation ($n = 4$)		
Aerosol[d]							
1	1.198 μg m^{-3}	5.01	−6.4	1.134 μg m^{-3}	5.38	1.034	0.043
2	3.120 μg m^{-3}	5.13	4.0	3.160 μg m^{-3}	5.06	1.000	0.114
3	2.790 μg m^{-3}	4.83	−8.0	2.710 μg m^{-3}	4.43	1.264	0.096
4	2.180 μg m^{-3}	5.76	2.0	2.200 μg m^{-3}	5.91	1.071	0.090
5	3.980 μg m^{-3}	3.77	4.0	4.020 μg m^{-3}	2.99	1.563	0.107
6	4.639 μg m^{-3}	4.10	5.1	4.690 μg m^{-3}	3.41	1.410	0.136
7	5.970 μg m^{-3}	4.36	−8.6	5.884 μg m^{-3}	2.72	2.641	0.186
8	5.780 μg m^{-3}	3.11	3.0	5.810 μg m^{-3}	3.10	1.000	0.129
Dry deposits[e]							
1	3.884 μg/m^2/d	7.75	4.1	3.843 μg/m^2/d	6.29	1.455	0.155
2	1.408 μg/m^2/d	6.69	-6.6	1.474 μg/m^2/d	4.61	2.041	0.215
3	3.093 μg/m^2/d	7.14	−3.3	3.126 μg/m^2/d	5.47	1.848	0.079
4	1.036 μg/m^2/d	5.98	−5.8	1.094 μg/m^2/d	3.70	2.697	0.145
5	2.845 μg/m^2/d	5.84	5.3	2.791 μg/m^2/d	7.98	1.830	0.122
6	2.633 μg/m^2/d	4.05	−2.8	2.661 μg/m^2/d	4.68	1.361	0.172
Soil[g]							
1	26.39 μg/g	1.48	5.6	26.44 μg/g	1.02	2.086	0.279
2	18.09 μg/g	3.04	3.7	18.13 μg/g	1.21	6.250	0.393
3	15.82 μg/g	2.47	6.9	15.89 μg/g	1.70	2.086	0.279
4	19.25 μg/g	1.66	−4.0	19.21 μg/g	2.55	2.345	0.229
5	14.33 μg/g	2.37	−3.0	14.30 μg/g	3.36	1.993	0.243
6	20.32 μg/g	2.95	5.0	20.37 μg/g	2.00	2.155	0.429
7	13.32 μg/g	3.52	6.0	13.38 μg/g	2.32	2.289	0.336
8	23.63 μg/g	2.07	−2.0	23.61 μg/g	0.93	4.961	0.351

[a] Standard ion chromatographic method.
[b] Tabulated F-values at 95% confidence level are as follows: for $N_1 = 10$, $N_2 = 4$ (or $\upsilon_1 = 9$, $\upsilon_2 = 3$), 8.81.
[c] Tabulated t-values at 95% confidence level are as follows: for $N_1 = 10$ (i.e., for $\upsilon_1 = N_1 - 1$, 9 degrees of freedom), 2.262.
[d] Amount of sulphate in aerosols determined using calibration curve no. 2; aerosol samples, 1–8, were collected at Raipur, India for a sampling period of 24 h on 21 March 2006 on different stages with the following particle size ranges (μ) viz.: 1 = 10–9; 2 = 9–5.8; 3 = 5.8–4.7; 4 = 4.7–3.3; 5 = 3.3–2.1; 6 = 2.1–1.1; 7 = 1.1–0.7; 8 = 0.7–0.4.
[e] Amount of sulphate in dry deposits determined using calibration curve no. 2; dry deposition samples, 1–6, were collected from six representative locations of Raipur for a period 1–31 December 2005.
[f] Amount of sulphate in soil determined using calibration curve no. 3; soil samples, 1–8, were collected from the vicinity of industrial areas surrounding the Raipur city, India.
[g] Error calculated with respect to the values obtained by the standard method.

of substantially high amount of diverse ions the separation of sulphate by extracting the solid samples in pure distilled water and the spectra of the extract and the residue both were scanned. The rinsing was performed using soil samples only due to ease of sample availability. Upon successive rinsing with a fixed volume of water (10–15 ml), on one hand the sulphate peak height at 617 cm^{-1} increased for the combined extract and on the other hand there were proportionate decrease in the peak height for the residue. This indicates the simple extraction procedure of sulphate. The tested real soil sample before rinsing gave absorption peak value 0.5672 at 617 cm^{-1}. After rinsing the sample thrice, all the peaks of the sulphate disappeared, except the quantitative peak 617 cm^{-1} which gave absorbance 0.0409. This quantitative peak disappeared completely when rinsing for five times. The same was observed with a single ultrasonication of the sample for 15 min. Thus, the analysis of the rinses may be an alternative method for the quantitative analysis as the inter-ionic effect in solids is rigorous than in liquids.

3.6. Apparent molar extinction coefficient, limit of detection (LOD) and limit of quantification (LOQ)

Following the fundamental concentration-absorbance relationship, $A = \varepsilon cl$, the apparent molar extinction coefficient for the analysis of sulphate using DRS-FTIR was calculated to be 4.506×10^5 G/mol/cm.

Limit of detection (LOD) and limit of quantification (LOQ), standard deviation, relative standard deviation and correlation coefficient (R), of the method were calculated for sulphate for the CC no. 2. The LOD of the method is calculated to be 0.20 μg/g SO_4^{2-}. The LOQ value is calculated to be 2.5 μg/g SO_4^{2-}. The standard deviation value and the relative standard value at a level of 20 μg SO_4^{2-}/0.5 g KBr for $n = 10$ is found to be 0.19 μg SO_4^{2-} and 1.9%, respectively.

3.7. Sulphate in aerosols, dust fall-out and soil samples

Aerosol samples precipitated over 81 mm circular stainless steel plates in all segregation levels were recovered by rubbing the plates using a 0.1 mm PVC foil. Then the recovered solid samples (∼15 mg) were taken directly in diffuse reflectance FTIR (DRS-FTIR) spectrometer and the spectra were scanned and absorbance values were measured at 617 cm^{-1} against KBr substrate as blank. The CC no. 2 was used to calculate the sulphate content in aerosols.

The dried soils, sampled and prepared as above, were taken directly with the help of spatula and the sample holder was filled completely. Amount of sample introduced for analysis was obtained by subtracting the pre and post weighed values of the sample holder before and after filling the samples. The samples were scanned and absorption was measured at 617 cm^{-1}. The calibration curve no. 3 was used to calculate sulphate content in the soil samples.

In a similar way, the sample absorption value was measured at 617 cm^{-1} for dry deposits collected and prepared as described above. The calibration curve no. 2 was used to calculate sulphate content in the dry deposit samples. Table 4 shows the results of all three kinds of samples analyzed by DRS-FTIR technique. The relative standard deviation for the sulphate concentration in real samples were found to be in the range, 3.11–5.76% ($n = 16$), 4.05–7.75% ($n = 16$) and 1.48–3.52% ($n = 10$) for aerosol, dry deposits and soil, respectively. The results were compared with ion-chromatographic method and were found to be in good agreement, Table 4. Fig. 3(a–c) shows DRS-FTIR spectra of some of the real samples scanned in the range about 800–500 cm^{-1} and analyzed viz. aerosol, dry deposition and soil samples.

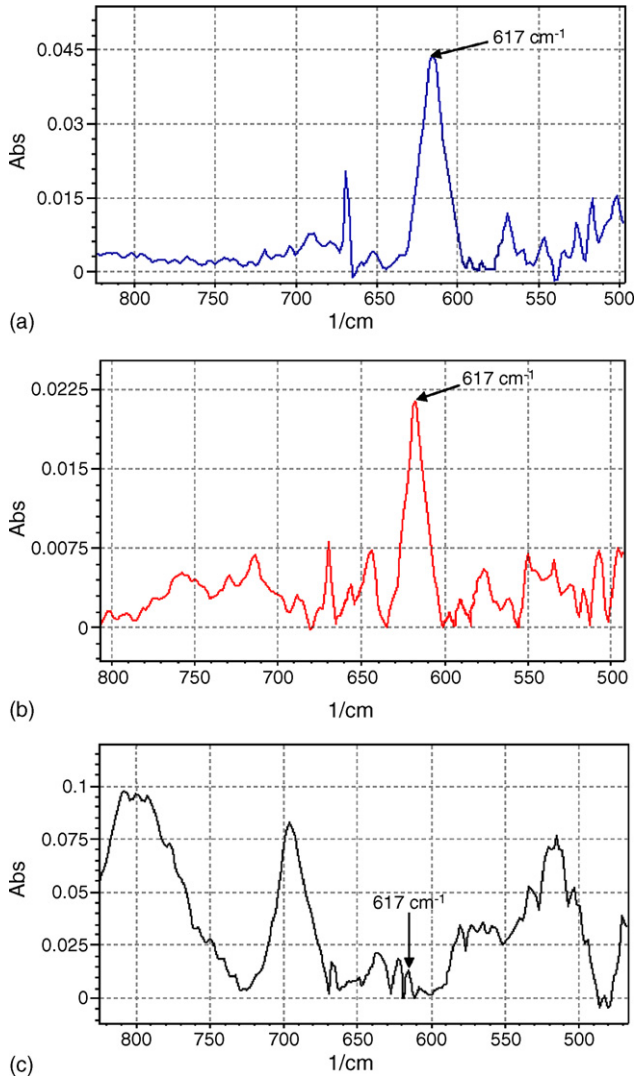

Fig. 3. (a–c) DRS-FTIR absorption spectrum of some real samples scanned using KBr substrate in the range 800–500 cm^{-1}; (a) aerosol sample collected at 0.7–0.4 μm size range on March 21, 2006 at Raipur city, India; (b) dry deposition sample collected during 1–31 December 2005 at Raipur; (c) soil sample collected from the vicinity of industrial area surrounding the Raipur city on December 23, 2005.

For all the tested real samples the two-point baseline corrections were performed between 650 and 550 cm^{-1} to obtain the quantitative absorption peak at around 617 cm^{-1} for sulphate.

3.8. Test of analytical quality assurance (AQA)

All the results were compared with the results obtained by the reference method statistically. It was shown that the difference between the results was insignificant

Different kinds of samples were analyzed for the sulphate by the proposed method for the purpose of AQA [17]. For samples with high concentration of sulphate 10 observations were made, whereas for samples with low concentration of sulphate 16 observations were made. A high correlation was observed between results obtained by the proposed method and the standard method.

The *F*-test was performed at 95% probability to compare the result of the present method with that of the standard method. Because in all cases the calculated values of F ($S.D._1^2/S.D._2^2$) were less than the tabulated F values at the 95% confidence level. The difference between the results of the present method and that of the standard method are not significant. The *t*-test was performed at 95% confidence level. Again in all the cases the calculated *t*-values were less than the tabulated values of *t*, indicating no statistical difference between the results obtained by the present method and the standard method.

3.9. Sample throughput

Once the sample is made ready for the analysis it hardly takes only few seconds or so for one analytical process. After the calibration curve is plotted, one sample could be analyzed within only 3–2 min for filling up of sample in sample holder, sample handling and cleaning, and 45 s for FTIR scanning of the sample in the range 200–4000 cm^{-1} for 45 scans. Thus, as much as 20 samples could be analyzed in an hour by using DRS-FTIR method. Time could be saved even more if the scan size and scan range is reduced. Diffuse reflectance-fourier transform infra red spectrometer (DRS-FTIR) is thus genuinely a time saving technique, additionally, being a non-destructive method; the analyzed samples could be preserved for further or advanced investigation.

4. Conclusions

The method described in this work is a simple and accurate analytical method for determining sulphate in environmental samples viz. aerosol, dry deposit and soil samples. This method eliminates the need for time consuming and costly sample pretreatment. The method has also high sample throughput value.

Quantitative analyses on the content of sulphate in aerosol, dry deposit and soil samples were performed using the non-destructive DRS-FTIR method. Analytical wavenumbers corresponding to the loading absorbance frequencies were established and the results were then calibrated with the loading concentrations as obtained from IC analyses of the same functional group. The DRS-FTIR/IC mean relative discrepancies for SO_4^{2-} in aerosol, dry deposit and soil samples are in the range 5.1% to −8.6%, 5.3% to −6.6% and 6.9% to −4.0%, respectively, indicating that the DRS-FTIR method developed in this work is a feasible method for quantitative analyses of nitrate in soil, dry deposit and aerosol samples.

Acknowledgements

The authors are grateful to Indian Space Research Organisation (ISRO), Bangalore, India for providing financial support under the RESPOND scheme (Grant-in-aid 287/10/2004). The authors are also thankful to the UGC, New Delhi for funding and Head, School of Studies in Chemistry, Pt. Ravishankar Shukla University, Raipur, India for providing laboratory facilities. At last, but not the least, the authors also express their heartfelt thanks to the anonymous reviewers for their valuable suggestions and guidance to upgrade the quality of our research work.

References

[1] L. Politi, R. Chiaraluce, V. Consalvi, N. Cerulli, R. Scandurra, Clin. Chim. Acta 184 (1989) 155.
[2] V.V. Egorov, V.A. Nazarov, E.B. Okaev, T.E. Pavlova, J. Anal. Chem. 61 (2006) 382.
[3] B. Butters, E.M. Chenery, Analyst 84 (1959) 239.
[4] J.W. O'Reilly, G.W. Dicinoski, M.J. Shaw, P.R. Haddad, Anal. Chim. Acta 432 (2001) 165.
[5] J.H. Poulsen, Scand. J. Clin. Lab. Invest. 43 (2) (1983) 157.
[6] R.A.S. Lapa, J.L.F.C. Lima, I.V.O.S. Pinto, J. Braz. Chem. Soc. 11 (2000) 333.
[7] S.M. Simkin, D.N. Lewis, K.C. Weathers, G.M. Lovett, K. Schwarz, Water, Air, Soil Pollut. 153 (2004) 343.
[8] A. Classen, W.D. Miersch, A. Hesse, J. Clin. Chem. Clin. Biochem. 28 (2) (1990) 91.
[9] J. Heland, K. Schafer, Atmos. Environ. 32 (1998) 3067.
[10] N.A. Saliba, H. Shaka, Atmos. Environ. 38 (2004) 523.
[11] H. Kouyoumdjian, N.A. Saliba, Atmos. Chem. Phys. Discuss. 5 (2005) 13053.
[12] C.C.K. Chou, S.H. Huang, T.K. Chen, C.Y. Lin, L.C. Wang, Atmos. Res. 75 (2005) 89.
[13] S.F. Mariaa, L.M. Russella, B.J. Turpinb, R.J. Porcjab, Atmos. Environ. 36 (2002) 5185.
[14] Y.I. Tsai, S.C. Kuo, Atmos. Environ. 40 (2006) 1781.
[15] R.A. Nyquist, R.O. Kagel, Infrared Spectra of Inorganic Compounds, Academic Press, New York, 1971.
[16] J.A. Gadsden, Inorganic Spectra of Minerals and Related Inorganic Compounds, Printed and bound by R.J. Acford Ltd., Industrial Estate, Chichester, Sussex, 1975.
[17] G.D. Christian, Analytical Chemistry, 5th ed, John Wiley and Sons, Inc., New York, 2001.

Available online at www.sciencedirect.com
ScienceDirect
Talanta 71 (2007) 1629–1636
Talanta
www.elsevier.com/locate/talanta

Comparison of different permanent chemical modifiers for lead determination in *Orujo* spirits by electrothermal atomic absorption spectrometry

M. Vilar, J. Barciela, S. García-Martín, R.M. Peña, C. Herrero *

Dpto Química Analítica, Nutrición y Bromatología, Facultad de Ciencias, Universidad de Santiago de Compostela, Augas Férreas s/n, Campus Universitario, 27002 Lugo, Spain

Received 25 May 2006; received in revised form 13 July 2006; accepted 24 July 2006
Available online 28 August 2006

Abstract

Different analytical methods for the determination of lead in *Orujo* spirits by electrothermal atomic absorption spectrometry (ETAAS) were developed using permanent modifiers (W, Ir, Ru, W-Ir and W-Ru) thermally deposited on platforms inserted in pyrolitic graphite tubes and Pd–$Mg(NO_3)_2$ conventional modifier mixture. In all cases, the Pb determination was performed without any sample pretreatment or preconcentration steps. The comparison between the chemical modifiers employed has been made in terms of pyrolysis and atomization temperatures, characteristic masses, detection limits, and atomization and background signal shapes. The limits of detection obtained were 0.375, 0.387, 0.109, 0.251 and 0.267 ng mL^{-1} for W, Ir, Ru, W–Ir and W–Ru, respectively and 0.710 ng mL^{-1} for Pd–$Mg(NO_3)_2$. The characteristic masses were 14.1, 11.2, 5.6, 8.3 and 9.3 pg for W, Ir, Ru, W–Ir and W–Ru, respectively and 22.2 pg for Pd–$Mg(NO_3)_2$. For all the developed procedures using the different modification systems, the relative standard deviations (<10%) and the analytical recoveries (95–103%) were acceptable. The more suitable methods for Pb determination in distillate spirits were those using permanent modifiers in contrast with classical Pd–$Mg(NO_3)_2$. The best analytical performance was achieved for W, Ir and W–Ir methods, which were applied to lead determination in *Orujo* spirit samples from Galicia (NW Spain). The Pb concentrations found in the analyzed samples were comprised in the range (<LOD to 1.5 μg mL^{-1}).

Keywords: *Orujo* spirits; Permanent chemical modifiers; Lead; Electrothermal atomic absorption spectrometry

1. Introduction

Galicia is a region located in North-West Spain with an important winegrowing tradition. *Orujo* is an alcoholic distillate from vinacce (skins, seeds and grape stalks) after alcoholic fermentation. *Orujo* spirits were traditionally considered an alcoholic beverage produced and consumed by common people; however, during the past few years, its productions and characteristics have been adapted to the quality demands of the market in order to assure authenticity.

Lead is a metal of public health interest because of several dangerous effects that it may cause to humans due to its toxicity after accumulation in multiple organs in the human body. Diet is the main source of Pb contamination for general public. Nowadays, there is a tendency to increase the beverage income, especially with regard to beers, wines, and soft drinks. Even though the lead quantity in these samples is low, its introduction in the daily diet may have significant physiological effects [1]. The presence of lead in alcoholic beverages mostly derives from copper alembics and lead welding repairs. This metal in alcoholic drinks might also proceed from fertilizers that are being used in phytosanitary treatments, from the equipment containers and utensils used for drink processing or storage, and lastly from massive industrial activity. Sometimes lead might also come from polluted water used for dilution of the distillates.

The determination of lead traces in alcoholic drinks requires the use of highly sensitive analytical techniques [2]. But only few ones have the required sensitivity to directly determine low quantities of this analyte: electrothermal atomic absorption spectrometry (ETAAS) [3–8], inductively coupled plasma mass spectrometry (ICP-MS) [9], flame atomic absorption and

* Corresponding author. Tel.: +34 982285900; fax: +34 982285872.
E-mail address: cherrero@lugo.usc.es (C. Herrero).

0039-9140/$ – see front matter © 2006 Elsevier B.V. All rights reserved.
doi:10.1016/j.talanta.2006.07.045

emission spectrometry (FAAS, FAES) [8,10,11] and anodic stripping voltametry (ASV) [12]. Other techniques such as reflection X-ray fluorescence (TXRF) [13], inductively coupled plasma-atomic emission spectrometry (ICP-AES) [14–19] and ultrasonic nebulization coupled to inductively coupled plasma optical emission spectrometry (UNS-ICP-OES) [20] are usually employed for multielemental beverages analysis. The application of stripping voltametry for lead determination in alcoholic drinks has been limited (particularly when this metal forms complex compounds that difficult a complete quantification), and TXRF has a high detection limit if it is compared to the ETAAS. In the techniques based in ICP (ICP-MS, ICP-AES or ICP-OES) the presence of ethanol in the samples can cause matrix interferences due to the deposition of coal in the sample introduction system, the uncertainty of the plasma and the increase of the sign for some elements. Furthermore, these techniques have a high purchase and maintenance costs, which limits its widespread use for routine analytical works. Flame atomic absorption and emission spectrometry have been broadly applied for the determination of most elements in different alcoholic drinks. But in the determination of trace metals, it is necessary to couple them with techniques of preconcentration and separation of the analyte due to their lack of sensibility. This fact causes an intense treatment of the sample, with the rising risk that this supposes. ETAAS is an attractive technique for the determination of metal traces in alcoholic beverages because it combines fast analysis time for alcoholic samples, relative simplicity, cheaper cost, and very low detection limits. All of these features have been responsible for its general use in the determination of trace amounts of heavy metals in alcoholic beverages such as *Orujo* spirits.

The aim of this study was to develop different analytical methods for the Pb determination in *Orujo* spirits by electrothermal atomic absorption spectrometry (ETAAS) using permanent modifiers, and to compare their analytical characteristics with those obtained with classical chemical modifier Pd–$Mg(NO_3)_2$. The use of a chemical modifier is required to allow Pb determination in real samples because it increases the analyte thermal stability [21] and decreases the matrix effects and the background signal. In previous studies, the use of Ir, Ru as well as carbide-forming elements, such as W and a mixture of both metals with W have been investigated for the determination of Pb in various samples [22–36]. In this work W, Ir, Ru, W–Ir and W–Ru were evaluated as permanent chemical modifiers for the stabilisation of Pb in *Orujo* spirits. For comparison purposes the universal modifier, the mixture of Pd–$Mg(NO_3)_2$ [37] was employed as a conventional chemical modifier.

Experimental design has been used to develop the ETAAS methods since its application offers a fast and appropriate tool to carry out the optimization of the different factors influencing the signal. Plackett–Burman design was applied as a screening method to evaluate the most significant factors with few experiments [38], and the optimum conditions for the significant parameters have been obtained using a central composite design developing with a two-level factorial and two central-points [39].

2. Experimental

2.1. Instrumentation

An atomic absorption spectrometer, Varian-SpectrAA-600 with Zeeman correction, equipped with a Varian GTA-100 electrothermal atomizer linked to an automatic sample dispenser was used for this work. Measurements were performed using a Varian hollow cathode lamp operating at 283.3 nm, with a current intensity of 5 mA. The bandwidth was 0.5 nm in all cases. Argon was employed as inert gas at 3 L min^{-1}, according to manufacturer recommendations [40]. Pyrolitic graphite-coated tubes with platform atomization were used.

2.2. Reagents

Stock standard solution of lead (10 g L^{-1}) was obtained from Panreac (Barcelona, Spain), and diluted as necessary to obtain working standard solutions. Palladium and magnesium nitrate were obtained from Fluka (Switzerland). Both working solutions were prepared by diluting the appropriate amount of a 10 g L^{-1} stock solutions with ultrapure water. The permanent modifier solutions of W, and Ir (1.0 g L^{-1}) were prepared from 179.4 mg $Na_2WO_4{\cdot}2H_2O$ powder (Sigma–Aldrich, Germany) dissolved in ultrapure water, and 62.7 mg $(NH_4)_3IrCl_6{\cdot}H_2O$ powder (Sigma–Aldrich, Germany) dissolved in 37% HCl solution and diluted to 25 mL with water. The permanent modifier solution of Ru (1.0 g L^{-1}) was purchased from Fluka (Switzerland). Nitric acid (65%, w/v) Suprapur reagent and Triton X-100 were obtained from Merck (Darmstadt, Germany). High-purity water was provided by a Milli-Q deionizing system (Millipore, Bedford, MA, USA).

All sampler containers, autosampler cups and other materials were washed with nitric acid (10%, v/v) for 24 h before rinsing with copious amount of ultrapure water and shaking dry prior to use. The cleaning solution employed to wash the sampling capillary contained HNO_3 (0.7, w/v) and Triton X-100 (0.2%, v/v).

2.3. Statistical software

Experimental design, surface and contour plots were carried out using Statgraphics 5.0 Plus software package.

2.4. Orujo samples

Thirty representative *Orujo* spirit samples from Galicia (NW Spain) were analysed, 25 of them were produced using traditional procedures in the producing region, the other five were commercial samples obtained from local stores. The identification code assigned to each sample includes information about CBO (Certified Brand of Origin "Specific Denomination of *Orujo* of Galicia") or non-CBO. The traditional elaboration method was coded as AQ for samples made with "Alquitara", S for samples made with still, U for unknown, C was used for commercial samples.

Table 1
Furnace heating programs using different modifiers

Step	Parameter	Modifier					
		Pd–Mg	W	Ru	Ir	W–Ru	W–Ir
Dry	Temperature (°C)	100	100	100	100	100	100
	Ramp (s)	15	14	17	6	3	16
	Hold (s)	10	9	6	30	25	19
Ash	Temperature (°C)	770	550	300	700	400	510
	Ramp (s)	22	1	5	7	10	5
	Hold (s)	19	24	14	15	5	25
Atomization	Temperature (°C)	1800	1570	1500	1950	1500	1890
	Ramp (s)	0	0	0	0	0	0
	Hold (s)	3	5	3	3	3	3
Clean	Temperature (°C)	2200	2200	2200	2200	2200	2200
	Ramp (s)	1	1	1	1	1	1
	Hold (s)	3	3	3	3	3	3
Cold	Temperature (°C)	40		40	40	40	40
	Ramp (s)	20		20	20	20	20
	Hold (s)	15		15	15	15	15

2.5. Analytical procedures

2.5.1. Palladium–magnesium nitrate method

Two-hundred and fifty microlitres of *Orujo* spirit were mixed in the autosampler cup and made up to 1000 μL with ultrapure water. An aliquot of 20 μL of this solution were introduced in the graphite tube together with 9 μL of Pd solution (2000 μg mL^{-1}) and 9 μL of $Mg(NO_3)_2$ solution (1200 μg mL^{-1}) and were subjected to ETAAS under the optimized conditions (see Table 1).

2.5.2. Permanent chemical modifiers method

Two-hundred and fifty microlitres of *Orujo* spirit were put into autosampler cup and made up to 1000 μL with ultrapure water. An aliquot of 20 μL of this solution were placed inside the graphite tube and subjected to ETAAS under the optimized conditions (see Table 1).

The treatment of the graphite tubes and the masses of permanent modifiers have been described in detail in previous studies [23]. In this work, the following quantities of permanent modifiers were used: 250 μg of W, 200 μg of Ru, 200 μg of Ir, 200 μg of Ru + 250 μg of W and 200 μg of Ir + 250 μg of W. The standard addition procedure was necessary in all cases.

3. Results and discussion

3.1. Optimization of ETAAS conditions

Experimental design was used to optimize all proposed methods. With the aim of establishing the statistically significant factors affecting the Pb signal, a Plackett–Burman fractional factorial design was applied as a screening approach in the case of palladium–magnesium nitrate method (nine factors optimized). For the permanent modifiers methods (six factors considered), a central composite design was performed to evaluate the response surfaces in order to establish the optimum conditions. Sometimes, univariate optimization procedure has been used with the purpose of obtaining additional useful information to carry out the optimization and in order to compare the stabilization effect of the different studied modifiers.

3.1.1. Pd–$Mg(NO_3)_2$ method optimization

In order to perform a preliminary factor screening, a Plackett–Burman design was carried out in a single block to study the effect of nine factors in 14 runs. Table 2 shows the factors evaluated and their high and low levels. Maximum and minimum levels were chosen according to our previous experience and taking into account the values reported in the literature. It was considered that an adequate strategy for a first screening involves working with a wide interval for the factors studied. The order of the experiments has been fully randomized to protect against the effect of uncontrolled variables. As it can be seen in the obtained Pareto plot represented in Fig. 1, atomization temperature (atom) has been the more significant factor. The effects of this factor, together with the concentrations of Pd and $Mg(NO_3)_2$, ash temperature and the ramp and hold ash have been studied by means of a central composite design 2^{6-1} + star with two central points (in 46 runs) with the purpose of obtaining the optimum value for these factors. Mineralization temperature was studied in the interval among 300 and 1200 °C. The Pb sig-

Table 2
Factors evaluated for Pd–$Mg(NO_3)_2$ modifier (high and low levels)

Factor	Code	Low	High
[Pd] (μg mL^{-1})	[Pd]	0	2000
[$Mg(NO_3)_2$] (μg mL^{-1})	[$Mg(NO_3)_2$]	0	2000
Dry temperature (°C)	Dry	70	200
Ash temperature (°C)	Ash	300	900
Atomization temperature (°C)	Atom	1100	2000
Dry ramp (s)	Dry ramp	1	10
Dry hold (s)	Dry hold	5	20
Ash ramp (s)	Ash ramp	1	10
Ash hold (s)	Ash hold	5	20

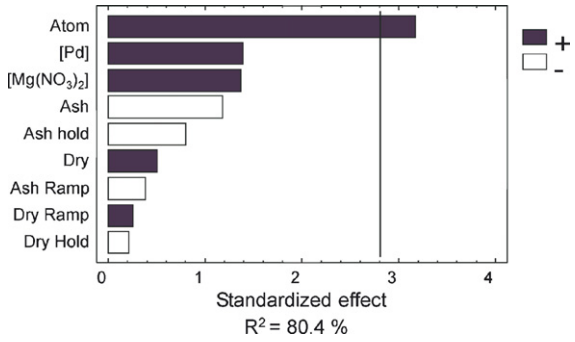

Fig. 1. Standardized Pareto chart. Pd–$Mg(NO_3)_2$ modifier.

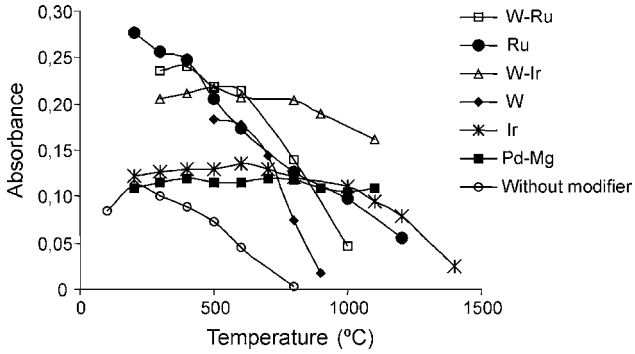

Fig. 3. Pyrolisis temperature curves for *Orujo* spirit dissolution (25%, v/v) with or without modifier.

nal fell slightly with the increase of ash temperature, but when temperature was higher than 770 °C, the signal fell abruptly. The studied atomization temperature was ranged between 1100 and 2000 °C (Table 2). A low value has been used, to be able to observe the effect of this variable clearly. For the atomization temperature, it was observed that the signal increase is significant up to optimum value of 1980 °C, while for higher atomization temperature the response signal remains constant. These ash and atomization temperatures are slightly lower than those reported in the bibliography for other samples (biological materials, sediments and soil samples) [41,25]. However, they allowed the removal of the volatile matrix during the ash stage and the complete atomization of lead. The effect of magnesium and palladium concentration in lead signal is slight. The Pb signal increases with the concentration of the two modifiers until reaching the optimum, and after diminished, being the optimum concentrations 2000 mg L^{-1} for palladium and 1200 mg L^{-1} for magnesium nitrate. In order to study the ramps and hold times, a response surface was obtained using the previous design. As it can be seen in Fig. 2, high times of ash hold and ramp are necessary to assure the complete removal of the *Orujo* matrix before atomization. Atomization ramp time was short, because it is advisable to rapidly heat the furnace up to the selected optimum temperature so that a difference between tube and platform can be achieved. The optimum furnace operation conditions for this method are given in Table 1. Values of dry temperature, dry

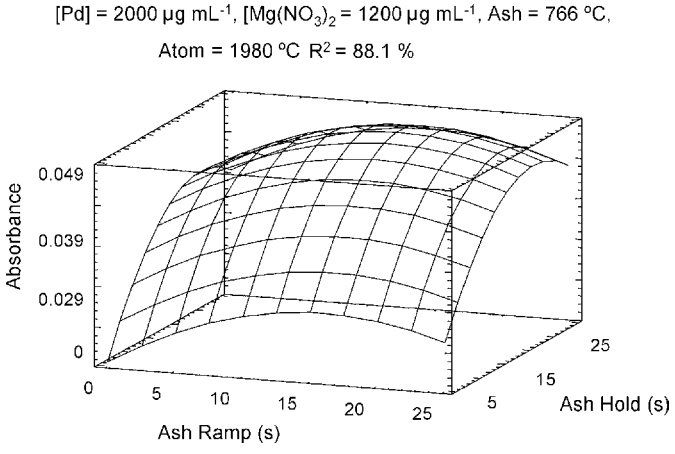

Fig. 2. Effect of ash ramp and hold on the Pb area response using Pd–$Mg(NO_3)_2$ as chemical modifier.

hold and ramp were chosen according to the values obtained with the Pareto plot and they were verified later.

An univariate study for mineralization and atomization temperatures has been carried out as the last stage of optimization with the purpose of choosing the optimum conditions according to the peak shape and sensitivity. Also, a comparison between the stabilization effect of all modifiers was carried out. In both cases, the same results were obtained using an univariate study and the central composite design when palladium was used as modifier. In Fig. 3, the ash temperature effect in the analytical signal is presented for all modifiers studied.

3.1.2. *Permanent chemical modifiers method optimization*

In this case, Plackett–Burman design has not been used to perform the optimization since dry temperature as well as modifier concentration have not been considered in the experimental design. Modifier mass has been used according to the literature, since the modifier mass has been sufficiently studied previously [3,22,23,41]. A dry temperature of 100 °C, was chosen according to the previous work with palladium and magnesium nitrate modifier because it was not a factor with significant influence. These data were verified carrying out several experiments with a wide interval of dry temperatures (70–110 °C), before and after the optimization with the experimental design.

The six remaining factors (ash and atomization temperature, dry ramp and hold, and ash ramp and hold) were studied and optimized by means of a central composite 2^{6-1} + star with two central points design (in 46 runs) for the different permanent modifiers (W, Ru, Ir, W–Ru and W–Ir) thermally deposited on the integrated platform. Table 3 shows the factors evaluated and their high and low levels. Again maximum and minimum levels

Table 3
Factors evaluated for permanent chemical modifiers method (high and low levels)

Factor	Code	Low	High
Ash temperature (°C)	Ash	400	900
Atomization temperature (°C)	Atom	1000	2000
Dry ramp (s)	Dry ramp	5	25
Dry hold (s)	Dry hold	5	30
Ash ramp (s)	Ash ramp	5	25
Ash hold (s)	Ash hold	5	25

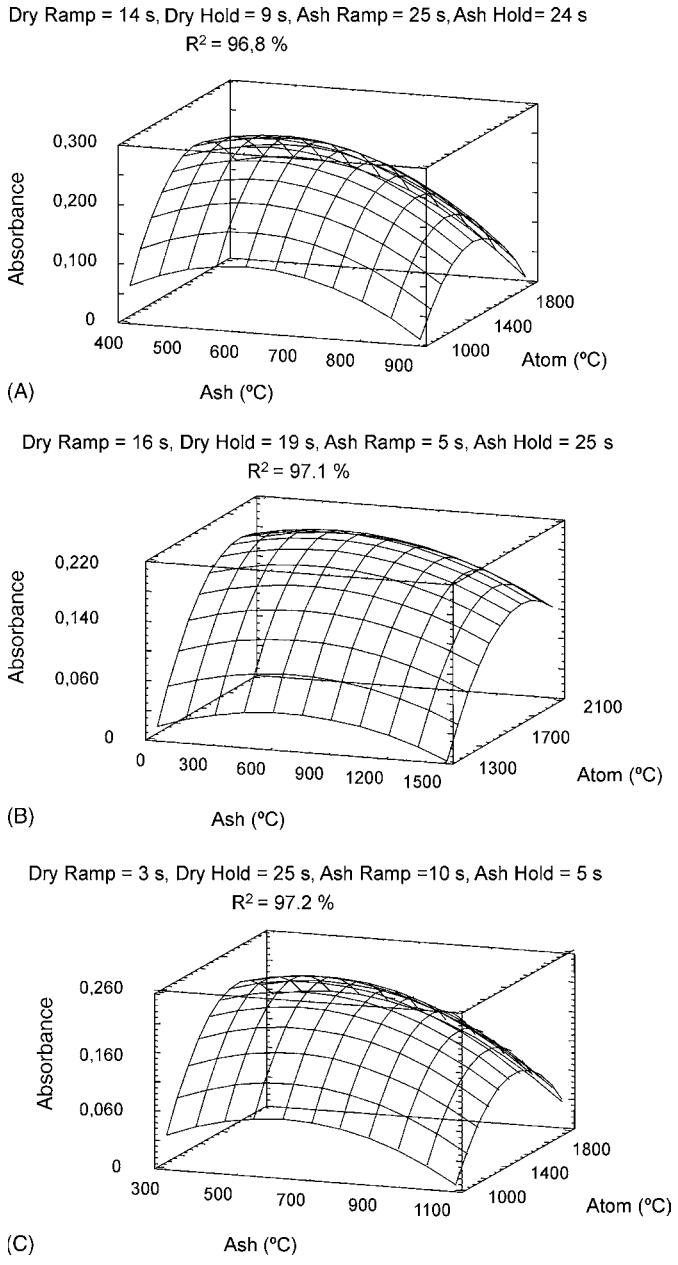

Fig. 4. Effect of ash and atomization temperature on the Pb area response using W (A), W–Ru (B), and W–Ir (C) as permanent chemical modifier.

were chosen according to our previous experience and taking into account the values reported in the literature. In Fig. 4, the obtained response surfaces for ash and atomization temperatures are presented. As can be seen, the area signal increased slightly up to maximum value when ash temperature was increased, higher ash temperatures produced a decrease of the response signal when W, W + Ru and W + Ir are used. Ash temperatures chosen as optimums for these modifiers were 550, 400 and 510 °C, respectively (see Fig. 4). It was also observed that the sensibility improved with the increase in the atomization temperature until reaching the ideal value while higher atomization temperatures produced a signal decrease. The optimum values of atomization temperatures for W, W + Ru and W + Ir were 1570, 1500 and 1890 °C, respectively. However, using experimental designs it was observed that when Ir and Ru were used as modifiers, the signal decayed for higher ash temperatures: 400 and 310 °C, respectively. Thus, these values were chosen as optimum. The optimum atomization temperatures for these permanent modifiers were 1950 °C for Ir and 1500 °C for Ru.

Also the hold and ramp times for the different steps in furnace heating program were studied using the developed experimental design. Low ash ramp times, next to 5 s, leaded to the maximum integrated absorbance signal. A long time periods in hold ash step were required in order to assure the total destruction of alcoholic matrix. Times comprised between 15 and 25 s were used, except in the case of the W–Ru in which 5 s in the ash step was sufficient.

An univariate study of mineralization and atomization temperatures was carried out in order to choose the optimum conditions compromise among peak shape and sensitivity (see Fig. 3). The obtained optimum for Ir determined by experimental design was different to the obtained with this univariate study. In this case, when all the variables remain constant, using the optimum conditions obtained in the previous study, and when ash temperature was modified, the area stayed constant up to 700 °C. In addition, ash temperature influences the peak shapes and when low ash temperatures were used, the peaks showed shoulders on its left faces indicating that there were two kind of compounds in the atomization process. Furthermore, using an ash temperature of 700 °C (univariate optimum), the signal difference compared to the one obtained operating under the optimum conditions established in the experimental design, was lower than 10%, value. Taking into account the previous data, ash temperature of 700 °C was considered as the optimum value. For the univariate study in the case of the Ru, the mineralization temperature achieved a similar value that the one obtained by experimental design. For the other modifiers, univariate values were comparable to those obtained previously, and the peak shape was always well defined. On the other hand, when the Pb stabilization is studied in an alcoholic matrix without modifier (Fig. 3), it was observed that the lead lost for ash temperatures lower than 200 °C. This temperature is similar to the one obtained when Ru or W–Ru were used as permanent modifiers. Therefore, these modifiers do not stabilize the analyte in this type of samples, and Ru and W–Ru were not appropriate for the determination of this metal in alcoholic matrix. The established optimum furnace operation conditions for the studied methods are summarized in Table 1.

3.2. Analytical characteristics

3.2.1. Calibration

Instrumental calibration was performed at different ranges for the permanent chemical modifier methods (0.0–7.5 ng mL^{-1} for Ir, and W–Ir; 0.0–15 ng mL^{-1} for W) in water solution and in the *Orujo* matrix. These intervals have been selected according to the concentrations found in the *Orujo* samples, in spite of calibration range has been demonstrated to be linear up to 80 ng mL^{-1} [28,29,35]. Table 4 shows the equations obtained for calibration and standard addition graphs. The comparison of

Table 4
Calibration and standard addition equations obtained for the four modifiers employed

Modifier	Calibration	Addition
W	$A = 3.9 \times 10^{-3}$ [Pb] + 8.4×10^{-3}	$A = 4.8 \times 10^{-3}$ [Pb] + 2.0×10^{-2}
Ir	$A = 4.2 \times 10^{-3}$ [Pb] + 1.8×10^{-3}	$A = 5.5 \times 10^{-3}$ [Pb] + 1.0×10^{-2}
W–Ir	$A = 5.5 \times 10^{-3}$ [Pb] + 0.3×10^{-3}	$A = 7.3 \times 10^{-3}$ [Pb] + 1.4×10^{-2}
Pd–$Mg(NO_3)_2$	$A = 1.8 \times 10^{-3}$[Pb] + 1.6×10^{-3}	$A = 3.0 \times 10^{-3}$ [Pb] + 1.1×10^{-2}

calibration and standard addition graph slopes for all permanent modifiers was indicative of a slight but significant matrix effect. For this reason, and in order to obtain accurate results, the samples were analysed in the standard addition mode when these matrix modifiers were used.

3.2.2. Detection limits

Detection limits (LOD) were calculated on the basis of 3S.D./*m*, where *m* is the slope of the addition graph and S.D. the standard deviation of 10 consecutive measurements of blank solutions. Quantification limit (LOQ) were calculated as 10S.D./*m*. The results obtained for LOD, LOQ, and characteristic masses (based on the integrated absorbance) are given in Table 5. In different ETAAS methods for Pb determination in sugar cane spirit [4] (without chemical modification) the LOD reported (0.6 ng mL^{-1}) was worse than the obtained in the present work with permanent chemical modifiers. Also, Pereira et al. [24] obtained a poorer LOD (3.6 ng mL^{-1}) for lead determination in marine sediment slurry samples using Zr, Ir, Ru and Rh as permanent modifiers. As can be seen in Table 4, the best detection limit was obtained for W–Ir in comparison with the rest of permanent modifiers. Nevertheless, the limits obtained for the other permanent chemical modifiers are not very different from that achieved with W–Ir, but this is very low in comparison with the value obtained for Pd–Mg. The methods with permanent chemical modifiers reached adequate sensibility to detect the studied metal at the levels present in *Orujo* spirit samples.

3.2.3. Precision

The within-run precision was studied using *Orujo* solutions spiked with lead (0.0, 5.0, 10.0 and 15.0 ng mL^{-1} using W and Pd–$Mg(NO_3)_2$ as modifiers; and 0.0, 2.5, 5.0 and 7.5 ng mL^{-1} with the rest of permanent modifiers used). The relative standard deviation for 10 determinations of each solution was below 10% for all modifiers. The coefficients of variation for the four concentration levels assayed by the different modifiers are showed in Table 5. In all cases, an acceptable precision was obtained. The repeatability of analytical signal obtained is similar for all the modifiers studied.

3.2.4. Accuracy

No *Orujo* spirits reference material with certified Pb concentration is currently available. Thus, the accuracy of the proposed methods was measured by evaluating the recovery on a real sample spiked with 0.0, 5.0, 10.0 and 15.0 ng mL^{-1} of Pb using W and Pd–$Mg(NO_3)_2$ as modifier; and spiked with 0.0, 2.5, 5.0 and 7.5 ng mL^{-1} of Pb when the rest of permanent modifiers were studied. The recoveries achieved were 97.7% for tungsten, 103.0% for iridium, 102.7% for tungsten–iridium and 98.0% for Pd–$Mg(NO_3)_2$. The results showed an acceptable accuracy for the proposed modifiers.

3.3. Application

The applicability of the developed methods for Pb determination at the levels present in alcoholic distillate spirits was demonstrated. Nine replicates of *Orujo* samples from Galicia were analysed using the three proposed permanent modifiers methods and Pd–$Mg(NO_3)_2$ method. The *t*-test for mean comparison and the *F*-test for variance comparison showed no significant differences among the developed methods at a 95% confidence level. The results provided by the different studied modifiers were comparable.

It is important to accurately know the concentration of Pb in *Orujo* spirit since it allows to evaluate the quality of the product. Lead determination was carried out for 30 representative *Orujo* spirit samples from Galicia (NW Spain). The determination was carried out using the W–Ir as chemical modifier, since this developed method presented the best detection limit and characteristic mass. Lead was found in the analysed samples at concentrations between <LOD and 1.5 μg mL^{-1} (see Table 6). The widespread range can be explained taking into account the diverse origin of the samples. Although it is necessary to point out that 60% of the studied samples had smaller concentrations than 20 ng mL^{-1} and that only one sample (non-CBOQ-AQ-11-HM) presented a concentration of Pb higher than 1 μg mL^{-1} (that is the upper limit for Pb level established for the Directive Council of Certified Brand of Origin Specific Denomination [42] *Orujo* from Galicia). This high value may be due to the use of

Table 5
Analytical parameters for Pb determination by the four proposed methods

Modifier	m_0 (pg)	LOD (ng mL^{-1})	LOQ (ng mL^{-1})	R.S.D.[a] (%)
W	14.1	0.375	1.25	4.5; 2.5; 1.6; 4.1
Ir	11.2	0.387	1.29	8.4; 7.0; 4.7; 4.1
W–Ir	8.3	0.251	0.84	5.8; 7.7; 6.3; 6.3
Pd–$Mg(NO_3)_2$	22.2	0.710	2.36	8.8; 4.8; 9.8; 5.4

[a] At the four concentration levels assayed (see text).

Table 6
Pb concentrations in the *Orujo* spirit samples from Galicia

Sample code[a]	[Pb] ± S.D. (ng mL^{-1})
Non-CBO-AQ-1-HM	6.92 ± 0.35
Non-CBO-AQ-2-HM	7.04 ± 0.18
Non-CBO-AQ-3-HM	<LOD
Non-CBO-AQ-4-HM	298 ± 11
Non-CBO-AQ-5-HM	19.3 ± 3.7
Non-CBO-AQ-6-HM	130 ± 6
Non-CBO-AQ-7-HM	199 ± 3
Non-CBO-AQ-8-HM	32.5 ± 1.6
Non-CBO-AQ-9-HM	41.9 ± 1.1
Non-CBO-AQ-10-HM	12.3 ± 1.2
Non-CBO-S-11-HM	1494 ± 34
Non-CBO-S-12-HM	54.8 ± 7.3
Non-CBO-S-13-HM	5.79 ± 0.18
Non-CBO-S-14-HM	0.67 ± 0.01
Non-CBO-S-15-HM	11.7 ± 0.1
Non-CBO-S-16-HM	1.17 ± 0.02
Non-CBO-S-17-HM	9.04 ± 0.18
Non-CBO-S-18-HM	0.42 ± 0.00
Non-CBO-S-19-HM	0.42 ± 0.00
Non-CBO-S-20-HM	15.7 ± 1.4
Non-CBO-S-21-HM	0.42 ± 0.00
Non-CBO-S-22-HM	<LOD
Non-CBO-S-23-HM	283 ± 16
Non-CBO-S-24-HM	<LOD
Non-CBO-S-25-HM	16.7 ± 1.8
Non-CBO-U-26-C	0.42 ± 0.00
Non-CBO-U-27-C	11.0 ± 0.18
Non-CBO-U-28-C	0.42 ± 0.00
Non-CBO-U-29-C	7.54 ± 0.53
CBO-U-30-C	<LOD

CBO: with Galician certified brand of origin; AQ: Alquitara; S: still; U: unknown; HM: homemade; C: commercial.
[a] Non-CBO: without Galician certified brand of origin.

an inadequate distillation recipient. Lead content in commercial *Orujo* samples was always very low (lower than 20 ng mL^{-1}).

The obtained Pb concentration range is higher than those published by other authors on other distillate products. For example, for traditional Greek fruit distillate "Mouro" [8] the concentration of lead obtained is between 8.1 and 399.0 ng mL^{-1}, for "Koumaro" (0.0–56.5 ng mL^{-1}). For Brazilian spirit samples, Nascimento et al. [7] reported concentrations between 36 and 92 ng mL^{-1} and for Spanish brandy Camean et al. [43], found values up to 224 ng mL^{-1}.

4. Conclusion

In the present work, various ETAAS methods for direct determination of lead in *Orujo* spirits samples without any sample pre-treatment or pre-concentration steps were developed using palladium-magnesium nitrate and permanent chemical modifiers (such as W, Ir, Ru, W–Ir and W–Ru). The permanent chemical modifier methods were the procedures selected for further direct Pb determinations in O*rujo* samples, since permanent modifier methods presented better analytical characteristics than Pd–Mg modifier method. It was also observed than the Pb determination methods based on Ru or W–Ru modifiers were not suitable for lead determination in alcoholic matrix, because they do not achieve an appropriate metal stabilization in this matrix. In all cases, the use of standard addition for the determination was necessary. Any of the other proposed permanent modifiers (W, Ir and W–Ir) allows lead determination in the majority of the samples, although W–Ir presents the better detection limit and characteristic mass. The W-Ir method has been applied to the determination of Pb content in 30 *Orujo* samples from Galicia (NW Spain), with comparable results between samples from different areas. Only one sample had a concentration of lead higher than the limit of 1 μg mL^{-1} that is considered as the maximum allowed by the established legislation for the Specific Denomination [42] of *Orujo* from Galicia.

References

[1] C. Cabrera, J. Anal. Atom Spectrom. 9 (1994) 1423.
[2] C. Mena, C. Cabrera, M. Lorenzo, C. López, J. Agric. Food Chem. 45 (1997) 1812.
[3] E.C. Lima, F. Barbosa Jr., F.J. Krug, J. Anal. Atom Spectrom. 14 (1999) 1913.
[4] H. Canuto, G.L. Siebald, M.B. Franco, J.B.B. da Silva, Atom Spectrosc. 25 (2004) 140.
[5] E.H. Soufleros, S. Ageliki, P. Miydalia, Food Chem. 86 (2004) 625.
[6] J. Kristl, M. Veber, M. Slekovec, Anal. Bioanal. Chem. 373 (2002) 200.
[7] R.F. Nascimento, C.W.B. Bezerra, S.M.B. Furuya, M.S. Schultz, L.R. Polastro, B.S. Lima, D.W. Franco, J. Food Comp. Anal. 12 (1999) 17.
[8] E.H. Soufleros, S.A. Mygdalia, P. Natskoulis, J. Food Comp. Anal. 18 (2005) 699.
[9] I. Rodushkin, F. Ódman, P.K. Appelblad, J. Food Comp. Anal. 12 (1999) 243.
[10] E.A. Hernández-Carballo, R.M. Avila-Gómez, N. Capote, F. Rivas, A.G. Pérez, Talanta 60 (2003) 1259.
[11] Y. Petit, B. Paredes, W. Rondón, M. Burguera, J.L. Burguera, C. Rondón, P. Carrero, T. Capote, Talanta 64 (2004) 1351.
[12] A.M. Green, A.C. Clark, G.R. Scollary, Fresen. J. Anal. Chem. 358 (1997) 711.
[13] S. Galani-Nikolakaki, N.S. Kallithrakas-Kontos, A.A. Katsanos, Sci. Total Environ. 285 (2002) 155.
[14] M. Aceto, O. Abollino, M.C. Bruzzoniti, E. Mentasti, C. Sarzanini, M. Malandrina, Food Addit. Contam. 19 (2002) 126.
[15] A. Alcázar, F. Pablos, M.J. Martín, A.G. González, Talanta 57 (2002) 45.
[16] R. Kokkinofta, P.V. Petrakis, T. Masuromoustakos, C.R. Theocharis, J. Agric. Food Chem. 51 (2003) 6233.
[17] G. Thiel, K. Danzer, Fresen. J. Anal. Chem. 357 (1997) 553.
[18] D.R. Cardoso, L.G. Andrad-Sobrinho, A.F. Leite-Neto, R.V. Reche, W.D. Isique, M.M.C. Ferreira, B.S. Lima-Neto, D.W. Franco, J. Agric. Food Chem. 52 (2004) 3429.
[19] R.A. Sousa, N. Baccan, S. Cadore, J. Braz. Chem. Soc. 16 (2005) 540.
[20] R. Lara, S. Cerutti, J.A. Sajonia, R.A. Olsina, L.D. Martínez, Food Chem. Toxicol. 43 (2005) 293.
[21] I.L. García, M.S. Sánchez, M.H. Córdoba, J. Anal. Atom Spectrom. 11 (1996) 1003.
[22] E.C. Lima, R.V. Barbosa, J.L. Brasil, A.H.D.P. Santos, J. Anal. Atom Spectrom. 17 (2002) 1523.
[23] E.C. Lima, J.L. Brasil, A.H.D.P. Santos, Anal. Chim. Acta 484 (2003) 233.
[24] L.A. Pereira, I. Amorim, J.B.B. da Silva, Talanta 68 (2006) 771.
[25] O. Acar, Anal. Chim. Acta 542 (2005) 280.
[26] J.B.B. da Silva, M.A.M. da Silva, A.J. Curtius, B. Welz, J. Anal. Atom Spectrom. 14 (1999) 1737.
[27] E. Vassileva, H. Baeten, M. Hoening, Fresen. J. Anal. Chem. 369 (2001) 491.
[28] O. Acar, J. Anal. Atom Spectrom. 19 (2004) 709.
[29] O. Acar, Anal. Chim. Acta 526 (2004) 103.
[30] C.J. Rademeyer, B. Radziuk, N. Romanova, Y. Thomassen, P. Tittarelli, J. Anal. Atom Spectrom. 12 (1997) 81.

[31] L.A. Pereira, I.G. Amorin, J.B.B. da Silva, Talanta 64 (2004) 395.
[32] C.J. Rademeyer, B. Radziuk, N. Romanova, N.P. Skaugset, A. Skogstad, Y. Thomassen, J. Anal. Atom Spectrom. 10 (1995) 739.
[33] O. Acar, A.R. Türker, Z. Kiliç, Spectrochim. Acta Part B 55 (2000) 1635.
[34] L. Jorhem, J. AOAC Int. 83 (2000) 1204.
[35] O. Acar, Z. Kiliç, A.R. Türker, Food Chem. 71 (2000) 117.
[36] Z. Kiliç, E. Kendüzler, O. Acar, Food Chem. 77 (2002) 85.
[37] P.B. Barrera, C.B. Alonso, A.B. Barrera, Mikrochim. Acta 124 (1996) 251.
[38] E. Morgan, Chemometrics: Experimental Design, John Wiley and Sons, London, 1991.
[39] D.L Massart, B.G. Vandeginste, L.M. Buydens, S. De Jong, P.J Lewi, J. Smeyers-Verkebe, Handbook of Chemometrics and Qualimetrics: Part A, Elsevier Science B.V., Amsterdam, 1998, pp. 711–716.
[40] Analytical Methods for Graphite tube atomizers, Varian Australia Pty Ltd., Australia, 1988.
[41] E.C. Lima, F. Barbosa, F.J. Drug, Fresen. J. Anal. Chem. 369 (2001) 496.
[42] Boletín Oficial del Estado (BOE) 194, ORDEN APA/2668/2005.
[43] A.M. Camean, I. Moreno, M. López, M.A. Repetto, A.G. González, Talanta 54 (2001) 53.

Available online at www.sciencedirect.com
ScienceDirect
Talanta 71 (2007) 1762–1768
Talanta
www.elsevier.com/locate/talanta

On-line organoselenium interference removal for inorganic selenium species by flow injection coprecipitation preconcentration coupled with hydride generation atomic fluorescence spectrometry

Hong Wu [a,b], Yan Jin [a], Yanqing Shi [a], Shuping Bi [a,*]

[a] *School of Chemistry and Chemical Engineering, State Key Laboratory of Coordination Chemistry & Key Laboratory of MOE for Life Science, Nanjing University, Nanjing 210093, PR China*

[b] *Department of Chemistry, Xuzhou Normal University, Xuzhou 221116, PR China*

Received 30 April 2006; received in revised form 4 August 2006; accepted 10 August 2006
Available online 15 September 2006

Abstract

The existence of dimethylselenium (DMSe) and dimethyldiselenium (DMDSe) in some environmental samples can cause serious interference on Se(IV) determination by hydride generation atomic fluorescence spectrometry (HG-AFS) due to their contribution on HG-response. A flow injection separation and preconcentration system coupled to HG-AFS was therefore developed by on-line coprecipitation in a knotted reactor (KR) for eliminating interference subjected from organoselenium. The sample, spiked with lanthanum nitrate, was merged with an ammonium buffer solution (pH 8.8), which promoted coprecipitation of Se(IV) and quantitative collection by 150 cm PTFE KR. DMSe and DMDSe, however, were unretained and expelled from the KR. An air flow was introduced to remove the residual solution from the KR, then a 1.2 mol l^{-1} HCl was pumped to dissolve the precipitates and merge with KBH_4 solution for HG-AFS detection. The interference of DMSe and DMDSe on the Se(IV) determination by conventional HG-AFS and its elimination by the developed separation and preconcentration system were evaluated. With optimal experimental conditions and with a sample consumption of 12.0 ml, an enhancement factor of 18 was obtained at a sample frequency of 24 h^{-1}. The limit of detection was 0.014 μg l^{-1} and the precision (R.S.D.) for 11 replicate measurements of 1.0 μg l^{-1} Se(IV) was 2.5%. The developed method was successfully applied to the determination of inorganic selenium species in a variety of natural water samples.

Keywords: Flow injection; Hydrider generation atomic fluorescence spectrometry; Selenium; Speciation; Knotted reactor; Coprecipitation

1. Introduction

Selenium is receiving special attention in recent years due to its dual role, as an essential nutrient at low concentrations or a highly toxic compound when in excess [1,2]. Its biogeochemical behavior, nutrition bioavailability and toxicity are largely dependent on its chemical species [3]. Inorganic species of selenium are more toxic than the organic forms [4]. In natural water samples inorganic species such as Se(VI) and Se(IV) are the most environmentally mobile and biogeochemically important oxidation states of selenium [5]. Methylation is an effective detoxification mechanism, and methylated forms, such as dimethylselenium (DMSe) and dimethyldiselenium (DMDSe), are formed during biomethylation processes by microorganisms in the aquatic environment [6]. Therefore, it is particularly imperative to develop rapid, sensitive and reliable analytical methods for better understanding of the biogeochemical cycle, mobility and toxicity of this element.

Hydride generation atomic absorption spectrometry (HG-AAS) [7–10] or hydride generation atomic fluorescence spectrometry (HG-AFS) [11–17] is one of the most effective techniques for trace selenium analysis. Inorganic Se species can be distinguished by direct determining Se(IV) and total Se after reduction of Se(VI) by 4–7 mol l^{-1} HCl at higher temperature [8–10], photoreduction [18], bromide in lower acidic medium [11,15] or microwave irradiation [13,14], from which Se(VI) being calculated by the difference. Therefore, accurate measurement of Se(IV) is the most important step in the Se speciation scheme based on HG-AAS or HG-AFS. Some attempts have been made to eliminate organic and inorganic interfer-

* Corresponding author. Tel.: +86 25 83594255; fax: +86 25 83317761.
E-mail address: bisp@nju.edu.cn (S.P. Bi).

0039-9140/$ – see front matter © 2006 Elsevier B.V. All rights reserved.
doi:10.1016/j.talanta.2006.08.011

ences on Se(IV) quantification. XAD resins have been used to remove interferences of organic matter (mostly humic substances) [19,20], although the fractional loss of Se(IV) may be caused due to its complexation with humic substances when an acidified sample was passed through the resin column [9,21,22]. The use of complexing agents [5,23,24] or Dowex 50W-X8 resin [25] has been reported to improve tolerance towards metal interferences. The interference of nitrite in the natural water and residual volatile nitrogen oxide in the sample matrix after acid digestion could be eliminated with addition of sulfanilamide [26] and sulfamic acid [27], respectively. Furthermore, the recent investigations proved the organoselenium compounds are HG active just like Se(IV) [28–30]. In particular, DMSe and DMDSe [31] have been shown to seriously interfere the determination of Se(IV) by HG-AFS. Since the presence of methylated selenium compounds in diverse natural aquatic systems suggests that biomethylation of selenium is a common process [6], there is a crucial need for the selective separation and preconcentration of trace amounts Se(IV) due to its complicated matrix and especially potential interferences subjected from DMSe and DMDSe in some real samples. However, to our knowledge, no simple and convenient method dealing with elimination interference from organoselenium has been reported before.

In order to enhance the sensitivity and selectivity of the measurement, several on-line column preconcentration and separation systems have been developed for selenium determination, including sorbent extraction [32–34], ion exchange [35–37] and coprecipitation [38]. A particular on-line coprecipitation scheme involving collection of precipitation on a PTFE or micro-line knotted reactor (KR) has been receiving considerable attention as an alternative preconcentration approach for atomic (mass) spectrometry [39]. The most salient advantages of this on-line preconcentration system are their tolerance to coexisting interferences and elimination the need for the use of a filter, due to a sustained centrifugal force caused by knots in the stream that lead the precipitate to be retained on the tube walls. Thus, flow injection on-line coprecipitation preconcentration systems using KR has been successfully applied to the determination of Pb [40] and Cd, Ni [41] by FAAS, Se(IV) [42,43] and As [44] by HG-AAS, Ba [45] by FAES and As, Sb by ICP-OES [46].

The aim of this work was to eliminate interference from DMSe and DMDSe on the determination of Se(IV) by HG-AFS. For this purpose, a FI on-line separation and preconcentration system using KR coupled to HG-AFS (FI-KR-HG-AFS) was therefore developed based on the selective collection of Se(IV) and its separation from organoselenium. The practical applicability of the proposed method was demonstrated by analyzing inorganic selenium species in a variety of natural water samples.

2. Experimental

2.1. Instrumentation

A non-dispersive atomic fluorescence spectrometer, model AF-610A (Beijing Rayleigh Analytical Instrument Co., Beijing, China), was used and controlled through a computer. A high-intensity selenium hollow cathode lamp (Beijing Tian-gong analytical instrumental factory, Beijing, China) was used as the radiation source at 196.0 nm. The volatile species and the hydrogen evolved from the reaction were swept by an argon carrier gas into the outlet of the electrically heated quarts furnace, where the gas mixture was self-ignited and a hydrogen–argon–air entrained flame was maintained without the addition of any auxiliary hydrogen. The gas–liquid separator made of glass was of three-stage separation design. The operating parameters of the AFS instrument are given in Table 1.

Table 1
Operating parameters of the AFS instrument

Parameter	Setting
Negative high voltage of photomultiplier	330 V
Lamp primary current	90 mA
Lamp boost current	30 mA
Flow rate of carrier gas (Ar)	600 ml min^{-1}
Atomizer temperature	200 °C
Atomizer height	7 mm
Signal recording mode	Peak area

The HG-AFS was coupled with a model FIA-3100 flow injection system (Vital Instrumentals Co. Ltd., Beijing, China), equipped with two peristaltic pumps and a standard rotary injection valve (8-channel 16-port multifunctional injector). The sample and reagents were delivered with Tygon pump tubes. The knotted reactors and all the connections consisted of 0.5 mm i.d. PTFE tubing.

2.2. Reagents

All chemicals were at least of analytical grade and were purchased from Nanjing Chemicals Co. (Nanjing, China) unless otherwise stated. Doubly de-ionized water (DDW) and polyethylene containers were used. A 0.5% (m/v) lanthanum nitrate solution was prepared by dissolving 0.6630 g of lanthanum nitrate hexahydrate (Shanghai Chemicals Co., Shanghai, China) in 100 ml DDW. The Se(IV) and Se(VI) stock solutions of 1000 mg l^{-1} were prepared by dissolving Na_2SeO_3 or Na_2SeO_4 (Aldrich, USA) in DDW. All the calibration standards, each spiked with $La(NO_3)_3$ (20 mg l^{-1}), were prepared by appropriate stepwise dilution of the stock standard solution to the required μg l^{-1} levels just before use, and the pH of the final solutions were adjusted to 3.0 with diluted hydrochloric acid. Organoselenium stock solution of 1000 mg l^{-1} (as Se) and intermediate solution of 10 mg l^{-1} (as Se) were prepared from DMSe and DMDSe (Alfa Aesar, USA) in methanol and stored frozen according to the reported procedure [31]. Aqueous working solutions were prepared daily and stored on ice until measurement. The buffer solution was prepared with 0.2 mol l^{-1} ammonium chloride adjusted to the appropriate pH (8.0–9.5) by addition of 0.2 mol l^{-1} ammonium solution. A 1.0% (m/v) KBH_4 solution was prepared freshly by dissolving KBH_4 in 0.2% (m/v) NaOH solution.

2.3. Sample pretreatment

One river water, one lake water, one pond water, and one ground water sample were collected locally (Nanjing, China).

One mineral water sample was obtained from commercial sources, and two sea water samples were taken from the Yellow Sea (Lianyungang, China). Immediately after sampling, all water samples were filtered through a 0.45 μm membrane. The filtered samples were subdivided into aliquots of 35 ml each for selective treatments. For Se(IV) determination, aliquots of samples were acidified to pH 3.0 with hydrochloric acid [42]. For total inorganic Se determination, aliquots were added to 2.0 g of NaBr, acidified with 4.5 ml of concentrated HCl, heated at 70 °C for 30 min to achieve a quantitative reduction of Se(VI) present in the sample [11,15] and cooled to room temperature prior to pH adjustment with diluted ammonia solution. All the resultant samples, each spiked with $La(NO_3)_3$ (20 mg l^{-1}), were diluted to 50 ml and stored in low density polyethylene (LDPE) bottles, which were precleaned with 8 mol l^{-1} HNO_3, then rinsed with DDW and dried at room temperature before use.

Certified reference materials GBW(E) 080394 (simulated natural water) and GBW(E) 080001 (tea leaf), all obtained from National Research Center of Standard Materials (NRCSM, Beijing, China), were used to validate the proposed method. Water sample was diluted to 50-fold just before analysis. Tea sample was dried at 80 °C, then around 0.5 g of the tea powder was accurately weighed and transferred to a PTFE microwave digestion vessel containing 3 ml concentrated HNO_3 and 2 ml 30% H_2O_2. Once sealed, the vessels were placed in the microwave chamber of closed microwave digester (Shanghai, China). The optimized digestion procedure runs through the following pressure program: 3 min at 0.5 MPa, 3 min at 1.0 MPa and 3 min at 1.5 MPa. After cooling, the clear digests were transferred into a 25 ml calibrated flask. The subsequent procedures were the same as indicated above for total inorganic Se determination. Blanks were subjected to the same procedures as samples.

2.4. Procedure

The manifold of the FI on-line KR coprecipitation preconcentration coupled with HG-AFS presented in Fig. 1 is a variation of the manifold proposed by Yan et al. [47]. The operation sequence runs through four steps. In step 1 (prefill, Fig. 1a), the injector valve was in the injection position, so that the sample or standard solution and the buffer solution were pumped to fill the PTFE tubing before entering the injection valve with pump 1 off and pump 2 on. This prefill stage was used only when a new sample was introduced but omitted for replicate preconcentration. In step 2 (preconcentration, Fig. 1b), the injection valve was in the fill position, the sample containing lanthanum nitrate was merged with an ammonium buffer solution. The generated lanthanum hydroxide induced selenium (IV) to coprecipitate, which were collected by KR. In step 3 (washing, Fig. 1b), the injection valve was still in the fill position, pump 1 was on and pump 2 was off to introduce an air segment into KR to remove residual reagents and matrix while the KBH_4 solution and the HCl solution were propelled to be mixed into GLS to define the base-line signal. In step 4 (dissolution, Fig. 1a), pump 1 was still on and pump 2 off while the injection valve was turned to the injection position, so that 1.2 mol l^{-1} HCl solution was pumped to dissolve the collected analyte precipitates and merge with

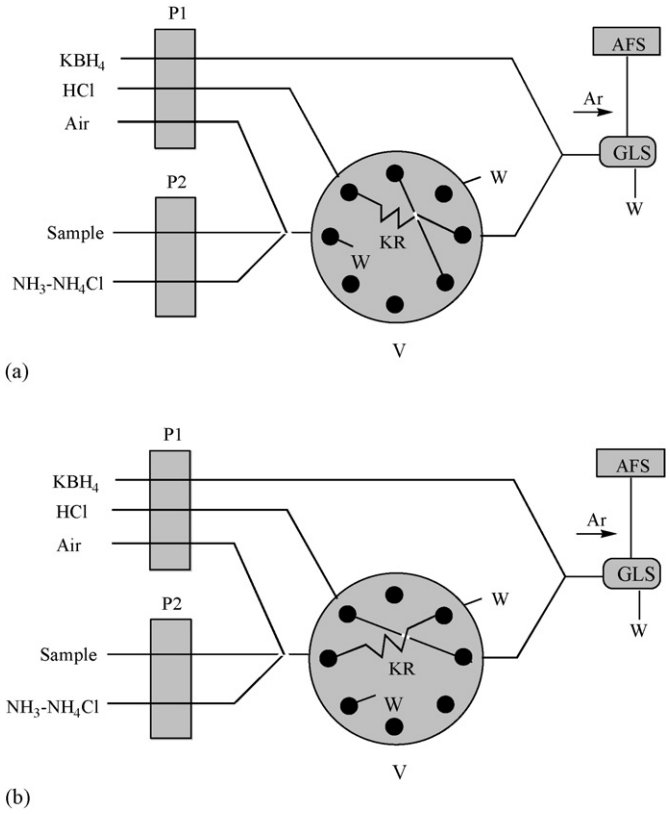

Fig. 1. FI manifold and operation for on-line coprecipitation preconcentration coupled with HG-AFS: (a) prefill/dissolution and (b) preconcentration/washing. P1, P2, peristaltic pump; W, waste; KR, knotted reactor (150 cm long × 0.5 mm i.d. PTFE tubing); V, injector valve; GLS, gas–liquid separator; AFS, atomic fluorescence spectrometry.

KBH_4 solution just before entering GLS to generate gaseous selenium hydride and hydrogen. The generated volatile mixture was swept into the AFS system by an argon flow for detection. Peak area of signal intensity was used for the sake of quantitative analysis.

3. Results and discussion

3.1. Principle of elimination interference of organoselenium on the determination of Se(IV) by the developed FI-KR-HG-AFS system

The existence of DMSe and DMDSe in some environmental samples can cause serious interference on Se(IV) determination by hydride generation atomic spectrometry [31]. As shown in Fig. 2, the developed flow injection on-line coprecipitation preconcentration in a knotted reactor coupled with HG-AFS is effective in eliminating interference subjected from organoselenium. The interference of DMSe and DMDSe on the Se(IV) determination by conventional HG-AFS and its elimination by the developed FI-KR-HG-AFS system are elucidated as follows:

(a) The effect of DMSe and DMDSe on the determination of Se(IV) by conventional HG-AFS was evaluated in the present work. Fig. 2(a) shows the calibration graphs of

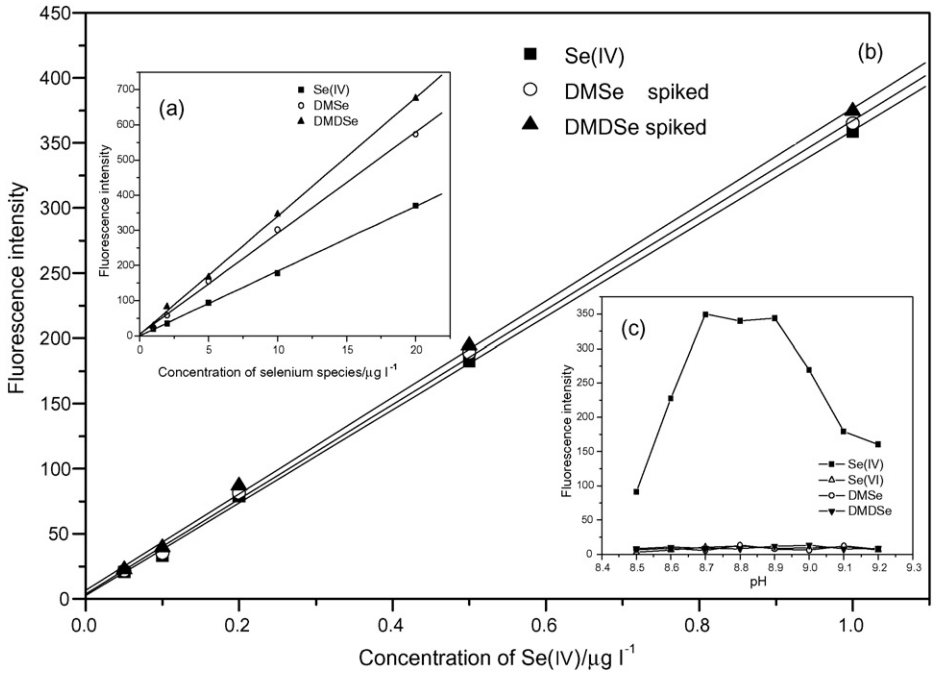

Fig. 2. (a) Calibration curves of Se(IV), DMSe and DMDSe obtained by conventional HG-AFS. HCl concentration 1.2 mol l^{-1}; KBH_4 concentration 1.0% (m/v); sample consumption 0.5 ml; all other conditions as in Table 1. (b) Calibration curves of Se(IV) (■), Se(IV) spiked with 100 μg l^{-1} DMSe (◯) and Se(IV) spiked with 100 μg l^{-1} DMDSe (▲) obtained by FI-KR-HG-AFS. $La(NO_3)_3$ concentration 20 mg l^{-1}; buffer pH 8.8; elute concentration 1.2 mol l^{-1} HCl; KBH_4 concentration 1.0% (m/v); sample flow rate 6.0 ml min^{-1}; buffer flow rate 1.2 ml min^{-1}; HCl flow rate 10.7 ml min^{-1}; KBH_4 flow rate 8.0 ml min^{-1}; sample loading time 120 s; KR length 150 cm. (c) The effect of buffer pH on the fluorescence intensity of 1.0 μg l^{-1} each of Se(IV), Se(VI), DMSe and DMDSe in the FI-KR-HG-AFS system. $La(NO_3)_3$ concentration 20 mg l^{-1}; all other conditions as in (b).

Se(IV), DMSe and DMDSe achieved by conventional HG-AFS, with regression equation of $I = -0.29 + 18.45C_{Se(IV)}$, $I = 3.98 + 28.79C_{DMSe}$ and $I = 3.39 + 33.70C_{DMDSe}$, respectively. Clearly, under the same experimental conditions, the slopes of calibration curves for DMSe and DMDSe were 1.6 and 1.8 times as that for Se(IV), respectively. This observation was similar to the results obtained by Moreno et al. [31]. During Se(IV) measurements by conventional HG-AFS, the presence of DMSe and DMDSe can cause an overestimation in Se(IV) concentration due to their higher AFS response. Therefore, the accuracy of Se(IV) quantification could not be guaranteed in some environmental samples if DMSe and/or DMDSe exist, thus further affecting the reliability of Se speciation analysis by HG-AFS.

(b) The developed preconcentration system of FI-KR-HG-AFS is effective in eliminating interference subjected from organoselenium. Fig. 2(b) shows the calibration graphs of Se(IV), Se(IV) spiked with 100 μg l^{-1} DMSe and Se(IV) spiked with 100 μg l^{-1} DMDSe achieved by FI-KR-HG-AFS under the optimal conditions, with regression equation of $I = 2.45 + 357.1C$, $I = 3.93 + 363.2C$ and $I = 6.73 + 369.9C$, respectively. No significant slope differences for Se(IV) with and without DMSe or DMDSe addition indicates that the existence of organoselenium compounds have no interference on the Se(IV) determination by the developed FI-KR-HG-AFS.

(c) The reason for the elimination interference of organoselenium on the determination of Se(IV) by the developed system is based on the selective preconcentration of Se(IV). The concentration of $La(NO_3)_3$ was kept at an optimal value of 20 mg l^{-1}, the effect of buffer pH on preconcentration efficiency of 1.0 μg l^{-1} (as Se) each of selenium species in the FI-KR-HG-AFS system was investigated. As shown in Fig. 2(c), optimal conditions for coprecipitation Se(IV) on the wall of KR was found in pH range 8.7–8.9, which was nearly in agreement with the observation obtained by HG-AAS [42] and HG-ICP-OES [46] systems. However, no fluorescence signal of Se(VI), DMSe or DMDSe was observed under the same conditions. The reason for the selective collection Se(IV) on the KR inner wall is due to the formation of basic lanthanum selenite, presumably reacting as follows [48]:

$$4H_2SeO_3 + 3La(NO_3)_3 + 9NH_4OH \rightarrow La_2(SeO_3)_3{\cdot}La(OH)SeO_3 + 9NH_4NO_3 + 8H_2O$$

DMSe and DMDSe do not participate in the above coprecipitation reaction and are not retained on the KR under the same working conditions. Therefore, selective preconcentration and separation of Se(IV) from DMSe and DMDSe could be performed with buffer pH kept at 8.8.

3.2. Optimization of experimental parameters

The chemical and flow conditions were optimized to achieve good sensitivity and precision.

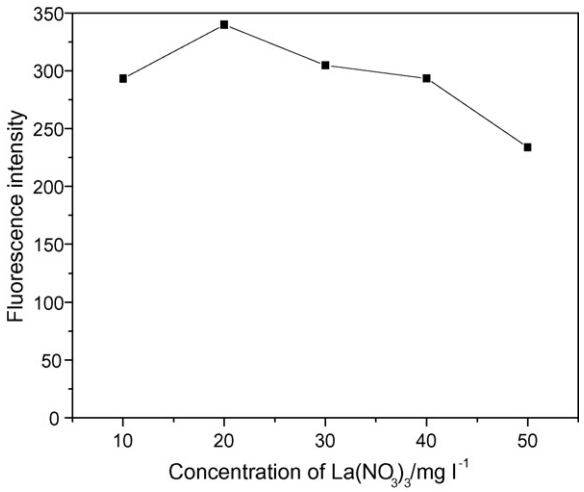

Fig. 3. Effect of concentration of $La(NO_3)_3$ on the fluorescence intensity of 1.0 μg l^{-1} Se(IV). Buffer pH 8.8; all other conditions as in Fig. 2(b).

3.2.1. $La(NO_3)_3$ concentration

The influence of $La(NO_3)_3$ concentration on the signal intensity of 1.0 μg l^{-1} Se(IV) standard was studied from 10 to 50 mg l^{-1} with the buffer pH kept at 8.8. As shown in Fig. 3, it is interesting to observe that the efficiency of Se(IV) preconcentration decreased at higher concentration of $La(NO_3)_3$. One reason is probably contributed to the large particles formed under these precipitation conditions, whereby the efficiency of adherence to the inner walls of KR might be reduced as larger particles are dislodged and carried to waste [42]. Another explanation might be that La^{3+} is adsorbed prior to Se(IV) under the conditions of excess $La(NO_3)_3$, which restrains Se(IV) from coprecipitation. Thus, the concentration of $La(NO_3)_3$ of 20 mg l^{-1} was used throughout.

3.2.2. Sample and buffer flow rates

The signal intensity of 1.0 μg l^{-1} Se(IV) standard increased almost linearly with increasing sample flow rate up to 6.0 ml min^{-1}, indicating quantitative precipitation. Above this level, the curve gradually leveled off, evidencing a lack of sufficient capacity of the knotted reactor at these sample rates. It should be noted that leakage caused by the build-up of high back-pressure appeared owing to the accumulated precipitate on the inner walls of the KR when the sample flow rate was above 8.4 ml min^{-1}. For this reason, a sample flow rate of 6.0 ml min^{-1} was selected, and the flow of the buffer solution should be kept as low as possible in order to minimize the total flow rate through KR and avoid leakage in the precipitation process. A buffer flow of 1.2 ml min^{-1} was thereby chosen for further work.

3.2.3. Sample loading time

The sample loading time must be selected as a compromise between sensitivity and sample throughput. It was observed that the intensity signal of Se(IV) increased linearly up to 120 s and then leveled off with further increase of loading time as a result of insufficient capacity of the KR. Hence, a sample loading time of 120 s was fixed.

3.2.4. Eluent concentration and flow rate

In the on-line flow injection coprecipitation preconcentration system coupled with HG-AFS, the eluent has two functions: firstly, it has sufficiently strong elution capability, completely dissolving the analyte precipitates collected in the inner walls of the KR, and secondly, it provides the required acidic medium for hydride generation. Thus, the eluent concentration is one of the most important instrumental parameters. In this study, hydrochloric acid, which has often been used as the acid medium for Se determination, was tested as eluent. The flow rate of HCl was fixed at 10.7 ml min^{-1} as recommended by the instrumental manufacture. The optimal fluorescence signal was obtained at the HCl concentration of 1.2 mol l^{-1}. Above this level, no sensitivity improvement was observed. Therefore, a 1.2 mol l^{-1} HCl was sufficient for the fast elution of the analyte precipitate and employed throughout.

3.2.5. KBH_4 concentration and flow rate

KBH_4 was used as both a reductant and a hydrogen supplier, which was necessary to sustain the argon–hydrogen flame. The flow rate of KBH_4 was fixed at 8.0 ml l^{-1} as recommended by the instrumental manufacture. The experimental results indicated that low concentrations of KBH_4 (<0.5%) could not effectively reduce the analyte to hydride or not sustain the argon–hydrogen flame while too high concentrations (>2.0%) caused very high background signals, which yielded worse detection limits. Therefore, a KBH_4 concentration of 1.0% (m/v) was chosen.

3.2.6. KR length and KR washing

It is important to keep the KR as short as possible with respect to quantitative coprecipitation and complete collection of the precipitate formed. In this work, a KR length of 150 cm was used as the optimum as longer KR length implies generation of increased back-pressure. Washing the KR and connecting tubing before elution aims at removing non-precipitated constituents of the matrix, but it should not strip the collected precipitates from the KR. In this work, DDW and air were tested as the washing solution. Although DDW could remove the residual

Table 2
Analytical performance of the FI on-line coprecipitation preconcentration system for HG-AFS determination of Se(IV)

Preconcentration time (s)	120
Sample consumption (ml)	12.0
Regent consumption (ml)	
0.2 mol l^{-1} NH_3–NH_4Cl	2.4
1.0% (m/v) KBH_4	4.0
1.2 mol l^{-1} HCl	5.3
Sampling frequency (h^{-1})	24
Linear range (μg l^{-1})	0.05–10
Regression equation (six standards; I, signal intensity; C, μg l^{-1})	$I = 360.6C + 2.51$
Correlation coefficient	0.9991
Detection limit (3 s) (μg l^{-1})	0.014
Precision (R.S.D., $n = 11$) (%)	2.5
Enhancement factor	18

Table 3
Analytical results for the determination of selenium in CRMs and spiked CRMs obtained by FI-KR-HG-AFS and by conventional HG-AFS (mean value ± standard deviation, $n = 5$)

Sample	Added ($\mu g\,l^{-1}$)		Certified value	Found		Unit
	DMSe	DMDSe		FI-KR-HG-AFS	HG-AFS	
GBW(E) 080394	0.00	0.00	100 ± 4	98 ± 3	103 ± 4	$\mu g\,l^{-1}$
	1.00[a]	0.00		97 ± 4	178 ± 12	$\mu g\,l^{-1}$
	0.00	1.00[a]		104 ± 4	189 ± 11	$\mu g\,l^{-1}$
	0.50[a]	0.50[a]		97 ± 3	183 ± 10	$\mu g\,l^{-1}$
GBW(E) 080001	0.00	0.00	40 ± 6	37 ± 2	38 ± 3	$\mu g\,kg^{-1}$
	0.50[b]	0.00		44 ± 3	71 ± 6	$\mu g\,kg^{-1}$
	0.00	0.50[b]		43 ± 2	80 ± 6	$\mu g\,kg^{-1}$
	0.25[b]	0.25[b]		42 ± 3	77 ± 8	$\mu g\,kg^{-1}$

[a] Spiked in the adequately diluted (50-fold) aliquot.
[b] Spiked in the digest just prior to pH adjustment.

matrix components completely, it also stripped the precipitates collected on the inner walls of the KR and decreased the Se signal by almost 15%. However, air was found to remove the residual matrix effectively while not stripping off the collected analyte with a washing flow rate of 5.0 ml min^{-1} for 10 s of washing time.

3.3. Analytical performance

Under the optimal conditions described above, the analytical characteristic data of FI on-line coprecipitation system for HG-AFS determination of ultra-trace selenium are summarized in Table 2. For 120 s preconcentration time the sampling throughput was 24 h^{-1} and the enhancement factor was 18 (as calculated by comparison with the direct injection of 0.5 ml aqueous standard solution). The detection limit was calculated on the basis of three-times the standard deviation of the blank and was found to be 0.014 $\mu g\,l^{-1}$ with the liner range of the method between 0.05 and 10 $\mu g\,l^{-1}$. The precision (R.S.D.) of the 11 replicate measurements of 1.0 $\mu g\,l^{-1}$ Se(IV) standard was 2.5%.

3.4. Real analytical application

3.4.1. Interferences

In this study, the influences of those potential coexisting ions on the signal of 1.0 $\mu g\,l^{-1}$ Se(IV) standard were investigated. The tolerance limits ($\mu g\,l^{-1}$) of the proposed method are presented as follows: Cu^{II} (300); Co^{II} (500); Ni^{II} (700); Fe^{III} (200); Pb^{II} (15); Sb^{III} (100); As^{III} (100); Bi^{III} (10); NO_2^- (>100,000); HCO_3^- (300,000); DMSe (>100); DMDSe (>100). The tolerance of Cu^{II} and Ni^{II} improved in this work due to the masking effect of ammonium compared to that of FI-HG-AFS mode [15] and flow injection on-line sorption preconcentration system [34]. The existence of nitrite in aquatic environments can interfere significantly in the determination of selenium species by hydride generation [26,27]. However, in our experiment, at least 100 mg l^{-1} nitrite may be tolerated thanks to the generation of precipitate that causes the analyte to be separated from the matrix. In particular, at least 100 $\mu g\,l^{-1}$ DMSe and DMDSe caused no appreciable interference. Since the concentration of the total organoselenium in environmental matrices, such as soils, biologically active lake sediments, sewage sludge and oxic groundwater [49], is far less than 100 $\mu g\,l^{-1}$ [6,9,49], the developed system was found to be free of interference from DMSe and DMDSe, and can be used for Se speciation analysis in a variety of environmental samples.

3.4.2. Method validation

Certified reference materials GBW(E) 080394 (simulated natural water) and GBW(E) 080001 (tea leaf) were used to evaluate the accuracy for selenium determination. As shown in Table 3, the determined value of the CRMs by both meth-

Table 4
Analytical results for Se(IV) and Se(VI) determination in natural water samples (mean value ± standard deviation, $n = 5$)

Sample	Found ($\mu g\,l^{-1}$)		Calculated ($\mu g\,l^{-1}$)	Recovery (%)	
	Se(IV)	Total Se	Se(VI)	Se(IV)[a]	Se(VI)[b]
River water	0.36 ± 0.02	0.52 ± 0.02	0.16 ± 0.02	107.4	92.5
Lake water	0.12 ± 0.02	0.19 ± 0.02	0.07 ± 0.02	103.7	97.2
Mineral water	0.07 ± 0.02	0.28 ± 0.01	0.21 ± 0.02	95.0	96.4
Pond water	0.21 ± 0.02	0.32 ± 0.02	0.11 ± 0.02	94.5	95.2
Ground water	0.40 ± 0.04	0.60 ± 0.05	0.20 ± 0.04	100.3	95.7
Sea water 1	0.07 ± 0.01	0.13 ± 0.01	0.06 ± 0.01	97.4	93.8
Sea water 2	0.06 ± 0.01	0.11 ± 0.01	0.05 ± 0.01	98.7	94.7

[a] Recovery for spiking with 0.50 $\mu g\,l^{-1}$ Se(IV).
[b] Recovery for spiking with 0.50 $\mu g\,l^{-1}$ Se(VI).

ods agreed well with the certified values. For the spiked CRMs analysis, however, an error in the selenium determination by conventional HG-AFS was observed due to the interference from DMSe and/or DMDSe, while the accuracy of the selenium determination by FI-KR-HG-AFS could be guaranteed all the same.

3.4.3. Determination of Se(IV) and Se(VI) in real natural water samples

The developed method was applied to the Se(IV) and Se(VI) determination in several types of natural water samples. The analytical results and recoveries for spiking with 0.50 $\mu g\,l^{-1}$ Se(IV) and Se(VI) are shown in Table 4. The recoveries of the spiked samples varied from 94.5 to 107.4% for Se(IV) and from 92.5 to 97.3% for Se(VI), indicating that the low levels of Se(IV) and Se(VI) originally present were determined with a comfortable degree of confidence.

4. Conclusions

On-line coprecipitation in a KR coupled with HG-AFS is shown to be an efficient and effective approach for eliminating interference from DMSe and DMDSe on the determination of Se(IV). Compared with other potential methods for organoselenium interference removal, such as pervaporation [31] and anion exchange resin column [22], the proposed system is very simple and cost-effective because of the ease of construction and the unlimited lifetime of the KR. In addition, the developed method improves tolerance towards nitrite interference. It is expected that this non-chromatographic method offers an inexpensive, reliable and sensitive alternative for the fast determination trace inorganic selenium of different oxidation states.

Acknowledgements

This project is supported by the National Natural Science Foundation of China (no. 20575025), Research Founding from the State Education Administration of China for PhD program (20050284030) and Excellent Young Teacher, Natural Science Foundation of Jiangsu Province (BK 2005083) and Grant of Analytical Measurements of Nanjing University.

References

[1] N. Maleki, A. Safavi, M.M. Doroodmand, Talanta 66 (2005) 858.
[2] M.S. El-Shahawi, M.A. El-Sonbati, Talanta 67 (2005) 806.
[3] C.-H. Yu, Q.-T. Cai, Z.-X. Guo, Z.-G. Yang, S.B. Khoo, J. Anal. At. Spectrom. 19 (2004) 410.
[4] B.D. Wake, A.R. Bowie, E.C.V. Butler, P.R. Haddad, Trends Anal. Chem. 23 (2004) 491.
[5] L.B. Xia, B. Hu, Z.C. Jiang, Y.L. Wu, R. Chen, L. Li, J. Anal. At. Spectrom. 21 (2006) 362.
[6] T.D. Cooke, K.W. Bruland, Environ. Sci. Technol. 21 (1987) 1214.
[7] A. D'Ulivo, L. Gianfranceschi, L. Lampugnani, R. Zamboni, Spectrochim. Acta, Part B 57 (2002) 2081.
[8] J. Stripeikis, P. Costa, M. Tudino, O. Troccoli, Anal. Chim. Acta 408 (2000) 191.
[9] Y.Q. Zhang, J.N. Moore, W.T. Frankenberger, Environ. Sci. Technol. 33 (1999) 1652.
[10] K.J. Reddy, Z.H. Zhang, M.J. Blaylock, G.F. Vance, Environ. Sci. Technol. 29 (1995) 1754.
[11] P. Cava-Montesinos, A. de la Guardia, C. Teutsch, M.L. Cervera, M. de la Guardia, J. Anal. At. Spectrom. 19 (2004) 696.
[12] Y. Wang, M.L. Chen, J.H. Wang, J. Anal. At. Spectrom. 21 (2006) 535.
[13] A.E. Moreno, C. Perez-Conde, C. Camara, J. Anal. At. Spectrom. 15 (2000) 681.
[14] Y.-Z. He, H. El Azouzi, M.L. Cervera, M. de la Guardia, J. Anal. At. Spectrom. 13 (1998) 1291.
[15] Y.-Z. He, J. Moreda-Pineiro, M.L. Cervera, M. de la Guardia, J. Anal. At. Spectrom. 13 (1998) 289.
[16] J.B. Garcia, M. Krachler, B. Chen, W. Shotyk, Anal. Chim. Acta 534 (2005) 255.
[17] J.L. Capelo, C. Fernandez, B. Pedras, P. Santos, P. Gonzalez, C. Vaz, Talanta 68 (2006) 1442.
[18] H. Mendez, I. Lavilla, C. Bendicho, J. Anal. At. Spectrom. 19 (2004) 1379.
[19] D.R. Roden, D.E. Tallman, Anal. Chem. 54 (1982) 307.
[20] D.A. Martens, D.L. Suarez, Environ. Sci. Technol. 31 (1997) 133.
[21] K. Pyrzynska, Analyst 120 (1995) 1933.
[22] Y.Q. Zhang, W.T. Frankenberger Jr., J.N. Moore, Sci. Total Environ. 229 (1999) 183.
[23] T. Wickstrom, W. Lund, R. Bye, J. Anal. At. Spectrom. 10 (1995) 803.
[24] K. Marcucci, R. Zamboni, A. D'Ulivo, Spectrochim. Acta, Part B 56 (2001) 393.
[25] L.D. Martinez, M. Baucells, E. Pelfort, M. Roura, R. Olsina, Fresenius J. Anal. Chem. 357 (1997) 850.
[26] G.A. Cutter, Anal. Chim. Acta 149 (1983) 391.
[27] D.L. Nunes, E.P. dos Santos, J.S. Barin, S.R. Mortari, V.L. Dressler, E.M.M. Flores, Spectrochim. Acta, Part B 60 (2005) 731.
[28] A. Chatterjee, Y. Shibata, Anal. Chim. Acta 398 (1999) 273.
[29] A. Chatterjee, K.J. Irgolic, Anal. Commun. 35 (1998) 337.
[30] A. Chatterjee, Y. Shibata, M. Yoneda, R. Banerjee, M. Uchida, H. Kon, M. Morita, Anal. Chem. 73 (2001) 3181.
[31] M.E. Moreno, C. Pérez-Conde, C. Cámara, Anal. Bioanal. Chem. 375 (2003) 666.
[32] V.M.C. Dias, S. Cadore, N. Baccan, J. Anal. At. Spectrom. 18 (2003) 783.
[33] X.-P. Yan, M. Sperling, B. Welz, Anal. Chem. 71 (1999) 4353.
[34] C.-Y. Lu, X.-P. Yan, Z.-P. Zhang, Z.-P. Wang, L.-W. Liu, J. Anal. At. Spectrom. 19 (2004) 277.
[35] D.W. Bryce, A. Izquierdo, M.D. Luque de Castro, J. Anal. At. Spectrom. 10 (1995) 1059.
[36] P.E. Carrero, J.F. Tyson, Analyst 122 (1997) 915.
[37] J. Stripeikis, J. Pedro, A. Bonivardi, M. Tudino, Anal. Chim. Acta 502 (2004) 99.
[38] X.-D. Tang, Z.-R. Xu, J.-H. Wang, Spectrochim. Acta, Part B 60 (2005) 1580.
[39] J.L. Burguera, M. Burguera, Spectrochim. Acta, Part B 56 (2001) 1801.
[40] Z.-L. Fang, M. Sperling, B. Welz, J. Anal. At. Spectrom. 6 (1991) 301.
[41] Z.-L. Fang, L.-P. Dong, J. Anal. At. Spectrom. 7 (1992) 439.
[42] G.-H. Tao, E.H. Hansen, Analyst 119 (1994) 333.
[43] S. Nielsen, J.J. Sloth, E.H. Hansen, Analyst 121 (1996) 31.
[44] S. Nielsen, J.J. Sloth, E.H. Hansen, Talanta 43 (1996) 867.
[45] C. Plamboeck, H.C. Westtoft, S.A. Pedersen, J.E.T. Andersen, J. Anal. At. Spectrom. 18 (2003) 49.
[46] E. Peña-Vázquez, A. Bermejo-Barrera, P. Bermejo-Barrera, J. Anal. At. Spectrom. 20 (2005) 1344.
[47] X.-P. Yan, X.-B. Yin, X.-W. He, Y. Jiang, Anal. Chem. 74 (2002) 2162.
[48] W. Reichel, B.G. Bleakley, Anal. Chem. 46 (1974) 59.
[49] X. Dauchy, M. Potin-Gautier, A. Astruc, M. Astruc, Fresenius J. Anal. Chem. 348 (1994) 792.

Available online at www.sciencedirect.com
ScienceDirect
Talanta 71 (2007) 1553–1559
Talanta
www.elsevier.com/locate/talanta

Simultaneous analysis of naltrexone and its major metabolite, 6-β-naltrexol, in human plasma using liquid chromatography–tandem mass spectrometry: Application to a parent-metabolite kinetic model in humans

Hwi-yeol Yun [a], Seong-chul Bang [a], Ki-cheol Lee [a], In-hwan Baek [a], Seo-pan Lee [a], Wonku Kang [b], Kwang-il Kwon [a,*]

[a] *College of Pharmacy, Chungnam National University, Daejeon, Republic of Korea*
[b] *College of Pharmacy, Catholic University of Daegu, Kyungbuk, Republic of Korea*

Received 14 June 2006; received in revised form 20 July 2006; accepted 20 July 2006
Available online 30 August 2006

Abstract

We developed a method for simultaneously determining naltrexone, an opioid antagonist, and its major metabolite (6-β-naltrexol) in plasma using LC/MS/MS. Three compounds, and naloxone as an internal standard, were extracted from plasma using a mixture of methyl-tertiary-butyl ether. After drying the organic layer, the residue was reconstituted in a mobile phase (0.1% formic acid–acetonitrile:0.1% formic acid buffer, 95:5, v/v) and injected onto a reversed-phase C_{18} column. The isocratic mobile phase was eluted at 0.2 ml/min. The ion transitions monitored in multiple reaction-monitoring modes were *m/z* 342 → 324, 344 → 326, and 328 → 310 for naltrexone, 6-β-naltrexol, and naloxone, respectively. The coefficient of variation of the assay precision was less than 11.520%, and the accuracy exceeded 93.465%. The limit of quantification was 2 ng/ml for naltrexone and 7.2 ng/ml for 6-β-naltrexol. And the limit of detection was 0.1 ng/ml for naltrexone and 0.36 ng/ml for 6-β-naltrexol. This method was used to measure the plasma concentration of naltrexone and 6-β-naltrexol in healthy subjects after a single oral 50 mg dose of naltrexone. This analytical method is a simple, sensitive, and accurate way of determining the pharmacokinetic profiles of naltrexone and its metabolites. The pharmacokinetic parameters were analyzed using both non-compartmental analysis performed for each subject according to standard methods and compartmental analysis with a parent-metabolite pharmacokinetic model that was fitted to the data, simultaneously, using the program ADAPT II. The tested parent-metabolite pharmacokinetic model successfully described the relationship between the plasma concentration of naltrexone and one of its major metabolites, 6-β-naltrexol.

Keywords: Naltrexone; 6-β-Naltrexol; LC/MS/MS; Parent-metabolite pharmacokinetic model

1. Introduction

The competitive narcotic antagonist naltrexone is increasingly considered an important aid in the detoxification of opiate addicts [1]. The effectiveness of naltrexone as an adjunct treatment for individuals with alcohol dependence undergoing psychosocial treatment programs was demonstrated recently [2]. In humans, naltrexone undergoes extensive hepatic metabolism, primarily via reduction to its major metabolite, 6-β-naltrexol (Fig. 1). 6-β-Naltrexol is believed to be a major contributor to the pharmacological effect of naltrexone. For this reason, it is prudent to characterize the disposition of both naltrexone and 6-β-naltrexol [3].

Many other methods, including the high performance liquid chromatography (HPLC)–mass–mass detection (MS–MS) [1], thin-layer chromatography (TLC) [3], HPLC–electrochemical detection (ECD) [4], and gas-chromatography (GC)–mass detection (MS) [5,6], have been published for determination of naltrexone and 6-β-naltrexol, in biological fluid. However, in spite of their general administration to alcohol dependence patients, there were no reports about simultaneous compartmental analysis and pharmacokinetic analysis of naltrexone and 6-β-naltrexol in humans.

This report describes the development of a LC–MS/MS method for simultaneously determining naltrexone and 6-β-naltrexol in human plasma. This study sought to develop a robust

* Corresponding author. Tel.: +82 42 821 5937; fax: +82 42 823 6781.
E-mail address: kwon@cnu.ac.kr (K.-i. Kwon).

0039-9140/$ – see front matter © 2006 Elsevier B.V. All rights reserved.
doi:10.1016/j.talanta.2006.07.035

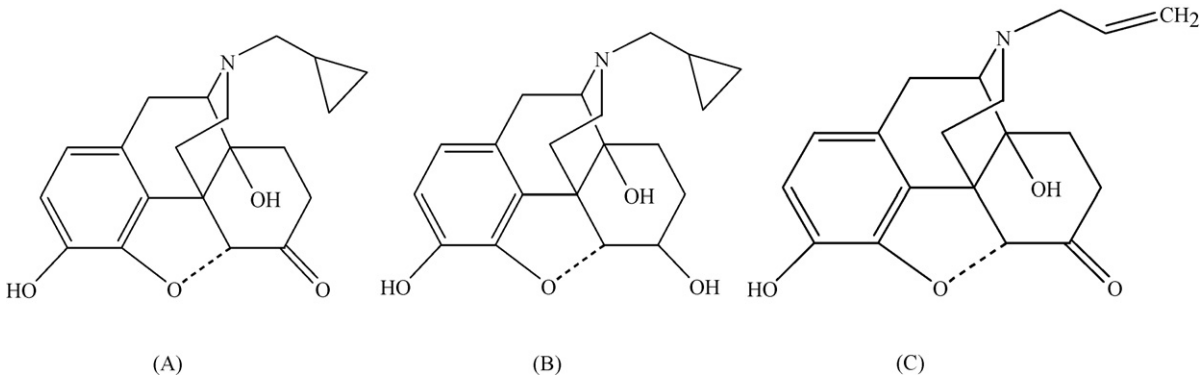

Fig. 1. Molecular structures of naltrexone (A), its active metabolite, 6-β-naltrexol (B) and internal standard, naloxone (C).

LC–MS/MS method for naltrexone and 6-β-naltrexol determination in human plasma, thereby enabling pharmacokinetic studies based on plasma data, and to characterize the metabolism of naltrexone and 6-β-naltrexol using non-compartmental pharmacokinetic analysis and compartmental parent-metabolite pharmacokinetic modeling.

2. Experimental

2.1. Reagents and materials

Naltrexone, naloxone (IS, internal standard), and HPLC-grade organic solvents (dichloromethane and diethylether) were purchased from Sigma Chemical (St. Louis, MO, USA) and Merck (Darmstadt, Germany), respectively. 6-β-Naltrexol was synthesized in the medicinal organic chemistry laboratory at Chungnam National University (Daejeon, Korea) [7,8]. All other chemicals and solvents were of the highest analytical grade available.

2.2. Preparation of standards and quality controls

Naltrexone, 6-β-naltrexol, and IS were dissolved in methanol at 1, 3.6, and 0.1 mg/ml, respectively. The naltrexone standard solution was serially diluted with methanol and added to drug-free plasma to obtain concentrations of 2, 5, 10, 20, 30, and 50 ng/ml. The 6-β-naltrexol standard solution was diluted with methanol and added to drug-free plasma to obtain concentrations of 7.2, 18, 36, 72, 360, and 720 ng/ml. A calibration graph was derived from the peak area ratios of naltrexone and 6-β-naltrexol to IS using a linear regression. All solutions were stored at 4 °C and protected from light.

Quality controls were prepared daily in 1 ml of blank human plasma by adding 100 μl of standard solution. Controls were prepared for low (2 ng/ml naltrexone, 7.2 ng/ml 6-β-naltrexol), intermediate (5 and 30 ng/ml naltrexone, 18 and 360 ng/ml 6-β-naltrexol), and high (50 ng/ml naltrexone, 720 ng/ml 6-β-naltrexol) concentrations to evaluate the inter- and intra-day precision and accuracy of the assay method. The calibration equation was validated when the relative difference between the theoretical and back-calculated concentrations of each sample of the calibration set did not exceed 20% at the lowest concentration and 15% at the other concentrations.

2.3. Characterization of the product ions using tandem mass spectrometry

Solutions containing 1 μg/ml of naltrexone, 6-β-naltrexol, and IS were infused separately into the mass spectrometer at a flow rate of 10 μl/min to characterize the product ions of each compound. The precursor ions, $[M+H]^+$, and pattern of fragmentation were monitored using positive ion mode. The major peaks observed in the MS–MS scan were used to quantify naltrexone, 6-β-naltrexol, and IS.

2.4. Analytical system

The plasma naltrexone and 6-β-naltrexol concentrations were quantified using LC–MS with a PE SCIEX API 2000 LC/MS/MS system (Sciex Division of MDS, Toronto, Canada) equipped with an electrospray ionization interface used to generate positive ions $[M+H]^+$. The compounds were separated on a reversed-phase column (Eclipse XDB-C_{18}, 2.1 mm × 100 mm internal diameter, 3.5 μm particle size; Agilent Technology, Wilmington, DE, USA) with an isocratic mobile phase consisting of 0.1% formic acid in acetonitrile and 0.1% formic acid in purified water (95:5%, v/v). The mobile phase was eluted at 0.2 ml/min using an Agilent 1100 series pump (Agilent Technology).

The turboion spray interface was operated in positive ion mode at 5500 V and 500 °C. The operating conditions were optimized by flow injection of a mixture of all of the analytes and were determined as follows: nebulizing gas flow, 1.04 l/min; auxiliary gas flow, 4.0 l/min; curtain gas flow, 1.44 l/min; collision gas (nitrogen) pressure, 5×10^{-5} Torr; orifice voltage (declustering potential), 76 V; ring voltage (focusing potential), 320 V; entrance potential, 12 V; collision energy, 25 V; and collision exit potential, 8.0 V. Quantification was performed by multiple reaction-monitoring (MRM) of the protonated precursor ion and the related product ion for naltrexone and 6-β-naltrexol, using the internal standard method with peak area ratios. The mass transitions used for naltrexone, 6-β-naltrexol, and the internal standards were m/z 342 → 324, 344 → 326, and 328 → 310,

respectively (dwell time, 150 ms). Quadrupoles Q1 and Q3 were set on unit resolution. The analytical data were processed using Analyst software (version 1.2).

2.5. Sample preparation

One hundred microliters of internal standard (1 μg/ml) were added to 1 ml of plasma, followed by a 10-min liquid–liquid extraction with 5 ml of methyl-*tert*-butyl ether. The organic layer was separated and evaporated under a gentle stream of nitrogen at about 40 °C. The residue was reconstituted into 100 μl of mobile phase by vortex mixing for 15 s; 5 μl of this solution was injected onto the column.

2.6. Validation procedure

The validation parameters were selectivity, precision, and accuracy. Ten batches of blank heparinized human plasma were screened to determine the specificity. The extraction recoveries of naltrexone and 6-β-naltrexol were calculated by comparing the peak area ratio measured for the standard solution considering condensation with that obtained for plasma extracts after the extraction procedure. The precision and accuracy of the intra- and inter-day assay validation were estimated using the inverse prediction of the concentration of the quality controls from the calibration curve [9,10].

2.7. Clinical application

Eight healthy subjects who gave written informed consent took part in this study. Health problems, drug or alcohol abuse, and abnormalities in laboratory screening values were exclusion criteria. The study protocol was approved by the Food and Drug Administration of Korea and the Ethics Committee of the Institute of Drug Research and Development at Chungnam National University (Daejeon, Korea).

After an overnight fast, all the subjects were given a single oral 50 mg dose of naltrexone. Blood samples (6 ml) were taken before and at 0.25, 0.5, 0.75, 1, 1.5, 2, 3, 4, 6, 9, and 12 h after drug administration. The plasma was separated by centrifugation at 1360 × *g* for 10 min and stored at −80 °C until analysis.

2.8. Pharmacokinetic analysis

The pharmacokinetic analysis was performed using non-compartmental and compartmental methods. The area under the plasma concentration-versus-time curve (AUC) was calculated using the trapezoidal rule and extrapolated to infinity. The time course of the plasma naltrexone and 6-β-naltrexol concentrations was used to determine the maximum plasma concentration (C_{max}) and the time (T_{max}) to reach C_{max}. The elimination rate constant (K_{el}) was obtained by the linear regression of the terminal phase, and the calculated elimination half-life ($t_{1/2}$) was $0.693/K_{el}$ [11].

In addition, we used a parent-metabolite compartmental model. Models were constructed as a series of differential equations that were solved numerically and were fitted to the data using ADAPT II (Biomedical Simulation Resource, Los Angeles, CA, USA). Fitting was performed using maximum likelihood estimation under the assumption that the standard deviation of the measurement error was a linear function of the measured quantity. The following information (obtained with ADAPT II) was used to evaluate the goodness of fit and the quality of the parameter estimates: coefficients of variation of parameter estimates, parameter correlation matrix, sums of squares of residuals, visual examination of the distribution of residuals, and the Akaike information criterion. We used a coefficient of variation of <0.5 and a correlation coefficient threshold of 0.9 as criteria for evaluating the numeric identifiability of the parameter estimates [12].

3. Results and discussion

3.1. Mass spectra

Precursor ions for naltrexone, 6-β-naltrexol, and naloxone, and their corresponding product ions, were determined from spectra obtained during the infusion of standard solutions into a mass spectrometer using an electrospray ionization source, which operated in positive ionization mode with collision nitrogen gas in Q2 of a MS/MS system. Naltrexone, 6-β-naltrexol, and naloxone produced mainly protonated molecules at *m/z* 342, 344, and 328, respectively. Both product ions were scanned in Q3 after collision with nitrogen in Q2 at *m/z* 324, 326, and 310 for naltrexone, 6-β-naltrexol, and naloxone, respectively (Fig. 2).

3.2. Determination of naltrexone, 6-β-naltrexol

The retention times of naltrexone, 6-β-naltrexol, and internal standard (naloxone) in human were approximately 0.2 min. Fig. 3A and B show typical chromatograms for blank plasma and plasma spiked with the three compounds (2 ng/ml naltrexone, limit of quantitation; 7.2 ng/ml 6-β-naltrexol, limit of quantitation; and IS), respectively. The plasma sample from a volunteer is shown in Fig. 3C.

Reconstitution of the final residue with methanol, acetonitrile, and 0.1% formic acid in water produced tailing with naltrexone and 6-β-naltrexol. In order to improve the peak shape, we reconstituted the residue with the mobile phase. The total run time for each sample was about 1 min.

3.3. Linearity and detection limit

The calibration curve of naltrexone gave a reliable response from 2 to 50 ng/ml. The mean equation of the regression line was $y = 0.044080x - 0.008236$ (slope range, 0.03865–0.04680; intercept range, −0.034794 to 0.007298; $r^2 > 0.997$). The limit of detection was 0.1 ng/ml at a signal-to-noise (S/N) ratio of 3, which is as sensitive as the previous LC–MS/MS method.

The calibration curve of 6-β-naltrexol provided a reliable response from 7.2 to 720 ng/ml. The mean equation of the regression line was $y = 0.0012x - 0.0072$ (slope range, 0.0011–0.0014; intercept range, 0.005–0.0156; $r^2 > 0.997$). The

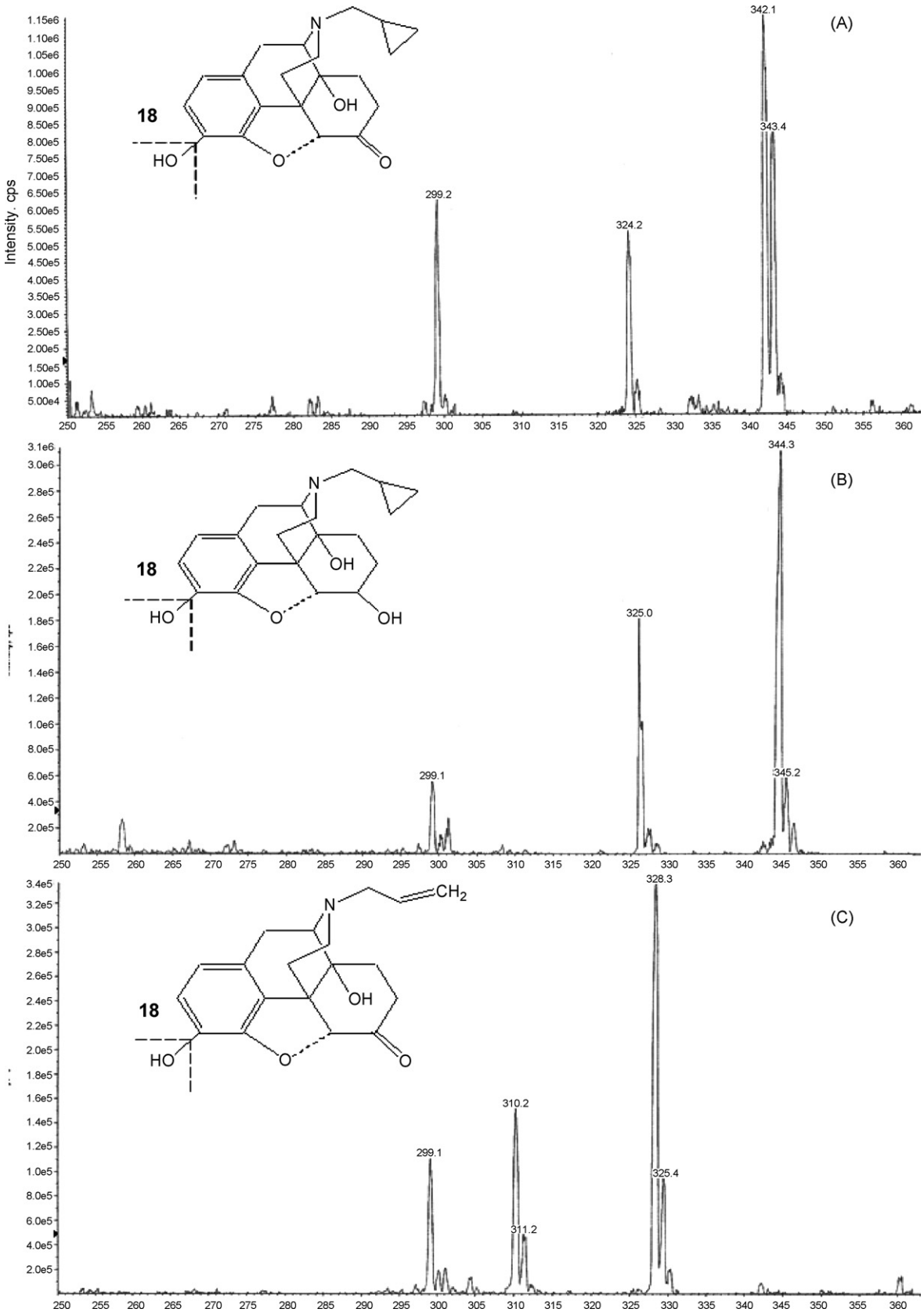

Fig. 2. Mass–mass spectra of naltrexone (A), 6-β-naltrexol (B), and naloxone (C) using electrospray ionization mode.

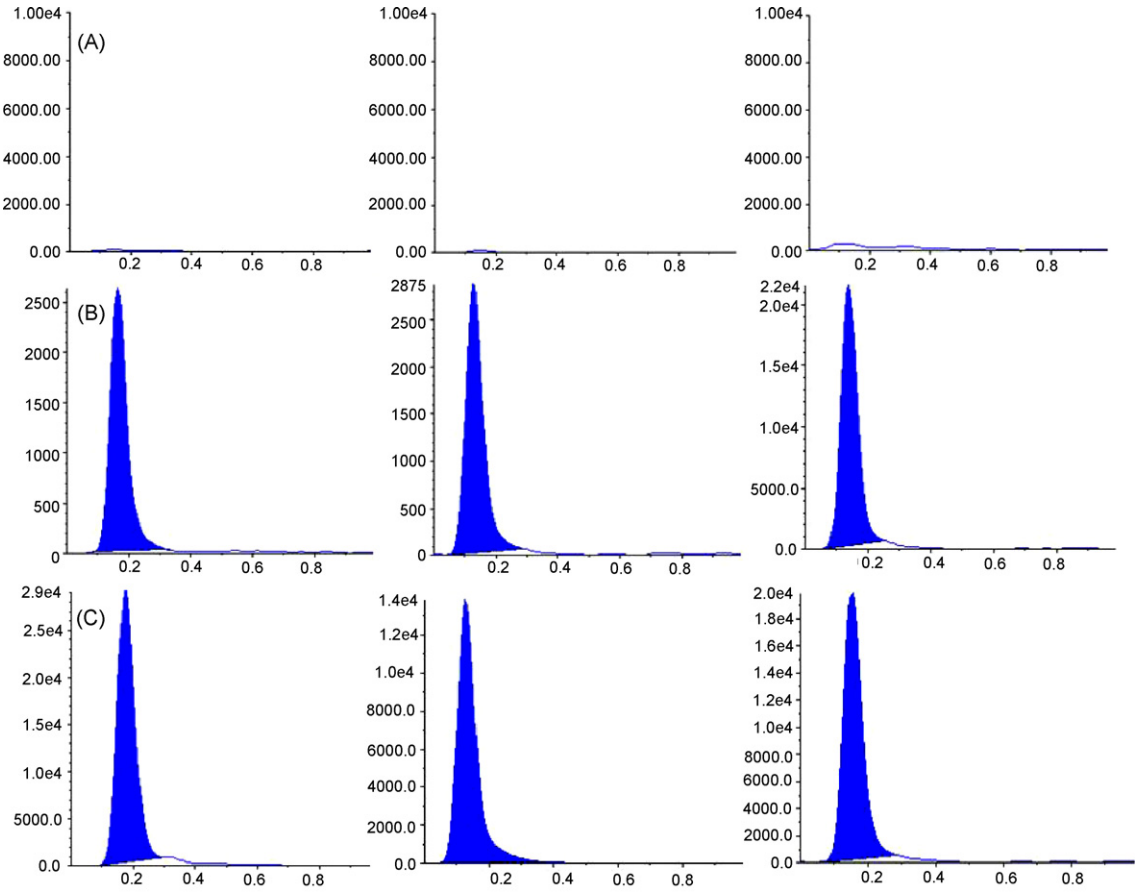

Fig. 3. Chromatograms of naltrexone (left), 6-β-naltrexol (center), and naloxone (right). (A) Blank plasma; (B) plasma spiked with 20 ng/ml naltrexone, 72 ng/ml 6-β-naltrexol, and 1 μg/ml internal standard; (C) plasma sample of subject #1, 1 h after a single oral 50 mg dose of naltrexone.

limit of detection was 0.36 ng/ml at a S/N ratio of 3, which is as sensitive as the previous LC–MS/MS method.

3.4. Precision and accuracy

The intra- and inter-day precision and accuracy of our method for naltrexone and 6-β-naltrexol are listed in Tables 1 and 2, respectively. The naltrexone coefficients of variation of the precision of the intra- and inter-day validation were less than 11.5% and 9.76%, respectively. The method exceeded 97.23% accuracy for naltrexone. The 6-β-naltrexol coefficients of variation of the precision of the intra- and inter-day validation were less than 7.59% and 6.38%, respectively. The method exceeded 92.89% accuracy for 6-β-naltrexol.

3.5. Assessment of the matrix effect in bioanalysis

Matrix effect was checked with total five different lots of normal control heparinised plasma. Each of low quality control (LQC) and high quality control (HQC) were prepared from

Table 1
The precision and accuracy of the intra-day naltrexone and 6-β-naltrexol assay ($n = 5$)

Added (ng/ml)	Measured (ng/ml) (mean ± S.D.)	CV (%)	Accuracy (mean% ± S.D.)
Naltrexone			
2	2.023 ± 0.122	6.649	101.175 ± 6.106
5	5.100 ± 0.566	11.520	102.002 ± 11.320
30	29.172 ± 1.699	5.863	97.239 ± 5.665
50	50.609 ± 4.239	8.406	101.210 ± 8.477
6-β-Naltrexol			
7.2	7.002 ± 0.381	2.709	97.246 ± 5.299
18	16.824 ± 1.252	5.239	93.465 ± 6.959
360	355.996 ± 9.924	2.733	98.888 ± 2.757
720	742.696 ± 56.828	7.589	103.013 ± 7.893

Table 2
The precision and accuracy of the inter-day naltrexone and 6-β-naltrexol assay ($n = 5$)

Added (ng/ml)	Measured (ng/ml) (mean ± S.D.)	CV (%)	Accuracy (mean% ± S.D.)
Naltrexone			
2	2.155 ± 0.077	0.781	107.774 ± 3.845
5	5.214 ± 0.491	9.762	104.280 ± 9.815
30	30.180 ± 1.444	4.815	100.600 ± 4.814
50	51.345 ± 4.209	8.227	102.690 ± 8.418
6-β-Naltrexol			
7.2	6.090 ± 0.501	3.636	92.919 ± 6.955
18	16.722 ± 1.440	6.049	92.898 ± 7.999
360	337.730 ± 13.259	3.845	93.814 ± 3.683
720	731.596 ± 47.190	6.388	101.611 ± 6.554

Table 3
Matrix effect in five different lot for plasma for naltrexone and 6-β-naltrexol

	Naltrexone LQC (2 ng/ml)					6-β-Naltrexol (7.2 ng/ml)				
	Lot-1	Lot-2	Lot-3	Lot-4	Lot-5	Lot-1	Lot-2	Lot-3	Lot-4	Lot-5
Calculated concentration (ng/ml)	1.849	2.149	1.975	2.130	2.011	7.174	6.380	6.987	7.404	7.063
RE (%)	−7.550	7.450	−1.250	6.500	0.550	−0.361	−11.389	−2.958	2.833	−1.902
	Naltrexone LQC (50 ng/ml)					6-β-Naltrexol (720 ng/ml)				
	Lot-1	Lot-2	Lot-3	Lot-4	Lot-5	Lot-1	Lot-2	Lot-3	Lot-4	Lot-5
Calculated concentration (ng/ml)	43.457	50.557	54.296	51.692	53.045	823.966	701.937	739.250	678.303	765.020
RE (%)	−13.086	1.114	8.592	3.384	6.090	14.440	−2.509	2.674	−5.791	6.253

Table 4
Stability results of naltrexone and 6-β-naltrexol

Stability experiments	Storage condition	Stability (%) ± S.D.	
		10 ng	20 ng
Naltrexone			
Bench top	Room temperature (6 h)	106.608 ± 0.430	109.893 ± 1.679
Process (extracted sample)	4 °C, for 48 h	92.165 ± 7.588	93.590 ± 4.605
Freeze and thaw stability in plasma	After third FT cycle at −70 °C	108.014 ± 0.292	109.393 ± 4.764
Long term stability in human plasma	For 30days at −70 °C	108.884 ± 0.036	95.437 ± 1.942
Stability experiments	Storage condition	Stability (%) ± S.D.	
		36 ng	72 ng
6-β-Naltrexol			
Bench top	Room temperature (6 h)	101.123 ± 0.543	98.632 ± 1.129
Process (extracted sample)	4 °C, for 48 h	96.842 ± 2.016	105.472 ± 0.536
Freeze and thaw stability in plasma	After third FT cycle at −70 °C	99.270 ± 0.823	96.913 ± 0.199
Long term stability in human plasma	For 30days at −70 °C	106.608 ± 0.248	95.003 ± 0.248

different lots of plasma and checked for the inaccuracy in all the QC samples. No matrix effect or interferences from endogenous compounds were detected from five different sources of human plasma (Table 3).

3.6. Stability

The stability of naltrexone and 6-β-naltrexol in plasma were investigated. The stability results are summarized in Table 4. Short-term stability (room temperature 6 h), long term stability (30 days at 70 °C), three freeze–thaw cycle stability, and stability of extraction sample (48 h at 4 °C) were stable in human plasma.

3.7. Pharmacokinetics of naltrexone and 6-β-nalterexol

All enrolled subjects ($n = 8$) completed the study. The compound was tolerated very well under both fed and fasting conditions. No subject exhibited any clinically important changes in vital signs or electrocardiogram and blood chemistry parameters during the study.

Fig. 4 shows the time course of the naltrexone and 6-β-naltrexol plasma concentrations after a single oral 50 mg dose of naltrexone. The pharmacokinetic parameters are listed in Table 5. The C_{max} of naltrexone was 11.44 ± 5.44 ng/ml at 1.19 ± 0.44 h. The AUC_{12h} and AUC_{inf} of naltrexone were 44.46 ± 12.17 and 58.56 ± 18.42 ng h/ml, respectively. The half-life calculated from the terminal phase was 5.89 ± 2.33 h. The C_{max} of 6-β-naltrexol was 322.93 ± 78.72 ng/ml at

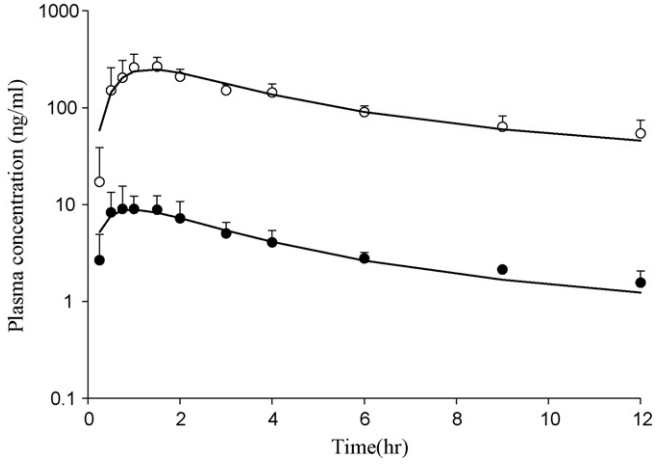

Fig. 4. Time course of the plasma concentration in healthy subjects after a single oral 50 mg dose of naltrexone. Each point represents the mean ± standard deviation ($n = 8$). (●) Observed plasma concentration of naltrexone and (○) observed plasma concentration of 6-β-naltrexol. The solid line is the result of the maximum likelihood fitting using the program ADAPT II.

Table 5
Pharmacokinetic parameters of naltrexone and 6-β-naltrexol after a single 50 mg dose ($n = 8$)

	Mean ± S.D.	
	Naltrexone	6-β-Naltrexol
Model independent parameters		
AUC_{12h} (ng h/ml)	44.460 ± 12.171	1158.839 ± 208.479
AUC_{inf} (ng h/ml)	58.564 ± 18.423	1712.155 ± 504.030
C_{max} (ng/ml)	11.443 ± 5.442	322.928 ± 78.724
T_{max} (h)	1.188 ± 0.438	1.281 ± 0.411
$V_{z(terminal)}/F$ (l)	7364.217 ± 1972.070	211.995 ± 50.923
$t_{1/2}$ (h)	5.894 ± 2.330	5.127 ± 15.586
		Mean ± S.D.
Model dependent parameters		
K_{el} (h^{-1})		0.074 ± 0.004
K_{cp} (h^{-1})		1.133 ± 0.052
K_{pc} (h^{-1})		0.150 ± 0.032
K_m (ng)		204 ± 12
V_m (ng/h)		25960 ± 3165
K_{mel} (h^{-1})		3.268 ± 0.452
K_{mcp} (h^{-1})		0.518 ± 0.0248
K_{mpc} (h^{-1})		0.100 ± 0.0296
V_1 (l)		779.100 ± 62.345
V_2 (l)		7.085 ± 0.482

1.28 ± 0.41 h. The AUC_{12h} and AUC_{inf} of 6-β-naltrexol were 1158.84 ± 208.48 and 1712.16 ± 504.03 ng h/ml, respectively. The half-life calculated from the terminal phase was 5.13 ± 2.26 h.

The solid line represents the best fit of the pharmacokinetic model to the measured concentration; based on the maximum likelihood criterion and visual inspection of the fits, a two-compartment open model, non-linear metabolism, and first-order elimination were chosen to describe the data (Fig. 5). The estimated pharmacokinetic parameters are listed in Table 5.

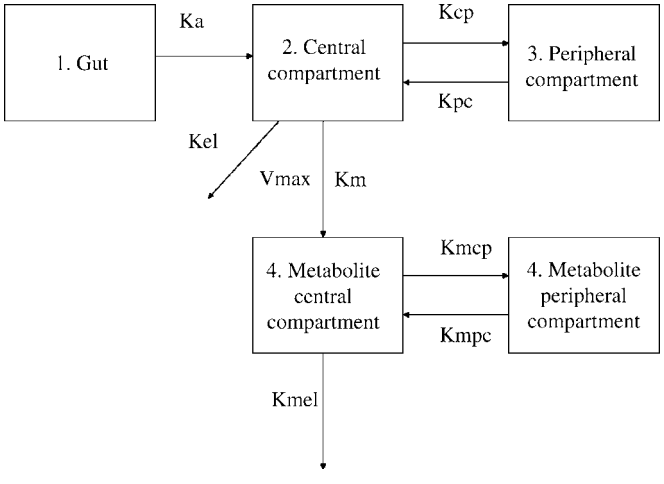

Fig. 5. The model scheme selected to describe the relationship between naltrexone and its major metabolite, 6-β-naltrexol, in healthy volunteers.

The Michaelis–Menten type metabolism rate into the central compartment of metabolite V_{max} and the apparent Michaelis constant K_m were 25,960 ng/h and 204 ng, respectively. The Michaelis–Menten kinetic analysis of the data indicated the existence of an enzymatic metabolic pathway. A previous study showed that at least two enzymatic pathways are involved in these transformations, and the 6-β-metabolite is predominant in humans. The administration of naltrexone in humans is followed by extensive biotransformation, which was more extensive after oral administration than after i.v. administration.

4. Conclusion

In conclusion, our LC/MS/MS method is a simple, sensitive, and accurate way of determining the plasma concentrations of naltrexone and its major metabolite (6-β-naltrexol), and is suitable for clinical pharmacokinetic studies of this drug at low doses. The established parent-metabolite pharmacokinetic model predicted the plasma levels of naltrexone and 6-β-naltrexol under new conditions, such as multiple doses or increasing or decreasing doses, and this model explained the non-linear metabolism between naltrexone and 6-β-naltrexol. However, this study was limited to healthy volunteers. To overcome the limitation, we need more pharmacokinetics data on patients.

Acknowledgment

This study was supported by a contract, “Bioequivalence assessment of naltrexone 50 mg tablets after administering a single oral dose to healthy Korean volunteers”, with Myung-In Pharmaceuticals, Seoul, Korea.

References

[1] S. Valiveti, B.N. Nalluri, D.C. Hammell, K.S. Paudel, A.L. Stinchcomb, J. Chromatogr. B. 810 (2004) 259–267.
[2] B.J. Mason, A.M. Goodman, R.M. Dixon, M.H.A. Hameed, T. Hulot, K. Wesens, J.A. Hunter, M.G. Boyeson, Neuropsychopharmacol 27 (4) (2002) 596–606.
[3] M.E. Wall, D.R. Brine, M. Perez-Reyes, Drug Metab. Dispos. 9 (4) (1981) 369–375.
[4] A.F. Davidson, T.A. Emm, H.J. Pieniaszek, J. Pharmaceut. Biomed. 14 (1996) 1717–1725.
[5] K. Verebey, M.J. Kogan, A. DePace, S.J. Mulle, J. Chromatogr. 118 (1976) 331–334.
[6] S.W. Toennes, D.F. Kauert, S.M. Grusser, W. Jakel, G. Partecke Jr., J. Pharmaceut. Biomed. 35 (2004) 169–176.
[7] K. Uwai, H. Uchiyama, S. Sakurada, C. Kabuto, M. Takeshida, Bioorg. Med. Chem. 12 (2004) 417–421.
[8] N. Chatterjie, C.E. Inturrisi, J. Med. Chem. 18 (5) (1975) 490–492.
[9] W. Kang, H.Y. Yun, K.H. Liu, K.I. Kwon, J.G. Shin, J. Chromatogr. B 805 (2004) 311–314.
[10] M.H. Yun, K.I. Kwon, J. Pharmaceut. Biomed. 40 (2006) 168–172.
[11] L. Shargel, A. Yu, Applied Biopharmaceutics and Pharmacokinetics, 4th ed., Appleton and Lange, Stamford, 1999.
[12] S.K. Woo, W. Kang, K.I. Kwon, Clin. Pharm. Ther. 71 (4) (2002) 246–252.

Available online at www.sciencedirect.com
ScienceDirect
Talanta 71 (2007) 1610–1615
Talanta
www.elsevier.com/locate/talanta

Analysis of wine primary aroma compounds by stir bar sorptive extraction

A. Zalacain [a], J. Marín [b], G.L. Alonso [a], M.R. Salinas [a,*]

[a] *Cátedra de Química Agrícola, E.T.S.I. Agrónomos, Universidad de Castilla-La Mancha, Campus Universitario, E-02071 Albacete, Spain*
[b] *Departamento de Química Analítica y Electroquímica, Universidad de Extremadura, Facultad de Ciencias, Campus Universitario, E-06071 Badajoz, Spain*

Received 28 March 2006; received in revised form 19 July 2006; accepted 24 July 2006
Available online 8 September 2006

Abstract

Due to the great importance of some primary aroma compounds on wine quality, these compounds which includes terpenes, C_{13}-norisoprenoids and C_6 compounds, have been analyzed by stir bar sorptive extraction (SBSE) followed by a thermal desorption-gas chromatography–mass spectrometry analysis. The stir bar sorptive extraction method was optimized in terms of temperature, time, pH and NaCl addition. The best SBSE sorption kinetics for the target analytes were obtained after submitting the solutions to 60 °C during 90 min. The addition of sodium chloride did not enhance the volatile extraction. The method proposed showed good linearity over the concentration range tested, with correlation coefficients higher than 0.98 for all the analytes. The reproducibility and repeatability of the method was estimated between 0.22 and 9.11%. The detection and quantification limits of all analytes were lower than their respective olfactory threshold values. The application of this SBSE method revealed that monovarietal white wines were clearly separated by two canonic discriminating functions when grape varieties were used as differentiating variable, the first of which explained 98.4% of the variance. The compounds which contributed most to the differentiation were limonene, linalool, nerolidol and 1-hexanol.

Keywords: Stir bar sorptive extraction (SBSE); Primary aroma; Wines

1. Introduction

Analysis of aroma compounds is one of the most important steps in the evaluation of wine quality. The low concentration of the volatile compounds responsible of wine aroma makes enrichment as a basis for identification and quantification [1], among them liquid–liquid extraction [2–4] or solid phase extraction [5,6] using organic solvents prior to analysis by GC–MS have been the most widely used. These analytical methods have some drawbacks such as the possibility of contamination with solvents and later solvent concentration, generation of artifacts and the length of time of analysis. Techniques which requires neither solvents nor sample preparation such as solid phase microextraction (SPME) [7–10] or a most powerful technique, the stir bar sportive extraction (SBSE) [11], have been successfully been applied for flavour profiling of different types of matrix because it combines ease of use, ruggedness, precision and sensitivity [12–18].

Today, there is an increasing demand for wines with a fresh and fuity aroma, which can also be used to identify the *Vitis vinifera* used for winemaking. One of the most important factors in determining wine typicity and quality. Wine primary aroma compounds, which are also defined as varietal aroma compounds and represent the typical aroma of the grapes noted in wines, are present as free forms, which may contributed directly to odour and, in much larger concentrations as non-volatile forms, among them the sugar-bound conjugates being the most abundant. The hydrolysis of these glycoconjugates mainly by acids, enzymes or while wine aging, can yield odour-active aglycones such as terpenes, C_{13}-norisoprenids, benzene derivates, and aliphatic alcohols [19,20] that are not always present in all *V. vinifera* varieties. These compounds have a great importance because they play a key role in the differentiation of the wines according to the different grape varieties used for winemaking [19,21].

* Corresponding author.
E-mail address: Rosario.Salinas@uclm.es (M.R. Salinas).

0039-9140/$ – see front matter © 2006 Elsevier B.V. All rights reserved.
doi:10.1016/j.talanta.2006.07.051

However, not all compounds contribute to the same extent to wine aroma. In fact, if the concentration/olfactory threshold ratio of each compound known as the "odour activity value" (OAV) is ≥1, this allows estimating the contribution of each compound to the wine aroma. According to Güth [22] this concept is therefore necessary to quantify the levels of flavour differences between wines obtained from the different grape varieties or origins.

The analysis of some wine aroma compounds by SBSE was first carried out by Hayasaka et al. [23], although there are only few papers that optimized the sorptive extraction procedure in wine matrixes for cork taint, oak volatiles and pesticides [14,16,24]. In this paper, the wine primary aroma compounds analysis by SBSE have been optimized for first time in terms of ionic strength, temperature and extraction time. The primary aroma compounds that can have a great contribution on wine and are closely related to quality in white wines and may be used to differentiate monovarietal wines are: terpenes such as limonene, linalool, α-terpineol, β-citronellol, nerol, geraniol, nerolidol; C_6 compounds such as *trans*-2-hexenal, 1-hexanol, *cis*-3-hexen-1-ol, *trans*-2-hexen-1-ol; and C_{13}-norisoprenoids such as β-damascenone, α and β-ionone. As well, this SBSE method has been applied to the differentiation of six different monovarietal white commercial wines elaborated with Chardonnay, Macabeo, Muscat, Eva, Cayetana and Pardina varieties from Extremadura, in the Spanish Southwest region.

2. Experimental

2.1. Chemicals and reagents

Standards: β-citronellol, geraniol, α and β-ionone, limonene, linalool, nerol, nerolidol, γ-hexalactone (IS), 1-hexanol, *trans*-2-hexenal, *trans*-2-hexen-1-ol, *cis*-3-hexen-1-ol, α-terpineol, were obtained from Sigma–Aldrich (Madrid, Spain). β-Damascenone was a gift from Firmenich (Barcelona, Spain). Exact masses of the chemical standards were dissolved in absolute ethanol.

Solvents: ethanol (analytical-reagent grade) was obtained from Merck (Damstard, Germany), while water was purified through a Milli-Q system (Millipore, Bedfords, MA, USA).

Synthetic wine samples were prepared by an ethanol solution at 12% (v/v) to which 5 g/L tartaric acid were added. Solution pH was adjusted to 3.6 with 1 M sodium hydroxide (Panreac, Barcelona, Spain).

2.2. Proposed extraction method

A sample of 25 mL of wine, to which 250 μL of internal standard γ-hexalactone solution at 1 μL/mL in absolute ethanol was added, was poured into a 25 mL volumetric flask. Compounds were extracted by introducing the polydimethylsiloxane coated stir bar (0.5 mm film thickness, 10 mm length, Twister, Gerstel GmbH, Mülheim and der Ruhr, Germany) into the sample (either commercial wine or synthetic wine solution). Samples were stirred at 700 rpm at 60 °C for 90 min. The stir bar was then removed from the sample, rinsed with distilled water and dried with a cellulose tissue, and later transferred into a thermal desorption tube for GC/MS analysis.

2.3. GC/MS analysis

In the thermal desorption tube, the volatile compounds were desorbed from the stir bar at the following conditions: oven temperature at 290 °C; desorption time, 4 min; cold trap temperature, −30 °C; helium inlet flow, 45 mL/min. The compounds were transferred into the Hewlett-Packard 6890 gas chromatograph coupled to an Hewlett-Packard LC 3D mass detector (Palo Alto, USA) with a fused silica capillary column (BP21 stationary phase 50 m length, 0.22 mm i.d., and 0.25 μm film thickness) (SGE, Ringwood, Australia). The chromatographic program was set at 50 °C (held for 2 min), raised to 230 °C at 12 °C/min and held for 20 min. For mass spectrometry analysis, electron impact mode (EI) at 70 eV was used. The mass range varied from 35 to 500 u and the detector temperature was 150 °C. Identification was carried out using the NIST library and quantification was based on the calibration curves of respective standards in the synthetic wines.

2.4. Analytical method validation

For linearity study, calibration graphs were established with five standard solutions in synthetic wine ranged from their OAV 0.5 to 10 which level of concentration has been included in Table 1. Each level of concentration was analyzed twice with two different stir bars, so there were a total of four replicates.

The detection and quantification limits (LOD and LOQ, respectively) were calculated with the data generated in the linearity studies. LOD was defined as $(a + 3S_a/b)$ and LOQ as $(a + 10S_a/b)$, "a" being the origin ordinate, "S_a" the origin ordinate variance and "b" the slope. The limit of quantification was taken to be validated when within-batch relative standard deviation, using three replicate samples spiked with known LOQs, was fewer than 20% according to Catice methodology [25].

The standard deviation for each compound (square root of the arithmetic mean of the variances) was calculated to obtain the repeatability (%R.S.D.). The standard deviation of the three values for each compound multiplied by the square root of 3 was taken as the reproducibility value (if this value was higher than repeatability; if not, this last value was also taken as reproducibility).

2.5. Wine samples differentiation

Six different commercial monovarietal white wines (Chardonnay, Muscat, Eva, Cayetana and Pardina) from Extremadura (Spanish Southwest region) were analyzed in duplicate in this study following the methodology proposed. Wine sample differentiation was performed with the SPSS Version 11.5 statistical package for Windows (SPSS, Chicago, IL).

Table 1
Odour threshold compounds and linearity data for wine primary aroma compounds ($n = 4$)

Volatile compound	Odour threshold	Linear range concentration	Selected ions (m/z)[a]	Slope	Intercept	Correlation coefficient (R^2)
Terpenes (μg/L)						
Limonene	15 [26]	7.5–150	68/**93**/121/136	0.116	0.359	0.998
Linalool	25 [27]	12.5–250	71/**93**/121/136	0.005	0.007	0.999
α-Terpineol	250 [27]	125–2500	**93**/121/136	0.002	0.097	0.996
β-Citronellol	18 [28]	9–180	**69**/123/138	0.014	0.011	0.999
Nerol	15 [26]	7.5–150	41/**69**/104	0.009	0.005	0.998
Geraniol	30 [22]	15–300	41/**69**/123	0.008	0.019	0.999
Nerolidol	15[b]	7.5–150	**69**/93/107	0.061	0.046	0.987
C_{13}-norisoprenoids (μg/L)						
β-Damascenone	0.05 [22]	0.025–0.5	69/**121**	43.141	0.741	0.999
α-Ionone	2.6 [29]	1.3–26	91/**121**/136	1.971	2.367	0.997
β-Ionone	0.09 [27]	0.045–0.9	**177**/192	6.684	0.071	0.989
C_6 compounds (mg/L)						
1-Hexanol	0.8 [22]	4–80	56/**69**	0.121	0.244	0.999
Trans-2-hexenal	0.6 [26]	0.3–6	41/55/**69**	0.304	0.039	0.999
Cis-3-hexen-1-ol	0.4 [22]	0.2–4	41/67/**82**	0.138	0.023	0.974
Trans-2-hexen-1-ol	15 [26]	7.5–150	41/57/**82**	0.077	0.174	0.992

[a] m/z used for quantification are given in bold.
[b] Nerolidol value is suppose to be the same as nerol.

3. Results and discussion

3.1. SBSE performance

Due to great number of aroma compounds identified in wine matrixes [12,14,23] and to avoid interferences with the target compounds, the MS analysis was carried out by using the selective ion monitoring mode at their characteristics m/z values. It is also important to point out the excellent signal-to-noise ratio observed for the individual ions. As there are a great odour threshold variability (Table 1) between the compounds, the standards solution concentration which have been submitted to the different SBSE extraction conditions correspond to an odour activity value (OAV) of 10 for each compound. Extraction conditions were studied by comparing the relative peak area compound (peak area of the target analyte/IS peak area ratio). As the diffusion of the analytes through the system phases is essential, the effect of the time and temperature in their extraction was firstly optimized. Extraction times such as 30, 60 and 90 min and extraction temperatures of 25 °C (room temperature) and 60 °C were evaluated by immersing the stir bar into the sample (Fig. 1a). It is apparent that the extraction time profile depends on individual analytes. Independently of the temperatures, the higher the extraction time the higher the absorption of compounds such as 1-hexenol, *trans*-2-hexenol, α-terpineol, α and β-ionone, whereas the rest of the compounds reached the equilibrium between 30 and 60 min. The temperature effect was not the same for all compounds under study. High temperatures are supposed to release more analytes, allowing better extraction. However, an excessive heating temperature and/or extraction time could lead to degradation of the analytes and/or the matrix with a consequent decrease in extraction recovery. Among both temperatures, 60 °C was been revealed as the most sensitive temperature condition for the absorption of most wine primary aroma compounds. No significant differences between both temperatures have been observed for β-citronellol, nerol, geraniol, and β-ionone. Other extraction parameter which can improve the extraction efficiency for many analytes is the addition of salt to the sample. The influence of ionic strength was

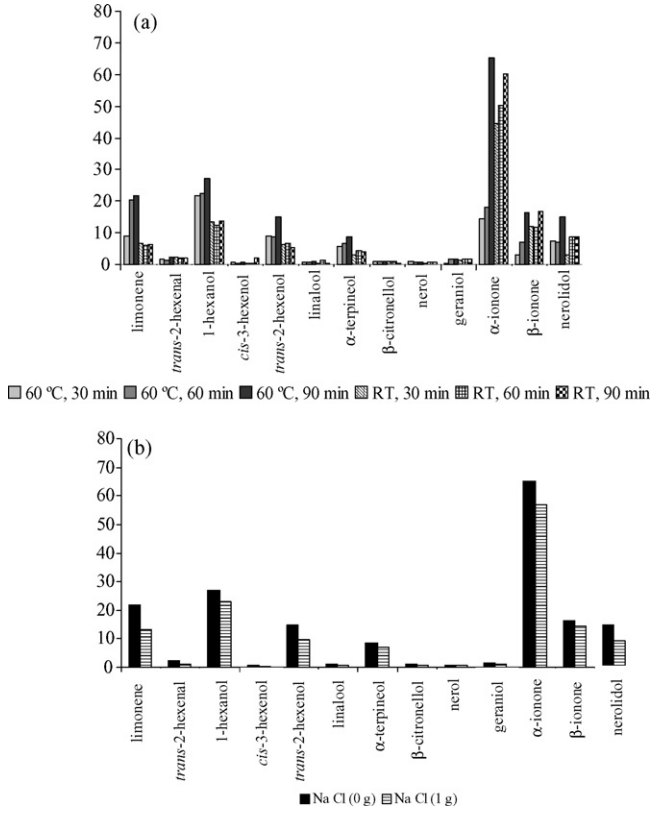

Fig. 1. Peak area vs. IS area: (a) at T^a (RT and 60 °C) and time (30, 60 and 90 min); (b) at 60 °C during 90 min with or without NaCl (1 g).

evaluated by addition of two different amounts of sodium chloride (0 or 1 g) into 25 mL (Fig. 1b), and not significant differences were observed for all compounds, then the extraction method will be carried out without adding sodium salt.

Neither higher extraction time nor higher temperatures have been tested to continue extraction until equilibrium as the conditions tested were enough to obtain a quantitative extraction with good analytical validation parameters. Then, the optimum stir bar sorptive extraction conditions were fixed as: 25 mL of the sample spiked with the target analytes and stirred at 700 rpm with a stir bar at 60 °C for 90 min, and not salt addition was needed. Blank runs of the stir bar were made before and after each analysis and no memory effect occurred for the target solutions.

3.2. Calibration curves and performance characteristics

Five levels of concentration were tested in duplicate and regression lines were calculated for each compound, calibration data are shown in Table 1. Linear range covered the volatile compound concentration expected in the samples with OAV of 0.5, 1.0, 5.0 and 10.0; good regression coefficient (R^2) was obtained in all the cases ranged from 0.974 (*cis*-3-hexen-1-ol) to 0.999 (linalool and geraniol) (Table 1). A saturation effect on the polydimethylsiloxane stir bar was observed for linalool when assaying higher concentration levels (up to 125 μg/L, OAV of 10). The precision of the experimental procedure was also evaluated. For the reproducibility of a method (%R.S.D.) to be considered acceptable, its value should be less than 20%. As can be seen in the results summarized in Table 2, this parameter ranged from 0.22% (β-damascenone) to 4.15% (1-hexanol). The same limit (20%) was taken to represent good repeatability; in this case ranging from 0.71% (limonene) to 9.11% (α-terpineol).

In the literature, many analytical methods have been described to determine the concentration of these wine aroma compounds, but only a few show the method validation parameters.

Table 2
Precision of the experimental procedure ($n = 4$)

Volatile compound	LOD	LOQ	Repetivity (%)	R.S.D. (%)
Terpenes (μg/L)				
Limonene	4.29	7.09	0.71	0.41
Linalool	1.41	1.72	2.70	1.56
α-Terpineol	48.17	50.10	9.11	5.26
β-Citronellol	5.19	5.21	0.48	0.84
Nerol	0.62	0.64	0.84	0.48
Geraniol	0.76	0.77	1.52	0.87
Nerolidol	0.76	0.77	1.52	0.87
C_{13}-norisoprenoids (μg/L)				
β-Damascenone	0.1×10^{-2}	0.2×10^{-2}	3.84	0.22
α-Ionone	1.22	1.31	0.25	0.44
β-Ionone	0.01	0.02	4.58	2.64
C_6 compounds (μg/L)				
1-Hexanol	0.46	0.47	1.74	3.02
Trans-2-hexenal	6.09×10^{-2}	7.08×10^{-2}	1.50	0.87
Cis-3-hexen-1-ol	0.26	0.28	4.31	2.49
Trans-2-hexen-1-ol	5.89	5.90	0.59	1.02

The terpene content of a wine is considered to be a quality factor. These compounds have a very pleasant aroma and very low olfactory thresholds, so that they can be perceived during wine tasting even in low concentrations due as well to several synergic and antagonist effects observed between them [30]. For all terpenes analyzed the detection and quantification limits were much lower than its olfactory threshold (Table 2). In comparison with SPME or ultrasound-assisted extraction [9,10], the limits obtained by SBSE in compounds such as linalool, nerol, citronellol and geraniol are between 73 and 92% lower; whereas for α-terpineol the values are higher than for SPME. When headspace-SPME was applied to the analysis of these compounds [7], the SBSE LOD and LOQ were lower for linalool, nerol and nerolidol whereas for α-terpineol (LOD 2.89 μg/L), citronellol (LOD 1.61 μg/L) and geraniol (LOD 1.45 μg/L) were better with HS-SPME.

A classical technique such as SPE has been successfully applied on the analysis of seven wine terpenoids [6], lower LOD were showed for most compounds ranged from 0.40 μg/L (linalool) to 2.10 μg/L (limonene), and being only nerol LODs lower in case of SBSE. SPE technique has also been used in grape distillate [31], being only α-terpineol the terpene with better LOD (17 μg/L) that with SBSE.

C_6 compounds have been described with herbaceous and greasy odours that have been related to deleterious effects in wines, although in white wines a small herbaceous perception can be appreciated by consumers [32]. Their origin was reported as being related mainly to the lipooxygenase activity of the grape [33] and/or must aeration [34]. All unsaturated C_6 compounds have olfactory threshold very low, but during fermentation these compounds may be transformed by yeast into 1-hexanol, being its olfactory threshold higher and therefore less aggressive. For this reason the analysis of this type of compounds may result very interesting together with the study of the strain yeast which are capable of this transformation. As well as in terpenes detection, the LOD and LOQ values obtained by SBSE were lower than their respective olfactory threshold (Table 2). Polydimethylsiloxane-SPME was applied to the characterization of varietal wines [35], only 1-hexanol and *cis*-3-hexanol as C_6 compounds were studied, but their respective LOD values were 0.15 and 0.49 mg/L, respectively, valued much higher than the ones obtained by SBSE. SPE technique has also been used in grape distillate [31], but with much worst results than SBSE. No other bibliographic references have been found in relation with validation method parameters of these compounds with any analytical technique.

Carotenoids and non-aromatic intermediates are known to be precursors of aroma-active C_{13}-norisoprenoids which are responsible for the typical aroma of some grapes varieties [36]. The presence of C_{13}-norisoprenoids is also considered to be a quality factor, as they supply an agreeable scent of flowers, fruits, tea, etc. [37]. Besides, the high quality grape viniferas of certain prestige areas have a higher C_{13}-norisoprenoids concentration than the ones with lower quality used for common wines [38,39]. Among these compounds, β-ionone stands-out as sup-

plies an aroma of violet, α-ionone with a woody, cedar wood like aroma or β-damascenone with a sweet and apple aroma descriptor.

Their detection and quantification limits obtained by SBSE were much lower than their respective olfactory threshold (Table 2) and the values reported by headspace-SPME [7] and SPE [5].

Although in some of the cited papers the limits obtained were better for some of the compounds analyzed, in this paper a compromise has been established between compounds with very different chemical characteristics. Then, the advantage of the SBSE is that in a single run, 13 primary volatile compounds can be quantified correctly at levels lower than their respective olfactory thresholds and no sample manipulation is necessary avoiding the possible artifact generation.

3.3. Wine differentiation

The proposed SBSE method was applied to six different monovarietal white wines. It has to be pointed out that although the SBSE method can detect values lower than their respective olfactory threshold, many of the compounds analyzed have not been found in these wine samples, with special evidence on C_{13}-norisoprenoids. Winemaking grapes are not very aromatic fruits and only some, denominated floral (e.g. Muscats), have enough aroma compounds to proportionate its particular typicity. The analyzed wines have been elaborated with non-floral varieties, except for Muscat. In this case, the aroma grape typicity is derived from their terpene content [40,41], specially related with linalool, α-terpienol, geraniol and nerolidol that are the compounds detected in higher amounts. From the wines analyzed it positively outstands, Eva which has the same terpenes as Muscat although in lower quantity, resulting in wines with a characteristic aroma. For this reason, in Extremadura area the use of this *V. vinifera* variety is being promotes.

It surprises the low content of this type of compounds, lower than their olfactory thershold) in Chardonnay and Macabeo wines except for nerolidol, although several authors points out the presence of these primary aroma compounds [42,43]. Nevertheless, the type of winemaking process has a great influence on aroma content and as these are young white wines no compounds could have been liberated while aging [44,45].

Evidently, the presence or absence of these compounds will allow the differentiation of the monovarietal wines. The obtained results where submitted to a discriminant analysis which revealed that monovarietal white wines were clearly separated by two canonic discriminating functions, when the different grape varieties were used as differentiating variable, the first of which explained 98.4% of the variance. Fig. 2 shows how Muscat wines are clearly separated from the other non-floral varieties. From the latest Eva wines are the most differentiate one, followed by Macabeo and Chardonnay. As it was expected, Pardina and Cayetana wines are very closed, as it is known that they are very similar and with a low varietal aroma content. The compounds which contributed most to the differentiation were limonene, linalool, nerolidol and 1-hexanol.

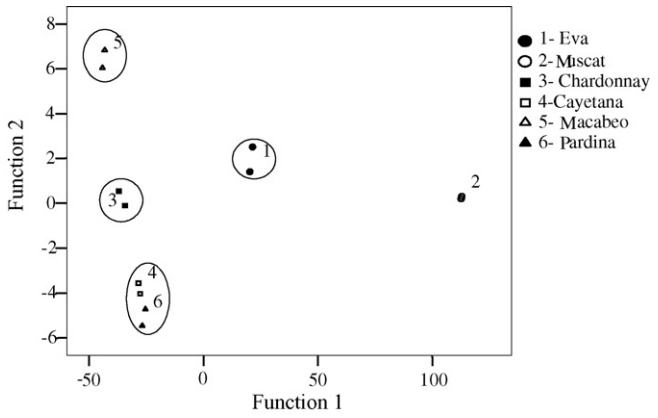

Fig. 2. Discriminant plot of the different wines when the primary aroma compounds were used as variables.

References

[1] L. Pillonel, J.O. Bosset, R. Tabacchi, Lebensm. Wiss. U-Technol. 35 (2002) 1.
[2] A. Calleja, E. Falqué, Food Chem. 90 (2005) 357.
[3] V. Ferreira, A. Rapp, J. Cacho, H. Hastrich, I. Yavas, J. Agric. Food Chem. 41 (1993) 1413.
[4] M. Ortega-Heras, M.L. González-San José, S. Beltrán, Anal. Chim. Acta 458 (2002) 85.
[5] R. López, M. Aznar, J. Cacho, V. Ferreira, J. Chromatogr. A 966 (2002) 167.
[6] Z. Piñeiro, M. Palma, C.G. Barroso, Anal. Chim. Acta 513 (2004) 209.
[7] J.S. Câmara, M.A. Alves, J.C. Marques, Anal. Chim. Acta 555 (2006) 191.
[8] D. De la Calle, K. Séller, M. Reichbacher, K. Danzer, C. Hurlbeck, C. Bartzech, J. High Resol. Chromatogr. 21 (1998) 368.
[9] R.M. Peña, J. Barciela, C. Herrero, S. García-Martín, Talanta 67 (2005) 129.
[10] R.M. Peña, J. Barciela, C. Herrero, S. García-Martín, J. Sci. Food Agric. 85 (7) (2005) 1227.
[11] E. Baltussen, P. Sandra, F. David, C.A. Cramers, J. Microcolumn Sep. 11 (1999) 737.
[12] R.F. Alves, A.M.D. Nascimento, J.M.F. Nogueira, Anal. Chim. Acta 546 (2005) 11.
[13] A. Hoffmann, A. Heiden, E. Pfannkoch, Appl. Note Gerstel 4 (2000) 1.
[14] J. Marín, A. Zalacain, C. De Miguel, G.L. Alonso, M.R. Salinas, J. Chromatogr. A 1098 (2005) 1.
[15] M.R. Salinas, A. Zalacain, F. Pardo, G.L. Alonso, J. Agric. Food Chem. 52 (2004) 4821.
[16] A. Zalacain, G.L. Alonso, C. Lorenzo, M. Iñiguez, M.R. Salinas, J. Chromatogr. A 1033 (2004) 173.
[17] D.J. Caven-Quantrill, A.J. Buglass, J. Chromatogr. A 1117 (2006) 121.
[18] F. Luan, A. Mosandl, M. Gubesch, M. Wust, J. Chromatogr. A 1112 (2006) 369.
[19] Y.Z. Günata, C. Bayonove, R. Baumes, R. Cordonnier, J. Chromatogr. 331 (1985) 83.
[20] P. Ribéreau-Gayon, Y. Glories, A. Naujean, D. Dubourdieu, Handbook of Enology, vol. 2, Wiley, UK, 2000.
[21] E. Dimitriadis, P.J. Williams, Am. J. Enol. Viticult. 35 (1984) 66.
[22] H. Güth, J. Agric. Food Chem. 45 (1997) 3027.
[23] Y. Hayasaka, K. MacNamara, G.A. Baldock, R.L. Taylor, A.P. Pollnitz, Anal. Bioanal. Chem. 375 (2003) 948.
[24] P. Sandra, B. Tienpont, J. Vercammen, T. Tredoux, F. David, J. Chromatogr. A 928 (2001) 117.
[25] Catice, Centro de Asistencia Técnica e Inspección del Comercio Exterior, Ministerio de Economía y Hacienda, Spain, 2003.
[26] P.X. Etiévant, in: H. Marse (Ed.), Volatile Compounds in Foods and Beverages, Marcel Dekker Inc., New York, USA, 1991, pp. 483–587.

[27] V. Ferreira, R. López, J.F. Cacho, J. Sci. Food Agric. 80 (2000) 1659.
[28] P. Ribéreau-Gayon, J.N. Boidron, A. Terrier, J. Agric. Food Chem. 23 (1975) 1042.
[29] R. López, El aroma del vino tinto joven. Caracterización química y métodos de análisis de sus principales odorantes, PhD Thesis, Zaragoza, Spain, 1999.
[30] P. Winterhalter, R. Rouseff, in: P. Winterhalter, R. Rousseff (Eds.), Carotenoid-derived Aroma Compounds, ACS Symposium Series 802, Washington, DC, 2002, pp. 1–79.
[31] I. Lukic, M. Banovic, D. Persuric, S. Radeka, B. Sladonja, J. Chromatogr. A 1101 (2006) 238.
[32] P. Dubois, Rev. Fr. Oenol. 145 (1994) 27.
[33] R. Cordonnier, Rev. Oenol. S 53 (1989) 25.
[34] R. Cordonnier, C. Bayonove, Parfums Cosmet Arômes 24 (1978) 67.
[35] M.A. Pozo-Bayon, E. Pueyo, P.J. Martin-Alvarez, M.C. Polo, J. Chromatogr. A 922 (2001) 267.
[36] P. Guedes de Pinho, A.C. Silva-Ferreira, M. Mendes, J. Gomez, T.A. How, J. Agric. Food Chem. 49 (2001) 5484.
[37] P. Schreier, Chromatographic Studies of Biogenesis of Plant Volatiles, Ed. Huething, Heidelberg, 1994.
[38] S. Bureau, R.L. Baumes, A.J. Razungles, J. Agric. Food Chem. 48 (2000) 1290.
[39] A. Razungles, C. Bayonove, R.E. Cordonnier, Am. J. Enol. Viticult. 39 (1988) 44.
[40] K.W.O. Wenzel, S. Afr. J. Agric. Sci. 11 (1968) 273.
[41] C. Bayonove, in: C. Flanzy (Ed.), Enología: Fundamentos Científicos y Tecnológicos, AMV Ediciones, Mundi-Prensa, Madrid, Spain, 2003, pp. 137–146.
[42] L. Castro, M.S. Pérez-Coello, M.D. Cabezudo, Anal. Chim. Acta 458 (2002) 39.
[43] A. Escudero, B. Gogorza, M.A. Melús, N. Ortín, J. Cacho, V. Ferreira, J. Agric. Food Chem. 52 (2004) 3516.
[44] A. Razungles, A. Günata, S. Pinatel, R. Baumes, C. Bayonove, Sci. Aliments 13 (1993) 59.
[45] E. Boido, A. Lloret, K. Medina, L. Fariña, F. Carrau, G. Versini, E. Dellacassa, J. Agric. Food Chem. 51 (2003) 5408.

Available online at www.sciencedirect.com
ScienceDirect
Talanta 71 (2007) 1594–1598
Talanta
www.elsevier.com/locate/talanta

Stripping voltammetry of silver ions at polythiophene-modified platinum electrodes

H. Zejli [a,b,*], J.L. Hidalgo-Hidalgo de Cisneros [c], I. Naranjo-Rodriguez [c], K.R. Temsamani [a]

[a] *Equipe de Recherche Bioelectrochemie et Systèmes Interfaciaux, University Abdelmalek Essaadi, Morocco*
[b] *Medical Bioinorganic Chemistry Laboratory, University Paul Sabatier, France*
[c] *Department of Analytical Chemistry, Faculty of Sciences, University of Cádiz, Spain*

Received 12 February 2006; received in revised form 15 July 2006; accepted 24 July 2006
Available online 11 October 2006

Abstract

The present work describes the development of a modified platinum electrode for stripping voltammetric determination of silver. The deposition of films based on electropolymerisation of the monomer thiophene was carried out by cycling the potential towards positive values between 0 and 1.6 V.

The preconcentration process of silver ions was initiated on the surface of the modified electrode by complexing silver with polythiophene (PTH) when a negative potential (−0.5 V) was applied; then the reduced products was oxidized by means of differential pulse stripping voltammetry and the peak was observed at 0.17 V. Parameters such as pH, supporting electrolyte and number of electropolymerisation cycles were studied. A linear relation between current peak and concentration of Ag(I) was obtained in the range 0.07–1.0 mg L^{-1}. The detection limit for Ag(I) was evaluated to be 0.06 mg L^{-1}. The reproducibility was tested carrying out 11 measurements at different electrodes and the relative standard deviation was 1.5%. The interference of several metals was investigated and showed negligible effect on the electrode response.

Keywords: Polylthiophene-modified electrode; Silver ion monitoring; Stripping voltammetry

1. Introduction

The polymer film deposition can be considered as one of the most versatile approaches for preparing chemically modified electrodes. The electropolymerisation of heteroaromatic compounds at electrodes surfaces has become one of the more effective ways to produce chemically modified electrodes with electrical conductivity. Among the various conducting polymers, polypyrrole (Ppy) is one of the most frequently investigated; it can be easily prepared by electrochemical oxidation of the pyrrole monomers [1] but the species loaded on a Ppy electrode surface containing chemically active counter-ions are difficult to remove resulting in poor reusability [2]. Wong at al. have reported the voltammetric extraction of silver species with Ppy film that had undergone a base–acid treatment but this was time consuming [3]. Song and Shiu found that silver species could be determined with Ppy film modified glassy carbon electrodes, but copper and mercury were also extracted onto Ppy film electrodes and caused significant interference in the determination of silver species. The Ppy electrode exposed to a binary mixture of silver and mercury showed only a large anodic peak at 0.53 V. According to the authors, this might be due to the reduction of both silver and mercuric ions at Ppy film to form the silver amalgam Ag(Hg) and simultaneous stripping of the two elements at the same potential during the anodic process [4]. Besides Ppy, the sulphur-containing polymers such as polythiocrown-ether, and poly-3-methylthiophene [5,6] are mostly used as modifiers for heavy metal due to their high affinity for different species. Some analytical technique have been employed in metal analysis, such as atomic absorption spectrometry (AAS) [7], X-ray fluorescence [8], UV-spectrophotometry [9], inductively coupled plasma atomic emission spectrometry (ICP–AES) [10] and inductively coupled plasma mass spectrometry (ICP–MS) [11]. These techniques, commonly used for trace measurement of heavy metal in the laboratory, are not suitable for the task of in situ testing and monitoring. Electrochemical methods are between the most favourable techniques for the determination of heavy metal ions because of its low cost, high sensitivity easy operation and the ability for carry out speciation analysis.

* Corresponding author.
E-mail address: zejlih@yahoo.fr (H. Zejli).

0039-9140/$ – see front matter © 2006 Elsevier B.V. All rights reserved.
doi:10.1016/j.talanta.2006.07.052

In this paper, we present results of detecting Ag(I) at a polythiophene (PTH)-modified platinum electrode by an electrochemical controlled release of silver in 0.2 M KNO_3 solution. This method features fast experimentation time, good suitability for field trace silver analysis and an acceptable electrode lifetime. Analytical performances of the method and the PTH/Ag interaction were investigated using cyclic voltammetry (CV), differential pulse anodic stripping voltammetry (DPASV), scanning electron microscopy (SEM) coupled to energy-dispersive analysis of X-ray (EDAX) and electrochemical impedance spectroscopy (EIS).

2. Experimental

2.1. Reagents and materials

Thiophene (98%), dithizone, Nafion, 2,3-dibromthiophene, pyrrole, acetonitrile (HPLC grade) and tetrabutylammonium hexafluorophosphate (TBAHFP) were obtained from Aldrich (Steinheim, Germany). $AgNO_3$, $Cr(NO_3)_3$, $Cd(NO_3)_2$, $CuSO_4$, $ZnCl_2$, $FeCl_3$, $Ni(NO_3)_2$ and $K_2Cr_2O_7$ were all purchased from Riedel de Haen (Germany). Supporting electrolyte KNO_3 was from Panreac (Barcelona, Spain). All other chemicals used were of reagent grade. Solutions were prepared using deionised doubly distilled water with a measured resistance less than 15 $\mu S\,cm^{-1}$. Nitrogen (98%) used to purge electrochemical reaction media was obtained from Air Liquide (France).

2.2. Voltammetric techniques

All the electrochemical measurements were performed with an Autolab PGSTAT20 (Ecochemie, Utrecht, The Netherlands). The experiments were carried out in a three-electrode cell of 25 mL at room temperature (298 K) under nitrogen atmosphere; the counter electrode was a platinum wire (0.3 mm) and a Ag/AgCl, 3 M KCl electrode was used as the reference. A platinum electrode (0.35 mm i.d.) was used as the working electrode; its surface was polished with 0.5 μm alumina powder and then cleaned by ultrasonication prior to polymer electropolymerisation. Differential pulse anodic stripping voltammetry and cyclic voltammetry were the electrochemical techniques applied to study the behaviour of the modified platinum electrode. Instrumental parameters for DPASV were as follow: pulse amplitude ±60 mV, pulse repetition time 0.4 s, modulation time 0.06 s; a preconcentration potential of −0.5 V was applied for 2 min under stirring and a rest period of 5 s, followed by a potential scan from 0 to 0.7 V. Cyclic scan for CV were carried out between −0.25 and 1.25 V at a scan rate of 100 $mV\,s^{-1}$. After each measurement, the cleaning of the modified electrode was carried out by application five cycles of a potential scan from −1 to 1 V.

2.3. Preparation of the polythiophene-modified platinum electrode

The electropolymerisation of PTH was carried out as described previously [12], with the following modifications: the polymer synthesis was realized at 273 K in a cell containing deaerated acetonitrile, 0.01 M TBAHFP and 0.1 M thiophene. The synthesis was initiated by CV, scanning toward positive potentials from 0 to 1.6 V at a scan rate of 100 $mV\,s^{-1}$. After electrosynthesis, the PTH films were kept for a few minutes at a reducing potential, in contact with the original electrolyte anion, for undoping.

2.4. Scanning electron microscopy (SEM) measurements

To carry out these measurements, the microscope, a JSM 5400 type (JEOL, Japan), was coupled to the analyser, a link type with a Si/Li detector and an ultra thin window. The PTH film electrode were washed then dried; the films were then introduced into a high vacuum system before application of electron beam.

2.5. Electrochemical impedance spectroscopy measurements

The electrochemical impedance spectroscopy (EIS) measurements were performed with a Voltalab 100 type PGZ 10 from Radiometer. The impedance spectra were set up as described previously [13]. The initial frequency used was 100 KHz and the final one was 4 mHz with an ac amplitude of 10 mV. In order to insure the inert effect of PTH electrode during the experiment, a potential of 0.8 V was chosen.

3. Results and discussion

3.1. Cyclic voltammetry

Cyclic voltammograms of a modified electrode in absence of Ag(I), as well as those of a bare platinum electrode and a modified electrode, both in presence of Ag(I), were carried out. Neither the bare platinum electrode in presence of Ag(I) nor the modified electrode in absence of the ion, exhibited detectable peaks. On the other hand, when a modified electrode is dipped into a solution containing silver ion, a sharp anodic peak at around 0.15 V are observed. These results indicate the accumulation of Ag on the surface of the modified electrode, as consequence of a complexing interaction between silver ions and the polymer, that has been well described in literature [4,5], following by reduction of entrapped silver(I). The inductive effect of the C–S dipole, that makes the sulphur very reactive toward positively charged species, is one of the factors that explains the different behaviour of the polythiophene-modified electrode and the bare platinum electrode.

3.2. DPASV measurements

In order to explore the analytical performances of our system, the PTH electrode was immersed in a cell containing 0.2 M KNO_3 at pH 5. Ten microliters of a solution of 100 $mg\,l^{-1}$ Ag(I) was injected and a scan from 0 to 0.7 V was carried out. The modulation time was 0.06 s, the interval time was 0.4 s; a preconcentration potential of −0.5 V was immediately applied during 2 min under stirring followed by a rest period of 5 s. The

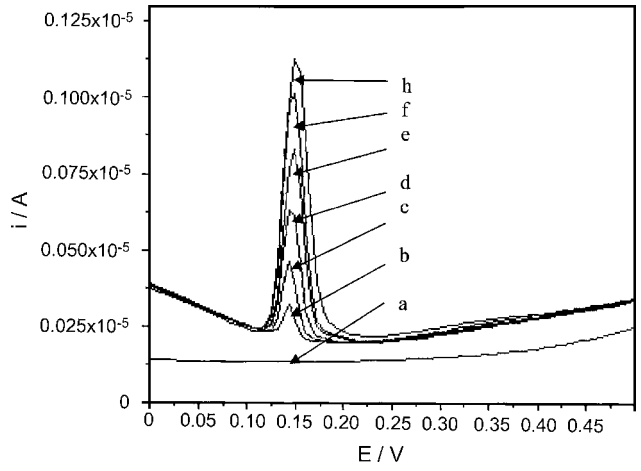

Fig. 1. DPASV response of the PTH-modified electrode in a solution of Ag(I); the concentration of the silver solution varies as follows: (a) supporting electrolyte; (b) 0.07; (c) 0.14; (d) 0.21; (e) 0.28; (f) 0.35; (h) 0.49 mg L^{-1}. Supporting electrolyte 0.2 M KNO_3 at pH 5.

stripping of silver(I) by a reoxidation process can be observed at 0.17 V thanks to the characteristic of the heavy metal anodic peaks. Fig. 1 shows the DPASV voltammograms obtained when increasing Ag(I) concentrations from 0.07 to 0.49 mg l^{-1}.

3.3. Influence of modifier and pH

The effect on the signal of Ag(I) of several polymers such as polypyrrole, polythiophene, Nafion, polydibromothiophene and dithizone, used as modifiers in the same conditions, were explored. PTH showed the higher peak current, consequently it was chosen to continue the studies.

The pH effect of the supporting electrolyte on the voltammetric behaviour of the PTH films versus Ag(I) species, was also investigated. Table 1 summarizes the results.

It clearly appears from these results that pH of supporting electrolyte plays an important role in the voltammetric response of the silver. Between pH 2 and 4 the peak of oxidation increased and reached a maximum value around pH 5; above pH 6 the peak height rapidly decreased, probably due to hydrolysis of the cation. Consequently, pH 5 was selected to carry out the determination. Finally it should be taken into consideration that hydrogen bonding between silver(I) and the sulphur atoms might also play a role in the electrochemical reduction of the cation.

Table 1
Effect of pH on the voltammetric response of the PTH-modified electrode

pH	I (A)
2	5.60×10^{-7}
3	7.00×10^{-7}
4	9.08×10^{-7}
5	1.04×10^{-6}
6	9.05×10^{-7}
7	7.05×10^{-7}
8	7.02×10^{-7}
9	6.59×10^{-7}
10	4.95×10^{-7}

Supporting electrolyte 0.2 M KNO_3; Ag(I) concentration 0.63 mg L^{-1}.

3.4. Calibration, reproducibility, detection limit and electrode stability

The reduction peak of the entrapped Ag(I) showed in the cyclic voltammogram of Fig. 1 was the signal used to determine the ion in solution. A calibration plot was carried out under the optimised conditions already described. A linear correlation between the concentration of Ag(I) and peak current for the range 0.07–1 mg L^{-1} was found, with a regression equation of $I_P = 3 \times 10^{-6} C - 2 \times 10^{-7}$ and a correlation coefficient, R^2, of 0.995. The test of reproducibility for 11 measurements of solutions containing a 0.63 mg L^{-1} concentration of Ag(I), carried out with electrodes polymerised each time, gave a relative standard deviation of 1.5%. Furthermore, there was no obvious deterioration of the electrodes during at least 2 weeks of successive operations. The detection limit, statistically calculated of the calibration plot as the concentration whose intensity is the intensity of the blank plus three times the standard deviation of the blank [14], was 0.06 mg L^{-1}. Such performance indicates that the modified electrode is very stable and reproducible and with a high response in addition with an easy and low cost preparation.

3.5. Study of interferences

The effect of several common metal ions on the Ag(I) signal was investigated. All the cations were submitted to the same preconcentration procedure described above; the scan in this occasion was realized from −1 to 0.75 V. The PTH-modified platinum electrode was immersed in a cell containing the support electrolyte and the procedure was run; then a standard addition of a solution containing Cr(III), Cd(II), Cu(II), Zn(II), Fe(III), Ag(I), Pb(II), Ni(II) (0.63 mg L^{-1} each) was done and the procedure again run. Fig. 2A shows the voltammogram of the

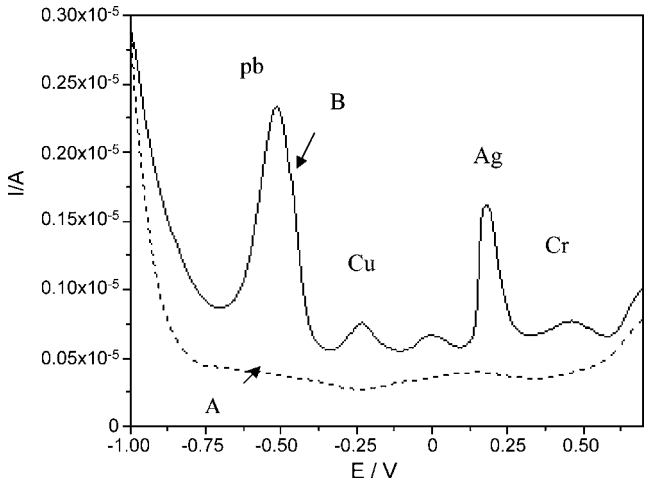

Fig. 2. DPASV on a PTH-modified electrode (A) solution of KNO_3 (0.2 M) supporting electrolyte; (B) solution containing a mixture of Cd(II), Cr(III), Cr(VI), Zn(II), Ni (II), Fe(III), Cu(II), and Ag(I) (0.63 mg L^{-1} each).

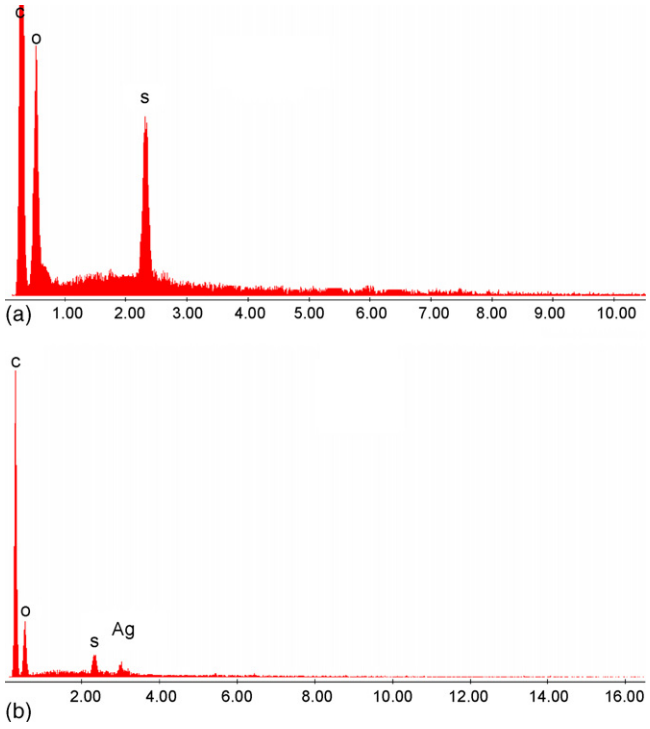

Fig. 3. EDAX spectra of (a) PTH film; (b) PTH film after being in contact with silver.

support electrolyte. Several well defined and separated peaks are observed in Fig. 2B; one of them can be attributed to silver (as compared to pure Ag(I) experiment) and another peaks attributed to other metals, but the values of their E_P are far from the position of Ag(I). This results clearly show the great selectivity of the modified electrode, which could be used to determine Ag(I) in waters without any harmful interference from other common metal ions.

3.6. SEM–EDAX measurements

To verify and confirm the silver presence in our polymer films, EDAX measurements were performed on both the silver-free and -containing PTH films. Fig. 3a shows the EDAX spectrum of the PTH film. As can be seen, no silver is detected in the film under the equipment sensitivity range. As expected, we can notice in the EDAX spectra a significant amount of sulphur coming from the thiophene structure of the PTH. On the other hand, Fig. 3b clearly shows silver content in the spectra of the films previously put in contact with Ag(I). It seems probably due to the strong silver–sulphur atom interaction. Fig. 4 is a scanning electron micrograph picture of the PTH film after exposure to a solution of Ag(I) 0.63 mg L^{-1}. It can be seen that the polymer maintains its regular and granular (porous) structure

3.7. EIS measurements

In order to confirm the mechanism suggested in the voltammetric part of this work regarding to the PTH/Ag(I) interaction, we have performed some EIS measurements. The impedance spectra (Fig. 5) were collected at 800 mV (versus SCE) in a frequency range from 100 to 4 mHz with an ac amplitude of 5 mV. The potential of 0.8 V was chosen in order to ensure the stability of the PTH/Ag(I) films during the measurements. Fig. 5a shows the Nyquist plot for the silver-free PTH-modified electrode. The high frequency arc observed may be associated to charge transfer at the PTH/solution interface. If we admit the Randel equivalent circuit model, the calculated (Voltamaster® 4.0 software) charge transfer resistance R_{ct} and the double layer capacitance C_d are, respectively: 38.92 kΩ cm^2 and 1 μF cm^{-2}. These data are typical of metal electrodes covered with polymeric films. On the other hand, Fig. 5b also exhibits an arc like Nyquist plot for the PTH/Ag(I) system. The electrical parameters calculated were: R_{ct} = 30.3 kΩ cm^2 and C_d = 1.3 μF cm^{-2}. It appears clearly from these data that the capacitance at the interface increases when the PTH film is exposed to Ag(I). The observed decrease of the charge transfer resistance means also that the modified electrode becomes more conductive which can be explained by the presence of silver on the electrode surface.

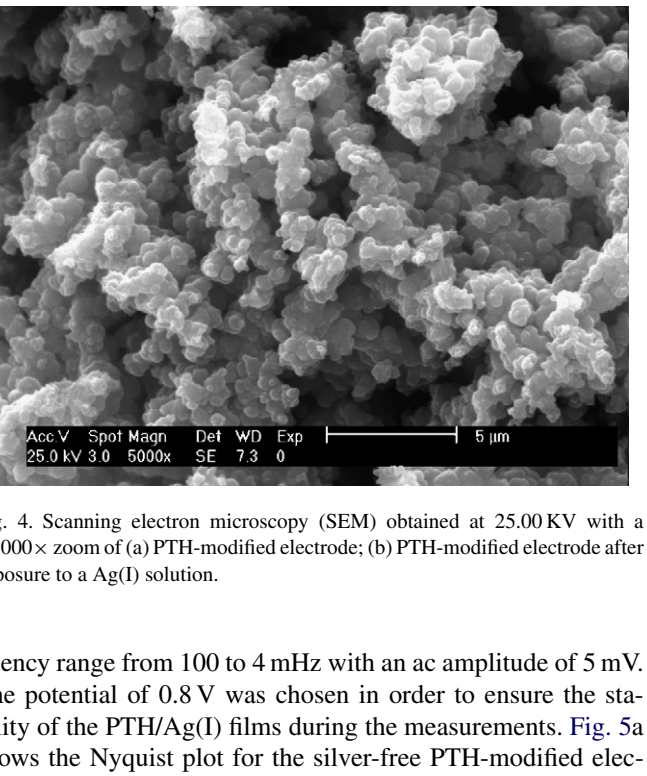

Fig. 4. Scanning electron microscopy (SEM) obtained at 25.00 KV with a 10,000× zoom of (a) PTH-modified electrode; (b) PTH-modified electrode after exposure to a Ag(I) solution.

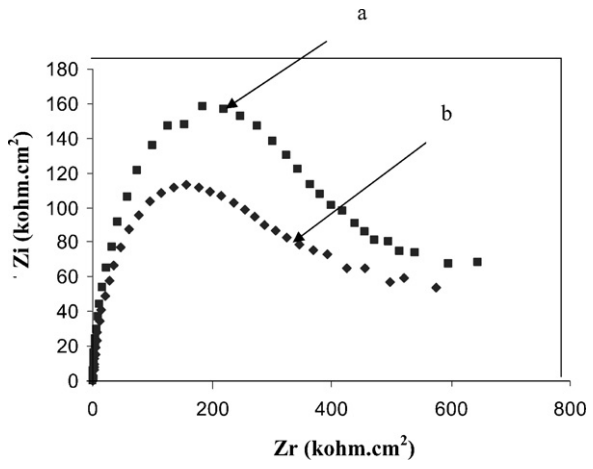

Fig. 5. Impedance spectra at 1000 V (vs. SCE): (a) PTH-modified electrode; (b) PTH/Ag(I).

3.8. Analysis of real samples

The analytical performance of the method was assessed by determination of silver in wastewaters, where possible interference due to complexity of the matrix can occurs. The samples were collected from four sites of the zone of Tangier, near to the places where the wastes were dumped: Oued El Kabire (S_1), Bay of Tangier (S_2), an industrial plant (S_3) and Malabata (S_4). The results were compared with those obtained by AAS; no silver was detected for samples S_1, S_2, S_4, as in electrochemical analysis; the concentration values obtained for sample S_3 by AAS ($0.11\,mg\,L^{-1}$) were similar than those obtained by electroanalysis ($0.12\,mg\,L^{-1}$), with a R.S.D. for the last technique of 1.9%.

4. Conclusion

The modified polythiophene platinum electrode proposed in this paper for the determination of ion silver shows good sensitivity and reproducibility and a great selectivity for Ag(I). Furthermore, it is of easy preparation, operation and regeneration, and can be used for more of 2 weeks of consecutive measurements. Its possibilities for field and on-site applications are being investigated.

Acknowledgements

We thank to the Agencia Española de Cooperación Internacional (AECI) for a grant to Hanane Zejli in the University of Cádiz, and to Mr. David Gómez, from the Institute of Polymer Science and Technology (CSIC, Madrid, Spain), for the SEM and EDAX results.

References

[1] M.D. Imisides, R. John, P.J. Riley, G. Wallace, Electroanalysis 3 (1991) 879.
[2] G.G. Wallace, Y.P. Lin, J. Electroanal. Chem. 247 (1988) 144.
[3] N.L. Pickup, J.S. Shapiro, D.K.Y. Wong, Anal. Chim. Acta 367 (1998) 41.
[4] F.Y. Song, K.K. Shiu, J. Electroanal. Chem. 498 (2001) 161–170.
[5] A.M. jiménz, J.C. Galvan, P. Ananda, Electrochim. Acta 47 (2002) 2281–2287.
[6] H. Zejli, P. Sharrock, J.L. Hidalgo-Hidalgo de Cisneros, I. Naranjo-Rodriguez, K.R. Temsamani, Talanta 68 (2005) 79–85.
[7] V.P.Y. Gadzekpo, P. Buhlman, K.P. Xiao, H. Aoki, Y. Umez, Anal. Chem. Acta 411 (2000) 343.
[8] I. Turgan, D. Mandler, Anal. Chem. 69 (1997) 894.
[9] I. Wittner, A. Riklin, Anal. Chem. 66 (1994) 1535.
[10] I.S. Krull, D.S. Bushee, R.G. Shleicher, S.B. Smith, Analyst 111 (1986) 345.
[11] C.F. Harrington, T. Catterick, J. Anal. Atom. Spectrom. 12 (1997) 1053.
[12] H.B. Mark Jr., N. Atta, Ma, Y.L. Pettiorew, K.L. Zimmer, H. ShiY, S.K. Lunsford, J.F. Rubinson, A. Galal, Bioelectrochem. Bioenerg. 38 (1995) 229.
[13] H. Zejli, N. Isoumen, D. Bouchta, M.E.L. Koutit, K.R. Temsamani, Anal. Lett. 37 (2004) 1737.
[14] H. Zejli, J.L. Hidalgo-Hidalgo de Cisneros, I. Naranjo-Rodriguez, K.R. Temsamani, Anal. Lett. 39 (2006) 1053–1063.

Available online at www.sciencedirect.com
ScienceDirect
Talanta 71 (2007) 1661–1668
Talanta
www.elsevier.com/locate/talanta

Determination of bioavailable fractions of Zn, Cu, Ni, Pb and Cd in soils and sludges by atomic absorption spectrometry

Mária Žemberyová *, Jana Barteková, Mária Závadská, Miriam Šišoláková

Comenius University in Bratislava, Faculty of Natural Sciences, Department of Analytical Chemistry, Mlynská dolina CH-2, 842 15 Bratislava, Slovak Republic

Received 23 February 2004; received in revised form 26 July 2006; accepted 27 July 2006
Available online 15 September 2006

Abstract

The single extraction procedures validated by the standards, measurement and testing programme (formerly BCR), extraction with 0.05 mol l^{-1} EDTA and 0.43 mol l^{-1} acetic acid, have been applied to reference materials of soils and sludges with certified total values of elements, in order to determine bioavailable contents of Cd, Cu, Ni, Pb and Zn. These soils, which represent uncontaminated pedologically different types of soils from Slovakia and sludges from city water treatment are characterized for the bioavailable fraction of the metals using the procedures followed by SM&T Programme. Concentrations of the elements under the study in the extracts were determined by flame (FAAS) using calibration curves in appropriate extractants and by electrothermal (ETAAS) atomic absorption spectrometry, using technique of standard additions for the evaluation of the results. The accuracy of the extraction procedures and determinations of the elements in the extracts was controlled using CRM 483 certified for EDTA- and acetic acid-extractable contents of Cd, Cu, Ni, Pb and Zn in sewage sludge amended soil.

Keywords: Single extraction; Zn, Cu, Ni, Pb, Cd; Soils; Sludges; Atomic absorption spectrometry; SM&T programme

1. Introduction

Considerable recent research effort in the field of environmental science has focused on the subject of chemical speciation. It is increasingly realized that the distribution, mobility and biological availability of chemical elements depend not simply on their concentrations but, critically, on the chemical and physical associations which they undergo in natural system. Changes in environmental conditions, whether natural or anthropogenic, can strongly influence the behaviour of both essential and toxic elements by altering the forms in which they occur [1,2]. Two different approaches are usually applied in speciation studies for solid samples: single and sequential extraction procedures [3–9]. Single step extraction procedures are mainly applied to soil samples to identify the "bioavailable" fraction, using a number of different reagents able to extract all, or part of the metals from soil [10–13]. The standards, measurements and testing programme—SM&T (formerly BCR) of the European Commission organized intercomparisons on determination of extractable trace elements [14]. The results showed that the most suitable approach for certification of a soil sample was a single step procedures using EDTA/acetic acid to characterize the bioavailable fraction of metals [15,16].

In the present contribution we utilized the single step extraction procedures recommended by SM&T, extraction with 0.05 mol l^{-1} EDTA and 0.43 mol l^{-1} acetic acid to three pedologically different soil reference materials Soil Eutric Cambisol; Soil Orthic Luvisols and Soil Rendzina, which represent basic soil types of Slovakia and are certified for total contents of the studied elements. The determined values of bioavailable copper, nickel, lead, cadmium and zinc in the studied soils could be recommended as indicative values for the similar types of soil for purposes of hygienic and soil laboratories. Copper in EDTA extracts and zinc in acetic acid and EDTA extracts could be determined by flame atomic absorption spectrometry (FAAS), but the technique proved to be insufficiently sensitive for the determination of copper in acetic acid extracts and nickel, lead, cadmium in both used extracts. Electrother-

* Corresponding author. Tel.: +421 2 60296309; fax: +421 2 60296706.
E-mail address: zemberyova@fns.uniba.sk (M. Žemberyová).

0039-9140/$ – see front matter © 2006 Elsevier B.V. All rights reserved.
doi:10.1016/j.talanta.2006.07.055

mal atomic absorption spectrometry was therefore applied for the determination of the mentioned analytes in acetic acid and EDTA extracts. Furnace conditions were optimized and matrix interferences could be overcome by the use of matrix modifier and analysing of the soil extracts by the technique of standard addition.

Determination of plant available contents of heavy metals in sewage sludges has received an increasing attention, since their agricultural use as fertilisers requires a strict information about the metal composition of the samples [17–19]. The mentioned single extraction procedures were applied to different sludges from city water treatment WT-L, WT-M and WT-H with the aim to study the leaching behaviour of the metals and also to predict their possible mobility when the sludges are disposed on the environment.

The accuracy of the heavy metal determinations based on the well-defined extraction procedures was verified using CRM 483, certified for EDTA- and acetic acid-extractable contents of Cd, Cu, Ni, Pb and Zn in sewage sludge amended soil. The choice of the CRM helps us to check the accuracy of the determination of the analytes in matrices of the reference materials of soils and sludges.

2. Materials and methods

2.1. Instrumentation

The system used for the measurements was a Perkin-Elmer atomic absorption spectrometer model 1100 B (Norwalk, Connecticut, USA) equipped with deuterium background correction and HGA 700 graphite furnace with automated sampler AS-70. The graphite tubes (Part No. 070699) and pyrolytically coated tubes (Part No. 137111) were used. A KS 125 basic IKA-shaker (IKA Labortechnik, Germany) and a K70D centrifuge (MLW, Germany) were used for extraction procedures and centrifugation. pH meter PHM 64 (Radiometer Copenhagen, Denmark) and analytical balances Sartorius 1702 (Germany) were used for another analytical procedures. PRO-PS Labconco (Kansas City, KS, USA) was used for producing of deionized water.

2.2. Reagents and standards

2.2.1. Extraction reagents

0.05 mol l^{-1} ethylenediamine tetraacetic acid (EDTA) as an ammonium salt. This is prepared by mixing 14.61 ± 0.05 g EDTA (free acid) with 80 ± 2 ml distilled water and dissolving by stirring in approximately 13 ml of ammonia solution until all the EDTA has dissolved. The filtered solution is adjusted to pH 7.00 ± 0.05 by addition of hydrochloric acid or ammonia.

0.43 mol l^{-1} acetic acid. This is prepared by adding, in a fume cupboard, 25 ml Suprapur grade glacial acetic acid to about 1 l of distilled water and making up to 1 l volume.

2.2.2. Calibration standards and modifiers

To prepare calibration solutions, aliquots were taken from stock standards solutions (1000 mg l^{-1} of Zn, Cu, Ni, Pb, Cd, E. Merck, Darmstadt, Germany). Standard solutions for FAAS sample analyses were prepared in appropriate extractants, for ETAAS in 0.2% HNO_3 (v/v). $NH_4H_2PO_4$ (0.2 mg) was used as matrix modifier for determination of Pb and Cd by ETAAS.

2.3. Working conditions

Two techniques of atomic absorption spectroscopy for determination of the selected elements were used:

FAAS—flame atomic absorption spectroscopy. A fuel–lean air–acetylene flame was used; acetylene flow rate 2.5 l min^{-1}, air flow rate 8.0 l min^{-1}.

ETAAS—electrothermal atomic absorption spectrometry. The instrumental conditions were optimized (pyrolysis and atomization temperatures were derived from the pyrolysis and atomization curves) for the standard solutions and soil extracts in the case of Cd and Pb without and in the presence of matrix modifier $NH_4H_2PO_4$ (Table 1).

2.4. Samples

The different types of soil reference materials (according to the FAO classification) [20] with certified total values of the elements, S-VM No. 12-1-07 Soil Eutric Cambisol (Hills of Medzev near the town Kosice), S-MS No. 12-1-08 Soil Orthic

Table 1
Measurement conditions for FAAS and ETAAS

Instrumental conditions	Cu	Ni	Pb	Cd	Zn
Wavelength (nm)	324.8	232.0	283.3	228.8	213.7
Lamp intensity (mA)	15	25	10	6	20
Slit-width (nm)	0.7	0.2	0.7	0.7	0.7
Programme of temperature					
Drying 1	90/10/20[a]	90/10/20	90/10/20	90/10/20	
Drying 2	130/20/25	130/20/20	130/20/20	130/20/25	
Pyrolysis 1	200/20/20	200/20/20	300/20/20	200/20/25	
Pyrolysis 2	900/20/35	1000/20/30	700/20/30	700/20/35	
Atomization	2000/0/3	2300/0/3	2000/0/3	2000/0/3	
Matrix modifier	No	No	$NH_4H_2PO_4$, 0.2 mg	$NH_4H_2PO_4$, 0.2 mg	
Type of signal	Peak area	Peak area	Peak area	Peak area	

[a] Temperature (°C)/ramp time (s)/hold time (s).

Table 2
Certified and recommended total values of the studied and major elements in the reference materials of the soils S-SP, S-MS, S-VM [20]

Element	S-SP content (μg g^{-1})		S-MS content (μg g^{-1})		S-VM content (μg g^{-1})	
	CV	CI	CV	CI	CV	CI
Al[a,b]	7.48		5.76		8.96[b]	
Ca[a]	6.34	6.09–6.59	0.49[b]		0.692[b]	
Fe[a]	3.73	3.55–3.92	2.70	2.59–2.81	3.73	3.56–3.89
K[a]	2.63	2.41–2.86	1.85	1.74–1.95	3.08	2.89–3.27
Mg[a,b]	1.19		0.627		0.593	
Mn	734	700–768	910	876–945	897	853–942
Na[a,b]	0.446		0.807		0.321	
P[b]	1370		1010		1350	
Si[a,b]	20.4		31.4		24.8	
Zn	119	112–125	63.7	59.5–67.8	88.8	85.6–92.1
Cu	30.9	29.1–32.8	21.2	19.5–22.9	30.0	27.9–32.1
Ni	37.4	34.2–40.7	40.0	37.5–42.5	30.8	28.7–32.9
Pb	41.3	36.9–45.7	18.9	16.7–21.2	19.6	17.5–21.8
Cd	0.285	0.226–0.343	0.198	0.169–0.227	0.214	0.176–0.253

CV: certified value; CI: confidence interval (95%).
[a] Values in %.
[b] Indicative values.

Luvisols (Interhill of Saris near the town Presov), S-SP No. 12-1-09 Soil Rendzina (Plateau of Silica near the town Roznava) and reference materials of sludges from city water treatment with certified total values of the elements: WT-L; WT-M; WT-H [21] produced by the Institute of Radioecology and Applied Nuclear Techniques, Kosice, Slovakia, were used for this study.

Certified and recommended total values of the studied and major elements in the reference materials of the soils S-SP, S-MS, S-VM are in Table 2 and of the sludges from city water treatment WT-L; WT-M; WT-H are in Table 3.

Certified reference material of sewage sludge amended soil. CRM 483 (BCR, Brussels), with the certified EDTA- and acetic acid-extractable contents of Cd, Cu, Ni, Pb and Zn, was used to verify the accuracy of the determinations based on the extraction procedures for the elements.

2.5. Extraction procedures

Extraction protocols were used according procedure described in report EUR 17127 [15] 2 g of soil (sludge) was transferred to an extraction bottle in which 20 ml of 0.05 mol l^{-1} EDTA was added. The obtained mixture was shaken on a shaker operating at 300 motions min^{-1} for 1 h in a room at 20 °C. For acetic acid extraction 1 g of soil (sludge) was transferred to an extraction bottle in which 40 ml of 0.43 mol l^{-1} acetic acid was added. The mixture was shaken for 16 h (overnight) by 300 motions min^{-1} in a room at 20 °C. The extracts were immediately filtered through a filter paper Whatman 42 previously rinsed with extractants. The extraction was performed in PTFE bottles. All laboratory glassware was cleaned with HNO_3 and rinsed with distilled water.

Table 3
Certified and recommended total values of the studied and major elements in the reference materials of the sludges WT-L, WT-M, WT-H [21]

Element	WT-L content (μg g^{-1})		WT-M content (μg g^{-1})		WT-H content (μg g^{-1})	
	CV	Uncertaity A	CV	Uncertaity A	CV	Uncertaity A
Al[a]	3.03	0.13	2.61	0.12	2.51	0.14
Ca[a]	8.80	0.35	5.15	0.16	4.83	0.16
Fe[a]	1.70	0.11	1.74	0.08	1.70	0.09
K[a]	0.695	0.15	0.589	0.040	0.582	0.049
Mg[a]	0.781	0.049	0.613	0.041	0.570	0.048
Mn	390	15	942	34	3660	163
Na[a,b]	0.414	0.109	0.303	0.072	0.282	0.075
P[a]	0.881	0.029	1.58	0.07	1.44	0.04
Si[a]	11.1	0.6	8.37[b]	1.36	8.20[b]	1.23
Zn	1310	40	3080	100	6360	140
Cu	136	7	959	32	3140	120
Ni	32.0	2.3	240	9	1140	50
Pb	122	7	841	46	2290	90
Cd	1.97	0.21	11.9	0.3	54.7	2.3

CV: certified value; uncertaity of Type A.
[a] Values in %.
[b] Indicative values.

Table 4
Comparison of calibration slopes of Zn and Cu in acetic acid extracts and Cu in EDTA extracts of soils using technique of standard addition and calibration curve for FAAS determination

Element/soil	Slopes				Difference in slopes (%)	
	Calibration curve		Technique of standard addition		EDTA	Acetic acid
	EDTA	Acetic acid	EDTA	Acetic acid		
Zn						
S-SP	0.186	0.206	0.195	0.198	+4.84	−3.88
S-VM	0.186	0.206	0.194	0.211	+4.30	+2.43
S-MS	0.186	0.206	0.193	0.209	+3.76	+1.46
Cu[a]						
S-SP	0.045		0.044		−2.22	
S-VM	0.045		0.046		+2.22	
S-MS	0.045		0.046		+2.22	

[a] FAAS only for the determination of Cu in EDTA extracts of soils was used.

3. Results

EDTA- and acetic acid-extractable contents of Cu, Ni, Pb, Cd and Zn were determined in different types of Slovak reference materials of soils and sludges.

Because the extractable major elements of soils and sludges could be a possible source of interferences by the trace element determinations, the method of calibration curve and the standard addition technique were critically compared in this work for both, flame atomic absorption technique and electrothermal atomic absorption spectrometry. Zinc contents in the acetic acid and EDTA extracts and copper contents in the EDTA extracts were determined by flame atomic absorption technique and the results were evaluated from calibration curves prepared in the used extractants and by the standard addition technique. Differences in plots obtained by the standard addition technique and calibration curve measurement modes are given in Table 4. In this case the differences in slopes between the calibration curves and standard addition technique, obtained for Zn determined in acetic acid and EDTA extracts by FAAS, and Cu in EDTA extracts were within ±5% of each other, so evaluation using calibration curves in appropriate extractants because of unsignificant matrix interferences could be recommended for FAAS method.

Since FAAS was insufficiently sensitive, except for the determination of zinc in EDTA and acetic acid extracts and copper in EDTA extracts, ETAAS was used for the determination of copper in acetic acid extracts, nickel, lead and cadmium in EDTA and acetic acid extracts. The optimal decomposition and atomization

Table 5
Comparison of calibration slopes of Cu, Ni, Pb, Cd in EDTA and Ni, Pb, Cd in acetic acid extracts of soils using technique of standard addition and calibration curve for ETAAS determination

Element/soil	Slopes			Difference in slope (%)	
	Calibration curve, 0.2% HNO_3 ($\times10^{-2}$)[a]	Technique of standard addition		EDTA	Acetic acid
		EDTA ($\times10^{-2}$)[a]	Acetic acid ($\times10^{-2}$)[a]		
Cu[b]					
S-SP	1.70		1.63		−4.12
S-VM	1.70		1.67		−1.76
S-MS	1.70		1.68		−1.18
Ni					
S-SP	0.510	0.620	0.560	+21.6	+9.80
S-VM	0.510	0.605	0.585	+18.6	+14.7
S-MS	0.510	0.585	0.605	+14.7	+18.6
Pb					
S-SP	0.310	0.280	0.290	−9.68	−6.45
S-VM	0.310	0.250	0.285	−19.4	−8.06
S-MS	0.310	0.240	0.270	−22.6	−12.9
Cd[a]					
S-SP	0.287	0.238	0.266	−17.1	−7.32
S-VM	0.287	0.243	0.233	−15.3	−18.8
S-MS	0.287	0.246	0.249	−14.3	−13.2

[a] ($\times10^{-2}$) except of Cd.
[b] ETAAS only for the determination of Cu in acetic acid extracts of soils was used.

Table 6
Analyte contents[a] ($\mu g\,g^{-1}$) in 0.05 mol l^{-1} EDTA and 0.43 mol l^{-1} acetic acid extract solutions of soil samples

Soil	EDTA extracts				Acetic acid extracts			
	Calibration curve		Technique of standard addition		Calibration curve		Technique of standard addition	
	Mean ± S.D.	R.S.D. (%)	Mean ± S.D.	R.S.D. (%)	Mean ± S.D.	R.S.D. (%)	Mean ± S.D.	R.S.D. (%)
Zn								
S-SP	5.1 ± 0.2	3.13	5.3 ± 0.3	4.75	5.3 ± 0.2	3.77	5.7 ± 0.2	3.67
S-VM	3.3 ± 0.1	3.96	3.7 ± 0.3	11.0	3.7 ± 0.1	3.92	3.6 ± 0.2	5.32
S-MS	2.17 ± 0.06	2.80	2.4 ± 0.3	7.50	2.0 ± 0.1	5.00	2.2 ± 0.2	7.38
Cu								
S-SP	4.07 ± 0.06	1.42	4.88 ± 0.07	1.48	0.231 ± 0.007	3.03	0.282 ± 0.010	3.55
S-VM	7.0 ± 0.4	5.71	7.7 ± 0.3	3.60	1.19 ± 0.03	2.71	1.28 ± 0.05	3.91
S-MS	4.1 ± 0.1	2.44	4.7 ± 0.1	2.25	0.67 ± 0.07	9.99	0.72 ± 0.06	7.66
Ni								
S-SP	0.79 ± 0.04	5.13	0.96 ± 0.04	3.63	2.46 ± 0.04	1.43	2.3 ± 0.1	5.24
S-VM	0.789 ± 0.008	0.95	1.07 ± 0.03.	2.62	1.37 ± 0.04	2.63	1.24 ± 0.04	3.22
S-MS	3.4 ± 0.2	5.97	3.5 ± 0.1	3.39	3.64 ± 0.09	2.34	3.2 ± 0.1	3.12
Pb								
S-SP	6.1 ± 0.2	3.37	7.27 ± 0.02	2.48	0.68 ± 0.02	2.22	0.75 ± 0.01	1.60
S-VM	6.0 ± 0.2	3.66	7.1 ± 0.2	2.81	0.56 ± 0.01	2.31	0.64 ± 0.02	2.34
S-MS	5.5 ± 0.1	2.31	6.7 ± 0.1	1.65	0.311 ± 0.003	1.11	0.37 ± 0.01	2.72
Cd								
S-SP	0.128 ± 0.002	1.56	0.178 ± 0.003	1.69	0.133 ± 0.002	1.57	0.163 ± 0.008	4.91
S-VM	0.123 ± 0.006	4.47	0.177 ± 0.005	2.82	0.125 ± 0.002	1.39	0.161 ± 0.003	1.86
S-MS	0.109 ± 0.002	1.41	0.138 ± 0.004	2.90	0.10 ± 0.01	11.5	0.146 ± 0.006	4.11

[a] Data are expressed as mean ± S.D. The number of extraction procedures replicates $n = 4$.

temperatures found for ETAAS determination of the elements in the extract solutions are in Table 1. For the determination of Cd and Pb in acetic acid and EDTA soil extracts the presence of 0.2 mg of $NH_4H_2PO_4$ as matrix modifier was used. Similarly using ETAAS technique for the determination of Cu in EDTA extract and Ni, Pb and Cd in EDTA and acetic acid extracts, matrix interference effects associated with the soil components extracted by acetic acid and EDTA were investigated by comparison of the method of calibration curves and the standard addition technique as well.

Differences in plots obtained by the standard addition technique and calibration curve measurement modes are given in Table 5. Besides of copper in acetic acid extracts, the differences in slopes of all the elements under the study determined by ETAAS are higher than ±5%, so the use of standard addition technique is recommended.

However, in order to increase the robustness of the method and reduce variations among the different types of soil samples and among laboratories which may employ single extraction procedures in the study of different soil matrices, it may be preferable to use the technique of standard additions in all cases.

Determined analyte contents in 0.05 mol l^{-1} EDTA and 0.43 mol l^{-1} acetic acid soil extracts using calibration curves and the technique of standard addition are in Table 6. The partitioning of analytes studied in extracts (%) comparing to the total contents (100%) is shown in Fig. 1.

The measurement conditions mentioned above for the soil extracts were also used for the extracts of sludges.

The acetic acid- and EDTA-extractable contents of Cu, Ni, Cd, Pb and Zn in reference materials of sludges were determined by FAAS and evaluated using calibration curves in appropriate extractants.

Determined analyte contents in 0.05 mol l^{-1} EDTA and 0.43 mol l^{-1} acetic acid extracts of sludges using calibration curves are in Table 7. The partitioning of analytes studied in extracts (%) comparing to the total contents (100%) is shown in Fig. 2.

The quality control of the determination of Cu, Ni, Pb, Cd and Zn Based on the well-defined extraction procedures was verified using the certified reference material CRM 483; certified for the EDTA- and acetic acid-extractable contents of Cd, Cu, Cr, Cu, Ni and Zn in sewage sludge amended soil [15]. Determined contents of the elements presented as mean values ± standard deviation (S.D.) of five replicate analyses (of five independent extraction procedures) were compared to the certi-

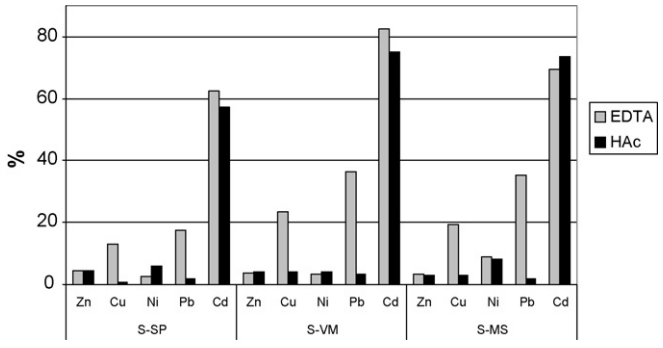

Fig. 1. Concentrations of extractable Zn, Cu, Ni, Pb, Cd in acetic acid (HAc) and EDTA extracts of soils S-SP, S-VM, S-MS in comparison to total contents—100%.

Table 7
Analyte contents[a] ($\mu g\,g^{-1}$) in 0.05 mol l^{-1} EDTA and 0.43 mol l^{-1} acetic acid extract solutions of sludge samples

Element	Sludge	Calibration curve			
		EDTA extracts		Acetic acid extracts	
		Mean ± S.D.	R.S.D. (%)	Mean ± S.D.	R.S.D. (%)
Zn	WT-L	686 ± 44	6.41	898 ± 11	1.22
	WT-M	1951 ± 110	5.64	2370 ± 56	2.36
	WT-H	4240 ± 240	5.66	5222 ± 316	6.05
Cu	WT-L	33 ± 2	6.40	3.2 ± 0.4	11.4
	WT.M	531 ± 9	1.69	138 ± 1	0.72
	WT-H	2049 ± 155	7.56	1280 ± 15	1.17
Ni	WT-L	4.5 ± 0.4	8.99	5.8 ± 0.4	7.64
	WT-M	100 ± 2	2.00	134 ± 2	1.49
	WT-H	817 ± 6	0.73	993 ± 24	2.42
Pb	WT-L	49 ± 3	6.33	0.99 ± 0.06[b]	5.58
	WT-M	551 ± 21	3.81	6.2 ± 0.3[b]	4.82
	WT-H	1545 ± 106	6.6	54 ± 3	5.03
Cd	WT-L	0.61 ± 0.04	6.28	0.7 ± 0.1[b]	1.55
	WT-M	7.9 ± 0.1	1.52	8.5 ± 0.2	1.89
	WT-H	46 ± 1	2.85	44 ± 1	3.17

[a] Data are expressed as mean ± S.D. The number of extraction procedures replicates $n = 4$.
[b] ETAAS, standard addition technique was used.

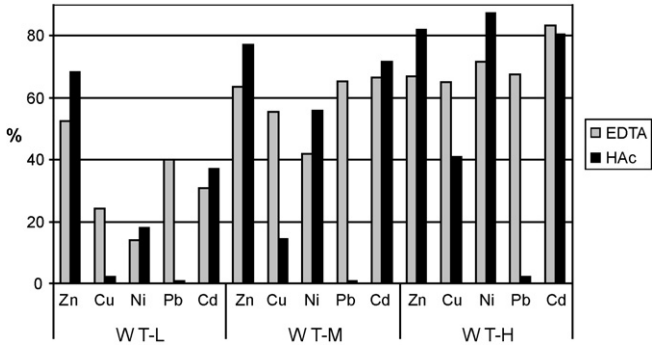

Fig. 2. Concentrations of extractable Zn, Cu, Ni, Pb, Cd in acetic acid (HAc) and EDTA extracts of sludges WT-L, WT-M, WT-H in comparison to total contents—100%.

Table 8
Comparison of determined contents[a] ($\mu g\,g^{-1}$) of the elements with the certified values of EDTA and acetic acid extractable trace elements in CRM 483-sewage sludge amended soil

Element	Acetic acid		EDTA	
	Determined	Certified	Determined	Certified
Zn	602 ± 21	620 ± 24	608 ± 7	612 ± 19
Cu	33 ± 2	34 ± 2	205 ± 15	215 ± 11
Ni	25 ± 1	26 ± 1	28 ± 1	29 ± 2
Pb[b]	2.2 ± 0.4	2.1 ± 0.3	230 ± 7	229 ± 8
Cd	18.0 ± 0.2	18.3 ± 0.6	22.7 ± 0.9	24 ± 1

[a] Data are expressed as mean ± S.D. The number of extraction procedures replicates $n = 5$.
[b] ETAAS, standard addition technique was used for acetic acid extractable Pb.

fied contents in Table 8. From the results very good agreement can be seen.

4. Discussion

4.1. Soils

Weak acids and strong complexant solutions are commonly used to determine trace-element mobility in soil sciences. Acetic acid extracts ion-exchangeable forms of elements and forms bound to carbonates. The exchangeable fractions may indicate the forms of metals that are most available to plant uptake. The elements bound to carbonates and specifically adsorbed phases can easily become mobile and become available under conditions of lower pH. Moreover, weak acids simulate the effect of an acid input (e.g. through acid rain or an accidental spill) onto soils and sediments [5]. From the results it yields that the availability for plant uptake in acetic acid extracts decreases in the order Cd > Ni > Zn > Cu > Pb generally in all studied soils, according to the type of soil. The most mobile element Cd represents 57–75%; Ni 4–8%; Zn 3–4%; Cu 1–4%; Pb 2–3%.

Chelating agents offer great promise for assessing readily available micronutrient cations in soils. These agents combine with free metal ions in solution forming soluble complexes and thereby reduce the activities of the free metal ions in solution. In response, metal ions desorb from soil surfaces or dissolve from labile solid phases to replenish the free metal ions in solution. The amount of chelated metals that accumulates in solution during the extraction is a function of the activity of metal ions in the soil (intensity factor) and the ability of the soil to replenish those ions (capacity factor). Both factors are important in determining the availability of elements to plants [22]. EDTA belongs to the best chelating agents, because it offers the most favourable

combination of stability constants for the complexing of the studied elements. EDTA extracts represents the content of the elements sorbed and organically bound to the soils. The amounts decreases in the order Cd > Pb > Cu > Ni > Zn. The most mobile element Cd represents 62–83%; Pb 17–36%; Cu 13–23%; Ni 2–9%; Zn 3–4%.

It is obvious that the sequence of EDTA-extractable elements is different from the sequence of acetic acid-extractable elements. The predominance of acidification or complexation processes can be studied from the plot (Fig. 1). For Cd, Ni and Zn it seems, that there is no predominance of one effect over the other. Different behaviour is observed for Pb and Cu, for which the extractability is higher when using the complexing agent. This fact can be explained by high complexation constants of Cu and Pb with EDTA ($\log K = 17.8$ and 18.3, respectively), these two metals are highly associated with Fe oxides and hydroxides and the elements can be remobilized because of the complexation of Fe with EDTA ($\log K = 25.1$).

4.2. Sludges

Sewage sludge is a good source of plant nutrients such as N and P and it has large amounts of organic matter that can improve physical and biological properties of the soil. The concentration and the availability of heavy metals is probably the main factor to consider, when sewage sludges are used as organic amendments. It has been suggested that applying sewage sludge to soil might provide metals in potentially toxic, labile forms [19,23]. As shown in Table 3 the studied sludges contain a wide range of concentrations of the studied elements. When considering inputs of metals to soils, it is important to know the leachability of the metals comparing to total contents. In this study we used the same extractants as were recommended for soil samples. Acetic acid-extractable contents of Zn, Cd, Ni, Cu and Pb in the sludges are in range of 68–82%, 37–81%, 18–87%, 2–41% and 1–2%, respectively. EDTA-extractable contents of Zn, Pb, Cd, Cu and Ni in the sludges are in the range of 52–67%, 40–68%, 30–83%, 24–65% and 18–87%, respectively (Table 7, Fig. 2). It is obvious from the total metal concentrations that Zn and Cu are predominant metals in the reference materials of sludges. Acetic acid-extractable Zn reaches 68–82% and EDTA-extractable Zn reaches 52–67%. This values indicate the high availability and thus the potential toxicity of Zn in these sludges, especially in WT-H. Pb and Cu show higher extraction values with EDTA, which indicates that these two elements are more easily remobilized by complexation than by acidification processes. On the contrary Zn and Ni show higher extraction values with acetic acid, which indicates that the elements are more easily remobilized by acidification than by complexation processes. For Cd there is no predominance of one effect over the other. Fig. 2 shows that Cd availability is large.

5. Conclusions

The single step extraction procedures validated by the standards, measurements and testing programme – SM&T (formerly BCR) – of the European Commission, were applied to the reference materials of soils, which represent uncontaminated pedologically different types of soils from regions of Slovakia and to the reference materials of sludges from city water treatment. The contents of Zn, Cu, Ni, Pb and Cd were determined in EDTA and acetic acid extracts of the soils by FAAS. Evaluation using calibration curves in appropriate extractants is possible for determination of Zn and Cu in EDTA extracts and Zn in acetic acid extracts. Electrothermal atomic absorption spectrometry (ETAAS) was used for the determination of copper in acetic acid extract, nickel, lead and cadmium in EDTA and acetic acid extracts. The technique of standard additions is preferable using ETAAS in all cases. For the determination of the analytes in the extracts of sludges mostly the FAAS with evaluation using calibration curves was used.

These procedures are recommended for hygienic and soil laboratories and the determined contents of zinc, copper, nickel, lead and cadmium could be indicative values for bioavailable forms of these elements for pedologically similar types of soils and similar types of sludges.

Acknowledgement

This work was financially supported by the Scientific Grant Agency of the Ministry of Education of the Slovak Republic VEGA 1/2466/05.

References

[1] E. Merian, Metals and Their Compounds in the Environment: Occurrence, Analysis and Biological Relevance, VCH, Weinheim, 1991.
[2] A.M. Ure, C.M. Davidson, Chemical Speciation in the Environment, Blackwell, Oxford, 2002.
[3] R. Morabito, Fresenius J. Anal. Chem. 351 (1995) 378.
[4] A.M. Ure, C.M. Davidson, R.P. Thomas, Single and sequential extraction schemes for trace metal speciation in soil and sediment, in: Ph. Quevauviller, E.A. Maier, B. Griepink (Eds.), Quality Assurance for Environmental Analysis, Elsevier, Amsterdam, 1995.
[5] A. Sahuquillo, A. Rigol, G. Rauret, Trends Anal. Chem. 22 (3) (2003) 152.
[6] G.A. Mitchell, F.T. Bingham, A.L. Page, J. Environ. Qual. 7 (1974) 165.
[7] A. Fuentes, M. Llorens, J. Saez, A. Soler, M.I. Aguilar, J.F. Ortuno, V.F. Meseguer, Chemosphere 54 (8) (2004) 1039.
[8] J.E. Sedberry, B.J. Miller, M.B. Sad, Commun. Soil Sci. Plant Anal. 10 (1979) 689.
[9] T.G. Kazi, M.K. Jamali, G.H. Kazi, M.B. Arain, H.I. Afridi, A. Siddiqui, Anal. Bioanal. Chem. 383 (2) (2005) 297.
[10] R.D. Davis, J. Sci. Food Agric. 30 (1979) 937.
[11] M. Žemberyová, M. Moskál'ová, M. Gregorová, CANAS'95 Colloquium Analytische Atomspektroskopie, Hrsg. B. Welz, Bodenseewerk Perkin-Elmer GmbH, Uberlingen, 1996.
[12] S.Z. Zhang, A.X. Lu, X. Shan, Z.W. Wang, S.X. Wang, Anal. Bioanal. Chem. 374 (5) (2002) 942.
[13] S. Tokalioglu, S. Kartal, A.A. Gunes, Int. J. Environ. Anal. Chem. 84 (9) (2004) 691.
[14] Ph. Quevauviller, G. Rauret, R. Rubio, J.F. Lopez- Sanchez, A.M. Ure, J. Bacon, H. Muntau, Fresenius J. Anal. Chem. 357 (1997) 611.
[15] Ph. Quevauviller, G. Rauret, A. Ure, J. Bacon, H. Muntau, Report EUR 17127 EN, Brussels, 1997.
[16] Ph. Quevauviller, Trends Anal. Chem. 17 (5) (1998) 289.
[17] B.J. Alloway, A.P. Jackson, Sci. Tot. Environ. 100 (1991) 151.
[18] B. Perez-Cid, C. Silva, C. Boia, Int. J. Environ. Anal. Chem. 82 (10) (2002) 721.

[19] I. Walter, F. Martinez, V. Cala, Environ. Pollut. 139 (3) (2006) 507.
[20] Š. Barta, M. Kalinčák, D. Kladeková, Report on Intercomparison of the Determination of Essential and Toxic Elements, Košice, 1992.
[21] Š. Barta, Report on Intercomparison of the Determination of Essential and Toxic Elements in Sludge from City Water Treatment, pb-anal, Košice, 1996.
[22] W.L. Lindsay, W.A. Norvell, Soil Sci. Soc. Am. J. 42 (1978) 421.
[23] B.R. Singh, R.P. Narwal, J. Environ. Qual. 13 (1984) 344.

Available online at www.sciencedirect.com
ScienceDirect
Talanta 71 (2007) 1481–1486
Talanta
www.elsevier.com/locate/talanta

A novel approach for simultaneous determination of polycyclic aromatic hydrocarbons by Shpol'skii non-linear variable-angle synchronous fluorescence spectrometry

Wei Zhang, Dan-Li Lin, Zhe-Xiang Zou, Yao-Qun Li *

Department of Chemistry and The Key Laboratory of Analytical Sciences of MOE, College of Chemistry and Chemical Engineering, Xiamen University, Xiamen, Fujian 361005, PR China

Received 4 May 2006; received in revised form 10 July 2006; accepted 10 July 2006

Abstract

A new method of combining low-temperature Shpol'skii effect with non-linear variable-angle synchronous fluorescence spectrometry (L-NLVASFS) has been proposed to increase spectral resolution. This coupled method was applied successfully to the simultaneous identification and quantification of some polycyclic aromatic hydrocarbons (PAHs) in mixtures, which cannot be determined by non-linear variable-angle synchronous fluorescence spectrometry at room-temperature (R-NLVASFS). The usefulness of this method is demonstrated by the analyses of synthetic mixtures and several real samples of airborne particulates.

Keywords: Low-temperature; Non-linear variable-angle synchronous fluorescence; PAHs; Shpol'skii spectroscopy

1. Introduction

Polycyclic aromatic hydrocarbons (PAHs) are a vast class of carcinogenic organic substances present in the environment, so the rapid screening and analysis of PAHs are of great significance. The strong native fluorescence of PAHs in liquid solutions has prompted the development of several room-temperature fluorescence methods for PAHs analyses [1]. Synchronous fluorescence spectrometry (SFS) may be the most popular solution for PAHs analysis to increase selectivity, while maintaining sensitivity [2].

Conventional SFS has been widely applied for the direct resolution of multi-component mixtures [3–7], but it is limited to a 45° section cut through the excitation–emission matrix. For making the scanning mode more flexible, some other synchronous fluorescence spectrometric approaches were developed such as constant-energy synchronous fluorescence spectrometry [8,9], variable-angle synchronous fluorescence spectrometry [10–12], non-linear variable-angle synchronous fluorescence spectrometry (NLVASFS) [13] and matrix isopotential synchronous fluorescence spectrometry [14]. Especially for NLVASFS [15,16], it provides most flexible scanning mode and can be achieved directly on a spectrofluorimeter by varying the relative scan speed of each monochromator. The increased selectivity afforded by the non-linear variable-angle synchronous scanning technique has been demonstrated in the simultaneous determination of some compounds in mixtures [16,17].

However, the broad-band nature of spectra obtained at room-temperature restricts the effective use in complex multi-component analysis. Combinations with other fluorescence approaches such as derivative techniques [17,18], excitation–emission matrices [19], Shpol'skii spectrometry [20] and time-resolved technique [21] are often needed. In this work, an evaluation was performed by combining the excellent band-narrowing features of low-temperature Shpol'skii effect with the flexibility of the non-linear variable-angle synchronous scanning technique (L-NLVASFS).

The Shpol'skii effect was reported in 1952 by Shpol'skii et al. Some aromatic compounds, when dissolved in selected *n*-alkane solvents and then frozen in liquid nitrogen (b.p. 77 K), exhibited extremely narrow-banded and line-rich "quasi-linear" fluorescence spectra [23]. Obviously, low-temperature spectroscopy

* Corresponding author. Tel.: +86 592 2185875; fax: +86 592 2185875.
E-mail address: yqlig@xmu.edu.cn (Y.-Q. Li).

0039-9140/$ – see front matter © 2007 Published by Elsevier B.V.
doi:10.1016/j.talanta.2006.07.022

demonstrates increasing selectivity advantages by the reduction of spectral bandwidths, offering fingerprint spectra with potential in analyses of complex mixtures [24]. However, since the first use of constant-energy synchronous luminescence techniques at low-temperature in 1982 [8], there are few reports about the application of this method [25].

In this work, the mixture of 1,2-benzoanthracene (1,2-BA), pyrene (Pyr), coronene (Cor), 3,4-benzopyrene (BaP) (mixture I) and the mixture of coronene, 3.4,8.9-dibenzopyrene (DBP) and perylene (Pery) (mixture II) were used as two examples for the evaluation of the coupled approach of the Shpol'skii effect and NLVASFS for multi-component analysis.

2. Materials and methods

2.1. Reagent

Stock solutions of 1,2-benzoanthracene (99%, Aldrich), pyrene (99%, Aldrich), coronene (99%, Sigma), 3,4-benzopyrene (97%, sigma) 3.4,8.9-dibenzopyrene (99%, Sigma), perylene (99+%, Aldrich) were prepared in cyclohexane (analytical-reagent grade, Shanghai Reagent), and diluted prior to fluorescence detection. The solutions in volumetic flasks covered with a black box were stored in a refrigerator with the temperature of 4–5°C.

The internal reference method was used for L-NLVASF spectrum intensity calibration in mixture I. The internal standard (Pery) compensated for variation of experimental conditions such as the position of the sample cell in the optical path, the rate of cooling, the inhomogeneity of the sample surface and the source intensity [22,23,26].

2.2. Sample preparation

The filter membranes absorbing airborne particulates from the Sanming (Fujian, the People's Republic of China) were spiked with different amounts of the three PAHs of mixture II and then extracted with 5 mL octane in test-tube directly.

2.3. Apparatus and software

Fig. 1 shows the structural diagram of the cryo-unit [27] which allows 12 samples to be frozen at one time for Shpol'skii fluorescence detection (LUMEX Corp., Russia). This unit was connected with spectrofluorimeter by the fiber.

The spectra of mixture I were obtained on a laboratory-constructed computer (IBM)-controlled spectrofluorimeter. It was equipped with a 350 W xenon lamp. Slit bandpasses were 5 nm for room-temperature detection and 3 nm for low-temperature detection. Mixture I was analyzed by a new laboratory-constructed spectrofluorimeter, which was equipped with a 150 W xenon lamp. The 2.5 nm slit bandpasses were used for the low-temperature detection (The resolution of this spectrofluorimeter was better than the former one). Excitation and emission grating monochromators were interfaced to the computer for controlling the instrument. A software package written in Turbo C 2.0 was used to control the data collection. A quartz cuvette with a path-length of 1 cm was used for room-temperature measurements. An electronic differentiator was connected to the spectrofluorimeter for direct recording the derivative spectra. The excitation–emission matrices calculated from the excitation and emission spectral data were used to acquire a suitable scan route with the aid of a program written in Visual Basic for Excel [28]. The NLVASF spectrum was recorded with the selected scan route. The procedures of selecting an optimum route are similar to our previous works [16,17].

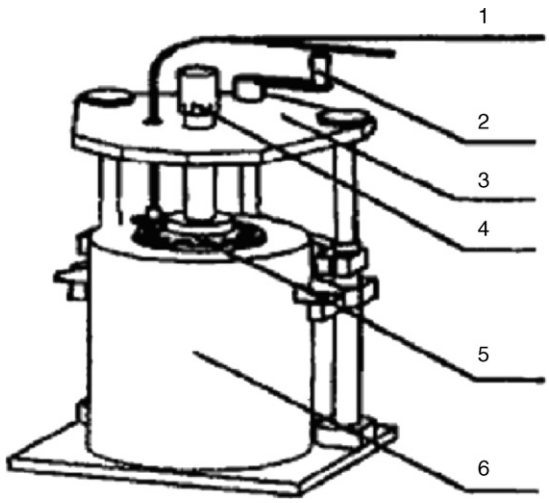

Fig. 1. Cryogenic unit (1) flexible fiber optical system, (2) handle of the turret drive screw, (3) cover of the cryogenic unit, (4) indexed head of the rod, (5) Turret wheel with samples and (6) Dewar vessel in the housing.

2.4. Freezing procedure

Carefully pouring liquid nitrogen to 3/4 of the dewar vessel, then putting the vessel under the other parts of the cryo-unit, the cylindrical cells with 0.5 mL sample solution were inserted in the turret wheel. Then the cells were set into liquid nitrogen by rotating handle. Complete sample freezing took less than 6 min. By moving the rod head, samples can be analyzed one by one. The 5 min procedure of probe cleanup involved removing the sample cells from the turret wheel, melting the frozen matrix and warming the resulting solution approximately to room-temperature with a heat gun.

3. Results and discussion

3.1. Selection of the optimum scan route

In order to produce the best NLVASFS scan spectrum (highest signal values, interference-free bands), it is necessary to select an optimum scan route for the application of the non-linear synchronous scan technique.

As the peak position should be changed from room-temperature to liquid nitrogen temperature, the different routes for each mixture should be found at these two temperatures. Figs. 2 and 3 show the overlaid contour plots of the individual components at room-temperature and at low-temperature. The three-dimensional spectra were derived from a pair of excita-

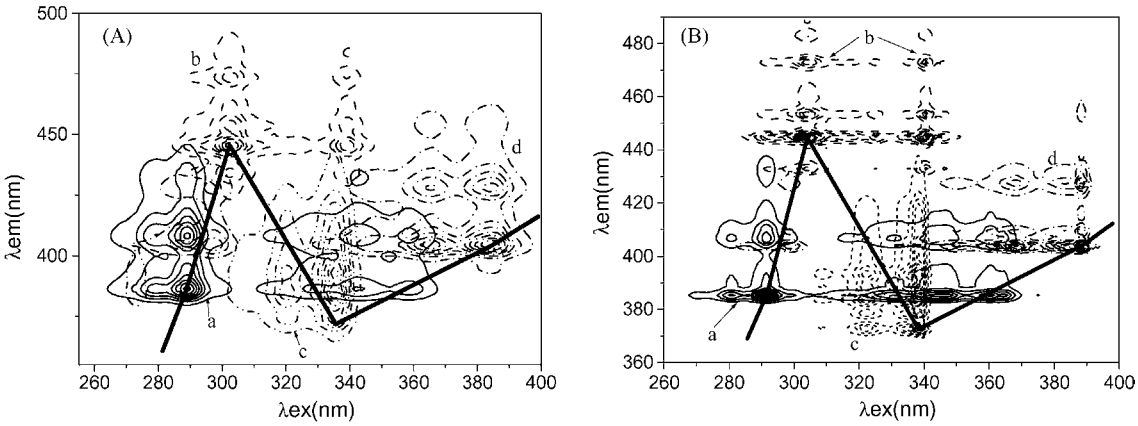

Fig. 2. Contour plot of 1,2-BA (a, 0.2 μg/mL), Cor (b, 0.5 μg/mL), Pyr (c, 0.3 μg/mL), BaP (d, 0.03 μg/mL) at room-temperature (A) and 1,2-BA (a, 1.5 μg/mL), Cor (b, 0.9 μg/mL), Pyr (c, 0.2 μg/mL), BaP (d, 0.05 μg/mL) at low-temperature (B). The bold folded lines are the selected NLVASFS scan routes.

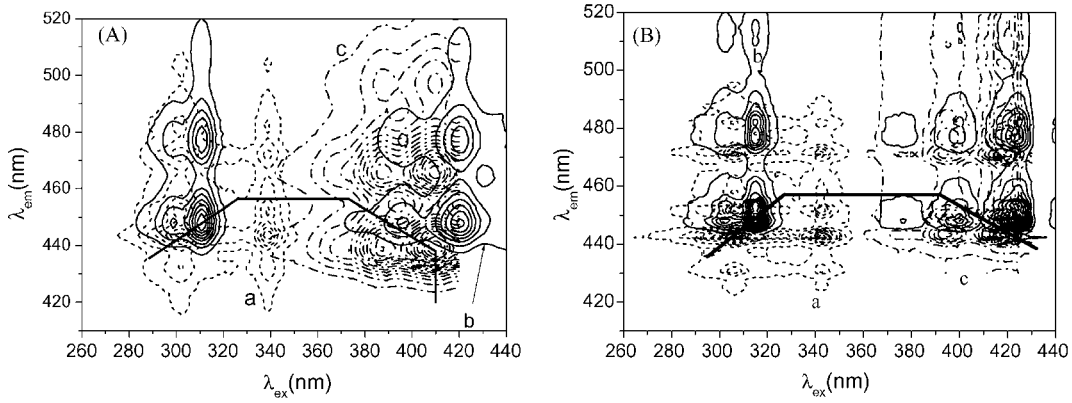

Fig. 3. Contour plot of Cor (a, 1.0 μg/mL), DBP (b, 0.3 μg/mL), Pery (c, 0.02 μg/mL) at room-temperature (A) and at low-temperature (B). The bold folded lines through the plot are the selected NLVASF scan routes.

tion and emission spectra. It is obvious that the fluorescence spectra of individual components overlap more seriously at room-temperature than at low-temperature. When plotting three-dimensional spectra of each component, it is better to keep spectral intensities of each compound similar for the convenience of observing three-dimensional spectra [16,17]. Therefore, the concentration levels indicated in the captions of Figs. 2 and 3 were selected.

The detection points of the PAHs in the two mixtures were chosen, where the spectrum of each component has a maximum signal value and a minimum interfering signal (Table 1).

Table 1
The detection points of each PAHs in mixture I and mixture II

	PAH	Detection points (λ_{ex}, λ_{em}) (nm) at room-temperature	Detection points (λ_{ex}, λ_{em}) (nm) at low-temperature
Mixture I	1,2-BA	289, 386	291, 385
	Cor	302, 445	304, 445
	Pyr	336, 372	338, 373
	BaP	384, 404	389, 404
Mixture II	Cor	302, 433	306, 443
	DBP	311, 448	315, 449
	Pery	410, 438	420, 444

At room-temperature, the strongest signal of Pyr at the point (λ_{ex} 336 nm, λ_{em} 380 nm) was overwhelmed by the spectrum of adjoining component (1,2-BA). Alternatively, the point (336 nm, 372 nm) was chosen as the detection point of Pyr where spectral interferences of other components are comparatively small and the signal intensity is still high. Similarly, at low-temperature, although Pyr has the highest signal at the point (338 nm, 383 nm), due to the interferences of other components, we choose another peak at (338 nm, 373 nm) as the detection point of Pyr. After the detection points were determined, other points were chosen to make up the whole scan routes as marked with the bold folded lines in Figs. 2 and 3.

3.2. Comparing spectral characteristics at room-temperature and low-temperature

By using the selected optimum routes in Fig. 2A and B, corresponding NLVASF spectra were obtained (Fig. 4A and B). For Pyr at room-temperature, only a small peak appeared near the detection point and the spectral interference from 1,2-BA could not be avoided (Fig. 4A). However, broad-banded emission peaks are concentrated into several narrow wavelength lines at liquid nitrogen temperature, especially for Pyr (Fig. 5). Using the optimum route in Fig. 2B, the four PAHs of

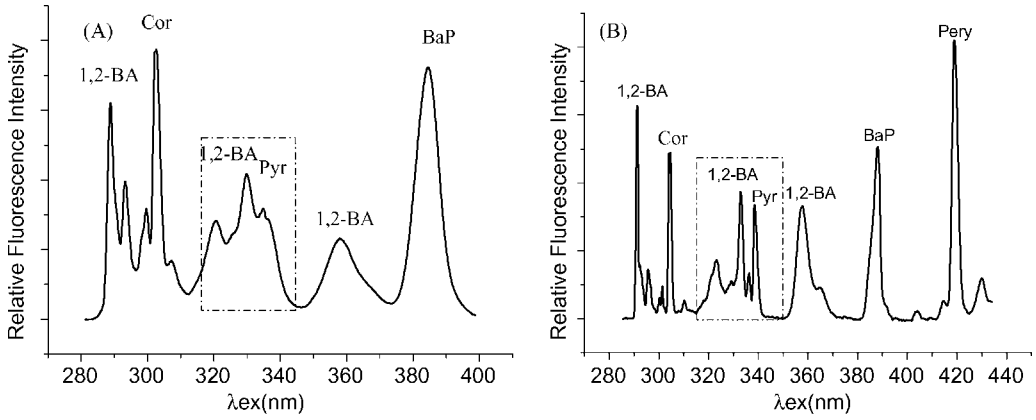

Fig. 4. Room-temperature non-linear variable-angle synchronous fluorescence spectrum of mixture I (A) which contains 1,2-BA (0.2 μg/mL), Cor (0.5 μg/mL), Pyr (0.3 μg/mL) and BaP (0.03 μg/mL); low-temperature non-linear variable-angle synchronous fluorescence spectrum of mixture I (B) which contains 1,2-BA (1.5 μg/mL), Cor (0.9 μg/mL), Pyr (0.2 μg/mL), BaP (0.05 μg/mL) and pery (0.1 μg/mL, internal standard).

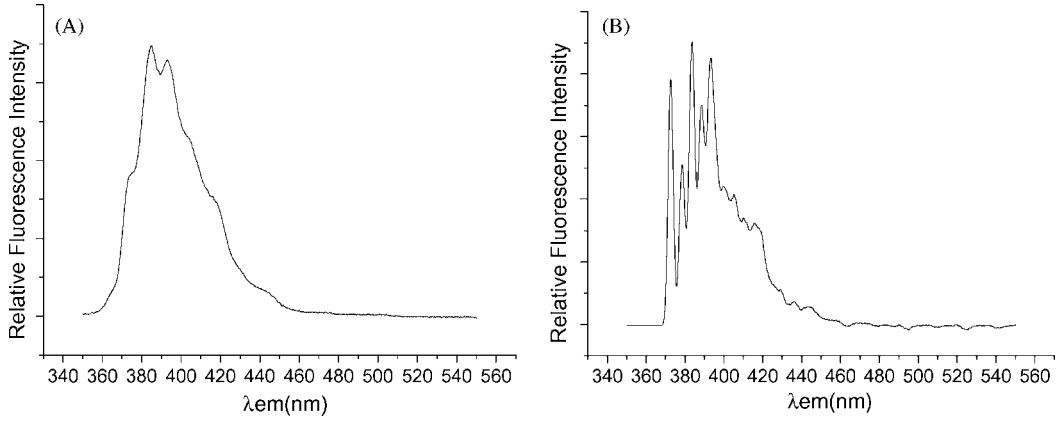

Fig. 5. Emission spectra of Pyr at room-temperature (A, λ_{ex} = 335 nm) and at low-temperature (B, λ_{ex} = 338 nm).

mixture I are all well identified (Fig. 4B). In comparison with the room-temperature non-linear variable-angle synchronous fluorescence (R-NLVASF) spectrum, it is obvious that Pyr in the low-temperature non-linear variable-angle synchronous fluorescence (L-NLVASF) spectrum is well resolved with a smooth baseline. This spectral characteristic makes the spectral interval of each component become larger, and suggests that more PAHs in these wavelength regions could be detected.

As to mixture II, the derivative technique was combined with NLVASFS in order to obtain better resolution. However,

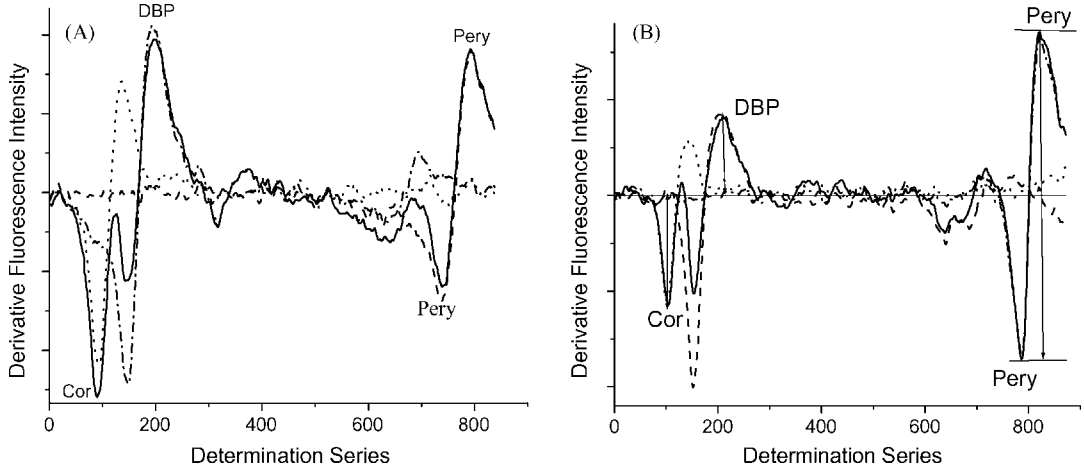

Fig. 6. Derivative room-temperature non-linear variable-angle synchronous fluorescence spectra (A) and derivative low-temperature non-linear variable-angle synchronous fluorescence spectra (B) of mixture II and individual components of Cor (1.0 μg/mL), DBP (0.3 μg/mL) and pery (0.02 μg/mL). Determination series denote the spatial order of appearance of all dots forming spectra [12].

Table 2
Linear ranges and detection limits of the PAHs in mixture I (by L-NLVASFS) and mixture II (by derivative L-NLVASFS)

		Liner range (μg/mL)	Component present (μg/mL))		$y = a + bx$				DL (ng/mL)
					a	b	γ	S.D. of estimation	
PAHs in mixture I	1,2-BA	0.01-1.0	Cor	0.20	2.63	809	0.9912	4.36	1.2
			Pyr	0.20					
			BaP	0.05					
	Cor	0.01-0.60	1,2-BA	0.20	5.53	156	0.9948	4.16	1.3
			Pyr	0.20					
			BaP	0.05					
	Pyr	0.005-0.80	1,2-BA	0.20	5.97	487	0.9996	4.67	1.4
			Cor	0.20					
			BaP	0.05					
	BaP	0.005-1.80	1,2-BA	0.20	44.01	514	0.9941	40.85	3.7
			Cor	0.20					
			Pyr	0.20					
PAHs in mixture II	Cor	0.05-0.85	DBP	0.10	19	327	0.9964	8.67	29.6
			Pery	0.10					
	DBP	0.01-0.14	Cor	0.50	5.5	938	0.9974	3.71	6.4
			Pery	0.10					
	Pery	0.01-0.17	Cor	0.50	5.6	5253	0.9961	29.3	5.7
			DBP	0.10					

1,2-BA: 1,2-benzofluorathene; Cor: coronene; Pyr: pyrene; BaP: 3,4-benzopyrene; DBP: 3.4,8.9-dibenzopyrene, Pery: perylene; γ: correlation coefficient; DL: detection limit based on three times the standard deviation of the blank of 11 replicate determinations.

Table 3
Recoveries of the four PAHs of mixture I in synthetic samples

Mixture sample	Amount added (ng/mL)				Amount found (ng/mL)				Recovery (%)			
	1,2-BA	Cor	Pyr	BaP	1,2-BA	Cor	Pyr	BaP	1,2-BA	Cor	Pyr	BaP
1	20.0	80.0	30.0	50.0	16.9	77.5	25.8	55.6	84.5	96.9	86.0	111.2
2	40.0	60.0	40.0	40.0	39.4	57.9	40.4	46.6	98.5	96.5	101.0	116.5
3	60.0	40.0	50.0	30.0	68.7	44.9	43.1	32.6	114.5	112.0	86.2	108.7
4	80.0	20.0	60.0	20.0	84.2	22.7	48.2	17.7	105.3	113.5	80.3	88.5

1,2-BA: 1,2-benzofluorathene; Cor: coronene; Pyr: pyrene; BaP: 3,4-benzopyrene.

it is still difficult to detect each component of mixture II at room-temperature with the derivative R-NLVASFS technique. As shown in Fig. 6A, Cor at the detection point is interfered by DBP and cannot be detected in the mixture, and Pery is influenced by the small peak of DBP and cannot be quantified accurately by peak-to-peak method. With the derivative L-NLVASFS technique, the spectral interferences of three components were apparently reduced and a single spectrum can be used for the simultaneous identification and quantification of these components in mixture II. The peak-to-peak distance was used for quantitative determination of Pery and zero-to-peak measurements were adopted for Cor and DBP (Fig. 6B).

Table 4
Recoveries of the three PAHs of mixture II in synthetic samples and in the samples of airborne particulates

PAHs	Samples	Amount added (ng/mL)			Amount found (ng/mL)			Recovery (%)		
		Cor	DBP	Pery	Cor	DBP	Pery	Cor	DBP	Pery
In synthetic samples	1	850	20.0	20.0	836	17.0	22.0	98.4	85.0	110.0
	2	550	110	110	601	109	107	109.3	88.0	97.2
	3	100	20.0	170	108	18.0	169	108.0	90.0	99.6
	4	50.0	10.0	10.0	43.4	9.78	10.7	86.7	97.8	107.0
In the samples of airborne particulates	1	400	20.0	10.0	382	17.5	10.2	95.5	87.3	101.7
	2	200	50.0	20.0	194	43.3	22.2	97	86.5	110.8
	3	50.0	20.0	20.0	42.2	19.0	21.3	84.4	94.8	106.3
	4	100	30.0	30.0	112	31.2	27.2	112.0	103.9	90.6
	5	300	10.0	15.0	256	10.6	13.2	85.3	105.6	87.9

The amount of Pery in the un-spiked samples of airborne particulates has been subtracted.

3.3. Analytical figures of merit

In order to test the mutual independence of the analytical signal of each component, a calibration graph was constructed from low-temperature non-linear variable-angle synchronous signals for each one in the presence of the other components. When plotting a graph for a particular component, the concentrations of the other three components were chosen within their calibration concentration ranges. At these concentration ranges, the other components have zero or negligible effects on the component.

The proposed method has been evaluated by a statistical analysis of the experimental data by fitting the least-squares line according to $y = a + bx$. By applying the IUPAC definition, based on three times of the standard deviation of the blank ($n = 11$), detection limits of each component are obtained. Tables 2 and 3 show the satisfactory results.

In order to check its usefulness, the method was applied to the analyses of the samples of synthetic mixtures and airborne particulates. The synthetic samples were prepared by mixing known amounts of the solutions of the PAHs. The recovery results for the synthetic samples are shown in Table 4. The samples of airborne particulates were spiked with different amounts of the PAHs of mixture II to check the recoveries.

4. Conclusion

Shpol'skii spectroscopy offers fingerprint spectra with increasing selectivity advantages by the reduction of spectral bandwidths, and the combination of flexible synchronous scanning technique at low-temperature can provide an effective screening method for PAHs. We demonstrated the first successful use of NLVASFS at low-temperature. Comparing with R-NLVASFS, L-NLVASFS manifests better resolution and has the potential of analyzing more PAHs in the same wavelength region. Therefore L-NLVASFS is very hopeful to become a new method for the analyses of complex PAHs mixtures.

Acknowledgements

We thank the National Natural Science Foundation of China (No. 20575055), the Natural Science Foundation of Fujian Province (No. B0410002) and the Science and Technology Project of Xiamen for their financial support.

References

[1] T. Vo-Dinh, J. Fetzer, A.D. Campiglia, Talanta 47 (1998) 943–969.
[2] A.A. Eiroa, E.V. Blanco, P.L. Mahía, S.M. Lorenzo, D.P. Rodriguez, Analyst 123 (1998) 2113–2117.
[3] M.F. Pistonesi, M.S.D. Nezio, M.E. Centurion, M.E. Palomeque, A.G. Lista, B.S.F. Band, Talanta 69 (2006) 1265–1268.
[4] D. Patra, Luminescence 18 (2003) 97–102.
[5] A.M.B. Giessing, Marine Environ. Res. 56 (2003) 599–615.
[6] Y.N. Ni, D.Q. Lin, Talanta 65 (2005) 1295–1320.
[7] D. Patra, A.K. Mishra, Trends Anal. Chem. 21 (2002) 787–798.
[8] E.L. Inman, J.D. Winefordner, Anal. Chem. 54 (1982) 2018–2022.
[9] Y.Q. Li, X.Z. Huang, J.G. Xu, G.Z. Chen, Anal. Chim. Acta 256 (1992) 285–291.
[10] Y.Q. Li, X.Z. Huang, J.G. Xu, G.Z. Chen, Talanta 41 (1994) 695–701.
[11] J.J.B. Nevado, J.A.M. Pulgarin, O.I.R. Escudero, Appl. Spectrosc. 54 (2000) 1678–1683.
[12] F.G. Sanchez, A.F. Gutierrez, C.C. Blanco, Anal. Chim. Acta 306 (1995) 313–321.
[13] Y.Q. Li, X.Z. Huang, Fresenius J Anal. Chem. 357 (1997) 1072–1075.
[14] D.L. Lin, L.F. He, Y.Q. Li, Clin. Chem. 50 (2004) 1797–1803.
[15] J.J.B. Nevado, J.A.M. Pulgarin, Analyst 123 (1998) 483–848.
[16] W. Sui, C. Wu, Y.Q. Li, Fresenius J. Anal. Chem. 368 (2000) 669–675.
[17] D.L. Lin, Z.X. Zou, L.F. He, Y.Q. Li, Luminescence 20 (2005) 292–297.
[18] J.A.M. Pulgarin, L.F.G. Bermejo, Anal. Chim. Acta 373 (1998) 119–129.
[19] R.D. JiJi, G.A. Cooper, K.S. Booksh, Anal. Chim. Acta 397 (1999) 61–72.
[20] C. Gooijer, I. Kozin, N.H. Velthorst, Mikrochim. Acta 127 (1997) 149–182.
[21] N. Furuta, A. Otsuki, Anal. Chem. 55 (1983) 2407–2413.
[22] G.F. Kirkbright, C.G. DE Lima, Analyst 99 (1974) 338–354.
[23] E.P. Lai, E.L. Inman, Talanta 29 (1982) 601–608.
[24] E.L. Inman, J.D. Winefordner, Anal. Chim. Acta 141 (1982) 241–254.
[25] J.W. Hofstraat, U.P. Wild, J. Fluoresc. 8 (1998) 319–325.
[26] G. Luthe, H. Es-Sbai, C. Gooijer, U.A.T. Brinkman, F. Ariese, Anal. Chim. Acta 459 (2002) 53–59.
[27] L.J. Yu, Y.Q. Li, W. Sui, Spectrosc. Spectr. Anal. 22 (2002) 819–821.
[28] C. Wu, W. Sui, Y.Q. Li, Chem. J. Chin. Univ. 20 (Suppl.) (1999) 422.

Available online at www.sciencedirect.com
ScienceDirect
Talanta 71 (2007) 1530–1535
Talanta
www.elsevier.com/locate/talanta

A novel immunoassay strategy based on combination of chitosan and a gold nanoparticle label

Song-Bai Zhang, Zai-Sheng Wu, Meng-Meng Guo, Guo-Li Shen *, Ru-Qin Yu

State Key Laboratory for Chemo/Biosensing and Chemometrics, College of Chemistry and Chemical Engineering, Hunan University, Changsha 410082, PR China

Received 7 April 2006; received in revised form 15 July 2006; accepted 18 July 2006
Available online 7 September 2006

Abstract

A novel immunoassay strategy based on combination of chitosan (CHIT) and a gold nanoparticle (GNP) label has been developed. The susceptibility of CHIT to further chemical modifications due to the abundant amino groups is explored in order to covalently immobilize antibody (Ab) onto the (3-aminopropyl) triethoxysilane derivatized glass slide by cross-linking with glutaraldehyde (GA). After incubating in antigen (Ag) solution, the obtained substrate is immersed in GNP labeled antibody solution for signal generation. The two steps were repeated alternatively for three times, forming multilayer of gold nanoparticles via antigen–antibody specific reaction. Ultraviolet-visible (UV–vis) absorption spectrum is recorded to obtain quantitative information about the specific antigen. The presented immunoassay strategy is applied for determination of human serum albumin (HSA) as a model analyte. The immunoassay of HSA is specific. Compared to previous correlative work, the proposed immunosensing strategy shows some advantages, such as improved sensitivity as much more gold nanoparticles can be coupled to the functionalized surface making use of the abundant amino groups of CHIT. Moreover, a significantly extended linear detection range of 8.0–512.0 μg/mL is gained under the optimized experimental conditions. In particular, the presented biosensing method shows low cost and simplicity, and only a conventional UV–vis detector is involved.

Keywords: Gold nanoparticles; Chitosan; Human serum albumin; UV–vis absorption spectrum

1. Introduction

Immunoassay, which is based on the use of an antibody (Ab) that reacts specifically with the antigen (Ag), has been widely used in clinical diagnoses, environmental control and biochemical studies because of its extremely high sensitivity and selectivity. The quantification is generally achieved by measuring the specific activity of a label, i.e., its radioactivity, enzyme activity, fluorescence, chemiluminescence or bioluminescence [1]. However, for these labels, each of them has its own advantages and disadvantages. In order to overcome the problems associated with the common radioisotopic, fluorescent or enzyme labels, immunoassays involving metal-based labels were developed in the 1970s [1]. Among these metal-based labels, gold nanoparticle (GNP) label is an ideal one in biotechnological systems due to its inherent advantages: gold nanoparticles (GNPs) could be easily prepared in a wide range of sizes from 2 to 100 nm [2]; the biochemical activity of the biomolecules, such as antigen or antibody, would be well retained when adsorbing on the surfaces of gold nanoparticles. The use of gold nanoparticles for the determination of biomolecules and some biological metabolites has received great attention in recent years [3–8] due to their peculiar optical and electronic properties [9]. It has been extensively employed to label different biological receptors, such as protein A, immunoglobulin G and glucose oxidase [10]. In the present study, we employed gold nanoparticle to label antibody for optical signal generation.

In the visible range, the ultraviolet-visible (UV–vis) spectrum of spherical gold nanoparticles is generally dominated by the plasmon band due to the excitation of surface plasmons. The resonance band alters with the change of the size, shape, composition of the nanoparticles, the distance between nanoparticles and the refractive index of the environmental medium [11]. Nath and Chilkoti described an optical method for studying

* Corresponding author. Fax: +86 731 8821355.
E-mail address: glshen@hnu.cn (G.-L. Shen).

0039-9140/$ – see front matter © 2006 Elsevier B.V. All rights reserved.
doi:10.1016/j.talanta.2006.07.036

biomolecular interactions in real-time on the surface of an optically transparent substrate. The UV–vis absorbance spectrum of a self-assembled monolayer of colloidal gold on glass surface was studied as a function of biomolecular binding to the surface of the immobilized colloids, and the absorbance at a fixed wavelength changed as a function of refractive index [12]. Inspired by their work, we tried to develop a novel immunoassay strategy employing gold nanoparticles, which were assembled onto the surface of a transparent glass slide.

To amplify the optical response, chitosan (CHIT) was used in the present work making use of its abundant amino groups. Chitosan, which has been found to be a very useful functional material [13], has attracted much attention from scientists [14,15]. Chitosan is a polysaccharide biopolymer comprising of glucosamine (Gln) and *N*-acetyl-glucosamine (GlcNAc) [16]. It is soluble in aqueous acidic media, adopting an extended conformation because of the strong electrostatic segment–segment repulsion [17]. CHIT exhibits excellent film-forming ability, good adhesion, high water permeability and susceptibility to further chemical modifications due to the presence of abundant reactive amino and hydroxyl functional groups [18]. These unique properties prompted extensive investigations of chitosan in fabricating biosensors [19,20]. Zhang et al. designed a carbon nanotube–chitosan system for electrochemical sensing of glucose [18]. The susceptibility of CHIT to chemical modifications was explored in order to covalently immobilize glucose dehydrogenase. In the present work, using this technique, we designed an immunosensor employing the abundant amino groups of CHIT, which is easy for covalent immobilization of antibody via glutaraldehyde (GA).

Herein, a novel immunoassay method was proposed for the measurement of a model analyte of human serum albumin (HSA) based on ultraviolet-visible spectrometry of gold nanoparticles, which were selectively adsorbed on a glass slide. Firstly, the glass slide was derivatized with (3-aminopropyl) triethoxysilane (APTES). After CHIT was covalently bound to the resulting substrate via cross-linking with GA, the anti-human serum albumin (anti-HSA) antibody was coupled with the substrate, and the sensing interface was thus formed. Before UV–vis spectroscopic measurement, the resulting substrate was incubated in a HSA solution and then in a GNP labeled anti-HSA solution. The UV–vis absorption spectrum of substrate surface in the range of 400–750 nm was recorded. The intensity of 530 nm peak was used for the detection of the specific antigen. The peak intensity was found to increase with the increasing concentration of the specific antigen in the range of 8.0–512.0 μg/mL. The immunoassay system was depicted in Fig. 1.

2. Experimental

2.1. Instrumentation

UV–vis spectroscopic measurements were performed by a MultiSpec-1501 UV–vis spectrophotometer (Shimadzu, Japan) with the software of Hyper UV Version 1.50 at room temperature in the range of 400–750 nm. Solution spectra were gained by

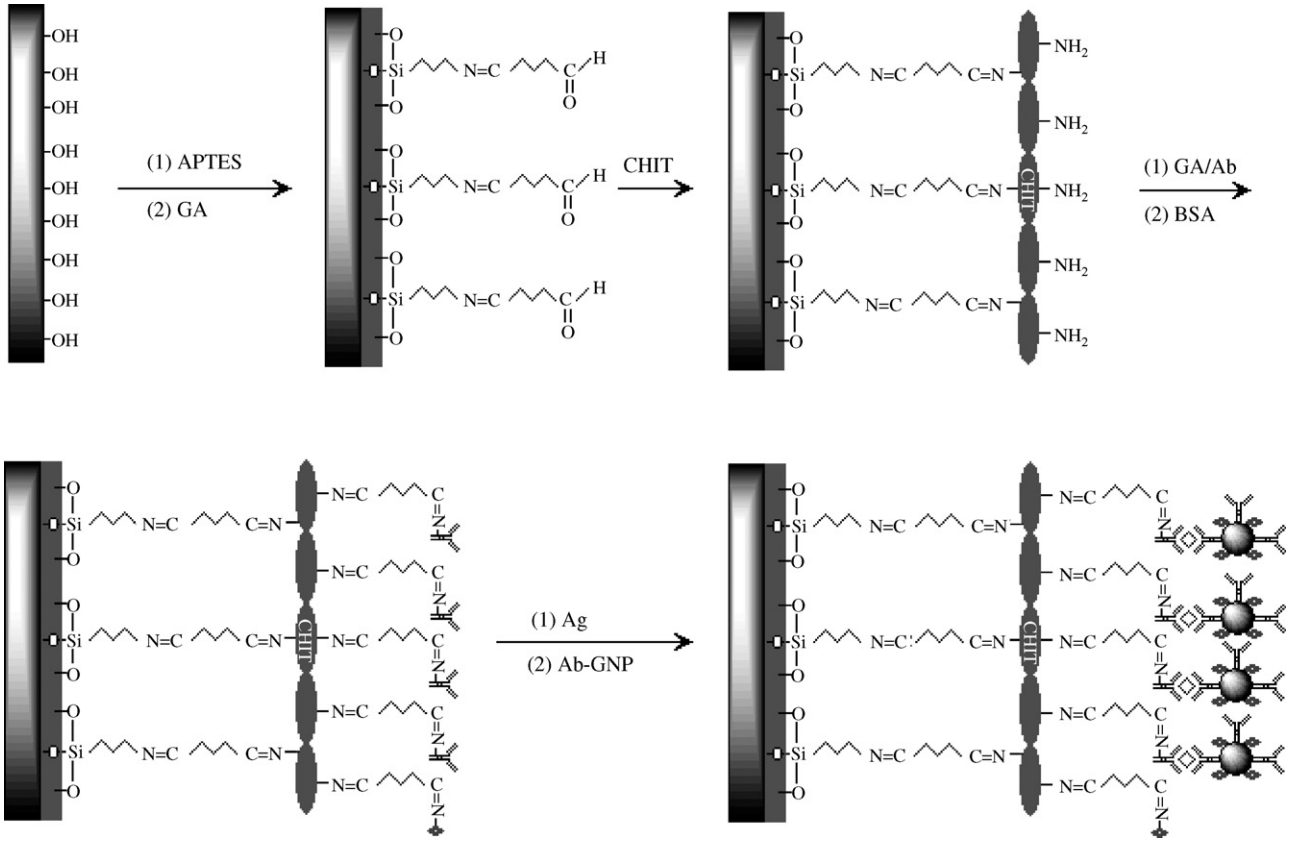

Fig. 1. Schematic illustrations of the operating principle and the assembly strategy for the sensor.

measuring the absorption of solution in a quartz cell with a path length of 1 cm. The spectra of the functionalized glass slides were measured by placing the substrates vertically to the light beam. A baseline correction procedure was carried out prior to each measurement session.

2.2. Materials

Human serum albumin, anti-human serum albumin antibody and bovine serum albumin (BSA) were obtained from the Health Department of institute of Biological Products (Shanghai, China). Glutaraldehyde solution (25%) was purchased from Changsha Chemical Reagents Co. (Changsha, China). Chitosan (CHIT, 75–85% deacetylation) and (3-aminopropyl) triethoxysilane were obtained from Sigma. Phosphate buffer solution (PBS, 10 mM, pH 7.4) was used as working solution. All other chemicals were of analytical reagent grade and used as received, and doubly distilled water was used throughout the experiments.

2.3. Synthesis of gold nanoparticles

All glassware were thoroughly cleaned with freshly prepared aqua regia (HNO_3:HCl = 1:3, by volume) and rinsed extensively with doubly distilled water (electric resistivity > 18 MΩ cm) before use. The GNPs used in this work were prepared according to reported methods with a slight modification [21]. Briefly, 100 mL of 0.01% $HAuCl_4$ solution was heated under reflux. After 1 mL of 1% trisodium citrate solution was added, the solution was heated under reflux for 10 min. The color of the solution changed from purple to blue and to red in the end, which indicated that the GNPs were formed. The solution was stirred continuously until it was cooled to room temperature. Finally, the cooled solution was stored in the refrigerator at 4 °C in a brown bottle until use. The particle was examined by the UV–vis absorption spectra with a surface plasmon resonance band at 528 nm, which corresponds to the particle size of ca. 32 nm [21].

2.4. Surface derivatization of substrates

The microscope glass slides were cut to a size of 9 mm × 50 mm and the derivatization was carried out as reported [12,22–24]: first, the glass slides were cleaned in a bath of seven parts H_2SO_4 to three parts 30% H_2O_2 (*Caution! Piranha solution is highly corrosive. Extreme care should be taken when handling Piranha solution, and only small quantities should be prepared.*) at 60 °C for 10 min and then rinsed with distilled water for several times followed by sonicating in distilled water for 10 min. Second, the glass slides were dipped into 1 M NaOH solution for 20 min at 80 °C. After rinsing with distilled water and spectrophotometric grade CH_3OH, the cleaned substrates were submerged into a 1% (v/v) solution of APTES in spectrophotometric grade CH_3OH for overnight. The substrates were subsequently rinsed with sonication in CH_3OH to take off the unbound monomer from substrates. Finally, the substrates were rinsed with distilled water and baked at 120 °C for at least 2 h.

2.5. Gold labeling of anti-HSA

The procedure of GNP labeling was performed as following: 100 μL of anti-human serum albumin antibody was added into 50 mL of gold nanoparticle suspension and continuously stirred for 1 h. Then, 100 μL of 10 mg/mL BSA solution was added to cover the non-specific sites. After stirring for at least 1 h, the solution was centrifugated at 8000 rpm for 15 min. The supernatant including the excess reagents was removed, and the red precipitate was redispersed in 50 mL of PBS solution. The GNP-labeled antibody solution was stored in refrigeratory at 4 °C until use.

2.6. Fabrication of the immunosensor

The APTES derivatized glass slide was dipped in a 2.5% GA solution for 40 min in a glass cell. Then, the substrate was soaked in 0.5 mg/mL chitosan solution. UV–vis absorption spectrum of the APTES/CHIT functionalized substrate was collected over the range of 400–750 nm (the primary absorption spectrum). To obtain the sensing interface, anti-HSA antibody (anti-HSA:PBS solution = 1:50, by volume) was coupled onto the surface of the APTES/GA/CHIT functionalized substrate with the cross-linker of GA. Finally, the glass slide was ready for the HSA detection after blocking the non-specific reactive sites using 10 mg/mL BSA solution. Note that the glass slide was washed with distilled water after each step.

2.7. The detection of HSA

The process of HSA detection was depicted as follows: after incubating the sensor in 2 mL of PBS buffer containing different concentrations of HSA antigen for 30 min and washing with PBS buffer, the resulting substrates were submerged in 2 mL of GNP labeled anti-HSA antibody solution for the generation of optical signal. The two steps were repeated alternatively for three times to form multilayer of gold nanoparticles. After rinsing thoroughly with distilled water to remove the unbound GNPs, the UV–vis absorption spectrum was recorded over the range of 400–750 nm. All UV–vis absorbance spectra reported in this study were subtracted from the corresponding primary absorption spectrum as the baseline unless specified otherwise.

3. Results and discussion

3.1. Surface modification of glass slides

We developed an optical biosensor on an optically transparent substrate functionalized with gold nanoparticles for several reasons: the gold colloid allowed the transmission of light in the visible region of the electromagnetic spectrum; it is easy to fabricate the sensing interface via covalent binding of a specific antibody on the substrate; antibody–gold nanoparticle conjugates is evenly adsorbed from solution onto a functionalized glass surface by specific interactions and laterally by the repulsive conjugate–conjugate electrostatic interactions; as only an UV–vis spectrophotometer was needed to perform

the measurements, it is simple enough to implement in most laboratories.

The glass surface treatment with NaOH solution leaded to a high concentration of hydroxyl group and facilitated the subsequent derivatization of APTES. The removal of the unbound monomer from substrate surfaces via abundant rinsing after the derivatization and baking of the substrates at 120 °C were necessary to prevent the formation of multilayers.

3.2. Amplification of CHIT

In the present work, CHIT was explored for the amplification of optical response making use of its abundant amino groups. The dependence of optical response on CHIT was investigated. Both the APTES-derivatized glass slide and the same slide modified with CHIT via GA were incubated in gold nanoparticle solution. The GNPs were adsorbed on amino group terminated glass substrates due to the high-affinity of gold nanoparticle for amino functional group. After rinsing thoroughly with distilled water to remove the unbound GNPs, the UV–vis absorption spectra of the two substrates were recorded. The substrate modified with CHIT exhibited a much stronger surface plasmon resonance absorption band than that of the other one. This result was expected as much more gold nanoparticles were coupled to the functionalized glass surface due to plenty of amino groups when the substrate was modified with CHIT.

3.3. Wavelength shift

Particles on the nanoscale exhibit interesting and unique optical responses in the ultraviolet-visible region, where the absorbance shows an exponential decay with decreasing photon energy. Therefore, for the particle materials, a surface plasmon resonance band is superimposed [25]. The surface plasmon energy and intensity have been found to be altered with the change of the size, shape, composition of the nanoparticles, the refractive index of the environmental medium as well as the distance between nanoparticles. It has been found experimentally that the surface plasmon oscillation of gold nanoparticles red shifted from 520 to 530 nm as the particle diameter increased from 5 to 400 nm [26]. In our study, the gold nanoparticles showed a surface plasmon resonance band at 528 nm in UV–vis absorption spectrum. Upon the binding of antibody, a new absorption band at longer wavelengths was recorded. As shown in Fig. 2, red shift of about 4 nm (line b) in the absorbance maximum was found compared to the bare GNPs (line a). It seemed that this behavior was due to the change in the refractive index as a result of the addition of ligand layers to the surface of gold nanoparticles [27–31]. When UV–vis measurements were performed on the surfaces of the glass slide, which was functionalized with GNP labeled anti-HSA, a red shift of the surface plasmon absorance peak was also found. Considering the phenomenon of wavelength shift, we used the absorbance intensity at 530 nm for HSA detection in our study.

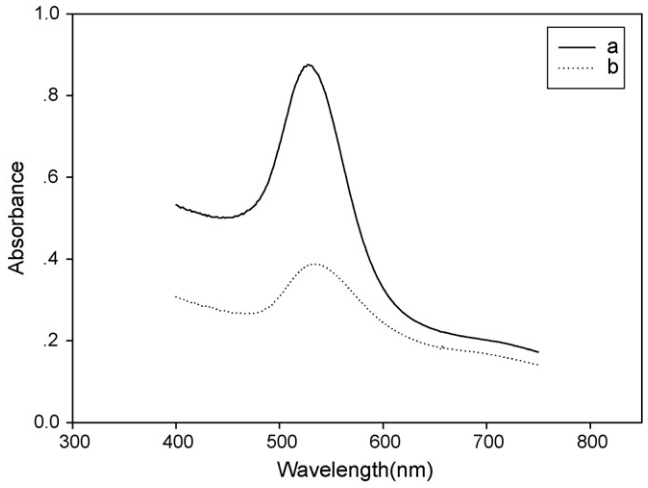

Fig. 2. Absorption spectra of: (a) gold colloidal solution and (b) GNP labeled anti-HAS solution.

3.4. Investigation of non-specific adsorption

Non-specific adsorption of proteins present in real matrices is a formidable factor, which limits the performance of a sensor. Therefore, we chose 10 mg/mL BSA to replace HSA for investigating the degree of the non-specific absorption. No obvious absorption at 530 nm in the UV–vis spectrum was found. The maximum absorbance intensity generated from non-specific adsorption of BSA was ca. 9.88×10^{-4}, which had a negligible effect on absorbance intensity of 2.78×10^{-2} caused by the interaction of GNP labeled antibody and target antigens, though the concentration of BSA was much higher than that of HSA (256.0 μg/mL). The experimental results obtained indicate that the designed sensor exhibits good specificity to HSA and is applicable to the selective determination of the target analyte.

3.5. The detection of HSA

To abtain the calibration curve, a series of different concentrations of human serum albumin were detected. The operations were performed as demonstrated in the experimental section. The UV–vis spectra of the glass slides were recorded as shown in Fig. 3. We found that as the concentration of the HSA increased, the absorbance intensity ascended. The results showed that the change of absorbance intensity and the concentration of HSA possessed a linear relationship in the concentration range from 8.0 to 512.0 μg/mL as depicted in Fig. 4. The calibration equation was $\Delta A = 0.01 \log X + 4.01 \times 10^{-3}$ with a correlation coefficient of 0.9936 (shown in the inset of Fig. 4). The detection limit of 2.0 μg/mL can be obtained, which was taken as three times the standard deviation of the blank signal. Saturation was encountered due to complete binding of antibodies fixed on the substrate when the concentration of HSA was more than 512.0 μg/mL. Comparing with a correlative work [19], in which a biosensing strategy was designed based on quartz-crystal microbalance (QCM) modified with multilayers of the positively charged CHIT and negatively charged alginate-HSA antibodies, a significantly extended linear detection range was obtained with our

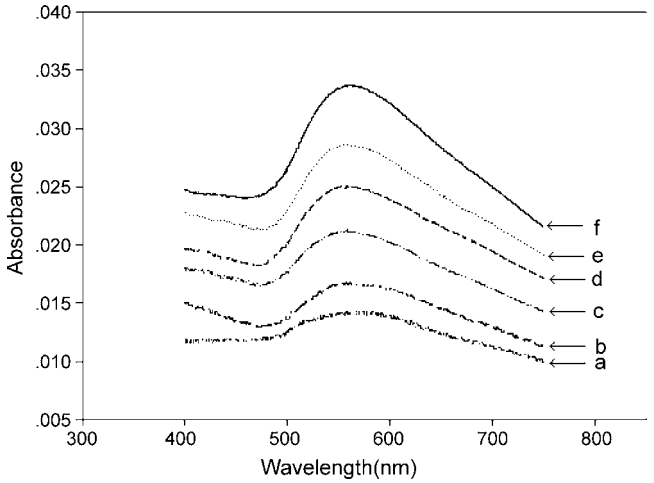

Fig. 3. Absorption spectra of substrates with different concentration of HSA: (a) 8.0 μg/mL; (b) 16.0 μg/mL; (c) 64.0 μg/mL; (d) 128.0 μg/mL; (e) 256.0 μg/mL; (f) 512.0 μg/mL.

proposed strategy. Moreover, by making use of the abundant amino groups of CHIT, the optical response was amplified due to much more GNP/anti-HSA conjugates could be immobilized onto the functionalized substrate. Therefore, improved sensitivity was gained compared to some previous correlative work [32–34].

3.6. Reproducibility

Reproducibility is important for practical application. To test the reproducibility of this method, seven different substrates were incubated in HSA solution at a concentration of 128.0 μg/mL under the same experimental conditions, and the UV–vis absorption spectra were recorded. The mean absorbance intensity at 530 nm for the seven glass slides was 0.0241. The relative standard deviation (R.S.D.) is ca. 2.18%. This indicated that the developed immunoassay technique had an excellent reproducibility.

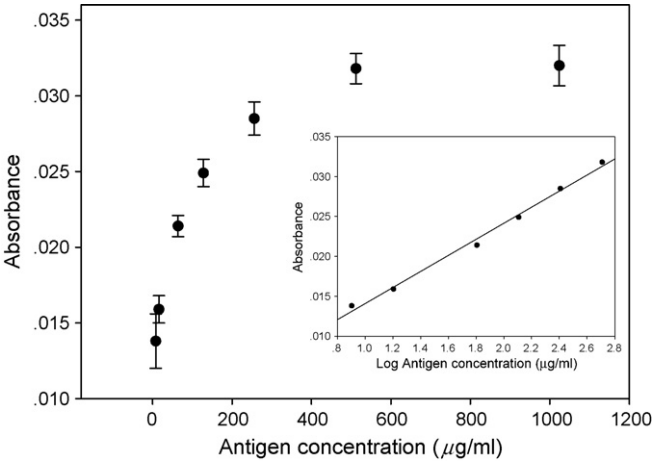

Fig. 4. Absorbance intensity at 530 nm vs. the HSA concentration. Inset: linear relationship between change of the absorbance intensity at 530 nm and the logarithm of HSA concentration. The standard deviations obtained by five repeated measurements were shown as the error bars.

Table 1
Recovery study of HSA for different concentrations

Sample no.	Mean HSA added (μg/mL)	Mean HSA found (μg/mL)	Recovery (%)	R.S.D. (%)
1	16.0	15.2	95	8.6
2	32.0	33.1	103	6.1
3	64.0	68.1	106	5.8
4	128.0	125.4	98	2.2

Measurement for each sample was repeated for five times. The percent recovery was calculated as follows: recovery (%) = [mean HSA found (μg/mL)]/[mean HSA added (μg/mL)] × 100.

3.7. Recovery

To assess the recovery of the assay, the glass slides were incubated in HSA solution of varying known amounts (16.0–128.0 μg/mL). UV–vis measurements were repeated for five times for each sample. The analytical recovery was calculated as the ratio between the mean HSA found and the mean HSA added, expressed as percentage. As shown in Table 1, the R.S.D.s of 2.2–8.6% and the quantitative recovery of 95–106% were obtained.

4. Conclusion

A cost-efficient immunoassay method based on UV–vis spectrometry of gold nanoparticles is demonstrated in the present study. The strategy is successfully applied in the quantification for a model analyte of HSA. The change of the absorption spectrum is associated with HSA. The intensity of 530 nm peak is linearly related to the HSA concentration in the range from 8.0 to 512.0 μg/mL. The detection limit is estimated as 2.0 μg/mL. The specificity of the HSA immunoassay is satisfactory. In addition, the reproducibility of the immunoreaction is investigated. Satisfactory recovery test values are realized, which confirms that the method presented in this paper is feasible to practical application.

Acknowledgments

The work was financially supported by the National Natural Science Foundation of China (Grant Nos. 20435010, 20205005 and 20375012), and the Science Commission of Hunan Province.

References

[1] M. Dequaire, C. Degrand, B. Limoges, Anal. Chem. 72 (2000) 5521.
[2] C. Zhang, Z.Y. Zhang, B.B. Yu, J.J. Shi, X.R. Zhang, Anal. Chem. 74 (2002) 96.
[3] L.A. Dykman, V.A. Bogatyrev, Biochemistry 62 (1997) 350.
[4] Y.C. Cao, R.C. Jin, C.S. Thaxton, C.A. Mirkin, Talanta 67 (2005) 449.
[5] S.H. Liu, Z.H. Zhang, Y.B. Wang, F.K. Wang, M.Y. Han, Talanta 67 (2005) 456.
[6] A.J. Wang, J.J. Xu, Q. Zhang, H.Y. Chen, Talanta 69 (2006) 210.
[7] X. Liu, Y. Sun, D.Q. Song, Q.L. Zhang, Y. Tian, H.Q. Zhang, Talanta 68 (2006) 1026.
[8] H.S. Guo, N.Y. He, S.X. Ge, D. Yang, J.N. Zhang, Talanta 68 (2005) 61.
[9] K. Aslan, C.C. Luhrs, V.H. Pérez-Luna, J. Phys. Chem. B 108 (2004) 15631.

[10] A.P. Fan, C.W. Lau, J.Z. Lu, Anal. Chem. 77 (2005) 3238.
[11] S. Hrapovic, Y.L. Liu, G. Enright, F. Bensebaa, J.H.T. Luong, Langmuir 19 (2003) 3958.
[12] N. Nath, A. Chilkoti, Anal. Chem. 74 (2002) 504.
[13] T. Masuko, A. Minami, N. Iwasaki, T. Majima, S.-I. Nishimura, Y.C. Lee, Biomacromolecules 6 (2005) 880.
[14] D.J. Macquarrie, J.J.E. Hardy, Ind. Eng. Chem. Res. 44 (2005) 8499.
[15] J.K. Francis Suh, H.W.T. Matthew, Biomaterials 21 (2000) 2589.
[16] X. Wei, M.G. Zhang, W. Gorski, Anal. Chem. 75 (2003) 2060.
[17] C.A. Constantine, S.V. Mello, A. Dupont, X.H. Cao, D. Santos Jr., O.N. Oliveira Jr., F.T. Strixino, E.C. Pereira, V. Rastogi, T.-C. Cheng, J.J. Defrank, R.M. Leblanc, J. Am. Chem. Soc. 125 (2003) 6595.
[18] M.G. Zhang, A. Smith, W. Gorski, Anal. Chem. 76 (2004) 5045.
[19] T. Deng, H. Wang, J.S. Li, G.L. Shen, R.Q. Yu, Anal. Chim. Acta 532 (2005) 137.
[20] Y.J. Liu, Y.L. Li, S.C. Liu, J. Li, S.Z. Yao, Biomaterials 25 (2004) 5725.
[21] M.F. Huang, Y.C. Kuo, C.C. Huang, H.T. Chang, Anal. Chem. 76 (2004) 192.
[22] Y.G. Sun, Y.M. Xia, Anal. Chem. 74 (2002) 5297.
[23] K.C. Grabar, R.G. Freeman, M.B. Hommer, M.J. Natan, Anal. Chem. 67 (1995) 735.
[24] N. Nath, A. Chilkoti, Anal. Chem. 76 (2004) 5370.
[25] S.W. Chen, K. Huang, Langmuir 16 (2000) 2014.
[26] T. Morris, H. Copeland, E. McLinden, S. Wilson, G. Szulczewski, Langmuir 18 (2002) 7261.
[27] K. Aslan, C.C. Luhrs, V.H. Pérez-Luna, J. Phys. Chem. B 108 (2004) 15631.
[28] C.S. Weisbecker, M.V. Merritt, G.M. Whitesides, Langmuir 12 (1996) 3763.
[29] P. Mulvaney, Langmuir 12 (1996) 788.
[30] D. Eck, C.A. Helm, N.J. Wagner, K.A. Vaynberg, Langmuir 17 (2001) 957.
[31] K.S. Mayya, V. Patil, M. Sastry, Langmuir 13 (1997) 3944.
[32] M.J. Doyle, H.B. Halsall, W.R. Heineman, Anal. Chem. 54 (1982) 2318.
[33] M.J. Doyle, H.B. Halsall, W.R. Heineman, Anal. Chem. 54 (1982) 2318.
[34] M. Rodríguez Alvarez, R. Badía Laíño, M.E. Díaz-García, J. Lumin. 118 (2006) 193.

Available online at www.sciencedirect.com
ScienceDirect
Talanta 71 (2007) 1769–1773
Talanta
www.elsevier.com/locate/talanta

Flow-injection analysis of glucose without enzyme based on electrocatalytic oxidation of glucose at a nickel electrode

Changzhi Zhao *, Changli Shao, Minghua Li, Kui Jiao

College of Chemistry and Molecular Engineering, Qingdao University of Science and Technology, Qingdao 266042, China

Received 26 April 2006; received in revised form 8 August 2006; accepted 13 August 2006
Available online 18 September 2006

Abstract

This paper reports a flow-injection analysis (FIA) of glucose not using enzyme based on the electrocatalytic oxidation of glucose at a nickel electrode. The electrocatalytic mechanism and quantificational method of glucose have been investigated. The current intensity of the electrocatalytic oxidation to glucose at the potential of 550 mV is proportional to the concentration of glucose over the range of 0.10–2.50 mmol l^{-1}, with a 0.04 mmol l^{-1} detection limit (S/N = 3) and a correlation coefficient of 0.9991. The relative standard deviation (R.S.D.) is less than 4.3% ($n = 5$) for the determination of practical serum samples. The biologic compounds probably existed in the sample, such as ascorbic acid, uric acid, dopamine and epinephrine, do not disturb the determination of glucose. The result is satisfactory for the determination of glucose in human serum sample as comparison to that from the routine hexokinase method.

Keywords: Flow-injection analysis; Glucose; Electrocatalytic oxidation; Nickel electrode

1. Introduction

The studies of modern pathology and medicine have demonstrated that in persons with diabetes, the risk for renal, retinal and neural complications is directly related to the magnitude of chronic elevations of blood glucose [1]. The accurate, rapid and automatic determination of glucose is necessary in clinical laboratories. Numerous methods by using enzyme have been reported for the determination of glucose, including amperometry [2–4], voltammetry [5], photometry [6–7], chemiluminescence and electrochemiluminescence [8,9]. In these methods, glucose oxidase (GOD) catalyzes the oxidation of glucose to gluconic acid in the presence of mediator and brings about change of current, absorbance or light intensity. Accordingly, the concentration of glucose can be determined by way of monitoring these signal changes. The hexokinase method is a representative spectrophotometry for the determination of glucose in clinical laboratories. It is well known that the enzyme reaction of glucose with hexokinase (HK)/glucose-6-phosphate dehydrogenase (G6PDH)-pair as the catalyzer in place of GOD takes place in an aqueous medium as follows [10,11]:

$$\text{Glucose} + \text{ATP} \xrightarrow{\text{HK}} \text{Glucose-6-phosphate} + \text{ADP}$$

By following another enzyme reaction:

$$\text{Glucose-6-phosphate} + \text{NAD}^{+} \xrightarrow{\text{G6PDH}} \text{6-PG} + \text{NADH} + \text{H}^{+}$$

where ATP, ADP, NADH, 6-PG are adenosine triphosphate, adenosine diphosphate, nicotinamide adenine dincleotide and 6-phosphate gluconic acid, respectively. The concentration of glucose can be determined in blood serum, because absorbance enhanced by producing NADH at wavelength of 340 nm is proportional to the concentration of glucose. Biosensor [12–15] is a current method for the determination of glucose. Actually, a great many glucose sensors were glucose electrodes based on immobilizing GOD and electronic mediator, detecting concentration of glucose by way of monitoring the electronic transfer between the mediator and enzyme-catalyzed reaction [16].

Despite analytical methods used enzyme giving an excellent selectivity, active change of enzyme along with time could bring about unpleasant problem to get an accurate result. And use of enzyme is also a considerable cost for conventional glucose

* Corresponding author. Tel.: +86 532 84022729.
E-mail address: zhaocz@qust.edu.cn (C. Zhao).

0039-9140/$ – see front matter © 2006 Elsevier B.V. All rights reserved.
doi:10.1016/j.talanta.2006.08.013

monitoring. Consequently, developing a nonenzymatic method for the determination of glucose is a significant work. Many investigators have already studied the possibility of continuous in vivo glucose monitoring, using several metal electrode. These are mainly oxidizable metals, such as nickel [17–19], gold [20] and copper [21–22]. These metal electrodes can provide a simple and sensitive way for the catalytic oxidation of carbohydrates at constant applied potentials. As previously reported, Schick et al. [17] described a nonenzymatic method for determining serum glucose based upon the direct electrochemical oxidation of glucose by means of stable nickel-catalyst that is electrodeposited onto a lead dioxide electrode surface. The sample is added to 25.00 ml of pH 13 electrolytes containing 1 mmol of $NiSO_4$ per liter, the amount of increase in anodic current comprises the analytical signal. Linear calibration range for determining glucose is from 0.1 to 4500 mg l^{-1}. Ascorbic acid is rapidly decomposed in the electrolyte used and thus does not interfere. Uric acid is inactive at the concentrations present in serum samples. And result was compared with values reported by a hospital laboratory using the hexokinase method. Similarly, Morita et al. [18] developed a highly sensitive amperometric detector for the liquid chromatographic analysis of carbohydrates based on the optimization of the Ni content in a Ni–Ti alloy electrode. Wang et al. [19] reported the advantages of a nickel electrode detector prepared by electroless deposition for CE microchip for the separation and detection of sugars.

Since the nickel electrode prepared by electroplated or electroless deposition has widely been used in the determination of sugars and the electrochemical property of metallic nickel electrode has been investigated [23], we have considered that using directly a metallic nickel electrode as the detector is a more convenient and inexpensive method for practical glucose monitoring. On the other hand, FIA is well established as an excellent technique for rapid, automatic, quantitative analysis that combines on-line chemical sample treatment with a range of flow-through detection systems [24]. In this paper, we would like to report a no enzymatic FIA method for the determination of glucose based on the electrocatalytic oxidation of glucose at a nickel electrode. The rapid, cheap, convenient characteristics of the method have been investigated and the mechanism of electrocatalytic oxidation of glucose at the nickel electrode has been discussed.

2. Experimental

2.1. Apparatus

A FIA system was made from a flow-injection analyzer (Shandong Seventh Telecommunication Co., Ltd., Jining, China) and a CHI 660B electrochemical analyzer (CH Instruments, USA) connected to a PC for control and data storage. One peristaltic pump was used to deliver the carrier stream, and injection of both the standard solution of glucose and the sample solution was made using a six-way valve equipped with a 100 μl sample loop. The flow-through electrolytic cell utilized a conventional three-electrode set-up was arranged as shown in Fig. 1. The flow-cell was made of polytetrafluoroethylene block fitted with three electrodes system. The nickel electrode was used as the working electrode, which was prepared with a nickel rod (>99.9% purity, Aldrich Chem. Co. Inc., USA) of 1.0 mm diameter. The counter electrode was a stainless steel tube and an Ag/AgCl electrode was used as the reference electrode. The applied potential was controlled with the electrochemical system and the current intensity was registered synchronously. The comparison spectrophotometric analysis was performed with a RT–1904C Semi-auto Chemistry Analyzer (Rayto Life and Analytical Sciences Co., Ltd., USA) in accordance to the hexokinase method.

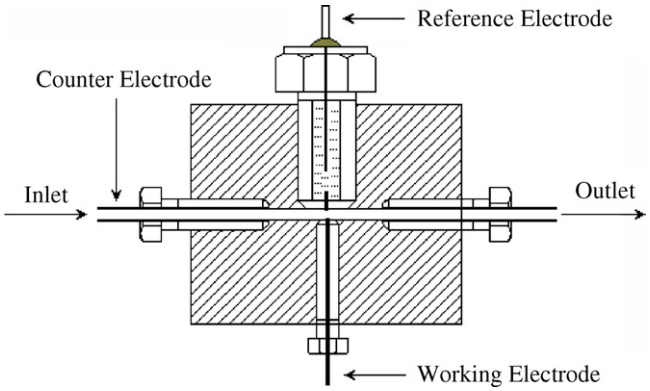

Fig. 1. Construction of the flow-through electrolytic cell.

2.2. Reagents

All solutions were prepared from analytical grade chemicals and deionised water (>15 MΩ) prepared from a KLUP-III water treatment system (Kang Ning Water Industry, China). A 0.01 mol l^{-1} glucose (99.9% purity, Kermel) stock solution was prepared, and stored in a refrigerator. Low concentration standard solutions of glucose were freshly prepared from the stock solution with 0.1 mol l^{-1} NaOH solution before experiment. Glucose reagent kit was used for the spectrophotometric measurement of glucose. The kit (compose from 1.30 mmol l^{-1} ATP, 0.65 mmol l^{-1} NAD, 1500 U l^{-1} HK, 2500 U l^{-1} G6PDH and 50 mmol l^{-1} triethanolamine) was purchased from Shanghai Fosun Long March Medical Science Co. Ltd. Serum samples were collected from a hospital (Qingdao, China).

2.3. Procedure

Before the first measurement was performed, the FIA system was allowed to run for 5 min to achieve good mechanical and thermal stability. The solution of the 0.1 mol l^{-1} NaOH as carrier stream was fed at a flow rate of 4.0 ml min^{-1}. A 550 mV potential was applied to the working electrode with the electrochemical system, and a stable blank baseline was observed. Then the standard glucose or sample solution was injected into the carrier stream, the current signal was recorded, and the concentration of glucose was quantified finally by the peak height of current intensity.

3. Results and discussion

3.1. Electrocatalytic oxidation of glucose at a nickel electrode

In alkaline solution, cyclic voltammetric curves of the nickel electrode in the absence and presence of glucose by scanning the potential from 0 to 630 mV are shown in Fig. 2, respectively. The cyclic voltammogram (Fig. 2b) of the nickel electrode in 0.1 mol l^{-1} NaOH showed a nonsymmetrical face wave, with an anodic peak potential at about 510 mV and a cathodic peak potential at about 400 mV versus Ag/AgCl, corresponding to the Ni(III)/(II) redox couple. The electrochemical reactions of peaks may be as follows:

$$NiO + OH^- - e^- \rightarrow NiO(OH) \quad (1)$$

$$\text{or } Ni(OH)_2 + OH^- - e^- \rightarrow NiO(OH) + H_2O \quad (2)$$

where NiO and $Ni(OH)_2$ are due to the oxidation of Ni(0) to Ni(II) at potential of less than −600 mV [25].

$$Ni + 2OH^- - 2e^- \rightarrow NiO + H_2O \quad (3)$$

$$\text{or } Ni + 2OH^- - 2e^- \rightarrow Ni(OH)_2 \quad (4)$$

Ep. (1) and (2) may be simply described by

$$Ni(II) - e^- \rightarrow Ni(III) \quad (5)$$

According to previous studies, carbohydrates can be oxidized at high pHs [26]. In this work, the Ni(III)/(II) species on the electrode surface acts as a catalyst for the oxidation of glucose, as can be seen clearly in Fig. 2(a). The peak potential of electrocatalytic oxidation appeared at about 550 mV, and its reduction peak potential appeared at about 420 mV. In aqueous solution when glucose diffuses from the bulk solution to the electrode surface, the glucose is quickly oxidized to glucolactone by the Ni(III) species on the electrode. As can be seen, upon glucose addition (1.00 mmol l^{-1}) there is an increase in the anodic peak current and the cathodic peak current (Fig. 2a). Because the

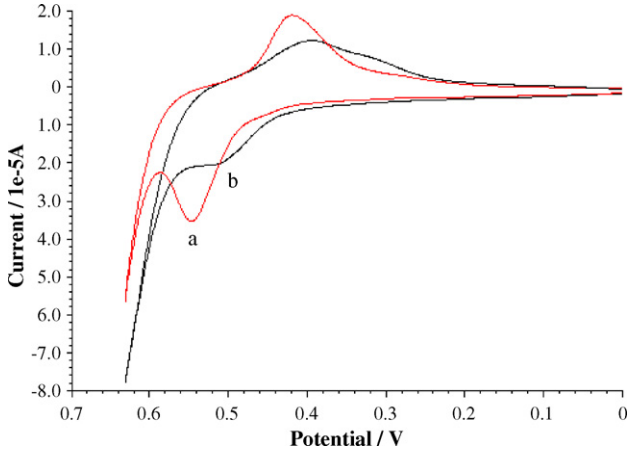

Fig. 2. Cyclic voltammograms of a nickel electrode in the absence (b) and presence (a) of 1.92×10^{-4} mol l^{-1} glucose in 0.1 mol l^{-1} NaOH. Scan rate was 100 mV s^{-1}.

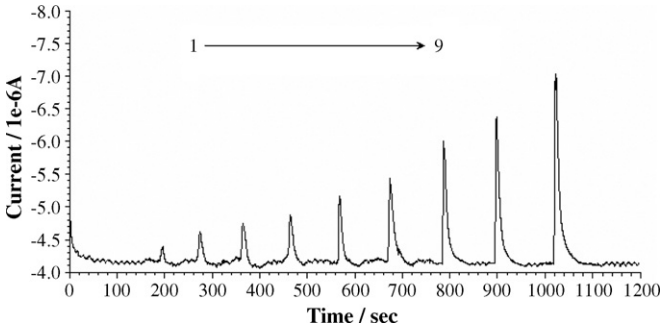

Fig. 3. Current responses for the injection of various concentrations of standard glucose solutions: (1) 0.10, (2) 0.20, (3) 0.40, (4) 0.60, (5) 0.80, (6) 1.00, (7) 1.50, (8) 2.00 and (9) 2.50 mmol l^{-1}. Flow rate of the carrier stream and applied potential were controlled at 4.0 ml min^{-1} and 550 mV, respectively.

Ni(III)/(II) redox couple serve double function of the electronical medium and enzyme, synchronously, this electrochemical behavior is different from typical mediated catalytic oxidation which the cathodic peak current is decreasing. The electrocatalytic oxidation mechanism of glucose at the nickel electrode surface may be simply described by

$$Ni(II) \rightarrow Ni(III) + e^- \quad (6)$$

$$Ni(III) + \text{Glucose} \rightarrow Ni(II) + \text{Glucolactone} \quad (7)$$

Based on above results, when applying a potential of 550 mV to the nickel electrode, the Ni(III) species produces on the electrode surface and oxidizes glucose to generate Ni(II) species, producing the glucolactone, simultaneously. Fig. 3 shows the response of anodic current dependent on the glucose concentration due to the oxidation of glucose.

3.2. Effect of flow rate and sample volume

An optimum flow rate is necessary to deliver the reactant for the maximum collection of the current response in the flow-through electrolytic cell. The effects of flow rate on the intensity of current were studied over the range 2.0–5.0 ml min^{-1} in each stream. The current intensities for glucose were increased with an increase in flow rate up to 4.5 ml min^{-1}. But current peaks became very narrow when flow rate was greater than 4.5 ml min^{-1}, resulting in a lower accuracy. The flow rate raised from 4.0 to 4.5 ml min^{-1}, the current intensities increased a little. So, an optimal flow rate of 4.0 ml min^{-1} was selected to maintain the maximum sensitivity and reproducibility for the subsequent experiments. After elaborating the electrochemical reaction conditions, the injection volume parameter was investigated. The variation of current response with the injected sample volume in the 50–150 μl range was studied. The results showed that relative higher current response was observed by increasing loop volumes up to 100 μl but current peaks appeared a trail when the loop volume exceeded 100 μl. Thus, in the present FIA system, a 100 μl sample loop was selected.

3.3. Amperometric response and calibration curve

Under the optimum conditions described above, Fig. 3 shows typical dynamic current responses to the injection of different concentration glucose at applied potential of 550 mV. The peak height of the current is proportional to the concentration of glucose over the range of 0.10–2.50 mmol l^{-1}. The calibration curve of $i = 4.26 + 1.09c$ (i and c express the height of peak current and concentration of glucose, respectively) was obtained with correlation coefficient of $r = 0.9991$. The detection limit (S/N = 3) was estimated to be 0.04 mmol l^{-1}, being low enough to apply to human serum sample. The determination of glucose could be performed in 1.5 min including sampling and washing, giving a throughput of ca. 40 h^{-1}. The relative standard deviation was 3.9% for five repeated determinations of 1.00 mmol l^{-1} glucose.

3.4. Interference study

The effect of foreign substances was tested by analyzing a standard solution of 1.00 mmol l^{-1} glucose to which increasing amounts of interfering substances was added. The concentration ratios for a 5% change of current response are stipulated for a tolerable limit. Experimental results revealed that the determination of 1.00 mmol l^{-1} glucose was not influenced by a less than 10^2-fold excess of the added general cations and anions, such as Ca(II), Mg(II), Cu(II), Cd(II), Pb(II), Fe(II), Fe(III), Al(III) and Cl^-, PO_4^{3-}, SO_4^{2-}, NO_3^-. It can be seen that the nickel electrode is highly selective toward electrocatalytic oxidation of glucose under present experimental conditions. However, more than five times MnO_4^- and eight times $Cr_2O_7^{2-}$ affect the determination of glucose, which is presumably due to the oxidation of glucose by oxidizing agent, leading to a decrease of the current response. Additionally, H_2O_2 (HO_2^-) possibly participating in the electrochemical process, and resulting in an increase of the current response interferes the determination of glucose. The biologic compounds probably existed in the sample, such as ascorbic acid, uric acid, dopamine, and epinephrine of two times as large as glucose have no arouse 5% change of the current signal (Fig. 4). These reducible substances do not disturb the determination of glucose in the present concentration, because they are rapidly decomposed in alkaline electrolyte used or are inactive at nickel electrode [17]. But other saccharine compounds in sample could bring on an increase of the current, resulting in a plus error.

3.5. Application

The detection limit of 0.04 mmol l^{-1}, and measurement range of 0.10–2.50 mmol l^{-1} allowed a direct determination of the glucose content in serum samples. To avoid the deterioration of sample, the serum was freshly diluted appropriately with 0.1 mol l^{-1} NaOH solution before measurement. For a sample containing 6.19 mmol l^{-1} glucose, the result obtained for five measurements was 6.17 ± 0.27 mmol l^{-1} (95% confidence interval), giving an acceptable accuracy and precision. Glucose quantities for five different blood samples were determined and summarized in Table 1 with the results of hexokinase method

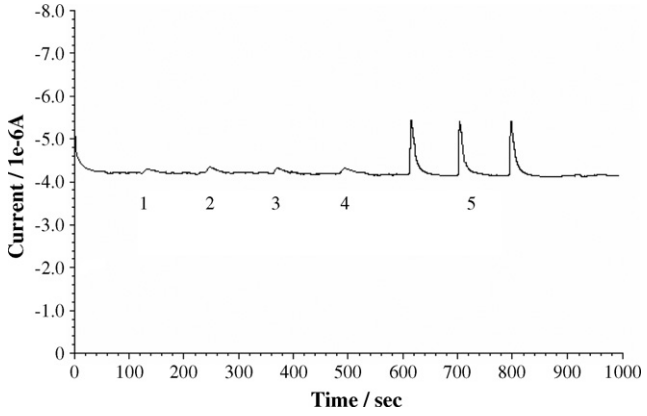

Fig. 4. Current changes for the injection of interferential compounds and glucose solutions: (1) 2.00 mmol l^{-1} ascorbic acid, (2) 2.00 mmol l^{-1} uric acid, (3) 4.00 mmol l^{-1} dopamine, (4) 4.00 mmol l^{-1} epinephrine and (5) 1.00 mmol l^{-1} glucose. The applied potential was 550 mV. Other experimental conditions were the same as in Fig. 3.

Table 1
Determination of glucose in human serum samples

Serum sample	This method (mmol l^{-1})	R.S.D. (%) ($n = 5$)	Hexokinase method (mmol l^{-1})
Sample 1	5.83	4.1	5.98
Sample 2	5.02	3.9	5.16
Sample 3	6.44	3.8	6.52
Sample 4	4.68	4.3	4.77
Sample 5	6.17	3.5	6.19

(spectrophotometry) for the comparison. The relative standard deviation was less than 4.3% to five parallel measurements of same sample.

4. Conclusions

Based on the electrocatalytic oxidation of glucose at a nickel electrode, a novel detection method of glucose in people serum without enzyme has been established. Linear range for monitoring glucose is 0.10–2.50 mmol l^{-1}, with a 0.04 mmol l^{-1} detection limit. The relative standard deviation (R.S.D.) is less than 4.3% for the determination of practical serum samples. No interference was observed even for these concentrations larger than the maximum physiological levels found in human serum blood (such as ascorbic acid level: $3.0–11.0 \times 10^{-5}$ mol l^{-1}, uric acid level: 3.5–6.0 mg dl^{-1}). The method exhibits a very convenient and inexpensive technique, which provides a simple, rapid and acceptable accuracy for determination of serum glucose level. And the established FIA system shows a short analysis time, a small volume of sample solution and a good reproducibility. Although other saccharine compounds interfere with determination of glucose, the method is satisfactory for the determination of glucose in human serum sample.

Acknowledgements

The authors are grateful for the financial support received from the National Nature Science Foundation of China (No.

20375020) and the National Nature Science Foundation of Qingdao City (No. 04-02-JZP-8).

References

[1] A.P. Turner, B. Chen, S. Piletsky, Clin. Chem. 45 (1999) 1596.
[2] M. Masoon, A. Townshend, Anal. Chim. Acta 166 (1984) 111.
[3] S.D. Kumar, A.V. Kulkarni, R. Kalyanraman, T.S. Krishnamoorthy, Anal. Chim. Acta 338 (1997) 135.
[4] J. Fei, K. Wu, F. Wang, S. Hu, Talanta 65 (2005) 918.
[5] J.M. Zen, C.W. Lo, Anal. Chem. 68 (1996) 2635.
[6] M. Zhu, X.M. Huang, H.X. Shen, Anal. Chim. Acta 349 (1997) 165.
[7] H. Katsumata, T. Sekine, N. Teshima, M. Kurihara, T. Kawashima, Talanta 51 (2000) 1197.
[8] P. Panoutsou, A. Economou, Talanta 67 (2005) 603.
[9] C.A. Marquette, L.J. Blum, Anal. Chim. Acta 381 (1999) 1.
[10] D.S. Young, D.W. Thomas, R.B. Friedman, L.C. Pestaner, Clin. Chem. 18 (1972) 1041.
[11] Y. Ye, Y. Wang, Operational Criterion for Countrywide Clinical Tests, second ed., Southeast University Press, Nanjing, 1997, p. 100.
[12] A. Cass, G. Davis, G. Francis, H.A. Hill, W. Aston, I.J. Higgins, E. Plotkin, L. Scott, A.P. Turner, Anal. Chem. 56 (1984) 667.
[13] J. Hodak, R. Etchenique, E. Calvo, P.N. Bartlett, Langmuir 13 (1997) 2708.
[14] W.K. Ward, L.B. Jansen, E. Anderson, G. Reach, J.-C. Klein, G.S. Wilson, Biosens. Bioelectron. 17 (2002) 181.
[15] S. Kalayci, G. Somer, G. Ekmekci, Talanta 65 (2005) 87.
[16] Y. Ito, S. Yamazaki, K. Kano, T. Ikeda, Biosens. Bioelectron. 17 (2002) 993.
[17] K.G. Schick, V.G. Magearu, C.O. Huber, Clin. Chem. 24 (1978) 448.
[18] M. Morita, O. Niwa, S. Tou, N. Watanabe, J. Chromatogr. A 837 (1999) 17.
[19] J. Wang, G. Chen, M.P. Chatrathi, Electroanalysis 16 (2004) 1603.
[20] A. Hilmi, J.H.T. Luong, Anal. Chem. 72 (2000) 4677.
[21] L.A. Colon, R. Dadoo, R.N. Zare, Anal. Chem. 65 (1993) 476.
[22] K. Kano, K. Takagi, K. Inoue, T. Ikeda, T. Ueda, J. Chromatogr. A 721 (1996) 53.
[23] A.A. El-Shafei, J. Electroanal. Chem. 471 (1999) 89.
[24] E.H. Hansan, Anal. Chim. Acta 308 (1995) 3.
[25] P.F. Luo, T. Kuwana, Anal. Chem. 68 (1996) 3330.
[26] F.D. Eramo, J.M. Marioli, A.A. Arevalo, L.E. Sereno, Electroanalysis 11 (1999) 481.

Available online at www.sciencedirect.com
ScienceDirect
Talanta 71 (2007) 1541–1545
Talanta
www.elsevier.com/locate/talanta

Separation and determination of acrylamide in potato chips by micellar electrokinetic capillary chromatography

Xun Zhou, Liu-Yin Fan, Wei Zhang, Cheng-Xi Cao *

Laboratory of Analytical Biochemistry and Bioseparation, School of Life Science and Biotechnology, Shanghai Jiao Tong University, 800 Dongchuan Rd. Minhang, 200240 Shanghai, PR China

Received 29 April 2006; received in revised form 5 June 2006; accepted 19 July 2006
Available online 6 September 2006

Abstract

A simple and rapid method using micellar electrokinetic capillary chromatography (MEKC) was developed for the separation and determination of acrylamide in potato chips at low levels for the first time. The experimental conditions for the separation and quantification of acrylamide were optimized at first. The optimized conditions were: 50 mmol/L $Na_2B_4O_7$ and 40 mmol/L SDS at pH 10.0, 12 kV applied voltage, 76 cm total length (67 cm effective length) and 75 μm i.d. capillary, 198 nm wavelength, 15 cm high 25 s hydrodynamics sample injection, 20 °C air-cooling. The linear response of acrylamide concentration ranges from 0.5 to 100 μg/mL with high correlation coefficient ($r = 0.9986$, $n = 9$). The LOD and LOQ were estimated to be 0.1 and 0.33 μg/mL based on S/N = 3 and 10. The precision values (expressed as R.S.D.) of intra- and inter-day were 0.86–4.35% and 2.61–9.65%, respectively. Recoveries spiked at levels 2, 20, 60 μg/mL ranged between 90.86% and 99.6% with R.S.D. less than 6.5%. Finally, the developed method has been applied to the analysis of real samples and has achieved satisfactory results. All of these indicated that it was a reliable method for the quantification of acrylamide in potato chips.

Keywords: Acrylamide; MEKC; Potato chips; Quantification; Capillary electrophoresis

1. Introduction

In April 2002, researchers from the University of Stockholm and the Swedish National Food Administration (NFA) reported the presence of acrylamide (2-propenamide) in a wide range of fried and oven-cooked foods [1]. These findings have attracted considerable attention worldwide because acrylamide has been classified as "probably carcinogenic to humans" by the International Agency for Research on Cancer (IARC) [2]. Recent studies have shown that acrylamide (see Fig. 1) was formed during the Maillard reaction, and that the major reactants leading to the release of acrylamide were sugars and asparagine [3,4]. The potential health risk of acrylamide in food has been considered by a number of government agencies and national authorities [5]. Thus, simple and sensitive analytical methods for the separation and determination of acrylamide are of great interest.

So far, methods based on gas chromatography (GC)–mass spectrometry (MS) [6–10] and liquid chromatography with tandem mass spectrometry (LC–MS/MS) [11–18] techniques have been reported. Although acknowledged as the most useful and authoritative method for the determination of acrylamide [19], these methods have some connatural disadvantages, such as complex procedure, expensive consume of instrument and reagents, pollution of organic reagents in laboratory, etc. [20]. Capillary electrophoresis (CE) has been successfully applied to the analysis of the complex matrices [21–23] because of its advantages of excellent separation efficiency, rapid analysis and minimal use of the samples and solvents [24,25]. Micellar electrokinetic capillary chromatography (MEKC) is an important separation mode of CE, and it can be employed for the separation of not only charged but also neural compounds by means of its capacity to partition molecules between the aqueous phase and the pseudo-stationary micellar phase [26,27]. It has been proven that MEKC can compete with HPLC with regard to the efficiency and selectivity [28,29], and several MEKC methods have been developed for the analysis of natural products [30,31].

* Corresponding author. Tel.: +86 21 34205820; fax: +86 21 34205820.
E-mail address: cxcao@sjtu.edu.cn (C.-X. Cao).

0039-9140/$ – see front matter © 2006 Elsevier B.V. All rights reserved.
doi:10.1016/j.talanta.2006.07.037

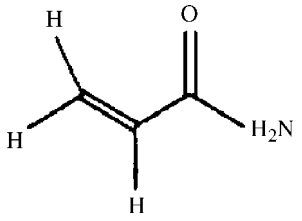

Fig. 1. Chemical structure of acrylamide. 71. 08 g/mol, CAS: 79-06-1.

In this paper, we had an innovative try and took the lead in developing a simple, fast and low-cost analytical method for the determination of acrylamide in potato chips by MEKC. Our work was based on the systematic investigation of the influences of pH value, concentration of buffer and SDS, applied voltage and the validation of method.

2. Experimental

2.1. Apparatus

The analysis of acrylamide was performed by an ACS 2000 HPCE apparatus (Beijing Cailu Scientific Inc., Beijing, China). The apparatus were comprised of a digital power supply (up to voltage 30 kV), a HW-2000 chromatography workstation and a UV–vis detector that could perform wavelength scanning from 190 to 740 nm. A fused-silica capillary (Factory of Yongnian Optical Fiber, Heibei, China), which was with 75 μm i.d. × 76 cm (67 cm effective length) was used. An Ultra-pure Water System (SG Ultra Clear system, Wasseraufbereitung und Regenerierstation Gmbh, Germany) was used to produce ultra pure water. pH meter (METTLER TOLEDO, Switzerland) was used for the pH measurement.

2.2. Chemicals

Acrylamide and sodium dodecyl sulfate (biochemical reagent, BC) were purchased from the Shanghai Shisheng Cell and Bio-technology Company (Shanghai, China). Sodium tetraborate (guarantee reagent, GR) was purchased from the Shanghai Chemistry Reagent Company (Shanghai, China). Methacrylamide (≥98% purity) and hexane (analytical reagent, AR) were obtained from the Sinopharm Chemical Reagent Co., Ltd. (Shanghai, China). Methanol (analytical reagent, AR) was purchased from the First Chemical Plant of Zhenxing (Shanghai, China).

2.3. Standards and reagents

$Na_2B_4O_7$-SDS solutions were chosen as the background electrolyte in our experiment. The pH value of the buffers ranged from 8.5 to 10.5 and the concentrations of $Na_2B_4O_7$ changed from 10 to 60 mmol/L as well as the SDS was from 10 to 50 mmol/L.

Stock solution of acrylamide (1 mg/mL) and methacrylamide (1 mg/mL) were prepared by dissolving in MeOH. Working standards for HPCE analysis were prepared according to the following procedures. 200, 120, 80, 40, 20, 10, 4, 2 and 1 μL of acrylamide solution (1 mg/mL) and 100 μL methacrylamide solution (1 mg/mL) were added into blank sample, respectively. Corresponding volume of MeOH were added afterwards and then the working standards were conducted in accordance with the procedures in Section 2.4. The final concentrations of working standards were 100, 60, 40, 20, 10, 5, 1 and 0.5 μg/mL.

2.4. Sample preparation

Finely ground potato chips (4 g) were weighed into a 50 mL centrifuge tube, and then 20 mL MeOH [32] and 100 μL internal standard (methacrylamide, 1 mg/mL) were added into the tube which would be strongly vibrated with a vibrator for 2 min later. After that, the mixture in the tube was centrifuged at 10,000 rpm (11,180 × *g*) and 10 °C for 10 min. The extraction was repeated for three times and the clear supernatants were combined together and were transferred into a beaker placed in a water bath at 70 °C for evaporation. The residue was dissolved in 1 mL ultra-pure water, and then the same volume hexane was added for defatting for two times. Before injection the sample solution was diluted two times with background electrolyte. All solutions were stored at 4 °C in a refrigerator until use.

2.5. Analytical procedures

HPCE was carried out with the following procedures. Before using, the new capillary was conditioned by rinsing with 1 mol/L NaOH for 20 min, ultra-pure water for 20 min, 1 mol/L HCl for 20 min, ultra-pure water for 20 min, and equilibrated for 30 min with the background electrolyte, in order. Between injections, the capillary was rinsed with the background electrolyte for 3 min. Since acrylamide is a derivative of carboxylic acid, the detection wavelength was set at 198 nm, which is the maximum absorbance wavelength of acrylamide [32]. Hydrodynamics injection (15 cm high, 25 s) was chosen to load samples. The working voltage was 12 kV. Temperature control of capillary was carried out with 20 °C air-cooling. Detection data were collected and processed with the HW-2000 Chromatography Workstation Software.

3. Results and discussions

3.1. Optimization of conditions

3.1.1. Effect of running voltage

Applied voltage had a great important effect on migration time, current strength and resolution. It indicated that with the increase of applied voltage, the migration time decreased due to the increasing of electroosmotic flow (EOF). However, it would induce a poor resolution of peaks as well as a deteriorated baseline due to the much higher Joule's heating and electric current at higher voltage. In order to obtain better resolution and faster detection of acrylamide, 12 kV was chosen as the working voltage.

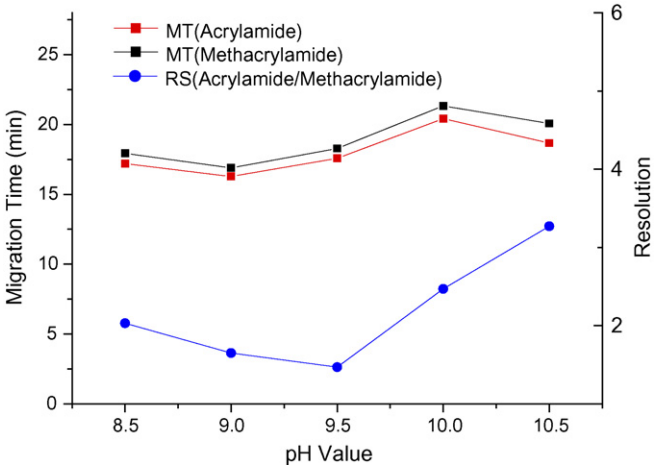

Fig. 2. Effect of pH value on migration time and resolution of acrylamide and methacrylamide. Conditions: pH 8.5–10.5 $Na_2B_4O_7$ (50 mmol/L)-SDS (40 mmol/L), 12 kV voltage, 76 cm total length (67 cm effective length) and 75 μm i.d. capillary, 198 nm wavelength, 15 cm high 25 s hydrodynamics sample injection, 20 °C air-cooling.

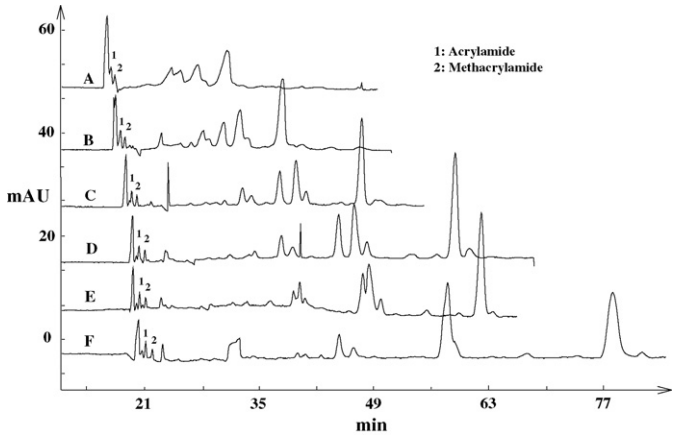

Fig. 3. Electropherograms of acrylamide at different concentrations of $Na_2B_4O_7$. (A) 10 mmol/L; (B) 20 mmol/L; (C) 30 mmol/L; (D) 40 mmol/L; (E) 50 mmol/L; (F) 60 mmol/L. Conditions: pH 10.0 $Na_2B_4O_7$-SDS (40 mmol/L), 12 kV voltage, other conditions are the same as those in Fig. 2.

3.1.2. *Effect of pH value of buffer*

In this experiment, the choice of pH value was very important to the separation of acrylamide and internal standard. As shown in Fig. 2, pH did not have an obvious influence on the migration time of acrylamide and internal standard. The changes of migration time were kept within about 3 min. The resolution of acrylamide and internal standard decreased with increasing buffer pH up to 9.5, and then increased at higher pH. There was no baseline separation between acrylamide and internal standard at pH lower than 10.0. Furthermore, at lower pH, acrylamide could not be separated from other components in potato chip. Although it had a better resolution at pH 10.5, the wavy baseline and high current went against the analysis on HPCE. Considering on better separation and peak shape, pH 10.0 was chosen as the optimized pH value.

3.1.3. *Effect of buffer concentration*

Buffer concentration played an important part in our research to the effect on resolution, peak shape, and electric current. Electropherograms with different concentrations of $Na_2B_4O_7$ (10–60 mmol/L) were shown in Fig. 3. The result indicated that the resolution of analytes were increased with the increasing of buffer concentration, but when it was higher than 50 mmol/L, the separation of internal standard to other components became worse. At the same time the increased ionic strength led to much higher current and the peak shape became wider. With 50 mmol/L buffer, the baseline separation of acrylamide and methacrylamide was achieved and the current level was acceptable. Finally, 50 mmol/L $Na_2B_4O_7$ was selected in the following experiments for better separation.

3.1.4. *Effect of SDS concentration*

The effect of SDS concentration on the separation was tested in the range of 10–50 mmol/L (see Fig. 4). Because of the superior water-solubility, acrylamide had weak retention in the micellar phase and moved faster than most of other components. With increasing SDS concentration up to 40 mmol/L, not only the resolution of acrylamide and internal standard but also the separation of analytes to other components was increased. But it would lower the detection sensitivity and overlap the peak of acrylamide with other components at 50 mmol/L SDS, because capillary would be absorbed in part at a higher concentration. It was obvious that the SDS concentration had evident influence on separation and detection sensitivity, so 40 mmol/L SDS was the better choice.

3.1.5. *Optimized results*

As the results mentioned above, the optimized separation condition was obtained with the background electrolyte containing 50 mmol/L $Na_2B_4O_7$ and 40 mmol/L SDS at pH 10.0, 12 kV applied voltage, 76 cm total length (67 cm effective length) and 75 μm i.d. capillary, 198 nm wavelength, 15 cm high 25 s hydrodynamics sample injection, 20 °C air-cooling.

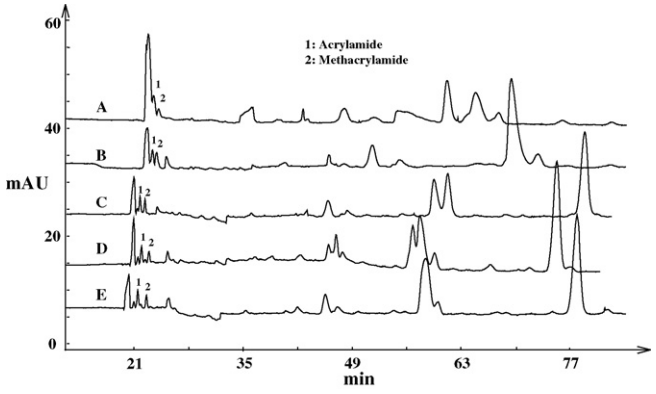

Fig. 4. Electropherograms of acrylamide at different concentrations of SDS. (A) 10 mmol/L; (B) 20 mmol/L; (C) 30 mmol/L; (D) 40 mmol/L; (E) 50 mmol/L. Conditions: pH 10.0 $Na_2B_4O_7$(50 mmol/L)-SDS, 12 kV voltage, other conditions are the same as those in Fig. 2.

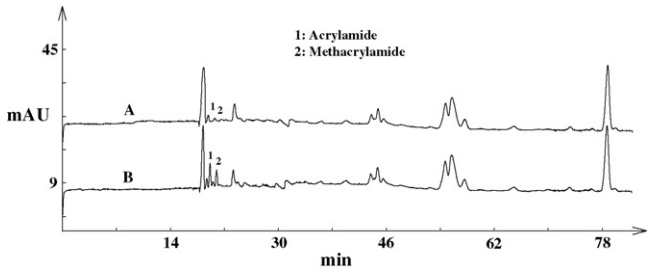

Fig. 5. Electropherograms of MEKC: (A) blank sample; (B) acrylamide and internal standard extracted from the blank sample. Conditions: 12 kV applied voltage, pH 10.0 $Na_2B_4O_7$ (50 mmol/L)-SDS (40 mmol/L) buffer, others are the same as those in Fig. 2.

3.2. Validation

In order to validate the feasibility and validity of our developed method in the analysis of acrylamide, routine criteria such as specificity, linearity, precision, accuracy and LOD, etc. were assessed as described below.

3.2.1. Specificity of method

The components of potato chips are very complex. Except the basal components of food such as starch, lipids and protein etc., there are some food additive in potato chips. So not only the acrylamide but also some other components were extracted out during sample preparation. The purpose of the analyses was to make sure whether the optimized conditions mentioned above could provide an effective system for the separation of acrylamide in potato chips. It was found that the peaks of acrylamide and internal standard were not interfered and the target analytes were separated on baseline from other components as shown in Fig. 5. Fig. 5A is the electropherograms of blank sample and no interferential peaks appeared at marker 1 and 2. Fig. 5B displays the peaks of acrylamide and internal standard extracted from the blank sample.

3.2.2. Linearity and detection limits

The response of detector was linearly changed with the concentration of standard solutions of acrylamide extracted from blank sample in the range of 0.5–100 μg/mL. The calibration curves ($y = 0.03246x + 0.00988$, y is the ratio of peak area, x is the concentration) revealed good linear behavior over the investigated concentration range ($r = 0.9986$, $n = 9$). Taking into account the instrumental noise recorded at 198 nm, the limit of detection (LOD) and limit of quantification (LOQ) was calculated to be 0.1 and 0.33 μg/mL, respectively, on the basis of a signal-to-noise ratio of 3 and 10.

3.2.3. Precision

Precision was evaluated by measuring intra- and inter-day relative standard deviations (R.S.D.) of peak areas ratio between acrylamide and internal standard extracted from blank sample. The intra-assay precision was performed by analyzing samples with the interval of 2 h in 1 day for five times at three different concentrations of 2, 20 and 60 μg/mL, and the inter-assay precision was performed over 5 days with the same three concentrations. The values of R.S.D. of intra-day were ranged from 0.86% to 4.35% as well as the inter-day was from 2.61 to 9.65%. The results implied that the operating conditions selected above could provide a stable background with good repeatability.

Table 1
The recovery of acrylamide under different concentrations ($r = 3$, $n = 3$)

Spiking level (μg/mL)	Recovery (%)	S.D.	R.S.D. (%)
2	90.86	0.05	5.50
20	92.77	0.06	6.47
60	99.60	0.04	4.01

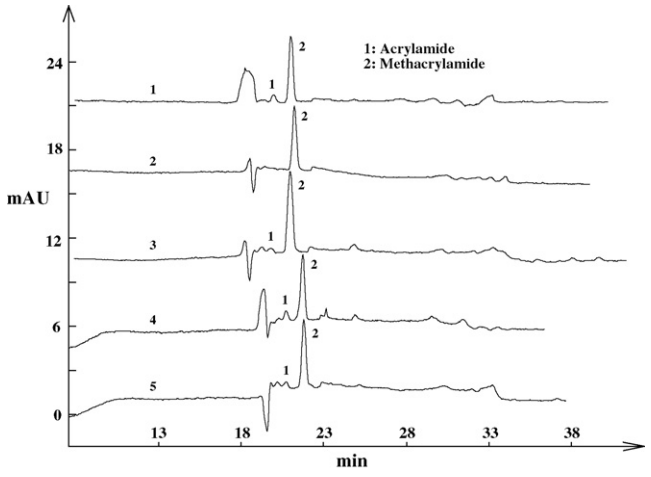

Fig. 6. Electropherograms of potato chips samples. 1–5 were different brands of potato chips. Conditions are the same as those in Fig. 5.

3.2.4. Accuracy

The recovery experiments were performed on sample with three different concentrations. Acrylamide standard solution was added to the blank sample and prepared as described in Section 2.4 to achieve the spiking level: 2, 20 and 60 μg/mL. The recovery was calculated by the ratio value of acrylamide and methacrylamide extracted from blank sample to the ratio of them resolved in the background electrolyte directly. The results were all acceptable and given in Table 1.

3.2.5. Analysis of real samples

In order to evaluate the applicability of this method for the determination of acrylamide in real samples, the analysis of potato chips were performed as described in Section 2. Five brands of potato chips belonged to different manufactures were

Table 2
Content of acrylamide in potato chips ($n = 3$)

Potato chips	Determined results (mg/kg) ($P = 0.90$)	R.S.D. (%)
Sample 1	1.505 ± 0.119	4.7
Sample 2	[a]	[a]
Sample 3	0.887 ± 0.099	6.7
Sample 4	2.393 ± 0.230	5.7
Sample 5	1.518 ± 0.109	4.3

[a] Not detected in the sample.

purchased from the supermarket in Shanghai, China. The electropherograms were shown in Fig. 6. The measurement results were given in Table 2 and the values were in agreement with the results reported in FDA, which was ranged from 0.693 to 2.510 mg/kg in potato chips [33].

4. Concluding remarks

A new MEKC method has been developed for the quantitative analysis of acrylamide in potato chips. Compared with other traditional chromatographic methods used, capillary electrophoresis shows several advantages. On one hand, it was more convenient, especially leaved out the clean-up procedures on solid phase extraction column, which was absolutely necessarily in chromatographic analysis so that the operation was more simple. On the other hand, the retention time of acrylamide was controlled within 20 min so that a rapid and time-saving monitoring could be achieved. On the third hand, less consumption of apparatus and chemicals made CE more economical. It was our first attempt to use MEKC to the analysis of acrylamide and we hoped that our research can give promotion to the found of detection ways of acrylamide in food matrix. Certainly, the better detection sensitivity and clean-up are waiting to be developed under further research.

Acknowledgement

The authors are grateful for the funding provided by the National Natural Science Foundation of China (No. 20475036, 20245004).

References

[1] Swedish National Food Administration, Information About Acrylamide in Food, 24 April 2002. http://www.slv.se.
[2] IARC Monographs on the Evaluation of Carcinogen Risk to Humans, International Agency for Research on Cancer, vol. 60, Lyon, 1994, p. 389.
[3] D.S. Mottram, B.L. Wedzicha, A.T. Dodson, Nature 419 (2002) 448.
[4] R.H. Stadler, I. Blank, N. Varga, F. Robert, J. Hau, P.A. Guy, M.-C. Robert, S. Riediker, Nature 419 (2002) 449.
[5] Y. Zhang, G.Y. Zhang, Y. Zhang, J. Chromatogr. A 1075 (2005) 1.
[6] L. Castle, M.-J. Campos, J.J. Gilbert, Sci. Food Agric. 54 (1991) 549.
[7] M. Biedermann, S. Biedermann-Brem, A. Noti, K. Grob, Mitt. Lebensm. Hyg. 93 (2002) 638.
[8] F. Tateo, M. Bononi, Ital. J. Food Sci. 15 (2003) 149.
[9] H. Ono, Y. Chuda, M. Ohnishi-Kameyama, H. Yada, M. Ishizaka, H. Kobayashi, M. Yoshida, Food Addit. Contam. 20 (2003) 215.
[10] S. Nemoto, S. Takatsuki, K. Sasaki, T. Maitani, J. Food Hyg. Soc. Jpn. 43 (2002) 371.
[11] J. Rosen, K.-E. Hellenas, Analyst 127 (2002) 880.
[12] E. Tareke, P. Rydberg, P. Karlsson, S. Eriksson, M. Tornqvist, J. Agric. Food Chem. 50 (2002) 4998.
[13] J.S. Ahn, L. Castle, D.B. Clarke, A.S. Lloyd, M.R. Philo, D.R. Speck, Food Addit. Contam. 19 (2002) 1116.
[14] D.V. Zyzak, R.A. Sanders, M. Stojanovich, D.H. Tallmadge, B.L. Eberhart, D.K. Ewald, D.C. Gruber, T.R. Morsch, M.A. Strothers, G.P. Rizzi, M.D. Villagran, J. Agric. Food Chem. 51 (2003) 4782.
[15] A. Becalski, B.P.Y. Lau, D. Lewis, S.W. Seaman, J. Agric. Food Chem. 51 (2003) 802.
[16] J.A.G. Roach, D. Andrzejewski, M.L. Gay, D. Nortrup, S.M. Musser, J. Agric. Food Chem. 51 (2003) 7547.
[17] M. Jezussek, P. Schieberle, J. Agric. Food Chem. 51 (2003) 7866.
[18] S. Riediker, R.H. Stadler, J. Chromatogr. A 1020 (2003) 121.
[19] T. Wenzl, M.B. de la Calle, E. Anklam, Food Addit. Contam. 20 (2003) 885.
[20] Q.L. Wang, X.H. Zhang, L.Y. Fan, W. Zhang, Y.Q. Xu, H.B. Hu, C.X. Cao, J. Chromatogr. B 826 (2005) 252.
[21] A. Nicole, W.B. Neil, W.L. Simon, Talanta 67 (2005) 269.
[22] S.L. Zhao, Y.R. Song, Y.M. Liu, Talanta 67 (2005) 212.
[23] G.H. Kristy, L. Holly, R.M. Bruce, Talanta 67 (2005) 304.
[24] S.F. Wang, Y.Y. Cheng, J. Pharm. Biomed. Anal. 40 (2006) 1137.
[25] Y. Zheng, Y. Sun, J.C. Ren, Talanta 69 (2006) 107.
[26] K. Yu, Y.W. Wang, Y.Y. Cheng, J. Pharm. Biomed. Anal. 40 (2006) 1257.
[27] S.L. He, Y.F. Zhao, Z.W. Zhu, H.W. Liu, M.X. Li, Y.H. Shao, Q.K. Zhuang, Talanta 69 (2006) 166.
[28] L. Clohs, K.M. McErlane, J. Pharm. Biomed. Anal. 31 (2003) 407.
[29] N. Anastos, N.W. Barnett, S.W. Lewis, Talanta 67 (2005) 269.
[30] Y.Q. Li, S.D. Qi, X.G. Chen, Z.D. Hu, Electrophoresis 25 (2004) 3003.
[31] J.Z. Song, H.X. Xu, S.J. Tian, P.P.H. But, J. Chromatogr. A 857 (1999) 303.
[32] V. Gökmen, H.Z. Şenyuva, J. Acar, K. Sarıoğlu, J. Chromatogr. A 1088 (2005) 193.
[33] FDA Centers for Disease Control and Prevention. Exploratory data on acrylamide in foods, February 2003 update [EB/OL]. http://www.cfsan.fda.gov/∼dms.